

# METABOLISM MEETS FUNCTION: THE MULTIFACED ROLE OF METABOLISM IN CANCER

EDITED BY: Andrea Morandi, Lorenzo Galluzzi, Miriam Martini and  
Monica Montopoli  
PUBLISHED IN: Frontiers in Oncology







# frontiers

## Frontiers eBook Copyright Statement

The copyright in the text of individual articles in this eBook is the property of their respective authors or their respective institutions or funders. The copyright in graphics and images within each article may be subject to copyright of other parties. In both cases this is subject to a license granted to Frontiers.

The compilation of articles constituting this eBook is the property of Frontiers.

Each article within this eBook, and the eBook itself, are published under the most recent version of the Creative Commons CC-BY licence.

The version current at the date of publication of this eBook is CC-BY 4.0. If the CC-BY licence is updated, the licence granted by Frontiers is automatically updated to the new version.

When exercising any right under the CC-BY licence, Frontiers must be attributed as the original publisher of the article or eBook, as applicable.

Authors have the responsibility of ensuring that any graphics or other materials which are the property of others may be included in the CC-BY licence, but this should be checked before relying on the CC-BY licence to reproduce those materials. Any copyright notices relating to those materials must be complied with.

Copyright and source acknowledgement notices may not be removed and must be displayed in any copy, derivative work or partial copy which includes the elements in question.

All copyright, and all rights therein, are protected by national and international copyright laws. The above represents a summary only. For further information please read Frontiers' Conditions for Website Use and Copyright Statement, and the applicable CC-BY licence.

ISSN 1664-8714

ISBN 978-2-88976-243-9

DOI 10.3389/978-2-88976-243-9

## About Frontiers

Frontiers is more than just an open-access publisher of scholarly articles: it is a pioneering approach to the world of academia, radically improving the way scholarly research is managed. The grand vision of Frontiers is a world where all people have an equal opportunity to seek, share and generate knowledge. Frontiers provides immediate and permanent online open access to all its publications, but this alone is not enough to realize our grand goals.

## Frontiers Journal Series

The Frontiers Journal Series is a multi-tier and interdisciplinary set of open-access, online journals, promising a paradigm shift from the current review, selection and dissemination processes in academic publishing. All Frontiers journals are driven by researchers for researchers; therefore, they constitute a service to the scholarly community. At the same time, the Frontiers Journal Series operates on a revolutionary invention, the tiered publishing system, initially addressing specific communities of scholars, and gradually climbing up to broader public understanding, thus serving the interests of the lay society, too.

## Dedication to Quality

Each Frontiers article is a landmark of the highest quality, thanks to genuinely collaborative interactions between authors and review editors, who include some of the world's best academicians. Research must be certified by peers before entering a stream of knowledge that may eventually reach the public - and shape society; therefore, Frontiers only applies the most rigorous and unbiased reviews.

Frontiers revolutionizes research publishing by freely delivering the most outstanding research, evaluated with no bias from both the academic and social point of view. By applying the most advanced information technologies, Frontiers is catapulting scholarly publishing into a new generation.

## What are Frontiers Research Topics?

Frontiers Research Topics are very popular trademarks of the Frontiers Journals Series: they are collections of at least ten articles, all centered on a particular subject. With their unique mix of varied contributions from Original Research to Review Articles, Frontiers Research Topics unify the most influential researchers, the latest key findings and historical advances in a hot research area! Find out more on how to host your own Frontiers Research Topic or contribute to one as an author by contacting the Frontiers Editorial Office: [frontiersin.org/about/contact](http://frontiersin.org/about/contact)

# METABOLISM MEETS FUNCTION: THE MULTIFACED ROLE OF METABOLISM IN CANCER

Topic Editors:

**Andrea Morandi**, University of Florence, Italy

**Lorenzo Galluzzi**, Cornell University, United States

**Miriam Martini**, University of Turin, Italy

**Monica Montopoli**, University of Padua, Italy

**Citation:** Morandi, A., Galluzzi, L., Martini, M., Montopoli, M., eds. (2022).

Metabolism Meets Function: The Multifaced Role of Metabolism in Cancer.

Lausanne: Frontiers Media SA. doi: 10.3389/978-2-88976-243-9

# Table of Contents

- 06 Editorial: Metabolism Meets Function: The Multifaced Role of Metabolism in Cancer**  
Isabella Giacomini and Monica Montopoli
- 08 Metabolomic Markers of Colorectal Tumor With Different Clinicopathological Features**  
Zhiping Long, Junde Zhou, Kun Xie, Zhen Wu, Huihui Yin, Volontovich Daria, Jingshen Tian, Nannan Zhang, Liangliang Li, Yashuang Zhao, Fan Wang, Maoqing Wang and Yunfu Cui
- 18 Targeting SREBP-2-Regulated Mevalonate Metabolism for Cancer Therapy**  
Linyuan Xue, Hongyu Qi, He Zhang, Lu Ding, Qingxia Huang, Daqing Zhao, Boyang Jason Wu and Xiangyan Li
- 38 GC1qR Cleavage by Caspase-1 Drives Aerobic Glycolysis in Tumor Cells**  
Annika Sünderhauf, Annika Raschdorf, Maren Hicken, Heidi Schlichting, Franziska Fetzer, Ann-Kathrin Brethack, Sven Perner, Claudia Kemper, Berhane Ghebrehiwet, Christian Sina and Stefanie Derer
- 54 Deregulation of Lipid Metabolism: The Critical Factors in Ovarian Cancer**  
Zhaodong Ji, Yan Shen, Xu Feng, Yue Kong, Yang Shao, Jiao Meng, Xiaofei Zhang and Gong Yang
- 64 Identification of Metabolism-Associated Prostate Cancer Subtypes and Construction of a Prognostic Risk Model**  
Yanlong Zhang, Ruiqiao Zhang, Fangzhi Liang, Liyun Zhang and Xuezhi Liang
- 81 Metabolism-Associated Molecular Classification of Colorectal Cancer**  
Meng Zhang, Hai-zhou Wang, Ru-yi Peng, Fei Xu, Fan Wang and Qiu Zhao
- 93 The Implications of PDK1–4 on Tumor Energy Metabolism, Aggressiveness and Therapy Resistance**  
Emine Atas, Monika Oberhuber and Lukas Kenner
- 102 Heterozygous P32/C1QBP/HABP1 Polymorphism rs56014026 Reduces Mitochondrial Oxidative Phosphorylation and Is Expressed in Low-grade Colorectal Carcinomas**  
Annika Raschdorf, Annika Sünderhauf, Kerstin Skibbe, Berhane Ghebrehiwet, Ellinor I. Peerschke, Christian Sina and Stefanie Derer
- 119 The Mevalonate Pathway, a Metabolic Target in Cancer Therapy**  
Borja Guerra, Carlota Recio, Haidée Aranda-Tavío, Miguel Guerra-Rodríguez, José M. García-Castellano and Leandro Fernández-Pérez
- 140 Asparagine Synthetase-Mediated L-Asparagine Metabolism Disorder Promotes the Perineural Invasion of Oral Squamous Cell Carcinoma**  
Yong Fu, Liang Ding, Xihu Yang, Zhuang Ding, Xiaofeng Huang, Lei Zhang, Sheng Chen, Qingang Hu and Yanhong Ni

- 151 *Biological Roles and Therapeutic Applications of IDH2 Mutations in Human Cancer***  
Jinxu Guo, Ruyue Zhang, Zhe Yang, Zhenfeng Duan, Detao Yin and Yubing Zhou
- 163 *Cholesterol Metabolic Reprogramming in Cancer and Its Pharmacological Modulation as Therapeutic Strategy***  
Isabella Giacomini, Federico Gianfanti, Maria Andrea Desbats, Genny Orso, Massimiliano Berretta, Tommaso Prayer-Galetti, Eugenio Ragazzi and Veronica Cocetta
- 186 *Lactate Modulates Cellular Metabolism Through Histone Lactylation-Mediated Gene Expression in Non-Small Cell Lung Cancer***  
Jun Jiang, DengLiang Huang, Yuan Jiang, Jing Hou, MeiYuan Tian, JianHua Li, Li Sun, YaoGang Zhang, Tao Zhang, ZhiQin Li, ZhongCheng Li, SiXian Tong and YanYan Ma
- 199 *Normalization of Enzyme Expression and Activity Regulating Vitamin A Metabolism Increases RAR-Beta Expression and Reduces Cellular Migration and Proliferation in Diseases Caused by Tuberous Sclerosis Gene Mutations***  
Elhusseiny Mohamed Mahmoud Abdelwahab, Judit Bovari-Biri, Gabor Smuk, Tunde Harko, Janos Fillinger, Judit Moldvay, Vera P. Krymskaya and Judit E. Pongracz
- 210 *Energy Metabolic Plasticity of Colorectal Cancer Cells as a Determinant of Tumor Growth and Metastasis***  
Leenu Reinsalu, Marju Puurand, Vladimir Chekulayev, Sten Miller, Igor Shevchuk, Kersti Tepp, Egle Rebane-Klemm, Natalja Timohhina, Anton Terasmaa and Tuuli Kaambre
- 221 *SNAP25 Inhibits Glioma Progression by Regulating Synapse Plasticity via GLS-Mediated Glutaminolysis***  
Qiongzheng Huang, Changlin Lian, Yaoyuan Dong, Huijun Zeng, Boyang Liu, Ningbo Xu, Zhenyan He and Hongbo Guo
- 235 *Regulation of Extracellular Matrix Production in Activated Fibroblasts: Roles of Amino Acid Metabolism in Collagen Synthesis***  
Emily J. Kay, Grigorios Koulouras and Sara Zanivan
- 246 *Mechanisms Governing Metabolic Heterogeneity in Breast Cancer and Other Tumors***  
Sayani Patra, Naveed Elahi, Aaron Armorer, Swathi Arunachalam, Joshua Omala, Iman Hamid, Anthony W. Ashton, David Joyce, Xuanmao Jiao and Richard G. Pestell
- 265 *Oncogenic Integration of Nucleotide Metabolism via Fatty Acid Synthase in Non-Hodgkin Lymphoma***  
Dashnamoorthy Ravi, Afshin Beheshti, Nasséra Abermil, Frederick Lansigan, William Kinlaw, Nirupa R. Matthan, Maisarah Mokhtar, Frank C. Passero Jr., Patrick Puliti, Kevin A. David, Gregory G. Dolnikowski, Xiaoyang Su, Ying Chen, Mahboubi Bijan, Rohan R. Varshney, Baek Kim, Sandeep S. Dave, Michael C. Rudolph and Andrew M. Evens
- 281 *Metabolic Reprogramming of Thyroid Cancer Cells and Crosstalk in Their Microenvironment***  
Lisha Bao, Tong Xu, Xixuan Lu, Ping Huang, Zongfu Pan and Minghua Ge

**297   *The Metabolism Symbiosis Between Pancreatic Cancer and Tumor Microenvironment***

Ying Li, Ju Zhang, Jie Xu and Shanglong Liu

**307   *Effects of Metformin Combined With Antifolates on HepG2 Cell Metabolism and Cellular Proliferation***

Sherouk M. Tawfik, Maha R. A. Abdollah, Mohey M. Elmazar,  
Hassan A. N. El-Fawal and Anwar Abdelnaser

**324   *Tryptophan Metabolites as Biomarkers for Esophageal Cancer Susceptibility, Metastasis, and Prognosis***

Yun Chen, Jianliang Chen, Dainian Guo, Peixuan Yang, Shuang Chen,  
Chengkuan Zhao, Chengcheng Xu, Qiuzhen Zhang, Chaoxian Lin,  
Shilong Zhong and Shuyao Zhang



# Editorial: Metabolism Meets Function: The Multifaced Role of Metabolism in Cancer

Isabella Giacomini<sup>1</sup> and Monica Montopoli<sup>1,2,3\*</sup>

<sup>1</sup> Department of Pharmaceutical and Pharmacological Sciences, University of Padova, Padova, Italy, <sup>2</sup> Veneto Institute of Molecular Medicine, VIMM, Padova, Italy, <sup>3</sup> Institute of Oncology Research (IOR), Bellinzona, Switzerland

**Keywords:** cancer, cancer metabolism, tumor microenvironment (TME), drug resistance, metabolic reprogramming, targeting metabolism

## Editorial on the Research Topic

### Metabolism Meets Function: The Multifaced Role of Metabolism in Cancer

#### OPEN ACCESS

##### Edited and reviewed by:

Michael P. Lisanti,  
University of Salford, United Kingdom

##### \*Correspondence:

Monica Montopoli  
monica.montopoli@unipd.it

##### Specialty section:

This article was submitted to  
Cancer Metabolism,  
a section of the journal  
Frontiers in Oncology

**Received:** 28 March 2022

**Accepted:** 08 April 2022

**Published:** 04 May 2022

##### Citation:

Giacomini I and Montopoli M  
(2022) Editorial: Metabolism  
Meets Function: The Multifaced  
Role of Metabolism in Cancer.  
Front. Oncol. 12:906421.  
doi: 10.3389/fonc.2022.906421

Cancer cells are highly proliferative cells and it has been reported that they are continuously rewiring their metabolism to support tumor growth and the enhanced energy supply.

Alterations of cancer metabolism involved several pathways, such as altered glycolysis, unbalanced lipid synthesis, or glutamine exploitation, as well as a shift toward pentose phosphate pathway or mitochondrial dysfunctions (1, 2). All these metabolic changes are known as metabolic reprogramming.

Emerging evidence reported that metabolic reprogramming of cancer cells is considered a hallmark of cancer and of drug resistance (3).

Although new discoveries in this field, there is still the need of understanding the mechanisms adopted by cancer cells that support metabolic changes, untangling the cross-link between metabolic reprogramming and tumor initiation and progression. Figuring out the molecular mechanisms that lead to alterations in cancer metabolism appears as a promising strategy for cancer therapy and to overcome drug resistance.

This Research Topic is aimed to investigate the metabolic aspects in cancer cells including (but not limited to):

- Crosstalk between metabolic reprogramming and tumor microenvironment in cancer;
- To assess whether metabolites with non-metabolic function could play a role in tumor initiation and progression;
- Characterize the phenotype of cancers establishing a correlation with metabolic reprogramming.

In addition, discussions about the promising approach of targeting metabolic alterations both alone and combined with standard therapeutic regimens will be appreciated in this Research Topic.

Authors are welcome to submit original research or review articles to provide the readers with up-to-date knowledge of the role of metabolic reprogramming in supporting and driving all the aspects of cancer biology.

## REFERENCES

1. Desbats MA, Giacomini I, Prayer-Galett T, Montopoli M. Metabolic Plasticity in Chemotherapy Resistance. *Front Oncol* (2020) 10:281. doi: 10.3389/fonc.2020.00281
2. Cocetta V, Ragazzi E, Montopoli M. Mitochondrial Involvement in Cisplatin Resistance. *Int J Mol Sci* (2019) 20:3384. doi: 10.3390/ijms20143384
3. Giacomini I, Ragazzi E, Pasut G, Montopoli M. The Pentose Phosphate Pathway and Its Involvement in Cisplatin Resistance. *Int J Mol Sci* (2020) 21:937. doi: 10.3390/ijms21030937

**Conflict of Interest:** The authors declare that the research was conducted in the absence of any commercial or financial relationships that could be construed as a potential conflict of interest.

## AUTHOR CONTRIBUTIONS

IG wrote the editorial. MM conceived and edit the editorial. All authors contributed to the article and approved the submitted version.

**Publisher's Note:** All claims expressed in this article are solely those of the authors and do not necessarily represent those of their affiliated organizations, or those of the publisher, the editors and the reviewers. Any product that may be evaluated in this article, or claim that may be made by its manufacturer, is not guaranteed or endorsed by the publisher.

*Copyright © 2022 Giacomini and Montopoli. This is an open-access article distributed under the terms of the Creative Commons Attribution License (CC BY). The use, distribution or reproduction in other forums is permitted, provided the original author(s) and the copyright owner(s) are credited and that the original publication in this journal is cited, in accordance with accepted academic practice. No use, distribution or reproduction is permitted which does not comply with these terms.*



# Metabolomic Markers of Colorectal Tumor With Different Clinicopathological Features

Zhiping Long<sup>1†</sup>, Junde Zhou<sup>2†</sup>, Kun Xie<sup>1</sup>, Zhen Wu<sup>1</sup>, Huihui Yin<sup>1</sup>, Volontovich Daria<sup>1</sup>, Jingshen Tian<sup>1</sup>, Nannan Zhang<sup>1</sup>, Liangliang Li<sup>1</sup>, Yashuang Zhao<sup>1</sup>, Fan Wang<sup>1\*</sup>, Maoqing Wang<sup>3\*</sup> and Yunfu Cui<sup>4\*</sup>

<sup>1</sup> Department of Epidemiology, School of Public Health, Harbin Medical University, Harbin, China, <sup>2</sup> Department of Colorectal Surgery, The Second Affiliated Hospital of Harbin Medical University, Harbin, China, <sup>3</sup> Department of Nutrition and Food Hygiene, School of Public Health, Harbin Medical University, Harbin, China, <sup>4</sup> Department of General Surgery, The Second Affiliated Hospital of Harbin Medical University, Harbin, China

## OPEN ACCESS

### Edited by:

Miriam Martini,  
University of Turin, Italy

### Reviewed by:

Eugenio Ragazzi,  
University of Padova, Italy  
Alessandra Castegna,  
University of Bari Aldo Moro, Italy

### \*Correspondence:

Fan Wang  
yifan.701@163.com  
Maoqing Wang  
wang\_maoqing@126.com  
Yunfu Cui  
yfcui777@hotmail.com

<sup>†</sup>These authors have contributed  
equally to this work

### Specialty section:

This article was submitted to  
Cancer Metabolism,  
a section of the journal  
Frontiers in Oncology

**Received:** 15 March 2020

**Accepted:** 18 May 2020

**Published:** 17 June 2020

### Citation:

Long Z, Zhou J, Xie K, Wu Z, Yin H,  
Daria V, Tian J, Zhang N, Li L, Zhao Y,  
Wang F, Wang M and Cui Y (2020)  
Metabolomic Markers of Colorectal  
Tumor With Different  
Clinicopathological Features.  
Front. Oncol. 10:981.  
doi: 10.3389/fonc.2020.00981

**Background:** Colorectal cancer (CRC) is the result of complex interactions between the tumor's molecular profile and metabolites produced by its microenvironment. Despite recent studies identifying CRC molecular subtypes, a metabolite classification system is still lacking. We aimed to explore the distinct phenotypes and subtypes of CRC at the metabolite level.

**Methods:** We conducted an untargeted metabolomics analysis of 51 paired tumor tissues and adjacent mucosa using ultra-performance liquid chromatography/quadrupole time-of-flight mass spectrometry. Multivariate analysis including principal component analysis, orthogonal partial least squares discriminant analysis and heat maps, univariate analysis, and pathway analysis were used to identify potential metabolite phenotypes of CRC. Unsupervised consensus clustering was used to identify robust metabolite subtypes, and evaluated their clinical relevance.

**Results:** A total of 173 metabolites (including nucleotides, carbohydrates, free fatty acids, and choline) were identified between CRC tumor tissue and adjacent mucosa. We found that lipid metabolism was closely related to the occurrence and progression of CRC. In particular, CRC tissues could be divided into three subtypes, and statistically significant correlations between different subtypes and clinical prognosis were observed.

**Conclusions:** CRC tumor tissue exhibits distinct metabolite phenotypes. Metabolite differences between subtypes may provide a basis and direction for further clinical individualized treatment planning.

**Keywords:** metabolomics, subtypes, CRC, prognosis, lipid metabolism

## INTRODUCTION

Colorectal cancer (CRC) is one of the leading causes of cancer-related death, both in China and worldwide. More than one million individuals develop CRC every year and most patients are diagnosed at advanced stages that correspond to poor prognosis (1). With the advances in the treatment of CRC over the past 20 years, median overall survival has been steadily increasing (2). Although the progress made thus far is encouraging, the existing treatment paradigm usually



employs a “one-size-fits-all” approach based on the histopathological diagnosis of CRC, which translates into demonstrable clinical benefit from any given chemotherapeutic regimen in only a small subset of treated patients (3).

It is now being increasingly realized that CRC is not a single disease entity, but a heterogeneous group of tumors, both at the inter-tumoral and intra-tumoral level (2). A major hallmark of CRC is its association with various types of etiological factors and its high heterogeneity in clinical presentation and underlying tumor biology (4). Consequently, most patients with CRC are refractory to treatment and have a dismal outcome. One of the essential requirements to improve their outcome is to provide biomarkers that are capable of accurately defining homogenous molecular subtypes; each displays unique tumor biology linked to potentially druggable driver genes to implement rational treatment choices (5).

Nowadays, tumor genomic profiling is routinely used to classify tumor types, identify driver or germline mutations, perform prognostic assessments, and make therapeutic decisions (6, 7). However, the notable heterogeneity of genomes in cancer tissues makes it difficult to determine the underlying causes or ascertain the optimal treatment. Furthermore, the elevated number of mutations and multiple combinations of tumor suppressors and oncogenes make individualized tumor classification or customized therapy almost impossible (8). Metabolomics is a rapidly growing field of study that endeavors to measure the complete set of metabolites (generally considered to be the intermediates and products of cellular metabolism <1 kDa in size) within a biological sample (that is, the metabolome) to achieve a global view of the state of the system (9). In general, multiple biochemical pathways are affected, owing to the fact that as cancer progresses, multiple defects in biochemical pathways arise as cancer subverts normal metabolism in an effort to survive (10). Furthermore, the metabolite requirements of cancer cells are different from those of most normal differentiated cells, exhibiting different metabolite phenotypes (11). Using metabolomics to identify the specific metabolite subtype of a particular tumor would enable better customization or informed adjustment of cancer therapies (12).

To present, metabolomics-based CRC phenotypic research and molecular typing have been rarely described, and little is known about how changes in metabolite levels relate to the characteristics of tumor tissue. In this study, we described a metabolomics analysis of CRC tissue samples from a group of CRC patients with different clinicopathological features. We aimed to analyze the differential metabolism of tumor tissues with different clinicopathological features, and to explore molecular typing methods for CRC based on metabolomics markers.

**Abbreviations:** CRC, colorectal cancer; ESI<sup>−</sup>, negative electrospray ionization; ESI<sup>+</sup>, positive electrospray ionization; VIP, variable important for the projection; mClusters, metabolite clusters; FFA, free fatty acids; ANIT, adjacent non-involved tissues.

## METHODS

### Study Design and Subject Recruitment

We designed a self-control study to detect the differential metabolites between tumor tissue and adjacent non-malignant mucosa tissue. Fifty-one pairs of tissue were obtained from surgical resection of CRC patients.

All patients were diagnosed and recruited at the Third Affiliated Hospital of Harbin Medical University. Any patients with neuroendocrine carcinoma, malignant melanoma, non-Hodgkin's lymphoma, gastrointestinal stromal tumors, and Lynch syndrome CRC were excluded. Only newly diagnosed histopathologically confirmed cases were retained. Tissue sampling included the deepest infiltration of the tumor and the adjacent non-malignant mucosa tissues. All tissues were immediately soaked in formaldehyde solution until use.

All procedures performed in studies involving human participants were in accordance with the ethical standards of the Human Research and Ethics Committee of Harbin Medical University and with the 1964 Helsinki declaration and its later amendments or comparable ethical standards. Informed consent was obtained from all individual participants included in the study.

### Metabolite Profiling

A detailed description of the experimental protocol of metabolite profiling analysis by UPLC/Q-TOF-MS/MS and the data processing, multivariate and univariate analysis of metabolites, as well as identification of differential metabolites, are provided in the **Supplementary Materials**.

### Pathway Analysis

Using an accurate *m/z* search under 50 ppm, metabolites from positive and negative ionization were matched in Mummichog software, which included metabolites from KEGG and other databases. Mummichog software (version 1.0.9) was used to further test pathway enrichment patterns using permutations, and to compute the probability for each pathway (13).

### Metabolite Clustering

Consensus clustering (cCluster; hierarchical clustering; Pearson distance; complete linkage; 1,000 resampling iteration) and unsupervised hierarchical clustering were performed to define subtypes of CRC tumor tissue samples (14, 15). Heatmaps were generated using the Complex Heatmap package in R to determine the relationship among samples or cCluster-defined subgroups (16).

### Clinical Relevance Analysis of Metabolite Subtypes

We assessed whether the metabolite subtypes had significant associations with overall survival. The R packages “survival” and “survminer” were used to perform the overall survival analysis and to produce Kaplan-Meier survival plots. A log-rank test was used to assess the significance ( $P < 0.05$ ). We further assessed whether the metabolite subtypes remained significantly associated with overall survival after adjusting for age, sex,

clinical stage, postoperative chemotherapy, and immunotherapy as covariates in the Cox model.

## RESULTS

### Metabolite Profiling of 51 Pairs of Tumor Tissue and Adjacent Mucosa Tissue

To identify the differential metabolites of CRC, the metabolomes of tumor tissues were compared with that of matched adjacent mucosa. **Supplementary Table 1** shows the demographic characteristics and clinicopathological features of 51 CRC patients. Mass spectrometry detected 4,526 and 4,765 variables in negative electrospray ionization (ESI-) and positive electrospray ionization (ESI+), respectively. Multivariate analysis was performed on the result of mass spectrometry to find metabolites that mostly discriminated the study groups. Principal component analysis (PCA) was the unsupervised analysis method, which was used for dimension reduction of data through making a linear combination of variables known as principal components. PCA analysis can reveal trends in the data and groups of observations and find outliers. Although a weak trend in clustering according to the PCA plot based on tumor tissue and adjacent mucosa was observed, the PCA analysis results showed a separation of tumor tissue and adjacent mucosa into two clusters (**Figures 1A,D**). To further study the differences between tumor tissue and adjacent mucosa and to find potential biomarkers, the supervised multivariate statistical method OPLS-DA was subsequently used. OPLS-DA is a supervised analysis method that is employed to divide the samples into different groups, including tumor tissue and adjacent mucosa, which was performed to find metabolites that mostly discriminated the studied groups in each comparison. The classification results are shown in **Figures 1B,E**. To guard against model overfitting, permutation tests (100 random permutations) were performed. These permutation tests were used to contrast the goodness of fit of the original model with the goodness of fit of randomly permuted models. As shown in **Figures 1C,F**, the validation plots strongly indicated that the original combined models were valid. No overfitting was observed.

A total of 373 metabolites (296 higher and 77 lower) were identified with the criteria of Variable important for the projection (VIP) score  $>1.5$  and  $P$ -values of  $<0.05$  in the false detection rate (FDR)-corrected Mann-Whitney U tests, which displayed differential abundance between tumor and adjacent mucosa samples (**Supplementary Figure 1**). The Human Metabolome Database (<http://www.hmdb.ca/>) mass search feature was used as to aid metabolite identification. A total of 173 metabolites were identified as shown in **Supplementary Table 2**. Interestingly, nucleotides, carbohydrates, free fatty acids, and choline were overrepresented and highly abundant in tumors, such as D-ribulose 5-phosphate, D-glucose, xylulose 5-phosphate, 3'-AMP, hypoxanthine, palmitoleic acid, and cytidine monophosphate (**Supplementary Table 2**).

### Metabolite Landscape of CRC Tumors

Pathway analysis was performed to systematically investigate the metabolite alterations associated with CRC pathogenesis.

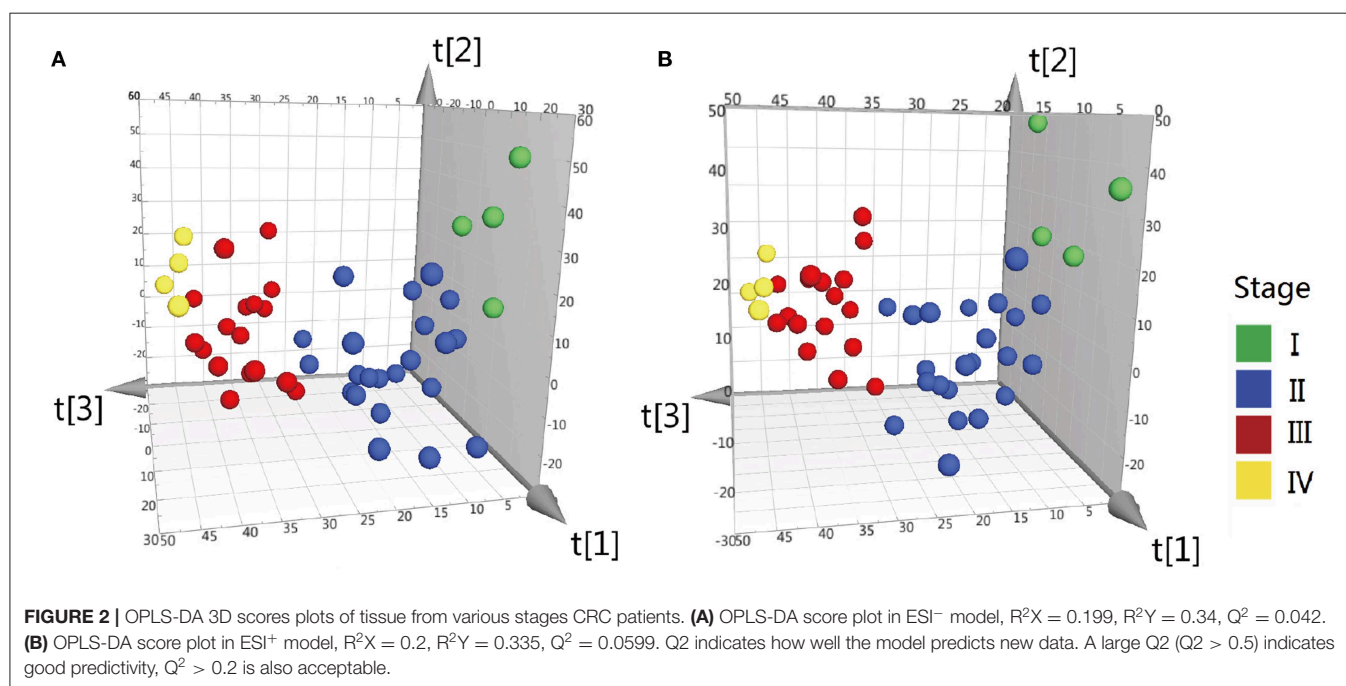
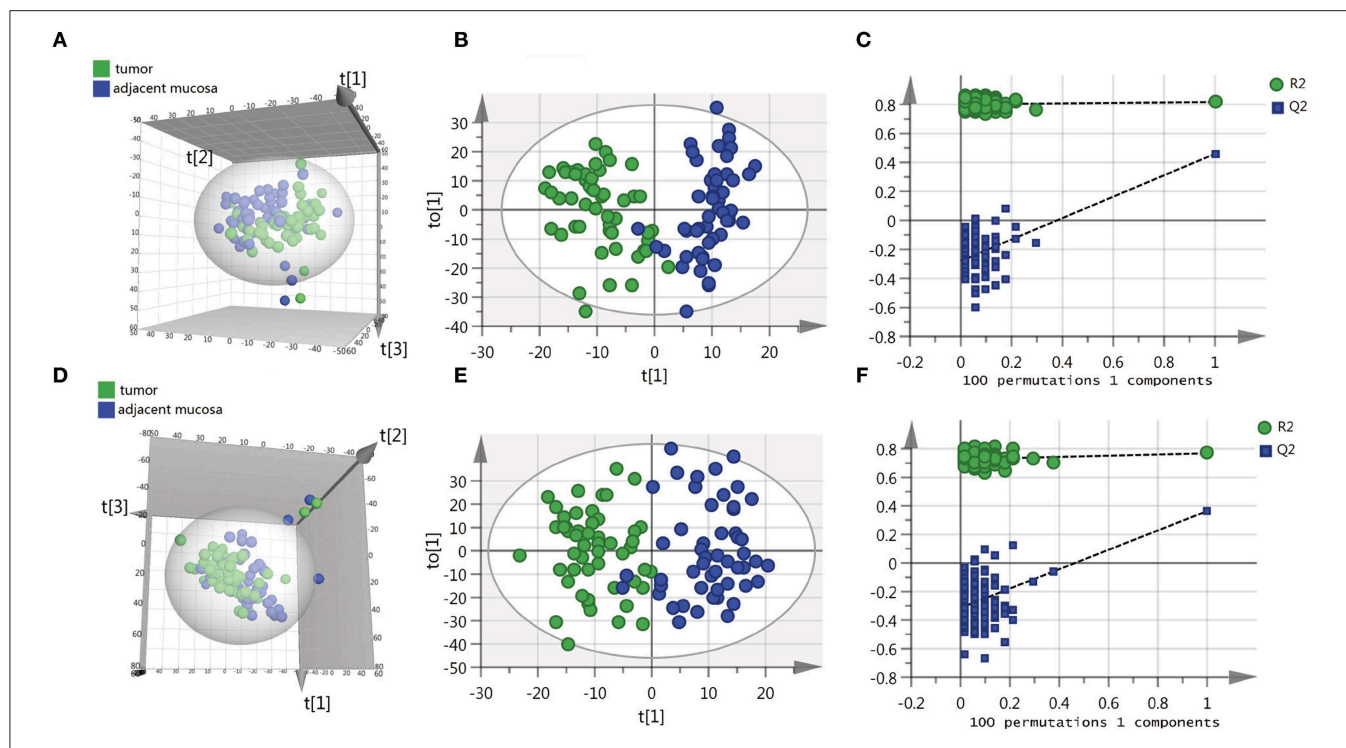
Mummichog software, a pathway tool designed for untargeted metabolomics data [13], was used to evaluate the significant metabolite pathways utilizing metabolites that were present at differential abundance between CRC tissues and adjacent mucosa. The mummichog analysis was performed on the previously identified 373 positive and negative ions, and the results are shown in **Supplementary Table 3**; interestingly, among the 34 metabolite pathways, most were involved in lipid metabolism ( $n = 7$ ) and glycan biosynthesis and metabolism ( $n = 8$ ). Other metabolite pathways included glycolysis/gluconeogenesis, pentose phosphate pathway, and tryptophan metabolism.

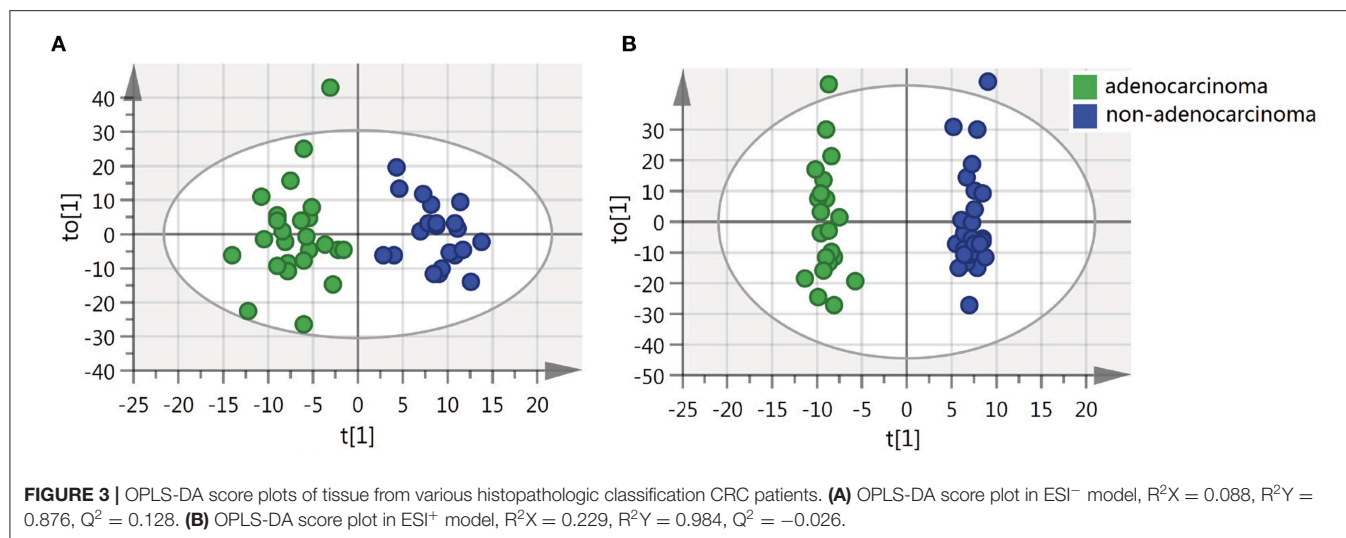
### Metabolite Changes Upon CRC Progression

Difference stage-distributed CRC samples allowed us to investigate the association between metabolite shifts and CRC progression. Based on the 4,526 and 4,765 variables in ESI- and ESI+, using American Joint Committee on Cancer (AJCC) clinical staging, the OPLS-DA analysis of the metabolite profiles of tumor tissue could separate clusters for each stage (**Figure 2**). Validation of the OPLS-DA model was performed here by permutation testing. Although the permutation test indicates that the OPLS-DA model is valid, the model fitting is not very satisfactory (**Supplementary Figure 2**). There were 94 metabolites exhibiting statistically significant differential abundance between early- (I, II) and late-stage (III, IV) tumors (VIP  $> 1.5$  and Mann-Whitney U-test FDR corrected  $P$ -value  $< 0.01$ ), and a total of 48 metabolites were identified (**Supplementary Table 3**). Most lipid metabolites showed an increase in late-stage tumors, while dipeptides also showed a decrease in late-stage tumors (**Supplementary Figure 3**). The results of pathway analysis by Mummichog software indicated that significant features are enriched for pathways involved in lipid metabolism (**Supplementary Table 4**).

### Metabolite Alterations of CRC Pathologic Characteristics

We also sought to determine whether we could identify the differences in metabolite features among various histopathological classifications of CRC. The separation of adenocarcinoma and non-adenocarcinoma CRCs was observed using OPLS-DA (**Figure 3**). Similarly, the permutation test indicates that the OPLS-DA model is valid, but, the model fitting is also unsatisfactory (**Supplementary Figure 4**). Forty-three metabolites exhibited statistically significant differential abundance between adenocarcinoma and non-adenocarcinoma tumors (VIP  $> 1.5$  and  $P < 0.01$ ). Furthermore, a total of 26 metabolites were identified (**Supplementary Table 5**) and almost all these 26 metabolites were lipids. Mummichog indicated that pathways involved in lipid metabolism were also significantly enriched (**Supplementary Table 5**).





### Unsupervised Clustering Reveals Three Metabolite Clusters (mClusters) With Prognostic Value

The results of cCluster showed that CRC tumor samples can be partitioned into clusters with distinct metabolite phenotypes using the differential metabolites among tumor and adjacent mucosa samples. cCluster revealed three major subtypes of CRC according to consensus distributions and the corresponding consensus matrices (Figure 4). Especially, the CRC subtypes defined by cCluster can be obviously observed through unsupervised hierarchical clustering (Figure 5), which is much clearer than the classification effect according to the pathological stages of tumor in Supplementary Figure 3. The rough estimate by chi-square tests indicated that there was no statistically significant consistency between the three mClusters and clinicopathological features, respectively (as shown in Figure 5). This analysis revealed unique subtypes of CRC cases with distinct metabolite patterns that were independent of known clinicopathological features.

For each metabolite cluster (mCluster), the clinical stages at presentation are summarized in Supplementary Figure 5. mCluster 1 had the highest percentage (66.7%) of early-stage (I & II) tumors and was characterized by the low abundance of carbohydrates, nucleotide metabolites, dipeptides, and lipids; mCluster 2 had the highest percentage (51.9%) of late-stage (III & IV) tumors and displayed medium levels of all metabolites; mCluster 3, characterized by the highest abundance of carbohydrates, nucleotide metabolites, dipeptides, and lipids, accounted for 62.5% early-stage tumors (Figure 5 and Supplementary Figure 5).

Additionally, we further determined the correlations of mClusters with patients' overall survival. As shown in Figure 6A, the result did not reach statistical significance, likely due to the relatively small number of events during follow-up (log-rank  $P = 0.099$ ). However, regardless of clinical staging, mCluster 1 and 3 (the two groups with similar prognostic survival) were combined,

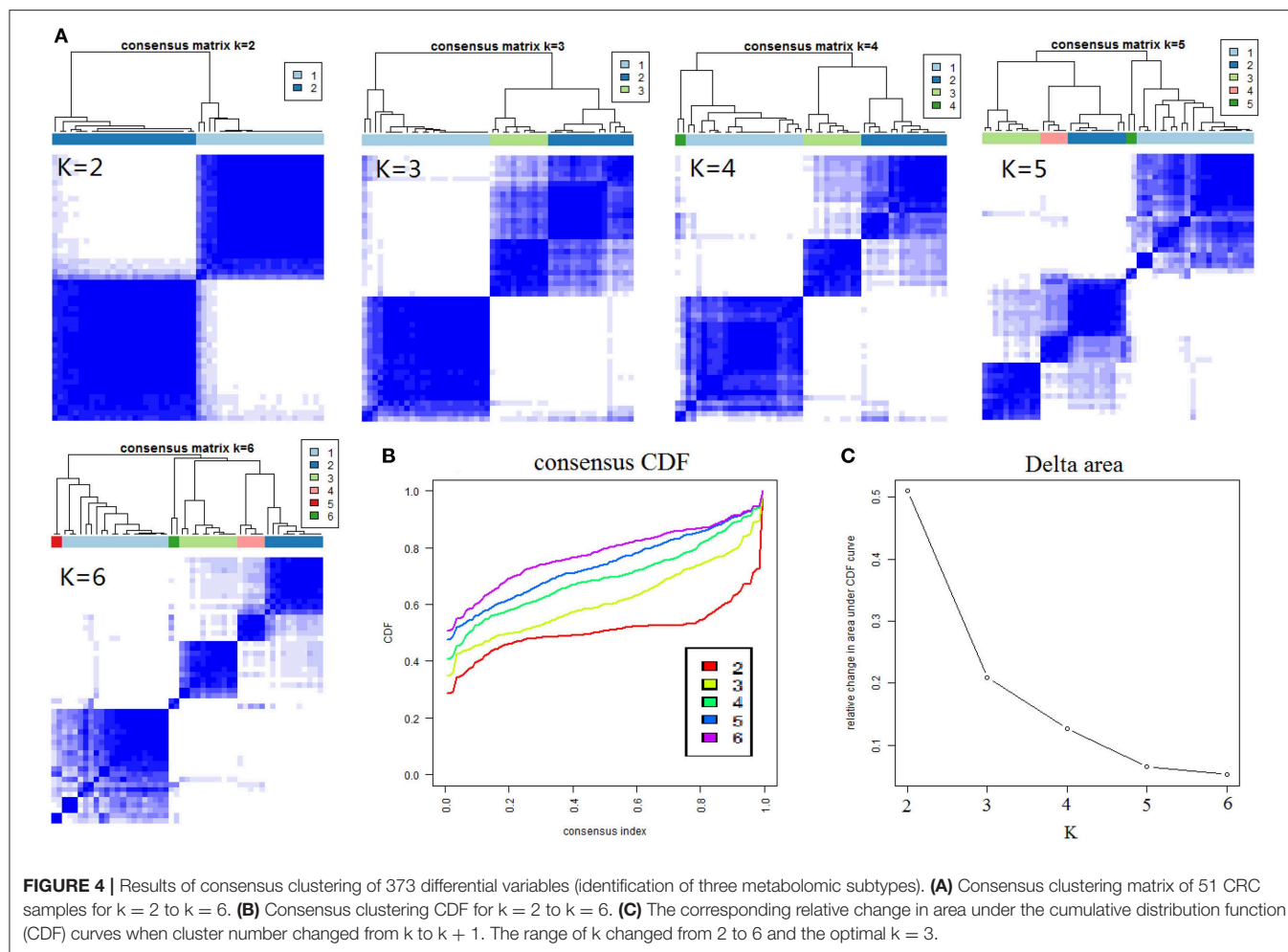
cases defined as mCluster 2 showed statistically significant poor survival (log-rank  $P = 0.032$ , Figure 6B). More importantly, we obtained the same results using Cox regression models adjusting by age, sex, clinical stage, and postoperative chemotherapy and immunotherapy ( $P = 0.027$ , Figure 6C).

### DISCUSSION

Metabolomics analysis of CRC can not only distinguish tumor tissue from adjacent mucosa, but can also discriminate CRC patients with different clinicopathological features. What's more, through the high-throughput metabolomics analysis using UPLC/Q-TOF MS mass spectrometry platform, metabolite profiling allows a more comprehensive understanding of CRC phenotyping. We are the first time defined molecular subtypes of CRC based on metabolomics. The results of our study indicated the molecular subtyping based on differential metabolites showed much better classification effect than according to pathological stages of tumor; especially, significant differences in survival was observed of the metabolic subtypes. It suggested us individualized treatment guided by molecular typing based on metabolites may be more reasonable and effective than treatment based on the same stage or morphological type.

Tian et al. analyzed the metabolomic signatures of 50 human CRC tissues and their adjacent non-involved tissues (ANIT) using high-resolution magic-angle spinning (HRMAS) <sup>1</sup>H NMR spectroscopy together with the fatty acid compositions of these tissues using GC-FID/MS (17). In this study, metabolomic phenotypes of CRC tissues differed significantly from that of ANIT in energy metabolism, membrane biosynthesis and degradation, and osmotic regulation together with the metabolism of proteins and nucleotides. Diverse metabolite pathways including N-glycan biosynthesis and degradation, linoleate metabolism, leukotriene metabolism, butanoate metabolism, glycosphingolipid biosynthesis, drug metabolism-cytochrome P450 and vitamin B5-CoA biosynthesis from





pantothenate significantly differed between tumor and normal tissues. The UPLC/Q-TOF MS-based metabolomics approach of this study provided additional information that complements our current understanding of the metabolomic characteristics between CRC tumor tissues and adjacent mucosa.

The Warburg effect is a known feature of cancer metabolism that describes maintenance of a high aerobic glycolysis rate and high levels of glucose uptake and lactate production during tumor growth (18, 19). Our findings are consistent with the Warburg effect. The difference in energy metabolism can be clearly observed between CRC tumor tissues and adjacent mucosa. Compared with adjacent mucosa, carbohydrates in colorectal cancer tissues were significantly increased and the pentose phosphate pathway and glycolysis/gluconeogenesis pathways were identified. In cancer metabolism, glycolysis is the preferred pathway to produce metabolite intermediates used to support cell proliferation during *de novo* biosynthesis (20), which can lead to higher levels of free fatty acids (FFA) and nucleic acid-related metabolites. In our current study, higher levels of nucleotides, palmitoleic acid, and hypoxanthine were observed in tumor tissues. Nucleotides are critical components of DNA and RNA structures, and disorders in their biosynthesis

have profound effects on cell physiology, which may lead to tumor transformation in cells (21). CRC tumor tissues showed higher levels of choline metabolites such as choline, PC, and PE than adjacent mucosa, which have also been reported in other malignancies (22–24).

Glycosylation changes are some of the most common post-translational modifications of proteins and are considered markers of cancer. N-glycans can regulate cell migration, cell adhesion, cell signaling, proliferation, and metastasis. Many carbohydrate-mediated cellular mechanisms, including those important for tumor progression, are regulated by N-glycans (25). Stephanie et al. compared the glycosylation profiles of tumor tissues and corresponding control tissues in 13 CRC patients (26). Multivariate data analysis showed significant differences in glycosphingolipids between tumors and corresponding adjacent tissues using MALDI-TOF/(TOF)-MS and 2-dimensional LC-MS/MS; the main changes included elevated fucosylation, reduced acetylation and sulfation, and reduced expression of globular glycans, as well as disialyl gangliosides. In our study, seven metabolite pathways were identified as being involved in the biosynthesis and metabolism of glycans, including biosynthesis of N-glycans, degradation of N-glycans, and

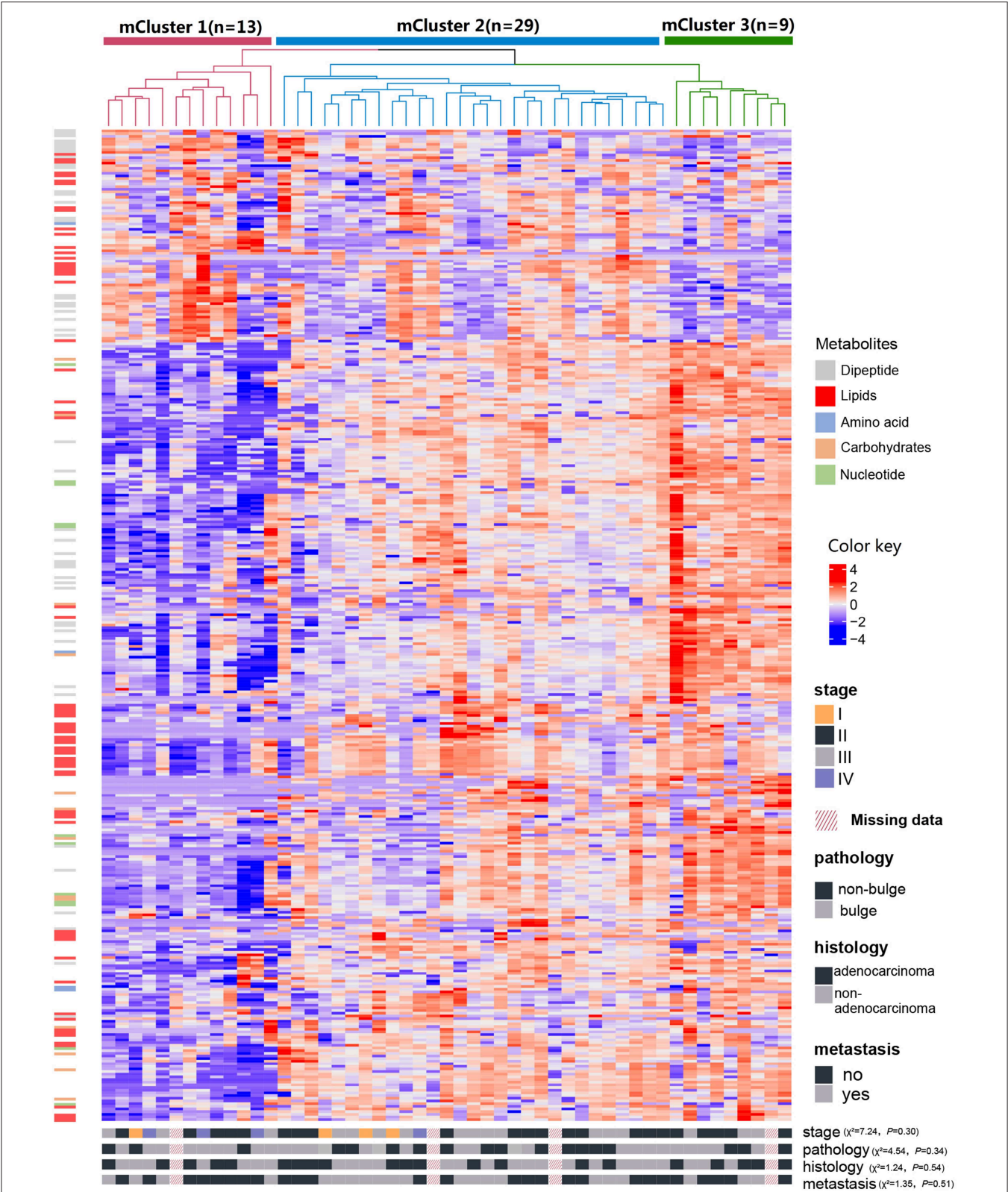
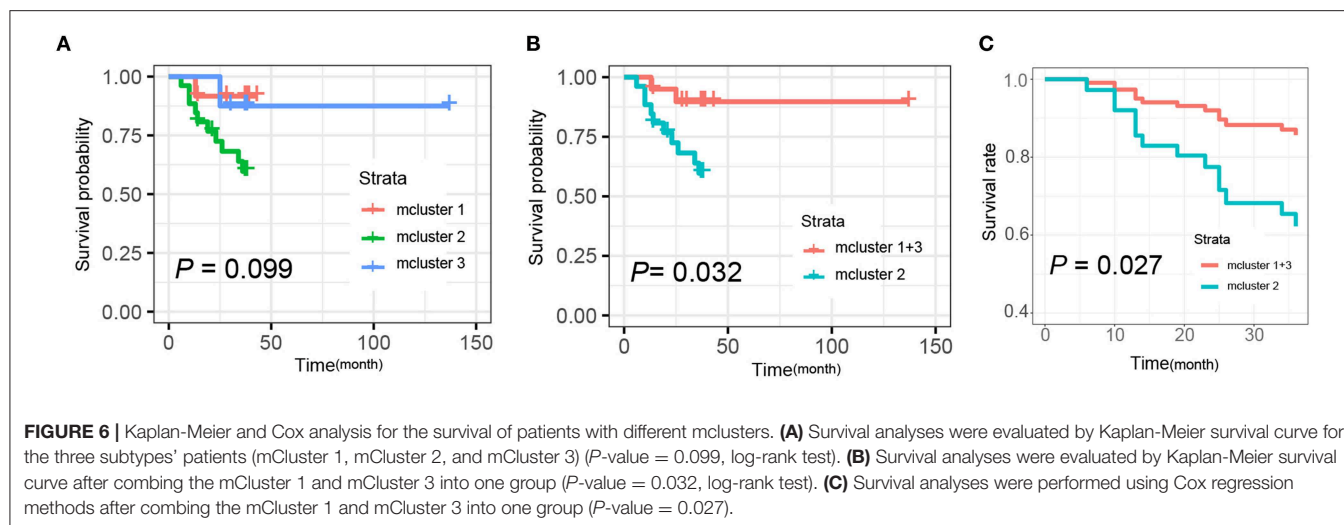


**FIGURE 5 |** Identification of CRC metabolite-based tumor subtypes. A heatmap of CRC subtypes is shown based on consensus clustering. The x-axis represents CRC subtype consensus clusters. CRC samples are represented in columns, grouped by the dendrogram into three main clusters, and metabolites ( $n = 373$ ) are represented in rows. Clinical data of the samples are included below the heatmap and the chi-square tests were used to estimate the difference between the three mClusters and clinicopathological features, respectively.



metabolism and biosynthesis of glycosphingolipids, confirming the changes in characteristic tumor-associated glycosylation.

To date, there have been few studies analyzing the differences in the metabolism of CRC with different clinicopathological features. In this study, it was reported for the first time that the early tumors of CRC have higher abundance of dipeptide characteristics. A large increase in dipeptides may be produced through protein degradation/reutilization processes, such as lysosomal degradation, phagocytosis, endocytosis, pinocytosis, and autophagy (27–30). Brauns et al. (31) have shown that cyclic dipeptides, especially those containing proline, have important biological activities. Their results indicated that phenylalanine-proline inhibits the proliferation of HT-29, MCF-7, and HeLa cells, as well as inducing apoptosis in HT-29 colon cancer cells, which has potential anti-tumor activity (31).

Higher levels of lipid metabolites observed in the current study in advanced CRC tissues have been reported in other studies (17, 32). Results of the Mummichog software pathway analysis showed that most pathways are lipid metabolism-related, consistent with previous studies by Zhang et al. and Tian et al. (17, 33). Abnormal lipid metabolism is a metabolite marker of cancer cells (34, 35), and many studies have reported that cancer cells have strong lipid and cholesterol affinities (35), by activating the exogenous (or dietary) lipid and lipoprotein uptake or by enhancing the reticular fat from the cytosol acetyl-CoA Biosynthesis of cholesterol and cholesterol, highly proliferative. Changes in lipid metabolism in CRC tumor tissues suggest enhanced lipogenesis is one of the most important features in CRC tumor tissues (36). Recent studies have also found that tumor tissue can use fatty acids and lipolytic pathways to obtain fatty acids to promote tumor cell proliferation (37).

We further observed that the metabolite differences between adenocarcinoma and non-adenocarcinoma CRCs were mainly related to lipid metabolism. Lipid metabolism is regulated by complex signaling networks in CRC tumor cells, which are closely related to cell growth, proliferation, differentiation, survival, and apoptosis (38). Several studies

have indicated that some fatty acid metabolism pathways are associated with the development and progression of colorectal adenocarcinoma (39, 40). Beatriz et al. also showed that changes in fatty acid metabolism are a crucial factor in the progression from colorectal adenoma to adenocarcinoma (41). Although our results are consistent with previous studies, there have been no studies on the metabolite differences of adenocarcinoma and non-adenocarcinoma thus far.

TNM staging system is currently recognized as an important independent indicator that can comprehensively reflect the progress of malignant tumor and judge the prognosis. It is also the main basis for determining the surgical resection scope, surgical method and formulation of adjuvant treatment plan. But, limitations cannot be ignored. TNM staging was determined based on the depth of invasion, lymph node metastasis and distant metastasis of the tumor in the intestinal wall. The essence of TNM staging is the clinical observable morphological index of the invasion and metastasis ability and degree of tumor, as well as adenocarcinoma and non-adenocarcinoma. Some recent studies have also indicated that, based on TNM staging and histological features, the sensitivity and prognosis of the same group of patients to the same treatment regimen vary greatly (42).

Our results, for the first time, showed that CRC could be divided into three subtypes at the metabolomics level, and the heterogeneity of metabolomic changes between different subtypes lead to inconsistent prognosis of tumors. Lipids, nucleotides, and carbohydrates have important roles in the biology of a subset of tumors. The differences in these metabolite levels between subtypes may point to different pathophysiological mechanisms for the development and progression of CRC. Understanding the pathogenesis of CRC is critical to developing personalized treatment strategies. As every CRC covers a specific, heterogeneous metabolite profile, the question rises if metabolomics (and other “omics”) approaches could become the new standard in adequately categorizing CRC on a molecular basis. This molecular classification could offer patients

a personalized therapy schedule, depending on the type of molecular defects that their colorectal tumor has acquired.

For example, many anticancer drugs are based on lipid metabolism, such as irinotecan, which can affect the accumulation of ceramide by inducing ceramide synthase to catalyze ceramide synthesis or by activating sphingomyelinase to catalyze the degradation of sphingomyelin (43, 44). At the same time, the use of drugs is also dependent on the sensitivity and intrinsic drug resistance of cancer cells. Studies have shown that omega-3 polyunsaturated fatty acids can improve the efficacy of chemotherapy and radiotherapy. Omega-3 fatty acids also reduce CD133+ colon cancer stem cell-like cells markers and increase sensitivity to chemotherapy (45). A eicosapentaenoic acid-free fatty acid (EPA-FFA) phase II double-blind, placebo-controlled trial of patients undergoing liver resection for CRC liver metastases showed that EPA-FFA treatment is anti-angiogenic, safe, and well tolerated (46). Backshall et al. evaluate the effect of pretreatment serum metabolite profiles generated by 1H NMR spectroscopy on toxicity in patients with inoperable CRC receiving single agent capecitabine (47). Their study suggests that metabolite profiles can delineate subpopulations susceptible to adverse events and have a potential role in the assessment of treatment viability for cancer patients prior to commencing chemotherapy.

This study still has some limitations. Our study is based on a relatively small sample of CRC patients in northeastern China. Tissue samples of patients with CRC are based on the continuous collection of clinical cases in the same hospital; the selection of samples may be biased. Moreover, the UPLC/Q-TOF MS metabolomics platform used in the study was used in isolation and some metabolites may not have been detected. Therefore, confirmation is necessary based on large samples from multiple populations and platforms.

In summary, our metabolomics study indicates that CRC tumor tissue exhibits distinct metabolite phenotypes. Metabolomics provides a new window into the study of CRC phenotypes and molecular typing as CRC can be divided into three subtypes at the metabolite level. When integrated with other platforms, we can provide a more comprehensive

explanation of the complex biology associated with CRC and malignant transformation. A deeper understanding of abnormal metabolism will provide a framework for the design and implementation of personalized approaches to CRC treatment through metabolite regulation.

## DATA AVAILABILITY STATEMENT

The datasets presented in this study can be found in online repositories. The names of the repository/repositories and accession number(s) can be found below: FigShare (<https://doi.org/10.6084/m9.figshare.12311315>).

## ETHICS STATEMENT

The studies involving human participants were reviewed and approved by the Ethics Committee of Harbin Medical University. The patients/participants provided their written informed consent to participate in this study.

## AUTHOR CONTRIBUTIONS

All authors listed have made a substantial, direct and intellectual contribution to the work, and approved it for publication.

## FUNDING

This work was supported by grants from National Nature Science Foundation of China (81773503, 81573147), Scientific Research Foundation for the Returned Overseas Scholars of Heilongjiang Province (LC2018033), and Dr. Wu Lien-teh Science Foundation of Harbin Medical University (WLD-QN1106).

## SUPPLEMENTARY MATERIAL

The Supplementary Material for this article can be found online at: <https://www.frontiersin.org/articles/10.3389/fonc.2020.00981/full#supplementary-material>

## REFERENCES

1. Siegel RL, Miller KD, Jemal A. Cancer statistics, 2018. *CA Cancer J Clin.* (2018) 68:7–30. doi: 10.3322/caac.21442
2. Kuipers EJ, Grady WM, Lieberman D, Seufferlein T, Sung JJ, Boelens PG, et al. Colorectal cancer. *Nat Rev Dis Primers.* (2015) 1:15065. doi: 10.1038/nrdp.2015.65
3. Goel G. Molecular characterization and biomarker identification in colorectal cancer: Toward realization of the precision medicine dream. *Cancer Manag Res.* (2018) 10:5895–908. doi: 10.2147/CMAR.S162967
4. Cunningham D, Atkin W, Lenz HJ, Lynch HT, Minsky B, Nordlinger B, et al. Colorectal cancer. *Lancet.* (2010) 375:1030–47. doi: 10.1016/S0140-6736(10)60353-4
5. Guinney J, Dienstmann R, Wang X, de Reyniès A, Schlicker A, Soneson C, et al. The consensus molecular subtypes of colorectal cancer. *Nat Med.* (2015) 21:1350–6. doi: 10.1038/nm.3967
6. Chaisaingmongkol J, Budhu A, Dang H, Rabibhadana S, Pupacdi B, Kwon SM, et al. Common molecular subtypes among asian hepatocellular carcinoma and cholangiocarcinoma. *Cancer Cell.* (2017) 32:57–70.e3. doi: 10.1016/j.ccell.2017.05.009
7. Choi W, Ochoa A, McConkey DJ, Aine M, Höglund M, Kim WY, et al. Genetic alterations in the molecular subtypes of bladder cancer: illustration in the cancer genome atlas dataset. *Eur Urol.* (2017) 72:354–65. doi: 10.1016/j.eururo.2017.03.010
8. Forbes SA, Beare D, Gunasekaran P, Leung K, Bindal N, Boutselakis H, et al. COSMIC: exploring the world's knowledge of somatic mutations in human cancer. *Nucleic Acids Res.* (2015) 43(Database issue):D805–11. doi: 10.1093/nar/gku1075
9. Johnson CH, Ivanisevic J, Siuzdak G. Metabolomics: beyond biomarkers and towards mechanisms. *Nat Rev Mol Cell Biol.* (2016) 17:451–9. doi: 10.1038/nrm.2016.25
10. Vander Heiden MG, DeBerardinis RJ. Understanding the intersections between metabolism and cancer biology. *Cell.* (2017) 168:657–69. doi: 10.1016/j.cell.2016.12.039



11. Levine AJ, Puzio-Kuter AM. The control of the metabolic switch in cancers by oncogenes and tumor suppressor genes. *Science*. (2010) 330:1340–4. doi: 10.1126/science.1193494
12. Wishart DS. Is cancer a genetic disease or a metabolic disease? *EBioMedicine*. (2015) 2:478–9. doi: 10.1016/j.ebiom.2015.05.022
13. Li S, Park Y, Duraisingham S, Strobel FH, Khan N, Soltow QA, et al. Predicting network activity from high throughput metabolomics. *PLoS Comp Biol*. (2013) 9:e1003123. doi: 10.1371/journal.pcbi.1003123
14. Monti S, Savage KJ, Kutok JL, Feuerhake F, Kurtin P, Mihm M, et al. Molecular profiling of diffuse large B-cell lymphoma identifies robust subtypes including one characterized by host inflammatory response. *Blood*. (2005) 105:1851–61. doi: 10.1182/blood-2004-07-2947
15. Wilkerson MD, Hayes DN. ConsensusClusterPlus: a class discovery tool with confidence assessments and item tracking. *Bioinformatics*. (2010) 26:1572–3. doi: 10.1093/bioinformatics/btq170
16. Gu Z, Eils R, Schlesner M. Complex heatmaps reveal patterns and correlations in multidimensional genomic data. *Bioinformatics*. (2016) 32:2847–9. doi: 10.1093/bioinformatics/btw313
17. Tian Y, Xu T, Huang J, Zhang L, Xu S, Xiong B, et al. Tissue metabolomic phenotyping for diagnosis and prognosis of human colorectal cancer. *Sci Rep*. (2016) 6:20790. doi: 10.1038/srep20790
18. Warburg O. [Origin of cancer cells]. *Oncologia*. (1956) 9:75–83. doi: 10.1159/000223920
19. Gatenby RA, Gillies RJ. Why do cancers have high aerobic glycolysis? *Nat Rev Cancer*. (2004) 4:891–9. doi: 10.1038/nrc1478
20. Vander Heiden MG, Cantley LC, Thompson CB. Understanding the Warburg effect: the metabolic requirements of cell proliferation. *Science*. (2009) 324:1029–33. doi: 10.1126/science.1160809
21. Tong X, Zhao F, Thompson CB. The molecular determinants of de novo nucleotide biosynthesis in cancer cells. *Curr Opin Genet Dev*. (2009) 19:32–7. doi: 10.1016/j.gde.2009.01.002
22. Chan EC, Koh PK, Mal M, Cheah PY, Eu KW, Backshall A, et al. Metabolic profiling of human colorectal cancer using high-resolution magic angle spinning nuclear magnetic resonance (HR-MAS NMR) spectroscopy and gas chromatography mass spectrometry (GC/MS). *J Proteome Res*. (2009) 8:352–61. doi: 10.1021/pr8006232
23. Chae YK, Kang W-Y, Kim SH, Joo JE, Han JK, Hong BW. Combining information of common metabolites reveals global differences between colorectal cancerous and normal tissues. *Bull Korean Chem Soc*. (2010) 31:379. doi: 10.5012/bkcs.2010.31.02.379
24. Griffin JL, Shockcor JP. Metabolic profiles of cancer cells. *Nat Rev Cancer*. (2004) 4:551. doi: 10.1038/nrc1390
25. de Freitas Junior JCM, Morgado-Diaz JA. The role of N-glycans in colorectal cancer progression: potential biomarkers and therapeutic applications. *Oncotarget*. (2016) 7:19395. doi: 10.18632/oncotarget.6283
26. Holst S, Stavenhagen K, Balog CI, Koelman CA, McDonnell LM, Mayboroda OA, et al. Investigations on aberrant glycosylation of glycosphingolipids in colorectal cancer tissues using liquid chromatography and matrix-assisted laser desorption time-of-flight mass spectrometry (MALDI-TOF-MS). *Mol Cell Proteomics*. (2013) 12:3081–93. doi: 10.1074/mcp.M113.030387
27. Comisso C, Davidson SM, Soydaner-Azeloglu RG, Parker SJ, Kamphorst JJ, Hackett S, et al. Macropinocytosis of protein is an amino acid supply route in Ras-transformed cells. *Nature*. (2013) 497:633. doi: 10.1038/nature12138
28. Kimmelman AC. Metabolic dependencies in RAS-driven cancers. *AACR*. (2015) 21:1828–34. doi: 10.1158/1078-0432.CCR-14-2425
29. Mizushima N, Komatsu M. Autophagy: renovation of cells and tissues. *Cell*. (2011) 147:728–41. doi: 10.1016/j.cell.2011.10.026
30. Settembre C, Ballabio A. Lysosome: regulator of lipid degradation pathways. *Trends Cell Biol*. (2014) 24:743–50. doi: 10.1016/j.tcb.2014.06.006
31. Brauns SC, Milne P, Naudé R, Van de Venter M. Selected cyclic dipeptides inhibit cancer cell growth and induce apoptosis in HT-29 colon cancer cells. *Anticancer Res*. (2004) 24:1713–20.
32. Liesenfeld DB, Grapov D, Fahrman JF, Salou M, Scherer D, Toth R, et al. Metabolomics and transcriptomics identify pathway differences between visceral and subcutaneous adipose tissue in colorectal cancer patients: the ColoCare study. *Am J Clin Nutr*. (2015) 102:433–43. doi: 10.3945/ajcn.114.103804
33. Zhang H, Qiao L, Li X, Wan Y, Yang L, Wang H. Tissue metabolic profiling of lymph node metastasis of colorectal cancer assessed by 1H NMR. *Oncol Rep*. (2016) 36:3436–48. doi: 10.3892/or.2016.5175
34. Glunde K, Bhujwala ZM, Ronen SM. Choline metabolism in malignant transformation. *Nat Rev Cancer*. (2011) 11:835. doi: 10.1038/nrc3162
35. Beloribi-Djefailia S, Vasseur S, Guillaumond F. Lipid metabolic reprogramming in cancer cells. *Oncogenesis*. (2016) 5:e189. doi: 10.1038/oncsis.2015.49
36. Zaidi N, Lupien L, Kuemmerle NB, Kinlaw WB, Swinnen JV, Smans K. Lipogenesis and lipolysis: the pathways exploited by the cancer cells to acquire fatty acids. *Progr Lipid Res*. (2013) 52:585–9. doi: 10.1016/j.plipres.2013.08.005
37. Nomura DK, Long JZ, Niessen S, Hoover HS, Ng S-W, Cravatt BF. Monoacylglycerol lipase regulates a fatty acid network that promotes cancer pathogenesis. *Cell*. (2010) 140:49–61. doi: 10.1016/j.cell.2009.11.027
38. Huang C, Freter C. Lipid metabolism, apoptosis and cancer therapy. *Int J Mol Sci*. (2015) 16:924–49. doi: 10.3390/ijms16010924
39. Gassler N, Herr I, Schneider A, Penzel R, Langbein L, Schirmacher P, et al. Impaired expression of acyl-CoA synthetase 5 in sporadic colorectal adenocarcinomas. *J Pathol*. (2005) 207:295–300. doi: 10.1002/path.1831
40. Pakiet A, Kobiela J, Stepnowski P, Sledzinski T, Mika A. Changes in lipids composition and metabolism in colorectal cancer: a review. *Lipids Health Dis*. (2019) 18:29. doi: 10.1186/s12944-019-0977-8
41. Carvalho B, Sillars-Hardebol AH, Postma C, Mongera S, Terhaar Sive Droste J, Obulkasim A, et al. Colorectal adenoma to carcinoma progression is accompanied by changes in gene expression associated with ageing, chromosomal instability, and fatty acid metabolism. *Cell Oncol*. (2012) 35:53–63. doi: 10.1007/s13402-011-0065-1
42. Brenner H, Bouvier AM, Foschi R, Hackl M, Larsen IK, Lemmens V, et al. Progress in colorectal cancer survival in Europe from the late 1980s to the early 21st century: the EUROcare study. *Int J Cancer*. (2012) 131:1649–58. doi: 10.1002/ijc.26192
43. Saddoughi SA, Ogretmen B. Diverse functions of ceramide in cancer cell death and proliferation. *Adv Cancer Res*. (2013) 117:37–58. doi: 10.1016/B978-0-12-394274-6.00002-9
44. Senchenkov A, Litvak DA, Cabot MC. Targeting ceramide metabolism—a strategy for overcoming drug resistance. *J Natl Cancer Inst*. (2001) 93:347–57. doi: 10.1093/jnci/93.5.347
45. De Carlo F, Witte TR, Hardman WE, Claudio PP. Omega-3 eicosapentaenoic acid decreases CD133 colon cancer stem-like cell marker expression while increasing sensitivity to chemotherapy. *PLoS ONE*. (2013) 8:e69760. doi: 10.1371/journal.pone.0069760
46. Cockbain AJ, Volpato M, Race AD, Munarini A, Fazio C, Belluzzi A, et al. Anticancer activity of the omega-3 polyunsaturated fatty acid eicosapentaenoic acid. *Gut*. (2014) 63:1760–8. doi: 10.1136/gutjnl-2013-306445
47. Backshall A, Sharma R, Clarke SJ, Keun HC. Pharmacometabolomic profiling as a predictor of toxicity in patients with inoperable colorectal cancer treated with capecitabine. *Clin Cancer Res*. (2011) 17:3019–28. doi: 10.1158/1078-0432.CCR-10-2474

**Conflict of Interest:** The authors declare that the research was conducted in the absence of any commercial or financial relationships that could be construed as a potential conflict of interest.

Copyright © 2020 Long, Zhou, Xie, Wu, Yin, Daria, Tian, Zhang, Li, Zhao, Wang, Wang and Cui. This is an open-access article distributed under the terms of the Creative Commons Attribution License (CC BY). The use, distribution or reproduction in other forums is permitted, provided the original author(s) and the copyright owner(s) are credited and that the original publication in this journal is cited, in accordance with accepted academic practice. No use, distribution or reproduction is permitted which does not comply with these terms.



# Targeting SREBP-2-Regulated Mevalonate Metabolism for Cancer Therapy

Linyuan Xue<sup>1</sup>, Hongyu Qi<sup>2</sup>, He Zhang<sup>1</sup>, Lu Ding<sup>3</sup>, Qingxia Huang<sup>1,2</sup>, Daqing Zhao<sup>2</sup>, Boyang Jason Wu<sup>4\*</sup> and Xiangyan Li<sup>2\*</sup>

<sup>1</sup> Research Center of Traditional Chinese Medicine, College of Traditional Chinese Medicine, Changchun University of Chinese Medicine, Changchun, China, <sup>2</sup> Key Laboratory of Active Substances and Biological Mechanisms of Ginseng Efficacy, Ministry of Education, Jilin Provincial Key Laboratory of Bio-Macromolecules of Chinese Medicine, Jilin Ginseng Academy, Changchun University of Chinese Medicine, Changchun, China, <sup>3</sup> College of Traditional Chinese Medicine, Changchun University of Chinese Medicine, Changchun, China, <sup>4</sup> Department of Pharmaceutical Sciences, College of Pharmacy and Pharmaceutical Sciences, Washington State University, Spokane, WA, United States

## OPEN ACCESS

### Edited by:

Miriam Martini,  
University of Turin, Italy

### Reviewed by:

Cinzia Domenicotti,  
University of Genoa, Italy  
Paola Defilippi,  
University of Turin, Italy

### \*Correspondence:

Boyang Jason Wu  
boyang.wu@wsu.edu  
Xiangyan Li  
xiangyan\_li1981@163.com

### Specialty section:

This article was submitted to  
Cancer Metabolism,  
a section of the journal  
Frontiers in Oncology

Received: 24 April 2020

Accepted: 14 July 2020

Published: 21 August 2020

### Citation:

Xue L, Qi H, Zhang H, Ding L,  
Huang Q, Zhao D, Wu BJ and Li X  
(2020) Targeting SREBP-2-Regulated  
Mevalonate Metabolism for Cancer  
Therapy. *Front. Oncol.* 10:1510.  
doi: 10.3389/fonc.2020.01510

Recently, targeting metabolic reprogramming has emerged as a potential therapeutic approach for fighting cancer. Sterol regulatory element binding protein-2 (SREBP-2), a basic helix-loop-helix leucine zipper transcription factor, mainly regulates genes involved in cholesterol biosynthesis and homeostasis. SREBP-2 binds to the sterol regulatory elements (SREs) in the promoters of its target genes and activates the transcription of mevalonate pathway genes, such as HMG-CoA reductase (HMGCR), mevalonate kinase and other key enzymes. In this review, we first summarized the structure of SREBP-2 and its activation and regulation by multiple signaling pathways. We then found that SREBP-2 and its regulated enzymes, including HMGCR, FPPS, SQS, and DHCR4 from the mevalonate pathway, participate in the progression of various cancers, including prostate, breast, lung, and hepatocellular cancer, as potential targets. Importantly, preclinical and clinical research demonstrated that fatostatin, statins, and N-BPs targeting SREBP-2, HMGCR, and FPPS, respectively, alone or in combination with other drugs, have been used for the treatment of different cancers. This review summarizes new insights into the critical role of the SREBP-2-regulated mevalonate pathway for cancer and its potential for targeted cancer therapy.

**Keywords:** SREBP-2, HMG-CoA reductase, mevalonate, cholesterol, cancer therapy

## INTRODUCTION

Sterol regulatory-element binding proteins (SREBPs) were first identified as a subclass of membrane-bound, basic helix-loop-helix leucine zipper (bHLH-LZ) transcription factors which regulate the promoters of genes involved in lipid synthesis and uptake pathways (1–3). In mammals, two genes, *SREBF1* and *SREBF2*, express three major SREBP proteins (SREBP-1a, SREBP-1c, and SREBP-2) with distinct but overlapping lipogenic transcriptional programs (3, 4). Most studies report that SREBP-1a and SREBP-1c primarily regulate fatty acid metabolism and that SREBP-2 is a main regulator of cholesterol metabolism (5–8). Over the past 30 years, the functions of SREBPs have been identified to participate in numerous crucial physiologic processes (9), highlighting metabolic integrators in cellular

homeostasis (10, 11). Accumulating evidence has revealed that SREBPs integrate multiple cell signals to control lipogenesis as well as unexpected pathways in type II diabetes, atherosclerosis, and a series of cancers (12, 13).

In particular, multiple SREBP-2-mediated pathways have been extensively studied as attractive potential targets for cancer therapy (14–16). As reported, SREBP-2 binds to the sterol regulatory elements (SREs) in the promoters of its target genes and activates the transcription of mevalonate pathway genes, such as 3-hydroxy-3-methyl-glutaryl-CoA (HMG-CoA) reductase (HMGCR), mevalonate kinase (MVK), and other key enzymes (1). Recent reports found that the mevalonate pathway and its metabolites are essential for cancer growth and malignant progression in a series of cancers, including prostate, breast, lung, and liver cancer (17, 18). Moreover, multiple key pathways, such as the p53 and phosphatidylinositol-3-kinase (PI3K)/Akt signaling pathways, lead to the activation of SREBP-2 to promote tumorigenesis (19–21). Based on the findings above, targeting SREBP-2 and mevalonate pathways has emerged as an encouraging strategy for cancer therapy.

In this review, we first summarized recent advances in the study of SREBP-2 structure, activation, and regulation, followed by SREBP-2, key enzymes of mevalonate pathway, their regulation by various signal pathways or metabolites, and their roles in different cancers. Finally, we focused on the inhibition of the SREBP-2-regulated mevalonate pathway by fatostatin, natural products, statins, or amino-bisphosphonates (N-BPs), alone or in combination with other drugs, as potential therapeutic strategies for various cancers. This review provides new insights into the critical role of SREBP-2-regulated mevalonate metabolism in cancer and its potential as a target for cancer therapy.

## SREBP-2 STRUCTURE, ACTIVATION, AND REGULATION

### SREBP-2 Structure

Human SREBP-2, identified by cDNA cloning in 1993, is produced from one gene, *SREBF-2*, 72kb, human chromosome 22q13, as the result of alternative promoter usage and transcription start sites (1). Similar to SREBP-1 structure, SREBP-2 contains 1,141 amino acids and includes an NH<sub>2</sub>-terminal transcription factor domain, a middle hydrophobic region and a COOH-terminal regulatory domain (3). The NH<sub>2</sub>-terminal domain with ~480 amino acids contains the bHLH-Zip motif (DNA binding) and an acidic transcriptional motif (transcriptional activity), which binds co-activator specificity protein 1 (SP1) or nuclear transcription factor Y (NF-Y) to regulate gene expression (22, 23). A middle hydrophobic region of SREBP-2 with approximately 80 amino acids, a membrane-binding region, consists of two hydrophobic membrane-spanning segments separated by a hydrophilic loop, which extends into the lumen of the endoplasmic reticulum (ER). The COOH-terminal regulatory domain contains approximately 590 amino acids responsible for SREBP-2 subcellular localization and translocation (**Figure 1A**) (24).

### SREBP-2 Activation

Generally, SREBP-2 is synthesized as 125kDa inactive precursors in the ER (9). The COOH-terminal domain of SREBP-2 binds to the WD-repeat domain of SREBP cleavage-activation protein (SCAP), while the NH<sub>2</sub>-terminal domain of SCAP binds to the ER-resident insulin-induced gene proteins (INSIG), including INSIG1 and INSIG2, to form a complex of INSIG/SCAP/SREBP-2 for maintaining SREBP-2 in the ER (25, 26). When sterol level decreases, SCAP dissociates from INSIGs and facilitates the incorporation of SCAP/SREBP into coatamer protein II (COPII)-coated vesicles, which then transports the complex from the ER to the Golgi apparatus (27, 28). In the Golgi, SREBP-2 is sequentially cleaved by two membrane-bound proteases, site-1 protease (S1P) (29) and site-2 protease (S2P) (30) to release the NH<sub>2</sub>-terminal form of this transcription factor (nuclear SREBP-2, nSREBP-2) (28). This form translocates to the nucleus and binds to the sterol regulatory element (SRE) of target genes, including key enzymes of cholesterol biosynthesis and uptake (4).

Many studies have shown that the INSIG/SCAP/SREBP-2 complex and the transport of SREBP-2 from ER to Golgi are regulated by multiple signaling proteins. When sterols in the ER membrane are high, they bind to loop 1 of SCAP and switch the conformation of SCAP to interact with INSIG protein, which blocks COPII binding and causes the maintenance of the SCAP/SREBP-2 complex in the ER (31) (**Figure 1B**, upper). Three different mutants within the sterol-sensing domain of SCAP (L315F, Y298C, and D443N) disrupt the interaction of SCAP/INSIG to abolish the sterol-mediated feedback regulation of SREBP processing (32). A recent report showed that heat shock protein 90 (HSP90) stabilized the SCAP/SREBP complex to facilitate SREBP activation (33). Another intrinsic protein encoding an E3 ubiquitin ligase in ER, TRC8 (translocation in renal cancer from chromosome 8), is capable of binding both SREBP-2 and SCAP to form a TRC8/SREBP-2/SCAP complex, which hampers the interaction between SCAP and Sec24, a COPII protein, to reduce the cleavage of SREBP-2 (34). Meanwhile, INSIG-1 binds to GP78, a membrane-bound ubiquitin ligase with high affinity, and is then ubiquitinated and rapidly degraded in sterol-depleted cells. However, INSIG-2 lacks interaction with GP78, which may be related to its slower degradation than INSIG-1 (35, 36). In addition, oxysterols such as 25-hydroxycholesterol bind directly to INSIGs to trigger ER retention of the SCAP/SREBP-2 complex. Mutations at F115A and T136A of the transmembrane helices of INSIG-2 are important for binding to oxysterols and SCAP (37).

For the transporting process, the mutant SCAP with aspartic acid replacement by alanine at 428 (D428A) fails to dissociate from INSIGs and impairs the transportation of SREBP-2 to the Golgi (38). Similar to INSIG-1, INSIG-2 binds SCAP to block the export of SREBPs in the absence of exogenous sterols (25), which is inhibited by microRNA-96 to increase the abundance of active SREBP-2 (39). Furthermore, several signaling proteins were reported to control the transport of SREBP-2. One study showed that Golgi-localized transmembrane protein prostegonin and adipoQ receptor 3 (PAQR3) interacted

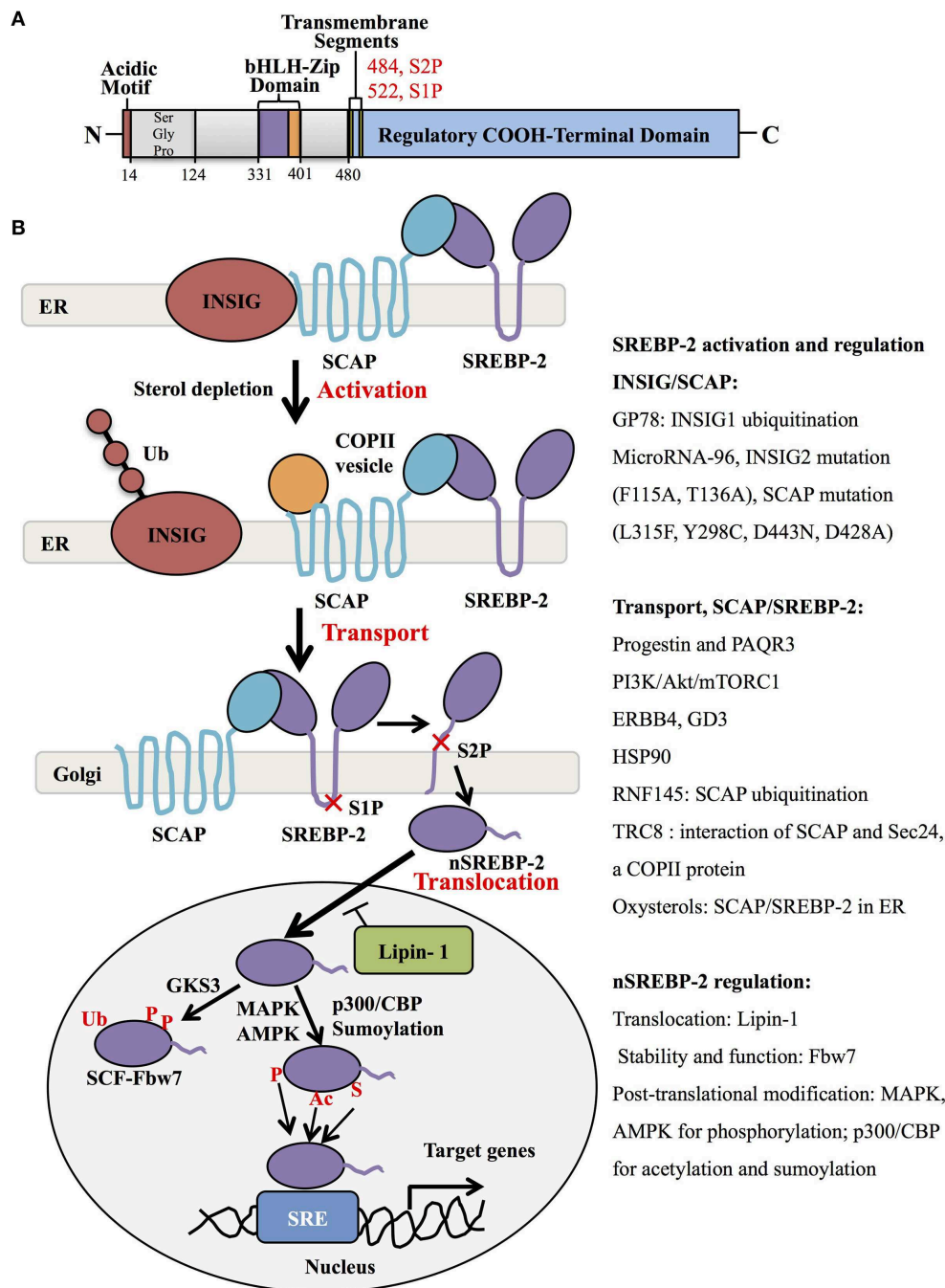


**FIGURE 1 |** SREBP-2 structure, activation, and regulation. **(A)** SREBP-2 protein consists of three domains, including an NH2-terminal regulatory domain, a middle hydrophilic region, and a COOH-terminal regulatory domain. The NH2-terminal domain contains the bHLH-Zip motif and an acidic transcriptional motif. **(B)** SREBP-2 activation, transport, and translocation. After INSIG dissociation from SCAP by sterol depletion, SREBP-2 translocates to the Golgi apparatus and is cleaved by S1P and S2P proteases to release the NH2-terminal fragment of SREBP-2 (nSREBP-2). nSREBP-2 translocation and stability are regulated by multiple signaling pathways at different levels. ER, endoplasmic reticulum; INSIG, insulin-induced gene protein; SCAP, SREBP cleavage-activation protein; COPII, coatamer protein II; S1P, site-1 protease; S2P, site-2 protease; Ub, ubiquitination; GSK3, glycogen synthase kinase 3; P, phosphorylation; SCF-Fbw7, SKP1-cullin-F-Box protein-F-box and WD repeat domain-containing 7; AMPK, adenosine monophosphate-activated protein kinase; MAPK, mitogen-activated protein kinase; p300/CBP, p300 and cyclic AMP response element-binding protein; Ac, acetylation; S, Sumoylation; SRE, sterol regulatory element; GP78, a membrane-anchored ubiquitin ligase; PAQR3, progesterin and adiponQ receptors member 3; ERBB4, Erb-b2 receptor tyrosine kinase 4; GD3, a dominant melanoma ganglioside; HSP90, heat shock protein 90; TRC8, translocation in renal cancer from chromosome 8; RNF145, RNF finger protein 145.



with the SCAP/SREBP-2 complex to remain in the Golgi, which was disrupted to reduce cholesterol biosynthesis (40). Another report demonstrated that a RING-finger ubiquitin ligase, RNF finger protein 145, triggered the ubiquitination of SCAP on lysine residues within a cytoplasmic loop, potentially inhibiting the transport of SREBP-2 to Golgi and subsequent SREBP-2 processing (41). Additionally, the PI3K/Akt/mTORC1 pathway is involved in SREBP-2 transport to the Golgi, contributing to SREBP-2 activation (42, 43), which can be activated by neuregulin-activated ERBB4 and melanoma antigen ganglioside GD3 (19, 44). Collectively, the INSIG/SCAP/SREBP-2 complex and SREBP-2 transportation from ER to Golgi are regulated by multiple signaling molecules, as summarized in **Figure 1B**.

## SREBP-2 Regulation at Different Levels

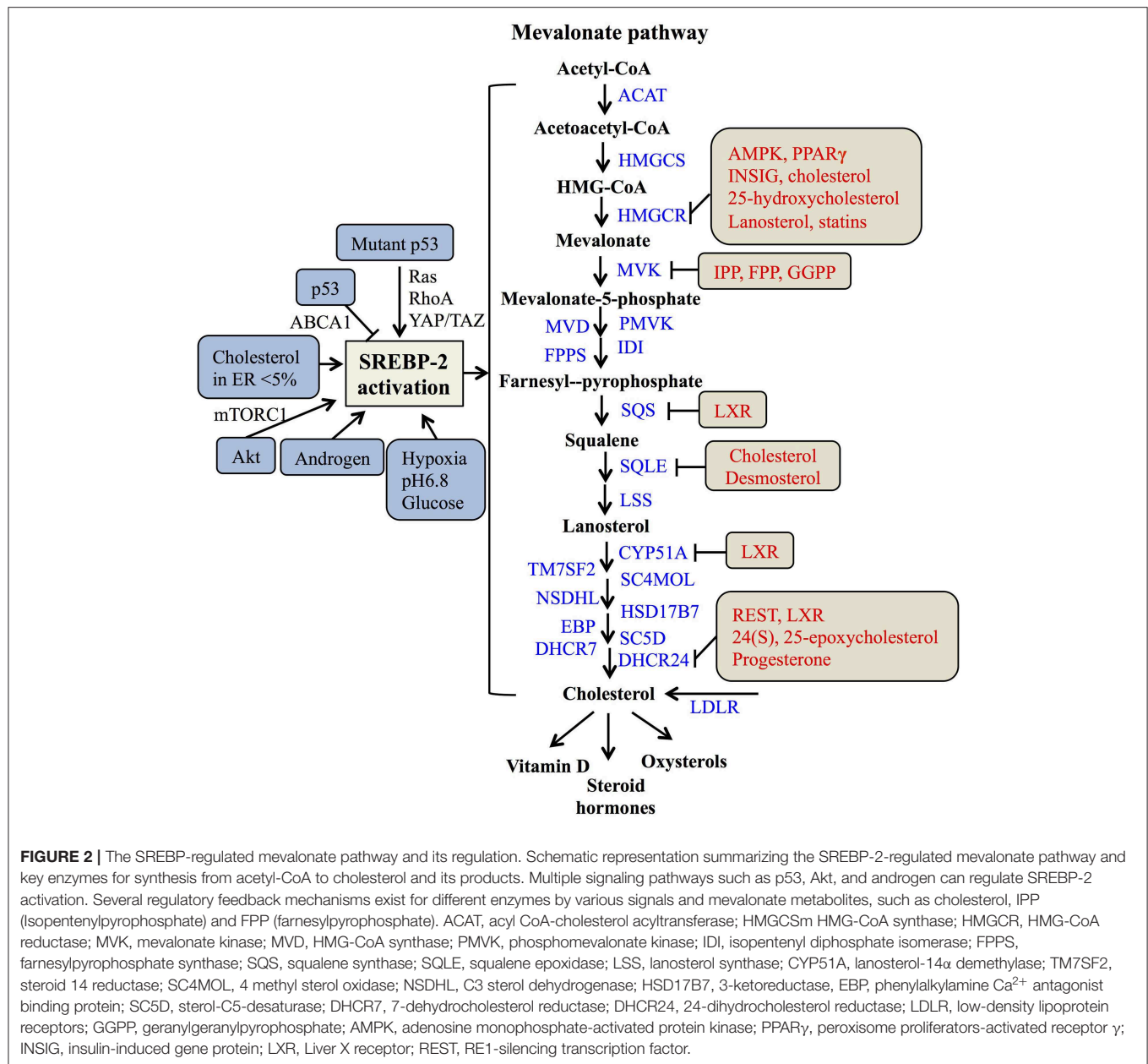
After the cleavage of full-length SREBP-2 by S1P and S2P in the Golgi, nSREBP-2 can translocate to the nucleus and be regulated at protein expression and transcription levels. The nutrient and growth factor-responsive kinase mTOR complex 1 (mTORC1) causes Lipin-1, a phosphatidic acid phosphatase, to reside in the cytoplasm, which increases the expression of nSREBP-2 protein (45, 46). mTORC1 can also suppress cholesterol delivery to lysosomes through the inhibition of autophagy and the maintenance of endosomal recycling, which reduces the level of cholesterol in ER to activate SREBP-2 (47). A nuclear receptor protein, peroxisome proliferator-activated receptor (PPAR)  $\alpha$  in rat liver cells, leads to a decrease of nSREBP-2 to lower cholesterol concentration (48). In addition, the stability and function of nuclear SREBP-2 are negatively regulated by a substrate receptor of the SCF ubiquitin ligase complex, Fbw7, through ubiquitination and proteasome-mediated degradation in a phosphorylation-dependent manner (49).

Importantly, the transcriptional activity of nSREBP-2 is also modulated by various post-translational modifications, including phosphorylation, acetylation, and sumoylation. For the phosphorylated regulation, insulin-activated Erk-mitogen-activated protein kinase (MAPK) increases SREBP-2 activity by phosphorylation at serine 432 and 455 (50). Glycogen synthase kinase 3 directly phosphorylates Ser443 on SREBP-2 to mediate Fbw7-induced ubiquitination and degradation of nSREBP-2 (49). A synthetic polyphenol, S17834, can promote AMP-activated protein kinase (AMPK) activation to decrease SREBP-2 transcription via its phosphorylation site on SREBP-2 (51). Aside from phosphorylation, histone acetyltransferase p300/CREB-binding protein (CBP) can bind and acetylate the N-terminus of SREBP-2 to enhance its expression and transcriptional activity (52), while sirtuin-1 (SIRT1) deacetylates SREBP-2 to decrease the abundance of SREBP-2 in the nucleus (53). Additionally, nSREBP-2 at Lys464 is also modified by sumoylation to decrease transcriptional activity (54). Taken together, SREBP-2 stability and activation are regulated by a series of key molecules and signaling pathways, which hold promise for understanding the role of SREBP-2 in physiological and pathological procedures.

## THE SREBP-2-REGULATED MEVALONATE PATHWAY

In the nucleus, nSREBP-2 binds to SREs in the promoter of target genes to activate the gene expression of most of the enzymes involved in the mevalonate pathway, including HMGCR, MVK, squalene synthase (SQS) (55), and 24-dihydrocholesterol reductase (DHCR24) (56), as well as increasing the expression of low-density lipoprotein receptors (LDLR) for exogenous cholesterol uptake (8, 57). For the mevalonate pathway, two molecules of acetyl-CoA from glucose metabolism or fatty acid degradation form acetoacetyl-CoA by acetoacetyl-CoA thiolase. In the presence of HMG-CoA synthase (HMGCS), acetyl-CoA and acetoacetyl-CoA form HMG-CoA, which is converted to mevalonate by HMGCR (58). Then, the mevalonate is phosphorylated sequentially to 5-phosphomevalonate by mevalonate kinase (MK) and to 5-pyrophosphomevalonate by phosphomevalonate kinase (PMK), which is further synthesized to isopentenylpyrophosphate (IPP) by mevalonate diphosphate decarboxylase (59). Furthermore, IPP and its isomer, dimethylallyl pyrophosphate (DMPP), can form geranyl pyrophosphate (GPP) by farnesylpyrophosphate synthase (FPPS, FDPS), which is condensed with another IPP to yield farnesylpyrophosphate (FPP). By the action of SQS, FPP is converted to squalene (60), which is converted sequentially to monooxidosqualene (MOS) and lanosterol by squalene monooxygenase (SM) and lanosterol synthase, respectively (18). Lastly, lanosterol is further metabolized to cholesterol by 19 enzymes, including CYP51A (lanosterol-14 $\alpha$  demethylase), TM7SF2 (steroid 14 reductase), SC4MOL (4 methyl sterol oxidase), NSDHL (C3 sterol dehydrogenase), HSD17B7 (3-ketoreductase), EBP (phenylalkylamine Ca<sup>2+</sup> antagonist binding protein), SC5D (sterol-C5-desaturase), 7-dehydrocholesterol reductase (DHCR7), and DHCR24 (17, 56, 61). As reported, cholesterol plays a crucial role in maintaining the structure and function of cellular membranes and is also a precursor of steroid hormones and vitamin D (62). Collectively, SREBP-2 controls cholesterol biosynthesis by regulating mevalonate metabolism enzymes (**Figure 2**).

As many studies reported, SREBP-2 activation and pathways are regulated by multiple signals. A major tumor suppressor, p53, can block activation of SREBP-2 to decrease the transcription of mevalonate pathway genes through transcriptional up-regulation of the ATP-binding cassette (ABC) transporter A1 (ABCA1) gene, which mediates tumor suppression (21). On the other hand, SREBP-2 can increase the generation of oxysterol ligands for liver X receptors (LXRs) to positively regulate ABCA1 gene transcription (63). LXRs play a potential role in maintaining cholesterol homeostasis through promoting cholesterol efflux and suppressing *de novo* synthesis and uptake (64, 65). Mutant p53 is recruited to the promoters of genes encoding mevalonate pathway enzymes by binding to the SREBP-2, which subsequently increases the activities of oncogenic pathways such as Ras, RhoA (66), and YAP/TAZ (67) to promote cancer progression (20, 68). Apart from p53, protein kinase B (Akt) acutely activates SREBP-2 (43) to induce the expression of genes involved in



cholesterol synthesis, which contributes to tumor development (19, 69). In addition, tumor microenvironments such as hypoxia, extracellular pH, and nutrient levels also play critical roles in the regulation of SREBP-2 activation. Hypoxia inducible factor-1 $\alpha$  is able to increase the activity of HMGCR by the translocation of SREBP-2 to the nucleus (70). Acidic extracellular pH (pH 6.8) triggers nuclear translocation of SREBP-2 to target acyl-CoA synthase short-chain family member 2 for maintaining overall survival of cancer patients (71). As a kind of nutrient, glucose promotes SCAP/SREBP complex trafficking from the ER to the Golgi and subsequent SREBP activation via N-glycosylation of SCAP (72). When cholesterol in the ER falls below 5% of total ER lipids, the cleavage of SREBP-2 is activated (31). A steroid

hormone, androgen, can induce SREBP-2 activation in normal physiological or pathological conditions, such as prostate cancer (73, 74). Taken together, either multiple signaling pathways or cellular nutrient levels can regulate SREBP-2 activation to control the mevalonate pathway (Figure 2).

Meanwhile, the enzymes participating in the mevalonate pathway, such as HMGCR, MVK, SQS, and DHCR24, are regulated by various molecules or the metabolites from mevalonate metabolism. Both the phosphorylation by AMP-activated protein kinase (AMPK) and dephosphorylation by protein phosphatase 2A regulate HMGCR activity (75, 76). The binding of INSIG on the sterol-sensing domain can lead to the ubiquitination and degradation of HMGCR (77, 78).

Interestingly, PPAR $\gamma$  can regulate multiple pathways, including decreasing the expressions of SREBP-2 and HMGCR and increasing the expression of LXR $\alpha$  to reduce cholesterol levels. Considering the role of LXR $\alpha$  on cholesterol efflux, the expression of ABC transporter G5 or G8 is increased by the PPAR $\gamma$ -LXR $\alpha$  pathway or their individual dependence, which needs to be further clarified (79). Two key enzymes of the post-squalene pathway, SQS and CYP51A are directly repressed by LXR $\alpha$  via negative binding with LXR DNA response elements (80). Moreover, DHCR24 as a final enzyme for cholesterol biosynthesis is regulated by RE1-silencing transcription factor, REST and LXR $\alpha$  through the binding of its promoter at the transcriptional level (56, 81). These findings suggest that LXR $\alpha$  plays an important role in regulating several enzymes of the mevalonate pathway, such as SQS, CYP51A, and DHCR24.

Additionally, key metabolites also can modulate metabolic enzymes of the SREBP-2-regulated mevalonate pathway. Cholesterol and 25-hydroxycholesterol can regulate HMGCR by increasing its alternative splicing (82). Mevalonate and certain of its derivatives such as dioxidolanosterol and geraniol regulate HMGCR mRNA translation or polysome distribution to reduce its synthesis and translation (83). Lanosterol and other C4-dimethylated sterol intermediates may regulate both HMGCR degradation and SREBP-2 cleavage (84). For geranylgeranyl diphosphate (GGPP), FPP and IPP, these intermediates post-transcriptionally inhibit MVK activity by negative feedback responses (85). Other metabolites, such as phytosterols, 24(S), 25-epoxycholesterol (24,25-EC) and steroid hormones (progesterone) can directly inhibit DHCR24 activity at the post-translational level (86–88). Overall, SREBP-2 and the enzymes for cholesterol biosynthesis, such as HMGCR, MVK, SQS, and DHCR24, can be regulated by various signaling pathways and mevalonate pathway metabolites at the transcriptional and post-translational levels (Figure 2).

## SREBP-2 SIGNALING AND THE ENZYMES FROM THE MEVALONATE PATHWAY IN THE CANCER CONTEXT

Reprogramming of lipid metabolism occurs in a variety of cancers and contributes to rapid tumor growth, which is regulated by SREBPs (89). SREBP-2 is markedly upregulated in various cancers, including prostate (14, 90), breast (15), and hepatocellular cancer (91). Moreover, SREBP-2-mediated mevalonate metabolism drives epithelial to mesenchymal transition (EMT) and supports cancer stemness, and has been suggested as a potential target for cancer treatment (17, 18, 92).

### Prostate Cancer

Lipid synthesis and uptake are significantly elevated in prostate cancer (PCa) as important energy resources to support tumor growth and progression (93, 94). As is well-known, androgens bind to and activate the androgen receptor (AR) to maintain the survival and proliferation of PCa (95). Androgen-induced activation of SREBPs occurs not only under normal physiological conditions but also in the setting of steroid-regulated cancers

(74, 96). Androgens markedly stimulate the expression of SCAP (97) and cause a switch in the isoform expression of INSIG, which play a pivotal role in the lipogenic effects of androgen in PCa (73). Meanwhile, dihydrotestosterone or R1881 marginally up-regulates the mRNA and protein levels of SREBP-2, which induces the expression of multiple genes encoding enzymes involved in cholesterol biosynthesis, including HMGCS, HMGCR, FPPS in PCa cells (98, 99). A recent report shows that an aberrant SREBP-dependent lipogenic program promotes PCa metastasis with double-null PML and PTEN (100). During the progression to androgen independence, nuclear SREBP-2 protein expression underwent a 3-fold increase in a PCa xenograft model (90). In addition, SREBP-2 expression is elevated in advanced pathologic grade and metastatic PCa and significantly associated with poor clinical outcomes. SREBP-2 promotes PCa cell growth, stemness and metastasis through transcriptional c-Myc activation mediated by direct interaction with a SREBP-2-binding element in the 5'-flanking c-Myc promoter region (14).

Key enzymes for mevalonate pathway such as HMGCS1, HMGCR, FPPS, and SQS also play important roles in PCa malignant progression. HMGCS1 and HMGCR are overexpressed in stroma of early stage PCa (101). Moreover, enzalutamide-resistant PCa cell lines express elevated HMGCR, and are more sensitive to statins, HMGCR inhibitors (102). FPPS is associated with increasing Gleason scores, PTEN functionally deficient status, and poor survival in PCa through modulation of the small GTPases/Akt axis (103, 104). SQS at rs2645429 is significantly associated with PCa risk and aggressive phenotypes (105). Taken together, SREBP-2 and key enzymes for the mevalonate pathway are potential targets for PCa treatment.

### Breast Cancer

In breast cancer, CtBP expression negatively correlates with SREBP-2 and HMGCR expressions. CtBP can form a complex with ZEB1 to transcriptionally repress SREBP-2 expression and activate TGF- $\beta$  signaling, which maintains intracellular cholesterol homeostasis in breast cancer (106). TP53 mutation correlates with elevated expression of a subset of mevalonate pathway genes in breast cancer patients. The levels of genes such as HMGCR, FPPS, SQS, and DHCR7 are positively associated with the risk of breast cancer. The functional interaction with SREBP-2 is critical for mutant p53-mediated up-regulation of the mevalonate pathway genes (20). Oncogenic PI3K (H1047R) or K-Ras (G12V) can induce *de novo* lipogenesis through convergent activation of mTORC1 to promote aberrant growth and proliferation of breast cancer, which is mediated by the activation of SREBP-2 or SREBP-1 (107). In addition, SREBP-2 is highly expressed in breast cancer tissues and correlated with a poor prognosis (15). SREBP-2 expression is increased during the early stages of osteoclast formation under the control of the RANKL/cAMP-CREB signaling cascade, which induces the expressions of NFATc1 and matrix metalloproteinase, thus contributing to breast cancer-induced osteolysis (15).

For patients with HER2<sup>+</sup> metastatic breast cancer, dual targeted therapy with a tyrosine kinase inhibitor, lapatinib or its combination with an anti-HER2 monoclonal antibody, trastuzumab can significantly improve pathological complete



response and overall survival (108). However, lapatinib and its combination with trastuzumab lead to the resistance of breast cancer cells to HER2-targeted therapy, which has been a clinical challenge (109). The mevalonate pathway has been considered as a new potential target for overcoming this acquired anti-HER2 treatment resistance, which may be mediated by activating the mTORC1-mediated YAP/TAZ pathway (110). Rate-limiting enzyme studies found that high levels of HMGCR are correlated with breast cancer risk (111) and poor survival (112, 113). Cholesterol is also implicated as a breast cancer risk factor and promotes breast tumor growth and metastasis (114). Another metabolite, 27-hydroxycholesterol, can increase the proliferation of estrogen receptor (ER)-positive breast cancer through the activation of ER and LXR (115). Therefore, inhibition of the SREBP-2-mediated mevalonate pathway has been recognized as a potential therapeutic approach for breast cancer.

## Lung Cancer

The single-nucleotide polymorphism of HMGCR, rs12916, is associated with the subgroups of attained age for lung cancer (111) and the C allele of the SQS rs2645429 polymorphism gene can be a risk factor for non-small cell lung cancer (NSCLC) (116). Three key enzymes of the mevalonate pathway, FPPS, SQS and GGPPS, are also associated with stage and metastasis of NSCLC (117–119). Of these enzymes, SQS is increased in invasive lung cancer cells and in the tumor regions of lung cancer specimens, and significantly associated with metastasis and poor prognosis by enhancing NF- $\kappa$ B-mediated up-regulation of matrix metalloproteinase-1 (117) or modulating extracellular signal-regulated kinase (ERK) signaling (120). FPPS plays an important role in promoting cell invasion and EMT through the RhoA/ROCK1 pathway (118). Although GGPPS knockdown has no effect on lung adenocarcinoma cell proliferation and apoptosis, it significantly inhibits invasion and migration by regulating EMT (119). Overall, several enzymes from the mevalonate pathway as mentioned above have been identified as potential targets for treating lung cancer (121).

## Hepatocellular Carcinoma

New studies reveal that several key molecules, such as p53 and fatty acid synthase (FASN), can activate SREBP-2 to promote cholesterol accumulation for maintaining the progression of hepatocellular carcinoma (HCC). In HCC, p53 tumor suppressor can induce the expression of MVA pathway enzymes through the accumulation and stabilization of mature SREBP-2 by transcriptionally inducing ABCA1, a cholesterol transporter gene. Like p53 loss, the ablation of ABCA1 promotes murine liver tumorigenesis and is associated with increased SREBP-2 maturation (21). In contrast to p53, a p53 activator, haplo-insufficient tumor suppressor ASPP2, can interact with SREBP-2 in the nucleus and negatively regulates the mevalonate pathway to mediate the inhibition of HCC tumor growth (122). Moreover, overexpression of Staphylococcal nuclease and tudor domain containing-1 (SND-1) in HCC results in the accumulation of cellular cholesterol esters due to the altered activation of SREBP-2 (123). Interestingly, SREBP-2 also binds to specific

sites in SND-1 promoter to induce its transcription, which contributes to lipid metabolism reprogramming in HCC (91). This suggests that there is a complex for the interaction of SND-1 and SREBP-2 in the lipid reprogramming of HCC, which needs to be clarified. Another molecule, FASN, contributes to *de novo* fatty acid synthesis in a murine HCC model induced by Pten loss and c-Met overexpression. Compared with the control group, genes such as HMGCR involved in cholesterol biosynthesis were obviously upregulated in HCC in FASN knockout mice, related to the promotion of nuclear SREBP-2 (124). Reportedly, the inhibition of FASN ubiquitination and disruption of the SREBP-1/SREBP-2 degradation complexes may be potential molecular mechanisms of Akt-induced lipogenesis and HCC tumor development in mice (69). In addition, Forkhead Box M1 has a positive correlation with SREBP-2 or HMGCR in HCC tissues, which links the mevalonate pathway through protein geranylgeranylation as novel targets (125). Based on the findings above, targeting the SREBP-2-mediated mevalonate pathway seems to have potential as a strategy for HCC treatment.

## Other Cancers

Similarly, SREBP-2 and its regulated mevalonate pathways also participate in other cancers. In esophageal squamous cell carcinoma, SREBP-2 is upregulated in clinical samples and promotes cell growth, migration and colony formation, which may be mediated by interaction with c-Myc to increase HMGCR expression (16). In renal carcinoma, Kruppel-like factor 6 (KLF6) activates mTOR signaling and its downstream lipid metabolism regulator, SREBP-2 to enhance tumor growth (126). In pancreatic cancer, the novel small nucleolar RNA host gene 16 directly regulates the miR-195/SREBP-2 axis to promote lipogenesis and accelerate tumor progression (127). Furthermore, increasing cellular cholesterol can drive intestinal stem cell proliferation and tumorigenesis through the activation of nuclear SREBP-2 (128). Also, SQS is frequently mutated and dysregulated in the liver metastatic cohort of colorectal cancer (129). The final enzyme of the cholesterol pathway, DHCR24, is significantly elevated and associated with advanced clinical stage and overall survival in bladder and endometrial cancer, which is mediated by several oncogenesis-associated biological processes (130, 131). Collectively, these findings in different cancers indicate that the SREBP-2-regulated mevalonate pathway significantly participates in tumor growth and metastasis and may be an attractive target in a variety of malignancies (Table 1).

## TARGETING THE SREBP-2-REGULATED MEVALONATE PATHWAY FOR CANCER THERAPY

Based on the above reports, we choose SREBP-2, HMGCR, and FPPS as potential targets for cancer therapy and summarized the findings so far regarding several inhibitors or miRNAs used to address these targets in preclinical and clinical studies.



**TABLE 1 |** The roles and molecular mechanisms of the SREBP-2-regulated mevalonate pathway in different cancers.

Cancer type	Targets	Molecular mechanism from the findings
Prostate cancer	SREBP-1, SREBP-2, HMGCS, HMGCR, FPPS	Androgen induces the activation of SREBPs and the expression of multiple enzyme genes, including HMGCS, HMGCR and FPPS in normal physiological conditions and steroid-regulated cancers (74, 96)
	SCAP, INSIG	Androgen stimulates SCAP expression and causes a switch in INSIG isoform for lipogenesis (73, 97)
	SREBP-2	Induced by a 3-fold increase during the progression to androgen independence (90)
	SREBP-2	Elevated in advanced pathologic grade and metastasis of prostate cancer and significantly associated with poor clinical outcomes (14)
	SREBP-2	Promotes cancer cell growth, stemness and metastasis through transcriptional c-Myc activation (14)
	HMGCS1, HMGCR	Overexpressed in stroma of early stage PCa (101)
	HMGCR	Elevated in enzalutamide-resistant cancer and more sensitive to statins (102)
	FPPS	Associated with increasing Gleason score and poor survival through modulation of small GTPase/Akt axis (103, 104)
Breast cancer	SQS	The allele at rs2645429 is significantly associated with cancer risk and aggressive phenotypes (105)
	SREBP-2	CtBP can form a complex with ZEB1 to transcriptionally repress SREBP-2 expression and activate TGF- $\beta$ signaling (106)
	SREBP-2, HMGCR, FPPS, SQS, DHCR7	TP53 mutation upregulates with the mevalonate pathway genes, HMGCR, FPPS, SQS, and DHCR7 through interaction with SREBP-2 (20)
	SREBPs	PI3K or K-Ras can induce mTORC1 signaling to promote cancer growth through SREBP-2 or SREBP-1 activation (107)
	SREBP-2	Highly expressed in cancer tissues and correlated with a poor prognosis (15)
	SREBP-2	Increased during the early stages of osteoclast formation under the control of the RANKL/cAMP-CREB signaling and induced the expressions of NFATc1 and matrix metalloproteinases for cancer-induced osteolysis (15)
	HMGCR	Correlated with the cancer risk and poor survival (111–113)
	Cholesterol 27-hydroxycholesterol	Implicated as a cancer, tumor growth and metastasis risk factor (114) Increases the proliferation of estrogen receptor (ER)-positive breast cancer through the activation of ER and LXR (115)
Lung cancer	HMGCR	The allele at rs12916 is significantly associated with the attained age for cancer patients (111)
	SQS	The allele at rs2645429 is a risk factor for non-small cell lung cancer (NSCLC) (116)
	SQS	Associated with the metastasis and poor prognosis by regulating NF- $\kappa$ B-mediated the up-regulation of matrix metalloproteinase-1 or extracellular signal-regulated kinase signaling (117, 120)
	FPPS	Promotes cell invasion and epithelial mesenchymal transition (EMT) through the RhoA/ROCK1 pathway (118)
	GGPPSS	Increases cancer invasion and migration by regulating EMT (119)
Hepatocellular carcinoma	SREBP-2	p53 induces the accumulation and stabilization of mature SREBP-2 by transcriptional ABCA1 induction (21)
	SREBP-2	ASPP2, a p53 activator interacts with SREBP-2 in the nucleus to negatively affect the mevalonate pathway (122)
	SREBP-2	Staphylococcal nuclease and tudor domain containing-1 (SND-1) results in the accumulation of cholesteryl esters through the activation of SREBP-2 (123)
	SREBP-2	Binds to specific sites in SND-1 promoter to contribute lipid metabolism reprogramming (91)
	SREBP-2, HMGCR	Fatty acid synthase ablation promotes nuclear localization of SREBP-2 and increases HMGCR expression to maintain carcinogenesis (124)
Esophageal squamous cell carcinoma	SREBP-2, HMGCR	Forkhead Box M1 has a positive correlation with SREBP-2 or HMGCR in hepatocellular carcinoma through protein geranylgeranylation (125)
	SREBP-2	Promotes cell growth, migration and colony formation through interaction with c-Myc; SREBP-2 is upregulated in clinical samples (16)
Renal carcinoma	SREBP-2	Kruppel-like factor 6 activates mTOR-SREBP-2 to enhance tumor growth (126)
Pancreatic cancer	SREBP-2	Small nucleolar RNA host gene 16 directly regulates the miR-195/SREBP-2 axis to promote cancer progression (127)
Colorectal cancer	SREBP-2	Increasing cellular cholesterol drives intestinal stem cell proliferation and tumorigenesis through SREBP-2 expression (128)
	SQS	Frequently mutated and dysregulated in liver metastasis (129)
Bladder and endometrial cancer	DHCR24	Significantly elevated and associated with advanced clinical stage and overall survival (130, 131)

## Targeting SREBP-2 for Cancer Therapy

As reported, SREBPs inhibition by small molecules such as fatostatin, natural products, and microRNAs such as miR-185, miR-342, and miR-33a have been extensively found to exert multiple anti-tumor effects in various cancers by reducing mevalonate metabolic dysfunction (132–136). Fatostatin, a non-sterol diarylthiazole derivative, was first reported to inhibit insulin-induced adipogenesis and reduce body weight by blocking nuclear translocation of SREBPs in obese mice (137, 138). Fatostatin has been used for treating prostate (133), breast (139), and endometrial cancers (140). Mechanistically, fatostatin directly binds SCAP and blocks its transport from ER to Golgi apparatus, then inhibits the activation of SREBPs (138). A recent study also showed that fatostatin inhibits cell proliferation through a SCAP-independent mechanism (141). In PCa, *in vitro* and *in vivo* studies reveal that fatostatin suppresses cell proliferation and induces apoptosis through blockade of SREBP-regulated metabolic pathways (133), similar to the findings in endometrial carcinoma (140). The combination of fatostatin with docetaxel significantly increases proliferation inhibition and apoptosis induction in metastatic PCa harboring p53 mutations, compared with fatostatin alone (142). Moreover, fatostatin also inhibits mitotic microtubule spindle assembly and cell division in aggressive cancers in addition to the inhibition of SREBP activity (136). Fatostatin also causes lipid accumulation as a response to endoplasmic reticulum stress rather than the inhibition of SREBP-mediated lipogenesis in ER<sup>+</sup> breast cancer cells (139). These studies suggest that the antitumor effects of fatostatin are multiple and dependent on cancer type.

Recent studies indicate that natural products can directly target SREBP-2 to inhibit the expression of key enzymes for the mevalonate pathway, to reduce tumor growth. Tocotrienol, a minor form of vitamin E, can degrade mature SREBP-2 without affecting LXR activity to maintain cholesterol homeostasis in PCa (143). In glioma, artesunate, initially developed as an anti-malaria drug, effectively inhibits cancer cell growth and distant metastasis, and further induces cell senescence by regulating the nuclear localization of SREBP-2 and the expression of HMGCR (144). As an anthraquinone derived from many plants, emodin inhibits SREBP-2 transcriptional activity to suppress cholesterol metabolism and Akt signaling, which sensitizes HCC cells to the anti-cancer effect of sorafenib *in vitro* and in xenograft models (145). Surprisingly, ursolic acid as a natural pentacyclic terpenoid activates SREBP-2 and increases the expression of cholesterol biosynthesis-related enzymes to induce cell cycle arrest and apoptosis in HCC cells (146). Additionally, archazolid B leads to the accumulation of free cholesterol and drastic disturbance in cholesterol homeostasis, which can activate nuclear SREBP-2 expression and up-regulate HMGCR for killing bladder cancer cells (147).

Some miRNAs, such as miR-98 and miR-33a, have been found to play critical roles in cholesterol metabolism by targeting SREBP-2 (134, 148, 149). Our previous study shows that miR-185 and miR-342 not only significantly block SREBP-2-mediated cholesterologenesis, but also inhibit SREBP-1-mediated lipogenesis in PCa (132). Another miRNA, miR-33a, an intronic miRNA

located within the SREBP-2 gene, inhibits EMT targeting of Twist1 to block invasion and metastasis in NSCLC (135). According to present studies, searching for miRNAs directly and specifically targeting SREBP-2 could be a future direction for new cancer treatment strategies. **Table 2** summarizes current SREBP-2 targeting by small molecules or miRNAs.

## Targeting HMGCR for Cancer Therapy

### Targeting HMGCR in Preclinical Cancer Therapy

Altered cholesterol metabolism is considered as a risk factor and driver of tumor growth, and is also associated with worse prognosis in a variety of cancers including breast, prostate, brain, and colorectal cancer (197, 198). Targeting HMGCR, a rate-limiting specific enzyme of cholesterol synthesis, has been identified as a potential therapeutic strategy for cancer treatment. Originally for treating cardiovascular diseases, statins like HMGCR inhibitors have become a standard of care for treating cancer patients with high cholesterol levels (199, 200) and also reduce the incidence and recurrence of various cancers, including colon (201), liver (202), and lung cancer (203). Statins can be divided mainly into two groups, depending on their origin by fungi fermentation or chemical syntheses, including type-1, mevastatin, lovastatin, simvastatin and type-2, fluvastatin, and atorvastatin (200). A number of studies have indicated that statins can inhibit cell proliferation, invasion and colony formation, and induce apoptosis to suppress tumorigenesis, tumor survival, angiogenesis and metastasis by regulating multiple signaling pathways (59, 199, 204).

In PCa xenograft mice models, simvastatin treatment at 25  $\mu$ M inhibited serum-induced Akt activity, cell migration and colony formation (150). Both simvastatin and fluvastatin inhibit cell proliferation and induce apoptosis in a dose- and time-dependent manner via the downregulation of Akt/Foxo1 phosphorylation in PCa (151). Simvastatin treatment also overcomes enzalutamide-induced resistance through the inhibition of mTOR-mediated AR degradation (102).

In breast cancer, both statins and HMGCR transcriptional regulation can overcome statin resistance through the regulation of SREBP-2 cleavage (205). The findings in a 2D co-culture and a splenic mouse model demonstrate that atorvastatin suppresses breast cancer proliferation, EMT and distant metastasis (152) and also induces autophagy (153), which is related to regulating PTEN/Akt and Ras homolog family member B pathways (154). In breast cancer stem-like cells, statins at non-toxic doses significantly alter a shared cluster of 37 genes, including the Hippo, Notch, and Wnt pathways, to hold back EMT processes (155). Simvastatin induces breast cancer cell death through the deactivation of PI3K/Akt and MAPK/Erk signals (156) and also prevents triple-negative breast cancer proliferation and metastasis through Foxo3a phosphorylation (157) or HSP90 acetylation (158). Another statin, pitavastatin, can slow breast cancer-induced bone metastasis and reduce urine-derived volatile organic compounds through the mevalonate pathway (159).

Increasing evidence demonstrates the anticancer effects of statins including atorvastatin, lovastatin, and fluvastatin against

**TABLE 2 |** Preclinical findings for targeting the SREBP-2-regulated mevalonate pathway in different cancers.

Treatment	Targets	Cancer type	Molecular mechanism
Fatostatin	SREBP-regulated metabolic pathway	Prostate cancer	Inhibits cell proliferation, colony formation, invasion and migration and causes G2/M cell cycle arrest and apoptosis <i>in vitro</i> and <i>in vivo</i> (133)
Fatostatin+ docetaxel	SREBP-regulated metabolic pathway	Prostate cancer	Results in greater proliferation inhibition and apoptosis induction in metastatic prostate cancer harboring p53 mutations, compared with fatostatin alone (142)
Fatostatin	SREBP-regulated metabolic pathway	Endometrial carcinoma	Inhibits cell viability, invasive and migratory capacities, and induces cell cycle arrest at the G2/M phase and stimulates caspase-mediated apoptosis (140)
Fatostatin	SREBP activity	Glioma, colorectal cancer, and others	Inhibits SREBP activity and mitotic microtubule spindle assembly and cell division (136)
Tocotrienol	SREBP-2	Prostate cancer	Degrades mature SREBP-2 and has no effect on LXR activity (143)
Artesunate	SREBP-2	Glioma	Inhibits cell growth, distant metastasis and induces cell senescence by regulating SREBP-2 nuclear localization and HMGCR expression (144)
Emodin	SREBP-2	Hepatocellular carcinoma	Inhibits SREBP-2 transcriptional activity to suppress cholesterol metabolism and Akt signaling (145)
Ursolic acid	SREBP-2	Hepatocellular carcinoma	Activates SREBP-2 and increases the expression of cholesterol biosynthesis-related enzymes to induce cell cycle arrest and apoptosis (146)
Archazolid B	SREBP-2	Bladder cancer	Activates nuclear SREBP-2 expression and up-regulates HMGCR for killing bladder cancer cells (147)
miRNA-185/342	SREBP-regulated metabolic pathway	Prostate cancer	Blocks SREBP-2-mediated cholesterol synthesis, and inhibits SREBP-1-mediated lipogenesis (132)
miRNA-33a	SREBP-2	Non-small cell lung cancer	Inhibits EMT targeting of Twist1 to block tumor progression (135)
Simvastatin	HMGCR	Prostate cancer	Inhibits Akt activity, cell migration and colony formation (150)
Simvastatin, fluvastatin	HMGCR	Prostate cancer	Inhibits cell proliferation and induces apoptosis via the downregulation of Akt/Foxo1 phosphorylation (151)
Simvastatin	HMGCR	Prostate cancer	Overcomes enzalutamide resistance by inhibiting mTOR-mediated AR degradation (102)
Atorvastatin	HMGCR	Breast cancer	Suppresses cancer proliferation, EMT and distant metastasis and induces autophagy by PTEN/Akt and Ras homolog family member B pathways (152–154)
Atorvastatin, lovastatin, simvastatin	HMGCR	Breast cancer (stem cells)	Significantly alters a shared cluster of 37 genes, including Hippo, Notch and Wnt pathways and holds back the EMT process (155)
Simvastatin	HMGCR	Breast cancer	Induces cell death through the deactivation of PI3K/Akt and MAPK/Erk signals (156)
Simvastatin	HMGCR	Triple negative breast cancer	Prevents cancer proliferation and metastasis through Foxo3a or heat shock protein 90 (157, 158)
Pitavastatin	HMGCR	Breast cancer	Slows bone metastasis and reduces urine-derived volatile organic compounds through the mevalonate pathway (159)
Atovastatin	HMGCR	Lung cancer	Inhibits TGF- $\beta$ 1-induced EMT by attenuating the upregulation of SphK1 (160)
Lovastatin	HMGCR	Lung cancer	Elicits cell apoptosis via a COX-2/PPAR $\gamma$ -dependent pathway (161)
Simvastatin	HMGCR	Lung cancer	Down-regulates TGF- $\beta$ RII expression and inhibits proliferation via Erk (162)
Fluvastatin	HMGCR	Lung cancer	Inhibits bone metastasis and the releases of RANKL, IL-6 and other factors through autophagy induction and osteoclastogenesis (163–165)
Simvastatin	HMGCR	Hepatocellular carcinoma	Induces G <sub>0</sub> /G <sub>1</sub> arrest by regulating p21 and p27, activating AMPK, and inhibiting STAT3-Skp2 axis (166)
Simvastatin, fluvastatin	HMGCR	Hepatocellular carcinoma	Attenuates cell proliferative ability via TAZ (167)
Simvastatin	HMGCR	Hepatocellular carcinoma	Induces growth inhibition and apoptosis via upregulation of Notch1 (168)
Simvastatin	HMGCR	Hepatocellular carcinoma	Modulates the adhesion and growth via decrease of integrin expression and ROCK (169)
Fluvastatin	HMGCR	Renal cell carcinoma	Has potent anti-cancer effects through suppression of the Akt/mTOR signaling cascade (170)
Fluvastatin	HMGCR	Lymphoma	Induces apoptosis by promoting ROS generation and regulating Akt, Erk and p38 signaling pathways (171)
Atovastatin + celecoxib	HMGCR	Prostate cancer	Inhibits the progression of androgen dependence to androgen independence (172)
Lovastatin + doxorubicin	HMGCR	Ovarian cancer	Induces apoptosis by blocking HMG-CoA reductase activity and inhibiting P-glycoprotein (173)

(Continued)

TABLE 2 | Continued

Treatment	Targets	Cancer type	Molecular mechanism
Statins + venetoclax	HMGCR	Leukemia and lymphoma	Enhances the proapoptotic activity of venetoclax by blocking mevalonate production and upregulating PUMA (174)
Simvastatin + Metformin	HMGCR	Endometrial carcinoma	Synergistically inhibits growth and induces apoptosis by upregulating AMPK phosphorylation and downregulating S6 phosphorylation (175)
Simvastatin + AZD6244	HMGCR	Pancreatic and Prostate cancer	Synergize to accumulate ROS production and cause apoptosis by targeting the compensatory xCT cystine importer (176)
Zoledronic acid	FPPS	Prostate cancer	Induces apoptosis through down-regulation of survivin (177)
Zoledronic acid	FPPS	Prostate cancer	Inhibits the RhoA-mediated amoeboid motility and impedes metastatic lung colonization (178)
Zoledronic acid	FPPS	Prostate cancer (stem cells)	Facilitates the intrinsic pathway of apoptosis to overcome chemoresistance (179)
Zoledronic acid	FPPS	Prostate cancer	Markedly induces autophagosome formation (180)
Zoledronic acid	FPPS	Prostate cancer	Inhibits protein prenylation (181)
Zoledronic acid	FPPS	Breast cancer	Significantly reduces the expression of cancer cell factors such as CCL2 and IDO to suppress regulatory T-cell function (182)
Zoledronic acid nanoparticle	FPPS	Breast cancer	Restores doxorubicin cytotoxic efficacy against chemo-immunoresistant tumors by reducing metabolic flux and also lowers the activity of Ras/Erk1/2-HIF-1 $\alpha$ axis to maintain cell death and immunosuppression (183)
Zoledronic acid	FPPS	Lung cancer	Causes arrest at S/G <sub>2</sub> /M phase with increases of cyclins and cyclin-related regulatory proteins, such as Ras (184)
Zoledronic acid	FPPS	Lung cancer	Inhibits the prenylations of Ras and Rap1A (185)
Zoledronic acid	FPPS	Hepatocellular carcinoma	Inhibits the translocation of Ras and Rho A to reduce cell growth and prevents progression to bone metastatic lesions (186)
Zoledronic acid	FPPS	Prostate cancer, primary effusion lymphoma	Reverts M2 macrophages to M1 phenotype for producing IFN- $\gamma$ and activates the V $\gamma$ 9V $\delta$ 2 T cells to suppress tumorigenesis through the immune modulation (187, 188)
YM529	FPPS	Prostate cancer	CXCR-4-induced invasion (189)
YM529	FPPS	Non-small cell lung cancer	Down-regulation of Erk1/2 phosphorylation (190)
YM529	FPPS	Bladder cancer	Inhibition of Rap1A prenylation (191)
Zoledronic acid + docetaxel	FPPS	Prostate cancer	The combination produces the greatest reduction in cell viability and increase in apoptosis through the reduction in the prenylation of GTPase Ras and Rho A (192)
Zoledronic acid + atorvastatin	FPPS, HMGCR	Breast cancer	Significantly impairs cancer cell adhesion on $\alpha$ v $\beta$ 3 expression (193)
Zoledronic acid + paclitaxel	FPPS	Breast cancer	Has synergistic effect on tumor cell number and apoptosis (194)
Zoledronic acid + atorvastatin	FPPS, HMGCR	Breast cancer	Combined inhibition achieves a meaningful anti-tumor effect by suppressed protein geranylation (195)
Zoledronic acid + gefitinib	FPPS, EGFR	Non-small cell lung cancer	Increases the antitumor effect of gefitinib by inhibiting STAT3 expression (196)

lung cancer by decreasing proliferative and migratory capacity and inducing apoptosis, which is mediated by SphK1 (160), COX-2/PPAR $\gamma$  (161), TGF- $\beta$  RII/Erk (162), and other key pathways (204). Lung cancer cells metastasize to the bone and release RANKL, IL-6, and other factors to stimulate osteoclasts, which can be inhibited by fluvastatin through autophagy induction and osteoclastogenesis (163–165).

In hepatocellular carcinoma, *in vitro* and *in vivo* studies reveal that simvastatin induces G<sub>0</sub>/G<sub>1</sub> arrest by upregulating p21 and p27, activating AMPK and inhibiting the STAT3-Skp2 axis in HCC (166). Other studies report that TAZ, Notch1 or ROCK expression are also involved in the anti-proliferative effects of statins against HCC (167–169).

Fluvastatin has potent anti-cancer effects against renal cell carcinoma through the suppression of the Akt/mTOR signaling cascade (170) and induces lymphoma cell apoptosis by

promoting ROS generation and regulating the Akt, Erk, and p38 signaling pathways via the inhibition of mevalonate metabolic products (171). Combination therapy studies demonstrated that statins combined with chemical molecules, including doxorubicin, celecoxib, venetoclax, metformin, or a MEK inhibitor, AZD6244, can synergistically suppress tumor growth in prostate, ovarian, endometrial, or pancreatic cancers, respectively (172–176). Overall, these findings suggest that statins alone or combined with other drugs inhibit the mevalonate pathway to achieve anti-cancer effects by a variety of molecular mechanisms (Table 2).

### Targeting HMGCR in Clinical Cancer Therapy

Currently, statins are in use for preventing or treating cancer patients with prostate (206), breast (207), lung (208), liver (209), and other cancers (210, 211). The safety, efficacy

and mortality benefits of statins have been assessed both alone and in combination therapy in clinical cancer patients studies (212–214).

In a 7.5 year follow-up of patients with PCa, statin use was associated with a decreased risk of death and delays in cancer progression, dependent on the increasing intensity of usage. However, statin use before diagnosis is not associated with PCa death risk (206). A meta-analysis of breast cancer patients indicates that statin can lower cancer-specific and all-cause mortality, which appears to be related to statin type (lipophilic or hydrophilic statin) and follow-up time (207). Seventeen studies in 98,445 patients indicate that statins potentially decrease cancer-specific mortality and promote the overall survival of patients with lung cancer in observational studies (215), which does not affect progression-free survival (208). In liver cancer, numerous studies have demonstrate decreased liver cancer mortality by statin treatment after adjusting for cholesterol level and body mass index, which is a novel approach for the prevention and treatment of HCC (209). In addition, post-diagnostic statin use is associated with improved survival of patients with other cancers, such as esophageal cancer (211) and ovarian cancer (210). Compared to statin alone, the combination of statins with therapeutic drugs such as thalidomide, idarubicin or tyrosine kinase inhibitor has synergistic effects for patients with refractory myeloma (216), acute myeloid leukemia (217) or NSCLC (218), respectively.

However, some contradictory studies indicate that statins have no protective effect on skin (219), colon (220), or other cancers in numerous clinical trials (221), which might be related to chemical nature, tumor stage and type, dose, use duration and patient characteristics. Therefore, well-defined patient information and clinical trial design need careful consideration in future studies of statins in cancer patients (222). **Table 3** summarizes the detailed information about tumor type, the number of patients, and main findings from clinical studies of statins alone or combined with other therapeutic agents in patients with various cancers.

## Targeting FPPS for Cancer Therapy

### Targeting FPPS in Preclinical Cancer Therapy

Amino-bisphosphonates (N-BPs), as FPPS inhibitors, represent another major class of inhibitors targeting the mevalonate pathway. Compared to original non-nitrogen containing bisphosphonates, N-BPs have an increased affinity to hydroxyapatite and interfere with FPPS in the mevalonate pathway (227), and are used for treating patients with osteoporosis (228) or osteolytic bone metastases (229). Several studies reveal anti-tumor effects of N-BPs apart from the inhibition of osteoclasts. Third-generation N-BPs, zoledronic acid (ZOL) and minodronate (YM529), are more potent inhibitors of FPPS than the first-generation bisphosphonates, and have been found to exhibit anti-tumor effects through inhibition of cell growth, induction of apoptosis, inhibition of angiogenesis, decrease in tumor cell adhesion to bone and other possible mechanisms in various cancers (230, 231).

In PCa, ZOL induces apoptosis through down-regulation of survivin (177), and inhibits RhoA-mediated amoeboid motility to impede metastatic lung colonization (178). In PCa stem

cells, ZOL can facilitate the intrinsic apoptosis pathway to overcome chemoresistance (179). Moreover, ZOL exposure markedly induces autophagosome formation and inhibits protein prenylation for anti-prostate cancer activity (180, 181). In breast cancer, ZOL can significantly reduce the expression of cancer cell factors such as CCL2 and IDO to suppress regulatory T-cell function (182). Especially, a formed ZOL-nanoparticle restores doxorubicin cytotoxic efficacy against chemo-immunoresistant tumors by reducing metabolic flux and also lowers Ras/Erk1/2/HIF-1 $\alpha$  axis activity to maintain cell death and immunosuppression (183). In lung cancer, *in vitro* and *in vivo* experiments demonstrate that ZOL-treated cells typically arrest the at S/G<sub>2</sub>/M phase with increases of cyclins and cyclin-related regulatory proteins such as Ras (184). ZOL can also inhibit Ras and Rap1A prenylation to target lung cancer (185). Similar findings in HCC demonstrate that ZOL inhibits the translocation of Ras and RhoA to reduce cell growth and prevent progression to bone metastatic lesions (186). Additionally, ZOL treatment reverts M2 macrophages to M1 phenotype for producing IFN- $\gamma$  (188) or activating V $\gamma$ 9V $\delta$ 2 T cells (187) to suppress tumorigenesis through the immune modulation.

Another N-BP, YM529, also exerts anti-tumor effects against various types of cancer cells, including PCa, NSCLC, and bladder cancer, by various mechanisms such as CXCR-4-induced invasion (189), down-regulation of Erk1/2 phosphorylation (190), and inhibition of Rap1A prenylation (191). In addition, N-BPs have been used in combination with chemotherapy, statins or enzyme inhibitors to achieve additive or synergistic effects by diverse mechanisms, including a reduction in protein prenylation, impairment of geranylgeranylation or inhibition of STAT3 in prostate (192), breast (193–195), and lung (196) cancers. The effects of FPPS inhibitors such as ZOL and YM529 alone and in combination with other drugs targeting multiple signaling pathways in cancer cell and xenograft models are summarized in **Table 2**.

### Targeting FPPS in Clinical Cancer Therapy

Based on their strong inhibitory effect on osteoclasts, N-BPs are used to treat osteolytic bone metastases, which are frequent in advanced cancer, especially prostate and breast cancer. In PCa, ZOL has become an established first-line or adjunctive treatment in bone-targeted therapy for metastatic castration-resistant progression (223, 232). Though ZOL delays skeletal-related events (SREs), it reportedly has no effect on overall survival, other disease-oriented parameters, or radiographic progression improvement. It remains an important adjunctive treatment strategy in the care of metastatic castrate-resistant PCa patients (223). Findings in clinical trials indicate that the beneficial effect of ZOL on bone metastasis from advanced prostate cancer might be related to long-term therapy, generally for more than 2 years (226). Similarly, ZOL can prevent the development of SREs in bone metastatic patients with breast cancer and improve quality of life, although with no effect on overall survival (224, 225). However, long-term side effects of ZOL, such as impaired renal function and bone pain need to be taken into consideration for treatment decisions (233).



**TABLE 3 |** Clinical findings for statins and N-BPs in different cancers.

Treatments	Tumor type	No. of patients	Findings
Statins before and after diagnosis	Prostate cancer	6,537	Statin use after diagnosis decreases the risk of cancer death only in men managed with androgen deprivation therapy (206)
Lipophilic statins	Breast cancer	197,048	Lipophilic statins are associated with decreased breast cancer-specific and all-cause mortality, which appears to be constrained by statin type and follow-up time (207)
Statins	Non-small cell lung cancer (Stage IV)	5,118	Statin use at the time of the diagnosis is associated with improved survival (215)
Statins	Lung cancer	98,445	Statins are potentially associated with the decreasing risk of mortality and the improvement of overall survival in observation studies, but not in randomized controlled trials (17 studies) (208)
Statins	Liver cancer	13,063	Statin use is associated with decreased liver cancer mortality by adjusting for cholesterol levels and body mass index (209)
Statins after diagnosis	Esophageal cancer	11,750	Statin use is associated with a decreased risk of cancer specific and all-cause mortality (211)
Statins after diagnosis	Ovarian cancer	5,416	Statin use is associated with improved survival in a large nation-wide cohort (210)
Lovastatin + Thalidomide + dexamethasone	Refractory myeloma	91	The addition of lovastatin to the regimen of thalidomide and dexamethasone improves the response rate (216)
Pravastatin + idarubicin + cytarabine	Acute myeloid leukemia	46	The combination demonstrates an impressive response rate and has therapeutic benefit by targeting the cholesterol pathway (217)
Statins + EGFR-TKIs therapy	Non-small cell lung cancer	20,717	Statin use potentially enhances the therapeutic effect and decreases mortality in patients receiving EGFR-tyrosine kinase inhibitors (218)
Statins	Skin cancer	114,708	Statin use is not associated with skin cancer risk from 29 studies (219)
Statins	Colon cancer	740	Statin use is not associated with improved cancer-specific survival (220)
Statins, lipophilic	Various cancers	175,000	Statin therapy has no effect on the incidence or mortality in 27 large-scale trials (221)
Zoledronic acid	Metastatic castration-resistant prostate cancer	7,346	Zoledronic acid remains an important adjunctive treatment strategy in the care of metastatic cancer patients from 6 of Phase III randomized controlled trials (223)
Zoledronic acid	Breast cancer, multiple myeloma	7,396	Zoledronic acid prevents the development of skeletal-related events in bone metastatic patients and improve life quality, but has no effect of overall survival from 10 clinical studies (224)
Zoledronic acid + radiopharmaceuticals	Osteoblastic metastases from lung, breast, and prostate cancer	261	The addition of radiopharmaceuticals to zoledronic acid does not alter time to skeletal-related events or overall survival (225)
Zoledronic acid + docetaxel	Prostate cancer	662	The addition of docetaxel to zoledronic acid shows no evidence for improving survival in men with local advanced or metastatic cancer from 3 randomized controlled trials (226)

Findings in clinical studies of ZOL treatment alone or in combination are summarized in **Table 3**.

Overall, the SREBP-2-regulated mevalonate pathway is a crucial regulator for tumor progression and a promising therapeutic target. Targeting SREBP-2, HMGCR or FPPS has become an attractive strategy for cancer therapy. Preclinical (**Table 2**) and clinical (**Table 3**) studies demonstrate that fatostatin, statins, ZOL, and YM529, alone or in combination with chemotherapy or other drugs, have anti-tumor effects through a variety of molecular mechanisms.

## CONCLUSIONS

This review has summarized the structure, activation and regulation of SREBP-2 by multiple signaling pathways. SREBP-2 and its regulated enzymes from the mevalonate pathway,

including HMGCR, FPPS, SQS, and DHCR4, participate in the progression of various cancers including prostate, breast, lung, and hepatocellular cancer, and thus are important potential therapeutic targets. Importantly, preclinical and clinical research has demonstrated that fatostatin, statins, and N-BPs targeting SREBP-2, HMGCR, and FPPS, respectively, alone or in combination with other drugs, are used for the treatment of different cancers. This review provides new insights into the critical role of the SREBP-2-regulated mevalonate pathway in cancer and its potential for targeted cancer therapy.

As a metabolic reprogramming process, the SREBP-2-regulated mevalonate pathway has a high-degree of similarity with glucose or glutamine metabolism and links them together to participate in cancer progression. Based on the function of SREBP-2 in cholesterol biosynthesis, it is necessary to develop new strategies specifically targeting SREBP-2 to treat various

cancers with dysfunctional cholesterol metabolism. Combination treatments simultaneously targeting SREBP-2 and its regulated enzymes from the mevalonate pathway may achieve beneficial effects for cancer treatment and prevention, and represent important future directions in ongoing research.

## AUTHOR CONTRIBUTIONS

LX, XL, and BW: conceptualization. LX: writing—original draft preparation. HQ, HZ, LD, and QH: writing—review and

editing of different sections. DZ, BW, and XL: supervision. All authors have read and agreed to the published version of the manuscript.

## FUNDING

This work was supported by the National Natural Science Foundation of China (81602257) and the Science and Technology Development Plan Project of Jilin Province (20190101010JH).

## REFERENCES

- Hua X, Yokoyama C, Wu J, Briggs MR, Brown MS, Goldstein JL, et al. SREBP-2, a second basic-helix-loop-helix-leucine zipper protein that stimulates transcription by binding to a sterol regulatory element. *Proc Natl Acad Sci USA*. (1993) 90:11603–7. doi: 10.1073/pnas.90.24.11603
- Yokoyama C, Wang X, Briggs MR, Admon A, Wu J, Hua X, et al. SREBP-1, a basic-helix-loop-helix-leucine zipper protein that controls transcription of the low density lipoprotein receptor gene. *Cell*. (1993) 75:187–97. doi: 10.1016/S0092-8674(05)80095-9
- Brown MS, Goldstein JL. The SREBP pathway: regulation of cholesterol metabolism by proteolysis of a membrane-bound transcription factor. *Cell*. (1997) 89:331–40. doi: 10.1016/S0092-8674(00)80213-5
- Goldstein JL, DeBose-Boyd RA, Brown MS. Protein sensors for membrane sterols. *Cell*. (2006) 124:35–46. doi: 10.1016/j.cell.2005.12.022
- Horton JD, Shimomura I, Brown MS, Hammer RE, Goldstein JL, Shimano H. Activation of cholesterol synthesis in preference to fatty acid synthesis in liver and adipose tissue of transgenic mice overproducing sterol regulatory element-binding protein-2. *J Clin Invest*. (1998) 101:2331–9. doi: 10.1172/JCI2961
- Shimano H, Yahagi N, Amemiya-Kudo M, Hasty AH, Osuga J, Tamura Y, et al. Sterol regulatory element-binding protein-1 as a key transcription factor for nutritional induction of lipogenic enzyme genes. *J Biol Chem*. (1999) 274:35832–9. doi: 10.1074/jbc.274.50.35832
- Amemiya-Kudo M, Shimano H, Hasty AH, Yahagi N, Yoshikawa T, Matsuzaka T, et al. Transcriptional activities of nuclear SREBP-1a, -1c, and -2 to different target promoters of lipogenic and cholesterol genes. *J Lipid Res*. (2002) 43:1220–35. doi: 10.1194/jlr.M100417-JLR200
- Horton JD, Goldstein JL, Brown MS. SREBPs: activators of the complete program of cholesterol and fatty acid synthesis in the liver. *J Clin Invest*. (2002) 109:1125–31. doi: 10.1172/JCI215593
- Osborne TF, Espenshade PJ. Evolutionary conservation and adaptation in the mechanism that regulates SREBP action: what a long, strange trip it's been. *Genes Dev*. (2009) 23:2578–91. doi: 10.1101/gad.1854309
- Jeon TI, Osborne TF. SREBPs: metabolic integrators in physiology and metabolism. *Trends Endocrinol Metab*. (2012) 23:65–72. doi: 10.1016/j.tem.2011.10.004
- Shao W, Espenshade PJ. Expanding roles for SREBP in metabolism. *Cell Metab*. (2012) 16:414–9. doi: 10.1016/j.cmet.2012.09.002
- Moon YA, Liang G, Xie X, Frank-Kamenetsky M, Fitzgerald K, Kotliansky V, et al. The Scap/SREBP pathway is essential for developing diabetic fatty liver and carbohydrate-induced hypertriglyceridemia in animals. *Cell Metab*. (2012) 15:240–6. doi: 10.1016/j.cmet.2011.12.017
- Griffiths B, Lewis CA, Bensaad K, Ros S, Zhang Q, Ferber EC, et al. Sterol regulatory element binding protein-dependent regulation of lipid synthesis supports cell survival and tumor growth. *Cancer Metab*. (2013) 1:3. doi: 10.1186/2049-3002-1-3
- Li X, Wu JB, Li Q, Shigemura K, Chung LW, Huang WC. SREBP-2 promotes stem cell-like properties and metastasis by transcriptional activation of c-Myc in prostate cancer. *Oncotarget*. (2016) 7:12869–84. doi: 10.18632/oncotarget.7331
- Jie Z, Xie Z, Xu W, Zhao X, Jin G, Sun X, et al. SREBP-2 aggravates breast cancer associated osteolysis by promoting osteoclastogenesis and breast cancer metastasis. *Biochim Biophys Acta Mol Basis Dis*. (2019) 1865:115–25. doi: 10.1016/j.bbdis.2018.10.026
- Zhong C, Fan L, Li Z, Yao F, Zhao H. SREBP2 is upregulated in esophageal squamous cell carcinoma and cooperates with cMyc to regulate HMGCR expression. *Mol Med Rep*. (2019) 20:3003–10. doi: 10.3892/mmr.2019.10577
- Gruenbacher G, Thurnher M. Mevalonate metabolism in cancer. *Cancer Lett*. (2015) 356(Pt. A):192–6. doi: 10.1016/j.canlet.2014.01.013
- Bathia SZ, Ashrafi M, Azizian M, Tamanoi F. Mevalonate pathway and human cancers. *Curr Mol Pharmacol*. (2017) 10:77–85. doi: 10.2174/1874467209666160112123205
- Yamauchi Y, Furukawa K, Hamamura K, Furukawa K. Positive feedback loop between PI3K-Akt-mTORC1 signaling and the lipogenic pathway boosts Akt signaling: induction of the lipogenic pathway by a melanoma antigen. *Cancer Res*. (2011) 71:4989–97. doi: 10.1158/0008-5472.CAN-10-4108
- Freed-Pastor WA, Mizuno H, Zhao X, Langerod A, Moon SH, Rodriguez-Barrueco R, et al. Mutant p53 disrupts mammary tissue architecture via the mevalonate pathway. *Cell*. (2012) 148:244–58. doi: 10.1016/j.cell.2011.12.017
- Moon SH, Huang CH, Houlihan SL, Regunath K, Freed-Pastor WA, Morris JP, et al. p53 represses the mevalonate pathway to mediate tumor suppression. *Cell*. (2019) 176:564–80 e519. doi: 10.1016/j.cell.2018.11.011
- Sato R, Yang J, Wang X, Evans MJ, Ho YK, Goldstein JL, et al. Assignment of the membrane attachment, DNA binding, and transcriptional activation domains of sterol regulatory element-binding protein-1 (SREBP-1). *J Biol Chem*. (1994) 269:17267–73.
- Shimano H, Horton JD, Shimomura I, Hammer RE, Brown MS, Goldstein JL. Isoform 1c of sterol regulatory element binding protein is less active than isoform 1a in livers of transgenic mice and in cultured cells. *J Clin Invest*. (1997) 99:846–54. doi: 10.1172/JCI119248
- Weber LW, Boll M, Stampfl A. Maintaining cholesterol homeostasis: sterol regulatory element-binding proteins. *World J Gastroenterol*. (2004) 10:3081–7. doi: 10.3748/wjg.v10.i21.3081
- Yabe D, Brown MS, Goldstein JL. Insig-2, a second endoplasmic reticulum protein that binds SCAP and blocks export of sterol regulatory element-binding proteins. *Proc Natl Acad Sci USA*. (2002) 99:12753–8. doi: 10.1073/pnas.162488899
- Yang T, Espenshade PJ, Wright ME, Yabe D, Gong Y, Aebersold R, et al. Crucial step in cholesterol homeostasis: sterols promote binding of SCAP to INSIG-1, a membrane protein that facilitates retention of SREBPs in ER. *Cell*. (2002) 110:489–500. doi: 10.1016/S0092-8674(02)00872-3
- Sun LP, Li L, Goldstein JL, Brown MS. Insig required for sterol-mediated inhibition of Scap/SREBP binding to COPII proteins *in vitro*. *J Biol Chem*. (2005) 280:26483–90. doi: 10.1074/jbc.M504041200
- Brown MS, Radhakrishnan A, Goldstein JL. Retrospective on cholesterol homeostasis: the central role of scap. *Annu Rev Biochem*. (2018) 87:783–807. doi: 10.1146/annurev-biochem-062917-011852
- Sakai J, Rawson RB, Espenshade PJ, Cheng D, Seegmiller AC, Goldstein JL, et al. Molecular identification of the sterol-regulated luminal protease that cleaves SREBPs and controls lipid composition of animal cells. *Mol Cell*. (1998) 2:505–14. doi: 10.1016/S1097-2765(00)80150-1

30. Rawson RB, Zelenski NG, Nijhawan D, Ye J, Sakai J, Hasan MT, et al. Complementation cloning of S2P, a gene encoding a putative metalloprotease required for intramembrane cleavage of SREBPs. *Mol Cell*. (1997) 1:47–57. doi: 10.1016/S1097-2765(00)80006-4
31. Radhakrishnan A, Goldstein JL, McDonald JG, Brown MS. Switch-like control of SREBP-2 transport triggered by small changes in ER cholesterol: a delicate balance. *Cell Metab*. (2008) 8:512–21. doi: 10.1016/j.cmet.2008.10.008
32. Yabe D, Xia ZP, Adams CM, Rawson RB. Three mutations in sterol-sensing domain of SCAP block interaction with insig and render SREBP cleavage insensitive to sterols. *Proc Natl Acad Sci USA*. (2002) 99:16672–7. doi: 10.1073/pnas.262669399
33. Kuan YC, Hashidume T, Shibata T, Uchida K, Shimizu M, Inoue J, et al. Heat shock protein 90 modulates lipid homeostasis by regulating the stability and function of Sterol Regulatory Element-binding Protein (SREBP) and SREBP cleavage-activating protein. *J Biol Chem*. (2017) 292:3016–28. doi: 10.1074/jbc.M116.767277
34. Irisawa M, Inoue J, Ozawa N, Mori K, Sato R. The sterol-sensing endoplasmic reticulum (ER) membrane protein TRC8 hampers ER to Golgi transport of sterol regulatory element-binding protein-2. (SREBP-2)/SREBP cleavage-activated protein and reduces SREBP-2 cleavage. *J Biol Chem*. (2009) 284:28995–9004. doi: 10.1074/jbc.M109.041376
35. Gong Y, Lee JN, Lee PC, Goldstein JL, Brown MS, Ye J. Sterol-regulated ubiquitination and degradation of Insig-1 creates a convergent mechanism for feedback control of cholesterol synthesis and uptake. *Cell Metab*. (2006) 3:15–24. doi: 10.1016/j.cmet.2005.11.014
36. Lee JN, Song B, DeBose-Boyd RA, Ye J. Sterol-regulated degradation of Insig-1 mediated by the membrane-bound ubiquitin ligase gp78. *J Biol Chem*. (2006) 281:39308–15. doi: 10.1074/jbc.M608999200
37. Radhakrishnan A, Ikeda Y, Kwon HJ, Brown MS, Goldstein JL. Sterol-regulated transport of SREBPs from endoplasmic reticulum to Golgi: oxysterols block transport by binding to Insig. *Proc Natl Acad Sci USA*. (2007) 104:6511–8. doi: 10.1073/pnas.0700899104
38. Feramisco JD, Radhakrishnan A, Ikeda Y, Reitz J, Brown MS, Goldstein JL. Intramembrane aspartic acid in SCAP protein governs cholesterol-induced conformational change. *Proc Natl Acad Sci USA*. (2005) 102:3242–7. doi: 10.1073/pnas.0500206102
39. Jo Y, Cha JY, Moon YA. Regulation of INSIG2 by microRNA-96. *Anim Cells Syst*. (2017) 21:263–8. doi: 10.1080/19768354.2017.1336483
40. Xu D, Wang Z, Zhang Y, Jiang W, Pan Y, Song BL, et al. PAQR3 modulates cholesterol homeostasis by anchoring Scap/SREBP complex to the Golgi apparatus. *Nat Commun*. (2015) 6:8100. doi: 10.1038/ncomms9100
41. Zhang L, Rajbhandari P, Priest C, Sandhu J, Wu X, Temel R, et al. Inhibition of cholesterol biosynthesis through RNF145-dependent ubiquitination of SCAP. *Elife*. (2017) 6:e28766. doi: 10.7554/eLife.28766
42. Du X, Kristiana I, Wong J, Brown AJ. Involvement of Akt in ER-to-Golgi transport of SCAP/SREBP: a link between a key cell proliferative pathway and membrane synthesis. *Mol Biol Cell*. (2006) 17:2735–45. doi: 10.1091/mbc.e05-11-1094
43. Luu W, Sharpe LJ, Stevenson J, Brown AJ. Akt acutely activates the cholesterologenic transcription factor SREBP-2. *Biochim Biophys Acta*. (2012) 1823:458–64. doi: 10.1016/j.bbamcr.2011.09.017
44. Haskins JW, Zhang S, Means RE, Kelleher JK, Cline GW, Canfran-Duque A, et al. Neuregulin-activated ERBB4 induces the SREBP-2 cholesterol biosynthetic pathway and increases low-density lipoprotein uptake. *Sci Signal*. (2015) 8:ra111. doi: 10.1126/scisignal.aac5124
45. Lewis CA, Griffiths B, Santos CR, Pende M, Schulze A. Regulation of the SREBP transcription factors by mTORC1. *Biochem Soc Trans*. (2011) 39:495–9. doi: 10.1042/BST0390495
46. Peterson TR, Sengupta SS, Harris TE, Carmack AE, Kang SA, Balderas E, et al. mTOR complex 1 regulates lipin 1 localization to control the SREBP pathway. *Cell*. (2011) 146:408–20. doi: 10.1016/j.cell.2011.06.034
47. Eid W, Dauner K, Courtney KC, Gagnon A, Parks RJ, Sorisky A, et al. mTORC1 activates SREBP-2 by suppressing cholesterol trafficking to lysosomes in mammalian cells. *Proc Natl Acad Sci USA*. (2017) 114:7999–8004. doi: 10.1073/pnas.1705304114
48. König B, Koch A, Spielmann J, Hilgenfeld C, Stangl GI, Eder K. Activation of PPARalpha lowers synthesis and concentration of cholesterol by reduction of nuclear SREBP-2. *Biochem Pharmacol*. (2007) 73:574–85. doi: 10.1016/j.bcp.2006.10.027
49. Sundqvist A, Bengoechea-Alonso MT, Ye X, Lukiyanchuk V, Jin J, Harper JW, et al. Control of lipid metabolism by phosphorylation-dependent degradation of the SREBP family of transcription factors by SCF(Fbw7). *Cell Metab*. (2005) 1:379–91. doi: 10.1016/j.cmet.2005.04.010
50. Kotzka J, Lehr S, Roth G, Avci H, Knebel B, Muller-Wieland D. Insulin-activated Erk-mitogen-activated protein kinases phosphorylate sterol regulatory element-binding Protein-2 at serine residues 432 and 455 *in vivo*. *J Biol Chem*. (2004) 279:22404–11. doi: 10.1074/jbc.M401198200
51. Li Y, Xu S, Mihaylova MM, Zheng B, Hou X, Jiang B, et al. AMPK phosphorylates and inhibits SREBP activity to attenuate hepatic steatosis and atherosclerosis in diet-induced insulin-resistant mice. *Cell Metab*. (2011) 13:376–88. doi: 10.1016/j.cmet.2011.03.009
52. Giandomenico V, Simonsson M, Gronroos E, Ericsson J. Coactivator-dependent acetylation stabilizes members of the SREBP family of transcription factors. *Mol Cell Biol*. (2003) 23:2587–99. doi: 10.1128/MCB.23.7.2587-2599.2003
53. Walker AK, Yang F, Jiang K, Ji JY, Watts JL, Purushotham A, et al. Conserved role of SIRT1 orthologs in fasting-dependent inhibition of the lipid/cholesterol regulator SREBP. *Genes Dev*. (2010) 24:1403–17. doi: 10.1101/gad.1901210
54. Hirano Y, Murata S, Tanaka K, Shimizu M, Sato R. Sterol regulatory element-binding proteins are negatively regulated through SUMO-1 modification independent of the ubiquitin/26S proteasome pathway. *J Biol Chem*. (2003) 278:16809–19. doi: 10.1074/jbc.M212448200
55. Inoue J, Sato R, Maeda M. Multiple DNA elements for sterol regulatory element-binding protein and NF-Y are responsible for sterol-regulated transcription of the genes for human 3-hydroxy-3-methylglutaryl coenzyme A synthase and squalene synthase. *J Biochem*. (1998) 123:1191–8. doi: 10.1093/oxfordjournals.jbchem.a022060
56. Zeretur EJ, Sharpe LJ, Brown AJ. Sterols regulate 3beta-hydroxysterol Delta24-reductase (DHCR24) via dual sterol regulatory elements: cooperative induction of key enzymes in lipid synthesis by Sterol Regulatory Element Binding Proteins. *Biochim Biophys Acta*. (2012) 1821:1350–60. doi: 10.1016/j.bbalip.2012.07.006
57. Horton JD, Shah NA, Warrington JA, Anderson NN, Park SW, Brown MS, et al. Combined analysis of oligonucleotide microarray data from transgenic and knockout mice identifies direct SREBP target genes. *Proc Natl Acad Sci USA*. (2003) 100:12027–32. doi: 10.1073/pnas.1534923100
58. Mizioroko HM. Enzymes of the mevalonate pathway of isoprenoid biosynthesis. *Arch Biochem Biophys*. (2011) 505:131–43. doi: 10.1016/j.abb.2010.09.028
59. Gobel A, Rauner M, Hofbauer LC, Rachner TD. Cholesterol and beyond - the role of the mevalonate pathway in cancer biology. *Biochim Biophys Acta Rev Cancer*. (2020) 1873:188351. doi: 10.1016/j.bbcan.2020.188351
60. Do R, Kiss RS, Gaudet D, Engert JC. Squalene synthase: a critical enzyme in the cholesterol biosynthesis pathway. *Clin Genet*. (2009) 75:19–29. doi: 10.1111/j.1399-0004.2008.01099.x
61. Luo J, Yang H, Song BL. Mechanisms and regulation of cholesterol homeostasis. *Nat Rev Mol Cell Biol*. (2019) 21:225–45. doi: 10.1038/s41580-019-0190-7
62. Narwal V, Deswal R, Batra B, Kalra V, Hooda R, Sharma M, et al. Cholesterol biosensors: a review. *Steroids*. (2019) 143:6–17. doi: 10.1016/j.steroids.2018.12.003
63. Tamehiro N, Shigemoto-Mogami Y, Takeya T, Okuhira K, Suzuki K, Sato R, et al. Sterol regulatory element-binding protein-2- and liver X receptor-driven dual promoter regulation of hepatic ABC transporter A1 gene expression: mechanism underlying the unique response to cellular cholesterol status. *J Biol Chem*. (2007) 282:21090–9. doi: 10.1074/jbc.M701228200
64. Wong J, Quinn CM, Brown AJ. SREBP-2 positively regulates transcription of the cholesterol efflux gene, ABCA1, by generating oxysterol ligands for LXR. *Biochem J*. (2006) 400:485–91. doi: 10.1042/BJ20060914
65. Hu YW, Zheng L, Wang Q. Regulation of cholesterol homeostasis by liver X receptors. *Clin Chim Acta*. (2010) 411:617–25. doi: 10.1016/j.cca.2009.12.027



66. Ingallina E, Sorrentino G, Bertolio R, Lisek K, Zannini A, Azzolin L, et al. Mechanical cues control mutant p53 stability through a mevalonate-RhoA axis. *Nat Cell Biol.* (2018) 20:28–35. doi: 10.1038/s41556-017-0009-8
67. Sorrentino G, Ruggeri N, Specchia V, Cordenonsi M, Mano M, Dupont S, et al. Metabolic control of YAP and TAZ by the mevalonate pathway. *Nat Cell Biol.* (2014) 16:357–66. doi: 10.1038/ncb2936
68. Parrales A, Thoenen E, Iwakuma T. The interplay between mutant p53 and the mevalonate pathway. *Cell Death Differ.* (2018) 25:460–70. doi: 10.1038/s41418-017-0026-y
69. Calvisi DF, Wang C, Ho C, Ladu S, Lee SA, Mattu S, et al. Increased lipogenesis, induced by AKT-mTORC1-RPS6 signaling, promotes development of human hepatocellular carcinoma. *Gastroenterology.* (2011) 140:1071–83. doi: 10.1053/j.gastro.2010.12.006
70. Pallottini V, Quantario B, Martini C, Totta P, Filippi I, Carraro F, et al. Regulation of HMG-CoA reductase expression by hypoxia. *J Cell Biochem.* (2008) 104:701–9. doi: 10.1002/jcb.21757
71. Kondo A, Yamamoto S, Nakaki R, Shimamura T, Hamakubo T, Sakai J, et al. Extracellular acidic pH activates the sterol regulatory element-binding protein 2 to promote tumor progression. *Cell Rep.* (2017) 18:2228–42. doi: 10.1016/j.celrep.2017.02.006
72. Guo D. SCAP links glucose to lipid metabolism in cancer cells. *Mol Cell Oncol.* (2016) 3:e1132120. doi: 10.1080/23723556.2015.1132120
73. Heemers H, Maes B, Foulfelle F, Heyns W, Verhoeven G, Swinnen JV. Androgens stimulate lipogenic gene expression in prostate cancer cells by activation of the sterol regulatory element-binding protein cleavage activating protein/sterol regulatory element-binding protein pathway. *Mol Endocrinol.* (2001) 15:1817–28. doi: 10.1210/mend.15.10.0703
74. Chen M, Chen LM, Chai KX. Androgen regulation of prostatic gene expression is mediated by sterol-regulatory element-binding proteins and SLUG. *Prostate.* (2006) 66:911–20. doi: 10.1002/pros.20325
75. Ching YP, Davies SP, Hardie DG. Analysis of the specificity of the AMP-activated protein kinase by site-directed mutagenesis of bacterially expressed 3-hydroxy 3-methylglutaryl-CoA reductase, using a single primer variant of the unique-site-elimination method. *Eur J Biochem.* (1996) 237:800–8. doi: 10.1111/j.1432-1033.1996.0800p.x
76. Gausin V, Skarlas P, Ching YP, Hardie DG, Hue L. Distinct type-2A protein phosphatases activate HMGCoA reductase and acetyl-CoA carboxylase in liver. *FEBS Lett.* (1997) 413:115–8. doi: 10.1016/S0014-5793(97)00890-9
77. Sever N, Yang T, Brown MS, Goldstein JL, DeBose-Boyd RA. Accelerated degradation of HMG CoA reductase mediated by binding of insig-1 to its sterol-sensing domain. *Mol Cell.* (2003) 11:25–33. doi: 10.1016/S1097-2765(02)00822-5
78. Tsai YC, Lechner GS, Pearce MM, Wilson GL, Wojcikiewicz RJ, Roitelman J, et al. Differential regulation of HMG-CoA reductase and Insig-1 by enzymes of the ubiquitin-proteasome system. *Mol Biol Cell.* (2012) 23:4484–94. doi: 10.1091/mbc.e12-08-0631
79. Han T, Lv Y, Wang S, Hu T, Hong H, Fu Z. PPARgamma overexpression regulates cholesterol metabolism in human L02 hepatocytes. *J Pharmacol Sci.* (2019) 139:1–8. doi: 10.1016/j.jphs.2018.09.013
80. Wang Y, Rogers PM, Su C, Varga G, Stayrook KR, Burris TP. Regulation of cholesterologenesis by the oxysterol receptor, LXRalpha. *J Biol Chem.* (2008) 283:26332–9. doi: 10.1074/jbc.M804808200
81. Tint GS, Pan L, Shang Q, Sharpe LJ, Brown AJ, Li M, et al. Desmosterol in brain is elevated because DHCR24 needs REST for Robust Expression but REST is poorly expressed. *Dev Neurosci.* (2014) 36:132–42. doi: 10.1159/000362363
82. Medina MW, Gao F, Naidoo D, Rudel LL, Temel RE, McDaniel AL, et al. Coordinately regulated alternative splicing of genes involved in cholesterol biosynthesis and uptake. *PLoS ONE.* (2011) 6:e19420. doi: 10.1371/journal.pone.0019420
83. Peffley DM, Gayen AK. Mevalonate regulates polysome distribution and blocks translation-dependent suppression of 3-hydroxy-3-methylglutaryl coenzyme A reductase mRNA: relationship to translational control. *Somat Cell Mol Genet.* (1995) 21:189–204. doi: 10.1007/BF02254770
84. Chen L, Ma MY, Sun M, Jiang LY, Zhao XT, Fang XX, et al. Endogenous sterol intermediates of the mevalonate pathway regulate HMGCR degradation and SREBP-2 processing. *J Lipid Res.* (2019) 60:1765–75. doi: 10.1194/jlr.RA119000201
85. Hinson DD, Chambliss KL, Toth MJ, Tanaka RD, Gibson KM. Post-translational regulation of mevalonate kinase by intermediates of the cholesterol and nonsterol isoprene biosynthetic pathways. *J Lipid Res.* (1997) 38:2216–23.
86. Metherall JE, Waugh K, Li H. Progesterone inhibits cholesterol biosynthesis in cultured cells. Accumulation of cholesterol precursors. *J Biol Chem.* (1996) 271:2627–33. doi: 10.1074/jbc.271.5.2627
87. Fernandez C, Suarez Y, Ferruelo AJ, Gomez-Coronado D, Lasuncion MA. Inhibition of cholesterol biosynthesis by Delta22-unsaturated phytosterols via competitive inhibition of sterol Delta24-reductase in mammalian cells. *Biochem J.* (2002) 366(Pt. 1):109–19. doi: 10.1042/bj20011777
88. Zerenturk EJ, Kristiana I, Gill S, Brown AJ. The endogenous regulator 24(S),25-epoxycholesterol inhibits cholesterol synthesis at DHCR24 (Seladin-1). *Biochim Biophys Acta.* (2012) 1821:1269–77. doi: 10.1016/j.bbalip.2011.11.009
89. Cheng C, Geng F, Cheng X, Guo D. Lipid metabolism reprogramming and its potential targets in cancer. *Cancer Commun.* (2018) 38:27. doi: 10.1186/s40880-018-0301-4
90. Ettinger SL, Sobel R, Whitmore TG, Akbari M, Bradley DR, Gleave ME, et al. Dysregulation of sterol response element-binding proteins and downstream effectors in prostate cancer during progression to androgen independence. *Cancer Res.* (2004) 64:2212–21. doi: 10.1158/0008-5472.CAN-2148-2
91. Armengol S, Arretxe E, Enzunza L, Llorente I, Mendibil U, Navarro-Imaz H, et al. SREBP-2-driven transcriptional activation of human SND1 oncogene. *Oncotarget.* (2017) 8:108181–94. doi: 10.18632/oncotarget.22569
92. Gruenbacher G, Thurnher M. Mevalonate metabolism in cancer stemness and trained immunity. *Front Oncol.* (2018) 8:394. doi: 10.3389/fonc.2018.00394
93. Suburu J, Chen YQ. Lipids and prostate cancer. *Prostaglandins Other Lipid Mediat.* (2012) 98:1–10. doi: 10.1016/j.prostaglandins.2012.03.003
94. Bull CJ, Bonilla C, Holly JM, Perks CM, Davies N, Haycock P, et al. Blood lipids and prostate cancer: a Mendelian randomization analysis. *Cancer Med.* (2016) 5:1125–36. doi: 10.1002/cam4.695
95. Fujita K, Nonomura N. Role of androgen receptor in prostate cancer: a review. *World J Mens Health.* (2019) 37:288–95. doi: 10.5534/wjmh.180040
96. Heemers HV, Verhoeven G, Swinnen JV. Androgen activation of the sterol regulatory element-binding protein pathway: current insights. *Mol Endocrinol.* (2006) 20:2265–77. doi: 10.1210/me.2005-0479
97. Heemers H, Verrijdt G, Organe S, Claessens F, Heyns W, Verhoeven G, et al. Identification of an androgen response element in intron 8 of the sterol regulatory element-binding protein cleavage-activating protein gene allowing direct regulation by the androgen receptor. *J Biol Chem.* (2004) 279:30880–7. doi: 10.1074/jbc.M401615200
98. Swinnen JV, Van Veldhoven PP, Esquenet M, Heyns W, Verhoeven G. Androgens markedly stimulate the accumulation of neutral lipids in the human prostatic adenocarcinoma cell line LNCaP. *Endocrinology.* (1996) 137:4468–74. doi: 10.1210/endo.137.10.8828509
99. Swinnen JV, Ulrix W, Heyns W, Verhoeven G. Coordinate regulation of lipogenic gene expression by androgens: evidence for a cascade mechanism involving sterol regulatory element binding proteins. *Proc Natl Acad Sci USA.* (1997) 94:12975–80. doi: 10.1073/pnas.94.24.12975
100. Chen M, Zhang J, Sampieri K, Clohessy JG, Mendez L, Gonzalez-Billalabeitia E, et al. An aberrant SREBP-dependent lipogenic program promotes metastatic prostate cancer. *Nat Genet.* (2018) 50:206–18. doi: 10.1038/s41588-017-0027-2
101. Ashida S, Kawada C, Inoue K. Stromal regulation of prostate cancer cell growth by mevalonate pathway enzymes HMGCS1 and HMGCR. *Oncol Lett.* (2017) 14:6533–42. doi: 10.3892/ol.2017.7025
102. Kong Y, Cheng L, Mao F, Zhang Z, Zhang Y, Farah E, et al. Inhibition of cholesterol biosynthesis overcomes enzalutamide resistance in castration-resistant prostate cancer (CRPC). *J Biol Chem.* (2018) 293:14328–41. doi: 10.1074/jbc.RA118.004442
103. Todenhofer T, Hennenlotter J, Kuhs U, Gerber V, Gakis G, Vogel U, et al. Altered expression of farnesyl pyrophosphate synthase in prostate cancer: evidence for a role of the mevalonate pathway in disease progression? *World J Urol.* (2013) 31:345–50. doi: 10.1007/s00345-012-0844-y
104. Seshacharyulu P, Rachagani S, Muniyan S, Siddiqui JA, Cruz E, Sharma S, et al. FDPS cooperates with PTEN loss to promote prostate cancer progression

- through modulation of small GTPases/AKT axis. *Oncogene*. (2019) 38:5265–80. doi: 10.1038/s41388-019-0791-9
105. Fukuma Y, Matsui H, Koike H, Sekine Y, Shechter I, Ohtake N, et al. Role of squalene synthase in prostate cancer risk and the biological aggressiveness of human prostate cancer. *Prostate Cancer Prostatic Dis.* (2012) 15:339–45. doi: 10.1038/pcan.2012.14
  106. Zhao Z, Hao D, Wang L, Li J, Meng Y, Li P, et al. CtBP promotes metastasis of breast cancer through repressing cholesterol and activating TGF- $\beta$  signaling. *Oncogene*. (2019) 38:2076–91. doi: 10.1038/s41388-018-0570-z
  107. Ricoult SJ, Yecies JL, Ben-Sahra I, Manning BD. Oncogenic PI3K and K-Ras stimulate de novo lipid synthesis through mTORC1 and SREBP. *Oncogene*. (2016) 35:1250–60. doi: 10.1038/ncr.2015.179
  108. Xu ZQ, Zhang Y, Li N, Liu PJ, Gao L, Gao X, et al. Efficacy and safety of lapatinib and trastuzumab for HER2-positive breast cancer: a systematic review and meta-analysis of randomised controlled trials. *BMJ Open*. (2017) 7:e013053. doi: 10.1136/bmjopen-2016-013053
  109. Wang YC, Morrison G, Gillihan R, Guo J, Ward RM, Fu X, et al. Different mechanisms for resistance to trastuzumab versus lapatinib in HER2-positive breast cancers—role of estrogen receptor and HER2 reactivation. *Breast Cancer Res.* (2011) 13:R121. doi: 10.1186/bcr3067
  110. Sethunath V, Hu H, De Angelis C, Veeraraghavan J, Qin L, Wang N, et al. Targeting the mevalonate pathway to overcome acquired anti-HER2 treatment resistance in breast cancer. *Mol Cancer Res.* (2019) 17:2318–30. doi: 10.1158/1541-7786.MCR-19-0756
  111. Orho-Melander M, Hindy G, Borgquist S, Schulz CA, Manjer J, Melander O, et al. Blood lipid genetic scores, the HMGCR gene and cancer risk: a Mendelian randomization study. *Int J Epidemiol.* (2018) 47:495–505. doi: 10.1093/ije/dyx237
  112. Clendening JW, Pandya A, Boutros PC, El Ghamrasni S, Khosravi F, Trentin GA, et al. Dysregulation of the mevalonate pathway promotes transformation. *Proc Natl Acad Sci USA.* (2010) 107:15051–6. doi: 10.1073/pnas.0910258107
  113. Di Benedetto A, Mottollese M, Sperati F, Ercolani C, Di Lauro L, Pizzuti L, et al. HMG-CoAR expression in male breast cancer: relationship with hormone receptors, Hippo transducers and survival outcomes. *Sci Rep.* (2016) 6:35121. doi: 10.1038/srep35121
  114. Baek AE, Nelson ER. The contribution of cholesterol and its metabolites to the pathophysiology of breast cancer. *Horm Cancer.* (2016) 7:219–28. doi: 10.1007/s12672-016-0262-5
  115. Nelson ER, Chang CY, McDonnell DP. Cholesterol and breast cancer pathophysiology. *Trends Endocrinol Metab.* (2014) 25:649–55. doi: 10.1016/j.tem.2014.10.001
  116. Dehghani M, Samani S, Abidi H, Manzouri L, Mahmoudi R, Hosseini Teshnizi S, et al. Relationship of SNP rs2645429 in farnesyl-diphosphate farnesyltransferase 1 gene promoter with susceptibility to lung cancer. *Int J Genomics.* (2018) 2018:4863757. doi: 10.1155/2018/4863757
  117. Yang YF, Jan YH, Liu YP, Yang CJ, Su CY, Chang YC, et al. Squalene synthase induces tumor necrosis factor receptor 1 enrichment in lipid rafts to promote lung cancer metastasis. *Am J Respir Crit Care Med.* (2014) 190:675–87. doi: 10.1164/rccm.201404-0714OC
  118. Lin L, Li M, Lin L, Xu X, Jiang G, Wu L. FPPS mediates TGF- $\beta$ 1-induced non-small cell lung cancer cell invasion and the EMT process via the RhoA/Rock1 pathway. *Biochem Biophys Res Commun.* (2018) 496:536–41. doi: 10.1016/j.bbrc.2018.01.066
  119. Wang X, Xu W, Zhan P, Xu T, Jin J, Miu Y, et al. Overexpression of geranylgeranyl diphosphate synthase contributes to tumour metastasis and correlates with poor prognosis of lung adenocarcinoma. *J Cell Mol Med.* (2018) 22:2177–89. doi: 10.1111/jcmm.13493
  120. Ge H, Zhao Y, Shi X, Tan Z, Chi X, He M, et al. Squalene epoxidase promotes the proliferation and metastasis of lung squamous cell carcinoma cells through extracellular signal-regulated kinase signaling. *Thorac Cancer.* (2019) 10:428–36. doi: 10.1111/1759-7714.12944
  121. Fatehi Hassanabad A, Mina F. Targeting the mevalonate pathway for treating lung cancer. *Am J Clin Oncol.* (2020) 43:69–70. doi: 10.1097/COC.0000000000000630
  122. Liang B, Chen R, Song S, Wang H, Sun G, Yang H, et al. ASPP2 inhibits tumor growth by repressing the mevalonate pathway in hepatocellular carcinoma. *Cell Death Dis.* (2019) 10:830. doi: 10.1038/s41419-019-2054-7
  123. Navarro-Imaz H, Chico Y, Rueda Y, Fresnedo O. Channeling of newly synthesized fatty acids to cholesterol esterification limits triglyceride synthesis in SMD1-overexpressing hepatoma cells. *Biochim Biophys Acta Mol Cell Biol Lipids.* (2019) 1864:137–46. doi: 10.1016/j.bbalip.2018.11.004
  124. Che L, Chi W, Qiao Y, Zhang J, Song X, Liu Y, et al. Cholesterol biosynthesis supports the growth of hepatocarcinoma lesions depleted of fatty acid synthase in mice and humans. *Gut.* (2019) 69:177–86. doi: 10.1136/gutjnl-2018-317581
  125. Ogura S, Yoshida Y, Kurahashi T, Egawa M, Furuta K, Kiso S, et al. Targeting the mevalonate pathway is a novel therapeutic approach to inhibit oncogenic FoxM1 transcription factor in human hepatocellular carcinoma. *Oncotarget.* (2018) 9:21022–35. doi: 10.18632/oncotarget.24781
  126. Syafruddin SE, Rodrigues P, Vojtasova E, Patel SA, Zaini MN, Burge J, et al. A KLF6-driven transcriptional network links lipid homeostasis and tumour growth in renal carcinoma. *Nat Commun.* (2019) 10:1152. doi: 10.1038/s41467-019-09116-x
  127. Yu Y, Dong JT, He B, Zou YF, Li XS, Xi CH, et al. LncRNA SNHG16 induces the SREBP2 to promote lipogenesis and enhance the progression of pancreatic cancer. *Future Oncol.* (2019) 15:3831–44. doi: 10.2217/fon-2019-0321
  128. Wang B, Rong X, Palladino END, Wang J, Fogelman AM, Martin MG, et al. Phospholipid remodeling and cholesterol availability regulate intestinal stemness and tumorigenesis. *Cell Stem Cell.* (2018) 22:206–20. e204. doi: 10.1016/j.stem.2017.12.017
  129. Ma YS, Wu ZJ, Zhang HW, Cai B, Huang T, Long HD, et al. Dual regulatory mechanisms of expression and mutation involving metabolism-related genes FDF1 and UQR5 during CLM. *Mol Ther Oncolytics.* (2019) 14:172–8. doi: 10.1016/j.omto.2019.04.008
  130. Dai M, Zhu XL, Liu F, Xu QY, Ge QL, Jiang SH, et al. Cholesterol synthetase DHCR24 induced by insulin aggravates cancer invasion and progesterone resistance in endometrial carcinoma. *Sci Rep.* (2017) 7:41404. doi: 10.1038/srep41404
  131. Liu XP, Yin XH, Meng XY, Yan XH, Cao Y, Zeng XT, et al. DHCR24 predicts poor clinicopathological features of patients with bladder cancer: a STROBE-compliant study. *Medicine.* (2018) 97:e11830. doi: 10.1097/MD.00000000000011830
  132. Li X, Chen YT, Jossan S, Mukhopadhyay NK, Kim J, Freeman MR, et al. MicroRNA-185 and 342 inhibit tumorigenicity and induce apoptosis through blockade of the SREBP metabolic pathway in prostate cancer cells. *PLoS ONE.* (2013) 8:e70987. doi: 10.1371/journal.pone.0070987
  133. Li X, Chen YT, Hu P, Huang WC. Fatostatin displays high antitumor activity in prostate cancer by blocking SREBP-regulated metabolic pathways and androgen receptor signaling. *Mol Cancer Ther.* (2014) 13:855–66. doi: 10.1158/1535-7163.MCT-13-0797
  134. Yang M, Liu W, Pellicane C, Sahyoun C, Joseph BK, Gallo-Ebert C, et al. Identification of miR-185 as a regulator of de novo cholesterol biosynthesis and low density lipoprotein uptake. *J Lipid Res.* (2014) 55:226–38. doi: 10.1194/jlr.M041335
  135. Yang L, Yang J, Li J, Shen X, Le Y, Zhou C, et al. MicroRNA-33a inhibits epithelial-to-mesenchymal transition and metastasis and could be a prognostic marker in non-small cell lung cancer. *Sci Rep.* (2015) 5:13677. doi: 10.1038/srep13677
  136. Gholkar AA, Cheung K, Williams KJ, Lo YC, Hamideh SA, Nnebe C, et al. Fatostatin inhibits cancer cell proliferation by affecting mitotic microtubule spindle assembly and cell division. *J Biol Chem.* (2016) 291:17001–8. doi: 10.1074/jbc.C116.737346
  137. Choi Y, Kawazoe Y, Murakami K, Misawa H, Uesugi M. Identification of bioactive molecules by adipogenesis profiling of organic compounds. *J Biol Chem.* (2003) 278:7320–4. doi: 10.1074/jbc.M210283200
  138. Kamisuki S, Mao Q, Abu-Elheiga L, Gu Z, Kugimiya A, Kwon Y, et al. A small molecule that blocks fat synthesis by inhibiting the activation of SREBP. *Chem Biol.* (2009) 16:882–92. doi: 10.1016/j.chembiol.2009.07.007
  139. Brovkovich V, Izhar Y, Danes JM, Dubrovskiy O, Sakalliglu IT, Morrow LM, et al. Fatostatin induces pro- and anti-apoptotic lipid accumulation in breast cancer. *Oncogenesis.* (2018) 7:66. doi: 10.1038/s41389-018-0076-0
  140. Gao S, Shi Z, Li X, Li W, Wang Y, Liu Z, et al. Fatostatin suppresses growth and enhances apoptosis by blocking SREBP-regulated metabolic

- pathways in endometrial carcinoma. *Oncol Rep.* (2018) 39:1919–29. doi: 10.3892/or.2018.6265
141. Shao W, Machamer CE, Espenshade PJ. Fatostatin blocks ER exit of SCAP but inhibits cell growth in a SCAP-independent manner. *J Lipid Res.* (2016) 57:1564–73. doi: 10.1194/jlr.M069583
  142. Li X, Wu JB, Chung LW, Huang WC. Anti-cancer efficacy of SREBP inhibitor, alone or in combination with docetaxel, in prostate cancer harboring p53 mutations. *Oncotarget.* (2015) 6:41018–32. doi: 10.18632/oncotarget.5879
  143. Krycer JR, Phan L, Brown AJ. A key regulator of cholesterol homeostasis, SREBP-2, can be targeted in prostate cancer cells with natural products. *Biochem J.* (2012) 446:191–201. doi: 10.1042/BJ20120545
  144. Wei S, Liu L, Chen Z, Yin W, Liu Y, Ouyang Q, et al. Artesunate inhibits the mevalonate pathway and promotes glioma cell senescence. *J Cell Mol Med.* (2019). doi: 10.1111/jcmm.14717
  145. Kim YS, Lee YM, Oh TI, Shin DH, Kim GH, Kan SY, et al. Emodin sensitizes hepatocellular carcinoma cells to the anti-cancer effect of sorafenib through suppression of cholesterol metabolism. *Int J Mol Sci.* (2018) 19:3127. doi: 10.3390/ijms19103127
  146. Kim GH, Kan SY, Kang H, Lee S, Ko HM, Kim JH, et al. Ursolic acid suppresses cholesterol biosynthesis and exerts anti-cancer effects in hepatocellular carcinoma cells. *Int J Mol Sci.* (2019) 20:4767. doi: 10.3390/ijms20194767
  147. Hamm R, Chen YR, Seo EJ, Zeino M, Wu CF, Muller R, et al. Induction of cholesterol biosynthesis by archazolid B in T24 bladder cancer cells. *Biochem Pharmacol.* (2014) 91:18–30. doi: 10.1016/j.bcp.2014.06.018
  148. Horie T, Ono K, Horiguchi M, Nishi H, Nakamura T, Nagao K, et al. MicroRNA-33 encoded by an intron of sterol regulatory element-binding protein 2 (Srebp2) regulates HDL *in vivo*. *Proc Natl Acad Sci USA.* (2010) 107:17321–6. doi: 10.1073/pnas.1008499107
  149. Geng C, Dong T, Jin W, Yu B, Yin F, Peng F, et al. MicroRNA-98 regulates hepatic cholesterol metabolism via targeting sterol regulatory element-binding protein 2. *Biochem Biophys Res Commun.* (2018) 504:422–6. doi: 10.1016/j.bbrc.2018.08.205
  150. Kochuparambil ST, Al-Husein B, Goc A, Soliman S, Somanath PR. Anticancer efficacy of simvastatin on prostate cancer cells and tumor xenografts is associated with inhibition of Akt and reduced prostate-specific antigen expression. *J Pharmacol Exp Ther.* (2011) 336:496–505. doi: 10.1124/jpet.110.174870
  151. Deng JL, Zhang R, Zeng Y, Zhu YS, Wang G. Statins induce cell apoptosis through a modulation of AKT/FOXO1 pathway in prostate cancer cells. *Cancer Manag Res.* (2019) 11:7231–42. doi: 10.2147/CMAR.S212643
  152. Beckwith CH, Clark AM, Ma B, Whaley D, Oltvai ZN, Wells A. Statins attenuate outgrowth of breast cancer metastases. *Br J Cancer.* (2018) 119:1094–105. doi: 10.1038/s41416-018-0267-7
  153. Hu MB, Zhang JW, Gao JB, Qi YW, Gao Y, Xu L, et al. Atorvastatin induces autophagy in MDA-MB-231 breast cancer cells. *Ultrastruct Pathol.* (2018) 42:409–15. doi: 10.1080/01913123.2018.1522406
  154. Ma Q, Gao Y, Xu P, Li K, Xu X, Gao J, et al. Atorvastatin inhibits breast cancer cells by downregulating PTEN/AKT pathway via promoting ras homolog family member B (RhoB). *Biomed Res Int.* (2019) 2019:3235021. doi: 10.1155/2019/3235021
  155. Koohestanimobarhan S, Salami S, Imeni V, Mohammadi Z, Bayat O. Lipophilic statins antagonistically alter the major epithelial-to-mesenchymal transition signaling pathways in breast cancer stem-like cells via inhibition of the mevalonate pathway. *J Cell Biochem.* (2018) 120:2515–31. doi: 10.1002/jcb.27544
  156. Wang T, Seah S, Loh X, Chan CW, Hartman M, Goh BC, et al. Simvastatin-induced breast cancer cell death and deactivation of PI3K/Akt and MAPK/ERK signalling are reversed by metabolic products of the mevalonate pathway. *Oncotarget.* (2016) 7:2532–44. doi: 10.18632/oncotarget.6304
  157. Wolfe AR, Debeb BG, Lacerda L, Larson R, Bambhroliya A, Huang X, et al. Simvastatin prevents triple-negative breast cancer metastasis in pre-clinical models through regulation of FOXO3a. *Breast Cancer Res Treat.* (2015) 154:495–508. doi: 10.1007/s10549-015-3645-3
  158. Kou X, Jiang X, Liu H, Wang X, Sun F, Han J, et al. Simvastatin functions as a heat shock protein 90 inhibitor against triple-negative breast cancer. *Cancer Sci.* (2018) 109:3272–84. doi: 10.1111/cas.13748
  159. Wang L, Wang Y, Chen A, Teli M, Kondo R, Jalali A, et al. Pitavastatin slows tumor progression and alters urine-derived volatile organic compounds through the mevalonate pathway. *FASEB J.* (2019) 33:13710–21. doi: 10.1096/fj.201901388R
  160. Fan Z, Jiang H, Wang Z, Qu J. Atorvastatin partially inhibits the epithelial-mesenchymal transition in A549 cells induced by TGF- $\beta$ 1 by attenuating the upregulation of SphK1. *Oncol Rep.* (2016) 36:1016–22. doi: 10.3892/or.2016.4897
  161. Walther U, Emmrich K, Ramer R, Mittag N, Hinz B. Lovastatin lactone elicits human lung cancer cell apoptosis via a COX-2/PPAR $\gamma$ -dependent pathway. *Oncotarget.* (2016) 7:10345–62. doi: 10.18632/oncotarget.7213
  162. Shang L, Jia SS, Jiang HM, Wang H, Xu WH, Lv CJ. Simvastatin downregulates expression of TGF- $\beta$ 2 and inhibits proliferation of A549 cells via ERK. *Tumour Biol.* (2015) 36:4819–24. doi: 10.1007/s13277-015-3134-7
  163. Nakashima Y, Haneji T. Stimulation of osteoclast formation by RANKL requires interferon regulatory factor-4 and is inhibited by simvastatin in a mouse model of bone loss. *PLoS ONE.* (2013) 8:e72033. doi: 10.1371/journal.pone.0072033
  164. Sarkar D. Statins as inhibitors of lung cancer bone metastasis. *EBioMedicine.* (2017) 19:6–7. doi: 10.1016/j.ebiom.2017.04.028
  165. Yang Z, Su Z, DeWitt JB, Xie L, Chen Y, Li X, et al. Fluvastatin prevents lung adenocarcinoma bone metastasis by triggering autophagy. *EBioMedicine.* (2017) 19:49–59. doi: 10.1016/j.ebiom.2017.04.017
  166. Wang ST, Ho HJ, Lin JT, Shieh JJ, Wu CY. Simvastatin-induced cell cycle arrest through inhibition of STAT3/SKP2 axis and activation of AMPK to promote p27 and p21 accumulation in hepatocellular carcinoma cells. *Cell Death Dis.* (2017) 8:e2626. doi: 10.1038/cddis.2016.472
  167. Higashi T, Hayashi H, Kitano Y, Yamamura K, Kaida T, Arima K, et al. Statin attenuates cell proliferative ability via TAZ (WWTR1) in hepatocellular carcinoma. *Med Oncol.* (2016) 33:123. doi: 10.1007/s12032-016-0845-6
  168. Huang X, Ma J, Xu J, Su Q, Zhao J. Simvastatin induces growth inhibition and apoptosis in HepG2 and Huh7 hepatocellular carcinoma cells via upregulation of Notch1 expression. *Mol Med Rep.* (2015) 11:2334–40. doi: 10.3892/mmr.2014.2976
  169. Relja B, Meder F, Wang M, Blaheta R, Henrich D, Marzi I, et al. Simvastatin modulates the adhesion and growth of hepatocellular carcinoma cells via decrease of integrin expression and ROCK. *Int J Oncol.* (2011) 38:879–85. doi: 10.3892/ijo.2010.892
  170. Woodard J, Sassano A, Hay N, Platanias LC. Statin-dependent suppression of the Akt/mammalian target of rapamycin signaling cascade and programmed cell death 4 up-regulation in renal cell carcinoma. *Clin Cancer Res.* (2008) 14:4640–9. doi: 10.1158/1078-0432.CCR-07-5232
  171. Qi XF, Zheng L, Lee KJ, Kim DH, Kim CS, Cai DQ, et al. HMG-CoA reductase inhibitors induce apoptosis of lymphoma cells by promoting ROS generation and regulating Akt, Erk and p38 signals via suppression of mevalonate pathway. *Cell Death Dis.* (2013) 4:e518. doi: 10.1038/cddis.2013.44
  172. Zheng X, Cui XX, Gao Z, Zhao Y, Lin Y, Shih WJ, et al. Atorvastatin and celecoxib in combination inhibits the progression of androgen-dependent LNCaP xenograft prostate tumors to androgen independence. *Cancer Prev Res.* (2010) 3:114–24. doi: 10.1158/1940-6207.CAPR-09-0059
  173. Martirosyan A, Clendening JW, Goard CA, Penn LZ. Lovastatin induces apoptosis of ovarian cancer cells and synergizes with doxorubicin: potential therapeutic relevance. *BMC Cancer.* (2010) 10:103. doi: 10.1186/1471-2407-10-103
  174. Lee JS, Roberts A, Juarez D, Vo TT, Bhatt S, Herzog LO, et al. Statins enhance efficacy of venetoclax in blood cancers. *Sci Transl Med.* (2018) 10:eaq1240. doi: 10.1126/scitranslmed.aq1240
  175. Kim JS, Turbov J, Rosales R, Thaete LG, Rodriguez GC. Combination simvastatin and metformin synergistically inhibits endometrial cancer cell growth. *Gynecol Oncol.* (2019) 154:432–40. doi: 10.1016/j.ygyno.2019.05.022
  176. McGregor GH, Campbell AD, Fey SK, Tumanov S, Sumpton D, Blanco GR, et al. Targeting the metabolic response to statin-mediated oxidative stress



- produces a synergistic antitumor response. *Cancer Res.* (2020) 80:175–88. doi: 10.1158/0008-5472.CAN-19-0644
177. Fragni M, Bonini SA, Stabile A, Bodei S, Cristinelli L, Simeone C, et al. Inhibition of survivin is associated with zoledronic acid-induced apoptosis of prostate cancer cells. *Anticancer Res.* (2016) 36:913–20.
  178. Pietrovito L, Comito G, Parri M, Giannoni E, Chiarugi P, Taddei ML. Zoledronic Acid inhibits the RhoA-mediated amoeboid motility of prostate cancer cells. *Curr Cancer Drug Targets.* (2019) 19:807–16. doi: 10.2174/1568009619666190115142858
  179. Rouhraz H, Turgan N, Oktem G. Zoledronic acid overcomes chemoresistance by sensitizing cancer stem cells to apoptosis. *Biotech Histochem.* (2018) 93:77–88. doi: 10.1080/10520295.2017.1387286
  180. Lin JF, Lin YC, Lin YH, Tsai TF, Chou KY, Chen HE, et al. Zoledronic acid induces autophagic cell death in human prostate cancer cells. *J Urol.* (2011) 185:1490–6. doi: 10.1016/j.juro.2010.11.045
  181. Coxon JP, Oades GM, Kirby RS, Colston KW. Zoledronic acid induces apoptosis and inhibits adhesion to mineralized matrix in prostate cancer cells via inhibition of protein prenylation. *BJU Int.* (2004) 94:164–70. doi: 10.1111/j.1464-4096.2004.04831.x
  182. Liu H, Wang SH, Chen SC, Chen CY, Lin TM. Zoledronic acid blocks the interaction between breast cancer cells and regulatory T-cells. *BMC Cancer.* (2019) 19:176. doi: 10.1186/s12885-019-5379-9
  183. Kopecka J, Porto S, Lusa S, Gazzano E, Salzano G, Pinzon-Daza ML, et al. Zoledronic acid-encapsulating self-assembling nanoparticles and doxorubicin: a combinatorial approach to overcome simultaneously chemoresistance and immunoresistance in breast tumors. *Oncotarget.* (2016) 7:20753–72. doi: 10.18632/oncotarget.8012
  184. Li YY, Chang JW, Liu YC, Wang CH, Chang HJ, Tsai MC, et al. Zoledronic acid induces cell-cycle prolongation in murine lung cancer cells by perturbing cyclin and Ras expression. *Anticancer Drugs.* (2011) 22:89–98. doi: 10.1097/CAD.0b013e328328340a05
  185. Xie F, Li P, Gong J, Zhang J, Ma J. The bisphosphonate zoledronic acid effectively targets lung cancer cells by inhibition of protein prenylation. *Biochem Biophys Res Commun.* (2015) 467:664–9. doi: 10.1016/j.bbrc.2015.10.089
  186. Honda Y, Takahashi S, Zhang Y, Ono A, Murakami E, Shi N, et al. Effects of bisphosphonate zoledronic acid in hepatocellular carcinoma, depending on mevalonate pathway. *J Gastroenterol Hepatol.* (2015) 30:619–27. doi: 10.1111/jgh.12715
  187. Goto H, Matsuda K, Srikoon P, Kariya R, Hattori S, Taura M, et al. Potent antitumor activity of zoledronic acid-induced Vgamma9Vdelta2 T cells against primary effusion lymphoma. *Cancer Lett.* (2013) 331:174–82. doi: 10.1016/j.canlet.2012.12.021
  188. Comito G, Pons Segura C, Taddei ML, Lanciotti M, Serni S, Morandi A, et al. Zoledronic acid impairs stromal reactivity by inhibiting M2-macrophages polarization and prostate cancer-associated fibroblasts. *Oncotarget.* (2017) 8:118–32. doi: 10.18632/oncotarget.9497
  189. Miwa S, Mizokami A, Keller ET, Taichman R, Zhang J, Namiki M. The bisphosphonate YM529 inhibits osteolytic and osteoblastic changes and CXCR-4-induced invasion in prostate cancer. *Cancer Res.* (2005) 65:8818–25. doi: 10.1158/0008-5472.CAN-05-0540
  190. Koshimune R, Aoe M, Toyooka S, Hara F, Ouchida M, Tokumo M, et al. Anti-tumor effect of bisphosphonate (YM529) on non-small cell lung cancer cell lines. *BMC Cancer.* (2007) 7:8. doi: 10.1186/1471-2407-7-8
  191. Sato K, Yuasa T, Nogawa M, Kimura S, Segawa H, Yokota A, et al. A third-generation bisphosphonate, minodronic acid (YM529), successfully prevented the growth of bladder cancer *in vitro* and *in vivo*. *Br J Cancer.* (2006) 95:1354–61. doi: 10.1038/sj.bjc.6603423
  192. Jones RM, Morgan C, Bertelli G. Effects of zoledronic acid and docetaxel on small GTP-binding proteins in prostate cancer. *Tumour Biol.* (2015) 36:4861–9. doi: 10.1007/s13277-015-3140-9
  193. Wilke M, Gobel A, Rauner M, Benad-Mehner P, Schutze N, Fussel S, et al. Zoledronic acid and atorvastatin inhibit alphavbeta3-mediated adhesion of breast cancer cells. *J Bone Oncol.* (2014) 3:10–7. doi: 10.1016/j.jbo.2014.02.001
  194. Jagdev SP, Coleman RE, Shipman CM, Rostami HA, Croucher PI. The bisphosphonate, zoledronic acid, induces apoptosis of breast cancer cells: evidence for synergy with paclitaxel. *Br J Cancer.* (2001) 84:1126–34. doi: 10.1054/bjoc.2001.1727
  195. Gobel A, Thiele S, Browne AJ, Rauner M, Zinna VM, Hofbauer LC, et al. Combined inhibition of the mevalonate pathway with statins and zoledronic acid potentiates their anti-tumor effects in human breast cancer cells. *Cancer Lett.* (2016) 375:162–71. doi: 10.1016/j.canlet.2016.03.004
  196. Feng C, Liu X, Li X, Guo F, Huang C, Qin Q, et al. Zoledronic acid increases the antitumor effect of gefitinib treatment for non-small cell lung cancer with EGFR mutations. *Oncol Rep.* (2016) 35:3460–70. doi: 10.3892/or.2016.4741
  197. Kuzu OF, Noory MA, Robertson GP. The role of cholesterol in cancer. *Cancer Res.* (2016) 76:2063–70. doi: 10.1158/0008-5472.CAN-15-2613
  198. Ding X, Zhang W, Li S, Yang H. The role of cholesterol metabolism in cancer. *Am J Cancer Res.* (2019) 9:219–27.
  199. Corcos L, Le Jossic-Corcos C. Statins: perspectives in cancer therapeutics. *Dig Liver Dis.* (2013) 45:795–802. doi: 10.1016/j.dld.2013.02.002
  200. Iannelli F, Lombardi R, Milone MR, Pucci B, De Rienzo S, Budillon A, et al. Targeting mevalonate pathway in cancer treatment: repurposing of statins. *Recent Pat Anticancer Drug Discov.* (2018) 13:184–200. doi: 10.2174/1574892812666171129141211
  201. Singh H, Mahmud SM, Turner D, Xue L, Demers AA, Bernstein CN. Long-term use of statins and risk of colorectal cancer: a population-based study. *Am J Gastroenterol.* (2009) 104:3015–23. doi: 10.1038/ajg.2009.574
  202. Chiu HF, Ho SC, Chen CC, Yang CY. Statin use and the risk of liver cancer: a population-based case-control study. *Am J Gastroenterol.* (2011) 106:894–8. doi: 10.1038/ajg.2010.475
  203. Khurana V, Bejanki HR, Caldito G, Owens MW. Statins reduce the risk of lung cancer in humans: a large case-control study of US veterans. *Chest.* (2007) 131:1282–8. doi: 10.1378/chest.06-0931
  204. Fatehi Hassanabad A, McBride SA. Statins as potential therapeutics for lung cancer: molecular mechanisms and clinical outcomes. *Am J Clin Oncol.* (2019) 42:732–6. doi: 10.1097/COC.0000000000000579
  205. Gobel A, Breining D, Rauner M, Hofbauer LC, Rachner TD. Induction of 3-hydroxy-3-methylglutaryl-CoA reductase mediates statin resistance in breast cancer cells. *Cell Death Dis.* (2019) 10:91. doi: 10.1038/s41419-019-1322-x
  206. Murtola TJ, Peltomaa AI, Talala K, Maattanen L, Taari K, Tammela TLJ, et al. statin use and prostate cancer survival in the finnish randomized study of screening for prostate cancer. *Eur Urol Focus.* (2017) 3:212–20. doi: 10.1016/j.euf.2016.05.004
  207. Liu B, Yi Z, Guan X, Zeng YX, Ma F. The relationship between statins and breast cancer prognosis varies by statin type and exposure time: a meta-analysis. *Breast Cancer Res Treat.* (2017) 164:1–11. doi: 10.1007/s10549-017-4246-0
  208. Xia DK, Hu ZG, Tian YF, Zeng FJ. Statin use and prognosis of lung cancer: a systematic review and meta-analysis of observational studies and randomized controlled trials. *Drug Des Devel Ther.* (2019) 13:405–22. doi: 10.2147/DDDT.S187690
  209. Kim GA, Shim JJ, Lee JS, Kim BH, Kim JW, Oh CH, et al. Effect of statin use on liver cancer mortality considering hypercholesterolemia and obesity in patients with non-cirrhotic chronic hepatitis B. *Yonsei Med J.* (2019) 60:1203–8. doi: 10.3349/ymj.2019.60.12.1203
  210. Couttenier A, Lacroix O, Vaes E, Cardwell CR, De Schutter H, Robert A. Statin use is associated with improved survival in ovarian cancer: a retrospective population-based study. *PLoS ONE.* (2017) 12:e0189233. doi: 10.1371/journal.pone.0189233
  211. Nguyen T, Khan A, Liu Y, El-Serag HB, Thrift AP. The association between statin use after diagnosis and mortality risk in patients with esophageal cancer: a retrospective cohort study of United States veterans. *Am J Gastroenterol.* (2018) 113:1310. doi: 10.1038/s41395-018-0169-6
  212. Mei Z, Liang M, Li L, Zhang Y, Wang Q, Yang W. Effects of statins on cancer mortality and progression: a systematic review and meta-analysis of 95 cohorts including 1,111,407 individuals. *Int J Cancer.* (2017) 140:1068–81. doi: 10.1002/ijc.30526
  213. Farooqi MAM, Malhotra N, Mukherjee SD, Sanger S, Dhesy-Thind SK, Ellis P, et al. Statin therapy in the treatment of active cancer: a systematic review and meta-analysis of randomized controlled trials. *PLoS ONE.* (2018) 13:e0209486. doi: 10.1371/journal.pone.0209486

214. Zaleska M, Mozenska O, Bil J. Statins use and cancer: an update. *Future Oncol.* (2018) 14:1497–509. doi: 10.2217/fon-2017-0543
215. Lin JJ, Ezer N, Sigel K, Mhango G, Wisnivesky JP. The effect of statins on survival in patients with stage IV lung cancer. *Lung Cancer.* (2016) 99:137–42. doi: 10.1016/j.lungcan.2016.07.006
216. Hus M, Grzasko N, Szostek M, Pluta A, Helbig G, Woszczyk D, et al. Thalidomide, dexamethasone and lovastatin with autologous stem cell transplantation as a salvage immunomodulatory therapy in patients with relapsed and refractory multiple myeloma. *Ann Hematol.* (2011) 90:1161–6. doi: 10.1007/s00277-011-1276-2
217. Advani AS, Li H, Michaelis LC, Medeiros BC, Liedtke M, List AF, et al. Report of the relapsed/refractory cohort of SWOG S0919: A phase 2 study of idarubicin and cytarabine in combination with pravastatin for acute myelogenous leukemia (AML). *Leuk Res.* (2018) 67:17–20. doi: 10.1016/j.leukres.2018.01.021
218. Hung MS, Chen IC, Lee CP, Huang RJ, Chen PC, Tsai YH, et al. Statin improves survival in patients with EGFR-TKI lung cancer: a nationwide population-based study. *PLoS ONE.* (2017) 12:e0171137. doi: 10.1371/journal.pone.0171137
219. Li X, Wu XB, Chen Q. Statin use is not associated with reduced risk of skin cancer: a meta-analysis. *Br J Cancer.* (2014) 110:802–7. doi: 10.1038/bjc.2013.762
220. Gray RT, Loughrey MB, Bankhead P, Cardwell CR, McQuaid S, O'Neill RF, et al. Statin use, candidate mevalonate pathway biomarkers, and colon cancer survival in a population-based cohort study. *Br J Cancer.* (2017) 116:1652–9. doi: 10.1038/bjc.2017.139
221. Cholesterol Treatment Trialists Collaboration, Emberson JR, Kearney PM, Blackwell L, Newman C, Reith C, et al. Lack of effect of lowering LDL cholesterol on cancer: meta-analysis of individual data from 175,000 people in 27 randomised trials of statin therapy. *PLoS ONE.* (2012) 7:e29849. doi: 10.1371/journal.pone.0029849
222. Abdullah MI, de Wolf E, Jawad MJ, Richardson A. The poor design of clinical trials of statins in oncology may explain their failure - lessons for drug repurposing. *Cancer Treat Rev.* (2018) 69:84–9. doi: 10.1016/j.ctrv.2018.06.010
223. Finianos A, Aragon-Ching JB. Zoledronic acid for the treatment of prostate cancer. *Expert Opin Pharmacother.* (2019) 20:657–66. doi: 10.1080/14656566.2019.1574754
224. Lluch A, Cueva J, Ruiz-Borrego M, Ponce J, Perez-Fidalgo JA. Zoledronic acid in the treatment of metastatic breast cancer. *Anticancer Drugs.* (2014) 25:1–7. doi: 10.1097/CAD.0000000000000020
225. Seider MJ, Pugh SL, Langer C, Wyatt G, Demas W, Rashtian A, et al. Randomized phase III trial to evaluate radiopharmaceuticals and zoledronic acid in the palliation of osteoblastic metastases from lung, breast, and prostate cancer: report of the NRG Oncology RTOG 0517 trial. *Ann Nucl Med.* (2018) 32:553–60. doi: 10.1007/s12149-018-1278-4
226. Vale CL, Burdett S, Rydzewska LHM, Albiges L, Clarke NW, Fisher D, et al. Addition of docetaxel or bisphosphonates to standard of care in men with localised or metastatic, hormone-sensitive prostate cancer: a systematic review and meta-analyses of aggregate data. *Lancet Oncol.* (2016) 17:243–56. doi: 10.1016/S1470-2045(15)00489-1
227. van Beek E, Pieterman E, Cohen L, Lowik C, Papapoulos S. Farnesyl pyrophosphate synthase is the molecular target of nitrogen-containing bisphosphonates. *Biochem Biophys Res Commun.* (1999) 264:108–11. doi: 10.1006/bbrc.1999.1499
228. Rakel A, Boucher A, Ste-Marie LG. Role of zoledronic acid in the prevention and treatment of osteoporosis. *Clin Interv Aging.* (2011) 6:89–99. doi: 10.2147/CIA.S7282
229. Van Acker HH, Anguille S, Willemen Y, Smits EL, Van Tendeloo VF. Bisphosphonates for cancer treatment: mechanisms of action and lessons from clinical trials. *Pharmacol Ther.* (2016) 158:24–40. doi: 10.1016/j.pharmthera.2015.11.008
230. Green JR. Antitumor effects of bisphosphonates. *Cancer.* (2003) 97:840–7. doi: 10.1002/cncr.11128
231. Zekri J, Mansour M, Karim SM. The anti-tumour effects of zoledronic acid. *J Bone Oncol.* (2014) 3:25–35. doi: 10.1016/j.jbo.2013.12.001
232. Pinkawa M. Zoledronic acid in first-line treatment of prostate cancer. *Int J Radiat Oncol Biol Phys.* (2017) 97:6–8. doi: 10.1016/j.ijrobp.2016.06.2453
233. Ressler S, Mlineritsch B, Greil R. Zoledronic acid for adjuvant use in patients with breast cancer. *Expert Rev Anticancer Ther.* (2011) 11:333–49. doi: 10.1586/era.11.13

**Conflict of Interest:** The authors declare that the research was conducted in the absence of any commercial or financial relationships that could be construed as a potential conflict of interest.

Copyright © 2020 Xue, Qi, Zhang, Ding, Huang, Zhao, Wu and Li. This is an open-access article distributed under the terms of the Creative Commons Attribution License (CC BY). The use, distribution or reproduction in other forums is permitted, provided the original author(s) and the copyright owner(s) are credited and that the original publication in this journal is cited, in accordance with accepted academic practice. No use, distribution or reproduction is permitted which does not comply with these terms.





# GC1qR Cleavage by Caspase-1 Drives Aerobic Glycolysis in Tumor Cells

Annika Sünderhauf<sup>1</sup>, Annika Raschdorf<sup>1</sup>, Maren Hicken<sup>1</sup>, Heidi Schlichting<sup>1</sup>, Franziska Fetzer<sup>1</sup>, Ann-Kathrin Brethack<sup>1</sup>, Sven Perner<sup>2,3</sup>, Claudia Kemper<sup>4,5,6</sup>, Berhane Ghebrehwet<sup>7</sup>, Christian Sina<sup>1,8</sup> and Stefanie Derer<sup>1\*</sup>

<sup>1</sup> Institute of Nutritional Medicine, University Hospital Schleswig-Holstein, Lübeck, Germany, <sup>2</sup> Institute of Pathology, University Hospital Schleswig-Holstein, Lübeck, Germany, <sup>3</sup> Pathology of the Research Center Borstel, Leibniz Lung Center, Borstel, Germany, <sup>4</sup> Immunology Center, National Heart, Lung, and Blood Institute, National Institutes of Health, Bethesda, MD, United States, <sup>5</sup> Faculty of Life Sciences and Medicine, School of Immunology and Microbial Sciences, King's College London, London, United Kingdom, <sup>6</sup> Institute for Systemic Inflammation Research, University of Lübeck, Lübeck, Germany, <sup>7</sup> Department of Medicine, Stony Brook University, Stony Brook, NY, United States, <sup>8</sup> 1st Department of Medicine, Division of Nutritional Medicine, University Hospital Schleswig-Holstein, Lübeck, Germany

## OPEN ACCESS

### Edited by:

Monica Montopoli,  
University of Padua, Italy

### Reviewed by:

Brandon Faubert,  
University of Texas Southwestern  
Medical Center, United States  
Maria Letizia Taddei,  
University of Florence, Italy

### \*Correspondence:

Stefanie Derer  
Stefanie.Derer@uksh.de

### Specialty section:

This article was submitted to  
Cancer Metabolism,  
a section of the journal  
Frontiers in Oncology

Received: 24 June 2020

Accepted: 28 August 2020

Published: 30 September 2020

### Citation:

Sünderhauf A, Raschdorf A, Hicken M, Schlichting H, Fetzer F, Brethack A-K, Perner S, Kemper C, Ghebrehwet B, Sina C and Derer S (2020) GC1qR Cleavage by Caspase-1 Drives Aerobic Glycolysis in Tumor Cells. *Front. Oncol.* 10:575854. doi: 10.3389/fonc.2020.575854

Self-sustained cell proliferation constitutes one hallmark of cancer enabled by aerobic glycolysis which is characterized by imbalanced glycolysis and mitochondrial oxidative phosphorylation (OXPHOS) activity, named the Warburg effect. The C1q binding protein (C1QBP; gC1qR) is pivotal for mitochondrial protein translation and thus OXPHOS activity. Due to its fundamental role in balancing OXPHOS and glycolysis, *c1qbp*<sup>-/-</sup> mice display embryonic lethality, while gC1qR is excessively up-regulated in cancer. Although gC1qR encompasses an N-terminal mitochondrial leader it is also located in other cellular compartments. Hence, we aimed to investigate mechanisms regulating gC1qR cellular localization and its impact on tumor cell metabolism. We identified two caspase-1 cleavage sites in human gC1qR. GC1qR cleavage by active caspase-1 was unraveled as a cellular mechanism that prevents mitochondrial gC1qR import, thereby enabling aerobic glycolysis and enhanced cell proliferation. *Ex vivo*, tumor grading correlated with non-mitochondrial-located gC1qR as well as with caspase-1 activation in colorectal carcinoma patients. Together, active caspase-1 cleaves gC1qR and boosts aerobic glycolysis in tumor cells.

**Keywords:** aerobic glycolysis, gC1qR, inflammasome, mitochondria, OXPHOS, caspase-1, C1qbp, p32/HABP1

## INTRODUCTION

Proliferation and differentiation of cells comprise cellular processes that require high energy levels. While it is most likely to be a general mechanism that proliferating cells generate their energy via aerobic glycolysis, differentiated post-mitotic cells are known to maintain their energy level via the mitochondrial oxidative phosphorylation (OXPHOS) system (1). Notably, the metabolic switch from cytosolic aerobic glycolysis to the mitochondrial OXPHOS system is suggested to influence the transition of transient amplifying cells into post-mitotic cells (2). However, mechanisms that enable the cells to switch between these metabolic pathways still remain elusive.

Further, it is thought that the metabolic switch from gaining energy primarily via balanced mitochondrial OXPHOS toward aerobic glycolysis, the so-called Warburg effect, is an important

driver of tumor formation and proliferation (1, 3–5). Initially, it was hypothesized that tumor cells are characterized mostly by mitochondria dysfunction, while it is now understood that tumor cells still display functional mitochondria (6).

Under chronic inflammation, high cellular proliferation rates are required for proper tissue repair, thereby increasing the possibility of dysregulated cell proliferation and hence inflammation-driven carcinogenesis. Indeed, many tumors and especially colorectal carcinomas (CRCs) develop as a result of a chronic inflammatory microenvironment mediated by pathologically sustained NLRP3 (NACHT, LRR, and PYD domains-containing protein 3) inflammasome activation. This enzymatic complex comprises of NLRP3, ASC (apoptosis-associated speck-like protein containing a CARD) and caspase-1, and is described to be activated by danger-associated molecular patterns including nutrition-derived metabolites such as glucose, fatty acids, cholesterol, ceramide, or uric acid (7) and has been shown to alter metabolic activities of cells by triggering aerobic glycolysis (8). Hence, high-fat or Western diets have been linked to constant NLRP3 inflammasome activation, thereby potentially triggering inflammation-driven carcinogenesis especially in the gut (9, 10).

The mitochondria-located gC1qR [receptor of the globular heads of C1q (11)] protein critically maintains OXPHOS and hence regulates cell metabolism in breast or cervical cancer cells (12–14). Furthermore, studies have shown increased gC1qR expression in most cancer types where it supports metastasis. Thus, augmented gC1qR levels correlate with poor prognosis in cancer patients (15–21). Until now, it is assumed that mitochondrial gC1qR protein maintains mitochondria function by regulating mitochondrial protein translation (22, 23). Of note, while gC1qR is mainly localized to the mitochondria via the presence of an N-terminal mitochondrial leader sequence in the protein (22), gC1qR is also present in other subcellular compartments and can be observed on the cell surface of distinct leukocytes (11, 24). However, mechanisms that modulate the mitochondrial localization and thereby metabolic activity of gC1qR in tumor progression still remain to be elusive. Here, we define a novel, caspase-1-mediated, molecular mechanism of controlling gC1qR activity in cells and demonstrate its perturbation in colorectal cancer.

## MATERIALS AND METHODS

### Study Population

Patients' characteristics are depicted in **Table 1**. Tissue samples collected from CRC patients utilized in qPCR and Sanger sequencing experiments were purchased from Origene (OriGene Technologies, Inc., Rockville, MD, USA). Colonic biopsy samples collected from CRC patients utilized in retrospective IHC analyses were obtained at the University Hospital Schleswig-Holstein, Campus Lübeck, Germany. Due to the low probability of patients' survival no written informed consents could be obtained retrospectively. The present study was approved by ethical committee of the University of Lübeck (AZ 20-206).

## Cell Culture

Human colorectal carcinoma cell line HT29-MTX-E12 (Sigma-Aldrich, St. Louis, MO, US) was kept in DMEM medium, the human acute monocytic leukemia cell line THP-1 (Deutsche Sammlung von Mikroorganismen und Zellkulturen, Braunschweig, Germany) was kept in RPMI 1640 medium and the human chronic myelogenous leukemia cell lines HAP1 or HAP1-gC1qR<sup>-/-</sup> (both from Horizon Discovery, Cambridge, UK) were kept in IMDM medium. All cell culture media were supplemented with 10% (v/v) heat-inactivated FCS, 100 U/ml penicillin, and 100 mg/ml streptomycin. Cells were incubated at 37°C and 5% CO<sub>2</sub> in a humidified incubator.

THP-1 monocytes were stimulated with 1 µM phorbol 12-myristate 13-acetate (PMA; InvivoGen, San Diego, CA, USA) for 24 h to induce differentiation to THP-1 macrophages. Cells were then pre-incubated with a specific caspase-1 inhibitor (10 µg/ml; Ac-YVAD-cmk from InvivoGen) or the respective control for 60 min. Afterwards, cells were further stimulated with or without lipopolysaccharides (LPS; 100 ng/ml; InvivoGen) for 24 h.

HT29-MTX cells were left untransfected or were transiently transfected with siRNAs (50 µM each) specific for *C1qbp* exon 3 (*C1qbp* siRNA; s2138; Thermo Fisher Scientific, Waltham, MA, USA) or a control siRNA as well as with plasmids encoding human Caspase-1, human NLRP3, and human ASC (all three from InvivoGen, San Diego, CA, USA) or with a mock plasmid by reverse lipofection using Lipofectamine 3000 reagent (Thermo Fisher Scientific) for 96 h. After 24 h of transfection, cells were stimulated for 72 h with 1.25 mM butyrate or were left untreated.

## Generation of HAP1-gC1qR Mutants

The expression plasmid for human wild-type (wt) gC1qR (Sino Biological Inc., Wayne, PA, USA) was utilized for substitution of aspartic acid (D) residues 77 or 229 by glutamic acid (E) (D77E, D229E, or D77E/D229E) using the QuikChange II XL site-directed mutagenesis kit (Agilent, Santa Clara, CA, USA).

HAP1-gC1qR<sup>-/-</sup> cells were stably transfected with these plasmids, encoding the sequences for gC1qR-wt, gC1qR-D77E, gC1qR-D229E, or gC1qR-D77E/D229E by lipofection using Lipofectamine 3000 reagent (Thermo Fisher Scientific), according to the manufacturer's instructions. Twenty-four hours after transfection, cells were put under selection by adding Hygromycin B (Thermo Fisher Scientific). Stable HAP1-gC1qR mutant cell lines were then further stably transfected with plasmids encoding human Caspase-1, human NLRP3, and human ASC (all three from InvivoGen, San Diego, CA, USA) or with a mock plasmid by lipofection as described above. Selection of successfully transfected cells was performed using Blasticidin (InvivoGen).

## RNA Extraction and Real-Time Quantitative PCR

RNA was extracted using the innuPREP RNA mini kit (Analytik Jena AG, Jena, Germany) and transcribed to cDNA (RevertAid H Minus reverse transcriptase, Thermo Scientific, Schwerte,

**TABLE 1** | Overview of study population.

		Male [n]	Female [n]	Median age [y]	TNM [n]	Tumor stage [n]	Tumor grade [n]	Tumor cells [%]
Paired samples from CRC patients for qPCR [n = 10]	Normal Tumor	5 5	5 5	74.5	n.a. pT3pN0pMX [10]	n.a. IIA [10]	n.a. G1 [3], G2 [7]	n.a. 60–89
Paired samples from CRC patients for IHC analyses [n = 5]	Normal Tumor	1 1	4 4	78	n.a. pT2pN0pM0 [1], pT4apN0pM0 [1], pT3pN0pM0 [1], pT4bN0pM0 [1], pT3pN2a M2 [1]	n.a. I [1], IIB [2], IIIB [1], IV [1]	n.a. G1 [2], G2 [1], G3 [1], G4 [1]	n.a.
Tumor samples from CRC patients for qPCR [n = 42]	Tumor	19	23	f 72 m 62	pT1pN0pMX [1], pT1pN1pM1 [1], pT2pN0pMX [2], pT2pN1pM1 [1], pT2pN2 MX [3], pT3pN0pM1 [2], pT3pN0pMX [14], pT3pN1pM1 [1], pT3pN1pMX [5], pT3pN2pM1 [2], pT3pN2pMX [4], pT4pN0pMX [2], pT4pN1pMX [3], pT4pN2pMX [1]	I [3], IIA [14], IIB [2], IIIB [8], IIIC [8], IV [7]	G1 [13], G2 [17], G3 [10], G4 [1]	50–95

CRC, colorectal carcinoma; n, number of patients; n.a., not applicable.

Germany) using the T Gradient thermocycler (Whatman Biometra, Göttingen, Germany). Real-time quantitative PCR (qPCR) was carried out using Perfecta SYBR Green Supermix, plus specific oligonucleotides using a 96-well-plate format. The amplification program consisted of: (i) preincubation at 95°C for 5 min; (ii) 40 cycles of denaturation at 95°C for 45 s and annealing at appropriate temperature (55°C) for 1 min using the StepOne Plus Real-Time PCR System (ThermoFisher Scientific, Darmstadt, Germany). Melting curve profiles were produced and analyzed following the  $2^{-dCt}$  algorithm. Expression levels were normalized to  $\beta$ -actin. The following oligonucleotides were used for analyses ( $\beta$ -actin: for: 5'-ACATCCGCAAAGACC TGTACG-3', rev: 5'-TTGCTGATCCACATCTGCTGG-3'; *Clqbp*: for: 5'-CTGCACACCGACGGAGACAA-3', rev: 5'-CATATAAGGCCAGTCCAAG-3'; *Caspase-1*: for: 5'-CAAGACCTCTGACAGCACGT-3', rev: 5'-GCATCTGCGCTCTA CCATCT-3'; *PYCARD*: for: 5'-GAGAACCTGACCGCCG AG-3', rev: 5'-CCTTCCCGTACAGAGCATCC-3'; *NLRP3*: for: 5'-CGTTCAGGGAGTCTGTTGA-3', rev: 5'-GGCCTTCC TTTTCCTCCTCC-3'; *Ldha*: for: 5'-GCACCCAGTTTCCACC ATGA-3', rev: 5'-GCACTCTTCTTCAAACGGGC-3'; *Slc2a1*: for: 5'-TGGCATCAACGCTGTCTTCT-3', rev: 5'-CTAGCGCG ATGGTCATGAGT-3'; *Ki67*: for: 5'-CCTGCTTGTGTTGGA AGGG-3', rev: 5'-CCTGCTTGTGTTGGAAGGG-3'; *Fis1*: for: 5'-CAAGGAGGAACAGCGGGATT-3', rev: 5'-TGCCACG AGTCCATCTTTC-3'.

## SDS-PAGE and Immunoblotting

Whole-protein extracts were prepared by lysing cells in denaturing lysis buffer containing 1% SDS, 10 mM Tris (pH 7.4), and 1% protease inhibitor mixture (Complete Protease Inhibitor Cocktail; Roche Applied Science, Mannheim, Germany). Protein fractions from the nucleus, the cytosol or the mitochondria/cell membrane were prepared by lysing cells in non-denaturing lysis buffer containing 1% protease inhibitor mixture (Complete Protease Inhibitor Cocktail) and different centrifugation steps. Protein extracts were separated by denaturing SDS-PAGE under reducing conditions and transferred onto polyvinylidene difluoride membranes. After blocking, membranes were probed with primary antibodies specific for human gC1qR (clone 60.11/ab24733 or clone EPR8871/ab131284 both from Abcam, Cambridge, MA, USA; Exon1/3/6 Abs kindly provided by Prof. Berhane Ghebrehwet), human KLF4 (AF3640, R&D Systems), human TOM20 (#42406), human Caspase-1 (#2225; mainly detects full-length Caspase-1; **Supplementary Figure 5E**), human NLRP3 (#15101), human ASC (#13833), human pAMPK $\alpha$  (#2535) or AMPK $\alpha$  (#2532), human pAKT (#4060) or AKT (#9272), human HSP60 pp44/42 (#4370) or p44/42 (#4695; all from Cell Signaling Technology, Danvers, MA, US), human VDAC (Sigma-Aldrich, St. Louis, MO), as well as for human HSP60 (#sc-13115; Santa Cruz Biotechnology), washed, and incubated with HRP-conjugated IgG as secondary Ab. Proteins were visualized by



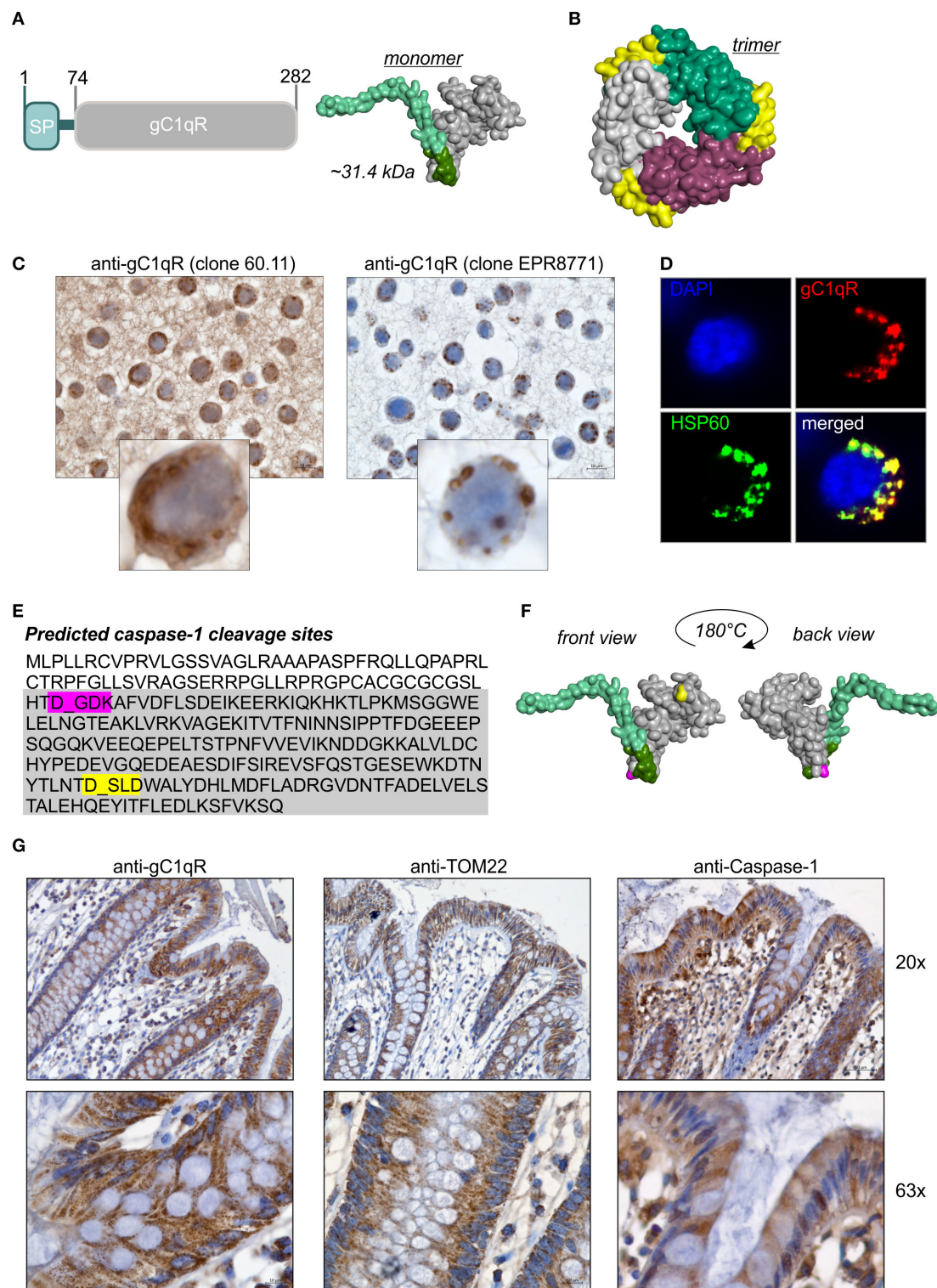


**FIGURE 1 |** GC1qR displays two caspase-1 cleavage sites. **(A)** Schematic structure model of the human gC1qR protein. SP, signal peptide sequence for mitochondrial import. Homology model of human gC1qR protein was generated using the PHYRE2 server. Bright green = predicted mitochondrial leader sequence, dark green = residual amino acid (aa) residues of exon 1, gray = mature gC1qR. **(B)** Crystal structure of trimeric human gC1qR was generated based on pdb file pdb1p32. **(C)** Immunohistochemistry analyses of paraffin-embedded formalin-fixed HT29 cells using anti-gC1qR Ab clone 60.11 or anti-gC1qR Ab clone EPR8771. **(D)** Co-localization of gC1qR with mitochondrial HSP60 protein in HAP1 cells was assessed by fluorescence microscopy using the anti-gC1qR clone EPR8771. **(E)**

(Continued)

**FIGURE 1 |** *In silico* prediction of potential protease cleavage sites was performed using the PeptideCutter software ([https://web.expasy.org/peptide\\_cutter/](https://web.expasy.org/peptide_cutter/)). Highlighted in pink = predicted caspase-1 cleavage site at amino acid D77; highlighted in yellow = predicted caspase-1 cleavage site at amino acid D229. **(F)** Predicted caspase-cleavage sites at D77 and D229 were highlighted in pink or yellow, respectively, in the generated homology model of gC1qR. **(G)** Representative pictures from immunohistochemistry analyses of five independent paraffin-embedded formalin-fixed human colonic biopsy samples collected from normal tissue sites from CRC patients using anti-gC1qR Ab (clone EPR8871), anti-TOM22 Ab or anti-Caspase-1 Ab.

chemiluminescence. To determine similar transfer and equal loading, membranes were stripped and reprobed with an Ab specific for  $\beta$ -actin (#4967, Cell Signaling Technology) or for alpha-tubulin (#2125, Cell Signaling Technology).

## ELISA

Supernatants of cell cultures were collected for measurement of IL-1 $\beta$  secretion by specific ELISA (R&D Systems, Inc., Minneapolis, MN, USA) according to the manufacturer's protocol. Release of gC1qR into the cell culture supernatant was determined by diluting the supernatant 1:2 in coating buffer (0.15 g NaH<sub>2</sub>CO<sub>3</sub>, 0.3 g NaHCO<sub>3</sub>, ad 50 ml dH<sub>2</sub>O; pH 9.6). Diluted cell culture supernatants were coated onto a 96-well-microtiter plate over night at 4°C. Next day, gC1qR was detected using a gC1qR-specific primary antibody (anti-Exon3 Ab) in combination with a respective HRP-conjugated secondary antibody. Optical density was measured at 450 nm with a reference wavelength at 540 nm.

## Immunohistochemistry

Immunohistochemical techniques were performed according to standard protocols. Briefly, paraformaldehyde-fixed and de-paraffinized tissue slides were stained with an anti-human gC1qR antibody (clone 60.11 or clone EPR8771; both from Abcam), an anti-human TOM22 antibody (#WH0056993M1, Sigma-Aldrich), an anti-human Caspase-1 antibody (#2225, Cell Signaling Technology) or with respective isotype control antibodies, washed, and incubated with respective HRP-conjugated IgG secondary Abs. Afterwards, tissue slides were incubated with DAB substrate (Dako) and counterstained with Mayer's hemalum solution. In the case of immunofluorescence analyses, slides were incubated with primary antibodies specific for human gC1qR (clone EPR8871; Abcam), HSP60 (#sc-13115; Santa Cruz Biotechnology, Dallas, Texas, USA) or an irrelevant antigen, washed, and incubated with respective fluorochrome-labeled IgG secondary Abs (HSP60: Alexa-Fluor 488 nm; gC1qR: Alexa-Fluor 594 nm; both from ThermoFisher Scientific). Afterwards, slides were counterstained with DAPI (Sigma-Aldrich).

## Caspase-1 Cleavage Assay

Cleavage of human gC1qR by active human caspase-1 was studied by incubating either recombinant human mature His-tagged gC1qR protein (aa 74-282; 30  $\mu$ g/ml; **Supplementary Figure 1F**; Prospec, East Brunswick NJ, USA), recombinant human full-length GST-tagged gC1qR protein (aa 1-282; 30  $\mu$ g/ml; **Figures 1D–G**; Abnova, Walnut, CA, USA) or native protein lysates isolated from HAP1 cells in the presence or absence of human active caspase-1 (600 U/ml; Enzo Life Sciences GmbH, Lörrach, Germany) for 4 h at 37°C in a water bath. The reaction was stopped by the addition of a reducing

SDS-buffer and heating at 95°C for 5 min. Reaction samples were then separated by denaturing SDS-PAGE and proteins were either transferred onto polyvinylidene difluoride membranes for immunoblot analyses or were stained with Coomassie blue. Protein bands were cut out of the Coomassie stained gel. Protein spots were in-gel digested by trypsin and analyzed by nanoHPLC-ESI-MS/MS method at the company Proteome Factory AG (Berlin, Germany).

## Analysis of Cell Proliferation

The CellTiter 96<sup>®</sup> Aqueous Non-Radioactive Cell Proliferation Assay (MTS) that measures metabolic activity of cells was performed using parental HAP1 cells or HAP1-gC1qR<sup>-/-</sup> cells ( $5 \times 10^3$  cells per well in a 96-well-microtiter plate, 72 h incubation at 37°C and 5% CO<sub>2</sub>) according to the manufacturer's instructions (Promega, Madison, WI, USA).

The neutral-red cytotoxicity assay was performed to determine viable cell mass in HAP1-gC1qR wt or mutant cell lines.  $5 \times 10^3$  cells per well were seeded into a 96-well-microtiter plate and incubated for 96 h at 37°C and 5% CO<sub>2</sub>. After incubation, cells were stained using a neutral red dye (Sigma-Aldrich), washed and destained to release incorporated dye into the supernatant. Neutral-red dye uptake of analyzed cells was then analyzed by measuring the absorbance at 540 and 690 nm in a microplate reader.

## Seahorse XF Cell Mito Stress Test

The Seahorse XF24 Cell Mito Stress Test was performed with parental HAP1 cells ( $3 \times 10^4$  cells/well), HAP1-gC1qR<sup>-/-</sup> cells ( $6 \times 10^4$  cells/well), HAP1-mock-NAC ( $4 \times 10^4$  cells/well), HAP1-gC1qR-wt-NAC ( $2 \times 10^4$  cells/well), or HAP1-gC1qR-D77E/D229E-NAC ( $2 \times 10^4$  cells/well), 5  $\mu$ M FCCP, 10  $\mu$ M oligomycin, and 5  $\mu$ M rotenone/antimycin A according to the manufacturer's instructions (Agilent). In the case of HAP1-gC1qR<sup>-/-</sup> and parental HAP1 cells, cells were seeded 24 h before running the Seahorse XF24 Cell Mito Stress Test. In the case of HAP1-mock-NAC, HAP1-gC1qR wt-NAC, and HAP1-gC1qR D77E/D229E-NAC transfectants, cells were seeded 48 h before running the Seahorse XF24 Cell Mito Stress Test. Cells were counted at the end of the assay and OCR and ECAR were normalized to cell count. In the case of HT29-MTX cells,  $5 \times 10^3$  cells/well were seeded in 5 mM glucose containing DMEM medium and were left untreated or stimulated with 1.25 mM butyrate for 24 h. Basal OCR and ECAR were measured in standard Seahorse medium according to the manufacturer's instructions (Agilent).

## Extracellular Oxygen Consumption Assay

The consumption of extracellular oxygen to drive oxidative phosphorylation was determined in HAP1-gC1qR wt or mutant



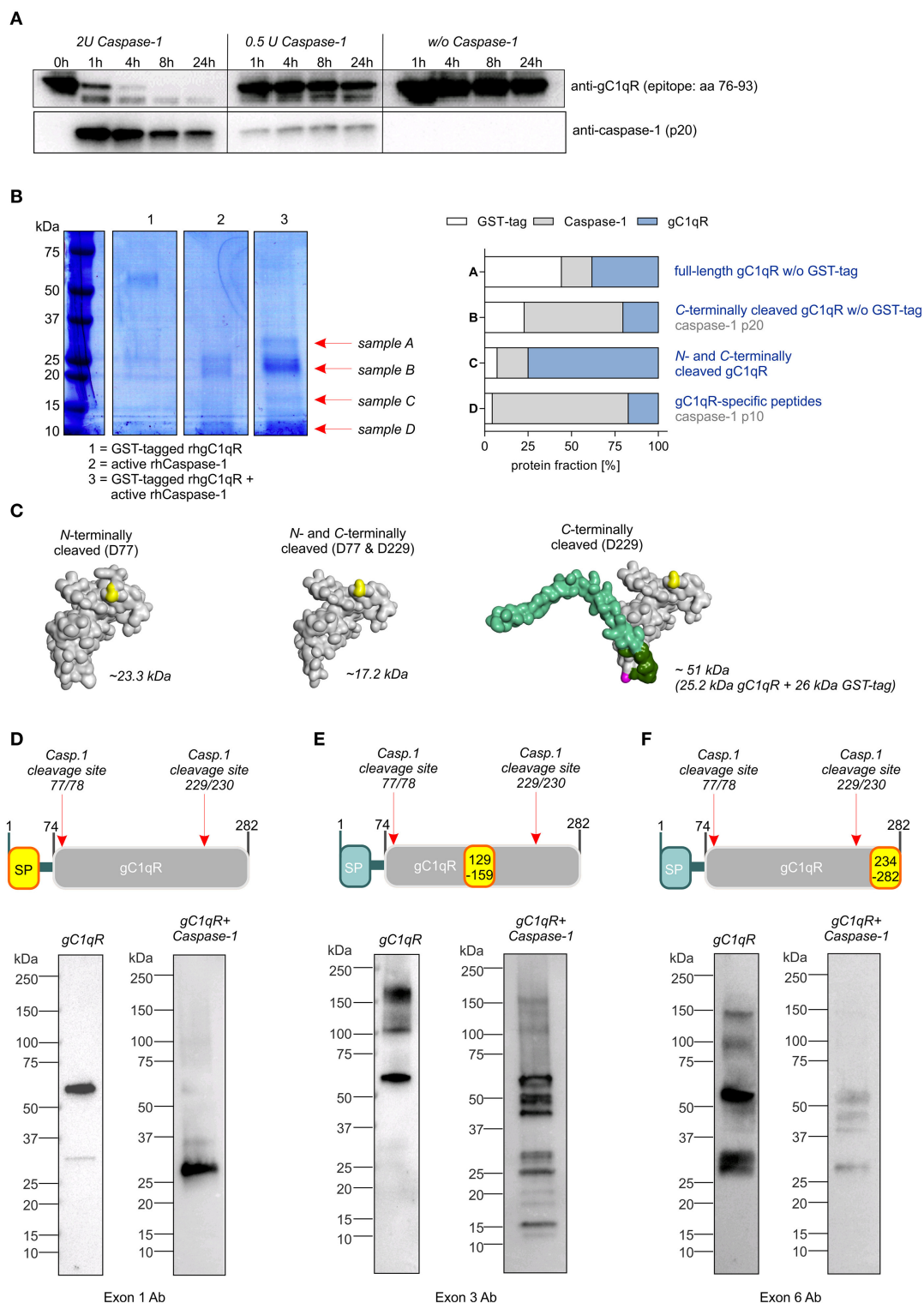


**FIGURE 2 |** Caspase-1 cleaves gC1qR at amino acid residues 77 and 229. **(A)** *In vitro* cleavage assay was performed by incubating human recombinant gC1qR (~32 kDa) in the presence or absence of human recombinant active caspase-1 (~10 and 20 kDa) at 37°C and indicated time periods. Afterwards, reduced protein samples were separated by SDS-PAGE. Western blot experiments were performed using an anti-gC1qR antibody (clone 60.11) or an anti-caspase-1 antibody. **(B)** *In vitro* cleavage assay was performed by incubating N-terminally GST-tagged human recombinant gC1qR (~58 kDa) in the presence or absence of human recombinant active caspase-1 (~10 and 20 kDa) at 37°C for 24 h. Afterwards, reduced protein samples were separated by SDS-PAGE and proteins were visualized by coomassie (Continued)

**FIGURE 2 |** blue staining. From lane 3 indicated protein bands were cut out of the gel. Protein spots were in-gel digested by trypsin and analyzed by nanoHPLC-ESI-MS/MS method. Fractions of peptides specific for cleaved or non-cleaved human gC1qR, for active caspase-1 or for GST in analyzed protein samples (A–D) are presented in the right panel. **(C)** Homology models of *N*-terminally cleaved, *N*- and *C*-terminally cleaved or *C*-terminally cleaved human gC1qR protein were generated using the PHYRE2 server. Full-length gC1qR has a calculated molar mass of 31.4 kDa, while *N*-terminally cleaved gC1qR has a calculated mass of 23.3 kDa. *C*-terminally cleaved gC1qR has a molar mass of 25.2 kDa (or in its GST-tagged form 51.2 kDa) and double-cleaved gC1qR has a molar mass of 17.2 kDa. **(D–F)** Western blot experiments using distinct gC1qR-directed primary antibodies with different binding epitopes located in exon 1, exon 3, or exon 6.

cell lines ( $1 \times 10^5$  cells per well in a 96-well-microtiter plate) using the Extracellular Oxygen Consumption Assay according to the manufacturer's instructions (Abcam).

## Determination of Lactate Production

The L-lactic acid assay was performed using supernatants (diluted 1:20 in  $1 \times$  PBS in the case of HAP1 cells or diluted 1:10 in  $1 \times$  PBS in the case of THP-1 cells) collected from indicated cell lines according to the manufacturer's instructions (Megazyme, Co Wicklow, Ireland). Data were normalized to the cell count in the case of THP-1 cells as well as to values received from respective neutral-red cytotoxicity assays in the case of HAP1 cells.

## Statistical Analysis

Data are displayed graphically and were statistically analyzed using GraphPad Prism 6.0. Curves were fitted using a non-linear regression model with a sigmoidal dose response (variable slope if applicable). Statistical significance was determined by the one-way or two-way ANOVA repeated measures test with the Bonferroni posttest. If not stated otherwise, the respective results were displayed as mean  $\pm$  SEM of at least three independent experiments. The *p*-values were calculated and null hypotheses were rejected when  $p \leq 0.05$ .

## RESULTS

### GC1qR Comprises Two Potential Caspase-1 Cleavage Sites

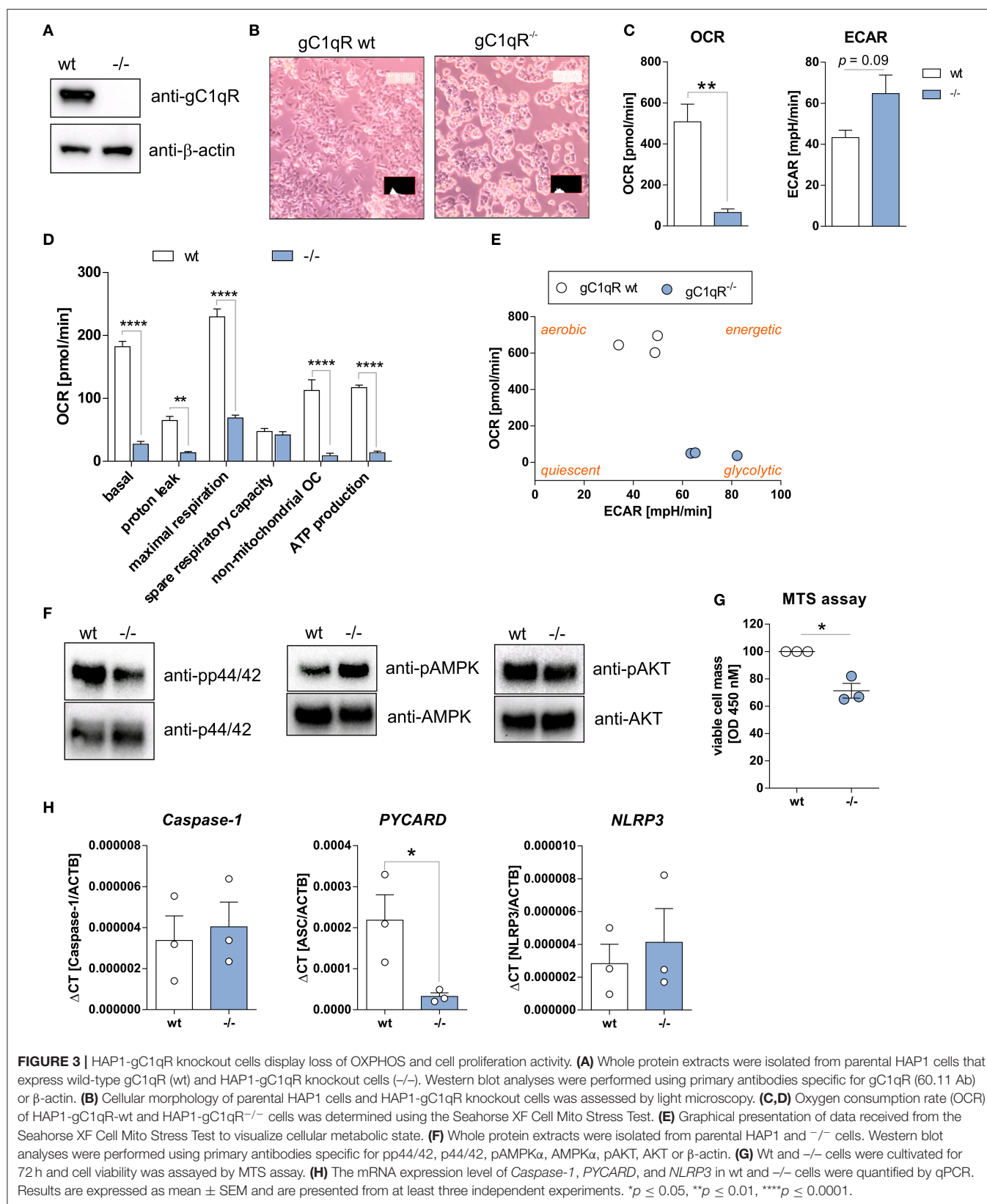
The full-length human gC1qR protein (282 amino acids; 31.4 kDa) includes an *N*-terminal signal leader sequence for mitochondrial import (**Figure 1A**) and forms trimeric complexes (**Figure 1B**) (11, 20, 25). Although the gC1qR activity on mitochondria is best studied, the protein is also found in the cytosol, the cell membrane and the extracellular compartment but its functional activity at these locations is unclear (24, 26). In the present study, distinct cellular localizations in the human colorectal carcinoma cell line HT29-MTX were visualized by immunohistochemistry (IHC) experiments utilizing gC1qR antibodies recognizing either the *N*-terminal residues 76–93 (clone 60.11) or the *C*-terminal residues 213–226 (clone EPR8871). As depicted in **Figure 1C**, the antibody clone 60.11 detected cytosolic and mitochondrial gC1qR, while the antibody clone EPR8871 mainly detected mitochondrial gC1qR in HT29-MTX cells (**Figure 1C**), indicating that gC1qR is present in distinct protein forms in these cells. Detection of mitochondrial gC1qR was further validated by co-localization experiments showing that fluorescence signals from the anti-gC1qR antibody

(clone EPR8871) overlaid with fluorescence signals from an anti-HSP60 antibody, a protein mainly localized to mitochondria (**Figure 1D**).

To unravel mechanisms regulating localization of gC1qR to distinct cellular compartments, we first hypothesized that the *N*-terminal mitochondrial leader (**Figure 1A**) may be removed to prevent mitochondrial localization and promote localization to other cellular compartments. Hence, we performed an *in silico* prediction analysis of potential protease cleavage sites in human gC1qR protein using the PeptideCutter server ([https://web.expasy.org/peptide\\_cutter/](https://web.expasy.org/peptide_cutter/)). Unexpectedly, caspase-1 was predicted to cleave at two distinct sites [amino acid (aa) residues 77 and 229] in the gC1qR protein sequence besides conventional protease cleavage sites. The first consensus sequence for caspase-1 cleavage was identified between aa 77–80 (DGDK) and the second one between aa 229–232 (DSL D) (**Figure 1E**). Notably, the first caspase-1 cleavage site in gC1qR is located directly after exon 1 (aa 1–74) that encodes the mitochondrial leader (**Figure 1F**). Next, we examined colonic expression of gC1qR, of the mitochondrial protein TOM22 as well as of caspase-1 by IHC experiments utilizing human normal biopsy samples. Indeed, high expression level of gC1qR, TOM22 as well as of caspase-1 were detected in colonic intestinal epithelial cells (IECs) as well as in lamina propria leukocytes, indicating a potential interaction between gC1qR and caspase-1 in these cells (**Figure 1G**, **Supplementary Figure 1**).

### Caspase-1 Cleaves gC1qR at Amino Acid Residues 77 and 229

To verify predicted caspase-1 cleavage sites in human gC1qR protein, an *in vitro* cleavage assay was performed using recombinant human gC1qR protein (rhgC1qR) in combination with different concentrations and incubation times of recombinant human active caspase-1. As presented in **Figure 2A**, Western blot experiments against gC1qR revealed gC1qR to be cleaved in a time- and concentration-dependent manner by active caspase-1 (**Figure 2A**). Additionally, an *in vitro* cleavage assay was performed utilizing *N*-terminally GST-tagged rhgC1qR that also included fractions of untagged full-length rhgC1qR (**Supplementary Figures 2A,B**). Samples derived from this *in vitro* cleavage assay that contained either rhgC1qR or active recombinant human caspase-1 alone as well as rhgC1qR combined with active rhcaspase-1 were separated by SDS-PAGE and stained with Coomassie blue. Afterwards, four specific protein bands (indicated as sample A–D) were isolated and peptide sequencing was performed that validated predicted caspase-1 cleavage sites in human gC1qR protein at amino acid residues 77 and 229 (**Figure 2B**, **Supplementary Figure 2C**). Cleavage of gC1qR by active caspase-1 was further verified



by Western blot experiments utilizing primary antibodies specific for exon 1 (aa1-74), exon 3 (aa129-159) and exon 6 (aa234-282). In the presence of active caspase-1, anti-exon1-Ab

only detected C-terminally cleaved gC1qR w/o GST-tag (~25.2 kDa; **Figures 2C,D**), anti-Exon3-Ab detected various cleavage products including N- and C-terminally cleaved fragments

(N-terminally cleaved gC1qR ~23.3 kDa; C-terminally cleaved gC1qR ~25.2 kDa or 51 kDa; N- and C-terminally cleaved gC1qR ~17.2 kDa; **Figures 2C,E**) and anti-Exon6-Ab displayed a mere loss of binding, potentially indicating caspase-1 to first cut at aa229 (**Figure 2F**).

## Deficiency of gC1qR Expression Induces Loss of OXPHOS Activity

To study functional consequences of the cleavage of gC1qR by active caspase-1 we utilized the human haploid HAP1 cell line system in which gC1qR was knocked-out by CRISPR/Cas9 technology. As demonstrated by Western blot experiments, we verified the loss of gC1qR protein in the HAP1-gC1qR knock-out cells (–/–) in comparison to the parental HAP1 cell line that expresses wild-type gC1qR (**Figure 3A**). Furthermore, HAP1-gC1qR<sup>–/–</sup> cells displayed a distinct cellular morphology (**Figure 3B**), a complete loss of basal and maximal OXPHOS activity as well as of non-mitochondrial respiration but similar spare respiratory capacity and enhanced extracellular acidification rate (ECAR) in comparison to the parental cell line as determined by Seahorse XF Cell Mito Stress test (**Figures 3C,D**).

Overall decrease in oxygen consumption together with significantly decreased ATP levels indicated low metabolic activity of HAP1-gC1qR<sup>–/–</sup> cells. Hence, while a highly balanced OXPHOS activity was detected in the parental HAP1 cell line, the HAP1-gC1qR<sup>–/–</sup> cells were found to preferentially perform anaerobic glycolysis (**Figure 3E**). These differences in cellular metabolism were reflected by decreased p44/42 and AKT but enhanced AMPK activation (**Figure 3F**), resulting in significantly diminished cell viability in HAP1-gC1qR<sup>–/–</sup> cells (**Figure 3G**). However, parental HAP1 cells as well as HAP1-gC1qR<sup>–/–</sup> cells were found to express extremely low mRNA level of the inflammasome components *Caspase-1*, *PYCARD*, or *NLRP3* (**Figure 3H**) that are fundamental for efficient caspase-1 activation.

## Cleavage of gC1qR by Active Caspase-1 Promotes Aerobic Glycolysis

To investigate functional consequences of gC1qR cleavage at aspartic acid residues 77 (D77) or 229 (D229) by active caspase-1, we established distinct HAP1-based cell lines stably expressing either a mock plasmid, wild-type gC1qR (wt), mutant gC1qR-D77E, mutant gC1qR-D229E, or mutant gC1qR-D77E/D229E. Of note, gC1qR protein was localized to the cellular organelle protein fraction, including the mitochondria protein fraction, but not to the cytosol or to the nucleus in all established HAP1-gC1qR mutant cell lines (**Supplementary Figures 3A–C**). As depicted in **Figure 4**, substitution of aspartic acid residues 77 and 229 by glutamic acid residues prevented active caspase-1 mediated cleavage of gC1qR in HAP1 cells in an *in vitro* cleavage assay utilizing recombinant human active caspase-1 in combination with native protein lysates isolated from indicated HAP1 cells (**Figure 4A**). Furthermore, generated HAP1 transfectants were additionally stably transfected with plasmids encoding human caspase-1 (C), human ASC (A)

and human NLRP3 (N), all three plasmids (NAC), or were left untransfected (w/o NAC) (**Figure 4B**). Constant overexpression of all three inflammasome components resulted in the release of gC1qR into the cell culture supernatant in gC1qR-wt cells that was significantly decreased in gC1qR-D77E and gC1qR-D77E/D229E but not in gC1qR-D229E mutant cell lines (**Figure 4C**). This suggests that cleavage of gC1qR by caspase-1 at amino acid residue D77 prevents mitochondria import and triggers release of gC1qR to the extracellular compartment.

Next, we studied extracellular oxygen consumption by these HAP1 transfectants. We detected highest oxygen consumption in HAP1-gC1qR-wt w/o NAC cells (RFU = 314,140 ± 85,329) in comparison to HAP1-gC1qR-D77E w/o NAC cells (RFU = 258,942 ± 84,888), to HAP1-gC1qR-D229E w/o NAC cells (RFU = 156,765 ± 55,276) or to HAP1-gC1qR-D77E/D229E w/o NAC cells (RFU = 135,065 ± 19,981), revealing aspartic acid residues 77 and 229 to be crucial for efficient mitochondrial respiratory capacity. Due to the findings that HAP1 cells endogenously express low level of the NLRP3 inflammasome components (**Figure 3H**), we cannot exclude low basal caspase-1 activity that may alter mitochondrial import of functional gC1qR protein. Hence, one may hypothesized that these stable transfectants have been adapted to metabolic changes, therefore potentially displaying lower OXPHOS activity, as mainly observed for the gC1qR-D229- and gC1qR-D77E/D229E-mutants, in comparison to gC1qR-wt cells. Of note, overexpression of all three inflammasome components NAC resulted in a significant loss of oxygen consumption in HAP1-gC1qR-wt or HAP1-gC1qR-D77E mutants (**Figures 4D,E**, **Supplementary Figures 4A,B**). Furthermore, lactate production was highest in gC1qR-wt-NAC cells, followed by gC1qR-D77E-NAC cells (fold change = –1.1) and was significantly reduced in gC1qR-D229-NAC (fold change = –1.5) and gC1qR-D77E/D229E-NAC cells (fold change = –1.3) compared to gC1qR-wt-NAC cells (**Figure 4F**, **Supplementary Figure 4C**). Hence, we hypothesized that gC1qR cleavage by active caspase-1 results in the loss of OXPHOS activity thereby inducing an imbalance between glycolysis and OXPHOS, potentially enabling increased activity of the pentose-phosphate pathway (1). These findings were further verified by the Seahorse XF Cell Mito Stress test that identified HAP1-gC1qR-wt NAC cells to perform aerobic glycolysis, while the double-mutant HAP1-gC1qR-D77E/D229E NAC cells displayed a loss of OXPHOS as well as of the ECAR, indicating that these cells were metabolically less active. Again, high anaerobic glycolysis activity was detected in mock-NAC transfected HAP1 cells (**Figure 4G**). Of note, higher lactate production in HAP1-gC1qR-wt NAC cells in comparison to double-mutant HAP1-gC1qR-D77E/D229E NAC cells (**Figure 4F**) was diminished by pharmacological inhibition of caspase-1 by about ~17% (**Figure 4H**). Additionally, overexpression of the inflammasome components NAC were identified to significantly boost cell proliferation in gC1qR-wt but not in gC1qR-D77E/D229E cells, pointing to a critical role of gC1qR cleavage by active caspase-1 in the induction of cell proliferation. On the other side, mock transfected HAP1 cells died in the presence of active caspase-1, further underlining the findings that gC1qR seems to



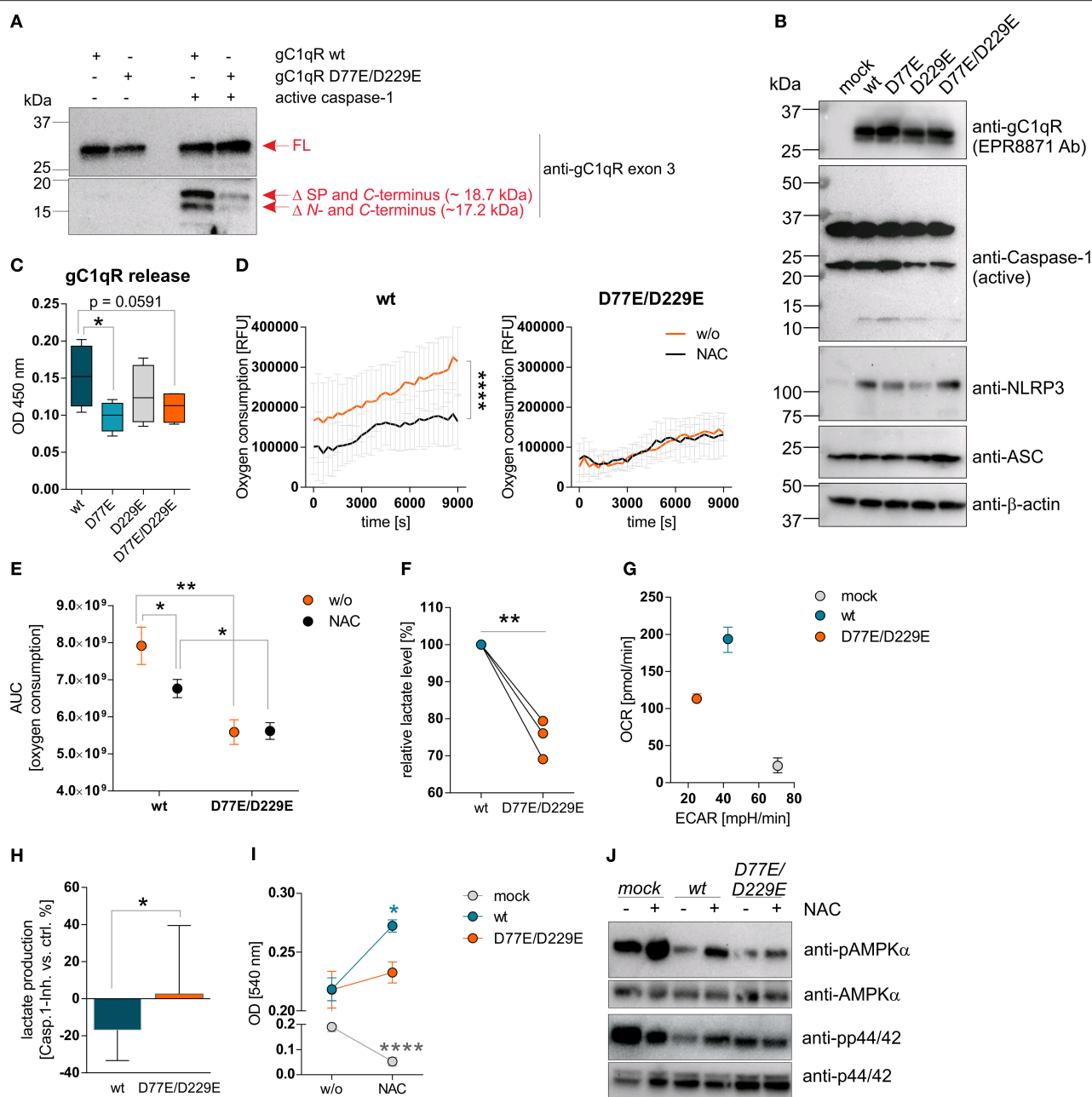


**FIGURE 4 |** Cleavage of gC1qR by active caspase-1 results in decreased OXPHOS activity and enhanced proliferation. **(A)** Site-directed mutagenesis of human *C1qbp* was performed using site-specific oligonucleotides to prevent caspase-1 cleavage of gC1qR. Aspartic acid (D) residues at aa77 and aa229 were substituted by glutamic acid (E) residues, resulting in the following gC1qR mutant D77E/D229E. HAP1-gC1qR<sup>-/-</sup> cells were stably transfected with generated plasmids encoding wt or mutated *C1qbp* variant D77E/D229E. *In vitro* cleavage assay was performed by incubating whole native protein lysates extracted from HAP1-gC1qR-wt or HAP1-gC1qR-D77E/D229E cells in the presence or absence of human recombinant active caspase-1 at 37°C for 4 h. Afterwards, reduced protein samples were separated by SDS-PAGE. Western blot experiments were performed using a primary antibody specific for exon 3 of human gC1qR. SP, signal peptide for mitochondrial import; Δ, cleavage; FL, full-length. **(B)** Plasmids encoding the human inflammasome components caspase-1 (C), NLRP3 (N) or ASC (A) were stably transfected into generated HAP1-gC1qR wt or mutant cell lines. Whole protein extracts were isolated and western blot analyses were performed using primary antibodies specific for gC1qR (clone EPR8871), caspase-1, NLRP3, ASC, or β-actin. **(C)** GC1qR release was measured by gC1qR-specific ELISA (exon 3 Ab) in supernatants from HAP1-gC1qR transfectants stably expressing all three inflammasome components NAC after 72 h of incubation. **(D)** Time-dependent measurement of oxygen consumption rate of indicated HAP1 transfectants in the presence or absence of over-expressed inflammasome components (NAC). **(E)** The area under the curve of data presented in **(D)** was calculated for each single experiment and each cell line. **(F)** Lactate production was measured in cell culture supernatants after 72 h of incubation of HAP1-gC1qR wt or D77E/D229E mutant cell lines stably transfected with NAC. Lactate levels generated by gC1qR-D77E/D229E mutant were related to lactate level produced by gC1qR-wt cells. **(G)** Oxygen consumption rate (OCR) as well as extracellular acidification rate (Continued)



**FIGURE 4 |** (ECAR) of HAP1-gC1qR-wt-NAC, HAP1-gC1qR-D77E/D229E-NAC as well as HAP1-mock-NAC cells were determined using the Seahorse XF Cell Mito Stress Test. Results from triplicates from one representative experiment are presented. **(H)** Lactate level were determined in cell culture supernatants collected from HAP1-gC1qR-wt-NAC or HAP1-gC1qR-D77E/D229E-NAC cells that have been incubated in the absence or presence of 100  $\mu$ g/ml caspase-1 inhibitor for 72 h. Results received from caspase-1 inhibitor treated cells were related to results from control treated cells for each cell line. **(I)** Cell viability of NAC expressing or NAC non-expressing HAP1-gC1qR-wt, HAP1-gC1qR-D77E/D229E, or HAP1-mock cells was determined after 72 h incubation by the neutral red assay. Optical density was measured at 540 nm. **(J)** Whole protein extracts were isolated from NAC expressing or NAC non-expressing HAP1-gC1qR-wt, HAP1-gC1qR-D77E/D229E, or HAP1-mock cells. Western blot analyses were performed using primary antibodies specific for pAMPK $\alpha$ , AMPK $\alpha$ , pp44/42, or p44/42. Results are expressed as mean  $\pm$  SEM and are presented from at least three independent experiments. \* $p \leq 0.05$ , \*\* $p \leq 0.01$ , \*\*\*\* $p \leq 0.0001$ .

be indispensable for maintaining OXPHOS activity for efficient energy supply under stress conditions (Figure 4I). These data were reflected by phosphorylation states of AMPK $\alpha$  and p44/42 (Figure 4J). Of note, if caspase-1 mediated cleavage of gC1qR cannot occur due to the knockout of respective cleavage site, cell proliferation should be reduced and the cells will shift to a more quiescent cell state, reflected by low OXPHOS and glycolysis activities. Indeed, this is what we observe for the single D229E-mutant and for the double-mutant D77E/D229E cells. Hence, we hypothesize that C-terminal cleavage of gC1qR by caspase-1 between aa 229 and 230 may be most critical for shifting the cells into a proliferative and metabolically active state.

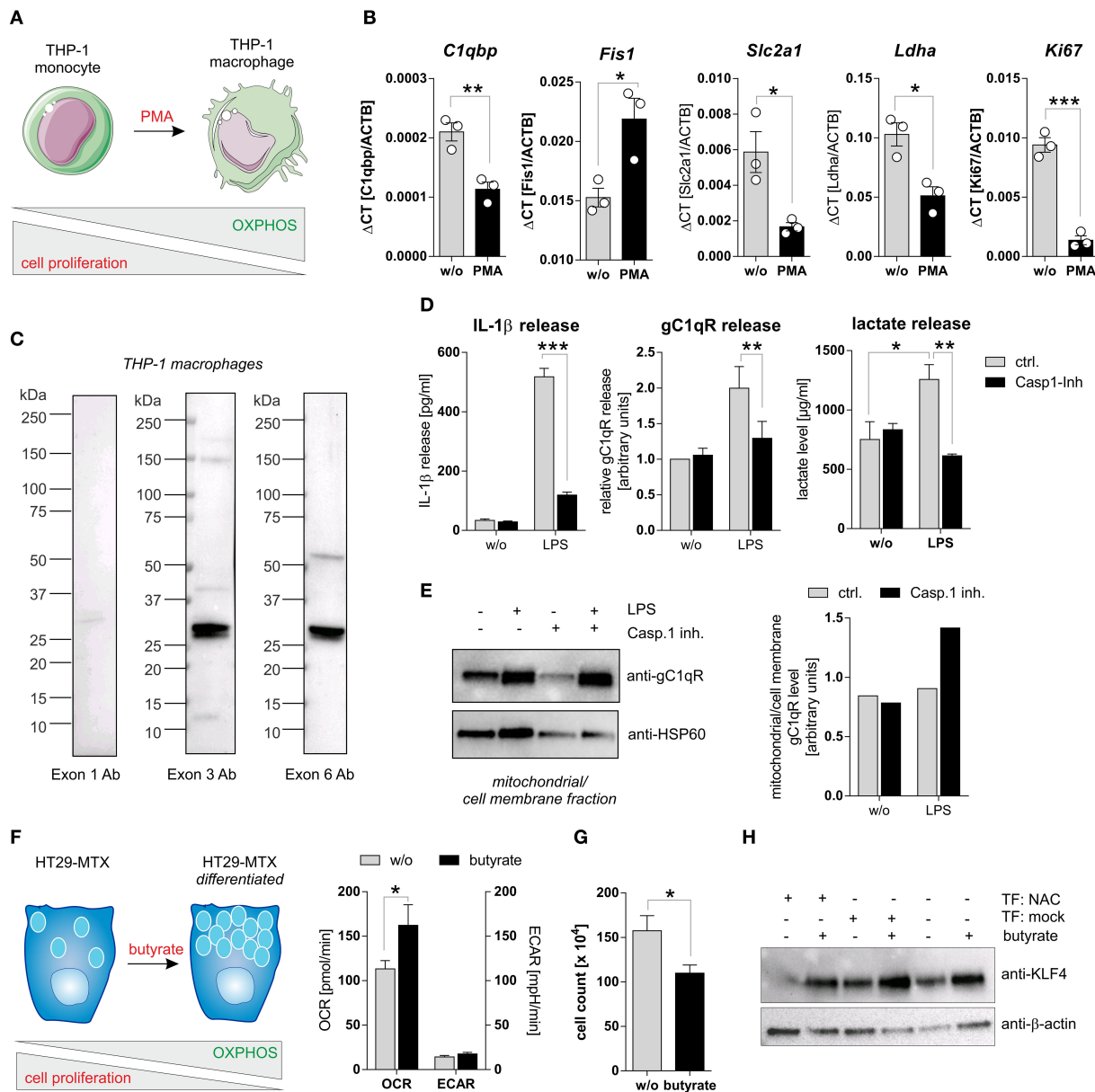
To study caspase-1 mediated cleavage of gC1qR in a second cell system that endogenously expresses wild-type gC1qR and all three inflammasome components (NAC) we utilized PMA-induced differentiated THP-1 macrophages (Figure 5A). Differentiated THP-1 macrophages in comparison to THP-1 monocytes were demonstrated to display significantly decreased mRNA expression levels of *C1qbp*, of the glucose transporter *Slc2a1*, of the lactate dehydrogenase A (*Ldha*) as well as of the proliferation marker *Ki67*. Of note, the mitochondria fission protein 1 (*Fis1*) was significantly upregulated in THP-1 macrophages (Figure 5B). Hence, PMA-induced differentiation of THP-1 monocytes into macrophages initiates metabolic reprogramming of THP-1 cells, characterized by diminished metabolic activity and reduced cell proliferation. Notably, low full-length gC1qR protein expression (anti-exon 1 Ab) but strong mature gC1qR protein expression (anti-exon 3 Ab and anti-exon 6 Ab) was detected in THP-1 macrophages by Western blot experiments (Figure 5C). These findings point to the loss of the mitochondria leader, located in exon 1, possibly due to mitochondria import but not to cleavage of gC1qR by active caspase-1 due to the presence of exon 6. Furthermore, LPS stimulation of THP-1 macrophages resulted in caspase-1 mediated induction of glycolysis, reflected by significantly increased secretion of IL-1 $\beta$  (Figure 5D, left panel), gC1qR (Figure 5D, middle panel) as well as of lactate (Figure 5D, right panel) that all were significantly blocked by pharmacological caspase-1 inhibition. The finding that active caspase-1 prevents gC1qR mitochondria localization being associated with enhanced glycolysis was supported by Western blot experiments demonstrating increased gC1qR localization to the mitochondrial/cell membrane protein fraction in LPS stimulated THP-1 macrophages in the presence of a caspase-1 inhibitor (Figure 5E).

## Activation of Caspase-1 Impairs Differentiation of Colorectal Carcinoma Cells

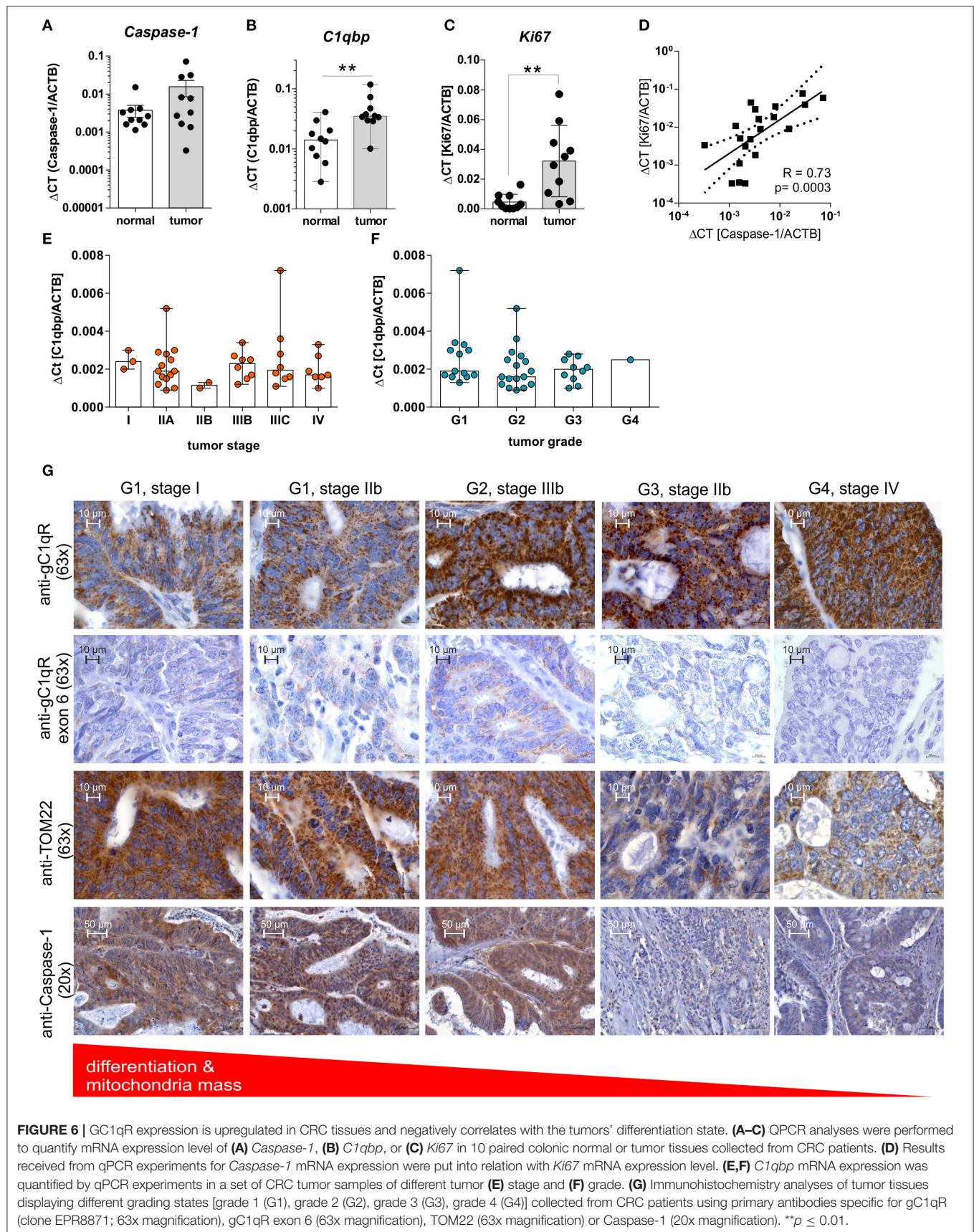
To strengthen the hypothesis that caspase-1 mediated cleavage of gC1qR protein prevents its localization to mitochondria and hence critically impacts cellular metabolism, we additionally utilized the colorectal carcinoma cell line HT29-MTX in functional analyses. Stimulation of HT29-MTX cells with the OXPHOS promoting short chain fatty acid (SCFA) butyrate has been previously demonstrated by our group and other groups to enhance differentiation of these cells into mucus-producing goblet cells [Figures 5F–H; unpublished data from our laboratory; (27, 28)]. Indeed, HT29-MTX cells stimulated with butyrate displayed a significantly enhanced OXPHOS activity, being reflected by an increased oxygen consumption rate, an unaltered extracellular acidification rate (Figure 5F) and significantly decreased cell proliferation (Figure 5G). To study the effect of caspase-1 activation on butyrate induced differentiation of HT29-MTX cells, cells were transiently transfected with plasmids encoding all three inflammasome components (NAC) before stimulation with butyrate. Of note, constant and butyrate-induced goblet cell differentiation was decreased in the presence of active NLRP3 inflammasome, indicated by reduced expression of the goblet cell marker KLF4 [(29); Figure 5H]. Together, these findings further highlight the critical role of active caspase-1 in mediating metabolic reprogramming of tumor cells, leading to the loss of tumor cells' differentiation state.

## Non-mitochondrial gC1qR Protein Expression Correlates With Grading of Colorectal Carcinoma Cells

Highly proliferating tumor cells are known to display an imbalance between glycolysis and OXPHOS activity, with a shift toward aerobic glycolysis, to ensure fast cell division (1). Based on our findings we demonstrated enhanced cell proliferation and a shift toward aerobic glycolysis after caspase-1 activation in gC1qR expressing cells (Figures 4, 5A–E) as well as decreased differentiation of colorectal carcinoma cells (Figures 5F–H), we hypothesized that grading and staging of colorectal carcinoma cells may be correlated with caspase-1 mediated cleavage of gC1qR. Therefore, we first analyzed mRNA expression of *Caspase-1*, *PYCARD*, and *NLRP3* in paired normal and tumor tissues collected from CRC patients (Table 1) by qPCR experiments. Unexpectedly, no differences between normal and



**FIGURE 5 |** Caspase-1 activation enhances glycolysis and impairs cell differentiation. **(A)** Schematic model of PMA induced differentiation of THP-1 monocytes into macrophages. This figure was generated using pictures provided by the Servier Medical Art homepage <https://smart.servier.com/>. Servier Medical Art by Servier is licensed under a Creative Commons Attribution 3.0 Unported License. **(B)** QPCR analyses were performed to quantify mRNA expression level of *C1qbp*, *Fis1*, *Slc2a1*, *Ldha*, and *Ki67*. **(C)** Western blot analysis of whole protein extracts from PMA-induced differentiated THP-1 macrophages using gC1qR-directed antibodies specific for epitopes located in exon 1, 3, or 6. **(D)** Secretion of IL-1β (left panel), gC1qR (middle panel) or lactate (right panel) was determined using specific ELISA using supernatants from untreated or LPS stimulated PMA-differentiated THP-1 cells in the presence or absence of caspase-1 inhibitor (10 μg/ml; Ac-YVAD-cmk from InvivoGen). **(E)** gC1qR protein expression in mitochondrial/ cell membrane protein fractions was quantified by Western blot experiments. PMA-differentiated THP-1 cells were stimulated with LPS in the presence or absence of caspase-1 inhibitor (10 μg/ml; Ac-YVAD-cmk) or were left untreated. Densitometry was performed using the software ImageJ (right panel). **(F)** Schematic model of butyrate induced goblet cell differentiation of HT29-MTX cells (left panel). Oxygen consumption rate (OCR) as well as extracellular acidification rate (ECAR) of HT29-MTX cells stimulated with 1.25 mM butyrate for 24 h or left untreated were determined using the Seahorse XF Cell Mito Stress Test (right panel). **(G)** HT29-MTX cells were incubated in the absence or presence of 1.25 mM butyrate for 72 h. After incubation, cells were counted. **(H)** HT29-MTX cells were transiently transfected for 96 h with plasmids encoding full-length human caspase-1 (C), human ASC (A), human NLRP3 (N) or with a mock plasmid in the presence or absence of 1.25 mM butyrate. Whole protein extracts were separated by SDS-PAGE under reducing conditions and Western blot experiments were performed using indicated primary antibodies. Results are presented as mean ± SEM from at least three independent experiments. \**p* ≤ 0.05, \*\**p* ≤ 0.01, \*\*\**p* ≤ 0.001.





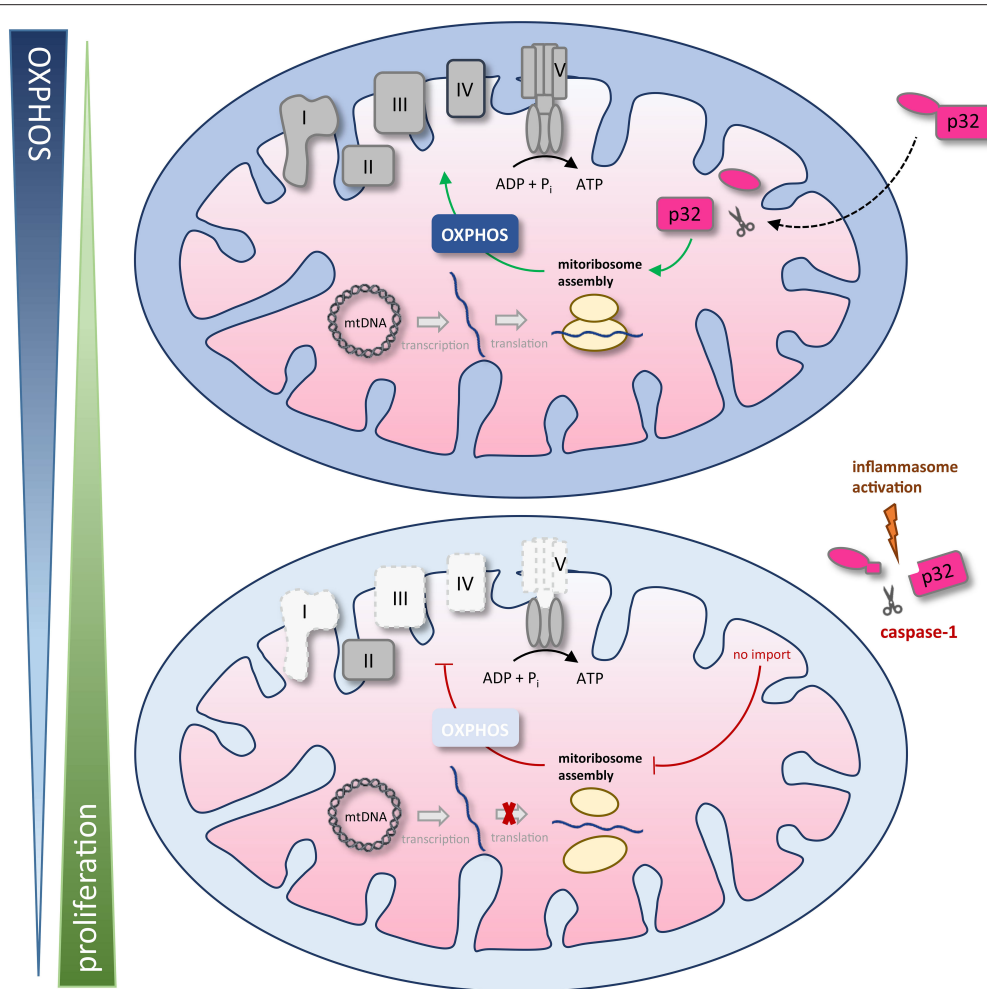


**FIGURE 7 |** Schematic model of caspase-1 reduction of mitochondrial OXPHOS activity via gC1qR cleavage. The gC1qR protein encompasses an N-terminal mitochondria leader that mediates its import into the mitochondrial matrix. Recently, mitochondria located gC1qR has been demonstrated to be part of the mitoribosome and hence critically regulate translation of mitochondria encodes proteins such as complexes I, III, IV, and V of the respiratory chain. In the present study, two specific caspase-1 cleavage sites at asparagine residues 77 and 229 were identified in the amino acid sequence of gC1qR, resulting in the cleavage of its N-terminal mitochondrial leader under conditions that activate the inflammasome. As a consequence of gC1qR cleavage by active caspase-1, cells display a loss of OXPHOS activity and a shift toward aerobic glycolysis, enabling increased cell proliferation. mtDNA, mitochondrial DNA; OXPHOS, oxidative phosphorylation; I – V, complexes I to V.

tumor tissues were detected for analyzed transcripts (**Figure 6A, Supplementary Figure 5A**). Notably, significant up-regulation of *C1qbp* and the cell proliferation marker *Ki67* mRNA expression level were determined in tumor tissues compared to paired normal tissues (**Figures 6B,C**), while no correlation was found in colonic tissues between *C1qbp* and *Ki67* mRNA level, between *NLRP3* and *Ki67* mRNA level as well as between *PYCARD* and *Ki67* mRNA level (**Supplementary Figures 5B–D**). However, *Ki67* mRNA expression highly correlated with *Caspase-1* mRNA expression in colonic tissues, supporting our hypothesis that caspase-1 may be critically involved in the regulation of cell proliferation (**Figure 6D**). Furthermore, we tested *C1qbp* mRNA expression in 42 distinct CRC tumor samples of different tumor grades and stages. Unexpectedly, *C1qbp* mRNA expression was not affected by tumor

stage or grade in analyzed CRC patient samples (**Table 1, Figures 6E,F**).

In the next set of experiments, protein expression level of gC1qR, TOM22, or full-length caspase-1 (**Supplementary Figure 5E**) were investigated by IHC experiments utilizing CRC tumor tissues of different grades (grade1-4) and stages (I-IV) (**Table 1**). Here, in contrast to healthy colonic tissue (**Figure 1G, Supplementary Figure 1**) protein expression of gC1qR negatively correlated with the mitochondrial marker TOM22 and was highest in grade 4 (G4) and lowest in grade 1 (G1) CRC (**Figure 6G**), although *C1qbp* mRNA expression did not correlate with tumor stage and grade (**Figures 6E,F**). Notably, staining of gC1qR-exon 6 and TOM22 protein correlated with inactive full-length caspase-1 staining (**Figure 6G, Supplementary Figure 5G**) in CRC samples

with lowest expression level detected in high-grade CRC samples. These findings in combination with results from IHC experiments demonstrating gC1qR-exon 6 being detectable in all paired normal colon tissues from analyzed CRC patient samples (**Supplementary Figure 5F**) point to a mere post-translational processing of gC1qR potentially by active caspase-1, leading to the loss of mitochondrial biogenesis and an increase of non-mitochondria localized gC1qR protein level (**Figure 6G**, **Supplementary Figure 5G**).

## DISCUSSION

Most tumor cells fine-tune their metabolism from balanced OXPHOS to fast but inefficient aerobic glycolysis, called the Warburg effect (3, 4). However, the question remains, whether regulation of the level of gC1qR localized in the mitochondria leads to a secondary regulation of energy provided by mitochondrial oxidative phosphorylation, thereby allowing the switch to aerobic glycolysis.

We found that the amino acid sequence of gC1qR presents two specific caspase-1 cleavage sites at aspartic acid residues 77 and 229, resulting in the cleavage of the N-terminal mitochondrial leader. Furthermore, we functionally verified these cleavage sites by an *in vitro* cleavage assay followed by mass spectrometry based peptide sequencing. As a consequence of gC1qR cleavage by active caspase-1, tumor cells displayed a loss of OXPHOS activity and thereby an imbalanced OXPHOS and glycolysis activity. Excessive aerobic glycolysis activity then enabled augmented cell proliferation that was prevented by mutated caspase-1 cleavage sites (**Figure 7**).

The salient finding of the present study is that cleavage of gC1qR by active caspase-1 promotes aerobic glycolysis in tumor cells and boosts carcinogenesis. These data are in line with data from recent studies that demonstrated the NLRP3 inflammasome to be critical for tissue homeostasis in the colonic intestine by driving intestinal epithelial cell (IEC) proliferation and tissue repair under DSS-induced colitis conditions (30–32). Of note, mice deficient in caspase-1 displayed a hypoproliferative intestinal epithelium, while mice deficient in the intrinsic caspase-1 inhibitor, caspase-12, displayed exacerbated colitis-associated colorectal carcinogenesis due to increased IEC proliferation (30). These data reveal the NLRP3 inflammasome to drive IEC proliferation that is beneficial in the resolution of colitis but is detrimental in CRC. However, contradicting studies regarding the role of NLRP3 inflammasome activation in CRC development have been published ranging from tumor promoting (33) to tumor-preventing modes of action (34). Due to findings that the NLRP3 inflammasome is continuously activated by nutrient excess (9, 10), we propose a novel mechanism explaining how the exposome –for example Western diet–triggers self-sustained cell proliferation via caspase-1 mediated cleavage of gC1qR, thereby boosting fast cell proliferation under chronic inflammation and potentially inflammation-driven carcinogenesis.

In summary, the present study presents for the first time, an explanation on how the metabolic activity of gC1qR is controlled by the NLRP3 inflammasome and how this interplay impacts cellular balance between OXPHOS activity and glycolysis. This study therefore opens new alleys for novel strategies in the therapy of inflammation-driven carcinogenesis, including nutritional interventions that prevent activation of the inflammasome.

## DATA AVAILABILITY STATEMENT

The original contributions presented in the study are publicly available. This data can be found here: FigShare ([https://figshare.com/articles/dataset/gC1qR\\_peptide\\_sequencing\\_data\\_pdf/12886709](https://figshare.com/articles/dataset/gC1qR_peptide_sequencing_data_pdf/12886709)).

## ETHICS STATEMENT

The studies involving human participants were reviewed and approved by ethical committee of the University of Lübeck. Written informed consent for participation was not required for this study in accordance with the national legislation and the institutional requirements.

## AUTHOR CONTRIBUTIONS

SD designed the concept of the present study and supervised it. CS and SP collected and provided human biopsy samples. BG provided primary antibodies specific for distinct epitopes of human gC1qR. AS, AR, MH, HS, FF, A-KB, and SD performed the experiments and acquired the data. AS, AR, and SD analyzed and interpreted the data. AS, AR, and SD drafted the article. CS, CK, BG, and SD critically revised the article for important intellectual content. All authors read and approved the final manuscript.

## FUNDING

This work was supported by the German Research Foundation (Research grants DE 1874/1-2 to SD and SI 1518/3-1 to CS).

## ACKNOWLEDGMENTS

The authors thank all the participating patients for agreeing to support this study and Prof. Jan Rupp for providing the Seahorse XF24 analyzer from Agilent.

## SUPPLEMENTARY MATERIAL

The Supplementary Material for this article can be found online at: <https://www.frontiersin.org/articles/10.3389/fonc.2020.575854/full#supplementary-material>



## REFERENCES

- Vander Heiden MG, Cantley LC, Thompson CB. Understanding the Warburg effect: the metabolic requirements of cell proliferation. *Science*. (2009) 324:1029–33. doi: 10.1126/science.1160809
- Ito K, Suda T. Metabolic requirements for the maintenance of self-renewing stem cells. *Nat Rev Mol Cell Biol*. (2014) 15:243–56. doi: 10.1038/nrm3772
- Warburg O, Wind F, Negelein E. The metabolism of tumors in the body. *J Gen Physiol*. (1927) 8:519–30. doi: 10.1085/jgp.8.6.519
- Warburg O. On the origin of cancer cells. *Science*. (1956) 123:309–14. doi: 10.1126/science.123.3191.309
- Hanahan D, Weinberg RA. Hallmarks of cancer: the next generation. *Cell*. (2011) 144:646–74. doi: 10.1016/j.cell.2011.02.013
- Koppenol WH, Bounds PL, Dang CV. Otto Warburg's contributions to current concepts of cancer metabolism. *Nat Rev Cancer*. (2011) 11:325–37. doi: 10.1038/nrc3038
- Camell C, Goldberg E, Dixit VD. Regulation of Nlrp3 inflammasome by dietary metabolites. *Semin Immunol*. (2015) 27:334–42. doi: 10.1016/j.smim.2015.10.004
- Wen H, Ting JP, O'Neill LA. A role for the NLRP3 inflammasome in metabolic diseases—did Warburg miss inflammation? *Nat Immunol*. (2012) 13:352–7. doi: 10.1038/ni.2228
- Ahechu P, Zozaya G, Marti P, Hernandez-Lizasoain JL, Baixauli J, Unamuno X, et al. NLRP3 inflammasome: a possible link between obesity-associated low-grade chronic inflammation and colorectal cancer development. *Front Immunol*. (2018) 9:2918. doi: 10.3389/fimmu.2018.02918
- Christ A, Gunther P, Lauterbach MAR, Duestel P, Biswas D, Pelka K, et al. Western diet triggers NLRP3-dependent innate immune reprogramming. *Cell*. (2018) 172:162–75 e114. doi: 10.1016/j.cell.2017.12.013
- Ghebrehewet B, Lim BL, Peerschke EI, Willis AC, Reid KB. Isolation, cDNA cloning, and overexpression of a 33-kD cell surface glycoprotein that binds to the globular “heads” of C1q. *J Exp Med*. (1994) 179:1809–21. doi: 10.1084/jem.179.6.1809
- Fogal V, Richardson AD, Karmali PP, Scheffler IE, Smith JW, Ruoslahti E. Mitochondrial p32 protein is a critical regulator of tumor metabolism via maintenance of oxidative phosphorylation. *Mol Cell Biol*. (2010) 30:1303–18. doi: 10.1128/MCB.01101-09
- Hu M, Crawford SA, Henstridge DC, Ng IH, Boey EJ, Xu Y, et al. p32 protein levels are integral to mitochondrial and endoplasmic reticulum morphology, cell metabolism and survival. *Biochem J*. (2013) 453:381–91. doi: 10.1042/BJ20121829
- Ghebrehewet B, Geisbrecht BV, Xu X, Savitt AG, Peerschke EIB. The C1q Receptors: Focus on gC1qR/p33. (C1qBP, p32, HABP-1)(1). *Semin Immunol*. (2019) 45:101338. doi: 10.1016/j.smim.2019.101338
- Kim KB, Yi JS, Nguyen N, Lee JH, Kwon YC, Ahn BY, et al. Cell-surface receptor for complement component C1q. (gC1qR) is a key regulator for lamellipodia formation and cancer metastasis. *J Biol Chem*. (2011) 286:23093–101. doi: 10.1074/jbc.M111.233304
- Dembitzer FR, Kinoshita Y, Burstein D, Phelps RG, Beasley MB, Garcia R, et al. gC1qR expression in normal and pathologic human tissues: differential expression in tissues of epithelial and mesenchymal origin. *J Histochem Cytochem*. (2012) 60:467–74. doi: 10.1369/0022155412440882
- Peerschke EI, Brandwijk RJ, Dembiter FR, Kinoshita Y, Ghebrehewet B. Soluble gC1qR in blood and body fluids: examination in a pancreatic cancer patient cohort. *Int J Cancer Res Mol Mech*. (2015) 1:10.16966/ijcrrm.110. doi: 10.16966/2381-3318.110
- Zhao J, Liu T, Yu G, Wang J. Overexpression of HABP1 correlated with clinicopathological characteristics and unfavorable prognosis in endometrial cancer. *Tumour Biol*. (2015) 36:1299–306. doi: 10.1007/s13277-014-2761-8
- Gao H, Yao Q, Lan X, Li S, Wu J, Zeng G, et al. Elevated HABP1 protein expression correlates with progression and poor survival in patients with gastric cancer. *Onco Targets Ther*. (2016) 9:6711–8. doi: 10.2147/OTT.S114756
- Li W, Zhang X, Wang W, Sun R, Liu B, Ma Y, et al. Quantitative proteomics analysis of mitochondrial proteins in lung adenocarcinomas and normal lung tissue using iTRAQ and tandem mass spectrometry. *Am J Transl Res*. (2017) 9:3918–34.
- Saha SK, Kim KE, Islam SMR, Cho SG, Gil M. Systematic multiomics analysis of alterations in C1QBP mRNA expression and relevance for clinical outcomes in cancers. *J Clin Med*. (2019) 8:513. doi: 10.3390/jcm8040513
- Muta T, Kang D, Kitajima S, Fujiwara T, Hamasaki N. p32 protein, a splicing factor 2-associated protein, is localized in mitochondrial matrix and is functionally important in maintaining oxidative phosphorylation. *J Biol Chem*. (1997) 272:24363–70. doi: 10.1074/jbc.272.39.24363
- Hillman GA, Henry MF. The yeast protein Mam33 functions in the assembly of the mitochondrial ribosome. *J Biol Chem*. (2019) 294:9813–29. doi: 10.1074/jbc.RA119.008476
- Saha P, Datta K. Multi-functional, multicompartmental hyaluronan-binding protein 1. (HABP1/p32/gC1qR): implication in cancer progression and metastasis. *Oncotarget*. (2018) 9:10784–807. doi: 10.18632/oncotarget.24082
- Jiang J, Zhang Y, Krainer AR, Xu RM. Crystal structure of human p32, a doughnut-shaped acidic mitochondrial matrix protein. *Proc Natl Acad Sci USA*. (1999) 96:3572–7. doi: 10.1073/pnas.96.7.3572
- Ghebrehewet B, Lim BL, Kumar R, Feng X, Peerschke EI. gC1q-R/p33, a member of a new class of multifunctional and multicompartmental cellular proteins, is involved in inflammation and infection. *Immunol Rev*. (2001) 180:65–77. doi: 10.1034/j.1600-065X.2001.1800106.x
- Gum JR, Kam WK, Byrd JC, Hicks JW, Sleisenger MH, Kim YS. Effects of sodium butyrate on human colonic adenocarcinoma cells. induction of placental-like alkaline phosphatase. *J Biol Chem*. (1987) 262:1092–7.
- Witt O, Schulze S, Kanbach K, Roth C, Pekrun A. Tumor cell differentiation by butyrate and environmental stress. *Cancer Lett*. (2001) 171:173–82. doi: 10.1016/S0304-3835(01)00628-0
- Katz JP, Perreault N, Goldstein BG, Lee CS, Labosky PA, Yang VW, et al. The zinc-finger transcription factor Klf4 is required for terminal differentiation of goblet cells in the colon. *Development*. (2002) 129:2619–28.
- Dupaul-Chicoine J, Yeretssian G, Doiron K, Bergstrom KS, McIntire CR, LeBlanc PM, et al. Control of intestinal homeostasis, colitis, and colitis-associated colorectal cancer by the inflammatory caspases. *Immunity*. (2010) 32:367–78. doi: 10.1016/j.immuni.2010.02.012
- Zaki MH, Boyd KL, Vogel P, Kastan MB, Lamkanfi M, Kanneganti TD. The NLRP3 inflammasome protects against loss of epithelial integrity and mortality during experimental colitis. *Immunity*. (2010) 32:379–91. doi: 10.1016/j.immuni.2010.03.003
- Hirota SA, Ng J, Lueng A, Khajah M, Parhar K, Li Y, et al. NLRP3 inflammasome plays a key role in the regulation of intestinal homeostasis. *Inflamm Bowel Dis*. (2011) 17:1359–72. doi: 10.1002/ibd.21478
- Du Q, Wang Q, Fan H, Wang J, Liu X, Wang H, et al. Dietary cholesterol promotes AOM-induced colorectal cancer through activating the NLRP3 inflammasome. *Biochem Pharmacol*. (2016) 105:42–54. doi: 10.1016/j.bcp.2016.02.017
- Dupaul-Chicoine J, Arabzadeh A, Dagenais M, Douglas T, Champagne C, Morizot A, et al. The Nlrp3 inflammasome suppresses colorectal cancer metastatic growth in the liver by promoting natural killer cell tumoricidal activity. *Immunity*. (2015) 43:751–63. doi: 10.1016/j.immuni.2015.08.013

**Conflict of Interest:** BG receives royalties from the sale of monoclonal antibodies 60.11 and 74.5.2

The remaining authors declare that the research was conducted in the absence of any commercial or financial relationships that could be construed as a potential conflict of interest.

Copyright © 2020 Sünderhauf, Raschdorf, Hicken, Schlichting, Fetzer, Brethack, Perner, Kemper, Ghebrehewet, Sina and Derer. This is an open-access article distributed under the terms of the Creative Commons Attribution License (CC BY). The use, distribution or reproduction in other forums is permitted, provided the original author(s) and the copyright owner(s) are credited and that the original publication in this journal is cited, in accordance with accepted academic practice. No use, distribution or reproduction is permitted which does not comply with these terms.



# Deregulation of Lipid Metabolism: The Critical Factors in Ovarian Cancer

Zhaodong Ji<sup>1,2†</sup>, Yan Shen<sup>3†</sup>, Xu Feng<sup>1,2†</sup>, Yue Kong<sup>1,2</sup>, Yang Shao<sup>1,2</sup>, Jiao Meng<sup>1,2</sup>, Xiaofei Zhang<sup>4\*</sup> and Gong Yang<sup>1,2,5\*</sup>

<sup>1</sup> Cancer Institute, Fudan University Shanghai Cancer Center, Shanghai, China, <sup>2</sup> Department of Oncology, Shanghai Medical College, Fudan University, Shanghai, China, <sup>3</sup> Department of Pharmacy, Nantong Health College of Jiangsu Province, Nantong, China, <sup>4</sup> Department of Gynecology, Shanghai First Maternity and Infant Hospital, Tongji University School of Medicine, Shanghai, China, <sup>5</sup> Central Laboratory, The Fifth People's Hospital of Shanghai Fudan University, Shanghai, China

## OPEN ACCESS

### Edited by:

Monica Montopoli,  
University of Padua, Italy

### Reviewed by:

Mariafrancesca Scalise,  
University of Calabria, Italy  
Amilcare Barca,  
University of Salento, Italy

### \*Correspondence:

Xiaofei Zhang  
sophia\_will@163.com  
Gong Yang  
yanggong@fudan.edu.cn

<sup>†</sup>These authors have contributed  
equally to this work

### Specialty section:

This article was submitted to  
Cancer Metabolism,  
a section of the journal  
Frontiers in Oncology

**Received:** 09 August 2020

**Accepted:** 28 September 2020

**Published:** 19 October 2020

### Citation:

Ji Z, Shen Y, Feng X, Kong Y, Shao Y,  
Meng J, Zhang X and Yang G (2020)  
Deregulation of Lipid Metabolism: The  
Critical Factors in Ovarian Cancer.  
Front. Oncol. 10:593017.  
doi: 10.3389/fonc.2020.593017

Ovarian cancer is one of the most malignant gynecological cancers around the world. In spite of multiple treatment options, the five-year survival rate is still very low. Several metabolism alterations are described as a hallmark in cancers, but alterations of lipid metabolism in ovarian cancer have been paid less attention. To explore new markers/targets for accurate diagnosis, prognosis, and therapeutic treatments based on metabolic enzyme inhibitors, here, we reviewed available literature and summarized several key metabolic enzymes in lipid metabolism of ovarian cancer. In this review, the rate limiting enzymes associated with fatty acid synthesis (FASN, ACC, ACLY, SCD), the lipid degradation related enzymes (MAGL, CPT, 5-LO, COX2), and the receptors related to lipid uptake (FABP4, CD36, LDLR), which promote the development of ovarian cancer, were analyzed and evaluated. We also focused on the review of application of current metabolic enzyme inhibitors for the treatment of ovarian cancer through which the potential therapeutic agents may be developed for ovarian cancer therapy.

**Keywords:** ovarian cancer, lipid metabolism, potential target, fatty acid synthesis, metabolic enzyme

## INTRODUCTION

Ovarian cancer, as one malignant gynecological cancer, is the eighth leading cause in cancer-related death around world (1). According to the latest statistical cohort from the Surveillance, Epidemiology and End Results (SEER) in 2017, there was an annual incidence of 11.6 cases/100,000 women per year, with an estimated 224,940 women living with this disease in the world (2). Because of hidden symptoms and lack of effective diagnostic methods, about 70% of patients are diagnosed in advanced stage when they receive treatment for the first time (3), which underlines the status of ovarian cancer as a serious public health concern for women. Based on the various research and epidemiological investigations, the pathogenesis of ovarian cancer mainly include viral infection, endocrine disorders, genetics, and environmental pollution (4–7). Ovarian cancer is characterized by widespread and rapid metastasis in the peritoneal cavity, which facilitates metastatic dissemination and poor disease progression. Malignant ascites constitute a unique tumor microenvironment providing a physical structure for the accumulation of many components. A large number of cancer-promoting components such as cytokines, proteins, and metabolites in

ascites are reported to promote cancer invasion and resistance to chemotherapy through surface-specific receptors on tumor cells (8–10). Meanwhile, the malignant progress of ovarian cancer also brings a series of changes in its own metabolism including glycometabolism, lipid metabolism, and amino acid metabolism, which may further strengthen the malignancy of the disease (11–14).

Lipids, as important nutrients for the body, are a class of water-insoluble substances including triacylglycerol, glycerol phosphates, sterols, and sphingolipids. In addition to providing a large amount of energy, lipids are also widely distributed in cellular organelles and used as biologically vital active molecules in a variety of signaling pathways to participate in process of inflammation, immunity, cell proliferation, and differentiation (15, 16). Four major routes demonstrate how lipids are routed and used in the cell: uptake, lipogenesis, storage, and degradation. The lipogenesis refers to the fatty acid synthesis pathway and the mevalonate pathway, the latter mainly leading to cholesterol and isoprenoid synthesis. The important raw material for the *de novo* synthesis of fatty acids is acetyl-CoA, which comes from two approaches: one is citric acid from the tricarboxylic acid cycle. Citrate is transported across the inner mitochondrial membrane by the transport protein CIC (citrate carrier) and then catalyzed by ATP-citrate lyase (ACLY) to produce acetyl-CoA and oxaloacetate. The other is that cells uptake acetic acid directly from the outside and catalyze the production of acetyl CoA through acetyl CoA synthetase (17, 18). Deregulation of lipid metabolism including the increasing *de novo* synthesis and degradation of fatty acid often occurs in a variety of cancer diseases, which could provide cancer cell a strong support for proliferation, invasion and metastasis. A large number of studies have found that in multiple cancers, the expression and activity of various enzymes involved in the synthesis and catabolic pathways of fatty acids (phospholipids and cholesterol) are significantly up-regulated. In addition, other lipid-metabolizing enzymes such as lipoxygenase (LOX) and cyclooxygenase (COX) gradually become cancer research hotspots in recent years. Oncogenes highly expressed in cancer cells can activate the PI3K/AKT/mTOR signaling pathway to allow the related proteins such as ErbB2 and HIF-1 to promote the expression of lipid synthetases (19–21).

Lipid droplets (LDs) occurring in specialized cytoplasm are considered to be special lipid storage organelles because they can synthesize and store triglycerides. LDs are composed of a core of neutral lipids, surrounded by phospholipids and cholesterol, and specific proteins are embedded or associated with their surroundings. More and more evidence shows that LDs are not only passive reservoirs of lipids, but are actually dynamic organelles that play a central role in lipid and energy metabolism (22).

Since fatty acids are essential for cancer malignant progression, the availability of rate limiting enzymes in lipid metabolism could be therapeutic targets. Lipid metabolism could be regulated by suppressing fatty acid synthesis, accelerating fatty acid degradation *via* oxidation, diverting fatty acid to storage, retarding fatty acid release from storage, and blocking fatty acids intake (23). Limiting lipid metabolism through these mechanisms could be

accomplished in alone or in a combinatorial manner, which could pave the way for the therapy of ovarian cancer (Table 1). This article summarizes the effects of lipid metabolism disorders in ovarian cancer from two aspects: exogenous lipid metabolism and endogenous lipid metabolism.

## ENDOGENOUS LIPID METABOLISM

In lipid metabolism of ovarian cancer cells, many metabolic enzymes are abnormally expressed, which can cause lipid metabolism disorders by participating in processes that affect lipid synthesis or degradation, thereby to provide raw materials and energy for cancer development. At present, the combination of inhibitors of rate limiting metabolic enzymes with first-line chemotherapy agents has become a new strategy for treatment of ovarian cancer.

### Rate Limiting Enzymes in Fatty Acid Synthesis

#### ATP-Citrate Lyase (ACLY)

ATP-citrate lyase (ACLY), the upstream enzyme in fatty acid biosynthesis, functions physiologically to catalyze the six-carbon citric acid from the tricarboxylic acid cycle, either from glucose by glycolysis or glutamine, to oxaloacetate and acetyl on the cytosolic side, which provides raw materials for the synthesis of fat acid and cholesterol (Figure 1). Therefore, it is considered as a bridge connecting glycometabolism and lipid metabolism (40). The AKT-mediated phosphorylation of ACLY could promote histone acetylation in cancer cells and immune cells to response to the oncogenic and cytokine-induced signaling, while ACLY is transcriptionally regulated by SREBP1 (sterol regulatory element binding transcription protein-1) (41, 42). In addition, other substances such as insulin, glucagon, and TGF- $\beta$  can promote the phosphorylation of ACLY.

Wang et al. found that ACLY expression was higher in malignant tissues than that in normal ovarian tissues. Immunohistochemical analysis showed that the increased expression level of phosphorylated ACLY in ovarian cancer tissues was related to cancer grade, FIGO stage, and poor prognosis. Mechanismly, by knockdown of ACLY expression could inhibit the proliferation of ovarian cancer A2780 cells and cause G1 phase arrest (43, 44), suggesting that ACLY promoted cancer cell proliferation through the regulation of cell cycle.

The ubiquitin-proteasome controls protein degradation and regulatory functions. Ubiquitin-specific proteases (USPs) are the largest family of deubiquitin, which can catalyze the removal of ubiquitin from different target proteins to regulate cell function. Studies have reported that ubiquitin-specific peptidase 13 (USP13) was the main regulator of ovarian cancer metabolism (45). ACLY can be one of deubiquitinase target proteins of USP13, removing K48-related ubiquitination on ACLY to improve the stability of ACLY. The *in vitro* experiments found that the inhibition of USP13 expression could significantly inhibit the progression of ovarian cancers and enhance the sensitivity of cancer cells to treatment with PI3K/AKT inhibitors. Therefore, the researchers proposed that ACLY may

**TABLE 1 |** Chemical Inhibitors targeting enzymes of lipid metabolism in ovarian cancer.

Enzyme	Chemical inhibitor	Notes	Pathway	Models(animal/cell line)	Reference
FASN	Orlistat	1. Reduce proliferation and promotes apoptosis 2. Platinum resensitization	---	1. Mouse 2. A2780	(24)
	Compound 34	Inhibits proliferation	---	A2780	(25)
	Cerulenin or C75	1. Induce apoptosis 2. Platinum resensitization	Receptor/PI3K/mTORC1	SKOV3, OVCAR3, A2780, HOC-7	(26) (27)
	(A cerulenin derived)				
	TVB-3664	1. Reduce tubulin palmitoylation 2. Inhibit proliferation	1. PI3K/AKT/mTOR 2. $\beta$ -catenin signal	OVCAR5/8	(28)
	C93	Induce apoptosis	NAC1-FASN	SKOV3, A2780, OVCAR3	(29)
SCD1	TVB-3166	Induce apoptosis and anchorage-independent cell growth	PI3K/AKT/mTOR	OVCAR5/8	(28)
	A939572	Cause cell death	---	1. SKOV3 2. Mouse	(30)
	CAY10566	Reduce the lipid unsaturation levels in OC spheroids	STAT/NF $\kappa$ B/SCD1	OVCAR5, COV362	(31)
	MF-438	Induce apoptosis and ferroptosis	---	SKOV3	(30)
ACC1	CAY10566	Induce apoptosis and ferroptosis	---	SKOV3	(30)
	TOFA	1. Suppress the proliferation and induce apoptosis. 2. Inhibit growth	1. Down-regulated the expression of cyclin D1, CDK4 and Bcl-2 2. Caspase-3 was cleaved and activated.	1. COC1 2. Mouse	(32)
MAGL	JZL184	Decrease cancer cell migration	---	SKOV3, OVCAR3	(33)
CPT	Etomoxir	Reduce tumor growth rate, ascites production	---	Mouse	(34)
5-LO	Zileuton	Reduce the MMP-7 expression and the number of macrophages infiltrating	P38 pathway	Mouse	(35)
COX2	Celecoxib	1. Reduce invasion 2. Inhibit proliferation 3. Induce cell cycle arrest in G0/G1 and apoptosis 4. Inhibit tumor growth	COX2/Snail/E-cadherin	1. SKOV3, ES-2 Hey, IGROV1 2. Mouse	(36) (37)
	Berberine	Inhibit the chemotherapy-induced repopulation of ovarian cancer cells	Caspase3/iPLA2/AA/COX2/PGE2	SKOV3	(38)
FABP4	BMS309403	1. Reduce tumor burden 2. Increase the sensitivity of carboplatin	---	1. Mouse 2. HeyA8, SKOV3	(39)

play an important role in the USP13-mediated deubiquitination to promote cancer development (45, 46).

## Acetyl-CoA Carboxylase (ACC)

The first committed step of fatty acid synthesis is mediated by acetyl- ACC, which in mammals is encoded by two subtype enzymes ACC1 (Acetyl-CoA Carboxylase Alpha) and ACC2 (Acetyl-CoA Carboxylase Beta) (47). ACC1 is generally expressed in lipogenic tissues, and the ACC1-generated malonyl-CoA is utilized for the synthesis of fatty acids in cytosol. In contrast, ACC2 is highly expressed in heart and muscle and to a lesser expressed in liver. Unlike ACC1 promoting fatty acid synthesis, ACC2 is anchored at outer membrane of mitochondria in subcellular where localized malonyl-CoA production blocks carnitine palmitoyltransferase-1 (CPT1) function to prevent fatty acids from entering the mitochondria to undergo fatty acid oxidation (48). ACC is a biotin-dependent multi-domain enzyme, which has biotin carboxylase (BC) and carboxyl transferase (CT) activities in most eukaryotes. In regard to these two enzyme activities, BC catalyzes the ATP-dependent carboxylation of biotin with bicarbonate as a CO<sub>2</sub> donor, and CT promotes the transfer of carboxyl groups from biotin to acetyl CoA. In recent years, ACC

activity is tightly regulated by reverse phosphorylation and gene expression. The phosphorylation of ACC by adenosine monophosphate-activated protein kinase (AMPK) has been identified (49). Notably, ACC1 has been shown to be elevated in a number of cancers, including liver cancer, lung cancer, breast cancer, and pancreatic cancer. Inhibitors targeting ACC1 were shown to reduce cell proliferation through inhibiting fatty acid synthesis (50, 51).

TOFA, an allosteric inhibitor of ACC1, was reported to suppress the proliferation of ovarian cancer *via* arresting the cells in G0/G1 cell cycle phase and inducing apoptosis (32). Meanwhile, TOFA could inhibit growth of ovarian cancer xenograft in mice. One study based on a randomized multicentre phase 3 trial (MITO2) found that carboplatin/PLD might be more effective than carboplatin/paclitaxel to ovarian cancer patients in the presence of pACC overexpression, suggesting that ACC might be a new biomarker for personalizing the choice of chemotherapy regimen in ovarian cancer (52).

## Fatty Acid Synthase (FASN)

FASN is a key enzyme for endogenous fatty acid synthesis. This cytosolic enzyme catalyzes the synthesis of 16-carbon palmitic acid by malonyl-CoA and acetyl-CoA under the action of



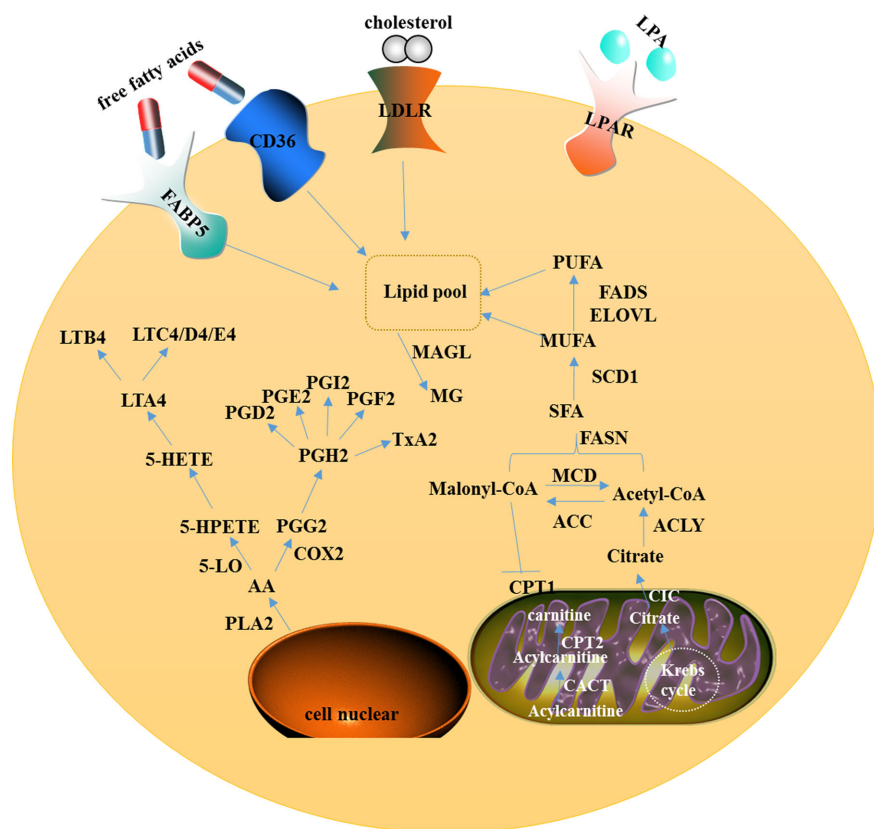


**FIGURE 1** | A model showing intracellular lipid metabolism and AA metabolism in ovarian cancer. In the cytoplasm of the cell, fatty acid metabolism includes uptake, *de novo* lipogenesis, and degradation. AA can be metabolized via two major pathways, namely the lipoxygenase pathway and the cyclooxygenase pathway. In mitochondria, CIC promotes the efflux of citrate from the mitochondria to the cytosol and CACT catalyzes acylcarnitine to translocate through the inner mitochondrial membrane.

reducing coenzyme II (53) (**Figure 1**). In normal condition, the physiological function of FASN is to convert excess carbohydrates into fatty acid, which will be further esterified into triacylglycerols, and finally stored or supplied for energy through  $\beta$  oxidation. As a downstream effector, FASN could be activated by the PI3K/AKT/mTOR signaling pathway and the transcription factors such as SREBP-1, ZBTB7A, and p53 (54, 55). FASN is highly expressed in ovarian cancer tissues and is associated with poor prognosis and survival rate (56). Because the majority of cancers rely on the FASN-mediated *de novo* fatty acid synthesis pathway, FASN could be an attractive therapeutic target, and inhibition of FASN has shown antitumor effects in ovarian cancer (25, 57).

In tumor cell lines, FASN overexpression was found to cause chemotherapy resistance induced by culture in drug-containing media. This means that FASN may be involved in chemoresistance of cancer cells. O Bauerschlag et al. treated HEY cells with cerulenin, an inhibitor of FASN, and found that cerulenin markedly decreased FASN expression and cell viability, and induced apoptosis. Unlike combined administrations, sequential cerulenin, and cisplatin treatment profoundly

reduced cisplatin's half maximal inhibitory concentration in a cisplatin-resistant cell line, suggesting that cerulenin had reinduce platinum sensitivity (26). Papaevangelou et al. conducted a metabolite analysis and histopathology of ovarian cancer xenograft mice treated with the combination of the anti-obesity drugs orlistat and cisplatin, and found that orlistat reduced cancers by inhibiting FASN. At the same time, cisplatin reduced the  $\beta$ -oxidation of fatty acids, and combined therapy delayed the cisplatin-resistant ovarian cancer cell growth and induced apoptosis. The combination therapy of the two drugs also reduced glycometabolism, biosynthesis of nucleotides and glutathione, and  $\beta$ -oxidation of fatty acids (24).

Overexpression of FASN was also reported to be associated with tumor cell proliferation, metastasis, poor prognosis, and high risk of recurrence in breast cancer, prostate cancer and gastric cancer (58–60). The FASN inhibitor TVB-3166 can destroy the lipid structure on membrane of cancer cell, inhibit lipid biosynthesis, and promote cancer cell apoptosis through the PI3K-AKT-mTOR and  $\beta$ -catenin signaling pathways in ovarian cancer. At the same time, this inhibitor can also block the expression of the oncogene c-Myc (28). Some studies have

pointed out that FASN inhibitors could also induce the cell cycle arrest at S/G2/M and apoptosis of cancer cells, but only caused cell cycle deceleration without apoptosis for normal cells (61). Therefore, FASN is proposed as a metabolic marker for ovarian cancer proliferation.

Recently, some scholars have found that the abnormal activation of FASN can blunt the anti-tumor immunity of host (62). The clinical data showed that, in the advanced stage of ovarian cancer, the abnormally increased expression of FASN was positively correlated with the state of immunosuppression. The immunosuppression was manifested in the lower number and dysfunction of infiltrating T cells. Mechanistic studies have found that FASN activation in ovarian cancer cells can induce the resulting lipid accumulation at high concentrations in the tumor microenvironment. High expression of FASN in ovarian cancer cells also caused defects in the ability of dendritic cells to present antigens and prime T cells in ascites. To further explore FASN inhibition effect in anti-tumor immune response *in vivo*, the use of FASN inhibitors could partially restore the immunostimulating activity of Tumor-Infiltrating DCs (TIDCs) and evoke protective anti-tumor immune responses.

### Stearoyl COA Desaturase (SCD)

Stearoyl COA desaturase (SCD) is an endoplasmic reticulum enzyme that promotes a balance of saturated fatty acids (SFA) and mono-unsaturated fatty acids (MUFA) in cell lipids. Specifically speaking, SCD catalyzes the synthesis of MUFA SFA, principally stearic acid (18:0) and palmitic acid (16:0), to their D9-monounsaturated counterparts, oleic acid (18:1) and palmitoleic acid (16:1; ref. 8) (63). These MUFAs are major components of cell membrane phospholipids and cholesterol esters. Two SCD isoforms SCD1 and SCD5 have been identified in human, whereas other four desaturases (SCD1-SCD4) share the same enzymatic function exist in mouse (64). Among of five isoforms, SCD1 is expressed ubiquitously among tissue with a 33-amino acid sequence at the N terminus that leads to the rapid degradation of this enzyme *via* an ubiquitin-dependent proteasome (65). It has been identified that the promoter of SCD1 contains several binding sites with the peroxisome proliferator-activated receptor (PPAR), NF-1, AP-2, and SREBP. The enzyme activity of SCD1 is either promoted by insulin, glucose, and fructose or inhibited by unsaturated fatty acids, ethanol, TNF $\alpha$ , IL-11, thyroid hormones, and some steroid hormones (66). Previous studies have shown that SCD1 was overexpressed in many malignant cancers to regulate cell proliferation, cell cycle, apoptosis, metastasis, and to modulate lipid metabolism through reducing fatty acid oxidation to foster lipogenesis (67).

Roongta et al. found that the expression of SCD1 was up-regulated in ovarian cancer tissues and stem cells (68). Inhibition of SCD1 expression can induce cancer cell death. Conversely, overexpression of SCD1 or exogenous addition of palmitoleic acid can protect cells from death. Ferroptosis is an iron-dependent oxidative damage causing cell death that greatly inhibits the growth of ovarian cancer cells (69). Overexpression of SCD1 protects cells from ferroptosis through the increase of

monounsaturated fatty acids, whereas inhibition of SCD1 significantly enhances the anticancer effect of ferroptosis-inducers on ovarian cancer cell lines and xenograft mouse tumors (30).

Scattering microscopy was used to observe an increase in unsaturated fatty acid level in ovarian cancer stem cells, and a significant increase in the mRNA level of SCD1 was detected by qRT-PCR. However, when SCD1 inhibitors were used to treat the primary ovarian cancer stem cells, the stemness markers were down-regulated. In addition, the treatment of ovarian cancer stem cells with SCD1 inhibitors retarded the tumor growth of cells when injected into athymic mice. Further study demonstrated that NF- $\kappa$ B may directly regulate the transcription of SCD1 (31).

### Limiting Enzymes in Fatty Acid Degradation

Cancer cells usually stimulate the degradation of fatty acids to provide energy for proliferation, and this degradation process can be achieved through mitochondrial  $\beta$ -oxidation. Within mitochondria, fatty acids continuously undergo cyclical series of reactions to produce acetyl-CoAs that were fed into the Krebs cycle and supply energy to tissues in demand when glycogen store is out of service (70).

### Monoacylglycerol Lipase (MAGL)

Monoacylglycerol lipase, a member of the serine hydrolase superfamily, mainly functions as a key enzyme to catalyze the decomposition of monoacylglycerol into free fatty acids and glycerol (Figure 1). Furthermore, MAGL controls several physiological processes including pain and nociception through hydrolysis of the endocannabinoid 2-arachidonoylglycerol (2-AG). MAGL was highly expressed in ovarian and breast cancer tissues, and identified to contribute to tumorigenesis and metastasis through up-regulation of free fatty acids (33). MAGL also promotes epithelial-mesenchymal transition (EMT) and may serve as a gene expression signature for cancer stem cells (71, 72).

Other studies also found that the multiple inhibitors of MAGL could inhibit the proliferation of ovarian cancer cells (73, 74). The knockdown of MAGL expression inhibited the proliferation, migration and invasion of ovarian cancer cells (33).

### Carnitine Palmitoyltransferase (CPT)

When cancer cells lack glucose, energy is generated through the increased  $\beta$ -oxidation. CPT is a key enzyme that catalyzes the conversion of long-chain fatty acids into acylcarnitine, which can be inhibited by malonyl-CoA (Figure 1). Two subtypes of CPT (CPT1 and CPT2) differently catalyze the decomposition of long-chain fatty acids and  $\beta$ -oxidation. CPT1 resides at the outer membrane of mitochondria and transports long-chain fatty acids into mitochondria for  $\beta$ -oxidation. CPT2 is located on the mitochondrial inner membrane and catalyzes the production of acyl-CoA from acyl-carnitine-derived acyl groups and free coenzymes to shuttle across the inner mitochondrial membrane CACT (carnitine acylcarnitine translocase), which helps acylcarnitine to translocate through

the inner mitochondrial membrane and to be converted back to acyl-CoA for  $\beta$ -oxidation and energy substrate generation. Increasing studies have reported that  $\beta$ -oxidation abnormality can be induced through the high expression of CPT1 to promote cancer progression (75).

Three different CPT1 isozymes are identified. CPT1A is widely distributed in multiple tissues with stronger enzyme activity. CPT1B is mainly expressed in skeletal muscle cells and cardiac muscle cells, while CPT1C is mainly found in testis and central nervous tissues. With the improvements of metabolic studies, it has revealed that CPT1 may promote cancer cell proliferation and survival (76).

Shao et al. found that CPT1A was highly expressed in ovarian cancer cell lines and primary ovarian serous carcinomas. Analysis of database revealed that overexpression of CPT1A was associated with poor survival in ovarian cancer patients. Knockdown of CPT1A expression reduced the cellular level of ATP and induced the cell cycle arrest at G0/G1 in ovarian cancer cells, indicating that the CPT1A-mediated  $\beta$ -oxidation controlled the proliferation through regulating cell cycle process. Knockdown of CPT1A stimulated the phosphorylation of the transcription factor FOXO through the AMPK/p38/JNK signaling pathway and up-regulated P21 to arrest cell cycle (77).

Roy et al. found that overexpression of CPT1A can increase the  $\beta$ -oxidation of fatty acids and ATP levels to promote cancer cell proliferation. In contrast, Etomoxir, a specific inhibitor of CPT1A, can inhibit the proliferation of ovarian cancer cells (34).

### 5-Lipoxygenase (5-LO)

Arachidonic acid (AA) is located in the phospholipid bilayer of the cell membrane and the precursor of main signal molecules. The metabolism of AA is closely associated with the development of cancer cells (78, 79). As a member of the arachidonic acid lipoxygenase family, 5-LO is composed of 674 amino acids and a monomeric enzyme containing iron ions. 5-LO can be transcriptionally regulated by *t* Egr, Sp1, nuclear factor- $\kappa$ B (NF- $\kappa$ B), and GATA (80).

5-LO is activated by 5-LO activating protein (ALOXAP) to catalyze AA which is released from the phospholipid bilayer by phospholipase A2. AA is transformed to 5-hydroxyeicosatetraenoic acid which can be metabolized by glutathione peroxidase into 5-hydroxyeicosatetraenoic acid (5-HETE), which is further converted into either 5-oxo-eicosatetraenoic acid or LTA4. LTA4 is further converted into LTB4, LTC4, LTD4, or LTE4 depending on the different catalytic enzymes (81) (Figure 1). By immunohistochemistry, researchers found that the expression of 5-LO was high in epithelial ovarian cancer tissues and was associated with poor prognosis (35).

Z Wen et al. found that the high expression of 5-LO was strongly correlated with the density of TAMs in hypoxic areas of human ovarian tumor tissues. Leukotrienes (LTs) from 5-LO metabolites promoted migration and invasion of macrophages, which was mediated by up-regulation of matrix metalloproteinase-7 (MMP7) expression (35). Zileuton, a selective and specific 5-LO inhibitor, can reduce the expression of MMP-7 and the number of infiltrating macrophages in xenograft tumor tissues.

### Cyclooxygenase-2 (COX-2)

As another rate-limiting enzyme in AA metabolism, cyclooxygenase mainly catalyzes AA to produce prostaglandins (PGs) (Figure 1). Cyclooxygenase includes two isozymes, COX-1 and COX-2. COX1 maintains the homeostasis, while COX-2 can be induced by various stimulants, including cytokines, mitogens, hormones, and hypoxia. Growing evidence proves that COX-2 is highly expressed in cancers such as skin cancer, liver cancer, and breast cancer. Some studies reported that COX-2 and its derivative prostaglandin E2 (PGE2) were highly expressed in ovarian cancer cells and might promote cancer cell proliferation and metastasis (36, 82).

Angiogenesis is the physiological basis of solid cancer growth and metastasis. The high expression of COX-2 and its metabolite PGE2 promote angiogenesis through up-regulating of the angiogenic factors such as vascular endothelial growth factor (VEGF) and basic fibroblast growth factor (bFGF). COX-2 can also promote the metastasis and invasion of ovarian cancer through induction of matrix metalloproteinases (MMPs) in extracellular matrix and the decomposition of collagen matrix which may be involved in activation of the PI3K/AKT signaling pathway (83). Inhibition of COX-2 with its specific inhibitor NS-398 can increase the expression of E-cadherin and inhibit the expression of slug, vimentin, MMP2, and MMP9, thereby to suppress invasion and metastasis of ovarian cancer cells under estrogen treatment (84). Moreover, overexpression of COX-2 in ovarian cancer cells can directly up-regulate Bcl-2 expression through the increased synthesis of PGs. Celecoxib, a selective COX-2 inhibitor, can decrease cell growth, increase the cleaved caspase-3 activity and induce cell cycle G1 phase arrest in a dose-dependent manner in ovarian cancer cells (37).

## EXOGENOUS LIPID METABOLISM

The interactions between ovarian cancer cells and human peritoneal adipocytes in ascites are believed to be important for tumor progression. Co-culture of human primary omental adipocytes with ovarian cancer cells could transfer lipids directly from adipocytes to ovarian cancer cells, indicating that adipocytes may serve as an energy source for cancer cells (57).

### Fatty Acid Binding Protein 4 (FABP4)

The family of FABPs is a type of intracellular lipid chaperones that coordinate cellular lipid responses through binding to and redistributing intracellular fatty acids, so FABPs are also called lipid chaperone proteins (85). The function of FABP4 is to promote the uptake of long-chain fatty acids and to participate in lipid transport and metabolic regulation. Overexpression of FABP4 is reported in various types of tumors such as ovarian cancer. As a key mediator in adipocytes and cancer progression, FABP4 can be a worthy predictor of residual disease in ovarian cancer. Recent studies have found that miR-409-3p can target the 3'UTR region of FABP4 and regulate the expression of FABP4 (86).

Nieman et al. compared primary ovarian cancers with corresponding omental metastatic tissues by immunohistochemical staining, and found that FABP4 was increased in ovarian cancer cells at the adipocyte-cancer interface, but was not detected in ovarian cancer cells and benign tissues adjacent to ovarian cancers far from the adipocyte-cancer interface (87). Co-culture of adipocytes with ovarian cancer cells showed that the adipocytes significantly promoted the metastasis of the ovarian cancer cells, whereas treatment of the co-cultured cells with FABP4 inhibitor, lipid accumulation and adipocyte-mediated invasion of the cancer cells were greatly reduced. In the latest research, knockdown of FABP4 in ovarian cancer cells resulted in the increasing level of 5-hydroxymethylcytosine, the downregulated expression of genes was associated with metastasis and the number of clone formation. BMS309403, a small molecule inhibitor of FABP4, was used and the results showed that it not only significantly reduced tumor burden in a syngeneic orthotopic mouse model but also increased the sensitivity of cancer cells towards carboplatin (39).

Taken together, these studies suggest that targeting FABP4 in ovarian cancer may inhibit the ability to adapt lipid-rich cancer microenvironment and to reduce tumor aggressiveness.

## CD36

CD36 is a transmembrane glycoprotein, which is one of the most abundantly expressed members in the class B scavenger receptor family. CD36 not only uptakes of free fatty acids and cholesterol, and the transfer of intracellular signals, but also pertains to the cancer-associated antigen presentation, inflammation, and angiogenesis (88). Studies have found that CD36 is highly expressed in ovarian cancer tissues and also metastatic tissues, which shows that CD36 may participate in the metastasis and proliferation of ovarian cancer.

Ladanyi et al. found that co-culture of ovarian cancer cells with human primary adipocytes (HPAs) increased the expression of CD36 in ovarian cancer cells. However, the inhibition of CD36 caused a decrease in fatty acid intake of cancer cells and reduced the accumulation of cholesterol and lipid droplets and the intracellular reactive oxygen species (ROS) in cancer cells. Knockdown of CD36 can also diminish adipocyte-mediated invasion and migration of cancer cells. Intraperitoneal injection of CD36-deficient cells significantly reduced the number of metastatic nodules in the abdominal of xenograft mouse tumor model (89). Thus, CD36 inhibition can effectively reduce fat acid uptake from microenvironment in ovarian cancer cells to suppress adipocyte-mediated tumor progression.

## Low Density Lipoprotein Receptor (LDLR)

LDLR is a trans-membrane protein that mediates the uptake of cellular cholesterol (90). Reports about LDLR mainly focus on the mechanism of LDLR-mediated chemo-resistance in ovarian cancer cells.

LDLR expression was reported to be correlated with the poor prognosis in patients with epithelial ovarian cancer (EOCs) treated with platinum-based drugs according to the cDNA chip database. Knockdown of LDLR can increase the sensitivity of cells to platinum, whereas overexpression of LDLR can promote chemotherapy resistance. The LDLR/LPC/FAM83B/FGFRs axis

is involved in the LDLR-mediated resistance to platinum based chemotherapy. Zheng et al. determined that both SREBP2 and LDLR expression levels were increased in ovarian cancer cisplatin-resistant cell lines. Bioinformatics analysis predicts that SREBP2 may mediate ovarian cancer resistance through binding to LDLR (91).

## Lysophosphatidic Acid Receptor (LPA)

Lysophosphatidic acid (LPA) is a kind of growth factor-like lipid signal molecule, and is secreted from platelets, nerve cells, and endothelial cells by endocrine and paracrine. LPA exerts its biological function through binding to the heterotrimeric transmembrane G protein coupled receptor (including  $G\alpha_q$ ,  $G\alpha_{12/13}$ ,  $G\alpha_{i/o}$ , and  $G\alpha_s$ ) on cell surface. At least six members of the receptor family are identified, named as LPA1-6 (92). These LPA receptors can be divided into two subfamilies, of which LPA1-3 are the member of vascular endothelial gene (edg) family and LPA4-6 belong to the family of non-vascular endothelial factors. LPA1 is widely distributed in heart, brain and kidney; LPA2 is distributed in testis, pancreas, and prostate; LPA3 is distributed in testis and prostate. All LPAs bind to cell surface receptors and are quickly degraded into inactive monoacylglycerol (MAG) and phosphatidic acid by phospholipase (93).

Ovarian cancer cells can uptake the lysophosphatidic acid through membrane receptors to promote proliferation (94). Studies have found that compared with normal ovarian tissues, LPA2 and LPA3 receptors were highly expressed in ovarian cancer tissues, while LPA1 receptor expression was still low. Inhibition of LPA2 or LPA3 receptor expression led to decreased cancer cell migration and invasiveness. Treatment of cells with LPA1 and LPA3 receptor-specific antagonist VPC32183 reduced the uptake of LPA and caused apoptosis through inhibition of the phosphorylation of ERK1/2. LPA and its receptors can regulate the promoter activity of cyclin D1 through the downstream signaling pathway of LTA receptor, which thereby promoting cell proliferation (95).

LPA and its receptors are also involved in cancer metastasis-related signaling pathways. Xu et al. found that the thyroid receptor interference protein 6 (TRIP6) can affect the LPA-induced cancer cell migration through directly binding to LPA2 receptor. The specific manifestation is that overexpression of TRIP6 enhanced the LPA-induced cell migration, while in contrast, inhibition of TRIP6 expression suppressed the LPA-induced cell migration, suggesting that TRIP6 may mediate the LPA2-induced cancer cell migration (96). Park et al. found that LPA could activate the downstream  $G\alpha_{12/13}$ /RhoA signaling pathway through LPA 1/2 receptor to induce the phosphorylation of ERM proteins (Ezrin/Radixin/Moesin), which promotes the metastasis of ovarian cancer cell line OVC-3 (97).

The combination of paclitaxel and cisplatin is a first-line chemotherapeutic strategy for ovarian cancer treatment. The researchers pretreated ovarian cancer cells with LPA followed by paclitaxel and found that LPA reduced mitochondrial ROS production while the LPA receptor agent VPC32183 increased the content of mitochondrial ROS. Further ROS could cause mitochondrial membrane damage and cancer cell apoptosis (98).



## CONCLUSION

Lipid metabolism of ovarian cancer is a complex process, including lipid uptake, lipid synthesis or storage, and fatty acid degradation by oxidation. So far, the researchers mainly clarified that the enzymes related to fatty acid synthesis (FASN, ACC, ACLY, SCD) and lipid degradation related enzymes (MAGL, CPT, 5-LO, COX2), and receptors related to lipid uptake (FABP4, CD36, LDLR) play important roles in promoting cancer development (Figure 1). However, the study of lipid metabolomics for ovarian cancer markers is still in the primary stage.

In this review, we systematically summarized the process metabolism of fatty acid and the rate-limiting enzymes in this framework. Meanwhile, a number of promising agents targeting the lipid metabolism axis are being developed and applied in clinical treatment, which can provide new strategies for clinical treatment of ovarian cancer.

## AUTHOR CONTRIBUTIONS

GY and XZ were responsible for the revision of the manuscripts. ZJ completed the writing. YShe and XF were involved in the design of the manuscripts. JM, YSha, and YK completed the

documentation and figure drawing. All authors contributed to the article and approved the submitted version.

## SUPPLEMENTARY MATERIAL

The Supplementary Material for this article can be found online at: <https://www.frontiersin.org/articles/10.3389/fonc.2020.593017/full#supplementary-material>

**SUPPLEMENTARY TABLE 1 |** Abbreviation List. AA, arachidonic acid; ACC, acetyl-CoA carboxylase; ACLY, ATP citrate lyase; CACT, carnitine-acylcarnitine translocase; CIC, citrate carrier protein; COX2, cyclooxygenase-2; CPT1, carnitine palmitoyl transferase 1; CPT2, carnitine palmitoyl transferase 2; DGAT, diacylglycerol acyltransferase; ELOVL, elongation of very long-chain fatty acids diacylglycerol acyltransferase; FADS, fatty acid desaturase; FASN, fatty acid synthase; FABP4, fatty acid binding protein 4; LDLR, low density lipoprotein receptor; LTA4, lipoxin A4; LTB4, leukotriene B4; LTC4, leukotriene C4; LTD4, leukotriene D4; LTE4, leukotriene E4; LPAR, lysophosphatidic acid receptor; MAGL, monoacylglycerol lipase; MCD, malonyl-CoA decarboxylase; MG, monoglyceride; MUFA, monounsaturated fatty acids; PGD2, prostaglandin D2; PGE2, prostaglandin E2; PGF2, prostaglandin F2; PGH2, prostaglandin H2; PGI2, prostaglandin I2; PLA2, phospholipase A2; PUFA, polyunsaturated fatty acids; SCD1, stearoyl CoA desaturase1; SFA, saturated fatty acids; TxA2, thromboxane A2; 5-HETE, 5-hydroxyeicosatetraenoic acid; 5-HPETE, 5-hydroperoxy-eicosatetraenoic acid; 5-LO, 5-Lipoxygenase.

## REFERENCES

- Torre LA, Trabert B, DeSantis CE, Miller KD, Goli S, Runowicz CD, et al. Ovarian cancer statistics, 2018. *CA Cancer J Clin* (2018) 68(4):284–96. doi: 10.3322/caac.21456
- Eisenhauer EA. Real-world evidence in the treatment of ovarian cancer. *Ann Oncol* (2017) 28:viii61–5. doi: 10.1093/annonc/mdx443
- Liu J, Matulonis UA. New strategies in ovarian cancer: translating the molecular complexity of ovarian cancer into treatment advances. *Clin Cancer Res* (2014) 20(20):5150–6. doi: 10.1158/1078-0432.CCR-14-1312
- Zhang P-P, Zhou L, Cao J-S. Possible Epithelial Ovarian Cancer Association with HPV18 or HPV33 Infection. *Asian Pac J Cancer Prev* (2016) 17(6):2959–64.
- Leung PC, Choi JH. Endocrine signaling in ovarian surface epithelium and cancer. *Hum Reprod Update* (2007) 13(2):143–62. doi: 10.1093/humupd/dml002
- Ilenkovan N, Gourley C. Pathogenesis, Genetics, and Genomics of Non-High Grade Serous Ovarian Cancers. *Hematol Oncol Clin North Am* (2018) 32(6):929–42. doi: 10.1016/j.hoc.2018.07.004
- Hanchette C, Zhang CH, Schwartz GG. Ovarian Cancer Incidence in the U.S. and Toxic Emissions from Pulp and Paper Plants: A Geospatial Analysis. *Int J Environ Res Public Health* (2018) 15(8):1619. doi: 10.3390/ijerph15081619
- Kipps E, Tan DSP, Kaye SB. Meeting the challenge of ascites in ovarian cancer: new avenues for therapy and research. *Nat Rev Cancer* (2013) 13(4):273–82. doi: 10.1038/nrc3432
- Ahmed N, Stenvers KL. Getting to know ovarian cancer ascites: opportunities for targeted therapy-based translational research. *Front Oncol* (2013) 3:256. doi: 10.3389/fonc.2013.00256
- Kim S, Kim B, Song YS. Ascites modulates cancer cell behavior, contributing to tumor heterogeneity in ovarian cancer. *Cancer Sci* (2016) 107(9):1173–8. doi: 10.1111/cas.12987
- Currie E, Schulze A, Zechner R, Walther TC, Farese RV Jr. Cellular fatty acid metabolism and cancer. *Cell Metab* (2013) 18(2):153–61. doi: 10.1016/j.cmet.2013.05.017
- Carracedo A, Cantley LC, Pandolfi PP. Cancer metabolism: fatty acid oxidation in the limelight. *Nat Rev Cancer* (2013) 13(4):227–32. doi: 10.1038/nrc3483
- Yang Y, Cao Y, Chen L, Liu F, Qi Z, Cheng X, et al. Cryptotanshinone suppresses cell proliferation and glucose metabolism via STAT3/SIRT3 signaling pathway in ovarian cancer cells. *Cancer Med* (2018) 7(9):4610–8. doi: 10.1002/cam4.1691
- Dillon EL, Volpi E, Wolfe RR. Amino Acid Metabolism and Inflammatory Burden in Ovarian Cancer Patients Undergoing Intense Oncological Therapy. *Clin Nutr* (2007) 26(6):736–43. doi: 10.1016/j.clnu.2007.07.004
- Fahy E, Cotter D, Sud M, Subramaniam S. Lipid classification, structures and tools. *Biochim Biophys Acta* (2011) 1811(11):637–47. doi: 10.1016/j.bbalip.2011.06.009
- Swinen JV, Brusselmans K, Verhoeven G. Increased lipogenesis in cancer cells: new players, novel targets. *Curr Opin Clin Nutr Metab Care* (2006) 9(4):358–65. doi: 10.1097/01.mco.0000232894.28674.30
- Kouba S, Ouldamer L, Garcia C, Fontaine D, Chantome A, Vandier C, et al. Lipid metabolism and Calcium signaling in epithelial ovarian cancer. *Cell Calcium* (2019) 81:38–50. doi: 10.1016/j.ceca.2019.06.002
- Schug ZT, Vande Voorde J, Gottlieb E. The metabolic fate of acetate in cancer. *Nat Rev Cancer* (2016) 16(11):708–17. doi: 10.1038/nrc.2016.87
- Mylonis I, Simos G, Paraskeva E. Hypoxia-Inducible Factors and the Regulation of Lipid Metabolism. *Cells* (2019) 8(3):214. doi: 10.3390/cells8030214
- Maiti P, Scott J, Sengupta D, Al-Gharaiheb A, Dunbar GL. Curcumin and Solid Lipid Curcumin Particles Induce Autophagy, but Inhibit Mitophagy and the PI3K-Akt/mTOR Pathway in Cultured Glioblastoma Cells. *Int J Mol Sci* (2019) 20(2). doi: 10.3390/ijms20020399
- Chen J, Chen J, Huang J. HIF-2 $\alpha$  upregulation mediated by hypoxia promotes NAFLD-HCC progression by activating lipid synthesis via the PI3K-AKT-mTOR pathway. *Aging (Albany NY)* (2019) 11(23):10839–60. doi: 10.18632/aging.102488
- Arrese EL, Soulages JL. Insect fat body: energy, metabolism, and regulation. *Annu Rev Entomol* (2010) 55:207–25. doi: 10.1146/annurev-ento-112408-085356
- Pavlova NN, Thompson CB. The Emerging Hallmarks of Cancer Metabolism. *Cell Metab* (2016) 23(1):27–47. doi: 10.1016/j.cmet.2015.12.006
- Papaevangelou E, Almeida GS, Box C, Desouza NM, Chuang YL. The effect of FASN inhibition on the growth and metabolism of a cisplatin-resistant ovarian carcinoma model. *Int J Cancer* (2018) 143(4):992–1002. doi: 10.1002/ijc.31392
- Lu T, Schubert C, Cummings MD, Bignan G, Connolly PJ, Smans K, et al. Design and synthesis of a series of bioavailable fatty acid synthase (FASN) KR

- domain inhibitors for cancer therapy. *Bioorg Med Chem Lett* (2018) 28 (12):2159–64. doi: 10.1016/j.bmcl.2018.05.014
26. Bauerschlag DO, Maass N, Leonhardt P, Verburg FA, Pecks U, Zeppernick F, et al. Fatty acid synthase overexpression: target for therapy and reversal of chemoresistance in ovarian cancer. *J Trans Med* (2015) 13(1):13535. doi: 10.1186/s12967-015-0511-3
  27. Wagner R, Stübiger G, Veigel D. Multi-level suppression of receptor-PI3K-mTORC1 by fatty acid synthase inhibitors is crucial for their efficacy against ovarian cancer cells. *Oncotarget* (2017) 8(7):11600–13. doi: 10.18632/oncotarget.14591
  28. Ventura R, Mordec K, Waszczuk J, Wang Z, Lai J, Fridlib M, et al. Inhibition of de novo Palmitate Synthesis by Fatty Acid Synthase Induces Apoptosis in Tumor Cells by Remodeling Cell Membranes, Inhibiting Signaling Pathways, and Reprogramming Gene Expression. *EBioMedicine* (2015) 2(8):808–24. doi: 10.1016/j.ebiom.2015.06.020
  29. Ueda SM, Yap KL, Davidson B, Tian Y, Murthy V, Wang TL, et al. Expression of Fatty Acid Synthase Depends on NAC1 and Is Associated with Recurrent Ovarian Serous Carcinomas. *J Oncol* (2010) 2010:285191. doi: 10.1155/2010/285191
  30. Tesfay L, Paul BT, Konstorum A. Steroyl-CoA Desaturase 1 (SCD1) protects ovarian cancer cells from ferroptotic cell death. *Cancer Res* (2019) 79 (20):5355–66. doi: 10.1158/0008-5472.CAN-19-0369
  31. Li J, Condello S, Thomes-Pepin J, Ma X, Xia Y, Hurley TD, et al. Lipid Desaturation Is a Metabolic Marker and Therapeutic Target of Ovarian Cancer Stem Cells. *Cell Stem Cell* (2017) 20(3):303–14. doi: 10.1016/j.stem.2016.11.004
  32. Li S, Qiu L, Wu B, Shen H, Zhu J, Zhou L, et al. TOFA suppresses ovarian cancer cell growth in vitro and in vivo. *Mol Med Rep* (2013) 8(2):373–8. doi: 10.3892/mmr.2013.1505
  33. Nomura DK, Long JZ, Niessen S, Hoover HS, Ng SW, Cravatt BF. Monoacylglycerol lipase regulates a fatty acid network that promotes cancer pathogenesis. *Cell* (2010) 140(1):49–61. doi: 10.1016/j.cell.2009.11.027
  34. Sawyer BT, Qamar L, Yamamoto TM, McMellen A, Watson ZL, Richer JK, et al. Targeting fatty acid oxidation to promote anoikis and inhibit ovarian cancer progression. *Mol Cancer Res* (2020) 18(7):1088–98. doi: 10.1158/1541-7786.MCR-19-1057
  35. Wen Z, Liu H, Li M, Li B, Gao W, Shao Q, et al. Increased metabolites of 5-lipoxygenase from hypoxic ovarian cancer cells promote tumor-associated macrophage infiltration. *Oncogene* (2014) 34(10):1241–52. doi: 10.1038/onc.2014.85
  36. Wang Y-P, Wang Q-Y, Li C-H, Li XW. COX-2 inhibition by celecoxib in epithelial ovarian cancer attenuates E-cadherin suppression through reduced Snail nuclear translocation. *Chem Biol Interact* (2018) 292:24–9. doi: 10.1016/j.cbi.2018.06.020
  37. Suri A, Sheng X. The effect of celecoxib on tumor growth in ovarian cancer cells and a genetically engineered mouse model of serous ovarian cancer. *Oncotarget* (2016) 7(26):39582–94. doi: 10.18632/oncotarget.8659
  38. Zhao Y, Cui L, Pan Y, Shao D, Zheng X, Zhang F, et al. Berberine inhibits the chemotherapy-induced repopulation by suppressing the arachidonic acid metabolic pathway and phosphorylation of FAK in ovarian cancer. *Cell Prolif* (2017) 50(6). doi: 10.1111/cpr.12393
  39. Mukherjee A, Chiang C-Y, Daifotis HA, Nieman KM, Fahrman JF, Lastra RR, et al. Adipocyte-induced FABP4 expression in ovarian cancer cells promotes metastasis and mediates carboplatin resistance. *Cancer Res* (2020) 80(8):1748–61. doi: 10.1158/0008-5472.CAN-19-1999
  40. Granchi C. ATP citrate lyase (ACLY) inhibitors: An anti-cancer strategy at the crossroads of glucose and lipid metabolism. *Eur J Med Chem* (2018) 157:1276–91. doi: 10.1016/j.ejmech.2018.09.001
  41. Xu H, Luo J, Ma G, Zhang X, Yao D, Li M, et al. Acyl-CoA synthetase short-chain family member 2 (ACSS2) is regulated by SREBP-1 and plays a role in fatty acid synthesis in caprine mammary epithelial cells. *J Cell Physiol* (2018) 233(2):1005–16. doi: 10.1002/jcp.25954
  42. Covarrubias AJ, Aksoylar HI, Yu J, Snyder NW, Worth AJ, Iyer SS, et al. Akt-mTORC1 signaling regulates Acly to integrate metabolic input to control of macrophage activation. *Elife* (2016) 5:e11612. doi: 10.7554/eLife.11612
  43. Wang Y, Wang Y, Shen L, Pang Y, Qiao Z, Liu P. Prognostic and therapeutic implications of increased ATP citrate lyase expression in human epithelial ovarian cancer. *Oncol Rep* (2012) 27(4):1156–62. doi: 10.3892/or.2012.1638
  44. Wojnarowicz PM, Breznan A, Arcand SL, Filali-Mouhim A, Provencher MD, Mes-Masson A-M, et al. Construction of a chromosome 17 transcriptome in serous ovarian cancer identifies differentially expressed genes. *Int J Gynecol Cancer* (2008) 18(5):963–75. doi: 10.1111/j.1525-1438.2007.01134.x
  45. Han C, Yang L. Amplification of USP13 drives ovarian cancer metabolism. *Nat Commun* (2016) 7:13525. doi: 10.1038/ncomms13525
  46. Han C, Lu X, Nagrath D. Regulation of protein metabolism in cancer. *Mol Cell Oncol* (2018) 5(5):e1285384. doi: 10.1080/23723556.2017.1285384
  47. Wakil SJ, Abu-Elheiga LA. Fatty acid metabolism: target for metabolic syndrome. *J Lipid Res* (2009) 50(Supplement):S138–43. doi: 10.1194/jlr.R800079-JLR200
  48. McGarry JD, Leatherman GF, Foster DW. The site of inhibition of hepatic fatty acid oxidation by malonyl-CoA. *J Biol Chem* (1978) 253:4128–36.
  49. Steinberg GR, Kemp BE. AMPK in Health and Disease. *Physiol Rev* (2009) 89 (3):1025–78. doi: 10.1152/physrev.00011.2008
  50. Brusselmans K, De Schrijver E, Verhoeven G, Swinnen JV. RNA Interference-Mediated Silencing of the Acetyl-CoA Carboxylase- $\alpha$  Gene Induces Growth Inhibition and Apoptosis of Prostate Cancer Cells. *Cancer Res* (2005) 65:6719–25. doi: 10.1158/0008-5472.CAN-05-0571
  51. Chajes V, Cambot M, Moreau K, Lenoir G, Joulin V. Acetyl-CoA carboxylase  $\alpha$  is essential to breast cancer cell survival. *Cancer Res* (2006) 66 (10):5287–94. doi: 10.1158/0008-5472.CAN-05-1489
  52. Perrone F, Baldassarre G, Indraco S. Biomarker analysis of the MITO2 phase III trial of first-line treatment in ovarian cancer: predictive value of DNA-PK and phosphorylated ACC. *Oncotarget* (2016) 7(45):72654–61. doi: 10.18632/oncotarget.12056
  53. Menendez JA, Lupu R. Fatty acid synthase and the lipogenic phenotype in cancer pathogenesis. *Nat Rev Cancer* (2007) 7(10):763–77. doi: 10.1038/nrc2222
  54. Jiang Y, Yin X, Wu L, Qin Q, Xu J. MAPK/P53-mediated FASN expression in bone tumors. *Oncol Lett* (2017) 13(6):4035–8. doi: 10.3892/ol.2017.6015
  55. Choi WI, Jeon BN, Park H, Yoo JY, Kim YS, Koh DI, et al. Proto-oncogene FBI-1 (Pokemon) and SREBP-1 synergistically activate transcription of fatty-acid synthase gene (FASN). *J Biol Chem* (2008) 283(43):29341–54. doi: 10.1074/jbc.M802477200
  56. Cai Y, Wang J, Zhang L, Wu D, Yu D, Tian X, et al. Expressions of fatty acid synthase and HER2 are correlated with poor prognosis of ovarian cancer. *Med Oncol* (2015) 32(1):391. doi: 10.1007/s12032-014-0391-z
  57. Chen RR, Yung MMH, Xuan Y, Zhan S, Leung LL, Liang RR, et al. Targeting of lipid metabolism with a metabolic inhibitor cocktail eradicates peritoneal metastases in ovarian cancer cells. *Commun Biol* (2019) 2:281. doi: 10.1038/s42003-019-0508-1
  58. Luu TH, Bard JM, Carbonnelle D, Chaillou C, Huvelin JM, Bobin-Dubigeon C, et al. Lithocholic bile acid inhibits lipogenesis and induces apoptosis in breast cancer cells. *Cell Oncol (Dordr)* (2018) 41(1):13–24. doi: 10.1007/s13402-017-0353-5
  59. Stoykova GE, Schlaepfer IR. Lipid Metabolism and Endocrine Resistance in Prostate Cancer, and New Opportunities for Therapy. *Int J Mol Sci* (2019) 20 (11):2626. doi: 10.3390/ijms20112626
  60. Ezzeddini R, Taghikhani M, Somi MH, Samadi N, Rasaee M. Clinical importance of FASN in relation to HIF-1 $\alpha$  and SREBP-1c in gastric adenocarcinoma. *Life Sci* (2019) 224:169–76. doi: 10.1016/j.lfs.2019.03.056
  61. Veigel D, Wagner R, Stubiger G, Wuczkowski M, Filipits M, Horvat R, et al. Fatty acid synthase is a metabolic marker of cell proliferation rather than malignancy in ovarian cancer and its precursor cells. *Int J Cancer* (2015) 136 (9):2078–90. doi: 10.1002/ijc.29261
  62. Jiang L, Fang X, Wang H, Li D, Wang X. Ovarian Cancer-Intrinsic Fatty Acid Synthase Prevents Anti-tumor Immunity by Disrupting Tumor-Infiltrating Dendritic Cells. *Front Immunol* (2018) 9:2927. doi: 10.3389/fimmu.2018.02927
  63. AlJohani AM, Syed DN, Ntambi JM. Insights into Stearoyl-CoA Desaturase-1 Regulation of Systemic Metabolism. *Trends Endocrinol Metab* (2017) 28 (12):831–42. doi: 10.1016/j.tem.2017.10.003
  64. Hodson L, Fielding BA. Stearoyl-CoA desaturase: rogue or innocent bystander? *Prog Lipid Res* (2013) 52(1):15–42. doi: 10.1016/j.plipres.2012.08.002
  65. Liu X, Ntambi JM. Stearoyl CoA Desaturase 1: Role in Cellular Inflammation and Stress. *Adv Nutr* (2011) 2:15–22. doi: 10.3945/an.110.000125. MS Strable.
  66. Koeberle A, Loser K, Thurmer M. Stearoyl-CoA desaturase-1 and adaptive stress signaling. *Biochim Biophys Acta* (2016) 1861(11):1719–26. doi: 10.1016/j.bbalip.2016.08.009

67. Igal RA. Stearoyl CoA desaturase-1: New insights into a central regulator of cancer metabolism. *Biochim Biophys Acta* (2016) 1861(12 Pt A):1865–80. doi: 10.1016/j.bbali.2016.09.009
68. Roongta UV, Pabalan JG, Wang X, Ryseck RP, Fargnoli J, Henley B, et al. Cancer cell dependence on unsaturated fatty acids implicates stearoyl-CoA desaturase as a target for cancer therapy. *Mol Cancer Res* (2011) 9(11):1551–61. doi: 10.1158/1541-7786.MCR-11-0126
69. Stockwell BR, Angeli JFP, Bayir H, Bush AI, Conrad M, Dixon S, et al. Ferroptosis: A Regulated Cell Death Nexus Linking Metabolism, Redox Biology, and Disease. *Cell* (2017) 171(2):273–85. doi: 10.1016/j.cell.2017.09.021
70. Currie E, Schulze A, Zechner R. Cancer metabolism fatty acid oxidation in the limelight. *Cell Metab* (2013) 18(2):153–61. doi: 10.1016/j.cmet.2013.05.017
71. Nomura DK, Lombardi DP, Chang JW, Niessen S, Ward A, Long J, et al. Monoacylglycerol lipase exerts dual control over endocannabinoid and fatty acid pathways to support prostate cancer. *Chem Biol* (2011) 18(7):846–56. doi: 10.1016/j.chembiol.2011.05.009
72. Zhu W, Zhao Y, Zhou J, Wang X, Pan Q, Zhang N, et al. Monoacylglycerol lipase promotes progression of hepatocellular carcinoma via NF- $\kappa$ B-mediated epithelial-mesenchymal transition. *J Hematol Oncol* (2016) 9(1). doi: 10.1186/s13045-016-0361-3
73. Poli G, Lapillo M, Jha V, Mouawad N, Caligiuri I, Macchia M, et al. Computationally driven discovery of phenyl(piperazin-1-yl)methanone derivatives as reversible monoacylglycerol lipase (MAGL) inhibitors. *J Enzyme Inhibit Med Chem* (2019) 34(1):589–96. doi: 10.1080/14756366.2019.1571271
74. Granchi C, Caligiuri I. A patent review of Monoacylglycerol Lipase (MAGL) inhibitors (2013–2017). *Expert Opin Ther Pat* (2017) 27(12):1341–51. doi: 10.1080/13543776.2018.1389899
75. Adeva-Andany MM, Calvo-Castro I, Fernández-Fernández C, Donapetry-García C, Pedre-Piñero AM. Significance of carnitine for human health. *IUBMB Life* (2017) 69(8):578–94. doi: 10.1002/iub.1646
76. Bonnefont JP, Djouadi F, Prip-Buus C, Gobin S, Munnich A, Bastin J. Carnitine palmitoyltransferases 1 and 2: biochemical, molecular and medical aspects. *Mol Aspects Med* (2004) 25(5–6):495–520. doi: 10.1016/j.mam.2004.06.004
77. Shao H, Mohamed EM, Xu GG. Carnitine palmitoyltransferase 1A functions to repress FoxO transcription factors to allow cell cycle progression in ovarian cancer. *Oncotarget* (2016) 7(4):3832–46. doi: 10.18632/oncotarget.6757
78. Mashima R, Okuyama T. The role of lipoxygenases in pathophysiology: new insights and future perspectives. *Redox Biol* (2015) 6:297–310. doi: 10.1016/j.redox.2015.08.006
79. Rocconi RP, Kirby TO, Seitz RS, Beck R, Straughn J, Alvarez RD, et al. Lipoxygenase pathway receptor expression in ovarian cancer. *Reprod Sci* (2008) 15(3):321–6. doi: 10.1177/1933719108316390
80. Moore G, Pidgeon G. Cross-Talk between Cancer Cells and the Tumour Microenvironment: The Role of the 5-Lipoxygenase Pathway. *Int J Mol Sci* (2017) 18(2):236. doi: 10.3390/ijms18020236
81. Das UN. Ageing: Is there a role for arachidonic acid and other bioactive lipids? A review. *J Advanced Res* (2018) 11:67–79. doi: 10.1016/j.jare.2018.02.004
82. Lin Y, Cui M, Xu T, Yu W, Zhang L. Silencing of cyclooxygenase-2 inhibits the growth, invasion and migration of ovarian cancer cells. *Mol Med Rep* (2014) 9(6):2499–504. doi: 10.3892/mmr.2014.2131
83. Gu P, Su Y, Guo S, Teng L, Xu Y, Qi J, et al. Over-Expression of COX-2 Induces Human Ovarian Cancer Cells (CAOV-3) Viability, Migration and Proliferation in Association with PI3-k/Akt Activation. *Cancer Invest* (2009) 26(8):822–9. doi: 10.1080/07357900801941860
84. Feng D, Zhao T, Yan K, Liang H, Liang J, Zhou Y, et al. Gonadotropins promote human ovarian cancer cell migration and invasion via a cyclooxygenase 2-dependent pathway. *Oncol Rep* (2017) 38(2):1091–8. doi: 10.3892/or.2017.5784
85. Lee D, Wada K, Taniguchi Y, Al-Shareef H, Masuda T, Usami Y, et al. Expression of fatty acid binding protein 4 is involved in the cell growth of oral squamous cell carcinoma. *Oncol Rep* (2014) 31(3):1116–20. doi: 10.3892/or.2014.2975
86. Gharpure KM, Pradeep S, Sans M, Rupaimoole R, Ivan C, Wu SY, et al. FABP4 as a key determinant of metastatic potential of ovarian cancer. *Nat Commun* (2018) 9(1):2923. doi: 10.1038/s41467-018-04987-y
87. Nieman KM, Kenny HA, Penicka CV, Ladanyi A, Buell-Gutbrod R, Marion Zillhardt M, et al. Adipocytes promote ovarian cancer metastasis and provide energy for rapid tumor growth. *Nat Med* (2011) 17(11):1498–503. doi: 10.1038/nm.2492
88. DeFilippis RA, Chang H, Dumont N, Rabban JT, Chen YY, Fontenay GV, et al. CD36 repression activates a multicellular stromal program shared by high mammographic density and tumor tissues. *Cancer Discovery* (2012) 2(9):826–39. doi: 10.1158/2159-8290.CD-12-0107
89. Ladanyi A, Mukherjee A, Kenny HA, Johnson A, Mitra AK, Sundaresan S, et al. Adipocyte-induced CD36 expression drives ovarian cancer progression and metastasis. *Oncogene* (2018) 37(17):2285–301. doi: 10.1038/s41388-017-0093-z
90. Chang XL, Liu L, Wang N, Chen ZJ, Zhang C. The function of high-density lipoprotein and low-density lipoprotein in the maintenance of mouse ovarian steroid balance. *Biol Reprod* (2017) 97(6):862–72. doi: 10.1093/biolre/iox134
91. Zheng L, Li L, Lu Y, Jiang F, Yang XA. SREBP2 contributes to cisplatin resistance in ovarian cancer cells. *Exp Biol Med* (2018) 243(7):655–62. doi: 10.1177/1535370218760283
92. Tsujiuchi T, Hirane M, Dong Y, Fukushima N. Diverse effects of LPA receptors on cell motile activities of cancer cells. *J Recept Signal Transd* (2014) 34(3):149–53. doi: 10.3109/10799893.2013.876042
93. Wang P, Wu X, Chen W, Liu J, Wang X. The lysophosphatidic acid (LPA) receptors their expression and significance in epithelial ovarian neoplasms. *Gynecol Oncol* (2007) 104(3):714–20. doi: 10.1016/j.ygyno.2006.10.016
94. Umez-Goto M, Tanyi J, Lahad J, Liu S, Yu S, Lapushin R, et al. Lysophosphatidic acid production and action: validated targets in cancer? *J Cell Biochem* (2004) 92(6):1115–40. doi: 10.1002/jcb.20113
95. Hu Y-L, Albanese C, Pestell RG, Jaffe RB. Dual Mechanisms for Lysophosphatidic Acid Stimulation of Human Ovarian Carcinoma Cells. *J Natl Cancer Inst* (2003) 95(10):733–40. doi: 10.1093/jnci/95.10.733
96. Xu J, Lai Y-J, Lin W-C, Lin F-T. TRIP6 Enhances Lysophosphatidic Acid-induced Cell Migration by Interacting with the Lysophosphatidic Acid 2 Receptor. *J Biol Chem* (2004) 279(11):10459–68. doi: 10.1074/jbc.M311891200
97. Park J, Jang JH, Oh S, Kim M, Shin C, Jeong M, et al. LPA-induced migration of ovarian cancer cells requires activation of ERM proteins via LPA1 and LPA2. *Cell Signal* (2018) 44:138–47. doi: 10.1016/j.cellsig.2018.01.007
98. Saunders JA, Rogers LC, Klomsiri C, Poole LB, Daniel LW. Reactive oxygen species mediate lysophosphatidic acid induced signaling in ovarian cancer cells. *Free Radic Biol Med* (2010) 49(12):2058–67. doi: 10.1016/j.freeradbiomed.2010.10.663

**Conflict of Interest:** The authors declare that the research was conducted in the absence of any commercial or financial relationships that could be construed as a potential conflict of interest.

Copyright © 2020 Ji, Shen, Feng, Kong, Shao, Meng, Zhang and Yang. This is an open-access article distributed under the terms of the Creative Commons Attribution License (CC BY). The use, distribution or reproduction in other forums is permitted, provided the original author(s) and the copyright owner(s) are credited and that the original publication in this journal is cited, in accordance with accepted academic practice. No use, distribution or reproduction is permitted which does not comply with these terms.



# Identification of Metabolism-Associated Prostate Cancer Subtypes and Construction of a Prognostic Risk Model

Yanlong Zhang<sup>1,2†</sup>, Ruiqiao Zhang<sup>1,2</sup>, Fangzhi Liang<sup>1,2</sup>, Liyun Zhang<sup>3\*†</sup> and Xuezhi Liang<sup>1\*†</sup>

<sup>1</sup> Department of Urology, First Hospital of Shanxi Medical University, Taiyuan, China, <sup>2</sup> First Clinical Medical College, Shanxi Medical University, Taiyuan, China, <sup>3</sup> Department of Rheumatology, Shanxi Bethune Hospital, Shanxi Academy of Medical Sciences, Taiyuan, China

## OPEN ACCESS

### Edited by:

Andrea Morandi,  
University of Florence, Italy

### Reviewed by:

Krishna Beer Singh,  
University of Pittsburgh, United States  
Amilcare Barca,  
University of Salento, Italy

### \*Correspondence:

Xuezhi Liang  
liangxz2008@sina.com  
Liyun Zhang  
1315710223@qq.com

<sup>†</sup>First author

<sup>†</sup>These authors have contributed  
equally to this work

### Specialty section:

This article was submitted to  
Cancer Metabolism,  
a section of the journal  
Frontiers in Oncology

**Received:** 01 September 2020

**Accepted:** 26 October 2020

**Published:** 26 November 2020

### Citation:

Zhang Y, Zhang R, Liang F, Zhang L  
and Liang X (2020) Identification of  
Metabolism-Associated Prostate  
Cancer Subtypes and Construction of  
a Prognostic Risk Model.  
Front. Oncol. 10:598801.  
doi: 10.3389/fonc.2020.598801

**Background:** Despite being the second most common tumor in men worldwide, the tumor metabolism-associated mechanisms of prostate cancer (PCa) remain unclear. Herein, this study aimed to investigate the metabolism-associated characteristics of PCa and to develop a metabolism-associated prognostic risk model for patients with PCa.

**Methods:** The activity levels of PCa metabolic pathways were determined using mRNA expression profiling of The Cancer Genome Atlas Prostate Adenocarcinoma cohort via single-sample gene set enrichment analysis (ssGSEA). The analyzed samples were divided into three subtypes based on the partitioning around medication algorithm. Tumor characteristics of the subsets were then investigated using t-distributed stochastic neighbor embedding (t-SNE) analysis, differential analysis, Kaplan–Meier survival analysis, and GSEA. Finally, we developed and validated a metabolism-associated prognostic risk model using weighted gene co-expression network analysis, univariate Cox analysis, least absolute shrinkage and selection operator, and multivariate Cox analysis. Other cohorts (GSE54460, GSE70768, genotype-tissue expression, and International Cancer Genome Consortium) were utilized for external validation. Drug sensibility analysis was performed on Genomics of Drug Sensitivity in Cancer and GSE78220 datasets. In total, 1,039 samples and six cell lines were concluded in our work.

**Results:** Three metabolism-associated clusters with significantly different characteristics in disease-free survival (DFS), clinical stage, stemness index, tumor microenvironment including stromal and immune cells, DNA mutation (*TP53* and *SPOP*), copy number variation, and microsatellite instability were identified in PCa. Eighty-four of the metabolism-associated module genes were narrowed to a six-gene signature associated with DFS, *CACNG4*, *SLC2A4*, *EPHX2*, *CA14*, *NUDT7*, and *ADH5* ( $p < 0.05$ ). A risk model was developed, and external validation revealed the strong robustness our risk model possessed in diagnosis and prognosis as well as the association with the cancer feature of drug sensitivity.



**Conclusions:** The identified metabolism-associated subtypes reflected the pathogenesis, essential features, and heterogeneity of PCa tumors. Our metabolism-associated risk model may provide clinicians with predictive values for diagnosis, prognosis, and treatment guidance in patients with PCa.

**Keywords:** prostate cancer, metabolism-associated subtype, risk model, tumor heterogeneity, immunotherapy

## INTRODUCTION

Prostate cancer (PCa) is the second most frequent urinary system-associated type of cancer, accounting for 13% of all malignant tumors in men (1). Radical prostatectomy (RP) has been used to cure PCa patients by removing the malignant prostate. However, the recurrence rates after the surgery are high. Recurrent cancer has risks of developing into castration-resistant PCa, which will either continue progressing the pre-existing PCa or spreading cancer to other parts of the body (2). Therefore, exploring the tumor characteristic and finding a new therapy for PCa remains crucial. Furthermore, identifying biomarkers for disease-free survival (DFS) is needed to improve patients' prognosis with PCa.

Due to the unrestricted multiplicative nature of cancer cells, tumors exhibit different metabolic statues from normal tissue, thus provide a possible way to identify tumors through the difference in metabolism. Recent studies have proven that some metabolisms, such as citrate and choline metabolism, are closely related to PCa (3). Studies have also shown that based on the variance in metabolites, such as increased urea cycle metabolites, PCa can be characterized (4).

Classification analysis based on a large number of samples that can better reflect tumor features and heterogeneity becomes possible with the advent of high-throughput sequencing. High-throughput sequencing has been successfully applied to classify subtypes in different cancers. Subtypes are then used to either guide immune therapy, portray multiple dimensions of tumor characteristics, or assist patient prognosis prediction (5, 6). Although many genome-wide analyses have been performed in regards to PCa, there has been a lack of hierarchical cluster analyses of the PCa transcriptome to exploring tumor metabolic features. Meanwhile, almost all previous studies were based on PCa tumor metabolism concentrated on individual tumor cells rather than mixed tissue, including tumor cells, stromal cells, and immune cells. These studies and therefore do not reflect the metabolic characteristics of PCa *in vivo* (7). So a hierarchical cluster analysis of the PCa transcriptome from a metabolic view to exploring tumor heterogeneity is therefore crucial.

Based on the information above, we performed unsupervised clustering to explore the potential metabolism-associated subtypes and explored the correlations between the subtypes and tumor heterogeneity. Biomarkers associated with subtypes were also selected. Finally, a risk model to predict PCa patients' prognosis was constructed. We hypothesize the metabolism-associated characteristics of PCa to understand the PCa metabolic mechanism better and further identify tumors. The risk model will be able to guide the PCa diagnosis, prognosis, and treatment.

## MATERIALS AND METHODS

### Data Collection

Gene expression files, DNA mutation data, and copy number variation (CNV) of prostate adenocarcinoma (PRAD) tissues were downloaded from TCGA (<https://portal.gdc.cancer.gov/>). Gene expression data were acquired using the Illumina HiSeq RNA Sequencing platform and expressed as fragments per kilobase of transcript per million fragments (FPKM). The cBioPortal for Cancer Genomics (<https://www.cbioportal.org/>) provided clinical data of the PRAD patients (8). RNA sequencing (RNA-seq) data of normal prostate tissues from testing cohorts for diagnosis were obtained from the Genotype-Tissue Expression (GTEx) (<https://www.gtexportal.org/>) and tumor tissue from the ICGC (<https://icgc.org/>). RNA-seq and microarray data of PRAD tissues and clinical information from testing cohorts for prognosis were obtained from the Gene Expression Omnibus (GEO) database (<https://www.ncbi.nlm.nih.gov/gds/>). The GEO search strategy of the GSE datasets was as follows: 1) Include "prostate cancer" and dataset types of RNA-seq or micro-array; 2) Include more than one hundred PRAD samples with survival data; and 3) Include expression information of six risk model genes. Two datasets that met these requirements were identified, GSE54460 and GSE70768. Microarray data of cell lines (including 22RV1, DU-145, LNCaP-Clone-FGC, PC-3, PWR-1E, and VCaP), and RNA-seq data of melanoma samples were downloaded from the Genomics of Drug Sensitivity in Cancer (GDSC) (<https://www.cancerrxgene.org/>) and GSE78220. We also acquired the immunohistochemistry (IHC) data for PRAD and normal prostate tissues from the Human Protein Atlas (HPA) data portal (<https://www.proteinatlas.org/>). Immune infiltrate data for PRAD tissues were downloaded from the Cistrome Project (<http://www.cistrome.org/>) using the Tumor IMMune Estimation Resource version 2.0 (TIMER2.0) (9).

### ssGSEA Assessment of Metabolism-Associated Pathways Expression Levels

Data for 41 metabolism pathway gene sets were acquired from Molecular Signatures Database (MSigDB; <https://www.gsea-msigdb.org/>) (10) and Kyoto Encyclopedia of Genes and Genomes (KEGG) (11) and the PCa related activity levels were calculated using ssGSEA and the gene set variance analysis (GSVA) R package 1.34.0 (10). The metabolism-associated signatures used included galactose metabolism, ascorbate and aldarate metabolism, fatty acid metabolism, purine metabolism, pyrimidine metabolism, alanine aspartate and glutamate metabolism, glycine serine and threonine metabolism, cysteine and methionine

metabolism, arginine and proline metabolism, histidine metabolism, tyrosine metabolism, phenylalanine metabolism, tryptophan metabolism, beta alanine metabolism, taurine and hypotaurine metabolism, selenoamino acid metabolism, glutathione metabolism, starch and sucrose metabolism, amino sugar and nucleotide sugar metabolism, glycerolipid metabolism, inositol phosphate metabolism, glycerophospholipid metabolism, ether lipid metabolism, arachidonic acid metabolism, linoleic acid metabolism, alpha linolenic acid metabolism, sphingolipid metabolism, pyruvate metabolism, glyoxylate and dicarboxylate metabolism, propanoate metabolism, butanoate metabolism, riboflavin metabolism, nicotinate and nicotinamide metabolism, retinol metabolism, porphyrin and chlorophyll metabolism, nitrogen metabolism, sulfur metabolism, metabolism of xenobiotics by cytochrome P450, drug metabolism cytochrome P450, and drug metabolism other enzymes (Table S1).

### Identification of PRAD Subtypes by Partitioning Around Medication (PAM) and T-Distributed Stochastic Neighbor Embedding (t-SNE) Analyses

Unsupervised clustering analysis using the PAM algorithm was performed based on the ssGSEA score of each sample using the R package ConsensusClusterPlus function (12). The samples were then divided into three subtypes. The t-SNE analysis of the ssGSEA scores using R package Rtsne identified three clusters. Kaplan–Meier (K–M) survival analysis of the three metabolism-associated subtypes was performed using R package survival.

### Stemness Index Calculation and Immune Infiltration Estimation of PRAD Tumors

To evaluate the tumor stemness index, we downloaded the mRNA expression-based stemness index (mrNasi) calculated by machine learning in previous studies (13). The stem cell gene set was obtained in a previous study (14), and the ssGSEA stemness index (ssGSEAsi) was calculated using the GSVA R package 1.34.0 (10). Tumor purity was calculated using R package ESTIMATE 1.0.13 (15) and then used to correct the stemness index. The immune scores, stromal scores, and ESTIMATION scores calculated using the R package ESTIMATE 1.0.13 (15) were used to evaluate immune cell and stromal cell abundance in the PRAD tumors.

### Metabolism-Associated Module Genes Filtered by WGCNA and Functional Enrichment Analysis

After selecting the metabolism-associated genes, we generated an adjacency matrix (AM) and topological overlap matrix (TOM) using the gradient method based on power values ranging from 1 to 20. When the correlation between the average degree of connectivity ( $k$ ) and  $p(k)$  reached 0.88, we obtained the optimal power value and constructed a scale-free topology network. Network connectivity of the genes was measured using a TOM transformed from an AM (16). Modules were calculated using a divided cluster tree (17). Finally, we linked the

module eigengenes (MEs) with the subtypes in the current study related to metabolism-associated status (C1, C2, and C3) and for the next analysis, selected the module with the highest correlation based on module-trait correlation coefficients and gene significance (GS) with C1 and C3 ( $|cor| > 0.3$ ). These genes were considered metabolism-associated module genes. To annotate the molecular functions of the genes, Gene Ontology (GO) and KEGG functional enrichment analyses of the metabolism-associated module genes were performed using the clusterProfiler R package 3.42.0 (18).

### Biomarker Selection and Risk Model Construction

The correlation between metabolism-associated genes and DFS of PRAD was calculated and analyzed using univariate Cox analysis with R package survival 3.1.8, and candidate biomarkers were screened at  $p$  values  $< 0.05$ . LASSO regression using R package glmnet 3.0.2 (19, 20) was then applied to resolve any multilinear problem that may have existed in the regression analysis, and the biomarkers were filtered. Multivariate Cox was used next to build a risk model and to obtain estimated regression coefficients. Finally, we calculated the risk score for each sample to quantify the prognosis risk of each patient with PRAD. Survival data were analyzed as K–M survival curves via R package survival 3.1.8. To evaluate the precision of the risk model and nomogram, time-dependent receiver operating characteristic (ROC) analysis was applied using the R package survival ROC 1.0.3. An area under the ROC curve (AUC)  $> 0.60$ , indicated the prediction ability of the model was meaningful, and an AUC  $> 0.70$  indicated an outstanding predictive value of the model. To investigate the function of risk model genes, we performed GSEA of the TCGA cohort according to the high-risk group and low-risk group divided by the risk score medium value. The correlation between clinical variates and the DFS of PRAD was analyzed and calculated using univariate and multivariate Cox with the R package survival v3.1.8. The nomogram was obtained with the R package survival v3.1.8. The C-index analysis was performed with the R package pec v2019.11.3 (21).

### HPA Analysis

Protein levels of six risk model genes expressed in PRAD and normal prostate samples were analyzed using IHC staining data obtained from the HPA database. Four categories of high, medium, low, and not detected were used to evaluate expression levels. These categories included a scoring system based on the proportion of positive-stained cells ( $>75$ ,  $25$ – $75$ , or  $<25\%$ ) and staining intensity (strong, moderate, weak, or negative).

### Statistical Analysis

All statistical analyses were conducted using R software (version 3.6.1). The Mann–Whitney U-test was used to compare two groups with a non-normal distribution of variables. For comparisons of three groups, Kruskal–Wallis tests of variance were used as nonparametric methods. Correlation analysis was

performed using the Person coefficient. All statistical tests were two-sided, and  $p$ -values < than 0.05 were considered statistically significant.

## RESULTS

### Metabolism-Associated Subtypes Identified by ssGSEA and PAM Analysis

A schematic of our research workflow is shown in **Figure 1A**, and the clinical information regarding the TCGA PRAD cases included in our study is summarized in **Table 1**. To determine the level of activity of the metabolic pathways in each PRAD sample, we calculated the enrichment scores of 41 metabolism-associated gene sets using ssGSEA (**Table S1**). We then performed PAM analysis of ssGSEA scores for 499 PRAD samples and determined the matrix heatmap of the ssGSEA scores retained sharp and clear sides when  $k = 3$ , which indicated there were three different metabolism-associated clusters, C1, C2, and C3 (**Figure 1B** and **Figures S1A–F**). To verify the subtype distribution, we performed t-SNE to dimensionally reduce the ssGSEA scores and found the subclass assignment was approximately accordant with the t-SNE coordinates designation (**Figure 1C**).

To explore the characterization of each subtype, we described the clustering hot map of the metabolic pathway scores (**Figure 2A**).

Compared to that of cluster C1, C2 had higher enrichment scores in most metabolic pathways, indicating that tumors from C2 exhibited higher metabolic activity than that of tumors from C1. Concomitantly, the highest specific metabolic pathways scores were observed for cluster C3 and included retinol metabolism, metabolism of xenobiotics by cytochrome P450, drug metabolism cytochrome\_P450, drug metabolism other enzymes, starch and sucrose metabolism, ascorbate and aldarate metabolism, and porphyrin and chlorophyll metabolism. The other pathway scores of C3 were higher compared to those of C1, but lower than those of C2. This indicated that tumors from C3 might have had a medium metabolic status at levels between those from C1 and C2 and, at the same time, exhibited some unique metabolic characteristics.

Clinical analysis comparing the different subtypes revealed patients from C1 and C3 had higher primary tumor (T) stage and Gleason scores than patients from C3, but the age and regional lymph nodes (N) stage differences of the patients among these subtypes were not significant (**Figures 2B, C** and **Figures S2A, B**). Prostate-specific antigen (PSA) is the most common index used in the diagnosis and prediction of prognosis for PCa (22). Differences in PSA levels among the three subtypes indicated the subtypes were independent of PSA without any detectable connection (**Figure S2C**). We then performed a K–M survival analysis of patients with PRAD from each subtype. The results suggested there were considerable differences in DFS among the three subtypes ( $p < 0.05$ ; **Figure 2D**). The patients from C1 had the shortest DFS compared to those from the other subtypes.

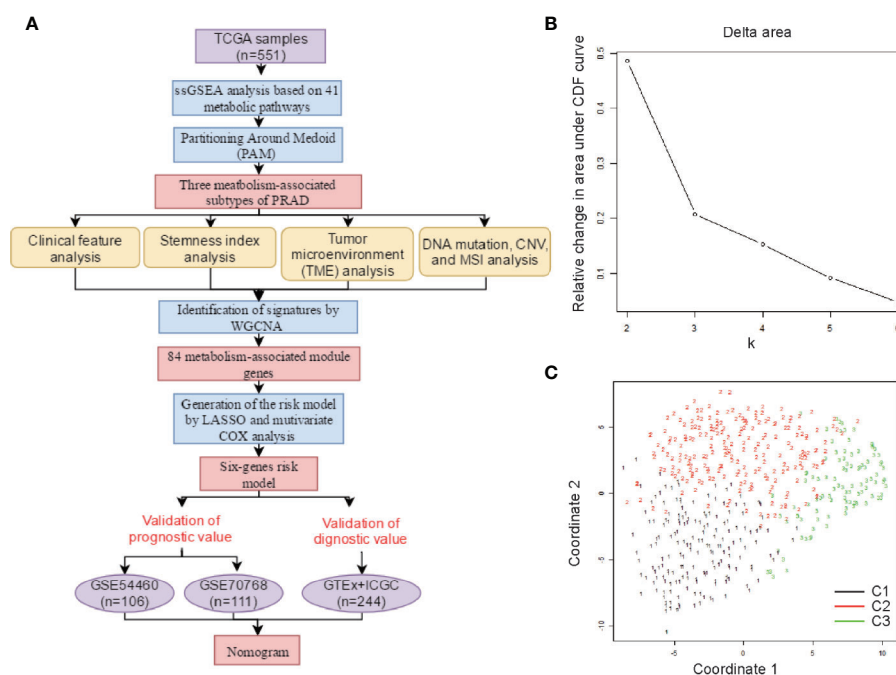


**FIGURE 1** | Identification of metabolism-associated subtypes of PRAD using PAM algorithm based on ssGSEA score. **(A)** Workflow in this study. **(B)** Delta area curves for consensus clustering indicating the relative change in area under the cumulative distribution function (CDF) curve for each category number  $k$  compared to  $k - 1$ . The horizontal axis represents the category number  $k$ , and the vertical axis represents the relative change in area under CDF curve. **(C)** t-SNE analysis supported the stratification into three metabolism-associated subtypes of PRAD.

**TABLE 1** | Clinical information from the 545 PCa patient of TCGA.

Clinical parameters	Variable	N (total = 545)	Percentages (%)
Age (years)	<=60	242	44.40%
	>60	303	55.60%
T/N grade	T2	188	34.50%
	T3	295	54.13%
	T4	10	1.83%
	unknow (T stage)	52	9.54%
	N0	348	63.85%
	N1	79	14.50%
Gleason score	unknow (N stage)	118	21.65%
	6	48	8.81%
	7	285	52.29%
	8	66	12.11%
Survival status	9 & 10	146	26.78%
	Dead	10	1.83%
	Alive	482	88.44%
	unknown	53	9.72%

This result indicated that the metabolism-associated subtypes would be associated with different prognoses, and tumors from the different subtypes exhibited considerable differences in their metabolic status.

## Correlation of PRAD Subtypes With Cancer Stem Cell Characteristics

In previous studies, cancer stem cell characteristics have been shown to represent the capability of tumor proliferation and are associated with the development and progression of PRAD (23, 24). To determine the heterogeneity of the current study subtypes, we compared the stemness index of each subtype that was calculated using one-class logistic regression (OCLR) machine learning and ssGSEA. We initially obtained two stemness indices, mRNAsi, and ssGSEAsi (**Table S2**).

Differential analysis of mRNAsi indicated there were significant differences among the three subtypes ( $p < 0.05$ ; **Figure 3A**). C1 had the highest stemness index, whereas C2 had the lowest. Moreover, ssGSEAsi analysis indicated that C3 had the highest stemness index ( $p < 0.05$ ; **Figure S3A**). To compensate for the impact of tumor purity on the stemness index, we recalculated the indices using corrected mRNAsi and ssGSEAsi values by dividing them by their respective tumor purity values and then re-performing the differential analysis. The results for the two corrected stemness indices were in approximate accordance with the original results (**Figure 3B** and **Figure S3B**). This suggested the tumors from clusters C1

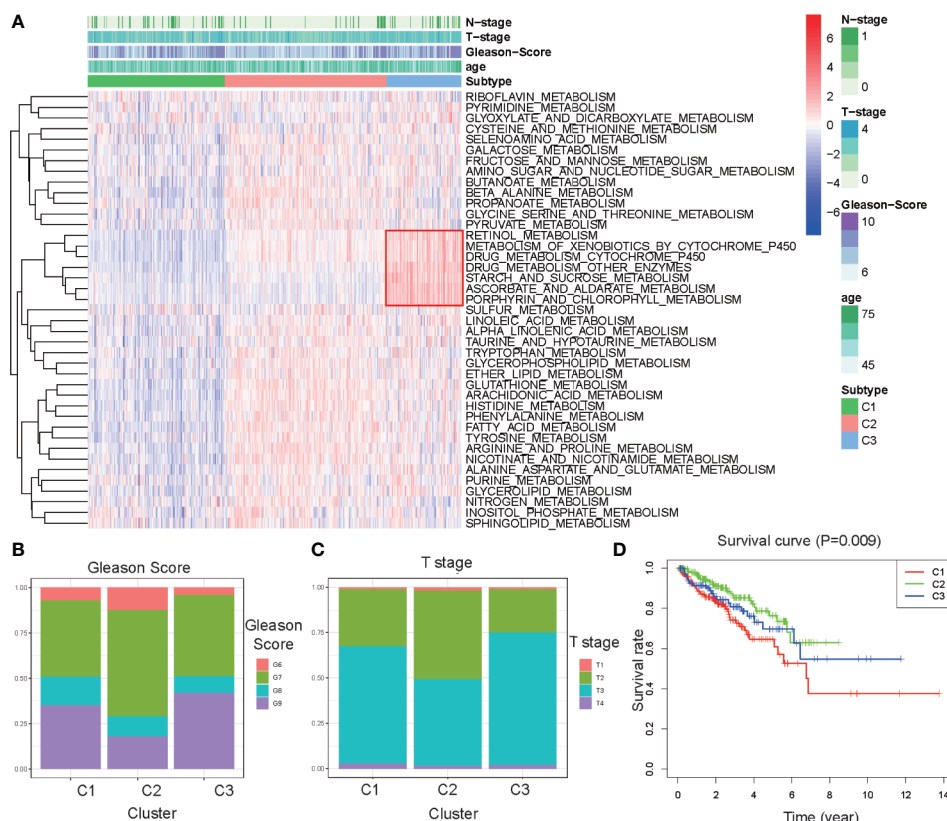


**FIGURE 2** | Association between clinical characteristics and the metabolism-associated subtypes. **(A)** Heatmap of the ssGSEA score calculated by metabolic pathways gene sets and specific metabolic pathways of C3 in the red frame. Gleason score **(B)** and Primary Tumor (T) stage **(C)** for each metabolism-associated subtype in the TCGA cohort. The P values are labeled above each boxplot with asterisks (ns represents no significance, \* $P < 0.05$ , \*\* $P < 0.01$ , \*\*\* $P < 0.001$ ). **(D)** Survival curves for each metabolism-associated subtype in the TCGA cohort. The horizontal axis represents survival time (year), and the vertical axis represents the probability of survival. The log-rank test was used to assess the statistical significance of the differences between the three subtypes.



and C3 had a stronger capacity for invasion, proliferation, and self-renewal compared to that for those from C2.

Because C3 demonstrated the highest ssGSEAsi and COssGSEAsi and had specific metabolic pathways, we performed a correlation analysis between COssGSEAsi/ssGSEAsi and the specific metabolic pathways. The results indicated the starch and sucrose metabolism and porphyrin and chlorophyll metabolism pathways were highly correlated with the PRAD stemness index ( $\text{cor} > 0.3$ ; **Figure S3C**).

## Relationship Between PRAD Subtypes and TME

To further investigate PRAD tumor heterogeneity, we compared the TME among the metabolism-associated subtypes. In previous studies, TME compounded by both stromal and immune cells played a crucial role in the occurrence and progression of PRAD (25, 26). Moreover, TME may reflect a tumor's sensitivity to immunotherapies (27, 28). Accordingly, we obtained stromal scores and immune scores for the PRAD tumors in the current study using the ESTIMATE algorithm and then performed a differential analysis of the three subtypes. The results showed that C1 tumors had lower stromal and immune scores compared to those C2 and C3 tumors (**Figures 4A–C**). This suggested that tumor tissue from C1 had higher tumor purity and lower immune infiltration compared to tumor tissues from C2 and C3. To further investigate the differences in stromal cells among the three clusters, we calculated ssGSEA

scores for epithelial-mesenchymal transition (EMT), extracellular matrix (ECM), and transforming growth factor-beta (TGF- $\beta$ ) using the corresponding gene sets downloaded from the Molecular Signatures Database (**Table S2**). Differential analysis of these ssGSEA scores suggested C1 tumors had the lowest scores for all three gene sets, which was consistent with the results from the comparison of the stromal scores for the three subtypes (**Figures 4D–F**).

Because of the significant difference in immune scores between PRAD subtypes, we explored immune infiltration to identify their respective immunologic landscapes. The abundance of six immune-related cell types, B cell, dendritic, macrophage, neutrophil, CD4+ T cell, and CD8+ T cell, was download from TIMER2.0. Significant differences for all six immune cell types were verified among the cluster subtypes, with the tumors from C2 having the highest abundance of all immune cells, except B cells. The cluster with the highest abundance of B cells was C3, whereas C1 tumors had the lowest abundance of all the immune cell types evaluated (**Figure 4G**). Our results indicated that the metabolism-associated subtypes of PRAD exhibited remarkably distinct characteristics with respect to immune infiltration.

## PRAD Subtype Relationship With DNA Mutations, CNV, and MSI

To determine the reason for cluster subtype heterogeneity, we investigated whether differences existed among the three

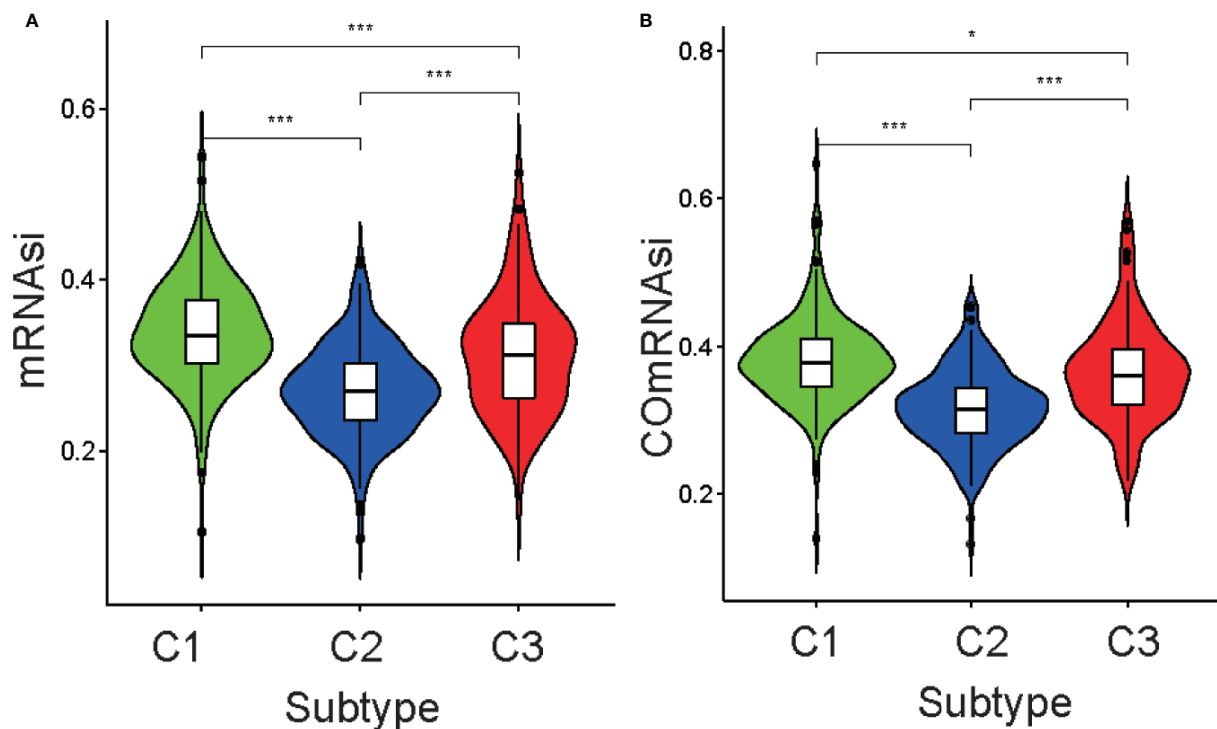


**FIGURE 3 |** Association between the stemness index and the metabolism-associated subtypes. The pairwise comparison of the mRNAasi (**A**) and COMRNAasi (**B**) between three subtypes. The P values are labeled above each boxplot with asterisks (ns represents no significance, \* $P < 0.05$ , \*\* $P < 0.01$ , \*\*\* $P < 0.001$ ).

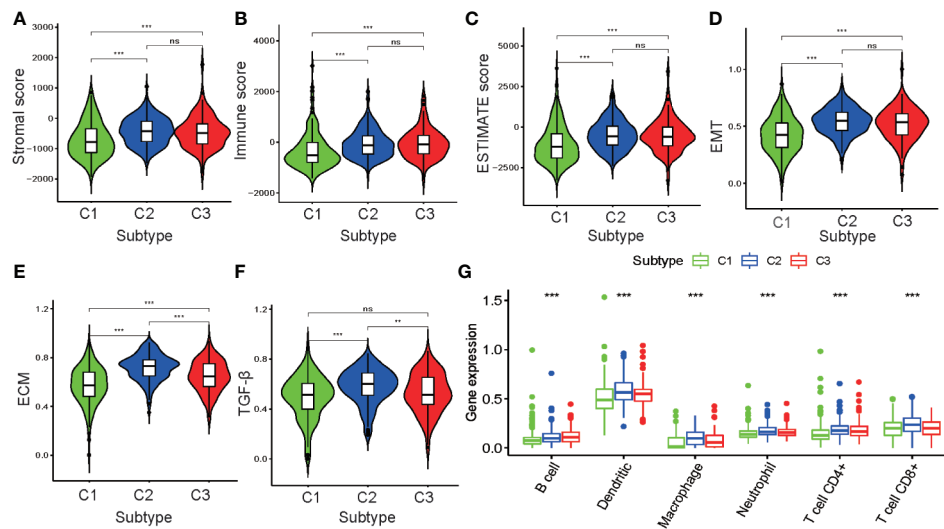


**FIGURE 4 |** Association between the tumor microenvironment and the metabolism-associated subtypes. The pairwise comparison of the stromal score (A), immune score (B), ESTIMATE score (C), ssGSEA score of EMT (D), ssGSEA score of ECM (E), and ssGSEA score of TGF- $\beta$  (F) between three subtypes. (G) The differential analysis of the abundance of immune cells between three subtypes. The P values are labeled above each boxplot with asterisks (ns represents no significance, \*P < 0.05, \*\*P < 0.01, \*\*\*P < 0.001).

subtypes in DNA mutation burdens and patterns of somatic mutation rates. By displaying the 15 genes determined to have the highest frequency of DNA mutations in PRAD in a waterfall plot, we observed remarkably different landscapes for each of the PRAD subtype (Figure 5A). Mutation of *TP53* was the most frequent DNA mutation in cluster C1 and mutation of *SPOP* was the most frequent in cluster C2. These results indicated that the *TP53* mutation was a characteristic mutation of C1 tumors, and the *SPOP* mutation was a characteristic mutation of C2 tumors. The C3 cluster had high mutation rates of both *SPOP* and *TP53*. This may explain why tumors from C3 exhibited a status between those of C1 and C2, regardless of the stemness index or TME analysis.

Tumor mutation burden (TMB) is considered to reflect the sensitivity of tumors to targeted drug therapies (29). To further investigate the features of DNA mutations and clinical treatment options for PRAD subtypes, we compared the differences in the number of DNA mutations among the subtypes. We found that tumors of subtypes C1 and C3 had higher mutation counts than those of subtype C2 (Figure 5B). This further indicated that tumors from C1 and C3 exhibited greater heterogeneity compared to those from C2.

CNV occurring upstream of genes regulates gene expression and influence tumor occurrence and development (30). To further explore whether this DNA element may lead to increased heterogeneity among the metabolism-associated subtypes, we downloaded a list of metabolism-relevant genes (31) and analyzed the number of amplifications and deletions regarding the CNV in these genes. We found that the number of CNV amplifications and deletions was highest in subset C1, followed by that in subset C3, with the fewest being observed in

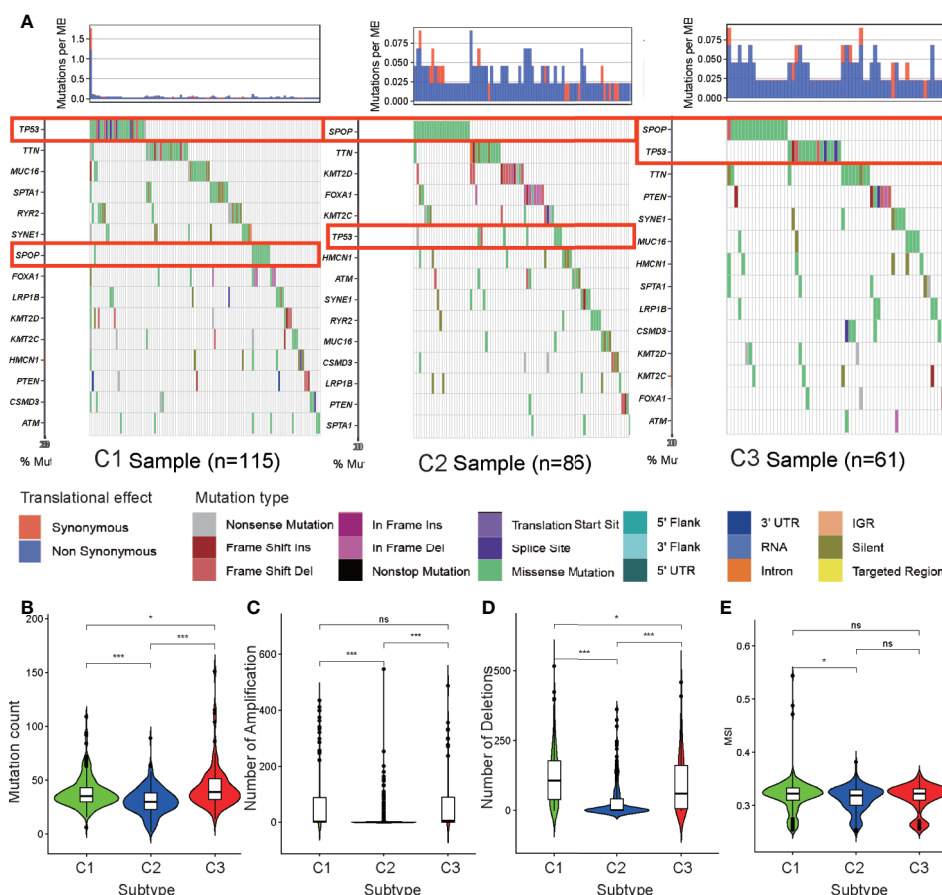
subset C2 (Figures 5C, D). These results suggest that CNV results in significant heterogeneity among the three subtypes.

Previous studies have shown that MSI is a crucial indicator of genome instability and is associated with many genetic diseases (32). In our studies, we obtained level data from MSI of each PRAD sample calculated in a previous study (33) and performed differential analysis. The results indicate that C1 has a higher level of MSI than C2 ( $p < 0.05$ ) (Figure 5E), suggesting that MSI may be the resource of tumor heterogeneity in C1.

## Identification of Metabolism-Associated Signatures

We selected 2,029 metabolism-associated genes among the TCGA PRAD cohort samples and constructed a co-expression network through co-expression analysis (31). Average linkage hierarchical clustering identified five modules. To realize the scale-free co-expression network, a power of  $\beta = 3$  was used (Figure S4A). We then adopted the dynamic hybrid tree cut method to combine highly similar modules using a cutoff value = 0.25 and module size = 50 (Figure S4B). Although we failed to identify a module associated with the C3 subtype, the green and blue modules showed a strong association with C1 and C2 subtypes ( $\text{cor} > 0.3$  or  $< -0.3$ ; Figures 6A and S4C). Ultimately, 489 associated genes were identified, including 388 genes in the blue module and 101 genes in the green module. Of the 489 genes, 84 ( $\text{cor}$  of GS with C1 and C2  $> 0.3$  or  $< -0.3$ ) were determined as metabolism-associated module genes (Figure 6B and Table S3).

To determine the biochemical functions of the metabolism-relevant module genes, we performed GO and KEGG function enrichment analyses. Some metabolic pathways, such as alcohol



metabolic process, sulfur compound metabolic process, cellular modified amino acid metabolic process, phenylalanine metabolism, drug metabolism cytochrome P450, and glutathione metabolism were significantly enriched by these genes (Figures 6C, D; Table S4). This further confirmed that the functions of the selected genes were closely associated with PRAD metabolism.

## Metabolism-Associated Risk Model Development and Validation

Patients with DFS <20 d and those without available DFS information were excluded. A total of 489 patients in the TCGA database were included in the training cohort of this study (Table 2). We performed a univariate Cox regression analysis of the 84 previously selected variables to identify potential optimal prognostic targets. A total of 23 genes that met the prognostic criteria were identified ( $p < 0.05$ ; Table S5). To avoid overfitting of the model. The prognostic biomarkers that highly correlated with one another were first removed using LASSO regression, resulting in six candidate prognostic genes (Figures S5A, B). These six genes were then analyzed using the

multivariate Cox proportional hazards regression method. Finally, metabolism-associated module genes related to DFS of PRAD were identified, including *CACNG4*, *SLC2A4*, *EPHX2*, *CA14*, *NUDT7*, and *ADH5* (Table 3). The formula used for calculating the risk score was as follows:

$$\begin{aligned} \text{Risk score} = & (-0.083 \times \text{FPKM of } CACNG4) \\ & + (-0.0980 \times \text{FPKM of } SLC2A4) \\ & + (-0.0161 \times \text{FPKM of } EPHX2) \\ & + (-0.2182 \times \text{FPKM of } CA14) \\ & + (-0.2055 \times \text{FPKM of } NUDT7) \\ & + (-0.0213 \times \text{FPKM of } ADH5) \end{aligned}$$

To verify the robustness of the risk model, two external cohorts available in the GEO repository, datasets GSE54460 and GSE70768, were obtained and used as validation cohorts. Each cohort was separated into two groups according to the median value of each risk score. To evaluate the differences in prognosis between the high-risk and low-risk groups, a K-M

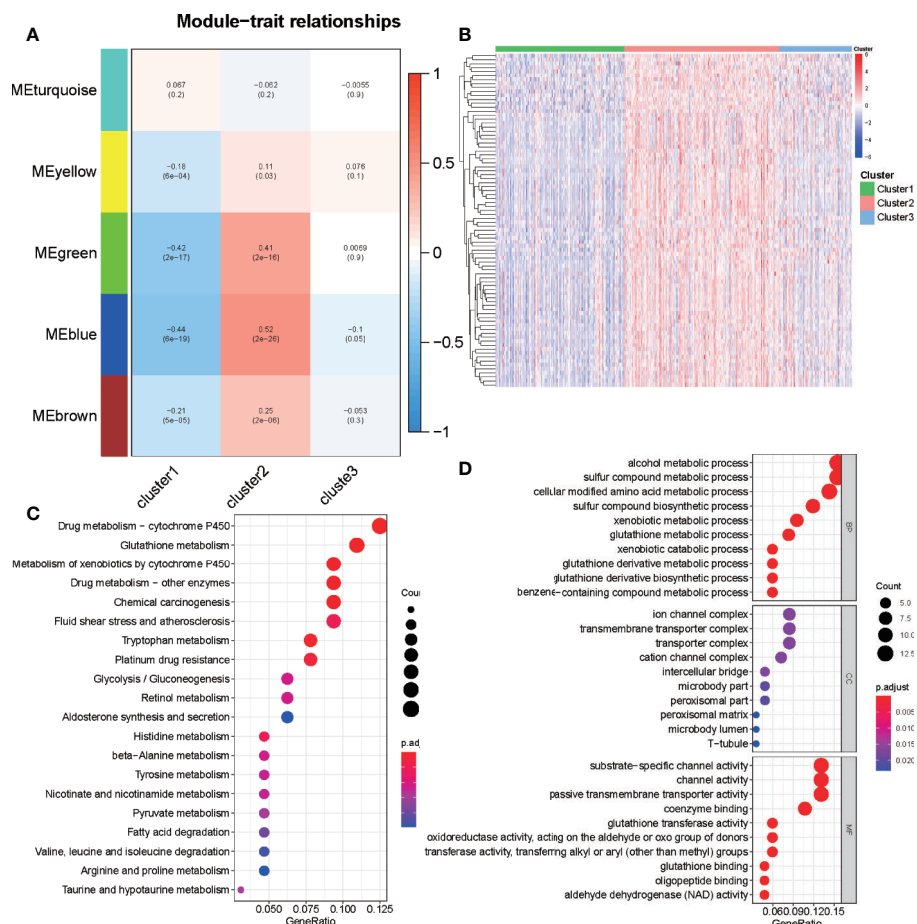


**FIGURE 6 |** Identification of metabolism-associated module genes of PRAD in the WGCNA and the functional enrichment analysis of these genes. **(A)** Heatmap of the correlation between module Eigengenes and metabolism-associated subtypes (C1, C2, and C3). **(B)** Heatmap of 84 metabolism-associated module genes in three subtypes. **(C)** The GO analysis of metabolism-associated module genes. **(D)** The KEGG analysis of metabolism-associated module genes.

**TABLE 2 |** Grouping of PCa patients for survival analysis.

Clinical parameter	Variable	TCGA	GSE 54460	GSE 70768
Recurrence or no	Recurrence	91 (18.61%)	51 (48.11%)	19 (17.11%)
	No recurrence	398 (81.39%)	55 (51.89%)	92 (82.88%)

survival curve was constructed based on the log-rank test. Patients in the high-risk group of the TCGA cohort GSE54460 dataset exhibited poorer outcomes compared to those in the low-risk group ( $p < 0.05$ ; **Figures 7A, B**). As for the GSE70768 cohort, the arrangement characteristic of microarray data differed from RNA-seq data. Therefore, we divided the cohort according to most cutoff value, which was calculated using X-tile, and found there was a significantly different prognosis between the high-risk and low-risk groups (**Figure 7C**). We used a time-dependent ROC curve to investigate the predictive accuracy of our model and determined the AUC of the prognostic model using the TCGA training cohort was 0.769 at one year, 0.702 at three years, and 0.705 at five years (**Figure 7D**). For the testing cohorts, the AUC of the prognostic model for the GSE54460

cohort was 0.703 at one year, 0.709 at three years, and 0.665 at five years and 0.668 at one year, 0.644 at three years, and 0.628 at five years for the GSE70768 cohort (**Figures 7E, F**).

## Identification of Risk Model Biomarkers Biological Functions and Construction of Nomogram

GSEA analysis was performed to explore the biological functions of the risk model genes. The results indicated the genes had a significant relationship with cell cycle, DNA replication, homologous recombination, RNA degradation, and spliceosome pathways in the high-risk group and with beta alanine metabolism, dilated cardiomyopathy, drug metabolism cytochrome P450, metabolism of xenobiotics by cytochrome\_P450, and vascular



**TABLE 3 |** Risk genes in the prognostic risk model.

GENE	Coef	HR	HR.95L	HR.95H	P value
CACNG4	-0.00837	0.991664	0.96811	1.015792	0.49494
SLC2A4	-0.09798	0.906668	0.768444	1.069754	0.245648
EPHX2	-0.01612	0.984005	0.960761	1.007812	0.18618
CA14	-0.21817	0.803992	0.352487	1.833836	0.604063
NUDT7	-0.20554	0.814211	0.501774	1.321193	0.405298
ADH5	-0.02131	0.978912	0.95889	0.999352	0.043232

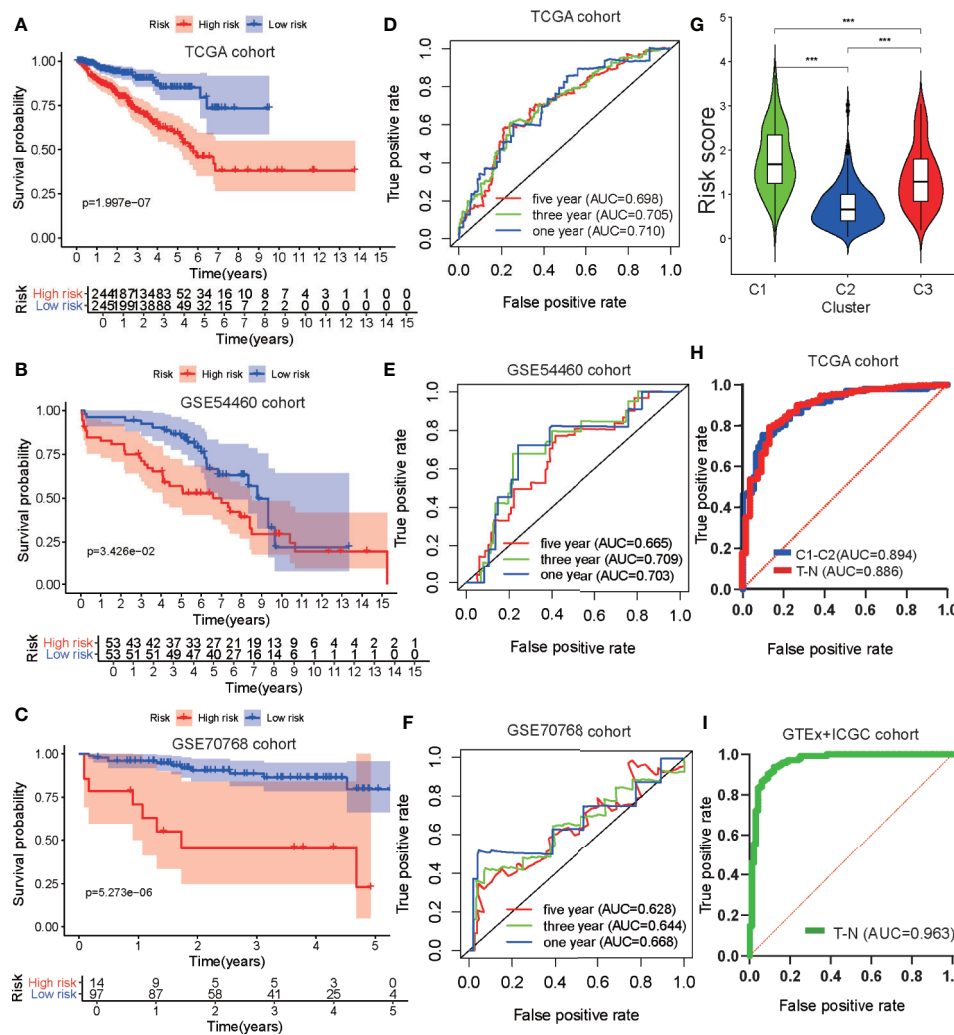


**FIGURE 7 |** Development and validation of the metabolism-associated risk model. Kaplan-Meier curve analysis of high-risk the low-risk groups in the TCGA cohort (A), in the GSE54460 cohort (B), and in the GSE70768 cohort (C). Time-dependent ROC curve analysis of the prognostic model in the TCGA cohort (D), in the GSE54460 cohort (E), and in the GSE70768 cohort (F). (G) The differential analysis of risk score between three subtypes in PRAD. The P values are labeled above each boxplot with asterisks (ns represents no significance, \* $P < 0.05$ , \*\* $P < 0.01$ , \*\*\* $P < 0.001$ ). (H) ROC curve analysis of risk score to predict sample types (tumor and normal tissue) and metabolism-associated subtypes (C1 and C2) in TCGA. (I) ROC curve analysis of risk score to predict sample types (tumor and normal tissue) in GTEx and ICGC cohorts.

smooth muscle contraction pathways in the low-risk group (Figures S5C, D; Table S6). This suggested our risk model genes influenced these pathways and that these pathways may impact PRAD DFS.

We then explored the relationship between clinical/metabolism-associated subtypes and risk scores and found there was a close relationship between risk score and age/Gleason score/T stage/N stage/metabolism-associated subtypes

(Figures S5E–H and Figure 7G). This suggested that our risk model had predictive value, not only in PRAD DFS, but also in tumor size, lymphatic node metastasis, and metabolism-associated subtype. Meanwhile, when we used ROC to determine whether our risk model could predict sample type (tumor vs. normal tissue) and metabolism-associated subtypes (C1 vs. C2), we observed that the AUC values of the risk model were 0.886 and 0.894, respectively, in TCGA cohort (Figure 7H). To determine the diagnostic value of our model, we used ROC to evaluate samples from the external group (GTEx and ICGC) and found that there was an outstanding predictor value for PCa diagnosis with our model (AUC = 0.963) (Figure 7I and Table 4).

Finally, we selected clinical variates with independent prognostic value to obtain a nomogram through univariate and multivariate Cox analyses (Figure S5I and Table S7). ROC analysis and C-index calculation assessed the clinical meaning of the nomogram and suggested that the clinical nomogram had a better net benefit than clinical variate or risk score only models (Figures S5J, K).

To determine the diagnostic and prognostic value of a single risk model gene, we performed differential analyses of six risk

model genes between different types, Gleason score, T- and N stage of samples, and K–M analyses of each risk model gene in the TCGA cohort. The findings indicated that six risk model genes have differing expression levels between normal and tumor tissue, and different Gleason score samples. Simultaneously, there was a significant difference in prognosis between PRAD patients with high-risk and low-risk model gene expression (Figures 8A–D and Figures S6A–F).

To confirm whether there was a differential abundance of proteins associated with the selected genes between normal prostate tissues and tumor tissues of patients with PRAD, we downloaded IHC micrographs from the HPA database. Three of the six risk model genes were found to exhibit differential staining between normal prostate tissue and PRAD tissue, those being *EPHX2*, *NUDT7*, and *ADH5* (Figures S7A–C). The results suggested that the expression of these proteins was decreased in PRAD tissues. This was in accordance with the differential analysis of expression for the six risk model genes of the TCGA cohort and further indicated these genes might play crucial roles in the occurrence and development of PRAD.

## Drug Sensibility Analysis With Metabolism-Associated Subtypes and Risk Model

Anti-androgen treatment is the first non-surgical treatment for PRAD (34). It has been shown that the level of the androgen receptor (AR) gene expression in tumor tissue is closely related to anti-androgen treatment sensitivity (35). Therefore, we also compared the expression levels of AR in the three subtypes and

**TABLE 4 |** Grouping of PCa patients for diagnostic analysis.

Clinical parameter	Variable	TCGA	GTEx + ICGC
Normal or tumor tissue	Normal	52 (10.60%)	100 (40.98%)
	Tumor	499 (89.40%)	144 (59.02%)

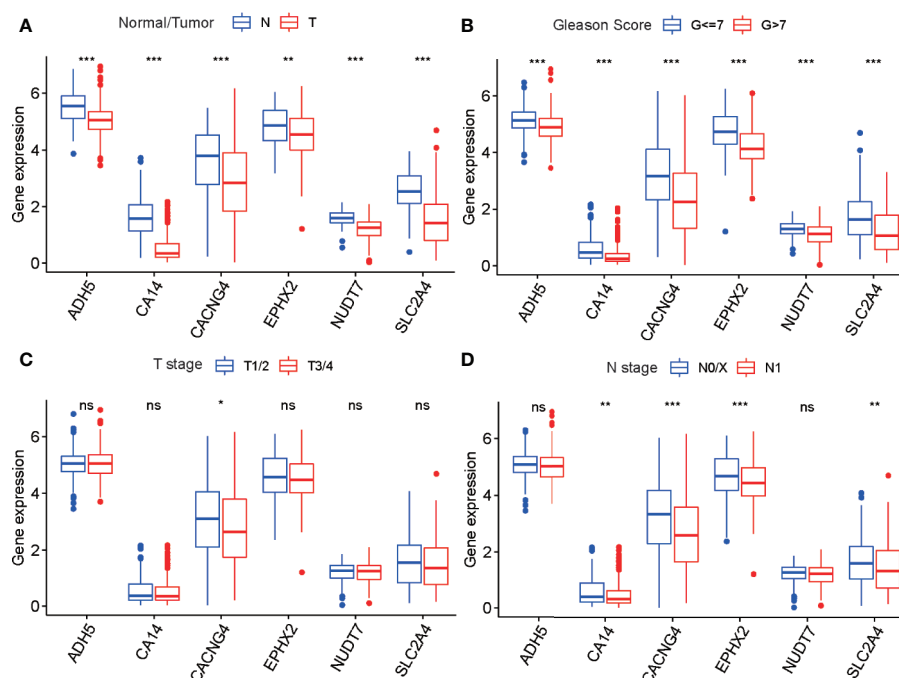


**FIGURE 8 |** The differential analysis of six risk model genes between PRAD tissue and normal prostate tissue (A), different Gleason score PRAD samples (B), different Primary Tumor (T) stage samples (C), and different Lymph Nodes (N) stage samples (D) in TCGA cohort. The P values are labeled above each boxplot with asterisks (ns represents no significance, \*P < 0.05, \*\*P < 0.01, \*\*\*P < 0.001).

found that tumors from C1 and C3 had higher AR expression levels than those from C2 (**Figure 9A**). This indicates that patients from C1 and C3 may be more sensitive to anti-androgen treatment than those from C2, and that there existed considerable tumor heterogeneity among the subtypes.

For castration-resistant prostate cancer, immunotherapy and chemotherapy are the preferred treatments. To explore the sensitivity of each cluster subtype to immunotherapies, we collected data for 14 immune checkpoints and compared the gene expression levels of these proteins. Significant differences in gene expression of the checkpoint proteins among the three

subtypes were observed, except for CTLA4 and IL1A. Cluster C1 exhibited lower expression of most the checkpoint genes relative to that cluster C2 and C3 (**Figure 9B**), which is in accordance with the immune infiltration status described above. Therefore, we were able to determine that tumors of the C1 subtype demonstrated lower immune infiltration and may, therefore, garner fewer benefits from treatment with immunotherapies.

Then, to evaluate the association between drug sensitivity and the metabolism-associated risk model, correlation analysis was performed using half-inhibitory concentration (IC<sub>50</sub>) of chemotherapeutic drugs, risk score, and gene expression data

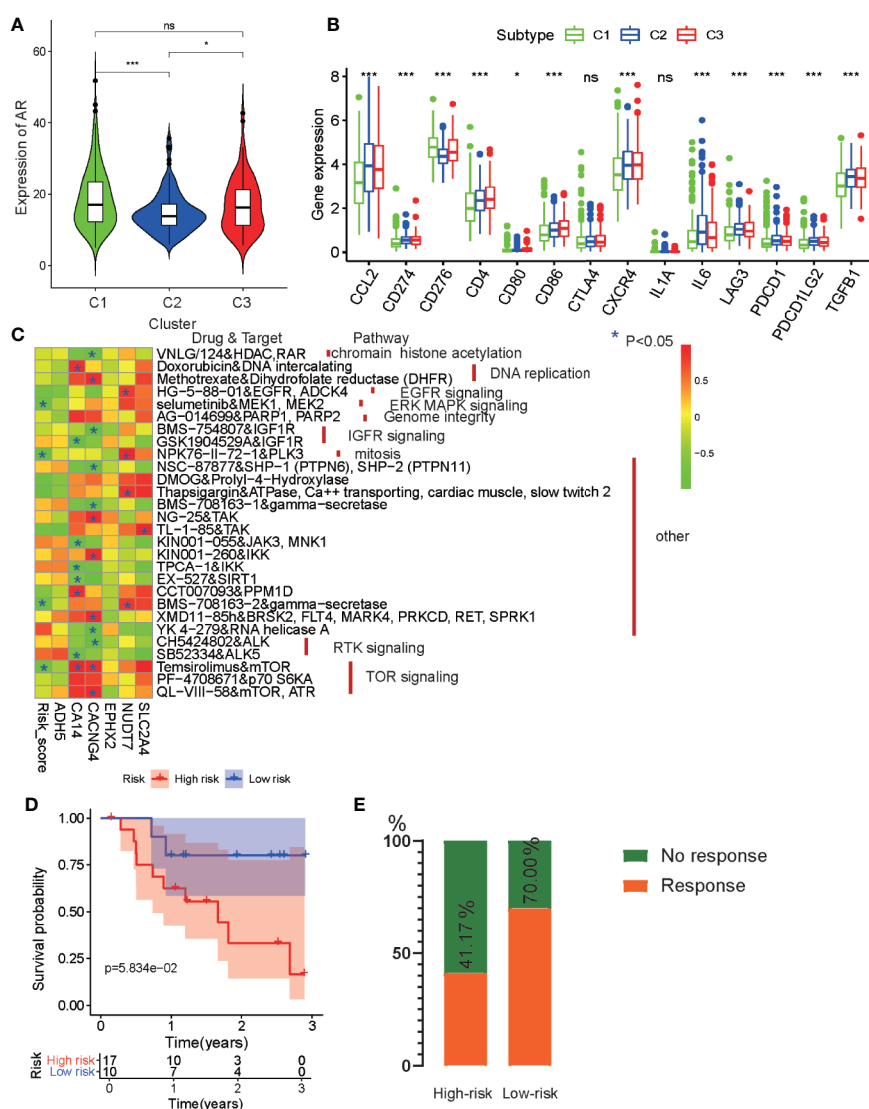


**FIGURE 9** | Drug sensibility analysis with metabolism-associated subtypes and risk model. **(A)** The pairwise comparison of the androgen receptor (AR) expression between three subtypes. **(B)** The differential analysis of the expression of 14 checkpoints between three subtypes. The P values are labeled above each boxplot with asterisks (ns represents no significance, \*P < 0.05, \*\*P < 0.01, \*\*\*P < 0.001). **(C)** Heatmap for correlation between drug sensitivity and expression levels of six risk model genes. \*p < 0.05. **(D)** Survival analyses for low-risk and high-risk scores patient groups in the anti-PD1 immunotherapy cohort using Kaplan-Meier curves. **(E)** The proportion of patients with response to PD-1 blockade immunotherapy in low-risk or high-risk scores groups.

from six PCa cell lines obtained from the GDSC database. As a result, four anti-tumor drugs (selumetinib, NPK76-11-72-1, BMS-708163, and temsirolimus) were negatively correlated with risk score (**Figure 9C** and **Table S8**). Among the six genes, CA14, CACNG4, and NUDT7 had associations with more than four drugs, indicating that these genes and risk scores may guide chemotherapy in drug choice.

Finally, immunotherapies represented by PD-L1 and PD-1 blockades have undoubtedly emerged as a breakthrough in cancer therapy (36, 37). We explored whether our risk model could predict patient responses to immune checkpoint blockade therapy based on the anti-PD-1 cohort (GSE78220). First, we performed K-M survival analysis and found that melanoma patients with high-risk scores had shorter OS than patients with low-risk scores, although no significant difference was observed ( $p = 0.058$ ) (**Figure 9D**). The proportion of beneficiaries with anti-PD-1 treatment in the high-risk cohort (41.17%) was lower than that of the low-risk cohort (70%) (**Figure 9E**). These results implied that patients with low-risk scores would get more benefits from immunotherapy than patients with high-risk scores.

## DISCUSSION

With the development of RNA-seq technology, many classical analyses based on gene expression data have been reported for most cancers (6, 38–40). However, few cluster studies have been performed on PCa to explore the tumor metabolic characteristics. Thus, we identified in our current work a metabolism-associated PRAD classification based on ssGSEA and 41 metabolic pathway gene sets. The PRAD cases included in the study were divided into three subtypes. The metabolic features, clinical characteristics, prognosis, TME, stemness index, DNA mutation, CNV, and MSI were then investigated in the different subtypes. Subtype C1 exhibited low metabolic levels and was similar to high-grade PCa with high tumor purity and low immune infiltration. Furthermore, patients from C1 had worst prognosis and the shortest DFS among the patients with PCa. In comparison, patients from C2 displayed high metabolic levels in most pathways and were similar to low-grade PCa with low tumor purity, low stemness index, and high immune cell infiltration. Patients with tumors from C2 had the best prognosis and longest DFS among the patients with PCa. Patients from C3 represented a medium state between the findings for those from C1 and C2 and demonstrated similar medium-grade PCa. Specifically, C3 had highly metabolic pathways activity and the highest stemness index. Accordingly, we believe there may be some connections between starch/sucrose/porphyrin/chlorophyll metabolism and a high stemness index.

Cancer stem cells play important roles in therapeutic responses and the progression of cancer (41). To further explore the reason C1 subset has the worst prognosis, we continued investigating the stem index between three subtypes. C1 and C3 had higher stemness indices, which indicates more

malignant tumors from these subsets compared to those from C2. This may partly explain why patients with PCa from subsets C1 and C3 presented with shorter DFS and worse prognosis compared to that of patients from subset C2. These results indicate a remarkable tumor heterogeneity among PRAD metabolism-associated subtypes. However, the reason for C3 tumors having the highest ssGSEAs is unclear. In previous studies, starch and sucrose metabolism is associated with the progression of colon cancer (42). Therefore, we believe that specific metabolic pathways, such as those for starch/sucrose/porphyrin/chlorophyll metabolism, have crucial roles in tumor progression. This hypothesis needs to be tested using *in vitro* experiments and single-cell sequencing.

TME is a remarkable factor impacting the occurrence and development of PCa. Many cancer-promoting factors play a role in the EMT pathway (43). For instance, the expression of PDL1 can affect the prognosis of adrenocortical carcinoma (44). Regardless of stromal or immune cells, the C2 and C3 subtypes displayed more characteristics of TME. Stromal scores indicated that C2 and C3 had greater stromal cell content than C1. ECM functions as cell scaffoldings and can induce EMT in stromal cells, with the TGF- $\beta$  pathway having a strong connection with this process (45). To further explore the features of stromal cells in PCa, ECM, EMT, and TGF- $\beta$ , ssGSEA scores were calculated for each gene set. Differential analysis suggests that C2 had the most significant activity in this process. EMT often has a close relationship with cell cancer and poor prognosis (46–48); however, C2 had the best prognosis among the three subtypes. Therefore, we believe that EMT does not have an obvious cancer-promoting function in PCa. As for the increase of EMT in C2, we believe this phenomenon was the result of increased stromal cell content in C2. The immune system is the most important anti-cancer system in the body (49). In a previous study, immune cells were found to be strongly lethal in fighting tumor cells. Natural killer cells can kill lung cancer tumor cells and are regulated by TME (50). Additional support that the immune system is important is demonstrated by T cells being able to be used in clinical settings for the treatment of cancer (51). Herein, our study shows that the levels of all immune cells (B cells, dendritic cells, macrophages, neutrophils, CD4+ T cells, and CD8+ T cells) were increased in C2, indicating that tumors from C2 were in a state of immune activation. We believe this is the reason C2 had the best prognosis among the three subtypes.

TMB is presumed to have a close relationship with tumor heterogeneity (52). *TP53* is the most prominent gene in pan-cancer investigations. For instance, *TP53* mutations lead to high-grade cancer and tumor heterogeneity of ovarian granulosa (53). At the same time, mutations in *TP53* were shown to be strongly associated with the occurrence and progression of PCa (54). *SPOP* mutations have also been considered for their impact on castration sensitivity in PCa (55). Gene mutation spectra were significantly different among the three metabolism-associated subtypes in our current study. For instance, in C1, the *TP53* mutation rate was higher than that of others, whereas C2 had a high mutation rate of *SPOP*. This indicates that the tumor features of C1 and C2 partly result from *TP53* and *SPOP*



mutations, respectively. C3 had high mutation rates of both *TP53* and *SPOP*, which further supported that C3 exhibited an intermediate state between C1 and C2. Meanwhile, many studies have investigated CNV in PCa, with the results indicating that CNV can affect tumor features and heterogeneity (56). MSI also has been regarded as a vital factor in DNA mismatches and can improve tumor heterogeneity in many types of cancer. Herein, we show that there is a significant difference in CNV of metabolic genes and MSI levels among the three subtypes. Our current work revealed that there was a significant difference in CNV of metabolic genes among the three subtypes. C1 had the highest number of amplifications and deletions. This indicates that the *TP53* mutation, *SPOP* mutation, and increased CNV and MSI were key factors contributing to the tumor heterogeneity observed among the subtypes.

A general opinion regarding tumor cells with high activity levels of one or more specific metabolic pathways is that they have a stronger capacity for invasion, proliferation, and self-renewal compared to cells with low metabolic activity. For instance, higher sulfur amino acid metabolic levels in liver cancer can accelerate the EMT process and cancer cell migration (57). Aldehyde oxidase 1 decreases the metabolic level and displays tumor inhibition activity in bladder cancer (58), whereas long intergenic non-coding RNA-nucleotide metabolism regulator upregulates nucleotide metabolism and increase the proliferation of tumor cells (59). Our results partly contradict these views in that we found tumors from C1 with the lowest metabolic activity level had the worst prognosis in patients with PCa. The samples from patients with PCa were mixed tissues, including tumor cells, normal prostate cells, stromal cells, and immune cells. Tumor malignancy was determined based on several factors, including tumor purity, tumor proliferation ability, and the TME *in vivo*. Thus, our results differed in part from those concluded *in vitro*, where tumor malignancy was determined by the tumor cells only. Normal prostate cells are smooth muscle cells that exhibit high metabolic levels, whereas tumor cells may show lower levels of metabolic activity compared to normal prostate cells. Meanwhile, ssGSEA scores based on mRNA-seq data from second-generation sequencing reflects the metabolic level of the whole sample, rather than only tumor cells. Therefore, in this study, we determined a lower metabolic level, and that greater tumor heterogeneity of the PCa samples was associated with a worse prognosis for the patient. This was in accordance with that reported for liver cancer (60). These specifications may partly explain why tumors from the C1 subset had the worst prognosis in PCa.

According to the above subtype analyses, we consider that C2 is the subtype that characterizes early PCa. In fact, during the early stage, the tumor metabolic status often resembles that of normal tissue. Besides, during the initial stage, the immune system exerts a strong anti-tumor response, and the tumor has low heterogeneity and stemness index. On the contrary, due to immune escape and the decrease of blood supply in the later stage of tumor progression, immune cells are not able to infiltrate the tumor. Thus, C1 has milder immune characteristics than C2.

Nevertheless, because C1 is an advanced tumor, it had the highest tumor heterogeneity and the lowest metabolic status among the three subtypes. As for C3, which is regarded as an intermediate between C1 and C2, we consider it to be the crucial status of PCa from early to advanced tumor stage. The unique metabolic pathways of C3 reportedly affect the malignant transformation of healthy tissue.

To predict prognosis, previous studies have developed prognostic risk models for PCa based on gene expression data (61–63). This indicates that risk models based on high-throughput data may accurately predict the prognosis of PCa. Therefore, we used WGCNA to identify the characteristic genes of C1 and C2. Using multiple algorithms, a six-gene risk model, including *CACNG4*, *SLC2A4*, *EPHX2*, *CA14*, *NUDT7*, and *ADH5*, was established using the TCGA cohort. Through the testing of four external datasets, our metabolism-associated risk model was demonstrated to have strong robustness. GSEA analysis provided further evidence that our risk genes are related to PCa metabolism. Finally, we combined risk score and clinical variates to obtain a nomogram to help clinicians predict the DFS for PCa patients.

Many studies have demonstrated that gene expression data can be used to predict drug treatment sensitivity. For instance, molecular profiling can be used to identify treatment-refractory metastatic castration-resistant prostate cancer (64). C1 had the highest AR expression. This indicates that C1 may exhibit high sensitivity to anti-androgenic therapy. With a high expression of immune checkpoints and significant features of immune cell infiltration, C2 tumors may benefit more from immune-targeted therapy, whereas C3, with an active status of specific drug metabolism pathways, may facilitate the development of tolerance to traditional chemotherapy (65). In the drug sensitivity analysis of the risk model, our study suggests that patients with low-risk scores may benefit more from anti-PD-1 treatment, and this is consistent with C2 being more suitable for immune target therapy. All of these conclusions need to be validated *in vitro*.

In contrast to previous research that focused on the metabolic level of single tumor cell types, we explored the metabolic features of mixed cancer samples. We first investigated the characteristics of metabolic pathways using cluster analysis and explored tumor heterogeneity in multiple dimensions employing multi-omics. Finally, our risk model of PCa was constructed and verified using a large number of samples and multiple datasets. However, our research also had limitations. First, the data we studied were from public databases rather than our database. Second, we did not perform *in vitro* or *in vivo* experiments to further investigate the mechanism of metabolism-associated genes in PCa. These are what we plan to do next.

## CONCLUSIONS

Three metabolism-associated subtypes were first identified by unsupervised cluster and ssGSEA analyses in PCa. Differential analyses indicated these subtypes could reflect tumor

heterogeneity in the stemness index, tumor microenvironment, TMB, CNV, MSI, and clinical features. So our metabolism-associated subtypes can better represent the metabolic characteristics of PCa and can be beneficial in exploring the metabolic mechanism of occurrence and development of PCa. Meanwhile, a six-gene metabolism-associated risk score model by using four separate datasets and demonstrated strong robustness in the prediction of sample types (tumor and normal tissue), DFS, metabolism-associated subtypes, and anti-tumor therapeutic effect. Therefore our model can powerfully help clinicians evaluate the prognosis and develop personalized treatment for PCa patients. Although the six prognostic markers still require experimental verification, they may provide insight and a prospect for further investigation and clinical work regarding PCa.

## DATA AVAILABILITY STATEMENT

Publicly available datasets were analyzed in this study. This data can be found here: <https://portal.gdc.cancer.gov/> (PRAD); <https://www.ncbi.nlm.nih.gov/gds/> (GSE54460, 70768, 78220); <https://www.cancerrxgene.org/> (22RV1, DU-145, LNCaP-Clone-FGC, PC-3, PWR-1E, and VCaP); <https://www.gtexportal.org/> (Prostate); [https://icgc.org/\(PRAD\)](https://icgc.org/(PRAD)).

## AUTHOR CONTRIBUTIONS

YZ designed the study and analyzed the data. YZ and RZ revised the images. YZ, RZ, and FL performed the literature search and collected data for the manuscript. XL and LZ revised the manuscript. All authors contributed to the article and approved the submitted version.

## FUNDING

This work was supported by the National Natural Science Foundation of China (No. 81771768).

## ACKNOWLEDGMENTS

The authors thank all the patients who participated in the study.

## SUPPLEMENTARY MATERIAL

The Supplementary Material for this article can be found online at: <https://www.frontiersin.org/articles/10.3389/fonc.2020.598801/full#supplementary-material>

**SUPPLEMENTARY FIGURE 1** | The PAM analysis of ssGSEA score based on metabolism-associated pathways. (A) Consensus among clusters for each category number K. Color-coded heatmap corresponding to the consensus matrix

for  $k = 2$  (B),  $K = 3$  (C),  $K = 4$  (D),  $K = 5$  (E), and  $K = 6$  (F) obtained by applying consensus clustering.

**SUPPLEMENTARY FIGURE 2** | Association between clinical characteristics and the metabolism-associated subtypes. Age (A) and Lymph Nodes (N) stage (B) for each metabolism-associated subtype in the TCGA cohort. (C) The pairwise comparison of the PSA between three subtypes. The P values are labeled above each boxplot with asterisks (ns represents no significance, \* $P < 0.05$ , \*\* $P < 0.01$ , \*\*\* $P < 0.001$ ).

**SUPPLEMENTARY FIGURE 3** | Association between the stemness index and the metabolism-associated subtypes. The pairwise comparison of the ssGSEA (A) and COSSGSEA (B) between three subtypes. The P values are labeled above each boxplot with asterisks (ns represents no significance, \* $P < 0.05$ , \*\* $P < 0.01$ , \*\*\* $P < 0.001$ ). (C) The correlation analysis between specific metabolic pathways of C3 and ssGSEA in the TCGA cohort.

**SUPPLEMENTARY FIGURE 4** | The WGCNA analysis of metabolism-associated genes among three subtypes. (A) Analysis of the scale-free fit index and the mean connectivity for various soft-thresholding powers, and checking the scale-free topology when  $\beta = 3$ . K represents the logarithm of whole network connectivity,  $p(k)$  represents the logarithm of the corresponding frequency distribution. K is negatively correlated with  $p(k)$  (correlation coefficient = 0.88), which represents scale-free topology. (B) Identification of a co-expression module in PCa. The branches of the cluster dendrogram correspond to the five different gene modules. Each piece of the leaves on the cluster dendrogram corresponds to a gene. (C) Scatter plot of module eigengenes in the blue and green modules.

**SUPPLEMENTARY FIGURE 5** | Identification of risk model functions and development of the nomogram. (A, B) prognostic genes selected through Lasso regression. (C, D) Enrichment plots of the top five KEGG pathways in the high-risk score and low-risk score groups in PRAD. The relationship between the age (E)/Gleason score (F)/N stage (G)/T stage (H) and risk score in the TCGA cohort. (I) Nomogram for predicting the probability of 1, 3, and 5 disease-free survival times for PCa patients. (J) ROC analysis for nomogram in 1, 3, and 5 years. (K) The C-index analysis for clinical variates, risk model, and nomogram.

**SUPPLEMENTARY FIGURE 6** | The K-M survival analysis of six risk model genes. (A) ADH5. (B) CA14. (C) CACNG4. (D) EPHX2. (E) NUDT7. (F) SLC2A4.

**SUPPLEMENTARY FIGURE 7** | The protein expression of three risk model genes in normal prostate tissues and PRAD tissues from the Human Protein Atlas (HPA) database. (A) ADAH5. (B) EPHX2T. (C) NUDT7N.

**SUPPLEMENTARY TABLE 1** | The 41 metabolism pathway gene sets collected to evaluate the metabolic status of PRAD samples.

**SUPPLEMENTARY TABLE 2** | The ssGSEA score of each sample of PRAD in TCGA based on metabolic pathways, stem cell, EMT, ECM, and TGF- $\beta$  gene sets.

**SUPPLEMENTARY TABLE 3** | The WGCNA analysis between the expression of metabolism-associated genes and metabolism-associated subtypes in PRAD.

**SUPPLEMENTARY TABLE 4** | The GO and KEGG functional enrichment analysis of metabolism-associated module genes.

**SUPPLEMENTARY TABLE 5** | The Univariable Cox analysis of metabolism-associated prognostic genes.

**SUPPLEMENTARY TABLE 6** | The GSEA analysis of risk score in TCGA.

**SUPPLEMENTARY TABLE 7** | The Univariable and Multivariable Cox analysis of clinical variates and risk score.

**SUPPLEMENTARY TABLE 8** | Drug sensitivity analysis of risk model genes and risk score.

## REFERENCES

1. Ferlay J, Ervik M, Lam F, Colombet M, Mery L, Piñeros M, et al. *Global Cancer Observatory: Cancer Today*. Lyon, France: International Agency for Research on Cancer (2018). Available at: <https://gco.iarc.fr/today>.
2. Culp MB, Soerjomataram I, Efstathiou JA, Bray F, Jemal A. Recent Global Patterns in Prostate Cancer Incidence and Mortality Rates. *Eur Urol* (2020) 77:38–52. doi: 10.1016/j.eururo.2019.08.005
3. Nassar ZD, Mah CY, Dehairs J, Burvenich IJ, Irani S, Centenera MM, et al. Human DECR1 is an androgen-repressed survival factor that regulates PUFA oxidation to protect prostate tumor cells from ferroptosis. *Elife* (2020) 9: e54166. doi: 10.7554/eLife.54166
4. Franko A, Shao Y, Heni M, Hennenlotter J, Hoene M, Hu C, et al. Human Prostate Cancer is Characterized by an Increase in Urea Cycle Metabolites. *Cancers (Basel)* (2020) 12(7):1814. doi: 10.3390/cancers12071814
5. Song B-N. Identification of an immunotherapy-responsive molecular subtype of bladder cancer. *EBioMedicine* (2019) 50:238–45. doi: 10.1016/j.ebiom.2019.10.058
6. Chen W, Zhuang J, Wang PP, Jiang J, Lin C, Zeng P, et al. DNA methylation-based classification and identification of renal cell carcinoma prognosis subgroups. *Cancer Cell Int* (2019) 19:185. doi: 10.1186/s12935-019-0900-4
7. Xiao H, Wang J, Yan W, Cui Y, Chen Z, Gao X, et al. GLUT1 regulates cell glycolysis and proliferation in prostate cancer. *Prostate* (2018) 78:86–94. doi: 10.1002/pros.23448
8. Cerami E, Gao J, Dogrusoz U, Gross BE, Sumer SO, Aksoy BA, et al. The cBio cancer genomics portal: an open platform for exploring multidimensional cancer genomics data. *Cancer Discovery* (2012) 2:401–404. doi: 10.1158/2159-8290.CD-12-0095
9. Bhattacharya S, Andorf S, Gomes L, Dunn P, Schaefer H, Pontius J, et al. ImmPort: disseminating data to the public for the future of immunology. *Immunol Res* (2014) 58:234–239. doi: 10.1007/s12026-014-8516-1
10. Subramanian A, Tamayo P, Mootha VK, Mukherjee S, Ebert BL, Gillette MA, et al. Gene set enrichment analysis: a knowledge-based approach for interpreting genome-wide expression profiles. *Proc Natl Acad Sci USA* (2005) 102:15545–15550. doi: 10.1073/pnas.0506580102
11. Ogata H, Goto S, Sato K, Fujibuchi W, Bono H, Kanehisa M. KEGG: Kyoto Encyclopedia of Genes and Genomes. *Nucleic Acids Res* (1999) 27:29–34. doi: 10.1093/nar/27.1.29
12. Wilkerson MD, Hayes DN. ConsensusClusterPlus: a class discovery tool with confidence assessments and item tracking. *Bioinformatics* (2010) 26:1572–1573. doi: 10.1093/bioinformatics/btq170
13. Malta TM, Sokolov A, Gentles AJ, Burzykowski T, Poisson L, Weinstein JN, et al. Machine Learning Identifies Stemness Features Associated with Oncogenic Dedifferentiation. *Cell* (2018) 173:338–54.e15. doi: 10.1016/j.cell.2018.03.034
14. Miranda A, Hamilton PT, Zhang AW, Pattnaik S, Becht E, Mezheyeuski A, et al. Cancer stemness, intratumoral heterogeneity, and immune response across cancers. *Proc Natl Acad Sci USA* (2019) 116:9020–9. doi: 10.1073/pnas.1818210116
15. Yoshihara K, Shahmoradgol M, Martínez E, Vegesna R, Kim H, Torres-García W, et al. Inferring tumour purity and stromal and immune cell admixture from expression data. *Nat Commun* (2013) 4:2612. doi: 10.1038/ncomms3612
16. Botia JA, Vandrovicova J, Forabosco P, Guelfi S, D'Sa K United Kingdom Brain Expression Consortium, et al. An additional k-means clustering step improves the biological features of WGCNA gene co-expression networks. *BMC Syst Biol* (2017) 11:47. doi: 10.1186/s12918-017-0420-6
17. Langfelder P, Horvath S. WGCNA: an R package for weighted correlation network analysis. *BMC Bioinf* (2008) 9:559. doi: 10.1186/1471-2105-9-559
18. Yu G, Wang L-G, Han Y, He Q-Y. clusterProfiler: an R package for comparing biological themes among gene clusters. *OMICS* (2012) 16:284–7. doi: 10.1089/omi.2011.0118
19. Friedman J, Hastie T, Tibshirani R. Regularization Paths for Generalized Linear Models via Coordinate Descent. *J Stat Softw* (2010) 33:1–22.
20. Simon N, Friedman J, Hastie T, Tibshirani R. Regularization Paths for Cox's Proportional Hazards Model via Coordinate Descent. *J Stat Softw* (2011) 39:1–13. doi: 10.18637/jss.v039.i05
21. Mogensen UB, Ishwaran H, Gerds TA. Evaluating Random Forests for Survival Analysis using Prediction Error Curves. *J Stat Softw* (2012) 50:1–23. doi: 10.18637/jss.v050.i11
22. Tikkinen KAO, Dahm P, Lytvyn L, Heen AF, Vernooij RWM, Siemieniuk RAC, et al. Prostate cancer screening with prostate-specific antigen (PSA) test: a clinical practice guideline. *BMJ* (2018) 362:k3581. doi: 10.1136/bmj.k3581
23. Lytle NK, Barber AG, Reya T. Stem cell fate in cancer growth, progression and therapy resistance. *Nat Rev Cancer* (2018) 18:669–680. doi: 10.1038/s41568-018-0056-x
24. Wang L, Zi H, Luo Y, Liu T, Zheng H, Xie C, et al. Inhibition of Notch pathway enhances the anti-tumor effect of docetaxel in prostate cancer stem-like cells. *Stem Cell Res Ther* (2020) 11:258. doi: 10.1186/s13287-020-01773-w
25. Qian J, Olbrecht S, Boeckx B, Vos H, Laoui D, Etioglu E, et al. A pan-cancer blueprint of the heterogeneous tumor microenvironment revealed by single-cell profiling. *Cell Res* (2020) 30(9):745–62. doi: 10.1038/s41422-020-0355-0
26. Chen Q, Gu M, Cai Z-K, Zhao H, Sun S-C, Liu C, et al. TGF- $\beta$ 1 promotes epithelial-to-mesenchymal transition and stemness of prostate cancer cells by inducing PCBP1 degradation and alternative splicing of CD44. *Cell Mol Life Sci* (2020) doi: 10.1007/s00018-020-03544-5
27. Li N, Kang Y, Wang L, Huff S, Tang R, Hui H, et al. ALKBH5 regulates anti-PD-1 therapy response by modulating lactate and suppressive immune cell accumulation in tumor microenvironment. *Proc Natl Acad Sci USA* (2020) 117(33):20159–170. doi: 10.1073/pnas.1918986117
28. Goliwas KF, Deshane JS, Elmetts CA, Athar M. Moving Immune Therapy Forward Targeting TME. *Physiol Rev* (2020). doi: 10.1152/physrev.00008.2020
29. Rizvi NA, Hellmann MD, Snyder A, Kvistborg P, Makarov V, Havel JJ, et al. Cancer immunology. Mutational landscape determines sensitivity to PD-1 blockade in non-small cell lung cancer. *Science* (2015) 348:124–8. doi: 10.1126/science.aaa1348
30. Vagner T, Spinelli C, Minciaccchi VR, Balaj L, Zandian M, Conley A, et al. Large extracellular vesicles carry most of the tumour DNA circulating in prostate cancer patient plasma. *J Extracell Vesicles* (2018) 7:1505403. doi: 10.1080/20013078.2018.1505403
31. Possemato R, Marks KM, Shaul YD, Pacold ME, Kim D, Birsoy K, et al. Functional genomics reveal that the serine synthesis pathway is essential in breast cancer. *Nature* (2011) 476:346–50. doi: 10.1038/nature10350
32. Niu B, Ye K, Zhang Q, Lu C, Xie M, McLellan MD, et al. MSIsensor: microsatellite instability detection using paired tumor-normal sequence data. *Bioinformatics* (2014) 30:1015–6. doi: 10.1093/bioinformatics/btt755
33. Cortes-Ciriano I, Lee S, Park W-Y, Kim T-M, Park PJ. A molecular portrait of microsatellite instability across multiple cancers. *Nat Commun* (2017) 8:15180. doi: 10.1038/ncomms15180
34. Attard G. Anti-androgen monotherapy for metastatic prostate cancer. *Lancet Oncol* (2014) 15:543–4. doi: 10.1016/S1470-2045(14)70159-7
35. Kokal M, Mirzakhani K, Pungsrinont T, Banihammad A. Mechanisms of Androgen Receptor Agonist- and Antagonist-Mediated Cellular Senescence in Prostate Cancer. *Cancers (Basel)* (2020) 12(7):1833. doi: 10.3390/cancers12071833
36. Mariathasan S, Turley SJ, Nickles D, Castiglioni A, Yuen K, Wang Y, et al. TGF $\beta$  attenuates tumour response to PD-L1 blockade by contributing to exclusion of T cells. *Nature* (2018) 554:544–8. doi: 10.1038/nature25501
37. Topalian SL, Taube JM, Anders RA, Pardoll DM. Mechanism-driven biomarkers to guide immune checkpoint blockade in cancer therapy. *Nat Rev Cancer* (2016) 16:275–87. doi: 10.1038/nrc.2016.36
38. Robertson AG, Kim J, Al-Ahmadie H, Bellmunt J, Guo G, Cherniack AD, et al. Comprehensive Molecular Characterization of Muscle-Invasive Bladder Cancer. *Cell* (2018) 174:1033. doi: 10.1016/j.cell.2018.07.036
39. Tan TZ, Ye J, Yee CV, Lim D, Ngoi NYL, Tan DSP, et al. Analysis of gene expression signatures identifies prognostic and functionally distinct ovarian clear cell carcinoma subtypes. *EBioMedicine* (2019) 50:203–10. doi: 10.1016/j.ebiom.2019.11.017
40. Yang C, Zhang Y, Xu X, Li W. Molecular subtypes based on DNA methylation predict prognosis in colon adenocarcinoma patients. *aging* (2019) 11:11880–92. doi: 10.18632/aging.102492
41. Najafi M, Farhood B, Mortezaee K. Cancer stem cells (CSCs) in cancer progression and therapy. *J Cell Physiol* (2019) 234:8381–95. doi: 10.1002/jcp.27740

42. Zhang Z, Zhang S, Yang J, Yi P, Xu P, Yi M, et al. Integrated transcriptomic and metabolomic analyses to characterize the anti-cancer effects of (-)-epigallocatechin-3-gallate in human colon cancer cells. *Toxicol Appl Pharmacol* (2020) 401:115100. doi: 10.1016/j.taap.2020.115100
43. Rennier K, Shin WJ, Krug E, Virdi G, Pachynski RK. Chemerin Reactivates PTEN and Suppresses PD-L1 in Tumor Cells via Modulation of a Novel CMKLR1-mediated Signaling Cascade. *Clin Cancer Res* (2020) 26(18):5019–35. doi: 10.1158/1078-0432.CCR-19-4245
44. Billon E, Finetti P, Bertucci A, Niccoli P, Birnbaum D, Mamessier E, et al. PDL1 expression is associated with longer postoperative, survival in adrenocortical carcinoma. *Oncoimmunology* (2019) 8:e1655362. doi: 10.1080/2162402X.2019.1655362
45. Park J, Kim D-H, Shah SR, Kim H-N, Kshitiz, Kim P, et al. Switch-like enhancement of epithelial-mesenchymal transition by YAP through feedback regulation of WT1 and Rho-family GTPases. *Nat Commun* (2019) 10:2797. doi: 10.1038/s41467-019-10729-5
46. Yang J, Antin P, Berx G, Blanpain C, Brabletz T, Bronner M, et al. Guidelines and definitions for research on epithelial-mesenchymal transition. *Nat Rev Mol Cell Biol* (2020) 21:341–52. doi: 10.1038/s41580-020-0237-9
47. Su Y, Feng W, Shi J, Chen L, Huang J, Lin T. circRIP2 accelerates bladder cancer progression via miR-1305/Tgf- $\beta$ 2/smad3 pathway. *Mol Cancer* (2020) 19:23. doi: 10.1186/s12943-019-1129-5
48. Wu N, Jiang M, Liu H, Chu Y, Wang D, Cao J, et al. LINC00941 promotes CRC metastasis through preventing SMAD4 protein degradation and activating the TGF- $\beta$ /SMAD2/3 signaling pathway. *Cell Death Differ* (2020). doi: 10.1038/s41418-020-0596-y
49. Bruni D, Angell HK, Galon J. The immune contexture and Immunoscore in cancer prognosis and therapeutic efficacy. *Nat Rev Cancer* (2020) 20(11):662–80. doi: 10.1038/s41568-020-0285-7
50. Ren J, Nie Y, Lv M, Shen S, Tang R, Xu Y, et al. Estrogen upregulates MICA/B expression in human non-small cell lung cancer through the regulation of ADAM17. *Cell Mol Immunol* (2015) 12:768–76. doi: 10.1038/cmi.2014.101
51. Waldman AD, Fritz JM, Lenardo MJ. A guide to cancer immunotherapy: from T cell basic science to clinical practice. *Nat Rev Immunol* (2020) 20(11):651–68. doi: 10.1038/s41577-020-0306-5
52. Salem ME, Bodor JN, Puccini A, Xiu J, Goldberg RM, Grothey A, et al. Relationship between MLH1, PMS2, MSH2 and MSH6 gene-specific alterations and tumor mutational burden in 1057 microsatellite instability-high solid tumors. *Int J Cancer* (2020) 147(10):2948–56. doi: 10.1002/ijc.33115
53. Roze J, Monroe G, Kutzera J, Groeneweg J, Stelloo E, Paijens S, et al. Whole Genome Analysis of Ovarian Granulosa Cell Tumors Reveals Tumor Heterogeneity and a High-Grade TP53-Specific Subgroup. *Cancers (Basel)* (2020) 12(5):1308. doi: 10.3390/cancers12051308
54. Nyquist MD, Corella A, Coleman I, De Sarkar N, Kaipainen A, Ha G, et al. Combined TP53 and RB1 Loss Promotes Prostate Cancer Resistance to a Spectrum of Therapeutics and Confers Vulnerability to Replication Stress. *Cell Rep* (2020) 31:107669. doi: 10.1016/j.celrep.2020.107669
55. Swami U, Isaacsson Velho P, Nussenzweig R, Chipman J, Sacristan Santos V, Erickson S, et al. Association of SPOP Mutations with Outcomes in Men with De Novo Metastatic Castration-sensitive Prostate Cancer. *Eur Urol* (2020) 78(5):652–6. doi: 10.1016/j.eururo.2020.06.033
56. Su F, Zhang W, Zhang D, Zhang Y, Pang C, Huang Y, et al. Spatial Intratumor Genomic Heterogeneity within Localized Prostate Cancer Revealed by Single-nucleus Sequencing. *Eur Urol* (2018) 74:551–9. doi: 10.1016/j.eururo.2018.06.005
57. Xu Q, Li Y, Gao X, Kang K, Williams JG, Tong L, et al. HNF4 $\alpha$  regulates sulfur amino acid metabolism and confers sensitivity to methionine restriction in liver cancer. *Nat Commun* (2020) 11:3978. doi: 10.1038/s41467-020-17818-w
58. Vantaku V, Putluri V, Bader DA, Maity S, Ma J, Arnold JM, et al. Epigenetic loss of AOX1 expression via EZH2 leads to metabolic deregulations and promotes bladder cancer progression. *Oncogene* (2019) 39(40):6265–85. doi: 10.1038/s41388-019-0902-7
59. Gandhi M, Groß M, Holler JM, Coggins SA, Patil N, Leupold JH, et al. The lncRNA lincNMR regulates nucleotide metabolism via a YBX1 - RRM2 axis in cancer. *Nat Commun* (2020) 11:3214. doi: 10.1038/s41467-020-17007-9
60. Yang C, Huang X, Liu Z, Qin W, Wang C. Metabolism-associated molecular classification of hepatocellular carcinoma. *Mol Oncol* (2020) 14:896–913. doi: 10.1002/1878-0261.12639
61. Zhang E, Hou X, Hou B, Zhang M, Song Y. A risk prediction model of DNA methylation improves prognosis evaluation and indicates gene targets in prostate cancer. *Epigenomics* (2020) 12:333–52. doi: 10.2217/epi-2019-0349
62. Cao Z-X, Xiao G-A, Zhang W, Ji J, Ye C, Liu D, et al. Comprehensive investigation of alternative splicing and development of a prognostic risk score for prostate cancer based on six-gene signatures. *J Cancer* (2019) 10:5585–96. doi: 10.7150/jca.31725
63. Hu D, Jiang L, Luo S, Zhao X, Hu H, Zhao G, et al. Development of an autophagy-related gene expression signature for prognosis prediction in prostate cancer patients. *J Transl Med* (2020) 18:160. doi: 10.1186/s12967-020-02323-x
64. Labrecque MP, Coleman IM, Brown LG, True LD, Kollath L, Lakely B, et al. Molecular profiling stratifies diverse phenotypes of treatment-refractory metastatic castration-resistant prostate cancer. *J Clin Invest* (2019) 129:4492–505. doi: 10.1172/JCI128212
65. Brecht K, Schäfer AM, Meyer Zu Schwabedissen HE. Uptake Transporters of the SLC21, SLC22A, and SLC15A Families in Anticancer Therapy-Modulators of Cellular Entry or Pharmacokinetics? *Cancers (Basel)* (2020) 12(8):2263. doi: 10.3390/cancers12082263

**Conflict of Interest:** The authors declare that the research was conducted in the absence of any commercial or financial relationships that could be construed as a potential conflict of interest.

Copyright © 2020 Zhang, Zhang, Liang, Zhang and Liang. This is an open-access article distributed under the terms of the Creative Commons Attribution License (CC BY). The use, distribution or reproduction in other forums is permitted, provided the original author(s) and the copyright owner(s) are credited and that the original publication in this journal is cited, in accordance with accepted academic practice. No use, distribution or reproduction is permitted which does not comply with these terms.





# Metabolism-Associated Molecular Classification of Colorectal Cancer

Meng Zhang<sup>1,2†</sup>, Hai-zhou Wang<sup>1,2†</sup>, Ru-yi Peng<sup>1,2†</sup>, Fei Xu<sup>1,2\*</sup>, Fan Wang<sup>1,2\*</sup> and Qiu Zhao<sup>1,2\*</sup>

<sup>1</sup> Department of Gastroenterology, Zhongnan Hospital of Wuhan University, Wuhan, China, <sup>2</sup> Hubei Clinical Center & Key Lab of Intestinal & Colorectal Diseases, Wuhan University, Wuhan, China

## OPEN ACCESS

### Edited by:

Monica Montopoli,  
University of Padua, Italy

### Reviewed by:

Weiting Ge,  
Zhejiang University, China  
Barbara Marengo,  
University of Genoa, Italy

### \*Correspondence:

Qiu Zhao  
qiu Zhao@whu.edu.cn  
Fan Wang  
fandywang@foxmail.com  
Fei Xu  
2017103030003@whu.edu.cn

<sup>†</sup>These authors have contributed  
equally to this work

### Specialty section:

This article was submitted to  
Cancer Metabolism,  
a section of the journal  
Frontiers in Oncology

**Received:** 03 September 2020

**Accepted:** 28 October 2020

**Published:** 04 December 2020

### Citation:

Zhang M, Wang H-z, Peng R-y, Xu F,  
Wang F and Zhao Q (2020)  
Metabolism-Associated Molecular  
Classification of Colorectal Cancer.  
Front. Oncol. 10:602498.  
doi: 10.3389/fonc.2020.602498

The high heterogeneity of colorectal cancer (CRC) is the main clinical challenge for individualized therapies. Molecular classification will contribute to drug discovery and personalized management optimizing. Here, we aimed to characterize the molecular features of CRC by a classification system based on metabolic gene expression profiles. 435 CRC samples from the Genomic Data Commons data portal were chosen as training set while 566 sample in GSE39582 were selected as testing set. Then, a non-negative matrix factorization clustering was performed, and three subclasses of CRC (C1, C2, and C3) were identified in both training set and testing set. Results showed that subclass C1 displayed high metabolic activity and good prognosis. Subclass C2 was associated with low metabolic activities and displayed high immune signatures as well as high expression of immune checkpoint genes. C2 had the worst prognosis among the three subtypes. Subclass C3 displayed intermediate metabolic activity, high gene mutation numbers and good prognosis. Finally, a 27-gene metabolism-related signature was identified for prognosis prediction. Our works deepened the understanding of metabolic hallmarks of CRC, and provided valuable information for “multi-molecular” based personalized therapies.

**Keywords:** colorectal cancer, classification, metabolism, immune signatures, non-negative matrix factorization

## INTRODUCTION

Colorectal cancer (CRC) is one of the most frequently diagnosed cancers all around the world. There are over 1.8 million new cases and almost 900,000 deaths annually (1, 2). Although new treatment options, such as targeted therapy and immunotherapy, have been developed, the average 5-year survival probability for advanced CRC patients is still dismal, lower than 15% (3, 4). What's worse is that the incidence of CRC in patients who are younger than 50 years is rising sharply, and the mortality of CRC has ranked the first for men in age 20–49 during 2012 to 2016 (5, 6). As we were known, CRC is a heterogeneous disease, therefore, more researches should be conducted for precisely understanding the molecular properties of CRC (7).

Besides the classic TNM staging based on histopathology, CRC also has several molecular traits, such as chromosomal instability (CIN), microsatellite instability (MSI) and CpG island methylator phenotype (CIMP) (8). With the accumulation of multiple kinds of “omics” data, CRC samples have been classified into four consensus molecular subtypes (CMS) in 2015, including CMS1 (MSI Immune, 14%), CMS2 (Canonical, 37%), CMS3 (Metabolic, 13%), and CMS4 (Mesenchymal, 23%).

The CMS groups had distinct characteristics, which contributed to targeted interventions for CRC patients. For example, KRAS mutations were overrepresented in CMS3, therefore, epidermal growth factor receptor (EGFR) antibodies should be avoided for these CRC patients (9, 10). More recently, some signatures, especially immune alterations, were utilized for molecular subtyping in many kinds of cancers. Three immune subtypes were identified and validated in lower-grade diffuse glioma, and they were characterized with different lymphocyte signatures, somatic DNA alterations and clinical outcomes (11). Microsatellite instability-high (MSI-H) CRC patients were separated into two different subtypes by consensus clustering, which showed distinct molecular profiles (12).

Metabolism reprogramming is one of the hallmarks of cancer (13). In order to meet the growing demands for energy requirement for cell proliferation, tumor cells owned unique metabolic way of glucose, glutamine, fatty acids, amino acid and many other kinds of nutrients and metabolites, such as aerobic glycolysis, *de novo* synthesis of fatty acids (14). Nowadays, targeting the metabolic differences between tumor and normal cells have become a promising anticancer strategy. Moreover, a deeply exploring of molecular changes induced by metabolism rewiring can contribute to the development of targeted therapies (15). Recently, a study had classified hepatocellular carcinoma (HCC) samples into three subclasses based on a panel of metabolic genes, including active (C1), intermediate (C2), and exhausted (C3) metabolic subtype. Each subtype had distinct molecular, immune and clinical features. For instance, C1 had the best prognosis and matched the characteristics of non-proliferative HCCs. C2 exhibited high immune infiltration and sensitivity toward immune blockade as well as chemotherapy. What's more, a meaningful 90-gene classifier was provided, which may help to predict the prognosis of HCC patients and prospective therapies (16). However, research on metabolism-relevant molecular classification of CRC has not yet been reported.

In the present study, a non-negative matrix factorization (NMF) clustering based on metabolic genes was performed and validated in CRC datasets. Three distinct subtypes were identified, namely C1, C2, and C3. Then, we revealed the prognosis traits, metabolic signatures, transcriptome features, clinical characteristics, immune infiltration as well as gene mutation alterations among the three subclasses. Furthermore, a metabolism-related signature was also identified and validated.

## METHODS

### Data Source and Processing

The CRC clinical and molecular data (including RNA expression and mutation) were extracted from the Genomic Data Commons (GDC) Data Portal (<https://portal.gdc.cancer.gov/>). Normal samples, repeated samples and samples without key clinical features were excluded for further analyses. After procession, there were 435 patients in GDC TCGA COAD project included in training study. 375 of the above 435 patients had mutation data. For validation, the human CRC mRNA expressing data

were downloaded from Gene Expression Omnibus (GEO) database (<http://www.ncbi.nlm.nih.gov/geo/>). Dataset GSE39582, containing 585 CRC samples, was chosen as testing set, and 556 of which were finally selected after data filtration.

### Identification of CRC Subclasses

In the present study, we prepared a total of 2,752 metabolism-related genes involved in all metabolic process for non-negative matrix factorization (NMF) clustering (17). Before classification, a filtering procedure was conducted. Firstly, some candidate genes, whose expression value was zero in any analyzed sample and whose median absolute deviation (MAD) value was lower than 0.5 across all the samples, were excluded. Next, Cox proportional hazards model was conducted by “survival” R package to screen meaningful genes for overall survival (OS). Finally, metabolism-associated genes with relatively high variable (MAD > 0.5) and significant prognostic value ( $P < 0.05$ ) were chosen for subsequent clustering analysis. The way of unsupervised NMF clustering was implemented by “NMF” R package on the training and testing datasets (18). The corresponding codes were provided in supplementary methods. The value was determined by the cophenetic correlation coefficient, the magnitude of which began to fall was chosen as the optimal number of clusters (19). Principal components analysis (PCA) was used to access expression differences between the subtypes.

### Gene Set Variation Analysis

Gene set variation analysis (GSVA), a nonparametric and unsupervised gene set enrichment method, can calculate the score of a certain pathway or a signature based on transcriptomic data (20). We acquired the 115 metabolism-associated gene signatures from previously published works (21). Several CRC progression relevant signatures were also downloaded from the Kyoto Encyclopedia of Genes and Genomes (KEGG) database. Then, each sample got a score corresponding to the above signatures by “GSVA” R package. Utilizing “limma” R package, differential analyses were subsequently conducted based on the signature cores, and the signatures with an absolute log2 fold change (FC) > 0.4 (adjusted  $P < 0.05$ ) were defined as significant differentially expressed signatures. The results were visualized by using “ComplexHeatmap” R package.

### Differentially Expressed Gene and Gene Ontology Analyses of CRC Subclasses

The “limma” R package was also utilized to calculate the DEGs among CRC subclasses. Adjusted  $P$  value < 0.05 and  $|\log_2\text{FC}| > 0.5$  were set to choose significant DEGs. Then, GO enrichment analysis and visualization were performed *via* “clusterProfiler” R package (22).

### Immune Infiltration Estimation and Immunotherapy Prediction of CRC Subclasses

Firstly, the immune score, stromal score and tumor purity were calculated by the ESTIMATE algorithm, which can reflect the

enrichment of stromal and immune cell gene signatures (23). Then, the online CIBERSORT method (<https://cibersortx.stanford.edu/>) was used to evaluate the LM22 gene signatures in CRC subtypes (24). Furthermore, the other signature contained 17 immune cell types was provided, and the single-sample GSEA (ssGSEA) algorithm was applied to estimate the immune infiltration. Differential analyses were conducted as described above, and data were visualized by the heatmap. The expression data from melanoma patients treated with immunotherapies were extracted from the published work (25). SubMap analysis (Gene Pattern) was applied to compare the correlation of gene expression profiles between our subclasses and melanoma patients.

## Mutation Differences of CRC Subclasses

The MAF files contained the mutation information of training set were downloaded and processed. The “maftools” R package was utilized to analyze gene mutations among CRC subclasses (26).

## Metabolism-Related Signature Construction

LASSO penalized Cox regression model was built by “glmnet” R package (27), and the lambda.1se, a penalty parameter for prevention of overfitting, was selected to construct an optimal and prognostic gene set. Finally, the risk scores of each samples was calculated by the formula: Risk score =  $\sum_{i=1}^N Exp_i * \beta_i$ .

## Statistical Analysis

Survival analyses were performed by Kaplan–Meier methods and compared by the log-rank test. ROC curve was analyzed, and the area under the curve (AUC) was calculated using the “survivalROC” package. The relationship between CRC subclasses and the clinical features was estimated by Chi-square analysis. Unpaired Student’s t-test was used to compare two groups with normally distributed variables, one-way analysis of variance was used for three group comparison. A two-tailed P value < 0.05 was statistically significant.

## RESULTS

### NMF Identifies Three Metabolism Subclasses in CRC

First of all, a flow chart was shown to introduce this study design (Figure 1A). Clinical characteristics of training set and testing set were listed in Table 1, and there was no significant difference in general features between two datasets. The training set had 435 valid CRC samples with complete clinical traits. For clustering, the mRNA expression matrix of the initial 2,752 metabolism-relevant genes in training set was acquired. After primary filtering, 1,514 genes were excluded for undetectable expression or low MAD, and 1,238 genes were selected for subsequent analysis. To get the metabolic genes with prognostic value for classification, univariate cox proportional hazards model was

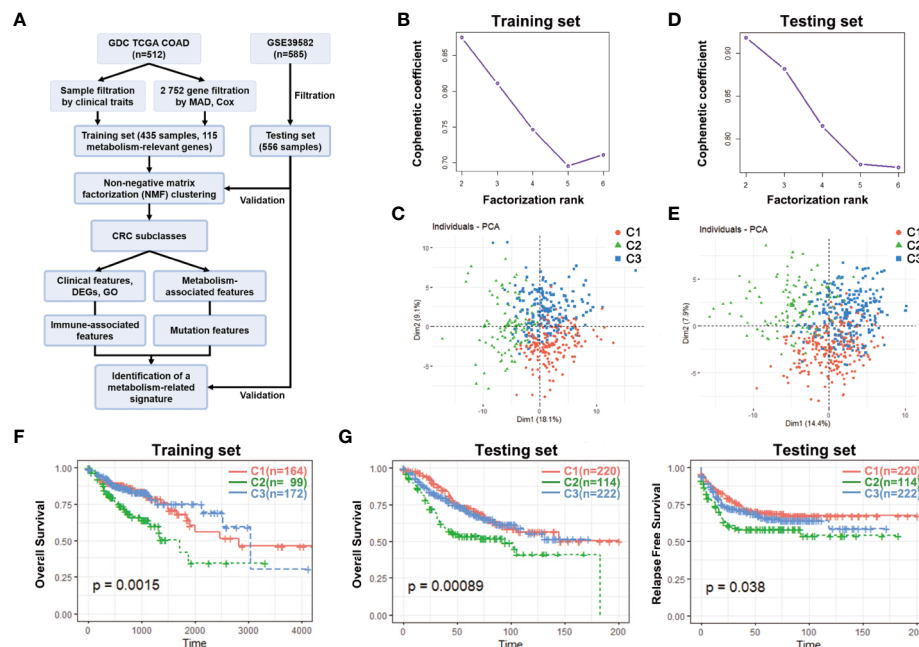


**FIGURE 1 |** Identification of CRC subclasses using NMF consensus clustering. (A) A flow chart of the study. (B) NMF clustering using 115 metabolism-associated genes in training set. Cophenetic correlation coefficient for  $k = 2-6$  is shown. (C) PCA showed the distribution of three CRC subclasses in training set. (D) Cophenetic correlation coefficient in testing set. (E) The distribution of three CRC subclasses in testing set. (F) OS of three subclasses (C1, C2, and C3) in training set. (G) OS and RFS of three subclasses in testing set. CRC, Colorectal cancer; NMF, Non-negative matrix factorization; MAD, Median absolute deviation; PCA, Principal components analysis; OS, Overall survival; RFS, Relapse free survival; DEGs, Differentially expressed genes; GO, gene ontology.

**TABLE 1 |** Clinical characteristics of training and testing sets.

Clinical characteristics		Training set (n=435) n(%)	Testing set (n=556) n(%)	Chi-square	P value
Gender	male	233(53.6)	306(55.0)	0.213	0.653
	female	202(46.4)	250(45.0)		
Age	<65	171(39.3)	210(37.8)	0.245	0.645
	≥65	264(60.7)	346(62.2)		
TNM stage	1–2	239(55.0)	295(53.1)	1.063	0.332
	3–4	185(42.5)	261(46.9)		
	NA	11(2.5)	0(0.0)		

conducted. Results showed that only 115 of the above metabolic genes had significant risks on survival of patients in training set (**Table S1**). Moreover, multiple permutation testing was performed to confirm the robustness of the selected genes for classification (**Figure S1**) (28, 29). Therefore, a total of 115 genes were identified for NMF clustering. GO analysis showed that the 115 genes were mostly enriched in small molecule, oxoacid, organophosphate, lipid and some other metabolite metabolic process (**Figure S2A**). To find the optimal k value, cophenetic correlation coefficients were calculated. Data showed that the cophenetic correlation coefficient fell sharply when k = 3 (**Figure 1B**). Moreover, the consensus matrix heatmap also kept crisp boundaries at k = 3 (**Figure S2B**). Therefore, k = 3 was chosen as the optimal number of clusters. Namely, three clusters were identified in training set. There were 164 samples in the cluster 1 (C1), 99 in the C2 and 172 in the C3. To access the subclasses' assignments, we performed PCA. Data showed that the three clusters were distributed in different corners of the two dimensional coordinate systems (**Figure 1C**). Furthermore, we extracted the expression data of the above selected 115 genes in testing dataset with 556 eligible CRC samples from GEO database (GSE39582). A similar NMF consensus clustering was performed. Consistently, the optimal K value was also 3 in testing set and three distinct subclasses were identified, which also showed the same distribution as that in training set by PCA (**Figures 1D, E, and S1C**).

To explore the differences among the three subclasses, the survival analyses were firstly performed. In the training set, the C2 had the shortest median survival time (MST) while the C3 had the longest. The OS probability within the three subclasses had significant differences ( $p = 0.0015$ ) (**Figure 1F**). What's more, the OS probability levels of the three subclasses in testing set had the same tendency as that in training set. The OS probability and relapse free survival (RFS) probability of the C2 was the lowest, and both had significant differences ( $p = 0.00089$  for OS,  $p = 0.038$  for RFS) (**Figure 1G**). These results demonstrated that the three subclasses had obviously different prognosis.

## Correlation of the CRC Subclasses With Metabolism-Associated Signatures

The CRC classification was based on metabolism-relevant genes, therefore, we further studied whether distinct subclasses in training set had different metabolic characteristics. Firstly, 115 metabolism processes were listed and quantified by GSVA R package (**Table S2**). Each sample got a score for the correspondingly metabolic pathway. Then, differential analyses

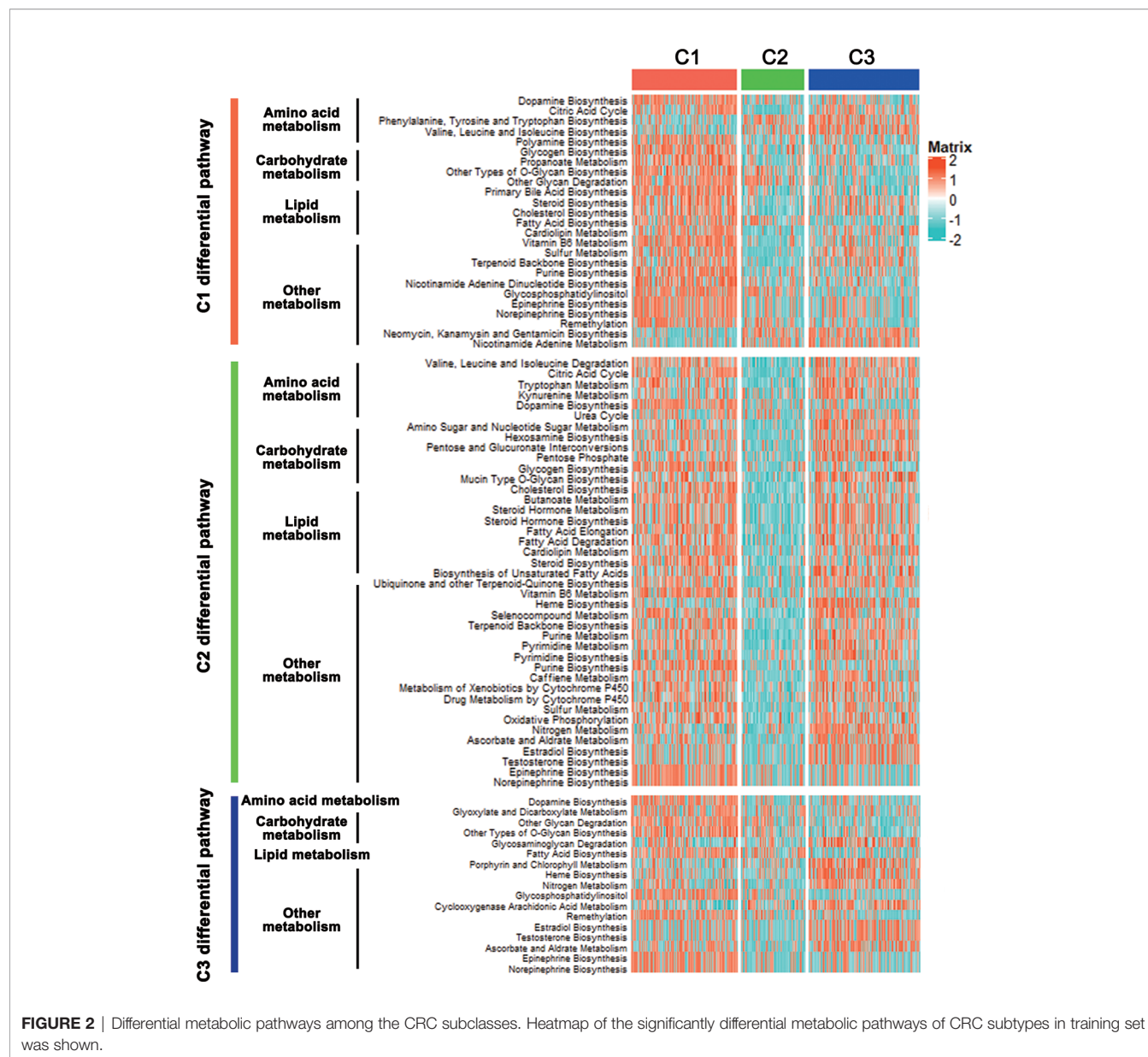
were performed to dig out subtype-specific metabolism signatures (**Figure 2**). Compared with C2 and C3, results showed that C1 had 25 kinds of significantly differential metabolic pathways, 5 of them were related to amino acid metabolism while 5 belonged to lipid metabolism. At the same time, most differential metabolism pathways were enriched in C1. Compared with C1 and C3, C2 had 41 kinds of significantly differential metabolic pathways, but all of which were downregulated, including amino acid, carbohydrate, lipid and other metabolism-related signatures. Moreover, there were 17 kinds of differential metabolic pathways in C3. Some other metabolism pathways, such as porphyrin and chlorophyll metabolism, heme biosynthesis, related to metabolism of cofactors and vitamins, were enriched in this subtype (**Figure 2, Table S3**). After merging duplicate pathways in three subtypes, a total of 58 metabolism-associated signatures were shown by a heatmap (**Figure 3A**). It clearly showed that C1 was metabolic active while C2 was metabolic exhausted, and C3 displayed intermediate activity. The above data demonstrated that the three subclasses were enriched with diverse metabolism pathways and had different levels of metabolic activity.

For further investigation, several CRC progression relevant pathways were also evaluated. Results exhibited that C1 had significantly higher Cell cycle signature than C2 and C3, and C2 displayed higher expression for PI3K-AKT, WNT, MAPK, RAS, NOTCH and ECM pathways, while C3 was especially enriched with HIF-1, P53 and Apoptosis pathways (**Figure 3B**). Moreover, the expressions of some key genes participated in glucose, fatty acid and glutamine metabolic process were analyzed. Data showed that C1 and C3 harbored a higher expression of these key metabolic genes, which was consistent with the metabolic pathway results (**Figure 3C**).

## Clinical Characteristics and DEGs of the CRC Subclasses

To better clarify the three CRC subclasses, the relationship with clinical features was studied by Chi-square test. The results in training set was shown in **Table 2**, which demonstrated that the proportion of samples in "TNM stage", "T stage", "N stage" and "M stage" were significantly different within distinct subtypes. Consistently, the difference of "T stage" and "M stage" within distinct subtypes of testing set also had significance. However, "TNM stage" and "N stage" had no significance. Furthermore, subtypes in testing set had significantly diverse proportion of "TP53 mutation", "KRAS mutation" and "BRAF mutation" (**Table 3**).





To gain deeper insights into the molecular characteristics of the three CRC subclasses, the DEGs and their GO analysis were identified in training dataset. Under a threshold of Adjusted P value < 0.05 and  $|\log_2FC| > 0.5$ , a total of 5 271 DEGs were identified for the three subclasses. In detail, 1 893 DEGs were obtained for C1 compared with C2 and C3, 2,064 DEGs for C2 while 1,314 genes for C3 (Table S4). The DEG expressions among the three subclasses were shown by a heatmap (Figure 4A). Genes with significant expression differences in all three possible comparisons were considered as subclass-specific genes. After merging, 263 subclass-specific genes were acquired (Figure 4B). GO analysis showed that the subclass-specific genes were mostly enriched in immune-related pathways, which suggested that the three subclasses may have different immune signatures (Figure 4C).

## Correlation of the CRC Subclasses With Immune Infiltration

To initially evaluate the tumor heterogeneity among these three subtypes, ESTIMATE algorithm was used to calculate the stromal score, immune score and tumor purity both in training and testing sets. Results showed that the three subtypes had significantly different stromal score, immune score and tumor purity (Figure 5). The C2 has the highest stromal score and the lowest tumor purity in training and testing sets. The immune scores of the C2 and C3 were relatively higher than that of the C1 in training set, while there was no significant difference between the C2 and C3. For testing set, the C2 has the highest immune score, which was a little different from the training set (Figures 5A, B).

**TABLE 2 |** Clinical Characteristics of patients with distinct classification in training set.

Clinical characteristics		Total	C1	C2	C3	Chi-square	P value
		n = 435	n = 164	n = 99	n = 172		
Gender	male	233	83	58	92	1.58	0.454
	female	202	81	41	80		
Age	<65	171	67	40	64	0.532	0.767
	≥65	264	97	59	108		
TNM stage	1–2	239	89	38	112	18.399	<0.0001***
	3–4	185	69	59	57		
	NA	11	6	2	3		
T stage	Tis–T2	87	42	10	35	9.302	0.01*
	T3–T4	348	122	89	137		
N stage	N0	255	96	43	116	16.122	0.003**
	N1	102	42	30	30		
	N2	78	26	26	26		
M stage	M0	320	114	66	140	17.651	0.001**
	M1	61	25	23	13		
	MX	47	24	7	16		
	NA	7	1	3	3		

\* $P < 0.05$ , \*\* $P < 0.01$ , \*\*\* $P < 0.001$ . NA, Not Available.

With the significant difference in immune score identified among subclasses, immune infiltration was investigated to characterize their immunologic landscape. Firstly, the CIBERSORT algorithm was performed to show the differences of the LM22 gene signature within the three subtypes. There were 9 kinds of immune cell populations significantly differently enriched in the three subtypes. Plasma cells, Macrophages M2, Neutrophils and T cells CD8 were enriched in the C3 while T

cells regulatory (Tregs) and Macrophages M0 were enriched in the C2, T cells CD4 memory activated and T cells CD4 naïve in the C1 (**Figure 6A**). Based on an additionally signature of 17 immune cell type (**Table S5**), more kinds of immune cells were analyzed by ssGSEA algorithm. The heatmap showed that the C2 and C3 were enriched with more immune cells, which was consistent with the result that the two had higher immune scores (**Figure 6B**). We further investigated the association

**TABLE 3 |** Clinical Characteristics of patients with distinct classification in testing set.

Clinical characteristics		Total	C1	C2	C3	Chi-square	P value
		n = 556	n = 220	n = 114	n = 222		
Gender	male	306	113	62	131	2.634	0.268
	female	250	107	52	91		
Age	<65	210	84	39	87	0.821	0.663
	≥65	346	136	75	135		
TNM stage	1–2	295	123	50	122	4.911	0.086
	3–4	261	97	64	100		
T stage	Tis–T2	57	28	1	28	13.239	0.001**
	T3–T4	479	185	106	188		
	NA	20	7	7	6		
N stage	N0	296	124	51	121	9.36	0.053
	N1	131	53	23	55		
	NX	109	36	33	40		
	NA	20	7	7	6		
M stage	M0	473	194	84	195	12.298	0.002**
	M1–MX	63	19	23	21		
	NA	20	7	7	6		
TP53	M	188	89	34	65	7.931	0.019*
Mutation	WT	156	51	32	73		
	NA	212	80	48	84		
KRAS	M	213	72	39	102	8.307	0.016*
	WT	322	136	72	114		
	NA	21	12	3	6		
BRAF	M	49	2	23	24	34.24	<0.0001***
	WT	453	192	85	176		
	NA	54	26	6	22		

\* $P < 0.05$ , \*\* $P < 0.01$ , \*\*\* $P < 0.001$ . M, Mutation; WT, Wild Type. NA, Not Available.

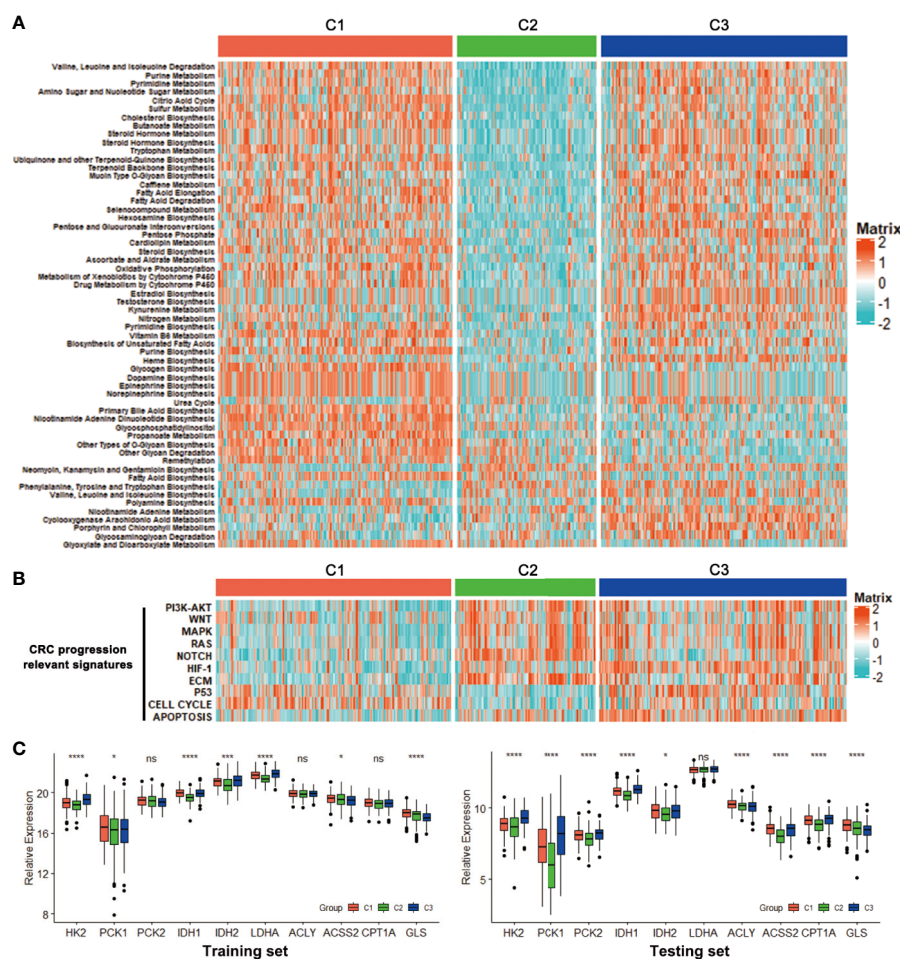


**FIGURE 3 |** Association with metabolism and progression-associated signatures among the CRC subclasses. **(A)** Heatmap of the specific metabolism-associated signatures of CRC subtypes in training set. **(B)** Heatmap of the CRC progression relevant signatures in training set. **(C)** Expression differences of several key metabolic genes among three subclasses in training and testing sets. \* $P < 0.05$ , \*\*\* $P < 0.001$ , \*\*\*\* $P < 0.0001$ ; ns, no significance.

between subclasses and the expression of several potentially targetable immune checkpoint genes. In training set, the expressions of checkpoint gene CCL2, CD276, CD4, CXCR4, LAG3, and TGFBI were analyzed. The C2 and C3, especially C2, exhibited higher expression for the above immune checkpoint genes (Figure 6C). In testing set, additional checkpoint gene CD274, CTLA4, IL1A, and IL6 were also tested. The results coincided with that in training set, except for no significant differences with CTLA4 and IL1A (Figure 6C).

Considering the difference in immune infiltration patterns and expression levels of immune checkpoint genes among CRC subclasses, the probability of responding to immunotherapy was investigated by subclass mapping. We compared the expression profiles of three CRC subclasses with a published dataset (25), which included a number of 47 melanoma patients that received programmed cell death protein-1 (PD-1) immune checkpoint inhibitor or cytotoxic T-lymphocyte-associated protein-4 (CTLA-4) immune checkpoint inhibitor treatment. Data

showed that the expression profile of C3 group has significant correlation with PD-1-response group ( $P = 0.000999$ ), indicating that patients within C3 group were promising to respond to anti-PD-1 therapy (Figure 6D).

## Correlation of the CRC Subclasses With Mutations

Recent studies have linked the gene mutations with metabolism phenotype (30). We further explored the difference of gene mutations among these three subtypes. The genes with high mutation frequency in CRC, such as APC, TP53, TTN and KRAS were examined. Results showed that distinct subclasses tended to have different mutation proportion of each gene. For example, 80 percent samples in C1 had APC mutation while only 67% in C2 and 59 percent in C3 (Figure 7A). What's more, the C3 subtype had the most mutation numbers (Figure 7B). These data could protect samples in different clusters from choosing resistant chemotherapeutic drugs.

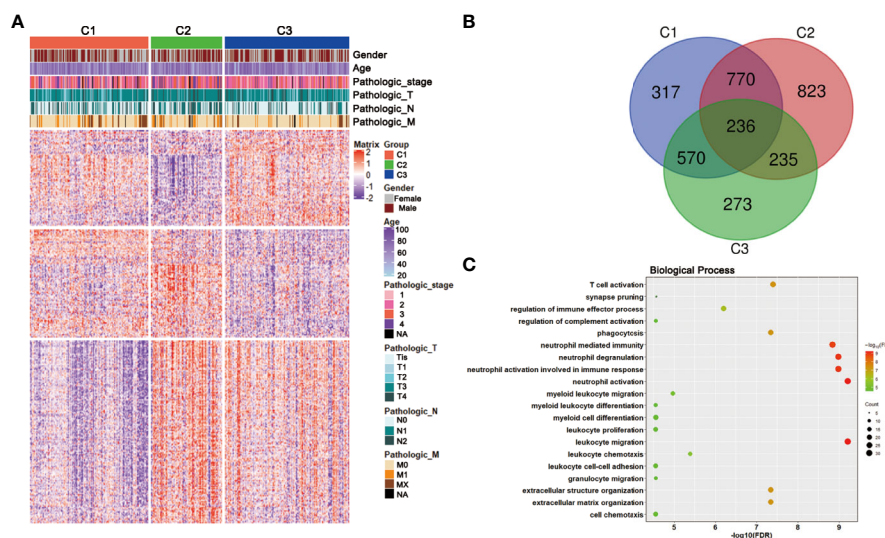


**FIGURE 4** | DEGs and GO analysis in the CRC subclasses. **(A)** DEG heatmap of CRC subtypes in training set, annotated by clinical traits. **(B)** Venn diagram showed the number of DEGs among three subtypes in training set. **(C)** GO results of the subclass-specific genes in training set.

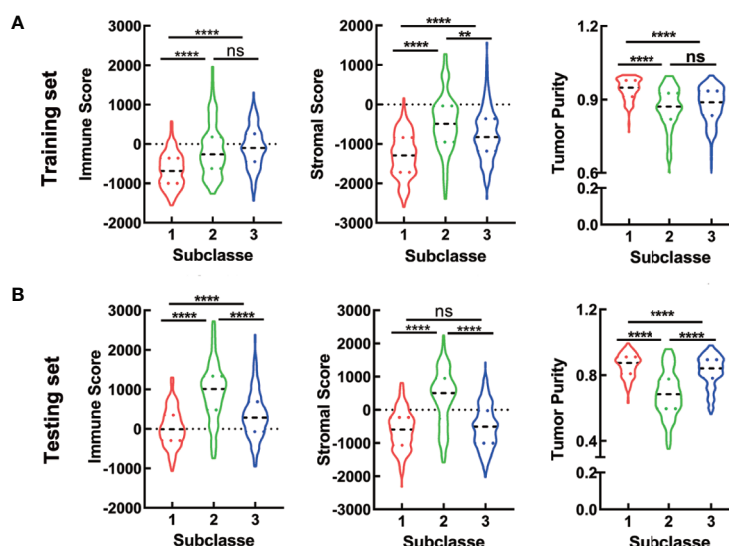


**FIGURE 5** | ESTIMATE analyses in the CRC subclasses. **(A, B)** The violin plot of immune score, stromal score and tumor purity from ESTIMATE of three subclasses in training set **(A)** and testing set **(B)**. For violin plots, the three lines within the boxes represent the 25th percentile, median value and the 75th percentile, respectively. The bottom and top of the plots represent the min and max value. \*\* $P < 0.01$ , \*\*\*\* $P < 0.0001$ ; ns, no significance.

## Development and Validation of a Metabolism-Related Signature Using LASSO Regression Model

To build a signature for clinical use, it is necessary to select the most representative genes of each subclass. The above data showed that a total of 3,244 DEGs were obtained among three subclasses in the training set, wherein 66 genes were significantly correlated with patients' overall survival and had been used for

metabolism-associated clustering (**Figure 8A**). Then, we applied the LASSO penalized Cox regression to identify a signature with best prognostic value (**Figure 8B**). A twenty-seven gene metabolic signature was obtained and the expression profile was distinct in three subclasses (**Figure 8C**). Furthermore, the risk scores of the metabolism-related signature were calculated with the regression coefficients (**Table S6**). The subtype C2 has the highest scores while C1 had the lowest (**Figure 8D**). Survival



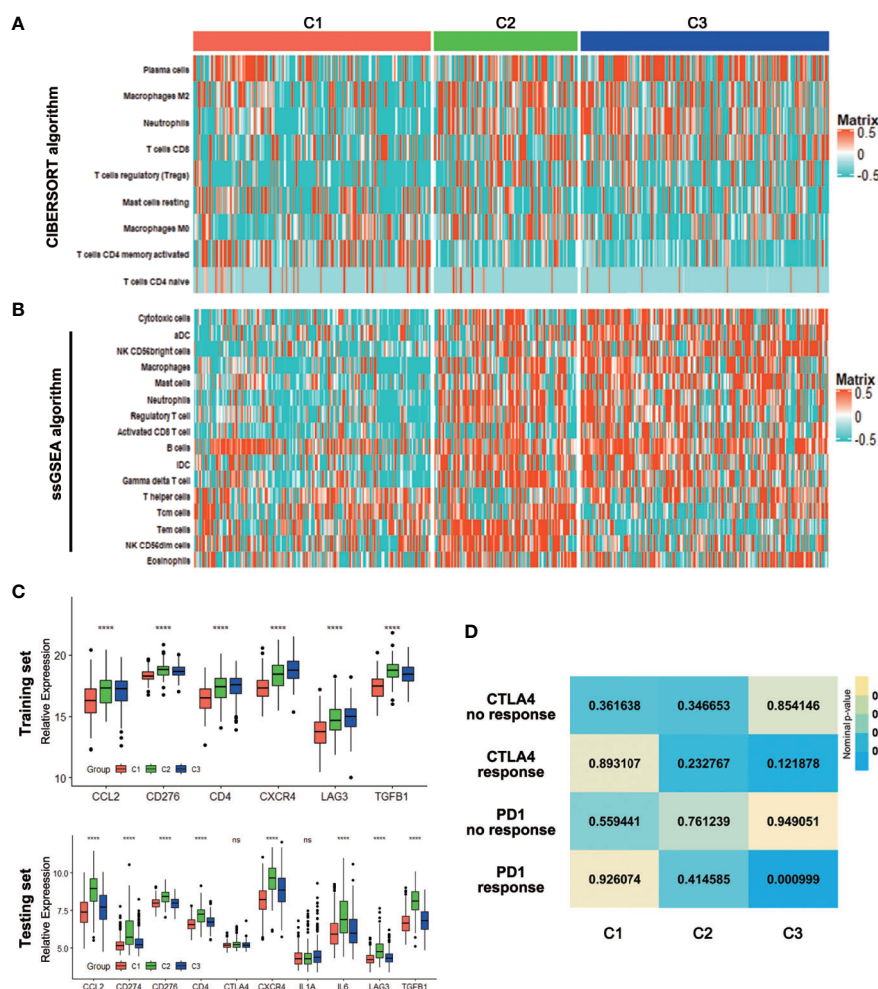


**FIGURE 6** | Association with immune signatures among the CRC subclasses. **(A, B)** Heatmap describing the abundance of immune cell populations in C1, C2, and C3 by CIBERSORT **(A)** and ssGSEA algorithms **(B)**. **(C)** Expression differences of several immune checkpoint genes among three subclasses in training and testing sets. **(D)** SubMap analysis for immunotherapy prediction in training set. \*\*\*\* $P < 0.0001$ ; ns, no significance.

analysis revealed that high scores exhibited significantly poorer prognosis of CRC patients or each metabolism-associated subtype in training set (**Figures 8E, F**). The results coincided with the above data that C2 had the worst prognosis. To further explore the prognostic accuracy of our signature, we performed ROC analysis to compare AUC with other factors (age and stage). It showed that the AUC of metabolism-related signature was 76.3%, higher than that of age and stage (**Figure 8G**). In addition, multivariate Cox regression analysis also confirmed the independent prognostic value of this signature (**Figure 8H**). We further applied this signature into testing set and found consistent results. Data showed that C2 has the highest scores and CRC patients with high scores had poorer prognosis (**Figures S3A, B**). These data demonstrated the superior performance of metabolism-related signature for prognosis prediction, highlighting the importance of the metabolism in determining survival of CRC.

## DISCUSSION

With the revealing of the heterogeneity in CRC, traditional paradigm of precision medicine, “one gene, one drug”, has gradually translated to “multi-gene, multi-drug” model. Better characterization of the transcriptomic subtypes, stromal and immune components for CRC may help to improve the “multi-molecular” perspective for more precise therapies (10, 31). Here, we presented a comprehensive classification of metabolism profile of CRC samples. Our results showed that CRC could be classified into three distinct metabolism-relevant subtypes, and the reproducibility of this subtyping was validated in testing set. Each subtype was associated with different clinical traits, molecular features, functions, immune cell fractions as well as gene mutation alterations.

In detail, results showed that C2 had the most kinds of differential metabolic pathways, almost all of which were downregulated in this

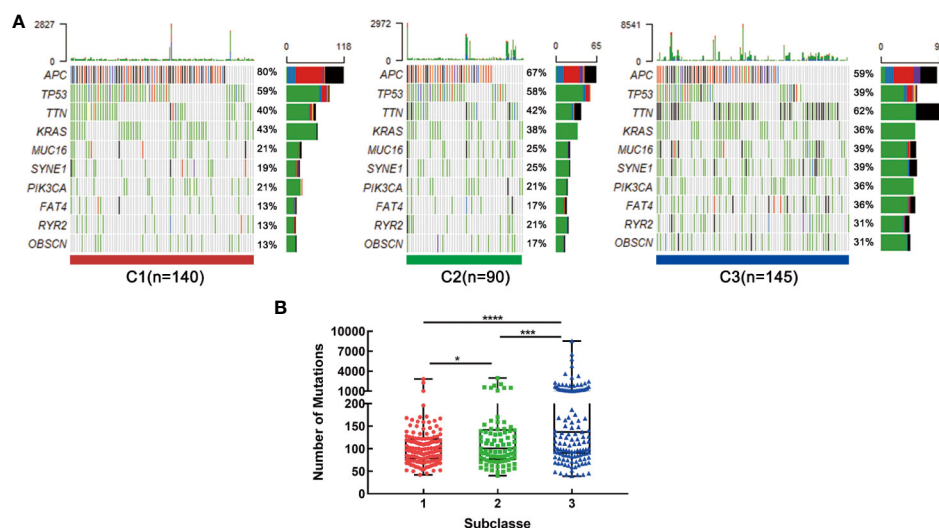


**FIGURE 7** | Association with mutation alterations among the CRC subclasses in training set. **(A)** OncoPrint of mutation status of top 10 genes in C1, C2, and C3. **(B)** The number of mutations in three subtypes. \*P < 0.05, \*\*\*P < 0.001, \*\*\*\*P < 0.0001.

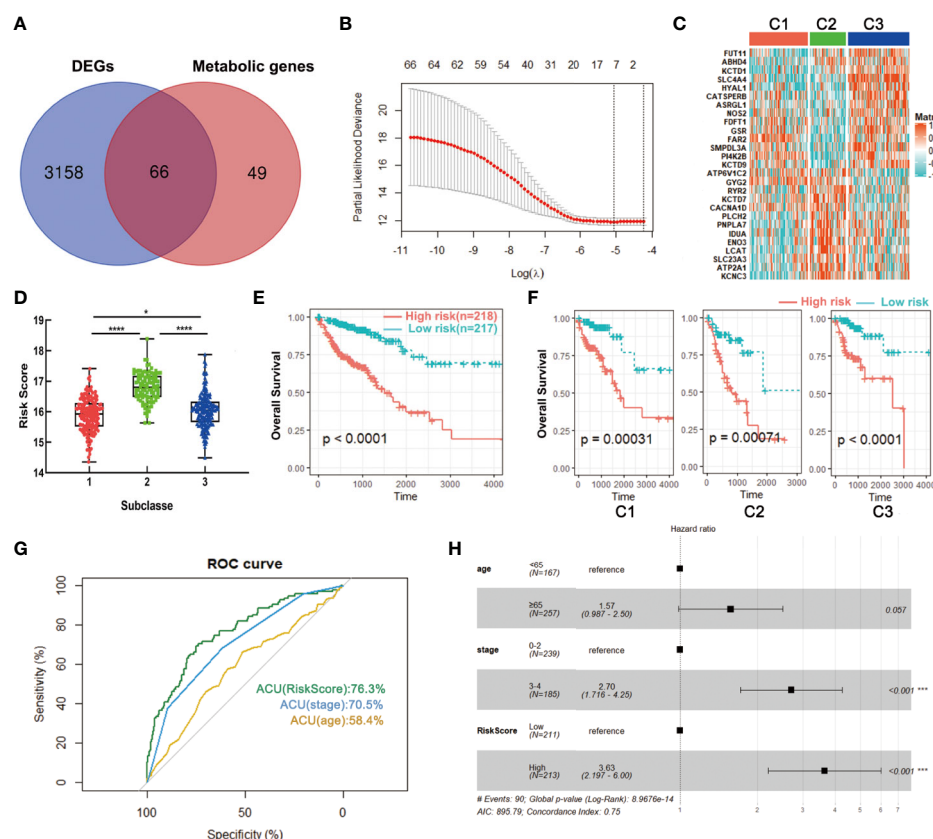


**FIGURE 8** | Identification of a metabolism-related signature by LASSO regression model. **(A)** Venn diagram of DEGs among three subclasses which are prognosis-related metabolic genes. **(B)** Cross-validation for tuning parameter selection in the proportional hazards model. **(C)** Heatmap of the expression levels of signature genes. **(D)** Distribution of risk scores in CRC subclasses. **(E, F)** Survival analysis of the metabolism-related signature in CRC or CRC subclasses. **(G)** ROC curve analysis of age, stage and risk score. **(H)** Multivariate Cox regression analysis of age, stage and risk score. \*P < 0.05, \*\*\*P < 0.001, \*\*\*\*P < 0.0001. AUC, area under the curve.

subtype. Therefore, we defined C2 as metabolic exhausted subtype. Inversely, the majority of the metabolic pathways were enriched in C1, thus defining as metabolic active subtype. At the same time, C3 displayed intermediate metabolic activity. Our classification in CRC coincided with that in HCC, a work published recently (16). Clinical feature analyses showed that most samples in C2 were in advanced pathological stage. CRC progression signatures, such as PI3K-AKT, WNT, were also enriched in C2. Moreover, tumor microenvironment relevant estimation demonstrated that C2 had the higher immune score, stromal score and the lowest tumor purity. These data suggested that C2 subclass was of high heterogeneity and might be refractory. Our opinion was also consistent with the results that metabolic exhausted subtype C2 had the worst prognosis in both training and testing sets. The C2 subtype was somewhat similar to CMS4, one of the reported consensus molecular subtypes in CRC. CMS4 CRCs are mesenchymal prominent and characterized by activation of pathways related to epithelial-mesenchymal transition (EMT) and stemness (9). Consistently, ECM and NOTCH pathways were upregulated in our subtyped C2. Moreover, CMS4 CRCs exhibit a worse relapse-free and overall survival. A variety of immune cells were filled in C2, and C2 was presented with higher expressions of immune checkpoint genes, especially for CCL2, CD274 (also known as PD-L1), CD276, CD4, CXCR4, and TGFB, demonstrating a probably drug sensitivity toward PD-L1 antibodies (such as Nivolumab, Durvalumab) and other promising checkpoint inhibitors (32).

Compared with C2, C1, and C3 were more active in metabolism. Some key genes participated in glucose, fatty acid and glutamine metabolic process were upregulated in these two subtypes, which could be potential treatment targets. Results further revealed that C3 had the most number of mutations and accounted for the highest proportion of TTN, MUC16, SYNE1, PIK3CA, FAT4, RYR2, and OBSCN mutation compared with C1 and C2. Usually, approximately 15%–20% of CRCs harbored activating mutations in PIK3CA (33), but the mutant proportion of PIK3CA for C2 was almost doubled. As we were known, gene mutation may induce treatment resistance. A study proved that the PIK3CA mutations may potentially contribute to acquired cetuximab resistance in patients with metastatic CRC (34). Therefore, combining a PIK3CA inhibitor with an anti-EGFR antibody in the treatment of C3 subtype was recommended. What's more, our data also has demonstrated that patients in C3 subtype might be promising to respond to anti-PD-1 therapy.

At the end of our study, we developed a metabolism-related signature that had better performance for prognosis prediction in CRC. The signature was consisted of 27 metabolic genes, which

were not only expressed differentially among the three CRC subtypes but also significantly correlated with patients' overall survival in CRC. Tumors with high risk-score displayed significantly poor prognosis in both training and testing sets.

So far, the present study was a pioneer work for CRC classification based on metabolism signature. However, we have to mention some flaws in the present study. Firstly, datasets of larger sample size are urgently needed to verify our classification. Then, the validation of our classification in clinical samples is necessary. Moreover, basic experiments are important to understand the mechanism differences among the three metabolism-relevant subtypes in CRC.

Overall, our works deepened the understanding of metabolic hallmarks of CRC, and provided valuable information for "multi-molecular" based personalized therapies and prognosis prediction.

## DATA AVAILABILITY STATEMENT

Publicly available datasets were analyzed in this study. This data can be found here: TCGA data extracted from GDC data portal (<https://portal.gdc.cancer.gov/>), GEO (<https://www.ncbi.nlm.nih.gov/geo/>) (GSE39582).

## AUTHOR CONTRIBUTIONS

QZ designed and conceived the study. MZ analyzed data and drafted the manuscript. H-ZW completed and revised the manuscript. R-YP, FX, and FW provided advice and technical assistance. All authors contributed to the article and approved the submitted version.

## FUNDING

This study was supported by the National Natural Science Foundation of China (QZ, No. 81870390); Natural Science Foundation of Hubei Province (QZ, No. 2016CFA101).

## SUPPLEMENTARY MATERIAL

The Supplementary Material for this article can be found online at: <https://www.frontiersin.org/articles/10.3389/fonc.2020.602498/full#supplementary-material>

## REFERENCES

- Bray F, Ferlay J, Soerjomataram I, Siegel RL, Torre LA, Jemal A. Global cancer statistics 2018: GLOBOCAN estimates of incidence and mortality worldwide for 36 cancers in 185 countries. *CA Cancer J Clin* (2018) 68(6):394–424. doi: 10.3322/caac.21492
- Siegel RL, Miller KD, Jemal A. Cancer statistics, 2019. *CA Cancer J Clin* (2019) 69(1):7–34. doi: 10.3322/caac.21551
- Dekker E, Tanis PJ, Vleugels JLA, Kasi PM, Wallace MB. Colorectal cancer. *Lancet* (2019) 394(10207):1467–80. doi: 10.1016/S0140-6736(19)32319-0
- Miller KD, Nogueira L, Mariotto AB, Rowland JH, Yabroff KR, Alfano CM, et al. Cancer treatment and survivorship statistics, 2019. *CA Cancer J Clin* (2019) 69(5):363–85. doi: 10.3322/caac.21565
- Kasi PM, Shahjehan F, Cochuyl JJ, Li Z, Colibaseanu DT, Merchea A. Rising Proportion of Young Individuals With Rectal and Colon Cancer. *Clin Colorectal Canc* (2019) 18(1):e87–95. doi: 10.1016/j.clcc.2018.10.002

6. Wolf AMD, Fontham ETH, Church TR, Flowers CR, Guerra CE, LaMonte SJ, et al. Colorectal cancer screening for average-risk adults: 2018 guideline update from the American Cancer Society. *CA Cancer J Clin* (2018) 68 (4):250–81. doi: 10.3322/caac.21457
7. Punt CJA, Koopman M, Vermeulen L. From tumour heterogeneity to advances in precision treatment of colorectal cancer. *Nat Rev Clin Oncol* (2017) 14(4):235–46. doi: 10.1038/nrclinonc.2016.171
8. Fedorova MS, Krasnov GS, Lukyanova EN, Zaretsky AR, Dmitriev AA, Melnikova NV, et al. The CIMP-high phenotype is associated with energy metabolism alterations in colon adenocarcinoma. *BMC Med Genet* (2019) 20 (S1):52. doi: 10.1186/s12881-019-0771-5
9. Guinney J, Dienstmann R, Wang X, de Reyniès A, Schlicker A, Soneson C, et al. The consensus molecular subtypes of colorectal cancer. *Nat Med* (2015) 21(11):1350–6. doi: 10.1038/nm.3967
10. Dienstmann R, Vermeulen L, Guinney J, Kopetz S, Tejpar S, Tabernero J. Consensus molecular subtypes and the evolution of precision medicine in colorectal cancer. *Nat Rev Cancer* (2017) 17(2):79–92. doi: 10.1038/nrc.2016.126
11. Wu F, Wang ZL, Wang KY, Li GZ, Chai RC, Liu YQ, et al. Classification of diffuse lower-grade glioma based on immunological profiling. *Mol Oncol* (2020) 14(9):2081–95. doi: 10.1002/1878-0261.12707. Online ahead of print.
12. Hu W, Yang Y, Qi L, Chen J, Ge W, Zheng S. Subtyping of microsatellite instability-high colorectal cancer. *Cell Commun Signal* (2019) 17(1):79. doi: 10.1186/s12964-019-0397-4
13. Pavlova NN, Thompson CB. The Emerging Hallmarks of Cancer Metabolism. *Cell Metab* (2016) 23(1):27–47. doi: 10.1016/j.cmet.2015.12.006
14. La Vecchia S, Sebastián C. Metabolic pathways regulating colorectal cancer initiation and progression. *Semin Cell Dev Biol* (2020) 98:63–70. doi: 10.1016/j.semcdb.2019.05.018
15. Martinez-Outschoorn UE, Peiris-Pagès M, Pestell RG, Sotgia F, Lisanti MP. Cancer metabolism: a therapeutic perspective. *Nat Rev Clin Oncol* (2017) 14 (1):11–31. doi: 10.1038/nrclinonc.2016.60
16. Yang C, Huang X, Liu Z, Qin W, Wang C. Metabolism-associated molecular classification of hepatocellular carcinoma. *Mol Oncol* (2020) 14(4):896–913. doi: 10.1002/1878-0261.12639
17. Possemato R, Marks KM, Shaul YD, Pacold ME, Kim D, Birsoy K, et al. Functional genomics reveal that the serine synthesis pathway is essential in breast cancer. *Nature* (2011) 476(7360):346–50. doi: 10.1038/nature10350
18. Gaujoux R, Seoighe C. A flexible R package for nonnegative matrix factorization. *BMC Bioinf* (2010) 11:367. doi: 10.1186/1471-2105-11-367
19. Brunet JP, Tamayo P, Golub TR, Mesirov JP. Metagenes and molecular pattern discovery using matrix factorization. *Proc Natl Acad Sci - PNAS* (2004) 101(12):4164–9. doi: 10.1073/pnas.0308531101
20. Hanzelmann S, Castelo R, Guinney J. GSVA: gene set variation analysis for microarray and RNA-seq data. *BMC Bioinf* (2013) 14:7. doi: 10.1186/1471-2105-14-7
21. Rosario SR, Long MD, Affronti HC, Rowsam AM, Eng KH, Smiraglia DJ. Pan-cancer analysis of transcriptional metabolic dysregulation using The Cancer Genome Atlas. *Nat Commun* (2018) 9(1):5330. doi: 10.1038/s41467-018-07232-8
22. Yu G, Wang L, Han Y, He Q. clusterProfiler: an R Package for Comparing Biological Themes Among Gene Clusters. *OMICS: A J Integr Biol* (2012) 16 (5):284–7. doi: 10.1089/omi.2011.0118
23. Yoshihara K, Shahmoradgoli M, Martínez E, Vegesna R, Kim H, Torres-García W, et al. Inferring tumour purity and stromal and immune cell admixture from expression data. *Nat Commun* (2013) 4(1):2612. doi: 10.1038/ncomms3612
24. Newman AM, Steen CB, Liu CL, Gentles AJ, Chaudhuri AA, Scherer F, et al. Determining cell type abundance and expression from bulk tissues with digital cytometry. *Nat Biotechnol* (2019) 37(7):773–82. doi: 10.1038/s41587-019-0114-2
25. Roh W, Chen P, Reuben A, Spencer CN, Prieto PA, Miller JP, et al. Integrated molecular analysis of tumor biopsies on sequential CTLA-4 and PD-1 blockade reveals markers of response and resistance. *Sci Transl Med* (2017) 9(379):h3560. doi: 10.1126/scitranslmed.aah3560
26. Mayakonda A, Lin D, Assenov Y, Plass C, Koeffler HP. Maftools: efficient and comprehensive analysis of somatic variants in cancer. *Genome Res* (2018) 28 (11):1747–56. doi: 10.1101/gr.239244.118
27. Wu F, Li GZ, Liu HJ, Zhao Z, Chai RC, Liu YQ, et al. Molecular subtyping reveals immune alterations in IDH wild-type lower-grade diffuse glioma. *J Pathol* (2020) 251(3):272–83. doi: 10.1002/path.5468
28. Smith JJ, Deane NG, Wu F, Merchant NB, Zhang B, Jiang A, et al. Experimentally Derived Metastasis Gene Expression Profile Predicts Recurrence and Death in Patients With Colon Cancer. *Gastroenterology* (2010) 138(3):958–68. doi: 10.1053/j.gastro.2009.11.005
29. Ge W, Hu H, Cai W, Xu J, Hu W, Weng X, et al. High-risk Stage III colon cancer patients identified by a novel five-gene mutational signature are characterized by upregulation of IL-23A and gut bacterial translocation of the tumor microenvironment. *Int J Cancer* (2019) 146(7):2027–35. doi: 10.1002/ijc.32775
30. Thakur C, Chen F. Connections between metabolism and epigenetics in cancers. *Semin Cancer Biol* (2019) 57:52–8. doi: 10.1016/j.semcancer.2019.06.006
31. Wang W, Kandimalla R, Huang H, Zhu L, Li Y, Gao F, et al. Molecular subtyping of colorectal cancer: Recent progress, new challenges and emerging opportunities. *Semin Cancer Biol* (2019) 55:37–52. doi: 10.1016/j.semcancer.2018.05.002
32. Moehler M, Delic M, Goepfert K, Aust D, Grabsch HI, Halama N, et al. Immunotherapy in gastrointestinal cancer: Recent results, current studies and future perspectives. *Eur J Cancer* (2016) 59:160–70. doi: 10.1016/j.ejca.2016.02.020
33. Mei ZB, Duan CY, Li CB, Cui L, Ogino S. Prognostic role of tumor PIK3CA mutation in colorectal cancer: a systematic review and meta-analysis. *Ann Oncol* (2016) 27(10):1836–48. doi: 10.1093/annonc/mdw264
34. Xu J, Wang Y, Wang Y, Wang Y, Liu T, Ni M, et al. PIK3CA Mutations Contribute to Acquired Cetuximab Resistance in Patients with Metastatic Colorectal Cancer. *Clin Cancer Res* (2017) 23(16):4602–16. doi: 10.1158/1078-0432.CCR-16-2738

**Conflict of Interest:** The authors declare that the research was conducted in the absence of any commercial or financial relationships that could be construed as a potential conflict of interest.

Copyright © 2020 Zhang, Wang, Peng, Xu, Wang and Zhao. This is an open-access article distributed under the terms of the Creative Commons Attribution License (CC BY). The use, distribution or reproduction in other forums is permitted, provided the original author(s) and the copyright owner(s) are credited and that the original publication in this journal is cited, in accordance with accepted academic practice. No use, distribution or reproduction is permitted which does not comply with these terms.





# The Implications of PDK1–4 on Tumor Energy Metabolism, Aggressiveness and Therapy Resistance

Emine Atas<sup>1‡</sup>, Monika Oberhuber<sup>1,2‡</sup> and Lukas Kenner<sup>1,2,3,4\*</sup>

<sup>1</sup> Department of Pathology, Medical University of Vienna, Vienna, Austria, <sup>2</sup> Area 'Data & Technologies', CBmed—Center for Biomarker Research in Medicine GmbH, Graz, Austria, <sup>3</sup> Unit of Pathology of Laboratory Animals, University of Veterinary Medicine Vienna, Vienna, Austria, <sup>4</sup> Christian Doppler Laboratory for Applied Metabolomics (CDL AM), Division of Nuclear Medicine, Department of Biomedical Imaging and Image-Guided Therapy, Medical University of Vienna, Vienna, Austria

## OPEN ACCESS

### Edited by:

Monica Montopoli,  
University of Padua, Italy

### Reviewed by:

Cinzia Domenicotti,  
Università di Genova, Italy  
Gopinath Sutendra,  
University of Alberta, Canada

### \*Correspondence:

Lukas Kenner  
lukas.kenner@meduniwien.ac.at

### †ORCID:

Monika Oberhuber,  
orcid.org/0000-0002-5691-3605

<sup>‡</sup>These authors have contributed  
equally to this work

### Specialty section:

This article was submitted to  
Cancer Metabolism,  
a section of the journal  
Frontiers in Oncology

**Received:** 14 July 2020

**Accepted:** 13 November 2020

**Published:** 15 December 2020

### Citation:

Atas E, Oberhuber M and Kenner L  
(2020) The Implications of PDK1–4 on  
Tumor Energy Metabolism,  
Aggressiveness and  
Therapy Resistance.  
Front. Oncol. 10:583217.  
doi: 10.3389/fonc.2020.583217

A metabolic shift from oxidative phosphorylation (OXPHOS) to glycolysis—known as the Warburg effect—is characteristic for many cancers. It gives the cancer cells a survival advantage in the hypoxic tumor microenvironment and protects them from cytotoxic effects of oxidative damage and apoptosis. The main regulators of this metabolic shift are the pyruvate dehydrogenase complex and pyruvate dehydrogenase kinase (PDK) isoforms 1–4. PDK is known to be overexpressed in several cancers and is associated with bad prognosis and therapy resistance. Whereas the expression of PDK1–3 is tissue specific, PDK4 expression is dependent on the energetic state of the whole organism. In contrast to other PDK isoforms, not only oncogenic, but also tumor suppressive functions of PDK4 have been reported. In tumors that profit from high OXPHOS and high *de novo* fatty acid synthesis, PDK4 can have a protective effect. This is the case for prostate cancer, the most common cancer in men, and makes PDK4 an interesting therapeutic target. While most work is focused on PDK in tumors characterized by high glycolytic activity, little research is devoted to those cases where PDK4 acts protective and is therefore highly needed.

**Keywords:** pyruvate dehydrogenase kinase, tricarboxylic acid cycle, oxidative phosphorylation, Warburg effect, aerobic glycolysis, prostate cancer, cancer metabolism, therapy resistance

**Abbreviations:** 5-FU, 5-fluorouracil; ACAT1, Acetyl-CoA acetyltransferase 1; AML, Acute myeloid leukemia; AR, Androgen receptor; ATP, Adenosine triphosphate; BrCa, Breast cancer; BlCa, Bladder cancer; ChCa, Cholangiocarcinoma; CoA, Coenzyme-A; CoCa, Colon cancer; CRCa, Colorectal cancer; CRPCa, Castration resistant prostate cancer; CREB, CAMP response element binding protein; DCA, Dichloroacetate; E1, Pyruvate dehydrogenase; E2, Dihydrolipoamide acetyltransferase; E3, Dihydrolipoamide dehydrogenase; E3BP, E3 binding protein; EMT, Epithelial-mesenchymal transition; FASN, Fatty acid synthase; FGFR1, Fibroblast growth factor receptor 1; GCA, Gastric cancer; GLUT, Glucose transporters; HCCa, Hepatocellular carcinoma; HIF1 $\alpha$ , Hypoxia inducible factor 1 alpha; HNSCCa, Head and neck squamous cell carcinoma; LDHA, Lactate dehydrogenase A; mTORC1, Mechanistic target of rapamycin complex 1; NAD<sup>+</sup>, Nicotinamide adenine dinucleotide; NADH, Reduced form of NAD<sup>+</sup>; NF- $\kappa$ B, Nuclear factor kappa-light-chain-enhancer; NSCLCa, Non-small cell lung cancer; OCa, Ovarian cancer; OXPHOS, Oxidative phosphorylation; PCa, Prostate cancer; PDK, Pyruvate dehydrogenase kinase; PDP, Pyruvate dehydrogenase phosphatase; RHEB, Ras homolog enriched in brain; ROS, Reactive oxygen species; SIRT, Sirtuin; STAT3, Signal transducer and activator of transcription 3; SCD, Stearoyl-CoA desaturase; TCA cycle, Tricarboxylic acid cycle; TNF, Tumor necrosis factor.

## INTRODUCTION

Besides other hallmarks of cancer, such as sustained proliferative signaling, resistance to cell death, invasiveness and increased angiogenesis, tumors are characterized by their altered metabolic features (1, 2). The two major metabolic pathways providing energy in the form of adenosine triphosphate (ATP) are glycolysis and oxidative phosphorylation (OXPHOS) (1, 3). Under aerobic conditions, glucose is metabolized to pyruvate *via* glycolysis in the cytosol (4). Pyruvate is then processed to CO<sub>2</sub> in the mitochondria *via* the tricarboxylic acid (TCA) cycle and OXPHOS (1, 3) (**Figure 1**). On the contrary, under anaerobic conditions glycolysis is favored, where pyruvate is mostly converted to lactate and only minimal amounts enter the TCA cycle (1, 3). Cancer cells typically present a metabolic shift from the TCA cycle/OXPHOS to glycolysis or lactate fermentation regardless of the presence of oxygen, a phenomenon known as the “Warburg effect” (7, 8). Hereby, cancer cells obtain survival advantages in hypoxic tumor microenvironments where OXPHOS is compromised (3). However, the switch to aerobic glycolysis in the cancer cell is not only limited to hypoxia but is also activated by deregulated signals enhancing glycolysis or hindering OXPHOS (3, 9, 10).

The metabolic shift from TCA cycle/OXPHOS to aerobic glycolysis is tightly regulated (11). The following review focuses on the key players in this regulation—the mitochondrial pyruvate dehydrogenase complex (PDC) and the pyruvate dehydrogenase kinases (PDK). PDK have been associated with tumor aggressiveness, proliferation, anti-apoptotic effects and

therapy resistance in numerous malignancies (12–16). We here provide a compact overview on the latest research on the cancer specific levels of PDK isoforms and their associations with tumor aggressiveness and therapy resistance. We will also address the remarkable energy metabolism of prostate cancer (PCa) and the resulting effects of PDK on tumor growth. A detailed discussion of metabolic pathways intersecting with the TCA cycle and their interplay with the PDC/PDK axis is beyond the scope of this review but can be found here: Gray et al., Hirschey et al., Martínez-Reyes and Chandel et al., Vander Heiden and DeBerardinis et al. (4, 17–19).

## REGULATION OF THE METABOLIC SHIFT BY PDC/PDK ACTIVITY

One of the main enzymes regulating the metabolic shift in mammals is the mitochondrial PDC (20, 21). It is composed of the pyruvate dehydrogenase (E1), dihydrolipoamide acetyl-transferase (E2), dihydrolipoamide dehydrogenase (E3) and the E3 binding protein (E3BP) (4, 22). The PDC catalyzes the irreversible conversion of pyruvate, nicotinamide adenine dinucleotide (NAD<sup>+</sup>) and coenzyme-A (CoA) into acetyl-CoA, NADH and CO<sub>2</sub> (4). The converted acetyl-CoA then enters the TCA cycle (4). Thus, PDC represents an important link between glycolysis and TCA cycle/OXPHOS (20, 21, 23) (**Figure 1**). PDC is more active in the healthy and well-nourished state, whereas its activity is decreased during fasting or low glucose levels, but also in diabetes and most cancer types (21, 24). The activity of the

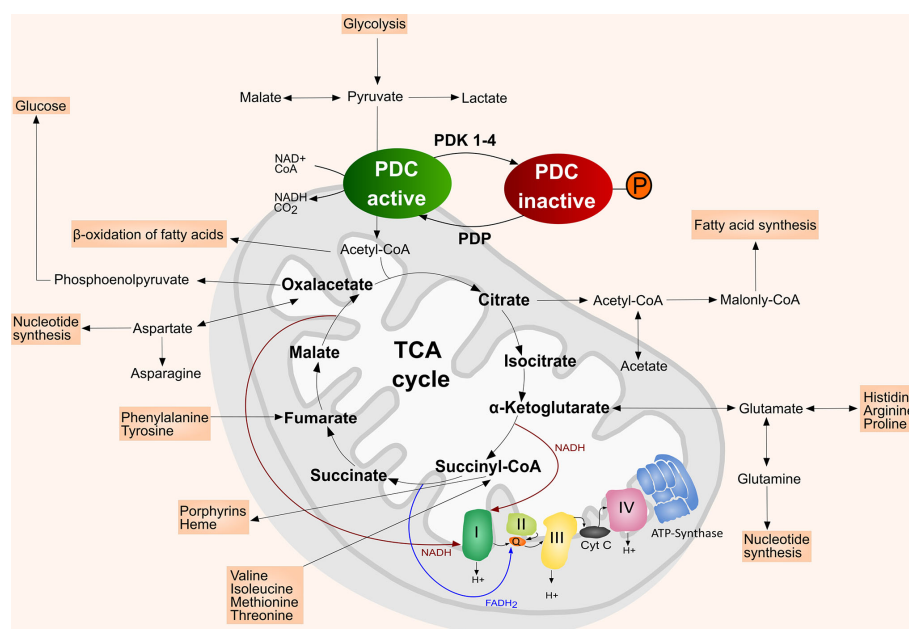


**FIGURE 1** | Simplified scheme of the mitochondrion with TCA cycle and the intersecting anaplerotic and cataplerotic reactions, OXPHOS complexes I–IV, and ATP synthase (complex V). In the mitochondrial matrix the PDC catalyzes the irreversible conversion of pyruvate, NAD<sup>+</sup> and CoA into acetyl-CoA, NADH and CO<sub>2</sub>. PDK inactivate the PDC by phosphorylating its E1α subunit, which hinders the entrance of acetyl-CoA into the TCA cycle. The PDC is reactivated upon dephosphorylation by PDP. Adapted from (5). Inspiration (4, 6).

PDC is mainly regulated by four PDK isoenzymes (PDK1–4) that are located in the mitochondrial matrix (20, 25). PDK1–4 achieve a reversible downregulation of the PDC by phosphorylating specific serine residues (Ser293, Ser300, and Ser232) of its E1 $\alpha$  subunit, thereby reducing the metabolic flux through the PDC and downstream pathways (4, 20, 23, 25). The E1 $\alpha$  subunit of the PDC can be dephosphorylated by pyruvate dehydrogenase phosphatase (PDP), which leads to the reactivation of the PDC (4, 22, 23) (**Figure 1**). In addition, PDC can also be reversely acetylated and succinylated (26, 27). Acetylation of the PDC E1 $\alpha$  subunit by acetyl-CoA acetyltransferase 1 (ACAT1) results in dissociation of PDP1 from the PDC and PDK1 recruitment, thereby suppressing PDC activity (26, 28, 29). Lysine desuccinylation of PDC subunits by sirtuin (SIRT) 3 and SIRT5 also results in suppression of PDC activity (26).

Besides generating reductive equivalents for OXPHOS, the TCA cycle provides precursors for biosynthetic processing of lipids, amino acids, and nucleotides (17, 19). Anaplerotic (carbon replenishing) and cataplerotic (carbon expending) pathways intersecting the TCA cycle balance the carbon flux (4). Pyruvate provides carbon either *via* the PDC or alternatively *via* conversion to oxaloacetate (4, 17, 30). Furthermore, glutamine contributes glutamate,  $\alpha$ -ketoglutarate, aspartate, CO<sub>2</sub>, pyruvate, lactate, alanine and citrate to the TCA cycle, which makes it a key player in the mitochondrial metabolism supporting proliferation of cancer cells (**Figure 1**) (4, 17, 19, 30).

A detailed discussion of the role of glutamine metabolism in cancer was published by Masisi et al. (31).

## PDK1–4 LEVELS IN DIFFERENT CANCERS AND THEIR PROGNOSTIC IMPLICATIONS

PDK1–4 are differentially expressed in several metabolic tissues (32). PDK1 is abundant in the cardiac muscle, pancreatic islets, and skeletal muscle and is expressed at lower levels in other tissues (20, 22, 23, 33–35). PDK2 on the contrary is ubiquitously expressed, with the highest expression levels in the heart, diaphragm, kidney, and red skeletal muscles (22). Other tissues such as liver, brain, testis, ovaries, and lung show lower PDK2 protein levels (22). While PDK3 has a weak expression pattern in kidney, brain, testis, and lung, PDK4 is mainly expressed in the heart, skeletal muscle, pancreatic islets and at intermediate levels in the liver, lung, and kidney (20, 22, 23, 33–35).

PDK1, a downstream target of hypoxia inducible factor 1 alpha (HIF1 $\alpha$ ), is upregulated in a number of cancers including ovarian cancer (OCa) (36), gastric cancer (GCa) (37, 38), colorectal cancer (CRCa) (39), PCa (40), and acute myeloid leukemia (AML) (41). Involvement of PDK1 has also been implicated in cancer cell epithelial–mesenchymal transition (EMT) and metastasis, for example in metastasis of liver aggressive 4T1 breast cancer (BrCa) cells to the liver, which implies an oncogenic role (12) (**Table 1**). PDK1 can be tyrosine phosphorylated and thereby activated

**TABLE 1** | Overview of PDK1–4 expression levels in different cancer types, their effect on prognosis upon up-regulation and tumorigenesis.

Expression level in cancer			Prognosis upon up-regulation	Effect on tumorigenesis	References	
PDK1	AML	↑	p. bad	oncogenic	(41)	
	BrCa	↑	bad	oncogenic	(12, 42)	
	CRCa	↑	p. bad	oncogenic	(39)	
	GCa	↑	bad	p. oncogenic	(37, 38)	
	HNSCCa	↑	bad	oncogenic	(43, 44)	
	NSCLCa	↑	bad	oncogenic	(45)	
	OCa	↑	bad	oncogenic	(36)	
	PCa	↑	p. bad	oncogenic	(40)	
PDK2	AML	↑	bad	p. oncogenic	(46)	
	CRCa	↑	bad	p. oncogenic	(14)	
	GCa	↑	p. bad	oncogenic	(47)	
	HCCa	↑	p. bad	oncogenic	(48)	
	HNSCCa	↑	p. bad	oncogenic	(49, 50)	
PDK3	AML	↑	bad	p. oncogenic	(46)	
	ChCa	↑	bad	p. oncogenic	(51)	
	CRCa	↑	bad	oncogenic	(15)	
	GCa	↑	p. bad	oncogenic	(52)	
	Glioma	↑	p. bad	oncogenic	(53)	
	Melanoma	↑	p. bad	oncogenic	(54)	
	PCa	↑	p. bad	oncogenic	(40)	
PDK4	AML	↑	p. bad	oncogenic	(55)	
	BiCa	↑	p. bad	oncogenic	(56)	
	BrCa	↑	bad	p. oncogenic	(57, 58)	
	CRCa	↑	bad	oncogenic	(13, 59)	
	HCCa		↓	good	suppressive	(16, 60)
	NSCLCa		↓	p. good	suppressive	(61)
	OCa	↑	bad	oncogenic	(62)	
	PCa		↓	good	p. suppressive	(63)

p. = presumably, ↑ = high, ↓ = low.

by tyrosine kinase fibroblast growth factor receptor 1 (FGFR1), which localizes to mitochondria (64). Interestingly, both the PDC and PDK1 were also detected in the outer mitochondrial matrix, where PDK1 can be directly phosphorylated by tyrosine kinases (64).

PDK2 is the only PDK enzyme that has been confirmed as p53 target (65). P53 downregulates and controls PDK2 expression on transcriptional and posttranscriptional level and thereby reduces the Warburg effect (25, 65). In hepatocellular carcinoma (HCCa) (48) and GCa cells (47) proliferation and migration were suppressed after downregulation of PDK2. PDK2 has also been associated with therapy resistance in CRCa cells (14), in head and neck squamous cell carcinoma (HNSCCa) cells (49), and in non-small cell lung cancer (NSCLCa) patients (66) (Table 1).

PDK3, which has the highest binding affinity to the PDC, is the least studied isoenzyme of the PDK (25). Similarly to PDK1, PDK3 is induced by HIF-1 $\alpha$ , and higher expression is associated with higher tumor stage in many cancers (15, 67). In GCa (52), glioma (53), PCa (40), AML (46), and melanoma (54), high expression of PDK3 has been shown. Knockdown of PDK3 in the GCa cell lines SGC7901 and AGS (52), and the PCa cell line LNCaP (40) inhibited proliferation and induced apoptosis. Moreover, elevated expression of PDK3 is associated with chemo resistance in GCa cells (68), increased drug resistance in CoCa cells (15) and correlates with poor prognosis in cholangiocarcinoma (ChCa) (51), and AML (46) (Table 1).

While the regulation of PDK1–3 reflects the immediate energy demands of the cell, PDK4 reflects whole organism energy balance and is upregulated during excessive exercise (69), starvation (70), in insulin resistant states and diabetes (6, 57). PDK4 is also involved in the control of muscle size in cancer stages or after chemotherapy treatment, which renders it interesting as a target to combat cancer-associated cachexia (20). Based on the metabolic function of the respective tissue, the cancer type and stage, high PDK4 expression can act either oncogenic or tumor suppressive, as described below (Table 1).

The overexpression of PDK4 is associated with poorer prognosis in BrCa patients, irrespective of their molecular or histological subtype (58) and is associated with antiestrogen resistance (57). Duan et al. showed that PDK4 expression induced by benzyl butyl phthalate promotes glycolysis and proliferation in AML cells (55). In human metastatic CoCa cells, knockdown of PDK4 reduced their migratory and invasive properties (13). Furthermore, HIF1 $\alpha$  expression was reduced in PDK4 knockdown cells, suggesting a correlation between PDK4 and HIF1 $\alpha$  (13). PDK4 is also linked to enhanced cell proliferation and invasion in OCa (62) and bladder cancer (BlCa) (56). In addition, PDK4 has been identified as a positive regulator and activator of mechanistic target of rapamycin complex 1 (mTORC1) by cAMP response element binding protein (CREB)-mediated transcriptional regulation of the small GTPase Ras homologue enriched in brain (RHEB) (71). Additionally, Wu et al. suggested that PDK4 is essential for tumor necrosis factor alpha (TNF- $\alpha$ ) to execute its pro-survival function *via* nuclear factor 'kappa-light-

chain-enhancer' of activated B-cells (NF- $\kappa$ B), and consequently PDK4 deficiency in HCCa cells results in apoptosis (72).

In contrast, a tumor suppressive effect of PDK4 was observed in lung cancer (61, 73) and HCCa (16, 60). Sun et al. described that a metabolic switch from glycolysis to OXPHOS was observed in NSCLCa cells that underwent EMT, which was induced by knockdown of PDK4 (73). In the liver, PDK4 expression is associated with increased survival and liver function of patients undergoing liver resection due to colorectal liver metastases, and its downregulation predicted poor prognosis in HCCa patients (59). Besides that, loss of PDK4 resulted in enhanced lipogenesis and more aggressive tumors in HCCa (16). In PCa, Oberhuber et al. showed the association of low PDK4 with a risk of earlier disease recurrence in PCa, independent of tumor grading and tumor stage (63).

## PDK1–4 ARE ASSOCIATED WITH THERAPY RESISTANCE IN SEVERAL CANCERS

PDK1–4 have been associated with therapy resistance in several cancers. Qian et al. revealed that miR-4290 improved the sensitivity of GCa cells to cisplatin and induced apoptosis by downregulating PDK1 expression (38). Moreover, genetic knockdown of PDK1 abolished hypoxia-induced 5-fluorouracil (5-FU) resistance in GCa cells (74) and sensitized resistant OCa cells to cisplatin-induced cell death and apoptosis (75). Recently, PDK2 has been shown to induce resistance to 5-FU in chemo resistant CRCa cells (14), to be associated with cisplatin resistance in HNSCCa cells (49) and acquired paclitaxel-resistance in NSCLCa patients (66). PDK3 is associated with chemo resistance in GCa cells (68) and increased drug resistance in CoCa cells (15). Altered regulation of PDK4 is suggested to play a role in antiestrogen resistance in BrCa cells (57). In tamoxifen resistant MCF-7 breast cancer cells, PDK4 mRNA overexpression, but not enhanced protein levels, have been shown (57). Wang et al. described PDK4-induced chemo resistance in OCa (62). Sun et al. showed that downregulation of PDK4 in lung cancer drives EMT and promotes erlotinib resistance in EGFR mutant lung cancer cells (73). The combination of chemotherapeutic drugs with dichloroacetate (DCA), a PDK inhibitor, have been shown to enhance therapeutic efficacy (76). In addition, DCA has been described to increase radiosensitivity by increasing tumor oxygenation and reactive oxygen species (ROS) activity (76).

The association of PDK to therapy resistance can be explained by the anti-apoptotic and ROS protective benefits of the Warburg effect, which results in proliferative advantages (27, 76). The Warburg effect is supported by activated oncogenes and HIF1 $\alpha$ , which induce the expression of glycolytic enzymes and transporters, such as glucose transporters (GLUTs) or lactate dehydrogenase A (LDHA) that are involved in glucose uptake, lactate production, and lactate secretion (27, 77). As a result, tumors are characterized by high levels of glycolysis and lactate



production, and low levels of PDC activity and OXPHOS (27, 77). High accumulation of lactate and low OXPHOS activity lead to reduced activation of the apoptotic cascade and ROS, which protect cancer cells from cytotoxic effects of oxidative damage and apoptosis (3, 9, 10, 27, 76). Although aerobic glycolysis generates less energy (2 ATP per glucose molecule) than OXPHOS (36 ATP per oxidized glucose molecule) a high rate of glucose uptake of the tumor can compensate the tumor's energetic demands (10, 11). DeBerardinis et al. suppose that generation of energy *via* glycolysis is faster and therefore more attractive than the more energy efficient but slower OXPHOS (77).

## THE PECULIAR ENERGY METABOLISM OF PCa AND ITS IMPLICATIONS ON THE ROLE OF PDK4

Primary PCa is lacking the Warburg effect and has a very distinctive energy metabolism compared to most other cancer types, showing high TCA cycle/OXPHOS activity (78, 79). The energy metabolism of the normal prostate cell is a result of its biological function, where the glandular epithelial cells secrete prostatic fluid and its main component—citrate—into the lumen (79, 80). Prostate epithelial cells accumulate extensive amounts of zinc, which inhibit the TCA cycle enzyme m-aconitase (78–80). Thereby citrate cannot be converted to isocitrate, the TCA cycle is truncated, and citrate is secreted by the prostatic epithelial cells (**Figure 2A**). As the prostatic epithelial cells have low OXPHOS activity, they mainly rely on aerobic

glycolysis and are therefore energetically inefficient (78–80). In contrast, PCa cells no longer present zinc-accumulation and citrate-secretion, but activated TCA cycle/OXPHOS, thereby generating additional ATP (78, 80) (**Figure 2B**). Latonen et al. and Xue et al. show an increase in aconitase expression in PCa cells compared to non-cancerous tissue, which indicates their citrate oxidizing ability (81, 82). Acetyl-CoA provided by the TCA cycle serves as substrate for lipogenesis, which is known to be hyper-activated in PCa and associated with androgen resistance and tumor aggressiveness (17, 83–85). Lipogenic enzymes, as well as genes involved in cholesterol synthesis, have been shown to be regulated by androgen signaling (84). In turn, inhibition of fatty acid synthase (FASN), a key enzyme of *de novo* fatty acid synthesis, led to reduced androgen receptor (AR) expression in castration-resistant PCa (CRPCa) (85). PDK4 is not only a regulator of PDC activity, but can also alter fatty acid metabolism, as has been shown in HCCa cells (16). Here, knockdown of PDK4 did not alter OXPHOS, but resulted in enhanced expression of FASN and stearoyl-CoA desaturase (SCD) (16). Similarly, PDK4 was shown to enhance lipogenesis in lung cancer cells (61).

Since low levels of PDK4 result in enhanced OXPHOS and/or enhanced lipogenesis, both of which are associated with poor prognosis in PCa, PDK4 should have a tumor suppressive effect in primary PCa. Recently, a protective effect of high *PDK4*-expression in PCa in a transcriptomic patient dataset was demonstrated (63). In accordance with these data, augmented gene expression and protein levels of the PDC subunit E1 (*PDHA1*) and the PDC activator PDP1 were identified in PCa (86). In contrast, Wang et al. reported lower proliferation and

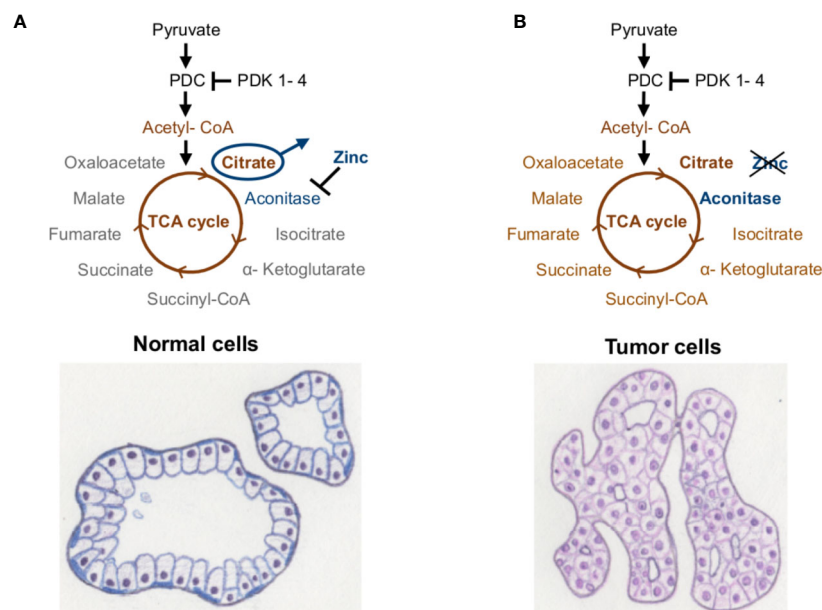


**FIGURE 2 |** Energy metabolism of the prostate. **(A)** Healthy prostate cells accumulate high amounts of zinc, which inhibit the enzyme m-aconitase and thereby truncate the TCA cycle. **(B)** Prostate tumor cells show lower levels of zinc, whereby the enzyme aconitase remains active and citrate can be metabolized *via* the TCA cycle and OXPHOS. Taken from (5), inspired by (78).

increased apoptosis in PCa cells upon knockdown of all PDK isoforms (40). While PDK4 and PDK2 are expressed at lower levels, PDK1 and PDK3 are supposedly overexpressed in PCa and associated with advanced tumor stages (40).

The specific effects of PDK1–4 on PCa energy and fatty acid metabolism have not been investigated yet. In addition to their direct implications on pyruvate provided carbon use and OXPHOS, also compensative mechanisms must be considered. These were shown to be active in metformin treated PCa cells (87). Here, metformin reduces entry of glucose-derived carbon into the TCA cycle due to complex I inhibition (87). The loss of glucose as carbon source was compensated by increased reductive glutamine metabolism, which provides  $\alpha$ -ketoglutarate to the TCA cycle (87). Additional inhibition of the reductive glutamine pathway resulted in enhanced PCa cell sensitivity to metformin (87).

Given the importance of the hyperactive FASN and the unique dependence on OXPHOS in primary PCa, we are convinced that the action of PDK4 in PCa has a profound clinical significance and therefore requires immediate research.

## SUMMARY AND CONCLUSION

PDK1–3 are described as oncogenes in different cancer types where their high expression is associated with EMT and metastasis, higher proliferation and migration, and most relevantly with therapy resistances, such as to 5-FU in CRCa and GCa, cisplatin in HNSCCa and OCa or paclitaxel in NSCLCa. In contrast to PDK1–3, data suggest either oncogenic or tumor suppressive function of PDK4, dependent on the metabolic profile of the tumor. It acts as an oncogene and is linked to therapy resistance in tumors that benefit from high glycolytic activity, such as in BrCa, AML, CoCa, OCa and BlCa. However, PDK4 can act as tumor suppressor in cancers that depend on high OXPHOS activity and/or high amounts of TCA cycle intermediates, as has been shown in PCa. Also in NSCLCa and HCCa low PDK4 levels are described to lead to more aggressive tumors and therapy resistance. We conclude that the combinatorial treatment of DCA with chemotherapeutic drugs might enable overcoming therapy resistances only in cancer types with a fitting metabolic profile (76). A large body of research is directed to tumors that profit from high glycolysis/lactate

accumulation, whereas far less is known about those cases, where high OXPHOS contributes to tumor aggressiveness. Especially for PCa, where only little research is available on the mechanistic regulation and effects of PDK4, more research is needed in this regard.

## AUTHOR CONTRIBUTIONS

All authors contributed to the conception and design of the review. EA and MO conducted literature research. EA wrote the first draft of the manuscript. All authors contributed to editing and rewriting of the manuscript. EA and MO created the figures for the manuscript. All authors contributed to the article and approved the submitted version.

## FUNDING

EA and LK are funded by the Austrian Science Fund (FWF): IPPTO project number DOC 59-B33. MO and LK were funded by the COMET Competence Center CBmed-Center for Biomarker Research in Medicine (FA791A0906.FFG). The COMET Competence Center CBmed is funded by the Austrian Federal Ministry for Transport, Innovation and Technology (BMVIT); the Austrian Federal Ministry for Digital and Economic Affairs (BMDW); Land Steiermark (Department 12, Business and Innovation); the Styrian Business Promotion Agency (SFG); and the Vienna Business Agency. The COMET program is executed by the FFG. LK was in addition funded by the FWF grant P26011 and the Christian-Doppler Lab for Applied Metabolomics. The financial support by the Austrian Federal Ministry for Transport, Innovation and Technology and the National Foundation for Research, Technology and Development is gratefully acknowledged.

## ACKNOWLEDGMENTS

We thank Assoc. Prof. Dr. Brigitte Hantusch for proof-reading the manuscript.

## REFERENCES

- Hanahan D, Weinberg RA. Hallmarks of Cancer: The Next Generation. *Cell* (2011) 144(5):646–74. doi: 10.1016/j.cell.2011.02.013
- Pavlova NN, Thompson CB. The Emerging Hallmarks of Cancer Metabolism. *Cell Metab* (2016) 23(1):27–47. doi: 10.1016/j.cmet.2015.12.006
- Bhattacharya B, Mohd Omar MF, Soong R. The Warburg effect and drug resistance: The Warburg effect and drug resistance. *Br J Pharmacol* (2016) 173(6):970–9. doi: 10.1111/bph.13422
- Gray LR, Tompkins SC, Taylor EB. Regulation of pyruvate metabolism and human disease. *Cell Mol Life Sci* (2014) 71(14):2577–604. doi: 10.1007/s00018-013-1539-2
- Oberhuber M. *Prostate cancer biomarker identification through proteomic and transcriptomic analyses. Doctoral thesis.* Vienna, Austria: Medical University of Vienna (2020).
- Lee I-K. The Role of Pyruvate Dehydrogenase Kinase in Diabetes and Obesity. *Diabetes Metab J* (2014) 38(3):181. doi: 10.4093/dmj.2014.38.3.181
- Warburg O. On the Origin of Cancer Cells. *Science* (1956) 24123(3191):309–14. doi: 10.1126/science.123.3191.309
- Weinhouse S, Warburg O, Burk D, Schade AL. On Respiratory Impairment in Cancer Cells. *Science* (1956) 10124(3215):267–72. doi: 10.1126/science.124.3215.267
- Orang AV, Petersen J, McKinnon RA, Michael MZ. Micromanaging aerobic respiration and glycolysis in cancer cells. *Mol Metab* (2019) 23:98–126. doi: 10.1016/j.molmet.2019.01.014

10. Zhang W, Zhang S-L, Hu X, Tam KY. Targeting Tumor Metabolism for Cancer Treatment: Is Pyruvate Dehydrogenase Kinases (PDKs) a Viable Anticancer Target? *Int J Biol Sci* (2015) 11(12):1390–400. doi: 10.7150/ijbs.13325
11. Jang M, Kim SS, Lee J. Cancer cell metabolism: implications for therapeutic targets. *Exp Mol Med* (2013) 45(10):e45–5. doi: 10.1038/emmm.2013.85
12. Dupuy F, Tabariès S, Andrzejewski S, Dong Z, Blagih J, Annis MG, et al. PDK1-Dependent Metabolic Reprogramming Dictates Metastatic Potential in Breast Cancer. *Cell Metab* (2015) 22(4):577–89. doi: 10.1016/j.cmet.2015.08.007
13. Leclerc D, Pham DNT, Lévesque N, Truongcao M, Foulkes WD, Sapienza C, et al. Oncogenic role of PDK4 in human colon cancer cells. *Br J Cancer* (2017) 116(7):930–6. doi: 10.1038/bjc.2017.38
14. Liang Y, Hou L, Li L, Li L, Zhu L, Wang Y, et al. Dichloroacetate restores colorectal cancer chemosensitivity through the p53/miR-149-3p/PDK2-mediated glucose metabolic pathway. *Oncogene* (2020) 39(2):469–85. doi: 10.1038/s41388-019-1035-8
15. Lu C-W, Lin S-C, Chien C-W, Lin S-C, Lee C-T, Lin B-W, et al. Overexpression of Pyruvate Dehydrogenase Kinase 3 Increases Drug Resistance and Early Recurrence in Colon Cancer. *Am J Pathol* (2011) 179(3):1405–14. doi: 10.1016/j.ajpath.2011.05.050
16. Yang C, Wang S, Ruan H, Li B, Cheng Z, He J, et al. Downregulation of PDK4 Increases Lipogenesis and Associates with Poor Prognosis in Hepatocellular Carcinoma. *J Cancer* (2019) 10(4):918–26. doi: 10.7150/jca.27226
17. Hirschey MD, DeBerardinis RJ, Diehl AME, Drew JE, Frezza C, Green MF, et al. Dysregulated metabolism contributes to oncogenesis. *Semin Cancer Biol* (2015) 35:S129–50. doi: 10.1016/j.semcancer.2015.10.002
18. Martínez-Reyes I, Chandel NS. Mitochondrial TCA cycle metabolites control physiology and disease. *Nat Commun* (2020) 11(1):102. doi: 10.1038/s41467-019-13668-3
19. Vander Heiden MG, DeBerardinis RJ. Understanding the Intersections between Metabolism and Cancer Biology. *Cell* (2017) 168(4):657–69. doi: 10.1016/j.cell.2016.12.039
20. Pin F, Novinger LJ, Huot JR, Harris RA, Couch ME, O'Connell TM, et al. PDK4 drives metabolic alterations and muscle atrophy in cancer cachexia. *FASEB J* (2019) 33(6):7778–90. doi: 10.1096/fj.201802799R
21. Zhang S, Hulver MW, McMillan RP, Cline MA, Gilbert ER. The pivotal role of pyruvate dehydrogenase kinases in metabolic flexibility. *Nutr Metab (Lond)* (2014) 11(1):10. doi: 10.1186/1743-7075-11-10
22. Klyuyeva A, Tuganova A, Kedishvili N, Popov KM. Tissue-specific kinase expression and activity regulate flux through the pyruvate dehydrogenase complex. *J Biol Chem* (2019) 18294(3):838–51. doi: 10.1074/jbc.RA118.006433
23. Kolobova E, Tuganova A, Boulatnikov I, Popov KM. Regulation of pyruvate dehydrogenase activity through phosphorylation at multiple sites. (2001) 9:69–77. doi: 10.1042/0264-6021:3580069
24. Connaughton S, Chowdhury F, Attia RR, Song S, Zhang Y, Elam MB, et al. Regulation of pyruvate dehydrogenase kinase isoform 4 (PDK4) gene expression by glucocorticoids and insulin. *Mol Cell Endocrinol* (2010) 315(1–2):159–67. doi: 10.1016/j.mce.2009.08.011
25. Woolbright BL, Rajendran G, Harris RA, Taylor JA. Metabolic Flexibility in Cancer: Targeting the Pyruvate Dehydrogenase Kinase:Pyruvate Dehydrogenase Axis. *Mol Cancer Ther* (2019) 18(10):1673–81. doi: 10.1158/1535-7163.MCT-19-0079
26. Saunier E, Benelli C, Bortoli S. The pyruvate dehydrogenase complex in cancer: An old metabolic gatekeeper regulated by new pathways and pharmacological agents: Pyruvate dehydrogenase complex in cancer. *Int J Cancer* (2016) 15138(4):809–17. doi: 10.1002/ijc.29564
27. Stacpoole PW. Therapeutic Targeting of the Pyruvate Dehydrogenase Complex/Pyruvate Dehydrogenase Kinase (PDC/PDK) Axis in Cancer. *JNCI: J Natl Cancer Institute* (2017) 109(11):dx071. doi: 10.1093/jnci/djx071
28. Fan J, Shan C, Kang H-B, Elf S, Xie J, Tucker M, et al. Tyr Phosphorylation of PDP1 Toggles Recruitment between ACAT1 and SIRT3 to Regulate the Pyruvate Dehydrogenase Complex. *Mol Cell* (2014) Feb53(4):534–48. doi: 10.1016/j.molcel.2013.12.026
29. Shan C, Kang H-B, Elf S, Xie J, Gu T-L, Aguiar M, et al. Tyr-94 Phosphorylation Inhibits Pyruvate Dehydrogenase Phosphatase 1 and Promotes Tumor Growth. *J Biol Chem* (2014) 289(31):21413–22. doi: 10.1074/jbc.M114.581124
30. Luengo A, Gui DY, Vander Heiden MG. Targeting Metabolism for Cancer Therapy. *Cell Chem Biol* (2017) 24(9):1161–80. doi: 10.1016/j.chembiol.2017.08.028
31. Masisi BK, El Ansari R, Alfarsi L, Rakha EA, Green AR, Craze ML. The role of glutaminase in cancer. *Histopathology* (2020) 76(4):498–508. doi: 10.1111/his.14014
32. Yang R, Guo C. Discovery of potent pyruvate dehydrogenase kinase inhibitors and evaluation of their anti-lung cancer activity under hypoxia. *Med Chem Commun* (2018) 9(11):1843–9. doi: 10.1039/C8MD00453F
33. Kato M, Li J, Chuang JL, Chuang DT. Distinct Structural Mechanisms for Inhibition of Pyruvate Dehydrogenase Kinase Isoforms by AZD7545, Dichloroacetate, and Radicol. *Structure* (2007) 5(8):992–1004. doi: 10.1016/j.str.2007.07.001
34. Park B-Y, Jeon J-H, Go Y, Ham HJ, Kim J-E, Yoo EK, et al. PDK4 Deficiency Suppresses Hepatic Glucagon Signaling by Decreasing cAMP Levels. *Diabetes* (2018) 67(10):2054–68. doi: 10.2337/db17-1529
35. Tao R, Xiong X, Harris RA, White MF, Dong XC. Genetic Inactivation of Pyruvate Dehydrogenase Kinases Improves Hepatic Insulin Resistance Induced Diabetes. *Zang M editor PloS One* (2013) 8(8):e71997. doi: 10.1371/journal.pone.0071997
36. Siu MKY, Jiang Y, Wang J, Leung THY, Ngu SF, Cheung ANY, et al. PDK1 promotes ovarian cancer metastasis by modulating tumor-mesothelial adhesion, invasion, and angiogenesis via  $\alpha 5 \beta 1$  integrin and JNK/IL-8 signaling. *Oncogenesis* (2020) 9(2):1–16. doi: 10.1038/s41389-020-0209-0
37. HUR H, XUAN Y, KIM YB, LEE G, SHIM W, YUN J, et al. Expression of pyruvate dehydrogenase kinase-1 in gastric cancer as a potential therapeutic target. *Int J Oncol* (2012) 42(1):44–54. doi: 10.3892/ijo.2012.1687
38. Qian Y, Wu X, Wang H, Hou G, Han X, Song W. MicroRNA-4290 suppresses PDK1-mediated glycolysis to enhance the sensitivity of gastric cancer cell to cisplatin. *Braz J Med Biol Res* (2020) 53(5):e9330. [cited 2020 Jun 18]. doi: 10.1590/1414-431x20209330
39. Qin W, Tian Y, Zhang J, Liu W, Zhou Q, Hu S, et al. The double inhibition of PDK1 and STAT3-Y705 prevents liver metastasis in colorectal cancer. *Sci Rep* (2019) 9(1):12973. doi: 10.1038/s41598-019-49480-8
40. Wang L-Y, Hung C-L, Chen Y-R, Yang JC, Wang J, Campbell M, et al. KDM4A Coactivates E2F1 to Regulate the PDK-Dependent Metabolic Switch between Mitochondrial Oxidation and Glycolysis. *Cell Rep* (2016) 16(11):3016–27. doi: 10.1016/j.celrep.2016.08.018
41. Qin L, Tian Y, Yu Z, Shi D, Wang J, Zhang C, et al. Targeting PDK1 with dichloroacetophenone to inhibit acute myeloid leukemia (AML) cell growth. *Oncotarget* (2015) 7(2):1395–407. doi: 10.18632/oncotarget.6366
42. Peng F, Wang J-H, Fan W-J, Meng Y-T, Li M-M, Li T-T, et al. Glycolysis gatekeeper PDK1 reprograms breast cancer stem cells under hypoxia. *Oncogene* (2018) 37(8):1119. doi: 10.1038/ncr.2017.407
43. McFate T, Mohyeldin A, Lu H, Thakar J, Henriques J, Halim ND, et al. Pyruvate Dehydrogenase Complex Activity Controls Metabolic and Malignant Phenotype in Cancer Cells. *J Biol Chem* (2008) 283(33):22700–8. doi: 10.1074/jbc.M801765200
44. Wigfield SM, Winter SC, Giatromanolaki A, Taylor J, Koukourakis ML, Harris AL. PDK-1 regulates lactate production in hypoxia and is associated with poor prognosis in head and neck squamous cancer. *Br J Cancer* (2008) 98(12):1975–84. doi: 10.1038/sj.bjc.6604356
45. Liu T, Yin H. PDK1 promotes tumor cell proliferation and migration by enhancing the Warburg effect in non-small cell lung cancer. *Oncol Rep* (2017) 37(1):193–200. doi: 10.3892/or.2016.5253
46. Cui L, Cheng Z, Liu Y, Dai Y, Pang Y, Jiao Y, et al. Overexpression of PDK2 and PDK3 reflects poor prognosis in acute myeloid leukemia. *Cancer Gene Ther* (2020) 27(1–2):15–21. doi: 10.1038/s41417-018-0071-9
47. He Z, Li Z, Zhang X, Yin K, Wang W, Xu Z, et al. miR-422a regulates cellular metabolism and malignancy by targeting pyruvate dehydrogenase kinase 2 in gastric cancer. *Cell Death Dis* (2018) 9(5):505. doi: 10.1038/s41419-018-0564-3
48. Yu Q, Zhou J, Jian Y, Xiu Z, Xiang L, Yang D, et al. MicroRNA-214 suppresses cell proliferation and migration and cell metabolism by targeting PDK2 and PHF6 in hepatocellular carcinoma. *Cell Biol Int* (2020) 44(1):117–26. doi: 10.1002/cbin.11207
49. Roh J-L, Park JY, Kim EH, Jang HJ, Kwon M. Activation of mitochondrial oxidation by PDK2 inhibition reverses cisplatin resistance in head and neck cancer. *Cancer Lett* (2016) 371(1):20–9. doi: 10.1016/j.canlet.2015.11.023
50. Sun W, Zhou S, Chang SS, McFate T, Verma A, Califano JA. Mitochondrial Mutations Contribute to HIF1 $\alpha$  Accumulation via Increased Reactive Oxygen Species and Up-regulated Pyruvate Dehydrogenase Kinase 2 in Head and



- Neck Squamous Cell Carcinoma. *Clin Cancer Res* (2009) 15(2):476–84. doi: 10.1158/1078-0432.CCR-08-0930
51. Sanmai S, Prongvitaya T, Limpaboon T, Chua-On D, Seubwai W, Roytrakul S, et al. Serum pyruvate dehydrogenase kinase as a prognostic marker for cholangiocarcinoma. *Oncol Lett* (2019) 17:5275–82. cited 2020 Apr 24. doi: 10.3892/ol.2019.10185
  52. Feng L, Cheng K, Zang R, Wang Q, Wang J. miR-497-5p inhibits gastric cancer cell proliferation and growth through targeting PDK3. *Biosci Rep* (2019) 39(9):BSR20190654. doi: 10.1042/BSR20190654
  53. Xie Z, Li X, Chen H, Zeng A, Shi Y, Tang Y. The lncRNA-DLEU2/miR-186-5p/PDK3 axis promotes the progress of glioma cells. *Am J Transl Res* (2019) 11(8):4922–34.
  54. Kluzja J, Corazao-Rozas P, Touil Y, Jendoubi M, Maire C, Guerreschi P, et al. Inactivation of the HIF-1 /PDK3 Signaling Axis Drives Melanoma toward Mitochondrial Oxidative Metabolism and Potentiates the Therapeutic Activity of Pro-Oxidants. *Cancer Res* (2012) 72(19):5035–47. doi: 10.1158/0008-5472.CAN-12-0979
  55. Duan X-L, Ma C-C, Hua J, Xiao T-W, Luan J. Benzyl butyl phthalate (BBP) triggers the malignancy of acute myeloid leukemia cells via upregulation of PDK4. *Toxicol Vitro* (2020) 62:104693. doi: 10.1016/j.tiv.2019.104693
  56. Woolbright BL, Choudhary D, Mikhalyuk A, Trammel C, Shanmugam S, Abbott E, et al. The Role of Pyruvate Dehydrogenase Kinase-4 (PDK4) in Bladder Cancer and Chemoresistance. *Mol Cancer Ther* (2018) 17(9):2004–12. doi: 10.1158/1535-7163.MCT-18-0063
  57. Walter W, Thomalla J, Bruhn J, Fagan DH, Zehowski C, Yee D, et al. Altered regulation of PDK4 expression promotes antiestrogen resistance in human breast cancer cells. *SpringerPlus* (2015) 4(1):689. doi: 10.1186/s40064-015-1444-2
  58. Guda MR, Asuthkar S, Labak CM, Tsung AJ, Alexandrov I, Mackenzie MJ, et al. Targeting PDK4 inhibits breast cancer metabolism. *Am J Cancer Res* (2018) 8(9):1725–38.
  59. Strowitzki MJ, Radhakrishnan P, Pavicevic S, Scheer J, Kimmer G, Ritter AS, et al. High hepatic expression of PDK4 improves survival upon multimodal treatment of colorectal liver metastases. *Br J Cancer* (2019) 120(7):675–88. doi: 10.1038/s41416-019-0406-9
  60. Choiniere J, Wu J, Wang L. Pyruvate Dehydrogenase Kinase 4 Deficiency Results in Expedited Cellular Proliferation through E2F1-Mediated Increase of Cyclins. *Mol Pharmacol* (2017) 91(3):189–96. doi: 10.1124/mol.116.106757
  61. Li G, Li M, Hu J, Lei R, Xiong H, Ji H, et al. The microRNA-182-PDK4 axis regulates lung tumorigenesis by modulating pyruvate dehydrogenase and lipogenesis. *Oncogene* (2017) 36(7):989–98. doi: 10.1038/onc.2016.265
  62. Wang J, Qian Y, Gao M. Overexpression of PDK4 is associated with cell proliferation, drug resistance and poor prognosis in ovarian cancer. *CMAR* (2018) Volume 11:251–62. doi: 10.2147/CMAR.S185015
  63. Oberhuber M, Pecoraro M, Rusz M, Oberhuber G, Wieselberg M, Haslinger P, et al. STAT 3 -dependent analysis reveals PDK 4 as independent predictor of recurrence in prostate cancer. *Mol Syst Biol* (2020) 16(4):e9247. doi: 10.15252/msb.20199247 cited 2020 May 15.
  64. Hitosugi T, Fan J, Chung T-W, Lythgoe K, Wang X, Xie J, et al. Tyrosine Phosphorylation of Mitochondrial Pyruvate Dehydrogenase Kinase 1 Is Important for Cancer Metabolism. *Mol Cell* (2011) 44(6):864–77. doi: 10.1016/j.molcel.2011.10.015
  65. Contractor T, Harris CR. p53 Negatively Regulates Transcription of the Pyruvate Dehydrogenase Kinase Pdk2. *Cancer Res* (2012) 72(2):560–7. doi: 10.1158/0008-5472.CAN-11-1215
  66. Sun H, Zhu A, Zhou X, Wang F. Suppression of pyruvate dehydrogenase kinase-2 re-sensitizes paclitaxel-resistant human lung cancer cells to paclitaxel. *Oncotarget* (2017) 8(32):52642–50. doi: 10.18632/oncotarget.16991
  67. Lu C-W, Lin S-C, Chen K-F, Lai Y-Y, Tsai S-J. Induction of Pyruvate Dehydrogenase Kinase-3 by Hypoxia-inducible Factor-1 Promotes Metabolic Switch and Drug Resistance. *J Biol Chem* (2008) 283(42):28106–14. doi: 10.1074/jbc.M803508200
  68. Xu J, Shi Q, Xu W, Zhou Q, Shi R, Ma Y, et al. Metabolic enzyme PDK3 forms a positive feedback loop with transcription factor HSF1 to drive chemoresistance. *Theranostics* (2019) 9(10):2999–3013. doi: 10.7150/thno.31301
  69. Wang L, Sahlin K. The effect of continuous and interval exercise on PGC-1 $\alpha$  and PDK4 mRNA in type I and type II fibres of human skeletal muscle: Exercise and single fibres genes expression. *Acta Physiol* (2012) 204(4):525–32. doi: 10.1111/j.1748-1716.2011.02354.x
  70. Wu P, Blair PV, Sato J, Jaskiewicz J, Popov KM, Harris RA. Starvation Increases the Amount of Pyruvate Dehydrogenase Kinase in Several Mammalian Tissues. *Arch Biochem Biophys* (2000) 381(1):1–7. doi: 10.1006/abbi.2000.1946
  71. Liu Z, Chen X, Wang Y, Peng H, Wang Y, Jing Y, et al. PDK4 Protein Promotes Tumorigenesis through Activation of cAMP-response Element-binding Protein (CREB)-Ras Homolog Enriched in Brain (RHEB)-mTORC1 Signaling Cascade. *J Biol Chem* (2014) 289(43):29739–49. doi: 10.1074/jbc.M114.584821
  72. Wu J, Zhao Y, Park Y-K, Lee J-Y, Gao L, Zhao J, et al. Loss of PDK4 switches the hepatic NF- $\kappa$ B/TNF pathway from pro-survival to pro-apoptosis. *Hepatology* (2018) 68(3):1111–24. doi: 10.1002/hep.29902
  73. Sun Y, Daemen A, Hatzivassiliou G, Arnott D, Wilson C, Zhuang G, et al. Metabolic and transcriptional profiling reveals pyruvate dehydrogenase kinase 4 as a mediator of epithelial-mesenchymal transition and drug resistance in tumor cells. *Cancer Metab* (2014) 2(1):20. doi: 10.1186/2049-3002-2-20
  74. Xuan Y, Hur H, Ham I-H, Yun J, Lee J-Y, Shim W, et al. Dichloroacetate attenuates hypoxia-induced resistance to 5-fluorouracil in gastric cancer through the regulation of glucose metabolism. *Exp Cell Res* (2014) 321(2):219–30. doi: 10.1016/j.yexcr.2013.12.009
  75. Zhang M, Cong Q, Zhang X-Y, Zhang M-X, Lu Y-Y, Xu C-J. Pyruvate dehydrogenase kinase 1 contributes to cisplatin resistance of ovarian cancer through EGFR activation: ZHANG et al. *J Cell Physiol* (2019) 234(5):6361–70. doi: 10.1002/jcp.27369
  76. Tataranni T, Piccoli C. Dichloroacetate (DCA) and Cancer: An Overview towards Clinical Applications. *Oxid Med Cell Longevity* (2019) 2019:1–14. doi: 10.1155/2019/8201079
  77. DeBerardinis RJ, Lum JJ, Hatzivassiliou G, Thompson CB. The Biology of Cancer: Metabolic Reprogramming Fuels Cell Growth and Proliferation. *Cell Metab* (2008) 7(1):11–20. doi: 10.1016/j.cmet.2007.10.002
  78. Cutruzzola F, Giardina G, Marani M, Maccone A, Paiardini A, Rinaldo S, et al. Glucose Metabolism in the Progression of Prostate Cancer. *Front Physiol* (2017) 8:97. cited 2020 Mar 27. doi: 10.3389/fphys.2017.00097
  79. Eidelman E, Twum-Ampofo J, Ansari J, Siddiqui MM. The Metabolic Phenotype of Prostate Cancer. *Front Oncol* (2017) 7:131. doi: 10.3389/fonc.2017.00131
  80. Costello LC, Franklin RB. The clinical relevance of the metabolism of prostate cancer; zinc and tumor suppression: connecting the dots Leslie. *Mol Cancer* (2006) 5(1):17. doi: 10.1186/1476-4598-5-17
  81. Latonen L, Afyounian E, Jylhä A, Näntinen J, Aapola U, Annala M, et al. Integrative proteomics in prostate cancer uncovers robustness against genomic and transcriptomic aberrations during disease progression. *Nat Commun* (2018) 9(1):1176. doi: 10.1038/s41467-018-03573-6
  82. Xue Y, Liu Y, Su J, Li J, Wu Y, Guo R, et al. Zinc cooperates with p53 to inhibit the activity of mitochondrial aconitase through reactive oxygen species accumulation. *Cancer Med* (2019) 8(5):2462–73. doi: 10.1002/cam4.2130
  83. Grunt TW. Interacting Cancer Machineries: Cell Signaling, Lipid Metabolism, and Epigenetics. *Trends Endocrinol Metab* (2018) 29(2):86–98. doi: 10.1016/j.tem.2017.11.003
  84. Swinnen JV, Roskams T, Joniau S, Van Poppel H, Oyen R, Baert L, et al. Overexpression of fatty acid synthase is an early and common event in the development of prostate cancer. *Int J Cancer* (2002) 98(1):19–22. doi: 10.1002/ijc.10127
  85. Zadra G, Ribeiro CF, Chetta P, Ho Y, Cacciatore S, Gao X, et al. Inhibition of de novo lipogenesis targets androgen receptor signaling in castration-resistant prostate cancer. *Proc Natl Acad Sci USA* (2019) 116(2):631–40. doi: 10.1073/pnas.1808834116
  86. Chen J, Guccini I, Di Mitri D, Brina D, Revandkar A, Sarti M, et al. Compartmentalized activities of the pyruvate dehydrogenase complex sustain lipogenesis in prostate cancer. *Nat Genet* (2018) 50(2):219–28. doi: 10.1038/s41588-017-0026-3
  87. Fendt S-M, Bell EL, Keibler MA, Davidson SM, Wirth GJ, Fiske B, et al. Metformin Decreases Glucose Oxidation and Increases the Dependency of Prostate Cancer Cells on Reductive Glutamine Metabolism. *Cancer Res* (2013) 73(14):4429–38. doi: 10.1158/0008-5472.CAN-13-0080



**Conflict of Interest:** LK is a member of the scientific advisory board of CBmed—Center for Biomarker Research in Medicine GmbH. Author MO was employed by COMET centre (K1) CBmed—Center for Biomarker Research in Medicine GmbH.

The remaining authors declare that the research was conducted in the absence of any commercial or financial relationships that could be construed as a potential conflict of interest.

*Copyright © 2020 Atas, Oberhuber and Kenner. This is an open-access article distributed under the terms of the Creative Commons Attribution License (CC BY). The use, distribution or reproduction in other forums is permitted, provided the original author(s) and the copyright owner(s) are credited and that the original publication in this journal is cited, in accordance with accepted academic practice. No use, distribution or reproduction is permitted which does not comply with these terms.*



# Heterozygous *P32/C1QBP/HABP1* Polymorphism *rs56014026* Reduces Mitochondrial Oxidative Phosphorylation and Is Expressed in Low-grade Colorectal Carcinomas

Annika Raschdorf<sup>1</sup>, Annika Sünderhauf<sup>1</sup>, Kerstin Skibbe<sup>1</sup>, Berhane Ghebrehwet<sup>2</sup>, Ellinor I. Peerschke<sup>3</sup>, Christian Sina<sup>1,4</sup> and Stefanie Derer<sup>1\*</sup>

<sup>1</sup> Institute of Nutritional Medicine, University Hospital Schleswig-Holstein, Campus Lübeck, Lübeck, Germany, <sup>2</sup> Department of Medicine, Stony Brook University, Stony Brook, NY, United States, <sup>3</sup> Department of Laboratory Medicine, Memorial Sloan Kettering Cancer Center, New York, NY, United States, <sup>4</sup> 1<sup>st</sup> Department of Medicine, Division of Nutritional Medicine, University Hospital Schleswig-Holstein, Campus Lübeck, Lübeck, Germany

## OPEN ACCESS

### Edited by:

Monica Montopoli,  
University of Padua, Italy

### Reviewed by:

Jun Fan,  
Jinan University, China  
Juan Carlos Gallardo,  
Instituto Nacional de  
Cardiología, Mexico

### \*Correspondence:

Stefanie Derer  
Stefanie.Derer@uksh.de

### Specialty section:

This article was submitted to  
Cancer Metabolism,  
a section of the journal  
Frontiers in Oncology

**Received:** 20 November 2020

**Accepted:** 21 December 2020

**Published:** 08 February 2021

### Citation:

Raschdorf A, Sünderhauf A, Skibbe K, Ghebrehwet B, Peerschke EI, Sina C and Derer S (2021) Heterozygous *P32/C1QBP/HABP1* Polymorphism *rs56014026* Reduces Mitochondrial Oxidative Phosphorylation and Is Expressed in Low-grade Colorectal Carcinomas. *Front. Oncol.* 10:631592. doi: 10.3389/fonc.2020.631592

Rapid proliferation of cancer cells is enabled by favoring aerobic glycolysis over mitochondrial oxidative phosphorylation (OXPHOS). *P32* (*C1QBP/gC1qR*) is essential for mitochondrial protein translation and thus indispensable for OXPHOS activity. It is ubiquitously expressed and directed to the mitochondrial matrix in almost all cell types with an excessive up-regulation of *p32* expression reported for tumor tissues. We recently demonstrated high levels of non-mitochondrial *p32* to be associated with high-grade colorectal carcinoma. Mutations in human *p32* are likely to disrupt proper mitochondrial function giving rise to various diseases including cancer. Hence, we aimed to investigate the impact of the most common single nucleotide polymorphism (SNP) *rs56014026* in the coding sequence of *p32* on tumor cell metabolism. *In silico* homology modeling of the resulting p.Thr130Met mutated *p32* revealed that the single amino acid substitution potentially induces a strong conformational change in the protein, mainly affecting the mitochondrial targeting sequence (MTS). *In vitro* experiments confirmed an impaired mitochondrial import of mutated *p32*-T130M, resulting in reduced OXPHOS activity and a shift towards a low metabolic phenotype. Overexpression of *p32*-T130M maintained terminal differentiation of a goblet cell-like colorectal cancer cell line compared to *p32*-wt without affecting cell proliferation. Sanger sequencing of tumor samples from 128 CRC patients identified the heterozygous SNP *rs56014026* in two well-differentiated, low proliferating adenocarcinomas, supporting our *in vitro* data. Together, the SNP *rs56014026* reduces metabolic activity and proliferation while promoting differentiation in tumor cells.

**Keywords:** colorectal cancer, metabolism, mitochondria, OXPHOS, *p32*, single nucleotide polymorphism, *C1QBP*

## INTRODUCTION

One of the major differences between differentiated and proliferating tissues is their cell metabolism as a result of different metabolic requirements of the cells. While differentiated post-mitotic cells maintain their energy level primarily *via* mitochondrial oxidative phosphorylation (OXPHOS), most proliferating cells rely on aerobic glycolysis for energy production (1). Although much less energy efficient than OXPHOS (up to 36 mole ATP per mole glucose), aerobic glycolysis (approximately 4 mole ATP per mole glucose) can rapidly provide macromolecular precursors for anabolic pathways needed for cell division (2).

The metabolic switch from gaining energy *via* balanced OXPHOS towards aerobic glycolysis, or the so-called Warburg effect, is considered to be an important driver of proliferation and tumor formation (1, 3–5).

Initially, it was proposed that tumor cells manifest a mitochondria dysfunction (4), but in contrast to prior assumption it has been shown that functional mitochondria are essential for rapid cancer cell proliferation (6, 7). ATP production by OXPHOS is required for tumors to progress *in vivo* (8, 9) and some cancer cell lines have even revealed to mainly depend on OXPHOS for ATP supply under normoxia (10, 11). The question whether mutations affecting mitochondrial function promote or inhibit colorectal tumor growth is still controversial. A study by Ericson *et al.* reported the frequency of mitochondrial mutations to be decreased in colorectal cancer relative to normal tissues, suggesting that mutagenesis in mitochondrial DNA (mtDNA) is disadvantageous for tumor development and may even impede it (12). Conversely, a recent study indicated accumulation of mtDNA mutations in colon cancer to cause OXPHOS dysfunction and metabolic rewiring characterized by specific upregulation of the *de novo* serine synthesis pathway, conferring a distinct metabolic advantage for tumor growth (13).

The single nucleotide polymorphism (SNP) *rs56014026* is the most prominent SNP in the coding sequence (CDS) of the gene *P32* on chromosome 17 p13.2. Full-length p32 (282 aa) possesses an N-terminal mitochondrial targeting sequence (MTS) directing the protein to the mitochondria (14), although it has also been found in the cytosol (15), the nucleus (15) on the cell surface (16) or in the extracellular compartment (17). Apart from an enormous functional diversity in the fields of inflammation and infection, in recent years, p32 has emerged to play a pivotal role in the overall growth, survival and metastasis of tumor cells (14). Studies have shown that most tumor types exhibit increased expression levels of p32 (18), which often correlate with tumor stage and poor prognosis in cancer patients (19–23). For colorectal carcinomas we recently found that non-mitochondrial p32 is associated with increasing tumor grade (24). Until now, it is assumed that mitochondrial p32 is essential for mitochondrial protein synthesis, thereby critically maintaining OXPHOS, as complexes I, III, IV and V of the electron transport chain (ETC) contain subunits encoded by the mtDNA (14, 25, 26).

Short-hairpin RNA (shRNA)-induced knockdown of p32 in human breast cancer cells has been shown to reduce total oxygen consumption by about one third with concomitant increase in glycolysis, resulting in decreased cell proliferation and tumorigenicity *in vivo*. When p32 expression was restored to the original level in the knockdown cells, metabolic phenotype, proliferation rate and tumorigenicity could be rescued (25). By virtue of its regulatory impact on mitochondria activity, we hypothesized that mutations in p32 are likely to disrupt balanced cell metabolism giving rise to various diseases including cancer.

The SNP *rs56014026* indicates the exchange of cytosine (C) by thymine (T) at nucleotide position 389 of the human *p32* mRNA, resulting in substitution of threonine at amino acid position 130 into methionine (p.Thr130Met) in p32. Given its pivotal role for mitochondrial function, we aimed to decipher the impact of the SNP *rs56014026* on tumor cells' metabolism and differentiation in the context of colorectal cancer.

## MATERIALS AND METHODS

### Study Population

Complementary DNA (cDNA) samples derived from tumor tissues of CRC patients utilized in Sanger sequencing experiments were purchased from OriGene Technologies Inc. (Rockville, MD, USA). The gender- and age-matched cohort comprised 128 CRC patients (59 male, 69 female) with a median age [ $\pm$  SD] of 70 [ $\pm$  13.51] years. Diagnosed tumors ranged from well differentiated G1 to undifferentiated G4 adenocarcinomas, being classified as stage I to IV. Twenty matched RNA samples from tumor and normal tissue of ten CRC patients analyzed by qPCR experiments depicted in heatmaps were purchased from OriGene Technologies Inc. The cohort was gender- and age-matched with a median age [ $\pm$  SD] of 74.50 [ $\pm$  8.45] years and comprised ten G1 or G2 adenocarcinomas of the colon, all classified as stage IIA. Detailed patients' characteristics are depicted in **Table 1**.

### Sanger Sequencing

To screen for the SNP *rs56014026* in *p32* transcripts, 128 colonic tumor samples collected from CRC patients (OriGene Technologies, Rockville, MD, USA; see **Table 1**) were analyzed by Sanger sequencing. Therefore, part of the *p32* cDNA was amplified by PCR using the oligonucleotides *p32\_forward*: 5'-CTGCACACCGACGGAGACAA-3' and *p32\_reverse*: 5'-CATATAAGGCCCAAGTCCAAG-3'. Sanger sequencing of amplicons was performed by Eurofins Genomics GmbH using the oligonucleotide *p32\_reverse*.

For sequencing of *p32* transcripts in paired normal and tumor samples from ten CRC patients (OriGene Technologies; see **Table 1**), *p32* cDNA was amplified by PCR using the oligonucleotides *p32\_nt1\_forward*: 5'-ATGCTGCCTCTGCTGCG-3' and *p32\_reverse*. Subsequently, amplicons were Sanger sequenced by Eurofins Genomics GmbH using the oligonucleotides *hp32\_nt1\_forward* and *hp32\_reverse*.

**TABLE 1 |** Overview of study population.

		Male [n]	Female [n]	Median age [y]	TNM[n]	Tumor stage [n]	Tumor grade [n]	Tumor cells [%]
<b>Tumor samples from CRC patients for Sanger sequencing</b> [n=128]	tumor	59	69	male: 68 female: 72	pT1pN0pMX [3] pT1pN1pMX [3] pT1pN1pM1 [1] pT2pN0pMX [17] pT2pN1pMX [2] pT2pN2pMX [3] pT2pN1pM1 [1] pT3pN0pM0 [1] pT3pN0pMX [36] pT3pN0pM1 [4] pT3pN1pMX [15] pT3pN1pM1 [3] pT3pN2pMX [10] pT3pN2pM1 [3] pT4pN0pMX [9] pT4pN0pM1 [1] pT4pN1pMX [7] pT4pN2pMX [4] pT4pN2pM1 [2] pTXpNXpM1 [3]	I [19] II [1] IIA [37] IIB [9] III [7] IIIA [4] IIIB [17] IIIC [16] IV [18]	G1 [52] G2 [54] G3 [16] G4 [2] not reported [4]	72 (40–98)
	Paired samples from CRC patients for qPCR	5	5	74.5	n.a.	n.a.	n.a.	n.a.
	normal	5	5					
	tumor	5	5		pT3pN0pMX [10]	IIA [10]	G1 [3] G2 [7]	73 (60–89)

CRC, colorectal carcinoma; n, number of patients; n.a., not applicable.

## Cell Culture

The human chronic myelogenous leukemia cell line HAP1-p32<sup>-/-</sup> with a CRISPR/Cas9 induced knockout for P32 (Horizon Discovery, Cambridge, UK) was cultivated in IMDM medium and the human colorectal carcinoma cell lines HT29 (American Type Culture Collection (ATCC), Manassas, VA, USA) and HT29-MTX-E12 (Sigma-Aldrich, St. Louis, MO, USA) were kept in DMEM medium. Both cell culture media were supplemented with 10% (v/v) FBS, 100 U/ml penicillin and 100 µg/ml streptomycin. Additionally, 1% non-essential amino acids (NEAA) was added to the medium for HT29-MTX-E12 cells. Cells were incubated at 37°C and 5% CO<sub>2</sub> in a humidified incubator and confirmed to be negative for mycoplasma contamination every three months. For experiments, cells have been cultivated up to a maximum of 20 passages.

## Site-directed Mutagenesis of Human p32

The expression plasmid pCMV3-p32 for human wild type (wt) p32 (Sino Biological, Beijing, China) was utilized for substitution of cytosine (C) at nucleotide position 389 by thymine (T) using the Quik Change II XL site-directed mutagenesis kit (Agilent, Santa Clara, CA, USA) and the mutagenic oligonucleotides p32\_T130M\_forward: 5'-GTTGCCGGGGAAAAAATCATGGTCACTTTCAACATTAACAACAGC-3' and p32\_T130M\_reverse: 5'-GCTGTTGTTAATGTTGA AAGTGACCATGATTTTTTCCCCGGCAAC-3', resulting in substitution of threonine (T) at amino acid position 130 by methionine (M) in p32. The mutated plasmid was Sanger sequenced by Eurofins Genomics GmbH (Ebersberg,

Germany) using the oligonucleotide p32\_exon2\_forward: 5'-ATGTCTGGAGGTTGGGAG-3'.

## Transfection of Cell Lines

For stable transfection, HAP1-p32<sup>-/-</sup> cells were seeded at a density of 0.8 × 10<sup>6</sup> cells per well in a 6-well-plate in IMDM medium supplemented with 10% (v/v) FBS. Twenty-four hours after seeding, knockout cells were transfected with plasmids encoding the sequences for p32-wt or p32-T130M or with an empty vector by lipofection using the Lipofectamine<sup>TM</sup> 3000 kit (Thermo Fisher Scientific, Waltham, MA, USA), according to the manufacturer's instructions. Twenty-four hours after transfection, cells were put under selection by adding 200 µg/ml Hygromycin B (Thermo Fisher Scientific). For transient transfection, HT29-MTX cells were reverse transfected with p32-wt or p32-T130M plasmids or with an empty vector at a density of 0.5 × 10<sup>6</sup> cells per well. Cells were cultivated for 72 h in DMEM medium supplemented with 10% (v/v) FBS.

## Growing of Spheroids

Stable HAP1 transfectants were grown as spheroids using the hanging drop technique. Drops with a volume of 30 µl IMDM medium supplemented with 10% (v/v) FBS, 100 U/ml penicillin, 100 µg/ml streptomycin and 200 µg/ml Hygromycin B containing 10,000 cells per drop were placed on the bottom side of the lid of a 10 cm cell culture dish. To minimize evaporation, 10 ml of supplemented IMDM medium were placed in the bottom of the dish. Spheroids were grown for 8 days and medium was changed on day 4 and 6. Finally, spheroids



were imaged with the Axio Scope.A1 microscope (2.5× magnification; Carl Zeiss, Oberkochen, Germany) and the area of each spheroid was determined using the ImageJ software (National Institutes of Health, Bethesda, MD, USA).

## RNA Extraction and Real-time Quantitative PCR

RNA was isolated from cell pellets utilizing the innuPREP RNA Mini Kit 2.0 (Analytik Jena AG, Jena, Germany) according to the manufacturer's instructions and transcribed to cDNA using the RevertAid H Minus Reverse Transcriptase (Thermo Fisher Scientific) and Oligo(dT)<sub>18</sub> primers. Real-time quantitative PCR (qPCR) was performed using Perfecta SYBR Green FastMix (Quanta BioSciences Inc., Gaithersburg, MD, USA) plus specific oligonucleotides in a 96-well plate format. The amplification program consisted of (i) preincubation at 95°C for 5 min and (ii) 40 cycles of denaturation at 95°C for 45 sec, annealing at 55°C for 30 sec and elongation at 72°C for 30 sec using the StepOnePlus Real-Time PCR System (Thermo Fisher Scientific). The following oligonucleotides were used for analyses (*ATOH1*: for: 5'-CCAGCTGCGCAATGTTATCC-3', rev: 5'-TGCTGTTTTCTCTGCACT-3'; *HES1*: for: 5'-CTACCCCAGCCAGTGTC AAC-3', rev: 5'-GGTCACCTCGTTCATGCAC-3'; *Ki67*: for: 5'-CCTGCTTGTGGAGGG-3', rev: 5'-GCTGGCTCCTGTTACGTAT-3'; *KLF4*: for: 5'-CCATCTTTCTCCACGTTTCG-3', rev: 5'-ATCGGATAGGTGAAGCTGCA-3'; *LDHA*: for: 5'-GCACCCAGTTTCCACCATGA-3', rev: 5'-GCACTCTTCTCAAACGGGC-3'; *LGR5*: for: 5'-CACACACTGTCATTGCGAG-3', rev: 5'-GCTTCTGTGGGTACGTGTCTT-3'; *p32*: for: 5'-CTGCACACCGACGGAGACAA-3', rev: 5'-CATATAAGGCCCAGTCCAAG-3'; *Slc2a1*: for: 5'-TGGCATCAACGCTGTCTTCT-3', rev: 5'-CTAGCGCGATGGTCATGAGT-3'; *SPDEF1*: for: 5'-GATTCACTACTGTGCCTCGAC-3', rev: 5'-ATGTC TGGCTTCCGGATGAT-3'; *β-actin*: for: 5'-ACATCCGC AAAGACCTGTACG-3', rev: 5'-TTGCTGATCCACA TCTGCTGG-3'). After melting curve profiling, amplification curves were analyzed according to the 2<sup>-dCt</sup> algorithm and expression levels were normalized to *β-actin*.

Expression of complement components in paired CRC samples was additionally analyzed by Taqman probes according to manufacturer's instructions using the StepOnePlus Real-Time PCR System. The following cycling conditions were applied: (i) preincubation at 50°C for 2 min and 95°C for 10 min and (ii) 40 cycles of denaturation at 95°C for 15 sec and annealing and elongation at 60°C for 1 min. The following Taqman probes (Thermo Fisher Scientific) were used: *C1QA* (Hs00381122\_m1), *C1QB* (Hs00608019\_m1), *C1QC* (Hs00757779\_m1), *C1R* (Hs00357637\_m1), *C1S* (Hs01043794\_m1), *C2* (Hs00918862\_m1), *C3* (Hs00163811\_m1), *C4A* (Hs00416393\_g1), *C5* (Hs00156197\_m1), *C6* (Hs01110040\_m1), *C7* (Hs00940408\_m1), *CFB* (Hs00156060\_m1), *C3AR1* (Hs00377780\_m1), *C5AR1* (Hs00383718\_m1), *C5AR2* (Hs00218495\_m1), *CR1* (Hs00559348\_m1), *CR2* (Hs00153398\_m1), *P32* (Hs00241825\_m1), *CD93* (Hs00362607\_m1), *CD46* (Hs00611257\_m1), *CD55* (Hs00892618\_m1), *CD59* (Hs00174141\_m1), *C4BPB*

(Hs00361221\_m1), *ITGAM* (Hs00355885), *ITGAX* (Hs00174217) and *ACTB* (Hs99999903\_m1). Expression levels of complement transcripts determined *via* the 2<sup>-dCt</sup> algorithm were normalized to *β-actin*.

## Cell Fractionation

For cell fractionation of stable HAP1 transfectants, cell pellets were resuspended in 250 µl of cold non-denaturing lysis buffer containing 1% phosphatase inhibitor cocktail II (Th. Geyer, Renningen, Germany) and cells were disrupted by drawing cell suspensions up and down through a 26 G needle causing shear force. Cell lysates were fractionated by different successive centrifugation steps.

## Western Blot and Antibodies

Cell pellets were lysed by resuspension in denaturing lysis buffer containing Tris and SDS supplemented with 2% phosphatase inhibitor cocktail II (Th. Geyer) and 3 (Sigma-Aldrich) and 1% protease inhibitor cocktail (Sigma-Aldrich). Samples were heated at 100°C for 5 min, cooled on ice, mixed and treated twice by ultrasonication for 20 s. Supernatants were collected after centrifugation at 12,000 × g at 4°C for 15 min.

Ten to 20 µg of whole-protein extracts or protein fractions were separated by denaturing SDS-PAGE utilizing a 4% to 15% gradient gel (Bio-Rad Laboratories, Hercules, CA, USA) under reducing conditions.

After separation, proteins were transferred to a PVDF membrane (GE Healthcare, Chicago, IL, USA) using a Trans-Blot<sup>®</sup> semi-dry transfer cell (Bio-Rad Laboratories). After blocking with 5% w/v non-fat milk in TBS buffer with 0.1% Tween 20 (T-TBS), membranes were probed with primary antibodies diluted 1:1,000 in 5% w/v non-fat milk or 5% w/v BSA at 4°C over night. Primary antibodies specific for human p32 (clone EPR8871, ab131284 or clone 60.11, ab24733; both from Abcam, Cambridge, UK), *β-actin* (Cell Signaling Technology (CST), Danvers, MA, USA, #4967), Tom20 (CST, #42406), AMPKα (CST, #2532), phospho-AMPKα (CST, #2535) or KLF4 (R&D Systems, Minneapolis, MN, USA, #AF3640) were utilized. The next day, membranes were incubated with the corresponding secondary antibody conjugated to horseradish peroxidase (HRP). Proteins were visualized by chemiluminescence. To determine similar transfer and equal loading, membranes were reprobed with an antibody specific for *β-actin*.

## Determination of Kinase Phosphorylation Levels

Relative level of phosphorylation at 37 kinase phosphorylation sites and two related proteins were detected in stable HAP1-p32-wt and HAP1-p32-T130M transfectants using the Proteome Profiler<sup>™</sup> Human Phospho-Kinase Array Kit (R&D Systems, Minneapolis, MN, USA). For each set of membranes (A and B) 600 µg of protein isolated from the respective cell pellets (see *Western blot and antibodies*) were used and the array was performed according to the manufacturer's instructions. Spot intensity was analyzed densitometrically using ImageJ and was normalized to the reference spots.

## Immunofluorescence Staining

Immunofluorescence staining was performed according to standard protocols. Briefly, paraformaldehyde-fixed and deparaffinized slides of cell pellets were incubated with primary antibodies specific for human p32 (clone 60.11; Abcam) or HSP60 (#sc-13115; Santa Cruz Biotechnology, Dallay, TX, USA), washed and incubated with respective fluorochrome-labelled IgG secondary antibodies (HSP60: Alexa-Fluor 488 nm; p32: Alexa-Fluor 594 nm; both from Thermo Fisher Scientific). Afterwards, slides were counterstained with DAPI (Sigma-Aldrich).

## Extracellular Oxygen Consumption Assay

To determine respiration rates of HAP1 or HT29-MTX transfectants, consumption of extracellular oxygen was measured. Therefore, cells were seeded in a 96-well microtiter plate at a density of  $1 \times 10^5$  cells per well and incubated at 37°C and 5% CO<sub>2</sub> in a humidified incubator for 4 to 6 h. Real-time measurement of oxygen consumption was performed using the MitoXpress Xtra Oxygen Consumption Assay (Agilent) according to the manufacturer's instructions.

## Determination of Lactate Production

Measurement of lactate produced by HAP1 or HT29-MTX transfectants was performed using the L-Lactic acid assay kit (Megazyme, Bray, Ireland), according to the manufacturer's instructions. Supernatants from indicated cells (HAP1 transfectants:  $5 \times 10^3$  cells per well in a 96-well microtiter plate, incubation at 37°C and 5% CO<sub>2</sub> for 96 h under normoxia or hypoxia; HT29-MTX transfectants:  $0.5 \times 10^6$  cells per well in a 6-well plate, incubation at 37°C and 5% CO<sub>2</sub> for 72 h) were diluted 1:20 in 1× PBS. Amounts of lactate measured were normalized to the viable cell mass determined in the corresponding neutral red assay or to cell counts, respectively.

## Cell Viability Assay

The neutral red cell viability assay was performed to determine the viable cell mass in HAP1-p32-wt, HAP1-p32-T130M and HAP1-mock cultures.  $5 \times 10^3$  cells per well were seeded into a 96-well microtiter plate and incubated at 37°C and 5% CO<sub>2</sub> for 96 h. To determine the effect of oxygen depletion, transfectants were cultivated under normoxia with 21% oxygen or under hypoxia in an incubator providing hypoxic conditions of 2% oxygen for 72 h.

After incubation, cells were stained using a neutral red dye (Sigma-Aldrich) diluted 1:100 in IMDM for 2 h, washed and destained with a solution consisting of 50% pure ethanol, 49% bidistilled water and 1% pure acetic acid to release the incorporated dye into the supernatant. To analyze the neutral red dye uptake, absorbance was measured at 540 nm against a background absorbance of 690 nm in a spectrophotometer.

## Statistical Analysis

Data are displayed graphically and were statistically analyzed using GraphPad Prism version 6.0. Statistical significance was determined by appropriate statistical tests, which are indicated in the corresponding figure legends. Results are displayed as mean

± SD of at least three independent experiments. P-values were calculated and null hypotheses were rejected when  $p \leq 0.05$ .

## RESULTS

### The SNP rs56014026 Is the Most Common Coding Mutation of p32

Mitochondrial p32 plays an essential role in OXPHOS, as it functions in the assembly of the mitoribosome, thereby enabling translation of the mitochondrially encoded subunits of the complexes of the electron transport chain (26, 27) (**Figure 1A**). Among many other polymorphisms, rs56014026 is the most common SNP in the CDS of p32 with an estimated minor allele frequency (MAF) of 0.0148 (1.48%), as reported in the SNP database (dbSNP) of the National Center for Biotechnology Information (NCBI) (**Figure 1B**). The SNP rs56014026 identifies the substitution of guanine by adenine at genome locus chr17:5434961 (GRCh 38.p12) in the P32 gene (**Figure 1C**). Following transcription, the resulting cytosine to uracil exchange is located at nucleotide position 389 in exon 3 of the human p32 mRNA, translating in the amino acid substitution p.Thr130Met (T130M) in p32 (**Figure 1D**).

### P.T130M Mutated p32 Decreases Mitochondrial OXPHOS Activity

To model the impact of the polymorphism on protein structure, we performed homology modeling *in silico* using the Phyre2 server. Full-length human p32 protein (282 amino acids; 31.4 kDa) comprises an N-terminal targeting sequence for mitochondrial import (MTS), whose conformation was predicted to be strongly affected by the p.T130M mutation. While in wild type protein the MTS is accessible for mitochondrial import (**Figure 2A**), in mutated p32-T130M the conformation of the MTS is predicted to be altered, potentially preventing p32 binding to receptors for mitochondrial import (**Figure 2B**). Hence, we hypothesized that mitochondrial import of p32 may be reduced by the polymorphism rs56014026. To functionally analyze the effect of the polymorphism on mitochondrial import of p32 and possible consequences on cell metabolism *in vitro*, a plasmid encoding 389 C>U mutated p32 was generated by a site-directed mutagenesis PCR using the plasmid encoding human wild type p32. Successful introduction of the SNP was verified by Sanger sequencing (**Supplementary Figure S1**). The near-haploid human chronic myelogenous leukemia (CML)-derived HAP1 cell line with a CRISPR/Cas9 induced knockout for p32 (HAP1-p32<sup>-/-</sup>) was stably transfected with plasmids encoding wild type or mutated p32-T130M or with an empty vector. Successful transfection was visualized by Western blot experiments utilizing a primary antibody specific for human p32 (**Figure 2C**). Western blot experiments of fractionated cell lysates confirmed decreased mitochondrial import of mutated p32-T130M by displaying reduced amounts of p32 in the mitochondria/cell membrane fraction of HAP1-p32-T130M mutants compared to HAP1-p32-wt cells (**Figure 2D**). Of note, in cytosolic protein fractions no differences in p32 level were observed between p32-T130M and p32-wt

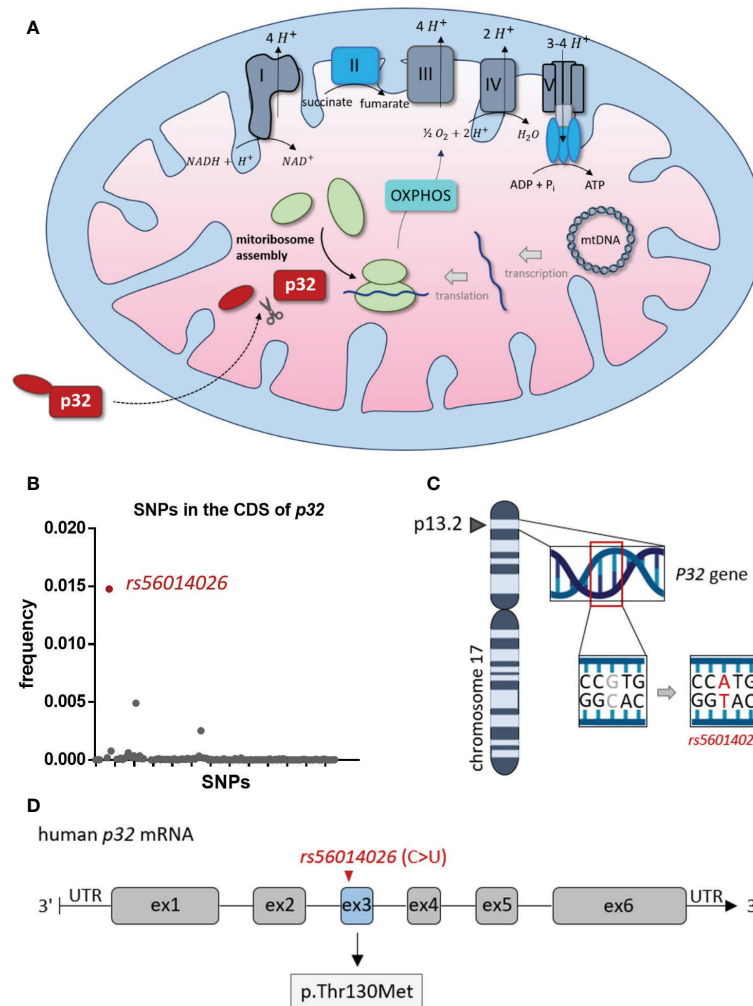


**FIGURE 1** | *Rs56014026* is the most common SNP in the CDS of P32. **(A)** Mitochondrial p32 functions in the assembly of the mitoribosome, which makes it essential for translation of the mitochondrially encoded subunits of the complexes I, III, IV and V of the electron transport chain (depicted in grey) [26, 27]. **(B)** Frequency of SNPs ( $n=124$ ) located in the coding sequence (CDS) of human P32. Data are based on the SNP database (dbSNP) of the National Center for Biotechnology Information (NCBI). **(C)** The P32 gene is located at position 13.2 of the short (p) arm of human chromosome 17 (17p13.2). **(D)** Schematic model of human p32 mRNA (exons 1–6). The SNP *rs56014026*, leading to substitution of cytosine by uracil (C>U), is localized in exon 3 and results in the missense mutation p.Thr130Met (T130M) in p32.

transfectants. Additionally, co-localization of p32 and the mitochondrial heat shock protein 60 (HSP60) was assessed using immunofluorescence microscopy. While p32-wt was mainly localized to the mitochondria, mitochondrial localization of p32-T130M was decreased (**Figure 2E**). Notably, HAP1-mock transfectants depicted diminished mitochondrial mass as reflected by reduced and more diffuse HSP60 staining compared to the HAP1-p32<sup>-/-</sup> cells transfected with p32. To investigate the consequence of diminished mitochondrial p32 localization on cell metabolism, we performed Western blot experiments to determine the phosphorylation state of 5'-AMP-activated protein kinase (AMPK $\alpha$ ). AMPK $\alpha$  acts as a cellular energy sensor, as it is phosphorylated by sensing increases in the ratios of AMP/ATP and ADP/ATP and hence indicates energy deficiency in cells. In

response to phosphorylation, it regulates energy balance by activating catabolic and downregulating anabolic pathways (28). Highest AMPK $\alpha$  activation was observed in mock transfected cells lacking p32 with decreasing activation level in p32-T130M mutants and lowest one in p32-wt cells (**Figure 2F**). Hence, decreased mitochondrial import of p.T130M mutated p32 was accompanied by an energy deficiency in HAP1 cells (**Figure 2G**). In line, oxygen consumption of p32-T130M mutants was decreased compared to p32-wt cells (**Figure 3H**). As expected, HAP1 cells deficient for p32 showed the lowest oxygen consumption with the area under the curve (AUC) displaying a significant 76% reduction compared to the p32-wt cells (**Figure 2I**). In the course of aerobic glycolysis, L-lactate is built from pyruvate by the lactate dehydrogenase (LDH) and is secreted into the extracellular compartment. HAP1-p32-T130M

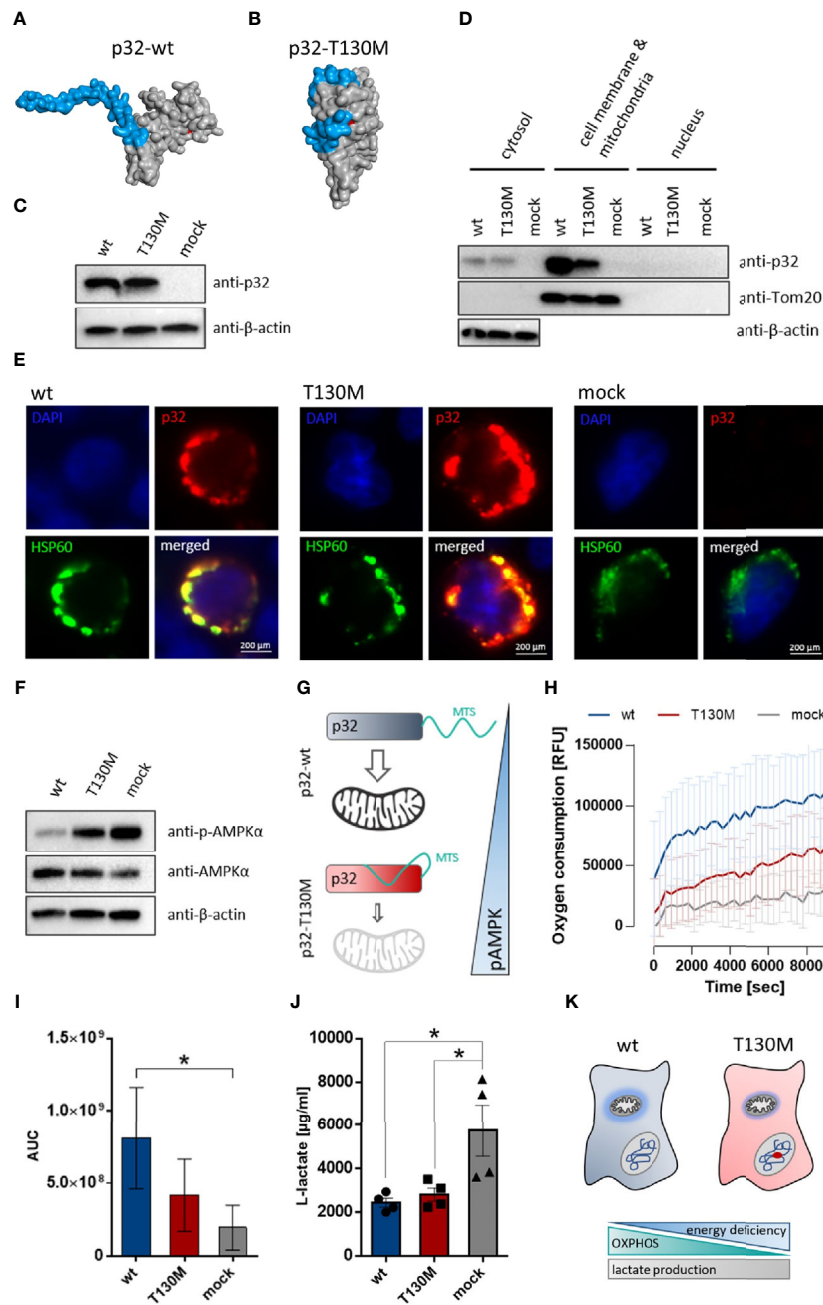


**FIGURE 2 |** P32-T130M impairs mitochondrial OXPHOS activity in HAP1 cells. (A+B) Schematic structure model of the human (A) wild type and (B) T130M mutated p32 protein. Homology modeling of p32 was performed using Phyre2. The proteins are depicted as surface representations with the predicted mitochondrial targeting sequence (MTS) and amino acid 130 highlighted in blue and red, respectively. (C) Western blot experiment with whole protein extracts of stable HAP1-p32-wt, HAP1-p32-T130M and HAP1-mock transfectants was performed using the anti-p32 antibody clone 60.11 or an anti-β-actin antibody. (D) Cytosolic, mitochondrial/cell membrane and nuclear protein fractions of the stable HAP1 transfectants were analyzed by Western blotting using primary antibodies against p32 (clone 60.11), Tom20 or β-actin. (E) Representative fluorescence microscopy images of colocalization of p32 (antibody clone 60.11) with mitochondrial HSP60 protein in HAP1 transfectants. (F) Western blot analyses were performed with whole protein lysates of the stable HAP1 transfectants using primary antibodies against phospho-AMPKα, AMPKα or β-actin. (G) Impaired mitochondrial import of p32-T130M is accompanied by increased phospho-AMPK in HAP1 cells. MTS; mitochondrial targeting sequence (H) Time-dependent measurement of oxygen consumption of the stable HAP1 transfectants. (I) The AUC was calculated for each single experiment and each cell line. For statistical analysis of significance, Friedman test was performed followed by Dunn's multiple comparison test. (J) L-lactate production was measured in cell culture supernatants from stable HAP1 transfectants after 96 h of incubation and normalized to the number of viable cells. Statistical significance was determined using a one-way ANOVA followed by Tukey's multiple comparison test. (K) P.T130M mutated p32 decreases OXPHOS activity in HAP1 cells, while lactate production is unaffected. \* $p \leq 0.05$ .



and HAP1-p32-wt transfectants displayed similar lactate production  $\pm$  SEM of  $2,800 \pm 298.6$   $\mu\text{g/ml}$  and  $2,400 \pm 206.4$   $\mu\text{g/ml}$ , respectively, while p32 deficient cells exhibited significantly higher lactate concentrations of an average  $\pm$  SEM of  $5,800 \pm 1,180$   $\mu\text{g/ml}$  (**Figure 2J**). Notably, neither the p32-T130M nor the mock transfectants compensated energy deficiency by upregulating expression of the glucose transporter 1 (*Slc2a1*) or the glycolytic enzyme *LDHA* (**Supplementary Figures S2A, B**). These experiments demonstrated that HAP1 cells expressing p32-wt are highly energetic performing aerobic glycolysis, while in HAP1-p32-T130M cells OXPHOS is impaired. As mitochondrial dysfunction is not compensated by anaerobic glycolysis, HAP1-p32-T130M cells are reduced in their energy status, producing less ATP compared to p32-wt expressing HAP1 cells. (**Figure 2K**).

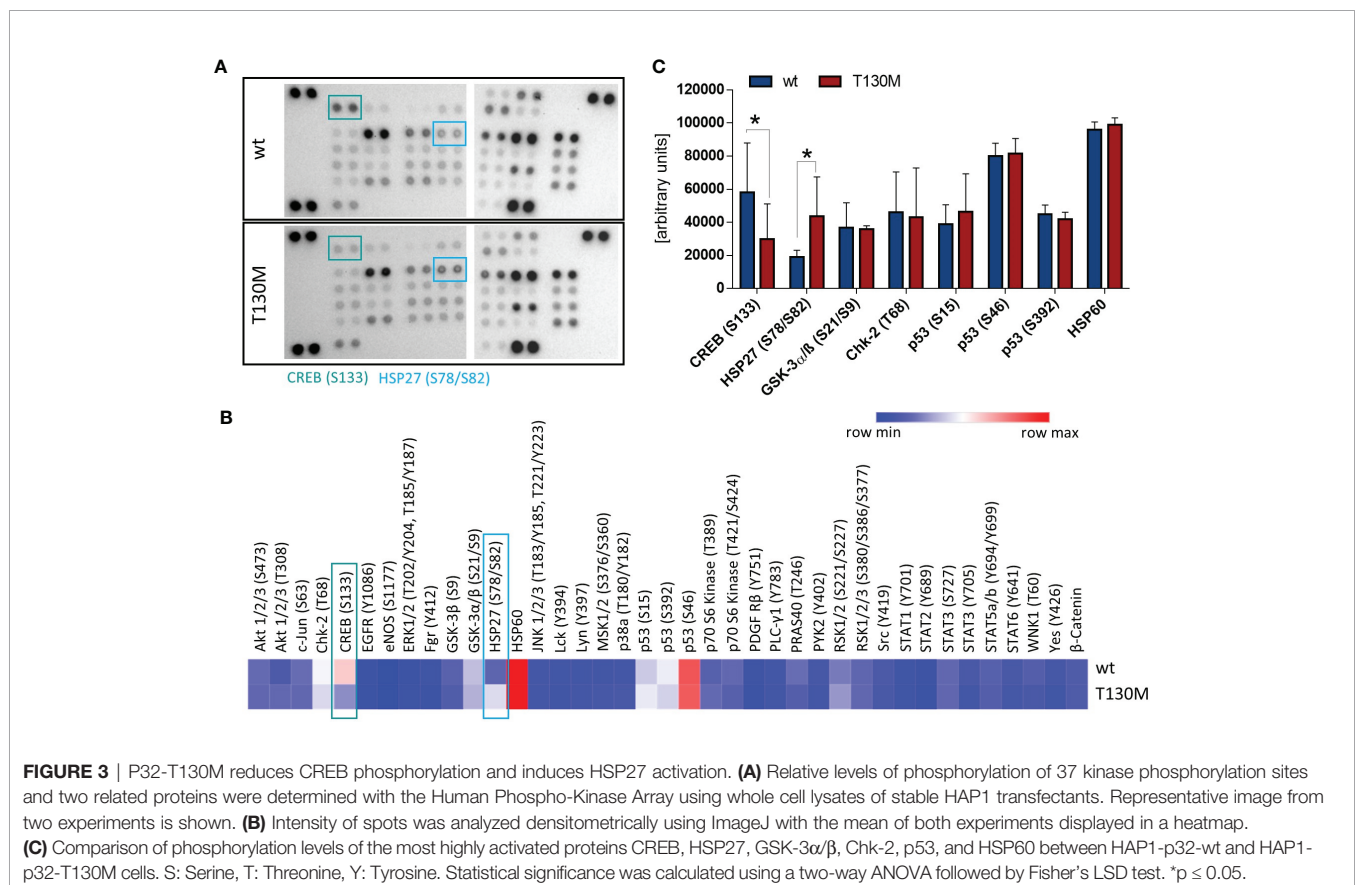
### P32-T130M Decreases CREB Phosphorylation and Increases HSP27 Activation

To unravel the impact of *rs56014026* associated energy deficiency on cellular signal transduction, we studied activation of different critical signaling pathways in the HAP1 transfectants. Therefore, we determined the phosphorylation level of 37 kinase phosphorylation sites and two related proteins (**Figures 3A, B**). Comparison of the most highly activated proteins in HAP1 cells revealed that

phosphorylation of the transcription factor cAMP response element-binding protein (CREB) at serine 133 (S133) was significantly reduced in HAP1-p32-T130M transfectants (**Figure 3C**). As CREB is overexpressed and constitutively phosphorylated in a number of human cancers, promoting survival and proliferation *via* different pathways (29), p32-T130M expression potentially triggers tumor-inhibiting signaling pathways as a result of decreased CREB activation. In contrast, phosphorylation of the heat shock protein 27 (HSP27) at serine 78/82 (S78/S82) was significantly increased in p32-T130M compared to p32-wt expressing HAP1 cells. Phosphorylation of HSP27 is induced in response to a variety of cellular stress stimuli and has been shown to prevent apoptosis (30). Hence, increased HSP27 activation in energy deficient HAP1-p32-T130M cells may potentially result in a cytoprotective effect.

### P32-T130M Increases Glycolytic Rate and Reduces Cell Proliferation Under Hypoxia

To analyze whether the detected mitochondrial dysfunction induced by expression of the polymorphism affects cell proliferation, HAP1 transfectants were incubated at normoxic conditions (21% oxygen) in a cell culture medium containing 25 mM glucose. Under normoxia, p32-T130M did not reduce cell proliferation compared to p32-wt cells, while the viable cell mass of HAP1 cells deficient for p32 was significantly decreased by 43% (**Figure 4A**). Additionally, HAP1 transfectants



were grown in spheroids under normoxic conditions using the hanging drop technique, presenting an intermediate between monolayer cell culture and tumor growth *in vivo* (Figure 4B). HAP1-p32-wt and HAP1-p32-T130M transfectants formed significantly larger spheroids than HAP1-mock transfectants (Figure 4C). Calculation of the mean area of the spheroids showed that p32-wt and p32-T130M spheroids displayed the same size (mean  $\pm$  SEM) of  $1.15 \pm 0.06 \text{ mm}^2$  to  $1.17 \pm 0.09 \text{ mm}^2$ , while mock spheroids revealed a significantly smaller size of  $0.49 \pm 0.04 \text{ mm}^2$  (Figure 4D). Similar to the results from monolayer cell culture, these experiments in 3D culture confirmed that p32-T130M mutants do not differ from p32-wt cells in cell proliferation under normoxic conditions.

Since the majority of tumor cells are present in a hypoxic microenvironment, HAP1 cells were investigated under more physiological oxygen conditions. Under hypoxia (2%  $\text{O}_2$ ), lactate release of HAP1-p32-wt and HAP1-p32-T130M transfectants increased threefold from  $4,602 \pm 557 \text{ }\mu\text{g/ml}$  to  $14,208 \pm 2,037 \text{ }\mu\text{g/ml}$  or more than fourfold from  $5,478 \pm 694 \text{ }\mu\text{g/ml}$  to  $22,918 \pm 2,048 \text{ }\mu\text{g/ml}$  compared to normoxia (21%  $\text{O}_2$ ), respectively (Figure 5A). In the case of p32 deficient HAP1 cells no difference in lactate production was observed between normoxic or hypoxic conditions. Comparing p32-wt cells and p32-T130M mutants under normoxia, there was no significant difference in glycolytic rate (Figure 5B). Though, cultivation under hypoxia induced a significant increase in glycolysis in p32-T130M

mutants ( $22,918 \pm 2,048 \text{ }\mu\text{g/ml}$ ) in comparison to p32-wt cells ( $14,208 \pm 2,037 \text{ }\mu\text{g/ml}$ ; Figure 5C).

Cell viability assays revealed that hypoxia significantly reduced proliferation of p32-wt and p32-T130M cells compared to normoxic conditions, while oxygen concentration had no impact on proliferation of HAP1 cells deficient for p32 (Figure 5D). Although cell proliferation did not differ between p32-T130M and p32-wt cells under normoxia (Figure 5E), it was reduced by 21% for p32-T130M mutants in comparison to p32-wt cells under hypoxia (Figure 5F). These experiments indicate that HAP1-p32-T130M cells shift more towards anaerobic glycolysis accompanied by reduced cell proliferation under physiological oxygen conditions compared to HAP1-p32-wt cells (Figure 5G). Hence, these data highlight the importance of efficient mitochondria function in cell proliferation.

### P32-T130M Decreases OXPHOS Activity and Promotes Differentiation in HT29-MTX Cells

Since recent studies have shown that loss of mitochondrial activity drives colorectal tumor growth (13, 24), we further investigated the impact of the SNP *rs56014026* on the metabolism of the human colorectal carcinoma cell line HT29-MTX. HT29-MTX cells derive from the colon cancer cell line HT29 by differentiating into goblet cells under methotrexate

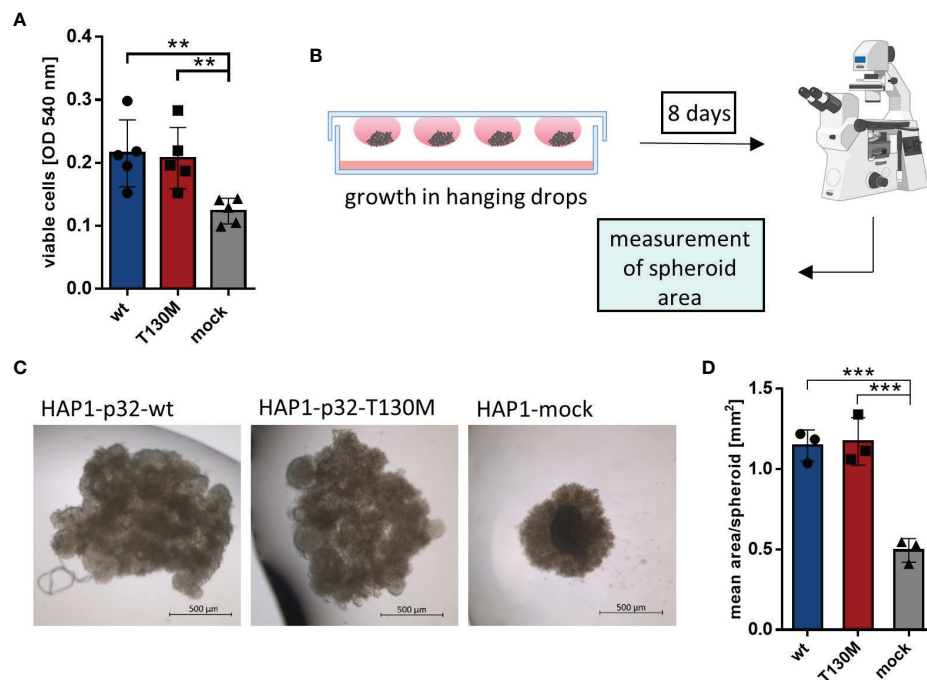


**FIGURE 4 |** P32-T130M does not affect proliferation of HAP1 cells and growth of HAP1 cell-derived spheroids. **(A)** HAP1 transfectants were incubated for 72 h and cell viability was determined by a neutral red assay, measuring the optical density (OD) at 540 nm. **(B)** Graphical setup of HAP1 transfectants grown as spheroids in hanging drops. **(C)** Representative pictures of HAP1-p32-wt, HAP1-p32-T130M and HAP1-mock spheroids after 8 days of incubation (brightfield, 2.5 $\times$  magnification). **(D)** Mean area of the HAP1 spheroids was determined using ImageJ. The three independent experiments comprise 10 to 12 spheroids each. For **(A)** and **(D)** statistical significance was determined using a one-way ANOVA followed by Tukey's multiple comparison test. \*\* $p \leq 0.01$ , \*\*\* $p \leq 0.001$ .

(MTX) selection (31) (**Figure 6A**) and display numerous mucous vacuoles (**Figure 6B**). Differentiated HT29-MTX cells display reduced expression of endogenous p32 on protein level compared to parental HT29 cells, reflecting the reduced p32 expression described for low grade colorectal carcinomas (24) (**Figures 6C, D**). For the subsequent analyses, HT29-MTX cells were transiently transfected with plasmids encoding p32-wt, p32-T130M or with an empty vector and transfection efficiency was verified by Western blot experiments (**Figure 6E**). Counting of cells after 72 h of cultivation revealed no differences in cell proliferation between the transient transfectants (**Figure 6F**). Notably, overexpression of p32-wt induced a significant induction of OXPHOS activity, while overexpression of p32-T130M did not affect OXPHOS activity in comparison to mock transfected HT29-MTX cells (**Figure 6G**). Oxygen consumption of HT29-MTX + p32-T130M transfectants was significantly lower (–68%) in comparison to

HT29-MTX + p32-wt transfectants (**Figure 6H**). Lactate production was increased in HT29-MTX cells overexpressing p32-T130M mutated p32 ( $3,214 \pm 182$ ) compared to HT29-MTX cells overexpressing p32-wt ( $2,641 \pm 290$   $\mu\text{g/ml}$ ) or mock transfected cells ( $2,388 \pm 278$ ) (**Figure 6I**). As expected, p32-wt transfectants performing high OXPHOS had an increased energy level compared to p32-T130M and mock transfected cells, displayed by lower AMPK $\alpha$  phosphorylation (**Figure 6J**). Thus, p32-T130M overexpressing HT29-MTX cells turned out to be metabolically less active compared to p32-wt transfected HT29-MTX cells, partially compensating the lower OXPHOS rate by an increase in aerobic glycolysis (**Figure 6K**).

To study the impact of the polymorphism on cell differentiation, we performed Western blot experiments utilizing a primary antibody specific for human *Kruppel-like factor 4* (KLF4), a goblet cell-specific differentiation marker in the colon (32). P32-T130M overexpressing and mock transfected HT29-MTX cells showed

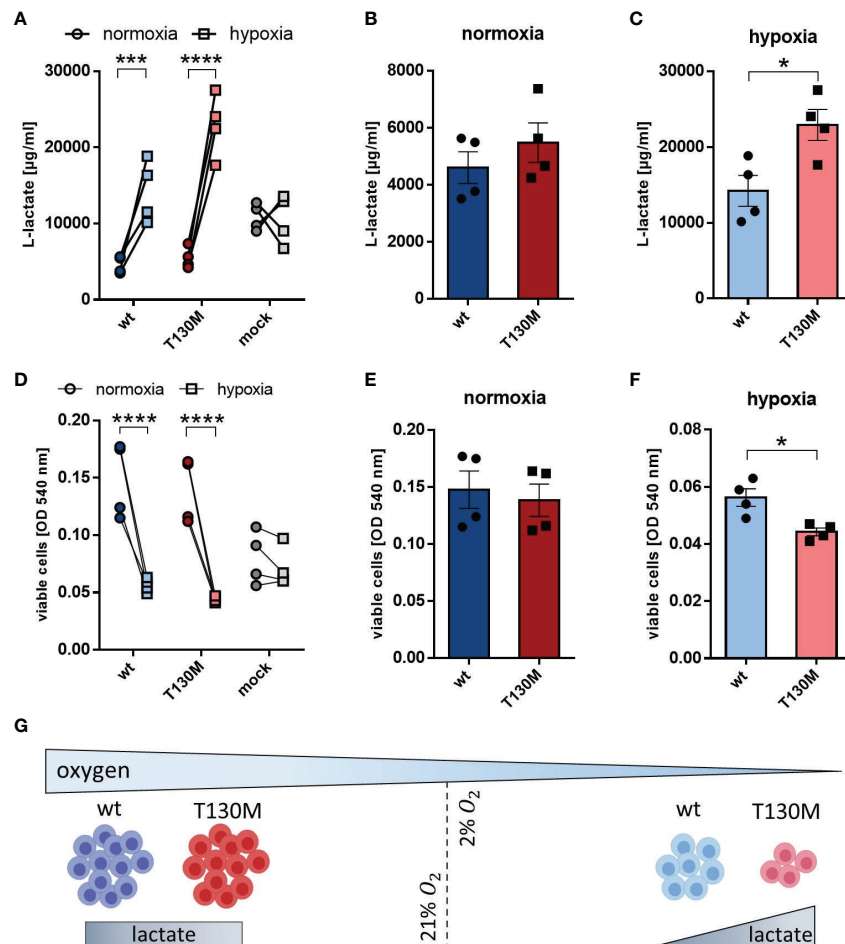


**FIGURE 5 |** P32-T130M increases glycolysis and decreases proliferation of HAP1 cells under hypoxia. **(A–C)** HAP1 transfectants were cultivated under **(B)** normoxic or **(C)** hypoxic conditions for 72 h. L-lactate production was measured in cell culture supernatant and normalized to the number of viable cells. **(D–F)** Cell viability of HAP1 transfectants being cultivated for 72 h under **(E)** normoxia or **(F)** hypoxia was determined by a neutral red assay. **(G)** Under hypoxic conditions glycolysis is increased and cell proliferation is decreased for HAP1-p32-T130M compared to HAP1-p32-wt cells. For **(A, D)** and **(C, F)** statistical significance was determined using a two-way ANOVA followed by Sidak's multiple comparison test or an unpaired t-test, respectively. \* $p \leq 0.05$ , \*\*\*\* $p \leq 0.0001$ .

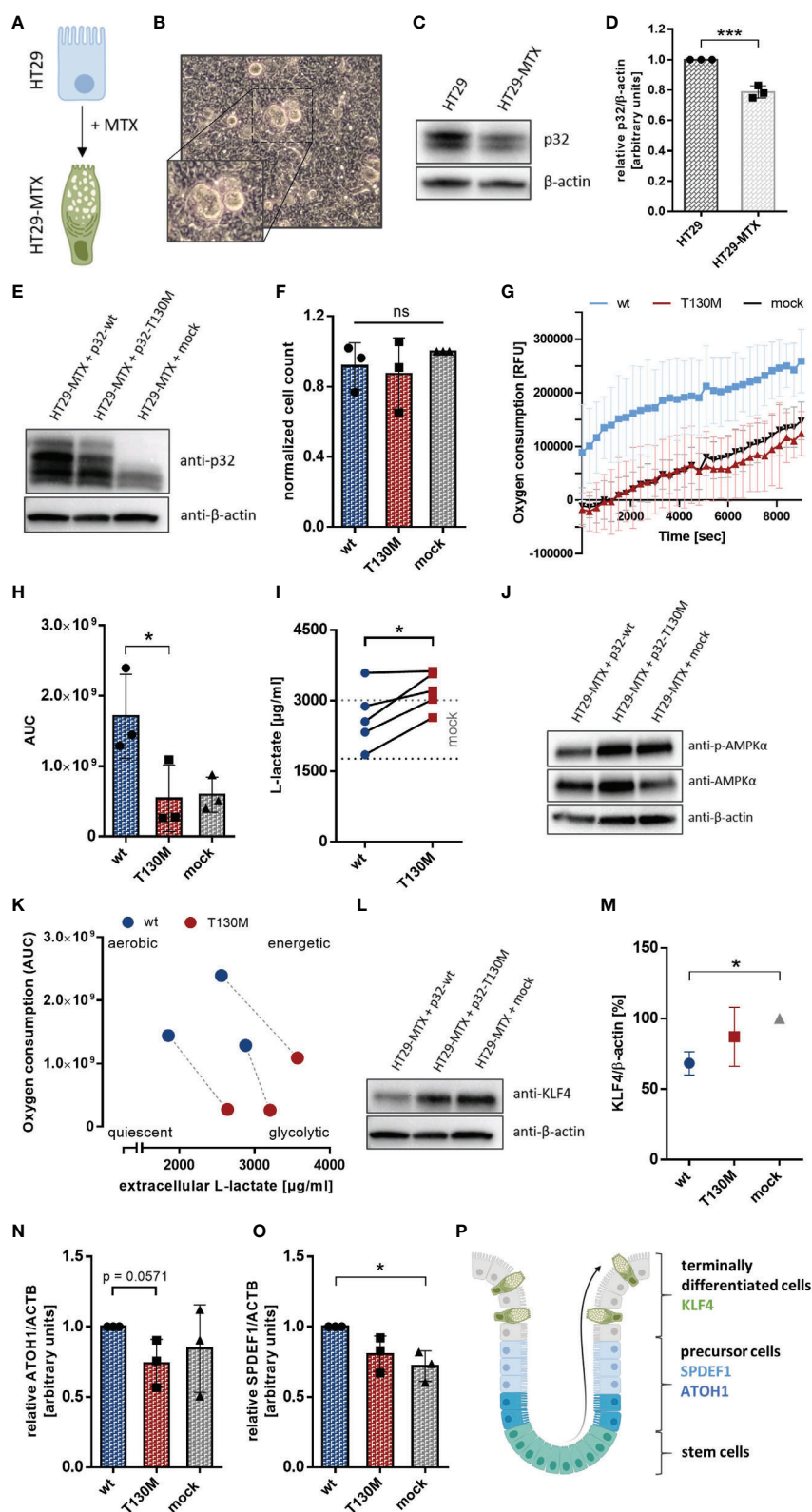


FIGURE 6 | Continued



**FIGURE 6** | P32-T130M reduces OXPHOS activity and maintains efficient differentiation in HT29-MTX cells. **(A)** HT29-MTX cells derive from HT29 cells following differentiation induced by methotrexate (MTX). **(B)** Representative image of HT29-MTX cell growth characteristics displaying mucous vacuoles. **(C)** Protein level of p32 was compared between HT29 and HT29-MTX cells by Western blot experiments using primary antibodies against p32 (clone EPR8871) or  $\beta$ -actin. **(D)** Amount of p32 was quantified densitometrically using Western Blots of HT29 and HT29-MTX cell lysates. **(E)** Western blot experiment with whole protein extracts of transient HT29-MTX + p32-wt, HT29-MTX + p32-T130M and HT29-MTX + mock transfectants was performed using the anti-p32 antibody clone EPR8871. **(F)** Cell count of transient HT29-MTX transfectants was determined after 72 h of incubation and normalized to mock transfected HT29-MTX cells. **(G)** Time-dependent measurement of oxygen consumption of transient HT29-MTX transfectants. **(H)** The AUC was calculated for each single experiment and each cell line. **(I)** L-lactate production was measured in cell culture supernatants from transient HT29-MTX transfectants after 72 h of incubation and normalized to the cell count. Mean  $\pm$  SD of HT29-MTX + mock transfectants is depicted by dotted gray lines. **(J)** Western blot experiment with whole protein extracts of transient HT29-MTX transfectants was performed using primary antibodies against phospho-AMPK $\alpha$ , AMPK $\alpha$  or  $\beta$ -actin. **(K)** Schematic representation of energy metabolism of HT29-MTX cells overexpressing p32-wt or p32-T130M using data displayed in **(H, I)**. Transfectants from the same experiment are connected by a dashed line. **(L)** Western blot analyses were performed with whole protein lysates of transient HT29-MTX transfectants using primary antibodies against KLF4 or  $\beta$ -actin. **(M)** For relative quantification bands were analyzed densitometrically using ImageJ and the amount of KLF4 was normalized to the amount of  $\beta$ -actin. **(N, O)** Expression of **(N)** ATOH1 and **(O)** SPDEF1 mRNA was quantified in transient HT29-MTX transfectants by qPCR. **(P)** Schematic model for goblet cell differentiation in the colonic crypt. Statistical analysis of significance for **(D, N, I)** was performed using an unpaired or paired t-test, respectively. For **(F, H, M, O)** statistical significance was determined using a one-way ANOVA followed by Tukey's multiple comparison test. \* $p \leq 0.05$ , \*\*\* $p \leq 0.001$ .

increased expression of KLF4 in comparison to HT29-MTX cells overexpressing p32-wt (**Figure 6L**). Densitometric analysis revealed a reduction of KLF4 expression in p32-wt transfectants of about 32% in comparison to mock transfected HT29-MTX cells (**Figure 6M**). In line with reduced KLF4 expression, mRNA expression of the precursor markers of the secretory lineage *Atonal Homolog 1* (*ATOH1*) and *SAM pointed domain-containing Ets transcription factor 1* (*SPDEF1*) (**Figure 6P**) was slightly increased in p32-wt compared to p32-T130M overexpressing HT29-MTX cells (**Figures 6N, O**). Since *SPDEF1* and *ATOH1* are markers for goblet cell progenitors, p32-T130M seems to maintain terminal goblet cell differentiation in contrast to overexpression of p32-wt. Hence, heterozygous expression of the polymorphism rs56014026 results in reduced metabolic activity, characterized by balanced glycolysis and OXPHOS activities and thus in increased differentiation of HT29-MTX cells.

## Sequencing Study and Characterization of Human Colorectal Tumor Samples

The previous *in vitro* experiments suggested that the SNP rs56014026 in *P32* shifts the metabolism of cancer cells into a more quiescent phenotype, accompanied by a decrease in the proliferation rate. To determine the rate of appearance of the SNP rs56014026 in a pure CRC cohort, we Sanger sequenced *p32* in tumor samples of 128 CRC patients. The cohort comprised 59 male and 69 female CRC patients with a median age of 68 or 72 years, respectively, harboring poorly or well differentiated colorectal adenocarcinomas from grade 1 (G1) to grade 4 (G4) with staging between I and IV (**Table 1**). As expected from the MAF available in the dbSNP (1.48%; **Figure 1B**), we found the heterozygous SNP rs56014026 in two out of 128 colorectal cancer patients (#1 and #2; 1.56%) being diagnosed with a G2 or G1 tumor, respectively (**Figure 7A**). Noteworthy, to determine and validate the frequency of this polymorphism in colorectal carcinoma patients more precisely, further studies utilizing larger CRC cohorts have to be performed. Both SNP rs56014026 expressing tumors were classified as stage IIA and stage pT3pN0pMX according to the TNM staging system and were localized in the cecum. Comparing the expression of *p32* between tumors encoding wt or p.T130M mutated protein revealed no difference on mRNA level (**Figure 7B**). Reflecting the low

grading of both tumors harboring the polymorphism, colonic tumor biopsies from patients #1 and #2 exhibit well defined epithelial structures in contrast to poorly differentiated G3 or G4 tumors (**Figure 7C**). To investigate the impact of the polymorphism on metabolism and differentiation of colorectal adenocarcinomas *ex vivo*, paired cDNA samples collected from normal and tumor tissue of ten CRC patients were analyzed by qPCR. While no mutation was detected in analyzed normal tissues, mutations in the coding sequence of *p32* were identified in paired tumor samples of CRC patient #2 and #4 (**Figure 7D**). While the tumor tissue of patient #2 expressed the heterozygous SNP rs56014026, the carcinoma of patient #4 exhibited multiple mutations (D77E, F82L, V83I, K91Q, G108V, E127G, aa 129 to 161 missense, E161 stop) in *p32*. One may hypothesize that the expression of non-functional *p32* in the tumor of patient #4 will result in mitochondrial dysfunction and thus in a low energetic phenotype, similar to *P32* deficient cells (**Figures 2F–J**). First, we quantified expression of three key metabolic markers, with the expression in the tumor given as fold change compared to the respective normal tissue. As depicted by low *Ki-67* expression, the tumor harboring the polymorphism rs56014026 (#2) was less proliferative compared to most of the other tumors (**Figure 7E**) and clustered with the tumor expressing non-functional *p32* (#4) as well as with tumor #8. Reduced proliferative capacity of tumors #2, #4 and #8 might be explained by relatively low carbohydrate metabolism in these tumors, depicted by modest expression levels of lactate dehydrogenase A (*LDHA*) and solute carrier family 2, facilitated glucose transporter member 1 (*Slc2a1*), encoding the glucose transporter 1 (GLUT1). Further, we quantified the absolute expression levels of several colonic differentiation markers to determine the cellular origin of the tumors, as gene expression patterns were reported to be conserved during colorectal carcinogenesis (33). Most of the analyzed tumors displayed high expression of the stem cell marker *leucine-rich repeat-containing G-protein coupled receptor 5* (*LGR5*) as well as of *hairy and enhancer of split-1* (*HES1*), which is a marker of the absorptive epithelial cell lineage (**Figure 7F**). Reflecting the mucinous phenotype described for the tumors of patient #8 and #10, these tumors revealed high expression of the secretory progenitor marker *SPDEF1*, accompanied by low *LGR5* expression. Notably, tumor #2 exhibited only low *LGR5* intestinal

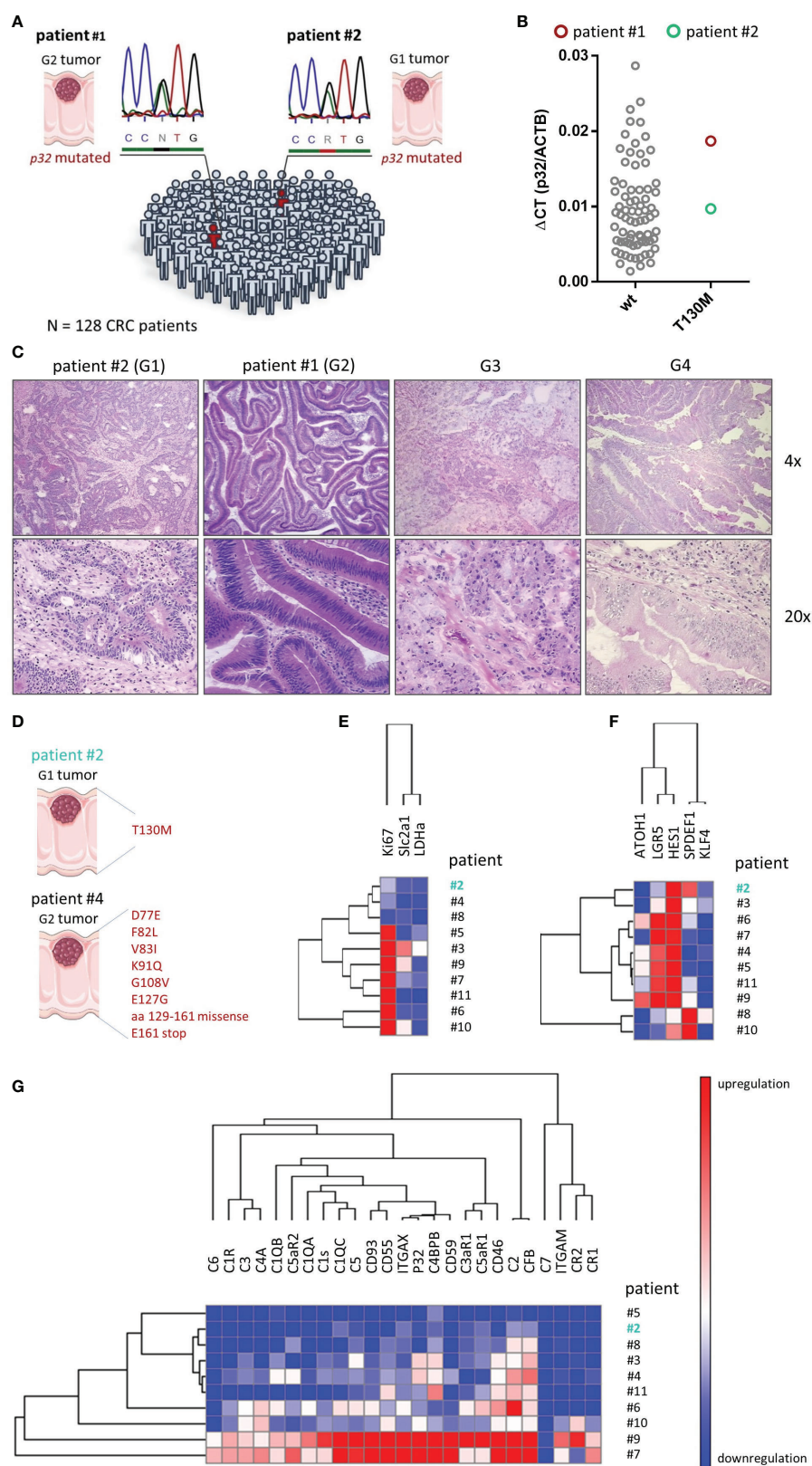


**FIGURE 7 |** Continued

**FIGURE 7** | Screening for the SNP *rs56014026* in colon cancer patients. **(A)** The heterozygous SNP *rs56014026* was identified in two tumor samples of a total of 128 CRC patients by Sanger sequencing. Chromatograms depict sections of the reverse sequencing reactions. **(B)** *P32* mRNA expression in colorectal tumor samples encoding wt *p32* ( $n=74$ ) or heterozygous T130M mutated *p32* (patient #1 and #2) was quantified by qPCR. **(C)** Pictures of hematoxylin and eosin (HE) staining of colonic tumor biopsies harboring the polymorphism collected from patient #2 (G1) and #1 (G2) as well as of a G3 and a G4 tumor (from OriGene Technologies). **(D)** Identified *p32* mutations in cDNA samples from tumor tissues of patient #2 and #4. **(E)** Heatmap displaying mRNA expression levels of different metabolic proteins in ten colorectal tumor samples (patient #2 to #11) normalized to respective non-malignant colonic epithelium. **(F)** Heatmap showing mRNA expression levels of colonic differentiation markers in ten colorectal tumor samples (patient #2 to #11). **(G)** Quantification of mRNA expression of the components of the complement system in ten colorectal tumor samples (patient #2 to #11) normalized to respective non-malignant colonic epithelium. **(D–G)** Patient #2 (depicted in turquoise) carries the heterozygous SNP *rs56014026* in tumor, but not in normal tissue. Hierarchical clustering was performed by **(E)** city-block distance or **(F, G)** one minus Pearson correlation utilizing GENE-E (software.broadinstitute.org/GENE-E/).

stem cell marker expression, but consisted of substantial amounts of enterocytes and secretory progenitor cells as depicted by high *HES1* and *SPDEF1* as well as moderate *KLF4* expression, respectively. Hence, according to published data (33) one may conclude that composition of tumor #2 mostly resembled the cellular distribution found in normal colonic epithelium, suggesting that the tumor originated from the differentiated compartment in the upper part of the crypt rather than from the colonic stem cell compartment at the bottom of the crypt. Furthermore, *p32* has also been characterized as a receptor for the globular heads of the complement component 1q (C1q) (34) and recent studies have reported that the presence of different factors of the complement system in the tumor microenvironment promote tumorigenesis (35–37). Products of the complement cascade have turned out to be major determinants of myeloid-derived suppressor cell recruitment into the tumor microenvironment, which promote tumor growth and create an immunosuppressive environment (38, 39). Hence, we additionally determined expression levels of complement components in these CRC samples. Therefore, mRNA expression of 25 complement components, receptors or inhibitors was studied utilizing target specific TaqMan arrays in qPCR experiments. As depicted in **Figure 7G**, expression of most complement system members was increased at least in some tumors, while mRNA of *C7* was reduced in each of the ten investigated adenocarcinomas compared to the respective normal tissue (**Figure 7G**). Complement components that were most frequently upregulated in tumor tissues were *CD46*, *C2* and *complement factor B* (*CFB*). Quantification revealed that expression of all analyzed compounds of the complement system was downregulated in the tumor tissue of patient #2 compared to most of the other tumors, suggesting that this tumor lacks high complement expression and associated pro-tumorigenic effects. In line with low *Ki-67* expression, the tumors of patient #2, #4 and #8 displayed low to moderate mRNA levels of the growth-promoting complement proteins C1q (40), *p32* (41), *CFB* (42) as well as *C3*, *C5*, *C3aR1* and *C5aR1/2* (43, 44). Hence, analysis of the CRC cohort suggested that the SNP *rs56014026* is associated with differentiated G1 or G2 adenocarcinomas exhibiting low metabolic activity and complement expression, which potentially may explain the observed moderate cell proliferation in these colorectal tumors.

## DISCUSSION

Tumor cell metabolism is characterized by a switch from balanced OXPHOS to aerobic glycolysis, allowing for rapid cell proliferation

(1, 3–5). Mitochondrial *p32* is pivotal for OXPHOS maintenance, as it essentially supports translation of the mitochondria encoded proteins of the complexes I, III, IV and V of the respiratory chain (14, 25, 26). In recent years, a crucial role for *p32* in cancer has emerged, since expression is enhanced in most human cancer types, affecting growth, survival and metastasis (14). In this study the most common SNP in the CDS of *P32* (*rs56014026*) was analyzed to unravel potential effects on cell metabolism and thus on proliferation and tumor growth.

Our *in vitro* study revealed that mitochondrial import of p.T130M mutated *p32* is impaired, potentially caused by a conformational change affecting the MTS, which leads to decreased OXPHOS activity. Respective cells showed an energy deficiency, resulting in a compensatory increase in glycolysis and reduced proliferation under hypoxia. By Sanger sequencing we found the polymorphism in two of 128 colorectal tumors, being characterized by low CRC grading and low expression of the cell proliferation marker *Ki-67*, which has to be further verified in larger patient cohorts.

While for many tumor types expression of *p32* has been reported to correlate with tumor grade, stage and poor prognosis in patients (21, 24), we here propose the SNP *rs56014026* in *P32* to be associated with reduced proliferation and low grading in colorectal carcinomas through insufficient mitochondrial respiration. Although OXPHOS activity is strongly reduced by impaired mitochondrial import of mutated *p32*, aerobic glycolysis is not increased under optimal cell culture conditions, as cells probably do not have the need to optimize their energy metabolism. However, the polymorphism induces an increase in glycolysis under hypoxia, which is much closer to the tumor microenvironment *in vivo*, given that most solid tumors rapidly outgrow their blood supply (45). Thus, the heterozygous SNP *rs56014026* results in a shift from a highly energetic phenotype characterized by high OXPHOS and glycolysis activity to a more quiescent metabolic phenotype with only basal mitochondrial respiration. In line with OXPHOS being the major source of cellular energy, our data indicate that cancer cells carrying the heterozygous SNP *rs56014026* display an energy deficit, resulting in decreased proliferation under hypoxia. Additionally, we observed that mutated *p32* is associated with enhanced differentiation in colorectal carcinoma cells *in vitro* and *ex vivo*, which supports the hypothesis, that the SNP is associated with low grading of colorectal tumors.

Despite metabolism being shifted towards aerobic glycolysis, mitochondrial OXPHOS is still essential in highly glycolytic cancer cells. Using [ $^{13}\text{C}$ ] glucose labeling, Scott *et al.* verified that metabolism of melanoma cells was not strictly glycolytic,



even under hypoxia, as the tricarboxylic acid cycle was still functional Scott et al. (9). Moreover, as the expression of p32 is strongest in hypoxic regions within tumors, it is likely that p32 balances between OXPHOS and glycolysis to attenuate the otherwise detrimental switch to aerobic glycolysis (25).

As protein synthesis of p32 is not affected by the SNP *rs56014026* and mitochondrial import of p.T130M mutated p32 is impaired without concomitant increase in cytosolic protein, the question where the remaining extramitochondrial p32 is located instead awaits further investigation. Considering recent studies reporting different cancer cell lines to shed p32 into the extracellular compartment (46, 47), one could hypothesize that p.T130M mutated p32 may be increasingly secreted into the extracellular milieu.

Recently, our group suggested a mechanism for inflammation-driven carcinogenesis induced by caspase-1 cleavage of human p32 in response to NLRP3 inflammasome activation (24). In consequence of caspase-1-mediated cleavage of the N-terminal mitochondrial leader of p32, cell metabolism is shifted from balanced OXPHOS to excessive glycolysis activity boosting cell proliferation. Here, we show that cells encoding the SNP *rs56014026* compensate the reduction in OXPHOS only by a slight increase in glycolysis under oxygen depletion, giving rise to a rather quiescent metabolic phenotype with diminished proliferative capacity.

In many human cancer types overexpression and persistent activity of CREB promote survival and proliferation *via* upregulation of downstream genes, which leads to CREB being discussed as a target in cancer therapy (48). Interestingly, we could show that phosphorylation of CREB (S133) is significantly reduced in cancer cells carrying the SNP *rs56014026 in vitro*, further supporting an anti-tumorigenic potential of this polymorphism.

In conclusion, our data indicate that the heterozygous SNP *rs56014026* is disadvantageous for tumor growth while ensuring differentiation of tumor cells. The question whether changes in cell metabolism and signaling pathways induced by the polymorphism may in turn affect sensitivity towards certain chemotherapeutic drugs awaits further investigation. Although detailed impact of the SNP on tumor growth has not been identified *in vivo* yet, the present study highlights the significance of mutations in *P32* in the context of cancer metabolism. The functional analysis of this polymorphism opens up a broad field of research on many other SNPs in *P32* that may lead to similarly striking effects on tumor metabolism. This raises perspectives for new cancer treatment strategies targeting p32, potentially resulting in impaired mitochondrial energy production and cancer cell proliferation.

## REFERENCES

1. Vander Heiden MG, Cantley LC, Thompson CB. Understanding the Warburg effect: the metabolic requirements of cell proliferation. *Science* (2009) 324:1029–33. doi: 10.1126/science.1160809
2. Patra KC, Hay N. The pentose phosphate pathway and cancer. *Trends Biochem Sci* (2014) 39:347–54. doi: 10.1016/j.tibs.2014.06.005
3. Hanahan D, Weinberg RA. Hallmarks of cancer: the next generation. *Cell* (2011) 144:646–74. doi: 10.1016/j.cell.2011.02.013
4. Warburg O. On the origin of cancer cells. *Science* (1956) 123:309–14. doi: 10.1126/science.123.3191.309

## DATA AVAILABILITY STATEMENT

The original contributions presented in the study are included in the article/**Supplementary Material**, further inquiries can be directed to the corresponding author.

## ETHICS STATEMENT

Ethical review and approval was not required for the study on human participants in accordance with the local legislation and institutional requirements. Written informed consent for participation was not required for this study in accordance with the national legislation and the institutional requirements.

## AUTHOR CONTRIBUTIONS

SD conceived the concept of the present study and supervised it. BG and EP provided the primary antibody 60.11 specific for human p32. AR and KS performed the experiments. AR and SD analyzed and interpreted the acquired data and drafted the article. AS, BG, CS, EP, and SD critically revised the article. All authors contributed to the article and approved the submitted version.

## FUNDING

This work was supported by the German Research Foundation (research grant DE 1874/1-2 to SD) and in part by the NIH/NCI Cancer Center Support Grant P30 CA008748. CS is Fresenius Kabi endowed professor of nutritional medicine.

## ACKNOWLEDGMENTS

The authors thank Maren Hicken and Heidi Schlichting for technical support and Prof. Jan Rupp from the Department of Infectious Diseases and Microbiology at the University of Lübeck for providing the hypoxic cell incubator from Thermo Fisher Scientific.

## SUPPLEMENTARY MATERIAL

The Supplementary Material for this article can be found online at: <https://www.frontiersin.org/articles/10.3389/fonc.2020.631592/full#supplementary-material>

5. Warburg O, Wind F, Negelein E. The Metabolism of Tumors in the Body. *J Gen Physiol* (1927) 8:519–30. doi: 10.1085/jgp.8.6.519
6. Rodriguez-Enriquez S, Hernandez-Esquivel L, Marin-Hernandez A, El Hafidi M, Gallardo-Perez JC, Hernandez-Resendiz I, et al. Mitochondrial free fatty acid beta-oxidation supports oxidative phosphorylation and proliferation in cancer cells. *Int J Biochem Cell Biol* (2015) 65:209–21. doi: 10.1016/j.biocel.2015.06.010
7. Weinhouse S. The Warburg hypothesis fifty years later. *Z Krebsforsch Klin Onkol Cancer Res Clin Oncol* (1976) 87:115–26. doi: 10.1007/BF00284370



8. Porporato PE, Filigheddu N, Pedro JMB, Kroemer G, Galluzzi L. Mitochondrial metabolism and cancer. *Cell Res* (2018) 28:265–80. doi: 10.1038/cr.2017.155
9. Scott DA, Richardson AD, Filipp FV, Knutzen CA, Chiang GG, Ronai ZA, et al. Comparative metabolic flux profiling of melanoma cell lines: beyond the Warburg effect. *J Biol Chem* (2011) 286:42626–34. doi: 10.1074/jbc.M111.282046
10. Moreno-Sanchez R, Marin-Hernandez A, Saavedra E, Pardo JP, Ralph SJ, Rodriguez-Enriquez S. Who controls the ATP supply in cancer cells? Biochemistry lessons to understand cancer energy metabolism. *Int J Biochem Cell Biol* (2014) 50:10–23. doi: 10.1016/j.biocel.2014.01.025
11. Pacheco-Velazquez SC, Robledo-Cadena DX, Hernandez-Resendiz I, Gallardo-Perez JC, Moreno-Sanchez R, Rodriguez-Enriquez S. Energy Metabolism Drugs Block Triple Negative Breast Metastatic Cancer Cell Phenotype. *Mol Pharm* (2018) 15:2151–64. doi: 10.1021/acs.molpharmaceut.8b00015
12. Ericson NG, Kulawiec M, Vermulst M, Sheahan K, O'Sullivan J, Salk JJ, et al. Decreased mitochondrial DNA mutagenesis in human colorectal cancer. *PLoS Genet* (2012) 8:e1002689. doi: 10.1371/journal.pgen.1002689
13. Smith AL, Whitehall JC, Bradshaw C, Gay D, Robertson F, Blain AP, et al. Age-associated mitochondrial DNA mutations cause metabolic remodelling that contributes to accelerated intestinal tumorigenesis. *Nat Cancer* (2020) 1:976–89. doi: 10.1038/s43018-020-00112-5
14. Ghebrehwet B, Geisbrecht BV, Xu X, Savitt AG, Peerschke EIB. The C1q Receptors: Focus on gC1qR/p33 (C1qBP, p32, HABP-1)(1). *Semin Immunol* (2019) 45:101338. doi: 10.1016/j.smim.2019.101338
15. van Leeuwen HC, O'Hare P. Retargeting of the mitochondrial protein p32/gC1qR to a cytoplasmic compartment and the cell surface. *J Cell Sci* (2001) 114:2115–23.
16. Soltys BJ, Kang D, Gupta RS. Localization of P32 protein (gC1q-R) in mitochondria and at specific extramitochondrial locations in normal tissues. *Histochem Cell Biol* (2000) 114:245–55. doi: 10.1007/s004180000191
17. Ghebrehwet B, Jesty J, Peerschke EI. gC1q-R/p33: structure-function predictions from the crystal structure. *Immunobiology* (2002) 205:421–32. doi: 10.1078/0171-2985-00143
18. Rubinstein DB, Stortchevoi A, Boosalis M, Ashfaq R, Ghebrehwet B, Peerschke EI, et al. Receptor for the globular heads of C1q (gC1q-R, p33, hyaluronan-binding protein) is preferentially expressed by adenocarcinoma cells. *Int J Cancer* (2004) 110:741–50. doi: 10.1002/ijc.20105
19. Gao H, Yao Q, Lan X, Li S, Wu J, Zeng G, et al. Elevated HABP1 protein expression correlates with progression and poor survival in patients with gastric cancer. *Oncotargets Ther* (2016) 9:6711–8. doi: 10.2147/OTT.S114756
20. Li W, Zhang X, Wang W, Sun R, Liu B, Ma Y, et al. Quantitative proteomics analysis of mitochondrial proteins in lung adenocarcinomas and normal lung tissue using iTRAQ and tandem mass spectrometry. *Am J Trans Res* (2017) 9:3918–34.
21. Saha P, Datta K. Multi-functional, multicompartamental hyaluronan-binding protein 1 (HABP1/p32/gC1qR): implication in cancer progression and metastasis. *Oncotarget* (2018) 9:10784–807. doi: 10.18632/oncotarget.24082
22. Saha SK, Kim KE, Islam SMR, Cho SG, Gil M. Systematic Multiomics Analysis of Alterations in C1QBP mRNA Expression and Relevance for Clinical Outcomes in Cancers. *J Clin Med* (2019) 8. doi: 10.3390/jcm8040513
23. Zhao J, Liu T, Yu G, Wang J. Overexpression of HABP1 correlated with clinicopathological characteristics and unfavorable prognosis in endometrial cancer. *Tumour Biol* (2015) 36:1299–306. doi: 10.1007/s13277-014-2761-8
24. Sünderhauf A, Raschdorf A, Hicken M, Schlichting H, Fetzter F, Brethack AK, et al. gC1qR Cleavage by Caspase-1 Drives Aerobic Glycolysis in Tumor Cells. *Front Oncol* (2020) 10:575854:575854. doi: 10.3389/fonc.2020.575854
25. Fogal V, Richardson AD, Karmali PP, Scheffler IE, Smith JW, Ruoslahti E. Mitochondrial p32 protein is a critical regulator of tumor metabolism via maintenance of oxidative phosphorylation. *Mol Cell Biol* (2010) 30:1303–18. doi: 10.1128/MCB.01101-09
26. Hillman GA, Henry MF. The yeast protein Mam33 functions in the assembly of the mitochondrial ribosome. *J Biol Chem* (2019) 294:9813–29. doi: 10.1074/jbc.RA119.008476
27. Yagi M, Uchiyama T, Takazaki S, Okuno B, Nomura M, Yoshida S, et al. p32/gC1qR is indispensable for fetal development and mitochondrial translation: importance of its RNA-binding ability. *Nucleic Acids Res* (2012) 40:9717–37. doi: 10.1093/nar/gks774
28. Hardie DG, Ross FA, Hawley SA. AMPK: a nutrient and energy sensor that maintains energy homeostasis. *Nat Rev Mol Cell Biol* (2012) 13:251–62. doi: 10.1038/nrm3311
29. Sakamoto KM, Frank DA. CREB in the pathophysiology of cancer: implications for targeting transcription factors for cancer therapy. *Clin Cancer Res* (2009) 15:2583–7. doi: 10.1158/1078-0432.CCR-08-1137
30. Concannon CG, Gorman AM, Samali A. On the role of Hsp27 in regulating apoptosis. *Apoptosis* (2003) 8:61–70. doi: 10.1023/a:1021601103096
31. Lesuffleur T, Barbat A, Dussaulx E, Zweibaum A. Growth adaptation to methotrexate of HT-29 human colon carcinoma cells is associated with their ability to differentiate into columnar absorptive and mucus-secreting cells. *Cancer Res* (1990) 50:6334–43.
32. Katz JP, Perreault N, Goldstein BG, Lee CS, Labosky PA, Yang VW, et al. The zinc-finger transcription factor Klf4 is required for terminal differentiation of goblet cells in the colon. *Development* (2002) 129:2619–28.
33. Bormann F, Rodriguez-Paredes M, Lasitschka F, Edelman D, Musch T, Benner A, et al. Cell-of-Origin DNA Methylation Signatures Are Maintained during Colorectal Carcinogenesis. *Cell Rep* (2018) 23:3407–18. doi: 10.1016/j.celrep.2018.05.045
34. Ghebrehwet B, Lim BL, Peerschke EI, Willis AC, Reid KB. Isolation, cDNA cloning, and overexpression of a 33-kD cell surface glycoprotein that binds to the globular “heads” of C1q. *J Exp Med* (1994) 179:1809–21. doi: 10.1084/jem.179.6.1809
35. Rutkowski MJ, Sughrue ME, Kane AJ, Mills SA, Parsa AT. Cancer and the complement cascade. *Mol Cancer Res* (2010) 8:1453–65. doi: 10.1158/1541-7786.MCR-10-0225
36. Downs-Canner S, Magge D, Ravindranathan R, O'Malley ME, Francis L, Liu Z, et al. Complement Inhibition: A Novel Form of Immunotherapy for Colon Cancer. *Ann Surg Oncol* (2016) 23:655–62. doi: 10.1245/s10434-015-4778-7
37. Reis ES, Mastellos DC, Ricklin D, Mantovani A, Lambris JD. Complement in cancer: untangling an intricate relationship. *Nat Rev Immunol* (2018) 18:5–18. doi: 10.1038/nri.2017.97
38. Lin Y, Xu J, Lan H. Tumor-associated macrophages in tumor metastasis: biological roles and clinical therapeutic applications. *J Hematol Oncol* (2019) 12:76. doi: 10.1186/s13045-019-0760-3
39. Kim J, Bae JS. Tumor-associated macrophages and neutrophils in tumor microenvironment. *Mediators Inflamm* (2016) 2016:6058147. doi: 10.1155/2016/6058147
40. Bulla R, Tripodo C, Rami D, Ling GS, Agostinis C, Guarnotta C, et al. C1q acts in the tumour microenvironment as a cancer-promoting factor independently of complement activation. *Nat Commun* (2016) 7:10346. doi: 10.1038/ncomms10346
41. McGee AM, Douglas DL, Liang Y, Hyder SM, Baines CP. The mitochondrial protein C1qbp promotes cell proliferation, migration and resistance to cell death. *Cell Cycle* (2011) 10:4119–27. doi: 10.4161/cc.10.23.18287
42. Riihila P, Nissinen L, Farshchian M, Kallajoki M, Kivisaari A, Meri S, et al. Complement Component C3 and Complement Factor B Promote Growth of Cutaneous Squamous Cell Carcinoma. *Am J Pathol* (2017) 187:1186–97. doi: 10.1016/j.ajpath.2017.01.006
43. Markiewski MM, DeAngelis RA, Benencia F, Ricklin-Lichtsteiner SK, Koutoulaki A, Gerard C, et al. Modulation of the antitumor immune response by complement. *Nat Immunol* (2008) 9:1225–35. doi: 10.1038/ni.1655
44. Cho MS, Vasquez HG, Rupaimoole R, Pradeep S, Wu S, Zand B, et al. Autocrine effects of tumor-derived complement. *Cell Rep* (2014) 6:1085–95. doi: 10.1016/j.celrep.2014.02.014
45. Bensaad K, Harris AL. Hypoxia and metabolism in cancer. *Adv Exp Med Biol* (2014) 772:1–39. doi: 10.1007/978-1-4614-5915-6\_1
46. Kandov E, Kaur A, Kishore U, Ji P, Williams J, Peerschke E, et al. C1q and C1q receptors (gC1qR and cC1qR) as potential novel targets for therapy against breast cancer. *Trends Immunol* (2018) 19:59–76.

47. Peerschke E, Stier K, Li X, Kandov E, de Stanchina E, Chang Q, et al. gC1qR/HABP1/p32 Is a Potential New Therapeutic Target Against Mesothelioma. *Front Oncol* (2020) 10:1413:1413. doi: 10.3389/fonc.2020.01413
48. Steven A, Seliger B. Control of CREB expression in tumors: from molecular mechanisms and signal transduction pathways to therapeutic target. *Oncotarget* (2016) 7:35454–65. doi: 10.18632/oncotarget.7721

**Conflict of Interest:** The authors declare that the research was conducted in the absence of any commercial or financial relationships that could be construed as a

potential conflict of interest with the exception of BG and EP who receive royalties from the sale of the monoclonal anti-p32 antibody 60.11.

Copyright © 2021 Raschdorf, Sünderhauf, Skibbe, Ghebrehiwet, Peerschke, Sina and Derer. This is an open-access article distributed under the terms of the Creative Commons Attribution License (CC BY). The use, distribution or reproduction in other forums is permitted, provided the original author(s) and the copyright owner(s) are credited and that the original publication in this journal is cited, in accordance with accepted academic practice. No use, distribution or reproduction is permitted which does not comply with these terms.



# The Mevalonate Pathway, a Metabolic Target in Cancer Therapy

**Borja Guerra<sup>\*</sup>, Carlota Recio, Haidée Aranda-Tavío, Miguel Guerra-Rodríguez, José M. García-Castellano and Leandro Fernández-Pérez<sup>\*</sup>**

*Molecular and Translational Pharmacology Lab, Institute for Biomedical and Health Research (IUIBS), University of Las Palmas de Gran Canaria, Las Palmas de Gran Canaria, Spain*

## OPEN ACCESS

### Edited by:

Miriam Martini,  
University of Turin, Italy

### Reviewed by:

Khalid Omer Alfarouk,  
Alfarouk Biomedical Research LLC,  
United States

Parames C. Sil,  
Bose Institute, India

### \*Correspondence:

Borja Guerra  
borja.guerra@ulpgc.es  
Leandro Fernández-Pérez  
leandrofco.fernandez@ulpgc.es

### Specialty section:

This article was submitted to  
Cancer Metabolism,  
a section of the journal  
Frontiers in Oncology

**Received:** 07 November 2020

**Accepted:** 18 January 2021

**Published:** 25 February 2021

### Citation:

Guerra B, Recio C, Aranda-Tavío H, Guerra-Rodríguez M, García-Castellano JM and Fernández-Pérez L (2021) The Mevalonate Pathway, a Metabolic Target in Cancer Therapy. *Front. Oncol.* 11:626971. doi: 10.3389/fonc.2021.626971

A hallmark of cancer cells includes a metabolic reprogramming that provides energy, the essential building blocks, and signaling required to maintain survival, rapid growth, metastasis, and drug resistance of many cancers. The influence of tumor microenvironment on cancer cells also results an essential driving force for cancer progression and drug resistance. Lipid-related enzymes, lipid-derived metabolites and/or signaling pathways linked to critical regulators of lipid metabolism can influence gene expression and chromatin remodeling, cellular differentiation, stress response pathways, or tumor microenvironment, and, collectively, drive tumor development. Reprogramming of lipid metabolism includes a deregulated activity of mevalonate (MVA)/cholesterol biosynthetic pathway in specific cancer cells which, in comparison with normal cell counterparts, are dependent of the continuous availability of MVA/cholesterol-derived metabolites (i.e., sterols and non-sterol intermediates) for tumor development. Accordingly, there are increasing amount of data, from preclinical and epidemiological studies, that support an inverse association between the use of statins, potent inhibitors of MVA biosynthetic pathway, and mortality rate in specific cancers (e.g., colon, prostate, liver, breast, hematological malignances). In contrast, despite the tolerance and therapeutic efficacy shown by statins in cardiovascular disease, cancer treatment demands the use of relatively high doses of single statins for a prolonged period, thereby limiting this therapeutic strategy due to adverse effects. Clinically relevant, synergistic effects of tolerable doses of statins with conventional chemotherapy might enhance efficacy with lower doses of each drug and, probably, reduce adverse effects and resistance. In spite of that, clinical trials to identify combinatory therapies that improve therapeutic window are still a challenge. In the present review, we revisit molecular evidences showing that deregulated activity of MVA biosynthetic pathway has an essential role in oncogenesis and drug resistance, and the potential use of MVA pathway inhibitors to improve therapeutic window in cancer.

**Keywords:** mevalonate, cholesterol, oxysterols, isoprenoids, sterol regulatory element binding protein, cancer, statins

## INTRODUCTION

Adaptive metabolic reprogramming is often observed in cancer cells. It is widely accepted that metabolic disruptions of carbohydrates, proteins, and lipids are one of the hallmarks of cancer (1–3). Metabolic adaptations provide energy and the crucial building blocks needed to maintain abnormal survival, rapid growth, metastasis, and drug resistance in many tumors. In addition to tumor microenvironment, they are main driving forces for cancer progression (4, 5). Lipid metabolism reprogramming involves lipid-related enzymes, metabolites, and signaling pathways linked to key regulators that can directly influence gene expression and chromatin remodeling, cellular differentiation, stress response pathways, or tumor microenvironment that collectively drive tumor development (6). An elevated or deregulated activity of mevalonate (MVA)/cholesterol biosynthetic pathway in specific cancer cells suggests that they are dependent of the continuous availability of MVA-derived metabolites (7–10). Furthermore, the aberrant activity of 3-hydroxy-3-methylglutaryl coenzyme A (HMGCoA) reductase (HMGCR), the rate-limiting enzyme of MVA pathway, can promote malignant transformation (7) and provides essential metabolites (i.e., sterols and non-sterol intermediates) that collectively drive tumor growth and development. Despite clinical evidences supporting the use of MVA pathway inhibitors (i.e., statins) for limiting cancer morbimortality are relatively low, increasing preclinical (11–19) and epidemiological (20–28) studies sustain the inverse association between statins and cancer-specific mortality rate. This beneficial effects of statins have been described in several types of cancer, including osteosarcoma/chondrosarcoma (16–18), prostate (24, 26), colon (29, 30), breast (19, 31), liver (32, 33), pancreas (34), ovarian (35, 36), esophageal (37, 38), lung (39), and hematological malignances (40). Interestingly, statins may suppress epithelial-mesenchymal transition (EMT) program together with the inhibition of cancer stem cell generation, maintenance, and expansion (6, 41). Unluckily, the use of statins in cancer is currently limited by the requirement of using high doses for prolonged periods, thus generating adverse effects. Therefore, studies focused on elucidating new strategies targeting the MVA signaling pathway to improve the therapeutic window in cancer are urgently needed (42). Clinically relevant, synergistic effects of tolerable doses of statins with conventional chemotherapy could enhance treatment efficacy, by reducing doses of each drug and, probably, adverse effects. To date, clinical trials that identify combinatory therapies (statins-chemotherapy) that improve therapeutic window in different cancer types are still a challenge. In this review, we revisit preclinical and molecular evidences showing that aberrant MVA biosynthetic pathway may have an essential role in oncogenesis and we discuss how potent inhibitors of MVA pathway may best be applied to improve cancer therapy.

## THE MVA BIOSYNTHETIC PATHWAY

In normal cells, cellular cholesterol can arise from receptor-mediated uptake of LDL-cholesterol from circulation, or be *de novo* synthesized

from acetyl-CoA by the MVA biosynthetic pathway. The precise regulation of MVA pathway is essential to guarantee continuous production of MVA-derived products, and to guard cells from accumulation of toxic end products, including cholesterol (43, 44). MVA pathway produces lipoproteins, dolichol, ubiquinone or cholesterol derived products (i.e., steroid hormones, oxysterols, vitamin D, bile acids) which are essential regulators of cellular metabolism. Cholesterol is essential for the buildup and maintenance of the structure and function of cellular membranes, cholesterol-rich microdomains or membrane rafts (lipid rafts). These structures constitute a core of organization for several signaling pathways and intracellular transport systems where cholesterol acts as a signaling molecule. The MVA biosynthetic pathway (**Figure 1**) starts with the formation of HMGCoA from three molecules of acetyl-CoA (43, 45), the end product of glycolysis. This reaction is catalyzed by the enzyme HMGCoA synthase. Subsequently, HMGCR converts HMGCoA to MVA which is the rate-limiting step of whole MVA pathway. The MVA is phosphorylated by the MVA kinase and converted to isopentenyl pyrophosphate (IPP). This step is decisive for the biosynthesis of farnesyl pyrophosphate (FPP) and geranylgeranyl pyrophosphate (GGPP) and is regulated by a cascade of different synthases including the farnesyl diphosphate synthase (FDPS) and the GGPP synthase (GGPS). Then, FPP can be converted to squalene and, subsequently, by further enzymes such as squalene synthase and squalene epoxidase, to cholesterol. Further lipid products FPP downstream include dolichol and ubiquinone, both with antioxidant properties, and crucial for glycosylation and mitochondrial electron transport processes. The synthesis of FPP and GGPP is essential for protein prenylation, a key posttranslational modification for localization, membrane anchoring and function of many signaling proteins. Protein prenylation is mediated by the enzymes farnesyltransferase (FTase) I and geranylgeranyl transferases (GGTase) I and II. The MVA pathway also participates in other biological mechanisms including long-term memory of innate immune cells, survival, and polarization of effector immune cells (i.e., macrophages) or metabolic reprogramming in cancer cells (46–48).

## REGULATION OF THE MVA BIOSYNTHETIC PATHWAY

The MVA biosynthetic pathway is regulated by transcriptional and post-transcriptional mechanisms including modulation of gene transcription, mRNA translation, protein degradation, and enzymatic activity (44, 49). The HMGCR enzyme, which regulates the rates of cholesterol synthesis, is in turn controlled by very fine-tuned regulatory mechanisms. Transcriptional regulation of HMGCR is mediated by two members of the sterol regulatory element binding proteins (SREBP) family called SREBP1 and SREBP2 (44, 49). SREBP proteins are encoded by two separate genes, SREBP-1 and -2. An alternative splicing of SREBP-1 can be produced, driving the



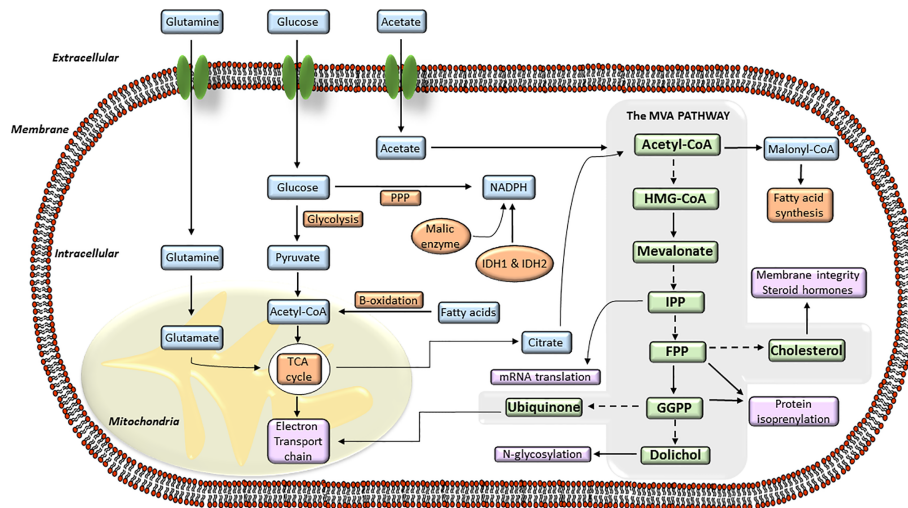


**FIGURE 1 |** The mevalonate (MVA) pathway and its connection with the intracellular energy metabolism signaling. Diagram of the different steps of the intracellular MVA anabolic pathway, from the entry of acetyl-coenzyme A (CoA) to the production of isoprenoid metabolites. Acetyl-CoA is transformed into hydroxy-methylglutaryl-CoA (HMG-CoA) which is used by the enzyme hydroxy-methyl-glutaryl-CoA reductase (HMGCR) to synthesize MVA. MVA is further metabolized to farnesyl pyrophosphate (FPP), a precursor of cholesterol and sterols. FPP is also converted to geranylgeranyl pyrophosphate (GGPP), and these lipids are used for post-translational modification of proteins, including N-glycosylation and protein prenylation.

synthesis of two isoforms, SREBP-1a and -1c. Whereas SREBP-1 has been clearly associated with homeostasis of cholesterol and fatty acids, SREBP-2 is mainly involved in synthesis and uptake of cholesterol. Thus, in response to intracellular sterol levels, SREBPs regulate the MVA biosynthetic pathway. Briefly, when the amount of intracellular sterol increases, SREBPs are held in an inactive form at the endoplasmic reticulum (ER) by their binding partner SREBP cleavage-activating protein (SCAP) and the insulin-induced genes (INSIG)-1 and -2. However, in response to sterol deprivation (e.g., when HMGCR activity is inhibited), intracellular end products of the MVA biosynthetic pathway are depleted. As the number of sterols diminishes, they no longer bind SCAP, thus producing a conformational change that triggers the SCAP-SREBP complex dissociation from the INSIGs and translocation from the ER to the Golgi. The SREBPs are successively cleaved by Golgi-resident proteases and released on their activated form, so they can translocate to the nucleus where they bind to sterol regulatory elements (SRE). This initiates the transcription of target genes that translate into key proteins involved in the biosynthesis of MVA-derived metabolites (i.e., HMGCoA synthase, HMGCR, FPP synthase, Insig-1) and cholesterol uptake (i.e., LDLR) to restore intracellular isoprenoid and sterol levels. Intracellular sterol levels are also regulated by oxysterols, metabolites derived from cholesterol oxidation. The 7 $\alpha$ - and 27-hydroxycholesterols are synthesized in the liver by CYP7A1 and CYP27A1, the genes encoding the rate-limiting enzymes of neutral and acid bile synthetic pathways, respectively, which contribute to eliminate cholesterol. Oxysterols contribute to cholesterol homeostasis through activation of Liver X receptors (LXR) (50). LXR were originally characterized by their role in the positive regulation of the gene CYP7A. This relevant physiological

role was further confirmed by the phenotype of LXR $\alpha$  null mice, which appear healthy when fed on a standard mouse diet but, when fed with a cholesterol-enriched diet, failed to induce CYP7A (51). Consequently, LXR $\alpha$  null mice suffered from a dramatic accumulation of cholesteryl ester in the liver and a reduction in bile acid production. Upon binding to LXR, oxysterols induce the transcription of specific ATP-binding cassette (ABC) transporters A1 and G1, that increase cholesterol efflux from enterocytes and macrophages, respectively (52). In addition to LXR activation, oxysterols (e.g., 25-hydroxycholesterol (25HC)), and high sterol concentrations, lanosterol, or Insig, can provoke ubiquitination and proteasomal degradation of HMGCR (53). Furthermore, the sterol-accelerated degradation of HMGCR is strengthened by non-sterol isoprenoids, including derivatives from FPP and GGPP. Notably, lanosterol does not interact with the sterol-sensing domain of SCAP and, therefore, does not suppress the processing of SREBP. Thereby, oxysterols downregulate HMGCR by increasing its ubiquitination-mediated degradation as well as suppress HMGCR gene transcription by inhibiting the delivery of SREBP-SCAP complex from ER. In contrast, lanosterol enhances the HMGCR degradation rate, and cholesterol limits the translocation of SREBP-SCAP (54). Furthermore, negative feedback responses of IPP, FPP, and GGPP suppress the activity of the MVA kinase. Expression of HMGCR is further modulated at the translational level, where the translation rate of HMGCR mRNA is controlled by the demand of the cell for non-sterol isoprenoids (e.g., MVA). When HMGCR dependent-MVA production is inhibited by statins, HMGCR mRNA is efficiently translated, even in the presence of sterols, being in contrast reduced when MVA is added. Finally, as mentioned below, the catalytic activity of HMGCR can be inhibited *via* phosphorylation by AMPK, a sensor of cellular energy state (55).

## THE MVA PATHWAY IN CANCER

The Warburg phenomenon (56) is the best studied metabolic adaptation program developed by cancer cells. It was described as the preference of cancer cells to use aerobic glycolysis to obtain most of their energy, even in the presence of abundant oxygen supply, when normal cells would typically use the aerobic cellular respiration. Therefore, tumor cells will be highly dependent on glucose to produce large quantities of energy and provide other cells with intermediates necessary for the biosynthesis of amino acids, nucleic acids, and lipids (5, 57). This metabolic reprogramming provides energy, the crucial building blocks, and signaling required to keep survival, rapid growth, and drug resistance of many cancers (1–3). Glycolysis generates acetyl-CoA (45), a molecule that is derived from acetate and/or glutamine metabolism. Acetyl-CoA can be incorporated into the MVA biosynthetic pathway, into lipids by fatty acid synthase (FAS) or into phospholipids by the action of different enzymes, including the pro-oncogene choline kinase (CK) (58). Acetyl-CoA feeds the MVA biosynthetic pathway to generate metabolites that are essential to maintain survival and rapid growth of multiple tumors. Accordingly, transcriptional profiling studies support the hypothesis that genes involved in cholesterol and fatty acid metabolism are upregulated in cancer cells and play an essential role in transformation (59). Several studies suggest that an elevated requirement for cholesterol is an innate metabolic hallmark in cancer cells, which could be used in a prophylactic and therapeutic manner. However, the complexities of how lipid metabolism interconnects with oncogenesis and tumor progression are not yet well understood. The list of molecules functionally connected with the MVA biosynthetic pathway in cancer is wide and diverse. It includes: 1) enzymes [e.g., HMGCR (8, 60–62), small GTPases (63, 64), ATP citrate lyase (ACL) (5), AMPK (65–67), FAS (68), pyruvate kinase M2 (PKM2) (69)]; 2) CD36, a fatty acid transporter (68); 3) signaling pathways [e.g., PI3K-AKT-mTOR (70, 71), Hippo (72, 73), Hedgehog (74, 75)]; 4) transcriptional regulators [e.g., SREBPs (68, 76), HIF-1 (77), STAT3 (78–80)], c-MYC (6, 81), YAP/TAZ (72, 73); and 5) nuclear receptors such as LXRs (82), ER $\alpha$  (62, 83), and Estrogen-Related Receptor (ERR $\alpha$ ) (84, 85). Additionally, the loss-of-function of tumor suppressor proteins such as p53 (86, 87) and pRb (88–90) can also contribute to adapt lipid metabolism to tumor growth, metastasis, and drug resistance (Figure 2).

## HMGCR

Originally, the hypothesis that MVA-derived metabolites have a role in cancer cell biology was suggested by studying liver cancer (91) and primary chronic lymphocytic leukemia cells (92). Further gene expression profiling and immunohistochemical analysis identified that HMGCR expression can be associated with a molecular gene signature of certain subtypes of breast cancer (93). The proto-oncogenic role of HMGCR was functionally shown by overexpression of constitutively active HMGCR, which potentiated both anchorage-independent

cellular growth in soft agar as well as the development of xenografts (7). Furthermore, dysregulated HMGCR was shown to induce anchorage-independent growth of an immortalized, non-transformed cell line, and support the formation of myeloid colonies from normal hematopoietic progenitors. A link between MVA pathway and oncogenic signaling was also reported with the cooperation between HMGCR and the small GTPase Ras to promote cell transformation (7). Clinically relevant, increased levels of HMGCR were shown to correlate with poor prognosis in breast (93) and prostate cancer (94) patients. Several epidemiological studies have also evidenced that hypercholesterolemia and increased oxysterol production are associated with higher cancer risk (e.g., postmenopausal breast cancer, colon cancer, lung cancer, non-Hodgkin lymphoma, acute myeloid leukemia) (95). Accordingly, high levels of cholesterol could provide cancer cells with immune surveillance and/or resistance to drug therapy (9, 60). Thus, cholesterol is recognized as an inherent metabolic demand in cancer cells and increased rates of cholesterol synthesis can potentiate the progression of numerous types of cancer (7, 8). This is explained by the fact that highly proliferative cancer cells need to rapidly produce membranes, so requiring higher cholesterol availability than normal cells (8). Besides, cholesterol is an integral component of lipid rafts, which constitute a core of organization for several signaling pathways and intracellular transport systems (96), and is also a precursor of downstream products such as oxysterols and steroid hormones which can drive activation of nuclear receptors in several cancers (97). Thus, decreasing intracellular cholesterol biosynthesis could be a promising strategy to restrain cancer progression. Indeed, it was reported that acute myeloid leukemia (AML) cells exposed to high-cholesterol media *in vitro*, increased their cholesterol synthesis and influx compared to their normal, non-tumorigenic counterparts. Moreover, AML cells did not usually display efficient feedback repression of cholesterol synthesis and influx, and this appeared to be associated with increased survival of leukemic cells. Interestingly, synthetic LXR ligands can block tumor cell proliferation, tumorigenesis, and metastasis in multiple cancer models, which emphasizes the potential role of LXRs in cancer therapy (82, 98). Cholesterol is also the precursor of steroid hormones, responsible for driving the initiation and progression of hormone-dependent breast and prostate cancers. Recently, it has been shown that long-term E2 withdrawal of ER $\alpha$ -positive breast cancers triggers to the stable epigenetic activation of the MVA pathway and cholesterol synthesis (61). The resulting augmented level of 27-hydroxycholesterol was enough to induce ER $\alpha$  signaling in the absence of exogenous E2, promoting the activation of genes that give rise to an invasive phenotype (62). Likewise, in prostate cancer, the *de novo* biosynthesis of androgens from cholesterol activates androgen receptor (AR) activity in castration resistant disease (99), thus suggesting a role for the MVA pathway in prostate cancer progression, also considering the observations that SREBP expression is enhanced in advanced stages of prostate cancer. However, these findings require further research into the utility of inhibitors of the MVA pathway and/or SREBPs in the treatment of

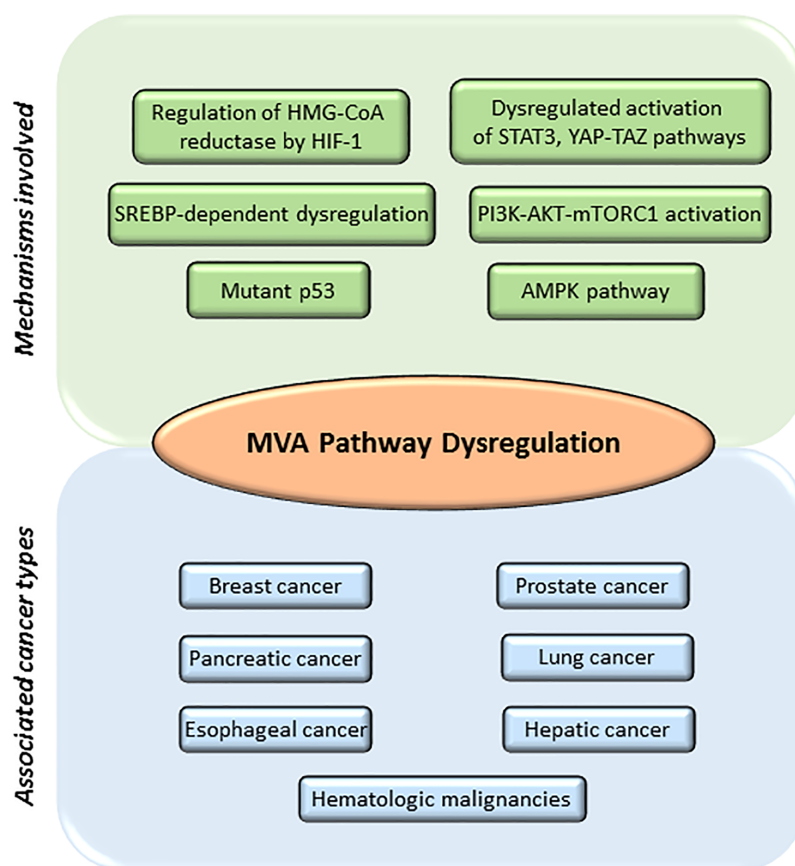


**FIGURE 2 |** Main mechanisms involved in mevalonate (MVA) pathway dysregulation and different cancers associated. MVA pathway is upregulated in several cancers including breast, prostate, pancreatic, lung, esophageal, hepatic, and leukemia. Main mechanisms involved in the dysregulation of MVA pathway include: abnormal regulation of the enzyme hydroxy-methyl-glutaryl-CoA reductase (HMGCR) by different transcription factors such as hypoxia-inducible factor 1 (HIF-1); mutations or abnormal activation of sterol regulatory element-binding proteins (SREBPs); mutations on tumor suppressor proteins such as tumor protein (p53); decreased AMP-activated protein kinase (AMPK) activation; increased activation of signaling pathways such as phosphoinositide 3-kinase (PI3K)—protein kinase B (AKT)—mammalian target of rapamycin complex 1 (mTORC1), Janus Kinase (JAK)/Signal Transducer and Activator of Transcription 3 (STAT3) or Hippo signaling pathway (YAP-TAZ).

hormone-driven cancers. All these evidences indicate that increased cellular cholesterol and/or oxysterols, represent another hallmark in many cancers, and suggest that limiting cellular cholesterol levels, or LXR activity, should be considered to improve therapeutic window and sensitivity of cancer cells to chemotherapy. Unluckily, the mechanisms by which HMGCR and the MVA pathway become dysregulated, or how precisely this deregulation promotes carcinogenesis, are still poorly understood, so further studies would be needed in order to elucidate these key questions.

## SMALL GTPases

Rho GTPases belong to the Ras superfamily which comprises more than 20 members classified into eight subfamilies (Rho, Rac, Cdc42, RhoD/RhoF, RhoH, RhoU/RhoV, Rnd, and RhoBTB) according to their structure and function (63, 64). Most Rho family proteins act as molecular switches cycling

between an inactive guanosine diphosphate GDP-bound state in the cytoplasm, and an active guanosine triphosphate (GTP)-bound state in the cell membrane. The activation state of Rho GTPases is tightly regulated and occurs in a cell-type and pathway-dependent manner. Although Rho GTPases are mostly known as master regulators of the actin cytoskeleton, they are also involved in cell proliferation, apoptosis, cell cycle progression, and genomic stability, and they are dysregulated in several human cancers (100). Notably, some Rho GTPases have been related to tumor metabolism through activation of glutaminase, which catalyzes the conversion of glutamine to glutamate and ammonia, a crucial step in glutamine metabolism and contributor to the Warburg phenomenon. As Rho GTPases need isoprenylation to properly function, their activity essentially depends on the HMGCR enzyme, thus providing a critical link between the MVA pathway and tumor cell metabolism. Specifically, the isoprenoids FPP and GGPP post-translationally modify proteins with C-terminal CAAX, CXC or CC motifs, such as small GTPases, with very well established roles in

carcinogenesis (100). Rho can only be geranylgeranylated, whereas H-Ras is purely farnesylated, and K-Ras and N-Ras can be both farnesylated and geranylgeranylated. Accordingly, inhibition of the MVA pathway can reduce the isoprenylation of these GTPases and promote apoptosis of cancer cells (100–102). This antitumoral effect can be prevented by the addition of GGPP, and sometimes FPP, suggesting that these MVA-derived metabolites are vital for cancer cell viability. Isoprenoids are also involved in the production of the ubiquinone (quinone coenzyme Q). In this case, the hydrophobic isoprenoid chain places the ubiquinone to the inner membrane of the mitochondria, where the quinone group transfers electrons from complex I or II to complex III of the electron transport chain (ETC) (103). Therefore, ubiquinone is essential for ATP production in cancer cells that rely on oxidative phosphorylation to generate energy. It seems that the depletion of isoprenoid pools, which potentially affect the many proteins that are isoprenylated, mediates the anticancer activity of HMGCR inhibitors (i.e., statins). However, despite dependency of isoprenoids, inhibitors that directly inhibit isoprenylation of small GTPases have not been a successful anticancer strategy to date because, in part, their narrow therapeutic window.

## CD36

The fatty acid transporter CD36 is considered as a novel connection between lipids and cancer. It may contribute to regulate cholesterol synthesis (88) and phenotypic changes linked to tumor growth and metastasis (68, 104, 105). In hepatocytes, activation of CD36 increases phosphorylation of Ser872 in HMGCR, and the recruitment of the Insig 1/2 contribute to degradation of HMGCR by the ubiquitin-proteasome pathway. In addition, genes encoding key enzymes involved in MVA pathway, and under the control of SREBP2, remained unresponsive to sterol depletion, due to retention of Scap by Insig-1/2. Interestingly, some fatty acids (e.g., palmitic acid), or a high-fat diet, enhance the metastatic potential of cells in a CD36-dependent manner, whereas blocking CD36 causes inhibition of metastasis in mouse models of human oral cancer, with no side effects (104). Relevant to the connection between oncogenic STAT3 and aberrant lipid metabolism, it has been shown that STAT3-activated CD36 contributes to fatty acid uptake in chronic lymphocytic leukemia cells (106), which supports a critical role of STAT3 in the regulation of CD36-dependent leukemia.

## AMPK

The AMP-activated protein kinase (AMPK) was originally described as a protein to lessen anabolic pathways activity when intracellular ATP levels are low (66). AMPK acts as an energy sensor and central regulator of glucose, lipid, and cholesterol metabolism in specialized tissues (e.g., liver, muscle, adipose). This function has placed AMPK as a key therapeutic target in cancer. Decreased AMPK activation can promote carcinogenesis, and the pharmacological induction of AMPK

has been reported to be cytotoxic to cancer cells (65, 67). This is in part, because AMPK can regulate the MVA pathway through phosphorylation and thereby inhibition of HMGCR (55) and SREBPs (107) activities. AMPK can phosphorylate the Ser872 within the catalytic domain of HMGCR, suppressing its enzymatic activity, independently of its feedback regulation by MVA-derived metabolites. Moreover, the transcription factors SREBPs are direct targets of AMPK phosphorylation, as AMPK inhibits the proteolytic processing, nuclear translocation, and transactivation activity of SREBPs, after their activation (e.g., under hyperglycemic and hyperinsulinemic conditions). Interestingly, activation of AMPK in the liver of insulin-resistant mice was shown to inhibit the transcription of enzymes that participate in lipid and cholesterol biosynthesis, including HMGCS1 and HMGCR, thereby reducing hepatic triglyceride and cholesterol levels. Thus, AMPK can inhibit the activity of MVA pathway both, directly, *via* HMGCR phosphorylation and, indirectly, through SREBPs inhibition. However, the relevance of this regulation in the context of cancer is still scarcely regarded. The MVA pathway may besides modulate AMPK activity, thereby forming a feedback loop (108). The discovery that the serine-threonine kinase Liver Kinase B1 (LKB1), a known tumor suppressor, was a crucial upstream activator of the AMPK, added a relevant piece of information to our understanding about the connection between cell metabolism and cancer (109). It is therefore feasible that the anticancer effects of AMPK activation and the tumor suppressor role of its upstream kinase LKB, are in part due to the inhibition of HMGCR and the MVA pathway. LKB1 is modified by protein farnesylation and it phosphorylates and activates AMPK. This suggests a negative feedback loop, where AMPK activation, in response to reduced cellular energy, results in the suppression of the MVA pathway *via* the phosphorylation of HMGCR and SREBPs. This reduces in turn the FPP pool inside the cell, thereby hampering LKB1 farnesylation and blocking activation of AMPK. Remarkably, AMPK activation has also been reported to suppress cell proliferation in normal and cancer cells by regulating cell cycle progression or inhibiting protein synthesis (110, 111). In line with this, recent studies have shown that simvastatin, a potent HMGCR inhibitor, induces apoptosis and cell cycle arrest by activating AMPK and inhibiting the Signal Transducer and Activator of Transcription 3 (STAT3) axis, both in liver cancer cells and tumor xenografts (112, 113). However, restoration of MVA reversed the activation of AMPK and the suppression of STAT3 caused by statin treatment. These findings contributed to demonstrate that AMPK induction and STAT3 inhibition in liver cancer cells are dependent on HMGCR activity. Thereby, MVA signaling pathway, AMPK and STAT3 activities may represent potential therapeutic targets in liver cancer.

## THE PI3K-AKT-mTORC1 AXIS

In normal cells, the mTORC1 activity can be activated by diverse stimuli (i.e., growth factors, nutrients, energy, and stress signals),



and key signaling pathways (i.e., PI3K-AKT, MAPK and AMPK), in order to regulate cell growth, proliferation and survival. Upon stimuli, PI3K produces PtdIns(3,4,5)P<sub>3</sub> which binds to AKT and 3-phosphoinositide-dependent protein kinase (PDK1). In contrast, the inactivation of AKT is regulated by PTEN that converts PtdIns(3,4,5)P<sub>3</sub> into PtdIns(4,5)P<sub>2</sub>, driving to a lower recruitment of AKT to the cell membrane (114, 115). An increased mTORC1 activity is observed in 40–90% of the most frequent human cancers. The aberrant activation of PI3K-AKT-mTORC1 signaling leads to an increase activity of the MVA biosynthetic pathway and lipogenesis, and the reprogramming of lipid metabolism contributes to potentiate tumor growth (70, 71). Several mechanisms are implicated, including the inactivating mutation of PTEN (116, 117), the mutation/amplification of PI3K-AKT (118), the hyperactivation of PI3K-AKT signaling pathway by growth factors (e.g., insulin, PDGF, VEGF, HER-2, IGF-I), the overexpression of mTORC1 targets (i.e., S6K1, 4BP1, eIF4E), or the loss of tumor suppressors (e.g., PTEN, LKB1, or TSC). These are common mechanisms that increase *de novo* cholesterol synthesis and fatty acid biosynthesis in cancer (119, 120). Upregulated PI3K-AKT activity increases glucose uptake and glycolysis rate in cancer cells, a mechanism that provides NADPH and acetyl-CoA to the MVA pathway. Conversely, inhibition of the MVA pathway can decrease PI3K activity. The PI3K-AKT-mTOR pathway connects with SREBP-mediated lipid biosynthesis by using complex protein-protein interactions and phosphorylation of regulatory elements (121, 122). Interestingly, AKT prevents proteasomal degradation of nuclear SREBPs which increases *de novo* cholesterol and fatty acid biosynthesis. This role of AKT on lipogenesis, and tumorigenesis, is blocked after gene silencing of SREBPs. Furthermore, the connection of mTOR with SREBPs was evidenced by enhanced lipogenesis in response to mTORC1 activation whereas inhibition of mTORC1 with rapamycin blocked both active SREBP and expression of SREBP target genes. In addition to a positive regulation of SREBP, mTORC1 has a main role in regulation of protein synthesis through phosphorylation of downstream effectors such as 4EBP1 and S6K1. Targets of S6K1 include 40S ribosomal protein S6, protein elongation factors, and IGF-II. Clinically relevant, human primary breast cancer samples with high levels of pS6K1, as a marker of mTORC1 activity, had high expression of SREBP target genes (e.g. FASN, LDLR, MVA kinase). In contrast, breast cancer cell lines with silenced SREBPs (1 and/or 2) showed reduced proliferation and increased cell death despite activation of mTORC1. Finally, mTORC1 activation has also been linked to proteins such as STAT3, STAT5 and PPAR $\gamma$ , in a rapamycin sensitive manner. Thereby, aberrant activation of PI3K-AKT-mTOR axis can reprogram protein and lipid biosynthesis in an orchestrated manner to provide efficient tumor growth.

## THE HIPPO PATHWAY

The Yes-associated protein (YAP) and the transcriptional co-activator with PDZ-binding motif (TAZ) are key downstream terminal effectors of the Hippo signaling pathway (123). In normal tissues, YAP-TAZ proteins are phosphorylated at

specific serine residues in order to confine their subsequent degradation in the cytoplasm (124). However, in cancer, YAP-TAZ proteins are translocated into the nucleus where they bind to TEA domain (TEAD) proteins which drive the transcriptional activation of proliferative genes, the repression of pro-apoptotic genes and the amplification of stem/progenitor cells. Increasing evidences have shown that deregulated Hippo pathway is significantly associated with cancer development (72, 73). Remarkably, YAP and TAZ require the MVA biosynthetic pathway to translocate into the nucleus and be fully functional (72). In fact, it has been reported that the concurrent knockdown of SREBPs (1 and 2) reduces nuclear localization of YAP-TAZ, suggesting the importance of SREBP-mediated induction of the MVA for YAP and TAZ nuclear localization (72). Interestingly, activation of both the MVA pathway and YAP-TAZ is correlated with mutant p53 expression in primary tumors, suggesting a dysfunctional mutant p53-SREBP-YAP-TAZ axis in cancer (72). Relevant to this review, the MVA pathway is an essential intermediate in the oncogenic activation of YAP and TAZ by mutant p53 (72). When statins are used to inhibit the HMGCR activity in the MVA pathway, the nuclear localization and transcriptional activity of YAP-TAZ are also inhibited. GGPP may be involved in this process, as it is known to promote YAP-TAZ nuclear translocation and increase their transcriptional activity *via* activation of Rho GTPases. Thus, when MVA pathway is inhibited, also GGPP is, thereby reducing YAP-TAZ activity. Additionally, it has been shown that YAP-TAZ can be activated by SREBPs, main regulators of MVA pathway, in a breast cancer cell line. Interestingly, mutant p53 promoted YAP-TAZ transcriptional activity and contributed to cancer cell malignancy by maintaining SREBP expression in MVA pathway. Taken together, these data clearly show that MVA participates in the regulation of YAP-TAZ expression and transcriptional activity and reveal an original process through which statins have anticancer effects.

## THE HEDGEHOG PATHWAY

Members of the Hedgehog (Hh) family of secreted signaling proteins have an essential role in the regulation of vertebrate development and adult tissue homeostasis, including regulation of stem cell physiology (74, 75). Reduced Hh pathway activity can cause development defects in mice and humans, and aberrant increased activity of this pathway is linked to tumorigenesis. The core components of the Hh pathway include: the secreted signaling ligand Hh, the twelve-pass transmembrane receptor Patched (PTCH), the seven-pass transmembrane co-receptor G-protein-coupled receptor (GPCR)-like transducer Smoothened (SMO), and the glioma associated-oncogene (GLI) (74, 75). After secreted from the producing cells, Hh binds to PTCH on the cell surface, and subsequently release suppression of PTCH on SMO. Then, activation of SMO triggers GLI-dependent expression of downstream target genes through a complex network of post-translational modifications and translocations. There are positive

and negative feedback loops that ensure a homeostatic regulation of Hh signaling pathway, which include an increment of GLI levels or the potentiation of the activity of negative regulators such as PTCH1, respectively. Relevant to this review, the Hh signaling pathway is regulated by cholesterol and oxysterols, main products of MVA biosynthetic pathway (74). It has been established that cellular cholesterol is an endogenous ligand of SMO. Thereby, cholesterol levels can modulate the Hh signaling pathway by direct binding to GPCR-SMO (50). Thus, cholesterol itself can be used as a substrate for the post-translational modification of Hh ligands, required for biological activities of Hh, as well as a molecule for long-distance and local Hh signal communication. Thereby, inhibitors of MVA pathway (e.g., statins) that modulate Hh pathway activity could represent potential drugs in Hh pathway-related cancers.

## HYPOXIA-INDUCIBLE FACTORS (HIF)

Under hypoxic conditions, cells respond by suppressing energy-consuming processes to preserve energy, including mitochondrial respiration (125, 126). These conditions promote the activation of the Hypoxia-Inducible Factors (HIF). The HIF protein family consists of three  $\alpha$  members (i.e., HIF-1 $\alpha$ , HIF-2 $\alpha$ , and HIF-3 $\alpha$ ) and two  $\beta$  members (i.e., HIF- $\beta$  and ARNT2), which have a similar domain structure (127). Under hypoxic conditions, HIF-1 $\alpha$  is stabilized, binds DNA, and regulates the transcription of glycolytic target genes in cancer cells (125, 128). Several observations have shown that the MVA pathway can be directly or indirectly modulated under hypoxic conditions, in part, because HMGCR expression is regulated through the transcriptional activity of HIF-1 $\alpha$  (129, 130). It has been reported that HIF-1 $\alpha$  connects pathways for oxygen sensing and feedback regulation of cholesterol synthesis in human fibroblasts by directly inducing the transcription of the INSIG-2 gene. INSIG-2 is an ER membrane protein that inhibits cholesterol synthesis by mediating sterol-induced ubiquitination and subsequent degradation of the HMGCR. Furthermore, pharmacologic stabilization of HIF-1 $\alpha$  in the liver was shown to trigger accelerated HMGCR degradation by prior ubiquitination (131). Pharmacologically relevant, in other pathologic fields such as Alzheimer's disease, statins (simvastatin) have been shown to reduce intracellular levels of HIF-1 expression (132). Likewise, fluvastatin was shown to accelerate ubiquitin/proteasome-dependent degradation of HIF-1, effect that was reversed by concomitant treatment with mevalonate, farnesyl pyrophosphate, or geranylgeranyl pyrophosphate (133). While HIF has been broadly studied as an essential protein for modulation of transcriptional program during the hypoxia response, many other transcription factors (e.g., NF $\kappa$ B, Nrf2, Myc, STAT3) and/or tumor suppressors also function under hypoxic conditions to promote the acquisition and maintenance of metabolic reprogramming phenotype in cancer. Further understanding about the connections between these transcription factors and the MVA pathway constitutes an ongoing challenge.

## SIGNAL TRANSDUCERS AND ACTIVATORS OF TRANSCRIPTION (STAT)

The STAT family of transcription factors consists of 7 members within STAT3 highlights by its oncogenic activity. STAT3 appears constitutively active in a broad variety of cancers that often become addicted to its activity (78–80). In contrast to normal STAT3 activity, which is transient, constitutively active STAT3 is associated with abnormal cell growth and survival, angiogenesis and metastasis, tumor immune evasion, and aberrant mitochondrial function. While tyrosine phosphorylation by Janus Kinases (JAK), represents the main activation mechanism of STATs, alternative mechanisms, such as the interaction with HIF signaling pathway, phosphorylation of STAT3 on S727 (134), and regulation of activity and nuclear traffic by small GTPases (135), appear to play important roles that connect STAT3 oncogenic activities with deregulated metabolism in cancer cells. An important component of STAT3 oncogenic activity resides in the induction of aerobic glycolysis, making cancer cells highly sensitive to glucose deprivation, whereas they are protected from apoptosis and senescence. Accordingly, inhibition of STAT3 tyrosine phosphorylation in several cancer cells down-regulates glycolysis prior to leading to growth arrest and cell death. STAT3-addicted cancer cells can develop a switch towards aerobic glycolysis program through two mechanisms: a) the up-regulation of HIF-1 $\alpha$ , which in turn mediates the induction of several glycolytic genes [e.g., hexokinase 2, LDH-A, pyruvate dehydrogenase kinase 1 (PDH), PKM2] (136); and b) the down-regulation of mitochondrial activity, which is totally or partially independent of HIF-1 $\alpha$ . HIF-1 $\alpha$  induces PKM2 expression, which maintains STAT3 tyrosine phosphorylation, a mechanism that initiates a positive feedback loop that leads breast cancer cells to adapt and grow into hypoxia conditions (137). Similarly, hypoxia can activate oncogenic STAT3 in prostate cancers cells, and, together with the AKT and HIF-pathways, induces an androgen-independent and invasive phenotype (138). In addition, STAT3 phosphorylation on S727 has emerged as a crucial regulator of metabolic processes in the mitochondria. Indeed, S727-STAT3 was found to enhance Complex I and II activities and reduce ROS production within the mitochondria (139, 140). This function appears to be essential for cellular survival under certain stress conditions such as heart ischemia, where mitochondrial STAT3 protects cardiac cells from apoptosis (140). Furthermore, mitochondrial STAT3 potentiates RAS-mediated oncogenic transformation. This finding supports the role of STAT3 in maintaining cell survival and oncogenesis, linked to a metabolic adaptation of cancer cells. In contrast, mitochondrial expression of an inactive mutant S727A-STAT3 was shown to inhibit growth and metastatic capacity of the breast cancer cell line 4T1, and this inhibition correlated with reduction of Complex I activity under hypoxia (141). The form S727-STAT3 can also be induced by the mTOR pathway to potentiate the expression of STAT3 target genes (e.g., Bcl-xL, VEGF, cyclin D2) (142, 143). Moreover, activated forms of small GTPases such as Rac1, Cdc42 or RhoA directly or indirectly promote the phosphorylation and activation of STAT3 (134, 144, 145). Particularly, Rac1 specifically induces an increase in Rac1 and Cdc42 protein levels and activities, and stimulates

autocrine IL6 secretion, which contributes to an increase of STAT3 activity. Interestingly, the activated form of Rac1, but not its inactive variant, forms a complex with STAT3 to regulate its phosphorylation and activity (146, 147). Interestingly, the Rac (and Cdc42) GTPase activating protein MgcRacGAP plays also a critical role in STAT3 activation (148, 149). When activated, the complex MgcRacGAP-Rac-GTP interacts with STAT3 to promote its binding to the IL6 receptor thus facilitating that JAK phosphorylates and activates STAT3. These observations suggest that MgcRacGAP, a core regulator of cytokinesis, and other Rho proteins, support oncogenic properties of STAT3. All observations indicate that STAT3 can integrate different pro-survival and growth signals in a context of energy and respiratory metabolism, emerging as a key molecule to target within the mitochondrial metabolism.

Tumor immune microenvironment (TIM), including surrounding (niche) and inflammatory cells, plays a key role in the development of angiogenesis, proliferation, immunosuppression, and tumor progression (150). These biological effects depend, at least in part, on the aberrant activation of STAT pathway which is an immuno-inflammatory-carcinogenic pathway. Thus, in addition to their roles in adaptive metabolism of cancer cells, aberrant STAT activity can drive cancer development through the regulation of TIM. This is particularly relevant for STAT3 and STAT5 which are highly expressed in Tumor-Associated Macrophages (TAMs), a critical cellular component of TIM. It is well known that TAMs are recruited into tumor formation by chemo-attractant cytokines and, once inside the tumor, tumor cells secrete cytokines that prolong the survival of TAMs; these cells, in turn, express multiple factors that promote tumor development and immunosuppression. STAT3 and STAT5 have been reported to act by inhibiting the antitumor immune response by activating, at least in part, the production of inflammatory cytokines (IL-1, IL-17, IL-10, TGF- $\beta$ , or VEGF) and promoting tumor growth and metastasis (150). Moreover, it has been described that TAMs could favor the development of tumor resistance to conventional chemotherapy, highlighting the importance of the microenvironment in tumor development. In addition to TAMs, the influence of niche stem cells on tumor development and drug resistant is also relevant. Interestingly, many studies have shown that STAT activity is essential to localize, maintain, and renew Hematopoietic Stem/Progenitors cells (HSPC) into tumoral niche and that STAT hyperactivation is associated with uncontrolled proliferation of HSPC (151–155). Thereby, dual strategies targeting both tumor cell proliferation and tumor niche and/or regulation of TIM represent a promising therapeutic strategy (156, 157). Interestingly, the effects of MVA biosynthetic pathway inhibitors (i.e., statins, bisphosphonates) on TAMs suggest that TIM can be regulated by MVA biosynthetic pathway (158–160). However, despite TIM is known to be highly dependent of cholesterol biosynthesis (10, 161–164), its interplay with MVA biosynthetic pathway and STAT signaling, remains unexplored.

## MYC

MYC belongs to the Myc gene family that is comprised by C-MYC, N-MYC, and L-MYC, and they have been shown to influence

almost all aspects of carcinogenesis, including rapid cell growth, inhibition of cell differentiation, genomic instability, metastasis, or angiogenesis (165–167). Aberrant regulation of MYC is observed in more than 50% of cancers, where this oncoprotein is overexpressed, either due to enhanced transcription of the Myc gene or to dysregulated stability of MYC protein. The stability of MYC can be modulated by a) the ubiquitin/26S proteasome pathway, and b) the sequential phosphorylation of MYC at S62 and T58. The phosphorylation of S62 is controlled by the MAPK/ERK pathway and leads to the stabilization of MYC, whereas its phosphorylation on T58 is mediated by GSK3 $\beta$  and promotes ubiquitin-dependent MYC degradation once S62 is dephosphorylated by, for example, the serine/threonine-protein phosphatase 2A (PP2A) (165, 168). Mutations on the phosphorylation sites that stabilize MYC have been identified in human cancers, thus highlighting the relevance of S62 and T58 phosphorylation as regulators of MYC tumorigenic activity (169). MYC is a major driver of metabolic reprogramming in cancer, where this transcription factor regulates the expression of genes involved in anabolic metabolism, cellular bioenergetics and lipid metabolism (167, 170, 171). This oncoprotein can reprogram cancer cell metabolism toward glycolysis and MVA pathway to drive the proliferation and survival of cancer cells. Accordingly, it has been reported that knockdown of c-Myc in gastric cancer cells suppresses glycolysis rates and cell proliferation capacity. MYC can also bind SREBP to drive somatic cell reprogramming into induced pluripotent stem cells (171), or bind to promoters of MVA pathway genes in close proximity to SREBPs (8), suggesting that MYC may contribute to the expression of MVA pathway enzymes. Notably, HMGCR is a positive regulator of phosphorylation, activation, and tumorigenic properties of MYC in a MYC-driven model of hepatocellular carcinoma where exogenous mevalonate deliver can enhance cancer growth (168). In agreement with the positive role of MVA pathway in MYC-induced oncogenic activities, the antitumoral effects of statin were prevented by mevalonate. This effect was associated with a reduction of small GTPase RAC isoprenylation levels and PP2A activation. Moreover, when tumors that expressed active phosphorylated mutants of MYC at S62 or T58 were studied, there was an increase of tumor resistance to statin treatment which supported the role of serine/threonine phosphatase PP2A as a negative regulator of MYC (168). Recently, studies on MYC null mice showed that mice had improved lifespan, which was linked to the decreased expression of MVA pathway genes, including HMGCR and SREBP2, and most likely to caloric restriction (172). Finally, RAS, whose activity is also regulated by the MVA pathway is thought to modulate MYC activity and enhance levels of HIF-1, independently of hypoxia conditions (173, 174). These findings reinforce the hypotheses that MYC dependent oncogenesis is linked to a deregulated MVA biosynthetic pathway.

## THE ERR $\alpha$ PATHWAY

Estrogen-Related Receptors (ERRs) are a group of nuclear receptors with three isoforms ( $\alpha$ ,  $\beta$ , and  $\gamma$ ) (84, 85, 175). ERR $\alpha$  is mainly expressed in high-energy demanding tissues where it associates with the co-regulator peroxisome proliferator-activated receptor- $\gamma$  co-



activator 1 (PGC-1). In differentiated cells,  $ERR\alpha$ , together with PGC, controls cellular metabolism, assists the growth of rapidly proliferating cells, directs metabolic programs necessary for cell differentiation, and keeps cellular energy homeostasis. In several cancer cells, the expression, and the activity of  $ERR\alpha$ , and its cofactor PGC-1, is further influenced by oncogenic signals (e.g., IGF1 receptor pathway, estrogen signaling, mTOR pathway) and induces metabolic programs favoring cell growth and tumor progression. This is particularly relevant when there is a functional relation between augmented cholesterol levels and certain cancer phenotypes, with an overexpression of  $ERR\alpha$  [i.e. colorectal cancer (176), prostatic, and breast cancers (177)]. Notably,  $ERR\alpha$  activity promotes an inflammatory environment by the production of cytokines that supports a protumoral microenvironment (178). Recently, affinity chromatography and transcriptional assays have identified cholesterol as an endogenous ligand and agonist of  $ERR\alpha$  (84). A functional link between cholesterol (or MVA pathway) and  $ERR\alpha$  has been described in bone, muscle, and in the immune system (macrophages). Particularly, cholesterol-induced bone loss or bisphosphonate osteoprotection are lost in  $ERR\alpha$  knockout mice. In addition, statin induction of muscle toxicity and cholesterol suppression of macrophage cytokine secretion are impaired by loss or inhibition of  $ERR\alpha$ . These findings showed that cholesterol is an  $ERR\alpha$  agonist and that the MVA biosynthetic pathway impacts biological functions of  $ERR\alpha$  (85). Thereby, the use of therapeutic strategies that aim to decrease cholesterol levels (e.g., statins, bisphosphonates) could be an encouraging way to counteract metabolic reprogramming in cancer cells where  $ERR\alpha$  plays a critical role.

## **$ERR\alpha$**

The MVA biosynthesis pathway was recently reported to be up-regulated in  $ER\alpha$ -positive breast cancer cells lines that are resistant to E2 withdrawal (61, 62, 83). This suggests that dysregulation of cholesterol biosynthesis may be a mechanism of anti-estrogen resistance in  $ER$ -positive breast cancer. Mechanistically relevant, chronic estrogen removal in  $ER\alpha$ -positive breast cancer cells seems to stabilize the epigenetic activation of the MVA pathway and cholesterol biosynthesis (61). This leads to the accumulation of cholesterol-derivative metabolites (i.e., 27HC) which, in the absence of estrogens, acts as  $ER\alpha$  agonist, and then potentiates  $ER\alpha$  signaling to induce the transcription of genes involved in proliferation and invasion. Therefore, statins might act as anti-breast cancer drug by reducing circulating cholesterol and 27HC, and the availability of these  $ER\alpha$  agonists in breast cancer cells. Furthermore, direct suppression of HMGCR by statins depletes intratumoral levels of isoprenoids, which are also key modulators of breast cancer cell proliferation and metastasis.

## **TUMOR SUPPRESSOR PROTEINS**

Loss-of-function of tumor suppressor protein p53 (TP53) (86, 87) and cyclin-dependent kinases (cdks)- retinoblastoma suppressor

protein (Rb)- transcription factor E2F Transcription Factor 1 (E2F1) pathway (88–90), novel regulators of metabolism, promotes the acquisition and maintenance of glucose and/or lipid metabolism reprogramming phenotype in cancer. The mutated forms of the tumor suppressor protein TP53 confer oncogenic properties to p53 in a broad range of cancer types (87). Specific oncogenic mutations lead p53 to functionally interact with nuclear SREBP2 and enhance the transcription of MVA genes (86) (**Figure 3**). Furthermore, an increased expression of mutant p53 in primary breast cancer tissues has been associated to the augmented expression of MVA pathway genes. In contrast, wild-type p53 can decrease lipid synthesis under glucose starving conditions by inducing the expression of phosphatide phosphatase LPIN1, a protein that can prevent SREBPs-DNA binding. Thus, the interaction between p53 and the MVA axis suggests that this pathway may be a novel therapeutic target for tumors with specific p53 gain-of-function mutations. Another example of mutated tumor suppressor gene that leads to an oncogenic phenotype is the *cdks-Rb-E2F1* pathway. Analysis of genetically engineered mice deficient in *cdk*, *E2F1*, or *Rb* protein, showed an adaptive reprogramming to metabolism of glucose and/or lipids, including MVA biosynthetic pathway. This showed that the *cdk-Rb-E2F1* pathway acts as a key regulator of cell growth, proliferation, and development by sensing external signals that require a particular adaptive metabolic reprogramming. Particularly, this cell cycle regulatory pathway is an essential regulator for decreasing oxidative metabolism and, at the same time, to increase lipid synthesis and glycolytic metabolism. Interestingly, loss of *Rb* causes abnormal expression of the farnesyl diphosphate synthase (FDPS), many prenyltransferases, and their upstream regulators SREBPs, in an E2F-dependent manner, leading to an increased isoprenylation and activation of N-Ras (89). Additionally, loss of *Rb* reduces the suppression of E2F (1 and 3), a mechanism that leads to promoter activation of prenyltransferase genes. Conversely, the presence of active *Rb* prevents the association of SREBPs with the FDPS promoter, suggesting that *Rb* negatively modulates the MVA pathway at both the transcriptional and the post-translational level.

## **CHOLESTEROL CONTRIBUTES TO CHEMOTHERAPY RESISTANCE**

Upregulated MVA pathway contributes to chemotherapy resistance by increasing both isoprenoids and cholesterol levels (10), thus generating a serious problem that arises in the treatment of many cancers. It has been shown that, in response to chemotherapy *in vitro*, some leukemic cells (i.e., AML cells) abnormally increased their cholesterol levels, whereas when this response is blocked with HMGCR inhibitors (i.e., statins), they increased its sensitivity to cytotoxic drugs (179). Interestingly, apoptosis resistance, typically observed in cancer (i.e., hepatocellular carcinoma (HCC), colon cancer and HeLa cells), has been related to cholesterol accumulation in mitochondria, resulting in decreased membrane fluidity (180–182). These data



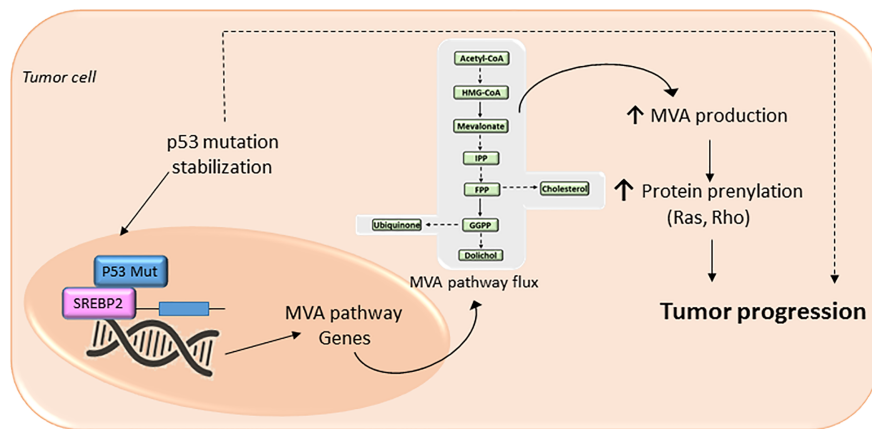


**FIGURE 3** | The mevalonate (MVA) pathway in cancer progression. The MVA pathway is dysregulated in several cancer cells due to mutations or abnormal signaling of different proteins/pathways. Upregulation of MVA pathway drives to increased protein prenylation thus promoting a malignant phenotype of cancer cells with an uncontrolled cell invasive growth and survival. In cancer cells expressing a mutation of tumor protein p53, there is a positive-feedback loop where p53 interacts with sterol regulatory element-binding protein (SREBP), leading to increased activation of the MVA pathway activity, and therefore higher levels of MVA. This MVA leads to the stabilization of p53 mutation as well as promotes protein prenylation, thus accelerating cancer progression.

suggest that high mitochondrial cholesterol content contributes to chemotherapeutic resistance, especially to chemotherapeutic agents targeting mitochondria (182). On the other hand, as deeply discussed in a later section of the present review, it has been reported that HMGCR inhibitors (i.e., simvastatin) are able to overcome resistance or to potentiate the antitumoral effects of conventional chemotherapy in several models of cancer (*in vitro* and *in vivo*), such as, non-small cell lung cancer (183), resistant colorectal tumors (184) and human gastric cancer (39, 185). Therefore, inhibition of *de novo* cholesterol synthesis by statins may restore the efficacy and overcome resistance to conventional chemotherapy.

## EFFICACY AND RESISTANCE TO MVA PATHWAY INHIBITORS IN HUMAN TUMORS

MVA biosynthetic pathway is considered a potential drug target to improve therapeutic window in cancer (11) (**Figure 4**). However, despite mounting body of preclinical and epidemiological evidences suggesting MVA pathway inhibitors (i.e., statins) as anticancer agents, many patients remained non-responsive to drug treatment in some cancer clinical trials (13, 20, 23, 30, 33, 186). This is, in part, because cancer cell selectivity, as well as predictive biomarkers of drug efficacy and drug resistance, is still poorly understood. Therefore, clinical trials are still required to further characterize the subset of cancers that are especially sensitive to MVA pathway inhibitors. The major limitation for the development of MVA pathway-based therapy is the absence of predictive biomarkers of efficacy and chemotherapy resistance, which is due to, at least in part, the lack of routine genotyping of human tumors. Therefore, predictive biomarkers, stratifications of patients, and selection

of drug combination-based therapies may lead to a more effective MVA pathway-based therapy in cancer. Nowadays, there are a few completed clinical trials in which statins are used as monotherapy. Some of them have exhibited promising evidence of therapeutic potential and survival benefit mainly in breast cancer (187–189) and multiple myeloma (MM) (190, 191) (**Table 1**). Breast cancer clinical trials, using atorvastatin and fluvastatin, have shown decreased proliferation index marker in a subset of patients who were treated with cholesterol-management doses of statins between cancer diagnosis and surgery (187, 189) (**Table 1**). Moreover, a phase II window-of-opportunity trial has shown that high-dose atorvastatin (80 mg/day) induced anti-proliferative effects in breast cancer through cell cycle regulation *via* cyclin D1 and p27 (188) (**Table 1**). Although the molecular mechanisms are still unknown, hepatocarcinoma also seems to be particularly responsive to statins (193). Exposition to simvastatin has also been associated to reduced risk of hematological malignancies (194). Although clinical trials with statins show that some tumors may be more sensitive to statins than others, few of them have specifically enriched for subsets of patients whose tumors are preferentially sensitive to statins. As described above, tumors harboring an aberrant MVA pathway may be more sensitive to the antitumoral action of statins. This hypothesis follows the general principles of oncogene addiction and may provide the basis on which patients should be treated with statins. However, follow-up studies are still needed before validating those biomarkers to predict which cancers will be specifically sensitive to statin therapy. For example, certain phases of cancer progression, such as breast cancer recurrence, are particularly sensitive to the antitumoral effects of statins (195, 196). This is in line with the current paradigm of inter-patient cancer biodiversity. This lack of response might also be expected considering the evidence that the MVA pathway is regulated by many critical oncogenic signals. For example, a poor outcome

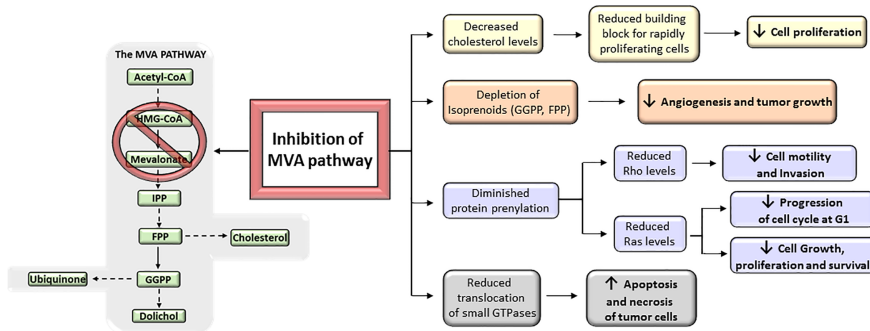


**FIGURE 4 |** Antitumoral effects of mevalonate (MVA) pathway inhibition. The inhibition of MVA pathway triggers a series of anticancer events that get to inhibit tumor growth and progression. These include the reduction of MVA synthesis, which in turn decreases the levels of downstream products (isoprenoids) and therefore prevents protein prenylation; the reduction in the translocation of small GTPases such as Rho and Ras to the cell membrane; and the inhibition of cholesterol synthesis. All these inhibitory actions suggest that targeting the MVA pathway could represent a key mechanism to prevent cancer progression.

has been reported in clinical breast cancer samples that carry a mutant form of p53 that stimulates the activity of MVA pathway (86). A molecular hallmark of basal transcriptome has been developed to forecast statin response in breast cancer *in vitro* (197) and aberrant MYC expression has been proposed as an indicator of statin response in specific cancer types (198). Notably, subsets of statin-sensitive and statin-insensitive cells were described in MM cell lines (199, 200). Remarkably, insensitive cells exhibited a robust feedback response, like normal cells, with an immediate up-regulation of different SREBP target genes, including HMGCR. In fact, recently, it has been reported that resistance of breast cancer cells to statins is, at least in part, due to the induction of HMGCR (201). Although the sterol feedback response tried to reinstate the MVA pathway, sensitive cells appear to show, in comparison with statin-insensitive cells, a weaker feedback response. This suggest that statin-sensitive cells have either lost checkpoint controls maintaining the MVA pathway intact, or that the pathway is deregulated and decreased HMGCR activity was not detected by the common intracellular sensors (i.e., SCAP, INSIGs). It appears that the sterol feedback response may serve as a protective mechanism, warranting that normal or statin-insensitive tumor cells are protected from the effect of statins. However, the loss of this sterol feedback response may not be a universal phenomenon across all statin-sensitive cancer types as it has been shown an intact sterol feedback response in AML cells (202). Moreover, tumor cholesterol may also be used as a biomarker of statin sensitivity in many AML cells exposed to chemotherapy *in vitro* (202, 203). All these observations suggest that aberrant MVA pathway may be both a promoter of transformation and an indicator of statin sensitivity. Moreover, these data also establish the bases to further developing biomarker tools that could allow to predict which cancers are more sensitive to statins. That may provide a personalized medicine approach in which statins, and/or other inhibitors of MVA pathway, would constitute a successful class of anti-cancer drugs.

## SREBP, A DRUG TARGET TO INCREASE STATIN EFFICACY AND OVERCOME DRUG RESISTANCE

Inhibition of the MVA pathway leads to the activation of the SREBPs and the increased expression of MVA pathway genes, an effect that may be intensified in cancer cells and be responsible of statin resistance (201, 204). This SREBP-mediated feedback mechanism also increases the expression of the LDLR, and LDL-cholesterol uptake, which has been shown relevant in cancer cells (205, 206). Thus, the SREBPs work to replenish MVA-derived metabolites, which can depress the apoptotic response following statin treatment. Recent studies targeting the maturation or transcriptional activities of SREBPs supply proof of concept for the efficacy of SREBP inhibition in cancer therapy (204). Inhibiting the SREBP-regulated feedback response together with statin therapy could prevent drug resistance and increase the antitumoral efficacy of statins. In addition to HMGCR, the MVA pathway genes HMGCoAS1, GGPS1, SCAP, and SREBP2 are also good candidates to either suppressing other enzymes in the MVA pathway or blocking the SREBP-mediated feedback response in combination with statin therapy (207). Particularly, the clinically approved agent dipyridamole may be repurposed as an inhibitor of statin (fluvastatin)-induced SREBP processing and blocks the SREBP-regulated feedback response. This mechanism can potentiate antitumoral efficacy of statins, at least in prostate cancer, and most likely prevent drug resistance (208). However, preclinical and clinical investigations performed in order to investigate the utility of this combinatory drug strategy in cancer (i.e., HMGCR inhibitors *plus* SREBP inhibitors), are still a pharmacological challenge. Hopefully, other molecules can be repurposed as potentially antitumoral candidates in combination with statins. Thereby, fatostatin, a nonsterol diarylthiazole derivative originally developed to inhibit insulin-induced adipogenesis, suppresses (*in vitro* and *in vivo*) prostate cancer cell proliferation and induces apoptosis through inhibition of

**TABLE 1 |** Completed clinical trials with statins used in mono- or in combination therapy for cancer treatment.

Cancer type	Drugs	Research findings and conclusions	Study phase	References and ClinicalTrials.gov Identifier
Breast Cancer (BC)	Fluvastatin	Fluvastatin reduces tumor proliferation and increases apoptosis in high-grade, stage 0/1 BC. These data support further evaluation of statins as chemoprevention for ER-negative high-grade BC	Phase II	(187) NCT00416403
Breast Cancer (BC)	Atorvastatin	High-dose atorvastatin (HD-Atorv) induces anti-proliferative effects through up-regulation of tumor suppressor p27 and down-regulation of oncogene cyclin D1 in BC	Phase II	(188) NCT00816244
Breast Cancer (BC)	Atorvastatin	Atorvastatin and its metabolites are detectable in breast fine needle aspiration biopsies and its use is associated with decreased C-reactive protein (CRP). These results support atorvastatin further evaluation in phase II BC prevention studies	Phase I	(189) NCT100637481
Multiple Myeloma (MM)	Simvastatin	Standard-dose simvastatin (SD-Sim) is well tolerated without grade 3/4 toxicity and shows reduction of cell adhesion-mediated drug resistance in MM by inhibition of HMG-CoA-reductase. Moreover, authors suggest that SD-Sim efficacy needs to be improved either by dose escalation and/or by combination with other mevalonate pathway inhibitors	Phase II	(190) NCT00399867
Multiple Myeloma (MM)	Simvastatin	High-dose simvastatin (HD-Sim) has not beneficial effect on markers of bone turnover in MM. In fact, HD-Sim seems to be harmful rather than beneficial for MM patients due a transient stimulation of osteoclast activity	Phase II	(191) NCT00281476
Pancreatic Cancer (PC)	Simvastatin/ Gemcitabine	Adding low-dose simvastatin (LD-Sim) to gemcitabine in treatment of advanced pancreatic cancer does not provide additional benefit but it also does not result in greater toxicity compared to gemcitabine alone. Since data point to an emerging role of statins in overcoming resistance to anti-epidermal growth factor receptor (EGFR) treatments, these results support further evaluation of efficacy and safety of combined LD-Sim and anti-EGFR agents (e.g., erlotinib or cetuximab) plus gemcitabine for treating advanced and metastatic PC	Phase II	(34) NCT00944463
Small-Cell Lung Cancer (SCLC)	Pravastatin/ Etoposide/ Cisplatin or Carboplatin	Pravastatin combined with standard platinum chemotherapy in patients with SCLC, although safe, does not benefit patients. Authors concluded that ongoing and future trials of statins used for either cancer prevention or treatment should monitor clinical efficacy and ensure that preclinical data are strong enough to warrant large-scale randomized studies	Phase III	(39) NCT00433498
Advanced Gastric Cancer (AGC)	Simvastatin/ Capecitabine – Cisplatin (XP)	Addition of low-dose simvastatin (LD-Sim) to XP does not increase median progression free survival (PFS) in AGC, but it does not increase toxicity. Authors concluded that LD-Sim to chemotherapy is not recommended in untargeted patients with AGC. However, given the emerging role of statins as anti-cancer agents, this study also suggest that intermediate or high-dose simvastatin synergistically combined with standard chemotherapy regimens should be further evaluated in AGC	Phase III	(192) NCT01099085

SREBP-regulated pathways, such as MVA pathway (209). Moreover, the combination of the anti-chronic myelogenous leukemia (CML) drug imatinib and simvastatin resulted in a synergistic killing effect on imatinib-resistant CML cells (210).

## COMBINATORY THERAPY, A STRATEGY TO IMPROVE THERAPEUTIC WINDOWS OF MVA PATHWAY INHIBITORS IN CANCER

Monotherapy with statins (e.g., simvastatin) displays anticancer activity *in vitro* (11). However, it is undefined whether lipophilic statins accumulate in tumor tissues at concentrations in which they are cytotoxic to cancer cells and efforts are still underway to determine tolerable and therapeutic dose of statins that could potentially be used in cancer (211). This is particularly jumbling as statins are also known to exert effects on certain normal cells. For example, myopathy is a rare but potentially dangerous side effect of statin treatment that is thought to be consequence of the induction of apoptosis in skeletal muscle cells (212). Interestingly, many studies have shown that statins can directly and specifically trigger the apoptosis of cancer cells (213, 214). Noteworthy, statins trigger apoptosis of cells derived from AML,

whereas normal myeloid progenitors do not suffer apoptosis and keep a proliferative phenotype (213). This optimal therapeutic index may be result of the altered metabolic reprogramming of AML cells leading to an increased dependence on MVA-derived metabolites for survival and proliferation. These findings and the widespread use of statins for hypercholesterolemia control strongly suggest that these drugs might have a high therapeutic window to target tumors *in vivo*, despite the MVA pathway is active in both normal and cancer cells. Therefore, the therapeutic window of statins in cancer patients is being explored in several clinical trials that have been conducted to study the tolerability of high dose statins in cancer patients. Phase I–II clinical trials have shown that statins can be given to cancer patients in relatively high dosages (i.e., 15 mg/kg/day for simvastatin; 25 mg/kg/day for lovastatin). In these studies, the maximum tolerated dose of simvastatin was defined to be 15 mg/kg/day, 25-fold higher compared to a typical dose. However, response may not be satisfactory because to treat human cancer high doses of statins (10–100  $\mu$ M) need to be used. Moreover, statins can cause anorexia and death in some individuals when serum concentrations reached levels higher than 20–25  $\mu$ M (215, 216). An efficient strategy that might increase therapeutic window of statins in cancer patients is its combination with conventional chemotherapy in those cancers where altered aberrant cholesterol metabolism is linked to oncogenic

signaling. This strategy can improve antitumor efficacy, by taking advantage of the synergistic effects of these drugs, and, potentially, reduces therapy-associated toxicity (8, 13, 217). For example and related to hematological cancers, cholesterol levels are abnormally elevated in many AML cells exposed to chemotherapy *in vitro* (202, 203). Suppressing this cholesterol response was further shown to sensitize AML cells to drug treatment, suggesting that MVA pathway inhibition by statins may improve the efficacy of conventional chemotherapy (203, 218). Thus, when pravastatin was combined with conventional treatment in AML resulted in complete or partial response in 60% of patients with AML (218). Furthermore, simvastatin also has potential application in oncohematology as it is able to potentiate the effects of imatinib in CML cells, inducing cell cycle arrest and apoptosis through the inactivation of STAT3 and STAT5 (210). Interestingly, lovastatin can enhance the antitumor effects of the antiretroviral drug saquinavir against human lymphoma cells, decreasing some of its side effects while potentiating the antitumor effectiveness (219). In another study, the combination of lovastatin with thalidomide and dexamethasone in patients with relapsed or refractory multiple myeloma prolonged overall survival and progression-free survival (220). Recently, it has been reported that combination of statins (atorvastatin, fluvastatin and simvastatin) and conventional chemotherapy (topotecan, paclitaxel and doxorubicin) acted synergistically to inhibit cell proliferation and to induce cytotoxicity in an aggressive natural killer cell leukemia (221). On the other hand, and related to solid tumors, a combinatory strategy has also been safely used to increase statin efficacy and security in HCC. Thus, pravastatin was combined with conventional treatment in HCC, resulting in significantly longer median survival (193). Moreover, promising results from both epidemiological studies (222, 223) and clinical trials (187, 224) suggest that patients with hormone dependent breast and prostate cancers, may benefit from the addition of statins to their conventional treatment regimens. Accordingly, it has been reported that simvastatin has additive effect with the antiandrogen enzalutamide promoting a greater inhibition of prostate cancer cells (225, 226). Moreover, simvastatin also enhances *ex vivo* the tumor cell inhibition effects of cisplatin or docetaxel in head and neck squamous carcinoma (HNSCC) (227) and sensitized human osteosarcoma cells to doxorubicin and cisplatin (228). Preclinical data have also shown that simvastatin in combination with cetuximab/irinotecan allows overcoming the resistance to irinotecan and oxaliplatin in KRAS mutant colorectal cancer (184). Moreover, simvastatin can potentiate the antitumor effect of capecitabine by suppressing proliferation and tumor invasion mediated by NF $\kappa$ B in a xenograft mouse model of human gastric cancer (185). In addition, it has been observed that lovastatin increases *in vitro* TNF- $\alpha$  -induced cell death in two gefitinib-resistant cholangiocarcinoma cell lines (229). Finally, statins can overcome the resistance to EGFR tyrosine kinase inhibitors in a non-small cell lung cancer cells (183) and to gefitinib in KRAS-mutant human non-small cell lung cancer cells (230). Paradoxically, several clinical trials have shown that combinatory therapy with statins does not add any benefit in comparison with conventional therapy. Clinical trials where simvastatin was combined with

capecitabine–cisplatin (XP) in patients with previously untreated advanced gastric cancer (AGC) showed that addition of low dose (40 mg) of simvastatin to XP does not increased the median progression free survival (PFS) (192) (**Table 1**). Moreover, it has been reported that using a combination of pravastatin, a hydrophilic statin, with etoposide plus cisplatin or carboplatin in order to treat small-cell lung cancer does not provide additional benefit for patients (39) (**Table 1**). Alike, a randomized double-blind phase II clinical trial in which patients with locally advanced and metastatic pancreatic cancer participated, reported no clinical benefits when low doses of simvastatin were added to gemcitabine (34). The limited effectiveness of statins in these and previous studies (231, 232), and in clinical trials mentioned above (34, 39, 192) (**Table 1**) might be linked to low statin biodisponibility in cancer cells. Pharmacokinetic studies in chronic lymphocytic leukemia patients have shown that when simvastatin is administered at the maximum tolerated dose of 7.5 mg/kg, twice daily, plasma concentrations were dose proportional relative to the hypolipidemic doses, but lower than those required for *in vitro* cytotoxicity on cancer cells (231). This lower drug bioavailability in cancer cells might explain, at least in part, the absent or low efficacy of statins in cancer patients.

## CONCLUSIONS AND FUTURE PERSPECTIVES

Nowadays, an increasing amount of data, from preclinical and epidemiological studies, support an inverse association between the use of potent inhibitors of MVA pathway and the mortality rate in specific cancers (e.g., breast, colon, prostate, liver, hematological malignances). Furthermore, inhibitors of MVA pathway seem to have potential features that overcome main limitations of current chemotherapy: drug resistance and toxicity. Cancer treatment demands the use of relatively high doses of single inhibitors of MVA pathway for a prolonged period, thereby limiting this therapeutic strategy due to adverse effects. Clinically relevant, synergistic effects of tolerable doses of MVA inhibitors with conventional chemotherapy might enhance efficacy with lower doses of each drug and, probably, reduce adverse effects and resistance. In spite of that, clinical trials to identify combinatory therapies that improve therapeutic window are still a challenge. Dual strategies targeting both tumor cell proliferation and tumor niche and/or regulation of TIM represent a promising therapeutic strategy. However, despite TIM is known to be highly dependent of cholesterol biosynthesis, interplay of MVA biosynthetic pathway and TIM remains unexplored. Therefore, research needs to be performed in order to identify an effective MVA pathway inhibitor that may be clinically used, individually or in combination with conventional chemotherapy, in the treatment of cancers with addiction to cholesterol biosynthetic pathway.

## AUTHOR CONTRIBUTIONS

All authors listed have made a substantial, direct, and intellectual contribution to the work, and approved it for publication.



## FUNDING

The Ministry of Science, Innovation and Universities (MCIU, SAF2015-65113-C2-2) with the funding of European Regional Development Fund-European Social Fund, SODECAN (Canary Islands Government; ET/15020), and FIISC (FUNCANIS2017; FIISC-DISA2018) supported research to Molecular and Translational Pharmacology Lab at University Institute for Biomedical and Health Research (IUIBS). Molecular and Translational Pharmacology Lab was also supported by grant-in-aid from Alfredo Martin-Reyes Foundation (Arehucas S.A.). MCIU-FPU16/00233 and ULPGC-2016 supported pre-doctoral

programs to MG-R. and HA-T, respectively. The post-doctoral program Juan de la Cierva (MCIU2017; MCIU2019) supported to CR.

## ACKNOWLEDGMENTS

We thank all the authors that have made a contribution to the understanding of the crosstalk between MVA pathway and cancer. We apologize to those whose work deserves to be cited but unfortunately are not quoted because of space limitations.

## REFERENCES

- Cairns RA, Harris IS, Mak TW. Regulation of cancer cell metabolism. *Nat Rev Cancer* (2011) 11(2):85–95. doi: 10.1038/nrc2981
- Boroughs LK, DeBerardinis RJ. Metabolic pathways promoting cancer cell survival and growth. *Nat Cell Biol* (2015) 17(4):351–9. doi: 10.1038/ncb3124
- Pavlova NN, Thompson CB. The Emerging Hallmarks of Cancer Metabolism. *Cell Metab* (2016) 23(1):27–47. doi: 10.1016/j.cmet.2015.12.006
- Sullivan LB, Gui DY, Vander Heiden MG. Altered metabolite levels in cancer: implications for tumour biology and cancer therapy. *Nat Rev Cancer* (2016) 16(11):680–93. doi: 10.1038/nrc.2016.85
- Altman BJ, Stine ZE, Dang CV. From Krebs to clinic: glutamine metabolism to cancer therapy. *Nat Rev Cancer* (2016) 16(10):619–34. doi: 10.1038/nrc.2016.71
- Li Z, Kang Y. Lipid Metabolism Fuels Cancer's Spread. *Cell Metab* (2017) 25(2):228–30. doi: 10.1016/j.cmet.2017.01.016
- Clendening JW, Pandya A, Boutros PC, El Ghamrasni S, Khosravi F, Trentin GA, et al. Dysregulation of the mevalonate pathway promotes transformation. *Proc Natl Acad Sci U S A* (2010) 107(34):15051–6. doi: 10.1073/pnas.0910258107
- Mullen PJ, Yu R, Longo J, Archer MC, Penn LZ. The interplay between cell signalling and the mevalonate pathway in cancer. *Nat Rev Cancer* (2016) 16(11):718–31. doi: 10.1038/nrc.2016.76
- Oguro H. The Roles of Cholesterol and Its Metabolites in Normal and Malignant Hematopoiesis. *Front Endocrinol* (2019) 10:204. doi: 10.3389/fendo.2019.00204
- Huang B, Song BL, Xu C. Cholesterol metabolism in cancer: mechanisms and therapeutic opportunities. *Nat Metab* (2020) 2(2):132–41. doi: 10.1038/s42255-020-0174-0
- Gazzerro P, Proto MC, Gangemi G, Malfitano AM, Ciaglia E, Pisanti S, et al. Pharmacological actions of statins: a critical appraisal in the management of cancer. *Pharmacol Rev* (2012) 64(1):102–46. doi: 10.1124/pr.111.004994
- Clendening JW, Penn LZ. Targeting tumor cell metabolism with statins. *Oncogene* (2012) 31(48):4967–78. doi: 10.1038/onc.2012.6
- Chimento A, Casaburi I, Avena P, Trotta F, De Luca A, Rago V, et al. Cholesterol and Its Metabolites in Tumor Growth: Therapeutic Potential of Statins in Cancer Treatment. *Front Endocrinol* (2018) 9:807. doi: 10.3389/fendo.2018.00807
- Mo H, Jeter R, Bachmann A, Yount ST, Shen CL, Yeganehjoo H. The Potential of Isoprenoids in Adjuvant Cancer Therapy to Reduce Adverse Effects of Statins. *Front Pharmacol* (2018) 9:1515. doi: 10.3389/fphar.2018.01515
- Iannelli F, Lombardi R, Milone MR, Pucci B, De Rienzo S, Budillon A, et al. Targeting Mevalonate Pathway in Cancer Treatment: Repurposing of Statins. *Recent Pat Anticancer Drug Discov* (2018) 13(2):184–200. doi: 10.2174/1574892812666171129141211
- Kamel WA, Sugihara E, Nobusue H, Yamaguchi-Iwai S, Onishi N, Maki K, et al. Simvastatin-Induced Apoptosis in Osteosarcoma Cells: A Key Role of RhoA-AMPK/p38 MAPK Signaling in Antitumor Activity. *Mol Cancer Ther* (2017) 16(1):182–92. doi: 10.1158/1535-7163.MCT-16-0499
- Kany S, Woschek M, Kneip N, Sturm R, Kalbitz M, Hanschen M, et al. Simvastatin exerts anticancer effects in osteosarcoma cell lines via geranylgeranylation and c-Jun activation. *Int J Oncol* (2018) 52(4):1285–94. doi: 10.3892/ijo.2018.4288
- Cecen B, Keles D, Oktay G, Kozaci LD. Effects of simvastatin on matrix metalloproteinase regulation in IL-1 $\beta$ -induced SW1353 cells. *Chem Biol Interact* (2019) 310:108730. doi: 10.1016/j.cbi.2019.108730
- Beckwitt CH, Clark AM, Ma B, Whaley D, Oltvai ZN, Wells A. Statins attenuate outgrowth of breast cancer metastases. *Br J Cancer* (2018) 119(9):1094–105. doi: 10.1038/s41416-018-0267-7
- Demierre MF, Higgins PD, Gruber SB, Hawk E, Lippman SM. Statins and cancer prevention. *Nat Rev Cancer* (2005) 5(12):930–42. doi: 10.1038/nrc1751
- Kuoppala J, Lamminpää A, Pukkala E. Statins and cancer: A systematic review and meta-analysis. *Eur J Cancer* (2008) 44(15):2122–32. doi: 10.1016/j.ejca.2008.06.025
- Mei Z, Liang M, Li L, Zhang Y, Wang Q, Yang W. Effects of statins on cancer mortality and progression: A systematic review and meta-analysis of 95 cohorts including 1,111,407 individuals. *Int J Cancer* (2017) 140(5):1068–81. doi: 10.1002/ijc.30526
- Jeong GH, Lee KH, Kim JY, Eisenhut M, Kronbichler A, van der Vliet HJ, et al. Statin and Cancer Mortality and Survival: An Umbrella Systematic Review and Meta-Analysis. *J Clin Med* (2020) 9(2):326. doi: 10.3390/jcm9020326
- Alfaqi MA, Allott EH, Hamilton RJ, Freeman MR, Freedland SJ. The current evidence on statin use and prostate cancer prevention: are we there yet? *Nat Rev Urol* (2017) 14(2):107–19. doi: 10.1038/nrurol.2016.199
- Liu B, Yi Z, Guan X, Zeng YX, Ma F. The relationship between statins and breast cancer prognosis varies by statin type and exposure time: a meta-analysis. *Breast Cancer Res Treat* (2017) 164(1):1–11. doi: 10.1007/s10549-017-4246-0
- Chen YA, Lin YJ, Lin CL, Lin HJ, Wu HS, Hsu HY, et al. Simvastatin Therapy for Drug Repositioning to Reduce the Risk of Prostate Cancer Mortality in Patients With Hyperlipidemia. *Front Pharmacol* (2018) 9:225. doi: 10.3389/fphar.2018.00225
- Borgquist S, Broberg P, Tojjar J, Olsson H. Statin use and breast cancer survival - a Swedish nationwide study. *BMC Cancer* (2019) 19(1):54. doi: 10.1186/s12885-018-5263-z
- Feng JL, Qin X. Does adherence to lipid-lowering medications improve cancer survival? A nationwide study of breast and colorectal cancer, and melanoma. *Br J Clin Pharmacol* (2020). doi: 10.1111/bcp.14573
- Poynter JN, Gruber SB, Higgins PD, Almog R, Bonner JD, Rennert HS, et al. Statins and the risk of colorectal cancer. *N Engl J Med* (2005) 352(21):2184–92. doi: 10.1056/NEJMoa043792
- Ibanez-Sanz G, Guino E, Pontes C, Quijada-Manuitt MA, de la Pena-Negro LC, Aragon M, et al. Statin use and the risk of colorectal cancer in a population-based electronic health records study. *Sci Rep* (2019) 9(1):13560. doi: 10.1038/s41598-019-49877-5
- Ehmsen S, Pedersen MH, Wang G, Terp MG, Arslanagic A, Hood BL, et al. Increased Cholesterol Biosynthesis Is a Key Characteristic of Breast Cancer Stem Cells Influencing Patient Outcome. *Cell Rep* (2019) 27(13):3927–38 e6. doi: 10.1016/j.celrep.2019.05.104

32. Zhong GC, Liu Y, Ye YY, Hao FB, Wang K, Gong JP. Meta-analysis of studies using statins as a reducer for primary liver cancer risk. *Sci Rep* (2016) 6:26256. doi: 10.1038/srep26256
33. Facciorusso A, Abd El Aziz MA, Singh S, Pusceddu S, Milione M, Giacomelli L, et al. Statin Use Decreases the Incidence of Hepatocellular Carcinoma: An Updated Meta-Analysis. *Cancers (Basel)* (2020) 12(4):874. doi: 10.3390/cancers12040874
34. Hong JY, Nam EM, Lee J, Park JO, Lee SC, Song SY, et al. Randomized double-blinded, placebo-controlled phase II trial of simvastatin and gemcitabine in advanced pancreatic cancer patients. *Cancer Chemother Pharmacol* (2014) 73(1):125–30. doi: 10.1007/s00280-013-2328-1
35. Goldman AR, Bitler BG, Schug Z, Conejo-Garcia JR, Zhang R, Speicher DW. The primary effect on the proteome of ARID1A-mutated ovarian clear cell carcinoma is downregulation of the mevalonate pathway at the post-transcriptional level. *Mol Cell Proteomics* (2016) 15(11):3348–60. doi: 10.1074/mcp.M116.062539
36. Kobayashi Y, Kashima H, Rahmanto YS, Banno K, Yu Y, Matoba Y, et al. Drug repositioning of mevalonate pathway inhibitors as antitumor agents for ovarian cancer. *Oncotarget* (2017) 8(42):72147–56. doi: 10.18632/oncotarget.20046
37. Alexandre L, Clark AB, Bhutta HY, Chan SS, Lewis MP, Hart AR. Association Between Statin Use After Diagnosis of Esophageal Cancer and Survival: A Population-Based Cohort Study. *Gastroenterology* (2016) 150(4):854–65 e1; quiz e16–7. doi: 10.1053/j.gastro.2015.12.039
38. Alexandre L, Clark AB, Bhutta HY, Holt S, Lewis MP, Hart AR. Statin use is associated with reduced risk of histologic subtypes of esophageal cancer: a nested case-control analysis. *Gastroenterology* (2014) 146(3):661–8. doi: 10.1053/j.gastro.2013.11.046
39. Seckl MJ, Ottensmeier CH, Cullen M, Schmid P, Ngai Y, Muthukumar D, et al. Multicenter, Phase III, Randomized, Double-Blind, Placebo-Controlled Trial of Pravastatin Added to First-Line Standard Chemotherapy in Small-Cell Lung Cancer (LUNGSTAR). *J Clin Oncol* (2017) 35(14):1506–14. doi: 10.1200/JCO.2016.69.7391
40. Pradelli D, Soranna D, Zamboni A, Catapano A, Mancini G, La Vecchia C, et al. Statins use and the risk of all and subtype hematological malignancies: a meta-analysis of observational studies. *Cancer Med* (2015) 4(5):770–80. doi: 10.1002/cam4.411
41. Warita K, Warita T, Beckwith CH, Schurdak ME, Vazquez A, Wells A, et al. Statin-induced mevalonate pathway inhibition attenuates the growth of mesenchymal-like cancer cells that lack functional E-cadherin mediated cell cohesion. *Sci Rep* (2014) 4:7593. doi: 10.1038/srep07593
42. Pandya AA, Mullen PJ, Goard CA, Ericson E, Sharma P, Kalkat M, et al. Genome-wide RNAi analysis reveals that simultaneous inhibition of specific mevalonate pathway genes potentiates tumor cell death. *Oncotarget* (2015) 6(29):26909–21. doi: 10.18632/oncotarget.4817
43. Edwards PA, Ericsson J. Sterols and isoprenoids: signaling molecules derived from the cholesterol biosynthetic pathway. *Annu Rev Biochem* (1999) 68:157–85. doi: 10.1146/annurev.biochem.68.1.157
44. Shimano H, Sato R. SREBP-regulated lipid metabolism: convergent physiology - divergent pathophysiology. *Nat Rev Endocrinol* (2017) 13(12):710–30. doi: 10.1038/nrendo.2017.91
45. Pietrocchi F, Galluzzi L, Bravo-San Pedro JM, Madeo F, Kroemer G. Acetyl coenzyme A: a central metabolite and second messenger. *Cell Metab* (2015) 21(6):805–21. doi: 10.1016/j.cmet.2015.05.014
46. Greenwood J, Steinman L, Zamvil SS. Statin therapy and autoimmune disease: from protein prenylation to immunomodulation. *Nat Rev Immunol* (2006) 6(5):358–70. doi: 10.1038/nri1839
47. Gruenbacher G, Thurnher M. Mevalonate Metabolism in Cancer Stemness and Trained Immunity. *Front Oncol* (2018) 8:394. doi: 10.3389/fonc.2018.00394
48. Bekkering S, Arts RJW, Novakovic B, Kourtzelis I, van der Heijden C, Li Y, et al. Metabolic Induction of Trained Immunity through the Mevalonate Pathway. *Cell* (2018) 172(1–2):135–46 e9. doi: 10.1016/j.cell.2017.11.025
49. Horton JD, Goldstein JL, Brown MS. SREBPs: activators of the complete program of cholesterol and fatty acid synthesis in the liver. *J Clin Invest* (2002) 109(9):1125–31. doi: 10.1172/JCI0215593
50. Luu W, Sharpe LJ, Capell-Hattam I, Glissen IC, Brown AJ. Oxysterols: Old Tale, New Twists. *Annu Rev Pharmacol Toxicol* (2016) 56:447–67. doi: 10.1146/annurev-pharmtox-010715-103233
51. Peet DJ, Turley SD, Ma W, Janowski BA, Lobaccaro JM, Hammer RE, et al. Cholesterol and bile acid metabolism are impaired in mice lacking the nuclear oxysterol receptor LXR alpha. *Cell* (1998) 93(5):693–704. doi: 10.1016/S0092-8674(00)81432-4
52. Sontag TJ, Reardon CA, Getz GS. ABC transporters: lipid transport and inflammation. *Curr Opin Lipidol* (2010) 21(2):159–60. doi: 10.1097/MOL.0b013e3283376910
53. Lechner GS, Avner R, Harats D, Roitelman J. Dislocation of HMG-CoA reductase and Insig-1, two polytopic endoplasmic reticulum proteins, en route to proteasomal degradation. *Mol Biol Cell* (2009) 20(14):3330–41. doi: 10.1091/mbc.e08-09-0953
54. Hinson DD, Chambliss KL, Toth MJ, Tanaka RD, Gibson KM. Post-translational regulation of mevalonate kinase by intermediates of the cholesterol and nonsterol isoprene biosynthetic pathways. *J Lipid Res* (1997) 38(11):2216–23. doi: 10.1016/S0022-2275(20)34935-X
55. Clarke PR, Hardie DG. Regulation of HMG-CoA reductase: identification of the site phosphorylated by the AMP-activated protein kinase in vitro and in intact rat liver. *EMBO J* (1990) 9(8):2439–46. doi: 10.1002/j.1460-2075.1990.tb07420.x
56. Warburg O. On respiratory impairment in cancer cells. *Science* (1956) 124(3215):269–70. doi: 10.1126/science.124.3215.267
57. Grunt TW. Interacting Cancer Machineries: Cell Signaling, Lipid Metabolism, and Epigenetics. *Trends Endocrinol Metab* (2018) 29(2):86–98. doi: 10.1016/j.tem.2017.11.003
58. Ramirez de Molina A, Gallego-Ortega D, Sarmentero J, Banez-Coronel M, Martin-Cantalejo Y, Lacal JC. Choline kinase is a novel oncogene that potentiates RhoA-induced carcinogenesis. *Cancer Res* (2005) 65(13):5647–53. doi: 10.1158/0008-5472.CAN-04-4416
59. Hirsch HA, Iliopoulos D, Joshi A, Zhang Y, Jaeger SA, Bulky M, et al. A transcriptional signature and common gene networks link cancer with lipid metabolism and diverse human diseases. *Cancer Cell* (2010) 17(4):348–61. doi: 10.1016/j.ccr.2010.01.022
60. Yang J, Wang L, Jia R. Role of de novo cholesterol synthesis enzymes in cancer. *J Cancer* (2020) 11(7):1761–7. doi: 10.7150/jca.38598
61. Nguyen VT, Barozzi I, Faronato M, Lombardo Y, Steel JH, Patel N, et al. Differential epigenetic reprogramming in response to specific endocrine therapies promotes cholesterol biosynthesis and cellular invasion. *Nat Commun* (2015) 6:10044. doi: 10.1038/ncomms10044
62. Silvente-Poirot S, Dalenc F, Poirot M. The Effects of Cholesterol-Derived Oncometabolites on Nuclear Receptor Function in Cancer. *Cancer Res* (2018) 78(17):4803–8. doi: 10.1158/0008-5472.CAN-18-1487
63. Hafizz A, Zin RRM, Aziz NHA, Kampan NC, Shafiee MN. Beyond lipid-lowering: role of statins in endometrial cancer. *Mol Biol Rep* (2020) 47(10):8199–207. doi: 10.1007/s11033-020-05760-5
64. Hodge RG, Ridley AJ. Regulating Rho GTPases and their regulators. *Nat Rev Mol Cell Biol* (2016) 17(8):496–510. doi: 10.1038/nrm.2016.67
65. Shackelford DB, Shaw RJ. The LKB1-AMPK pathway: metabolism and growth control in tumour suppression. *Nat Rev Cancer* (2009) 9(8):563–75. doi: 10.1038/nrc2676
66. Carling D. The AMP-activated protein kinase cascade—a unifying system for energy control. *Trends Biochem Sci* (2004) 29(1):18–24. doi: 10.1016/j.tibs.2003.11.005
67. Han F, Li CF, Cai Z, Zhang X, Jin G, Zhang WN, et al. The critical role of AMPK in driving Akt activation under stress, tumorigenesis and drug resistance. *Nat Commun* (2018) 9(1):4728. doi: 10.1038/s41467-018-07188-9
68. Nickels JJJ. New links between lipid accumulation and cancer progression. *J Biol Chem* (2018) 293(17):6635–6. doi: 10.1074/jbc.H118.002654
69. Zahra K, Dey T, Ashish, Mishra SP, Pandey U. Pyruvate Kinase M2 and Cancer: The Role of PKM2 in Promoting Tumorigenesis. *Front Oncol* (2020) 10:159. doi: 10.3389/fonc.2020.00159
70. Rodon J, Dienstmann R, Serra V, Tabernero J. Development of PI3K inhibitors: lessons learned from early clinical trials. *Nat Rev Clin Oncol* (2013) 10(3):143–53. doi: 10.1038/nrclinonc.2013.10
71. Song M, Bode AM, Dong Z, Lee MH. AKT as a Therapeutic Target for Cancer. *Cancer Res* (2019) 79(6):1019–31. doi: 10.1158/0008-5472.CAN-18-2738
72. Sorrentino G, Ruggeri N, Specchia V, Cordenonsi M, Mano M, Dupont S, et al. Metabolic control of YAP and TAZ by the mevalonate pathway. *Nat Cell Biol* (2014) 16(4):357–66. doi: 10.1038/ncb2936

73. Zhao Y, Yang X. The Hippo pathway in chemotherapeutic drug resistance. *Int J Cancer* (2015) 137(12):2767–73. doi: 10.1002/ijc.29293
74. Eaton S. Multiple roles for lipids in the Hedgehog signalling pathway. *Nat Rev Mol Cell Biol* (2008) 9(6):437–45. doi: 10.1038/nrm2414
75. Wu F, Zhang Y, Sun B, McMahon AP, Wang Y. Hedgehog Signaling: From Basic Biology to Cancer Therapy. *Cell Chem Biol* (2017) 24(3):252–80. doi: 10.1016/j.chembiol.2017.02.010
76. Cheng X, Li J, Guo D. SCAP/SREBPs are Central Players in Lipid Metabolism and Novel Metabolic Targets in Cancer Therapy. *Curr Top Med Chem* (2018) 18(6):484–93. doi: 10.2174/1568026618666180523104541
77. Cook CC, Kim A, Terao S, Gotoh A, Higuchi M. Consumption of oxygen: a mitochondrial-generated progression signal of advanced cancer. *Cell Death Dis* (2012) 3:e258. doi: 10.1038/cddis.2011.141
78. Yu H, Lee H, Herrmann A, Buettner R, Jove R. Revisiting STAT3 signalling in cancer: new and unexpected biological functions. *Nat Rev Cancer* (2014) 14(11):736–46. doi: 10.1038/nrc3818
79. Poli V, Camporeale A. STAT3-Mediated Metabolic Reprograming in Cellular Transformation and Implications for Drug Resistance. *Front Oncol* (2015) 5:121. doi: 10.3389/fonc.2015.00121
80. Huynh J, Chand A, Gough D, Ernst M. Therapeutically exploiting STAT3 activity in cancer - using tissue repair as a road map. *Nat Rev Cancer* (2019) 19(2):82–96. doi: 10.1038/s41568-018-0090-8
81. Li X, Wu JB, Li Q, Shigemura K, Chung LW, Huang WC. SREBP-2 promotes stem cell-like properties and metastasis by transcriptional activation of c-Myc in prostate cancer. *Oncotarget* (2016) 7(11):12869–84. doi: 10.18632/oncotarget.7331
82. Lin CY, Gustafsson JA. Targeting liver X receptors in cancer therapeutics. *Nat Rev Cancer* (2015) 15(4):216–24. doi: 10.1038/nrc3912
83. Kulkoyluoglu-Cotul E, Arca A, Madak-Erdogan Z. Crosstalk between Estrogen Signaling and Breast Cancer Metabolism. *Trends Endocrinol Metab* (2019) 30(1):25–38. doi: 10.1016/j.tem.2018.10.006
84. Wei W, Schwaib AG, Wang X, Chen S, Chu Q, Saghatelian A, et al. Ligand Activation of ERRalpha by Cholesterol Mediates Statin and Bisphosphonate Effects. *Cell Metab* (2016) 23(3):479–91. doi: 10.1016/j.cmet.2015.12.010
85. Casaburi I, Chimento A, De Luca A, Nocito M, Sculco S, Avena P, et al. Cholesterol as an Endogenous ERRalpha Agonist: A New Perspective to Cancer Treatment. *Front Endocrinol* (2018) 9:525. doi: 10.3389/fendo.2018.00525
86. Freed-Pastor WA, Mizuno H, Zhao X, Langerod A, Moon SH, Rodriguez-Barrueco R, et al. Mutant p53 disrupts mammary tissue architecture via the mevalonate pathway. *Cell* (2012) 148(1–2):244–58. doi: 10.1016/j.cell.2011.12.017
87. Bykov VJN, Eriksson SE, Bianchi J, Wiman KG. Targeting mutant p53 for efficient cancer therapy. *Nat Rev Cancer* (2018) 18(2):89–102. doi: 10.1038/nrc.2017.109
88. Kitajima S, Yoshida A, Kohno S, Li F, Suzuki S, Nagatani N, et al. The RB-IL-6 axis controls self-renewal and endocrine therapy resistance by fine-tuning mitochondrial activity. *Oncogene* (2017) 36(36):5145–57. doi: 10.1038/onc.2017.124
89. Shamma A, Takegami Y, Miki T, Kitajima S, Noda M, Obara T, et al. Rb Regulates DNA damage response and cellular senescence through E2F-dependent suppression of N-ras isoprenylation. *Cancer Cell* (2009) 15(4):255–69. doi: 10.1016/j.ccr.2009.03.001
90. Wu Q, Ba-Alawi W, Deblois G, Cruickshank J, Duan S, Lima-Fernandes E, et al. GLUT1 inhibition blocks growth of RB1-positive triple negative breast cancer. *Nat Commun* (2020) 11(1):4205. doi: 10.1038/s41467-020-18020-8
91. Siperstein MD. Cholesterol and cancer. *Trans Am Clin Climatol Assoc* (1970) 81:107–18.
92. Larson RA, Yachnin S. Mevalonic acid induces DNA synthesis in chronic lymphocytic leukemia cells. *Blood* (1984) 64(1):257–62. doi: 10.1182/blood.V64.1.257.bloodjournal641257
93. Bjarnadottir O, Feldt M, Inasu M, Bendahl PO, Elebro K, Kimbung S, et al. Statin use, HMGR expression, and breast cancer survival - The Malmo Diet and Cancer Study. *Sci Rep* (2020) 10(1):558. doi: 10.1038/s41598-019-57323-9
94. Ashida S, Kawada C, Inoue K. Stromal regulation of prostate cancer cell growth by mevalonate pathway enzymes HMGCS1 and HMGR. *Oncol Lett* (2017) 14(6):6533–42. doi: 10.3892/ol.2017.7025
95. Hu J, La Vecchia C, de Groh M, Negri E, Morrison H, Mery L. Dietary cholesterol intake and cancer. *Ann Oncol* (2012) 23(2):491–500. doi: 10.1093/annonc/mdr155
96. Sezgin E, Levental I, Mayor S, Eggeling C. The mystery of membrane organization: composition, regulation and roles of lipid rafts. *Nat Rev Mol Cell Biol* (2017) 18(6):361–74. doi: 10.1038/nrm.2017.16
97. Zhao L, Zhou S, Gustafsson JA. Nuclear Receptors: Recent Drug Discovery for Cancer Therapies. *Endocr Rev* (2019) 40(5):1207–49. doi: 10.1210/er.2018-00222
98. Bovenga F, Sabba C, Moschetta A. Uncoupling nuclear receptor LXR and cholesterol metabolism in cancer. *Cell Metab* (2015) 21(4):517–26. doi: 10.1016/j.cmet.2015.03.002
99. Locke JA, Guns ES, Lubik AA, Adomat HH, Hendy SC, Wood CA, et al. Androgen levels increase by intratumoral de novo steroidogenesis during progression of castration-resistant prostate cancer. *Cancer Res* (2008) 68(15):6407–15. doi: 10.1158/0008-5472.CAN-07-5997
100. Jung H, Yoon SR, Lim J, Cho HJ, Lee HG. Dysregulation of Rho GTPases in human cancers. *Cancers (Basel)* (2020) 12(5):1179. doi: 10.3390/cancers12051179
101. Berndt N, Hamilton AD, Sefti SM. Targeting protein prenylation for cancer therapy. *Nat Rev Cancer* (2011) 11(11):775–91. doi: 10.1038/nrc3151
102. Cox AD, Fesik SW, Kimmelman AC, Luo J, Der CJ. Drugging the undruggable RAS: Mission possible? *Nat Rev Drug Discov* (2014) 13(11):828–51. doi: 10.1038/nrd4389
103. Ernster L, Dallner G. Biochemical, physiological and medical aspects of ubiquinone function. *Biochim Biophys Acta* (1995) 1271(1):195–204. doi: 10.1016/0925-4439(95)00028-3
104. Pascual G, Avgustinova A, Mejetta S, Martin M, Castellanos A, Attolini CS, et al. Targeting metastasis-initiating cells through the fatty acid receptor CD36. *Nature* (2017) 541(7635):41–5. doi: 10.1038/nature20791
105. Horton BL, Spranger S. CD36 - the Achilles' heel of Treg cells. *Nat Immunol* (2020) 21(3):251–3. doi: 10.1038/s41590-020-0601-0
106. Rozovski U, Harris DM, Li P, Liu Z, Jain P, Ferrajoli A, et al. STAT3-activated CD36 facilitates fatty acid uptake in chronic lymphocytic leukemia cells. *Oncotarget* (2018) 9(30):21268–80. doi: 10.18632/oncotarget.25066
107. Li Y, Xu S, Mihaylova MM, Zheng B, Hou X, Jiang B, et al. AMPK phosphorylates and inhibits SREBP activity to attenuate hepatic steatosis and atherosclerosis in diet-induced insulin-resistant mice. *Cell Metab* (2011) 13(4):376–88. doi: 10.1016/j.cmet.2011.03.009
108. Collins SP, Reoma JL, Gamm DM, Uhler MD. LKB1, a novel serine/threonine protein kinase and potential tumour suppressor, is phosphorylated by cAMP-dependent protein kinase (PKA) and prenylated in vivo. *Biochem J* (2000) 345 Pt 3:673–80. doi: 10.1042/bj3450673
109. Alessi DR, Sakamoto K, Bayascas JR. LKB1-dependent signaling pathways. *Annu Rev Biochem* (2006) 75:137–63. doi: 10.1146/annurev.biochem.75.103004.142702
110. Rao S, Porter DC, Chen X, Herliczek T, Lowe M, Keyomarsi K. Lovastatin-mediated G1 arrest is through inhibition of the proteasome, independent of hydroxymethyl glutaryl-CoA reductase. *Proc Natl Acad Sci U S A* (1999) 96(14):7797–802. doi: 10.1073/pnas.96.14.7797
111. Motoshima H, Goldstein BJ, Igata M, Araki E. AMPK and cell proliferation-AMPK as a therapeutic target for atherosclerosis and cancer. *J Physiol* (2006) 574(Pt 1):63–71. doi: 10.1113/jphysiol.2006.108324
112. Kochuparambil ST, Al-Husein B, Goc A, Soliman S, Somanath PR. Anticancer efficacy of simvastatin on prostate cancer cells and tumor xenografts is associated with inhibition of Akt and reduced prostate-specific antigen expression. *J Pharmacol Exp Ther* (2011) 336(2):496–505. doi: 10.1124/jpet.110.174870
113. Wang ST, Ho HJ, Lin JT, Shieh JJ, Wu CY. Simvastatin-induced cell cycle arrest through inhibition of STAT3/SKP2 axis and activation of AMPK to promote p27 and p21 accumulation in hepatocellular carcinoma cells. *Cell Death Dis* (2017) 8(2):e2626. doi: 10.1038/cddis.2016.472
114. Inoki K, Li Y, Zhu T, Wu J, Guan KL. TSC2 is phosphorylated and inhibited by Akt and suppresses mTOR signalling. *Nat Cell Biol* (2002) 4(9):648–57. doi: 10.1038/ncb839
115. Inoki K, Li Y, Xu T, Guan KL. Rheb GTPase is a direct target of TSC2 GAP activity and regulates mTOR signaling. *Genes Dev* (2003) 17(15):1829–34. doi: 10.1101/gad.1110003



116. Stambolic V, Suzuki A, de la Pompa JL, Brothers GM, Mirtsos C, Sasaki T, et al. Negative regulation of PKB/Akt-dependent cell survival by the tumor suppressor PTEN. *Cell* (1998) 95(1):29–39. doi: 10.1016/S0092-8674(00)81780-8
117. Milella M, Falcone I, Conciatori F, Matteoni S, Sacconi A, De Luca T, et al. PTEN status is a crucial determinant of the functional outcome of combined MEK and mTOR inhibition in cancer. *Sci Rep* (2017) 7:43013. doi: 10.1038/srep43013
118. Gris-Oliver A, Palafox M, Monserrat L, Braso-Maristany F, Odena A, Sanchez-Guix M, et al. Genetic alterations in the PI3K/AKT pathway and baseline AKT activity define AKT inhibitor sensitivity in breast cancer patient-derived xenografts. *Clin Cancer Res* (2020) 26(14):3720–31. doi: 10.1158/1078-0432.CCR-19-3324
119. Shimobayashi M, Hall MN. Making new contacts: the mTOR network in metabolism and signalling crosstalk. *Nat Rev Mol Cell Biol* (2014) 15(3):155–62. doi: 10.1038/nrm3757
120. Ricoult SJ, Yecies JL, Ben-Sahra I, Manning BD. Oncogenic PI3K and K-Ras stimulate de novo lipid synthesis through mTORC1 and SREBP. *Oncogene* (2016) 35(10):1250–60. doi: 10.1038/ncr.2015.179
121. Lee G, Zheng Y, Cho S, Jang C, England C, Dempsey JM, et al. Post-transcriptional Regulation of De Novo Lipogenesis by mTORC1-S6K1-SRPK2 Signaling. *Cell* (2017) 171(7):1545–58 e18. doi: 10.1016/j.cell.2017.10.037
122. Siess KM, Leonard TA. Lipid-dependent Akt-ivity: where, when, and how. *Biochem Soc Trans* (2019) 47(3):897–908. doi: 10.1042/BST20190013
123. Bacciera T, Azzolin L, Cordenonsi M, Piccolo S. Mechanobiology of YAP and TAZ in physiology and disease. *Nat Rev Mol Cell Biol* (2017) 18(12):758–70. doi: 10.1038/nrm.2017.87
124. Zhao B, Tumaneng K, Guan KL. The Hippo pathway in organ size control, tissue regeneration and stem cell self-renewal. *Nat Cell Biol* (2011) 13(8):877–83. doi: 10.1038/ncb2303
125. Semenza GL. Targeting HIF-1 for cancer therapy. *Nat Rev Cancer* (2003) 3(10):721–32. doi: 10.1038/nrc1187
126. Pugh CW, Ratcliffe PJ. New horizons in hypoxia signaling pathways. *Exp Cell Res* (2017) 356(2):116–21. doi: 10.1016/j.yexcr.2017.03.008
127. Bersten DC, Sullivan AE, Peet DJ, Whitelaw ML. bHLH-PAS proteins in cancer. *Nat Rev Cancer* (2013) 13(12):827–41. doi: 10.1038/nrc3621
128. Koyasu S, Kobayashi M, Goto Y, Hiraoka M, Harada H. Regulatory mechanisms of hypoxia-inducible factor 1 activity: Two decades of knowledge. *Cancer Sci* (2018) 109(3):560–71. doi: 10.1111/cas.13483
129. Pallottini V, Guantario B, Martini C, Totta P, Filippi I, Carraro F, et al. Regulation of HMG-CoA reductase expression by hypoxia. *J Cell Biochem* (2008) 104(3):701–9. doi: 10.1002/jcb.21757
130. Thompson JM, Alvarez A, Singha MK, Pavesic MW, Nguyen QH, Nelson LJ, et al. Targeting the Mevalonate Pathway Suppresses VHL-Deficient CC-RCC through an HIF-Dependent Mechanism. *Mol Cancer Ther* (2018) 17(8):1781–92. doi: 10.1158/1535-7163.MCT-17-1076
131. Hwang S, Nguyen AD, Jo Y, Engelking LJ, Brugarolas J, DeBose-Boyd RA. Hypoxia-inducible factor 1alpha activates insulin-induced gene 2 (Insig-2) transcription for degradation of 3-hydroxy-3-methylglutaryl (HMG)-CoA reductase in the liver. *J Biol Chem* (2017) 292(22):9382–93. doi: 10.1074/jbc.M117.788562
132. Jeong JH, Yum KS, Chang JY, Kim M, Ahn JY, Kim S, et al. Dose-specific effect of simvastatin on hypoxia-induced HIF-1alpha and BACE expression in Alzheimer's disease cybrid cells. *BMC Neurol* (2015) 15:127. doi: 10.1186/s12883-015-0390-5
133. Hisada T, Ayaori M, Ohru N, Nakashima H, Nakaya K, Uto-Kondo H, et al. Statin inhibits hypoxia-induced endothelin-1 via accelerated degradation of HIF-1alpha in vascular smooth muscle cells. *Cardiovasc Res* (2012) 95(2):251–9. doi: 10.1093/cvr/cvs110
134. Aznar S, Valeron PF, del Rincon SV, Perez LF, Perona R, Lacal JC. Simultaneous tyrosine and serine phosphorylation of STAT3 transcription factor is involved in Rho A GTPase oncogenic transformation. *Mol Biol Cell* (2001) 12(10):3282–94. doi: 10.1091/mbc.12.10.3282
135. Raptis L, Arulanandam R, Geletu M, Turkson J. The R(h)oads to Stat3: Stat3 activation by the Rho GTPases. *Exp Cell Res* (2011) 317(13):1787–95. doi: 10.1016/j.yexcr.2011.05.008
136. Jiang S, Zhang LF, Zhang HW, Hu S, Lu MH, Liang S, et al. A novel miR-155/miR-143 cascade controls glycolysis by regulating hexokinase 2 in breast cancer cells. *EMBO J* (2012) 31(8):1985–98. doi: 10.1038/emboj.2012.45
137. Demaria M, Poli V. PKM2, STAT3 and HIF-1alpha: The Warburg's vicious circle. *JAKSTAT* (2012) 1(3):194–6. doi: 10.4161/jkst.20662
138. Yamasaki M, Nomura T, Sato F, Mimata H. Chronic hypoxia induces androgen-independent and invasive behavior in LNCaP human prostate cancer cells. *Urol Oncol* (2013) 31(7):1124–31. doi: 10.1016/j.urolonc.2011.12.007
139. Wegrzyn J, Potla R, Chwae YJ, Sepuri NB, Zhang Q, Koeck T, et al. Function of mitochondrial Stat3 in cellular respiration. *Science* (2009) 323(5915):793–7. doi: 10.1126/science.1164551
140. Szczepanek K, Chen Q, Derecka M, Salloum FN, Zhang Q, Szelag M, et al. Mitochondrial-targeted Signal transducer and activator of transcription 3 (STAT3) protects against ischemia-induced changes in the electron transport chain and the generation of reactive oxygen species. *J Biol Chem* (2011) 286(34):29610–20. doi: 10.1074/jbc.M111.226209
141. Zhang Q, Raju V, Yakovlev VA, Yacoub A, Szczepanek K, Meier J, et al. Mitochondrial localized Stat3 promotes breast cancer growth via phosphorylation of serine 727. *J Biol Chem* (2013) 288(43):31280–8. doi: 10.1074/jbc.M113.505057
142. Zhou J, Wulffkuhle J, Zhang H, Gu P, Yang Y, Deng J, et al. Activation of the PTEN/mTOR/STAT3 pathway in breast cancer stem-like cells is required for viability and maintenance. *Proc Natl Acad Sci U S A* (2007) 104(41):16158–63. doi: 10.1073/pnas.0702596104
143. Yang F, Zhang W, Li D, Zhan Q. Gadd45a suppresses tumor angiogenesis via inhibition of the mTOR/STAT3 protein pathway. *J Biol Chem* (2013) 288(9):6552–60. doi: 10.1074/jbc.M112.418335
144. Arulanandam R, Vultur A, Cao J, Carefoot E, Elliott BE, Truesdell PF, et al. Cadherin-cadherin engagement promotes cell survival via Rac1/Cdc42 and signal transducer and activator of transcription-3. *Mol Cancer Res* (2009) 7(8):1310–27. doi: 10.1158/1541-7786.MCR-08-0469
145. Faruqi TR, Gomez D, Bustelo XR, Bar-Sagi D, Reich NC. Rac1 mediates STAT3 activation by autocrine IL-6. *Proc Natl Acad Sci U S A* (2001) 98(16):9014–9. doi: 10.1073/pnas.161281298
146. Simon AR, Vikis HG, Stewart S, Fanburg BL, Cochran BH, Guan KL. Regulation of STAT3 by direct binding to the Rac1 GTPase. *Science* (2000) 290(5489):144–7. doi: 10.1126/science.290.5489.144
147. Tonozyuka Y, Minoshima Y, Bao YC, Moon Y, Tsubono Y, Hatori T, et al. A GTPase-activating protein binds STAT3 and is required for IL-6-induced STAT3 activation and for differentiation of a leukemic cell line. *Blood* (2004) 104(12):3550–7. doi: 10.1182/blood-2004-03-1066
148. Kawashima T, Bao YC, Minoshima Y, Nomura Y, Hatori T, Hori T, et al. A Rac GTPase-activating protein, MgcRacGAP, is a nuclear localizing signal-containing nuclear chaperone in the activation of STAT transcription factors. *Mol Cell Biol* (2009) 29(7):1796–813. doi: 10.1128/MCB.01423-08
149. van Adrichem AJ, Wennerberg K. MgcRacGAP inhibition stimulates JAK-dependent STAT3 activity. *FEBS Lett* (2015) 589(24 Pt B):3859–65. doi: 10.1016/j.febslet.2015.11.013
150. Owen KL, Brockwell NK, Parker BS. JAK-STAT Signaling: A Double-Edged Sword of Immune Regulation and Cancer Progression. *Cancers (Basel)* (2019) 11(12):2002–27. doi: 10.3390/cancers11122002
151. Krause DS, Scadden DT. A hostel for the hostile: the bone marrow niche in hematologic neoplasms. *Haematologica* (2015) 100(11):1376–87. doi: 10.3324/haematol.2014.113852
152. Cartledge Wolf DM, Langhans SA. Moving Myeloid Leukemia Drug Discovery Into the Third Dimension. *Front Pediatr* (2019) 7:314. doi: 10.3389/fped.2019.00314
153. Irey EA, Lassiter CM, Brady NJ, Chuntova P, Wang Y, Knutson TP, et al. JAK/STAT inhibition in macrophages promotes therapeutic resistance by inducing expression of protumorigenic factors. *Proc Natl Acad Sci U S A* (2019) 116(25):12442–51. doi: 10.1073/pnas.1816410116
154. Petty AJ, Yang Y. Tumor-Associated Macrophages in Hematologic Malignancies: New Insights and Targeted Therapies. *Cells* (2019) 8(12):1526–40. doi: 10.3390/cells8121526
155. Teodorescu P, Pasca S, Dima D, Tomuleasa C, Ghiaur G. Targeting the Microenvironment in MDS: The Final Frontier. *Front Pharmacol* (2020) 11:1044. doi: 10.3389/fphar.2020.01044
156. Genard G, Lucas S, Michiels C. Reprogramming of Tumor-Associated Macrophages with Anticancer Therapies: Radiotherapy versus Chemo- and Immunotherapies. *Front Immunol* (2017) 8:828. doi: 10.3389/fimmu.2017.00828



157. Tabraue C, Lara PC, De Mirecki-Garrido M, De La Rosa JV, Lopez-Blanco F, Fernandez-Perez L, et al. LXR Signaling Regulates Macrophage Survival and Inflammation in Response to Ionizing Radiation. *Int J Radiat Oncol Biol Phys* (2019) 104(4):913–23. doi: 10.1016/j.ijrobp.2019.03.028
158. Al Dujaily E, Baena J, Das M, Sereno M, Smith C, Kamata T, et al. Reduced Protumorigenic Tumor-Associated Macrophages With Statin Use in Premalignant Human Lung Adenocarcinoma. *JNCI Cancer Spectr* (2020) 4(2):pkz101. doi: 10.1093/jncics/pkz101
159. Comito G, Pons Segura C, Taddei ML, Lanciotti M, Serni S, Morandi A, et al. Zoledronic acid impairs stromal reactivity by inhibiting M2-macrophages polarization and prostate cancer-associated fibroblasts. *Oncotarget* (2017) 8(1):118–32. doi: 10.18632/oncotarget.9497
160. Coscia M, Quaglini E, Iezzi M, Curcio C, Pantaleoni F, Riganti C, et al. Zoledronic acid repolarizes tumour-associated macrophages and inhibits mammary carcinogenesis by targeting the mevalonate pathway. *J Cell Mol Med* (2010) 14(12):2803–15. doi: 10.1111/j.1582-4934.2009.00926.x
161. Gruenbacher G, Thurnher M. Mevalonate metabolism governs cancer immune surveillance. *Oncoimmunology* (2017) 6(10):e1342917. doi: 10.1080/2162402X.2017.1342917
162. Baek AE, Yu YA, He S, Wardell SE, Chang CY, Kwon S, et al. The cholesterol metabolite 27 hydroxycholesterol facilitates breast cancer metastasis through its actions on immune cells. *Nat Commun* (2017) 8(1):864. doi: 10.1038/s41467-017-00910-z
163. Kopecka J, Godel M, Riganti C. Cholesterol metabolism: At the cross road between cancer cells and immune environment. *Int J Biochem Cell Biol* (2020) 129:105876. doi: 10.1016/j.biocel.2020.105876
164. Mok EHK, Lee TKW. The Pivotal Role of the Dysregulation of Cholesterol Homeostasis in Cancer: Implications for Therapeutic Targets. *Cancers (Basel)* (2020) 12(6):1410–31. doi: 10.3390/cancers12061410
165. Yeh E, Cunningham M, Arnold H, Chasse D, Monteith T, Ivaldi G, et al. A signalling pathway controlling c-Myc degradation that impacts oncogenic transformation of human cells. *Nat Cell Biol* (2004) 6(4):308–18. doi: 10.1038/ncb1110
166. Adhikary S, Eilers M. Transcriptional regulation and transformation by Myc proteins. *Nat Rev Mol Cell Biol* (2005) 6(8):635–45. doi: 10.1038/nrm1703
167. Stine ZE, Walton ZE, Altman BJ, Hsieh AL, Dang CV. MYC, Metabolism, and Cancer. *Cancer Discov* (2015) 5(10):1024–39. doi: 10.1158/2159-8290.CD-15-0507
168. Cao Z, Fan-Minogue H, Bellovin DI, Yevtodiyenko A, Arzeno J, Yang Q, et al. MYC phosphorylation, activation, and tumorigenic potential in hepatocellular carcinoma are regulated by HMG-CoA reductase. *Cancer Res* (2011) 71(6):2286–97. doi: 10.1158/0008-5472.CAN-10-3367
169. Bhatia K, Huppi K, Spangler G, Siwarski D, Iyer R, Magrath I. Point mutations in the c-Myc transactivation domain are common in Burkitt's lymphoma and mouse plasmacytomas. *Nat Genet* (1993) 5(1):56–61. doi: 10.1038/ng0993-56
170. Dang CV. MYC on the path to cancer. *Cell* (2012) 149(1):22–35. doi: 10.1016/j.cell.2012.03.003
171. Wu Y, Chen K, Liu X, Huang L, Zhao D, Li L, et al. Srebp-1 Interacts with c-Myc to Enhance Somatic Cell Reprogramming. *Stem Cells* (2016) 34(1):83–92. doi: 10.1002/stem.2209
172. Hofmann JW, Zhao X, De Cecco M, Peterson AL, Pagliaroli L, Manivannan J, et al. Reduced expression of MYC increases longevity and enhances healthspan. *Cell* (2015) 160(3):477–88. doi: 10.1016/j.cell.2014.12.016
173. Kikuchi H, Pino MS, Zeng M, Shirasawa S, Chung DC. Oncogenic KRAS and BRAF differentially regulate hypoxia-inducible factor-1 $\alpha$  and -2 $\alpha$  in colon cancer. *Cancer Res* (2009) 69(21):8499–506. doi: 10.1158/0008-5472.CAN-09-2213
174. Sears R, Leone G, DeGregori J, Nevins JR. Ras enhances Myc protein stability. *Mol Cell* (1999) 3(2):169–79. doi: 10.1016/S1097-2765(00)80308-1
175. Giguere V. Transcriptional control of energy homeostasis by the estrogen-related receptors. *Endocr Rev* (2008) 29(6):677–96. doi: 10.1210/er.2008-0017
176. Wang C, Li P, Xuan J, Zhu C, Liu J, Shan L, et al. Cholesterol enhances colorectal cancer progression via ROS elevation and MAPK signaling pathway activation. *Cell Physiol Biochem* (2017) 42(2):729–42. doi: 10.1159/000477890
177. Gutierrez-Pajares JL, Ben Hassen C, Chevalier S, Frank PG. SR-BI: linking cholesterol and lipoprotein metabolism with breast and prostate cancer. *Front Pharmacol* (2016) 7:338. doi: 10.3389/fphar.2016.00338
178. Mantovani A, Marchesi F, Malesci A, Laghi L, Allavena P. Tumour-associated macrophages as treatment targets in oncology. *Nat Rev Clin Oncol* (2017) 14(7):399–416. doi: 10.1038/nrclinonc.2016.217
179. Gritsman K, Yuzugullu H, Von T, Yan H, Clayton L, Fritsch C, et al. Hematopoiesis and RAS-driven myeloid leukemia differentially require PI3K isoform p110 $\alpha$ . *J Clin Invest* (2014) 124(4):1794–809. doi: 10.1172/JCI69927
180. Lucken-Ardjomande S, Montessuit S, Martinou JC. Bax activation and stress-induced apoptosis delayed by the accumulation of cholesterol in mitochondrial membranes. *Cell Death Differ* (2008) 15(3):484–93. doi: 10.1038/sj.cdd.4402280
181. Montero J, Morales A, Llacuna L, Lluis JM, Terrones O, Basanez G, et al. Mitochondrial cholesterol contributes to chemotherapy resistance in hepatocellular carcinoma. *Cancer Res* (2008) 68(13):5246–56. doi: 10.1158/0008-5472.CAN-07-6161
182. Garcia-Ruiz C, de la Rosa LC, Ribas V, Fernandez-Checa JC. Mitochondrial cholesterol and cancer. *Semin Cancer Biol* (2020). doi: 10.1016/j.semcancer.2020.07.014
183. Hwang KE, Kwon SJ, Kim YS, Park DS, Kim BR, Yoon KH, et al. Effect of simvastatin on the resistance to EGFR tyrosine kinase inhibitors in a non-small cell lung cancer with the T790M mutation of EGFR. *Exp Cell Res* (2014) 323(2):288–96. doi: 10.1016/j.yexcr.2014.02.026
184. Lee J, Hong YS, Hong JY, Han SW, Kim TW, Kang HJ, et al. Effect of simvastatin plus cetuximab/irinotecan for KRAS mutant colorectal cancer and predictive value of the RAS signature for treatment response to cetuximab. *Invest New Drugs* (2014) 32(3):535–41. doi: 10.1007/s10637-014-0065-x
185. Manu KA, Shanmugam MK, Li F, Chen L, Siveen KS, Ahn KS, et al. Simvastatin sensitizes human gastric cancer xenograft in nude mice to capecitabine by suppressing nuclear factor-kappa B-regulated gene products. *J Mol Med* (2014) 92(3):267–76. doi: 10.1007/s00109-013-1095-0
186. Jeong GH, Lee KH, Kim JY, Eisenhut M, Kronbichler A, van der Vliet HJ, et al. Effect of statin on cancer incidence: an umbrella systematic review and meta-analysis. *J Clin Med* (2019) 8(6):819. doi: 10.3390/jcm8060819
187. Garwood ER, Kumar AS, Baehner FL, Moore DH, Au A, Hylton N, et al. Fluvastatin reduces proliferation and increases apoptosis in women with high grade breast cancer. *Breast Cancer Res Treat* (2010) 119(1):137–44. doi: 10.1007/s10549-009-0507-x
188. Feldt M, Bjarnadottir O, Kimbung S, Jirstrom K, Bendahl PO, Veerla S, et al. Statin-induced anti-proliferative effects via cyclin D1 and p27 in a window-of-opportunity breast cancer trial. *J Transl Med* (2015) 13:133. doi: 10.1186/s12967-015-0486-0
189. Arun BK, Gong Y, Liu D, Litton JK, Gutierrez-Barrera AM, Jack Lee J, et al. Phase I biomarker modulation study of atorvastatin in women at increased risk for breast cancer. *Breast Cancer Res Treat* (2016) 158(1):67–77. doi: 10.1007/s10549-016-3849-1
190. Schmidmaier R, Baumann P, Bumeder I, Meinhardt G, Straka C, Emmerich B. First clinical experience with simvastatin to overcome drug resistance in refractory multiple myeloma. *Eur J Haematol* (2007) 79(3):240–3. doi: 10.1111/j.1600-0609.2007.00902.x
191. Sondergaard TE, Pedersen PT, Andersen TL, Soe K, Lund T, Ostergaard B, et al. A phase II clinical trial does not show that high dose simvastatin has beneficial effect on markers of bone turnover in multiple myeloma. *Hematol Oncol* (2009) 27(1):17–22. doi: 10.1002/hon.869
192. Kim ST, Kang JH, Lee J, Park SH, Park JO, Park YS, et al. Simvastatin plus capecitabine-cisplatin versus placebo plus capecitabine-cisplatin in patients with previously untreated advanced gastric cancer: a double-blind randomised phase 3 study. *Eur J Cancer* (2014) 50(16):2822–30. doi: 10.1016/j.ejca.2014.08.005
193. Graf H, Jungst C, Straub G, Dogan S, Hoffmann RT, Jakobs T, et al. Chemoembolization combined with pravastatin improves survival in patients with hepatocellular carcinoma. *Digestion* (2008) 78(1):34–8. doi: 10.1159/000156702

194. Yi X, Jia W, Jin Y, Zhen S. Statin use is associated with reduced risk of haematological malignancies: evidence from a meta-analysis. *PLoS One* (2014) 9(1):e87019. doi: 10.1371/journal.pone.0087019
195. Ahern TP, Pedersen L, Tarp M, Cronin-Fenton DP, Garne JP, Silliman RA, et al. Statin prescriptions and breast cancer recurrence risk: a Danish nationwide prospective cohort study. *J Natl Cancer Inst* (2011) 103(19):1461–8. doi: 10.1093/jnci/djr291
196. Boudreau DM, Yu O, Chubak J, Wirtz HS, Bowles EJ, Fujii M, et al. Comparative safety of cardiovascular medication use and breast cancer outcomes among women with early stage breast cancer. *Breast Cancer Res Treat* (2014) 144(2):405–16. doi: 10.1007/s10549-014-2870-5
197. Goard CA, Chan-Seng-Yue M, Mullen PJ, Quiroga AD, Wasylshen AR, Clendening JW, et al. Identifying molecular features that distinguish fluvastatin-sensitive breast tumor cells. *Breast Cancer Res Treat* (2014) 143(2):301–12. doi: 10.1007/s10549-013-2800-y
198. Shachaf CM, Perez OD, Youssef S, Fan AC, Elchuri S, Goldstein MJ, et al. Inhibition of HMGCoA reductase by atorvastatin prevents and reverses MYC-induced lymphomagenesis. *Blood* (2007) 110(7):2674–84. doi: 10.1182/blood-2006-09-048033
199. Wong WW, Clendening JW, Martirosyan A, Boutros PC, Bros C, Khosravi F, et al. Determinants of sensitivity to lovastatin-induced apoptosis in multiple myeloma. *Mol Cancer Ther* (2007) 6(6):1886–97. doi: 10.1158/1535-7163.MCT-06-0745
200. Clendening JW, Pandya A, Li Z, Boutros PC, Martirosyan A, Lehner R, et al. Exploiting the mevalonate pathway to distinguish statin-sensitive multiple myeloma. *Blood* (2010) 115(23):4787–97. doi: 10.1182/blood-2009-07-230508
201. Gobel A, Breining D, Rauner M, Hofbauer LC, Rachner TD. Induction of 3-hydroxy-3-methylglutaryl-CoA reductase mediates statin resistance in breast cancer cells. *Cell Death Dis* (2019) 10(2):91. doi: 10.1038/s41419-019-1322-x
202. Banker DE, Mayer SJ, Li HY, Willman CL, Appelbaum FR, Zager RA. Cholesterol synthesis and import contribute to protective cholesterol increments in acute myeloid leukemia cells. *Blood* (2004) 104(6):1816–24. doi: 10.1182/blood-2004-01-0395
203. Li HY, Appelbaum FR, Willman CL, Zager RA, Banker DE. Cholesterol-modulating agents kill acute myeloid leukemia cells and sensitize them to therapeutics by blocking adaptive cholesterol responses. *Blood* (2003) 101(9):3628–34. doi: 10.1182/blood-2002-07-2283
204. Xue L, Qi H, Zhang H, Ding L, Huang Q, Zhao D, et al. Targeting SREBP-2-regulated mevalonate metabolism for cancer therapy. *Front Oncol* (2020) 10:1510. [Review]. doi: 10.3389/fonc.2020.01510
205. Ho YK, Smith RG, Brown MS, Goldstein JL. Low-density lipoprotein (LDL) receptor activity in human acute myelogenous leukemia cells. *Blood* (1978) 52(6):1099–114. doi: 10.1182/blood.V52.6.1099.1099
206. Guillaumond F, Bidaut G, Ouassii M, Servais S, Gouirand V, Olivares O, et al. Cholesterol uptake disruption, in association with chemotherapy, is a promising combined metabolic therapy for pancreatic adenocarcinoma. *Proc Natl Acad Sci U S A* (2015) 112(8):2473–8. doi: 10.1073/pnas.1421601112
207. Gobel A, Rauner M, Hofbauer LC, Rachner TD. Cholesterol and beyond - The role of the mevalonate pathway in cancer biology. *Biochim Biophys Acta Rev Cancer* (2020) 1873(2):188351. doi: 10.1016/j.bbcan.2020.188351
208. Longo J, Mullen PJ, Yu R, van Leeuwen JE, Masoomian M, Woon DTS, et al. An actionable sterol-regulated feedback loop modulates statin sensitivity in prostate cancer. *Mol Metab* (2019) 25:119–30. doi: 10.1016/j.molmet.2019.04.003
209. Li X, Chen YT, Hu P, Huang WC. Fatostatin displays high antitumor activity in prostate cancer by blocking SREBP-regulated metabolic pathways and androgen receptor signaling. *Mol Cancer Ther* (2014) 13(4):855–66. doi: 10.1158/1535-7163.MCT-13-0797
210. Oh B, Kim TY, Min HJ, Kim M, Kang MS, Huh JY, et al. Synergistic killing effect of imatinib and simvastatin on imatinib-resistant chronic myelogenous leukemia cells. *Anticancer Drugs* (2013) 24(1):20–31. doi: 10.1097/CAD.0b013e32835a0fbdb
211. Moon H, Hill MM, Roberts MJ, Gardiner RA, Brown AJ. Statins: protectors or pretenders in prostate cancer? *Trends Endocrinol Metab* (2014) 25(4):188–96. doi: 10.1016/j.tem.2013.12.007
212. Dirks AJ, Jones KM. Statin-induced apoptosis and skeletal myopathy. *Am J Physiol Cell Physiol* (2006) 291(6):C1208. doi: 10.1152/ajpcell.00226.2006
213. Dimitroulakos J, Nohynek D, Backway KL, Hedley DW, Yeger H, Freedman MH, et al. Increased sensitivity of acute myeloid leukemias to lovastatin-induced apoptosis: A potential therapeutic approach. *Blood* (1999) 93(4):1308–18. doi: 10.1182/blood.V93.4.1308.404k08\_1308\_1318
214. Wong WW, Dimitroulakos J, Minden MD, Penn LZ. HMG-CoA reductase inhibitors and the malignant cell: the statin family of drugs as triggers of tumor-specific apoptosis. *Leukemia* (2002) 16(4):508–19. doi: 10.1038/sj.leu.2402476
215. Baigent C, Keech A, Kearney PM, Blackwell L, Buck G, Pollicino C, et al. Efficacy and safety of cholesterol-lowering treatment: prospective meta-analysis of data from 90,056 participants in 14 randomised trials of statins. *Lancet* (2005) 366(9493):1267–78. doi: 10.1016/S0140-6736(05)67394-1
216. Adnan M, Mohammad KI, Manik MEH. Anticancer agents in combination with statins. *J Bioequiv Availab* (2017) 9(4):463–6. doi: 10.4172/jbb.1000345
217. Ashburn TT, Thor KB. Drug repositioning: identifying and developing new uses for existing drugs. *Nat Rev Drug Discov* (2004) 3(8):673–83. doi: 10.1038/nrd1468
218. Kornblau SM, Banker DE, Stirewalt D, Shen D, Lemker E, Verstovsek S, et al. Blockade of adaptive defensive changes in cholesterol uptake and synthesis in AML by the addition of pravastatin to idarubicin + high-dose Ara-C: a phase 1 study. *Blood* (2007) 109(7):2999–3006. doi: 10.1182/blood-2006-08-044446
219. Issat T, Nowis D, Jakobsiak M, Golab J. Lovastatin potentiates antitumor effects of saquinavir against human lymphoma cells. *Oncol Rep* (2004) 12(6):1371–5. doi: 10.3892/or.12.6.1371
220. Hus M, Grzasko N, Szostek M, Pluta A, Helbig G, Woszczyk D, et al. Thalidomide, dexamethasone and lovastatin with autologous stem cell transplantation as a salvage immunomodulatory therapy in patients with relapsed and refractory multiple myeloma. *Ann Hematol* (2011) 90(10):1161–6. doi: 10.1007/s00277-011-1276-2
221. Henslee AB, Steele TA. Combination statin and chemotherapy inhibits proliferation and cytotoxicity of an aggressive natural killer cell leukemia. *Biomark Res* (2018) 6:26. doi: 10.1186/s40364-018-0140-0
222. Hamilton RJ, Banez LL, Aronson WJ, Terris MK, Platz EA, Kane CJ, et al. Statin medication use and the risk of biochemical recurrence after radical prostatectomy: results from the Shared Equal Access Regional Cancer Hospital (SEARCH) Database. *Cancer* (2010) 116(14):3389–98. doi: 10.1002/cncr.25308
223. Harshman LC, Wang X, Nakabayashi M, Xie W, Valenza L, Werner L, et al. Statin Use at the Time of Initiation of Androgen Deprivation Therapy and Time to Progression in Patients With Hormone-Sensitive Prostate Cancer. *JAMA Oncol* (2015) 1(4):495–504. doi: 10.1001/jamaoncol.2015.0829
224. Bjarnadottir O, Romero Q, Bendahl PO, Jirstrom K, Ryden L, Loman N, et al. Targeting HMG-CoA reductase with statins in a window-of-opportunity breast cancer trial. *Breast Cancer Res Treat* (2013) 138(2):499–508. doi: 10.1007/s10549-013-2473-6
225. Syvala H, Pennanen P, Blauer M, Tammela TL, Murtola TJ. Additive inhibitory effects of simvastatin and enzalutamide on androgen-sensitive LNCaP and VCaP prostate cancer cells. *Biochem Biophys Res Commun* (2016) 481(1–2):46–50. doi: 10.1016/j.bbrc.2016.11.021
226. Pennanen P, Syvala H, Blauer M, Savinainen K, Ylikomi T, Tammela TLJ, et al. The effects of metformin and simvastatin on the growth of LNCaP and RWPE-1 prostate epithelial cell lines. *Eur J Pharmacol* (2016) 788:160–7. doi: 10.1016/j.ejphar.2016.06.036
227. Stoehr M, Mozet C, Boehm A, Aigner A, Dietz A, Wichmann G. Simvastatin suppresses head and neck squamous cell carcinoma ex vivo and enhances the cytostatic effects of chemotherapeutics. *Cancer Chemother Pharmacol* (2014) 73(4):827–37. doi: 10.1007/s00280-014-2412-1
228. Fromigue O, Hamidouche Z, Marie PJ. Statin-induced inhibition of 3-hydroxy-3-methyl glutaryl coenzyme A reductase sensitizes human osteosarcoma cells to anticancer drugs. *J Pharmacol Exp Ther* (2008) 325(2):595–600. doi: 10.1124/jpet.108.136127
229. Yang SH, Lin HY, Chang VH, Chen CC, Liu YR, Wang J, et al. Lovastatin overcomes gefitinib resistance through TNF-alpha signaling in human cholangiocarcinomas with different LKB1 statuses in vitro and in vivo. *Oncotarget* (2015) 6(27):23857–73. doi: 10.18632/oncotarget.4408
230. Chen J, Bi H, Hou J, Zhang X, Zhang C, Yue L, et al. Atorvastatin overcomes gefitinib resistance in KRAS mutant human non-small cell lung carcinoma cells. *Cell Death Dis* (2013) 4:e814. doi: 10.1038/cddis.2013.312
231. Ahmed TA, Hayslip J, Leggas M. Pharmacokinetics of high-dose simvastatin in refractory and relapsed chronic lymphocytic leukemia patients. *Cancer Chemother Pharmacol* (2013) 72(6):1369–74. doi: 10.1007/s00280-013-2326-3

232. van der Spek E, Bloem AC, Sinnige HA, Lokhorst HM. High dose simvastatin does not reverse resistance to vincristine, adriamycin, and dexamethasone (VAD) in myeloma. *Haematologica* (2007) 92(12):e130–1. doi: 10.3324/haematol.12071

**Conflict of Interest:** The authors declare that the research was conducted in the absence of any commercial or financial relationships that could be construed as a potential conflict of interest.

Copyright © 2021 Guerra, Recio, Aranda-Tavío, Guerra-Rodríguez, García-Castellano and Fernández-Pérez. This is an open-access article distributed under the terms of the Creative Commons Attribution License (CC BY). The use, distribution or reproduction in other forums is permitted, provided the original author(s) and the copyright owner(s) are credited and that the original publication in this journal is cited, in accordance with accepted academic practice. No use, distribution or reproduction is permitted which does not comply with these terms.



# Asparagine Synthetase-Mediated L-Asparagine Metabolism Disorder Promotes the Perineural Invasion of Oral Squamous Cell Carcinoma

Yong Fu<sup>1,2†</sup>, Liang Ding<sup>1†</sup>, Xihu Yang<sup>3</sup>, Zhuang Ding<sup>1,2</sup>, Xiaofeng Huang<sup>4</sup>, Lei Zhang<sup>4</sup>, Sheng Chen<sup>4</sup>, Qingang Hu<sup>1,2\*</sup> and Yanhong Ni<sup>1\*</sup>

<sup>1</sup> Central Laboratory of Stomatology, Nanjing Stomatological Hospital, Medical School of Nanjing University, Nanjing, China,

<sup>2</sup> Department of Oral and Maxillofacial Surgery, Nanjing Stomatological Hospital, Medical School of Nanjing University, Nanjing, China, <sup>3</sup> Department of Oral and Maxillofacial Surgery, Affiliated Hospital of Jiangsu University, Zhenjiang, China,

<sup>4</sup> Department of Oral Pathology, Nanjing Stomatological Hospital, Medical School of Nanjing University, Nanjing, China

## OPEN ACCESS

### Edited by:

Miriam Martini,  
University of Turin, Italy

### Reviewed by:

Mariafrancesca Scalise,  
University of Calabria, Italy

Victoria Bunik,  
Lomonosov Moscow State University,  
Russia

### \*Correspondence:

Yanhong Ni  
niyanhong12@163.com  
Qingang Hu  
qghu@nju.edu.cn

<sup>†</sup>These authors have contributed  
equally to this work

### Specialty section:

This article was submitted to  
Cancer Metabolism,  
a section of the journal  
Frontiers in Oncology

Received: 03 December 2020

Accepted: 04 February 2021

Published: 10 March 2021

### Citation:

Fu Y, Ding L, Yang X, Ding Z,  
Huang X, Zhang L, Chen S,  
Hu Q and Ni Y (2021) Asparagine  
Synthetase-Mediated L-Asparagine  
Metabolism Disorder Promotes  
the Perineural Invasion of Oral  
Squamous Cell Carcinoma.  
Front. Oncol. 11:637226.  
doi: 10.3389/fonc.2021.637226

Dysregulated amino acids metabolism reciprocally interplays with evolutionary phenotypic characteristics of cancer cells to enhance metastasis. The high metastasis potential of oral squamous cell carcinoma (OSCC) can manifest with perineural invasion (PNI). We here aimed to determine the role of amino acids metabolism in OSCCs with different PNI statuses. Targeted metabolomics was used to quantify 48 amino acids in 20 fresh OSCC samples and 25 amino acids were successfully detected, within which 9 were significantly up-regulated in PNI positive (PNI<sup>+</sup>) samples. As its highest area under the curve value (0.9063), L-asparagine was selected as the biomarker to distinguish PNI<sup>+</sup> from PNI negative (PNI<sup>-</sup>). Then, the key enzyme of L-asparagine, asparagine synthetase (ASNS), was investigated using immunohistochemistry with 86 OSCC patients. The results showed that ASNS mainly expressed in tumor epitheliums and positively correlated with lymph node metastasis and PNI. Moreover, subgroup survival analysis revealed that ASNS expression combined with PNI status significantly improved their prognostic value, which was confirmed by the TCGA OSCC cohort (n = 279). To validate whether ASNS promotes PNI, we determined ASNS expression levels in five OSCC cell lines and one normal oral keratinocyte, and HSC3 showed the lowest ASNS level but CAL33 had the highest. Therefore, HSC3 and CAL33 (or PBS as control) were selected and injected separately into sciatic nerves to construct the *in vivo* PNI mouse models. Although both models eventually developed the hind-limb paralysis, nerve dysfunction in the CAL33 model progressed significantly earlier than HSC3 (Day 9 vs. Day 24). Besides, CAL33 migrated significantly farther than HSC3 in the nerve microenvironment ( $P = 0.0003$ ), indicating high ASNS expression is indispensable for OSCC progression, especially PNI formation, through L-asparagine metabolism alteration. This study provides novel insights into how amino acids metabolism disorders alter tumor neurotropism which helps cancer metastasis.

**Keywords:** amino acids metabolism, asparagine synthetase (ASNS), L-asparagine, perineural invasion (PNI), oral squamous cell carcinoma (OSCC)



## INTRODUCTION

Lip and oral cavity cancers are ranked among the top 15 most common cancers in the world, accounting for 500 550 cases out of which 177 384 patients succumbed (1). As the most common type of oral cancer, the 5-year overall survival rate of treated patients with oral squamous cell carcinoma (OSCC) remains approximately 60% because of its highly invasive and metastatic potential even at the early stage (2–4). Perineural invasion (PNI), as one of the significant oncologic features, has been strongly associated with the aggressive behavior leading to a poor prognosis (5).

PNI, the process of neoplastic invasion of nerves, also has been called neurotropic carcinomatous spread and perineural spread. The definition of PNI that widely accepted is that tumor cells are in close proximity to a nerve involving at least 33% of its circumference or within any of the 3 layers (the epineurium, perineurium and the endoneurium) of the nerve sheath (6). Different phenotypes meeting the current criteria of PNI have been well illustrated: Tumor cells inside nerve sheaths; Tumor cells surrounding at least 33% of the nerve circumference, thus the prevalence of PNI in OSCC was reported up to 82% (7).

In addition to OSCC, PNI indicates poor prognosis in various solid cancers, such as pancreatic ductal adenocarcinoma, prostate cancer, gastric carcinoma and cervical cancer et al., but the mechanism behind is still unclear (8). For example, Schwann cells the important components of peripheral nerves were shown to promote cancer dispersion along nerves through direct contact with cancer cells (9). Furthermore, neurotrophins and their receptors, chemokines, and matrix metalloproteinase have been demonstrated as the molecular mechanism driving PNI (10–14). However, few studies have focused on the metabolism dysregulation behind PNI.

Metabolic reprogramming has been shown to be an important hallmark of cancers. Most of the metabolomics studies in oral cancers focus on the metabolic profiles of saliva, serum, and tumor tissues in order to identify potential biomarkers for screening and early diagnosis (15). In addition to increased glucose and fatty acids metabolism during cancer progression, amino acid metabolism also increases to match demands for cancer cells growth and metastasis (16). For example, by a combination of non-targeted and targeted metabolomics, a panel including three amino acids (L-glutamate, L-aspartic acid, and L-proline) was identified as potential diagnostic biomarkers of OSCC (17). L-tryptophan metabolism promotes tumor invasion, metastasis and dysregulates immune cells infiltration thereby accelerating cancer progression (18, 19). Moreover, amino acids metabolism was also distinct at different distances from surgical margins in OSCC (20). Here, we hoped to further elucidate the amino acid metabolism alteration behind different PNI statuses.

In this study, 20 prospectively collected primary OSCC tissues were used for quantification of 48 amino acids using ultra-high-performance liquid chromatography-tandem mass spectrometer (UHPLC-MS/MS). After the differential amino acids analysis, the metabolite with the highest area under the curve (AUC) value to distinguish different PNI statuses was selected and its key

enzyme were evaluated for its clinical value. Meanwhile, a mouse model was successfully constructed by injecting cancer cells into the sciatic nerves to study PNI *in vivo*. The hypothesis for this study is that dysregulated amino acids metabolism affects PNI and ultimately promotes OSCC progression.

## MATERIALS AND METHODS

### Patients and Tissue Samples

Written informed consent for participation, including use of tissue samples, was obtained from each patient prior to inclusion. The protocol was reviewed and approved by the Medical Ethics Committee of Nanjing Stomatological Hospital and the study conforms to the declaration of Helsinki. To quantitatively investigate the amino acids concentration of OSCC samples, frozen tumor tissues from 20 primary OSCC patients were prospectively collected (Table 1). There were 13 men and 7 women who had ages ranging from 37 to 73 years (median, 60.5 years). Within these tumor tissues, 8 were judged as PNI positive (PNI<sup>+</sup>, Figure 1) by two independent oral pathologists with Hematoxylin and Eosin (H&E) staining.

To retrospectively evaluate ASNS expression, we conducted a cohort including 86 primary OSCC patients. All patients with complete follow-up information were admitted at Nanjing Stomatological Hospital during 2013 to 2014 and diagnosed with primary OSCC by experienced pathologists from the Department of Pathology (Table 2). There were 52 men and 34 women included with ages ranging from 28 to 83 years (median, 55 years). The follow-up time ranged from 4 to 79 months (median, 71 months). Patients who had received chemotherapy or radiation therapy before surgery were excluded. All OSCC samples were evaluated according to the

**TABLE 1 |** Baseline characteristics of 20 prospectively collected OSCC patients.

Patient ID	Gender	Age	Tumor site	Differentiation	pT	pN	PNI
#01	Male	56	Floor of mouth	Well	T3	N1	No
#02	Female	37	Tongue	Well	T3	N0	No
#03	Male	73	Tongue	Well	T2	N1	No
#04	Female	64	Tongue	Poor	T2	N0	No
#05	Female	60	Buccal mucosa	Well	T2	N1	No
#06	Male	63	Floor of mouth	Well	T3	N0	No
#07	Female	62	Buccal mucosa	Well	T4	N0	No
#08	Male	70	Hard Palate	Moderately	T3	N0	No
#09	Male	48	Buccal mucosa	Well	T3	N0	No
#10	Male	71	Gingiva	Well	T4	N0	No
#11	Female	55	Tongue	Well	T2	N0	No
#12	Female	71	Buccal mucosa	Well	T2	N0	No
#13	Male	50	Floor of mouth	Moderately	T4	N1	Yes
#14	Male	61	Tongue	Well	T2	N1	Yes
#15	Male	48	Tongue	Well	T2	N1	Yes
#16	Female	61	Gingiva	Well	T4	N1	Yes
#17	Male	40	Tongue	Well	T2	N0	Yes
#18	Male	68	Tongue	Well	T3	N2	Yes
#19	Male	52	Tongue	Well	T2	N0	Yes
#20	Male	54	Tongue	Moderately	T4	N2	Yes

pT, pathologic T stage; pN, pathologic N stage; PNI, perineural invasion; OSCC, oral squamous cell carcinoma.

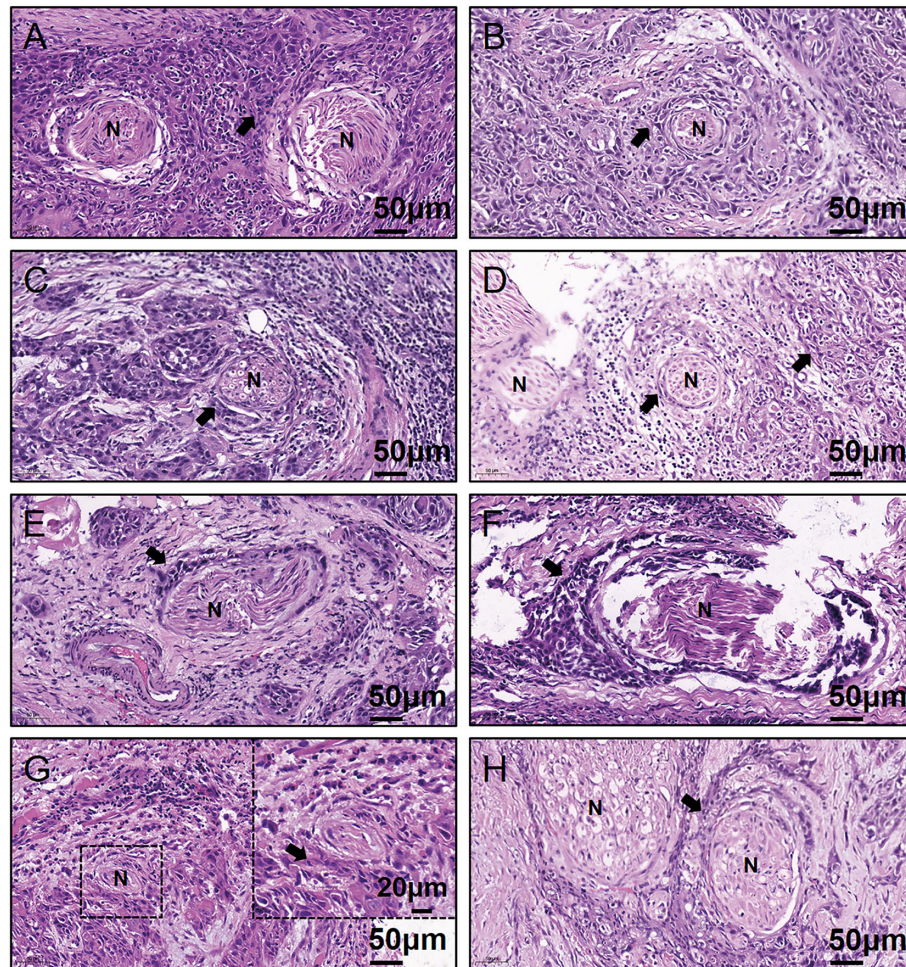


**FIGURE 1** | Representative H&E-stained images for the eight PNI<sup>+</sup> OSCC samples. (A–H) Patient #13 to #20. N, Nerve; H&E, hematoxylin & eosin; PNI, perineural invasion; OSCC, oral squamous cell carcinoma; +, positive; The black arrow indicates the tumor.

WHO classification and the UICC tumor–node–metastasis (TNM) staging system, for which “T” describes the extent of primary tumor (T), “N” refers to absence or presence and extent of overt regional lymph node(s), and “M” depicts the absence or presence of distant metastasis.

Another cohort with 279 OSCC patients from The Cancer Genome Atlas (TCGA) was also conducted (**Supplementary Table 1**). Phenotype and survival data retrieved from the TCGA-HNSC dataset were downloaded from the UCSC Xena website (<https://xenabrowser.net/>). There were 187 men and 92 women with ages ranging from 19 to 90 years (median, 61 years). The follow-up time was from 11 to 5480 days (median, 641 days). H&E-stained images from the Cancer Digital Slide Archive website (<https://cancer.digitalarchive.org/>) were reviewed for their PNI statuses. Additionally, RNA-seq data (FPKM-UQ) of ASNS were downloaded and the cutoff value 17.72 (the third quantile) was selected in order to separate these patients into ASNS expression low (<17.72, ASNS<sup>low</sup>) or high (≥17.72, ASNS<sup>high</sup>).

## Ultra-High-Performance Liquid Chromatography-Tandem Mass Spectrometer Targeted Quantitative Analysis

The specific operation steps for UHPLC-MS/MS could refer to our previous work (20). Shortly described as follows: Equipped with a Waters ACQUITY UPLC BEH Amide column (100 × 2.1 mm, 1.7 μm; Waters Corporation, USA), an Agilent 1290 Infinity II series UHPLC system (Agilent Technologies, California, USA) was used for the UHPLC separation. Mobile phase A and B were respectively made up of 1% formic acid in water and 1% formic acid in acetonitrile. The column temperature was set to 35°C while the auto-sampler temperature was set to 4°C. For assay development, Agilent 6460 Triple Quadrupole mass spectrometer was connected with an Agilent Jet Stream electrospray ionization interface (Agilent Technologies, California, USA).

Isotope standards used for the quantifications were applied and the optimal Multiple Reaction Monitoring (MRM) parameters of the target metabolites were obtained. Agilent



**TABLE 2 |** ASNS expression and baseline characteristics of 86 primary OSCC patients.

Characteristics	Total N=86	ASNS expression		$\chi^2$	P
		Low, n (%)	High, n (%)		
Age				0.247	0.619
<60	39 (45.3%)	22 (56.4%)	17 (43.6%)		
≥60	47 (54.7%)	29 (61.7%)	18 (38.3%)		
Gender				0.943	0.332
Female	34 (39.5%)	18 (52.9%)	16 (47.1%)		
Male	52 (60.5%)	33 (63.5%)	19 (36.5%)		
Site				3.58	0.472
Tongue	33 (38.4%)	18 (54.5%)	15 (45.5%)		
Gingiva	18 (20.9%)	10 (55.6%)	8 (44.4%)		
Buccal mucosa	17 (19.8%)	11 (64.7%)	6 (35.3%)		
Floor of mouth	10 (11.6%)	5 (50.0%)	5 (50.0%)		
Others	8 (9.3%)	7 (87.5%)	1 (12.5%)		
T				0.032	0.859
T1 + T2	73 (84.9%)	43 (58.9%)	30 (41.1%)		
T3 + T4	13 (15.1%)	8 (61.5%)	5 (38.5%)		
N				6.32	<b>0.012</b>
N-	53 (61.6%)	37 (69.8%)	16 (30.2%)		
N+	33 (38.4%)	14 (42.4%)	19 (57.6%)		
Stage				4.316	<b>0.038</b>
I + II	46 (53.5%)	32 (69.6%)	14 (30.4%)		
III + IV	40 (46.5%)	19 (47.5%)	21 (52.5%)		
Grade				1.105	0.293
Well	25 (29.1%)	17 (68.0%)	8 (32.0%)		
Moderately + Poor	61 (70.9%)	34 (55.7%)	27 (44.3%)		
PNI				21.395	<b>&lt;0.001</b>
No	38 (44.2%)	33 (86.8%)	5 (13.2%)		
Yes	48 (55.8%)	18 (37.5%)	30 (62.5%)		
Radiation therapy				1.489	0.222
Without	58 (67.4%)	37 (63.8%)	21 (36.2%)		
With	28 (32.6%)	14 (50.0%)	14 (50.0%)		
Chemotherapy				0.884	0.347
Without	78 (90.7%)	48 (61.5%)	30 (38.5%)		
With	8 (9.3%)	3 (37.5%)	5 (62.5%)		

Chi-square test was used between each baseline characteristic and ASNS expression and  $P < 0.05$  in bold was viewed as significant. -, negative; +, positive; PNI, perineural invasion; ASNS, asparagine synthetase; OSCC, oral squamous cell carcinoma.

MassHunter Work Station Software (B.08.00, Agilent Technologies, California, USA) was used for the MRM data acquisition and processing. The raw data of amino acids concentration in PNI was in the **Supplementary Table 2**.

## Immunohistochemistry

IHC of formalin fixed paraffin-embedded tissues was performed as previously described (21). ASNS rabbit polyclonal antibody (Sigma-Aldrich Cat# HPA029318, RRID: AB\_10602389) was used with the dilution ratio 1:200. The intensity of ASNS immunoreaction was scored as follows: 0 = absence of stained cells; 1 = weak staining; 2 = moderate staining; and 3 = strong staining. The percentage of stained cells was scored as follows: 0 = 0–5% stained cells; 1 = 6–33% stained cells; 2 = 34–66% stained cells; 3 = 67–100% stained cells. ASNS immunoreaction index was calculated by multiplying the staining intensity and the percentage of stained cells. Then, OSCC tissues were divided into low or high group: score = 0–4, ASNS low (ASNS<sup>low</sup>); score = 6–9, ASNS high (ASNS<sup>high</sup>).

## Cell Culture and Reagents

The human OSCC cell lines Cal27, HSC3, CAL33, SCC9, SCC131 and immortalized human oral keratinocyte (HOK) were kept in our lab and were maintained in the Dulbecco's Modified Eagle Medium, high glucose (DMEM-H) supplemented with 10% fetal bovine serum and 1% penicillin-streptomycin. All cell lines were authenticated using Short Tandem Repeat (STR) analysis and cultured at 37 °C in a standard humidified atmosphere of 5% CO<sub>2</sub>. All cell culture reagents were obtained from Gibco (ThermoFisher, USA).

## Western Blotting

After cells in six-well plate reached a confluency of 80% to 90%, cells were washed three times with ice-cold PBS and then lysed on ice with SDS lysis buffer (Beyotime, China). Equal amounts of protein lysates (25 µg per lane) were separated by 4% to 12% gradient SDS-polyacrylamide gels (GenScript, USA) for 40 min at 200 V and then transferred onto polyvinylidene difluoride (PVDF) membranes (Millipore, USA) using a wet transfer system (Bio-Rad, USA). Membranes were blocked with 5% bovine serum albumin for 1 h at room temperature. Then PVDF membranes were probed with β-Actin mouse monoclonal antibody (dilution ratio 1:10000, Proteintech Cat# 66009-1-Ig, RRID: AB\_2687938) and ASNS rabbit polyclonal antibody (dilution ratio 1:500, Proteintech Cat# 14681-1-AP, RRID: AB\_2060119) at 4°C overnight with gentle shaking. After incubation, PVDF membranes were washed three times with PBST (0.05% Tween20 in PBS) and detected with secondary antibodies conjugated with horseradish peroxidase (dilution ratio 1:20000, Invitrogen, USA). Images were captured using Tanon-5200 Chemiluminescent Imaging System (Tanon, China).

## Reverse Transcription and Quantitative Real-Time PCR

Total RNA was extracted from cells using TRIzol reagent (Invitrogen, USA) following the manufacturer's instructions. The concentration and purity of the RNA were determined by measuring the absorbance at 260 nm and 280 nm using NanoDrop One (ThermoFisher, USA). Total RNA (1 µg) was reverse transcribed in a 20 µL system using HiScript III RT SuperMix (Vazyme, China). Subsequently, qRT-PCR was performed using ChamQ SYBR qPCR Master Mix (Vazyme, China) and LightCycler 96 (Roche, Switzerland). The primer sequences used were as follows: forward primer 5'-GGAAGACAGCCCCGATTACT-3' and reverse primer 5'-AGCACGAAGTGTGTAATGTCA-3' for human ASNS; forward primer 5'-CATGTACGTTGCTATCCAGGC-3' and reverse primer 5'-CTCCTTAATGTCACGCACGAT-3' for human β-Actin. All primer sequences were purchased from Invitrogen (USA).

## In Vivo Perineural Invasion Mouse Model

All of the procedures with animal subjects were approved by the Institutional Animal Care and Use Committee at Medical School of Nanjing University. In this study, 6-week-old male BALB/c nu/nu mice were used. The surgical procedure and cancer cells injection

in detail were previously described (22). Briefly, mice were anesthetized and maintained with isoflurane and a 1 cm incision with small scissors was made on the hind limb of the injection side. Then, sciatic nerves were exposed and injected with cancer cells ( $3 \times 10^4$  in 3  $\mu$ L PBS) or the same volume PBS with a 10  $\mu$ L syringe (Hamilton, USA). Put the nerve back and close the skin with 5-0 Nylon sutures. Mice were closely watched for its recovery from anesthesia and wound healing. Sciatic nerve function was measured every three days as previously described (23). The sciatic function index indicates the distance between the first and fifth toes of the mouse hind limbs. In the *in vivo* model, disease progression was recorded when the mouse hind limb became complete nerve paralysis. At the end of the experiment, mice were sacrificed and sciatic nerves and tumor tissues were isolated, measured, and fixed for histological analysis.

## Statistical Analysis

For the identification of significant differentially expressed amino acids in UHPLC-MS/MS, the MetaboAnalyst method was applied with a *P*-value threshold of 0.05 and fold-change (FC) threshold of 1.5. For the heatmap, the clustering distances in X-axes and Y-axes were “Correlation” and “Euclidean” respectively, and the clustering method was “Complete”. The clustering distances in X-axes and Y-axes were “Correlation” and “Euclidean” respectively, and the clustering method was “Complete”. To compare how well each amino acid can distinguish between PNI<sup>+</sup> and PNI<sup>−</sup> statuses, receiver operating characteristics (ROC) curves with the Area Under the Curve (AUC) value were drawn. Statistical significance of ASNS IHC staining between PNI<sup>+</sup> and PNI<sup>−</sup> samples was determined using unpaired two-tailed Student's *t*-test. Quantitative analysis of distance between the 1st and 5th toes of mice was determined using pairwise two-tailed Student's *t*-test. For comparison of the migration distance in nerve environment between HSC3 and CAL33, *P*-value was derived from an unpaired two-tailed Student's *t*-test. Bar graphs represent as the mean  $\pm$  the standard error of the mean (s.e.m.).

Survival curves were calculated using the Kaplan–Meier method and compared using the log-rank test. Overall survival (OS) was defined as the time from surgery to death from any cause while disease-specific survival (DSS) was defined as the time from surgery to OSCC caused death. On the other hand, progression-free survival (PFS) was defined as the time from surgery to the time evidence of recurrent or progressive disease was obtained based on clinical diagnosis of recurrence or confirmation of recurrence using imaging, or in instances where patients died from OSCC prior to the censoring date.

## RESULTS

### L-Asparagine Provides the Optimal Diagnostic Efficacy for Perineural Invasion

As shown in **Figure 1**, 40% (8/20) prospectively collected OSCC samples were diagnosed with PNI<sup>+</sup>. Targeted quantitative

metabolomics analyses were performed for 48 amino acids using UHPLC-MS/MS and 25 amino acids were detected robustly, among which 9 significantly up-regulated in the PNI<sup>+</sup> samples (**Figures 2A, B**). The ability of single amino acid marker distinguishing the PNI<sup>+</sup> samples from the PNI negative (PNI<sup>−</sup>) was tested using ROC curve analysis. With the results shown that only one amino acid marker (L-asparagine, AUC > 0.9) displayed high sensitivity and specificity in diagnosing the PNI (**Figure 2C**). In addition, two amino acid markers displayed the least sensitivity and specificity (AUC < 0.8, **Figures 2D, E**) and six displayed moderate sensitivity and specificity (AUC = 0.8–0.9, **Figures 2F–K**). Since its well-known role in the patients with acute lymphoblastic leukemia, the new discovery of L-asparagine dysregulation behind PNI deserves further exploration (24).

### High Expression of Asparagine Synthetase in Tumor Cells Positively Correlated With Perineural Invasion

Since ASNS is the key enzyme for L-asparagine metabolism (**Figure 3A**), ASNS expression in OSCC samples was evaluated by IHC staining. As shown in **Figures 3B, C**, ASNS was mainly located in the tumor epithelium while there was low or no expression in the lymphocytes and fibroblasts. With regards to the ASNS expression in the lymphocytes and fibroblasts, there was no significant difference between the PNI<sup>+</sup> and PNI<sup>−</sup> samples (**Figure 3D**). However, the intensity of ASNS expression in the tumor epithelium varied apparently among individuals (**Figure 3E**).

The clinicopathological data in **Table 2** indicated that ASNS expression was positively correlated with the pathologic N stage ( $\chi^2 = 6.32$ ,  $P = 0.012$ ), TNM stage ( $\chi^2 = 4.316$ ,  $P = 0.038$ ), and PNI ( $\chi^2 = 21.395$ ,  $P < 0.001$ ), but not T stage ( $\chi^2 = 0.032$ ,  $P = 0.859$ ). Obtained IHC images showed that PNI<sup>+</sup> OSCC samples had an upregulated ASNS expression in the tumor epithelium (**Figures 4A, B**) with significantly increased IHC score (**Figure 4C**,  $P = 0.0008$ ). TCGA data confirmed our results that PNI<sup>+</sup> OSCCs had significantly elevated ASNS expression at the mRNA level (**Figure 4D**).

### The PNI<sup>+</sup>ASNS<sup>high</sup> Oral Squamous Cell Carcinoma Patients Had the Worst Survival Outcome

Regarding that PNI positively correlated with ASNS expression, OSCC patients were classified into three groups: I, PNI<sup>−</sup>ASNS<sup>low</sup>; II, PNI<sup>−</sup>ASNS<sup>high</sup>/PNI<sup>+</sup>ASNS<sup>low</sup>; III, PNI<sup>+</sup>ASNS<sup>high</sup>. Kaplan–Meier analysis revealed that patients in group III had the worst OS ( $P < 0.0001$ , **Figure 5A**), DSS ( $P = 0.0001$ , **Figure 5B**), and PFS ( $P = 0.0007$ , **Figure 5C**). TCGA data with larger population indicated that combinations of the PNI status and ASNS expression robustly distinguished three groups of patients with varied prognosis (**Figures 5D–F**). In detail, comparative to the patients in group II, individuals in group I always had significantly better OS ( $P = 0.0032$ ), DSS ( $P = 0.0030$ ), and PFS ( $P = 0.0212$ ), while ones in group III had relatively worse OS ( $P = 0.2169$ ), DSS ( $P = 0.0441$ ), and PFS ( $P = 0.0773$ ).



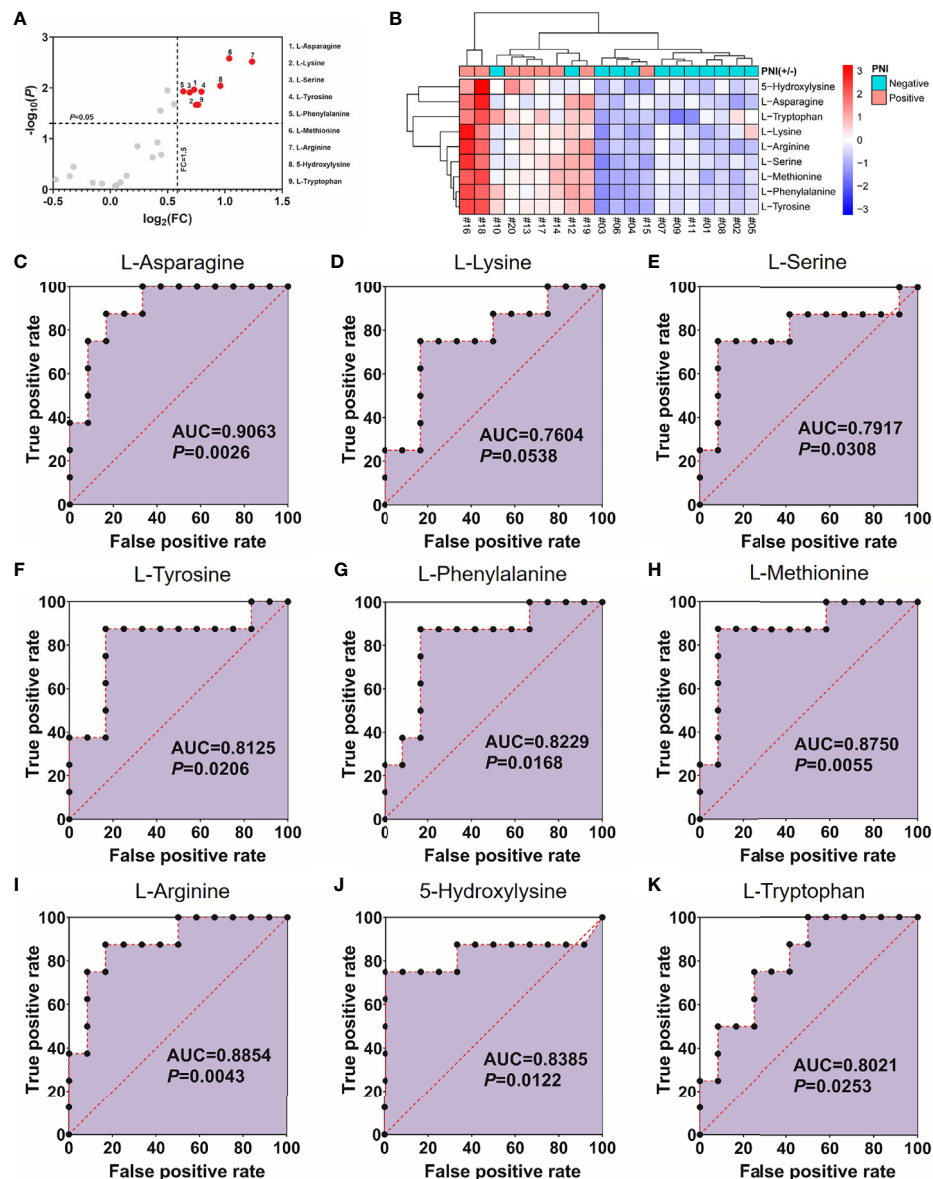


**FIGURE 2 |** Nine amino acids significantly up-regulated in the PNI<sup>+</sup> tissues. **(A)** Volcano plot with fold change (FC) threshold = 1.5 and *P* value threshold = 0.05. The red dots represent features above the threshold. Note that both FC and *P* values are log transformed. **(B)** Heatmap visualization of the differential amino acids between samples with different PNI statuses. Automatic clustering by samples (X-axes) and amino acids (Y-axes). The clustering distances in X-axes and Y-axes were “Correlation” and “Euclidean” respectively, and the clustering method was “Complete”. **(C–K)** Receiver operating characteristics curves for each of the nine amino acids above. FC, fold change; AUC, area under the curve; PNI, perineural invasion; OSCC, oral squamous cell carcinoma. +, positive; –, negative.

## Asparagine Synthetase Promoted Nerve Invasion of Oral Squamous Cell Carcinoma Cells in the Mouse Perineural Invasion Model *In Vivo*

We next compared ASNS expression levels across 6 cell lines. As shown in **Figures 6A, B**, when compared to immortalized human oral keratinocyte (HOK), OSCC cell lines (CAL27, HSC3, CAL33, SCC9, and SCC131) had significantly higher

expression of ASNS. Among these five cancer cell lines, we finally chose HSC3 and CAL33 to construct the *in vivo* PNI mouse model as HSC3 had the lowest ASNS expression while CAL33 had the highest. As demonstrated in **Figure 6C**, with cancer cells or PBS injection into the sciatic nerves, mice eventually developed the hind-limb paralysis or kept normal (**Figure 6D**, upper panel). What is more, comparative to the control mice (injection with PBS), the experimental mice

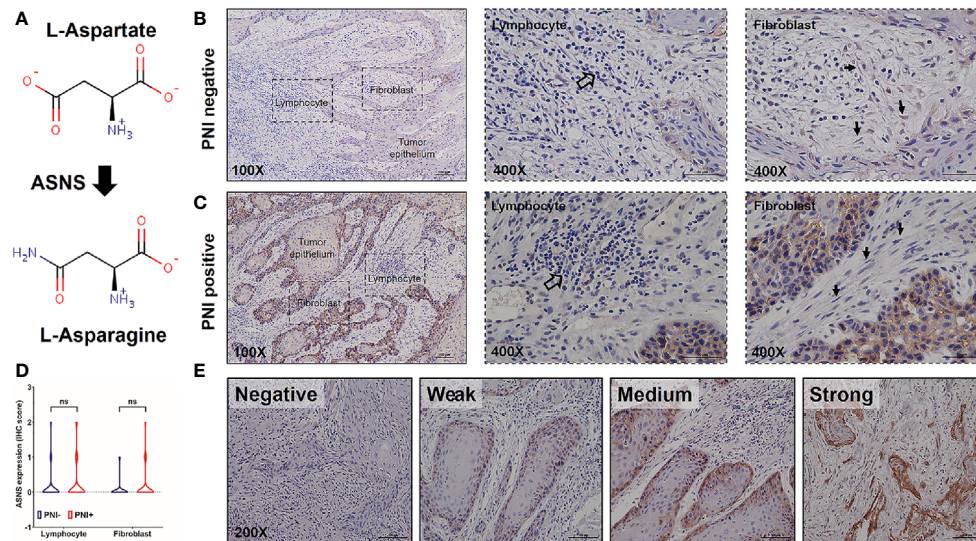


**FIGURE 3 |** The expression pattern of ASNS in the OSCC tissues. **(A)** ASNS catalyzed the synthesis of L-asparagine from L-aspartate. **(B, C)** Representative IHC images of ASNS separately in the PNI<sup>+</sup> **(B)** and PNI<sup>-</sup> **(C)** tissues. Note that the open arrows indicate the lymphocytes and solid arrows indicate the fibroblasts. **(D)** Comparison of ASNS expression in the lymphocytes (or fibroblasts) between the PNI<sup>+</sup> and PNI<sup>-</sup> OSCC tissues. Statistical significance of ASNS IHC staining between PNI<sup>+</sup> and PNI<sup>-</sup> samples was determined using unpaired two-tailed Student's *t*-test. **(E)** Illustration of the intensity of ASNS expression in the tumor epitheliums. ASNS, asparagine synthetase; IHC, immunohistochemistry; PNI, perineural invasion; OSCC, oral squamous cell carcinoma. ns, not statistically significant ( $P \geq 0.05$ ). +, positive; -, negative.

successfully developed tumors in the sciatic nerves (**Figure 6D**, lower panel).

With the *in vivo* PNI mouse models successfully constructed, we subsequently compared the sciatic function index among three groups of mice: the control group with PBS injection, the HSC3 group with HSC3 injection, and the CAL33 group with CAL33 injection. As shown in **Figure 6E**, the control group did not show any nerve dysfunctions during the entire experimental period while 4/5 mice in the HSC3 group developed nerve dysfunction at Day 24. Importantly, in the CAL33 group 1/5 mice became hind-limb paralysis at Day 9 and all mice developed nerve dysfunction at Day 15. Distances between the first and fifth toes confirmed that mice in the CAL33 group eventually had more severe sciatic nerves dysfunction than the HSC3 group ( $P < 0.0001$  vs.  $P = 0.0092$ , **Figure 6F**). As demonstrated in **Figure 6G**, tumor burden in the CAL33 group was larger than that in HSC3 group. H&E-stained images of the injected nerves (long axis) revealed that cancer cells invasion distance in the nerve microenvironment varied between the HSC3 and CAL33 groups (**Figure 6H**). Quantification results indicated that CAL33 had significantly longer nerve invasion distance than HSC3 ( $P = 0.0003$ , **Figure 6I**).

## DISCUSSION

Although a combination of non-targeted and targeted metabolomics have revealed the aberrant levels of several amino acids from normal epithelium to OSCC, the potential function of dysregulated amino acids metabolism behind OSCC metastasis is

still unclear (17). PNI, as a third route for tumor dissemination besides the local invasion and lymphovascular metastasis, was demonstrated in this study to have correlations with the amino acids metabolism disorder. We found that L-asparagine was significantly enriched in the PNI<sup>+</sup> samples and its key enzyme ASNS overexpression accelerated nerve dysfunction and promoted cancer cells invasion in the nerve microenvironment.

PNI as a well-known pathological feature has been recognized widely as an indicator of poor prognosis and we here investigated the metabolism change between PNI<sup>+</sup> and PNI<sup>-</sup> samples, thus two groups were divided in first parts of this study, whereas the amino acid L-asparagine and its key enzyme ASNS was found to be significantly correlated with PNI statuses, and three groups was divided based on both PNI status and ASNS expression in further study to emphasize the potential role of ASNS during the PNI development.

Although there were total 9 amino acids displaying upregulated in the PNI<sup>+</sup> OSCC samples, we finally chose L-asparagine as the marker to distinguish different PNI statuses. As one of the non-essential amino acids (NEAAs), L-asparagine strongly influences tumor metastatic potential (25, 26). Supplementing the culture medium with L-asparagine increased the invasiveness of breast cancer cells twofold when compared with other NEAAs (25). Moreover, concentrations of L-asparagine gradually increased with progression from normal oral tissues to OSCC (20). As illustrated in **Figure 2B**, the expressions of amino acids in patients #10, #12, and #15 were indeed the outliers, indicating the existence of individual differences. One possible explanation is that individual factors such as drug history, dietary habit et al. may affect their amino acids

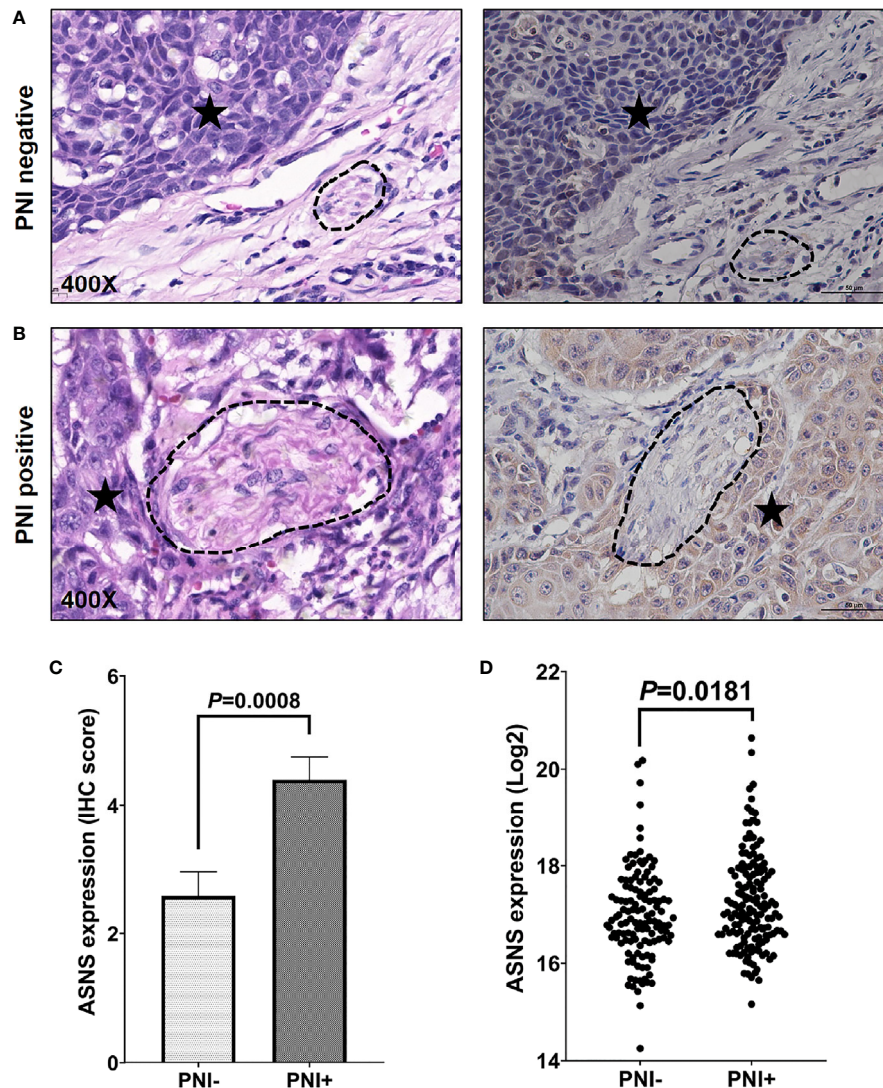


**FIGURE 4 |** ASNS expression significantly upregulated in the PNI<sup>+</sup> OSCC tissues. **(A, B)** Comparison of ASNS expression in the tumor epithelium of the PNI<sup>+</sup> **(B)** and PNI<sup>-</sup> **(A)** tumors by the IHC staining (Right panel). The left panel shows the same tumor area as the right panel by the H&E staining and the dark asterisk indicates the tumor while the dashed circle shows the nerve trunk. **(C)** The IHC scores of ASNS expression between the PNI<sup>+</sup> and PNI<sup>-</sup> tumors. Data are presented as mean  $\pm$  s.e.m. **(D)** Comparison of the ASNS mRNA expression from the TCGA between the PNI<sup>+</sup> and PNI<sup>-</sup> tumors. Statistical significance of ASNS expression between PNI<sup>+</sup> and PNI<sup>-</sup> samples was determined using unpaired two-tailed Student's *t*-test. ASNS, asparagine synthetase; IHC, immunohistochemistry; H&E, hematoxylin eosin; PNI, perineural invasion; OSCC, oral squamous cell carcinoma. +, positive; -, negative.

metabolism levels and the other possibility may be due to the limited sample size ( $n = 20$ ) of this study. Although we believed that these three cases should not be deleted, the AUC value after deletion confirmed that L-asparagine still had an optimal diagnostic efficacy (AUC = 0.9571,  $P = 0.0018$ ) for PNI, suggesting that elevated L-asparagine level promoted OSCC progression through enhanced PNI formation.

ASNS regulates the metabolism level of L-asparagine. To verify that whether ASNS associated with PNI the same pattern as its substrate L-asparagine, we investigated the relationship between the clinicopathological data of OSCC

patients and ASNS expression at the protein or mRNA level. Consistently, ASNS expression was positively correlated with PNI and negatively with the survival outcome. Recently, a phase IIb open-label study evaluated the effect of L-asparaginase combined with chemotherapy in the second-line treatment of advanced pancreatic ductal adenocarcinomas (PDACs) showing that the combination was associated with improvements in OS and PFS (27). According to the human protein atlas data (HPA, <https://www.proteinatlas.org/ENSG00000070669-ASNS/tissue>), ASNS expression was high in the normal pancreas but low in the normal oral mucosa. In cancer tissues, high ASNS expression was



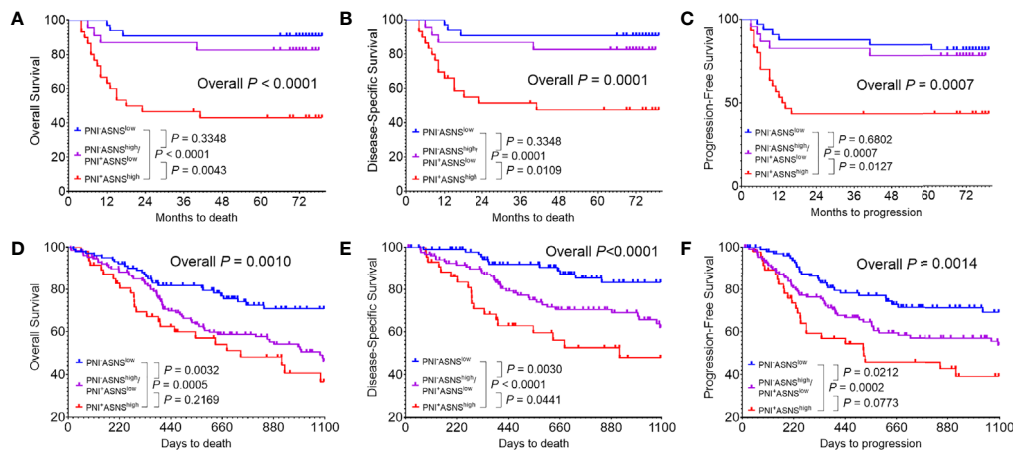


**FIGURE 5 |** Evaluation of the prognostic value of combinations of the PNI status and ASNS expression (A–C) Kaplan-Meier analysis in the 86 OSCC patients cohort from our hospital for the overall survival (A), disease-specific survival (B), and progression-free survival (C). (D–F) Survival analysis in the 279 OSCC patients cohort from the TCGA. Survival curves were calculated using the Kaplan–Meier method and compared using the log-rank test. ASNS, asparagine synthetase; PNI, perineural invasion; OSCC, oral squamous cell carcinoma. +, positive; –, negative.

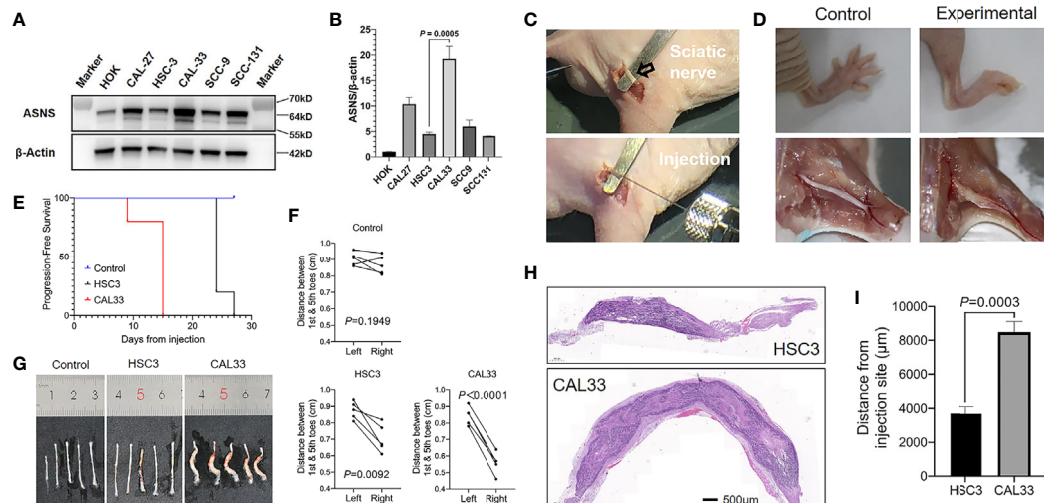


**FIGURE 6 |** ASNS promotes cancer cells nerve invasion *in vivo* (A, B) ASNS levels in several cell lines were screened by the western blotting (A) and the quantitative real-time PCR (B). (C) Exposure of the sciatic nerve (open arrow) and injection. (D) Comparison of the nerve functions (upper panel) and appearances (lower panel) between the control mice (left panel, injected with PBS) and experimental mice (right panel, injected with cancer cells). (E) Time to nerve dysfunction among three groups of mice (Control, HSC3 and CAL33) were compared. (F) The distance between the 1st and 5th toes of mice was recorded to represent the sciatic function index. Quantitative analysis of distance between the 1st and 5th toes of mice was determined using pairwise two-tailed Student's *t*-test. (G) Images showing the sciatic nerves of the three groups of mice. (H) Representative H&E-stained images of the cancer cells in the sciatic nerves (HSC3, upper panel; CAL33, lower panel). (I) Quantitative comparison of the distance of cancer cells (HSC3 vs. CAL33) migration from the injection sites. Five mice were used in each *in vivo* model. For comparison of the migration distance in nerve environment between HSC3 and CAL33, *P*-value was derived from an unpaired two-tailed Student's *t*-test. Bar graphs represent as the mean ± the standard error of the mean (s.e.m.) ASNS, asparagine synthetase.

found in only 20% to 50% of the resected PDACs (28, 29). Similarly, in this study of the resected OSCCs 41% (35/86) at the protein level and 25% (71/279) at the mRNA level showed high expression of ASNS. Considering the similar expression pattern as the PDAC, L-asparaginase has excellent therapeutic potential for OSCC treatment.

The mechanism of ASNS promoting OSCC nerve invasion still needs to be further explored. In order to construct the *in vivo* PNI mouse models using oral cancer cells with different ASNS baseline expressions, we screened 5 OSCC cell lines and 1 normal human oral keratinocyte cell line in our lab. Consistent with our previous work, cancer cells had significantly elevated ASNS expression than



the normal cell (HOK) but varied distinctly among OSCC cell lines (20). Besides selecting two OSCC cell lines (HSC3 and CAL33) with different ASNS levels, knockdown or overexpression of ASNS in cancer cells through genetic modification was another reliable way to construct the *in vivo* PNI model. Although we could not explain at present through which signaling pathway ASNS promotes PNI, the amino acids metabolism alterations behind the nerve invasion of OSCC need be noticed. As reported, the activating transcription factor (ATF)-4 targeted ASNS and knockdown of ATF-4 significantly reduced ASNS expression (30–32). Moreover, induction of ATF-4 is dependent on the activation of the PI3K-AKT-mTOR signaling (31, 33). Interestingly, PNI<sup>+</sup> tumors had increased activation levels of the AKT and mTOR kinases (34). Therefore, ASNS regulating PNI may be involved in the PI3K-AKT-mTOR-ATF4 signaling pathway.

In conclusion, L-asparagine and its key enzyme ASNS are involved in the process of PNI which is validated based on the clinicopathological data and an *in vivo* PNI mouse model. Elucidation of ASNS-mediated L-asparagine metabolism alteration behind PNI in the future would provide novel therapeutic targets for inhibiting OSCC early dissemination.

## DATA AVAILABILITY STATEMENT

Publicly available datasets were analyzed in this study. These data can be found here: [https://gdc.xenahubs.net/download/TCGA-HNSC.htseq\\_fpkm-uc.tsv.gz](https://gdc.xenahubs.net/download/TCGA-HNSC.htseq_fpkm-uc.tsv.gz).

## ETHICS STATEMENT

The studies involving human participants were reviewed and approved by the Research Ethics Committee of Nanjing

Stomatological Hospital. The patients/participants provided their written informed consent to participate in this study. The animal study was reviewed and approved by the Institutional Animal Care and Use Committee at Medical School of Nanjing University.

## AUTHOR CONTRIBUTIONS

QH and YN designed this study. YF and LD performed all the experiments. YF, LD, and ZD collected the clinical data. YF, LD, and XY interpreted the data. XH, LZ, and SC offered technical support. YF and LD wrote the manuscript. All authors contributed to the article and approved the submitted version.

## FUNDING

This work was supported by the National Natural Science Foundation of China (grant nos. 81902754, 81772880, 81700939, and 81902759), Fundamental Research Funds for the Central Universities (no. 021014380161), Natural Science Foundation of Jiangsu Province (no. BK20190304), China Postdoctoral Science Foundation (no. 2019M651789), and Nanjing Medical Science and Technology Development Foundation, Nanjing Department of Health (no. YKK18123).

## SUPPLEMENTARY MATERIAL

The Supplementary Material for this article can be found online at: <https://www.frontiersin.org/articles/10.3389/fonc.2021.637226/full#supplementary-material>

## REFERENCES

- Bray F, Ferlay J, Soerjomataram I, Siegel RL, Torre LA, Jemal A. Global cancer statistics 2018: GLOBOCAN estimates of incidence and mortality worldwide for 36 cancers in 185 countries. *CA Cancer J Clin* (2018) 68:394–424. doi: 10.3322/caac.21492
- Peres MA, Macpherson LMD, Weyant RJ, Daly B, Venturelli R, Mathur MR, et al. Oral diseases: a global public health challenge. *Lancet* (2019) 394:249–60. doi: 10.1016/S0140-6736(19)31146-8
- Zanoni DK, Montero PH, Migliacci JC, Shah JP, Wong RJ, Ganly I, et al. Survival outcomes after treatment of cancer of the oral cavity (1985–2015). *Oral Oncol* (2019) 90:115–21. doi: 10.1016/j.oraloncology.2019.02.001
- Oliveira DT, Biassi TP, Faustino SE, Carvalho AL, Landman G, Kowalski LP. Eosinophils may predict occult lymph node metastasis in early oral cancer. *Clin Oral Invest* (2012) 16:1523–8. doi: 10.1007/s00784-011-0651-7
- Marchesi F, Piemonti L, Mantovani A, Allavena P. Molecular mechanisms of perineural invasion, a forgotten pathway of dissemination and metastasis. *Cytokine Growth Factor Rev* (2010) 21:77–82. doi: 10.1016/j.cytogfr.2009.11.001
- Liebig C, Ayala G, Wilks JA, Berger DH, Albo D. Perineural invasion in cancer: a review of the literature. *Cancer* (2009) 115:3379–91. doi: 10.1002/cncr.24396
- Schmidt LB, Scanlon CS, D'Silva NJ. Perineural Invasion in Head and Neck Cancer. *J Dent Res* (2018) 97:742–50. doi: 10.1177/0022034518756297
- Chen SH, Zhang BY, Zhou B, Zhu CZ, Sun LQ, Feng YJ. Perineural invasion of cancer: a complex crosstalk between cells and molecules in the perineural niche. *Am J Cancer Res* (2019) 9:1–21.
- Deborde S, Omelchenko T, Lyubchik A, Zhou Y, He S, McNamara WF, et al. Schwann cells induce cancer cell dispersion and invasion. *J Clin Invest* (2016) 126:1538–54. doi: 10.1172/JCI82658
- Frydenlund N, Mahalingam M. Desmoplastic melanoma, neurotropism, and neurotrophin receptors—what we know and what we do not. *Adv Anat Pathol* (2015) 22:227–41. doi: 10.1097/PAP.0000000000000076
- Yu EH, Lui MT, Tu HF, Wu CH, Lo WL, Yang CC, et al. Oral carcinoma with perineural invasion has higher nerve growth factor expression and worse prognosis. *Oral Dis* (2014) 20:268–74. doi: 10.1111/odi.12101
- Marchesi F, Piemonti L, Fedele G, Destro A, Roncalli M, Albarello L, et al. The chemokine receptor CX3CR1 is involved in the neural tropism and malignant behavior of pancreatic ductal adenocarcinoma. *Cancer Res* (2008) 68:9060–9. doi: 10.1158/0008-5472.CAN-08-1810
- Bakst RL, Xiong H, Chen CH, Deborde S, Lyubchik A, Zhou Y, et al. Inflammatory Monocytes Promote Perineural Invasion via CCL2-Mediated Recruitment and Cathepsin B Expression. *Cancer Res* (2017) 77:6400–14. doi: 10.1158/0008-5472.CAN-17-1612
- Huang C, Li Y, Guo Y, Zhang Z, Lian G, Chen Y, et al. MMP1/PAR1/SP1/NK1R paracrine loop modulates early perineural invasion of pancreatic cancer cells. *Theranostics* (2018) 8:3074–86. doi: 10.7150/thno.24281
- Chen X, Yu D. Metabolomics study of oral cancers. *Metabolomics* (2019) 15:22. doi: 10.1007/s11306-019-1483-8
- Li Z, Zhang H. Reprogramming of glucose, fatty acid and amino acid metabolism for cancer progression. *Cell Mol Life Sci* (2016) 73:377–92. doi: 10.1007/s00018-015-2070-4

17. Yang XH, Jing Y, Wang S, Ding F, Zhang XX, Chen S, et al. Integrated Non-targeted and Targeted Metabolomics Uncovers Amino Acid Markers of Oral Squamous Cell Carcinoma. *Front Oncol* (2020) 10:426:426. doi: 10.3389/fonc.2020.00426
18. Platten M, Nollen EAA, Rohrig UF, Fallarino F, Opitz CA. Tryptophan metabolism as a common therapeutic target in cancer, neurodegeneration and beyond. *Nat Rev Drug Discovery* (2019) 18:379–401. doi: 10.1038/s41573-019-0016-5
19. Lemos H, Huang L, Prendergast GC, Mellor AL. Immune control by amino acid catabolism during tumorigenesis and therapy. *Nat Rev Cancer* (2019) 19:162–75. doi: 10.1038/s41568-019-0106-z
20. Yang XH, Zhang XX, Jing Y, Ding L, Fu Y, Wang S, et al. Amino acids signatures of distance-related surgical margins of oral squamous cell carcinoma. *EBioMedicine* (2019) 48:81–91. doi: 10.1016/j.ebiom.2019.10.005
21. Liang D, Xiao-Feng H, Guan-Jun D, Er-Ling H, Sheng C, Ting-Ting W, et al. Activated STING enhances Tregs infiltration in the HPV-related carcinogenesis of tongue squamous cells via the c-jun/CCL22 signal. *Biochim Biophys Acta* (2015) 1852:2494–503. doi: 10.1016/j.bbdis.2015.08.011
22. Deborde S, Yu Y, Marcadis A, Chen CH, Fan N, Bakst RL, et al. An In Vivo Murine Sciatic Nerve Model of Perineural Invasion. *J Vis Exp* (2018) 134: e56857. doi: 10.3791/56857
23. Gil Z, Rein A, Brader P, Li S, Shah JP, Fong Y, et al. Nerve-sparing therapy with oncolytic herpes virus for cancers with neural invasion. *Clin Cancer Res* (2007) 13:6479–85. doi: 10.1158/1078-0432.CCR-07-1639
24. Garcia-Bermudez J, Williams RT, Guarecuco R, Birsoy K. Targeting extracellular nutrient dependencies of cancer cells. *Mol Metab* (2020) 33:67–82. doi: 10.1016/j.molmet.2019.11.011
25. Knott SRV, Wagenblast E, Khan S, Kim SY, Soto M, Wagner M, et al. Asparagine bioavailability governs metastasis in a model of breast cancer. *Nature* (2018) 554:378–81. doi: 10.1038/nature25465
26. Du F, Chen J, Liu H, Cai Y, Cao T, Han W, et al. SOX12 promotes colorectal cancer cell proliferation and metastasis by regulating asparagine synthesis. *Cell Death Dis* (2019) 10:239. doi: 10.1038/s41419-019-1481-9
27. Hammel P, Fabienne P, Mineur L, Metges JP, Andre T, De La Fouchardiere C, et al. Erythrocyte-encapsulated asparaginase (eryaspase) combined with chemotherapy in second-line treatment of advanced pancreatic cancer: An open-label, randomized Phase IIb trial. *Eur J Cancer* (2020) 124:91–101. doi: 10.1016/j.ejca.2019.10.020
28. Bachet JB, Gay F, Marechal R, Galais MP, Adenis A, Ms CD, et al. Asparagine Synthetase Expression and Phase I Study with L-Asparaginase Encapsulated in Red Blood Cells in Patients with Pancreatic Adenocarcinoma. *Pancreas* (2015) 44:1141–7. doi: 10.1097/MPA.0000000000000394
29. Dufour E, Gay F, Aguera K, Scoazec JY, Horand F, Lorenzi PL, et al. Pancreatic tumor sensitivity to plasma L-asparagine starvation. *Pancreas* (2012) 41:940–8. doi: 10.1097/MPA.0b013e318247d903
30. Ye J, Kumanova M, Hart LS, Sloane K, Zhang H, De Panis DN, et al. The GCN2-ATF4 pathway is critical for tumour cell survival and proliferation in response to nutrient deprivation. *EMBO J* (2010) 29:2082–96. doi: 10.1038/emboj.2010.81
31. Gwinn DM, Lee AG, Briones-Martin-Del-Campo M, Conn CS, Simpson DR, Scott AI, et al. Oncogenic KRAS Regulates Amino Acid Homeostasis and Asparagine Biosynthesis via ATF4 and Alters Sensitivity to L-Asparaginase. *Cancer Cell* (2018) 33:91–107 e6. doi: 10.1016/j.ccell.2017.12.003
32. Jiang J, Srivastava S, Seim G, Pavlova NN, King B, Zou L, et al. Promoter demethylation of the asparagine synthetase gene is required for ATF4-dependent adaptation to asparagine depletion. *J Biol Chem* (2019) 294:18674–84. doi: 10.1074/jbc.RA119.010447
33. Fujiki K, Inamura H, Matsuoka M. PI3K signaling mediates diverse regulation of ATF4 expression for the survival of HK-2 cells exposed to cadmium. *Arch Toxicol* (2014) 88:403–14. doi: 10.1007/s00204-013-1129-y
34. Saidak Z, Clatot F, Chatelain D, Galmiche A. A gene expression profile associated with perineural invasion identifies a subset of HNSCC at risk of post-surgical recurrence. *Oral Oncol* (2018) 86:53–60. doi: 10.1016/j.oraloncology.2018.09.005

**Conflict of Interest:** The authors declare that the research was conducted in the absence of any commercial or financial relationships that could be construed as a potential conflict of interest.

Copyright © 2021 Fu, Ding, Yang, Ding, Huang, Zhang, Chen, Hu and Ni. This is an open-access article distributed under the terms of the Creative Commons Attribution License (CC BY). The use, distribution or reproduction in other forums is permitted, provided the original author(s) and the copyright owner(s) are credited and that the original publication in this journal is cited, in accordance with accepted academic practice. No use, distribution or reproduction is permitted which does not comply with these terms.



# Biological Roles and Therapeutic Applications of IDH2 Mutations in Human Cancer

Jinxu Guo<sup>1,2</sup>, Ruyue Zhang<sup>1,2</sup>, Zhe Yang<sup>1,2</sup>, Zhenfeng Duan<sup>1,2</sup>, Detao Yin<sup>3\*</sup> and Yubing Zhou<sup>1,2\*</sup>

<sup>1</sup> Department of Pharmacy, The First Affiliated Hospital of Zhengzhou University, Zhengzhou, China, <sup>2</sup> Henan Key Laboratory for Precision Clinical Pharmacy, The First Affiliated Hospital of Zhengzhou University, Zhengzhou, China, <sup>3</sup> Department of Thyroid Surgery, The First Affiliated Hospital of Zhengzhou University, Zhengzhou, China

## OPEN ACCESS

### Edited by:

Monica Montopoli,  
University of Padua, Italy

### Reviewed by:

Domenica Scumaci,  
Magna Graecia University of  
Catanzaro, Italy  
Hongliang Zhang,  
Guangxi Medical University, China

### \*Correspondence:

Yubing Zhou  
fcczhouyb@zzu.edu.cn  
Detao Yin  
detaoyin@zzu.edu.cn

### Specialty section:

This article was submitted to  
Cancer Metabolism,  
a section of the journal  
Frontiers in Oncology

Received: 22 December 2020

Accepted: 01 April 2021

Published: 26 April 2021

### Citation:

Guo J, Zhang R, Yang Z, Duan Z, Yin D  
and Zhou Y (2021) Biological Roles  
and Therapeutic Applications of IDH2  
Mutations in Human Cancer.  
Front. Oncol. 11:644857.  
doi: 10.3389/fonc.2021.644857

Isocitrate dehydrogenase (IDH) is a key metabolic enzyme catalyzing the interconversion of isocitrate to  $\alpha$ -ketoglutarate ( $\alpha$ -KG). Mutations in IDH lead to loss of normal enzymatic activity and gain of neomorphic activity that irreversibly converts  $\alpha$ -KG to 2-hydroxyglutarate (2-HG), which can competitively inhibit  $\alpha$ -KG-dependent enzymes, subsequently induces cell metabolic reprogramming, inhibits cell differentiation, and initiates cell tumorigenesis. Encouragingly, this phenomenon can be reversed by specific small molecule inhibitors of IDH mutation. At present, small molecular inhibitors of IDH1 and IDH2 mutant have been developed, and promising progress has been made in preclinical and clinical development, showing encouraging results in patients with IDH2 mutant cancers. This review will focus on the biological roles of IDH2 mutation in tumorigenesis, and provide a proof-of-principle for the development and application of IDH2 mutant inhibitors for human cancer treatment.

**Keywords:** IDH2 mutation, cancer metabolism, 2-HG, cancers, IDH2 inhibitors

## INTRODUCTION

Abnormal metabolism has been established as one of the ten characteristics of cancer cells (1). Metabolic pathways such as glycolysis pathway, tricarboxylic acid cycle and pentose phosphate pathway are important molecular events of life activities. Mutations of key enzyme genes involved in metabolic pathways are the main cause of abnormal metabolism by changing the expression and activity of metabolic enzymes (2). In recent years, genomic mutations of succinate dehydrogenase, pyruvate kinase and isocitrate dehydrogenase have been found in many cancer types (3). Metabolic reprogramming of tumor cells seems to be the result of carcinogenic transformation of human cancer, which may also be one of the causes of oncogenic transformation. In addition, the abnormal accumulation of some metabolites (tumor metabolites) caused by genetic mutations in metabolic genes further supports the importance of metabolic disorders in cancer occurrence and cancer cell survival (4).

Isocitrate dehydrogenase (IDH) is an important metabolic enzyme in the tricarboxylic acid cycle, whose mutated genes are associated with a variety of tumors, including acute myeloid leukemia (AML), glioma, cholangiocarcinoma, colon cancer and chondrosarcoma (5). IDH mutation can catalyze the conversion of  $\alpha$ -ketoglutarate ( $\alpha$ -KG) to 2-hydroxyglutarate (2-HG) (Figure 1), and studies have found that the level of 2-HG in cancer patients is higher than that in normal or non-mutated cancer patients (6–8). The increased level of 2-HG and the resulting epigenetic disorders and cell differentiation show the

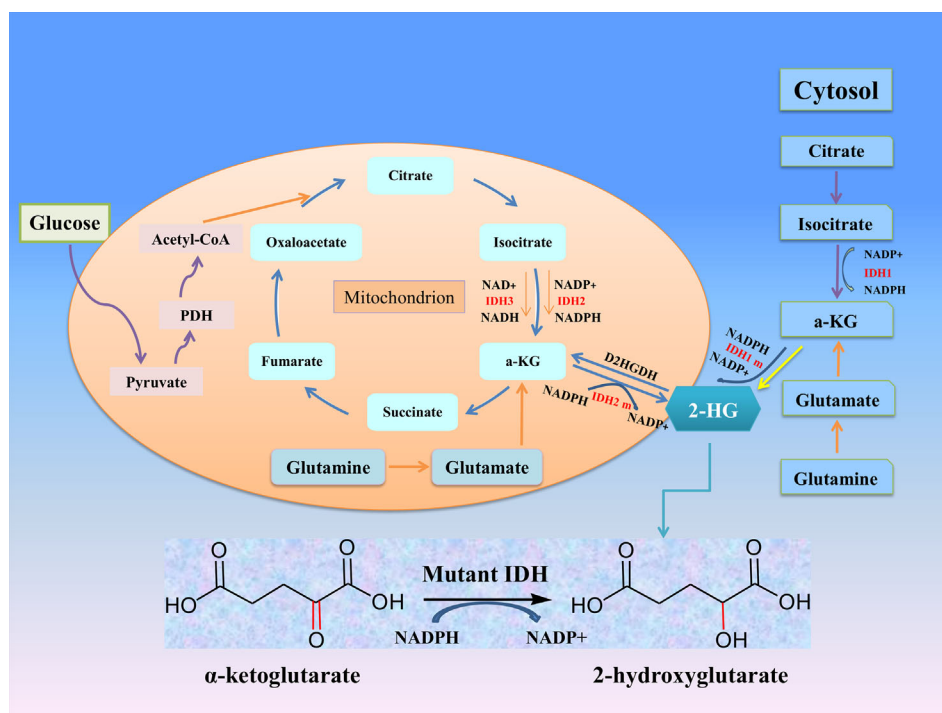


**FIGURE 1** | The roles of IDHs in cancer metabolism. Mutation of either IDH1 or IDH2 imparts a neomorphic enzymatic activity upon the encoded enzymes resulting in the ability to convert  $\alpha$ -ketoglutarate ( $\alpha$ -KG) into the oncometabolite 2-hydroxyglutarate (2-HG), and simultaneously converts NADPH to NADP+.

potential carcinogenicity of IDH mutations (9). These mutations attracted considerable interest due to the potential consequences of the neo-enzymatic conversion of  $\alpha$ -KG to 2-HG and provided a proof of concept for the development of mutant IDH small molecule inhibitors. The targeted drugs developed according to IDH mutations have entered clinical trials, and some drugs have been involved in clinical treatment (10–12). In this review, we discuss the biological roles and therapeutic applications of IDH2 mutations in human cancers.

## IDH STRUCTURE AND FUNCTIONS

IDH metabolic enzyme family includes three subtypes: IDH1, IDH2 and IDH3, which are the most important metabolic enzymes in the Krebs cycle. The structure and function

information of IDH metabolic enzymes are introduced below (Table 1). The active forms of IDH1 and IDH2, which depend on nicotinamide adenine dinucleotide phosphate (NADP +), are homodimers with similar structures: a large domain, a small domain and a clasp domain (13). And human IDH1 and IDH2 genes are located on chromosomes 2q33.3 and 15q26.1, which encode a 414-amino-acid and a 452-amino-acid (14). IDH3 is a heterooctamer whose activities are dependent on nicotinamide adenine dinucleotides (NAD+), formed by two  $\alpha$  subunits (IDH3 $\alpha$ ), one  $\beta$  subunit (IDH3 $\beta$ ), and one  $\gamma$  subunit (IDH3 $\gamma$ ), which are encoded by the IDH3A (15q25.1-2), IDH3B (20p13), and IDH3G (Xq28) genes, respectively (15, 16). Subcellular localized, IDH1 is mainly located in cytoplasm and peroxidase, while IDH2 and IDH3 are mainly located in mitochondria.

IDH subtypes can catalyze the oxidation of decarboxylated isocitrate to tricarboxylic acid cycle intermediates  $\alpha$ -KG and

**TABLE 1** | IDH Structures and Biochemical characteristics.

Subtypes	Isomers	Genes	Chromosome location	Amino acids	Subcellular localization	Co-enzymes	Amino acid substitutions
IDH1	Homodimer	IDH1	2q33.3	414 aa	Cytoplasm Peroxidase	NADP+	R132H, R132C, R132L, R132S, R132G
IDH2	Homodimer	IDH2	15q26.1	452 aa	Mitochondrion	NADP+	R140Q, R140W R172S, R172T, R172K, R172G, R172I, R172M
IDH3	Heterotetramer	IDH3A IDH3B IDH3G	15q25.1-2 20p13 Xq28	366 aa 385 aa 393 aa	Mitochondrion	NAD+	unknown unknown unknown



NADPH, which are involved in other metabolic processes (**Figure 1**).  $\alpha$ -KG is an intermediate of the tricarboxylic acid cycle, participates in epigenetic modification as an important cofactor, and regulates hypoxia-inducible factor-1  $\alpha$  and dioxygenase (17). NADPH plays an important role in keeping reduced glutathione and peroxidase, which can maintain the redox balance and protect cells from oxidative damage caused by various cellular stresses. Studies have confirmed that NADPH produced by IDH1 is involved in lipid metabolism and helps cells defend against lipid oxidation-induced reactive oxygen species (ROS) (18). IDH3 $\alpha$  was also considered to be an upstream activator of hypoxia-inducible factor-1, which promotes metabolic reprogramming of cancer cells and angiogenesis of malignant tumors by improving the stability and transactivation of hypoxia-inducible factor-1 (19).

## IDH MUTATION AND NEOMORPHIC ACTIVITY

IDH has found frequent genetic mutations in many tumors. IDH1 mutations were first discovered in glioblastoma genome-wide analysis (20). With the development of sequencing technology, IDH1 or IDH2 mutations have been found in various malignant tumors, such as AML, glioma, chondrosarcoma. At present, the IDH3 mutant gene has not been found in tumors, but its abnormal expression was related to the occurrence and development of a few cancers (19). This phenomenon may be related to the unique heterotetramer structure of IDH3 (15). Cancer-related IDH1 and IDH2 mutations occur almost entirely on different arginine residues at the active site of the enzyme. Missense mutation in IDH1Arg132 codon leads to single amino acid substitution.

The most common is histidine, but also lead to cysteine, serine, glycine, leucine or isoleucine substitutions (9). The mutation site of IDH1 gene is located at R132, and the mutation sites mainly include R132H, R132C, R132L, R132S, and R132G (**Table 1**). For IDH2, two mutation hotspots have been described. One was codon 140 (IDH2 R140) and the other at codon 172 (IDH2 R172), including R140Q, R172S, R172T, R172K and R172M (21) (**Table 1**).

After IDH mutation, the catalytic activity decreased, and the yield of corresponding enzymatic reactants NADPH and  $\alpha$ -KG decreased, but at the same time, a new enzymatic activity was obtained, which catalyzed NADPH and  $\alpha$ -KG to produce a new enzyme active metabolite 2-HG (22) (**Figure 1**). The expression level of 2-HG is related to different mutation sites, and IDH2 R172 mutations usually lead to a very high level of 2-HG accumulation (23, 24). At present, 2-HG is considered to be a tumor metabolite because it is involved in a variety of biological processes related to tumorigenesis (25, 26) (**Figure 2**). Although more than 60 different  $\alpha$ -KG-dependent dioxygenases have been described, there seem to be two main targets for 2-HG: the KDM family of histone lysine demethylases and the TET family of 5-methylcytosine hydroxylase (27). Because of its structural affinity to  $\alpha$ -KG, 2-HG competitively inhibits histone demethylase and Tet family methylcytosine hydroxylase (25), resulting enzyme block leads to increased histone H3 lysine methylation and global DNA hypermethylation (28, 29). Hypermethylation has been shown to lead to changes in gene expression, many of which are related to cell differentiation. The decrease of  $\alpha$ -ketoglutarate also leads to the decrease of proline hydroxylase and the up-regulation of HIF-1  $\alpha$ , which destroys the adaptability to hypoxia (30, 31). In addition, 2-HG can increase the level of vascular endothelial growth factor (VEGF) secreted by cancer cells and promote endothelial cell proliferation in a concentration-

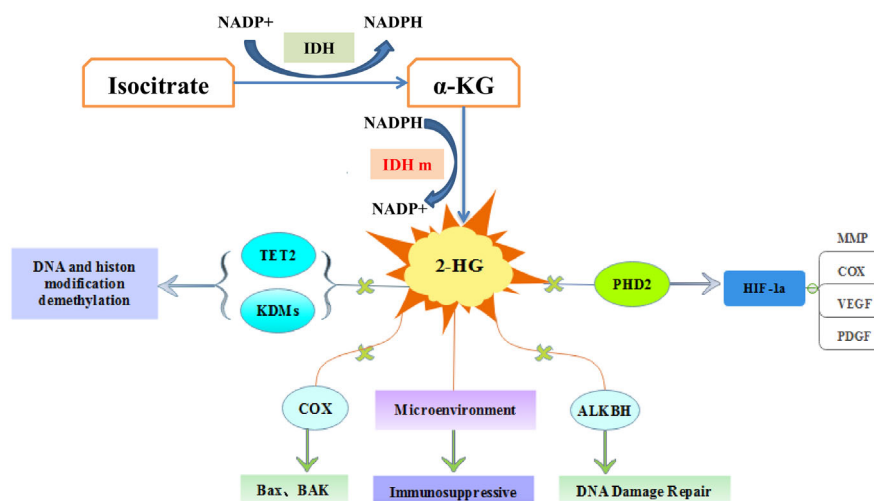


**FIGURE 2 |** The molecular pathways of IDH mutations in tumorigenesis. 2-hydroxyglutarate competitively inhibits multiple  $\alpha$ -ketoglutarate dependent dioxygenases, thereby causing widespread epigenetic changes that result in a global dysregulation of gene expression. 2-HG inhibits prolyl hydroxylases (PHD) and increases HIF-1 $\alpha$  stabilization and result in impairment of collagen maturation. 2-HG can promote apoptosis by inhibiting cytochrome c oxidase (COX), and associate with tumor microenvironment.

dependent manner. Some results suggest that 2-HG induces angiogenesis activity and increases MMP2 activity through VEGFR2 signal (32). The researchers found that 2-HG not only directly regulates a variety of  $\alpha$ -KG-dependent dioxygenases, but also directly inhibits cytochrome c oxidase (COX) in the mitochondrial electron transport chain (ETC). This leads to the activation of pro-apoptotic Bax and BAK, which triggers hypoxia-induced cell death (33). 2-HG released from the microenvironment may also alter the function of non-tumor cells around the tumor, such as neurons and immune cells (34). In fact, there is now direct evidence that 2-HG accumulation plays an immunosuppressive role. In the presence of high levels of 2-HG, the proliferation ability of activated CD4+ and CD8+T cells decreased (35).

## IDH2 MUTATIONS IN HUMAN CANCER

IDH mutations have been detected in multiple tumor types, including various solid tumors and several myeloid malignancies. High frequent mutations in IDH2 have been found in AML, glioma, chondrosarcoma, angioimmunoblastic T cell lymphoma (AITL) and solid papillary carcinoma with reverse polarity (SPCRP), and IDH2 mutations were also reported in other malignant tumors (Table 2, Figure 3).

### AML

Whole-genome sequencing of IDH2 gene mutations have found that the genes encoding epigenetic regulators in AML samples are frequently mutated, about 20% of patients with AML have IDH gene mutations (36, 46). IDH1 and IDH2 mutations occur at comparable frequencies in AML, but no patient had both IDH1 and IDH2 mutations (37). IDH2 mutation has the clinical characteristics of older age, lower white blood cell count; higher platelets and NPM1 mutations in patients with AML (47, 48). In addition, researchers found that R172 IDH2 mutations had potential adverse prognostic significance, and that R172 IDH2 mutations are mutually exclusive with any other prognosis-related mutations. IDH2 mutant AML patients are associated with a resistance to treatment as illustrated by a low rate of CR and a high RR (36, 47). A predictive analysis of the leave-one-out cross-validation further explains this phenomenon (47). The results showed that the genes up-regulated in patients with R172 IDH2 mutation were ID1, ABCB1 and KRAS2 associated with the poor prognosis of AML. The down-regulated genes are KYN1 involved in NAD cofactor biosynthesis, SUCLG2 involved in the Krebs cycle; and CD93 involved in the regulation of phagocytosis and angiogenesis of apoptotic cells. These genomic changes in AML usually have a clear correlation with the clinical diagnosis and prognosis of patients, and are widely used to guide the clinical use of drugs and indicate the prognosis of AML.

With the continuous deepening of understanding of the role of IDH2 mutations and their metabolites in AML, IDH2 inhibitor targeted therapy for AML patients has gradually been applied in clinical practice. Inhibitors of mutant IDH2 may reduce the level of 2-HG to reverse cell differentiation (49),

**TABLE 2 |** IDH2 Mutations in Human Cancer.

Cancer types	Mutation modes	Co-occurring mutations	Detection methods	Refs
AML	R140L	NPM1	Next-generation sequencing	(36)
	R140G	DNMT3A	Gene scan	
	R140Q	SRSF2	Quantitative PCR	
	R140W	FLT3-ITD	Sanger sequencing	
	R172K	ASXL1	Direct sequencing	
	R172S	NRAS		
Glioma	R172W	RUNX1		(37, 38)
	R172G	TP53	Genomewide mutation analysis	
	R172M	PTEN	The direct DNA sequencing	
	R172S	EGFR	Mutation-specific mAbs	
	R172K	CDKN2A		
	R172W	CDKN2B		
DDCHS	R172S	TERT	Sanger sequencing	(39–41)
	R172T	TP53	qPCR genotyping	
	R172G	CDKN2A/2B	MSK-IMPACT sequencing	
	R172M			
AITL	R140G	TET2	Sanger sequencing	(42)
	R172K	DNMT3A	Sequenom	
	R172G			
	R172S			
	R172T			
SPCRP	R172S	TET2	Next-generation sequencing	(43, 44)
	R172T	PIK3CA	Sanger sequencing	
	R172G		SNaPshot genotyping	
	R172I		Whole exome and targeted massively parallel sequencing	
	R172W		Next-generation sequencing	
SNUC	R172M	TP53	Next-generation sequencing	(45)
	R172S	PIK3CA	Sanger sequencing	
	R172T		MSK-IMPACT sequencing	
	R172G			

and indirectly destroy the bone marrow microenvironment induced by 2-HG by blocking the proliferation of AML cells (21). Enasidenib (AG-221) is the first IDH inhibitor approved by the FDA for the treatment of relapsed or refractory acute myeloid leukemia (RR-AML) with IDH2 mutations and achieved good therapeutic effects (50).

### Glioma

Somatic mutations of IDH2 were first discovered in gliomas (51). Gliomas are a large and diverse group of primary brain tumors that include those that are diffusely infiltrative and others that are well-circumscribed and low grade (52). More recently, based on the sequencing results of large samples, it was found that about 60% to 80% of patients with grade II and III gliomas and most patients with secondary glioblastoma (GBM) had somatic mutations encoding isocitrate dehydrogenase genes, mainly IDH1 R132 mutation (53, 54). IDH2 mutations are mutually exclusive with IDH1 mutations, and thus far, have been found rarely (3.3%) in WHO grade II or III gliomas (55) and much rarely (less than 1%) in GBMs (38). In contrast, IDH2 mutations are most common in AML and residue R140, while IDH2 R140 mutations have not been detected in early gliomas or cartilage tumors

The prognostic effect of tumor was related to many factors. The prognosis of gliomas with IDH mutation was better than that of AML with IDH mutation, which is related to the

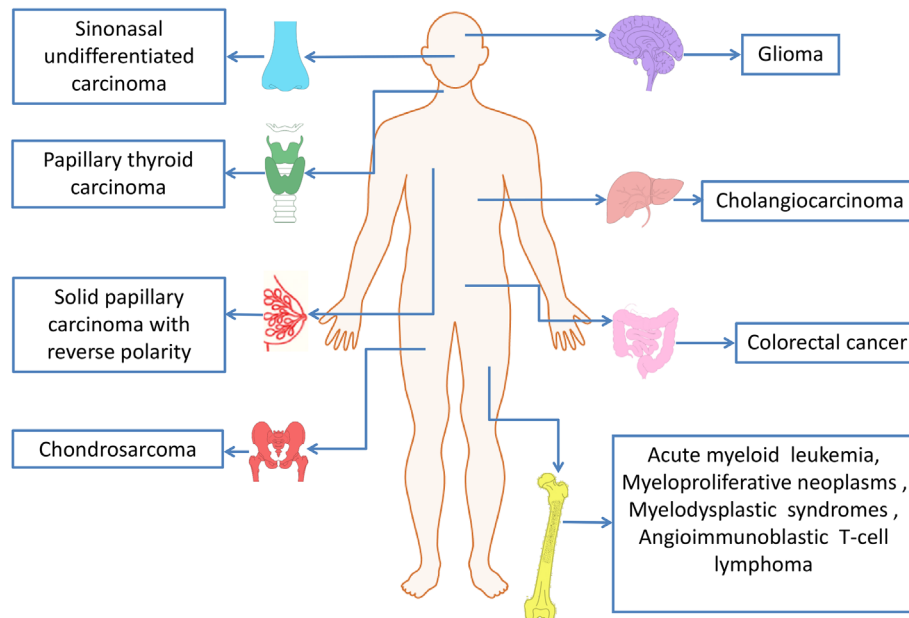


**FIGURE 3** | IDH2 mutations in human cancers.

difference of susceptible mutation sites between the two kinds of tumors. In gliomas, there is a close relationship between grade and prognosis. The latest study found that the prognosis of grade II and grade III was good, while the prognosis of grade IV was controversial (40). At the same time, compared with wild-type IDH tumors, glioma patients with IDH1/2 mutation had better prognosis and better therapeutic effect as they were younger. Neuropathologic assessment of gliomas increasingly relies on ancillary testing of molecular alterations for proper classification and patient management. Lower-grade gliomas with both an IDH mutation (a mutation in either IDH1 or IDH2) and deletion of chromosome arms 1p and 19q (1p/19q codeletion), which occurs most often in oligodendrogliomas, had better responses to radio chemotherapy and were associated with longer survival than diffuse gliomas without these alterations (56). The presence of IDH mutations failed to demonstrate a significant influence on survival in the multivariate analysis of low-grade astrocytomas (LGA) patients. Early RT appears to be beneficial only LGA patients with IDH-mutations (53). Lower-grade gliomas with an IDH mutation either had 1p/19q codeletion or carried TP53 mutation (56). Among patients with IDH mutant gliomas, those in the double-mutant subset had better survival and a lower incidence of malignant degeneration than those in the IDH-only subset (57). Noteworthy, although IDH mutation is associated with longer patient overall survival, IDH mutant accompanied with MGMT methylation subsets consistently showed higher risks of malignant transformation in low-grade glioma, compared to IDH wild type (58).

## Chondrosarcoma

Recently, researchers have discovered IDH2 R140 mutation in three advanced chondrosarcoma samples (59). Patients with

chondrosarcoma carry more than 50% of IDH1/2 mutant heterozygotes (41), and IDH1 R132 is the most common mutation, followed by IDH2 R172. Interestingly, in chondrosarcomas, the frequency of IDH2 mutations increases with grade. IDH2 is present in 22% of high-grade chondrosarcomas and only about 7% in low-grade tumors (59). Therefore, it is worth noting that many studies have suggested that the grade of chondrosarcoma is related to many tumor-related factors. IDH1/2 mutant cells need  $\alpha$ -KG to produce 2-HG, which can be produced by glycolysis and glutamine decomposition (60). A comparative study found that compared with low-grade chondrosarcoma, the expression of glycolysis-related genes is increased, and glutaminase is also high in high-chondrosarcoma, but glutamine degradation has nothing to do with IDH1/2 mutation (61). Hypermethylation of the nicotinic acid phosphoribosyl transferase (NAPRT) promoter was observed in advanced chondrosarcom. TP53 mutates in approximately 30% of chondrosarcomas (62), and this mutation mainly occurs in advanced chondrosarcomas. Some genes encoding energy metabolic components will change with increasing grade, but due to the influence of a series of complex factors, such as tumor type, tumor microenvironment and so on, whether the difference of high-grade chondrosarcoma is related to IDH mutation needs further study.

Dedifferentiated chondrosarcoma (DDCHS) is a kind of high-grade chondrosarcoma, which is transformed from low grade and has strong invasiveness (63). The frequency of IDH2 mutations in dedifferentiated chondrosarcoma is much higher than that of other chondrosarcomas (64). Researchers have found that up to 76% of IDH heterozygous mutations in DDCH, 39.1% of which are IDH2 mutations, 2-HG levels in tumor tissues are significantly higher than normal tissues (64). Given the high incidence of IDH2

mutations in DDCHS, IDH2 can be used as a diagnostic marker for DDCHS. And the distinction between DDCHS and osteosarcoma is very important for clinical treatment, IDH2 mutation analysis can be regarded as a suitable auxiliary test for the diagnosis of DDCHS (63).

Although IDH1 and IDH2 mutations are associated with better OS in glioma patients, it is controversial whether OS has a good correlation with chondrosarcoma patients (65, 66). A recent study showed that the OS of chondrosarcoma patients with IDH2 mutation was significantly shorter than that of patients without mutation. IDH mutation status is not related to overall survival, but IDH2 mutation is associated with longer recurrence-free survival (RFS) and metastasis-free survival (MFS) in high-grade chondrosarcomas (41). The coexistence of TERT mutations, CDKN2A/2B and TP53 changes in high-grade chondrosarcomas may explain this phenomenon (41).

### Angioimmunoblastic T-Cell Lymphoma (AITL)

AITL is a subtype of PTCL, which is characterized by high frequency of epigenetic factor overlap mutation and poor prognosis (67). TET2, RHOA, IDH2 R172 and DNMT3A are widespread genetic damages in AITL, in which the mutation rate of TET2 is the highest, and IDH2 R172 mutation can be different from other entities of PTCL (42). At present, there are only IDH2 R172 heterozygous mutations in AITL, and there are no other IDH mutants. Recently, IDH2 R172 mutations are described in AITL, and the prevalence rate is about 20%-45% (68). Sanger sequencing was used to detect mutations in all exons, and the mutation spectrum showed that IDH2 mutations at R172 were R172K, R172S, R172T and R172G (69). In patients with IDH2 mutated angioimmunoblastic T-cell lymphoma, the levels of intracellular and plasma 2-HG were not the same thing, and the level of intracellular 2-HG was higher than that in plasma (70). Some studies have provided another evidence for this: the R172 mutation in IDH2 has a greater ability to produce 2-HG in lymphoid cells and can damage the development of lymphoid cells, which may explain the advantage of this mutation in AITL (71). In addition, RHOAG17V and TET2 mutations coexist frequently in AITL patients with IDH2 mutations, suggesting that multiple mutations may work together to drive the transformation of this cell type (43). The overlapping mutations of epigenetic factors may be closely related to the poor prognosis of AITL. Further study of the combined effect of TET2, IDH2 and RHOA mutations may be more beneficial to the treatment of AITL patients.

### Solid Papillary Carcinoma With Reverse Polarity (SPCRP)

SPCRP, also known as resembling the tall cell variant of papillary thyroid neoplasms (BPTC), is a rare breast cancer subtype with unusual histopathological features (44). SPCRP are uniquely characterized by harbor recurrent IDH2 R172 hotspot mutations or TET2 mutations, and IDH2 R172 hotspot mutations often in combination with mutations in PI3K pathway genes, in particular in the form of PIK3CA hotspot mutations. Studies have shown that IDH2 R172 hotspot mutations coexisted with PIK3CA mutations in 50% of cases (72). IDH2 R172 mutations

in solid papillary carcinoma with reverse polarity most of which are in the form of R172S or R172T mutations, IDH2 R172G, R172I and R172W mutations have also been identified.

Through immunohistochemical characterization, Complete exon group (WES), targeting and Sanger sequencing of 13 SPCRP, 10 SPCRP were found to have hot spot mutations at R172 of IDH2, of which 8 SPCRP showed pathogenic mutations affecting PIK3CA or PIK3R1, and one IDH2 wild type SPCRP contained TET2Q548 truncated mutation and PIK3CA H1047R hot spot mutation. At the same time, functional studies also showed that a high concentration of 2-HG was detected in the SPCRP with IDH2 mutation, and global DNA hypermethylation and H3K27 trimethylation were observed in the SPCRP with IDH1/IDH2 mutations (72), which was consistent with the cancer characteristics of IDH1/IDH2 mutation. There was research reported that researchers sequenced the whole exon of 9 cases of SPCRP and used IDH1/IDH2 mutant (R132/R172) antibody in resected specimens for immunohistochemical analysis (73). At present, the main detection methods of IDH mutation gene are immunohistochemical detection and gene sequencing. SPCRP with IDH2 R172 hot spot mutation can be detected with high sensitivity and specificity by immunohistochemical staining with monoclonal antibody against IDH2 R172 mutation (74, 75). In view of the development of IDH2 mutation inhibitors, IDH2 mutations in SPCRP may become a new target for breast cancer treatment and intervention.

### Other Cancers

In addition to the above tumors, IDH2 mutations in sinonasal undifferentiated carcinoma (SNUC) are also common, with a mutation rate of about 48-82.4% (45, 75). The currently reported mutation is the R172 mutation, and no R140 mutation has been found. TP53 and PI3K mutations in cancer patients with IDH2 mutations are a common phenomenon. Although IDH2-mutated SNUC were associated with a trend of improved free survival and overall survival, such trend did not reach significant level (75).

IDH2 mutations have been reported in cholangiocarcinoma, an aggressive cancer associated with epithelial cells lining the bile duct. IDH2-R172K mutations in adult hepatocytes can cause the production of 2-HG and create a transformable pre-tumor state through other carcinogenic changes. The expression of IDH2 R172K is negatively correlated with OS, which is specifically expressed as a precursor oval cell population expansion and multistage intrahepatic cholangiocarcinoma (IHCC) (39). In addition, in patients with IDH1/2 mutant IHCC, the circulating level of 2-HG is directly related to tumor burden (76). IDH2 mutations in lower frequencies have also been identified in other malignant tumors, including myeloproliferative neoplasms (MPN) and myelodysplastic syndromes (MDS) (77).

Although IDH2 mutation sites were not found in some cancers, the levels of some landmark metabolites changed significantly after IDH2 overexpression. Some results demonstrate the potential role of IDH2 in the biological mechanisms and progression and also indicate IDH2 as



oncogene. Clinical specimens and cell experiments of papillary thyroid carcinoma provide effective evidence for this (78). IDH2 is associated with the occurrence and prognosis of gastric cancer (79). It was found that the expression level of IDH2 in gastric cancer was significantly decreased, and the low expression level of IDH2 was significantly correlated with the survival rate of patients with gastric cancer. The overexpression of IDH2 can increase the level of 5hMC in gastric cancer cells, while the low expression of IDH2 may lead to the depletion of 5hMC in gastric cancer cells. The down-regulation of IDH2 inhibited the growth and movement of gastric cancer cells. This phenomenon suggests that IDH2 plays a carcinogenic role in gastric cancer cells, which is similar to the effect of IDH2 on low-grade gliomas.

## IDH2 MUTANT INHIBITORS

In view of the important roles of mutant IDH1, IDH2 and their products in tumorigenesis and progression, another strategy of tumor therapy is to target mutant enzymes and products. In the past few years, a variety of IDH mutant enzyme inhibitors have been developed, including one PAN inhibitor and several inhibitors targeting specific IDH mutant subtypes (Table 3). A large number of preclinical studies have shown that IDH mutant inhibitors can significantly reduce the level of 2-HG and have great effects on cell metabolism, growth and tumorigenicity. For many of these inhibitors, the eutectic structure of enzyme-binding inhibitors has been determined by X-ray crystallography, and their

inhibition mechanism has been elucidated at the molecular level. Most inhibitors regulate the activity of the enzyme through allostery, rather than competing for the binding of the substrate and the active site. Several of them have been used in clinical trials, and Enasidenib (AG-221) and Ivosidenib (AG-120) have been approved by FDA for human cancer treatment (Table 3).

### AG-221

AG-221 has been approved by FDA for the treatment of RR-AML with IDH2 mutations. AG-221 was obtained through high-throughput screening and chemical structure optimization (80). Its precursor form is a triazine compound (Figure 4). After a series of chemical modification steps, the oral bioavailability, solubility and clearance rate of the precursor were optimized, and AG-221 which can be used in clinical development was obtained (81). Initial preclinical studies have shown that AG-221 can reduce the secretion of 2-HG in IDH2 R140Q mutant cells, thereby inhibiting cell proliferation, inducing cell differentiation (82), reversing histone hypermethylation associated with IDH2 mutations. In vivo experiments, oral administration of AG-221 can significantly improve the survival rate of nude mice. Based on the good preclinical results of AG-221, the clinical trial of AG-221 started quickly. In clinical trials, AG-221 has been used in patients with advanced hematological malignant tumors and known IDH2 mutations, and clinical trials have been conducted to test the safety and effectiveness of AG-221 (50, 83). The plasma concentration of AG-221 was stable, and the content of 2-HG decreased most significantly when the dose was

**TABLE 3 |** Development of IDH Mutant Inhibitors for Cancer Treatment.

Inhibitors	Targets	Cancers with IDH mutation	R & D status	Clinical trial identifiers
<b>AG-221</b> (FDA approved)	IDH2 mutant	Glioma	Phase 1/2	NCT02273739
		Angioimmunoblastic T-cell lymphoma	Phase 1/2	NCT02273739
		Cholangiocarcinoma	Phase 1/2	NCT02273739
		Chondrosarcoma	Phase 1/2	NCT02273739
		MDS	Phase 3	NCT03839771
<b>AG-120</b> (FDA approved)	IDH1 mutant	AML	Phase 3	NCT03839771
		AML	Phase 3	NCT03839771
		Glioma	Phase 2	NCT04056910
		Chondrosarcoma	Phase 2	NCT04278781
		MDS	Phase 2	NCT04044209
<b>AG-881</b>	IDH1/IDH2 mutant	Chondrosarcoma	Phase 2	NCT04278781
		Cholangiocarcinoma	Phase 3	NCT02989857
		AML	Phase 1	NCT02492737
		Glioma	Phase 3	NCT04164901
		AML	Phase 1	NCT02826642
<b>IDH305</b>	IDH1 mutant	Glioma	Phase 2	NCT02977689
		MDS	Phase 1	NCT02381886
		Solid Tumors	Phase 1	NCT02746081
<b>BAY1436032</b>	IDH1 mutant	AML	Phase 1	NCT03127735
		AML	Phase 1/2	NCT04013880
		MDS	Phase 1/2	NCT04013880
<b>FT-2102</b>	IDH1 mutant	Glioma	Phase 1/2	NCT03684811
		Chondrosarcoma	Phase 1/2	NCT03684811
		Glioma	Preclinical	/
<b>AGI-5198</b>	IDH1 mutant	Glioma	Preclinical	/
<b>AGI-6780</b>	IDH2 mutant	AML	Preclinical	/
<b>MRK-A</b>	IDH1 mutant	Glioma	Preclinical	/
<b>GSK321</b>	IDH1 mutant	AML	Preclinical	/
<b>GSK864</b>	IDH1 mutant	AML	Preclinical	/
		Glioma		

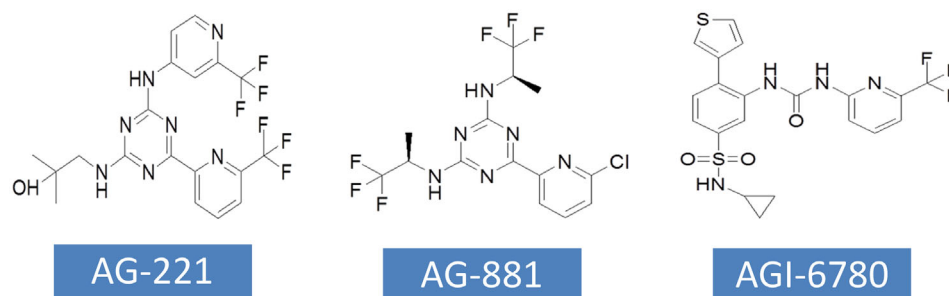


**FIGURE 4** | The chemical structures of currently developed inhibitors targeting IDH2 mutations.

100mg-d-1. The median survival time of refractory recurrent acute myeloid leukemia was 9.3 months, and the median survival time of patients with complete remission and partial remission after AG-221 was 19.7 months and 14.4 months, respectively. The study by Amatangelo et al. have shown that myeloblast differentiation, neutrophil recovery and platelet recovery are obvious in AML patients treated with IDH mutation inhibitors (83). The reduction of 2-HG level eliminates the obstacle of myeloid differentiation and promotes the differentiation of primordial cells expressing mutations (84).

It has been recently reported that in a small number of patients with recurrent or refractory AML, treatment with mutant IDH1 or mutant IDH2 inhibitors may lead to clinical differentiation syndrome, which is characterized by leukocytosis and exuberant neutrophil recovery. In addition, the most common treatment-related adverse events were indirect hyperbilirubinemia and nausea, and differentiation syndrome associated with IDH inhibitors was one of the most common highly adverse events (85). These findings suggest that clinicians must be aware that mutated IDH inhibitors may cause complications such as differentiation syndrome in AML patients. Since Enasidenib received approval for AML indications for recurrent/refractory IDH2 mutations in 2017, there have been many clinical trials investigating the efficacy of mutant IDH2 inhibitors (mainly Enasidenib) in different AML subtypes and solid tumors (Table 3). The combination of AG-221 and other inhibitors has become one of the main research directions.

### AG-881

AG-881 is the first PAN inhibitor developed by Celgene in cooperation with Agios Pharmaceuticals (86) (Figure 4). AG-881 is a small molecular inhibitor of IDH1 and IDH2 mutations, oral administration can reduce the formation of tumor metabolite 2-HG. At present, there are two mechanisms of AG-881 inhibition. One inhibition mechanism is that the triazine part of AG-881 can effectively inhibit the allosteric activity of the enzyme, and crystallographic studies have shown that AG-881 binds to the allosteric pocket of the two enzymes and locks the enzyme in an inactive conformation (86). Another inhibition mechanism is the direct interaction between mutant IDH1 inhibitors and Asp279, and the binding of compounds

prevents the catalytic active conformation of Mg/Mn<sup>2+</sup> binding with Asp279 from playing a role. Interestingly, the effects of AG-881 on these two mutations are different. Existing studies have confirmed that the binding of AG-881 to IDH1 mutant is more effective than the interaction between AG-881 and IDH2 mutant, especially with IDH1 R132H (87). In preclinical studies, primary human AML cells treated with AG-881 *in vitro* can induce myeloid differentiation, and it also shows good blood-brain barrier penetration in rodents. Currently, AG-881 is conducting a phase I clinical study in patients with advanced solid tumors and advanced hematological malignant tumors in muIDH1/2.

### AGI-6780

AGI-6780 is a urea sulfonamide inhibitor obtained by high-throughput screening and drug design (88). It has been found that AGI-6780 is an allosteric inhibitor, which binds to the substrate noncompetitively and plays a role at the dimer interface, which can effectively and selectively inhibit IDH2 R140Q mutation (88). At present, the research on the biological effects of AGI-6780 is limited to the environment related to acute myeloid leukemia (89). There are two confirmed mechanisms for AGI-6780: one is to induce the differentiation of TF-1 erythroleukemia cells and primary human AML cells, and the other is to reverse the hypermethylation of DNA and histones induced by 2-HG (49). Although AGI-6780 was developed early, its functions are limited.

Additionally, the potential drug side effects and treatment resistance has promoted the production of novel IDH2 mutant inhibitors with specific targeting and improved selectivity. Gao et al. reported TQ05310 as mutant IDH2 inhibitor targeting both IDH2 R140Q and IDH2 R172K mutants, and found that TQ05310 inhibited mutant IDH2 enzymatic activity, suppressed 2-HG production and induced differentiation in cells expressing IDH2 R140Q and IDH2 R172K, but not in cells expressing wild-type IDH1/2 or mutant IDH1. TQ05310 also had favorable pharmacokinetic characteristics in a tumor xenografts model (90). A heterocyclic urea amide compound, CP-17, was identified as a potent inhibitor of IDH2 R140Q mutant by *in silico* screening and enzymatic assay, exhibited excellent inhibitory activity against IDH2 R140Q and showed dramatic improvement over previously developed inhibitors

such as AGI-6780 and AG-221. Cellular assay results demonstrated that CP-17 inhibited intracellular 2-HG production and suppressed the proliferation of TF-1 erythroleukemia cells carrying IDH2 R140Q mutant (91). Li and colleagues designed and synthesized a series of novel 2-arylbenzimidazoles and evaluated their inhibitory activity against IDH2 R140Q mutant. The preliminary results indicated that four compounds 7b, 7c, 7m and 7r displayed the potent inhibitory activity against IDH2 R140Q mutant. Among them, compound 7c showed the highest inhibitory activity, which was more active than positive control AG-221, according to the IC<sub>50</sub> values (92). These selective IDH2 mutant inhibitors will provide promising candidates for the clinical development of IDH2-targeted drugs.

## CONCLUSION

A number of studies have provided strong evidence for the carcinogenic potential of IDH2 mutations, leading to the production of tumor metabolite 2-HG, which changes epigenetic regulation, cancer cell differentiation and cell metabolism. In addition, the mutation status of IDH2 genes is associated with the prognosis of tumor patients. Preclinical studies *in vitro* and *in vivo* have shown that inhibition of mutated IDH2 enzyme can reduce the level of intracellular 2-HG, reverse the loss of epigenetic control, and release the differentiation block of cancer cells. More importantly, the selective IDH2 mutant inhibitor AG-221 has achieved promising results in clinical practice. Therefore, further study on the biological roles of IDH2 mutations in tumorigenesis and development of potent IDH2 mutant inhibitors will improve the clinical treatment of certain cancer types.

## REFERENCES

- Hanahan D, Weinberg RA. Hallmarks of Cancer: The Next Generation. *Cell* (2011) 144(5):646–74. doi: 10.1016/j.cell.2011.02.013
- Nagarajan A, Malvi P, Wajapeyee N. Oncogene-Directed Alterations in Cancer Cell Metabolism. *Trends Cancer* (2016) 2(7):365–77. doi: 10.1016/j.trecan.2016.06.002
- Martinez-Outschoorn UE, Peiris-Pagès M, Pestell RG, Sotgia F, Lisanti MP. Cancer Metabolism: A Therapeutic Perspective. *Nat Rev Clin Oncol* (2017) 14(1):11–31. doi: 10.1038/nrclinonc.2016.60
- Nowicki S, Gottlieb E. Oncometabolites: Tailoring Our Genes. *FEBS J* (2015) 282(15):2796–805. doi: 10.1111/febs.13295
- Bhargava R, Florea AV, Pelmus M, Jones MW, Bonaventura M, Wald A, et al. Breast Tumor Resembling Tall Cell Variant of Papillary Thyroid Carcinoma: A Solid Papillary Neoplasm With Characteristic Immunohistochemical Profile and Few Recurrent Mutations. *Am J Clin Pathol* (2017) 147(4):399–410. doi: 10.1093/ajcp/aqx016
- Ward PS, Patel J, Wise DR, Abdel-Wahab O, Bennett BD, Collier HA, et al. The Common Feature of Leukemia-Associated IDH1 and IDH2 Mutations is a Neomorphic Enzyme Activity Converting Alpha-Ketoglutarate to 2-Hydroxyglutarate. *Cancer Cell* (2010) 17(3):225–34. doi: 10.1016/j.ccr.2010.01.020
- Kotredes KP, Razmpour R, Lutton E, Alfonso-Prieto M, Ramirez SH, Gamero AM. Characterization of Cancer-Associated IDH2 Mutations That Differ in Tumorigenicity, Chemosensitivity and 2-Hydroxyglutarate Production. *Oncotarget* (2019) 10(28):2675–92. doi: 10.18632/oncotarget.26848
- Li L, Hu X, Eid JE, Rosenberg AE, Wilky BA, Ban Y, et al. Mutant IDH1 Depletion Downregulates Integrins and Impairs Chondrosarcoma Growth. *Cancers (Basel)* (2020) 12(1):141. doi: 10.3390/cancers12010141
- Evans B, Griner E. Registered Report: Oncometabolite 2-Hydroxyglutarate is a Competitive Inhibitor of  $\alpha$ -Ketoglutarate-Dependent Dioxygenases. *Elife* (2015) 4:e07420. doi: 10.7554/eLife.07420
- Cho YS, Levell JR, Liu G, Caferro T, Sutton J, Shafer CM, et al. Discovery and Evaluation of Clinical Candidate IDH305, a Brain Penetrant Mutant IDH1 Inhibitor. *ACS Med Chem Lett* (2017) 8(10):1116–21. doi: 10.1021/acsmchemlett.7b00342
- Kim ES. Enasidenib: First Global Approval. *Drugs* (2017) 77(15):1705–11. doi: 10.1007/s40265-017-0813-2
- Lowery MA, Burris HA, Janku F, RT S, JM C, NS A, et al. Safety and Activity of Ivosidenib in Patients With IDH1-Mutant Advanced Cholangiocarcinoma: A Phase 1 Study. *Lancet Gastroenterol Hepatol* (2019) 4(9):711–20. doi: 10.1016/S2468-1253(19)30189-X
- Xu Y, Liu L, Nakamura A, Someya S, Miyakawa T, Tanokura M. Studies on the Regulatory Mechanism of Isocitrate Dehydrogenase 2 Using Acetylation Mimics. *Sci Rep* (2017) 7(1):9785. doi: 10.1038/s41598-017-10337-7
- Dang L, Jin S, Su SM. IDH Mutations in Glioma and Acute Myeloid Leukemia. *Trends Mol Med* (2010) 16(9):387–97. doi: 10.1016/j.molmed.2010.07.002
- Bzymek KP, Colman RF. Role of Alpha-Asp181, Beta-Asp192, and Gamma-Asp190 in the Distinctive Subunits of Human NAD-Specific Isocitrate Dehydrogenase. *Biochemistry* (2007) 46(18):5391–7. doi: 10.1021/bi700061t
- Zhang C, Moore LM, Li X, Yung WK, Zhang W. IDH1/2 Mutations Target a Key Hallmark of Cancer by Deregulating Cellular Metabolism in Glioma. *Neuro Oncol* (2013) 15(9):1114–26. doi: 10.1093/neuonc/not087
- Zdzisińska B, Żurek A, Kandefers-Szerszeń M. Alpha-Ketoglutarate as a Molecule With Pleiotropic Activity: Well-Known and Novel Possibilities of

## AUTHOR CONTRIBUTIONS

This review was designed by YZ and JG. The original manuscript was written by JG. The data was analyzed by RZ and ZY. ZD, DY and YZ are responsible for supervising and revising the manuscript. Funding was obtained by YZ and DY. All authors contributed to the article and approved the submitted version.

## FUNDING

This work was supported by the National Natural Science Foundation of China (No.: 81402266), Henan Scientific and Technological Research Projects (No.: 202102310044), the Outstanding Young Talent project of Scientific and Technological Innovation in Henan Health (No.: YXKC2020032), and the Medical Science and Technology Research Projects of Henan Province (No.: SBGJ202002082). Support has also been provided by the Clinical Pharmacy Branch of Chinese Medical Association-Wu Jieping Medical Foundation (No.: 320.6750.19090-3), Bethune exploration Project in Pharmaceutical Research (B-19-H-20200622), the International Talent Cooperation Project of Henan Province (No.: GH2019015), Major Scientific Research Projects of Traditional Chinese Medicine in Henan Province (No.20-21ZYZD14), and Cultivation of Young and Middle-aged Health Science and Technology Innovation Leading Talents in Henan Province (YXKC2020015).

## ACKNOWLEDGMENTS

We thank all the participants who were involved in this study.

- Therapeutic Use. *Arch Immunol Ther Exp (Warsz)* (2017) 65(1):21–36. doi: 10.1007/s00005-016-0406-x
18. Koh HJ, Lee SM, Son BG, Lee SH, Ryoo ZY, Chang KT, et al. Cytosolic NADP +-Dependent Isocitrate Dehydrogenase Plays a Key Role in Lipid Metabolism. *J Biol Chem* (2004) 279(38):39968–74. doi: 10.1074/jbc.M402260200
  19. Zeng L, Morinibu A, Kobayashi M, Zhu Y, Wang X, Goto Y, et al. Aberrant IDH3 $\alpha$  Expression Promotes Malignant Tumor Growth by Inducing HIF-1-Mediated Metabolic Reprogramming and Angiogenesis. *Oncogene* (2015) 34(36):4758–66. doi: 10.1038/onc.2014.411
  20. Parsons DW, Jones S, Zhang X, Lin JC, Leary RJ, Angenendt P, et al. An Integrated Genomic Analysis of Human Glioblastoma Multiforme. *Science* (2008) 321(5897):1807–12. doi: 10.1126/science.1164382
  21. Chen JY, Lai YS, Tsai HJ, Kuo CC, Yen BL, Yeh SP, et al. The Oncometabolite R-2-Hydroxyglutarate Activates NF- $\kappa$ B-Dependent Tumor-Promoting Stromal Niche for Acute Myeloid Leukemia Cells. *Sci Rep* (2016) 6:32428. doi: 10.1038/srep32428
  22. Popovici-Muller J, Saunders JO, Salituro FG, Travins JM, Yan S, Zhao F, et al. Discovery of the First Potent Inhibitors of Mutant IDH1 That Lower Tumor 2-HG in Vivo. *ACS Med Chem Lett* (2012) 3(10):850–5. doi: 10.1021/ml300225h
  23. Dang L, White DW, Gross S, Bennett BD, Bittinger MA, Driggers EM, et al. Cancer-Associated IDH1 Mutations Produce 2-Hydroxyglutarate. *Nature* (2010) 465(7300):966. doi: 10.1038/nature09132
  24. Ragon BK, DiNardo CD. Targeting IDH1 and IDH2 Mutations in Acute Myeloid Leukemia. *Curr Hematol Malign Rep* (2017) 12(6):537–46. doi: 10.1007/s11899-017-0418-6
  25. Xu W, Yang H, Liu Y, Yang Y, Wang P, Kim SH, et al. Oncometabolite 2-Hydroxyglutarate is a Competitive Inhibitor of  $\alpha$ -Ketoglutarate-Dependent Dioxygenases. *Cancer Cell* (2011) 19(1):17–30. doi: 10.1016/j.ccr.2010.12.014
  26. Molenaar RJ, Radivoyevitch T, Maciejewski JP, van Noorden CJ, Bleeker FE. The Driver and Passenger Effects of Isocitrate Dehydrogenase 1 and 2 Mutations in Oncogenesis and Survival Prolongation. *Biochim Biophys Acta* (2014) 1846(2):326–41. doi: 10.1016/j.bbcan.2014.05.004
  27. Ye D, Xiong Y, Guan KL. The Mechanisms of IDH Mutations in Tumorigenesis. *Cell Res* (2012) 22(7):1102–4. doi: 10.1038/cr.2012.51
  28. Figueroa ME, Abdel-Wahab O, Lu C, Ward PS, Patel J, Shih A, et al. Leukemic IDH1 and IDH2 Mutations Result in a Hypermethylation Phenotype, Disrupt TET2 Function, and Impair Hematopoietic Differentiation. *Cancer Cell* (2010) 18(6):553–67. doi: 10.1016/j.ccr.2010.11.015
  29. Chowdhury R, Yeoh KK, Tian YM, Hillringhaus L, Bagg EA, Rose NR, et al. The Oncometabolite 2-Hydroxyglutarate Inhibits Histone Lysine Demethylases. *EMBO Rep* (2011) 12(5):463–9. doi: 10.1038/embor.2011.43
  30. Chen C, Zhou H, Wei F, Jiang L, Liu X, Liu Z, et al. Increased Levels of Hypoxia-Inducible Factor-1 $\alpha$  are Associated With Bcl-XL Expression, Tumor Apoptosis, and Clinical Outcome in Chondrosarcoma. *J Orthop Res* (2011) 29(1):143–51. doi: 10.1002/jor.21193
  31. Bruick RK, McKnight SL. A Conserved Family of Prolyl-4-Hydroxylases That Modify HIF. *Science* (2001) 294(5545):1337–40. doi: 10.1126/science.1066373
  32. Seok J, Yoon SH, Lee SH, Jung JH, Lee YM. The Oncometabolite D-2-Hydroxyglutarate Induces Angiogenic Activity Through the Vascular Endothelial Growth Factor Receptor 2 Signaling Pathway. *Int J Oncol* (2019) 54(2):753–63. doi: 10.3892/ijo.2018.4649
  33. Chan SM, Thomas D, Corces-Zimmerman MR, Xavy S, Rastogi S, Hong WJ, et al. Isocitrate Dehydrogenase 1 and 2 Mutations Induce BCL-2 Dependence in Acute Myeloid Leukemia. *Nat Med* (2015) 21(2):178–84. doi: 10.1038/nm.3788
  34. Picca A, Berzoro G, Di Stefano AL, Sanson M. The Clinical Use of IDH1 and IDH2 Mutations in Gliomas. *Expert Rev Mol Diagn* (2018) 18(12):1041–51. doi: 10.1080/14737159.2018.1548935
  35. Zhang L, Sorensen MD, Kristensen BW, Reifemberger G, McIntyre TM, Lin F. D-2-Hydroxyglutarate is an Intercellular Mediator in IDH-Mutant Gliomas Inhibiting Complement and T Cells. *Clin Cancer Res* (2018) 24(21):5381–91. doi: 10.1158/1078-0432.CCR-17-3855
  36. Boissel N, Nibourel O, Renneville A, Gardin C, Reman O, Contentin N, et al. Prognostic Impact of Isocitrate Dehydrogenase Enzyme Isoforms 1 and 2 Mutations in Acute Myeloid Leukemia: A Study by the Acute Leukemia French Association Group. *J Clin Oncol* (2010) 28(23):3717–23. doi: 10.1200/JCO.2010.28.2285
  37. Im AP, Sehgal AR, Carroll MP, Smith BD, Tefferi A, Johnson DE, et al. DNMT3A and IDH Mutations in Acute Myeloid Leukemia and Other Myeloid Malignancies: Associations With Prognosis and Potential Treatment Strategies. *Leukemia* (2014) 28(9):1774–83. doi: 10.1038/leu.2014.124
  38. Stancheva G, Goranova T, Laleva M, Kamenova M, Mitkova A, Velinov N, et al. IDH1/IDH2 But Not TP53 Mutations Predict Prognosis in Bulgarian Glioblastoma Patients. *BioMed Res Int* (2014) 2014:654727. doi: 10.1155/2014/654727
  39. Saha SK, Parachoniak CA, Ghanta KS, Fitamant J, Ross KN, Najem MS, et al. Mutant IDH Inhibits HNF-4 $\alpha$  to Block Hepatocyte Differentiation and Promote Biliary Cancer. *Nature* (2014) 513(7516):110–4. doi: 10.1038/nature13441
  40. Eckel-Passow JE, Lachance DH, Molinaro AM, Walsh KM, Decker PA, Sicotte H, et al. Glioma Groups Based on 1p/19q, IDH, and TERT Promoter Mutations in Tumors. *N Engl J Med* (2015) 372(26):2499–508. doi: 10.1056/NEJMoa1407279
  41. Zhu GG, Nafa K, Agaram N, Zehir A, Benayed R, Sadowska J, et al. Genomic Profiling Identifies Association of IDH1/IDH2 Mutation With Longer Relapse-Free and Metastasis-Free Survival in High-Grade Chondrosarcoma. *Clin Cancer Res* (2020) 26(2):419–27. doi: 10.1158/1078-0432.CCR-18-4212
  42. Odejide O, Weigert O, Lane AA, Toscano D, Lunning MA, Kopp N, et al. A Targeted Mutational Landscape of Angioimmunoblastic T-Cell Lymphoma. *Blood* (2014) 123(9):1293–6. doi: 10.1182/blood-2013-10-531509
  43. Steinhilber J, Mederake M, Bonzheim I, Serinsöz-Linke E, Müller I, Fallier-Becker P, et al. The Pathological Features of Angioimmunoblastic T-Cell Lymphomas With IDH2(R172) Mutations. *Mod Pathol* (2019) 32(8):1123–34. doi: 10.1038/s41379-019-0254-4
  44. Zhong E, Scognamiglio T, D'Alfonso T, Song W, Tran H, Baek I, et al. Breast Tumor Resembling the Tall Cell Variant of Papillary Thyroid Carcinoma: Molecular Characterization by Next-Generation Sequencing and Histopathological Comparison With Tall Cell Papillary Carcinoma of Thyroid. *Int J Surg Pathol* (2019) 27(2):134–41. doi: 10.1177/1066896918800779
  45. Mito JK, Bishop JA, Sadow PM, Stelow EB, Faquin WC, Mills SE, et al. Immunohistochemical Detection and Molecular Characterization of IDH-Mutant Sinusoidal Undifferentiated Carcinomas. *Am J Surg Pathol* (2018) 42(8):1067–75. doi: 10.1097/PAS.0000000000001064
  46. Meggendorfer M, Cappelli LV, Walter W, Haferlach C, Kern W, Falini B, et al. IDH1R132, IDH2R140 and IDH2R172 in AML: Different Genetic Landscapes Correlate With Outcome and May Influence Targeted Treatment Strategies. *Leukemia* (2018) 32(5):1249–53. doi: 10.1038/s41375-018-0026-z
  47. Marcucci G, Maharry K, Wu YZ, Radmacher MD, Mrózek K, Margeson D, et al. IDH1 and IDH2 Gene Mutations Identify Novel Molecular Subsets Within De Novo Cytogenetically Normal Acute Myeloid Leukemia: A Cancer and Leukemia Group B Study. *J Clin Oncol* (2010) 28(14):2348–55. doi: 10.1200/JCO.2009.27.3730
  48. Paschka P, Schlenk RF, Gaidzik VI, Habdank M, Krönke J, Bullinger L, et al. IDH1 and IDH2 Mutations are Frequent Genetic Alterations in Acute Myeloid Leukemia and Confer Adverse Prognosis in Cytogenetically Normal Acute Myeloid Leukemia With NPM1 Mutation Without FLT3 Internal Tandem Duplication. *J Clin Oncol* (2010) 28(22):3636–43. doi: 10.1200/JCO.2010.28.3762
  49. Wang F, Travins J, DeLaBarre B, Penard-Lacronique V, Schalm S, Hansen E, et al. Targeted Inhibition of Mutant IDH2 in Leukemia Cells Induces Cellular Differentiation. *Science* (2013) 340(6132):622–6. doi: 10.1126/science.1234769
  50. Stein EM. Enasidenib, a Targeted Inhibitor of Mutant IDH2 Proteins for Treatment of Relapsed or Refractory Acute Myeloid Leukemia. *Future Oncol* (2018) 14(1):23–40. doi: 10.2217/fon-2017-0392
  51. Yan H, Parsons DW, Jin G, McLendon R, Rasheed BA, Yuan W, et al. IDH1 and IDH2 Mutations in Gliomas. *N Engl J Med* (2009) 360(8):765–73. doi: 10.1056/NEJMoa0808710
  52. Amary MF, Bacci K, Maggiani F, Damato S, Halai D, Berisha F, et al. IDH1 and IDH2 Mutations are Frequent Events in Central Chondrosarcoma and Central and Periosteal Chondromas But Not in Other Mesenchymal Tumours. *J Pathol* (2011) 224(3):334–43. doi: 10.1002/path.2913
  53. Juratli TA, Kirsch M, Robel K, Soucek S, Geiger K, von Kummer R, et al. IDH Mutations as an Early and Consistent Marker in Low-Grade Astrocytomas



- WHO Grade II and Their Consecutive Secondary High-Grade Gliomas. *J Neurooncol* (2012) 108(3):403–10. doi: 10.1007/s11060-012-0844-1
54. Kato Y. Specific Monoclonal Antibodies Against IDH1/2 Mutations as Diagnostic Tools for Gliomas. *Brain Tumor Pathol* (2015) 32(1):3–11. doi: 10.1007/s10014-014-0202-4
  55. Fathi AT, Nahed BV, Wander SA, Iafraite AJ, Borger DR, Hu R, et al. Elevation of Urinary 2-Hydroxyglutarate in IDH-Mutant Glioma. *Oncologist* (2016) 21(2):214–9. doi: 10.1634/theoncologist.2015-0342
  56. Brat DJ, Verhaak RG, Aldape KD, Yung WK, Salama SR, Cooper LA, et al. Comprehensive, Integrative Genomic Analysis of Diffuse Lower-Grade Gliomas. *N Engl J Med* (2015) 372(26):2481–98. doi: 10.1056/NEJMoa1402121
  57. Akcyerli CB, Yüksel Ş, Can Ö, Erson-Omay EZ, Oktay Y, Coşgun E, et al. Use of Telomerase Promoter Mutations to Mark Specific Molecular Subsets With Reciprocal Clinical Behavior in IDH Mutant and IDH Wild-Type Diffuse Gliomas. *J Neurosurg* (2018) 128(4):1102–14. doi: 10.3171/2016.11.JNS16973
  58. Leu S, von Felten S, Frank S, Boulay JL, Mariani L. IDH Mutation is Associated With Higher Risk of Malignant Transformation in Low-Grade Glioma. *J Neurooncol* (2016) 127(2):363–72. doi: 10.1007/s11060-015-2048-y
  59. Lugowska I, Tetrycz P, Mikula M, Kulecka M, Kluska A, Balabas A, et al. IDH1/2 Mutations Predict Shorter Survival in Chondrosarcoma. *J Cancer* (2018) 9(6):998–1005. doi: 10.7150/jca.22915
  60. Rozeman LB, Hameetman L, van Wezel T, Taminiau AH, Cleton-Jansen AM, Hogendoorn PC, et al. Cdna Expression Profiling of Chondrosarcomas: Ollier Disease Resembles Solitary Tumours and Alteration in Genes Coding for Components of Energy Metabolism Occurs With Increasing Grade. *J Pathol* (2005) 207(1):61–71. doi: 10.1002/path.1813
  61. Peterse EFP, Niessen B, Addie RD, de Jong Y, Cleven AHG, Kruisselbrink AB, et al. Targeting Glutaminolysis in Chondrosarcoma in Context of the IDH1/2 Mutation. *Br J Cancer* (2018) 118(8):1074–83. doi: 10.1038/s41416-018-0050-9
  62. Nazeri E, Gouran Savadkoobi M, Majidzadeh AK, Esmaeili R. Chondrosarcoma: An Overview of Clinical Behavior, Molecular Mechanisms Mediated Drug Resistance and Potential Therapeutic Targets. *Crit Rev Oncol Hematol* (2018) 131:102–9. doi: 10.1016/j.critrevonc.2018.09.001
  63. Chen S, Fritchie K, Wei S, Ali N, Curless K, Shen T, et al. Diagnostic Utility of IDH1/2 Mutations to Distinguish Dedifferentiated Chondrosarcoma From Undifferentiated Pleomorphic Sarcoma of Bone. *Hum Pathol* (2017) 65:239–46. doi: 10.1016/j.humpath.2017.05.015
  64. Mohammad N, Wong D, Lum A, Lin J, Ho J, Lee CH, et al. Characterisation of Isocitrate Dehydrogenase 1/Isocitrate Dehydrogenase 2 Gene Mutation and the D-2-Hydroxyglutarate Oncometabolite Level in Dedifferentiated Chondrosarcoma. *Histopathology* (2020) 76(5):722–30. doi: 10.1111/his.14018
  65. Christians A, Adel-Horowski A, Banan R, Lehmann U, Bartels S, Behling F, et al. The Prognostic Role of IDH Mutations in Homogeneously Treated Patients With Anaplastic Astrocytomas and Glioblastomas. *Acta Neuropathol Commun* (2019) 7(1):156. doi: 10.1186/s40478-019-0817-0
  66. Cleven AHG, Suijker J, Agrogianis G, Braire-de Bruijn IH, Frizzell N, Hoekstra AS, et al. IDH1 or -2 Mutations Do Not Predict Outcome and Do Not Cause Loss of 5-Hydroxymethylcytosine or Altered Histone Modifications in Central Chondrosarcomas. *Clin Sarcoma Res* (2017) 7:8. doi: 10.1186/s13569-017-0074-6
  67. de Leval L, Gisselbrecht C, Gaulard P. Advances in the Understanding and Management of Angioimmunoblastic T-Cell Lymphoma. *Br J Haematol* (2010) 148(5):673–89. doi: 10.1111/j.1365-2141.2009.08003.x
  68. Fukumoto K, Nguyen TB, Chiba S, Sakata-Yanagimoto M. Review of the Biologic and Clinical Significance of Genetic Mutations in Angioimmunoblastic T-Cell Lymphoma. *Cancer Sci* (2018) 109(3):490–6. doi: 10.1111/cas.13393
  69. Cairns RA, Iqbal J, Lemonnier F, Kucuk C, de Leval L, Jais JP, et al. IDH2 Mutations are Frequent in Angioimmunoblastic T-Cell Lymphoma. *Blood* (2012) 119(8):1901–3. doi: 10.1182/blood-2011-11-391748
  70. Churchill H, Naina H, Boriack R, Rakheja D, Chen W. Discordant Intracellular and Plasma D-2-Hydroxyglutarate Levels in a Patient With IDH2 Mutated Angioimmunoblastic T-Cell Lymphoma. *Int J Clin Exp Pathol* (2015) 8(9):11753–9.
  71. Lemonnier F, Cairns RA, Inoue S, Li WY, Dupuy A, Broutin S, et al. The IDH2 R172K Mutation Associated With Angioimmunoblastic T-Cell Lymphoma Produces 2HG in T Cells and Impacts Lymphoid Development. *Proc Natl Acad Sci U.S.A.* (2016) 113(52):15084–9. doi: 10.1073/pnas.1617929114
  72. Chiang S, Weigelt B, Wen HC, Pareja F, Raghavendra A, Martelotto LG, et al. IDH2 Mutations Define a Unique Subtype of Breast Cancer With Altered Nuclear Polarity. *Cancer Res* (2016) 76(24):7118–29. doi: 10.1158/0008-5472.CAN-16-0298
  73. Pareja F, da Silva EM, Frosina D, Geyer FC, Lozada JR, Basili T, et al. Immunohistochemical Analysis of IDH2 R172 Hotspot Mutations in Breast Papillary Neoplasms: Applications in the Diagnosis of Tall Cell Carcinoma With Reverse Polarity. *Mod Pathol* (2020) 33(6):1056–64. doi: 10.1038/s41379-019-0442-2
  74. Tang X, Lin CC, Spasojevic I, Iversen ES, Chi JT, Marks JR. A Joint Analysis of Metabolomics and Genetics of Breast Cancer. *Breast Cancer Res* (2014) 16(4):415. doi: 10.1186/s13058-014-0415-9
  75. Dogan S, Chute DJ, Xu B, Ptashkin RN, Chandramohan R, Casanova-Murphy J, et al. Frequent IDH2 R172 Mutations in Undifferentiated and Poorly-Differentiated Sinonasal Carcinomas. *J Pathol* (2017) 242(4):400–8. doi: 10.1002/path.4915
  76. Borger DR, Goyal L, Yau T, Poon RT, Ancukiewicz M, Deshpande V, et al. Circulating Oncometabolite 2-Hydroxyglutarate is a Potential Surrogate Biomarker in Patients With Isocitrate Dehydrogenase-Mutant Intrahepatic Cholangiocarcinoma. *Clin Cancer Res* (2014) 20(7):1884–90. doi: 10.1158/1078-0432.CCR-13-2649
  77. Kosmider O, Gelsi-Boyer V, Slama L, Dreyfus F, Beyne-Rauzy O, Quesnel B, et al. Mutations of IDH1 and IDH2 Genes in Early and Accelerated Phases of Myelodysplastic Syndromes and MDS/Myeloproliferative Neoplasms. *Leukemia* (2010) 24(5):1094–6. doi: 10.1038/leu.2010.52
  78. Zhang J, Hu L, Wang H, Zhi J, Hou X, Wu Y, et al. Functional Analysis and Clinical Significance of the Isocitrate Dehydrogenase 2 Gene in Papillary Thyroid Carcinoma. *Cancer Manag Res* (2019) 11:3765–77. doi: 10.2147/CMAR.S194920
  79. Chou NH, Tsai CY, Tu YT, Wang KC, Kang CH, Chang PM, et al. Isocitrate Dehydrogenase 2 Dysfunction Contributes to 5-Hydroxymethylcytosine Depletion in Gastric Cancer Cells. *Anticancer Res* (2016) 36(8):3983–90.
  80. Kats LM, Reschke M, Taulli R, Pozdnyakova O, Burgess K, Bhargava P, et al. Proto-Oncogenic Role of Mutant IDH2 in Leukemia Initiation and Maintenance. *Cell Stem Cell* (2014) 14(3):329–41. doi: 10.1016/j.stem.2013.12.016
  81. Andronesi OC, Arrillaga-Romany IC, Ly KI, Bogner W, Ratai EM, Reitz K, et al. Pharmacodynamics of Mutant-IDH1 Inhibitors in Glioma Patients Probed by in Vivo 3D MRS Imaging of 2-Hydroxyglutarate. *Nat Commun* (2018) 9(1):1474. doi: 10.1038/s41467-018-03905-6
  82. Yen K, Travins J, Wang F, David MD, Artin E, Straley K, et al. AG-221, a First-in-Class Therapy Targeting Acute Myeloid Leukemia Harboring Oncogenic IDH2 Mutations. *Cancer Discovery* (2017) 7(5):478–93. doi: 10.1158/2159-8290.CD-16-1034
  83. Waitkus MS, DiPlas BH, Yan H. Biological Role and Therapeutic Potential of IDH Mutations in Cancer. *Cancer Cell* (2018) 34(2):186–95. doi: 10.1016/j.ccell.2018.04.011
  84. Golub D, Iyengar N, Dogra S, Wong T, Bready D, Tang K, et al. Mutant Isocitrate Dehydrogenase Inhibitors as Targeted Cancer Therapeutics. *Front Oncol* (2019) 9:417. doi: 10.3389/fonc.2019.00417
  85. Stein EM, DiNardo CD, Pollyea DA, Fathi AT, Roboz GJ, Altman JK, et al. Enasidenib in Mutant IDH2 Relapsed or Refractory Acute Myeloid Leukemia. *Blood* (2017) 130(6):722–31. doi: 10.1182/blood-2017-04-779405
  86. Chen J, Yang J, Cao P. The Evolving Landscape in the Development of Isocitrate Dehydrogenase Mutant Inhibitors. *Mini Rev Med Chem* (2016) 16(16):1344–58. doi: 10.2174/1389557516666160609085520
  87. Ma R, Yun CH. Crystal Structures of Pan-IDH Inhibitor AG-881 in Complex With Mutant Human IDH1 and IDH2. *Biochem Biophys Res Commun* (2018) 503(4):2912–7. doi: 10.1016/j.bbrc.2018.08.068
  88. Chen J, Yang J, Sun X, Wang Z, Cheng X, Lu W, et al. Allosteric Inhibitor Remotely Modulates the Conformation of the Orthosteric Pockets in Mutant IDH2/R140Q. *Sci Rep* (2017) 7(1):16458. doi: 10.1038/s41598-017-16427-w
  89. Tommasini-Ghelfi S, Murnan K, Kouri FM, Mahajan AS, May JL, Stegh AH. Cancer-Associated Mutation and Beyond: The Emerging Biology of Isocitrate Dehydrogenases in Human Disease. *Sci Adv* (2019) 5(5):eaaw4543. doi: 10.1126/sciadv.aaw4543

90. Gao M, Zhu H, Fu L, Li Y, Bao X, Fu H, et al. Pharmacological Characterization of TQ05310, a Potent Inhibitor of Isocitrate Dehydrogenase 2 R140Q and R172K Mutants. *Cancer Sci* (2019) 110(10):3306–14. doi: 10.1111/cas.14152
91. Chen J, Yang J, Wei Q, Weng L, Wu F, Shi Y, et al. Identification of a Selective Inhibitor of IDH2/R140Q Enzyme That Induces Cellular Differentiation in Leukemia Cells. *Cell Commun Signal* (2020) 18(1):55. doi: 10.1186/s12964-020-00536-7
92. Li Z, Wu X, Jia L, Li J, Zhang R, Tang H, et al. Design and synthesis of novel 2-arylbenzimidazoles as selective mutant isocitrate dehydrogenase 2 R140Q inhibitors. *Bioorg Med Chem Lett* (2020) 30(9):127070. doi: 10.1016/j.bmcl.2020.127070

**Conflict of Interest:** The authors declare that the research was conducted in the absence of any commercial or financial relationships that could be construed as a potential conflict of interest.

Copyright © 2021 Guo, Zhang, Yang, Duan, Yin and Zhou. This is an open-access article distributed under the terms of the Creative Commons Attribution License (CC BY). The use, distribution or reproduction in other forums is permitted, provided the original author(s) and the copyright owner(s) are credited and that the original publication in this journal is cited, in accordance with accepted academic practice. No use, distribution or reproduction is permitted which does not comply with these terms.



# Cholesterol Metabolic Reprogramming in Cancer and Its Pharmacological Modulation as Therapeutic Strategy

Isabella Giacomini<sup>1†</sup>, Federico Gianfanti<sup>1,2†</sup>, Maria Andrea Desbats<sup>2</sup>, Genny Orso<sup>1</sup>, Massimiliano Berretta<sup>3</sup>, Tommaso Prayer-Galetti<sup>4</sup>, Eugenio Ragazzi<sup>1\*</sup> and Veronica Cocetta<sup>1</sup>

<sup>1</sup> Department of Pharmaceutical and Pharmacological Sciences, University of Padova, Padova, Italy, <sup>2</sup> Veneto Institute of Molecular Medicine, VIMM, Padova, Italy, <sup>3</sup> Department of Clinical and Experimental Medicine, University of Messina, Messina, Italy, <sup>4</sup> Department of Surgery, Oncology and Gastroenterology - Urology, University of Padova, Padova, Italy

## OPEN ACCESS

### Edited by:

Miriam Martini,  
University of Turin, Italy

### Reviewed by:

Alessandro Carrer,  
Veneto Institute of Molecular Medicine  
(VIMM), Italy  
Paola Defilippi,  
University of Turin, Italy  
Paolo E. Porporato,  
University of Turin, Italy

### \*Correspondence:

Eugenio Ragazzi  
eugenio.ragazzi@unipd.it

<sup>†</sup>These authors have contributed  
equally to this work and  
share first authorship

### Specialty section:

This article was submitted to  
Cancer Metabolism,  
a section of the journal  
Frontiers in Oncology

Received: 19 March 2021

Accepted: 06 May 2021

Published: 24 May 2021

### Citation:

Giacomini I, Gianfanti F, Desbats MA,  
Orso G, Berretta M, Prayer-Galetti T,  
Ragazzi E and Cocetta V  
(2021) Cholesterol Metabolic  
Reprogramming in Cancer and  
Its Pharmacological Modulation  
as Therapeutic Strategy.  
Front. Oncol. 11:682911.  
doi: 10.3389/fonc.2021.682911

Cholesterol is a ubiquitous sterol with many biological functions, which are crucial for proper cellular signaling and physiology. Indeed, cholesterol is essential in maintaining membrane physical properties, while its metabolism is involved in bile acid production and steroid hormone biosynthesis. Additionally, isoprenoids metabolites of the mevalonate pathway support protein-prenylation and dolichol, ubiquinone and the heme a biosynthesis. Cancer cells rely on cholesterol to satisfy their increased nutrient demands and to support their uncontrolled growth, thus promoting tumor development and progression. Indeed, transformed cells reprogram cholesterol metabolism either by increasing its uptake and *de novo* biosynthesis, or deregulating the efflux. Alternatively, tumor can efficiently accumulate cholesterol into lipid droplets and deeply modify the activity of key cholesterol homeostasis regulators. In light of these considerations, altered pathways of cholesterol metabolism might represent intriguing pharmacological targets for the development of exploitable strategies in the context of cancer therapy. Thus, this work aims to discuss the emerging evidence of *in vitro* and *in vivo* studies, as well as clinical trials, on the role of cholesterol pathways in the treatment of cancer, starting from already available cholesterol-lowering drugs (statins or fibrates), and moving towards novel potential pharmacological inhibitors or selective target modulators.

**Keywords:** cholesterol, cancer, metabolic reprogramming, cancer therapy, pharmacological targeting, pharmacological modulation, metabolic targeting agents

## INTRODUCTION

In the last decades, the study of metabolic reprogramming has been revealed as one of the hallmarks of cancer and chemotherapy resistance. It has been demonstrated that cancer cells change their metabolism, increasing glucose demand, glutamine or lipid synthesis, exploiting the pentose phosphate pathway or altering their mitochondrial function, in order to support a higher proliferation rate leading to tumor progression and chemotherapy resistance (1–10). Among

these altered pathways, cholesterol metabolic reprogramming has acquired a pivotal role in the field of cancer research.

The discovery of cholesterol dates back to the second half of the eighteenth century, when Poulletier de la Salle isolated for the first time this molecule from human gallstone and bile. Since then, a huge number of researches were undertaken, which eventually led to the understanding of key molecular events of cholesterol biology, such as transport in blood and cellular metabolism. Nowadays, this peculiar lipid is still extensively studied for its involvement in several pathophysiological processes (11, 12). Cholesterol is a ubiquitous sterol found in vertebrate organisms with a plethora of biological functions that are essential for proper cellular growth and activity (13, 14). Due to its alicyclic nature, cholesterol is highly hydrophobic and resides predominantly within the phospholipidic bilayer of cell membranes, where it preserves the barrier function by modulating permeability, fluidity and rigidity (15, 16). In this setting, cholesterol preferentially interacts with the saturated acyl chains of adjacent sphingolipids and glycosphosphatidylinositol-anchored proteins of the outer leaflet, forming small ordered and tightly packed microdomains, physically separated from the shorter and unsaturated phospholipids of the bilayer (16–18). These assemblies, usually called lipid rafts, are involved in several biological processes, such as biosynthetic and endocytic vesicular trafficking (19), ceramide-mediated apoptosis (20), host-pathogen interactions (pathogen binding and uptake) (21), cytoskeletal dynamics and rearrangement, cellular polarization (22) and signal transduction (IgE signaling, T-cell antigen receptor signaling, Ras signaling, Hedgehog signaling) (23). Although the most known role of cholesterol as a structural and functional component of cellular membranes is unquestionable (15, 16, 18), it also represents the precursor of bile acids, and its oxidation allows the biosynthesis of steroid hormones in steroid-producing tissues. In addition, the isoprenoid intermediates of the mevalonate pathway can be diverted toward the biosynthesis of dolichol, ubiquinone and the side tail of heme *a* (24, 25), or exploited as substrates for protein-prenylation (26). Lastly, cholesterol has also been found to interact with a large variety of proteins, including receptors, enzymes, etc. by both covalent and non-covalent binding, thus regulating protein stability, localization, and activity. These interactions indicate cholesterol as an important element in the regulation of many biochemical pathways, through the control of protein localization and activity (27).

Due to the crucial role played by this sterol in several physiological settings, disruption of cholesterol homeostasis and metabolic reprogramming may be responsible for the development of cardiovascular disorders and is implicated in the pathogenesis of diabetes, Alzheimer disease and many types of cancer (28–32). Intracellular and systemic cholesterol concentrations are tightly regulated by the balance between *de novo* biosynthesis, uptake, efflux, and storage, and metabolic alterations in lipid/cholesterol pathways have been shown to modulate cancer cells' sensitivity to chemotherapeutic agents. The dependence of cancer cells on aberrant lipid and cholesterol metabolism could point to these pathways as an attractive target

to treat cancer as well as to sensitize them to anticancer therapies (33). Many cholesterol-lowering drugs are approved and used for the treatment of hypercholesterolemia and for the control of pathologies and metabolic disorders. This work focuses on the correlation between cholesterol metabolism and cancer, considering the importance of these pathways in sustaining cell growth, invasion or migration. Furthermore, starting from the relatively recent findings on the role of sterol in tumor progression and chemotherapy response, we will consider how the pharmacological targeting of increased cholesterol metabolism pathways could represent a promising approach for cancer treatment.

## CHOLESTEROL METABOLISM

Cholesterol metabolism in humans is complex. Cholesterol is either supplied from the diet (exogenous) or synthesized *de novo* (~70% of total body cholesterol, endogenous). Here below we provide a brief section on the main aspects related to cholesterol metabolism, introductory to understanding the reprogramming aspect observed in cancer cells. For a more accurate description of the fine regulation of cellular processes involving cholesterol, we refer to several specific reviews (34–37).

### Cholesterol Biosynthesis

The biosynthetic cascade which leads to cholesterol production (**Figure 1**) occurs virtually in every mammalian cell, with liver and intestine being the anatomical sites responsible for more than 50% of total cholesterol biosynthesis (38, 39). This process is orchestrated by more than 20 enzymes which are distributed between the cytosol and the endoplasmic reticulum (ER) (40). The first step is catalyzed by the cytoplasmatic enzyme acetylacetyl-CoA thiolase which allows the condensation of two acetyl-CoA molecules to obtain acetylacetyl-CoA. In the second reaction, the enzyme 3-hydroxy-3-methylglutaryl-CoA synthase (HMGCS) allows the introduction of the third molecule of acetyl-CoA for the formation of the branched-chain molecule 3-hydroxy-3-methylglutaryl-CoA, which is then reduced to mevalonate in the first rate-limiting step of cholesterol biosynthesis by 3-hydroxy-3-methylglutaryl-CoA reductase (HMGCR). Afterwards, mevalonate undergoes two subsequent phosphorylations performed by mevalonate kinase (MVK) and phosphomevalonate kinase (PMVK) and an ATP-dependent decarboxylation which eventually yields the isoprenoid precursor isopentenyl pyrophosphate (IPP). This intermediate is converted into its isomer dimethylallyl pyrophosphate (DMAPP) in a reversible reaction catalyzed by isopentenyl pyrophosphate isomerase. The condensation of one molecule of IPP with one molecule of DMAPP allows the formation of geranyl pyrophosphate (GPP), which is in turn combined with another IPP molecule by the enzyme farnesyl diphosphate synthase to yield farnesyl pyrophosphate (FPP), a key isoprenoid. At this point, the mevalonate pathway diverts toward the formation of either non-sterol isoprenoids, such as geranylgeranyl pyrophosphate (GGPP), or sterols, through the



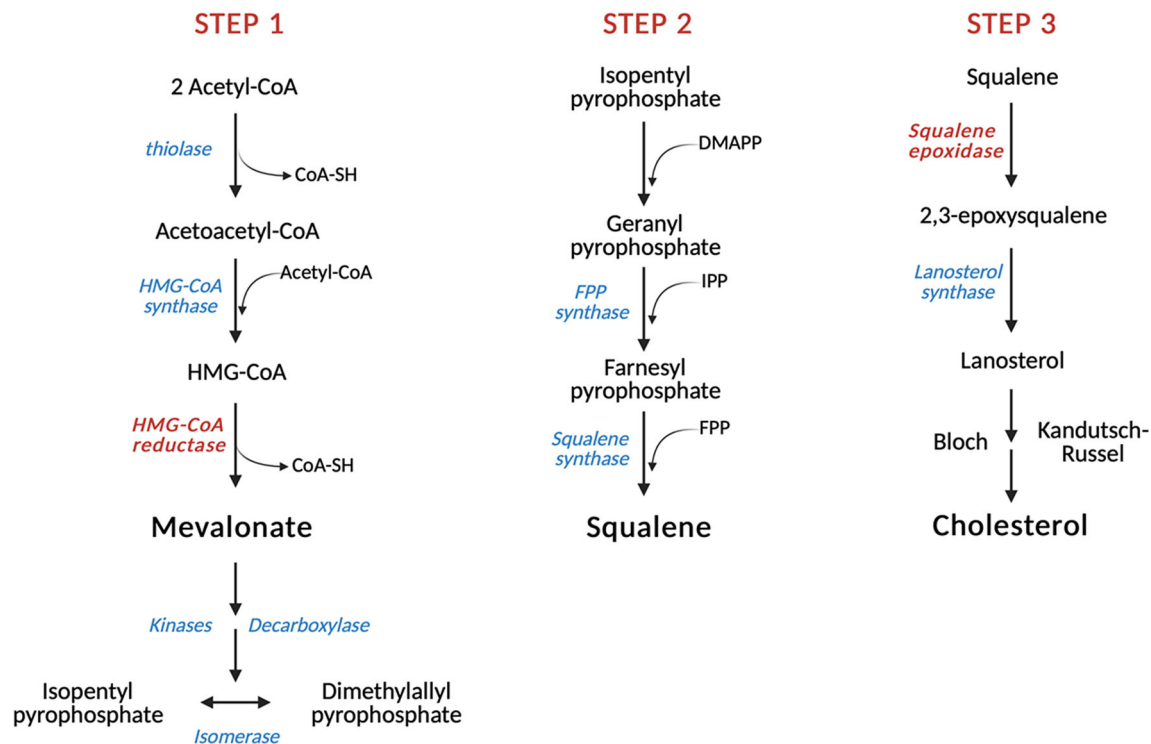


**FIGURE 1** | Schematic representation of cholesterol biosynthesis. In the first step of cholesterol biosynthesis, three molecules of acetyl-CoA condense to form HMG-CoA, which is then reduced to mevalonate by the first step-limiting enzyme HMG-CoA reductase (HMGCR). Subsequent reactions allow the conversion of mevalonate into FPP, an isoprenoid that gives rise to squalene in a reaction catalyzed by squalene synthase (SQS). Squalene is then converted by the second rate-limiting enzyme squalene epoxidase (SQLE) into its epoxidic form, which is eventually cyclized to lanosterol by the enzyme lanosterol synthase. Further oxygen-based reactions lead to the formation of cholesterol. Red: rate-limiting enzymes. HMG-CoA, 3-hydroxy-3-methylglutaryl-CoA; IPP, Isopentenyl pyrophosphate; DMAPP, Dimethylallyl pyrophosphate; FPP, Farnesyl pyrophosphate.

head-to-head condensation of two FPP molecules, mediated by squalene synthase, which gives rise to squalene. Intracellular accumulation of non-sterol products is required for post-translational modification processes (N-glycosylation and Cys-prenylation) of diverse proteins that play important roles in cellular growth and signal transduction (24, 41). On the other hand, squalene epoxidase (SQLE), the other rate-limiting enzyme of cholesterol biosynthesis, converts squalene into its epoxydic form 2,3-epoxysqualene, which is then cyclized to lanosterol by the enzyme lanosterol synthase. The last phase of cholesterol biosynthesis involves 19 oxygen-based reactions which include demethylations, double-bond reductions, and double bond replacements. In this context, lanosterol enters the Bloch branch or the Kandutsch–Russell pathway and is processed through the formation of several intermediates which yields desmosterol and 7-dehydrocholesterol, the direct precursors of cholesterol (42–44). Recently, the existence of a third hybrid pathway has also been suggested for the conversion of lanosterol into cholesterol (45).

## Cholesterol Uptake and Efflux

The dietary intake of cholesterol is extremely important to ensure the maintenance of its homeostasis (46, 47). In the

small intestinal lumen, dietary sterols are solubilized into micelles by bile acids and adsorbed in a process facilitated by the Niemann–Pick C1-like-1 (NPC1L1) protein, which is localized in the apical membrane of enterocytes and allows cholesterol uptake in a clathrin-mediated endocytosis fashion (48, 49). Once inside the enterocyte, cholesterol is mainly converted to cholesteryl esters by the ER enzyme acyl-coenzymeA cholesterol acetyltransferase 2 (ACAT2) and then packed into nascent chylomicrons, together with dietary triglycerides and apolipoprotein B-48 (50, 51). Through the lymphatic system, chylomicrons are poured into the bloodstream and metabolized by the endothelial enzyme lipoprotein lipase, which hydrolyzes the triglycerides contained in the core to yield chylomicron remnants. The released fatty acids are used by peripheral tissues including muscles and adipose tissue either for storage or oxidation, while dietary cholesterol is delivered to the liver by chylomicron remnants (52, 53). Hepatic cholesterol and triglycerides are coupled to apolipoprotein B and incorporated into VLDL particles, which are secreted into the blood and hydrolyzed by plasma lipases to yield IDL. IDLs are further converted into LDLs, particles rich in cholesterol and cholesteryl esters which are captured by LDL receptor-expressing tissues, including the liver and other

extrahepatic tissues (54, 55). On the other hand, LDL is driven towards the lysosomal compartment where lysosomal lipases hydrolyze the cholesteryl esters stored in the core to cholesterol, which eventually exits from the lysosome lumen aided by the coordinated action of NPC1, NPC2 and LAMP2 and reaches other cellular organelles, mostly *via* non-vesicular transport mediated by sterol transfer proteins (STPs) (56–58). Cholesterol elimination also significantly impacts cellular homeostasis. Therefore, the excess of cellular cholesterol in peripheral tissues has to be stored as less-toxic cholesteryl esters in lipid droplets or disposed and moved towards the liver for recycling or excretion, by a process usually referred to as reverse cholesterol transport (59, 60). Cholesterol removal from extrahepatic cells is driven by HDL particles, which accumulate and transport cholesteryl esters to the liver, the adrenal glands, and the gonads (61). Cholesteryl esters are then converted to free cholesterol by cholesteryl ester hydrolase (CEH) for either steroid hormones synthesis in steroid-producing organs or cholesterol excretion and bile acids synthesis in the liver (62, 63). Cellular cholesterol efflux is controlled by four regulatory proteins belonging to the ATP-binding cassette (ABC) transporter superfamily, namely ABCA1, ABCG1, ABCG5 and ABCG8. ABCA1 mediates the transport of cholesterol and phospholipids to lipid-free apolipoprotein A-I (apo A-I) in the blood allowing the generation of nascent discoidal HDL particles, which are converted into globular and mature HDLs under the action of lecithin:cholesterol acyl transferase (LCAT) by accepting further cholesterol from ABCG1 (63, 64).

## Cholesterol Storage

Intracellular cholesterol excess is usually esterified by the ER enzyme acyl coenzyme A cholesterol acetyltransferase (ACAT), which catalyzes the transfer of a fatty acyl group to cholesterol (65). Indeed, ACAT-produced cholesteryl esters can be easily stored into lipid droplets preventing free-cholesterol lipotoxicity (66). Cholesterol esterification is also involved in lipoprotein and steroid hormone production, as well as in chylomicrons assembly for cholesterol absorption (67). Two ACAT isoenzymes have been identified in mammals so far, consistent with their different tissue distribution. ACAT1 is widely expressed throughout the body, suggesting its involvement in maintaining cholesterol homeostasis, while ACAT2 expression is exclusive in enterocytes and hepatocytes, where it contributes to lipoprotein biosynthesis and assembly (68, 69).

## Regulation of Cholesterol Homeostasis

In order to ensure the maintenance of cellular and systemic cholesterol homeostasis, mammalian cells must carefully orchestrate the set of molecular pathways involved in cholesterol biosynthesis, uptake, storage and efflux (70, 71). This is accomplished by sterol-sensitive systems, which couple variations in cellular sterol levels with adaptive responses. Particularly, three adaptive factors are considered as key regulators of cholesterol homeostasis, namely sterol regulatory element-binding protein-2 (SREBP2), liver X receptors (LXRs) and nuclear factor erythroid 2 related factor-1 (NRF1) (40).

SREBP2 belongs to the basic-helix-loop-helix-leucine zipper (bHLH-Zip) family of transcription factors and lies within the ER membrane associated with SREBP-cleavage activating protein (SCAP) through its C-terminal portion (72). The N-terminal transcription factor portion, usually referred to as nuclear SREBP2 (nSREBP2), undergoes dimerization and is then imported inside the nucleus, where binds to sterol responsive elements (SREs) in the promoter regions of target genes, inducing their transcription (73, 74). Conversely, when ER-membrane cholesterol levels increase above the threshold, the sterol sensitive domain (SSD) of SCAP binds to cholesterol and SCAP switches to an open conformation promoting its interaction with insulin-induced gene 1 (INSIG1) protein (75). nSREBP2 binds to and induces the transcription of HMGCR and SQLE genes, which encode for the two rate-limiting enzymes of cholesterol biosynthesis, increasing sterols intracellular levels (76, 77). HMGCR levels are also regulated either by direct interaction with ER-sterols through its SSD (INSIG1-mediated ubiquitination) or by covalent modification (AMPK-mediated phosphorylation) (78, 79). SREBP2 activation also increases the expression of NPC1L1 and LDLR genes, two master regulators of cholesterol intestinal absorption and cholesterol intake by peripheral cells, respectively (80, 81). Moreover, a SRE motif is contained upstream of SREBP2 gene, suggesting that nSREBP2 promotes the activation of its own gene (feed-forward mechanism) (82). Under increasing cholesterol levels, the ER preserves cellular homeostasis by recruiting the adaptive factor NRF1 (61). NRF1 resides within the ER-membrane but is rapidly activated by proteolysis, released from the ER and translocated into the nucleus, where it regulates the transcription of its target genes by binding to anti-oxidant response elements (AREs) (83). Particularly, when NRF1 is activated and enters the nucleus, it represses the transcriptional activity of LXR, which promotes cholesterol excretion, export and storage, while inhibiting *de novo* biosynthesis. Differentially to SREBP2 and NRF1, LXRs are nuclear receptors which, upon heterodimerization with the retinoid X receptor- $\alpha$  (RXR  $\alpha$ ), bind to LXR responsive elements (LXRE) and regulate the expression of several genes involved in lipid homeostasis (84). Once activated, LXRs promotes the activation of genes involved in bile acids production (CYP7A1), cholesterol excretion (ABCG5, ABCG8) and reverse cholesterol transport (ABCA1, ABCG1) (85–87). Moreover, LXRs impair cholesterol intestinal absorption by down-regulating NPC1L1 expression and inhibit cholesterol cellular uptake by promoting IDOL-mediated LDLR degradation (88–90). Overall, LXRs activity prevents lipotoxicity induced by intracellular accumulation of sterols.

## Cholesterol Lowering Drugs

Since cholesterol plays a key role in many cellular processes, disruption of cholesterol homeostasis is linked to the onset of several diseases, including metabolic disorders, atherosclerosis, cancer, etc. Several therapeutic classes of drugs are currently used to treat hypercholesterolemia (Table 1) and to prevent associated cardiovascular diseases (110). Statins are the first-line treatment of hypercholesterolemia and they have an important role in the prevention of cardiovascular diseases. Statins are competitive

**TABLE 1** | Current cholesterol-lowering drugs and relative mechanism of action, main effects on cholesterol metabolism, adverse effects and therapeutic indications.

Therapeutic class	Drug	Mechanism of action	Effects on cholesterol metabolism	Main adverse effects	Clinical indications	References
<b>Statins</b>	Lovastatin	Competitive inhibitors of HMGCR		Myalgia, myositis, rhabdomyolysis	Primary H, Mixed dyslipidemia	(91–96)
	Simvastatin		↑HDL			
	Pravastatin		↓plasma triglycerides			
	Fluvastatin		↑LDLR			
	Rosuvastatin		↓LDL			
	Atorvastatin					
	Pitavastatin					
<b>Bempedoic acid</b>	Bempedoic acid (prodrug)	Inhibitor of ATP citrate lyase	↓LDL	Myalgia, muscular disorders, gout	Primary H, Mixed dyslipidemia	(97)
<b>Fibrates</b>	Gemfibrozil	PPAR $\alpha$ agonists	↑HDL	Nausea, abdominal pain	Primary H, Mixed dyslipidemia	(98–100)
	Fenofibrate		↓serum triglycerides			
	Fenofibric acid		↓VLDL			
<b>Selective cholesterol absorption inhibitors</b>	Ezetimibe	Selective block of NPC1L1	↑LDLR ↓serum LDL ↑HDL ↓triglycerides	Myopathy, acute pancreatitis (when it is combined with statins)	Dyslipidemia, FH	(101, 102)
<b>Resins</b>	Cholestyramine	Bile acid binders	↑HDL	Gastrointestinal effects	Dyslipidemia, Primary H, H associated with mild HT	(103, 104)
	Colesevelam		↓LDL			
	Colestipol		↑serum triglycerides			
<b>Apolipoprotein B synthesis inhibitor</b>	Mipomersen	Second-generation antisense oligonucleotide inhibitor of apoB-100	↓apoB ↓LDL ↓VLDL ↓lipoprotein	Injections site reactions; flu-like symptoms; elevated transaminasis (alanine aminotransferase) → reversible; hepatic steatosis → reversible	FH, Severe H	(105–107)
<b>Microsomal transfer protein inhibitor</b>	Lomitapide	Inhibitor of the microsomal triglyceride transfer protein (MTTP)	↓VLDL ↓LDL	Diarrhoea, nausea, dyspepsia, vomiting; elevated liver aminotransferase	Adult HoFH	(108)
<b>PCSK9 inhibitors</b>	Alirocumab	Inhibition of PCSK9	↓LDLR	Nasopharyngitis	FH	(109)
	Evolocumab		↓LDL			

HMGCR, 3-hydroxy-3-methyl-glutaryl-coenzyme A reductase; PPAR $\alpha$ , Peroxisome proliferator-activated receptor alpha; LDLR, low density lipoprotein receptor; HDL, High Density Lipoproteins; LDL, Low Density Lipoproteins; VLDL, Very Low Density Lipoproteins; MTTP, microsomal triglyceride transfer protein; HoFH, Homozygous familial hypercholesterolaemia; FH, familial hypercholesterolaemia; H, hypercholesterolaemia; PCSK9, proprotein convertase subtilisin/kexin type 9; HT, hypertriglyceridemia.

inhibitors of 3-hydroxy-3-methylglutaryl-CoA reductase (HMGCR), the enzyme responsible for the reduction of HMG-CoA into mevalonate (91). This specific block causes effects on cholesterol metabolism, such as diminished plasma triglycerides, enhanced HDL, and upregulation of LDL receptor (LDLR) expression, which leads to increased LDL uptake in hepatocytes and decreased blood LDL content (92). Fibrates are another therapeutic class of drugs prescribed to treat hypercholesterolemia (98, 99). They are agonists of the transcription factor PPAR $\alpha$ , that once activated, translocates in the nucleus, heterodimerizes with the retinoid X receptor (RXR) and binds to peroxisome proliferator response elements (PPREs) starting the gene's transcription (100). The effects on lipoprotein metabolism and cellular cholesterol homeostasis are decreased hepatic synthesis and decreased serum levels of triglycerides, reduced synthesis of VLDL, increased HDL cholesterol, and regulation in fatty acid synthesis and uptake, such as regulation of FAT or CD-36 (98, 99). Other therapeutic classes of cholesterol-lowering drugs are represented by selective cholesterol absorption inhibitors, such as ezetimibe; resins, such as cholestyramine, colestipol and colesevelam, which are bile acid sequestrants (103); apolipoprotein B synthesis inhibitors, such as mipomersen (105); microsomal transfer protein inhibitors, such as

lomitapide (105). A new promising therapeutic class of cholesterol-lowering drugs is represented by PCSK9 inhibitors. PCSK9 is predominantly produced in hepatocytes, where it decreases LDLR number. When PCSK9 binds LDLR there is a consequent block of LDLR in an open conformation and its recycling is blocked. Then, LDLR is degraded by lysosomes (109). Another recently approved cholesterol-lowering drug is bempedoic acid (8-hydroxy-2,2,14,14-tetramethylpentadecanedioic acid) (97), acting as ATP citrate lyase inhibitor, an enzyme upstream from 3-hydroxy-3-methylglutaryl-CoA. Since the focus of this review is the repositioning of cholesterol-lowering drugs in oncology, we refer to **Table 1** for a schematic explanation of the mechanisms of action, effects on cholesterol metabolism, and possible side effects of the drugs.

## CHOLESTEROL METABOLIC REPROGRAMMING IN CANCER: PHARMACOLOGICAL TARGETING

Cancer cells are highly proliferative and therefore strongly dependent on cholesterol to satisfy their increasing demand of

substrates for membrane biosynthesis (111). Accordingly, cholesterol is generally beneficial for cancer growth and development, as it promotes oncogenic signaling and evasion of apoptosis, as well as cell migration and invasion (112–115). Notably, cancer cells increase their cholesterol demand by enhancing *de novo* biosynthesis or uptake, by altering the cholesterol efflux, or by increasing its storage, as will be described in the following sections. Also, cholesterol homeostasis is largely compromised in cancer development and progression, as will be discussed below. In line with this, the differential cholesterol requirements of tumors provide novel therapeutic strategies for the treatment of several malignancies. As above mentioned, the purpose of this review is to sum up the main alterations in cholesterol-related metabolic pathways observed in *in vitro* and *in vivo* cancer models. The current scientific evidence highlights the reprogramming of lipid/cholesterol pathways in many cancers, thus suggesting intriguing targets exploitable for a combined therapy with conventional chemotherapeutic agents in the fight against cancer. In the following sections we will describe the main alterations observed in cancer cells in the context of cholesterol metabolism, pointing out the more interesting targets identified since now. The identification of specific targets has opened the possibility to exploit them for a pharmacological approach by using cholesterol lowering/modulating drugs. Here we will review the current literature focused on the use of cholesterol targeting drugs in the context of cancer treatment. Results from *in vitro* and *in vivo* studies have allowed the translation into clinical trials of some drugs that are discussed in the following sections, highlighting the potential of this combined approach for cancer treatment (Table 2).

## Enhanced Cholesterol *de novo* Biosynthesis

Many cancers upregulate *de novo* cholesterol biosynthesis, thereby fueling the oncogenic machinery and sustaining tumor progression (155). Aberrant cholesterol biosynthetic program can be considered as a hallmark of transformed cancer cells and has been correlated with lower overall patient survival in melanoma, acute myeloid leukemia and sarcoma (32). Consistently, in breast cancer cholesterol biosynthesis-related genes are considered reliable prognostic factors associated with shorter relapse-free survival (156). Cholesterol biogenesis is carried on through the mevalonate pathway (Figure 2), which leads to the production of farnesyl pyrophosphate (FPP), responsible for the formation of either the non-sterol isoprenoid geranylgeranyl pyrophosphate (GGPP) or squalene. The first rate-limiting enzyme HMGCR is overexpressed in many tumors, such as prostate cancer, gastric cancer and colon cancer (157–159). Indeed, the accumulation of non-sterol isoprenoids mediates several oncogenic activities by post-translationally modifying key proteins directly involved in the expression of oncogenes, cytoskeletal organization and cell survival/proliferation (24, 160). This process is collectively known as protein prenylation and allows the covalent attachment of lipid moieties to small oncogenic G proteins,

thereby promoting their activation and transforming function (26). GTP-binding proteins Rho, Rac, Rab, Rap, Ras (Ras, Rho, Rab superfamily of GTPases) are all dependent from farnesylation and geranylgeranylation to exert their tumorigenic activities, which eventually promote cell cycle progression and cellular survival, as well as tumor cells motility, migration and metastasis (41, 161, 162). Moreover, isoprenoids are involved in ubiquinone biogenesis. Ubiquinone (CoQ) is a redox active lipid that functions as electron carrier in the mitochondrial respiratory chain. CoQ sustains p53-deficient colon cancer cells growth and development by promoting *de novo* pyrimidine synthesis and maintaining the integrity of the electron transfer chain even under nutrients starvation and oxygen restriction (163). Differently from steroidogenic healthy tissues, HMGCR activity in tumors is refractory to sterol-mediated negative feedback regulation (36, 164). Therefore, HMGCR altered regulation allows the accumulation of isoprenoids even in cholesterol-enriched conditions, thereby sustaining the production of non-sterol mevalonate intermediates essential for the establishment of tumor malignant phenotype (41). The alternative branch of mevalonate pathway diverts towards the formation of sterols through the activity of squalene synthase (SQS), which gives rise to squalene. In lung cancer patients, SQS is frequently overexpressed and associated with poor prognosis and tumor metastasis. Indeed, the enhanced expression of SQS induces cholesterol biosynthesis, which in turn sustains Tumor Necrosis Factor Receptor 1 (TNFR1) accumulation into lipid rafts and subsequent NF- $\kappa$ B and MMP1 activation (165). Squalene epoxidase (SQLE) converts squalene into squalene-2,3-epoxide and represents the other rate-limiting enzyme in sterol biogenesis. SQLE activity is dysregulated in many tumors, such as breast, lung and colorectal cancer (166–168). Colorectal tumors are characterized by higher SQLE expression levels when compared with healthy tissues, which sustain tumor development by promoting extracellular signal-regulated kinase 1/2 (ERK1/2) oncogenic activity (169). Similarly, in breast cancer SQLE is frequently amplified at the gene level and strongly overexpressed in more aggressive and undifferentiated tumors, thereby demonstrating its oncogenic potential (170). On the other hand, a subset of tumors presents SQLE downregulation and subsequent cholesterol auxotrophy. Lymphoma SQLE-deficient cells accumulate squalene, which modifies cellular membranes and lipid droplets composition, thereby protecting neoplastic cells from the oxidative damage and ferroptosis (171, 172). In breast cancer cells, NAD(P)H-dependent steroid dehydrogenase-like protein (NSDHL) and sterol-C4-methyl oxidase (SC4MOL), two enzymes of the Kandutsch-Russell pathway, are overexpressed and translocate to the plasma membrane. Here, they promote metastasis development by modulating lipid rafts' sterol composition (173, 174). Another key post-squalenic enzyme is oxidosqualene cyclase (OSC), which mediates 2,3-oxidosqualene cyclization into lanosterol (175). In metastatic mouse models of human colorectal and pancreatic cancer, OSC promotes tumor neovascularization and metastatic potential. Consistently, OSC inhibitors hamper



**TABLE 2** | Sum up of drugs acting on cholesterol metabolism investigated as potential treatment in cancer therapy.

Target	Drug	Cancer	Preclinical/clinical phase	References
OSC	<b>Ro 48-8071</b>	Breast cancer	<i>In vitro</i> and <i>in vivo</i> studies	(116, 117)
		Colon carcinoma	<i>In vivo</i> studies	(118)
		Pancreatic ductal denocarcinoma	<i>In vivo</i> studies	(118)
		Hormone-dependent and castration-resistant prostate cancer	<i>In vitro</i> and <i>in vivo</i> studies	(119)
SQS	<b>Zaragozic acid</b>	Prostate cancer	<i>In vitro</i> studies	(120)
		RMA lymphoma	<i>In vivo</i> studies	(121)
		Lewis lung carcinoma	<i>In vivo</i> studies	(121)
		Breast cancer	<i>In vitro</i> studies	(122)
ACAT-1	<b>CP-113818</b>	Breast cancer	<i>In vivo</i> studies	(123)
	<b>Bitter melon extract</b>	Breast cancer	<i>In vivo</i> studies	(123)
	<b>Avasimin (nanoformulation with avasimibe)</b>	Prostate, pancreatic, colon and lung cancers	<i>In vitro</i> and <i>in vivo</i> studies	(124)
		Metastatic prostate cancer	<i>In vivo</i> studies	(125)
		Pancreatic cancer	<i>In vitro</i> and <i>in vivo</i> studies	(126)
	<b>Avasimibe</b>	Metastatic prostate cancer	<i>In vitro</i> studies	(125)
		Pancreatic ductal adenocarcinoma	<i>In vitro</i> studies	(126)
		Lewis lung cancer	<i>In vitro</i> and <i>in vivo</i> studies	(127)
	<b>Avasimibe + gemcitabine</b>	Pancreatic ductal adenocarcinoma	<i>In vitro</i> and <i>in vivo</i> studies	(128)
	<b>Avasimibe + cyclophosphamide</b>	Lewis lung cancer	<i>In vivo</i> studies	(127)
LXR	<b>T0901317</b>	Prostate cancer	<i>In vitro</i> and <i>in vivo</i> studies	(129)
		Breast cancer	<i>In vitro</i> studies	(130)
		Melanoma	<i>In vitro</i> and <i>in vivo</i> studies	(131)
		Multiple myeloma	<i>In vitro</i> and <i>in vivo</i> studies	(132)
		Oral squamous cell carcinoma	<i>In vitro</i> and <i>in vivo</i> studies	(133)
		Ovarian cancer	<i>In vitro</i> studies	(134)
		Lung cancer	<i>In vitro</i> and <i>in vivo</i> studies	(135)
		Hepatocellular carcinoma	<i>In vitro</i> and <i>in vivo</i> studies	(136)
		Breast cancer	<i>In vitro</i> studies	(130)
		Multiple myeloma	<i>In vitro</i> studies	(132)
	<b>T0901317 + Gefitinib</b> <b>T0901317 + Sorafenib</b> <b>22(R)-hydroxycholesterol</b> <b>GW3965</b>	Breast cancer	<i>In vitro</i> studies	(137, 138)
		Melanoma	<i>In vivo</i> studies	(139)
		Pancreatic ductal adenocarcinoma	<i>In vitro</i> studies	(140)
		Multiple myeloma	<i>In vitro</i> studies	(132)
		Colon cancers	<i>In vitro</i> studies	(138)
		Lung cancer	<i>In vitro</i> studies	(141)
		Prostate, lung, colon cancers and clear cell renal cell carcinoma	<i>In vitro</i> and <i>in vivo</i> studies	(142, 143)
		Clear cell renal cell carcinoma	<i>In vitro</i> studies	(143)
		Ishikawa endometrial cancer	<i>In vitro</i> studies	(144)
		Hepatoma	<i>In vitro</i> studies	(145)
PPAR $\alpha$	<b>Fenofibrate</b>	Oral cancer	<i>In vitro</i> and <i>in vivo</i> studies	(146)
		Gastric cancer	<i>In vitro</i> and <i>in vivo</i> studies	(147)
		Low-grade glioma and ependymoma	Phase-II clinical trial	(148)
		Ishikawa endometrial cancer	<i>In vitro</i> studies	(144)
		Prostate cancer	<i>In vitro</i> studies	(149)
		Prostate cancer	<i>In vitro</i> and <i>in vivo</i> studies	(150)
		Endometrial cancer	<i>In vitro</i> and <i>in vivo</i> studies	(151, 152)
		Breast cancer	<i>In vitro</i> and <i>in vivo</i> studies	(153)
SREBP	<b>Fatostatin</b>	Breast cancer	<i>In vitro</i> studies	(154)
		Breast cancer	<i>In vitro</i> studies	(154)

endothelial cell migration and promote cell apoptosis, thereby inhibiting tumor-associated angiogenesis and dissemination to distal organs (116, 118). Additionally, OSC plays an important role in cell self-renewal and its expression is increased in breast cancer stem cells (156, 176). In conclusion, the mevalonate pathway is oncogenic at many levels and frequently dysregulated in several cancers.

### Pharmacological Modulation of HMGCR

As mentioned, HMGCR is the rate-limiting enzyme of the mevalonate pathway, which produces cholesterol. Considering the overexpression of this enzyme in many tumors, targeting HMGCR could be a good strategy for cancer clinical therapy. As stated, statins are the commonest pharmacological inhibitors of

HMGCR and the repositioning of these drugs in the cancer field is well studied and established. Statins exerts antitumor activities with different molecular mechanisms, such as reducing cell proliferation or tumor cell survival (177), suppressing angiogenesis or causing apoptosis, and reducing tumor growth and metastasis (178–180). The efficacy of these drugs has been evaluated both in monotherapy and in combination therapy with standard chemotherapeutic agents. *In vitro* studies evidenced that statins are able to inhibit cell proliferation and viability, or causing apoptosis in different human cancer cell lines, such as breast, ovarian and prostate tumor cells. In particular, it has been demonstrated that the open-ring conformation of statins is responsible for the inhibition of HMGCR and apoptosis induction (181). *In vivo* studies evidenced that statins reduce

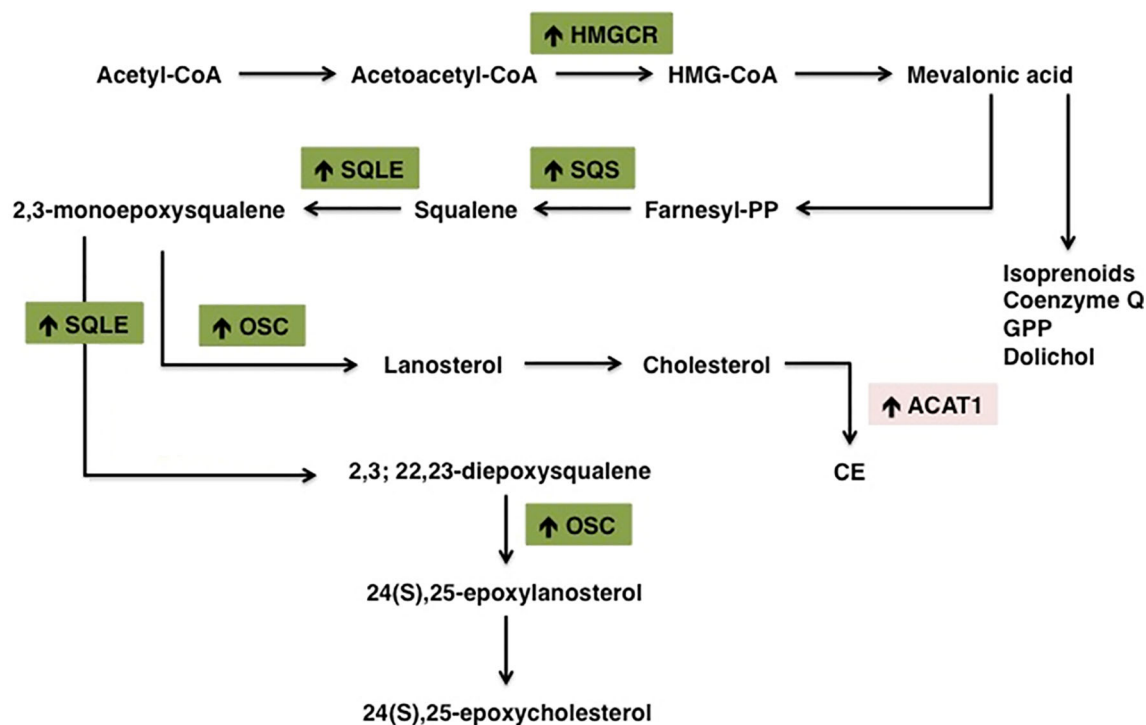


**FIGURE 2** | Schematic representation of the main alterations in cholesterol metabolism pathway in tumors. Cancer cells are highly proliferative and therefore strongly dependent on cholesterol to sustain the high demand of substrates for membrane biosynthesis. Cancer cells increase their cholesterol demand by enhancing *de novo* biosynthesis (or exogenous uptake). Increased/overexpressed enzymes in cholesterol biosynthesis pathway are indicated with (↑). HMGCR, 3-hydroxy-3-methylglutaryl-CoA reductase; SQS, Squalene synthase; SQLE, Squalene epoxidase; ACAT1, Acetyl-CoA Acetyltransferase 1.

tumor growth and arrest metastasis progression (113, 182–186). Terzi and co-workers (187) evaluated the effect of two statins, atorvastatin and simvastatin, combined with the standard chemotherapeutic agent, bortezomib, in human multiple myeloma. The results showed that statins are able to improve the effectiveness of bortezomib and reduce the adverse effects (187). The combined treatment of pivalastatin with gemcitabine synergically reduced cell proliferation of MIA PaCa-2 cells inducing cell cycle arrest. Moreover, the same combination reduced the tumor growth in *in vivo* xenograft models (188). A new formulation of atorvastatin was developed in order to cross the blood-brain barrier and target the glioblastoma tumor cells. This new nanoformulation was cytotoxic in mouse and human glioblastoma cells, and was able to reduce the growth in a three-dimensional (3D) tumor model (189). The anticancer role of statin treatment in combination with conventional anticancer drugs, has been tested in clinical trials for the treatment of different types of tumors, such as breast, prostate, ovarian or lung cancers, bringing to light controversial effects of the association (Table 3 summarizes some clinical trials on breast, ovarian and prostate cancer). Different clinical trials demonstrated that statins are able to reduce tumor progression and enhance the survival rate of patients with breast cancer (194). Farooqui reviewed different randomized controlled trials and concluded that the addition of statins to standard chemotherapy is not able

to enhance the survival in patients with advanced cancers and a prognosis of less than 2 years (195). A Swedish study, instead, concluded that statins use for 6 months in patients with multiple myeloma enhanced the survival rate of both men and women (196). In another study, atorvastatin was administered in patients with prostate cancer for 27 days before prostatectomy. In this case, drug administration was not able to decrease tumor proliferation with respect to placebo, however, a longer administration of atorvastatin showed beneficial effects (197). In light of this result, it could be interesting to define the specific chronic drug administration before surgery. In fact, other clinical trials evidenced that a chronic therapy of 6 months before surgery resulted to be more efficient compared with a 3 months therapy in reducing tumors (198). It is thus evident that the current knowledge obtained from several *in vitro* and *in vivo* studies in different types of tumors confirmed and deepened the molecular mechanisms of statins as anticancer drugs. Since statins were already approved for hypercholesterolemia treatment, their repositioning in the oncological field has benefited from an easier and faster translation into clinic. However, clinical trials evaluating the antitumor effect of these drugs are still few. Monotherapy studies highlight the potential of this class of drugs in cancer prevention, but the pharmacological differences among all statins, as well as the heterogeneity of tested tumors, lead to a lack of proven

**TABLE 3 |** Statins currently under evaluation in clinical trials for cancer treatment.

Type of statin	Cancer	Aim	Phase trial	ClinicalTrials.gov Identifier
<b>Simvastatin</b>	Breast cancer	Identify the molecular and genetic mechanisms by which statins influence breast cancer cell proliferation	Recruiting – Phase II	NCT03454529
		Preventive effect of a new breast cancer for women with high risk of a new breast cancer	Completed – phase II	NCT00334542 (190)
		Combined therapy with anti-HER2 to sensitize it in metastatic cancer	Recruiting-Phase II	NCT03324425
	Gastric cancer	Combined therapy with Capecitabine/cisplatin did not increase the progression-free survival of patients with advanced cancer	Completed-Phase III	NCT01099085 (191)
	Ovarian cancer	To evaluate the effect in women with ovarian cancer platinum sensitive	Recruiting – early phase I	NCT04457089
<b>Lovastatin</b>	Breast cancer	Chemoprevention effect of statin in women with high cancer risk	Completed – Phase II trial	NCT00285857 (192)
	Ovarian cancer	Combined therapy of paclitaxel and lovastatin in refractory or relapsed ovarian cancer	Completed – Phase II trial	NCT00585052
<b>Rosuvastatin</b>	Non-small cell lung cancer	Combined therapy with erlotinib in advanced incurable cancer	Completed – Phase I trial	NCT00966472
	Colorectal cancer	To study the effect in patients with stage I or II cancer after surgery	Terminated – Phase III	NCT01011478
	Rectal cancer	Combined with standard chemoradiation to enhance the patients' survival	Recruiting- phase II	NCT02569645
<b>Fluvastatin</b>	Breast cancer	Effect of statin on biomarkers in women who are undergoing surgery	Completed – Phase II trial	NCT00416403 (193)
<b>Atorvastatin</b>	Triple negative breast cancer	Antitumor effect of combined treatment of atorvastatin and zoledronate	Recruiting – Phase II trial	NCT03358017
	Prostate cancer	Effect of its administration before prostatectomy	Completed-Phase II trial	NCT01821404

positive outcomes. In addition, it has been demonstrated the impossibility to administer high doses because of their adverse effects (199). At the same time, relatively few clinical trials take into consideration the combined therapy with standard chemotherapeutic agents, a strategy allowing low dose administration and lower toxicity of the single agents. Thus, further studies evaluating the beneficial effect of statins in combination with conventional chemotherapy have to be conducted in order to assess their potential in cancer therapy.

### Pharmacological Modulation of OSC

2,3-Oxidosqualene cyclase (OSC) is the enzyme that catalyzes the conversion of 2, 3-monoepoxysqualene into lanosterol acting downstream of HMGCR (116). Since lanosterol is the precursor of cholesterol, the inhibition of OSC causes decreased cholesterol synthesis (175), but unlike statins the LDL catabolism is not affected. This suggests that OSC inhibitors act in a different way (200, 201). Staedler et al. (175) demonstrated the antitumor effect of OSC inhibitors in human glioblastoma and brain-derived endothelial cells. Moreover, the combined treatment with OSC inhibitors and atorvastatin showed an increased antitumor effect in human glioblastoma cells with respect to monotherapy (175). Among the OSC inhibitors, Ro 48-8071 ([4'-[6-(Allylmethylamino)hexyloxy]-4-bromo-2'-fluorobenzophenone fumarate]) emerged for its potential antitumor effect. Grinter and coworkers (117) demonstrated that this molecule was able to inhibit cell proliferation in BT-474 human breast cancer cells (117). Ro 48-8071 decreased cell viability of ER $\alpha$ -positive human breast cancer cells (BT-474 and MCF-7), without affecting normal AG1132A

cells. Moreover, this compound proved efficacy in reducing tumor growth in *in vivo* mouse xenograft model injected with BT-474 cells, without showing toxicity at doses administered (116). Maione et al. (118) demonstrated the antitumor effect of Ro 48-8071 in murine models of intestine and pancreas cancers. In fact, the role of this compound was investigated in mouse xenograft models injected with human colon carcinoma HCT116 cells, and pancreatic ductal adenocarcinoma HPAF-II cells. Results evidenced that Ro 48-8071 was able to weaken angiogenesis and inhibit tumor growth in the two mouse models previously mentioned (118). Hyder and coworkers (119) investigated the effect of Ro 48-8071 on cell viability and apoptosis in different lines of human prostate cancer cells. Data showed that this compound reduced cell viability in hormone-dependent LNCaP, castration-resistant PC-3 and DU145 prostate cancer cells, also causing apoptosis (119). Since several studies demonstrated the antiproliferative role of ER- $\beta$  (202–205), castration-resistant prostate cancer cells were treated with the combination of Ro 48-8071 and ER- $\beta$  agonist diarylpropionitrile showing enhanced activity in inhibiting cell viability. *In vivo* treatment with Ro 48-8071 was able to suppress the growth of prostate cancer PC-3 cell xenografts in mice (119).

### Pharmacological Modulation of SQS

Squalene synthase (SQS) is an enzyme that catalyzes the conversion of FPP into squalene, the precursor of cholesterol (206). Since squalene synthase is the enzyme responsible for the first committed step in cholesterol production, its targeting results of interest in clinical therapy (207). Zaragozic acids, natural products obtained from fungi, are pharmacological

inhibitors of SQS. Brusselmans et al. (120) demonstrated that the expression of squalene synthase was enhanced in LNCaP prostate cancer cells following androgen stimulation. Thus, the inhibition of the enzyme by downregulation or by treatment with zaragozic acid A, was able to cause both the arrest in growth and the induction of cytotoxicity in prostate cancer cells (120). Lanterna and coworkers (121) tested two different isoforms of zaragozic acid, A and B, in mouse models of RMA lymphoma and LLC Lewis lung carcinoma and results confirmed the ability of zaragozic acid in reducing tumor growth, without showing adverse effects (121).

## Enhanced Cholesterol Uptake

An alternative strategy exploited by cancer cells to promote sterol-mediated proliferation is to increase the uptake of exogenous cholesterol. NPC1L1 is a critical sterol transporter, essential for cholesterol intestinal uptake. In colorectal cancer, NPC1L1 promotes colitis-associated tumorigenesis by inducing cholesterol absorption and increasing its plasmatic levels (208). Malignant cells capture and internalize cholesterol through the activity of LDLRs. Indeed, LDLRs expression levels are increased in many cancers, including glioblastoma and leukemia, as well as in pancreatic and lung cancers (209). Also, higher levels of LDLRs negatively correlate with the survival of patients affected by pancreatic adenocarcinoma (210). HER2-positive and triple-negative breast tumors characterized by higher LDLRs intratumoral levels are associated with poorer prognosis, suggesting an important contribution of LDL cholesterol in breast cancer progression (211). LDLRs promote tumor development and progression, by modulating cancer cell invasive and migratory potential, as well as adhesivity and plasticity. Indeed, LDLRs foster epithelial-to-mesenchymal transition (EMT), the secretion of metalloproteinase MMP-9 and the activation of Wnt/ $\beta$ -catenin oncogenic signaling (212, 213). On the other hand, HDL cholesterol is accumulated by steroidogenic organs in a process mediated by scavenger receptor type B class 1 (SRB1). SRB1 is overexpressed in diverse human malignancies, such as prostate, breast, ovarian, and colorectal cancers (214). In lung adenocarcinoma, SRB1 represents an independent prognostic factor and its expression positively correlates with malignant tumor behavior and impaired overall survival (215). Consistently, cancer patients present lower levels of HDL cholesterol compared to healthy subjects, suggesting that cancer cells exploit HDL cholesterol from peripheral tissues to sustain their malignant phenotype by picking it up in a SRB1-mediated fashion (36). Indeed, high levels of SRB1 characterize highly undifferentiated and metastatic prostate tumors, which are usually associated with androgen independence. Accordingly, SRB1-mediated cholesterol supplying might provide sterol precursors, thereby promoting tumor self-production of androgens and the development of castration-resistant phenotypes (216). Currently, there are not pharmacological inhibitors targeting LDLR and SRB1. However, increasing evidence highlighted the correlation between high-cholesterol diet and increased tumor growth and development of metastasis (217–219). Dietary cholesterol, that represents only the 30% of total cholesterol in the human body is delivered to liver through

chylomicrons, which are hydrolyzed to fatty acids and stored in adipose tissue (220). Once cholesterol arrives at hepatocytes, it is removed either in form of free cholesterol or converted in bile acids. Excess of cholesterol is converted into cholesterol esters and stored in hepatocytes (221). Accumulating evidence, based on metabolic mechanisms, highlights that tissues enriched of stored fatty acids could be more prone to be related with increased cancer risk (222, 223). Pelton and coworkers (224) demonstrated that high-cholesterol diet enhances the tumor growth of human breast cancer injected in a mouse model. In light of this consideration, the administration of low-cholesterol diet or ezetimibe slightly decreased the growth of tumors by a reduction of cholesterol levels (224). Moreover, it has been shown that the inhibition of the xanthine oxidase with a pharmacological inhibitor was able to reduce both tumor growth and metastasis in breast mouse model fed with high-cholesterol diet (225). Thus, it appears that a low-cholesterol diet could be a promising strategy to counteract tumor growth. Furthermore, combining the low-cholesterol diet with anticancer drugs could become an exploitable field in clinical therapy.

## Dysregulated Cholesterol Efflux

In physiological conditions, the excess of cellular cholesterol is removed from peripheral tissues through a process controlled by ATP binding cassette transporters, mainly ABCA1. In general, malignant cells show decreased levels of ABCA1, thereby promoting intracellular cholesterol storage. Indeed, ABCA1 deregulation leads to cholesterol accumulation in the mitochondrial compartment, which in turn supports the malignant transformation (32, 155). Moreover, higher levels of intracellular cholesterol directly affect the lipid composition of plasma membranes, as well as their physical properties: cholesterol enrichment increases the phospholipids' degree of order in the bilayer while reducing its permeability, thereby promoting tumor resistance to membrane-active anticancer drugs (226). Peroxisome proliferator-activated receptors (PPAR)  $\alpha$  and  $\gamma$  play a pivotal role in modulating both intracellular and extracellular cholesterol fluctuations (227, 228). Indeed, PPAR $\alpha$  and PPAR $\gamma$  activation promotes LXR-mediated ABCA1 expression, thus inducing cholesterol efflux to the lipid-poor apolipoprotein A-I (229). Also, PPAR $\alpha$  blocks cholesterol biosynthesis by inhibiting sterol regulatory element-binding protein 2 (SREBP-2) activity (230). Accordingly, PPAR $\alpha$  and PPAR $\gamma$  are considered tumor suppressor genes which inhibit tumor progression (231). On the other hand, cholesterol integration within the plasma-membrane reduces malignant cell migration and metastatic potential. Specifically, increased plasma membrane-associated cholesterol reduces the fluidity of the bilayer, resulting in restricted cell motility and EMT, a critical event for the development of tumor metastasis (232). The variation in cholesterol content, in fact, affects membrane fluidity, permeability and rigidity, thus impacting several processes, such as invasion, migration or tumor development, growth and metastasis (233). In particular, different studies reported that increased cholesterol percentage deriving from higher *de novo* biosynthesis leads to enhanced rigidity and



decreased fluidity, thus contributing to decreased cell mobility (234), or to altered membrane permeability, which is involved in altered cancer cell response to drug treatments (226). In line with this, variations in intracellular cholesterol levels mediated by ABCA1 overexpression drive the onset of EMT and the promotion of tumor invasiveness, whilst human solid tumors at advanced stages are characterized by high levels of ABCA1 expression (235). Therefore, metastatic cancer cells substantially reduce their cholesterol levels in the plasma membrane compartment by overexpressing ABCA1, which eventually mediates cholesterol efflux (232). Conversely, the development of primary tumors requires pro-oncogenic and survival-stimulatory signaling pathways, which are dependent or modulated by lipid rafts (114). Accumulations of cholesterol in lipid rafts induce the aberrant activation of tyrosine kinase receptors, such as IGF1 and HER2, as well as PI3K/AKT-mediated tumorigenic signaling (234, 236, 237).

### Pharmacological Modulation of PPAR $\alpha$

Saidi and coworkers (144) tested fenofibrate, which is an agonist of PPAR $\alpha$ , in Ishikawa endometrial cancer cells. The results showed inhibition of cell viability and apoptosis induction. Moreover, the combined use of fenofibrate and retinoic acid, which is an agonist of retinoid-X-receptor (RXR), enhanced the inhibition of cell proliferation (144). The mechanism of action of fenofibrate still remains unclear. In fact, fenofibrate reduced the cell proliferation of human hepatoma cells through the inhibition of Akt phosphorylation and not through a PPAR $\alpha$ -dependent mechanism (145). Jan et al. (146) proposed metabolic reprogramming as the mechanism underpinning the anticancer effect of fenofibrate. In particular, this drug caused the reduction of oral cancer cell proliferation and activated the glycolysis pathway. Moreover, *in vivo* administration of fenofibrate in mice reduced the tumor growth (146). The antitumor effect of fenofibrate through the reprogramming of cancer metabolism is also confirmed in gastric carcinoma. In fact, the use of this drug reduced both *in vitro* cancer cell proliferation and *in vivo* tumor growth. In addition, Chen and coworkers (238) demonstrated that treating cells with fenofibrate causes mitochondrial dysfunction due to its accumulation too, suggesting also the PPAR $\alpha$  involvement in mitochondria reprogramming (238). Thus, targeting PPAR $\alpha$  could be an interesting tool for cancer treatment. Moreover, fenofibrate was also tested in combination with chemotherapeutic agents, suggesting that using the combined therapy could be a strategy to overcome drug resistance. In fact, treating prostate resistant cancer cells with fenofibrate is able to resensitize them to docetaxel (149).

### Enhanced Cholesterol Storage

The overload of free cholesterol inside the cell is extremely toxic (239). Therefore, in physiological conditions, the excess of free cholesterol is avoided by producing its esterified form, namely cholesteryl ester (240). Cholesteryl esters can be readily stored into lipid droplets, thus preventing the lipotoxic potential of free cholesterol (241). The accumulation of intracellular cholesterol is strongly oncogenic and represents a common hallmark of cancer (242, 243). For instance, the intracellular levels of cholesteryl

esters and lipid droplets are substantially increased in breast cancer, leukemia, and glioblastoma (244–246). In colorectal cancer, lipid droplet-enriched malignant stem cells are characterized by increased clonogenic and tumorigenic potentials (247). Consistently, the cholesteryl ester-producing enzyme acetyltransferase ACAT1 is upregulated in many cancers, including hepatocellular carcinoma, castration-resistant prostate cancer, and pancreatic cancer, whilst its expression positively correlates with reduced overall survival and recurrence-free survival in adrenocortical carcinoma (126, 248–250). ACAT1 overexpression and cholesteryl esters enrichment play a dual role in promoting cancer progression. Higher levels of cholesterol esterification lead to decreased contents of free cholesterol, thereby protecting malignant cells from ER stress and apoptosis (126, 251). On the other hand, esterified cholesterol represents an intracellular source of cholesterol, which can be exploited by cancer cells when needed to fuel the malignant phenotype. Consistently, the cholesteryl ester-metabolizing enzyme lysosomal acid lipase (LAL) is upregulated in tumor tissues, thus providing malignant cells with ready-to-use free cholesterol (243, 252). PTEN deficiency drives cholesteryl esters accumulation in pancreatic cancer through the activation of the downstream PI3K/Akt/mTOR/SREBP signaling pathway; increased content of esterified cholesterol promotes tumorigenesis and metastatic potential (126). Similarly, cholesterol reservoirs are enriched in advanced and metastatic human prostate cancer, while nearly absent in healthy prostate, benign prostatic hyperplasia, and prostatic intraepithelial neoplasia. Accumulation of cholesteryl esters is triggered by PTEN loss, which in turn induces the expression of SREBP and LDLR *via* PI3K/AKT/mTOR, thus promoting ACAT1-mediated cholesterol storage in lipid droplets (243). Thanks to cholesterol esterification and subsequent accumulation, prostate cancer cells reduce the intracellular levels of free cholesterol, thereby avoiding free cholesterol lipotoxicity and maintaining SREBP-induced cholesterol biogenesis and uptake (62, 253). Moreover, increased contents of esterified cholesterol might fuel the development of castration-refractory prostate tumors by providing androgen precursors for *de novo* steroidogenesis (125, 254, 255). The excess of lipid droplets accumulated in tumor cells is the leading cause of enhanced cell proliferation and the responsible of cancer aggressiveness. Thus, it appears that targeting enhanced cholesterol storage could be an interesting tool in cancer therapy (113).

### Pharmacological Modulation of ACAT-1

ACAT-1 is overexpressed in two ER<sup>+</sup> lines of human breast cancer, MDA-MB-231, and MDA-MB-436. Higher expression of this enzyme could be related to a higher cell proliferation rate (122). Treating cells with CP-113818, which is an ACAT-1 inhibitor, caused a reduction in cell proliferation and migration, suggesting the correlation mentioned above (122). Bitter melon extract, a natural ACAT-1 inhibitor, exerts antitumor effects towards breast cancer cells. Shim and coworkers (123) fed orthotopic mice models of MDA-MB-231 cells with this compound showing a reduction in tumor growth

through cholesterol metabolism modulation (123). It has also been demonstrated that *ACAT-1* is a metabolic “tumor promoter”, since it is overexpressed in human breast cancer cells leading to tumor formation and lung metastasis (256). Cancer cells use this mitochondrial enzyme to recycle ketone acids into acetyl-CoA enhancing the ATP production. Ozsvári and coworkers (257) investigated *ACAT-1* as a therapeutic target and the use of *in silico* drug design identified *mitoketoscins*. These molecules belong to a new therapeutic class of drugs that inhibits mitochondrial functions and *ACAT-1* (257). Lo et al. (258) demonstrated that *ACAT-1* is overexpressed in MES-SA/Dx doxorubicin-resistant uterine sarcoma cancer cells compared to the sensitive counterpart, suggesting a correlation with drug resistance. Thus, the *ACAT-1* knock-down caused a decrease in cell viability, showing an important role of this enzyme in the onset of drug resistance (258). Lee and coworkers (124) developed avasimin, which is a nanoformulation containing avasimibe, an *ACAT-1* inhibitor. They tested the formulation in different human cancer cell lines, showing that avasimin was able to reduce lipid droplets accumulation in PC3 prostate cancer cells. Concerning the effect on cell viability the nanoformulation was used to treat human PC3, MIA-PaCa2 pancreatic cancer cells, A549 lung cancer cells, and HCT116 colon cancer cells, showing a reduction in cell viability in all cell lines. Moreover, they evaluated *in vivo* the avasimin effect in PC3 and HCT116 cell xenograft mouse model. The results evidenced a decrease in both tumor growths after the avasimin intravenous treatment (124). Li et al. (126) demonstrated an overexpression of *ACAT-1* in MIA PaCa-2 and PANC-1 human pancreatic cancer cells compared to normal cells. Treating cells with avasimibe or genetic silencing of *ACAT-1* caused the block of cholesterol esterification that led to a reduction in cell invasion and migration. Results showed a higher sensitivity to the *ACAT-1* inhibition of cancer cells compared to the normal counterpart. A xenograft mouse model injected with MIA PaCa-2 cells was treated with avasimibe and results showed a reduction in tumor growth, decreased metastatic lesions in lymph nodes and in liver compared to untreated mice (126). Moreover, it has been suggested an important role of cholesteryl ester in the development of metastasis. Thus, Lee and coworkers (125) tested avasimibe in PC-3M metastatic prostate cancer cell lines derived from PC-3 xenografts liver metastasis. The treatment showed a decrease in cell migration rate. In addition, when they treated PC-3M xenograft mice with avasimin a reduction in tumor growth and metastasis development were observed. Taken together, these data suggested an implication of cholesteryl ester in the development of metastasis in prostate cancer. *ACAT-1* inhibition compromised Wnt/ $\beta$ -catenin signaling consequently overcoming metastasis formation (125). Li et al. (128) demonstrated a correlation between cholesterol metabolism and gemcitabine resistance, since it was found a higher accumulation of cholesteryl ester in gemcitabine-resistant pancreatic ductal adenocarcinoma cells compared to the sensitive counterpart. In addition, it has been demonstrated that Akt is implicated in cholesteryl ester accumulation. Treatment of resistant cells with avasimibe, an *ACAT-1*

inhibitor, caused a reduction in cell proliferation. Moreover, the combined treatment with gemcitabine and avasimibe showed synergic effect *in vitro* and resulted in decreasing tumor growth in *in vivo* xenograft mouse model injected with Mia PaCa-2 cells. Avasimibe treatment downregulates Akt contributing to resensitization of resistant cells (128). It has been demonstrated that the upregulation of *ACAT-1* is implicated in the development of metastasis in LLC Lewis lung cancer. Treatment of LLC cells with avasimibe caused a decrease in cell proliferation and migration. Moreover, avasimibe alone or in combination with cyclophosphamide was able to reduce both tumor growth and metastasis formation in xenograft mouse model (127).

## Oncogenic Signaling and Cholesterol Homeostasis

In physiological conditions, cholesterol homeostasis is maintained by sterol-sensitive systems, mainly SREBP2 and Liver X receptors (LXR). Oncogenic potential gaining and tumor suppressor activity loss in cancer cells deeply affect cholesterol metabolism. As a general rule, oncogenic pathways induce cholesterol biosynthesis and uptake, thus promoting increased intracellular levels of sterols, while tumor suppressor pathways lead to cholesterol lowering inside the cells (34). Indeed, the oncogenic *MYC* induces cholesterol biosynthesis by upregulating HMGCR expression, which is essential during oesophageal squamous cell carcinoma malignant transformation (259, 260). Similarly, aberrant EGFR oncogenic signaling is involved in SCAP-mediated SREBP-2 activation, thus promoting LDLR expression and subsequent cholesterol uptake (261, 262). In human hepatocellular carcinomas, the pro-oncogenic activity of c-FOS mediates LXR $\alpha$  downregulation, which leads to cholesterol retention and production of tumorigenic oxysterols (263). Oxysterols are oxygenated cholesterol metabolites which target and modulate the activity of many nuclear receptors, including LXRs, retinoid-related orphan receptors (RORs), as well as the Hedgehog signaling pathway (264, 265). Among them, 27-hydroxycholesterol (27HC) is an endogenous selective estrogen receptor modulator involved in breast and prostate cancers progression (266). 27HC promotes cell proliferation through *p53* inactivation, as well as cell migratory potential *via* Signal Transducer and Activator of Transcription-3 (STAT-3)-mediated MMP9 activation and subsequent EMT induction (267, 268). 27HC is also involved in tumor angiogenesis by inducing VEGF activation through ER $\alpha$  signaling or reactive oxygen species-mediated STAT-3 recruiting (269). Consistently, advanced breast cancers upregulate CYP27A1 while decreasing the expression of CYP7B1, thereby promoting 27HC accumulation (31, 270). Higher levels of intracellular cholesterol in cancer cells are determined by aberrant HMGCR activity, due to disrupted sterol-controlled feedback regulation or SREBP-mediated overexpression (271–273). In hypoxic tumor microenvironments, SREBPs and their downstream genes are strongly upregulated and support cell survival and tumor growth (274). The activity of SREBPs is promoted by many oncogenic

signaling pathways, including PI3K/Akt and Ras/ERK, which eventually induce cholesterol biosynthesis and uptake, while inhibiting its ABCA1-mediated efflux (275–277). In line with this, tumor suppressors genes *p53* and *PTEN* increase cholesterol clearance by increasing ABCA1 activity, while reducing cholesterol absorption and accumulation (126, 278). Indeed, *PTEN* and *p53* loss induce PI3K/Akt signaling, thereby promoting LDLR-induced cholesterol uptake and subsequent formation of cholesteryl esters (243, 279, 280).

### Pharmacological Modulation of LXR

Liver X receptors (LXR) are nuclear receptors involved in cholesterol metabolism. Targeting LXR could be a good strategy because its activation is able to modulate the cholesterol pathway. The consequence is decreased cholesterol levels into cells, causing limited cancer cell proliferation. As already explained above, LXR can be activated by endogenous ligands, such as oxysterols but also by agonists, such as T0901317 (130). Treating LNCaP human prostate cancer cells with LXR agonist T0901317 caused cell death through apoptosis. Moreover, the treatment with T0901317 in a xenograft mouse model injected with LNCaP cells was able to reduce tumor growth (129). It is known that increased levels of cholesterol activate Akt enhancing its phosphorylation besides improving tumor progression (281). Pommier and coworkers investigated the effect of LXR activation on cholesterol metabolism. T0901317 treatment was able to increase the expression of LXR target gene *Abcg1* and consequently causing a higher cholesterol efflux. Moreover, overexpression of *Abcg1* modulates reverse cholesterol transport causing cholesterol exhaustion in rafts and the inactivation of Akt signaling pathway (129). T0901317 showed anticancer properties also in ovarian cancer. In fact, treatment of ovarian cancer cells with this compound was able to inhibit cell proliferation and cause apoptosis (134). It was demonstrated that MCF-7 human breast cancer cells express LXR. Thus, treating these cells with the LXR synthetic agonist, T0901317, and the natural one, 22(R)-hydroxycholesterol, resulted in a reduction of cell proliferation besides both agonists caused cell death through apoptosis. In addition, T0901317 treatment was able to decrease intracellular cholesterol and LXR activation increased the expression of its target gene *Abcg1* in MCF-7 cells (130). Furthermore, it has been demonstrated that the combined therapy of T0901317 and gefitinib, an anticancer drug, was able to reduce cell and tumor growth both *in vitro* and *in vivo* in a lung cancer model (135). This agonist combined with sorafenib enhanced the antitumor effect of the chemotherapeutic agent in hepatocellular carcinoma. In fact, the activation of LXR blocks two pathways, MET and EGFR, avoiding their availability for lipid rafts and consequently enhancing the efflux of cholesterol (136). MCF-7, T-47D, SK-BR-3, or MDA-MB-231 human breast cancer cell lines, which are genetically different, expressed both LXR isoforms, LXR- $\alpha$  and LXR- $\beta$ . Treating these cell lines with GW3965 LXR ligand caused a reduction in proliferation. Nguyen-Vu and coworkers correlated decreased cell proliferation with the downregulation of genes involved in cell growth. For example, they showed that

the downregulation of E2F2, which is a transcription factor, caused a reduced proliferation of MCF-7 and T-47D ER<sup>+</sup> cancer cells (137). GW3965 treatment inhibited cell proliferation in both human MCF-7 breast and SW480 colon cancer cell lines. Investigating the molecular mechanisms underlying this anti-proliferative effect, Hassan and coworkers (138) demonstrated that the activation of LXR caused the decrease of Akt phosphorylation leading to its inactivation (138). The expression of the isoform LXR- $\beta$  was assessed in three different human pancreatic ductal adenocarcinoma cell lines, BxPC-3 and MIA-PaCa-2 and PANC-1. Treating cells with GW3965 increased the expression of the LXR target gene *Abca1*. Moreover, cell proliferation of human pancreatic ductal adenocarcinoma cell lines decreased after treatment with LXR agonist and the cell cycle was blocked (140).

The agonist GW3965 in combination with the standard chemotherapeutic agent gefitinib demonstrated synergic effect in resensitization of gefitinib-resistant lung cancer cells (141). Pencheva and her group (139) hypothesized that targeting LXR could be a strategy to block metastasis progression in melanoma. Treating melanoma cells with LXR agonists, GW3965 or T0901317, did not cause an impact on cell proliferation but affected cell invasion. In particular, the use of LXR agonists was able to block lung metastasis development and reduce brain metastasis progression in mouse melanoma models. In addition, it was also demonstrated that oral or diet administration of GW3965 to dacarbazine-resistant mice was able to strongly reduce melanoma tumor growth and that the combined treatment of LXR agonist with dacarbazine has proven to be more active compared to GW3965 alone. Moreover, the same agonist was able to reduce tumor growth in mouse melanoma models resistant to vemurafenib, and again, the combined treatment of GW3965 with vemurafenib had a higher effect compared to LXR alone (139). Zhang and coworkers (131) demonstrated that both LXR isoforms are expressed in murine B16F10 melanoma cells. When LXR is activated through the agonist T0901317 there was a decrease in melanoma cell proliferation and apoptosis through caspase-3 activation. Moreover, the treatment of mouse melanoma models with T0901317 reduced tumor growth. In order to confirm the involvement of LXR signaling in melanoma anti-tumor activity, the LXR target genes *Abca1* and *SREBF1* were checked confirming their increased expression in mice treated with T0901317 (131). Human multiple myeloma cells expressed both LXR isoforms, LXR- $\alpha$  and LXR- $\beta$ . Treating cells with LXR ligand, 22(R)-hydroxycholesterol and the two agonists, GW3965 and T0901317, strongly increased the expression of two target genes, *Abca1* and *Abcg1*, while slightly the one of the target gene *SREBP-1c* (132). The Hedgehog (Hh) signaling pathway is a regulator of proliferation, differentiation and it has been linked to carcinogenesis (282). Agarwal and coworkers showed that activating LXR represents a strategy to inhibit Hh signaling pathway in human multiple myeloma cells. Moreover, they showed that treating cells with LXR agonists was able to inhibit clonogenic growth both *in vitro* and *in vivo* (132). SR9243 is a specific inverse agonist of LXR. Flaveny et al. (142)



demonstrated that treatment of prostate, lung and colon cancer cells with SR9243 decreases cell proliferation, causes cell death through apoptosis and reduces tumor growth in mouse xenografts. Moreover, a combined treatment of SR9243 with cisplatin or 5'-fluorouracil sensitized cells to chemotherapeutic drugs. In particular, SR9243 treatment caused down-regulation of *GCK1*, *PFK2*, *PFK1*, and *LDH* Warburg genes, and decreased expression of *FASN*, *SREBP1-c*, and *SCD1* lipogenic gene both in *in vitro* and *in vivo* colon xenograft models (142). Similar results regarding lipid metabolism were obtained in clear renal cell carcinoma both *in vitro* and *in vivo* (143). SR9243 was also able to reduce the expression of LXR target gene *Abca1* involved in cholesterol transport (142). In addition, Wu et al. (143) tested the LXR agonist LXR623 in clear cell renal cell carcinoma demonstrating its role in decreasing cell proliferation and causing apoptosis. Considering that LXR is a transcription factor able to regulate the expression of different target genes, including those related to glycolysis and lipogenesis, targeting this receptor could represent a promising approach in cancer treatment. Kaneko and coworkers (133) demonstrated that LXR- $\alpha$  was expressed in human oral squamous cell carcinoma. Thus, activating LXR with T0901317 resulted in a reduction in cancer cell viability through the induction of the target gene *Abca1*. Moreover, SAS cells were injected in SCID mice and then they were treated with T0901317. The results evidenced a reduction in tumor growth after treatment (133).

The LXR agonist GW3965 was also used to target *LDLR* in glioblastoma. In fact, this pharmacological approach both inhibits the uptake of exogenous LDL and enhances the cholesterol excision from cells. Treating cancer cells with this drug induced apoptosis *in vitro* and reduced *in vivo* tumor growth (283).

### Pharmacological Modulation of SREBP

Fatostatin is a non-sterol diarylthiazole derivative and a specific inhibitor of SREBP. The mechanism of action of this drug consists in binding the SREBP cleavage activating protein (SCAP), and consequently blocking cholesterol biosynthesis (150, 151). Targeting SREBP could be a new pharmacological approach for cancer treatment. Fatostatin showed antitumor effect in both androgen-responsive and androgen-nonresponsive prostate cancer cells by the *in vitro* inhibition of cell proliferation and cell cycle arrest. In addition, it was able to reduce *in vivo* tumor growth (150). Gholkar and coworkers (284) investigated the mechanism underlying the antitumor effect of fatostatin in different types of tumors, such as human breast and cervix cells, showing its ability to block the tubulin polymerization and arrest cells in mitosis (284). Fatostatin reduced cell viability in endometrial cancer (151, 152) and decreased the tumor growth in xenograft mice enhancing their survival rate (151). ER-positive breast cancer cells treated with fatostatin showed decreased cell viability and higher lipid accumulation. In particular, increased ceramides' levels are strictly related to apoptosis. The xenograft volume decreased after treatment with fatostatin (153). Moreover, the combined treatment with tamoxifen resulted synergic in

reducing both *in vitro* cell proliferation and *in vivo* tumor growth in breast cancer (154).

## CONCLUSIONS

This review examined the most relevant aspects of the metabolic reprogramming that have been observed in cancer focusing on cholesterol metabolism. Understanding the metabolic vulnerabilities of tumor tissues can help in the identification of new therapeutic targets in order to develop a better cancer treatment. The large amount of literature of the last decades provided overwhelming evidence of lipid and cholesterol metabolism alterations in cancer. High levels of cholesterol are essential to sustain fast tumor cell proliferation and the complex role of cholesterol in cancer development, progression, and susceptibility to chemotherapy is firmly established. Intracellular cholesterol levels can be regulated by *de novo* synthesis, reduced degradation, increased uptake or storage. This review summarizes the current knowledge regarding the alteration in all these aspects of cholesterol metabolism, highlighting the molecular targets and the possible pharmacological approaches that are currently under investigation (Figure 3 and Table 2). Despite a large amount of *in vitro* and *in vivo* evidence suggesting the use of cholesterol-related drugs against cancer, the clinical translation is still limited (Table 3). To date, only statins and fenofibrate have resulted in clinical trials for cancer therapy showing promising results. Besides the treatment with a single agent, a common therapeutic strategy is the drug combination, which can affect simultaneously different pathways in cancers; thus, it is of interest to underline that the combination of conventional chemotherapeutic drugs with cholesterol-lowering agents is under investigation showing encouraging results.

A better understanding of the metabolic dependencies of tumors also provides new hints for therapeutic strategies in cancer therapy. Novel studies are focusing on the exploitation of lipid/cholesterol metabolic vulnerabilities of cancer to develop new drug delivery systems and strategies. Recent works make use of engineered lipids or adipocytes to deliver anticancer drugs to the tumors (285, 286). Moreover, LDL and HDL particles have been proposed as delivery systems for anticancer drugs. A work by Sobot et al. (287) proposed a chemical linkage of gemcitabine to squalene-moiety (the lipid precursors of cholesterol biosynthesis) assembled in nanoparticles. They showed that LDLR levels positively correlated with nanoparticle uptake and cytotoxic effect in cancer cells and in tumor-bearing mice (287). Mooberry and coworkers, instead, tested a formulation of paclitaxel encapsulated in synthetic/reconstituted high-density lipoprotein (rHDL). The increased uptake of anticancer drug is mediated by SR-B1, which is overexpressed in prostate cancer cells (288). Thus, conjugation of cholesterol moieties with anticancer drugs is an attractive approach (289) for cancer therapy, which can also improve the chemotherapy efficacy and reduce the cytotoxicity to normal cells.

The repurposing of cholesterol-lowering drugs for cancer therapy might be a promising approach to selectively affect cancer cells, highly dependent from cholesterol and to eventually improve the efficacy of conventional chemotherapy



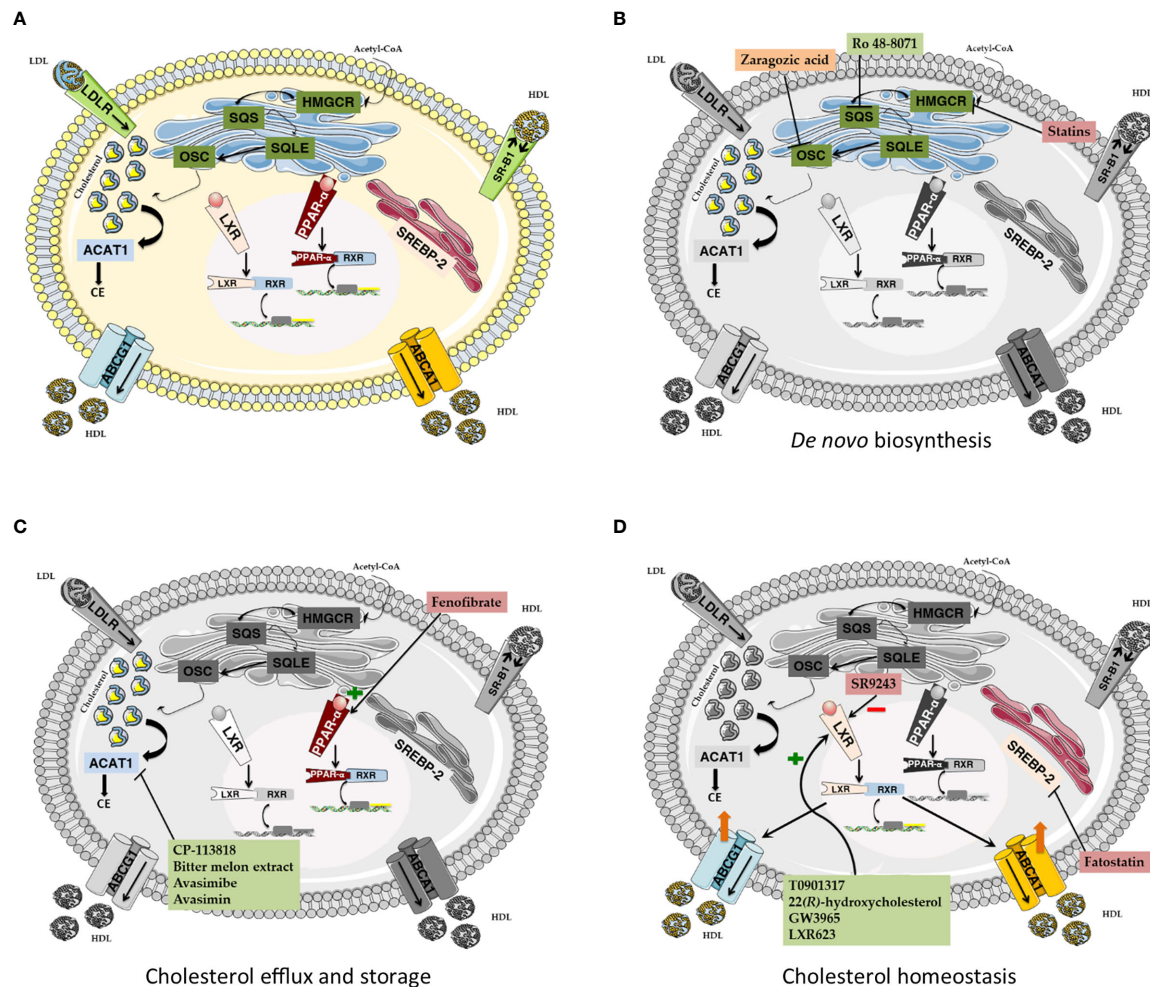


**FIGURE 3 | (A)** Cholesterol metabolism. *De novo* cholesterol biosynthesis mainly relies on the activity of four key enzymes. HMGCR catalyzes the formation of mevalonate. Mevalonate is essential for farnesyl pyrophosphate biosynthesis, which is in turn exploited by SQS for squalene production. SQL converts squalene into its epoxydic form, which is eventually cyclized to lanosterol by OSC. Lastly, lanosterol is converted to cholesterol. HDL particles collect extrahepatic cholesterol and allow its cellular uptake by interacting with SR-B1. Alternatively, LDL-associated cholesterol can be captured and internalized in coated endocytic vesicles in a LDLR-mediated fashion. Intracellular cholesterol excess is converted into cholesteryl esters by ACAT1 and stored into lipid droplets. Cellular cholesterol efflux is mainly controlled by ABCA1 and ABCG1, two regulatory proteins belonging to the ATP-binding cassette transporter superfamily. Cellular cholesterol homeostasis is maintained by sterol-sensitive systems, such as SREBP2 and LXR. SREBP2-mediated adaptive response promotes cholesterol biosynthesis and uptake. Conversely, LXR promotes cholesterol excretion while impairing its uptake and production. PPAR $\alpha$  activation promotes LXR-mediated ABCA1 expression and blocks cholesterol biosynthesis by inhibiting SREBP2. **(B)** Pharmacological targeting of *de novo* cholesterol biosynthesis pathway. Statins target and inhibit the activity of the rate-limiting enzyme HMGCR. Ro 48-8071 and Zaragozic acid act downstream of the mevalonate pathway, by inhibiting the activity of SQS and OSC, respectively. **(C)** Pharmacological targeting of cholesterol efflux and storage. The PPAR $\alpha$  agonist Fenofibrate promotes PPAR $\alpha$ -RXR interaction, thereby activating the PPAR $\alpha$  signaling cascade. Both synthetic (CP-113818, Avasimibe, Avasimin) and natural (Bitter melon extract) inhibitors of ACAT-1 block cholesterol esterification and intracellular overload. **(D)** Pharmacological targeting of cholesterol homeostasis. LXR agonists, such as GW3965, T0901317, 22(R)-hydroxycholesterol and LXR623, can activate LXR signaling cascade, leading to increased cholesterol efflux and reduced cholesterol uptake. HMGCR, 3-hydroxy-3-methylglutaryl-CoA reductase; SQS, Squalene synthase; SQLE, Squalene epoxidase; OSC, 2,3-oxidosqualene cyclase; SR B1, scavenger receptor type B class 1; LDLR, LDL receptor; ACAT1, Acetyl-CoA Acetyltransferase 1. PPAR-  $\alpha$ , peroxisome proliferator-activated receptor; LXR, liver X receptor; SREBP-2, sterol regulatory element-binding protein 2; ABCA1, ATP Binding Cassette Subfamily A Member 1; ABCG1, ATP Binding Cassette Subfamily G Member 1; HDL, High-density Lipoprotein; LDL, Low-density Lipoprotein.

by affecting different signaling/metabolic pathways. A deep elucidation of cholesterol-linked metabolic vulnerabilities in cancers may offer new opportunities to develop new drug delivery strategies, allowing a more selective targeting of cancer cells, thus improving the quality of cancer therapy in patients.

## AUTHOR CONTRIBUTIONS

VC and ER conceived the review. IG and FG wrote the literature review. VC, MB, GO, TP-G, MD, and ER supervised and edited the review. All authors contributed to the article and approved the submitted version.

## FUNDING

IG, FG, VC, GO, and ER are supported by the University of Padova.

## REFERENCES

- Yoshida GJ. Metabolic Reprogramming: The Emerging Concept and Associated Therapeutic Strategies. *J Exp Clin Cancer Res* (2015) 34:111. doi: 10.1186/s13046-015-0221-y
- Ward PS, Thompson CB. Metabolic Reprogramming: A Cancer Hallmark Even Warburg Did Not Anticipate. *Cancer Cell* (2012) 21:297–308. doi: 10.1016/j.ccr.2012.02.014
- Cocetta V, Ragazzi E, Montopoli M. Mitochondrial Involvement in Cisplatin Resistance. *Int J Mol Sci* (2019) 20:3384. doi: 10.3390/ijms20143384
- Zaal EA, Berkens CR. The Influence of Metabolism on Drug Response in Cancer. *Front Oncol* (2018) 8:500. doi: 10.3389/fonc.2018.00500
- Desbats MA, Giacomini I, Prayer-Galetti T, Montopoli M. Metabolic Plasticity in Chemotherapy Resistance. *Front Oncol* (2020) 10:281. doi: 10.3389/fonc.2020.00281
- Fendt S-M, Frezza C, Erez A. Targeting Metabolic Plasticity and Flexibility Dynamics for Cancer Therapy. *Cancer Discov* (2020) 10:1797–807. doi: 10.1158/2159-8290.CD-20-0844
- Giacomini I, Ragazzi E, Pasut G, Montopoli M. The Pentose Phosphate Pathway and Its Involvement in Cisplatin Resistance. *Int J Mol Sci* (2020) 21:937. doi: 10.3390/ijms21030937
- Morandi A, Indraccolo S. Linking Metabolic Reprogramming to Therapy Resistance in Cancer. *Biochim Biophys Acta BBA - Rev Cancer* (2017) 1868:1–6. doi: 10.1016/j.bbcan.2016.12.004
- Cocetta V, Ragazzi E, Montopoli M. Links Between Cancer Metabolism and Cisplatin Resistance. *Int Rev Cell Mol Biol* (2020) 354:107–64. doi: 10.1016/b.sircmb.2020.01.005
- Phan LM, Yeung S-CJ, Lee M-H. Cancer Metabolic Reprogramming: Importance, Main Features, and Potentials for Precise Targeted Anti-Cancer Therapies. *Cancer Biol Med* (2014) 11:1–19. doi: 10.7497/j.issn.2095-3941.2014.01.001
- Olson RE. Discovery of the Lipoproteins, Their Role in Fat Transport and Their Significance as Risk Factors. *J Nutr* (1998) 128:439S–43S. doi: 10.1093/jn/128.2.439S
- Schekman R. Discovery of the Cellular and Molecular Basis of Cholesterol Control. *Proc Natl Acad Sci* (2013) 110:14833–6. doi: 10.1073/pnas.1312967110
- Simons K, Ikonen E. How Cells Handle Cholesterol. *Science* (2000) 290:1721–6. doi: 10.1126/science.290.5497.1721
- Farese RV, Herz J. Cholesterol Metabolism and Embryogenesis. *Trends Genet* (1998) 14:115–20. doi: 10.1016/S0168-9525(97)01377-2
- Goldstein JL, Brown MS. History of Discovery: The LDL Receptor. *Arterioscler Thromb* (2010) 29:431–8. doi: 10.1161/ATVBAHA.108.179564.History
- Munro S. Lipid Rafts: Elusive or Illusive? *Cell* (2003) 115:377–88. doi: 10.1016/S0092-8674(03)00882-1
- Simons K, Ehehalt R. Cholesterol, Lipid Rafts, and Disease. *J Clin Invest* (2002) 110:597–603. doi: 10.1172/JCI0216390
- Sezgin E, Levental I, Mayor S, Eggeling C. The Mystery of Membrane Organization: Composition, Regulation and Roles of Lipid Rafts. *Nat Rev Mol Cell Biol* (2017) 18:361–74. doi: 10.1038/nrm.2017.16
- Simons K, Ikonen E. Functional Rafts in Cell Membranes. *Nature* (1997) 387:569–72. doi: 10.1038/42408
- Kolesnick R. The Therapeutic Potential of Modulating the Ceramide/Sphingomyelin Pathway. *J Clin Invest* (2002) 110:3–8. doi: 10.1172/JCI16127
- van der Goot FG, Harder T. Raft Membrane Domains: From a Liquid-Ordered Membrane Phase to a Site of Pathogen Attack. *Semin Immunol* (2001) 13:89–97. doi: 10.1006/smim.2000.0300
- Head BP, Patel HH, Insel PA. Interaction of Membrane/Lipid Rafts With the Cytoskeleton: Impact on Signaling and Function. *Biochim Biophys Acta* (2014) 1838:532–45. doi: 10.1016/j.bbamem.2013.07.018
- Simons K, Toomre D. Lipid Rafts and Signal Transduction. *Nat Rev Mol Cell Biol* (2000) 1:31–9. doi: 10.1038/35036052
- Buhaescu I, Izzedine H. Mevalonate Pathway: A Review of Clinical and Therapeutic Implications. *Clin Biochem* (2007) 40:575–84. doi: 10.1016/j.clinbiochem.2007.03.016
- Shi Z, Ruvkun G. The Mevalonate Pathway Regulates microRNA Activity in *Caenorhabditis Elegans*. *Proc Natl Acad Sci USA* (2012) 109:4568–73. doi: 10.1073/pnas.1202421109
- Berndt N, Hamilton AD, Sefti SM. Targeting Protein Prenylation for Cancer Therapy. *Nat Rev Cancer* (2011) 11:775–91. doi: 10.1038/nrc3151
- Hulce JJ, Cognetta AB, Niphakis MJ, Tully SE, Cravatt BF. Proteome-Wide Mapping of Cholesterol-Interacting Proteins in Mammalian Cells. *Nat Methods* (2013) 10:259–64. doi: 10.1038/nmeth.2368
- Martins IJ, Hone E, Foster JK, Sünram-Lea SI, Gnjec A, Fuller SJ, et al. Apolipoprotein E, Cholesterol Metabolism, Diabetes, and the Convergence of Risk Factors for Alzheimer's Disease and Cardiovascular Disease. *Mol Psychiatry* (2006) 11:721–36. doi: 10.1038/sj.mp.4001854
- Van Der Kant R, Goldstein LSB, Ossenkoppele R. Amyloid- $\beta$ -Independent Regulators of Tau Pathology in Alzheimer Disease. *Nat Rev Neurosci* (2020) 21:21–35. doi: 10.1038/s41583-019-0240-3
- Haase CL, Tybjaerg-Hansen A, Nordestgaard BG, Frikke-Schmidt R. HDL Cholesterol and Risk of Type 2 Diabetes: A Mendelian Randomization Study. *Diabetes* (2015) 64:3328–33. doi: 10.2337/db14-1603
- Silvente-Poirot S, Poirot M. Cholesterol and Cancer, in the Balance. *Science* (2014) 343:1445–6. doi: 10.1126/science.1252787
- Kuzu OF, Noory MA, Robertson GP. The Role of Cholesterol in Cancer. *Cancer Res* (2016) 76:2063–70. doi: 10.1158/0008-5472.CAN-15-2613
- Germain N, Dhayer M, Boileau M, Fovez Q, Kluz J, Marchetti P. Lipid Metabolism and Resistance to Anticancer Treatment. *Biology* (2020) 9:474. doi: 10.3390/biology9120474
- Huang B, Song B, Xu C. Cholesterol Metabolism in Cancer: Mechanisms and Therapeutic Opportunities. *Nat Metab* (2020) 2:132–41. doi: 10.1038/s42255-020-0174-0
- Ding X, Zhang W, Li S, Yang H. The Role of Cholesterol Metabolism in Cancer. *Am J Cancer Res* (2019) 9:219–27.
- Cruz PMR, Mo H, McConathy WJ, Sabnis N, Lacko AG. The Role of Cholesterol Metabolism and Cholesterol Transport in Carcinogenesis: A Review of Scientific Findings, Relevant to Future Cancer Therapeutics. *Front Pharmacol* (2013) 4:119. doi: 10.3389/fphar.2013.00119
- Xu H, Zhou S, Tang Q, Xia H, Bi F. Cholesterol Metabolism: New Functions and Therapeutic Approaches in Cancer. *Biochim Biophys Acta Rev Cancer* (2020) 1874:188394. doi: 10.1016/j.bbcan.2020.188394
- Repa JJ, Mangelsdorf DJ. The Role of Orphan Nuclear Receptors in the Regulation of Cholesterol Homeostasis. *Annu Rev Cell Dev Biol* (2000) 16:459–81. doi: 10.1146/annurev.cellbio.16.1.459
- Kruit JK, Groen AK, van Berkel TJ, Kuipers F. Emerging Roles of the Intestine in Control of Cholesterol Metabolism. *World J Gastroenterol* (2006) 12:6429–39. doi: 10.3748/wjg.v12.i40.6429
- Luo J, Yang H, Song B-L. Mechanisms and Regulation of Cholesterol Homeostasis. *Nat Rev Mol Cell Biol* (2020) 21:225–45. doi: 10.1038/s41580-019-0190-7
- Mo H, Elson CE. Studies of the Isoprenoid-Mediated Inhibition of Mevalonate Synthesis Applied to Cancer Chemotherapy and Chemoprevention. *Exp Biol Med* (2004) 229:567–85. doi: 10.1177/153537020422900701
- Ikonen E. Cellular Cholesterol Trafficking and Compartmentalization. *Nat Rev Mol Cell Biol* (2008) 9:125–38. doi: 10.1038/nrm2336
- Singh P, Saxena R, Srinivas G, Pande G, Chattopadhyay A. Cholesterol Biosynthesis and Homeostasis in Regulation of the Cell Cycle. *PLoS One* (2013) 8:e58833. doi: 10.1371/journal.pone.0058833
- Kandutsch AA, Russell AE. Preputial Gland Tumor Sterols. 3. A Metabolic Pathway From Lanosterol to Cholesterol. *J Biol Chem* (1960) 235:2256–61. doi: 10.1016/S0021-9258(18)64608-3

## ACKNOWLEDGMENTS

The authors thank Dr. Andrea Pagetta for graphical support.

45. Ačimović J, Goyal S, Košir R, Goličnik M, Perše M, Belić A, et al. Cytochrome P450 Metabolism of the Post-Lanosterol Intermediates Explains Enigmas of Cholesterol Synthesis. *Sci Rep* (2016) 6:28462. doi: 10.1038/srep28462
46. Jin U, Park SJ, Park SM. Cholesterol Metabolism in the Brain and Its Association With Parkinson's Disease. *Exp Neurobiol* (2019) 28:554–67. doi: 10.5607/en.2019.28.5.554
47. Goedeke L, Fernández-Hernando C. Regulation of Cholesterol Homeostasis. *Cell Mol Life Sci* (2012) 69:915–30. doi: 10.1007/s00018-011-0857-5
48. Jia L, Betters JL, Yu L. Niemann-Pick C1-Like 1 (NPC1L1) Protein in Intestinal and Hepatic Cholesterol Transport. *Annu Rev Physiol* (2011) 73:239–59. doi: 10.1146/annurev-physiol-012110-142233
49. Betters JL, Yu L. NPC1L1 and Cholesterol Transport. *FEBS Lett* (2010) 584:2740–7. doi: 10.1016/j.febslet.2010.03.030
50. Nguyen TM, Sawyer JK, Kelley KL, Davis MA, Rudel LL. Cholesterol Esterification by ACAT2 is Essential for Efficient Intestinal Cholesterol Absorption: Evidence From Thoracic Lymph Duct Cannulation. *J Lipid Res* (2012) 53:95–104. doi: 10.1194/jlr.M018820
51. Ko CW, Qu J, Black DD, Tso P. Regulation of Intestinal Lipid Metabolism: Current Concepts and Relevance to Disease. *Nat Rev Gastroenterol Hepatol* (2020) 17:169–83. doi: 10.1038/s41575-019-0250-7
52. Ginsberg HN. Lipoprotein Physiology. *Endocrinol Metab Clin North Am* (1998) 27:503–19. doi: 10.1016/s0889-8529(05)70023-2
53. Ramasamy I. Recent Advances in Physiological Lipoprotein Metabolism. *Clin Chem Lab Med* (2014) 52:1695–727. doi: 10.1515/cclm-2013-0358
54. Holmes MV, Ala-Korpela M. What Is “LDL Cholesterol”? *Nat Rev Cardiol* (2019) 16:197–8. doi: 10.1038/s41569-019-0157-6
55. Go GW, Mani A. Low-Density Lipoprotein Receptor (LDLR) Family Orchestrates Cholesterol Homeostasis. *Yale J Biol Med* (2012) 85:19–28.
56. Luo X, Cheng C, Tan Z, Li N, Tang M, Yang L, et al. Emerging Roles of Lipid Metabolism in Cancer Metastasis. *Mol Cancer* (2017) 16:76. doi: 10.1186/s12943-017-0646-3
57. Kwon HJ, Abi-Mosleh L, Wang ML, Deisenhofer J, Goldstein JL, Brown MS, et al. Structure of N-Terminal Domain of NPC1 Reveals Distinct Subdomains for Binding and Transfer of Cholesterol. *Cell* (2009) 137:1213–24. doi: 10.1016/j.cell.2009.03.049
58. Li J, Pfeffer SR. Lysosomal Membrane Glycoproteins Bind Cholesterol and Contribute to Lysosomal Cholesterol Export. *eLife* (2016) 5:e21635. doi: 10.7554/eLife.21635
59. Ouimet M, Barrett TJ, Fisher EA. HDL and Reverse Cholesterol Transport. *Circ Res* (2019) 124:1505–18. doi: 10.1161/CIRCRESAHA.119.312617
60. Brufau G, Groen AK, Kuipers F. Reverse Cholesterol Transport Revisited: Contribution of Biliary Versus Intestinal Cholesterol Excretion. *Arterioscler Thromb Vasc Biol* (2011) 31:1726–33. doi: 10.1161/ATVBAHA.108.181206
61. Röhrl C, Stangl H. HDL Endocytosis and Resecretion. *Biochim Biophys Acta* (2013) 1831:1626–33. doi: 10.1016/j.bbali.2013.07.014
62. Chang TY, Chang CCY, Ohgami N, Yamauchi Y. Cholesterol Sensing, Trafficking, and Esterification. *Annu Rev Cell Dev Biol* (2006) 22:129–57. doi: 10.1146/annurev.cellbio.22.010305.104656
63. Gelissen IC, Harris M, Rye KA, Quinn C, Brown AJ, Kockx M, et al. ABCA1 and ABCG1 Synergize to Mediate Cholesterol Export to ApoA-I. *Arterioscler Thromb Vasc Biol* (2006) 26:534–40. doi: 10.1161/01.ATV.0000200082.58536.e1
64. Ossoli A, Pavanello C, Calabresi L. High-Density Lipoprotein, Lecithin: Cholesterol Acyltransferase, and Atherosclerosis. *Endocrinol Metab* (2016) 31:223. doi: 10.3803/EnM.2016.31.2.223
65. Chang TY, Li BL, Chang CCY, Urano Y. Acyl-Coenzyme A:Cholesterol Acyltransferases. *Am J Physiol Endocrinol Metab* (2009) 297:E1–9. doi: 10.1152/ajpendo.90926.2008
66. Petan T, Jarc E, Jusović M. Lipid Droplets in Cancer: Guardians of Fat in a Stressful World. *Molecules* (2018) 23:1941. doi: 10.3390/molecules23081941
67. Miyazaki A, Sakashita N, Lee O, Takahashi K, Horiuchi S, Hakamata H, et al. Expression of ACAT-1 Protein in Human Atherosclerotic Lesions and Cultured Human Monocytes-Macrophages. *Arterioscler Thromb Vasc Biol* (1998) 18:1568–74. doi: 10.1161/01.ATV.18.10.1568
68. Chang CCY, Sakashita N, Ornvold K, Lee O, Chang ET, Dong R, et al. Immunological Quantitation and Localization of ACAT-1 and ACAT-2 in Human Liver and Small Intestine. *J Biol Chem* (2000) 275:28083–92. doi: 10.1074/jbc.M003927200
69. Joyce CW, Shelness GS, Davis MA, Lee RG, Skinner K, Anderson RA, et al. ACAT1 and ACAT2 Membrane Topology Segregates a Serine Residue Essential for Activity to Opposite Sides of the Endoplasmic Reticulum Membrane. *Mol Biol Cell* (2000) 11:3675–87. doi: 10.1091/mbc.11.11.3675
70. Steck TL, Lange Y. Cell Cholesterol Homeostasis: Mediation by Active Cholesterol. *Trends Cell Biol* (2010) 20:680–7. doi: 10.1016/j.tcb.2010.08.007
71. Wong J, Quinn CM, Brown AJ. SREBP-2 Positively Regulates Transcription of the Cholesterol Efflux Gene, ABCA1, by Generating Oxysterol Ligands for LXR. *Biochem J* (2006) 400:485–91. doi: 10.1042/BJ20060914
72. Brown MS, Radhakrishnan A, Goldstein JL. Retrospective on Cholesterol Homeostasis: The Central Role of Scap. *Annu Rev Biochem* (2018) 87:783–807. doi: 10.1146/annurev-biochem-062917-011852
73. Nagoshi E, Yoneda Y. Dimerization of Sterol Regulatory Element-Binding Protein 2 Via the Helix-Loop-Helix-Leucine Zipper Domain is a Prerequisite for Its Nuclear Localization Mediated by Importin  $\beta$ . *Mol Cell Biol* (2001) 21:2779–89. doi: 10.1128/MCB.21.8.2779-2789.2001
74. Zhao X, Yang F. Regulation of SREBP-Mediated Gene Expression. *Acta Biophys Sin* (2012) 28:287. doi: 10.3724/SP.J.1260.2012.20034
75. Radhakrishnan A, Sun LP, Kwon HJ, Brown MS, Goldstein JL. Direct Binding of Cholesterol to the Purified Membrane Region of SCAP: Mechanism for a Sterol-Sensing Domain. *Mol Cell* (2004) 15:259–68. doi: 10.1016/j.molcel.2004.06.019
76. Howe V, Sharpe LJ, Prabhu AV, Brown AJ. New Insights Into Cellular Cholesterol Acquisition: Promoter Analysis of Human HMGCR and SQLE, Two Key Control Enzymes in Cholesterol Synthesis. *Biochim Biophys Acta Mol Cell Biol Lipids* (2017) 1862:647–57. doi: 10.1016/j.bbalip.2017.03.009
77. Horton JD, Goldstein JL, Brown MS. SREBPs: Activators of the Complete Program of Cholesterol and Fatty Acid Synthesis in the Liver. *J Clin Invest* (2002) 109:1125–31. doi: 10.1172/JCI0215593
78. Theesfeld CL, Pourmand D, Davis T, Garza RM, Hampton RY. The Sterol-Sensing Domain (SSD) Directly Mediates Signal-Regulated Endoplasmic Reticulum-Associated Degradation (ERAD) of 3-Hydroxy-3-Methylglutaryl (HMG)-CoA Reductase Isozyme Hmg2. *J Biol Chem* (2011) 286:26298–307. doi: 10.1074/jbc.M111.244798
79. Clarke PR, Hardie DG. Regulation of HMG-CoA Reductase: Identification of the Site Phosphorylated by the AMP-Activated Protein Kinase In Vitro and in Intact Rat Liver. *EMBO J* (1990) 9:2439–46. doi: 10.1002/j.1460-2075.1990.tb07420.x
80. Alrefai WA, Annaba F, Sarwar Z, Dwivedi A, Saksena S, Singla A, et al. Modulation of Human Niemann-Pick C1-Like 1 Gene Expression by Sterol: Role of Sterol Regulatory Element Binding Protein 2. *Am J Physiol Gastrointest Liver Physiol* (2007) 292:G369–376. doi: 10.1152/ajpgi.00306.2006
81. Kotzka J, Müller-Wieland D, Roth G, Kremer L, Munck M, Schürmann S, et al. Sterol Regulatory Element Binding Proteins (SREBP)-1a and SREBP-2 are Linked to the MAP-kinase Cascade. *J Lipid Res* (2000) 41:99–108. doi: 10.1016/S0022-2275(20)32079-4
82. Sato R, Inoue J, Kawabe Y, Kodama T, Takano T, Maeda M. Sterol-Dependent Transcriptional Regulation of Sterol Regulatory Element-binding Protein-2. *J Biol Chem* (1996) 271:26461–4. doi: 10.1074/jbc.271.43.26461
83. Radhakrishnan SK, den Besten W, Deshaies RJ. p97-dependent Retrotranslocation and Proteolytic Processing Govern Formation of Active Nrf1 Upon Proteasome Inhibition. *eLife* (2014) 3:e01856. doi: 10.7554/eLife.01856
84. Wang B, Tontonoz P. Liver X Receptors in Lipid Signalling and Membrane Homeostasis. *Nat Rev Endocrinol* (2018) 14:452–63. doi: 10.1038/s41574-018-0037-x
85. Peet DJ, Turley SD, Ma W, Janowski BA, Lobaccaro JM, Hammer RE, et al. Cholesterol and Bile Acid Metabolism Are Impaired in Mice Lacking the Nuclear Oxysterol Receptor LXR Alpha. *Cell* (1998) 93:693–704. doi: 10.1016/s0092-8674(00)81432-4
86. Yvan-Charvet L, Wang N, Tall AR. Role of HDL, ABCA1, and ABCG1 Transporters in Cholesterol Efflux and Immune Responses. *Arterioscler Thromb Vasc Biol* (2010) 30:139–43. doi: 10.1161/ATVBAHA.108.179283



87. Venkateswaran A, Laffitte BA, Joseph SB, Mak PA, Wilpitz DC, Edwards PA, et al. Control of Cellular Cholesterol Efflux by the Nuclear Oxysterol Receptor LXR Alpha. *Proc Natl Acad Sci USA* (2000) 97:12097–102. doi: 10.1073/pnas.200367697
88. Duval C, Touche V, Tailleux A, Fruchart JC, Fievet C, Clavey V, et al. Niemann–Pick C1 Like 1 Gene Expression is Down-Regulated by LXR Activators in the Intestine. *Biochem Biophys Res Commun* (2006) 340:1259–63. doi: 10.1016/j.bbrc.2005.12.137
89. Zelcer N, Hong C, Boyadjian R, Tontonoz P. LXR Regulates Cholesterol Uptake Through Idol-Dependent Ubiquitination of the LDL Receptor. *Science* (2009) 325:100–4. doi: 10.1126/science.1168974
90. Zhang L, Reue K, Fong LG, Young SG, Tontonoz P. Feedback Regulation of Cholesterol Uptake by the LXR–IDOL–LDLR Axis. *Arterioscler Thromb Vasc Biol* (2012) 32:2541–6. doi: 10.1161/ATVBAHA.112.250571
91. Stancu C, Sima A. Statins: Mechanism of Action and Effects. *J Cell Mol Med* (2001) 5:378–87. doi: 10.1111/j.1582-4934.2001.tb00172.x
92. Bedi O, Dhawan V, Sharma PL, Kumar P. Pleiotropic Effects of Statins: New Therapeutic Targets in Drug Design. *Naunyn Schmiedeberg Arch Pharmacol* (2016) 389:695–712. doi: 10.1007/s00210-016-1252-4
93. Endo A. A Historical Perspective on the Discovery of Statins. *Proc Jpn Acad Ser B* (2010) 86:484–93. doi: 10.2183/pjab.86.484
94. Davies JT, Delfino SF, Feinberg CE, Johnson MF, Nappi VL, Olinger JT, et al. Current and Emerging Uses of Statins in Clinical Therapeutics: A Review. *Lipid Insights* (2016) 9:13–29. doi: 10.4137/LPI.S37450
95. Ramkumar S, Raghunath A, Raghunath S. Statin Therapy: Review of Safety and Potential Side Effects. *Acta Cardiol Sin* (2016) 32:631–9. doi: 10.6515/ACS20160611A
96. Liu A, Wu Q, Guo J, Ares I, Rodríguez J-L, Martínez-Larrañaga MR, et al. Statins: Adverse Reactions, Oxidative Stress and Metabolic Interactions. *Pharmacol Ther* (2019) 195:54–84. doi: 10.1016/j.pharmthera.2018.10.004
97. Ray KK, Bays HE, Catapano AL, Lalwani ND, Bloedon LT, Sterling LR, et al. Clear Harmony Trial. Safety and Efficacy of Bempedoic Acid to Reduce LDL Cholesterol. *N Engl J Med* (2019) 380:1022–32. doi: 10.1056/NEJMoA1803917
98. Fazio S, Linton MF. The Role of Fibrates in Managing Hyperlipidemia: Mechanisms of Action and Clinical Efficacy. *Curr Atheroscler Rep* (2004) 6:148–57. doi: 10.1007/s11883-004-0104-8
99. Backes JM, Gibson CA, Ruisinger JF, Moriarty PM. Fibrates: What Have We Learned in the Past 40 Years? *Pharmacotherapy* (2007) 27:412–24. doi: 10.1592/phco.27.3.412
100. Laganà A, Vitale S, Nigro A, Sofo V, Salmeri F, Rossetti P, et al. Pleiotropic Actions of Peroxisome Proliferator-Activated Receptors (PPARs) in Dysregulated Metabolic Homeostasis, Inflammation and Cancer: Current Evidence and Future Perspectives. *Int J Mol Sci* (2016) 17:999. doi: 10.3390/ijms170709993
101. Phan BA, Dayspring TD, Toth PP. Ezetimibe Therapy: Mechanism of Action and Clinical Update. *Vasc Health Risk Manag* (2012) 8:415–27. doi: 10.2147/VHRM.S33664
102. Florentin M, Liberopoulos EN, Elisaf MS. Ezetimibe-Associated Adverse Effects: What the Clinician Needs to Know: Ezetimibe and Side Effects. *Int J Clin Pract* (2007) 62:88–96. doi: 10.1111/j.1742-1241.2007.01592.x
103. Corsini A, Windler E, Farnier M, Colesevelam Hydrochloride: Usefulness of a Specifically Engineered Bile Acid Sequestrant for Lowering LDL-Cholesterol. *Eur J Cardiovasc Prev Rehabil* (2009) 16:1–9. doi: 10.1097/HJR.0b013e32831215db
104. Scadaferri F, Pizzoferrato M, Ponziani FR, Gasbarrini G, Gasbarrini A. Use and Indications of Cholestyramine and Bile Acid Sequestrants. *Intern Emerg Med* (2013) 8:205–10. doi: 10.1007/s11739-011-0653-0
105. Gouni-Berthold I, Berthold HK. Mipomersen and Lomitapide: Two New Drugs for the Treatment of Homozygous Familial Hypercholesterolemia. *Atheroscler Suppl* (2015) 18:28–34. doi: 10.1016/j.atherosclerosis.2015.02.005
106. Agarwala A, Jones P, Nambi V. The Role of Antisense Oligonucleotide Therapy in Patients With Familial Hypercholesterolemia: Risks, Benefits, and Management Recommendations. *Curr Atheroscler Rep* (2015) 17:467. doi: 10.1007/s11883-014-0467-4
107. Parhofer K. Mipomersen: Evidence-Based Review of its Potential in the Treatment of Homozygous and Severe Heterozygous Familial Hypercholesterolemia. *Core Evid* (2012) 7:29–38. doi: 10.2147/CE.S25239
108. Goulouze SC, Cohen AF, Rissmann R. Lomitapide: New Drug Mechanisms: Lomitapide. *Br J Clin Pharmacol* (2015) 80:179–81. doi: 10.1111/bcp.12612
109. Chaudhary R, Garg J, Shah N, Sumner A. PCSK9 Inhibitors: A New Era of Lipid Lowering Therapy. *World J Cardiol* (2017) 9:76. doi: 10.4330/wjc.v9.i2.76
110. Knopp RH. Drug Treatment of Lipid Disorders. *N Engl J Med* (1999) 341:498–511. doi: 10.1056/NEJM199908123410707
111. Gorin A, Gabitova L, Atsaturov I. Regulation of Cholesterol Biosynthesis and Cancer Signaling. *Curr Opin Pharmacol* (2012) 12:710–6. doi: 10.1016/j.coph.2012.06.011
112. Kuzu OF, Gowda R, Noory MA, Robertson GP. Modulating Cancer Cell Survival by Targeting Intracellular Cholesterol Transport. *Br J Cancer* (2017) 117:513–24. doi: 10.1038/bjc.2017.200
113. Gu L, Saha ST, Thomas J, Kaur M. Targeting Cellular Cholesterol for Anticancer Therapy. *FEBS J* (2019) 286:4192–208. doi: 10.1111/febs.15018
114. Li YC, Park MJ, Ye S-K, Kim C-W, Kim Y-N. Elevated Levels of Cholesterol-Rich Lipid Rafts in Cancer Cells Are Correlated With Apoptosis Sensitivity Induced by Cholesterol-Depleting Agents. *Am J Pathol* (2006) 168:1107–18. doi: 10.2353/ajpath.2006.050959
115. Liu Z, Liu X, Liu S, Cao Q. Cholesterol Promotes the Migration and Invasion of Renal Carcinoma Cells by Regulating the KLF5/miR-27a/FBXW7 Pathway. *Biochem Biophys Res Commun* (2018) 502:69–75. doi: 10.1016/j.bbrc.2018.05.122
116. Liang Y, Besch-Williford C, Aebi JD, Mafuvadze B, Cook MT, Zou X, et al. Cholesterol Biosynthesis Inhibitors as Potent Novel Anti-Cancer Agents: Suppression of Hormone-Dependent Breast Cancer by the Oxidosqualene Cyclase Inhibitor RO 48-8071. *Breast Cancer Res Treat* (2014) 146:51–62. doi: 10.1007/s10549-014-2996-5
117. Grinter SZ, Liang Y, Huang S-Y, Hyder SM, Zou X. An Inverse Docking Approach for Identifying New Potential Anti-Cancer Targets. *J Mol Graph Model* (2011) 29:795–9. doi: 10.1016/j.jmgm.2011.01.002
118. Maione F, Oliaro-Bosso S, Meda C, Di Nicolantonio F, Bussolino F, Balliano G, et al. The Cholesterol Biosynthesis Enzyme Oxidosqualene Cyclase is a New Target to Impair Tumour Angiogenesis and Metastasis Dissemination. *Sci Rep* (2015) 5:9054. doi: 10.1038/srep09054
119. Liang Y, Mafuvadze B, Aebi JD, Hyder SM. Cholesterol Biosynthesis Inhibitor RO 48-8071 Suppresses Growth of Hormone-Dependent and Castration-Resistant Prostate Cancer Cells. *Oncotargets Ther* (2016) 9:3223–32. doi: 10.2147/OTT.S105725
120. Brusselmans K, Timmermans L, Van de Sande T, Van Veldhoven PP, Guan G, Shechter I, et al. Squalene Synthase, a Determinant of Raft-Associated Cholesterol and Modulator of Cancer Cell Proliferation. *J Biol Chem* (2007) 282:18777–85. doi: 10.1074/jbc.M611763200
121. Lanterna C, Musumeci A, Raccosta L, Corna G, Moresco M, Maggioni D, et al. The Administration of Drugs Inhibiting Cholesterol/Oxysterol Synthesis is Safe and Increases the Efficacy of Immunotherapeutic Regimens in Tumor-Bearing Mice. *Cancer Immunol Immunother* (2016) 65:1303–15. doi: 10.1007/s00262-016-1884-8
122. Antalis CJ, Arnold T, Rasool T, Lee B, Buhman KK, Siddiqui RA. High ACAT1 Expression in Estrogen Receptor Negative Basal-Like Breast Cancer Cells Is Associated With LDL-induced Proliferation. *Breast Cancer Res Treat* (2010) 122:661–70. doi: 10.1007/s10549-009-0594-8
123. Shim SH, Sur S, Steele R, Albert CJ, Huang C, Ford DA, et al. Disrupting Cholesterol Esterification by Bitter Melon Suppresses Triple-Negative Breast Cancer Cell Growth. *Mol Carcinog* (2018) 57:1599–607. doi: 10.1002/mc.22882
124. Lee SSY, Li J, Tai JN, Ratliff TL, Park K, Cheng JX. Avasimibe Encapsulated in Human Serum Albumin Blocks Cholesterol Esterification for Selective Cancer Treatment. *ACS Nano* (2015) 9:2420–32. doi: 10.1021/nn504025a
125. Lee HJ, Li J, Vickman RE, Li J, Liu R, Durkes AC, et al. Cholesterol Esterification Inhibition Suppresses Prostate Cancer Metastasis by Impairing the Wnt/ $\beta$ -Catenin Pathway. *Mol Cancer Res* (2018) 16:974–85. doi: 10.1158/1541-7786.MCR-17-0665
126. Li J, Gu D, Lee SSY, Song B, Bandyopadhyay S, Chen S, et al. Abrogating Cholesterol Esterification Suppresses Growth and Metastasis of Pancreatic Cancer. *Oncogene* (2016) 35:6378–88. doi: 10.1038/onc.2016.168
127. Bi M, Qiao X, Zhang H, Wu H, Gao Z, Zhou H, et al. Effect of Inhibiting ACAT-1 Expression on the Growth and Metastasis of Lewis Lung Carcinoma. *Oncol Lett* (2019) 18:1548–56. doi: 10.3892/ol.2019.10427



128. Li J, Qu X, Tian J, Zhang JT, Cheng JX. Cholesterol Esterification Inhibition and Gemcitabine Synergistically Suppress Pancreatic Ductal Adenocarcinoma Proliferation. *PLoS One* (2018) 13:e0193318. doi: 10.1371/journal.pone.0193318
129. Pommier AJC, Alves G, Viennois E, Bernard S, Communal Y, Sion B, et al. Liver X Receptor Activation Downregulates AKT Survival Signaling in Lipid Rafts and Induces Apoptosis of Prostate Cancer Cells. *Oncogene* (2010) 29:2712–23. doi: 10.1038/onc.2010.30
130. Roz AE, Bard JM, Huvelin JM, Nazih H. LXR Agonists and ABCG1-dependent Cholesterol Efflux in MCF-7 Breast Cancer Cells: Relation to Proliferation and Apoptosis. *Anticancer Res* (2012) 32:3007–13.
131. Zhang W, Jiang H, Zhang J, Zhang Y, Liu A, Zhao Y, et al. Liver X Receptor Activation Induces Apoptosis of Melanoma Cell Through Caspase Pathway. *Cancer Cell Int* (2014) 14:16. doi: 10.1186/1475-2867-14-16
132. Agarwal JR, Wang Q, Tanno T, Rasheed Z, Merchant A, Ghosh N, et al. Activation of Liver X Receptors Inhibits Hedgehog Signaling, Clonogenic Growth, and Self-Renewal in Multiple Myeloma. *Mol Cancer Ther* (2014) 13:1873–81. doi: 10.1158/1535-7163.MCT-13-0997
133. Kaneko T, Kanno C, Ichikawa-Tomikawa N, Kashiwagi K, Yaginuma N, Ohkoshi C, et al. Liver X Receptor Reduces Proliferation of Human Oral Cancer Cells by Promoting Cholesterol Efflux Via Up-Regulation of ABCA1 Expression. *Oncotarget* (2015) 6:33345–57. doi: 10.18632/oncotarget.5428
134. Rough JJ, Monroy MA, Yerrum S, Daly JM. Anti-Proliferative Effect of LXR Agonist T0901317 in Ovarian Carcinoma Cells. *J Ovarian Res* (2010) 3:13. doi: 10.1186/1757-2215-3-13
135. Lou R, Cao H, Dong S, Shi C, Xu X, Ma R, et al. Liver X Receptor Agonist T0901317 Inhibits the Migration and Invasion of Non-Small-Cell Lung Cancer Cells *In Vivo* and *In Vitro*. *Anticancer Drugs* (2019) 30:495–500. doi: 10.1097/CAD.0000000000000758
136. Shao W, Zhu W, Lin J, Luo M, Lin Z, Lu L, et al. Liver X Receptor Agonism Sensitizes a Subset of Hepatocellular Carcinoma to Sorafenib by Dual-Inhibiting MET and EGFR. *Neoplasia* (2020) 22:1–9. doi: 10.1016/j.neo.2019.08.002
137. Nguyen-Vu T, Vedin LL, Liu K, Jonsson P, Lin JZ, Candelaria NR, et al. Liver x Receptor Ligands Disrupt Breast Cancer Cell Proliferation Through an E2F-Mediated Mechanism. *Breast Cancer Res* (2013) 15:R51. doi: 10.1186/bcr3443
138. Hassan TS, Panicia A, Russo V, Steffensen KR. LXR Inhibits Proliferation of Human Breast Cancer Cells Through the PI3K-Akt Pathway. *Nucl Recept Res* (2015) 2:1–10. doi: 10.11131/2015/101154
139. Pencheva N, Buss CG, Posada J, Merghoub T, Tavazoie SF. Broad-Spectrum Therapeutic Suppression of Metastatic Melanoma Through Nuclear Hormone Receptor Activation. *Cell* (2014) 156:986–1001. doi: 10.1016/j.cell.2014.01.038
140. Candelaria NR, Addanki S, Zheng J, Nguyen-Vu T, Karaboga H, Dey P, et al. Antiproliferative Effects and Mechanisms of Liver X Receptor Ligands in Pancreatic Ductal Adenocarcinoma Cells. *PLoS One* (2014) 9:e106289. doi: 10.1371/journal.pone.0106289
141. Wang Q, Shen B, Qin X, Liu S, Feng J. Akt/mTOR and AMPK Signaling Pathways are Responsible for Liver X Receptor Agonist GW3965-Enhanced Gefitinib Sensitivity in Non-Small Cell Lung Cancer Cell Lines. *Transl Cancer Res* (2019) 8:66–76. doi: 10.21037/tcr.2018.12.34
142. Flaveny CA, Griffett K, El-Gendy BE-DM, Kazantzis M, Sengupta M, Amelio AL, et al. Broad Anti-tumor Activity of a Small Molecule That Selectively Targets the Warburg Effect and Lipogenesis. *Cancer Cell* (2015) 28:42–56. doi: 10.1016/j.ccell.2015.05.007
143. Wu G, Wang Q, Xu Y, Li J, Zhang H, Qi G, et al. Targeting the Transcription Factor Receptor LXR to Treat Clear Cell Renal Cell Carcinoma: Agonist or Inverse Agonist? *Cell Death Dis* (2019) 10:416. doi: 10.1038/s41419-019-1654-6
144. Saidi SA, Holland CM, Charnock-Jones DS, Smith SK. *In Vitro* and *In Vivo* Effects of the PPAR-Alpha Agonists Fenofibrate and Retinoic Acid in Endometrial Cancer. *Mol Cancer* (2006) 5:13. doi: 10.1186/1476-4598-5-13
145. Yamasaki D, Kawabe N, Nakamura H, Tachibana K, Ishimoto K, Tanaka T, et al. Fenofibrate Suppresses Growth of the Human Hepatocellular Carcinoma Cell Via PPAR $\alpha$ -Independent Mechanisms. *Eur J Cell Biol* (2011) 90:657–64. doi: 10.1016/j.ejcb.2011.02.005
146. Jan CI, Tsai MH, Chiu CF, Huang YP, Liu CJ, Chang NW. Fenofibrate Suppresses Oral Tumorigenesis Via Reprogramming Metabolic Processes: Potential Drug Repurposing for Oral Cancer. *Int J Biol Sci* (2016) 12:786–98. doi: 10.7150/ijbs.13851
147. Chen X, Chen S, Yu D. Metabolic Reprogramming of Chemoresistant Cancer Cells and the Potential Significance of Metabolic Regulation in the Reversal of Cancer Chemoresistance. *Metabolites* (2020) 10:289. doi: 10.3390/metabo10070289
148. Robison NJ, Campigotto F, Chi SN, Manley PE, Turner CD, Zimmerman MA, et al. A Phase II Trial of a Multi-Agent Oral Antiangiogenic (Metronomic) Regimen in Children With Recurrent or Progressive Cancer. *Pediatr Blood Cancer* (2014) 61:636–42. doi: 10.1002/pbc.24794
149. Luty M, Piwowarczyk K, Łabędź-Masłowska A, Wróbel T, Szczygieł M, Catapano J, et al. Fenofibrate Augments the Sensitivity of Drug-Resistant Prostate Cancer Cells to Docetaxel. *Cancers* (2019) 11:77. doi: 10.3390/cancers11010077
150. Li X, Chen YT, Hu P, Huang WC. Fatostatin Displays High Antitumor Activity in Prostate Cancer by Blocking SREBP-Regulated Metabolic Pathways and Androgen Receptor Signaling. *Mol Cancer Ther* (2014) 13:855–66. doi: 10.1158/1535-7163.MCT-13-0797
151. Yao L, Chen S, Li W. Fatostatin Inhibits the Development of Endometrial Carcinoma in Endometrial Carcinoma Cells and a Xenograft Model by Targeting Lipid Metabolism. *Arch Biochem Biophys* (2020) 684:108327. doi: 10.1016/j.abb.2020.108327
152. Gao S, Shi Z, Li X, Li W, Wang Y, Liu Z, et al. Fatostatin Suppresses Growth and Enhances Apoptosis by Blocking SREBP-Regulated Metabolic Pathways in Endometrial Carcinoma. *Oncol Rep* (2018) 39:1919–29. doi: 10.3892/or.2018.6265
153. Brovkovich V, Izhar Y, Danes JM, Dubrovskiy O, Sakalliglu IT, Morrow LM, et al. Fatostatin Induces Pro- and Anti-Apoptotic Lipid Accumulation in Breast Cancer. *Oncogenesis* (2018) 7:66. doi: 10.1038/s41389-018-0076-0
154. Liu Y, Zhang N, Zhang H, Wang L, Duan Y, Wang X, et al. Fatostatin in Combination With Tamoxifen Induces Synergistic Inhibition in ER-Positive Breast Cancer. *Drug Des Devel Ther* (2020) 14:3535–45. doi: 10.2147/DDDT.S253876
155. Smith B, Land H. Anticancer Activity of the Cholesterol Exporter ABCA1 Gene. *Cell Rep* (2012) 2:580–90. doi: 10.1016/j.celrep.2012.08.011
156. Ehmsen S, Pedersen MH, Wang G, Terp MG, Arslanagic A, Hood BL, et al. Increased Cholesterol Biosynthesis Is a Key Characteristic of Breast Cancer Stem Cells Influencing Patient Outcome. *Cell Rep* (2019) 27:3927–38. doi: 10.1016/j.celrep.2019.05.104
157. Chushi L, Wei W, Kangkang X, Yongzeng F, Ning X, Xiaolei C. HMGCR is Up-Regulated in Gastric Cancer and Promotes the Growth and Migration of the Cancer Cells. *Gene* (2016) 587:42–7. doi: 10.1016/j.gene.2016.04.029
158. Ashida S, Kawada C, Inoue K. Stromal Regulation of Prostate Cancer Cell Growth by Mevalonate Pathway Enzymes HMGCS1 and HMGCR. *Oncol Lett* (2017) 14:6533–42. doi: 10.3892/ol.2017.7025
159. Wong W-LW, Dimitroulakos J, Minden M, Penn L. HMG-CoA Reductase Inhibitors and the Malignant Cell: The Statin Family of Drugs as Triggers of Tumor-Specific Apoptosis. *Leukemia* (2002) 16:508–19. doi: 10.1038/sj.leu.2402476
160. Goldstein JL, Brown MS. Regulation of the Mevalonate Pathway. *Nature* (1990) 343:425–30. doi: 10.1038/343425a0
161. Bonetti PO, Lerman LO, Napoli C, Lerman A. Statin Effects Beyond Lipid Lowering—are They Clinically Relevant? *Eur Heart J* (2003) 24:225–48. doi: 10.1016/S0195-668X(02)00419-0
162. Gimple RC, Wang X. RAS: Striking at the Core of the Oncogenic Circuitry. *Front Oncol* (2019) 9:965. doi: 10.3389/fonc.2019.00965
163. Kaymak I, Maier CR, Schmitz W, Campbell AD, Dankworth B, Ade CP, et al. Mevalonate Pathway Provides Ubiquinone to Maintain Pyrimidine Synthesis and Survival in P53-Deficient Cancer Cells Exposed to Metabolic Stress. *Cancer Res* (2020) 80:189–203. doi: 10.1158/0008-5472.CAN-19-0650
164. Chan KK, Oza AM, Siu LL. The Statins as Anticancer Agents. *Clin Cancer Res* (2003) 9:10–9.
165. Yang YF, Jan YH, Liu YP, Yang CJ, Su CY, Chang YC, et al. Squalene Synthase Induces Tumor Necrosis Factor Receptor 1 Enrichment in Lipid Rafts to Promote Lung Cancer Metastasis. *Am J Respir Crit Care Med* (2014) 190:675–87. doi: 10.1164/rccm.201404-0714OC
166. Parris TZ, Kovács A, Hajizadeh S, Nemes S, Semaan M, Levin M, et al. Frequent MYC Coamplification and DNA Hypomethylation of Multiple

- Genes on 8q in 8p11-p12-amplified Breast Carcinomas. *Oncogenesis* (2014) 3:e95. doi: 10.1038/oncsis.2014.8
167. Liu Y, Sun W, Zhang K, Zheng H, Ma Y, Lin D, et al. Identification of Genes Differentially Expressed in Human Primary Lung Squamous Cell Carcinoma. *Lung Cancer* (2007) 56:307–17. doi: 10.1016/j.lungcan.2007.01.016
  168. Yuen HF, McCrudden CM, Huang YH, Tham JM, Zhang X, Zeng Q, et al. TAZ Expression as a Prognostic Indicator in Colorectal Cancer. *PLoS One* (2013) 8:e54211. doi: 10.1371/journal.pone.0054211
  169. Sui Z, Zhou J, Cheng Z, Lu P. Squalene Epoxidase (SQLE) Promotes the Growth and Migration of the Hepatocellular Carcinoma Cells. *Tumor Biol* (2015) 36:6173–9. doi: 10.1007/s13277-015-3301-x
  170. Brown DN, Caffa I, Cirmena G, Piras D, Garuti A, Gallo M, et al. Squalene Epoxidase is a Bona Fide Oncogene by Amplification With Clinical Relevance in Breast Cancer. *Sci Rep* (2016) 6:19435. doi: 10.1038/srep19435
  171. Garcia-Bermudez J, Baudrier L, Bayraktar EC, Shen Y, La K, Guarecuco R, et al. Squalene Accumulation in Cholesterol Auxotrophic Lymphomas Prevents Oxidative Cell Death. *Nature* (2019) 567:118–22. doi: 10.1038/s41586-019-0945-5
  172. Viswanathan VS, Ryan MJ, Dhruv HD, Gill S, Eichhoff OM, Seashore-Ludlow B, et al. Dependency of a Therapy-Resistant State of Cancer Cells on a Lipid Peroxidase Pathway. *Nature* (2017) 547:453–7. doi: 10.1038/nature23007
  173. Murai T. Cholesterol Lowering: Role in Cancer Prevention and Treatment. *Biol Chem* (2014) 396:1–11. doi: 10.1515/hsz-2014-0194
  174. Xue T, Zhang Y, Zhang L, Yao L, Hu X, Xu LX. Proteomic Analysis of Two Metabolic Proteins With Potential to Translocate to Plasma Membrane Associated With Tumor Metastasis Development and Drug Targets. *J Proteome Res* (2013) 12:1754–63. doi: 10.1021/pr301100r
  175. Staedler D, Chapuis-Bernasconi C, Dehmlow H, Fischer H, Juillerat-Jeanneret L, Aebi JD. Cytotoxic Effects of Combination of Oxidosqualene Cyclase Inhibitors With Atorvastatin in Human Cancer Cells. *J Med Chem* (2012) 55:4990–5002. doi: 10.1021/jm300256z
  176. Mejia-Pous C, Damiola F, Gandrillon O. Cholesterol Synthesis-Related Enzyme Oxidosqualene Cyclase is Required to Maintain Self-Renewal in Primary Erythroid Progenitors. *Cell Prolif* (2011) 44:441–52. doi: 10.1111/j.1365-2184.2011.00771.x
  177. Beckwitt CH, Shiraha K, Wells A. Lipophilic Statins Limit Cancer Cell Growth and Survival, Via Involvement of Akt Signaling. *PLoS One* (2018) 13:e0197422. doi: 10.1371/journal.pone.0197422
  178. Hindler K, Cleland CS, Rivera E, Collard CD. The Role of Statins in Cancer Therapy. *Oncologist* (2006) 11:306–15. doi: 10.1634/theoncologist.11-3-306
  179. Pisanti S, Picardi P, Ciaglia E, D'Alessandro A, Bifulco M. Novel Prospects of Statins as Therapeutic Agents in Cancer. *Pharmacol Res* (2014) 88:84–98. doi: 10.1016/j.phrs.2014.06.013
  180. Gizzo S, Quaranta M, Nardelli GB, Noventa M. Lipophilic Statins as Anticancer Agents: Molecular Targeted Actions and Proposal in Advanced Gynaecological Malignancies. *Curr Drug Targets* (2015) 16:1142–59. doi: 10.2174/1389450116666150330113239
  181. Fatehi Hassanabad A. Current Perspectives on Statins as Potential Anti-Cancer Therapeutics: Clinical Outcomes and Underlying Molecular Mechanisms. *Transl Lung Cancer Res* (2019) 8:692–9. doi: 10.21037/tlcr.2019.09.08
  182. Osmak M. Statins and Cancer: Current and Future Prospects. *Cancer Lett* (2012) 324:1–12. doi: 10.1016/j.canlet.2012.04.011
  183. Ahmadi M, Amiri S, Pecic S, Machaj F, Rosik J, Łos MJ, et al. Pleiotropic Effects of Statins: A Focus on Cancer. *Biochim Biophys Acta BBA - Mol Basis Dis* (2020) 1866:165968. doi: 10.1016/j.bbdis.2020.165968
  184. Altwaigri AK. Statins Are Potential Anticancerous Agents (Review). *Oncol Rep* (2015) 33:1019–39. doi: 10.3892/or.2015.3741
  185. Di Bello E, Zwergel C, Mai A, Valente S. The Innovative Potential of Statins in Cancer: New Targets for New Therapies. *Front Chem* (2020) 8:516. doi: 10.3389/fchem.2020.00516
  186. Matuszewicz L, Meissner J, Toporkiewicz M, Sikorski AF. The Effect of Statins on Cancer Cells—Review. *Tumor Biol* (2015) 36:4889–904. doi: 10.1007/s13277-015-3551-7
  187. Terzi H, Altun A, Şencan M. In Vitro Comparison of the Cytotoxic Effects of Statins on U266 Myeloma Cell Line. *Indian J Med Res* (2019) 150:630–4. doi: 10.4103/ijmr.IJMR\_672\_18
  188. Chen YH, Chen YC, Lin CC, Hsieh YP, Hsu CS, Hsieh MC. Synergistic Anticancer Effects of Gemcitabine With Pitavastatin on Pancreatic Cancer Cell Line MIA PaCa-2 In Vitro and In Vivo. *Cancer Manag Res* (2020) 12:4645–65. doi: 10.2147/CMAR.S247876
  189. Lübtow MM, Oerter S, Quader S, Jeanclos E, Cubukova A, Krafft M, et al. In Vitro Blood–Brain Barrier Permeability and Cytotoxicity of an Atorvastatin-Loaded Nanoformulation Against Glioblastoma in 2D and 3D Models. *Mol Pharm* (2020) 17:1835–47. doi: 10.1021/acs.molpharmaceut.9b01117
  190. Higgins MJ, Prowell TM, Blackford AL, Byrne C, Khouri NF, Slater SA, et al. A Short-Term Biomarker Modulation Study of Simvastatin in Women at Increased Risk of a New Breast Cancer. *Breast Cancer Res Treat* (2012) 131:915–24. doi: 10.1007/s10549-011-1858-7
  191. Kim ST, Kang JH, Lee J, Park SH, Park JO, Park YS, et al. Simvastatin Plus Capecitabine–Cisplatin Versus Placebo Plus Capecitabine–Cisplatin in Patients With Previously Untreated Advanced Gastric Cancer: A Double-Blind Randomised Phase 3 Study. *Eur J Cancer* (2014) 50:2822–30. doi: 10.1016/j.ejca.2014.08.005
  192. Vinayak S, Schwartz EJ, Jensen K, Lipson J, Alli E, McPherson L, et al. A Clinical Trial of Lovastatin for Modification of Biomarkers Associated With Breast Cancer Risk. *Breast Cancer Res Treat* (2013) 142:389–98. doi: 10.1007/s10549-013-2739-z
  193. Garwood ER, Kumar AS, Baehner FL, Moore DH, Au A, Hylton N, et al. Fluvastatin Reduces Proliferation and Increases Apoptosis in Women With High Grade Breast Cancer. *Breast Cancer Res Treat* (2010) 119:137–44. doi: 10.1007/s10549-009-0507-x
  194. Beckwitt CH, Brufsky A, Oltvai ZN, Wells A. Statin Drugs to Reduce Breast Cancer Recurrence and Mortality. *Breast Cancer Res* (2018) 20:144. doi: 10.1186/s13058-018-1066-z
  195. Farooqi MAM, Malhotra N, Mukherjee SD, Sanger S, Dhesy-Thind SK, Ellis P, et al. Statin Therapy in the Treatment of Active Cancer: A Systematic Review and Meta-Analysis of Randomized Controlled Trials. *PLoS One* (2018) 13:e0209486. doi: 10.1371/journal.pone.0209486
  196. Brånvall E, Ekberg S, Eloranta S, Wästerlid T, Birmann BM, Smedby KE. Statin Use is Associated With Improved Survival in Multiple Myeloma: A Swedish Population-Based Study of 4315 Patients. *Am J Hematol* (2020) 95:652–61. doi: 10.1002/ajh.25778
  197. Murtola TJ, Syväälä H, Tolonen T, Helminen M, Riikonen J, Koskimäki J, et al. Atorvastatin Versus Placebo for Prostate Cancer Before Radical Prostatectomy—A Randomized, Double-blind, Placebo-Controlled Clinical Trial. *Eur Urol* (2018) 74:697–701. doi: 10.1016/j.eururo.2018.06.037
  198. Bono AV, Pagano F, Montironi R, Zattoni F, Manganelli A, Selvaggi FP, et al. Effect of Complete Androgen Blockade on Pathologic Stage and Resection Margin Status of Prostate Cancer: Progress Pathology Report of the Italian PROSIT Study. *Urology* (2001) 57:117–21. doi: 10.1016/S0090-4295(00)00866-9
  199. Matuszewicz L, Czogalla A, Sikorski AF. Attempts to Use Statins in Cancer Therapy: An Update. *Tumor Biol* (2020) 42:101042832094176. doi: 10.1177/1010428320941760
  200. Charlton-Menys V, Durrington PN. Squalene Synthase Inhibitors: Clinical Pharmacology and Cholesterol-Lowering Potential. *Drugs* (2007) 67:11–6. doi: 10.2165/00003495-200767010-00002
  201. Cenedella RJ, Jacob R, Borchman D, Tang D, Neely AR, Samadi A, et al. Direct Perturbation of Lens Membrane Structure may Contribute to Cataracts Caused by U18666A, an Oxidosqualene Cyclase Inhibitor. *J Lipid Res* (2004) 45:1232–41. doi: 10.1194/jlr.M300469-JLR200
  202. Dey P, Barros RPA, Warner M, Ström A, Gustafsson J-Å. Insight Into the Mechanisms of Action of Estrogen Receptor  $\beta$  in the Breast, Prostate, Colon, and CNS. *J Mol Endocrinol* (2013) 51:T61–74. doi: 10.1530/JME-13-0150101
  203. Dey P, Ström A, Gustafsson J-Å. Estrogen Receptor  $\beta$  Upregulates FOXO3a and Causes Induction of Apoptosis Through PUMA in Prostate Cancer. *Oncogene* (2014) 33:4213–25. doi: 10.1038/ncr.2013.384
  204. Singh V, Sharma V, Verma V, Pandey D, Yadav SK, Maikhuri JP, et al. Apigenin Manipulates the Ubiquitin–Proteasome System to Rescue Estrogen Receptor- $\beta$  From Degradation and Induce Apoptosis in Prostate Cancer Cells. *Eur J Nutr* (2015) 54:1255–67. doi: 10.1007/s00394-014-0803-z
  205. Pravettoni A, Mornati O, Martini PGV, Marino M, Colciago A, Celotti F, et al. Estrogen Receptor Beta (ERbeta) and Inhibition of Prostate Cancer Cell Proliferation: Studies on the Possible Mechanism of Action in DU145 Cells. *Mol Cell Endocrinol* (2007) 263:46–54. doi: 10.1016/j.mce.2006.08.008

206. Pandit J, Danley DE, Schulte GK, Mazzalupo S, Pauly TA, Hayward CM, et al. Crystal Structure of Human Squalene Synthase: A Key Enzyme in Cholesterol Biosynthesis. *J Biol Chem* (2000) 275:30610–7. doi: 10.1074/jbc.M004132200
207. Bergstrom JD, Dufresne C, Bills GF, Nallin-Omstead M, Byrne K. Discovery, Biosynthesis, and Mechanism of Action of the Zaragozic Acids: Potent Inhibitors of Squalene Synthase. *Annu Rev Microbiol* (1995) 49:607–39. doi: 10.1146/annurev.mi.49.100195.003135
208. He J, Shin H, Wei X, Kade Gowda AKG, Chen R, Xie SK. NPC1L1 Knockout Protects Against Colitis-Associated Tumorigenesis in Mice. *BMC Cancer* (2015) 15:189. doi: 10.1186/s12885-015-1230-0
209. Huang J, Li L, Lian J, Schauer S, Vesely PW, Kratky D, et al. Tumor-Induced Hyperlipidemia Contributes to Tumor Growth. *Cell Rep* (2016) 15:336–48. doi: 10.1016/j.celrep.2016.03.020
210. Gonias SL, Karimi-Mostowfi N, Murray SS, Mantuano E, Gilder AS. Expression of LDL Receptor-Related Proteins (LRPs) in Common Solid Malignancies Correlates With Patient Survival. *PloS One* (2017) 12: e0186649. doi: 10.1371/journal.pone.0186649
211. Gallagher EJ, Zelenko Z, Neel BA, Antoniou IM, Rajan L, Kase N, et al. Elevated Tumor LDLR Expression Accelerates LDL Cholesterol-Mediated Breast Cancer Growth in Mouse Models of Hyperlipidemia. *Oncogene* (2017) 36:6462–71. doi: 10.1038/onc.2017.247
212. Campion O, Al Khalifa T, Langlois B, Thevenard-Devy J, Salesse S, Savary K, et al. Contribution of the Low-Density Lipoprotein Receptor Family to Breast Cancer Progression. *Front Oncol* (2020) 10:882. doi: 10.3389/fonc.2020.00882
213. Roslan Z, Muhamad M, Selvaratnam L, Ab-Rahim S. The Roles of Low-Density Lipoprotein Receptor-Related Proteins 5, 6, and 8 in Cancer: A Review. *J Oncol* (2019) 2019:4536302. doi: 10.1155/2019/4536302
214. Mooberry LK, Sabnis NA, Panchoo M, Nagarajan B, Lacko AG. Targeting the SR-B1 Receptor as a Gateway for Cancer Therapy and Imaging. *Front Pharmacol* (2016) 7:466. doi: 10.3389/fphar.2016.00466
215. Feng H, Wang M, Wu C, Yu J, Wang D, Ma J, et al. High Scavenger Receptor Class B Type I Expression is Related to Tumor Aggressiveness and Poor Prognosis in Lung Adenocarcinoma: A STROBE Compliant Article. *Medicine (Baltimore)* (2018) 97:e0203. doi: 10.1097/MD.00000000000010203
216. Schörghofer D, Kinslechner K, Preitschopf A, Schütz B, Röhl C, Hengstschläger M, et al. The HDL Receptor SR-B1 is Associated With Human Prostate Cancer Progression and Plays a Possible Role In Establishing Androgen Independence. *Reprod Biol Endocrinol* (2015) 13:88. doi: 10.1186/s12958-015-0087-z
217. Wang C, Li P, Xuan J, Zhu C, Liu J, Shan L, et al. Cholesterol Enhances Colorectal Cancer Progression Via ROS Elevation and MAPK Signaling Pathway Activation. *Cell Physiol Biochem* (2017) 42:729–42. doi: 10.1159/000477890
218. Llaverrías G, Danilo C, Mercier I, Daumer K, Capozza F, Williams TM, et al. Role of Cholesterol in the Development and Progression of Breast Cancer. *Am J Pathol* (2011) 178:402–12. doi: 10.1016/j.ajpath.2010.11.005
219. Riscal R, Skuli N, Simon MC. Even Cancer Cells Watch Their Cholesterol! *Mol Cell* (2019) 76:220–31. doi: 10.1016/j.molcel.2019.09.008
220. Kapourchali FR, Surendiran G, Goulet A, Moghadasian MH. The Role of Dietary Cholesterol in Lipoprotein Metabolism and Related Metabolic Abnormalities: A Mini-Review. *Crit Rev Food Sci Nutr* (2016) 56:2408–15. doi: 10.1080/10408398.2013.842887
221. Püschel GP, Henkel J. Dietary Cholesterol Does Not Break Your Heart But Kills Your Liver. *Porto BioMed J* (2018) 3:e12. doi: 10.1016/j.pbj.0000000000000012
222. Quail DF, Dannenberg AJ. The Obese Adipose Tissue Microenvironment in Cancer Development and Progression. *Nat Rev Endocrinol* (2019) 15:139–54. doi: 10.1038/s41574-018-0126-x
223. Cedó L, Reddy ST, Mato E, Blanco-Vaca F, Escolà-Gil JC. HDL and LDL: Potential New Players in Breast Cancer Development. *J Clin Med* (2019) 8:853. doi: 10.3390/jcm8060853
224. Pelton K, Coticchia CM, Curatolo AS, Schaffner CP, Zurakowski D, Solomon KR, et al. Hypercholesterolemia Induces Angiogenesis and Accelerates Growth of Breast Tumors In Vivo. *Am J Pathol* (2014) 184:2099–110. doi: 10.1016/j.ajpath.2014.03.006
225. Oh SH, Choi SY, Choi HJ, Ryu HM, Kim YJ, Jung HY, et al. The Emerging Role of Xanthine Oxidase Inhibition for Suppression of Breast Cancer Cell Migration and Metastasis Associated With Hypercholesterolemia. *FASEB J* (2019) 33:7301–14. doi: 10.1096/fj.201802415RR
226. Heilos D, Röhl C, Pirker C, Englinger B, Baier D, Mohr T, et al. Altered Membrane Rigidity Via Enhanced Endogenous Cholesterol Synthesis Drives Cancer Cell Resistance to Destruxins. *Oncotarget* (2018) 9:25661–80. doi: 10.18632/oncotarget.25432
227. Han T, Lv Y, Wang S, Hu T, Hong H, Fu Z. PPAR $\gamma$  Overexpression Regulates Cholesterol Metabolism in Human L02 Hepatocytes. *J Pharmacol Sci* (2019) 139:1–8. doi: 10.1016/j.jphs.2018.09.013
228. Tachibana K, Yamasaki D, Ishimoto K, Doi T. The Role of PPARs in Cancer. *PPAR Res* (2008) 2008:102737. doi: 10.1155/2008/102737
229. Chinetti G, Lestavel S, Bocher V, Remaley AT, Neve B, Torra IP, et al. PPAR- $\alpha$  and PPAR- $\gamma$  Activators Induce Cholesterol Removal From Human Macrophage Foam Cells Through Stimulation of the ABCA1 Pathway. *Nat Med* (2001) 7:53–8. doi: 10.1038/83348
230. Grabacka M, Reiss K. Anticancer Properties of PPAR $\alpha$ -Effects on Cellular Metabolism and Inflammation. *PPAR Res* (2008) 2008:930705. doi: 10.1155/2008/930705
231. Gou Q, Gong X, Jin J, Shi J, Hou Y. Peroxisome Proliferator-Activated Receptors (PPARs) Are Potential Drug Targets for Cancer Therapy. *Oncotarget* (2017) 8:60704–9. doi: 10.18632/oncotarget.19610
232. Zhao W, Prijic S, Urban BC, Tisza MJ, Zuo Y, Li L, et al. Candidate Antimetastasis Drugs Suppress the Metastatic Capacity of Breast Cancer Cells by Reducing Membrane Fluidity. *Cancer Res* (2016) 76:2037–49. doi: 10.1158/0008-5472.CAN-15-1970
233. Preta G. New Insights Into Targeting Membrane Lipids for Cancer Therapy. *Front Cell Dev Biol* (2020) 8:571237. doi: 10.3389/fcell.2020.571237
234. Zhang J, Li Q, Wu Y, Wang D, Xu L, Zhang Y, et al. Cholesterol Content in Cell Membrane Maintains Surface Levels of ErbB2 and Confers a Therapeutic Vulnerability in ErbB2-Positive Breast Cancer. *Cell Commun Signal* (2019) 17:15. doi: 10.1186/s12964-019-0328-4
235. Aguirre-Portolés C, Feliu J, Reglero G, Ramírez de Molina A. ABCA1 Overexpression Worsens Colorectal Cancer Prognosis by Facilitating Tumour Growth and Caveolin-1-Dependent Invasiveness, and These Effects can be Ameliorated Using the BET Inhibitor Apabetalone. *Mol Oncol* (2018) 12:1735–52. doi: 10.1002/1878-0261.12367
236. Koundouros N, Poulogiannis G. Reprogramming of Fatty Acid Metabolism in Cancer. *Br J Cancer* (2020) 122:4–22. doi: 10.1038/s41416-019-0650-z
237. Adam RM, Mukhopadhyay NK, Kim J, Di Vizio D, Cinar B, Boucher K, et al. Cholesterol Sensitivity of Endogenous and Myristoylated Akt. *Cancer Res* (2007) 67:6238–46. doi: 10.1158/0008-5472.CAN-07-0288
238. Chen L, Peng J, Wang Y, Jiang H, Wang W, Dai J, et al. Fenofibrate-Induced Mitochondrial Dysfunction and Metabolic Reprogramming Reversal: The Anti-Tumor Effects in Gastric Carcinoma Cells Mediated by the PPAR Pathway. *Am J Transl Res* (2020) 12:428–46.
239. Ertunc ME, Hotamisligil GS. Lipid Signaling and Lipotoxicity in Metaflammation: Indications for Metabolic Disease Pathogenesis and Treatment. *J Lipid Res* (2016) 57:2099–114. doi: 10.1194/jlr.R066514
240. Wang YJ, Bian Y, Luo J, Lu M, Xiong Y, Guo SY, et al. Cholesterol and Fatty Acids Regulate Cysteine Ubiquitylation of ACAT2 Through Competitive Oxidation. *Nat Cell Biol* (2017) 19:808–19. doi: 10.1038/ncb3551
241. Jarc E, Petan T. Lipid Droplets and the Management of Cellular Stress. *Yale J Biol Med* (2019) 92:435–52.
242. Qiu B, Ackerman D, Sanchez DJ, Li B, Ochocki JD, Grazioli A, et al. HIF2 $\alpha$ -Dependent Lipid Storage Promotes Endoplasmic Reticulum Homeostasis in Clear-Cell Renal Cell Carcinoma. *Cancer Discov* (2015) 5:652–67. doi: 10.1158/2159-8290.CD-14-1507
243. Yue S, Li J, Lee SY, Lee HJ, Shao T, Song B, et al. Cholesteryl Ester Accumulation Induced by PTEN Loss and PI3K/AKT Activation Underlies Human Prostate Cancer Aggressiveness. *Cell Metab* (2014) 19:393–406. doi: 10.1016/j.cmet.2014.01.019
244. de Gonzalo-Calvo D, López-Vilaró L, Nasarre L, Perez-Olabarria M, Vázquez T, Escuin D, et al. Intratumor Cholesteryl Ester Accumulation is Associated With Human Breast Cancer Proliferation and Aggressive Potential: A Molecular and Clinicopathological Study. *BMC Cancer* (2015) 15:460. doi: 10.1186/s12885-015-1469-5
245. Mulas MF, Abete C, Pulisci D, Pani A, Massidda B, Dessì S, et al. Cholesterol Esters as Growth Regulators of Lymphocytic Leukaemia Cells. *Cell Prolif* (2011) 44:360–71. doi: 10.1111/j.1365-2184.2011.00758.x



246. Bemlih S, Poirier M-D, El Andaloussi A. Acyl-Coenzyme A: Cholesterol Acyltransferase Inhibitor Avasimibe Affect Survival and Proliferation of Glioma Tumor Cell Lines. *Cancer Biol Ther* (2010) 9:1025–32. doi: 10.4161/cbt.9.12.11875
247. Tirinato L, Liberale C, Di Franco S, Candeloro P, Benfante A, La Rocca R, et al. Lipid Droplets: A New Player in Colorectal Cancer Stem Cells Unveiled by Spectroscopic Imaging. *Stem Cells* (2015) 33:35–44. doi: 10.1002/stem.1837
248. Jiang Y, Sun A, Zhao Y, Ying W, Sun H, Yang X, et al. Proteomics Identifies New Therapeutic Targets of Early-Stage Hepatocellular Carcinoma. *Nature* (2019) 567:257–61. doi: 10.1038/s41586-019-0987-8
249. Saraon P, Cretu D, Musrap N, Karagiannis GS, Batruch I, Drabovich AP, et al. Quantitative Proteomics Reveals That Enzymes of the Ketogenic Pathway are Associated With Prostate Cancer Progression. *Mol Cell Proteomics* (2013) 12:1589–601. doi: 10.1074/mcp.M112.023887
250. Lacombe AMF, Soares IC, Mariani BM de P, Nishi MY, Bezerra-Neto JE, Charchar H da S, et al. Sterol O-Acyl Transferase 1 as a Prognostic Marker of Adrenocortical Carcinoma. *Cancers* (2020) 12:247. doi: 10.3390/cancers12010247
251. Warner GJ, Stoudt G, Bamberger M, Johnson WJ, Rothblat GH. Cell Toxicity Induced by Inhibition of Acyl Coenzyme A:Cholesterol Acyltransferase and Accumulation of Unesterified Cholesterol. *J Biol Chem* (1995) 270:5772–8. doi: 10.1074/jbc.270.11.5772
252. Wang J, Tan M, Ge J, Zhang P, Zhong J, Tao L, et al. Lysosomal Acid Lipase Promotes Cholesterol Ester Metabolism and Drives Clear Cell Renal Cell Carcinoma Progression. *Cell Prolif* (2018) 51:e12452. doi: 10.1111/cpr.12452
253. Chen Y, Hughes-Fulford M. Human Prostate Cancer Cells Lack Feedback Regulation of Low-Density Lipoprotein Receptor and its Regulator, SREBP2. *Int J Cancer* (2001) 91:41–5. doi: 10.1002/1097-0215(20010101)91:1<41::AID-IJC1009>3.0.CO;2-2
254. Locke JA, Guns ES, Lubik AA, Adomat HH, Hendy SC, Wood CA, et al. Androgen Levels Increase by Intratumoral De Novo Steroidogenesis During Progression of Castration-Resistant Prostate Cancer. *Cancer Res* (2008) 68:6407–15. doi: 10.1158/0008-5472.CAN-07-5997
255. Leon CG, Locke JA, Adomat HH, Etinger SL, Twiddy AL, Neumann RD, et al. Alterations in Cholesterol Regulation Contribute to the Production of Intratumoral Androgens During Progression to Castration-Resistant Prostate Cancer in a Mouse Xenograft Model. *Prostate* (2010) 70:390–400. doi: 10.1002/pros.21072
256. Martinez-Outschoorn UE, Lin Z, Whitaker-Menezes D, Howell A, Sotgia F, Lisanti MP. Ketone Body Utilization Drives Tumor Growth and Metastasis. *Cell Cycle* (2012) 11:3964–71. doi: 10.4161/cc.22137
257. Ozsvari B, Sotgia F, Simmons K, Trowbridge R, Foster R, Lisanti MP. Mitoketoscins: Novel Mitochondrial Inhibitors for Targeting Ketone Metabolism in Cancer Stem Cells (CSCs). *Oncotarget* (2017) 8:78340–50. doi: 10.18632/oncotarget.21259
258. Lo YW, Lin ST, Chang SJ, Chan CH, Lyu KW, Chang JF, et al. Mitochondrial Proteomics With siRNA Knockdown to Reveal ACAT1 and MDH2 in the Development of Doxorubicin-Resistant Uterine Cancer. *J Cell Mol Med* (2015) 19:744–59. doi: 10.1111/jcmm.12388
259. Dong Y, Tu R, Liu H, Qing G. Regulation of Cancer Cell Metabolism: Oncogenic MYC in the Driver's Seat. *Signal Transduct Target Ther* (2020) 5:124. doi: 10.1038/s41392-020-00235-2
260. Zhong C, Fan L, Yao F, Shi J, Fang W, Zhao H. HMGR is Necessary for the Tumorigenicity of Esophageal Squamous Cell Carcinoma and Is Regulated by Myc. *Tumor Biol* (2014) 35:4123–9. doi: 10.1007/s13277-013-1539-8
261. Cheng C, Geng F, Cheng X, Guo D. Lipid Metabolism Reprogramming and its Potential Targets in Cancer. *Cancer Commun Lond Engl* (2018) 38:27. doi: 10.1186/s40880-018-0301-4
262. Haskins JW, Zhang S, Means RE, Kelleher JK, Cline GW, Canfrán-Duque A, et al. Neuregulin-Activated ERBB4 Induces the SREBP-2 Cholesterol Biosynthetic Pathway and Increases Low-Density Lipoprotein Uptake. *Sci Signal* (2015) 8:ra111. doi: 10.1126/scisignal.aac5124
263. Bakiri L, Hamacher R, Graña O, Guio-Carrión A, Campos-Olivas R, Martínez L, et al. Liver Carcinogenesis by FOS-Dependent Inflammation and Cholesterol Dysregulation. *J Exp Med* (2017) 214:1387–409. doi: 10.1084/jem.20160935
264. Kloudova A, Guengerich PF, Soucek P. The Role of Oxysterols in Human Cancer. *Trends Endocrinol Metab* (2017) 28:485–96. doi: 10.1016/j.tem.2017.03.002
265. Olkkonen VM, Béaslas O, Nissilä E. Oxysterols and Their Cellular Effectors. *Biomolecules* (2012) 2:76–103. doi: 10.3390/biom2010076
266. He S, Nelson ER. 27-Hydroxycholesterol, an Endogenous Selective Estrogen Receptor Modulator. *Maturitas* (2017) 104:29–35. doi: 10.1016/j.maturitas.2017.07.014
267. Raza S, Ohm JE, Dhasarathy A, Schommer J, Roche C, Hammer KDP, et al. The Cholesterol Metabolite 27-Hydroxycholesterol Regulates p53 Activity and Increases Cell Proliferation Via MDM2 in Breast Cancer Cells. *Mol Cell Biochem* (2015) 410:187–95. doi: 10.1007/s11010-015-2551-7
268. Shen Z, Zhu D, Liu J, Chen J, Liu Y, Hu C, et al. 27-Hydroxycholesterol Induces Invasion and Migration of Breast Cancer Cells by Increasing MMP9 and Generating EMT Through Activation of STAT-3. *Environ Toxicol Pharmacol* (2017) 51:1–8. doi: 10.1016/j.etap.2017.02.001
269. Zhu D, Shen Z, Liu J, Chen J, Liu Y, Hu C, et al. The ROS-mediated Activation of STAT-3/VEGF Signaling is Involved in the 27-Hydroxycholesterol-Induced Angiogenesis in Human Breast Cancer Cells. *Toxicol Lett* (2016) 264:79–86. doi: 10.1016/j.toxlet.2016.11.006
270. Revilla G, Pons M de P, Baila-Rueda L, García-León A, Santos D, Cenarro A, et al. Cholesterol and 27-Hydroxycholesterol Promote Thyroid Carcinoma Aggressiveness. *Sci Rep* (2019) 9:10260. doi: 10.1038/s41598-019-46727-2
271. Clendening JW, Pandya A, Boutros PC, El Ghamrasni S, Khosravi F, Trentin GA, et al. Dysregulation of the Mevalonate Pathway Promotes Transformation. *Proc Natl Acad Sci* (2010) 107:15051–6. doi: 10.1073/pnas.0910258107
272. Xue L, Qi H, Zhang H, Ding L, Huang Q, Zhao D, et al. Targeting SREBP-2-Regulated Mevalonate Metabolism for Cancer Therapy. *Front Oncol* (2020) 10:1510. doi: 10.3389/fonc.2020.01510
273. Zhong C, Fan L, Li Z, Yao F, Zhao H. SREBP2 is Upregulated in Esophageal Squamous Cell Carcinoma and Co-Operates With C-Myc to Regulate HMGR Expression. *Mol Med Rep* (2019) 20:3003–10. doi: 10.3892/mmr.2019.10577
274. Lewis CA, Brault C, Peck B, Bensaad K, Griffiths B, Mitter R, et al. SREBP Maintains Lipid Biosynthesis and Viability of Cancer Cells Under Lipid- and Oxygen-Deprived Conditions and Defines a Gene Signature Associated With Poor Survival in Glioblastoma Multiforme. *Oncogene* (2015) 34:5128–40. doi: 10.1038/nc.2014.439
275. Porstmann T, Santos CR, Griffiths B, Cully M, Wu M, Leever S, et al. SREBP Activity is Regulated by mTORC1 and Contributes to Akt-Dependent Cell Growth. *Cell Metab* (2008) 8:224–36. doi: 10.1016/j.cmet.2008.07.007
276. Ricout SJH, Yecies JL, Ben-Sahra I, Manning BD. Oncogenic PI3K and K-Ras Stimulate De Novo Lipid Synthesis Through mTORC1 and SREBP. *Oncogene* (2016) 35:1250–60. doi: 10.1038/nc.2015.179
277. Dong F, Mo Z, Eid W, Courtney KC, Zha X. Akt Inhibition Promotes ABCA1-Mediated Cholesterol Efflux to ApoA-I Through Suppressing mTORC1. *PLoS One* (2014) 9:e113789. doi: 10.1371/journal.pone.0113789
278. Moon SH, Huang CH, Houlihan SL, Regunath K, Freed-Pastor WA, Morris JP4th, et al. P53 Represses the Mevalonate Pathway to Mediate Tumor Suppression. *Cell* (2019) 176:564–80.e19. doi: 10.1016/j.cell.2018.11.011
279. Peck B, Schulze A. Lipid Metabolism at the Nexus of Diet and Tumor Microenvironment. *Trends Cancer* (2019) 5:693–703. doi: 10.1016/j.trecan.2019.09.007
280. Ingallina E, Sorrentino G, Bertolio R, Lisek K, Zannini A, Azzolin L, et al. Mechanical Cues Control Mutant p53 Stability Through a Mevalonate-RhoA Axis. *Nat Cell Biol* (2018) 20:28–35. doi: 10.1038/s41556-017-0009-8
281. Zhuang L, Kim J, Adam RM, Solomon KR, Freeman MR. Cholesterol Targeting Alters Lipid Raft Composition and Cell Survival in Prostate Cancer Cells and Xenografts. *J Clin Invest* (2005) 115:959–68. doi: 10.1172/JCI200519935
282. Jia Y, Wang Y, Xie J. The Hedgehog Pathway: Role in Cell Differentiation, Polarity and Proliferation. *Arch Toxicol* (2015) 89:179–91. doi: 10.1007/s00204-014-1433-1
283. Guo D, Reinitz F, Youssef M, Hong C, Nathanson D, Akhavan D, et al. An LXR Agonist Promotes Glioblastoma Cell Death Through Inhibition of an EGFR/AKT/SREBP-1/LDLR-Dependent Pathway. *Cancer Discov* (2011) 1:442–56. doi: 10.1158/2159-8290.CD-11-0102



284. Gholkar AA, Cheung K, Williams KJ, Lo YC, Hamideh SA, Nnebe C, et al. Fatostatin Inhibits Cancer Cell Proliferation by Affecting Mitotic Microtubule Spindle Assembly and Cell Division. *J Biol Chem* (2016) 291:17001–8. doi: 10.1074/jbc.C116.737346
285. Wen D, Wang J, Van Den Driessche G, Chen Q, Zhang Y, Chen G, et al. Adipocytes as Anticancer Drug Delivery Depot. *Matter* (2019) 1:1203–14. doi: 10.1016/j.matt.2019.08.007
286. Shen H, Shi S, Zhang Z, Gong T, Sun X. Coating Solid Lipid Nanoparticles With Hyaluronic Acid Enhances Antitumor Activity Against Melanoma Stem-Like Cells. *Theranostics* (2015) 5:755–71. doi: 10.7150/thno.10804
287. Sobot D, Mura S, Rouquette M, Vukosavljevic B, Cayre F, Buchy E, et al. Circulating Lipoproteins: A Trojan Horse Guiding Squalenoylated Drugs to LDL-Accumulating Cancer Cells. *Mol Ther* (2017) 25:1596–605. doi: 10.1016/j.ymthe.2017.05.016
288. Mooberry LK, Nair M, Paranjape S, McConathy WJ, Lacko AG. Receptor Mediated Uptake of Paclitaxel From a Synthetic High Density Lipoprotein Nanocarrier. *J Drug Target* (2010) 18:53–8. doi: 10.3109/10611860903156419
289. Radwan AA, Alanazi FK. Targeting Cancer Using Cholesterol Conjugates. *Saudi Pharm J* (2014) 22:3–16. doi: 10.1016/j.jsps.2013.01.003

**Conflict of Interest:** The authors declare that the research was conducted in the absence of any commercial or financial relationships that could be construed as a potential conflict of interest.

The reviewer AC declared a shared affiliation with the authors to the handling editor at the time of review.

Copyright © 2021 Giacomini, Gianfanti, Desbats, Orso, Berretta, Prayer-Galetti, Ragazzi and Cocetta. This is an open-access article distributed under the terms of the Creative Commons Attribution License (CC BY). The use, distribution or reproduction in other forums is permitted, provided the original author(s) and the copyright owner(s) are credited and that the original publication in this journal is cited, in accordance with accepted academic practice. No use, distribution or reproduction is permitted which does not comply with these terms.



# Lactate Modulates Cellular Metabolism Through Histone Lactylation-Mediated Gene Expression in Non-Small Cell Lung Cancer

Jun Jiang<sup>1†</sup>, DengLiang Huang<sup>2†</sup>, Yuan Jiang<sup>2</sup>, Jing Hou<sup>2</sup>, MeiYuan Tian<sup>2</sup>, JianHua Li<sup>2</sup>, Li Sun<sup>2</sup>, YaoGang Zhang<sup>3</sup>, Tao Zhang<sup>4</sup>, ZhiQin Li<sup>5</sup>, ZhongCheng Li<sup>1</sup>, SiXian Tong<sup>5</sup> and YanYan Ma<sup>5\*</sup>

<sup>1</sup> Oncology Department, Affiliated Hospital of Qinghai University, Xining, China, <sup>2</sup> Central Laboratory, Affiliated Hospital of Qinghai University, Xining, China, <sup>3</sup> Qinghai Province Research Key Laboratory of Echinococcosis, Affiliated Hospital of Qinghai University, Xining, China, <sup>4</sup> Rehabilitation Department, Affiliated Hospital of Qinghai University, Xining, China, <sup>5</sup> Department of Scientific Research Office, Affiliated Hospital of Qinghai University, Xining, China

## OPEN ACCESS

### Edited by:

Andrea Morandi,  
University of Florence, Italy

### Reviewed by:

Sofia Avnet,  
University of Bologna, Italy  
Huakan Zhao,  
Xinqiao Hospital, China

### \*Correspondence:

YanYan Ma  
xnmayanyan@126.com

<sup>†</sup>These authors have contributed  
equally to this work

### Specialty section:

This article was submitted to  
Cancer Metabolism,  
a section of the journal  
Frontiers in Oncology

**Received:** 30 December 2020

**Accepted:** 26 March 2021

**Published:** 02 June 2021

### Citation:

Jiang J, Huang D, Jiang Y,  
Hou J, Tian M, Li J, Sun L,  
Zhang Y, Zhang T, Li Z, Li Z,  
Tong S and Ma Y (2021) Lactate  
Modulates Cellular Metabolism  
Through Histone Lactylation-  
Mediated Gene Expression in  
Non-Small Cell Lung Cancer.  
Front. Oncol. 11:647559.  
doi: 10.3389/fonc.2021.647559

Lactate has been observed to fuel TCA cycle and is associated with cancer progression in human lung cancer, the leading cause of cancer deaths worldwide, but the effect of lactate on lung cancer metabolism is rarely reported. In this study, disordered metabolism in non-small cell lung cancer was demonstrated by increased G6PD and SDHA protein levels *via* immunofluorescence, and up-regulated lactate dehydrogenase was found to be associated with poor prognosis. Then flow cytometry and Seahorse XFe analyzer were utilized to detect the effect of lactate on glycolysis and mitochondrial function in non-small cell lung cancer cells. The results show that in non-small cell lung cancer cells lactate attenuates glucose uptake and glycolysis while maintaining mitochondrial homeostasis as indicated by improved mitochondrial membrane potential. Further exploration found that mRNA levels of glycolytic enzymes (*HK-1*, *PKM*) and TCA cycle enzymes (*SDHA*, *IDH3G*) are respectively down-regulated and up-regulated by lactate, and increased histone lactylation was observed in promoters of *HK-1* and *IDH3G* *via* chromatin immunoprecipitation assay. Taken together, the above results indicate that lactate modulates cellular metabolism at least in part through histone lactylation-mediated gene expression in non-small cell lung cancer.

**Keywords:** lactate, lactylation, metabolism, gene expression, non-small cell lung cancer

## INTRODUCTION

Lung cancer has been reported as the most commonly diagnosed cancer and the leading cause of cancer deaths both in China and worldwide in two sexes combined. It was estimated that lung cancer accounted for 11.6% of 18.1 million new cancer cases and 18.4% of 9.6 million cancer deaths globally in 2018 (1), and 787 thousand diagnoses of lung cancer with 631 thousand lung cancer deaths were

estimated among Chinese population in 2015 (2). The two major histological forms of lung cancer are small-cell lung cancer (SCLC) and non-small-cell lung cancer (NSCLC), respectively making of about 85% and 15% of all lung cancer cases (3). Though significant progression has been achieved in targeted therapy and immunotherapy for lung cancer treatment, prognosis is still dismal, with a 5-year survival rate just being less than 17% (4).

Metabolic reprogramming is a hallmark of cancer cells (5). In addition to the common genetic alterations, such as mutations in *TP53*, *EGFR*, *KRAS*, and rearrangements in *RET*, *ROS1* and *ALK*, a subset of genes involved in modulating cellular metabolism were found to be dysregulated in NSCLC, including *CYP11B1*, *GPX7*, *GSTT2* and *BNIP3* (6). Disorders in cellular metabolism have been linked to the pathobiology of several common respiratory diseases and lung cancer (7); aberrantly activated pathways and genes, such as PI3K/Akt/mTOR, RAS/RAF and c-MYC, accelerate glucose and glutamine metabolism to meet the need of energy and building blocks for lung cancer proliferation, while abundant lactate accumulates due to anaerobic glycolysis (8). In recent years, the important pathological functions of lactate have been revealed, it goes in or out of cells dependent on MCT1, MCT4, SLC5A8 and SLC5A12 transporters; it also binds to NDRG3 protein or the membrane receptor GPCR81 to participate in hypoxia response and cellular metabolism, respectively (9, 10). Furthermore, lactate acts as a bona fide agonist to elicit magnesium from endoplasmic reticulum, leading to magnesium uptake by mitochondria and metabolic regulation (11). Through these ways, lactate is able to modulate cellular processes. Lactate was found to fuel TCA cycle in both lung cancer model mouse (12) and human lung cancer patients (13), and cell proliferation was suppressed when lactate utilization was blocked by MCT1 inhibition in lung cancer and colorectal cancer cells (14). Moreover, it was reported that lactate utilization triggered cancer stem cell-like transcriptional profile in human breast cancer cells (15). Recently, histone lactylation was identified as a novel type of epigenetic modification in macrophage, human NSCLC cell line A549 and mouse cells (16, 17), which induced altered gene expression and phenotype in macrophage. Lactate also contributes to the formation of immunosuppression microenvironment (18, 19). These studies demonstrated reprogrammed metabolism as well as the important role of lactate in lung cancer.

However, the regulatory effects of lactate on lung cancer cell metabolic processes are rarely investigated. In this study, we discovered that lactate inhibited glucose uptake and glycolysis while it maintained mitochondrial homeostasis in non-small-cell lung cancer cells. These effects are mainly mediated by altered expression levels of metabolic enzymes due to histone lactylation of the gene promoter.

## MATERIALS AND METHODS

### Instruments and Reagents

The main instruments in this study included flow cytometer (FACS Celesta, BD, USA), fluorescent quantitative analysis

system (Tissue FAXS-S Plus, Tissue Gnostics, Austria), cellular metabolism analysis system (Seahorse XFe96 Analyzer, Agilent, USA), Cytation 5 Cell Imaging Multi-Mode Reader (BioTek, USA), holographic tomographic microscopy 3D cell explorer (Nanolive, Switzerland) and real-time PCR instrument (Light Cycler 480 II, Roche, Switzerland). Antibodies against the following proteins were: G6PD (ab210702), SDHA (ab14715), histone H3 (ab12079) (all from Abcam, Cambridge, MA, USA). Anti-lactyllysine rabbit pAb (PTM-1401) and anti-lactyl-histone H4 (Lys8) antibody (PTM-1405) were purchased from Hangzhou PTM BIO, Co., LTD in China. Alexa Fluor 488 (ZF-0511) and Alexa Fluor 594 (ZF-0513) fluorescent secondary antibodies were purchased from ZSGB-BIO (Beijing, China). XF Cell Mito Stress Test kit (103015-100) and XF Glycolysis Stress Test kit (103020-100) were from Agilent Technologies Inc., and L- (+) lactic acid (L6402) was purchased from Sigma-Aldrich (St. Louis, MO, USA). SYBR-Green (0491850001) and mitochondrial membrane potential assay kit (551302) were respectively from Roche (Palo Alto, CA, USA) and BD (Becton, Dickinson and Company, USA). MitoTracker® Deep Red FAM (M22426) and 6-NBDG (N23106) for glucose-uptake assay were from Thermo Fisher Scientific (Waltham, MA, USA). Cell-light™ EdU Apollo567 In Vitro Kit (C10310-1) was purchased from Guangzhou RiboBio Co., LTD in China. Hoechst33258 (IH0060) was purchased from Solarbio (Beijing, China), and Lactic Acid assay kit (A019-2) was purchased from Nanjing Jiancheng Bioengineering Institute in China.

### Immunofluorescence

Clinical NSCLC samples were obtained from the Affiliated Hospital of Qinghai University. G6PD and SDHA were detected *via* immunofluorescence, with Alexa Fluor 488 (ZF-0511) and Alexa Fluor 594 (ZF-0513) fluorescent secondary antibodies against G6PD rabbit monoclonal antibody (ab210702) and SDHA mouse monoclonal antibody (ab14715), respectively. The dilution ration for the primary antibodies is 100, while that for fluorescent secondary antibodies is 400. Following immunofluorescent staining, the protein levels of G6PD and SDHA were analyzed with Tissue FAXS-S Plus system (Tissue Gnostics, Austria).

### Cell Culture and Treatment With Lactate

The human lung bronchial epithelial cell line BEAS-2B and NSCLC cell lines A549 and H1299 were purchased from the Cell Bank of the Chinese Academy of Sciences (Shanghai, China). The lung bronchial epithelial cells and NSCLC cells were respectively cultured in DMEM/F12 (1:1) and RPMI1640 supplemented with 10% fetal bovine serum at 37°C in a humidified incubator with 5% CO<sub>2</sub>. 1M lactate stock solution was added to the above cell media to reach a final lactate concentration of 5 mM or 10 mM; media with or without lactate were used to culture cells according to experiment requirement under normoxic or hypoxic (1% oxygen) conditions.

## Flow Cytometric Analysis

Control cells and cells treated with 10 mM lactate for 24 hour under normoxic or hypoxic conditions were subjected to flow cytometric analysis, and  $5 \times 10^5$  cells were used to perform each assay in triplicate. According to the manufacturer's instruction, 6-NBDG (N23106, Thermo Fisher Scientific) and mitochondrial membrane potential assay kit (551302, Becton, Dickinson and Company) were respectively utilized to examine the glucose uptake ability and mitochondrial membrane potential of each group of cells treated with different lactate and oxygen concentrations.

## Cell Metabolic Assays

BEAS-2B, A549 and H1299 cells were seeded in XF 96-well and cultured in media with 0, 5 or 10 mM lactate in quadruplicate, and the number of cells per well is  $1.5 \times 10^4$ ; in this way two 96-well plates were prepared and respectively incubated under normoxic and hypoxic conditions for 24 hours prior to cell metabolic analysis. The XF Cell Mito Stress Test kit (Cat# 103015-100) and XF Glycolysis Stress Test kit (Cat# 103020-100) were used following the manufacturer's instructions to assay glycolysis and mitochondrial metabolism of the cells treated with different lactate and oxygen concentrations. The cells in each well were stained with Hoechst33258 and counted with cytation5; then the raw data were normalized and processed with Wave Software (Version 2.6.1).

## Western Blotting and qPCR

Cultured cells were lysed with RIPA buffer containing proteinase inhibitor to extract total protein, which were quantified using BCA assay, and 20  $\mu$ g of total protein in each sample was loaded for detection of histone lactylation. For qPCR, total RNA was extracted using TRIzol reagent and 1  $\mu$ g of total RNA was used for reverse transcription; the reaction system was made according to the manufacturer's instruction and the assay was run on a Roche Light Cycler 480 II, detection system with the program: pre-degeneration by 95°C for 10 min followed with 40 cycles of 15 s at 95°C and 34 s at 60°C. The mitochondrial gene *mt-Cytb* (NC\_001665.2) was cloned into pEASY-T1 plasmid vector to generate pEASY-T1- *Cytb*, which was then used as standard sample to quantify the mitochondrial DAN (mtDNA) copy number; a series of standard samples containing 0, 10,  $10^2$ ,  $10^3$ ,  $10^4$ ,  $10^5$ ,  $10^6$ ,  $10^7$  copies of pEASY-T1-CYB were used to make standard curve, according to which mtDNA copy number in 50 ng of genomic DNA from each sample was examined. Sequences of primers for detecting each target gene are shown in **Table 1**.

## Cell Proliferation Assay

$10^4$  cells per well were seeded in 96-well plate and treated with or without lactate (10 mM) in triplicate for 24 hours. Then the cells were incubated in media containing EdU for 2 hours, followed by staining with Apollo fluorochrome according to manufacturer's instruction. Subsequently, cells were photographed and analyzed with Cytation 5 Cell Imaging Multi-Mode Reader. In addition, cells treated with or without lactate were continuously observed for 6 hours using holographic tomographic microscopy 3D cell explorer to examine cell division. In addition, proliferation and migration of cells treated with or without lactate (5 mM, 10 mM) in triplicate were examined *via* xCELLigence Real Time Cellular Analysis using RTCA DP instrument (Agilent, USA);  $5 \times 10^4$  and  $1.5 \times 10^4$  cells were seeded per well for proliferation and migration examination, respectively.

## Lactate Measurement in Cell Culture Supernatant

BEAS-2B, A549 and H1299 were seeded in 12-well plate in triplicate; the number of cells in each well is  $5 \times 10^4$ . Two 12-well plates prepared in the same way were incubated under normoxic and hypoxic conditions for 48 hours. Then Lactate concentration in culture supernatant of each cell was detected following the manufacturer's instruction.

## Chromatin Immunoprecipitation (ChIP) Assay

A549 cells were cross-linked with 1% (v/v) formaldehyde in phosphate-buffered saline for 10 min at 37°C with gentle shaking. After adding 0.125 M glycine to terminate the reaction, the cells were lysed with lysis buffer on ice. Chromatin DNA was sheared by sonication to obtain ~ 500 bp fragments that were then mixed with anti-lactyl-histone H4 (Lys8) antibody and protein G-agarose to enrich DNA fragments bound to lactylated histone H4 through immunoprecipitation. After decrosslinking, the precipitated DNA was analyzed by qPCR to assess the genomic DNA sequences in *HK-1* and *IDH3G* promoters. Sequences of primers for detecting each promoter site are shown in **Table 2**.

## Statistical Analysis

Quantitative data are presented as mean  $\pm$  SD of at least three experiments. Differences between groups were assessed with the Student's t-test or by one-way analysis of variance and were considered statistically significant at  $p < 0.05$  and highly significant at  $p < 0.01$ . Data were analyzed using SPSS v.17.0

**TABLE 1** | Primer sequences for qPCR.

gene	Forward primer	Reverse primer
HK-1	CTGCTGGTGAAATCCGTAAGTGG	GTCCAAGAAGTCAGAGATGCAGG
G6PD	CTGTTCCGTGAGGACACAGATCT	TGAAGGTGAGGATAACGCAGGC
PKM	ATGGCTGACACATTCTGGAGC	CCTTCAACGTCTCCACTGATCG
IDH3G	CCAGTGGACTTTGAAGAGGTGC	TTTGTGCGACGGTGGCAGGTTA
SDHA	GAGATGTGGTGTCTCGGTCCAT	GCTGTCTCTGAAATGCCAGGCA
B-actin	GAAGATCAAGATCATTGCTCCT	TACTCTGCTTGTCTGATCCA



**TABLE 2** | Primer sequences for ChIP-PCR.

Gene promoter	Forward primer	Reverse primer
HK-1 site 1	ATGTTTGGCAGGTTAGGGAG	TCTGGAGTTCTGGTTCTTGTC
HK-1 site 2	TGCCCTGACTTGTCTCAAAC	GGTAAATCTAGGACCTGTTACACG
IDH3G site 1	TCTGGAGTCCGATTGGCTAG	CAATCCCCTCAGTGACAGC
IDH3G site 2	ATTGTGACGTCTCTGGCAG	GGTCGCACCGATTACCG

software (SPSS Inc., Chicago, IL, USA). Survival analysis was performed using Kaplan-Meier analysis via “survival” and “survminer” R packages.

## RESULTS

### NSCLC Presents Altered Expression of Metabolic Enzymes With Aberrant Lactate Metabolism Being Associated With Poor Prognosis

Though metabolic disorders mainly demonstrated as altered nutrient uptake and utilization in lung cancer cells have been widely reported, the alteration in metabolic enzymes was much less investigated. In this study, we examined the expression level of glucose 6-phosphate dehydrogenase (G6PD) and succinate dehydrogenase (SDH) in NSCLC *via* immunofluorescence assay; the examined metabolic enzymes, respectively involved in pentose phosphate pathway and mitochondrial function, displayed higher protein level in cancerous tissues than in paired para-carcinoma tissues (**Figure 1**). In addition, our analysis of TCGA data on lung adenocarcinoma revealed that elevated expression of hypoxia-inducible factor 1A (*HIF1A*) (**Figure 2A**), lactate dehydrogenase A (*LDHA*) (**Figure 2B**), lactate dehydrogenase B (*LDHB*) (**Figure 2C**) and *SLC16A1* (**Figure 2D**) is significantly correlated with poor prognosis. While *LDHA* and *LDHB* directly regulate lactate metabolism, *HIF1A* can stimulate glycolysis (20) and *MCT1* encoded by *SLC16A1* can function as lactate transporter (9). These results revealed an increased expression level of metabolic enzymes and the correlation between aberrant lactate metabolism with poor prognosis in lung adenocarcinoma, strongly implying disordered cellular metabolism and an important role of lactate in NSCLC.

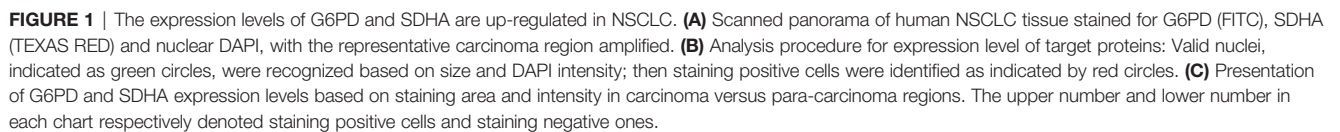
### Lactate Inhibits Glycolysis and Maintains Mitochondrial Homeostasis in NSCLC Cells

Based on the above results and the shortage of reported function of lactate in cellular metabolism, the lactate regulatory effects on glucose metabolism were analyzed, which is one of the principal nutrients for mammalian cells. The flow cytometric analysis showed decreased glucose uptake in lactate-treated A549 cells compared with the control group, while BEAS-2B presented increased glucose uptake when treated with lactate (**Figures 3A, B**), implying some difference in metabolic features between lung bronchial epithelial cells and NSCLC cells. In the following

investigation of how lactate influenced glycolysis and mitochondrial metabolism *via* Seahorse XFe Analyzer (**Figure 3C**), glycolysis (**Figure 3D**) and glycolytic capacity (**Figure 3E**) was dampened in BEAS-2B and A549 cells treated with lactate, while the effect of lactate on glycolytic reserve was not detected (**Figure 3F**). In Mito Stress Test (**Figure 4A**), both proton leak (**Figure 4B**) and ATP production (**Figure 4C**) were also observed to reduce in mitochondrial metabolism when the cells were treated with lactate. We presumed that the reduced proton leak is due to improved integrity of mitochondrial inner membrane after lactate treatment, and this was supported by the observation that the percentage of cells with decreased mitochondrial membrane potential fell in A549 and H1299 cells when they were treated with lactate (**Figures 4D, E**); however, lactate induced a decrease in mitochondrial membrane potential of BEAS-2B cell. The declined ATP production was likely supposed to result from reduced mitochondrial biomass, as demonstrated by the smaller mtDNA copy number (**Figure 4F**) and weaker mean fluorescence intensity (77.905 versus 70.764) (**Figure 4G**) when the cells were treated with lactate. It is also possible that lactate induced orchestration in mitochondrial function to produce more building blocks than energy for the cells. So lactate reduced the biomass but improved the membrane potential of mitochondria. Taken together, these results indicated that lactate plays a role in inhibiting glycolysis and maintaining mitochondrial homeostasis in NSCLC cells.

### Lactate Modulates Proliferation and Migration of NSCLC Cells

The effects of lactate on biological properties of NSCLC cells were detected *via* EdU incorporation assay. A larger proportion of EdU-positive cells going through S phase appeared in lactate-treated BEAS-2B and H1299 compared with the control groups (**Figures 5A–C**). In comparison to normal A549 cells (**Figure 5D**), lactate-treated A549 cells spent more time completing cell division, indicating that lactate slows down cell cycle progression of A549 cells (**Figure 5E**). In RTCA assay, while lactate had no effects on migration but promoted proliferation of BEAS-2B cell (**Figure 5F**), both migration and proliferation of A549 (**Figure 5G**) and H1299 (**Figure 5H**) cells were inhibited by lactate. The larger proportion of EdU-positive cells in lactate-treated H1299 cells is probably due to some retardation in S or the following phases. Therefore, lactate also plays a role in modulating cell cycle progression in NSCLC cells.



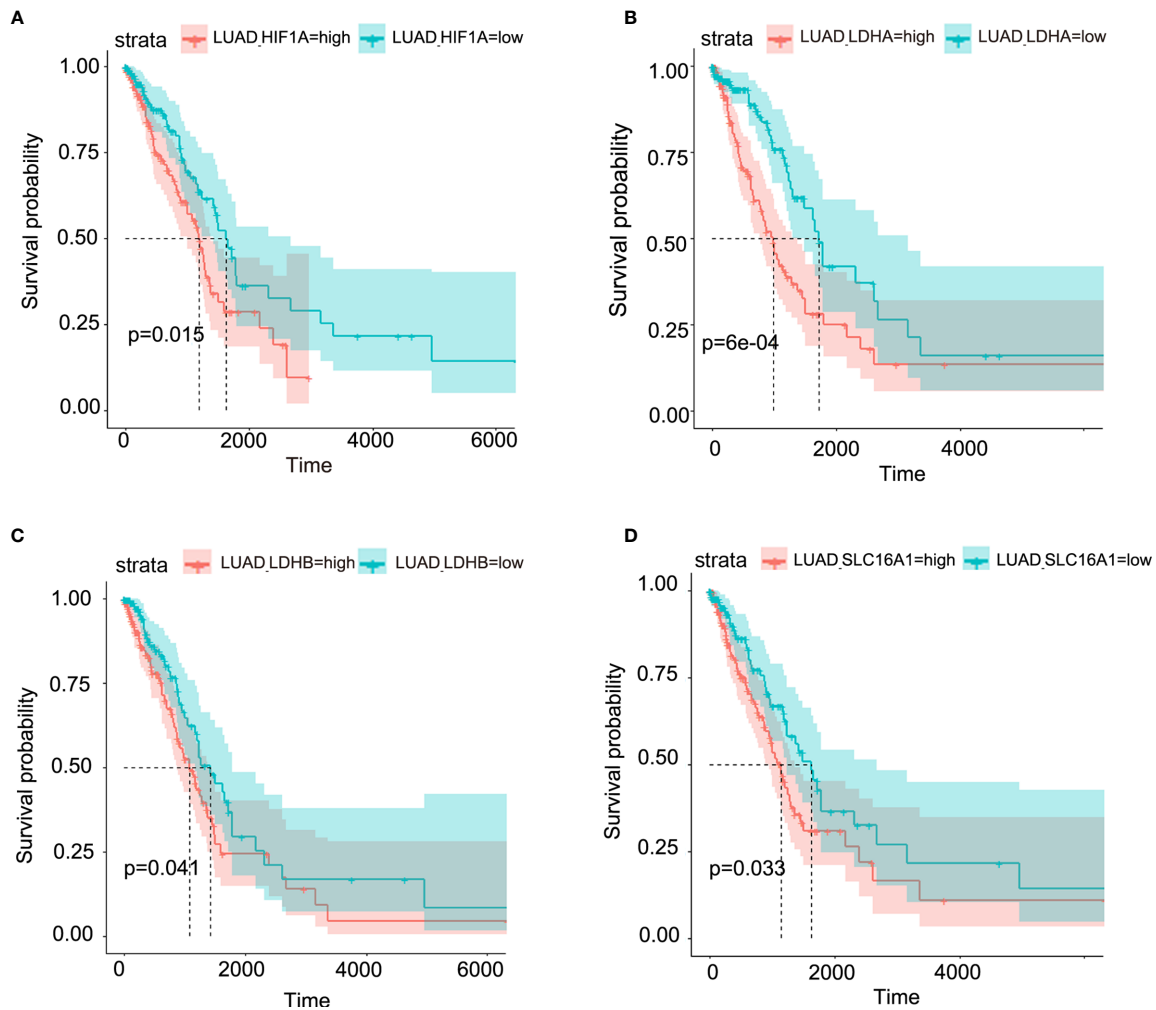


**FIGURE 2** | Aberrant lactate metabolism may contribute to human lung adenocarcinoma progression. Elevated expression levels of HIF-1A (A), LDHA (B), LDHB (C) and SLC16A1 (encoding MCT1, which can act as lactate transporter) (D) are all significantly associated with poor prognosis in human lung adenocarcinoma.

## Lactate Is Involved in Modulating the Biological Properties of NSCLC Cells Under Conditions That Mimic a Tumor's Internal Hypoxic Environment

Hypoxia is a hallmark of the interior of solid tumors (21), and is important to remodel cancer cell metabolism, generally resulting in lactate accumulation. To mimic the *in vivo* hypoxic environment, the NSCLC cells were cultured under hypoxic condition (1% oxygen) for 48 hours, and a higher lactate concentration was observed within the culture supernatant under hypoxia than that under normoxic condition (Figure 6A). Then lactate concentration was further elevated through addition of exogenous lactate to culture supernatant of NSCLC cells under hypoxia, and their metabolism were compared with that of the non-lactate-treated NSCLC cells under hypoxia. Consistent with the previous results, the metabolic level of glycolysis fell (Figures 6B–D), while the mitochondrial

membrane potential was maintained in lactate-treated cells under hypoxia (Figures 6E, F). So, lactate was able to function as metabolic modulator under both normoxic and hypoxic conditions.

## Histone Lactylation Regulates Expression of Genes Involved in Cellular Metabolism

Given the latest studies reporting lactate as a modulator of gene transcription through histone lactylation (16, 17), it was speculated that the effects of lactate on both cellular metabolism and biological properties in NSCLC cells may result from altered gene expression of critical metabolic enzymes or other factors mediated by histone lactylation. As we expected, when NSCLC cells were treated with lactate, histone lactylation level increased (Figure 7A), along with down-regulated transcription of *HK-1* (Figure 7B), *G6PD* (Figure 7C) and *PKM* (Figure 7D) as well as up-regulated transcription of *SDH* (Figure 7E) *IDH* and *HIF1A* (Figure 7F). Then ChIP assay using anti-lactylated histone H4

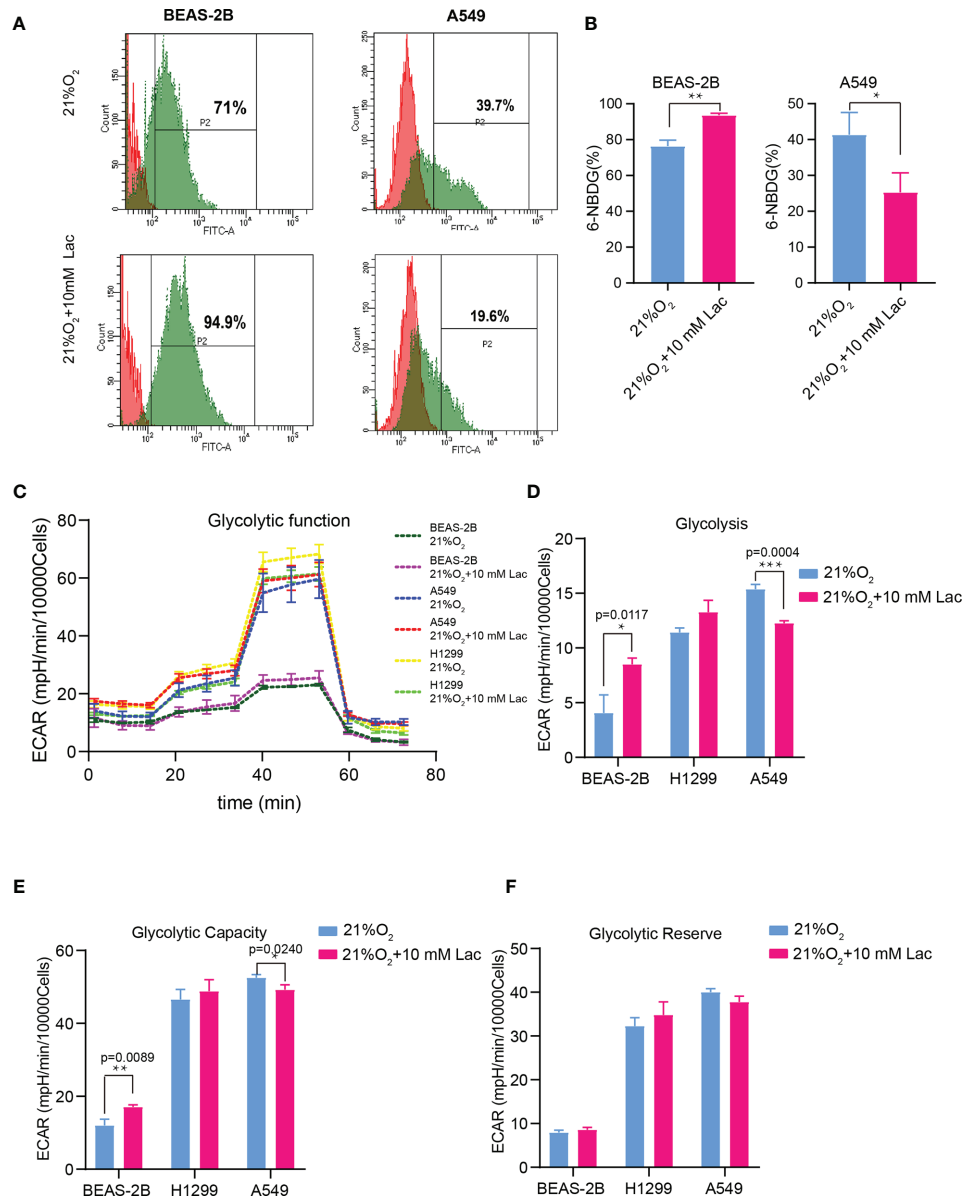


**FIGURE 3 |** Lactate exerted an inhibitory effect on glucose uptake and glycolysis in NSCLC cells. **(A)** Representative histograms showing distribution of FITC (6-NBDG) intensity among the indicated groups. The number in each histogram denotes the percentage of cells in "P2" that ingested 6-NBDG. **(B)** Comparison of glucose-uptake capability between lactate-treated cells and control ones, indicated as the percentage of 6-NBDG positive cells. **(C)** Glycolytic function curves from glycolysis stress test of BEAS-2B and A549 cells treated with or without lactate under normoxia. Based on glycolytic function curve, glycolysis level **(D)**, glycolytic capacity **(E)** and glycolytic reserve **(F)** of BEAS-2B and A549 treated with or without lactate were analyzed. (\* $p < 0.05$ , \*\* $p < 0.01$ , \*\*\* $p < 0.001$ ).

antibody was carried out to confirm lactylation of histone lactylation in *HK-1* and *IDH3G* promoters; more promoter DNA sequences of *HK-1* and *IDH* were enriched in the ChIP assay when A549 was treated with lactate (**Figure 7G**), indicating increased histone lactylation in *HK-1* and *IDH* promoters by lactate. Taken together, these results demonstrated that the regulatory effects of lactate on NSCLC cells were probably mediated by lactate-induced promoter histone lactylation of associated genes.

## DISCUSSION

Our findings demonstrated disordered metabolism in NSCLC, and that the metabolite lactate played an important role in modulating glycolysis, mitochondrial homeostasis as well as cell proliferation in NSCLC through histone lactylation-mediated expression of related genes. Disordered metabolism in lung cancer has been well established by remarkably altered metabolism of substances including lipid and glutamine (22, 23).



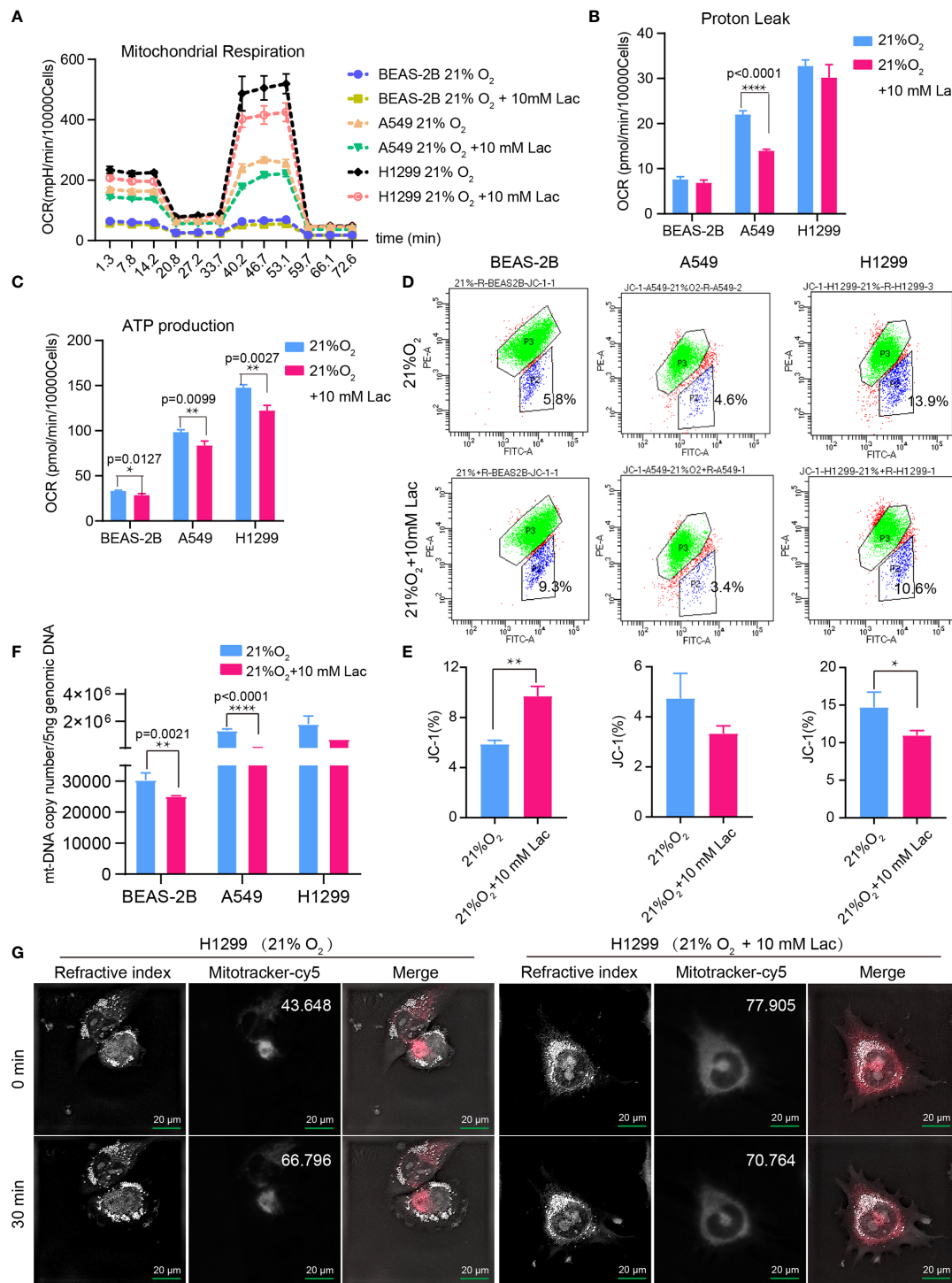


**FIGURE 4 |** Lactate involves in maintaining mitochondrial homeostasis in NSCLC cells. The cell mito stress test (A) was used to determine proton leak (B) and ATP production (C) levels in the indicated groups of cells via cell mito stress test. (D) Flow cytometric analysis of mitochondrial membrane potential of BEAS-2B, A549 and H1299 treated with indicated lactate concentration. Cells in “P2” were those with reduced mitochondrial membrane potential. (E) Percentage of cells with reduced mitochondrial membrane potential among BEAS-2B, A549 and H1299 cells treated with or without lactate. (F) Quantification of mt-Cytb gene copy number in 5 ng total DNA extracted from each of the indicated groups of cells. (G) Mitochondria stained with MitoTracker in H1299 cells treated with or without lactate under normoxia; number at the top-right corner denotes mean fluorescence intensity of MitoTracker-cy5. The images were photographed and processed with holographic tomographic microscopy 3D cell explorer. (\*p < 0.05, \*\*p < 0.01, \*\*\*\*p < 0.0001).

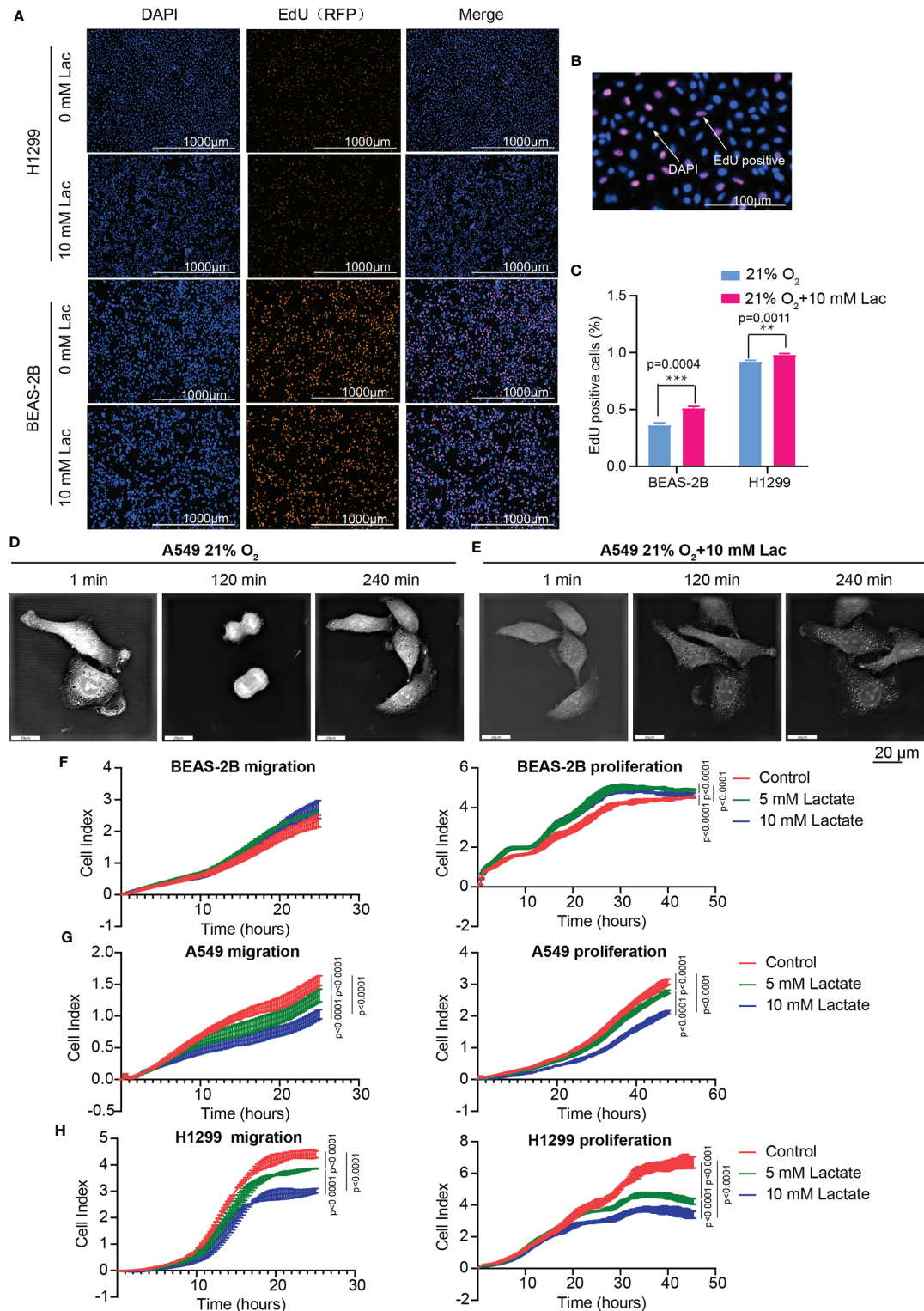


**FIGURE 5 |** Lactate modulated cell proliferation. **(A)** Representative cell images stained with nuclear DAPI and EdU (RFP) in EdU-incorporating assay. **(B)** Locally amplified image to clearly show EdU-positive cells, which were going through S phase of cell cycle. **(C)** The percentage of EdU-positive cells in the indicated groups. **(D, E)** Cell division progression of A549 cells observed via holographic tomographic microscopy 3D cell explorer for 6 hours, when the cells treated without **(D)** or with **(E)** lactate. **(F-H)** RTCA assays of cell migration and proliferation. Migration and proliferation of BEAS-2B **(F)**, A549 **(G)** and H1299 **(H)** when the cells were treated with the indicate concentrations of lactate. (\*\*p<0.01, \*\*\*p<0.001, \*\*\*\*p<0.0001).

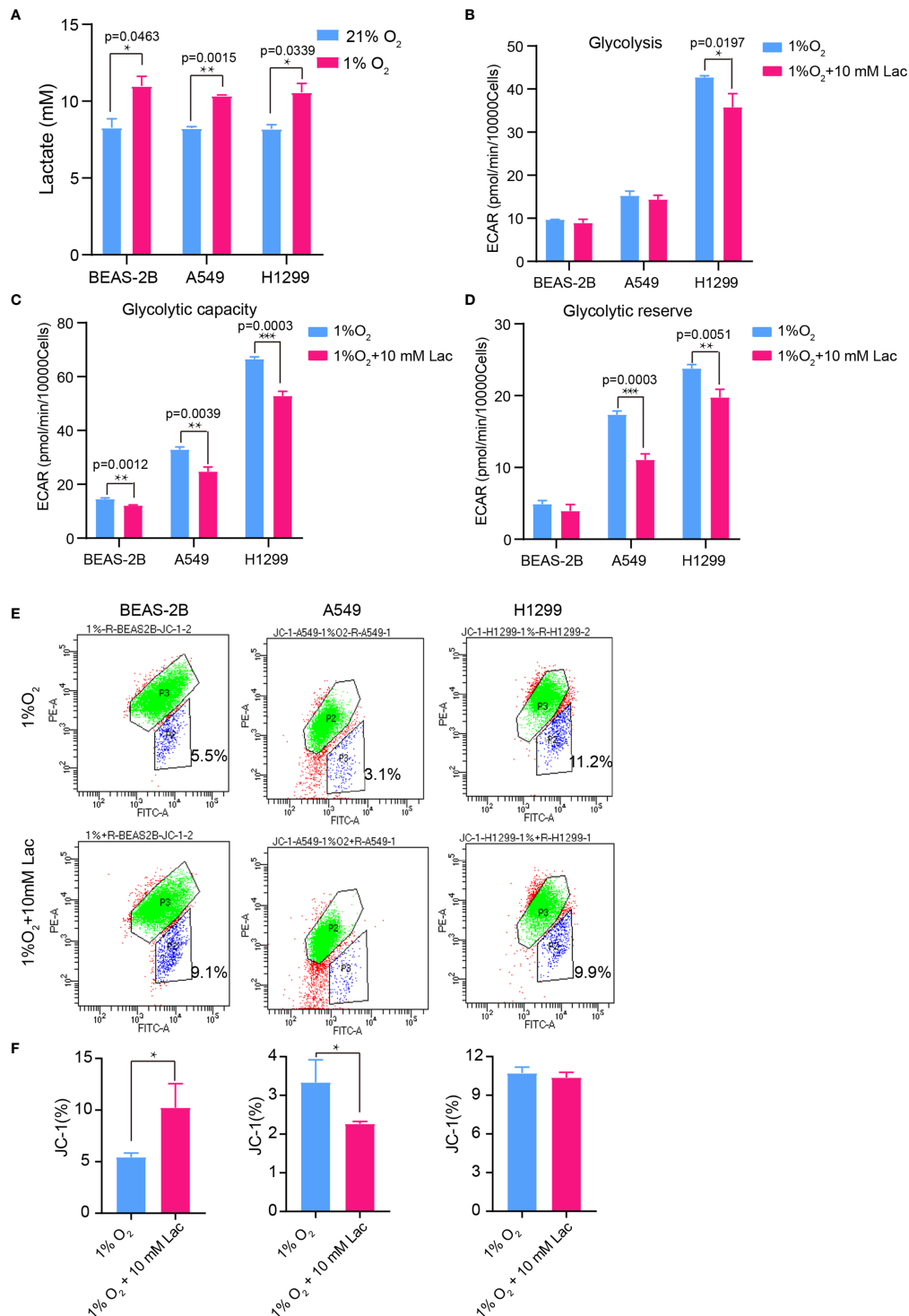


**FIGURE 6** | The glycolysis-inhibiting and mitochondrial homeostasis-maintaining effects were also observed under hypoxia. **(A)** Lactate concentration in culture supernatant of BEAS-2B, A549 and H1299 cells under normoxia (21% O<sub>2</sub>) and hypoxia (1% O<sub>2</sub>), respectively. Glycolysis **(B)**, glycolytic capacity **(C)** and glycolytic reserve **(D)** of BEAS-2B, A549 and H1299 cells treated with different concentrations of lactate under hypoxia. **(E)** Mitochondrial membrane potential of the indicated groups of cells assayed with flow cytometry. Cells in “P2” were those with reduced mitochondrial membrane potential. **(F)** Percentage of cells with reduced mitochondrial membrane potential among BEAS-2B, A549 and H1299 cells treated with or without lactate under hypoxia. (\*p<0.05, \*\*p<0.01, \*\*\*p<0.001).

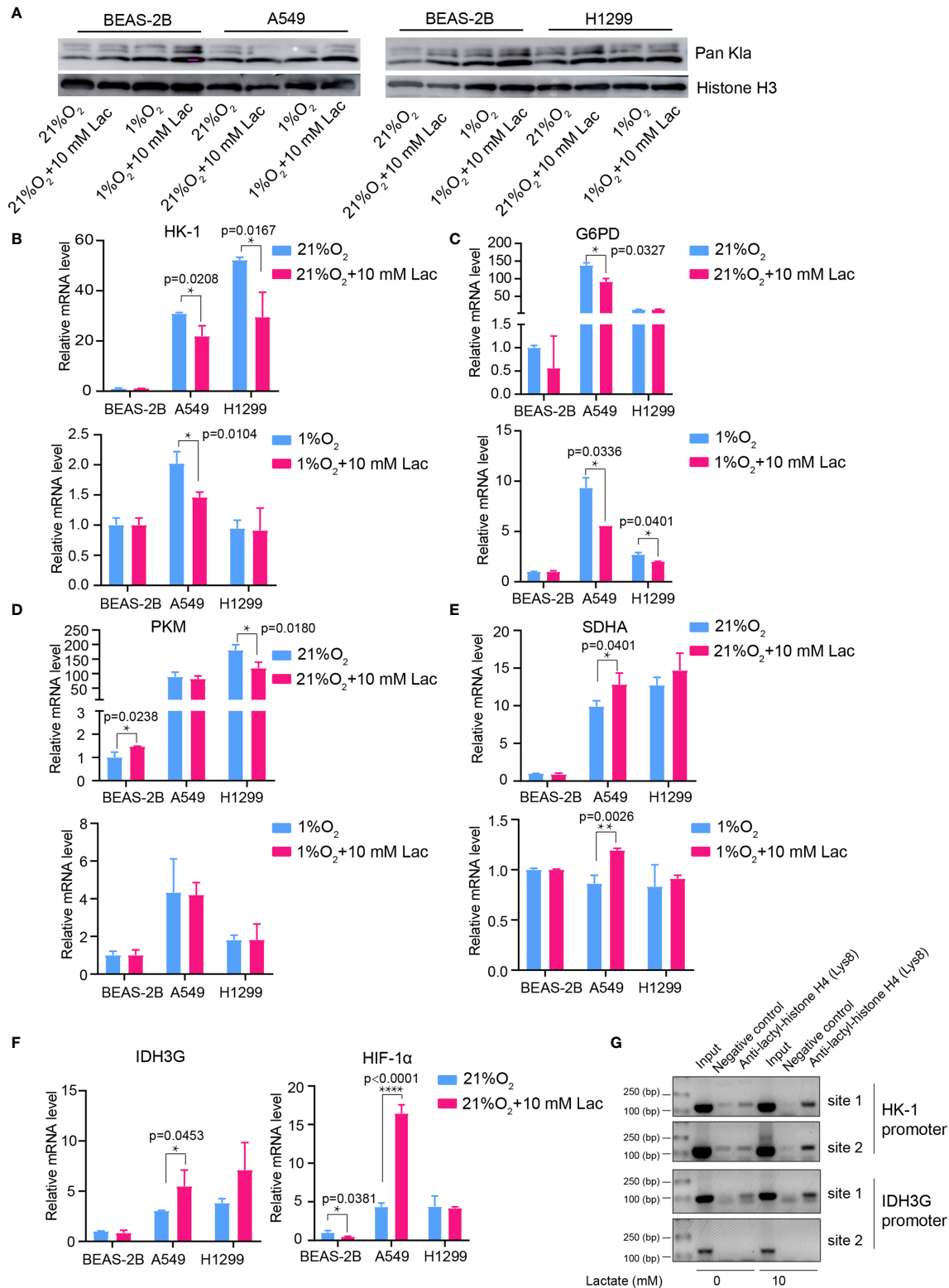


**FIGURE 7** | Lactate regulated gene expression through histone lactylation. **(A)** Pan K1a detection in cells treated with different concentrations of lactate under both normoxia and hypoxia. **(B–F)** mRNA levels of metabolic enzymes and HIF1A. HK-1 **(B)**, mRNA levels of G6PD **(C)**, PKM **(D)**, SDHA **(E)**, IDH3G and HIF-1A **(F)** in BEAS-2B, A549 and H1299 cells treated with the indicated conditions. **(G)** ChIP assay to detect histone lactylation level in HK-1 and IDH3G promoters. (\* $p<0.05$ , \*\* $p<0.01$ , \*\*\*\* $p<0.0001$ ).



In our study, the metabolic disorder in NSCLC was demonstrated by elevated expression levels of *G6PD* and *SDHA* in carcinoma tissues than in paired para-carcinoma tissues (Figure 1). In addition, compared with the human lung bronchial epithelial cell line BEAS-2B, the human NSCLC cell lines A549 and H1299 presented higher basal levels of glycolysis (Figures 3D, E) and metabolic enzymes (Figures 7B–F); lactate also induces disparate alterations in glucose uptake (Figures 3A, B) and mitochondrial membrane potential (Figures 4D, E) between BEAS-2B and NSCLC cells. These observations demonstrated that NSCLC cells possess a quite distinct metabolic status from that of normal cells, and the specific metabolic features may contribute to better tumor classification and discovery of therapeutic target (24).

Disordered metabolism in cancer is generally caused by hypoxia in interior of cancers and genetic mutations (21, 25, 26); however, the cellular metabolism is not passively affected, but actively reprogrammed to survive the harsh environment. Accumulated lactate resulting from reprogrammed metabolism can refuel TCA cycle in NSCLC (12, 13). Our study discovered that lactate attenuates glycolysis (Figure 3) while maintaining mitochondrial homeostasis (Figure 4) in NSCLC cells, and expression levels of the analyzed metabolic enzymes in glycolysis, pentose phosphate pathway and TCA cycle are respectively down-regulated and up-regulated by lactate (Figure 7). So TCA cycle is the preferential metabolic pathway in response to lactate in NSCLC cells. In human NSCLC, glucose is the main nutrient metabolized in less perfused regions, while highly perfused regions mainly utilize non-glucose nutrient, including lactate (27). Therefore, lactate probably mediates the symbiosis between less perfused and highly perfused regions, contributing to tumor progression. Furthermore, the involvement of lactate in modulating cellular metabolism is demonstrated by lactate-induced transcriptional activation of *HIF1A* in A549 cell (Figure 7F), and this effect of lactate on *HIF1A* transcription was also recently observed in human MCF7 breast cancer cell (28). HIF-1 can in turn activate transcription of multiple genes, including *SLC2A1*, *SLC2A3*, *LDHA* and *PDK1*, to facilitate glucose uptake and glycolysis (20), resulting in lactate generation. So there likely exists positive feedback between lactate and HIF-1 in reprogramming cancer cell metabolism.

Consistent with the effects of lactate on glycolysis and mitochondrial function, the mRNA levels of metabolic enzymes like *HK-1* and *PKM* in glycolysis as well as *SDHA* and *IDH3G* in TCA cycle were respectively down- and up-regulated by lactate (Figures 7B–F). This may involve increased histone lactylation in *HK-1* and *IDH3G* promoters (Figure 7G).

Based on these results, it can be concluded that lactate promotes cell proliferation and modulates cellular metabolism at least in part through histone lactylation-mediated gene expression in non-small cell lung cancer cells. But further investigation is needed to elucidate why histone lactylation is associated with both up-regulation and down-regulation of gene transcription.

## DATA AVAILABILITY STATEMENT

The original contributions presented in the study are included in the article/supplementary material. Further inquiries can be directed to the corresponding author.

## ETHICS STATEMENT

The study protocol was performed in accordance with the guidelines outlined in the Declaration of Helsinki. The Ethics Committee of Affiliated Hospital of Qinghai University approved the study.

## AUTHOR CONTRIBUTIONS

YM and DH: conceptualization. YM and JJ: funding acquisition, project administration and manuscript revision. YJ and JH: methodology. MT, JL, and YZ: data curation. TZ, ZhiL, ZhoL, and ST: software. DH: writing. All authors contributed to the article and approved the submitted version.

## FUNDING

This work was supported in part by grants from the Science and Technology Agency of Qinghai Province (2017-ZJ-710), Qinghai Health Committee (No. 2020-wjzd-03) and Qinghai University (2020-QYY-5).

## ACKNOWLEDGMENTS

This study was performed in Central Laboratory and Qinghai Province Research Key Laboratory of Echinococcosis, Affiliated Hospital of Qinghai University, Tongren Road 29, Xining, Qinghai Province, China, 810000.

## REFERENCES

- Bray F, Ferlay J, Soerjomataram I, Siegel RL, Torre LA, Jemal A. Global cancer statistics 2018: GLOBOCAN estimates of incidence and mortality worldwide for 36 cancers in 185 countries. *CA: Cancer J Clin* (2018) 68:394–424. doi: 10.3322/caac.21492
- Chen W, Zheng R, Baade PD, Zhang S, Zeng H, Bray F, et al. Cancer statistics in China, 2015. *CA: Cancer J Clin* (2016) 66:115–32. doi: 10.3322/caac.21338
- Herbst RS, Morgensztern D, Boshoff C. The biology and management of non-small cell lung cancer. *Nature* (2018) 553:446–54. doi: 10.1038/nature25183
- Miller KD, Siegel RL, Lin CC, Mariotto AB, Kramer JL, Rowland JH, et al. Cancer treatment and survivorship statistics, 2016. *CA: Cancer J Clin* (2016) 66:271–89. doi: 10.3322/caac.21349
- Hanahan D, Weinberg RA. Hallmarks of cancer: the next generation. *Cell* (2011) 144:646–74. doi: 10.1016/j.cell.2011.02.013
- Belinsky SA. Unmasking the lung cancer epigenome. *Annu Rev Physiol* (2015) 77:453–74. doi: 10.1146/annurev-physiol-021014-072018

7. Liu G, Summer R. Cellular Metabolism in Lung Health and Disease. *Annu Rev Physiol* (2019) 81:403–28. doi: 10.1146/annurev-physiol-020518-114640
8. Pavlova NN, Thompson CB. The Emerging Hallmarks of Cancer Metabolism. *Cell Metab* (2016) 23:27–47. doi: 10.1016/j.cmet.2015.12.006
9. Haas R, Cucchi D, Smith J, Pucino V, Macdougall CE, Mauro C. Intermediates of Metabolism: From Bystanders to Signalling Molecules. *Trends Biochem Sci* (2016) 41:460–71. doi: 10.1016/j.tibs.2016.02.003
10. Lee DC, Sohn HA, Park ZY, Oh S, Kang YK, Lee KM, et al. A lactate-induced response to hypoxia. *Cell* (2015) 161:595–609. doi: 10.1016/j.cell.2015.03.011
11. Daw CC, Ramachandran K, Enslow BT, Maity S, Bursic B, Novello MJ, et al. Lactate Elicits ER-Mitochondrial Mg(2+) Dynamics to Integrate Cellular Metabolism. *Cell* (2020) 183:474–89.e17. doi: 10.1016/j.cell.2020.08.049
12. Hui S, Ghergurovich JM, Morscher RJ, Jang C, Teng X, Lu W, et al. Glucose feeds the TCA cycle via circulating lactate. *Nature* (2017) 551:115–8. doi: 10.1038/nature24057
13. Faubert B, Li KY, Cai L, Hensley CT, Kim J, Zacharias LG, et al. Lactate Metabolism in Human Lung Tumors. *Cell* (2017) 171:358–71.e9. doi: 10.1016/j.cell.2017.09.019
14. Sonveaux P, Végran F, Schroeder T, Wergin MC, Verrax J, Rabbani ZN, et al. Targeting lactate-fueled respiration selectively kills hypoxic tumor cells in mice. *J Clin Invest* (2008) 118:3930–42. doi: 10.1172/JCI36843
15. Martinez-Outschoorn UE, Prisco M, Ertel A, Tsirogas A, Lin Z, Pavlides S, et al. Ketones and lactate increase cancer cell “stemness,” driving recurrence, metastasis and poor clinical outcome in breast cancer: achieving personalized medicine via Metabolo-Genomics. *Cell Cycle (Georgetown Tex)* (2011) 10:1271–86. doi: 10.4161/cc.10.8.15330
16. Zhang D, Tang Z, Huang H, Zhou G, Cui C, Weng Y, et al. Metabolic regulation of gene expression by histone lactylation. *Nature* (2019) 574:575–80. doi: 10.1038/s41586-019-1678-1
17. Izzo LT, Wellen KE. Histone lactylation links metabolism and gene regulation. *Nature* (2019) 574:492–3. doi: 10.1038/d41586-019-03122-1
18. Fischer K, Hoffmann P, Voelkl S, Meidenbauer N, Ammer J, Edinger M, et al. Inhibitory effect of tumor cell-derived lactic acid on human T cells. *Blood* (2007) 109:3812–9. doi: 10.1182/blood-2006-07-035972
19. Zhang W, Wang G, Xu ZG, Tu H, Hu F, Dai J, et al. Lactate Is a Natural Suppressor of RLR Signaling by Targeting MAVS. *Cell* (2019) 178:176–89.e15. doi: 10.1016/j.cell.2019.05.003
20. Semenza GL. HIF-1: upstream and downstream of cancer metabolism. *Curr Opin Genet Dev* (2010) 20:51–6. doi: 10.1016/j.gde.2009.10.009
21. Salem A, Asselin MC, Reymen B, Jackson A, Lambin P, West CML, et al. Targeting Hypoxia to Improve Non-Small Cell Lung Cancer Outcome. *J Natl Cancer Inst* (2018) 110:14–30. doi: 10.1093/jnci/djx160
22. Merino Salvador M, Gómez de Cedrón M, Moreno Rubio J, Falagán Martínez S, Sánchez Martínez R, Casado E, et al. Lipid metabolism and lung cancer. *Crit Rev Oncol/Hematol* (2017) 112:31–40. doi: 10.1016/j.critrevonc.2017.02.001
23. Mohamed A, Deng X, Khuri FR, Owonikoko TK. Altered glutamine metabolism and therapeutic opportunities for lung cancer. *Clin Lung Cancer* (2014) 15:7–15. doi: 10.1016/j.clcc.2013.09.001
24. Bobrovnikova-Marjon E, Hurov JB. Targeting metabolic changes in cancer: novel therapeutic approaches. *Annu Rev Med* (2014) 65:157–70. doi: 10.1146/annurev-med-092012-112344
25. Mullen AR, DeBerardinis RJ. Genetically-defined metabolic reprogramming in cancer. *Trends Endocrinol Metab: TEM* (2012) 23:552–9. doi: 10.1016/j.tem.2012.06.009
26. Berkers CR, Maddocks OD, Cheung EC, Mor I, Vousden KH. Metabolic regulation by p53 family members. *Cell Metab* (2013) 18:617–33. doi: 10.1016/j.cmet.2013.06.019
27. Hensley CT, Faubert B, Yuan Q, Lev-Cohain N, Jin E, Kim J, et al. Metabolic Heterogeneity in Human Lung Tumors. *Cell* (2016) 164:681–94. doi: 10.1016/j.cell.2015.12.034
28. San-Millán I, Julian CG, Matarazzo C, Martinez J, Brooks GA. Is Lactate an Oncometabolite? Evidence Supporting a Role for Lactate in the Regulation of Transcriptional Activity of Cancer-Related Genes in MCF7 Breast Cancer Cells. *Front Oncol* (2019) 9:1536. doi: 10.3389/fonc.2019.01536

**Conflict of Interest:** The authors declare that the research was conducted in the absence of any commercial or financial relationships that could be construed as a potential conflict of interest.

Copyright © 2021 Jiang, Huang, Jiang, Hou, Tian, Li, Sun, Zhang, Zhang, Li, Li, Tong and Ma. This is an open-access article distributed under the terms of the Creative Commons Attribution License (CC BY). The use, distribution or reproduction in other forums is permitted, provided the original author(s) and the copyright owner(s) are credited and that the original publication in this journal is cited, in accordance with accepted academic practice. No use, distribution or reproduction is permitted which does not comply with these terms.



# Normalization of Enzyme Expression and Activity Regulating Vitamin A Metabolism Increases RAR-Beta Expression and Reduces Cellular Migration and Proliferation in Diseases Caused by Tuberous Sclerosis Gene Mutations

Elhusseiny Mohamed Mahmoud Abdelwahab<sup>1,2</sup>, Judit Bovari-Biri<sup>1,2</sup>, Gabor Smuk<sup>3</sup>, Tunde Harko<sup>4</sup>, Janos Fillinger<sup>4,5</sup>, Judit Moldvay<sup>4,5</sup>, Vera P. Krymskaya<sup>6</sup> and Judit E. Pongracz<sup>1,2\*</sup>

## OPEN ACCESS

### Edited by:

Andrea Morandi,  
University of Florence, Italy

### Reviewed by:

Wojciech Jelski,  
Medical University of Białystok, Poland  
Gabor Halmos,  
University of Debrecen, Hungary

### \*Correspondence:

Judit E. Pongracz  
pongacz.e.judit@pte.hu

### Specialty section:

This article was submitted to  
Cancer Metabolism,  
a section of the journal  
Frontiers in Oncology

**Received:** 21 December 2020

**Accepted:** 25 May 2021

**Published:** 11 June 2021

### Citation:

Abdelwahab EMM, Bovari-Biri J, Smuk G, Harko T, Fillinger J, Moldvay J, Krymskaya VP and Pongracz JE (2021) Normalization of Enzyme Expression and Activity Regulating Vitamin A Metabolism Increases RAR-Beta Expression and Reduces Cellular Migration and Proliferation in Diseases Caused by Tuberous Sclerosis Gene Mutations. *Front. Oncol.* 11:644592. doi: 10.3389/fonc.2021.644592

<sup>1</sup> Departments of Pharmaceutical Biotechnology, University of Pecs, Pecs, Hungary, <sup>2</sup> Szentagothai Research Centre, University of Pecs, Pecs, Hungary, <sup>3</sup> Department of Pathology, University of Pecs, Pecs, Hungary, <sup>4</sup> Department of Pathology, Semmelweis University, Budapest, Hungary, <sup>5</sup> Department of Pulmonology, National Koranyi Institute of Pulmonology, Budapest, Hungary, <sup>6</sup> Pulmonary, Allergy and Critical Care Division, Department of Medicine, Perelman School of Medicine, University of Pennsylvania, Philadelphia, PA, United States

**Background:** Mutation in a tuberous sclerosis gene (TSC1 or 2) leads to continuous activation of the mammalian target of rapamycin (mTOR). mTOR activation alters cellular including vitamin A metabolism and retinoic acid receptor beta (RAR $\beta$ ) expression. The goal of the present study was to investigate the molecular connection between vitamin A metabolism and TSC mutation. We also aimed to investigate the effect of the FDA approved drug rapamycin and the vitamin A metabolite retinoic acid (RA) in cell lines with TSC mutation.

**Methods:** Expression and activity of vitamin A associated metabolic enzymes and RAR $\beta$  were assessed in human kidney angiomyolipoma derived cell lines, primary lymphangiomyomatosis (LAM) tissue derived LAM cell lines. RAR $\beta$  protein levels were also tested in primary LAM lung tissue sections. TaqMan arrays, enzyme activities, qRT-PCRs, immunohistochemistry, immunofluorescent staining, and western blotting were performed and analysed. The functional effects of retinoic acid (RA) and rapamycin were tested in a scratch and a BrDU assay to assess cell migration and proliferation.

**Results:** Metabolic enzyme arrays revealed a general deregulation of many enzymes involved in vitamin A metabolism including aldehyde dehydrogenases (ALDHs), alcohol dehydrogenases (ADHs) and Cytochrome P450 2E1 (CYP2E1). Furthermore, RAR $\beta$  downregulation was a characteristic feature of all TSC-deficient cell lines and primary tissues. Combination of the two FDA approved drugs -RA for acute myeloid leukaemia and rapamycin for TSC mutation- normalised ALDH and ADH expression and activity, restored RAR $\beta$  expression and reduced cellular proliferation and migration.

**Conclusion:** Deregulation of vitamin A metabolizing enzymes is a feature of TSC mutation. RA can normalize RAR $\beta$  levels and limit cell migration but does not have a significant effect on proliferation. Based on our data, translational studies could confirm whether combination of RA with reduced dosage of rapamycin would have more beneficial effects to higher dosage of rapamycin monotherapy meanwhile reducing adverse effects of rapamycin for patients with TSC mutation.

**Keywords:** tuberous sclerosis gene mutation, RAR $\beta$ , vitamin A metabolism, retinoic acid, rapamycin

## BACKGROUND

Tuberous sclerosis, angiomyolipoma and lymphangioleiomyomatosis (LAM) are diseases characterised by slow growing tumours that are affecting many parts of the body (1, 2) including the skin, brain, kidneys and the lungs. The above diseases are caused by the mutation of tumour suppressor genes tuberous sclerosis 1 or 2 (TSC or TSC2) (1). The above tumours were initially considered benign, but angiomyolipoma and LAM have recently been reclassified as “low grade, destructive, metastasizing neoplasms” characterised by  $\alpha$ -smooth muscle actin ( $\alpha$ -SMA), vimentin, desmin and melanoma gp100 (HMB45) markers. Diseases caused by TSC mutations bear all the hallmarks of cancers including genetic mutations, evasion of growth suppression, resistance to cell death, metabolic reprogramming to avoid immune detection, and capability of invasion (3). Loss of TSC activity results in continuous activation of the mTOR pathway, which is also characteristic to various neoplasms where upstream mutations or signalling malfunction both result in mTOR activation (4). mTOR activation alters various cellular functions including cellular proliferation, autophagy, mitochondrial biogenesis, and cellular metabolism. Activation of the mTOR pathway can change anabolic cell growth processes such as protein and lipid synthesis in correlation with external growth factor or nutrient intake (5). In our previous study of LAM, apart from detecting morphological abnormalities in mitochondria and suppression of ROS production, we identified downregulation of the proliferation suppressor nuclear receptors of the retinoic acid gene family both retinoic acid receptor (RAR) and retinoid x receptor (RXR) as well as several miRNA-s that regulate RAR expression including miR29b (6). RAR and RXR are receptors of retinoic acid (RA), a metabolite of vitamin A (7). Both classes of nuclear receptors have three subtypes ( $\alpha$ ,  $\beta$ , and  $\gamma$ ) and in-patient derived LAM cell lines RAR $\beta$  mRNA expression was found significantly reduced (6). Interestingly, RAR $\beta$  is the receptor that is associated with the anti-tumour effects of RA (8–10). In many neoplastic diseases, expression

of RAR $\beta$  is often downregulated or lost indicating that RAR $\beta$  plays an important role in tumour suppression (11). RA is a metabolite of the lipophilic vitamin A (retinol) which is obtained from plant or animal sources in the form of carotenoids and retinyl esters, respectively (12). RA is a lipophilic molecule with three isoforms: all-trans, 9-cis and 13-cis RA and is stored in forms of retinyl esters primarily in the liver as well as the kidneys, lungs and the bone marrow (12, 13). In circulation, retinol is bound to retinol-binding protein (RBP) which enters the cells through RBP receptors (STRA6) (12). In the cells, retinol-dehydrogenase (RDH) or alcohol-dehydrogenase (ADH) oxidize retinol to retinal which is irreversibly converted to RA by the aldehyde dehydrogenase (ALDH) family also known as retinaldehyde dehydrogenase (RALDH) (12). RA binds to cellular retinoic acid-binding protein (CRABP) in the cell that carries RA into the nucleus where it binds to nuclear RARs to function as transcription factors. RA signalling is dependent upon its nuclear availability, controlled among others by RBP1, which is the carrier protein involved in the transport of retinol from the storage site to peripheral tissues (12). Interestingly, the administration of RA not only activates the transcription factor RAR $\beta$  but also increases its expression (14, 15). As currently the only FDA approved drug to treat angiomyolipoma, tuberous sclerosis or LAM is rapamycin, search for additional therapeutic targets is important. Especially so, as rapamycin can only slow down disease progression and cannot offer a cure. Additionally, rapamycin has significant side effects therefore not all patients can tolerate the treatment (16, 17). Discontinuation of rapamycin, however, leads to rapid disease progression (17). Tissues affected by TSC mutation are low in RAR $\beta$  expression (18, 19). As, RAR $\beta$  is regulated by RA (6, 19–21), a product of vitamin A metabolism, we theorised that not just RAR $\beta$  expression is low in LAM, but it is likely that enzymes of vitamin A metabolism malfunction. To test the theory vitamin A metabolic enzyme expression and activity was tested. Simultaneously, the effect of the metabolic product RA was assessed in cell migration and proliferation alone or in combination with rapamycin using TSC mutant cell lines.

Based on our results, such combination of rapamycin with RA might offer a novel therapeutic strategy if our *in vitro* data could be confirmed in a clinical study.

## MATERIALS AND METHODS

### Ethical Statement

LAM tissue samples were obtained from lung transplant donors for generation of cell lines, in accordance with the Declaration of

**Abbreviations:** ADHs/RDHs, alcohol dehydrogenases/retinol dehydrogenases; ALDHs, aldehyde dehydrogenases; ATRA, all-trans retinoic acid/tretinoin; BSMC, human bronchial smooth muscle cell; CRABP, cellular retinoic acid-binding protein; CYP, Cytochrome P450; GFP, green fluorescent protein; H&E, hematoxylin and eosin; HMB45, melanoma marker; LAM, Lymphangioleiomyomatosis; mTOR, Mammalian target of rapamycin; NHLF, normal human lung fibroblast cell; RA, Retinoic acid; RALDH, retinaldehyde dehydrogenase; RAR, Retinoic acid receptor; RBP, retinol-binding protein; RXR, retinoid x receptors; S102, human female kidney angiomyolipoma cell line 621-102 TSC2-/-; S103, human female kidney angiomyolipoma cell line 621-103 TSC2+/-; STRA6, Stimulated by retinoic acid 6; TSC 1-2, Tuberous sclerosis 1-2.



Helsinki, approved by the Institutional Review Board at the University of Pennsylvania (22) and provided by the National Disease Research Interchange (NDRI, Philadelphia, PA). LAM patients had given written informed consent and all the collected samples were treated anonymously. Paraffin embedded tissue samples were obtained from the Departments of Pathology at Semmelweis University, Budapest, and from the University of Pecs, Pecs, Hungary and the National Koranyi Institute of Pulmonology, Budapest, Hungary. The study was approved by the Medical Research Council of Hungary (54034-4/2018/EKU).

## LAM Cell Lines, Bronchial Smooth Muscle Cells (BSMC), Normal Human Lung Fibroblast (NHLF) S102 and S103 Cell Lines and Cell Culture Conditions

Primary tissue derived cultures of human LAM cell lines were established in the Department of Medicine, University of Pennsylvania, Pennsylvania, USA (22). Briefly, LAM cells were dissociated from LAM nodules of transplant patients. Each LAM nodule was used to establish individual cell lines (characterized by alpha smooth muscle actin ( $\alpha$ -SMA) expression, mTORC1 activity, HMB45 immunoreactivity, DNA synthesis, and cell migration) (23). In the current study, four patient-derived individual LAM cell lines were used including LAM-100, LAM-111C, LAM-D9065 and LAM-HUP. As controls, primary cultures of normal, human bronchial smooth muscle cells (BSMC) and normal human lung fibroblasts (NHLF), were purchased from Lonza (Basel, Switzerland). Normal BSMC-s and LAM cell lines were cultured at 37°C, 5% CO<sub>2</sub> in SMC Growth Medium (insulin, hFGF, GA, FBS and hEGF) (Lonza, Basel, Switzerland). Two angiomyolipoma cell lines were also used in the study and cultured at the above-mentioned conditions. The 621-102 (S102)(TSC2-/-) cell line was generated by introduction of E6/E7 (pLXSN 16E6E7-neo) and human telomerase (pLXSN hTERT-hyg) into a primary culture of TSC2 null human angiomyolipoma cells (24–26). The 621-103 (S103)(TSC2+/+) was generated by stable transfection of TRI102 with wild-type TSC2 (pcDNA3.1 TSC2-zeo) into 621-101 cells (24).

## Haematoxylin Eosin Staining

5  $\mu$ m thick tissue sections of primary normal and LAM lungs (n=6 each, respectively) were stained in Mayer's haematoxylin solution (Sigma-Aldrich, St. Louis, USA) for 10 min, washed, then differentiated with 0.25% acetic acid and in eosin solution. Sections were mounted using Vectashield mounting medium (Vector Laboratories, Burlingame, USA). Images were taken using Nikon Eclipse Ti-U inverted microscope.

## Immunofluorescent Staining

Normal, BSMC, NHLF, LAM (four individual cell lines), S103 (TSC2+/+) and S102 (TSC2-/-) cells were cultured for 3 days using Falcon<sup>TM</sup> chambered cell culture slides (Thermo Fisher Scientific, Waltham, USA). Cell cultures were then fixed with 4% formaldehyde and permeabilized with PBS containing 0.1% Triton-X and 5% BSA. Slides were incubated with primary antibodies (**Table 1**) overnight at 4°C. Slides were washed with TBS for three times then incubated with corresponding secondary antibody (**Table 1**) for 90 min at RT. Nuclei were counter stained with DAPI. Images were acquired using an Olympus IX-81 (OLYMPUS Corporation, Tokyo, Japan) both light and fluorescence microscope.

## Immunohistochemistry

5  $\mu$ m thick tissue sections of primary normal and LAM lungs were stained using immunohistochemistry. First, the slides were rinsed in heated xylene and were washed with a descending series of alcohol to remove paraffin. After deparaffination the slides were rehydrated in distilled water and antigen retrieval was performed by heating the slides in Target Retrieval Solution (pH 6, DAKO, Produktionsvej, Denmark) at 97°C for 20–30 min. Subsequently slides were washed in dH<sub>2</sub>O and endogenous peroxidase activity was blocked with 3% H<sub>2</sub>O<sub>2</sub> containing TBS (pH 7.4) for 15 min. Then slides were washed three times with TBS containing Tween (0.05%, pH 7.4). Pre-blocking was carried out with 3% BSA in TBS for 20 min before overnight incubation with anti- Melanoma gp100 antibody (HMB-45) (1:100, HMB-45 mouse monoclonal antibody clone: Ab787, Abcam) and anti-RAR $\beta$  (1:100, anti-RAR $\beta$  rabbit monoclonal

**TABLE 1** | Antibodies used in western blot, immunofluorescent staining, and immunohistochemistry.

Antibody	Catalog number	Source	Dilution
Anti-alpha Smooth Muscle Actin	MAB1420	R&D Systems, Minneapolis, USA	10 $\mu$ g/mL
Anti-mTOR Antibody	Ab25880	Abcam, MA, USA	2 $\mu$ g/ml
Anti-p70 S6 kinase	Ab32529	Abcam, MA, USA	1:200
Anti-RPS6	Ab12864	Abcam, MA, USA	1:250
Ribosomal Protein S6 Antibody	sc-74459	Santa Cruz Biotechnology	1:100
Anti-RAR beta	ab25880	Abcam, MA, USA	2 $\mu$ g/ml
Anti-mouse Alexa 488	A28175	Thermo Fisher Scientific, Waltham, USA	1:200
Anti-rabbit Alexa 647	A27040	Thermo Fisher Scientific, Waltham, USA	1:200
Anti-rabbit Alexa 488	A11034	Thermo Fisher Scientific, Waltham, USA	1:200
Anti-mouse Alexa 647	A32728	Thermo Fisher Scientific, Waltham, USA	1:200
Anti- Melanoma gp100 antibody (HMB-45)	Ab787	Abcam, MA, USA	1 $\mu$ g/ml
anti-RAR $\beta$	Ab124701	Abcam, MA, USA	1:100
Goat Anti-Rabbit Immunoglobulins/HRP	P0448	DAKO, Produktionsvej, Denmark	1:50
Goat Anti-Mouse Immunoglobulins/HRP	P0447	DAKO, Produktionsvej, Denmark	1:50

antibody clone: Ab124701, Abcam) primary antibody at 4°C. Following incubation slides were washed with TBS for three times then incubated with peroxidase conjugated secondary antibody (1:100, Polyclonal Goat Anti-Rabbit IgG, DAKO) for 90 min. Antibody labelling was visualized with the help of liquid DAB Substrate Chromogen System (DAKO). For nuclear counterstaining, haematoxylin staining was performed. Finally, slides were mounted with Faramount Aqueous Mounting Medium (DAKO, Produktionsvej, Denmark). Histological evaluation was performed with the help of Panoramic MIDI digital slide scanner (3DHitech, Budapest, Hungary). Image analysis was performed using ImageJ software with IHC toolbox plug-in.

## Rapamycin and Retinoic Acid (RA) Treatments

BSMC, NHLF, LAM (four individual cell lines), S103 (TSC2+/+) and S102 (TSC2-/-) cell cultures were treated with rapamycin and/or RA. The two drugs were used in the following concentrations: 10 or 20 nM rapamycin catalogue: tlr-rap (InvivoGen, San Diego, USA) and 1 or 2  $\mu$ M RA (Sigma-Aldrich, St. Louis, USA) for 24h at 37°C, 5% CO<sub>2</sub>.

## Western Blot

Cells were lysed in ice-cold RIPA buffer (Sigma-Aldrich, St. Louis, USA) supplemented with protease inhibitors (Roche Diagnostics, Mannheim, Germany) for 30 min on ice and centrifuged at 16,000  $\times$  g for 20 min at 4° C. The supernatant was then used as the cell lysate. The protein content of each cell lysate was assessed using a Qubit protein assay kit (Thermo Scientific, Waltham, MA). 30  $\mu$ g of total protein was loaded onto Mini Protean gel (Bio-Rad, California, USA), then electrophoresis was followed by overnight blotting onto a nitrocellulose membrane using 10 mA current. The blots then were blocked in 5% non-fat skimmed milk blocking solution (Bio-Rad, California, USA) in TBS-T buffer for 1 h and incubated with primary antibodies (**Table 1**) diluted 1:1000 in 2.5% non-fat skimmed milk powder in TBS-T overnight at 4° C. After washing with TBS-T, the blots were incubated with rabbit anti-goat/HRP diluted in 2.5% non-fat skimmed milk powder in TBS-T for 1 h at room temperature. The immunoreaction was developed with a chemiluminescence HRP substrate and recorded with ImageQuant LAS-4000 imager (GE Healthcare Life Sciences, USA).

## RNA Isolation

Total RNA was extracted from normal BSMC, NHLF and LAM (four individual cell lines) cultures with MN NucleoSpin RNA isolation kit according to the manufacturer's protocol (Macherey-Nagel, Düren, Germany). The concentration of RNA samples was measured using NanoDrop (Thermo Fisher Scientific, Waltham, USA). Total RNA from human lung tissues were obtained using TRIzol reagent (Invitrogen, Thermo Fisher Scientific, Waltham, USA). RNA (1  $\mu$ g) was digested with DNase (Sigma-Aldrich, St. Louis, USA) to eliminate any DNA contamination. cDNA was

synthesized with high-capacity RNA to cDNA kit (Thermo Fisher Scientific, Waltham, USA). Reverse transcription was performed with random hexamer primers.

## Quantitative qRT-PCR

qRT-PCR was performed using SensiFAST SYBR Green reagent (BioLine, London, UK) in an ABI StepOnePlus system. Gene expressions using sequence specific primers (**S. Table 1**) were analysed with StepOne software and normalized to beta-actin. Changes in gene expression were calculated according to the 2<sup>-ddCt</sup> method.

## Metabolic Enzyme RT2 Array

cDNA was prepared using RT2 First Strand Kit (Qiagen, Hilden, Germany) according to manufacturers' protocol using 350ng-1000ng of total RNA as starting material. Metabolic enzymes mRNA expression levels were performed using Human Drug Metabolism: Phase I Enzymes arrays (Qiagen, Hilden, Germany), RT2 SYBR<sup>®</sup> Green qPCR Mastermix (Qiagen, Hilden, Germany) and results were acquired by Quantstudio 12k flex (Thermo Fisher Scientific, Waltham, USA).

## ALDH and ADH Activity Assay

ALDH Activity Assay Kit (Abcam, MA, USA, ab155893) and Alcohol Dehydrogenase Assay Kit (Abcam, MA, USA, ab102533) were used to test ALDH and ADH activity of LAM and S102 compared to their controls before and after treatments. Activity of cell lysates was assessed using a detection kit and following the manufacturer's instructions. Enzyme activity induced colour changes were measured at OD450 nm with EnSpire<sup>®</sup> Multimode Plate Reader (PerkinElmer, Waltham, Massachusetts, USA). Pierce<sup>™</sup> BCA Protein Assay Kit (Thermo Fisher Scientific, Waltham, USA) was used to measure protein content and results are presented as the fold change vs. control.

## Wound Healing Assay

Cells were grown to 90% confluence in 24 well plates and wound gap was made by scratching the cell with rapamycin (10 nM), RA (2  $\mu$ M) and rapamycin (10 nM) + RA (2  $\mu$ M) was after inducing the wound gap. The healing of the wound gap by cell migration and the centre of the gap was monitored with images taking with EVOS light microscopy (Thermo Fisher Scientific, Waltham, USA) and the gap area was quantified using ImageJ software.

## BrdU Click-Ti Proliferation Assay

S103 and S102 cells were cultured using Falcon<sup>™</sup> chambered cell culture slides (Thermo Fisher Scientific, Waltham, USA). Proliferation capacity was assessed using Click-iT<sup>™</sup> Plus EdU Cell Proliferation Kit for Imaging, Alexa Fluor<sup>™</sup> 488 dye (Thermo Fisher Scientific, Waltham, USA). Briefly, cell cultures were treated with rapamycin and/or RA then incubated with EDU solution

overnight. Following overnight incubation cells were fixed with 3.7% formaldehyde and permeabilized with PBS containing 0.5% Triton-X. Staining was performed following manufacture instructions using Alexa Fluor® 488 picolyl azide and nuclei were counter stained with Hoechst® 33342. Images were acquired using an Olympus IX-81 (OLYMPUS Corporation, Tokyo, Japan) both light and fluorescence microscope.

### 3D Co-Cultures

3D aggregates were formed as described previously (27, 28). Briefly, normal human lung fibroblasts (NHLF) and bronchial smooth muscle cells (BSMC) were isolated from anonymous donors of different ages and sexes and were purchased from Lonza (Basel, Switzerland). All cells were cultured at 37°C and 5% CO<sub>2</sub> in primary cell culture media. NHLF, BSMC and LAM cell types were sub-cultured and mixed at 1:1 ratio then dispensed 3\*10<sup>5</sup> cells/well onto a low-attachment 96-well U-bottom plates (Corning, New York, USA). The 3D aggregate co-cultures were incubated in the presence or absence of 10 nM rapamycin and/or 2 µM RA for 24 h, then collected into cryomold and sectioned for staining.

### Statistical Analysis

Unless otherwise noted, statistical analysis was performed with SPSS version 20 software. S102 and S103 data are presented as

mean ± technical error of three replicates and statistical analysis was performed using student t-test. In experiments using primary LAM lung derived cell lines and their controls (an average of BSMC n=4 and NHLF n=4 samples) data are presented as mean ± standard error of mean (SEM), and statistical analysis was performed using the one-way ANOVA. p<0.05 was considered as significant.

### RESULTS

To investigate the involvement of the enzyme cascades associated with vitamin A metabolism in TSC deficient cells, human enzyme profiler arrays (RT2 PCR) were used to compare mRNA levels of specific enzymes in the human kidney angiomyolipoma cell line S102 (TSC2<sup>-/-</sup>) and its control S103 (TSC2<sup>+/+</sup>). Out of the alcohol dehydrogenase family, four enzymes (ADH1A, ADH1B, ADH1C and ADH6) were significantly upregulated and one enzyme was downregulated (ADH4) in the mutant cell line (Figure 1A). In the aldehyde dehydrogenase family three enzymes (ALDH1A2, ALDH1A3, and ALDH3A1) were upregulated, while five enzymes were downregulated (ALDH1A1, ALDH3B1, ALDH3B2, ALDH4A1 and ALDH5A1) (Figure 1A). Additionally, analysis of the array data showed significant increase in CYP2E1 mRNA level (Figure 1A, S. Table 2). To predict the connection (expression, physical interaction, co-localization, etc) amongst the above

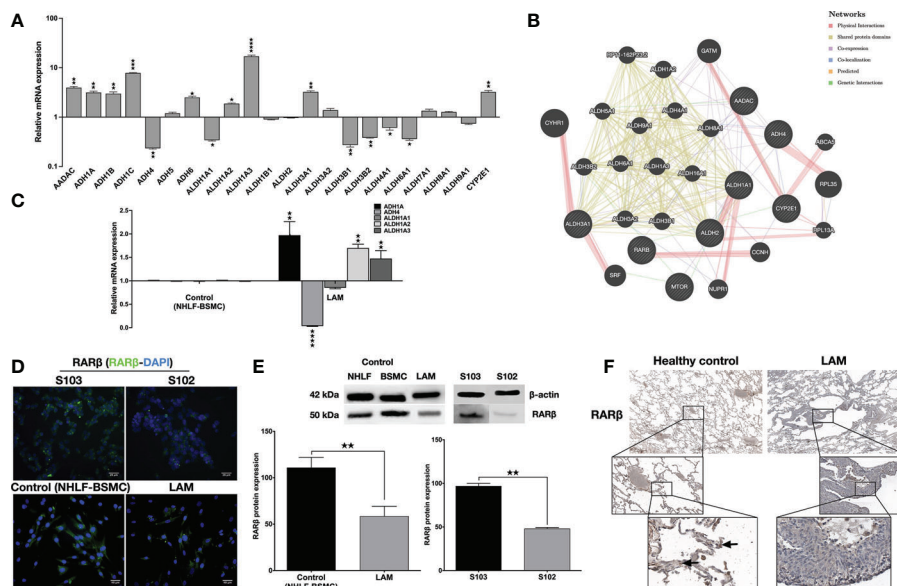


**FIGURE 1 |** Metabolic enzyme and retinoic acid receptor expression. **(A)** Human metabolic enzyme RT array analysis of S102 (TSC2<sup>-/-</sup>) compared to S103 (TSC2<sup>+/+</sup>) control. The figure presents Log RQ ± technical error of n=3 replicates (t-test). **(B)** Predictive analysis of co-expression, physical interactions between metabolic enzymes and RA in TSC mutant diseases groups using GeneMANIA database. **(C)** Gene expression of enzymes involved in vitamin A metabolism measured in LAM cell lines compared to primary healthy controls (BSMC and NHLF, 1:1). Data are presented as mean LogRQ ± SEM compared to untreated control. Significant changes are marked as ★, ★★, ★★★ and ★★★★★ (P<0.05, P<0.001, P<0.0002 and P<0.0001, respectively). **(D)** RARβ immunofluorescent staining (RARβ green, nuclei blue, magnification ×40, size bar 28–40 µm). **(E)** Western blot analysis of RARβ protein levels in LAM, control (NHLF and BSMC), S103 and S102 cell lines. WB protein expression levels were quantified by ImageJ and are presented as percentage compared to controls or S103. Significant changes are marked as ★, ★★ and ★★★ (P<0.05, P<0.001 and P<0.0002 respectively). **(F)** RARβ immunohistochemistry of a representative pair of primary LAM lung sections and healthy lung controls (size bar 100–500 µm), (n=6).



described enzymes and RA in TSC mutant cells, a linear regression-based prediction algorithm analysis was performed (GeneMANIA database) (29) (**Figure 1B**, **S. Table 3**). ADHs and ALDHs—especially ADH4, ALDH1A2 and ALDH1A3—were predicted to physically interact with molecules involved in the RA metabolic process and RAR $\beta$  binding (**Figure 1B**). To determine whether ADHs and ALDHs are present in TSC2-deficient LAM cells, ADHs and ALDHs mRNA expression levels were quantified by qRT-PCR in four patient derived LAM cell lines and normal individual primary human bronchial smooth muscle cell (BSMC) as well as primary normal human lung fibroblast cells (NHLF) as controls (**S. Figure 1**). Just as in the TSC2-/- angiomyolipoma cell line S102, in the primary LAM lung tissue derived cell lines the expression of ADH1, ADH4 and ALDH1A1-2-3 showed the same pattern (**Figure 1C**). Apart from vitamin A metabolism, the importance of ALDH and ADH were demonstrated in cancer cell proliferation, motility and metastasis (30, 31), due to their specific role in affecting mTOR dependent signalling. In a previous study it has been revealed that ALDH1A3 downregulation directly affects mTOR expression and its downstream signals *via* S6K (32). Result that ALDH1A3 mRNA was significantly upregulated in TSC2-/- S102 and patient derived LAM lung cell lines that leads to mTOR activation and downregulation of RAR $\beta$  expression (6) was confirmed by immunofluorescent staining (**Figure 1D**) and western blotting (**Figure 1E**). To confirm the cell line data, primary normal and LAM lung tissue sections (n=6) were stained for RAR $\beta$  protein by immunohistochemistry (**Figure 1F**, **S. Figure 2**). The staining of primary LAM tissues confirmed that reduced expression of RAR $\beta$  expression in the structural cells of the lung tissue is a feature of the TSC mutant LAM lungs (**Figure 1F**).

As RA is known to upregulate RAR $\beta$  expression (14, 15), we set out to investigate whether RA could restore normal levels of RAR $\beta$  in TSC2-/- cell lines. Four patient derived LAM lung cell lines were treated with 1  $\mu$ M or 2  $\mu$ M (33, 34) RA for 24 h, then RAR $\beta$  expression was quantified using qRT-PCR (**Figure 2A**) and immunofluorescent staining (**Figures 2B, C**). Following incubation with 2  $\mu$ M RA, RAR $\beta$  mRNA (**Figure 2A**) as well as protein expression (**Figures 2B, C**) was restored to normal levels. As patients with LAM disease are treated with rapamycin, and rapamycin is known to downregulate RAR $\beta$ , RAR $\beta$  protein expression levels were quantified in patient derived angiomyolipoma and LAM lung cell lines after 10 nM rapamycin treatment in the presence or absence of 2  $\mu$ M RA (**Figures 2D–G**). While 10 nM rapamycin mono treatment had no effect on RAR $\beta$  levels, 2  $\mu$ M RA increased RAR $\beta$  expression even in combination with rapamycin in the TSC2-/- cell lines (**Figures 2D–G**). The effects of the above treatments were tested on mTOR activity in the angiomyolipoma cell line S102 and its control S103 by western blotting of S6 and pS6 proteins (**Figure 2F**). While 10 nM rapamycin significantly reduced S6 phosphorylation close to control levels (**Figures 2F, G**), pS6 levels in the presence of 2  $\mu$ M RA mono treatment was not affected and remained just as high as in the untreated TSC2-/- control. Combination treatment with 10 nM rapamycin and 2  $\mu$ M RA resulted in middle ground. Significantly increased but not fully enhanced RAR $\beta$  protein expression and significantly

reduced pS6 levels but not as low as in the presence of 10 nM rapamycin mono treatment (**Figures 2D–G**).

Based on the data TSC mutation affects downstream signals including the vitamin A metabolic enzyme signalling cascades (**Figure 3A**). As the FDA approved rapamycin and RA in combination restored RAR $\beta$  and pS6 levels we also tested both drugs on vitamin A metabolic enzyme expression and activity. Mono treatment with 2  $\mu$ M RA normalised mRNA expression levels of ADH (1A, 4) and ALDH (1A1, 1A2, 1A3) (**Figure 3B**). Also, in RA treated TSC mutant S102 and primary LAM lung derived cell lines ADH and ALDH enzymes activity showed significant decrease compared to untreated controls (**Figure 3B**). Expression levels (**Figure 3B**) and enzymatic activity (**Figures 3C–F**) of metabolic enzymes were also quantified after 10 and 20 nM rapamycin and/or 2  $\mu$ M RA treatments. The cultures were assessed after 24 h incubation. While in mono treatment the 20 nM rapamycin was the most efficient in reducing ALDH (35) and ADH activity, combination treatment of 10 nM rapamycin and 2  $\mu$ M RA stabilised mRNA expression and activity of ADH and ALDH the most closely to TSC2+/+ control levels (**Figures 3B–F**).

To test whether normalization of enzyme levels and activity in vitamin A metabolism and suppression of mTOR activity would have an effect on cellular proliferation and migration, the effect of 2  $\mu$ M RA in combination with 10 nM rapamycin were tested in mono and combination treatment in a scratch and a BrdU assay (36, 37). The combined treatment of TSC2-/- cell lines with rapamycin (10 nM) and RA (2  $\mu$ M) decreased cellular migration significantly (**Figures 4A, B**). Furthermore, the combination significantly decreased the proliferation capacity detected in BrdU assay compared to rapamycin mono treatment (**Figures 4C, D**).

Apart from increased cell migration and proliferation, TSC-deficiency is characterized by structural changes of the affected tissues. Such changes cannot be detected in traditional 2D cell cultures, therefore a 3D tissue aggregates were used (27). The 3D aggregate tissues containing patient derived LAM lung cell lines developed empty sac formations after 24 h incubation which feature was reduced after 10 nM rapamycin and/or 2  $\mu$ M RA treatment making the LAM cell containing co-cultures structurally similar to the aggregate cultures containing only TSC+/+ BSMC and NHLF cells (**Figure 4E**). Additionally, 10 nM rapamycin and/or 2  $\mu$ M RA treatments increased RAR $\beta$  protein expression even in the 3D tissue structures containing TSC mutant cell lines (**S. Figure 3**).

## DISCUSSION

In our previous study of LAM, we detected correlation between mTOR activation, mitochondrial dysfunction and downregulation of the proliferation suppressor nuclear receptor family of RAR and RXR (6). Recent studies have also shown that rapamycin treatment induced upregulation of miR-29b in LAM affected cell growth, migration, and invasion *via* regulation of RAR $\beta$  activity (19).

In the present study, we confirmed that downregulation of RAR $\beta$  is not just a feature of TSC-deficient cell lines (angiomyolipoma, LAM primary cell lines) but it is characteristically present in primary



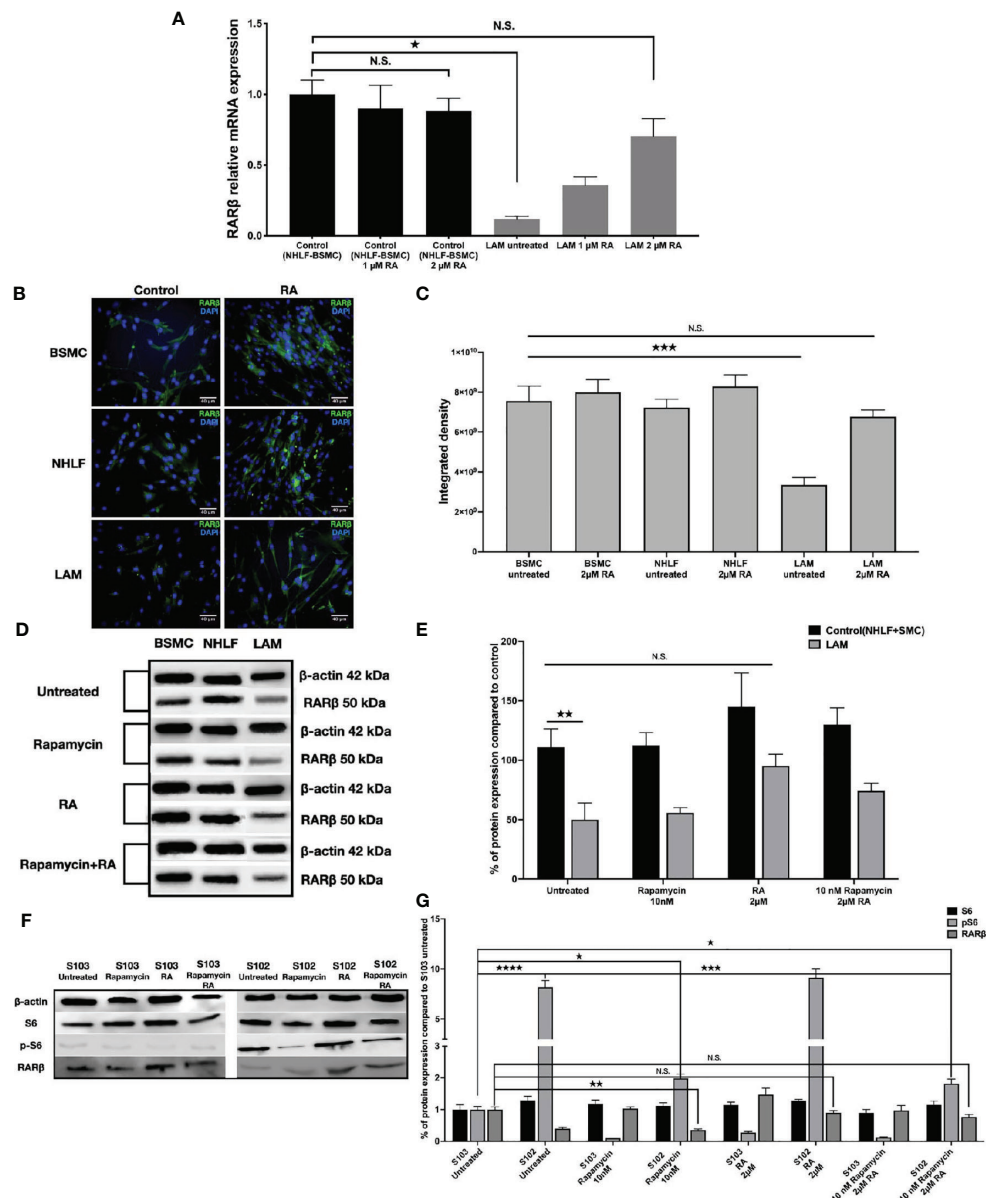


**FIGURE 2 |** Restoration of RARβ expression by RA. **(A)** mRNA expression levels of RARβ are significantly increased in LAM cell lines (n=4) compared to controls BSMC and NHLF after 2 μM RA treatment for 24 h. Significant changes are marked as ★ (P<0.05). **(B, C)**, Protein expression levels of RARβ using immunofluorescence staining in LAM cell lines compared to controls (BSMC and NHLF) after 2 μM RA treatment for 24 h. Immunofluorescence staining RARβ green, DAPI blue, magnification 40x, size-bar 40 μm. **(D, E)** Western blot analysis of RARβ protein levels in LAM cell lines and control cells (NHLF and BSMC). **(F, G)** Western blot analysis of RARβ, S6 and pS6 protein levels in S102 cell line compared to S103. WB protein expression levels were quantified by ImageJ and are presented as percentage compared to controls. Changes are marked as N.S. (Non Significant) or significant ★, ★★, ★★★ and ★★★★★ (P<0.05, P<0.001, P<0.0002 and P<0.0001, respectively).

LAM lung tissue sections (**Figures 1D–F**). In many cancers (38) the activity of RARβ itself is suppressed *via* various pathways leading up to mTOR activation (19, 39). As RARβ levels are strongly associated with alterations in the vitamin A metabolic pathway (11), clear understanding of vitamin A metabolism in connection with TSC mutation is important for better disease control.

In the present study, we used TSC mutant angiomyolipoma and primary LAM lung derived cell lines pre-dating the rapamycin era

to investigate enzyme expression and activity responsible for retinol metabolism. Based on our study the ability to metabolise retinol is seriously compromised in TSC-deficient cells (**Figure 1**). Many enzymes, including ADH1A, ADH1B, ADH1C, ADH6, ALDH1A2, ALDH1A3, and ALDH3A1 were drastically upregulated, while others including ADH4, ALDH1A1, ALDH3B1, ALDH3B2, ALDH4A1 and ALDH5A1 were significantly downregulated (**Figure 1**). The characteristic function of ALDHs is to oxidize

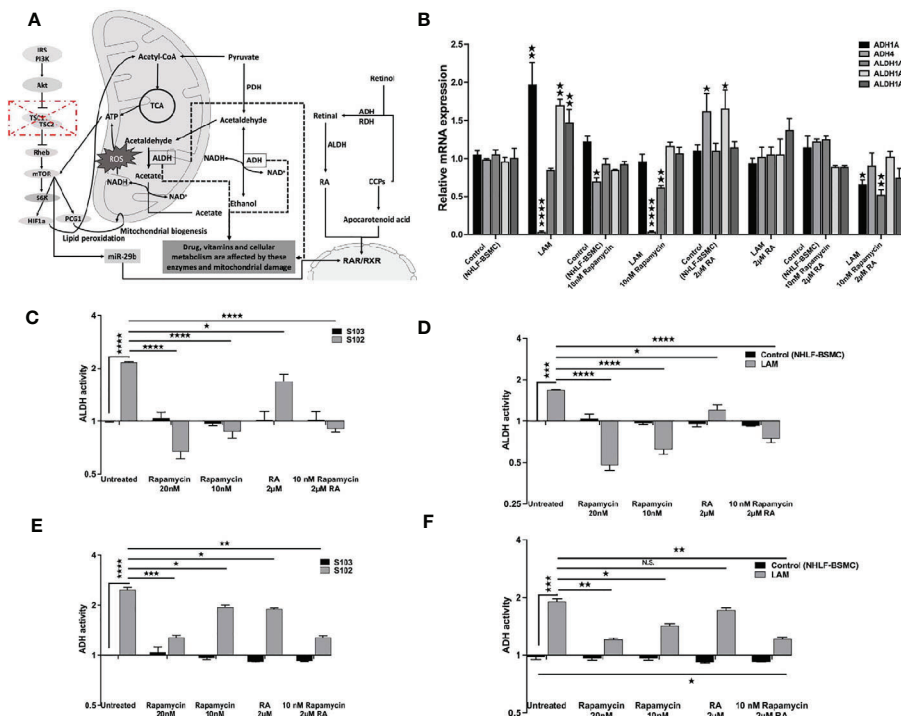


**FIGURE 3 |** The effect of RA on ALDH and ADH mRNA and enzyme activity levels. **(A)** Schematic figure explaining the connections between different pathways, TSC-mTOR, metabolic enzymes and energy production. **(B)** Gene expression levels of ALDH and ADH enzymes involved in RA metabolism following RA (2 μM) treatment of LAM cell lines compared to controls (BSMC and NHLF). Data are presented as mean LogRQ ± SEM compared to untreated controls. **(C)** ALDH enzyme activity fold changes in S102 (TSC-/-) cell lines compared to untreated S103 (TSC+/+) ± technical error of replicates (t-test). **(D)** ALDH enzyme activity fold changes in LAM cell lines compared to untreated BSMC and NHLF (1:1) ± SEM (ANOVA). **(E)** ADH enzyme activity fold changes in S102 (TSC-/-) cell lines compared to untreated S103 (TSC+/+) ± technical (t-test). **(F)** ADH enzyme activity fold changes in LAM cell lines compared to untreated BSMC and NHLF (1:1) ± SEM (ANOVA). Changes are marked as N.S. (Non Significant) or significant ★, ★★, ★★★ and ★★★★★ (P<0.05, P<0.001, P<0.0002 and P<0.0001, respectively).

aldehydes that would otherwise participate in signalling pathways to induce cellular, to minimize ROS production and to mediate RA signalling cascades (40). Other studies have also shown that in diseases caused by TSC mutation which increases mTORC1 activity is associated with deregulation of ALDH expression and activity, resistance to oxidative stress, greater proliferation, migration, and invasion as well as higher levels of VEGF expression (32, 35). These regulatory mechanisms are important in regulation of proliferation, tumorigenesis and resistance to therapy (41). Expression of ALDHs are also regulated by RA compounds including the chemotherapeutic vitamin A or chemically related molecules (retinoids) as well as oncogenic pathways including the WNT/β-catenin and the MUC1-C/ERK pathways (40). CYP2E1 degrades retinoic acid (RA) and retinol to polar metabolites with toxic and apoptotic properties (42). Imbalance in the level of alcohol dehydrogenases acts as a competitive inhibitor of retinol oxidation in the liver which may reduce the biosynthesis of retinoic acid (43). It is especially important that co-expression and physical interactions amongst the metabolic enzymes of retinol are tightly controlled and important in regulation of cellular differentiation, proliferation, and migration.

Our experiments have highlighted that patients might benefit from combination of RA with the routinely used treatment of

rapamycin in diseases affected by TSC mutation. In such treatment, reduction of rapamycin dosage and closely normalised vitamin A metabolic enzyme activities (Figure 3) could lead to beneficial physiological effects including reduced cellular proliferation and migration (Figure 4).

## CONCLUSION

Importantly, several enzymes of the vitamin A metabolism and the nuclear receptor RARβ can become potential therapeutic targets in TSC mutant or deregulated neoplasms (44, 45). RA for example is an FDA approved drug for acute myeloid leukaemia as RA can normalize RARβ levels and limit cancer cell migration and consequent disease progression (45). Based on our study we propose that clinical assessment of the combination of RA with reduced dosage of rapamycin might limit adverse reactions to rapamycin in rapamycin sensitive tuberous sclerosis, LAM and angiomyolipoma patients. With reduction of rapamycin levels, the inhibitory effect of rapamycin on ALDH can also become limited which allows better balance in vitamin A metabolism and consequently in RARβ activity. Increased expression and activity of RARβ might also lead to inhibition of cellular migration,

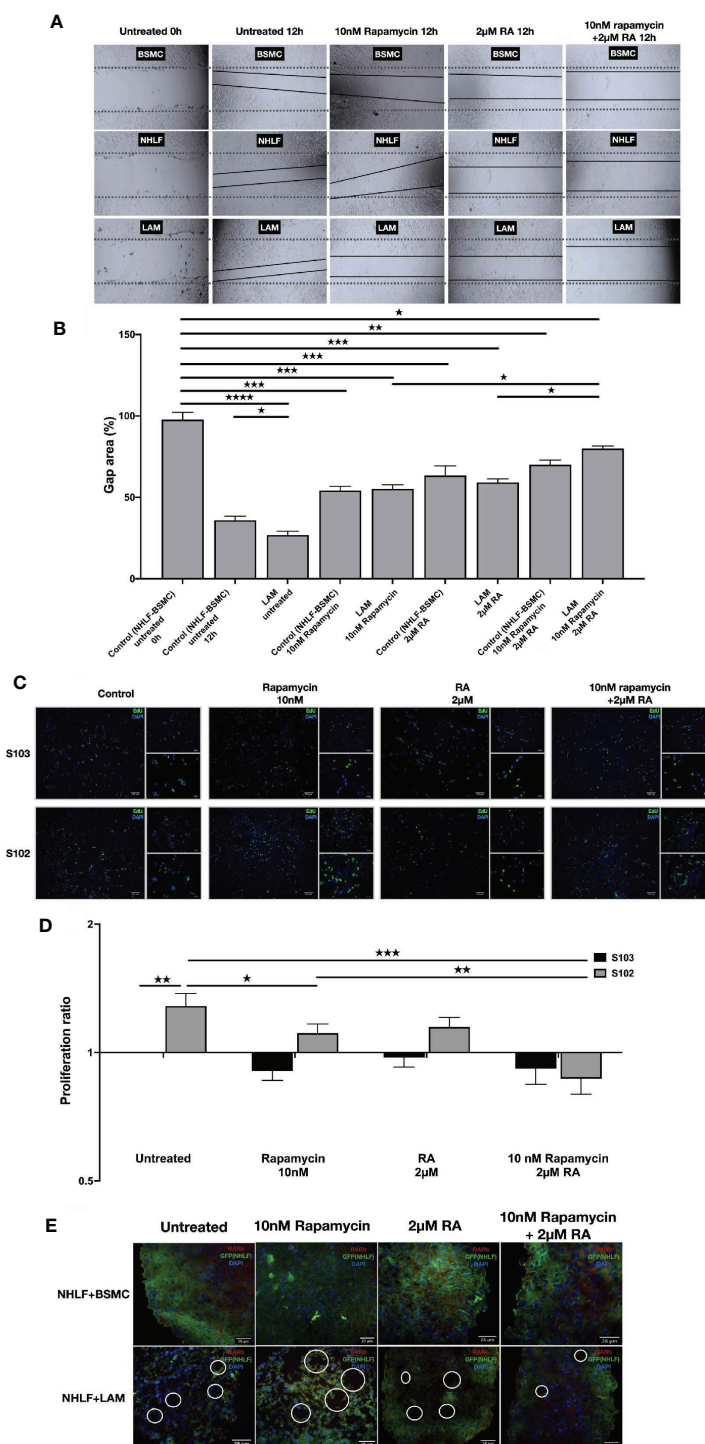


**FIGURE 4** | RA mono and RA and rapamycin combination treatment reduces cellular migration and proliferation in TSC-deficient cells. **(A)** Wound healing scratch assay following 10 nM rapamycin and/or 2 μM RA treatment for 24 h. **(B)** Wound gap area quantification, data are presented as gap area (%) compared to untreated control (BSMC and NHLF, 1:1) as 100%. Differences in gap closure % ± SEM. Significant changes are marked as ★, ★★, ★★★ and ★★★★★ ( $P < 0.05$ ,  $P < 0.001$ ,  $P < 0.0002$  and  $P < 0.0001$ , respectively). **(C, D)** Proliferation capacity of S102 compared to S103 using BrdU assay (BrdU green, DAPI blue, size-bar 100, 50, 25 μm). Proliferation ratio compared to untreated S103 ± technical error of replicates (t-test). Significant changes are marked as ★, ★★ and ★★★ ( $P < 0.05$ ,  $P < 0.001$  and  $P < 0.0002$  respectively). **(E)** Empty sac formation in NHLF-LAM co-cultures compared to NHLF-BSMC co-cultures in the presence or absence of 10 nM rapamycin and/or 2 μM RA treatment (24 h). Empty sac formation is marked with white circles in the staining where RARβ is red, NHLF-GFP is green and the nucleus is stained by DAPI (blue).

proliferation and as a result improved disease control. Further studies of improved drug concentrations and clinical assessment of our *in vitro* results are certainly required to modify treatment strategies for patients suffering from diseases affected by TSC mutations.

## DATA AVAILABILITY STATEMENT

The raw data supporting the conclusions of this article will be made available by the authors, without undue reservation.

## ETHICS STATEMENT

The study was approved by the Medical Research Council of Hungary (54034-4/2018/EKU). Written informed consent for participation was not required for this study in accordance with the national legislation and the institutional requirements.

## AUTHOR CONTRIBUTIONS

EA and JB-B: performed the experiments, isolated RNA and protein from NHLF, SMC and LAM, cellular staining, embedding of samples for microscopy, performed data analysis, and prepared

figures. VK: generated the LAM cell lines and performed experiments on angiomyolipoma cell lines. JM, JF, TH, and GS: selected the samples. JP designed the studies. EA and JP have written the manuscript. All authors contributed to the article and approved the submitted version.

## FUNDING

JP: TUDFO/51757-1/2019-ITM; 2020-4.1.1-TKP2020, GINOP 2.3.2-15-2016-00022; EFOP-3.6.1-16-2016-00004; and GINOP-2.3.3-15-2016-00012 HECRIN funds.

## ACKNOWLEDGMENTS

We would like to thank Professor Elizabeth Petri Henske (Brigham and Women's Hospital, Harvard Medical School, Boston, MA, USA) for the angiomyolipoma cell lines.

## SUPPLEMENTARY MATERIAL

The Supplementary Material for this article can be found online at: <https://www.frontiersin.org/articles/10.3389/fonc.2021.644592/full#supplementary-material>

## REFERENCES

- Leung AKC, Robson WLM. Tuberous Sclerosis Complex: A Review. *J Pediatr Heal Care* (2007) 21:108–14. doi: 10.1016/j.pedhc.2006.05.004
- Lin C, Jin L, Yang Y, Ding Y, Wu X, Ni L, et al. Tuberous Sclerosis-Associated Renal Angiomyolipoma: A Report of Two Cases and Review of the Literature. *Mol Clin Oncol* (2017) 7:706–8. doi: 10.3892/mco.2017.1377
- McCormack FX, Travis WD, Colby TV, Henske EP, Moss J. Lymphangioleiomyomatosis - Calling It What It Is: A Low-Grade, Destructive, Metastasizing Neoplasm. *Am J Respir Crit Care Med* (2012) 186:1210–2. doi: 10.1164/rccm.201205-0848OE
- Hammes SR, Krymskaya VP. Targeted Approaches Toward Understanding and Treating Pulmonary Lymphangioleiomyomatosis (Lam). *Horm Cancer* (2013) 4:70–7. doi: 10.1007/s12672-012-0128-4
- Laplante M, Sabatini DM. mTOR Signaling At a Glance. *J Cell Sci* (2009) 122:3589–94. doi: 10.1242/jcs.051011
- Abdelwahab EMM, Pal S, Kvell K, Karosi V, Bai P, Rue R, et al. Mitochondrial Dysfunction Is a Key Determinant of the Rare Disease Lymphangioleiomyomatosis and Provides a Novel Therapeutic Target. *Oncogene* (2019) 38:3093–101. doi: 10.1038/s41388-018-0625-1
- Altucci L, Leibowitz MD, Ogilvie KM, de Lera AR, Gronemeyer H. RAR and RXR Modulation in Cancer and Metabolic Disease. *Nat Rev Drug Discov* (2007) 6:793–810. doi: 10.1038/nrd2397
- Das BC, Thapa P, Karki R, Das S, Mahapatra S, Liu T-C, et al. Retinoic Acid Signaling Pathways in Development and Diseases. *Bioorg Med Chem* (2014) 22:673–83. doi: 10.1016/j.bmc.2013.11.025
- Li Y, Wongsiriroj N, Blaner WS. The Multifaceted Nature of Retinoid Transport and Metabolism. *Hepatobil Surg Nutr* (2014) 3:126–39. doi: 10.3978/j.issn.2304-3881.2014.05.04
- Tsuji M, Shudo K, Kagechika H. Identifying the Receptor Subtype Selectivity of Retinoid X and Retinoic Acid Receptors Via Quantum Mechanics. *FEBS Open Bio* (2017) 7:391–6. doi: 10.1002/2211-5463.12188
- Sun S-Y, Lotan R. Retinoids and Their Receptors in Cancer Development and Chemoprevention. *Crit Rev Oncol Hematol* (2002) 41:41–55. doi: 10.1016/S1040-8428(01)00144-5
- O'Byrne SM, Blaner WS. Retinol and Retinyl Esters: Biochemistry and Physiology. *J Lipid Res* (2013) 54:1731–43. doi: 10.1194/jlr.R037648
- Chelstowska S, Widjaja-Adhi MAK, Silvaroli JA, Golczak M. Molecular Basis for Vitamin A Uptake and Storage in Vertebrates. *Nutrients* (2016) 8:676. doi: 10.3390/nu8110676
- Sucov HM, Murakami KK, Evans RM. Characterization of an Autoregulated Response Element in the Mouse Retinoic Acid Receptor Type Beta Gene. *Proc Natl Acad Sci* (1990) 87:5392–6. doi: 10.1073/pnas.87.14.5392
- Leid M, Kastner P, Chambon P. Multiplicity Generates Diversity in the Retinoic Acid Signaling Pathways. *Trends Biochem Sci* (1992) 17:427–33. doi: 10.1016/0968-0004(92)90014-z
- Merkel S, Mogilevskaia N, Mengel M, Haller H, Schwarz A. Side Effects of Sirolimus. *Transplant Proc* (2006) 38:714–5. doi: 10.1016/j.transproceed.2006.01.044
- Salmon AB. About-Face on the Metabolic Side Effects of Rapamycin. *Oncotarget* (2015) 6:2585–6. doi: 10.18632/oncotarget.3354
- Kishton RJ, Rathmell JC. Novel Therapeutic Targets of Tumor Metabolism. *Cancer J* (2015) 21:62–9. doi: 10.1097/PPO.0000000000000099
- Liu HJ, Lam HC, Baglini CV, Nijmeh J, Cottrill AA, Chan SY, et al. Rapamycin-Upregulated miR-29b Promotes mTORC1-Hyperactive Cell Growth in TSC2-Deficient Cells by Downregulating Tumor Suppressor Retinoic Acid Receptor  $\beta$  (RAR $\beta$ ). *Oncogene* (2019) 38:7367–83. doi: 10.1038/s41388-019-0957-5
- Li C, Zhou X, Sun Y, Zhang E, Mancini JD, Parkhitko A, et al. Faslodex Inhibits Estradiol-Induced Extracellular Matrix Dynamics and Lung Metastasis in a Model of Lymphangioleiomyomatosis. *Am J Respir Cell Mol Biol* (2013) 49:135–42. doi: 10.1165/rcmb.2012-0476OC
- Boorjian SA, Sheinin Y, Crispen PL, Lohse CM, Kwon ED, Leibovich BC. Hormone Receptor Expression in Renal Angiomyolipoma: Clinicopathologic Correlation. *Urology* (2008) 72:927–32. doi: 10.1016/j.urolgy.2008.01.067



22. Goncharova EA, Goncharov DA, Eszterhas A, Hunter DS, Glassberg MK, Yeung RS, et al. Tuberin Regulates P70 S6 Kinase Activation and Ribosomal Protein S6 Phosphorylation: A Role for the TSC2 Tumor Suppressor Gene in Pulmonary Lymphangioleiomyomatosis (LAM). *J Biol Chem* (2002) 277:30958–67. doi: 10.1074/jbc.M202678200
23. Goncharova EA, Goncharov DA, Lim PN, Noonan D, Krymskaya VP. Modulation of Cell Migration and Invasiveness by Tumor Suppressor TSC2 in Lymphangioleiomyomatosis. *Am J Respir Cell Mol Biol* (2006) 34:473–80. doi: 10.1165/rcmb.2005-0374OC
24. Yu J, Astrinidis A, Howard S, Henske EP. Estradiol and Tamoxifen Stimulate LAM-Associated Angiomyolipoma Cell Growth and Activate Both Genomic and Nongenomic Signaling Pathways. *Am J Physiol - Lung Cell Mol Physiol* (2004) 286:694–700. doi: 10.1152/ajplung.00204.2003
25. Carsillo T, Astrinidis A, Henske EP. Mutations in the Tuberous Sclerosis Complex Gene TSC2 Are a Cause of Sporadic Pulmonary Lymphangioleiomyomatosis. *Proc Natl Acad Sci USA* (2000) 97:6085–90. doi: 10.1073/pnas.97.11.6085
26. Furukawa T, Duguid WP, Rosenberg L, Viallet J, Galloway DA, Tsao MS. Long-Term Culture and Immortalization of Epithelial Cells From Normal Adult Human Pancreatic Ducts Transfected by the E6E7 Gene of Human Papilloma Virus 16. *Am J Pathol* (1996) 148:1763–70.
27. Kovacs T, Csongei V, Feller D, Ernszt D, Smuk G, Sarosi V, et al. Alteration in the Wnt Microenvironment Directly Regulates Molecular Events Leading to Pulmonary Senescence. *Aging Cell* (2014) 13:838–49. doi: 10.1111/ace.12240
28. Abdelwahab EMM, Rapp J, Feller D, Csongei V, Pal S, Bartis D, et al. Wnt Signaling Regulates Trans-Differentiation of Stem Cell Like Type 2 Alveolar Epithelial Cells to Type 1 Epithelial Cells. *Respir Res* (2019) 20:204. doi: 10.1186/s12931-019-1176-x
29. Mostafavi S, Ray D, Warde-Farley D, Grouios C, Morris Q. Genemania: A Real-Time Multiple Association Network Integration Algorithm for Predicting Gene Function. *Genome Biol* (2008) 9:S4. doi: 10.1186/gb-2008-9-s1-s4
30. Moreb JS, Baker HV, Chang LJ, Amaya M, Lopez MC, Ostmark B, et al. ALDH Isozymes Downregulation Affects Cell Growth, Cell Motility and Gene Expression in Lung Cancer Cells. *Mol Cancer* (2008) 7:1–19. doi: 10.1186/1476-4598-7-87
31. Rodriguez-Torres M, Allan AL. Aldehyde Dehydrogenase as a Marker and Functional Mediator of Metastasis in Solid Tumors. *Clin Exp Metastasis* (2016) 33:97–113. doi: 10.1007/s10585-015-9755-9
32. Kawakami R, Mashima T, Kawata N, Kumagai K, Migita T, Sano T, et al. Aldh1a3-mTOR Axis as a Therapeutic Target for Anticancer Drug-Tolerant Persister Cells in Gastric Cancer. *Cancer Sci* (2020) 111:962–73. doi: 10.1111/cas.14316
33. Cheung Y-T, Lau WK-W, Yu M-S, Lai CS-W, Yeung S-C, So K-F, et al. Effects of All-Trans-Retinoic Acid on Human SH-SY5Y Neuroblastoma as In Vitro Model in Neurotoxicity Research. *Neurotoxicology* (2009) 30:127–35. doi: 10.1016/j.neuro.2008.11.001
34. Geisen C, Denk C, Gremm B, Baust C, Karger A, Bollag W, et al. High-Level Expression of the Retinoic Acid Receptor Beta Gene in Normal Cells of the Uterine Cervix Is Regulated by the Retinoic Acid Receptor Alpha and Is Abnormally Down-Regulated in Cervical Carcinoma Cells. *Cancer Res* (1997) 57:1460–7.
35. Mu X, Isaac C, Schott T, Huard J, Weiss K. Rapamycin Inhibits Aldh Activity, Resistance to Oxidative Stress, and Metastatic Potential in Murine Osteosarcoma Cells. *Sarcoma* (2013) 2013:480713. doi: 10.1155/2013/480713
36. Flamini MI, Gauna GV, Sottile ML, Nadin BS, Sanchez AM, Vargas-Roig LM. Retinoic Acid Reduces Migration of Human Breast Cancer Cells: Role of Retinoic Acid Receptor Beta. *J Cell Mol Med* (2014) 18:1113–23. doi: 10.1111/jcmm.12256
37. Varma S, Khandelwal RL. Effects of Rapamycin on Cell Proliferation and Phosphorylation of mTOR and p70S6K in HepG2 and HepG2 Cells Overexpressing Constitutively Active Akt/PKB. *Biochim Biophys Acta - Gen Subj* (2007) 1770:71–8. doi: 10.1016/j.bbagen.2006.07.016
38. Valastyan S, Weinberg RA. Tumor Metastasis: Molecular Insights and Evolving Paradigms. *Cell* (2011) 147:275–92. doi: 10.1016/j.cell.2011.09.024
39. Agudo M, Yip P, Davies M, Bradbury E, Doherty P, McMahon S, et al. A Retinoic Acid Receptor  $\beta$  Agonist (CD2019) Overcomes Inhibition of Axonal Outgrowth Via Phosphoinositide 3-Kinase Signalling in the Injured Adult Spinal Cord. *Neurobiol Dis* (2010) 37:147–55. doi: 10.1016/j.nbd.2009.09.018
40. Clark DW, Palle K. Aldehyde Dehydrogenases in Cancer Stem Cells: Potential as Therapeutic Targets. *Ann Transl Med* (2016) 4:40–40. doi: 10.21037/atm.2016.11.82
41. Singh S, Brocker C, Koppaka V, Chen Y, Jackson BC, Matsumoto A, et al. Aldehyde Dehydrogenases in Cellular Responses to Oxidative/Electrophilic Stress. *Free Radic Biol Med* (2013) 56:89–101. doi: 10.1016/j.freeradbiomed.2012.11.010
42. Orywal K, Szmikowski M. Alcohol Dehydrogenase and Aldehyde Dehydrogenase in Malignant Neoplasms. *Clin Exp Med* (2017) 17:131–9. doi: 10.1007/s10238-016-0408-3
43. Kedishvili NY. Retinoic Acid Synthesis and Degradation. *Subcell Biochem* (2016) 81:127–61. doi: 10.1007/978-94-024-0945-1\_5
44. Idres N, Marill J, Flexor MA, Chabot GG. Activation of Retinoic Acid Receptor-Dependent Transcription by All-Trans-Retinoic Acid Metabolites and Isomers. *J Biol Chem* (2002) 277:31491–8. doi: 10.1074/jbc.M205016200
45. Su M, Alonso S, Jones JW, Yu J, Kane MA, Jones RJ, et al. All-Trans Retinoic Acid Activity in Acute Myeloid Leukemia: Role of Cytochrome P450 Enzyme Expression by the Microenvironment. *PLoS One* (2015) 10:e0127790. doi: 10.1371/journal.pone.0127790

**Conflict of Interest Statement:** The authors declare that the research was conducted in the absence of any commercial or financial relationships that could be construed as a potential conflict of interest.

Copyright © 2021 Abdelwahab, Bovari-Biri, Smuk, Harko, Fillinger, Moldvay, Krymskaya and Pongracz. This is an open-access article distributed under the terms of the Creative Commons Attribution License (CC BY). The use, distribution or reproduction in other forums is permitted, provided the original author(s) and the copyright owner(s) are credited and that the original publication in this journal is cited, in accordance with accepted academic practice. No use, distribution or reproduction is permitted which does not comply with these terms.



# Energy Metabolic Plasticity of Colorectal Cancer Cells as a Determinant of Tumor Growth and Metastasis

Leenu Reinsalu<sup>1,2</sup>, Marju Puurand<sup>1</sup>, Vladimir Chekulayev<sup>1</sup>, Sten Miller<sup>1,2</sup>, Igor Shevchuk<sup>1</sup>, Kersti Tepp<sup>1</sup>, Egle Rebane-Klemm<sup>1,2</sup>, Natalja Timohhina<sup>1</sup>, Anton Terasmaa<sup>1</sup> and Tuuli Kaambre<sup>1\*</sup>

<sup>1</sup> Laboratory of Chemical Biology, National Institute of Chemical Physics and Biophysics, Tallinn, Estonia, <sup>2</sup> Department of Chemistry and Biotechnology, School of Science, Tallinn University of Technology, Tallinn, Estonia

## OPEN ACCESS

### Edited by:

Miriam Martini,  
University of Turin, Italy

### Reviewed by:

Tatiana Rostovtseva,  
National Institutes of Health (NIH),  
United States  
Wael Rabeh,  
New York University Abu Dhabi,  
United Arab Emirates

### \*Correspondence:

Tuuli Kaambre  
tuuli.kaambre@kbfi.ee

### Specialty section:

This article was submitted to  
Cancer Metabolism,  
a section of the journal  
Frontiers in Oncology

Received: 22 April 2021

Accepted: 08 July 2021

Published: 26 July 2021

### Citation:

Reinsalu L, Puurand M,  
Chekulayev V, Miller S,  
Shevchuk I, Tepp K,  
Rebane-Klemm E, Timohhina N,  
Terasmaa A and Kaambre T  
(2021) Energy Metabolic  
Plasticity of Colorectal  
Cancer Cells as a Determinant of  
Tumor Growth and Metastasis.  
Front. Oncol. 11:698951.  
doi: 10.3389/fonc.2021.698951

Metabolic plasticity is the ability of the cell to adjust its metabolism to changes in environmental conditions. Increased metabolic plasticity is a defining characteristic of cancer cells, which gives them the advantage of survival and a higher proliferative capacity. Here we review some functional features of metabolic plasticity of colorectal cancer cells (CRC). Metabolic plasticity is characterized by changes in adenine nucleotide transport across the outer mitochondrial membrane. Voltage-dependent anion channel (VDAC) is the main protein involved in the transport of adenine nucleotides, and its regulation is impaired in CRC cells. Apparent affinity for ADP is a functional parameter that characterizes VDAC permeability and provides an integrated assessment of cell metabolic state. VDAC permeability can be adjusted *via* its interactions with other proteins, such as hexokinase and tubulin. Also, the redox conditions inside a cancer cell may alter VDAC function, resulting in enhanced metabolic plasticity. In addition, a cancer cell shows reprogrammed energy transfer circuits such as adenylate kinase (AK) and creatine kinase (CK) pathway. Knowledge of the mechanism of metabolic plasticity will improve our understanding of colorectal carcinogenesis.

**Keywords:** tumor energy metabolism, aerobic glycolysis, oxidative phosphorylation, VDAC, creatine kinase, adenylate kinase, mitochondria

## INTRODUCTION

Analysis of mitochondrial function is central to the study of intracellular energy metabolism and pathophysiological mechanisms of various human diseases, including cancer. The metabolism of cancer cells is adapted to meet their needs to survive and proliferate in a hypoxic and also in a well-oxygenated microenvironment and thus must acquire metabolic flexibility. At the molecular level,

**Abbreviations:** ADP, adenosine diphosphate; AMPK, adenosine 5'-monophosphate-activated protein kinase; AK, adenylate kinase; ANT, adenine nucleotide translocator; CK, creatine kinase; CRC, colorectal cancer; HK, hexokinase; HIF, hypoxia-inducible factor; ISC, iron-sulfur clusters; OMM, outer mitochondrial membrane; TCA, tricarboxylic acid; OXPHOS, oxidative phosphorylation; ROS, reactive oxygen species; VDAC, voltage-dependent anion channel.

metabolic flexibility relies on the configuration of metabolic pathways, which are regulated by key metabolic enzymes and transcription factors. Reprogramming of cellular energetics is recognized as a distinctive hallmark of cancer (1). The first theory on the peculiarities of cancer metabolism was formulated by Otto Warburg in the early 20th century. He concluded that tumors, unlike normal cells, obtain their energy mainly from aerobic glycolysis, while normal cells usually favor oxidative phosphorylation (OXPHOS), which is much more efficient in terms of ATP gain. This observation is coined as the Warburg effect (2, 3) and became the central model for oncobiogenetics for most of the 20<sup>th</sup> century. The glycolytic part of the Warburg hypothesis was firmly and thoroughly confirmed for many cancer types, in contrast to the OXPHOS part, which was and still is a matter of intense research and controversy. Verified evidence indicates that in reality, both anaerobic (glucose to lactate) and aerobic (glucose to pyruvate) glycolysis operate in cancer cells simultaneously like in normal cells, although at higher rates than in non-tumor cells (4). In addition, tumor cells often exhibit high rates of OXPHOS (5, 6). Transcriptomics and end-product metabolites analyses of complex molecular pathways converge into a three-node minimum regulatory network consisting of hypoxia-inducible factor 1 (HIF-1), adenosine monophosphate-activated protein kinase (AMPK), and reactive oxygen species (ROS). Therefore, the coexistence of three distinct cellular metabolic phenotypes is revealed in cancer cells: 1) glycolytic, characterized by high activity of HIF-1 $\alpha$  and high activity of the glycolytic pathway; 2) OXPHOS state, characterized by high activity of AMPK and high activity of OXPHOS pathways such as glucose oxidation and fatty acid oxidation; 3) hybrid metabolic state, characterized by high activity of AMPK and HIF-1 $\alpha$  and concomitant functioning of glycolysis and OXPHOS pathways. In contrast, normal cells exhibit only two metabolic states, namely, glycolytic and OXPHOS, and lack the hybrid state (7, 8). In this regulatory network, HIF-1 and AMPK are the master regulators of glycolysis and OXPHOS, respectively (9), and both cytosolic and mitochondrial ROS mediate the complex interplay between AMPK and HIF-1. Accordingly, the hybrid metabolic state in cancer cells can be promoted by the stabilization of HIF-1 $\alpha$  and elevated production of mitochondrial ROS. Hypoxia activates glycolysis *via* stabilization of HIF-1 $\alpha$  and HIF-2 $\alpha$ , which in turn upregulates the activity of several members of the glycolytic pathway and increases glucose uptake (10, 11). In addition, the elevation of HIF-1 $\alpha$  levels could be induced by high concentrations of succinate (pseudohypoxia) (12). A striking feature of cancer cells is their ability to switch their metabolic phenotypes to glycolysis or OXPHOS in response to changes in their microenvironment or inhibition of one of these pathways, giving survival advantage during tumor progression (8, 13). This metabolic plasticity is promoted by the hybrid phenotype of cancer cells and is linked with metastasis and chemoresistance (14). However, it is still largely unknown how cancer cells regulate gene expression to maintain their hybrid metabolic state and metabolic plasticity.

Implementation of the hybrid metabolism paradigm may reveal new therapeutic targets and opportunities for the treatment of cancer. It was previously shown that administration of glycolytic inhibitors alone may be ineffective to eradicate tumors, and targeting the hybrid state to eliminate metabolic plasticity could be a new therapeutic strategy to eliminate cancer aggressiveness (15, 16). We review the changes in OMM permeability and intracellular energy transfer pathways in connection with the metabolic plasticity of CRC cells.

## METABOLIC REPROGRAMMING OF COLORECTAL CANCER

Colorectal cancer has been regarded as a purely hypoxic tumor of the Warburg phenotype for many years. This was confirmed by increased expression of several glycolytic enzymes, pentose phosphate pathway, and glucose transporters associated with elevated rates of glucose consumption and lactate production as compared with normal surrounding tissues (17–25). Normal colonocytes use the OXPHOS system as the primary energy source (26, 27). Short-chain fatty acids undergo  $\beta$ -oxidation to form acetyl-CoA, which enters into the tricarboxylic acid (TCA) cycle to yield citrate, NADH, and finally ATP. But, unlike normal colonocytes, colorectal carcinomas cannot utilize butyrate as an energy source and carbon donor (26, 28), implying the truncated TCA cycle in CRC. Importantly, some metabolites of the TCA cycle, such as succinate, fumarate, and  $\alpha$ -ketoglutarate, act as “oncometabolites” that support tumor growth *via* oncogenic signaling, *inter alia via* upregulation and stabilization of HIF-1 $\alpha$  (29).

Metabolic reprogramming during large intestine carcinogenesis is largely mediated by (a) altered expression of several oncogenes and a loss of tumor suppressor genes, encoding usually various transcriptional factors and protein kinases (30, 31), (b) adaptation to nutrient and oxygen availability in the local tumor microenvironment (metabolic plasticity) (32), and (c) metabolic cross-talk with stromal, adipose tissue and immune cells (31, 33–37).

Data on molecular mechanisms of the metabolic reprogramming of CRC are mostly obtained from studies using cell culture models, while the number of functional studies using clinical material is limited. Moreover, cell culture conditions have variations that could significantly affect the metabolic profile of the cells. For example, cells grown in glucose-free medium display a relatively high rate of oxygen consumption, while cultivation of cells in a high-glucose medium results in hyperglycolytic profile and declined respiratory flux (38–42). Our recent studies revealed remarkable differences in the regulation of outer mitochondrial membrane (OMM) permeability between cultured tumor cells and clinical material from cancer patients (5, 43). Comparative analysis of the biopsy or surgical cancer material and surrounding healthy tissue showed almost unchanged glycolytic activity and upregulation of OXPHOS in CRC, which is inconsistent with the data obtained by using cell culture (43–47). In addition, two widely

used breast cancer cell lines MCF7 and MCF-MDA-231 failed to replicate mitochondrial function in respect to metabolic activity and OXPHOS as seen in respective human samples (43, 46).

Why the CRC cells shift their metabolism in favor of OXPHOS? Perhaps, under normal conditions, the amount of ATP produced through aerobic glycolysis is insufficient to support cell proliferation and migration. There is a growing body of evidence that CRC is characterized by stimulated mitochondrial biogenesis expressed as an increase in mitochondrial DNA copy number (48) and elevated ADP-dependent oxygen consumption in CRC tissue (5, 6, 43–45). Activated mitochondrial biogenesis can be an adaptive response of tumor cells to overcome the chronic energy crisis caused by glucose starvation or defects in the function of their respiratory enzymes due to pathogenic nuclear or mtDNA mutations (49–51). The elevated lactate level may act as a signaling molecule to affect genes and proteins known to be involved in mitochondrial biogenesis (52), *via* upregulation of AMPK- and SIRT1-associated PGC-1 $\alpha$  activation (53). Nuclear Respiratory Factor 1 (NRF1) (54) and some cytokines, IL-6/8 (55, 56), activate the AMPK signaling pathway as well as apoptotic resistance of cancer cells (56–58). Some types of tumor cells support their high rates of OXPHOS and drug resistance by transferring mtDNA or even the entire mitochondria from surrounding healthy tissues; this intercellular mitochondrial transfer may occur through exosomes or tunnel nanotubes (59, 60). The signaling pathways responsible for the stimulation of mitochondrial biogenesis can have both intracellular and external origins.

## THE ROLE OF VDAC AND THE REGULATION OF OUTER MITOCHONDRIAL MEMBRANE PERMEABILITY IN METABOLIC PLASTICITY

The flux of water-soluble metabolites into and out of the mitochondria occurs through a variety of inner mitochondrial membrane (IMM) carriers, but the flux of ATP, ADP, and Pi across the OMM occurs through a single pathway, the VDAC, and therefore the regulation of OXPHOS is largely mediated by the VDAC permeability control (61). Based on studies of muscle permeabilized fibers, cellular respiration and associated ATP synthesis are regulated by a protein complex called Mitochondrial Interactosome (MI), which is located at the junction of mitochondrial membranes (62, 63). Restrictions for adenine nucleotides in VDAC are evident by measuring an apparent affinity of mitochondria for exogenous ADP [ $K_m$ (ADP)] in permeabilized cells and tissues by using high-resolution respirometry (64, 65). These barriers appear only in permeabilized cells and not in isolated mitochondria and disappear during mild proteolytic treatment with trypsin (66). Therefore, the metabolic plasticity of cancer cells is associated

with the protein-mediated control of VDAC permeability towards ADP.

## Cancer Metabolic Plasticity Is Functionally Defined by Changes in ADP Dependent Oxygen Consumption

Analysis of respirometry data provides instant functional profiling of metabolic plasticity. Dependence of mitochondrial O<sub>2</sub> consumption upon ADP concentration follows Michaelis-Menten kinetics and allows evaluation of apparent Michaelis-Menten constant for ADP  $K_m$ (ADP) in different tissues, cancers, and cell cultures (**Figure 1**). Determined in permeabilized cells and tissues,  $K_m$ (ADP) is the affinity of the mitochondria for exogenous ADP and characterizes permeability of OMM for adenine nucleotides and, thus, VDAC permeability. Measured  $K_m$ (ADP) values for human colon mucosa is ~110  $\mu$ M (47), ~100  $\mu$ M for CRC (5, 44, 47), ~60  $\mu$ M for colon polyps (47), and ~40  $\mu$ M for Caco2 CRC cell line (43), indicating the alteration of control mechanisms over VDAC permeability and OXPHOS during the progression of CRC. Thus, the regulation of OMM permeability to adenine nucleotides in cancer tissues is different from that in normal cells (5, 67, 68). Notably,  $K_m$ (ADP) values measured in cell cultures are much lower than in tissue biopsies and are similar to  $K_m$ (ADP) values for isolated mitochondria (69). This illustrates the shortcomings of cell culture studies and highlights the importance of using clinical material for the evaluation of the mechanism of cancer metabolic plasticity.

The cell-specific differences in  $K_m$ (ADP) are likely caused by the specific structural and functional organization of energy metabolism. For example, cells with a low  $K_m$ (ADP) value (~10  $\mu$ M), like glycolytic muscle, possess less structural and functional restrictions for ADP/ATP movement through OMM as compared to the oxidative muscles ( $K_m$ (ADP) ~300  $\mu$ M) (64). Thus, relatively low  $K_m$ (ADP) for colorectal polyps indicates a metabolic reprogramming towards the glycolytic phenotype with functional OXPHOS (as in glycolytic muscle), and an increase in  $K_m$  values in the CRC reflects a shift to OXPHOS phenotype with increased intracellular complexity (analogy with oxidative muscle). Hence,  $K_m$ (ADP) value is an important parameter describing metabolic plasticity. According to the model proposed by Saks V. et al, the proportion of mitochondria with low oxidative capacity in the tissue can be inferred from the  $K_m$ (ADP) value (70). For example, the proportion of mitochondria with high oxidative capacity is 67% in CRC tumors and only 38% in colorectal polyps (47).

In addition to  $K_m$ (ADP), the maximal ADP-dependent oxygen consumption ( $V_{max}$ ) is a defining characteristic of metabolic plasticity and is correlated to mitochondrial content (density) in the tissue.  $V_{max}$  values are higher in CRC than in normal colon tissue (5, 6, 47), indicating a vigorous metabolic activity. Moreover,  $V_{max}$  values in biopsy material from patients that succumbed to colon cancer were significantly higher than in patients staying in remission (5). However, the extent to which high  $V_{max}$  values correlate with tumor aggressiveness needs to be confirmed in further studies.



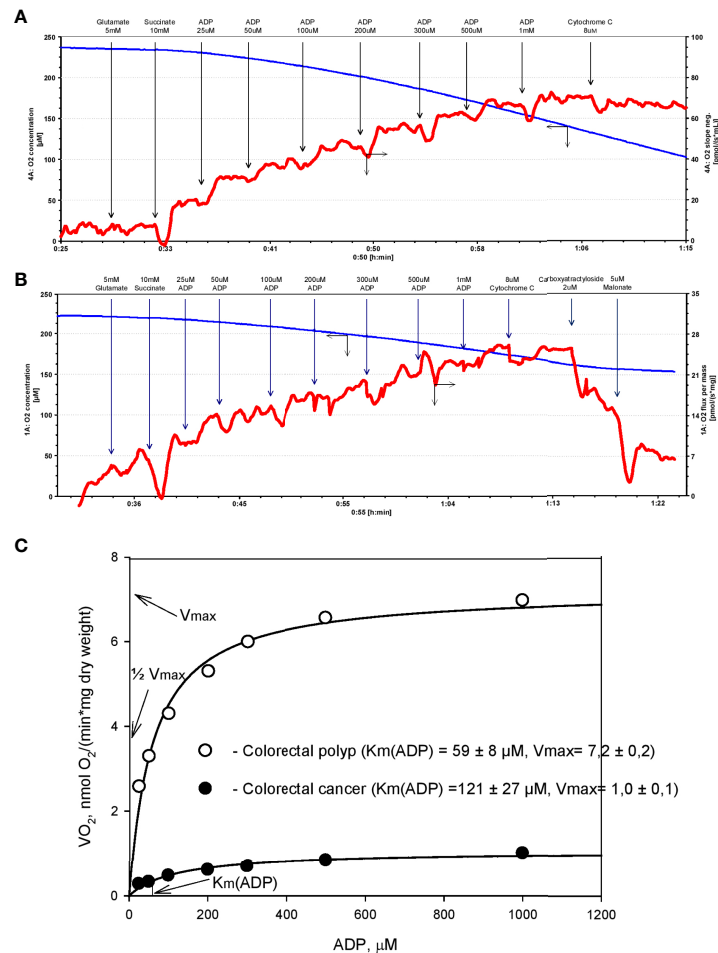


**FIGURE 1** | Michaelis-Menten kinetics of ADP-dependent respiration of human colorectal cancer and polyp biopsy material. Representative tracing of adenosine diphosphate (ADP)-activated oxygen consumptions rates in human permeabilized tissue of **(A)** colorectal polyp and **(B)** and colorectal cancer. **(C)** Corresponding K<sub>m</sub> (ADP) and V<sub>max</sub> values were calculated by non-linear regression using the Michaelis-Menten equation.

## The Possible Mechanisms of VDAC Permeability Regulation

Several studies show that VDAC isoform 1 (VDAC1) is the dominant isoform in most malignant tumors including CRC (44, 71, 72). VDAC1 is crucial in communication between the mitochondria and the cytosol. Cancer cells display high levels of metabolic flexibility combined with apoptosis resistance, which provides a survival advantage for these cells. VDAC1 is well recognized as a metabolic checkpoint at the crossroad of these two processes (72, 73). VDAC mediates and regulates the transport of metabolites, ions, and ROS across OMM. Thus, VDAC1 plays a major role in the control of mitochondrial function. Transport of ADP through OMM is mediated *via* VDAC1 and through the inner membrane *via* ANT. Metabolic control analysis of the OXPHOS system of CRC revealed that ANT does not exert exclusive control over the mitochondrial ADP-dependent oxygen consumption (5, 43). Therefore, the rate-limiting step of ADP transport into the mitochondria appears to be VDAC. Therefore, the alteration of K<sub>m</sub>(ADP)

value depends on the changes in interactions of VDAC1 with other proteins or on the modification of VDAC1 itself.

As the name implies, VDAC is regulated by a change of membrane potential. Studies of isolated VDAC1 reconstituted into planar lipid bilayers reveal sharp and symmetrical voltage dependence of VDAC1 permeability (72, 74, 75). At membrane potentials close to zero (between −20 to +20 mV), VDAC1 is open and displays low anionic selectivity. At more positive or more negative membrane potentials (+30.+60 mV or −30.–60 mV), VDAC1 shows diminished permeability to large anions and becomes more selective to small cations (72). However, it is unknown whether the voltage dependence of VDAC1 is relevant in physiological conditions, as the value of membrane potential across OMM is unknown. It is generally believed that any membrane potential generated at OMM will be offset by a relatively undisturbed movement of small ions across OMM. However, there is a theoretical possibility that OMM can be polarized to potentials large enough to alter the permeability of VDAC1 (2, 3). Although the role of OMM potential in the

regulation of VDAC1 permeability is unlikely, it remains to be investigated whether potential across OMM changes in CRC and whether such change can alter  $K_m(\text{ADP})$ .

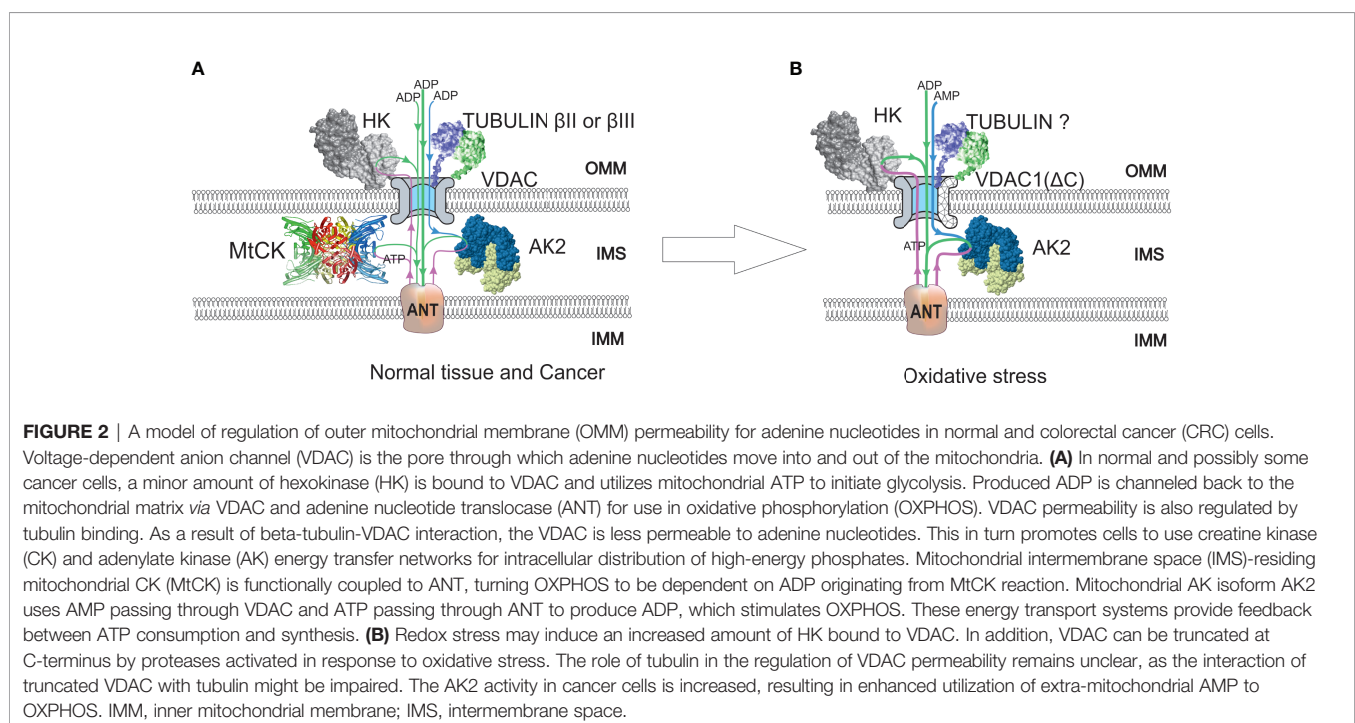
### Hexokinase-VDAC Interaction Regulates the Permeability of VDAC to Adenine Nucleotides

Although the VDAC-hexokinase (HK) binding was demonstrated by several groups using different experimental approaches, it still remains somewhat speculative, and there are different hypothesis on its functional consequences. Research activities of Prof. Pedersen and his colleagues resulted in the discovery of the binding of HK-II to VDAC with the conclusion that this phenomenon could play a pivotal role in the “Warburg Effect” (76–80). Review paper of V. Shoshan-Barmatz et al. proposed the hypothesis that HK-II binds to VDAC and promotes VDAC closing (81). Neumann et al. demonstrated the binding of the cytosolic protein HK-I to VDAC by two-color STED microscopy (82). Our group showed the colocalization of VDAC1 and hexokinase II in cell cultures and clinical cancer samples by confocal microscopy imaging (6, 67). Based on these studies, two models of VDAC permeability control have been proposed. The model proposed by Pedersen et al. states that the binding of HK-II to VDAC plays a pivotal role in maintaining the Warburg phenotype in cancer cells (77, 83). In such a setting, mitochondrial ATP is preferentially directed to glycolysis (HK reaction) and the produced ADP is channeled back to the OXPHOS (Figure 2). At the same time, VDAC is assumed to be in an open state and mitochondria have free access to exogenous ADP (84, 85), thus low  $K_m(\text{ADP})$  values are expected. Glucose-stimulated increase of mitochondrial respiration shows the amount of ADP released in the HK reaction that passes through VDAC and is utilized in

mitochondrial ATP synthesis (86). Such glucose effect comprises a fraction of total ADP-stimulated respiration and is higher in cancer cells as compared to normal cells. Accordingly, the glucose effect is about 20% for CRC tissue, about 12% for normal colon tissue samples (6), and about 48% for Caco-2 CRC cell line (43). These results show that the lower affinity of mitochondria for ADP could be related to the weaker ability for glucose to stimulate respiration. CRC displays elevated levels of VDAC1 as compared with surrounding healthy tissues (43), and this is in good agreement with the fact that  $V_{\max}$  for ADP-dependent respiration is higher in CRC (44). The total HK activity and expression levels of HK1 and HK2 in CRC do not differ from that of normal tissue (6, 44). In both the normal mucosa and the CRC, HK2 is colocalized with VDAC (6, 43). The interaction of HK1 or HK2 with VDAC1 gives numerous advantages to cancer cells: (1) it mediates the increased permeability of the OMM to adenine nucleotides; (2) it increases the rate of aerobic glycolysis and thereby allows the cells to adapt to hypoxic conditions; (3) it mediates elevated resistance to apoptosis and protection from oxidative stress as VDAC1-bound HK acts as an anti-apoptotic protein (73, 87–89). VDAC-HK interaction is reversed with inhibitors of HK2 (e.g., 3-bromopyruvate), and agents that disrupt the VDAC-HK interaction have been tested as anticancer drugs (73, 90–93). It was also reported that silencing of VDAC1 expression by siRNA inhibited the proliferation of several cancer cell lines (including CRC) (94).

### Free Beta-Tubulins Controlling VDAC Permeability in CRC

According to the free-tubulin model, the binding of free tubulin blocks VDAC and thereby regulates respiration (95). The



rationale behind this model is the observation that proliferating cancer cells have high levels of free tubulin for mitotic spindle formation. Free tubulin dimers bound to VDAC induce a closed state of VDAC (**Figure 2**) and cause a suppression of mitochondrial metabolism; thus, aerobic glycolysis will become the main source of energy. Maldonado and Lemasters's group shows at HepG2, A549, and UM-SCC-1 cells that tubulin binding closes the VDAC channel (95). It sounds like the hypothesis in this review contradicts Maldonado's publications (95, 96). However, in fact, the results of both works are in agreement. The amount of dimeric and polymerized tubulin in cells is nearly constant, but the ratio could change significantly. In both cases it is dimeric tubulin, which affects VDAC permeability, but this effect depends on the polymerization state. Also, it should be definitely noted that the regulation of VDAC permeability is tissue specific. Unlike striated muscles, where the main regulator of VDAC is beta-II tubulin (97), in CRC the VDAC and beta-II tubulin colocalization is absent (6). Instead, beta-III tubulin (TUBB3) could be the partner of VDAC in CRC cells. Beta-III tubulin overexpression has been reported in several intestinal cancers like carcinoids of the small intestine and rectal carcinoids (98), gastric cancer (99), colon neoplasias like polyps, and CRC (6, 100). *TUBB3* expression has been associated with the resistance to drugs perturbing the microtubule dynamics (e.g., paclitaxel) and studied as a prognostic biomarker in various cancers (101, 102). It has been demonstrated that in non-small-cell lung cancer, the expression of beta-III tubulin decreases the dependence of cells on glycolysis and thus improves the tumor's ability to cope with the changing nutrient supply in the microenvironment (103). From a functional analysis of the network of proteins forming disulfide bonds with beta-III tubulin, it appears that some of them are involved in oxidative stress and glucose deprivation response (104). It was shown that hypoxia *via* HIF-1 $\alpha$  can induce the expression of *TUBB3* (105). Beta-III tubulin is likely part of a complex pathway induced by hypoxia and shortage of nutrients (101). However, our recent study revealed that microtubule destabilizing (colchicine) and stabilizing (taxol) agents do not affect the  $K_m$ (ADP) in glioblastoma and sarcoma cells (67). Hence, the actual role of beta-tubulins in cancer metabolism and mitochondrial respiratory control needs further investigation.

### Regulation of VDAC1 by Protein-Protein Interactions and Redox Stress

In addition to the two previous models, the modifications of VDAC1 protein induced by oxidative stress could be responsible for alterations of apparent value of  $K_m$ (ADP). Tumor cells are well adapted to a hypoxic environment, and VDAC1 is regulated by oxygen tension in HIF-1 $\alpha$ -dependent manner at the levels of transcription and protein modification. Transcription of the *VDAC1* gene is regulated by HIF-1 $\alpha$  and NRF-1 (nuclear respiratory factor 1), which leads to increased levels of VDAC1 in response to hypoxia or nutrient deprivation of the cells (106). Along with VDAC1 expression regulation, HIF-1 $\alpha$  is also involved in the cleavage of VDAC1, resulting in a truncated form of VDAC1 (107). In normoxic conditions, VDAC1 is

expressed as a full-length protein of molecular weight of approximately 30 kDa, while in response to hypoxia, there is a larger proportion of a shorter VDAC1 variant lacking C-terminal part (VDAC1- $\Delta$ C) with a molecular weight of approximately 25 kDa (107). The shorter variant is a product of the cleavage of VDAC1 at asparagine 214 by the asparagine endopeptidase Legumain (LGMN), which in turn is activated in a HIF-1 $\alpha$ -dependent way upon hypoxia (107). The electrophysiological properties of VDAC1- $\Delta$ C are similar to full-length protein; however, its permeability is slightly reduced (107). Levels of VDAC1- $\Delta$ C were higher in late-stage lung tumors (107), and it was suggested that HIF-1 $\alpha$  mediated induction of VDAC1- $\Delta$ C provides protection from apoptosis and enhances cell survival in hypoxia (107, 108). Hypoxia-induced VDAC1- $\Delta$ C lacks a phosphorylation site at serine 215, and therefore its interaction with tubulin is impaired (108). Notably, *HIF-1 $\alpha$*  overexpression was significantly associated with higher CRC-specific mortality in a cohort of 731 patients (109). Consequently, inhibition of HIF-1 $\alpha$  is proposed as a possible treatment strategy for CRC (110). Moreover, the expression of endopeptidase LGMN is elevated in CRC and is associated with a poor prognosis (111). Furthermore, a meta-analysis revealed the overexpression of *LGMN* to be correlated with the aggressiveness of different cancer types, with higher levels of LGMN in late-stage tumors (112).

It is currently unknown whether VDAC1- $\Delta$ C is present in CRC cells and whether truncation-induced impairment of VDAC1 interaction with tubulin affects apparent affinity for ADP (**Figure 2**). Given the role of tubulin in the regulation of VDAC1 and the discovery of VDAC1- $\Delta$ C in lung cancer, VDAC1 truncation may also play a role in metabolic alterations of CRC. Future studies should reveal whether the truncated form of VDAC1 plays a role in metabolic adaptations of CRC.

Recent studies indicate a link between iron-sulfur cluster (ISC) synthesis and regulation of VDAC1. Biogenesis of ISC is an ancient process, and ISCs are important redox-sensitive cofactors for many enzymes involved in energy homeostasis. Synthesis of ISC starts within the mitochondrial matrix, and depletion of proteins involved in mitochondrial ISC assembly leads to accumulation of VDAC1- $\Delta$ C in normoxic conditions independent of HIF-1 $\alpha$  (113). Depletion of the iron-sulfur cluster containing protein Cisd2 also resulted in the accumulation of truncated VDAC1- $\Delta$ C (113). Therefore, mitochondria-associated membrane-localized Fe-S protein Cisd2 acts as a link between ISC machinery and accumulation of VDAC1- $\Delta$ C (113).

Another iron-sulfur cluster protein, mitoNEET, was found to interact with VDAC1 in a redox-sensitive way (114). MitoNEET harbors [2Fe-2S] cluster and binds to VDAC1 when its cluster is oxidized, thus inhibiting VDAC1 conductivity. Such interaction does not occur when mitoNEET-bound ISC cluster is reduced (114). Therefore, mitoNEET governs VDAC1 permeability in a redox-sensitive way, inhibiting VDAC1 in high redox stress conditions. Oxidative stress is increased in CRC (115); thus, the interaction of mitoNEET with VDAC1 can be altered in CRC.

It remains to be investigated whether such redox-sensitive mitoNEET-VDAC1 interaction can alter the apparent  $K_m$  (ADP) value and is involved in the metabolic plasticity of CRC.

There is a large number of proteins that were found to interact with VDAC1 and are therefore potentially able to modulate VDAC permeability. Interacting partners of VDAC1 are involved in the regulation of apoptosis (Bax, Bcl2, Bak, etc.), energy metabolism (HK1, HK2, ACSL, CPT1, ANT, etc.), cytoskeletal organization (Tubulin, actin, dynein, etc.), and other cellular functions [Parkin, alpha-synuclein, APP, gamma-secretase] [reviewed in (116)]. However, the role of these interactions in the modulation of cellular respiration needs to be further investigated.

## ENERGY TRANSPORT PATHWAYS IN CRC CELLS—THE PARTICIPANTS IN THE METABOLIC PLASTICITY

In addition to the altered transport of adenine nucleotides through OMM alterations of energy transport circuits formed from creatine kinase (CK) and adenylate kinase (AK) isoenzymes are also involved in the development of metabolic plasticity. Cancer cells have uncontrolled cell division, which is accompanied by a high energy need for anabolic processes and large cell structure rearrangements. Therefore, it is hypothesized that energy transport pathways are also reprogrammed in cancer cells to meet these demands. Previous data show downregulation of the CK pathway and mitochondrial CK (MtCK) in CRC cells, which results in functional uncoupling between the CK circuit and OXPHOS (6, 44). In contrast, total AK activity is higher in CRC than in normal intestinal tissue, and it also reflects enhanced coupling between AK and OXPHOS (i.e., AMP can affect the rate of oxygen consumption) (Figure 2) (6, 44). This is in agreement with the observation that expression of AK mitochondrial isoform AK2 is increased in several cancers including lung adenocarcinoma (117) and breast cancer (118, 119). Also, there is evidence that another mitochondrial isoform, AK4, is involved in the regulation of mitochondrial metabolism in cancer cells. In HeLa cells, AK4 forms complexes with ANT, VDAC, and HK2 for the efficient recycling of ADP (120). Further, AK4 expression is induced by hypoxia, and protein complex AK4-ANT-VDAC-HK2 complex supports the high glycolytic activity of cancer cells (120). Intestinal cells are able to switch off the CK circuit and turn on the AK pathway to establish metabolic plasticity. Such flexibility of phosphotransfer networks in Caco2 CRC cell lines depends on the availability of key metabolic substrates and is associated with the cell differentiation state (121). The abovementioned data indicate a possible role of the phosphotransfer networks related to the regulation of VDAC permeability for adenine nucleotides and metabolic plasticity.

The function of energy transfer pathways is well characterized in striated muscle cells where its role is to overcome the diffusion restrictions for ATP and ADP, thereby directing the energy-rich phosphate groups to the CK, AK, and glycolytic energy transfer circuits. This way of energy transfer allows the formation of micro-compartments at energy consumption sites where high ATP/ADP levels are maintained for maximal performance.

Similarly, in the compartment where energy is produced (e.g., mitochondrial membranes), favorable levels of ADP are maintained to ensure efficient ATP synthesis [reviewed in (65, 122)]. In the case of CRC, downregulation of MtCK leads to the inability to produce phosphocreatine and a loss of functional coupling between the VDAC-MtCK-ANT complex, accompanied by the formation of other regulating combinations like VDAC-HK-ANT. In this aspect, more studies are required to determine the profile of HK, AK, ANT, and VDAC isoform expression in human CRC.

In addition to their role in energy transfer among cellular processes, AKs are an integral part of intracellular energy sensing and metabolic signaling (123, 124). Due to its catalytic reaction ( $2\text{ADP} \leftrightarrow \text{AMP} + \text{ATP}$ ), it can amplify a small change in the ATP/ADP ratio into relatively large changes in AMP concentration. This relates AKs to the activation of cellular AMP-sensitive components like AMPK. In general, activation of AMPK switches on catabolic pathways that generate ATP, while switching off biosynthetic pathways and cell-cycle progress (125). The role of AMPK in cancer is controversial; it has been recognized as a tumor suppressor in some cancers (126–129) and in some cases described as a contextual oncogene, as the AMPK activation promotes tumor progression and chemoresistance (130–132). Downregulation of  $\text{AK} \rightarrow \text{AMP} \rightarrow \text{AMPK}$  signaling could lead to loss of control over the cell cycle, growth, and proliferation (124). A recent in-depth review about AKs and metabolic signaling in cancer cells by Klepinin et al. (124) highlights the role of suppression of AK phosphotransfer and signaling through AMPK as a potential target for cancer metabolism. How different AK isoforms are distributed in CRC cells and how their activities affect AMPK activation and metabolic plasticity need further investigation.

Adenylate kinases network promotes cancer growth and metastasis through participating in AMPK metabolic signaling and regulating mitochondrial adenine nucleotide exchange.

## CONCLUSION AND PROSPECTS

Metabolic plasticity is a defining characteristic of the cancer cells that allow undisturbed proliferation in changing environment. At the functional level, different metabolic states of the cancer cells can be identified and characterized by measuring the dependence of mitochondrial respiration upon ADP concentration using the classical Michaelis-Menten kinetic model. The apparent affinity of ADP provides an integrated assessment of cell metabolic state, which is functionally determined by the permeability of VDAC1. Regulation of VDAC1 involves many protein-protein interactions, as well as hypoxia- and redox-sensitive mechanisms. The regulation of OMM permeability for adenine nucleotides is presumably more complex than the binding between the VDAC1 channel and some single type of protein molecule. Unraveling the molecular mechanisms of metabolic plasticity will reveal new therapeutic targets for the development of novel cancer treatments. This knowledge combined with relatively simple



functional evaluation of cancer metabolism in biopsy material can form a new prospect for personalized medicine.

## AUTHOR CONTRIBUTIONS

Conceptualization, LT, MP, AT, and TK. Funding acquisition, TK. Project administration, AT and TK. Visualization, LR and IS. Writing—original draft, MP, AT, VC, and TK. Writing—

review and editing, LR, SM, ER-K, NT, KT, IS, and TK. All authors contributed to the article and approved the submitted version.

## FUNDING

This work was supported by the Estonian Research Council grant PRG1035 and NICPB institutional Development Fund grant.

## REFERENCES

- Hanahan D, Weinberg RA. Hallmarks of Cancer: The Next Generation. *Cell* (2011) 144(5):646–74. doi: 10.1016/j.cell.2011.02.013
- Lemeshko SV, Lemeshko VV. Metabolically Derived Potential on the Outer Membrane of Mitochondria: A Computational Model. *Biophys J* (2000) 79(6):2785–800. doi: 10.1016/S0006-3495(00)76518-0
- Lemeshko VV. Model of the Outer Membrane Potential Generation by the Inner Membrane of Mitochondria. *Biophys J* (2002) 82(2):684–92. doi: 10.1016/S0006-3495(02)75431-3
- Moreno-Sanchez R, Marin-Hernandez A, Saavedra E, Pardo JP, Ralph SJ, Rodriguez-Enriquez S. Who Controls the ATP Supply in Cancer Cells? Biochemistry Lessons to Understand Cancer Energy Metabolism. *Int J Biochem Cell Biol* (2014) 50:10–23. doi: 10.1016/j.biocel.2014.01.025
- Koiti A, Shevchuk I, Ounpuu L, Klepinin A, Chekulayev V, Timohhina N, et al. Mitochondrial Respiration in Human Colorectal and Breast Cancer Clinical Material Is Regulated Differently. *Oxid Med Cell Longev* (2017) 2017:1372640. doi: 10.1155/2017/1372640
- Kaldma A, Klepinin A, Chekulayev V, Mado K, Shevchuk I, Timohhina N, et al. An *in Situ* Study of Bioenergetic Properties of Human Colorectal Cancer: The Regulation of Mitochondrial Respiration and Distribution of Flux Control Among the Components of ATP Synthasome. *Int J Biochem Cell Biol* (2014) 55:171–86. doi: 10.1016/j.biocel.2014.09.004
- Yu L, Lu M, Jia D, Ma J, Ben-Jacob E, Levine H, et al. Modeling the Genetic Regulation of Cancer Metabolism: Interplay Between Glycolysis and Oxidative Phosphorylation. *Cancer Res* (2017) 77(7):1564–74. doi: 10.1158/0008-5472.CAN-16-2074
- Paudel BB, Quaranta V. Metabolic Plasticity Meets Gene Regulation. *Proc Natl Acad Sci USA* (2019) 116(9):3370–2. doi: 10.1073/pnas.1900169116
- Vander Heiden MG, Cantley LC, Thompson CB. Understanding the Warburg Effect: The Metabolic Requirements of Cell Proliferation. *Science* (2009) 324(5930):1029–33. doi: 10.1126/science.1160809
- Libby CJ, McConathy J, Darley-Usmar V, Hjelmeland AB. The Role of Metabolic Plasticity in Blood and Brain Stem Cell Pathophysiology. *Cancer Res* (2020) 80(1):5–16. doi: 10.1158/0008-5472.CAN-19-1169
- Berridge MV, Herst PM, Tan AS. Metabolic Flexibility and Cell Hierarchy in Metastatic Cancer. *Mitochondrion* (2010) 10(6):584–8. doi: 10.1016/j.mito.2010.08.002
- Garrigue P, Bodin-Hullin A, Balasse L, Fernandez S, Essamet W, Dignat-George F, et al. The Evolving Role of Succinate in Tumor Metabolism: An (18)F-FDG-Based Study. *J Nucl Med* (2017) 58(11):1749–55. doi: 10.2967/jnumed.117.192674
- Lin Y, Ma C, Bezabeh T, Wang Z, Liang J, Huang Y, et al. 1h NMR-Based Metabolomics Reveal Overlapping Discriminatory Metabolites and Metabolic Pathway Disturbances Between Colorectal Tumor Tissues and Fecal Samples. *Int J Cancer* (2019) 145(6):1679–89. doi: 10.1002/ijc.32190
- Jia D, Park JH, Jung KH, Levine H, Kaiparettu BA. Elucidating the Metabolic Plasticity of Cancer: Mitochondrial Reprogramming and Hybrid Metabolic States. *Cells* (2018) 7(3):21. doi: 10.3390/cells7030021
- Jia D, Lu M, Jung KH, Park JH, Yu L, Onuchic JN, et al. Elucidating Cancer Metabolic Plasticity by Coupling Gene Regulation With Metabolic Pathways. *Proc Natl Acad Sci* (2019) 116(9):3909–18. doi: 10.1073/pnas.1816391116
- Sotgia F, Ozsvari B, Fiorillo M, De Francesco EM, Bonuccelli G, Lisanti MP. A Mitochondrial Based Oncology Platform for Targeting Cancer Stem Cells (CSCs): MITO-ONC-Rx. *Cell Cycle* (2018) 17(17):2091–100. doi: 10.1080/15384101.2018.1515551
- Altenberg B, Greulich KO. Genes of Glycolysis Are Ubiquitously Overexpressed in 24 Cancer Classes. *Genomics* (2004) 84(6):1014–20. doi: 10.1016/j.ygeno.2004.08.010
- Kawada K, Toda K, Nakamoto Y, Iwamoto M, Hatano E, Chen FS, et al. Relationship Between F-18-FDG PET/CT Scans and KRAS Mutations in Metastatic Colorectal Cancer. *J Nucl Med* (2015) 56(9):1322–7. doi: 10.2967/jnumed.115.160614
- Iwamoto M, Kawada K, Nakamoto Y, Itatani Y, Inamoto S, Toda K, et al. Regulation of 18F-FDG Accumulation in Colorectal Cancer Cells With Mutated KRAS. *J Nucl Med* (2014) 55(12):2038–44. doi: 10.2967/jnumed.114.142927
- Rubie C, Kempf K, Hans J, Su T, Tilton B, Georg T, et al. Housekeeping Gene Variability in Normal and Cancerous Colorectal, Pancreatic, Esophageal, Gastric and Hepatic Tissues. *Mol Cell Probes* (2005) 19(2):101–9. doi: 10.1016/j.mcp.2004.10.001
- Shonk CE, Arison RN, Koven BJ, Majima H, Boxer GE. Enzyme Patterns in Human Tissues. 3. Glycolytic Enzymes in Normal and Malignant Tissues of the Colon and Rectum. *Cancer Res* (1965) 25:206–13.
- Hennipman A, Smits J, van Oirschot B, van Houwelingen JC, Rijkse G, Neyt JP, et al. Glycolytic Enzymes in Breast Cancer, Benign Breast Disease and Normal Breast Tissue. *Tumor Biol* (1987) 8(5):251–63. doi: 10.1159/000217529
- Hennipman A, van Oirschot BA, Smits J, Rijkse G, Staal GEJ. Glycolytic Enzyme Activities in Breast Cancer Metastases. *Tumor Biol* (1988) 9(5):241–8. doi: 10.1159/000217568
- Groheux D, Cochet A, Humbert O, Alberini J-L, Hindie E, Mankoff D. 18F-FDG PET/CT for Staging and Restaging of Breast Cancer. *J Nucl Med* (2016) 57(Supplement 1):17S–26S. doi: 10.2967/jnumed.115.157859
- Hirayama A, Kami K, Sugimoto M, Sugawara M, Toki N, Onozuka H, et al. Quantitative Metabolome Profiling of Colon and Stomach Cancer Microenvironment by Capillary Electrophoresis Time-of-Flight Mass Spectrometry. *Cancer Res* (2009) 69(11):4918–25. doi: 10.1158/0008-5472.CAN-08-4806
- Donohoe DR, Garge N, Zhang X, Sun W, O'Connell TM, Bunger MK, et al. The Microbiome and Butyrate Regulate Energy Metabolism and Autophagy in the Mammalian Colon. *Cell Metab* (2011) 13(5):517–26. doi: 10.1016/j.cmet.2011.02.018
- Fleming SE, Fitch MD, DeVries S, Liu ML, Kight C. Nutrient Utilization by Cells Isolated From Rat Jejunum, Cecum and Colon. *J Nutr* (1991) 121(6):869–78. doi: 10.1093/jn/121.6.869
- Donohoe DR, Collins LB, Wali A, Bigler R, Sun W, Bultman SJ. : The Warburg Effect Dictates the Mechanism of Butyrate-Mediated Histone Acetylation and Cell Proliferation. *Mol Cell* (2012) 48(4):612–26. doi: 10.1016/j.molcel.2012.08.033
- Martinez-Reyes I, Chandel NS. Mitochondrial TCA Cycle Metabolites Control Physiology and Disease. *Nat Commun* (2020) 11(1):102. doi: 10.1038/s41467-019-13668-3
- Rodriguez-Enriquez S, Marin-Hernandez A, Gallardo-Perez JC, Pacheco-Velazquez SC, Belmont-Diaz JA, Robledo-Cadena DX, et al. Transcriptional Regulation of Energy Metabolism in Cancer Cells. *Cells* (2019) 8(10):1225. doi: 10.3390/cells8101225

31. Neitzel C, Demuth P, Wittmann S, Fahrer J. Targeting Altered Energy Metabolism in Colorectal Cancer: Oncogenic Reprogramming, the Central Role of the TCA Cycle and Therapeutic Opportunities. *Cancers (Basel)* (2020) 12(7):1731. doi: 10.3390/cancers12071731
32. Epstein T, Gatenby RA, Brown JS. The Warburg Effect as an Adaptation of Cancer Cells to Rapid Fluctuations in Energy Demand. *PLoS One* (2017) 12(9):e0185085–e0185085. doi: 10.1371/journal.pone.0185085
33. Brown RE, Short SP, Williams CS. Colorectal Cancer and Metabolism. *Curr Colorectal Cancer Rep* (2018) 14(6):226–41. doi: 10.1007/s11888-018-0420-y
34. Gandhi N, Das MG. Metabolic Reprogramming in Breast Cancer and Its Therapeutic Implications. *Cells* (2019) 8(2):89. doi: 10.3390/cells8020089
35. Dai C, Arceo J, Arnold J, Sreekumar A, Dovichi NJ, Li J, et al. Metabolomics of Oncogene-Specific Metabolic Reprogramming During Breast Cancer. *Cancer Metab* (2018) 6:5. doi: 10.1186/s40170-018-0175-6
36. D'Esposito V, Ambrosio MR, Giuliano M, Cabaro S, Miele C, Beguinot F, et al. Mammary Adipose Tissue Control of Breast Cancer Progression: Impact of Obesity and Diabetes. *Front Oncol* (2020) 10(1554):1554. doi: 10.3389/fonc.2020.01554
37. Tian W, Zhang W, Zhang Y, Zhu T, Hua Y, Li H, et al. FABP4 Promotes Invasion and Metastasis of Colon Cancer by Regulating Fatty Acid Transport. *Cancer Cell Int* (2020) 20(1):512. doi: 10.1186/s12935-020-01582-4
38. Swerdlow RH, L E, Aires D, Lu J. Glycolysis-Respiration Relationships in a Neuroblastoma Cell Line. *Biochim Biophys Acta* (2013) 1830(4):2891–8. doi: 10.1016/j.bbagen.2013.01.002
39. Jose C, Rossignol R. Rationale for Mitochondria-Targeting Strategies in Cancer Bioenergetic Therapies. *Int J Biochem Cell Biol* (2013) 45(1):123–9. doi: 10.1016/j.biocel.2012.07.005
40. Gnaiger E, Kemp RB. Anaerobic Metabolism in Aerobic Mammalian Cells: Information From the Ratio of Calorimetric Heat Flux and Respirimetric Oxygen Flux. *Biochim Biophys Acta* (1990) 1016(3):328–32. doi: 10.1016/0005-2728(90)90164-y
41. Gstraunthaler G, Seppi T, Pfaller W. Impact of Culture Conditions, Culture Media Volumes, and Glucose Content on Metabolic Properties of Renal Epithelial Cell Cultures. Are Renal Cells in Tissue Culture Hypoxic? *Cell Physiol Biochem* (1999) 9(3):150–72. doi: 10.1159/000016312
42. Sherr CJ, DePinho RA. Cellular Senescence: Mitotic Clock or Culture Shock? *Cell* (2000) 102(4):407–10. doi: 10.1016/s0092-8674(00)00046-5
43. Ounpuu L, Truu L, Shevchuk I, Chekulayev V, Klepinin A, Koit A, et al. Comparative Analysis of the Bioenergetics of Human Adenocarcinoma Caco-2 Cell Line and Postoperative Tissue Samples From Colorectal Cancer Patients. *Biochem Cell Biol* (2018) 96(6):808–17. doi: 10.1139/bcb-2018-0076
44. Chekulayev V, Mado K, Shevchuk I, Koit A, Kaldma A, Klepinin A, et al. Metabolic Remodeling in Human Colorectal Cancer and Surrounding Tissues: Alterations in Regulation of Mitochondrial Respiration and Metabolic Fluxes. *Biochem Biophys Rep* (2015) 4:111–25. doi: 10.1016/j.bbrep.2015.08.020
45. Kaambre T, Chekulayev V, Shevchuk I, Karu-Varikmaa M, Timohhina N, Tepp K, et al. Metabolic Control Analysis of Cellular Respiration *In Situ* in Intraoperative Samples of Human Breast Cancer. *J Bioenerg Biomembr* (2012) 44(5):539–58. doi: 10.1007/s10863-012-9457-9
46. Koit A, Timohhina N, Truu L, Chekulayev V, Gudlawar S, Shevchuk I, et al. Metabolic and OXPHOS Activities Quantified by Temporal Ex Vivo Analysis Display Patient-Specific Metabolic Vulnerabilities in Human Breast Cancers. *Front Oncol* (2020) 10:1053. doi: 10.3389/fonc.2020.01053
47. Rebane-Klemm E, Truu L, Reinsalu L, Puurand M, Shevchuk I, Chekulayev V, et al. Mitochondrial Respiration in KRAS and BRAF Mutated Colorectal Tumors and Polyps. *Cancers (Basel)* (2020) 12(4):815. doi: 10.3390/cancers12040815
48. Feng S, Xiong LL, Ji ZN, Cheng W, Yang HJ. Correlation Between Increased Copy Number of Mitochondrial DNA and Clinicopathological Stage in Colorectal Cancer. *Oncol Lett* (2011) 2(5):899–903. doi: 10.3892/ol.2011.322
49. Richter C, Gogvadze V, Laffranchi R, Schlapbach R, Schweizer M, Suter M, et al. Oxidants in Mitochondria: From Physiology to Diseases. *Biochim Biophys Acta* (1995) 1271(1):67–74. doi: 10.1016/0925-4439(95)00012-S
50. Lee HC, Yin PH, Chi CW, Wei YH. Increase in Mitochondrial Mass in Human Fibroblasts Under Oxidative Stress and During Replicative Cell Senescence. *J BioMed Sci* (2002) 9(6 Pt 1):517–26. doi: 10.1007/BF02254978
51. Lee HC, Yin PH, Lu CY, Chi CW, Wei YH. Increase of Mitochondria and Mitochondrial DNA in Response to Oxidative Stress in Human Cells. *Biochem J* (2000) 348 Pt 2:425–32. doi: 10.1042/bj3480425
52. Genders AJ, Martin SD, McGee SL, Bishop DJ. A Physiological Drop in pH Decreases Mitochondrial Respiration, and HDAC and Akt Signaling, in L6 Myocytes. *Am J Physiol Cell Physiol* (2019) 316(3):C404–14. doi: 10.1152/ajpcell.00214.2018
53. Canto C, Auwerx J. PGC-1alpha, SIRT1 and AMPK, an Energy Sensing Network That Controls Energy Expenditure. *Curr Opin Lipidol* (2009) 20(2):98–105. doi: 10.1097/MOL.0b013e328328d0a4
54. Das KJ, Felty Q, Poppiti R, Jackson MR, Roy D. Nuclear Respiratory Factor 1 Acting as an Oncoprotein Drives Estrogen-Induced Breast Carcinogenesis. *Cells* (2018) 7(12):234. doi: 10.3390/cells7120234
55. Wang G, Wang Q, Huang Q, Chen Y, Sun X, He L, et al. Upregulation of mtSSB by Interleukin-6 Promotes Cell Growth Through Mitochondrial Biogenesis-Mediated Telomerase Activation in Colorectal Cancer. *Int J Cancer* (2018) 144:2516–28. doi: 10.1002/ijc.31978
56. Kumari N, Dwarakanath BS, Das A, Bhatt AN. Role of Interleukin-6 in Cancer Progression and Therapeutic Resistance. *Tumor Biol* (2016) 37(9):11553–72. doi: 10.1007/s13277-016-5098-7
57. Kumari N, Das A, Bhatt AN. Interleukin-6 Confers Radio-Resistance by Inducing Akt-Mediated Glycolysis and Reducing Mitochondrial Damage in Cells. *J Biochem* (2019) 167(3):303–14. doi: 10.1093/jb/mvz091
58. Ham I-H, Oh HJ, Jin H, Bae CA, Jeon S-M, Choi KS, et al. Targeting Interleukin-6 as a Strategy to Overcome Stroma-Induced Resistance to Chemotherapy in Gastric Cancer. *Mol Cancer* (2019) 18(1):68. doi: 10.1186/s12943-019-0972-8
59. Berridge MV, McConnell MJ, Grasso C, Bajzikova M, Kovarova J, Neuzil J. Horizontal Transfer of Mitochondria Between Mammalian Cells: Beyond Co-Culture Approaches. *Curr Opin Genet Dev* (2016) 38:75–82. doi: 10.1016/j.gde.2016.04.003
60. Sahinbegovic H, Jelinek T, Hrdinka M, Bago JR, Turi M, Sevcikova T, et al. Intercellular Mitochondrial Transfer in the Tumor Microenvironment. *Cancers (Basel)* (2020) 12(7):1787. doi: 10.3390/cancers12071787
61. Lemasters JJ, Holmuhamedov E. Voltage-Dependent Anion Channel (VDAC) as Mitochondrial Governor—Thinking Outside the Box. *Biochim Biophys Acta* (2006) 1762(2):181–90. doi: 10.1016/j.bbadis.2005.10.006
62. Guzun R, Kaambre T, Bagur R, Grichine A, Usson Y, Varikmaa M, et al. Modular Organization of Cardiac Energy Metabolism: Energy Conversion, Transfer and Feedback Regulation. *Acta Physiol (Oxf)* (2015) 213(1):84–106. doi: 10.1111/apha.12287
63. Saks V, Guzun R, Timohhina N, Tepp K, Varikmaa M, Monge C, et al. Structure-Function Relationships in Feedback Regulation of Energy Fluxes *In Vivo* in Health and Disease: Mitochondrial Interactosome. *Biochim Biophys Acta* (2010) 1797(6-7):678–97. doi: 10.1016/j.bbabi.2010.01.011
64. Kuznetsov AV, Tiivel T, Sikk P, Kaambre T, Kay L, Daneshrad Z, et al. Striking Differences Between the Kinetics of Regulation of Respiration by ADP in Slow-Twitch and Fast-Twitch Muscles *In Vivo*. *Eur J Biochem* (1996) 241(3):909–15. doi: 10.1111/j.1432-1033.1996.00909.x
65. Puurand M, Tepp K, Klepinin A, Klepinina L, Shevchuk I, Kaambre T. Intracellular Energy-Transfer Networks and High-Resolution Respirometry: A Convenient Approach for Studying Their Function. *Int J Mol Sci* (2018) 19(10):2933. doi: 10.3390/ijms19102933
66. Kay L, Li Z, Mericksay M, Olivares J, Tranqui L, Fontaine E, et al. Study of Regulation of Mitochondrial Respiration *In Vivo*. An Analysis of Influence of ADP Diffusion and Possible Role of Cytoskeleton. *Biochim Biophys Acta* (1997) 1322(1):41–59. doi: 10.1016/s0005-2728(97)00071-6
67. Klepinin A, Ounpuu L, Mado K, Truu L, Chekulayev V, Puurand M, et al. The Complexity of Mitochondrial Outer Membrane Permeability and VDAC Regulation by Associated Proteins. *J Bioenerg Biomembr* (2018) 50(5):339–54. doi: 10.1007/s10863-018-9765-9
68. Puurand M, Tepp K, Timohhina N, Aid J, Shevchuk I, Chekulayev V, et al. Tubulin betaII and betaIII Isoforms as the Regulators of VDAC Channel Permeability in Health and Disease. *Cells* (2019) 8(3):239. doi: 10.3390/cells8030239

69. Saks VA, Belikova YO, Kuznetsov AV. *In Vivo* Regulation of Mitochondrial Respiration in Cardiomyocytes: Specific Restrictions for Intracellular Diffusion of ADP. *Biochim Biophys Acta* (1991) 1074(2):302–11. doi: 10.1016/0304-4165(91)90168-g
70. Saks VA, Veksler VI, Kuznetsov AV, Kay L, Sikk P, Tiivel T, et al. Permeabilized Cell and Skinned Fiber Techniques in Studies of Mitochondrial Function *In Vivo*. *Mol Cell Biochem* (1998) 184(1-2):81–100. doi: 10.1023/A:1006834912257
71. Messina A, Reina S, Guarino F, De Pinto V. VDAC Isoforms in Mammals. *Biochim Biophys Acta (BBA) - Biomembr* (2012) 1818(6):1466–76. doi: 10.1016/j.bbame.2011.10.005
72. Shoshan-Barmatz V, Mizrahi D. VDAC1: From Structure to Cancer Therapy. *Front Oncol* (2012) 2:164. doi: 10.3389/fonc.2012.00164
73. Shoshan-Barmatz V, Ben-Hail D, Admoni L, Krelin Y, Tripathi SS. The Mitochondrial Voltage-Dependent Anion Channel 1 in Tumor Cells. *Biochim Biophys Acta (BBA) - Biomembr* (2015) 1848(10, Part B):2547–75. doi: 10.1016/j.bbame.2014.10.040
74. Mangan PS, Colombini M. Ultrastep Voltage Dependence in a Membrane Channel. *Proc Natl Acad Sci* (1987) 84(14):4896. doi: 10.1073/pnas.84.14.4896
75. Colombini M, Mannella CA. VDAC, The Early Days. *Biochim Biophys Acta (BBA) - Biomembr* (2012) 1818(6):1438–43. doi: 10.1016/j.bbame.2011.11.014
76. Mathupala SP, Ko YH, Pedersen PL. Hexokinase II: Cancer's Double-Edged Sword Acting as Both Facilitator and Gatekeeper of Malignancy When Bound to Mitochondria. *Oncogene* (2006) 25(34):4777–86. doi: 10.1038/sj.onc.1209603
77. Pedersen PL, Warburg, Me and Hexokinase 2: Multiple Discoveries of Key Molecular Events Underlying One of Cancers' Most Common Phenotypes, the "Warburg Effect", I.e., elevated glycolysis in the presence of oxygen. *J Bioenerg Biomembr* (2007) 39(3):211–22. doi: 10.1007/s10863-007-9094-x
78. Pedersen PL. The Cancer Cell's "Power Plants" as Promising Therapeutic Targets: An Overview. *J Bioenerg Biomembr* (2007) 39(1):1–12. doi: 10.1007/s10863-007-9070-5
79. Mathupala SP, Ko YH, Pedersen PL. Hexokinase-2 Bound to Mitochondria: Cancer's Stygian Link to the "Warburg Effect" and a Pivotal Target for Effective Therapy. *Semin Cancer Biol* (2009) 19(1):17–24. doi: 10.1016/j.semcancer.2008.11.006
80. Mathupala SP, Pedersen PL. Voltage Dependent Anion Channel-1 (VDAC-1) as an Anti-Cancer Target. *Cancer Biol Ther* (2010) 9(12):1053–6. doi: 10.4161/cbt.9.12.12451
81. Shoshan-Barmatz V, Maldonado EN, Krelin Y. VDAC1 at the Crossroads of Cell Metabolism, Apoptosis and Cell Stress. *Cell Stress* (2017) 1(1):11–36. doi: 10.15698/cst2017.10.104
82. Neumann D, Buckers J, Kastrop L, Hell SW, Jakobs S. Two-Color STED Microscopy Reveals Different Degrees of Colocalization Between Hexokinase-I and the Three Human VDAC Isoforms. *PMC Biophys* (2010) 3(1):4. doi: 10.1186/1757-5036-3-4
83. Pedersen PL, Mathupala S, Rempel A, Geschwind JF, Ko YH. Mitochondrial Bound Type II Hexokinase: A Key Player in the Growth and Survival of Many Cancers and an Ideal Prospect for Therapeutic Intervention. *Biochim Biophys Acta* (2002) 1555(1-3):14–20. doi: 10.1016/S0005-2728(02)00248-7
84. Rostovtseva TK, Tan W, Colombini M. On the Role of VDAC in Apoptosis: Fact and Fiction. *J Bioenerg Biomembr* (2005) 37(3):129–42. doi: 10.1007/s10863-005-6566-8
85. Majewski N, Nogueira V, Bhaskar P, Coy PE, Skeen JE, Gottlob K, et al. Hexokinase-Mitochondria Interaction Mediated by Akt Is Required to Inhibit Apoptosis in the Presence or Absence of Bax and Bak. *Mol Cell* (2004) 16(5):819–30. doi: 10.1016/j.molcel.2004.11.014
86. Eimre M, Paju K, Pelloux S, Beraud N, Roosimaa M, Kadaja L, et al. Distinct Organization of Energy Metabolism in HL-1 Cardiac Cell Line and Cardiomyocytes. *Biochim Biophys Acta* (2008) 1777(6):514–24. doi: 10.1016/j.bbabo.2008.03.019
87. Ahmad A, Ahmad S, Schneider BK, Allen CB, Chang LY, White CW. Elevated Expression of Hexokinase II Protects Human Lung Epithelial-Like A549 Cells Against Oxidative Injury. *Am J Physiol Lung Cell Mol Physiol* (2002) 283(3):L573–84. doi: 10.1152/ajplung.00410.2001
88. Zaid H, Abu-Hamad S, Israelson A, Nathan I, Shoshan-Barmatz V. The Voltage-Dependent Anion Channel-1 Modulates Apoptotic Cell Death. *Cell Death Differ* (2005) 12(7):751–60. doi: 10.1038/sj.cdd.4401599
89. Pastorino J, Hoek J. Regulation of Hexokinase Binding to VDAC. *J Bioenerg Biomembr* (2008) 40(3):171–82. doi: 10.1007/s10863-008-9148-8
90. Wei L, Zhou Y, Dai Q, Qiao C, Zhao L, Hui H, et al. Oroxynin A Induces Dissociation of Hexokinase II From the Mitochondria and Inhibits Glycolysis by SIRT3-Mediated Deacetylation of Cyclophilin D in Breast Carcinoma. *Cell Death Dis* (2013) 4:e601. doi: 10.1038/cddis.2013.131
91. Ikeda S, Abe F, Matsuda Y, Kitadate A, Takahashi N, Tagawa H. Hypoxia-Inducible Hexokinase-2 Enhances Anti-Apoptotic Function via Activating Autophagy in Multiple Myeloma. *Cancer Sci* (2020) 111:4088–101. doi: 10.1111/cas.14614
92. Fan T, Sun G, Sun X, Zhao L, Zhong R, Peng Y. Tumor Energy Metabolism and Potential of 3-Bromopyruvate as an Inhibitor of Aerobic Glycolysis: Implications in Tumor Treatment. *Cancers (Basel)* (2019) 11(3):317. doi: 10.3390/cancers11030317
93. Woldetsadik AD, Vogel MC, Rabeh WM, Magzoub M. Hexokinase II-derived Cell-Penetrating Peptide Targets Mitochondria and Triggers Apoptosis in Cancer Cells. *FASEB J* (2017) 31(5):2168–84. doi: 10.1096/fj.201601173R
94. Arif T, Vasilkovsky L, Refaely Y, Konson A, Shoshan-Barmatz V. Silencing VDAC1 Expression by siRNA Inhibits Cancer Cell Proliferation and Tumor Growth *In Vivo*. *Mol Ther - Nucleic Acids* (2014) 3:e159. doi: 10.1038/mtna.2014.9
95. Maldonado EN, Patnaik J, Mullins MR, Lemasters JJ. Free Tubulin Modulates Mitochondrial Membrane Potential in Cancer Cells. *Cancer Res* (2010) 70(24):10192–201. doi: 10.1158/0008-5472.CAN-10-2429
96. Maldonado EN, Lemasters JJ. ATP/ADP Ratio, the Missed Connection Between Mitochondria and the Warburg Effect. *Mitochondrion* (2014) 19 Pt A:78–84. doi: 10.1016/j.mito.2014.09.002
97. Varikmaa M, Bagur R, Kaambre T, Grichine A, Timohhina N, Tepp K, et al. Role of Mitochondria-Cytoskeleton Interactions in Respiration Regulation and Mitochondrial Organization in Striated Muscles. *Biochim Biophys Acta* (2014) 1837(2):232–45. doi: 10.1016/j.bbabo.2013.10.011
98. Jirasek T, Mandys V, Viklicky V. Expression of Class III Beta-Tubulin in Neuroendocrine Tumours of Gastrointestinal Tract. *Folia Histochem Cytobiol* (2002) 40(3):305–10.
99. Urano N, Fujiwara Y, Doki Y, Kim SJ, Miyoshi Y, Noguchi S, et al. Clinical Significance of Class III Beta-Tubulin Expression and Its Predictive Value for Resistance to Docetaxel-Based Chemotherapy in Gastric Cancer. *Int J Oncol* (2006) 28(2):375–81. doi: 10.3892/ijo.28.2.375
100. Oztop S, Isik A, Guner G, Gurdal H, Karabulut E, Yilmaz E, et al. Class III Beta-Tubulin Expression in Colorectal Neoplasms Is a Potential Predictive Biomarker for Paclitaxel Response. *Anticancer Res* (2019) 39(2):655–62. doi: 10.21873/anticancer.13160
101. Mariani M, Karki R, Spennato M, Pandya D, He S, Andreoli M, et al. Class III Beta-Tubulin in Normal and Cancer Tissues. *Gene* (2015) 563(2):109–14. doi: 10.1016/j.gene.2015.03.061
102. Mariani M, Shahabi S, Sieber S, Scambia G, Ferlini C. Class III Beta-Tubulin (TUBB3): More Than a Biomarker in Solid Tumors? *Curr Mol Med* (2011) 11(9):726–31. doi: 10.2174/156652411798062368
103. Parker AL, Turner N, McCarroll JA, Kavallaris M. betaIII-Tubulin Alters Glucose Metabolism and Stress Response Signaling to Promote Cell Survival and Proliferation in Glucose-Starved Non-Small Cell Lung Cancer Cells. *Carcinogenesis* (2016) 37(8):787–98. doi: 10.1093/carcin/bgw058
104. Cicchillitti L, Penci R, Di Michele M, Filippetti F, Rotilio D, Donati MB, et al. Proteomic Characterization of Cytoskeletal and Mitochondrial Class III Beta-Tubulin. *Mol Cancer Ther* (2008) 7(7):2070–9. doi: 10.1158/1535-7163.MCT-07-2370
105. Raspaglio G, Filippetti F, Prislei S, Penci R, De Maria I, Cicchillitti L, et al. Hypoxia Induces Class III Beta-Tubulin Gene Expression by HIF-1alpha Binding to its 3' Flanking Region. *Gene* (2008) 409(1-2):100–8. doi: 10.1016/j.gene.2007.11.015
106. Guarino F, Zinghirino F, Mela L, Pappalardo XG, Ichas F, De Pinto V, et al. NRF-1 and HIF-1alpha Contribute to Modulation of Human VDAC1 Gene Promoter During Starvation and Hypoxia in HeLa Cells. *Biochim Biophys Acta Bioenerg* (2020) 1861(12):148289. doi: 10.1016/j.bbabo.2020.148289



107. Brahimi-Horn MC, Ben-Hail D, Ilie M, Gounon P, Rouleau M, Hofman V, et al. Expression of a Truncated Active Form of VDAC1 in Lung Cancer Associates With Hypoxic Cell Survival and Correlates With Progression to Chemotherapy Resistance. *Cancer Res* (2012) 72(8):2140–50. doi: 10.1158/0008-5472.CAN-11-3940
108. Meyenberg Cunha-de Padua M, Fabbri L, Dufies M, Lacas-Gervais S, Contenti J, Voyton C, et al. Evidences of a Direct Relationship Between Cellular Fuel Supply and Ciliogenesis Regulated by Hypoxic VDAC1-DeltaC. *Cancers (Basel)* (2020) 12(11):3484. doi: 10.3390/cancers12113484
109. Baba Y, Noshio K, Shima K, Irahara N, Chan AT, Meyerhardt JA, et al. HIF1A Overexpression is Associated With Poor Prognosis in a Cohort of 731 Colorectal Cancers. *Am J Pathol* (2010) 176(5):2292–301. doi: 10.2353/ajpath.2010.090972
110. Ioannou M, Paraskeva E, Baxevanidou K, Simos G, Papamichali R, Papacharalambous C, et al. HIF-1alpha in Colorectal Carcinoma: Review of the Literature. *J BUON* (2015) 20(3):680–9.
111. Haugen MH, Boye K, Nesland JM, Pettersen SJ, Egeland EV, Tamhane T, et al. High Expression of the Cysteine Proteinase Legumain in Colorectal Cancer - Implications for Therapeutic Targeting. *Eur J Cancer* (2015) 51(1):9–17. doi: 10.1016/j.ejca.2014.10.020
112. Zhen Y, Chunlei G, Wenzhi S, Shuangtao Z, Na L, Rongrong W, et al. Clinicopathologic Significance of Legumain Overexpression in Cancer: A Systematic Review and Meta-Analysis. *Sci Rep* (2015) 5:16599. doi: 10.1038/srep16599
113. Ferecatu I, Canal F, Fabbri L, Mazure NM, Bouton C, Golinelli-Cohen MP. Dysfunction in the Mitochondrial Fe-S Assembly Machinery Leads to Formation of the Chemoresistant Truncated VDAC1 Isoform Without HIF-1alpha Activation. *PLoS One* (2018) 13(3):e0194782. doi: 10.1371/journal.pone.0194782
114. Lipper CH, Stoffleth JT, Bai F, Sohn YS, Roy S, Mittler R, et al. Redox-Dependent Gating of VDAC by mitoNEET. *Proc Natl Acad Sci USA* (2019) 116(40):19924–9. doi: 10.1073/pnas.1908271116
115. Basak D, Uddin MN, Hancock J. The Role of Oxidative Stress and Its Counteractive Utility in Colorectal Cancer (CRC). *Cancers (Basel)* (2020) 12(11):3336. doi: 10.3390/cancers12113336
116. Caterino M, Ruoppolo M, Mandola A, Costanzo M, Orru S, Imperlini E. Protein-Protein Interaction Networks as a New Perspective to Evaluate Distinct Functional Roles of Voltage-Dependent Anion Channel Isoforms. *Mol Biosyst* (2017) 13(12):2466–76. doi: 10.1039/c7mb00434f
117. Liu H, Pu Y, Amina Q, Wang Q, Zhang M, Song J, et al. Prognostic and Therapeutic Potential of Adenylate Kinase 2 in Lung Adenocarcinoma. *Sci Rep* (2019) 9(1):17757. doi: 10.1038/s41598-019-53594-4
118. Klepinin A, Ounpuu L, Guzun R, Chekulayev V, Timohhina N, Tepp K, et al. Simple Oxygraphic Analysis for the Presence of Adenylate Kinase 1 and 2 in Normal and Tumor Cells. *J Bioenerg Biomembr* (2016) 48(5):531–48. doi: 10.1007/s10863-016-9687-3
119. Speers C, Tsimelzon A, Sexton K, Herrick AM, Gutierrez C, Culhane A, et al. Identification of Novel Kinase Targets for the Treatment of Estrogen Receptor-Negative Breast Cancer. *Clin Cancer Res* (2009) 15(20):6327–40. doi: 10.1158/1078-0432.CCR-09-1107
120. Fujisawa K, Terai S, Takami T, Yamamoto N, Yamasaki T, Matsumoto T, et al. Modulation of Anti-Cancer Drug Sensitivity Through the Regulation of Mitochondrial Activity by Adenylate Kinase 4. *J Exp Clin Cancer Res* (2016) 35:48. doi: 10.1186/s13046-016-0322-2
121. Klepinina L, Klepinin A, Truu L, Chekulayev V, Vija H, Kuus K, et al. Colon Cancer Cell Differentiation by Sodium Butyrate Modulates Metabolic Plasticity of Caco-2 Cells via Alteration of Phosphotransfer Network. *PLoS One* (2021) 16(1):e0245348. doi: 10.1371/journal.pone.0245348
122. Dzeja PP, Terzic A. Phosphotransfer Networks and Cellular Energetics. *J Exp Biol* (2003) 206(Pt 12):2039–47. doi: 10.1242/jeb.00426
123. Dzeja P, Terzic A. Adenylate Kinase and AMP Signaling Networks: Metabolic Monitoring, Signal Communication and Body Energy Sensing. *Int J Mol Sci* (2009) 10(4):1729–72. doi: 10.3390/ijms10041729
124. Klepinin A, Zhang S, Klepinina L, Rebane-Klemm E, Terzic A, Kaambre T, et al. Adenylate Kinase and Metabolic Signaling in Cancer Cells. *Front Oncol* (2020) 10:660. doi: 10.3389/fonc.2020
125. Hardie DG, Ross FA, Hawley SA. AMPK: A Nutrient and Energy Sensor That Maintains Energy Homeostasis. *Nat Rev Mol Cell Biol* (2012) 13(4):251–62. doi: 10.1038/nrm3311
126. Wang W, Guan KL. AMP-Activated Protein Kinase and Cancer. *Acta Physiol* (2009) 196(1):55–63. doi: 10.1111/j.1748-1716.2009.01980.x
127. Faubert B, Boily G, Izreig S, Griss T, Samborska B, Dong Z, et al. AMPK Is a Negative Regulator of the Warburg Effect and Suppresses Tumor Growth *In Vivo*. *Cell Metab* (2013) 17(1):113–24. doi: 10.1016/j.cmet.2012.12.001
128. Rehman G, Shehzad A, Khan AL, Hamayun M. Role of AMP-Activated Protein Kinase in Cancer Therapy. *Archiv der Pharm* (2014) 347(7):457–68. doi: 10.1002/ardp.201300402
129. Hardie DG, Ross FA, Hawley SA. AMP-Activated Protein Kinase: A Target for Drugs Both Ancient and Modern. *Chem Biol* (2012) 19(10):1222–36. doi: 10.1016/j.chembiol.2012.08.019
130. Park HU, Suy S, Danner M, Dailey V, Zhang Y, Li H, et al. AMP-Activated Protein Kinase Promotes Human Prostate Cancer Cell Growth and Survival. *Mol Cancer Ther* (2009) 8(4):733–41. doi: 10.1158/1535-7163.MCT-08-0631
131. Khan AS, Frigo DE. Regulation, Role and Therapeutic Targeting of AMPK in Prostate Cancer. *Nat Rev Urol* (2017) 14(3):164–80. doi: 10.1038/nrurol.2016.272
132. Huang X, Li X, Xie X, Ye F, Chen B, Song C, et al. High Expressions of LDHA and AMPK as Prognostic Biomarkers for Breast Cancer. *Breast* (2016) 30:39–46. doi: 10.1016/j.breast.2016.08.014

**Conflict of Interest:** The authors declare that the research was conducted in the absence of any commercial or financial relationships that could be construed as a potential conflict of interest.

**Publisher's Note:** All claims expressed in this article are solely those of the authors and do not necessarily represent those of their affiliated organizations, or those of the publisher, the editors and the reviewers. Any product that may be evaluated in this article, or claim that may be made by its manufacturer, is not guaranteed or endorsed by the publisher.

Copyright © 2021 Reinsalu, Puurand, Chekulayev, Miller, Shevchuk, Tepp, Rebane-Klemm, Timohhina, Terasmaa and Kaambre. This is an open-access article distributed under the terms of the Creative Commons Attribution License (CC BY). The use, distribution or reproduction in other forums is permitted, provided the original author(s) and the copyright owner(s) are credited and that the original publication in this journal is cited, in accordance with accepted academic practice. No use, distribution or reproduction is permitted which does not comply with these terms.





# SNAP25 Inhibits Glioma Progression by Regulating Synapse Plasticity via GLS-Mediated Glutaminolysis

Qiongzen Huang<sup>†</sup>, Changlin Lian<sup>†</sup>, Yaoyuan Dong, Huijun Zeng, Boyang Liu, Ningbo Xu, Zhenyan He and Hongbo Guo<sup>\*</sup>

Guangdong Provincial Key Laboratory on Brain Function Repair and Regeneration, Zhujiang Hospital, Department of Neurosurgery, Guangzhou, China

## OPEN ACCESS

### Edited by:

Monica Montopoli,  
University of Padua, Italy

### Reviewed by:

Yuanping Xiong,  
First Affiliated Hospital of Nanchang  
University, China  
Stephen John Ralph,  
Griffith University, Australia

### \*Correspondence:

Hongbo Guo  
guohongbo911@126.com

<sup>†</sup>These authors have contributed  
equally to this work

### Specialty section:

This article was submitted to  
Cancer Metabolism,  
a section of the journal  
Frontiers in Oncology

**Received:** 26 April 2021

**Accepted:** 16 July 2021

**Published:** 16 August 2021

### Citation:

Huang Q, Lian C, Dong Y, Zeng H,  
Liu B, Xu N, He Z and Guo H (2021)  
SNAP25 Inhibits Glioma Progression  
by Regulating Synapse Plasticity via  
GLS-Mediated Glutaminolysis.  
Front. Oncol. 11:698835.  
doi: 10.3389/fonc.2021.698835

**Background:** Neuronal activity regulated by synaptic communication exerts an important role in tumorigenesis and progression in brain tumors. Genes for soluble N-ethylmaleimide-sensitive factor attachment protein receptors (SNAREs) annotated with the function ‘vesicle’ about synaptic connectivity were identified, and synaptosomal-associated protein 25 (SNAP25), one of those proteins, was found to have discrepant expression levels in neuropathies. However, the specific mechanism and prognostic value of SNAP25 during glioma progression remain unclear.

**Methods:** Using RNA sequencing data from The Cancer Genome Atlas (TCGA) database, the differential synaptosis-related genes between low grade glioma (LGG) and glioblastoma (GBM) were identified as highly correlated. Cox proportional hazards regression analysis and survival analysis were used to differentiate the outcome of low- and high-risk patients, and the Chinese Glioma Genome Atlas (CGGA) cohort was used for validation of the data set. RT-qPCR, western blot, and immunohistochemistry assays were performed to examine the expression level of SNAP25 in glioma cells and samples. Functional assays were performed to identify the effects of SNAP25 knockdown and overexpression on cell viability, migration, and invasion. Liquid chromatography-high resolution mass spectrometry (LC-MS)-based metabolomics approach was presented for identifying crucial metabolic disturbances in glioma cells. In situ mouse xenograft model was used to investigate the role of SNAP25 *in vivo*. Then, an immunofluorescence assay of the xenograft tissue was applied to evaluate the expression of the neuronal dendron formation marker-Microtubule Associated Protein 2 (MAP2).

**Results:** SNAP25 was decreased in level of expression in glioma tissues and cell lines, and low-level SNAP25 indicated an unfavorable prognosis of glioma patients. SNAP25 inhibited cell proliferation, migration, invasion and fostered glutamine metabolism of glioma cells, exerting a tumor suppressor role. Overexpressed SNAP25 exerted a lower expression level of MAP2, indicating poor neuronal plasticity and connectivity. SNAP25 could regulate glutaminase (GLS)-mediated glutaminolysis, and GLS knockdown could rescue the anti-tumor effect of SNAP25 in glioma cells. Moreover, upregulated

SNAP25 also decreased tumor volume and prolonged the overall survival (OS) of the xenograft mouse.

**Conclusion:** SNAP25, a tumor suppressor inhibited carcinogenesis of glioma *via* limiting glutamate metabolism by regulating GLS expression, as well as inhibiting dendritic formation, which could be considered as a novel molecular therapeutic target for glioma.

**Keywords:** SNAP25, synaptic plasticity, glutaminase, glioma progression, glutamine metabolism

## INTRODUCTION

Gliomas are among the most common primary brain tumors in adults and account for over 70% of malignant brain tumors, of which glioblastoma (GBM) is the most aggressive and deadly type with a median survival of 15 months and 5-year overall survival of 5.5% (1). Despite the conventional treatments (surgery followed by chemotherapy and radiotherapy), the prognosis of GBM has not been improved over the past years due to the highly invasive residual tumor cells and the incompletely resected tumors. Resistance of malignant gliomas to conventional therapies has been widely reported as a consequence of oncogene signaling activation and distinct metabolic mechanisms when cancer cells are exposed to various chemotherapeutic and/or cytostatic agents, thus, recurrent tumors usually become more aggressive (2, 3). Thus, the specific mechanism of glioma progression needs to be identified.

Previous studies have confirmed that gliomas occur in a striking spatiotemporal pattern highlighting the critical importance of the tumor microenvironment (4), as close relationships between glioma cells and neighboring microglia, astrocytes, and vascular cells have recently come to light (5, 6). Microenvironmental interaction, especially the aberrant interplay between glia and synapses, have been posted to contribute to neural pathology of Rett syndrome (7), Down syndrome (8), Spinal Muscular Atrophy (9) and others (10). More recent studies have identified that the communication between neurons and glial cells is associated with several neuropsychiatric and neurodegenerative disorders such as schizophrenia (11). Glia are active participants in synaptic plasticity and are known to modulate individual synapses and circuits (12). Importantly, the function of astrocytic glutamate transporters GLT-1 and GLAST is a classic example of how astrocytes regulate glutamatergic synaptic transmission by controlling the neurotransmitter levels at the synapse (13). Glutamate not only participates in synapse communication as one of the functional neurotransmitters but also functions as a signature metabolic product in tumor origination (14). Cancer cells typically rewire their metabolism to meet the bioenergetic and biosynthetic demands of uncontrolled cell growth, for example, many oncogenic mutations result in enhanced glutamate metabolism, reflecting its importance on tumor progression by generating tricarboxylic acid (TCA) cycle intermediates and amino acids, and maintaining redox homeostasis (15, 16). In this context, the rate-limiting enzyme

converting glutamine to glutamate, GLS, primarily enhances glutaminolysis and may provide a typical target in glutamate metabolism pathways (17). Therefore, targeting glutamate metabolism is an appealing therapeutic option in many cancer subtypes.

SNAP25 is a member of the SNARE family, associated with severe synaptopathies like Schizophrenia and also proteinopathies like Alzheimer's disease but its function in glioma is seldom studied (18–20). A recent study indicated that SNAP25 was a microenvironment-related gene that predicted poor outcomes in colon cancer, and gene set enrichment analysis (GSEA) suggested that SNAP25 was involved in metabolism progress (21).

In this study, SNAP25 was mined to have significantly lower expression levels in glioma from the mRNAs expression profiles in TCGA dataset and lower-expressed SNAP25 indicated an unfavorable prognosis of glioma patients. Then the lower expression of SNAP25 in glioma tissues and cell lines was validated. The effect of SNAP25 on glioma progression was studied, and the underlying metabolic and synaptic plasticity by which SNAP25 regulated glioma cell phenotype was also investigated.

## MATERIALS AND METHODS

### Datasets

We collected 693 and 512 gliomas with RNA-seq data and clinical information from TCGA and CGGA databases, respectively. All tissues and clinicopathologic information were obtained with written informed consents.

### Screening DEGs Through Integrated Analysis

The background correction, standardization, and log<sub>2</sub> conversion for raw data were conducted by the “affy” package of Bioconductor according to the annotation files. We used the “limma” package of the R software to investigate DEGs in LGG and GBM tissues. *P*-value < 0.05 along with |logFC| > 1 were considered significant.

### Patients and Specimens

All 40 glioma tissues samples and 8 normal samples were obtained from patients who had received surgery and chemotherapy at Zhujiang Hospital (Southern Medical

University, Guangzhou, China). These glioma specimens include 16 Grade IV (GBM), 14 Grade III, 8 Grade II, and 2 Grade I astrocytoma cases, and the histologic features of surgical resection specimens were independently examined by two neuropathologists according to the WHO criteria (**Supplementary Table 1**). The specimens were frozen in liquid nitrogen immediately after the surgery and then paraffin embedded for long time preservation. The project protocol was approved by the Ethics Committee of Zhujiang Hospital and written informed consents were obtained from all patients enrolled in this study.

## Cell Culture

The human GBM cell lines (U87, U251, A172, U118) were purchased from the Cell Bank of the Chinese Academy of Sciences (Shanghai, China), and were authenticated and examined for mycoplasma contamination. NHA cells were kindly provided by the Yongping You's lab of Nanjing medical university. U87MG-mCherry(U87MC) glioma cell line labelled with red fluorescent protein were kindly provided by the Ke Yichuan's lab of South medical university. The cells were routinely cultivated at 37°C in the 5% CO<sub>2</sub> humidification incubator (Thermo Scientific, Waltham, MA, USA) in Dulbecco's modified Eagle's medium (Invitrogen) with fetal bovine serum (10% v/v, Hyclone, Logan, UT, USA) penicillin (200 units/ml) and streptomycin (100 µg/ml).

## Cell Lentiviral Transfection

For lentiviral transfection, cells were seeded at 50% confluence in six-well cell culture plates and incubated with 1 ml medium overnight. Then medium was replaced with 500ul mixture of OPTI-MEM (Invitrogen, USA) with polybrene (4 µg/ml, Genechem, Shanghai, China). Cells were transfected by adding control shRNA lentiviral vectors, SNAP25 shRNA lentiviral vectors, GLS shRNA lentiviral vectors, Control lentiviral activation vectors, SNAP25 lentiviral activation vectors, GLS lentiviral activation vectors, respectively. All the lentiviral vectors were obtained from Obio (Obio, Shanghai, China). Medium was replaced with complete medium without polybrene 24h later after transfection. Transduced cells were selected for puromycin (2µg/ml, sc-108071, Santa Cruz) resistance for 10 days. The gene expression efficiency was detected by qRT-PCR and western blot.

## RNA Isolation, Reverse Transcription, and Quantitative Real-Time PCR

Total RNA from specimens or cells was extracted by using Trizol Reagent (Takara Bio, Shiga, Japan) and the absorbance was measured with OD260/280 ratio higher than 1.8. For qPCR analysis, cDNA was synthesized with the Prime Script™ RT reagent (Takara Bio, Shiga, Japan). Quantitative real-time PCR assay by using SYBR GREEN PCR Master Mix (Takara Bio, Shiga, Japan) was performed in triplicate with GAPDH as endogenous controls and the gene expression relative to control was calculated by  $2^{-\Delta\Delta CT}$ .

## Western Blot Assay

Total protein of cells was extracted by Cell Lysis and Protein Extraction kit (Keygen Biotech Co., China) and the western blot was performed in standard procedures. Specific antibodies were applied to the western blot: SNAP25(1:1000; Rat# ab5666; Abcam), Glutaminase(1:1000; Rat# ab156876; Abcam),  $\beta$ -catenin (1:1000; Rat#3700S; Cell Signaling Technology). Subsequently, the blots were incubated with goat anti-rabbit or mouse IgG (H+L) secondary antibody (Fdbio, China) at room temperature for 2 h. Then the blots were washed with TBST and visualized. The analysis of the protein expression was performed by the Image J software with  $\beta$ -actin as endogenous controls, and then the image is drawn according to the gray value using the software graphpad.

## Immunohistochemistry

The paraffin tissue was sliced continuously with a thickness of 4 microns and dried in an oven at 68°C, the slices were then dewaxed in three different concentrations of xylene solutions for 10 minutes each, then were placed in 100%, 95%, 85%, 75% alcohol for hydration, for 5 minutes each. The hydrated slices were rinsed slowly under running water for ten minutes and then dried. Fifty microliters of 3% hydrogen peroxide solution were added to each section, and the tissue on the section was evenly covered and incubated at room temperature for 15 minutes to seal, the slices were rinsed in running water for 10 minutes in the manner previously described, the antigenic repair solution was dropped into the rinsed section and then heated at 95°C to 99°C for 20 minutes. After the slices were naturally dried, they were rinsed twice with PBS buffer for 5 minutes each time, after the slices were dried again, a drop of 5% goat serum solution was added evenly to each slice, and the slices were incubated at room temperature for 30 minutes, then the serum was removed. 10 microliters anti-SNAP25 antibody (1:400; Rat# ab5666; Abcam) or anti-GLS antibody (1:400; Rat# ab156876; Abcam) was added to 1 mL PBS and diluted evenly, then the reagent is dripped onto the section at 4°C overnight, the next day, the sections were left at room temperature for 30 minutes and rinsed with PBS 3 times for 3 minutes each time. Then sections were incubated with secondary antibody at 37°C for 1 h, then rinsed three time with PBS buffer for 3 minutes each time. DAB colorimetric solution is added to the slices, when the chromogenation is observed under a microscope, the sections are washed with running water. The sections were stained with hematoxylin for 3 minutes, washed with running water for 3 minutes, differentiated in 1% alcohol for 1-3 seconds, washed with running water, placed in PBS, then washed with running water, and placed in 75%, 85%, 95%, 100% alcohol for dehydration, each dehydration for 5 minutes. The dehydrated sections were placed in a solution of xylene to make them transparent and then dried. Each section was dripped with 20 microliters of neutral resin and covered with cover glasses, sections were examined microscopically for staining.

## Immunofluorescence Staining

Glioma cells were respectively positioned on glass coverslips (0.17 mm thickness, 14 mm diameter) in a 6-well plate at room

temperature overnight. Then cells were washed by PBS, fixed by 4% paraformaldehyde for 30min, infiltrated by 0.1% Triton X-100 for 5min, and blocked by 2% bovine serum albumin (BSA) for 30min in sequence. Incubated with Specific primary antibodies: anti-SNAP25 (1:400; Rat# ab5666; Abcam), anti-GLS (1:400; Rat# ab156876; Abcam), anti-MAP2 (1:400; Rat# ab5392; Abcam) at 4°C overnight and rinsed by PBS 3 times, fluorescent secondary antibodies (Donkey anti-Rabbit IgG (H+L) Highly Cross-Absorbed Secondary Antibody, Alexa Fluor 488 (Thermo Fisher Scientific, catalog# A-21206, RRID AB\_2535792) were applied to specimens and incubated at 37°C in the darkness for 1h. Mounting medium with DAPI DNA counterstain was applied to the specimens followed by images capture (Nikon, Ti2-E).

## Tumor Xenograft Model

For the murine Intracranial tumors generation,  $5 \times 10^5$  specified cells (U87MC NC- SNAP25, U87MC oe-SNAP25, U87MC oe NC- GLS and U87MC oe sh05-GLS cells) expressing luciferase were independently injected into the randomly grouped mice and the bioluminescence was examined on the 0<sup>th</sup>, 7<sup>th</sup>, 14<sup>th</sup>, 21<sup>th</sup> day. Then the brains were dissected for immunohistochemistry and immunofluorescence staining. Procedures in experiments were performed according to the National Institutes of Health Guide for the Care and Use of Laboratory and approved by the Animal Experimental Committee of Southern Medical University.

## CCK-8 Assay

The cells were seeded in a 96-well plate for 24 h after stable transfection or transient transfection. Then followed by incubating with 10% CCK-8 (Dojindo, Japan) solution fresh medium solution for 2 h, the absorbance was measured at 450 nm using Ultra Multifunctional Microplate Reader (Tecan, Switzerland) according to the instructions.

## Wound Healing

The cells were cultured in a 6-well plate, scraped with cells to draw a line in the central area after the cells were scraped, and the cells in this line were mechanically removed. Then the cells were continued to be cultured in a serum-free medium, and the migration of cells to the scratch area without cells was observed to judge the migration ability of the cells.

## Transwell Migration Assay

The invasive abilities of cells were assessed through the transwell inserts (353097-Falcon, BD) with a 1:4 diluted Matrigel coating layer. After being suspended in a serum-free medium, the tumor cells were seeded into the upper well of the chamber for 24h and a medium with 10% FBS was supplied in The lower well. Then in the filter, the cells on the upper surface were removed and the cells on the lower surface were stained with 1% crystal violet after treated with 4% paraformaldehyde. The number of cells were calculated in 9 random fields using the microscope ( $\times 400$ ).

## Cancer Cell Spheroid Invasive Assay

Tumor cell invasion was assessed using a three-dimensional (3D) spheroid invasion assay (22). U118 and A172 cells formed

spheres in hanging drops of culture medium on the lid of cell culture dishes (approximately 500 cells per drop). After 48 hours, spheres from the lid were aliquoted into the same volume, mixed with rat tail type I collagen (final concentration is 1.7mg/ml), and embedded in wells to generate a 3D culture system. The invasion was concluded at 48 hours. Quantitative analyses were determined by measuring the maximal invasive distance (longest invasive distancespheroid radius) and invaded area (total invaded area-spheroid area) using the Image J software.

## LC-MS Analysis

For LC-MS analysis, in analytical triplicate, 5  $\mu$ L of the sample was injected on an XBridge BEH amide column through an Acquity H-class UPLC system (Waters Corporation). MS was done using a Waters Xevo-TQS-micro MS with polarity-switching (positive mode 3 kV, negative mode 2 kV), and multiple reaction monitoring modes were used to acquire data with a randomized injection order. Before, during, and after the run, quality control (QC) samples were injected. Data were processed through TargetLynx (v4.1) to identify peaks from Total Intensity Chromatograms. Peaks were then integrated, and ion counts were obtained and exported for further processing in R. Metabolites found in < 50% QC samples or those with a coefficient of variation > 30% were dropped. Besides, QC samples were used to fit a cross-validated locally estimated scatterplot smoothing (LOESS) function to each metabolite. This accounted for instrumental drift and was used for ion count normalization. The raw data of the LC-MS analysis was uploaded in Metabolights (<https://www.ebi.ac.uk/metabolights/index>) and the study number is MTBLS2806.

## Quantification and Statistical Analysis

All statistical analyses were conducted using GraphPad Prism 8.0. Data represent mean  $\pm$  s.e.m. unless otherwise noted and reported as biological replicates with technical replicates specified in figure legends. Unpaired two-tailed Student t-tests were used to determine *p*-values. Significance was defined as \**p* < 0.05, \*\**p* < 0.005, and \*\*\**p* < 0.0005.

## RESULTS

### A Screen of Candidate Genes Associated With Tumor Progression and Prognostic Validity of the Candidate Gene for Glioma

To identify the key genes involved in tumor progression of glioma, 527 cases of LGG patients and 166 GBM cases from the TCGA database were selected to perform differential expression analysis. As described in *Materials and Methods*, all cases were divided into two groups: the “LGG” group and the “GBM” group. A total of 24,991 differentially expressed genes (DEGs) were significantly upregulated and downregulated in LGG samples and GBM samples using adjusted *p* < 0.05 and  $|\log FC| \geq 1$  as the cut-off. Gene clustering using the R package ‘pheatmap’ found that the profile of synaptosome-related (SNARE) genes between



LGG and GBM showed obvious differences and SNAP25 was significantly down-expressed in GBM (**Figure 1A**). Violin plot showed the exact changing level of these genes as SNAP25 expression in glioma was significantly lower than that in normal brain tissue ( $p=0.001$ , **Figure 1B**). Next, the CGGA dataset was selected to show a negative correlation between the expression of SNAP25 and the WHO grades of glioma (**Figure 1C**). By performing univariate Cox regression analyses to determine the prognostic value of the acquired gene set, SNAP25 was indicated to be independently correlated with OS ( $p<0.001$ , **Figure 1D**). Then, based on the median SNAP25 expression score, patients were assigned to the high- or low-SNAP25 expression group. Kaplan-Meier analysis found the low-SNAP25 cases had a significantly shorter OS than high-SNAP25 ones ( $p=0.03$ , **Figure 1E**). To validate this, we also calculated patients' risk scores of the CGGA cohort. As expected, we acquired a consensus result (**Figure 1F**). Then, immunohistochemistry assay was applied to analyze the SNAP25 expression in surgical resection specimens, from which SNAP25 expression was negatively correlated with the tumor

grading ( $p<0.001$ , Mann-Whitney test) (**Figure 1G**). Taken together, these results suggest that SNAP25 downregulation is associated with poor clinical outcomes of glioma.

## Association of SNAP25 With Glioma Cell Proliferation

After we found a lower expression of SNAP25 in glioma, we explored its functional effects on glioma cells. First, we detected the expression of SNAP25 in glioma cell lines (U87, U251, U118, and A172), when compared to normal human astrocytes (NHAs) by RT-qPCR (**Figures 2A**) and western blot assays (**Figures 2B**). SNAP25 was decreased in level of expression in glioma cells, especially in U118 and A172 cells (**Figure 2A**). Therefore, we transfected U118, A172 cells with an shRNA targeting SNAP25 (U118-sh-SNAP25, A172-sh-SNAP25) and transfected them with functional SNAP25-cDNA (U118-Lv-SNAP25, A172-Lv-SNAP25). RT-qPCR and western blot assays confirmed that the expression of SNAP25 was effectively modulated in U118 and A172 cells (**Supplementary Figures 1A, B**).

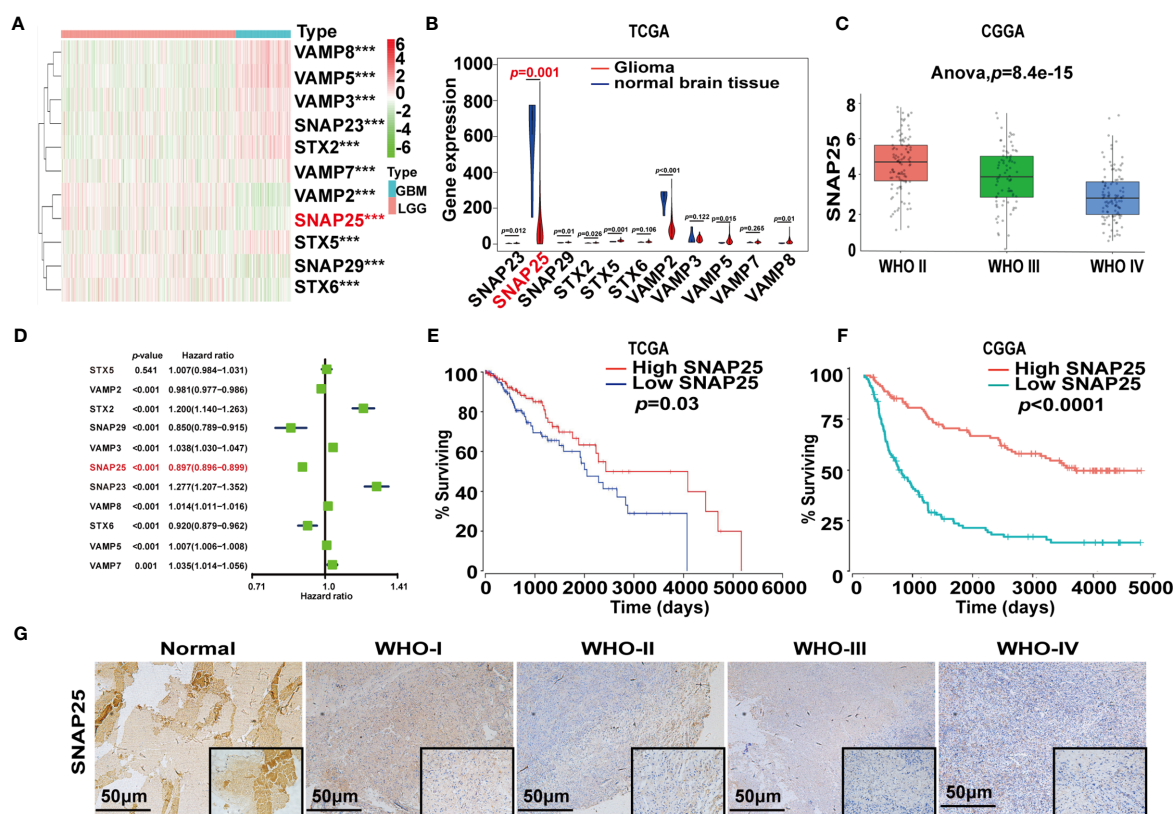


**FIGURE 1** | SNARE-related genes expression profiles and correlation between gene expression and clinical features in TCGA and CGGA datasets. **(A)** Heatmap show the different expression levels of 11 SNARE-related genes in TCGA dataset. Up-regulation is shown in red and downregulation is in blue. \*\*\* $p < 0.001$ . **(B)** Violin plot shows the expression of SNARE-related genes in normal tissue and gliomas. **(C)** Box plot shows SNAP25 expression in different glioma grades in CGGA database. **(D)** Hazard ratio values of the eleven selected genes. **(E, F)** Kaplan-Meier survival analysis for glioma patients with low and high risk scores in TCGA and CGGA datasets. Kaplan-Meier survival curve for glioma patients with a high risk score (red line) and a low risk score (blue line). **(G)** Representative images of SNAP25 expression from glioma tissues and nontumor tissues by IHC assays.

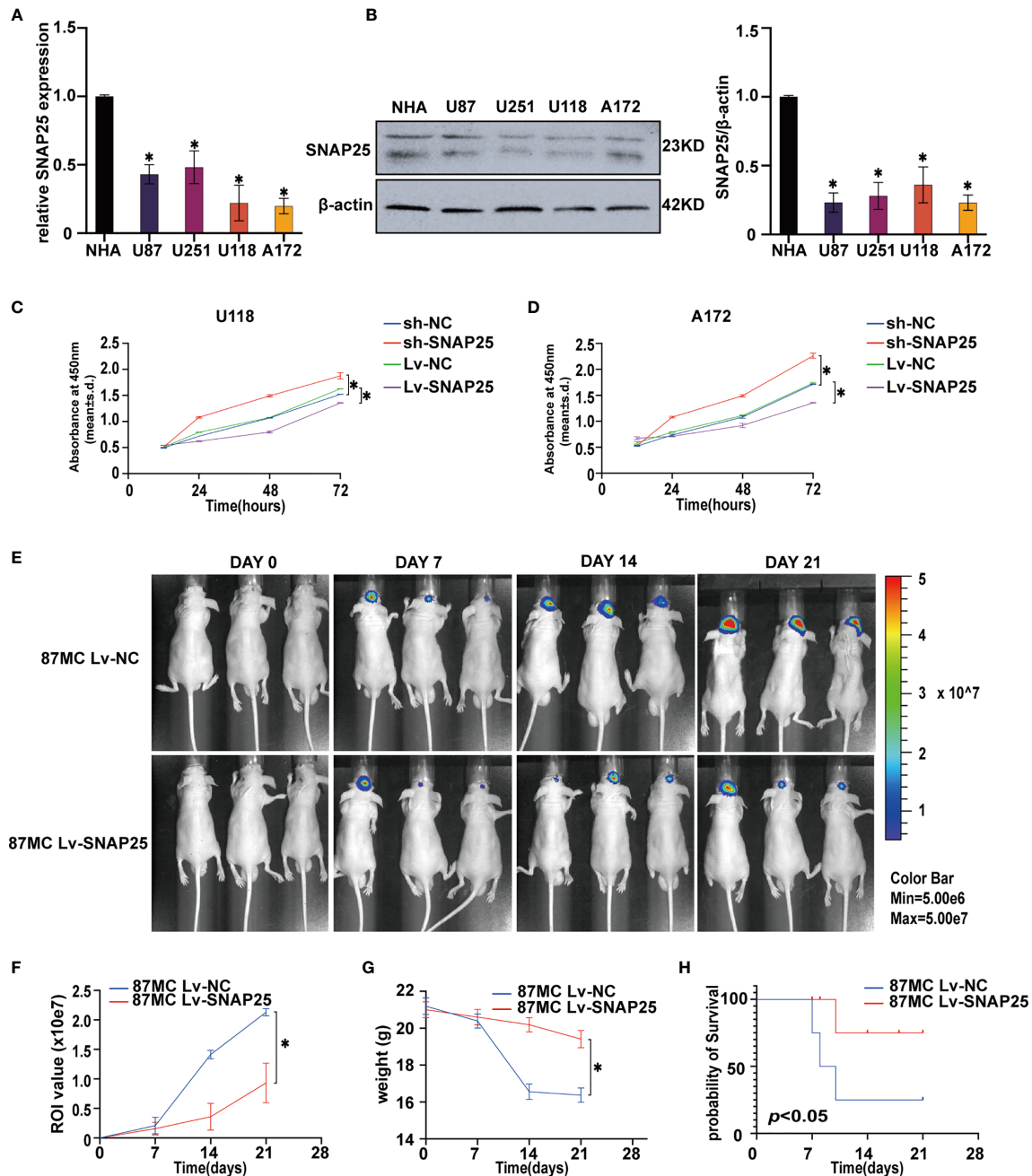


**FIGURE 2 |** Overexpression of SNAP25 inhibits glioma cell growth *in vitro* and *in vivo*. **(A)** Relative SNAP25 expression levels in various glioma cell lines, compared with the normal human astrocytes (NHA), \* $p < 0.05$  compared with NHA cells. GAPDH was used as a housekeeping gene. **(B)** The level of SNAP25 protein was detected in 4 glioma cell lines and NHA by western blot. \* $p < 0.05$  compared with NHA cells. B-actin was used as a control and the barplot besides shows the representative SNAP25/actin ratio regarding to the western blot. **(C, D)** Ectopic expression of SNAP25 inhibits cell growth as determined by CCK-8 assay. \* $p < 0.05$  compared with Lv-NC or sh-NC group. **(E)** Tumor growth was monitored over time (up to Day 21) by measuring luciferase emission (ROI). **(F–H)** The ROI value, weight of the mice and the probability of survival was recorded over time.

Functionally, the CCK-8 results showed that overexpression of SNAP25 significantly decreased cell proliferation in U118 and A172 cells, whereas knockdown of SNAP25 significantly increased cell proliferation in U118 and A172 cells (**Figures 2C, D**). Moreover, the effect of SNAP25 overexpression on tumor growth was also

examined by a nude-mouse transplanted tumor model. The results exhibited that U87Mcherry Lv-SNAP25 delayed tumor growth, decreased the weight-loss of vehicle mice, and prolonged the survival time compared with the U87Mcherry Lv-NC group (**Figures 2E–H**).

In summary, these results demonstrated that SNAP25 could significantly inhibit glioma cell proliferation *in vitro* and sponge tumor growth *in vivo*.

## Relationship Between SNAP25 and Glioma Cell Migration, Invasion, and Dendritic Formation

Subsequently, we examined the role of SNAP25 in glioma migration and invasion. The wound-healing assay indicated that the motility of glioma cells with stable SNAP25 silencing was significantly increased, while in SNAP25-upregulated cells was decreased ( $p < 0.05$ , **Figure 3A**). Transwell assays were implemented to evaluate the migration ability of glioma cells, and reduced migration ability of U118 and A172 cells with stable

SNAP25 overexpression was observed ( $p < 0.05$ , **Figure 3B**). Then we evaluated the effect of SNAP25 on tumor cell invasion using a 3-dimensional spheroid assay (22). Knockdown of SNAP25 increased invaded area and distance of both U118 and A172 cells ( $p < 0.05$ , **Figure 3C**). As SNAP25 acts as a classic role in synapse formation and transmission, we examined the roles of SNAP25 in neuron-glioma cells dendritic processes by immunofluorescence staining of MAP2, a neuron-specific cytoskeletal protein enriched in dendrites and perikarya, which implicates a biomarker of neuron development. As shown in the immunofluorescence staining results of the glioma xenograft in **Figure 3D**, U87Mcherry Lv-SNAP25 glioma cell-transplanted-xenograft expressed lower MAP2 expression than U87Mcherry Lv-NC group, indicating a negative function of SNAP25 in

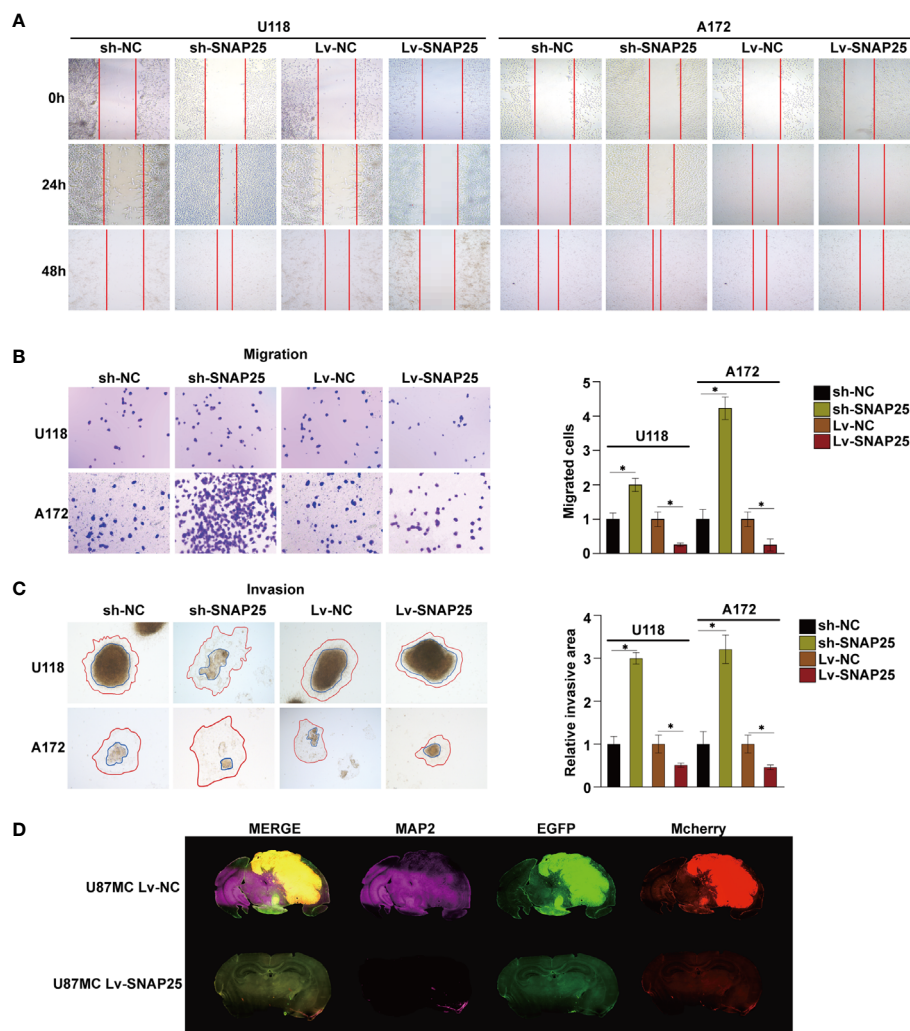


**FIGURE 3 |** SNAP25 inhibits migration and invasion of tumor cells, and inhibits dendron formation of glioma tissues. **(A)** Ectopic expression of SNAP25 inhibits cell migration as determined by wound healing assays. **(B)** Ectopic expression of SNAP25 inhibits cell migration as determined by transwell assays and analysis of representative migrated rates of glioma cells is shown below.  $*p < 0.05$  compared with Lv-NC or sh-NC group. **(C)** Representative pictures of glioma cell invasion (red curved line: invaded area, blue circle: spheroid) and analysis of quantitative invaded area of glioma cells using Image J software is shown below.  $*p < 0.05$  compared with Lv-NC or sh-NC group. **(D)** Glioma cell (Mcherry staining) and neuronal dendron (MAP2 staining) in the brains of indicated mice at the time of harvesting (Day 21).

synaptic plasticity. In general, SNAP25 overexpression inhibited cell migration and invasion of U118 and A172 cells, and SNAP25 knockdown promoted cell migration and invasion of glioma cells, and upregulation of SNAP25 could also inhibit the dendritic formation of the tumor *in vivo*.

## SNAP25 Activates GLS Expression in Glioma Cells

Metabolomic analysis was performed on A172 sh-NC, A172 sh-SNAP25, A172 Lv-NC, and A172 Lv-SNAP25 cells. We employed principal component analysis (PCA) to identify metabolic alternations between A172 Lv-NC and A172 Lv-SNAP25 cells, and each cohort separated into relative distinct clusters (Figure 4A). Subsequently, projections to latent structures

discriminant analysis (PLS-DA) defined metabolites contributing to the greatest separation between groups. Metabolites distinguishing Lv-NC and Lv-SNAP25 ( $VIP > 1$ ) were assessed and three metabolites (glutamate, glutamic acid and L-Glutathione) played important role in this process (Figure 4B). Moreover, cysteine and methionine metabolism, amino sugar and nucleotide sugar metabolism as well as alanine, aspartate and glutamate metabolism pathways were significantly differentiated in Lv-SNAP25 and Lv-NC tumor cells, suggesting that glutamine-related metabolism was highly activated (Figure 4C). Consistently, the pathway analysis showed that those involved in cysteine and methionine metabolism, amino sugar and nucleotide sugar metabolism, glutathione metabolism, alanine, aspartate and glutamate metabolism and D-glutamine and D-glutamate

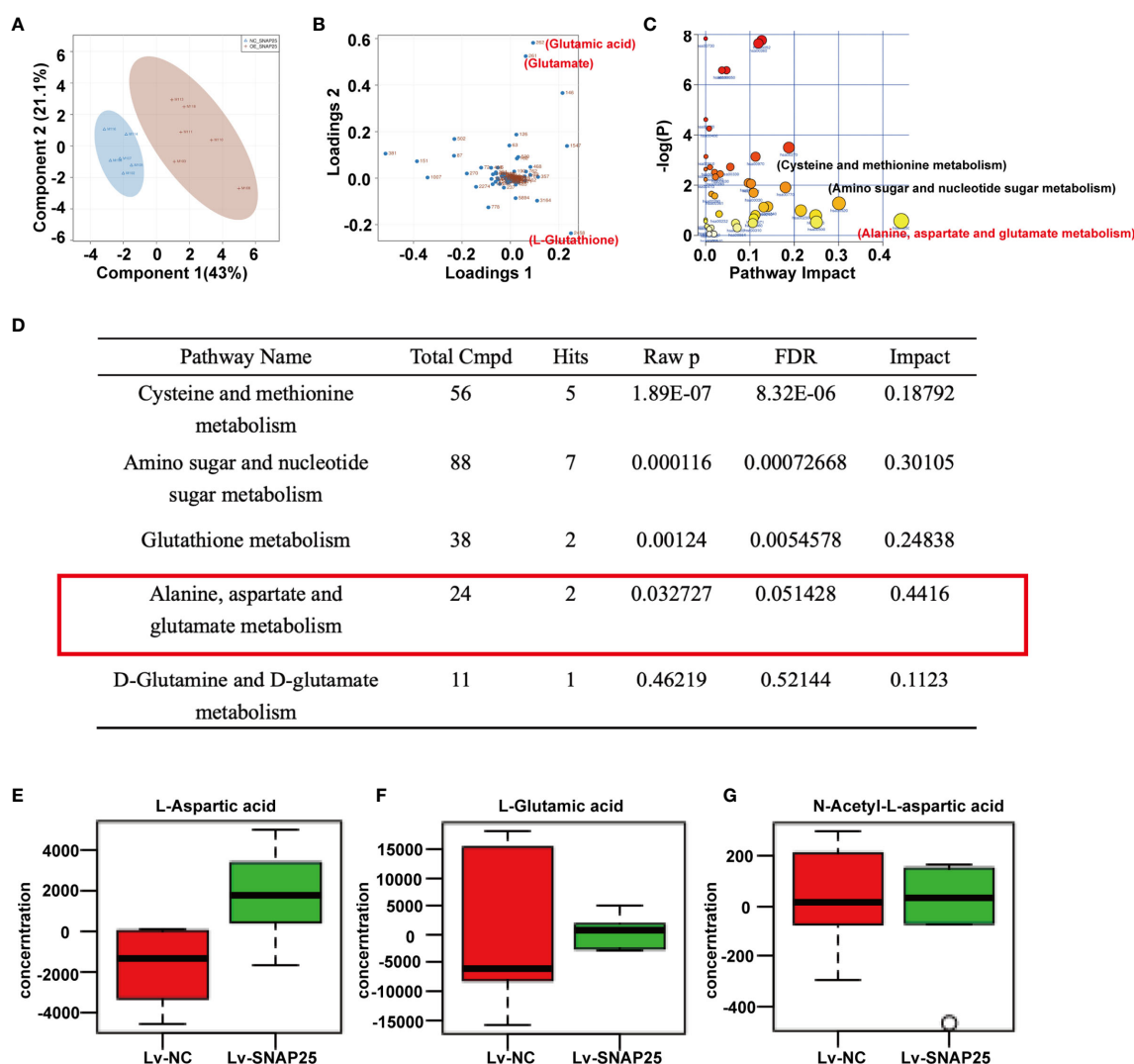


**FIGURE 4 |** SNAP25 regulates glutamine metabolism of glioma cells. (A) Plots of the principle component analysis results for LC-MS data obtained for Lv-NC and Lv-SNAP25 glioma cells. (B) Loading plots of the principle component analysis results for LC-MS data obtained for Lv-NC and Lv-SNAP25 glioma cells. Metabolites 261 (glutamate), 262 (glutamic acid), and 2458 (L-glutathione) contributed largely to their separation. (C, D) Pathway analysis results for LC-MS data obtained for Lv-NC and Lv-SNAP25 glioma cells. Alanine, aspartate and glutamate metabolism pathway shows a high pathway impact (0.4416),  $p=0.03$ . (E–G) The concentration of L-Aspartic acid (E), L-Glutamic acid (F), and N-Acetyl-L-aspartic acid.



metabolism largely contributed to their separation (**Figure 4D**). Finally, an LC-MS assay was performed to evaluate the levels of metabolic products of glutamine metabolism (L-Aspartic acid, L-Glutamic acid and N-Acetyl-aspartic acid), which indicated a positive effect of SNAP25 in glutamate metabolic ability (**Figures 4E–G**). Consistently, the metabonomic results in sh-SNAP25 vs sh-NC group showed glutamate and glutathione contributed largely to their metabolic differentiation in (**Supplementary Figures C–E**). The LC-MS analysis indicated that the levels of metabolic products of glutamine metabolism (L-Aspartic acid, L-Glutamic acid and N-Acetyl-aspartic acid) in sh-SNAP25 glioma cells were significantly higher than that in sh-NC cells (**Supplementary Figures F–H**). GLS catalyzes the conversion of glutamine to glutamate, acts as the rate-limiting enzyme for glutaminolysis, and exists in two isoforms, glutaminase 1 (GLS1) and 2 (GLS2) (23). Interestingly, recent findings support the function of GLS as a multifaceted protein which was not only involved in glutamate generation, but also in carcinogenesis and cancer progression as GLS2 acts as a transcriptional target of p53 and have been argued to have tumor suppressor properties, and re-expressing it in p53-deficient cells limits malignancy (24). But the exact role of GLS in SNAP25-regulated glioma progression has not been studied. By performing RT-qPCR and western blot assays, Glioma cell lines showed lower GLS expression compared to NHA cells ( $p < 0.05$ , **Figures 5A, B**). Negative correlation between GLS expression and WHO grading was observed by immunohistochemistry assay, reflecting the similar expression pattern of GLS and SNAP25 in glioma (**Figure 5C**). Also, SNAP25-knockdown glioma cells (A172 sh-SNAP25 and U118 sh-SNAP25) showed lower GLS expression compared to sh-NC cells and overexpression of SNAP25 witnessed an increased expression of GLS according to the western blot assay ( $p < 0.05$ , **Figure 5D**). Furthermore, the immunofluorescence assay showed consistent results (**Figure 5E**). Taken together, we demonstrated that SNAP25 contributed to boosting glutamate metabolism and it may work as a sponge to activate the rate-limiting enzyme-GLS-to make this process come true.

## SNAP25 Regulates Glioma Progression Through GLS-Mediated Glutamine Metabolism

Since SNAP25 has been shown to play a vital role in glioma progression and glutamate metabolism, we next investigated the way SNAP25 functioned in this process. We hypothesized that SNAP25 could regulate GLS-mediated glutamine metabolism to inhibit glioma progression. As we have found that SNAP25 and GLS showed the concurrent expression patterns in transfected glioma cells, there was a positive correlation ( $R^2 = 0.699$ ;  $p = 1.96 \times 10^{-10}$ , **Figure 6A**) between SNAP25 and GLS levels in glioma tissues according to CGGA database. To further prove that SNAP25 inhibited glioma progression through activating GLS, we applied GLS-shRNA to rescue the SNAP25 overexpressed cells. The proliferation, migration, and invasion assays proved that knockdown of GLS accelerated the proliferation, migration and invasion rate of glioma parental cells, and downregulation of GLS in SNAP25-overexpressed

glioma cells could rescue the tumor-suppressive function of SNAP25 in glioma cells (**Figures 6B–D**). Importantly, knockdown of GLS in SNAP25-upregulated cells encountered a low glutamate metabolic level (**Figure 6E**). Then xenograft model of glioma *in vivo* indicated a time-dependent aggressive growth of the xenograft in rat brains and SNAP25 acted as an efficient tumor suppressor as U87Mcherry Lv-SNAP25 rats showed lower growth rate, less weight-loss and longer survival time than U87Mcherry Lv-NC animals. Furthermore, downregulating the GLS in the U87MC Lv-SNAP25 group rescued the suppressive condition (**Figures 7A, B**). In the end, immunofluorescence assay was applied to demonstrate MAP2-indicated dendritic formation and synapse plasticity levels. As is shown in **Figure 7C**, SNAP25 inhibited MAP2 expression in xenograft glioma tissues and GLS-silencing reversed this process.

The above results indicated that SNAP25 functioned as an efficient GLS sponge in glioma and SNAP25 acted as a glioma suppressor through GLS-mediated glutamine metabolism.

## DISCUSSION

Glioma is the most devastating tumor in the central nervous system, and the exact pathogenesis of it is still unclear (25). Recent progress in molecular profiling has improved the diagnostics and classification system in which the most significant knowledge is that somatic mutations affecting the R132 residue of the isocitrate dehydrogenase 1 (IDH1) or R172 residue of the isocitrate dehydrogenase 2 (IDH2) are often detected in WHO II or III gliomas and oligodendrogliomas (26). SNAP25, a member of the SNARE family, is a membrane-binding protein in neurons that plays an indispensable role in the occurrence and development of various synaptopathies (18, 27). When comes to cancers, SNAP25 functions differently according to various cancer types. It was reported that SNAP25 was overexpressed in colon cancer samples, and abnormal expression of SNAP25 indicated a poor prognosis of colon cancer patients (21). Contradictorily, SNAP25 was identified to inhibit cancer progression as cleavage of SNAP25 could ameliorate cancer pain of a mouse melanoma model and a comprehensive bioinformatic analysis of GBM indicated that SNAP25 might act as a GBM suppressor and a biomarker in GBM treatment (28, 29). Furthermore, SNAP25 was found to have significantly lower expression levels in medulloblastoma and SNAP25 was crucial for dendrite formation which is associated with the effects of targeted chemotherapy (30). But the further mechanism of how SNAP25 regulates glioma progression remains unknown. In the present study, we first identified the expression of SNAP25 in the glioma tissues and cells. We found that SNAP25 was downexpressed in the glioma tissues and cells, and lower expression of SNAP25 showed an unfavorable prognosis in glioma patients. The effect of SNAP25 on cell proliferation, migration and invasion was also examined, and the results exhibited that SNAP25 overexpression effectively inhibited cell proliferation, migration, invasion and dendritic formation, and

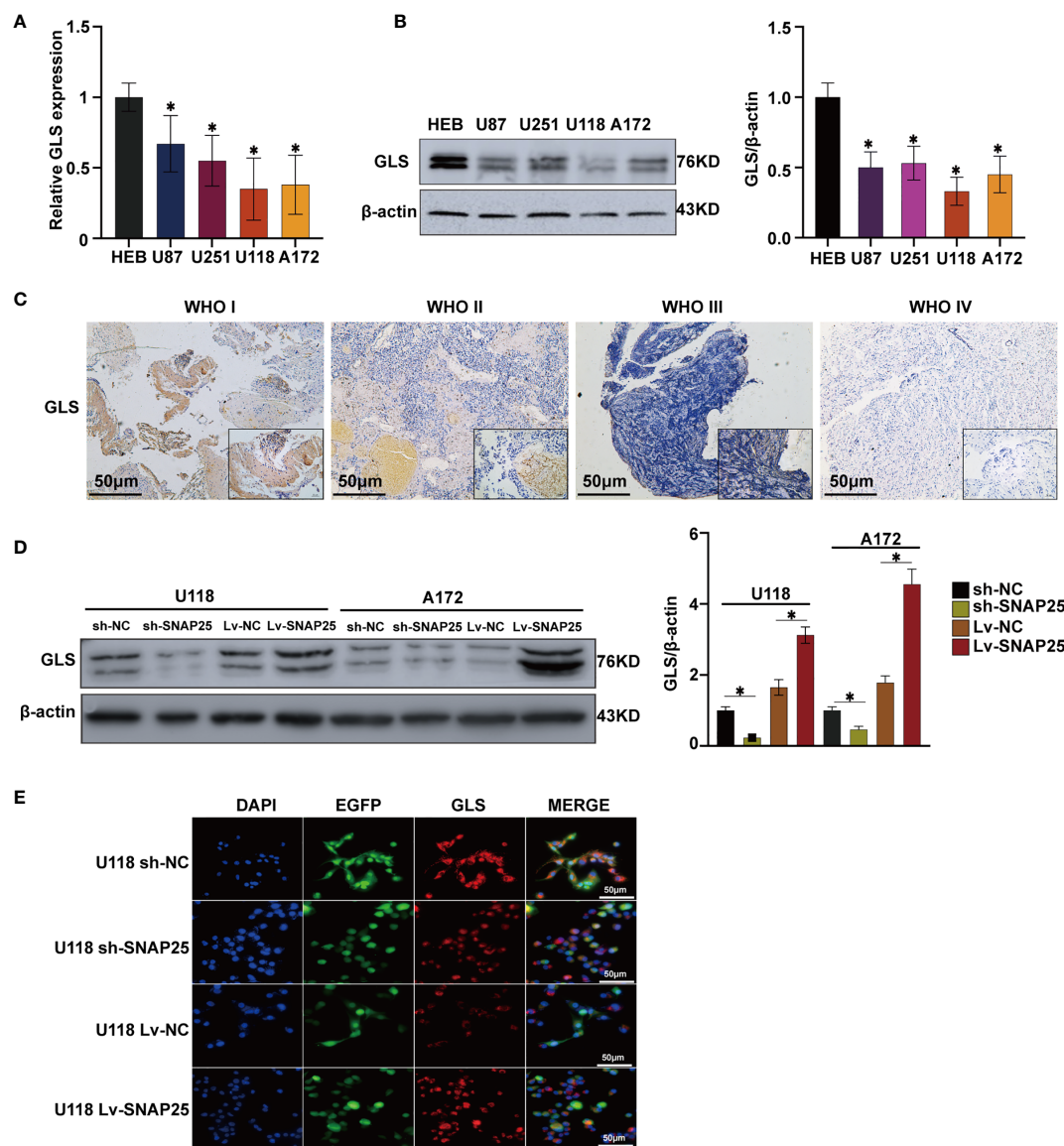


**FIGURE 5 |** SNAP25 functions as an efficient sponge in glioma. **(A, B)** RT-qPCR **(A)** and western blot **(B)** analysis of GLS expression level in glioma parental cell lines and NHA, \* $p < 0.05$  compared with NHA cells. **(C)** Representative images of SNAP25 expression from glioma tissues and nontumor tissues by ISH assays. **(D)** Western blot analysis of GLS expression level in U118 and A172 glioma cell lines transfected with sh-NC, sh-SNAP25, Lv-NC and Lv-SNAP25, \* $p < 0.05$  compared with Lv-NC or sh-NC group. **(E)** Immunofluorescence staining of GLS in SNAP25-transfected cells.

promoted cell glutaminolysis of glioma cells. Conversely, SNAP25 knockdown accelerated cell proliferation, migration and invasion, and decreased glutaminolysis of glioma cells. Besides, the upregulated SNAP25 could delay tumor growth and extent the overall survival time of the victims *in vivo*. The data above revealed that SNAP25 acted as a tumor suppressor in glioma and inhibited the progression of glioma.

Since SNAP25 basically functions as a critical role in synaptic activity regulating vesicle transfer between neighboring cells in the nervous system (31), SNAP25 was hypothesized to play a neuron-glioma cell interaction-activated role which can influence brain cancer growth. This represents a striking example of the

core physiological function of an organ promoting the growth of cancer arising within it. An important mechanism mediating this key microenvironmental interaction is the activity-regulated degradation of SNAP25. The importance of SNAP25 in glioma pathophysiology is underscored by the finding that SNAP25 expression strongly predicts survival in human glioma and discourages expression of MAP2, an abundant microtubule-associate protein that participates in the outgrowth of neuronal processes and synaptic plasticity (32). Also, reduced expression of SNAP25 not only fails to impair synaptic transmission but instead enhance evoked glutamatergic neurotransmission potentially rely on presynaptic voltage-gated calcium channel

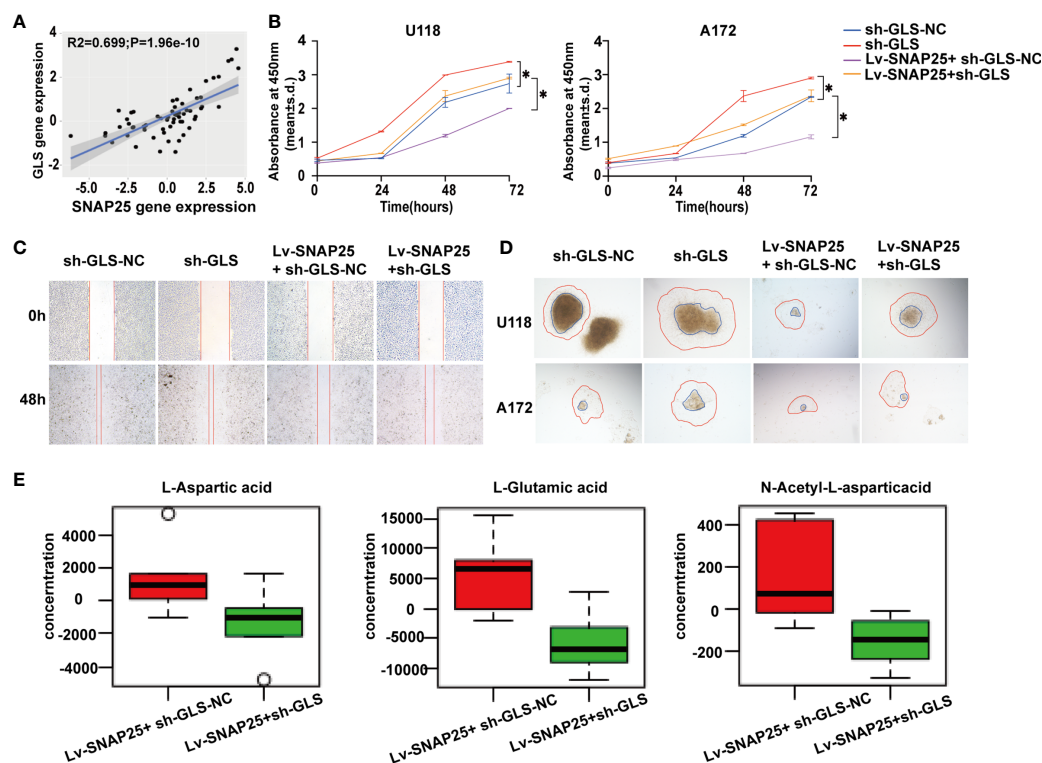


**FIGURE 6 |** GLS is positively correlated with SNAP25. **(A)** Correlation analysis of SNAP25 and GLS by Pearson's correlation coefficient. *P*-value is given on the figure. **(B)** CCK-8 assay of U118 and A172 glioma cells when transfected with Lv-NC, Lv-SNAP25 and/or sh-GLS-NC, sh-GLS, \**p* < 0.05 compared with Lv-NC or sh-GLS-NC group. **(C, D)** Wound healing assay and cancer cell spheroid invasive assay of U118 and A172 glioma cells when transfected with Lv-NC, Lv-SNAP25 and/or sh-GLS-NC, sh-GLS. **(E)** The concentration of L-Aspartic acid, L-Glutamic acid, and N-Acetyl-L-aspartic acid from LC-MS data obtained for Lv-SNAP25 glioma cells transfected with sh-GLS-NC or sh-GLS.

activity (27). Taken together, these studies elucidate a fundamental dimension of the glioma microenvironment and identify a robust and targetable mechanism of SNAP25 driving glioma proliferation and progression. However, a direct influence exerted by active parenchymal neurons upon the glioma environment has not been well appreciated. The critical role of neural elements in the cancer microenvironment has recently been elucidated for prostate, pancreatic and gastric cancers, in which peripheral innervation was found to potently promote cancer progression (33, 40). Furthermore, Venkatesh et al. suggest that abundant synaptic formation plays a critical role in the microenvironment of brain tumors through the malignant hijacking of mechanisms central to brain plasticity (35).

Interestingly, a wealth of elegant data illustrates that neurotransmitters and neuropeptides can affect glioma cell behavior. Glutamate secreted from glioma cells influences their proliferation and invasion through autocrine/paracrine signaling and subsequently increases the excitability of affected cortical networks (36). Tumorigenesis requires cancer cells to increase their metabolic output to support tumor growth (16, 37). Glutamine fuels cellular bioenergetics and supports multiple biosynthetic processes, making it an important nutrient for highly proliferative cells (38). Specifically, glutamine's carbon backbone can be utilized for the production of TCA cycle

intermediates, amino acids, and other metabolites, while glutamine-derived nitrogen also promotes nucleotide biosynthesis (39–41). Specifically, the abundance of glutamine in glioma further accelerates the tumor anabolism as glutamate converted from glutamine by glutaminase may be metabolized to D2HG in IDH1 mutated glioma cells accompanied by a loss of proper enzymatic activity (26). The proper function of glutaminase would be an important factor between the IDH1/2 mutational status and the WHO grade classification of gliomas.

In this study, the metabolic activity of glioma cells showed a significant discrepancy between SNAP25 overexpression and SNAP25 control cell groups and glutathione metabolism, alanine, aspartate and glutamate metabolism largely contributed to their separation. Moreover, glutamine-related metabolism was highly facilitated as increased L-aspartate acid, L-glutamate acid and N-acetyl-L-aspartic acid abundance was observed. Glutamatergic systems govern neuron-glia and glia-glia interactions and coordinate metabolic coupling of local cells (42, 43). Activation of the glutamine metabolism maintains synaptic homeostasis and regulates synaptic formation/plasticity. GLS, which deaminates glutamine to glutamate, reduces proliferation and tumorigenicity in certain cancer models (44). Conversely, GLS2 can be induced by the tumor suppressor p53 as a tumor suppressor (45). We confirmed that



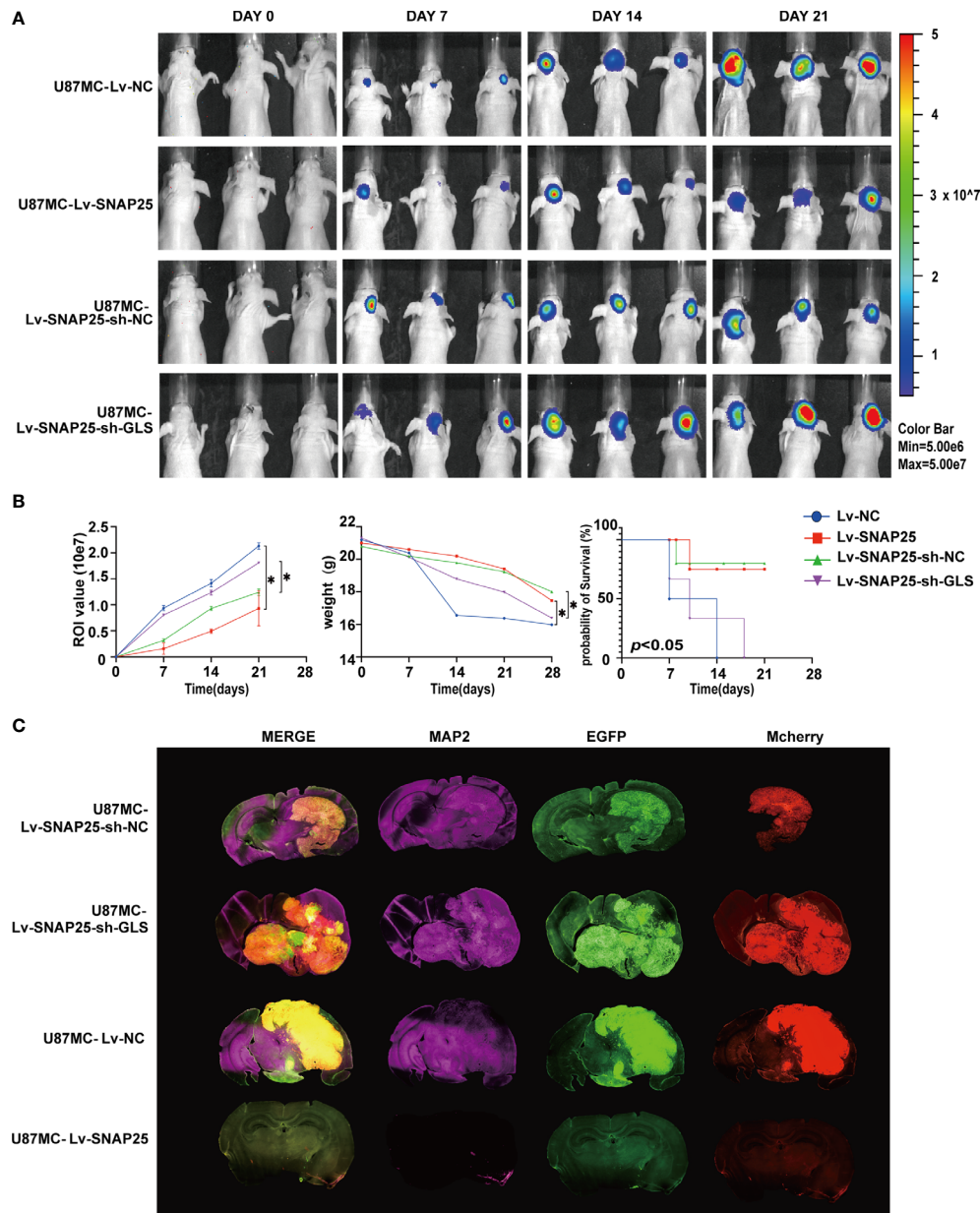


**FIGURE 7 | (A)** Tumor growth was monitored over time (up to Day 21) by measuring luciferase emission (ROI). **(B)** The ROI value, weight of the mice and the probability of survival was recorded over time.  $p < 0.05$  compared with Lv-NC or Lv-SNAP25-sh-NC group. **(C)** Glioma cell (Mcherry staining) and neuronal dendron (MAP2 staining) in the brains of indicated mice at the time of harvesting (Day 21).

GLS acted as a metabolic target of SNAP25 and consequently decelerated glioma progression. The correlation between SNAP25 and GLS is positive and the correlation coefficient is 0.699 ( $p=1.96 \times 10^{-10}$ ). Then further validation was applied in glioma tissues and cells and poor GLS expression was found in gliomas compared to normal tissues. Finally, knockdown of GLS could rescue the antitumor effect of SNAP25 *in vitro* and *in vivo*.

In summary, the present study is the first to investigate synapse-related gene expression patterns in glioma patients and

identify their relationship to patient outcome. The synaptic signature SNAP25 identified in our study exhibited potential as a biomarker of OS in glioma patients and indicated a relationship between neuron-glioma cell interaction and glioma progression. But the study just proved the positive correlation between SNAP25 and GLS, the cause effect of SNAP25 in regulation of GLS expression and the detail regulative mechanism was not figured out. Also, the relationship between SNAP25 and MAP2 was not well distinguished as the low expression of MAP2 in



U87Mcherry Lv-SNAP25 glioma cell-transplanted-xenograft may be simply related to the lack of tumor growth and size.

Understanding the microenvironmental mechanisms underlying synapse plasticity and its effect on tumor prognosis can provide insights into the identification of diagnostic and therapeutic targets for glioma.

## DATA AVAILABILITY STATEMENT

The original contributions presented in the study are publicly available. This data can be found here: [www.ebi.ac.uk/metabolights/MTBLS2806](http://www.ebi.ac.uk/metabolights/MTBLS2806) (Identifier MTBLS2806).

## ETHICS STATEMENT

The studies involving human participants were reviewed and approved by the ethical committee of Zhujiang Hospital. The patients/participants provided their written informed consent to participate in this study. The animal study was reviewed and approved by the ethical committee of Zhujiang Hospital.

## AUTHOR CONTRIBUTIONS

QH and CL: conception and design, experiments conduction, data analysis, and manuscript writing. YD, QH, and CL: experiments conduction and data analysis. ZH, BL, HZ, and NX: final approval of manuscript. HG: conception and design,

and final approval of manuscript. All authors contributed to the article and approved the submitted version.

## FUNDING

This study was supported by funds from the National Science Foundation of Guangdong Province (2017A030308001), Guangdong Province Science and Technology Innovation Strategy Special Fund (2018A030310422), the Guangdong Medical Science and Technology Research Fund (A2018542), and the National Nature Science Foundation of China (81874019, 82073193).

## SUPPLEMENTARY MATERIAL

The Supplementary Material for this article can be found online at: <https://www.frontiersin.org/articles/10.3389/fonc.2021.698835/full#supplementary-material>

**Supplementary Figure 1 | (A, B)** Knockdown and over-expression of endogenous SNAP25 in specific shRNA transduced glioma cells by RT-qPCR and western blot. \* $p < 0.05$  compared with the sh-NC cells. **(C)** Score plot of the principle component analysis results for LC-MS data obtained for sh-NC and sh-SNAP25 glioma cells. **(D)** Loading plots of the principle component analysis results for LC-MS data obtained for sh-NC and sh-SNAP25 glioma cells. Metabolites 261 (glutamate) and 262 (glutamic acid) contributed largely to their separation. **(E)** Pathway analysis results for LC-MS data obtained for sh-NC and sh-SNAP25 glioma cells. Alanine, aspartate and glutamate metabolism pathway shows a high pathway plot impact. **(F-H)** The concentration of L-Aspartic acid **(E)**, L-Glutamic acid **(F)**, and N-Acetyl-L-aspartic acid.

## REFERENCES

- Ostrom QT, Gittleman H, Fulop J, Liu M, Blanda R, Kromer C, et al. CBTRUS Statistical Report: Primary Brain and Central Nervous System Tumors Diagnosed in the United States in 2008–2012. *Neuro Oncol* (2015) 17(Suppl 4):iv1–62. doi: 10.1093/neuonc/now207
- Giering A, Psczolkowska D, Walentyrowicz KA, Rajan WD, Kaminska B. Immune Microenvironment of Gliomas. *Lab Invest* (2017) 97:498–518. doi: 10.1038/labinvest.2017.19
- Ma Q, Long W, Xing C, Chu J, Luo M, Wang HY, et al. Cancer Stem Cells and Immunosuppressive Microenvironment in Glioma. *Front Immunol* (2018) 9:2924. doi: 10.3389/fimmu.2018.02924
- Gu G, Gao T, Zhang L, Chen X, Pang Q, Wang Y, et al. NKAP Alters Tumor Immune Microenvironment and Promotes Glioma Growth via Notch1 Signaling. *J Exp Clin Cancer Res* (2019) 38:291. doi: 10.1002/jbbo.201900136
- Guo X, Xue H, Shao Q, Wang J, Guo X, Chen X, et al. Hypoxia Promotes Glioma-Associated Macrophage Infiltration via Periostin and Subsequent M2 Polarization by Upregulating TGF- $\beta$  and M-CSFR. *Oncotarget* (2016) 7:80521–42. doi: 10.18632/oncotarget.11825
- Klemm F, Maas RR, Bowman RL, Kornete M, Soukup K, Nassiri S, et al. Interrogation of the Microenvironmental Landscape in Brain Tumors Reveals Disease-Specific Alterations of Immune Cells. *Cell* (2020) 181:1643–60.e17. doi: 10.1016/j.cell.2020.05.007
- Derecki NC, Cronk JC, Lu Z, Xu E, Abbott SB, Guyenet PG, et al. Wild-Type Microglia Arrest Pathology in a Mouse Model of Rett Syndrome. *Nature* (2012) 484:105–9. doi: 10.1038/nature10907
- Garcia O, Torres M, Helguera P, Coskun P, Busciglio J. A Role for Thrombospondin-1 Deficits in Astrocyte-Mediated Spine and Synaptic Pathology in Down's Syndrome. *PLoS One* (2010) 5:e14200. doi: 10.1371/journal.pone.0014200
- Zhou C, Feng Z, Ko CP. Defects in Motoneuron-Astrocyte Interactions in Spinal Muscular Atrophy. *J Neurosci* (2016) 36:2543–53. doi: 10.1523/JNEUROSCI.3534-15.2016
- Higashimori H, Schin CS, Chiang MS, Morel L, Shoneye TA, Nelson DL, et al. Selective Deletion of Astroglial FMRP Dysregulates Glutamate Transporter GLT1 and Contributes to Fragile X Syndrome Phenotypes In Vivo. *J Neurosci* (2016) 36:7079–94. doi: 10.1523/JNEUROSCI.1069-16.2016
- Sekar A, Bialas AR, de Rivera H, Davis A, Hammond TR, Kamitaki N, et al. Schizophrenia Risk From Complex Variation of Complement Component 4. *Nature* (2016) 530:177–83. doi: 10.1038/nature16549
- Stogsdill JA, Eroglu C. The Interplay Between Neurons and Glia in Synapse Development and Plasticity. *Curr Opin Neurobiol* (2017) 42:1–8. doi: 10.1016/j.conb.2016.09.016
- Pajarillo E, Rizzor A, Lee J, Aschner M, Lee E. The Role of Astrocytic Glutamate Transporters GLT-1 and GLAST in Neurological Disorders: Potential Targets for Neurotherapeutics. *Neuropharmacology* (2019) 161:107559. doi: 10.1016/j.neuropharm.2019.03.002
- Rosati A, Poliani PL, Todeschini A, Cominelli M, Medicina D, Cenzato M, et al. Glutamine Synthetase Expression as a Valuable Marker of Epilepsy and Longer Survival in Newly Diagnosed Glioblastoma Multiforme. *Neuro Oncol* (2013) 15:618–25. doi: 10.1002/jnc.29152
- Maus A, Peters GJ. Erratum to: Glutamate and Alpha-Ketoglutarate: Key Players in Glioma Metabolism. *Amino Acids* (2017) 49:1143. doi: 10.1007/s00726-017-2414-5
- Vander Heiden MG, DeBerardinis RJ. Understanding the Intersections Between Metabolism and Cancer Biology. *Cell* (2017) 168:657–69. doi: 10.1016/j.cell.2016.12.039

17. Rumping L, Pras-Raves ML, Gerrits J, Tang YF, Willemsen MA, Houwen RHJ, et al. Metabolic Fingerprinting Reveals Extensive Consequences of GLS Hyperactivity. *Biochim Biophys Acta Gen Subj* (2020) 1864:129484. doi: 10.1016/j.bbagen.2019.129484
18. Wang Q, Wang Y, Ji W, Zhou G, He K, Li Z, et al. SNAP25 is Associated With Schizophrenia and Major Depressive Disorder in the Han Chinese Population. *J Clin Psychiatry* (2015) 76:e76–82. doi: 10.4088/JCP.13m08962
19. Carroll LS, Kendall K, O'Donovan MC, Owen MJ, Williams NM. Evidence That Putative ADHD Low Risk Alleles at SNAP25 may Increase the Risk of Schizophrenia. *Am J Med Genet B Neuropsychiatr Genet* (2009) 150B:893–9. doi: 10.1002/ajmg.b.30915
20. Jia L, Zhu M, Kong C, Pang Y, Zhang H, Qiu Q, et al. Blood Neuro-Exosomal Synaptic Proteins Predict Alzheimer's Disease at the Asymptomatic Stage. *Alzheimers Dement* (2021) 17:49–60. doi: 10.1002/alz.12166
21. Zou J, Duan D, Yu C, Pan J, Xia J, Yang Z, et al. Mining the Potential Prognostic Value of Synaptosomal-Associated Protein 25 (SNAP25) in Colon Cancer Based on Stromal-Immune Score. *PeerJ* (2020) 8:e10142. doi: 10.7717/peerj.10142
22. Hao J, Zhang Y, Yan X, Yan F, Sun Y, Zeng J, et al. Circulating Adipose Fatty Acid Binding Protein Is a New Link Underlying Obesity-Associated Breast/Mammary Tumor Development. *Cell Metab* (2018) 28:689–705.e5. doi: 10.1016/j.cmet.2018.07.006
23. Martin-Rufian M, Nascimento-Gomes R, Higuero A, Crisma AR, Campos-Sandoval JA, Gomez-Garcia MC, et al. Both GLS Silencing and GLS2 Overexpression Synergize With Oxidative Stress Against Proliferation of Glioma Cells. *J Mol Med (Berl)* (2014) 92:277–90, 465–71. doi: 10.1016/j.neuint.2005.10.015
24. Hu W, Zhang C, Wu R, Sun Y, Levine A, Feng Z. Glutaminase 2, a Novel P53 Target Gene Regulating Energy Metabolism and Antioxidant Function. *Proc Natl Acad Sci USA* (2010) 107:7455–60. doi: 10.1371/journal.pone.0038380
25. Ostrom QT, Cioffi G, Gittleman H, Patil N, Waite K, Kruchko C, et al. CBRUS Statistical Report: Primary Brain and Other Central Nervous System Tumors Diagnosed in the United States in 2012–2016. *Neuro Oncol* (2019) 21: v1–100. doi: 10.1093/neuonc/noz150
26. Obara-Michlewska M, Szeliga M. Targeting Glutamine Addiction in Gliomas. [In Eng]. *Cancers (Basel)* (2020) 12(2):310. doi: 10.3390/cancers12020310
27. Antonucci F, Corradini I, Morini R, Fossati G, Menna E, Pozzi D, et al. Reduced SNAP-25 Alters Short-Term Plasticity at Developing Glutamatergic Synapses. *EMBO Rep* (2013) 14:645–51. doi: 10.1038/embor.2013.75
28. Olbrich K, Costard L, Moser CV, Syhr KM, King-Himmelreich TS, Wolters MC, et al. Cleavage of SNAP-25 Ameliorates Cancer Pain in a Mouse Model of Melanoma. *Eur J Pain* (2017) 21:101–11. doi: 10.1002/ejp.904
29. Yu C, Yin J, Wang X, Chen L, Wei Y, Lu C, et al. Association Between SNAP25 and Human Glioblastoma Multiform: A Comprehensive Bioinformatic Analysis. *Biosci Rep* (2020) 40(6):BSR20200516. doi: 10.1042/BSR20200516
30. Choi J, Choi JA. Influence of Leisure Competence and Level of Leisure Activity on Life Satisfaction in Low-Income Older Adults in Rural South Korea. *Res Gerontol Nurs* (2017) 10:67–75. doi: 10.3928/19404921-20170224-01
31. Selak S, Paternain AV, Aller MI, Pico E, Rivera R, Lerma J. A Role for SNAP25 in Internalization of Kainate Receptors and Synaptic Plasticity. *Neuron* (2009) 63:357–71. doi: 10.1016/j.neuron.2009.07.017
32. D'Andrea MR, Howanski RJ, Saller CF. MAP2 IHC Detection: A Marker of Antigenicity in CNS Tissues. *Biotech Histochem* (2017) 92:363–73. doi: 10.1080/10520295.2017.1295169
33. Coarfa C, Florentin D, Putluri N, Ding Y, Au J, He D, et al. Influence of the Neural Microenvironment on Prostate Cancer. *Prostate* (2018) 78:128–39. doi: 10.18632/oncotarget.15019
34. Renz BW, Tanaka T, Sunagawa M, Takahashi R, Jiang Z, Macchini M, et al. Cholinergic Signaling via Muscarinic Receptors Directly and Indirectly Suppresses Pancreatic Tumorigenesis and Cancer Stemness. *Cancer Discov* (2018) 8:1458–73. doi: 10.1126/scitranslmed.3009569
35. Venkatesh HS, Morishita W, Geraghty AC, Silverbush D, Gillespie SM, Arzt M, et al. Electrical and Synaptic Integration of Glioma Into Neural Circuits. *Nature* (2019) 573:539–45. doi: 10.1038/s41586-019-1563-y
36. Venkataramani V, Tanev DI, Strahle C, Studier-Fischer A, Fankhauser L, Kessler T, et al. Glutamatergic Synaptic Input to Glioma Cells Drives Brain Tumour Progression. *Nature* (2019) 573:532–8. doi: 10.1038/s41586-019-1564-x
37. Lu J, Li D, Zeng Y, Wang H, Feng W, Qi S, et al. IDH1 Mutation Promotes Proliferation and Migration of Glioma Cells via EMT Induction. *J BUON* (2019) 24:2458–64.
38. Wang Y, Bai C, Ruan Y, Liu M, Chu Q, Qiu L, et al. Coordinative Metabolism of Glutamine Carbon and Nitrogen in Proliferating Cancer Cells Under Hypoxia. *Nat Commun* (2019) 10:201. doi: 10.1038/s41467-018-08033-9
39. DeBerardinis RJ, Mancuso A, Daikhin E, Nissim I, Yudkoff M, Wehrli S, et al. Beyond Aerobic Glycolysis: Transformed Cells Can Engage in Glutamine Metabolism That Exceeds the Requirement for Protein and Nucleotide Synthesis. *Proc Natl Acad Sci USA* (2007) 104:19345–50. doi: 10.1073/pnas.0709747104
40. Choi YK, Park KG. Targeting Glutamine Metabolism for Cancer Treatment. *Biomol Ther (Seoul)* (2018), 26(1):19–28. doi: 10.1016/j.cell.2018.07.019
41. Kim J, Hu Z, Cai L, Li K, Choi E, Faubert B, et al. CPS1 Maintains Pyrimidine Pools and DNA Synthesis in KRAS/LKB1-Mutant Lung Cancer Cells. *Nature* (2017) 546:168–72. doi: 10.1038/nature22359
42. Tasker JG, Oliet SH, Bains JS, Brown CH, Stern JE. Glial Regulation of Neuronal Function: From Synapse to Systems Physiology. *J Neuroendocrinol* (2012) 24:6920–7. doi: 10.1523/JNEUROSCI.0473-04.2004
43. von Blankenfeld G, Kettenmann H. Glutamate and GABA Receptors in Vertebrate Glial Cells. *Mol Neurobiol* (1991) 5:31–43. doi: 10.1007/BF02935611
44. Wang JB, Erickson JW, Fuji R, Ramachandran S, Gao P, Dinavahi R, et al. Targeting Mitochondrial Glutaminase Activity Inhibits Oncogenic Transformation. *Cancer Cell* (2010) 18:207–19. doi: 10.1016/j.ccr.2010.08.009
45. Suzuki S, Tanaka T, Poyurovsky MV, Nagano H, Mayama T, Ohkubo S, et al. Phosphate-Activated Glutaminase (GLS2), A P53-Inducible Regulator of Glutamine Metabolism and Reactive Oxygen Species. *Proc Natl Acad Sci USA* (2010) 107:7461–6. doi: 10.1073/pnas.1002459107

**Conflict of Interest:** The authors declare that the research was conducted in the absence of any commercial or financial relationships that could be construed as a potential conflict of interest.

**Publisher's Note:** All claims expressed in this article are solely those of the authors and do not necessarily represent those of their affiliated organizations, or those of the publisher, the editors and the reviewers. Any product that may be evaluated in this article, or claim that may be made by its manufacturer, is not guaranteed or endorsed by the publisher.

Copyright © 2021 Huang, Lian, Dong, Zeng, Liu, Xu, He and Guo. This is an open-access article distributed under the terms of the Creative Commons Attribution License (CC BY). The use, distribution or reproduction in other forums is permitted, provided the original author(s) and the copyright owner(s) are credited and that the original publication in this journal is cited, in accordance with accepted academic practice. No use, distribution or reproduction is permitted which does not comply with these terms.



# Regulation of Extracellular Matrix Production in Activated Fibroblasts: Roles of Amino Acid Metabolism in Collagen Synthesis

Emily J. Kay<sup>1\*</sup>, Grigorios Koulouras<sup>1,2</sup> and Sara Zanivan<sup>1,2\*</sup>

<sup>1</sup> Cancer Research UK Beatson Institute, Glasgow, United Kingdom, <sup>2</sup> Institute of Cancer Sciences, University of Glasgow, Glasgow, United Kingdom

## OPEN ACCESS

### Edited by:

Miriam Martini,  
University of Turin, Italy

### Reviewed by:

Lidia Avello,  
University of Turin, Italy  
Nadia Rucci,  
University of L'Aquila, Italy

### \*Correspondence:

Sara Zanivan  
s.zanivan@beatson.gla.ac.uk  
Emily J. Kay  
e.kay@beatson.gla.ac.uk

### Specialty section:

This article was submitted to  
Cancer Metabolism,  
a section of the journal  
Frontiers in Oncology

**Received:** 03 June 2021

**Accepted:** 27 July 2021

**Published:** 27 August 2021

### Citation:

Kay EJ, Koulouras G and Zanivan S  
(2021) Regulation of Extracellular  
Matrix Production in Activated  
Fibroblasts: Roles of Amino Acid  
Metabolism in Collagen Synthesis.  
Front. Oncol. 11:719922.  
doi: 10.3389/fonc.2021.719922

Cancer associated fibroblasts (CAFs) are a major component of the tumour microenvironment in most tumours, and are key mediators of the response to tissue damage caused by tumour growth and invasion, contributing to the observation that tumours behave as 'wounds that do not heal'. CAFs have been shown to play a supporting role in all stages of tumour progression, and this is dependent on the highly secretory phenotype CAFs develop upon activation, of which extracellular matrix (ECM) production is a key element. A collagen rich, stromal ECM has been shown to influence tumour growth and metastasis, exclude immune cells and impede drug delivery, and is associated with poor prognosis in many cancers. CAFs also extensively remodel their metabolism to support cancer cells, however, it is becoming clear that metabolic rewiring also supports intrinsic functions of activated fibroblasts, such as increased ECM production. In this review, we summarise how fibroblasts metabolically regulate ECM production, focussing on collagen production, at the transcriptional, translational and post-translational level, and discuss how this can provide possible strategies for effectively targeting CAF activation and formation of a tumour-promoting stroma.

**Keywords:** extracellular matrix, fibroblasts, CAF, tumour microenvironment, metabolism, amino acids

## INTRODUCTION

Fibroblasts are one of the most abundant cell types in the microenvironment of solid tumours, and have long been known to play multiple and varied roles in promoting tumour progression and metastasis. Fibroblasts are influenced by tumour cells to become 'activated', a process during which they develop a highly secretory phenotype involving production of growth factors, pro-angiogenic factors, immunomodulatory factors, metabolites, extracellular vesicles, and, crucially, ECM components and remodelling factors (1–5). Activated fibroblasts in the tumour microenvironment are known as cancer associated fibroblasts, or CAFs, however, fibroblasts undergo an extremely similar activation process during wound healing, or other fibrotic diseases (6, 7). Indeed, the role of activated fibroblasts is vital in the process of wound healing to stimulate cell proliferation, blood vessel repair and formation, immune cell recruitment to prevent infection and ECM production to provide

structural support for wound closure. However, following wound healing, fibroblasts revert to their quiescent state whereas in cancer or fibrotic disease, fibroblasts are aberrantly and continuously activated, leading to the description of tumours as ‘wounds that do not heal’ (8).

One of the main roles of fibroblasts in the healthy body is to produce and maintain turnover of the extracellular matrix (ECM), of which collagen proteins are one of the most highly abundant components, and indeed comprise approximately 30% of the total protein content of mammals (9). Upon fibroblast activation, however, production of ECM and collagen is vastly upregulated. In cancer, the production of excessive collagen-rich ECM by CAFs is a crucial step in tumour progression, and CAFs are the main source of structural ECM in tumours (10, 11). Studies have shown that a collagen-dense stromal compartment is a predictor of poor prognosis in many cancer types (12–14). ECM provides a substrate for integrin-mediated signalling supporting cancer cell adhesion and proliferation (15–18), acts as a reservoir of pro-angiogenic and growth factors, can be degraded to provide amino acids for tumour cells (19, 20) and also acts as a physical barrier to decrease tumour perfusion, drug delivery and infiltration of tumour suppressing immune cells (21, 22). Furthermore, collagen in the tumour microenvironment is more heavily cross-linked and linearised, leading to a stiffer ECM which is also known to increase tumour aggression (23, 24). The remodelling of the ECM and linearization of collagen fibres is an important step in the deposition of pro-tumorigenic ECM, since non-linearised collagen I can be anti-tumourigenic (25). *In vivo*, the effects of the ECM on tumour growth have been assessed in several studies. Ablation of Col6a1 or Col5a3 in the MMTV-PyMT mammary tumour model resulted in reduced hyperplasia and primary tumour growth (26, 27). Conversely, mice have been engineered to produce more collagen (Col1a1<sup>tm1jac</sup>) showed increased tumour growth in the MMTV-PyMT model

(12, 28). Inhibition of production of other ECM components such as hyaluronan, fibronectin and tenascin-C also suppresses tumour initiation and growth (29, 30). Therefore finding ways to target ECM production by CAFs could both reduce tumour growth and metastasis and improve tumour perfusion and drug delivery (**Figure 1**) (29–33).

## ENERGETIC COST OF ECM PRODUCTION

Of all the proteins that make up the ECM, collagen has a particularly unusual amino acid composition. The collagen protein is composed primarily of the Gly-X-Y motif, in which X and Y are most commonly proline and its modified form hydroxyproline (34). This is because small, flexible amino acids are required to fit into the helix conformation of collagen chains, and in particular glycine is the only amino acid small enough to fit into the centre of the triple helix. Furthermore, the hydroxyproline residues can form hydrogen bonds along the helix to stabilise it. As a result, collagens contain approximately 30% glycine and 15–20% proline or hydroxyproline residues, although this varies between different collagens (**Table 1**). Therefore, collagen synthesis has unique biosynthetic requirements and, given that it is a major output of CAFs, it is expected that they might remodel their metabolism accordingly to sustain it. Both proline and glycine are non-essential amino acids, and can therefore be obtained exogenously from blood or made endogenously. Glycine is the smallest amino acid and its production from larger molecules is actually an exogenic process. Glycine is produced from serine and its synthesis is therefore connected to the tetrahydrofolate cycle and to glycolysis, both of which produce ATP (**Figure 2**). Proline synthesis, on the other hand, is an ATP-consuming process. Proline can be synthesised either from glutamine *via* conversion to glutamate, or from

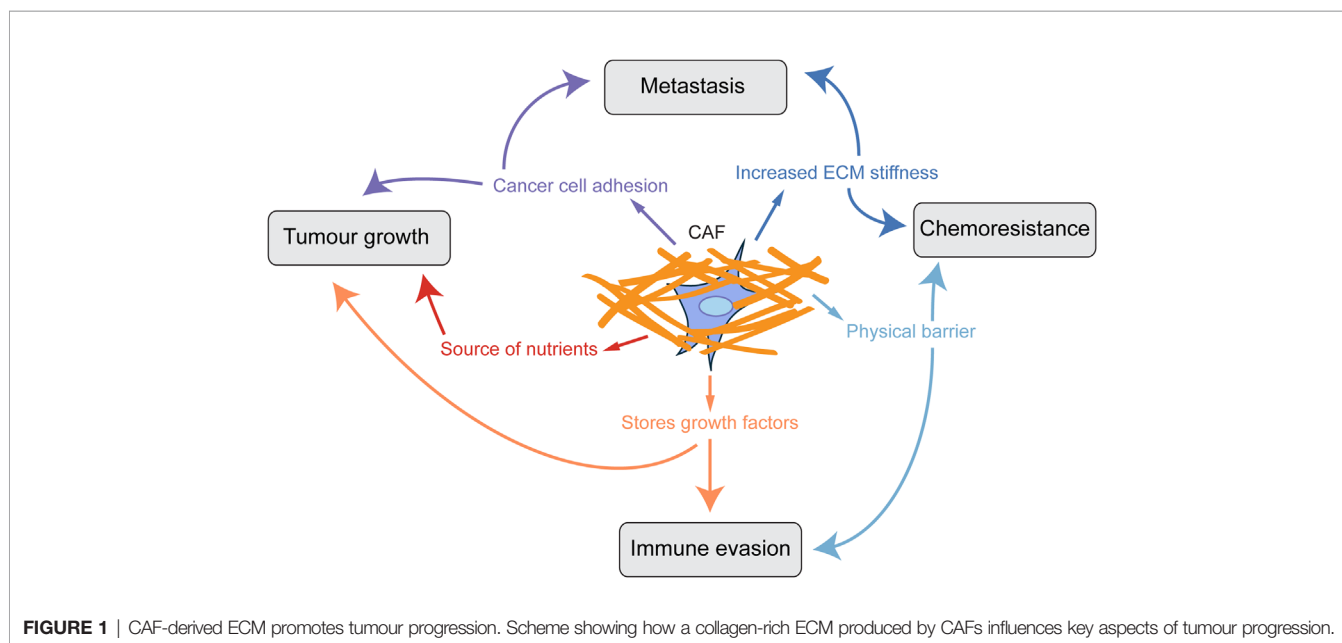




**TABLE 1 |** A list of collagens with the percentage of glycine and proline residues in each.

Collagen Type	Proline content (%)	Glycine content (%)
Collagen I	17.5	27.3
Collagen II	18.1	27.3
Collagen III	18.7	28.1
Collagen IV	21.7	27.7
Collagen V	17.6	24.8
Collagen VI	8.2	11.6
Collagen VII	14.4	21.2
Collagen VIII	22.4	26.5
Collagen IX	16.6	27.9
Collagen X	21.3	25.7
Collagen XI	16.7	24.0
Collagen XII	9.2	9.2
Collagen XIII	17.4	25.6
Collagen XIV	8.7	10.8
Collagen XV	13.8	15.9
Collagen XVI	17.5	24.3
Collagen XVII	13.6	18.8
Collagen XVIII	17.3	17.2

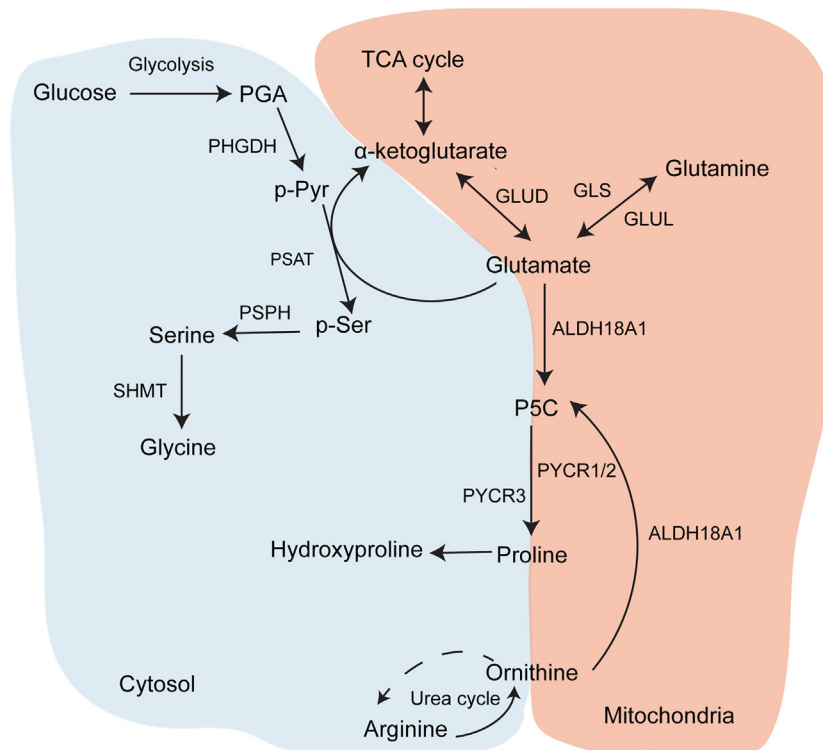


**FIGURE 2 |** Glycine and proline biosynthesis. Metabolic pathways contributing to synthesis of proline and glycine, which are the two most abundant amino acids in collagen.

arginine *via* conversion to ornithine. Synthesis of 1 mole proline from 1 mole glutamine or arginine requires 8 or 2.5 moles ATP, respectively (35). The arginine pathway for proline synthesis therefore has the least energetic cost.

Specific amino acid requirements aside, the increased production of ECM proteins has a more general energetic cost. Structural proteins such as collagens and fibronectin have a high number of amino acid residues, meaning that their translation is

costly in terms of ATP and GTP. Post-translational modification of proline to hydroxyproline also has a high energetic cost, with 4 mole of ATP required to produce 1 mole of hydroxyproline for collagen synthesis. Once translated and modified, ECM proteins are then secreted by exocytosis, itself an ATP-consuming process (36).

Although it has long been known that tumour cells undergo metabolic alterations, only in the last decade has the remodelling

of CAF metabolism been studied in detail. Most studies focus on the role of CAF metabolism in supporting tumour cell proliferation through secretion of metabolites such as lactate, pyruvate, and amino acids. Increased glycolysis and autophagy are the two mechanisms most commonly observed in CAF metabolic rewiring in the context of CAFs providing metabolites to fuel tumour cells (37–43). However, until recently there has been little research into how CAFs rewire their metabolism to support their own needs upon activation, and in particular to support ECM production. In addition to data available on how activated fibroblasts metabolically support ECM production in cancer, we can look to research on ECM production by fibroblasts in wound healing and fibrosis for further insights, since these behave similarly to CAFs (44). Indeed, studies show that there are metabolic similarities between CAFs and other types of activated fibroblasts, such as increased glycolysis (45–47).

## GLYCOLYSIS STIMULATES ECM PRODUCTION IN FIBROBLASTS

Increased TGF $\beta$  signalling is the most well-known and studied hallmark and master regulator of fibroblast activation, both in cancer and in other fibroblast activating conditions. Among its many roles, TGF $\beta$  signalling upregulates production of ECM, including collagens, in activated fibroblasts (48, 49). TGF $\beta$  has also been linked to metabolic reprogramming in CAFs; in particular, it has been shown to upregulate glycolysis in many studies. Although previous work has focussed on the role of TGF $\beta$ -induced glycolysis in CAFs in producing lactate as a metabolic fuel for tumour cells, termed the ‘Reverse Warburg effect’ (38, 50), it is important to note that glycolysis is also the major source of ATP production in cells. As discussed earlier, the process of ECM production is ATP consuming, through requirements for specific amino acids, protein translation and post-translational modification. Since ECM is such a significant output of CAFs, it is reasonable to predict that an increase in glycolysis may also support ECM synthesis *via* increased ATP production. In support of this, it has been shown that fibroblasts require an increase in glucose uptake and glycolysis to support TGF $\beta$ -induced collagen production in fibrosis (51, 52).

Glucose metabolism is also required for the synthesis of glycine, the most abundant amino acid in collagen, and therefore increased TGF $\beta$ -induced glycolysis in CAFs could also support collagen production through providing precursors for glycine synthesis. Although glycine is available exogenously (~400  $\mu$ M in plasma) (53), two studies have demonstrated that TGF $\beta$  signalling also increases serine and glycine synthesis in activated fibroblasts. Nigdegliogou and co-workers (51) demonstrated that the enzymes for serine and glycine synthesis from glucose, PDGDH and SHMT2 (**Figure 2**), were upregulated in TGF $\beta$ -treated human lung fibroblasts, in addition to glycolytic enzymes. Pharmacological inhibition or genetic deletion of PDGDH and SHMT2 both attenuated TGF $\beta$ -induced collagen I production. Since glycolysis provides precursors for both glycine and serine synthesis (**Figure 2**), this implies that

upregulated glycolysis in activated fibroblasts can also be used to fuel glycine biosynthesis, which is a requirement for collagen production. The mechanism for TGF $\beta$ -stimulated glycine production was further elucidated by Selvarajah and co-workers (54), who recently demonstrated that, in human lung fibroblasts, canonical TGF $\beta$  signalling through SMAD3 activated mTORC1 enhanced expression of glycine synthesis enzymes and the glucose transporter GLUT1 *via* upregulation of the transcription factor ATF4. Inhibition of this pathway reduced glycine incorporation into, and thereby production of, collagen I. A further study by Woodcock and co-workers (55) also found that pharmacological inhibition of the mTORC1/4EBP1 signalling pathway attenuated collagen I synthesis in TGF $\beta$ -treated human lung fibroblasts and in CAFs derived from lung adenocarcinoma patients. mTOR signalling was also found to be upregulated in CAFs isolated from human PDAC tumours, although its effect on ECM production was not investigated (56). These studies show firstly that there is a requirement for increased amino acid production to support collagen synthesis, and also suggest a further role for TGF $\beta$ -induced glycolysis and mTOR signalling in activated fibroblasts to support glycine synthesis for collagen production. The role of mTOR signalling in this pathway is also of interest, as mTORC1 has long been known to be regulated by availability of amino acids (57), including glutamine which is involved in collagen production. Therefore it is also possible that when amino acids are available in activated fibroblasts, activated mTOR signalling regulates transcription of genes involved in metabolic pathways that promote collagen synthesis, both through increasing ATP production *via* glycolysis and further synthesis of specific amino acids required for translation of collagen mRNA.

## PROLINE SYNTHESIS IS REQUIRED FOR COLLAGEN PRODUCTION IN ACTIVATED FIBROBLASTS

Collagen synthesis has often been hypothesised to be a metabolic ‘dump’ for excess proline. Both glutamine and arginine can be converted into 1-pyrroline-5-carboxylic acid (P5C) (*via* ALDH18A1 or OAT), which is the final precursor for proline synthesis by PYCR1, PYCR2 or PYCR3. It seems clear that proline synthesis is upregulated in activated fibroblasts and a limiting factor in collagen production. Hepatic stellate cells increase proline production from glutamine upon activation during liver fibrosis, and PYCR1 is upregulated and proline oxidase (PRODH), which recycles proline back to P5C, is downregulated, showing that fibroblast activation pushes cells towards proline synthesis, although whether this affected collagen production was not investigated (58). A recent study showed that TGF $\beta$ -activated fibroblasts increased expression of genes in the proline synthesis pathway as well as increasing proline labelling from  $^{13}$ C-glutamine. ALDH18A1 deletion decreased collagen production, which could be rescued with proline supplementation (52). PYCR1 deletion did not however affect collagen synthesis. Conversely, PYCR1

knockdown or inhibition reduced collagen production, and particularly collagen VI production, in patient derived mammary CAFs, and could be rescued with proline supplementation (59). P5C supplementation has also been shown to increase collagen synthesis by human fibroblasts (60). Furthermore, *Pycr1* KO zebrafish have reduced ECM content and proline and hydroxyproline levels in their tissues, demonstrating a link between proline availability and ECM production (61). Interestingly, mutations in *PYCR1* or *ALDH18A1* in patients give rise to a condition called cutis laxa, one of the symptoms of which is wrinkled skin. This could be due to a loss of ECM production by fibroblasts, and indeed abnormal collagen fibres and decreased collagen compactness, in addition to reduced elastin content, has been observed in some patients with *PYCR1* mutations (62). Reduced levels of collagens I and III has also been observed in patients with *ALDH18A1* mutations (63).

In addition to proline biosynthesis, extracellular proline is a potential source of proline for collagen synthesis. Several studies have investigated the effects of extracellular proline on collagen production in fibroblasts. Proline concentration is upregulated at wound sites, suggesting it is either actively imported to or synthesised at the wound and therefore there may be a requirement for extracellular proline (64). However, an early study found that proline supplementation does not increase collagen production in a range of cell lines in culture, although fibroblasts were not investigated (65). Although cirrhotic rat liver contains high levels of proline and collagen, a proline rich diet did not stimulate collagen production in the liver, suggesting the high proline concentration comes from proline synthesis (66). More recent research, including from our lab, has confirmed this observation (59). Proline supplementation did not increase collagen production in human mammary CAFs and human skin fibroblasts unless glutamine availability or proline synthesis was limited (59, 67). Furthermore, although exogenous proline increased Col1a1 expression and radiolabelled proline was incorporated into collagen in human dermal fibroblasts, this effect was more pronounced when the fibroblasts were cultured in the absence of glutamine (67). Therefore, it seems that fibroblasts preferentially synthesise their own proline. The study on dermal fibroblasts proposed that proline availability also regulates expression of collagen genes as well as being a substrate for collagen translation, which suggests there could be a feedback loop whereby intracellular proline concentration regulates collagen expression. However, this was not the case in the mammary CAFs, so this may not be a universal mechanism for activated fibroblasts.

The question of why fibroblasts prefer to synthesise their own proline for collagen production, even when free proline is available, has not yet been answered. One possibility is that proline synthesis plays an important role in producing reducing potential. The production of proline by *PYCR1* oxidises NADPH or NADH to NADP<sup>+</sup>/NAD<sup>+</sup>, which can support glycolysis and the pentose phosphate pathway (68), which could help to maintain the increase in glycolysis in activated fibroblasts. Equally, the interconversion of P5C and proline creates a shuttle of the redox equivalents NADPH/NADP<sup>+</sup> between the

mitochondria and cytosol, meaning that proline production can play a role in maintaining redox homeostasis (69). Proline itself is also an antioxidant through the secondary amine of the pyrrolidine ring (70). In support of this, upregulated proline synthesis protects cells from the reducing potential and ROS caused by increased TCA cycle activity in TGF- $\beta$  stimulated fibroblasts (52), and mitochondrial NADPH was required for proline biosynthesis and collagen production in MEFs (71). *PYCR1* loss in fibroblasts has been shown to increase their susceptibility to ROS-mediated apoptosis (72). Interestingly, both *PYCR1* and *PYCR2* have been found to interact with and promote the activity of RRM2B, a protein that supports DNA damage repair in response to oxidative stress, in fibroblasts, showing that the anti-oxidant properties of *PYCR1* are not solely due to its role in proline production but that it also plays a role in the wider cellular response to oxidative stress (73). Therefore fibroblasts may also maintain proline synthesis to counteract redox stress. Thus, in addition to reducing ECM production, targeting collagen production in CAFs through proline synthesis could also reduce their ability to cope with the increased levels of oxidative stress in the tumour microenvironment, and further research into the effects of proline synthesis inhibition on CAFs would be needed to verify this.

## PRECURSORS FOR PROLINE SYNTHESIS

### Glutamine Metabolism

Another major metabolic pathway, which has been found to regulate ECM production in fibroblasts, and in particular collagen production, is that of glutamine metabolism. Glutamine is converted to glutamate, and from there can enter the TCA cycle *via*  $\alpha$ -ketoglutarate to fuel oxidative phosphorylation. Glutamate is also a precursor for proline. Intraperitoneal administration of glutamine improved wound healing and increased the presence of immature collagen in parenchymal lung lesions in rats (74). Interestingly, dietary glutamine supplementation improved collagen density in colonic anastomoses in rats more than glycine supplementation (75), suggesting that fibroblasts are able to synthesise sufficient glycine for collagen production, whereas they require a source of extracellular glutamine. This is also reflected in a study showing that a much higher concentration of extracellular glycine was needed to increase collagen production in chondrocytes than that of glutamine or, indeed, proline (76). Conversely, inhibition of glutamine metabolism with the glutamine agonist 6-diazo-5-oxo-L-norleucine (DON) prevented aspects of fibrosis including collagen production in fibroblasts derived from patients with iatrogenic laryngotracheal stenosis (iLTS) (77). Conversion of glutamine into glutamate seems to be crucial for its collagen-promoting properties, as inhibition of glutamate synthase (GLS) with the inhibitor BPTES also decreased collagen production in iLTS derived fibroblasts (78). Furthermore, both glutamine and glutamate stimulated collagen biosynthesis in human skin fibroblasts (60), and glutamine synthesis has been shown to be upregulated in ovarian CAFs (79). However, although these studies show that glutamine

metabolism is important for collagen production both *in vivo* and in activated fibroblasts *in vitro*, the question remains as to whether glutamine enhances collagen production through incorporation into proline to sustain collagen translation, or through other metabolic pathways leading indirectly to increased collagen expression, or both.

A few studies have demonstrated that glutamine is required for proline production to sustain collagen synthesis in fibroblasts. Bellon and co-workers (80) first demonstrated that glutamine supplementation stimulates procollagen synthesis in human foreskin fibroblasts, and that glutamine-derived proline competed with extracellular  $^{14}\text{C}$ -labelled proline for incorporation into prolyl-tRNA and procollagen, showing that glutamine is an important intracellular source of proline for collagen production. Furthermore, procollagen synthesis was independent of the concentration of free proline in the media when glutamine was provided, suggesting that fibroblasts may prefer to synthesise their own proline from glutamine rather than use extracellular proline. A more recent study showed that conversion of glutamine into glutamate and thence to proline and glycine (Figure 2) is required for collagen production in human lung fibroblasts activated with TGF $\beta$  (81). TGF $\beta$  increased the expression of GLS, PSAT1 and enzymes in the proline synthesis pathway, and the intracellular concentrations of both proline and glycine, in addition to increasing collagen production. In the absence of glutamine, collagen production, but not *COL1A1* mRNA expression, was reduced, implying again that glutamine is required for collagen translation. siRNA mediated silencing of GLS, PSAT1 or ALDH18A1 attenuated TGF $\beta$ -induced collagen production, and interestingly ALDH18A1 knockdown could not be rescued by proline supplementation at physiological levels, suggesting again that proline synthesis from glutamine, rather than extracellular proline, is required for collagen synthesis in activated fibroblasts. This is concurrent with data showing only supraphysiological levels of proline could rescue PYCR1 knockdown (59), however another study was able to rescue ALDH18A1 depletion with sub physiological proline levels (52). This could be because the CRISPR mediated ALDH18A1 knockout in Schworer et al. has a more drastic effect on proline synthesis compared to the siRNA and shRNA knockdown in the other two studies, and can therefore a lower dose of proline will provide some rescue. Conversely, inhibition of glutamate metabolism by oxoglutarate dehydrogenase knockdown to decrease oxidative metabolism did not affect collagen production.

## Arginine and Ornithine

Aside from glutamine, cells can also make proline for collagen production from arginine *via* ornithine, a pathway which branches from the urea cycle (Figure 2). Much of the evidence that arginine metabolism supports collagen production comes from studies on wound healing and fibrosis, however there is some evidence that this pathway may be similarly regulated in CAFs. Glutamate, arginine and ornithine are all drained at burn sites (82, 83), suggesting a requirement for these specific amino acids during the wound healing process. Furthermore, arginase expression is upregulated in wound derived fibroblasts at all

stages of the wound healing process in rats (84) and local inhibition of arginase delayed healing of incisional wounds in C57Bl/6 mice (85). Arginine is also among the metabolites upregulated in the lungs of patients with idiopathic lung fibrosis (86), although the study did not investigate whether the increase in arginine levels was specifically in fibroblasts or in other cells in the lung. In an immunohistochemical analysis of PDAC patients, arginase has been found to be upregulated in CAFs, and is a predictor of poor outcome. Furthermore, arginase expression could be stimulated in cultured fibroblasts by exposure to hypoxia, which is a common feature of the tumour microenvironment (87). Therefore arginine and ornithine metabolism seems to be upregulated in conditions in which fibroblasts increase collagen production. But does it actually contribute to collagen synthesis? Dietary supplementation of both arginine and ornithine, but not citrulline, has been shown to improve collagen production in wounds in mice or rats (88–90). Furthermore, arginase is upregulated in fibroblasts in mice treated with bleomycin to stimulate fibrosis, and pharmacological inhibition of arginase with NG-hydroxy-L-arginine attenuated TGF $\beta$ -stimulated collagen deposition, without affecting collagen mRNA expression or SMAD signalling, suggesting that arginine is required for collagen translation, possibly through conversion to proline (91). Also linking TGF $\beta$ -induced collagen deposition by fibroblasts to arginase activity is a study showing that treating rats given lung orthotopic transplants with pirfenidone reduced collagen content and fibro-collagenous injury in the transplants, and that this was associated with both decreased endogenous TGF $\beta$  and arginase expression (92). TGF $\beta$  was also shown to stimulate arginine uptake and ornithine aminotransferase (OAT) expression in smooth muscle cells (93). Arginine-induced collagen production by smooth muscle cells was found to be dependent on conversion of arginine to proline (94), suggesting arginine's role in collagen synthesis is as a proline precursor. However, much of the research into arginine metabolism and collagen production has been done in the context of wound healing and fibrosis, and while activated fibroblasts in wounds and the TME share similarities, further research is required to verify whether targeting arginase also reduces collagen production in tumours. Arginase has already been proposed as a therapeutic target against tumour promoting immune cells, so if it also stimulates collagen production in CAFs it could be a useful means of targeting two aspects of the tumour microenvironment.

## ALTERNATIVE ROLES FOR AMINO ACID METABOLISM IN COLLAGEN PRODUCTION

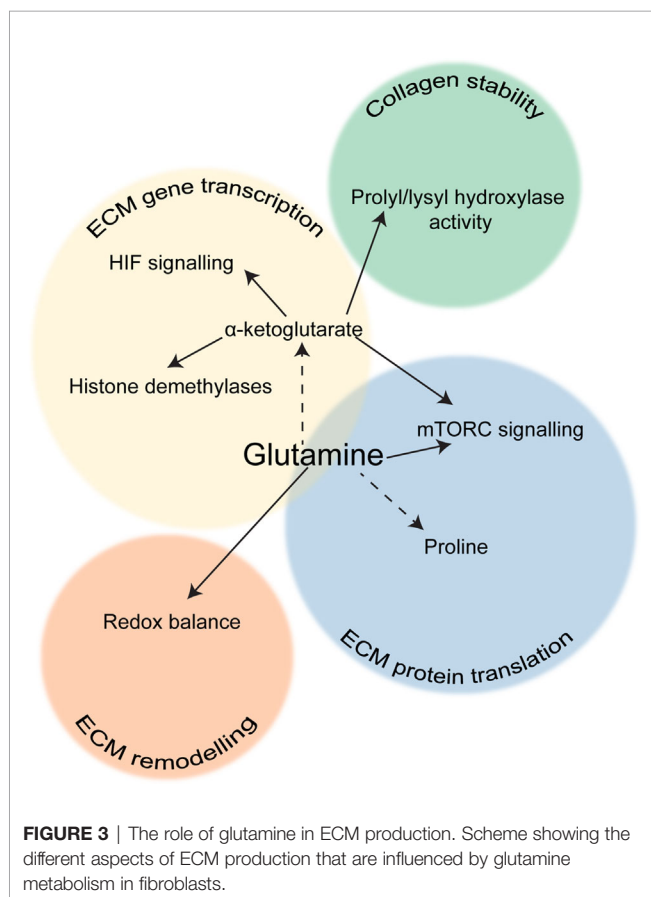
Many studies have shown that the role of glutamine metabolism in collagen synthesis is not limited to the translational level (Figure 3). Interestingly, glutamine availability can also regulate collagen mRNA expression in fibroblasts. Treatment of cultured fibroblasts with glutamine increased collagen mRNA levels (95), conversely, removal of glutamine from cell culture media or pharmacological inhibition of GLS reduced expression of



collagen I in hepatic stellate cells (58). It has also been shown that glutamine metabolism may regulate fibroblast activation at a more general level. Bernard and co-workers found that when murine lung fibroblasts are deprived of glutamine or GLS is inhibited, TGF $\beta$  treatment fails to increase not only the expression of *Colla1*, but also other markers of fibroblast activation including fibronectin, *Acta2* (which encodes for  $\alpha$ SMA) and *Hif1a*. Interestingly, the authors also found that glutamine depletion post-TGF $\beta$  treatment did not affect  $\alpha$ SMA protein levels but did affect the other markers, and that  $\alpha$ -ketoglutarate only restored *Acta2* and *Hif1a* expression under glutamine deprivation (96). On the other hand, another study showed that in human lung fibroblasts GLS inhibition did not affect collagen gene expression, but reduced collagen translation *via* loss of mTORC1 activation, which was regulated by  $\alpha$ -ketoglutarate production from glutamate (97). This therefore suggests that glutamine metabolism may support fibroblast activation through several different pathways. It is worth noting that  $\alpha$ -ketoglutarate is a cofactor for many enzymes, including histone demethylases, so it is possible that glutamine metabolism may promote expression of *Acta2* and *Hif1a* through an epigenetic switch, whereas perhaps expression of ECM proteins is part of a feedback loop regulated by amino acid availability. Conversion of  $\alpha$ -ketoglutarate to succinate could also inhibit prolyl hydroxylases that destabilise HIF1 $\alpha$ .

An alternative way that glutamine metabolism can affect collagen production is through  $\alpha$ -ketoglutarate-mediated activation of prolyl hydroxylases, which use it as a cofactor. Conversely, accumulation of succinate decreases prolyl hydroxylase activity. Proline hydroxylation is vital to maintain collagen stability, and GLS inhibition markedly increased degradation of collagens I and III in human lung fibroblasts (97). The requirement for  $\alpha$ -ketoglutarate by prolyl hydroxylases has also been linked to amino acid sensing by mTOR, since  $\alpha$ -ketoglutarate is a degradation product of several amino acids and the product of glutamine deamination (98). As previously discussed, mTOR activation has also been linked to collagen production through activation of glycine synthesis and glycolysis. A more recent study demonstrated that HIF1 $\alpha$  activation in chondrocytes led to increased glutaminolysis and thereby accumulation of  $\alpha$ -ketoglutarate. This enhanced proline and lysine hydroxylation on collagen, making the matrix more resistant to degradation by MMPs and ultimately resulting in skeletal dysplasia (99). Since HIF1 $\alpha$  signalling is also often activated in CAFs (100, 101), this mechanism could also be relevant for increased collagen modification in the tumour microenvironment. The  $\alpha$ -ketoglutarate: succinate ratio has also been shown to affect collagen stability in breast CAFs (102). Another aspect of glutamine metabolism is its effect on the redox balance of the cell, as glutamate is a precursor for GSH synthesis, and it has also been shown that glutamine or cancer cell-derived glutamate balances the redox state of fibroblasts, enabling ECM remodelling and increased ECM stiffness (103). Therefore glutamine metabolism clearly has a wider impact on CAF-derived ECM than solely the translation of ECM proteins. Although it is clear that glutamine metabolism has an important role to play in ECM production by CAFs, the mechanism(s) by which it promotes fibrosis are unclear and studies are conflicting as to whether glutamine affects both collagen transcription and translation. More research is needed to determine exactly how glutamine metabolism can regulate mRNA expression of collagen, fibronectin and other myofibroblast markers. Therefore the exact role of glutamine in fibroblast activation and ECM production has yet to be determined, and it seems likely that glutamine metabolism impacts upon many pathways that can affect ECM gene expression, synthesis and stability.

Arginine metabolism may also play a more complex role in collagen production besides that of a proline precursor. Arginine is involved in the production of nitric oxide (NO), which has been shown in several studies to inhibit fibrosis and collagen production by fibroblasts (104–106). Therefore arginase and NO synthase (NOS) may compete for arginine as a substrate, and metabolism of arginine by arginase may divert arginine away from NO production in addition to enabling proline synthesis to stimulate collagen synthesis. On the other hand, NO production has actually been found upregulated in breast CAFs due to downregulation of Caveolin 1, which binds and inhibits NOS. NO production led to increased glycolysis and ROS production, both features of CAF activation (107). Interestingly, arginine supplementation was unable to enhance wound healing and collagen production in inducible NOS knockout mice (108), whereas ornithine



supplementation still stimulated collagen production even in the absence of NOS (90). Therefore, while proline production from arginine and ornithine can be upregulated in activated fibroblasts to stimulate collagen production, whether or not arginine uptake regulates collagen production by reducing NO synthesis is still unclear and further research is required to elucidate the role of NO in fibroblast activation.

## CONCLUSIONS

TGF $\beta$  is well-known as a master regulator of CAF activation, but it is becoming clear that it is also a major architect of metabolic rewiring in fibroblasts. TGF $\beta$  stimulates glycolysis, serine and glycine metabolism, glutamine metabolism, and increased proline synthesis from glutamine and arginine. Therefore, in addition to increasing ECM gene expression, TGF $\beta$  also activates metabolic pathways that support ECM production by activated fibroblasts: by increasing ATP generation to support synthesis of ECM protein, increasing production of amino acids required for collagen translation and by enhancing collagen stability and post-translational modification.

Glycine, proline, glutamine and arginine metabolism are all potential targets for normalising collagen production in the tumour stroma to reduce tumour growth and improve tumour perfusion and drug delivery. However, there is still much research to be done and many unanswered questions. Firstly, many of the studies showing these metabolites affect collagen production have been carried out in the context of activated fibroblasts in wound healing, fibrotic disease and acutely TGF $\beta$ -treated fibroblasts, rather than CAFs derived from cancer patients, although gene expression data suggests these pathways are also upregulated in the tumour stroma. Therefore, further research is needed to verify that metabolic changes in CAFs are relevant and targetable pathways to regulate ECM production. Furthermore, there is a lack of studies investigating whether these metabolic pathways could be a viable therapeutic target against the tumour stroma *in vivo*, since the majority of research to date has focussed on the role of these pathways in 2D cell culture of activated fibroblasts and the only *in vivo* models have been of wound healing or fibrotic disease.

Therapeutically, there are already several possibilities for targeting metabolic regulation of ECM production in CAFs. The GLS inhibitor CB-839 is currently undergoing clinical trials in cancer patients, so it would be useful to ascertain whether this drug affects the stroma as well as targeting cancer cells. Arginase inhibitors are also available and undergoing clinical trials in cancer patients as an immunotherapeutic, again, it will be interesting to discover if they also have an impact on CAFs. However, the development of drugs targeting the proline synthesis pathway is still at an early stage, and inhibitors against PYCR1 have only recently been developed (109, 110). Since however, PYCR1 has recently been found to be upregulated in many cancer cells and to have tumour promoting effects both in cancer cells and CAFs (59, 111, 112), the development of new inhibitors may prove useful in targeting both tumour and stroma, killing two birds with one stone. Targeting stromal collagen production may also increase the effectiveness of immunotherapies. Collagen was shown to impede immune cell filtration, increase T-cell exhaustion and decrease sensitivity to PD-L1 blockade in lung tumours (113), although this may be tumour context dependent since in a *KRas*-induced PDAC mouse model, ablation of stromal collagen I enabled recruitment of tumour suppressing myeloid cells and promoted tumour progression (114). Finally, since normalisation of the tumour stroma is known to increase drug delivery to the tumour, it is likely that targeting the metabolic pathways discussed in this review will be most efficacious in combination with other cancer cell targeting therapies, and this should be borne in mind when designing future therapeutic strategies to target cancer-associated stroma and ECM production.

## AUTHOR CONTRIBUTIONS

Conceived the work: EJK and SZ. Writing the manuscript: EJK. Generated data for Figure: GK. All authors contributed to the article and approved the submitted version.

## FUNDING

This work was funded by Cancer Research UK (A29800 to SZ) and Breast Cancer Now (2019AugPR1307 to SZ).

## REFERENCES

- Cohen N, Shani O, Raz Y, Sharon Y, Hoffman D, Abramovitz L, et al. Fibroblasts Drive an Immunosuppressive and Growth-Promoting Microenvironment in Breast Cancer via Secretion of Chitinase 3-Like 1. *Oncogene* (2017) 36:4457–68. doi: 10.1038/onc.2017.65
- Hernandez-Fernaund JR, Ruengeler E, Casazza A, Neilson LJ, Pulleine E, Santi A, et al. Secreted CLIC3 Drives Cancer Progression Through Its Glutathione-Dependent Oxidoreductase Activity. *Nat Commun* (2017) 8:14206. doi: 10.1038/ncomms14206
- Kalluri R. The Biology and Function of Fibroblasts in Cancer. *Nat Rev Cancer* (2016) 16:582–98. doi: 10.1038/nrc.2016.73
- Liao D, Luo Y, Markowitz D, Xiang R, Reisfeld RA. Cancer Associated Fibroblasts Promote Tumor Growth and Metastasis by Modulating the Tumor Immune Microenvironment in a 4T1 Murine Breast Cancer Model. *PLoS One* (2009) 4:e7965. doi: 10.1371/journal.pone.0007965
- Zhao H, Yang L, Baddour J, Achreja A, Bernard V, Moss T, et al. Tumor Microenvironment Derived Exosomes Pleiotropically Modulate Cancer Cell Metabolism. *Elife* (2016) 5:e10250. doi: 10.7554/eLife.10250
- Darby IA, Laverdet B, Bonte F, Desmouliere A. Fibroblasts and Myofibroblasts in Wound Healing. *Clin Cosmet Investig Dermatol* (2014) 7:301–11. doi: 10.2147/CCID.S50046
- Khalil H, Kanisicak O, Prasad V, Correll RN, Fu X, Schips T, et al. Fibroblast-Specific TGF- $\beta$ 2/3 Signaling Underlies Cardiac Fibrosis. *J Clin Invest* (2017) 127:3770–83. doi: 10.1172/JCI94753
- Dvorak HF. Tumors: Wounds That Do Not Heal-Redux. *Cancer Immunol Res* (2015) 3:1–11. doi: 10.1158/2326-6066.CIR-14-0209
- Frantz C, Stewart KM, Weaver VM. The Extracellular Matrix at a Glance. *J Cell Sci* (2010) 123:4195–200. doi: 10.1242/jcs.023820
- Naba A, Clauser KR, Lamar JM, Carr SA, Hynes RO. Extracellular Matrix Signatures of Human Mammary Carcinoma Identify Novel Metastasis Promoters. *Elife* (2014) 3:e01308. doi: 10.7554/eLife.01308

11. Hebert JD, Myers SA, Naba A, Abbruzzese G, Lamar JM, Carr SA, et al. Proteomic Profiling of the ECM of Xenograft Breast Cancer Metastases in Different Organs Reveals Distinct Metastatic Niches. *Cancer Res* (2020) 80:1475–85. doi: 10.1158/0008-5472.CAN-19-2961
12. Provenzano PP, Inman DR, Eliceiri KW, Knittel JG, Yan L, Rueden CT, et al. Collagen Density Promotes Mammary Tumor Initiation and Progression. *BMC Med* (2008) 6:11. doi: 10.1186/1741-7015-6-11
13. Whatcott CJ, Diep CH, Jiang P, Watanabe A, LoBello J, Sima C, et al. Desmoplasia in Primary Tumors and Metastatic Lesions of Pancreatic Cancer. *Clin Cancer Res* (2015) 21:3561–8. doi: 10.1158/1078-0432.CCR-14-1051
14. Shimosato Y, Suzuki A, Hashimoto T, Nishiwaki Y, Kodama T, Yoneyama T, et al. Prognostic Implications of Fibrotic Focus (Scar) in Small Peripheral Lung Cancers. *Am J Surg Pathol* (1980) 4:365–73. doi: 10.1097/00000478-198008000-00005
15. Bae YH, Mui KL, Hsu BY, Liu SL, Cretu A, Razinia Z, et al. A FAK-Cas-Rac-Lamellipodin Signaling Module Transduces Extracellular Matrix Stiffness Into Mechanosensitive Cell Cycling. *Sci Signal* (2014) 7:ra57. doi: 10.1126/scisignal.2004838
16. Gilmore AP, Metcalfe AD, Romer LH, Streuli CH. Integrin-Mediated Survival Signals Regulate the Apoptotic Function of Bax Through Its Conformation and Subcellular Localization. *J Cell Biol* (2000) 149:431–46. doi: 10.1083/jcb.149.2.431
17. Schwartz MA, Assoian RK. Integrins and Cell Proliferation: Regulation of Cyclin-Dependent Kinases via Cytoplasmic Signaling Pathways. *J Cell Sci* (2001) 114:2553–60. doi: 10.1242/jcs.114.14.2553
18. Shibue T, Weinberg RA. Integrin Beta1-Focal Adhesion Kinase Signaling Directs the Proliferation of Metastatic Cancer Cells Disseminated in the Lungs. *Proc Natl Acad Sci USA* (2009) 106:10290–5. doi: 10.1073/pnas.0904227106
19. Gouirand V, Vasseur S. Fountain of Youth of Pancreatic Cancer Cells: The Extracellular Matrix. *Cell Death Discov* (2018) 4:1. doi: 10.1038/s41420-017-0004-7
20. Olivares O, Mayers JR, Gouirand V, Torrence ME, Gicquel T, Borge L, et al. Collagen-Derived Proline Promotes Pancreatic Ductal Adenocarcinoma Cell Survival Under Nutrient Limited Conditions. *Nat Commun* (2017) 8:16031. doi: 10.1038/ncomms16031
21. Mariathasan S, Turley SJ, Nickles D, Castiglioni A, Yuen K, Wang Y, et al. TGFbeta Attenuates Tumour Response to PD-L1 Blockade by Contributing to Exclusion of T Cells. *Nature* (2018) 554:544–8. doi: 10.1038/nature25501
22. Netti PA, Berk DA, Swartz MA, Grodzinsky AJ, Jain RK. Role of Extracellular Matrix Assembly in Interstitial Transport in Solid Tumors. *Cancer Res* (2000) 60:2497–503.
23. Rice AJ, Cortes E, Lachowski D, Cheung BCH, Karim SA, Morton JP, et al. Matrix Stiffness Induces Epithelial-Mesenchymal Transition and Promotes Chemoresistance in Pancreatic Cancer Cells. *Oncogenesis* (2017) 6:e352. doi: 10.1038/oncsis.2017.54
24. Wei SC, Fattet L, Tsai JH, Guo Y, Pai VH, Majeski HE, et al. Matrix Stiffness Drives Epithelial-Mesenchymal Transition and Tumour Metastasis Through a TWIST1-G3BP2 Mechanotransduction Pathway. *Nat Cell Biol* (2015) 17:678–88. doi: 10.1038/ncb3157
25. Maller O, Hansen KC, Lyons TR, Acerbi I, Weaver VM, Prekeris R, et al. Collagen Architecture in Pregnancy-Induced Protection From Breast Cancer. *J Cell Sci* (2013) 126:4108–10. doi: 10.1242/jcs.121590
26. Iyengar P, Espina V, Williams TW, Lin Y, Berry D, Jelicks LA, et al. Adipocyte-Derived Collagen VI Affects Early Mammary Tumor Progression *In Vivo*, Demonstrating a Critical Interaction in the Tumor/Stroma Microenvironment. *J Clin Invest* (2005) 115:1163–76. doi: 10.1172/JCI23424
27. Huang G, Ge G, Izzi V, Greenspan DS. Alpha3 Chains of Type V Collagen Regulate Breast Tumour Growth via Glypican-1. *Nat Commun* (2017) 8:14351. doi: 10.1038/ncomms14351
28. Esbona K, Inman D, Saha S, Jeffery J, Schedin P, Wilke L, et al. COX-2 Modulates Mammary Tumor Progression in Response to Collagen Density. *Breast Cancer Res* (2016) 18:35. doi: 10.1186/s13058-016-0695-3
29. Udagabe L, Brownlee GR, Waltham M, Blick T, Walker EC, Heldin P, et al. Antisense-Mediated Suppression of Hyaluronan Synthase 2 Inhibits the Tumorigenesis and Progression of Breast Cancer. *Cancer Res* (2005) 65:6139–50. doi: 10.1158/0008-5472.CAN-04-1622
30. Lingasamy P, Tobi A, Haugas M, Hunt H, Paiste P, Asser T, et al. Bi-Specific Tenascin-C and Fibronectin Targeted Peptide for Solid Tumor Delivery. *Biomaterials* (2019) 219:119373. doi: 10.1016/j.biomaterials.2019.119373
31. Pickup MW, Mouw JK, Weaver VM. The Extracellular Matrix Modulates the Hallmarks of Cancer. *EMBO Rep* (2014) 15:1243–53. doi: 10.15252/embr.201439246
32. Cox TR. The Matrix in Cancer. *Nat Rev Cancer* (2021) 21:217–38. doi: 10.1038/s41568-020-00329-7
33. Winkler J, Abisoye-Ogunniyan A, Metcalf KJ, Werb Z. Concepts of Extracellular Matrix Remodelling in Tumour Progression and Metastasis. *Nat Commun* (2020) 11:5120. doi: 10.1038/s41467-020-18794-x
34. Grant ME, Prockop DJ. The Biosynthesis of Collagen. *N Engl J Med* (1972) 286:194–9. doi: 10.1056/NEJM197201272860406
35. Li P, Wu G. Roles of Dietary Glycine, Proline, and Hydroxyproline in Collagen Synthesis and Animal Growth. *Amino Acids* (2018) 50:29–38. doi: 10.1007/s00726-017-2490-6
36. Malhotra V, Erlmann P. Protein Export at the ER: Loading Big Collagens Into COPII Carriers. *EMBO J* (2011) 30:3475–80. doi: 10.1038/emboj.2011.255
37. Capparelli C, Guido C, Whitaker-Menezes D, Bonuccelli G, Balliet R, Pestell TG, et al. Autophagy and Senescence in Cancer-Associated Fibroblasts Metabolically Supports Tumor Growth and Metastasis via Glycolysis and Ketone Production. *Cell Cycle* (2012) 11:2285–302. doi: 10.4161/cc.20718
38. Guido C, Whitaker-Menezes D, Capparelli C, Balliet R, Lin Z, Pestell RG, et al. Metabolic Reprogramming of Cancer-Associated Fibroblasts by TGF-Beta Drives Tumor Growth: Connecting TGF-Beta Signaling With "Warburg-Like" Cancer Metabolism and L-Lactate Production. *Cell Cycle* (2012) 11:3019–35. doi: 10.4161/cc.21384
39. Sousa CM, Biancur DE, Wang X, Halbrook CJ, Sherman MH, Zhang L, et al. Pancreatic Stellate Cells Support Tumour Metabolism Through Autophagic Alanine Secretion. *Nature* (2016) 536:479–83. doi: 10.1038/nature19084
40. Zhang D, Wang Y, Shi Z, Liu J, Sun P, Hou X, et al. Metabolic Reprogramming of Cancer-Associated Fibroblasts by IDH3alpha Downregulation. *Cell Rep* (2015) 10:1335–48. doi: 10.1016/j.celrep.2015.02.006
41. Sun K, Tang S, Hou Y, Xi L, Chen Y, Yin J, et al. Oxidized ATM-Mediated Glycolysis Enhancement in Breast Cancer-Associated Fibroblasts Contributes to Tumor Invasion Through Lactate as Metabolic Coupling. *EBioMedicine* (2019) 41:370–83. doi: 10.1016/j.ebiom.2019.02.025
42. Whitaker-Menezes D, Martinez-Outschoorn UE, Lin Z, Ertel A, Flomenberg N, Witkiewicz AK, et al. Evidence for a Stromal-Epithelial "Lactate Shuttle" in Human Tumors: MCT4 Is a Marker of Oxidative Stress in Cancer-Associated Fibroblasts. *Cell Cycle* (2011) 10:1772–83. doi: 10.4161/cc.10.11.15659
43. Yu T, Yang G, Hou Y, Tang X, Wu C, Wu XA, et al. Cytoplasmic GPER Translocation in Cancer-Associated Fibroblasts Mediates cAMP/PKA/CREB/glycolytic Axis to Confer Tumor Cells With Multidrug Resistance. *Oncogene* (2017) 36:2131–45. doi: 10.1038/onc.2016.370
44. Foster DS, Jones RE, Ransom RC, Longaker MT, Norton JA. The Evolving Relationship of Wound Healing and Tumor Stroma. *JCI Insight* (2018) 3(18):e99911. doi: 10.1172/jci.insight.99911
45. Zhao X, Psarianos P, Ghorraie LS, Yip K, Goldstein D, Gilbert R, et al. Metabolic Regulation of Dermal Fibroblasts Contributes to Skin Extracellular Matrix Homeostasis and Fibrosis. *Nat Metab* (2019) 1:147–57. doi: 10.1038/s42255-018-0008-5
46. Vincent AS, Phan TT, Mukhopadhyay A, Lim HY, Halliwell B, Wong KP. Human Skin Keloid Fibroblasts Display Bioenergetics of Cancer Cells. *J Invest Dermatol* (2008) 128:702–9. doi: 10.1038/sj.jid.5701107
47. Xie N, Tan Z, Banerjee S, Cui H, Ge J, Liu RM, et al. Glycolytic Reprogramming in Myofibroblast Differentiation and Lung Fibrosis. *Am J Respir Crit Care Med* (2015) 192:1462–74. doi: 10.1164/rccm.201504-0780OC
48. Casey TM, Eneman J, Crocker A, White J, Tessitore J, Stanley M, et al. Cancer Associated Fibroblasts Stimulated by Transforming Growth Factor Beta1 (TGF-Beta 1) Increase Invasion Rate of Tumor Cells: A Population Study. *Breast Cancer Res Treat* (2008) 110:39–49. doi: 10.1007/s10549-007-9684-7
49. Roberts AB, Sporn MB, Assoian RK, Smith JM, Roche NS, Wakefield LM, et al. Transforming Growth Factor Type Beta: Rapid Induction of Fibrosis



- and Angiogenesis In Vivo and Stimulation of Collagen Formation In Vitro. *Proc Natl Acad Sci USA* (1986) 83:4167–71. doi: 10.1073/pnas.83.12.4167
50. Pavlides S, Whitaker-Menezes D, Castello-Cros R, Flomenberg N, Witkiewicz AK, Frank PG, et al. The Reverse Warburg Effect: Aerobic Glycolysis in Cancer Associated Fibroblasts and the Tumor Stroma. *Cell Cycle* (2009) 8:3984–4001. doi: 10.4161/cc.8.23.10238
  51. Nigdelioglu R, Hamanaka RB, Meliton AY, O'Leary E, Witt LJ, Cho T, et al. Transforming Growth Factor (TGF)-Beta Promotes De Novo Serine Synthesis for Collagen Production. *J Biol Chem* (2016) 291:27239–51. doi: 10.1074/jbc.M116.756247
  52. Schworer S, Berisa M, Violante S, Qin W, Zhu J, Hendrickson RC, et al. Proline Biosynthesis Is a Vent for TGFbeta-Induced Mitochondrial Redox Stress. *EMBO J* (2020) 39:e103334. doi: 10.15252/embj.2019103334
  53. Schmidt JA, Rinaldi S, Scalbert A, Ferrari P, Achaintre D, Gunter MJ, et al. Plasma Concentrations and Intakes of Amino Acids in Male Meat-Eaters, Fish-Eaters, Vegetarians and Vegans: A Cross-Sectional Analysis in the EPIC-Oxford Cohort. *Eur J Clin Nutr* (2016) 70:306–12. doi: 10.1038/ejcn.2015.144
  54. Selvarajah B, Azuelos I, Plate M, Guillotin D, Forty EJ, Contento G, et al. Mtorc1 Amplifies the ATF4-Dependent De Novo Serine-Glycine Pathway to Supply Glycine During TGF-Beta1-Induced Collagen Biosynthesis. *Sci Signal* (2019) 12(582):eaav3048. doi: 10.1126/scisignal.aav3048
  55. Woodcock HV, Eley JD, Guillotin D, Plate M, Nanthakumar CB, Martufi M, et al. The Mtorc1/4E-BP1 Axis Represents a Critical Signaling Node During Fibrogenesis. *Nat Commun* (2019) 10:6. doi: 10.1038/s41467-018-07858-8
  56. Duluc C, Moatassim-Billah S, Chalabi-Dchar M, Perraud A, Samain R, Breibach F, et al. Pharmacological Targeting of the Protein Synthesis mTOR/4e-BP1 Pathway in Cancer-Associated Fibroblasts Abrogates Pancreatic Tumour Chemoresistance. *EMBO Mol Med* (2015) 7:735–53. doi: 10.15252/emmm.201404346
  57. Saxton RA, Sabatini DM. mTOR Signaling in Growth, Metabolism, and Disease. *Cell* (2017) 169:361–71. doi: 10.1016/j.cell.2017.03.035
  58. Li J, Ghazwani M, Liu K, Huang Y, Chang N, Fan J, et al. Regulation of Hepatic Stellate Cell Proliferation and Activation by Glutamine Metabolism. *PLoS One* (2017) 12:e0182679. doi: 10.1371/journal.pone.0182679
  59. Kay EJ, Paterson C, Riero Domingo C, Sumpton D, Daebritz H, Tardito S, et al. PYCR1-Dependent Proline Synthesis in Cancer-Associated Fibroblasts Is Required for the Deposition of Pro-Tumorigenic Extracellular Matrix. *BioRxiv* (2020). doi: 10.1101/2020.05.30.125237
  60. Karna E, Mityk W, Wolczynski S, Palka JA. The Potential Mechanism for Glutamine-Induced Collagen Biosynthesis in Cultured Human Skin Fibroblasts. *Comp Biochem Physiol B Biochem Mol Biol* (2001) 130:23–32. doi: 10.1016/S1096-4959(01)00400-6
  61. Liang ST, Audira G, Juniardi S, Chen JR, Lai YH, Du ZC, et al. Zebrafish Carrying Pycr1 Gene Deficiency Display Aging and Multiple Behavioral Abnormalities. *Cells* (2019) 8(5):453. doi: 10.3390/cells8050453
  62. Kretz R, Bozorgmehr B, Kariminejad MH, Rohrbach M, Haussler I, Baumer A, et al. Defect in Proline Synthesis: Pyrroline-5-Carboxylate Reductase 1 Deficiency Leads to a Complex Clinical Phenotype With Collagen and Elastin Abnormalities. *J Inher Metab Dis* (2011) 34:731–9. doi: 10.1007/s10545-011-9319-3
  63. Skidmore DL, Chitayat D, Morgan T, Hinek A, Fischer B, Dimopoulou A, et al. Further Expansion of the Phenotypic Spectrum Associated With Mutations in ALDH18A1, Encoding Delta(1)-Pyrroline-5-Carboxylate Synthase (P5CS). *Am J Med Genet A* (2011) 155A:1848–56. doi: 10.1002/ajmg.a.34057
  64. Albina JE, Abate JA, Mastrofrancesco B. Role of Ornithine as a Proline Precursor in Healing Wounds. *J Surg Res* (1993) 55:97–102. doi: 10.1006/jsre.1993.1114
  65. Baich A, Chen P, Cummings S. Effect of Proline on Synthesis of Collagen by Cells in Culture. *Physiol Chem Phys M* (1980) 12:63–7.
  66. Forsander OA, Pikkarainen JA, Salaspuro MP. A High Hepatic Concentration of Free Proline Does Not Induce Collagen Synthesis in Rat Liver. *Hepatogastroenterology* (1983) 30:6–8.
  67. Szoka L, Karna E, Hlebowicz-Sarat K, Karaszewski J, Palka JA. Exogenous Proline Stimulates Type I Collagen and HIF-1alpha Expression and the Process Is Attenuated by Glutamine in Human Skin Fibroblasts. *Mol Cell Biochem* (2017) 435:197–206. doi: 10.1007/s11010-017-3069-y
  68. Liu W, Hancock CN, Fischer JW, Harman M, Phang JM. Proline Biosynthesis Augments Tumor Cell Growth and Aerobic Glycolysis: Involvement of Pyridine Nucleotides. *Sci Rep* (2015) 5:17206. doi: 10.1038/srep17206
  69. Hagedorn CH, Phang JM. Transfer of Reducing Equivalents Into Mitochondria by the Interconversions of Proline and Delta 1-Pyrroline-5-Carboxylate. *Arch Biochem Biophys* (1983) 225:95–101. doi: 10.1016/0003-9861(83)90010-3
  70. Wondrak GT, Jacobson MK, Jacobson EL. Identification of Quenchers of Photoexcited States as Novel Agents for Skin Photoprotection. *J Pharmacol Exp Ther* (2005) 312:482–91. doi: 10.1124/jpet.104.075101
  71. Zhu J, Schworer S, Berisa M, Kyung YJ, Ryu KW, Yi J, et al. Mitochondrial NADP(H) Generation is Essential for Proline Biosynthesis. *Science* (2021) 372(6545):968–72. doi: 10.1126/science.abd5491
  72. Reversade B, Escande-Beillard N, Dimopoulou A, Fischer B, Chng SC, Li Y, et al. Mutations in PYCR1 Cause Cutis Laxa With Progeroid Features. *Nat Genet* (2009) 41:1016–21. doi: 10.1038/ng.413
  73. Kuo ML, Lee MB, Tang M, den Besten W, Hu S, Sweredoski MJ, et al. PYCR1 and PYCR2 Interact and Collaborate With RRM2B to Protect Cells From Overt Oxidative Stress. *Sci Rep* (2016) 6:18846. doi: 10.1038/srep18846
  74. Sanli A, Onen A, Sarioglu S, Sis B, Guneli E, Gokcen B, et al. Glutamine Administration Enhances the Healing of Lung Parenchymal Injuries and Reduces Air Leakage in Rats. *Tohoku J Exp Med* (2006) 210:239–45. doi: 10.1620/tjem.210.239
  75. da Costa MA, Campos AC, Coelho JC, de Barros AM, Matsumoto HM. Oral Glutamine and the Healing of Colonic Anastomoses in Rats. *J Parenter Enteral Nutr* (2003) 27:182–5. doi: 10.1177/0148607103027003182
  76. de Paz-Lugo P, Lupianez JA, Melendez-Hevia E. High Glycine Concentration Increases Collagen Synthesis by Articular Chondrocytes *In Vitro*: Acute Glycine Deficiency Could be an Important Cause of Osteoarthritis. *Amino Acids* (2018) 50:1357–65. doi: 10.1007/s00726-018-0211-x
  77. Murphy MK, Motz KM, Ding D, Yin L, Duvvuri M, Feeley M, et al. Targeting Metabolic Abnormalities to Reverse Fibrosis in Iatrogenic Laryngotracheal Stenosis. *Laryngoscope* (2018) 128:E59–67. doi: 10.1002/lary.26893
  78. Tsai HW, Motz KM, Ding D, Lina I, Murphy MK, Benner D, et al. Inhibition of Glutaminase to Reverse Fibrosis in Iatrogenic Laryngotracheal Stenosis. *Laryngoscope* (2020) 130:E773–81. doi: 10.1002/lary.28493
  79. Yang L, Achreja A, Yeung TL, Mangala LS, Jiang D, Han C, et al. Targeting Stromal Glutamine Synthetase in Tumors Disrupts Tumor Microenvironment-Regulated Cancer Cell Growth. *Cell Metab* (2016) 24:685–700. doi: 10.1016/j.cmet.2016.10.011
  80. Bellon G, Monboisse JC, Randoux A, Borel JP. Effects of Preformed Proline and Proline Amino Acid Precursors (Including Glutamine) on Collagen Synthesis in Human Fibroblast Cultures. *Biochim Biophys Acta* (1987) 930:39–47. doi: 10.1016/0167-4889(87)90153-4
  81. Hamanaka RB, O'Leary EM, Witt LJ, Tian Y, Gokalp GA, Meliton AY, et al. Glutamine Metabolism Is Required for Collagen Protein Synthesis in Lung Fibroblasts. *Am J Respir Cell Mol Biol* (2019) 61:597–606. doi: 10.1165/rcmb.2019-0008OC
  82. Yu YM, Ryan CM, Burke JF, Tompkins RG, Young VR. Relations Among Arginine, Citrulline, Ornithine, and Leucine Kinetics in Adult Burn Patients. *Am J Clin Nutr* (1995) 62:960–8. doi: 10.1093/ajcn/62.5.960
  83. Yu YM, Ryan CM, Castillo L, Lu XM, Beaumier L, Tompkins RG, et al. Arginine and Ornithine Kinetics in Severely Burned Patients: Increased Rate of Arginine Disposal. *Am J Physiol Endocrinol Metab* (2001) 280:E509–17. doi: 10.1152/ajpendo.2001.280.3.E509
  84. Witte MB, Barbul A, Schick MA, Vogt N, Becker HD. Upregulation of Arginase Expression in Wound-Derived Fibroblasts. *J Surg Res* (2002) 105:35–42. doi: 10.1006/jsre.2002.6443
  85. Campbell L, Saville CR, Murray PJ, Cruickshank SM, Hardman MJ. Local Arginase 1 Activity Is Required for Cutaneous Wound Healing. *J Invest Dermatol* (2013) 133:2461–70. doi: 10.1038/jid.2013.164
  86. Zhao YD, Yin L, Archer S, Lu C, Zhao G, Yao Y, et al. Metabolic Heterogeneity of Idiopathic Pulmonary Fibrosis: A Metabolomic Study. *BMJ Open Respir Res* (2017) 4:e000183. doi: 10.1136/bmjresp-2017-000183



87. Ino Y, Yamazaki-Itoh R, Oguro S, Shimada K, Kosuge T, Zavada J, et al. Arginase II Expressed in Cancer-Associated Fibroblasts Indicates Tissue Hypoxia and Predicts Poor Outcome in Patients With Pancreatic Cancer. *PLoS One* (2013) 8:e55146. doi: 10.1371/journal.pone.0055146
88. Wittmann F, Prix N, Mayr S, Angele P, Wichmann MW, van den Engel NK, et al. L-Arginine Improves Wound Healing After Trauma-Hemorrhage by Increasing Collagen Synthesis. *J Trauma* (2005) 59:162–8. doi: 10.1097/01.TA.0000171529.06625.A8
89. Seifert E, Rettura G, Barbul A, Levenson SM. Arginine: An Essential Amino Acid for Injured Rats. *Surgery* (1978) 84:224–30.
90. Shi HP, Fishel RS, Efron DT, Williams JZ, Fishel MH, Barbul A. Effect of Supplemental Ornithine on Wound Healing. *J Surg Res* (2002) 106:299–302. doi: 10.1006/jsre.2002.6471
91. Kitowska K, Zakrzewicz D, Konigshoff M, Chrobak I, Grimminger F, Seeger W, et al. Functional Role and Species-Specific Contribution of Arginases in Pulmonary Fibrosis. *Am J Physiol Lung Cell Mol Physiol* (2008) 294:L34–45. doi: 10.1152/ajplung.00007.2007
92. Liu H, Drew P, Gaugler AC, Cheng Y, Visner GA. Pirfenidone Inhibits Lung Allograft Fibrosis Through L-Arginine-Arginase Pathway. *Am J Transplant* (2005) 5:1256–63. doi: 10.1111/j.1600-6143.2005.00876.x
93. Durante W, Liao L, Reyna SV, Peyton KJ, Schafer AI. Transforming Growth Factor-Beta(1) Stimulates L-Arginine Transport and Metabolism in Vascular Smooth Muscle Cells: Role in Polyamine and Collagen Synthesis. *Circulation* (2001) 103:1121–7. doi: 10.1161/01.CIR.103.8.1121
94. Durante W, Liao L, Reyna SV, Peyton KJ, Schafer AI. Physiological Cyclic Stretch Directs L-Arginine Transport and Metabolism to Collagen Synthesis in Vascular Smooth Muscle. *FASEB J* (2000) 14:1775–83. doi: 10.1096/fj.99-0960.com
95. Bellon G, Chaqour B, Wegrowski Y, Monboisse JC, Borel JP. Glutamine Increases Collagen Gene Transcription in Cultured Human Fibroblasts. *Biochim Biophys Acta* (1995) 1268:311–23. doi: 10.1016/0167-4889(95)00093-8
96. Bernard K, Logsdon NJ, Benavides GA, Sanders Y, Zhang J, Darley-Usmar VM, et al. Glutaminolysis is Required for Transforming Growth Factor-Beta1-Induced Myofibroblast Differentiation and Activation. *J Biol Chem* (2018) 293:1218–28. doi: 10.1074/jbc.RA117.000444
97. Ge J, Cui H, Xie N, Banerjee S, Guo S, Dubey S, et al. Glutaminolysis Promotes Collagen Translation and Stability via Alpha-Ketoglutarate-Mediated mTOR Activation and Proline Hydroxylation. *Am J Respir Cell Mol Biol* (2018) 58:378–90. doi: 10.1165/rcmb.2017-0238OC
98. Duran RV, MacKenzie ED, Boulahbel H, Frezza C, Heiserich L, Tardito S, et al. HIF-Independent Role of Prolinyl Hydroxylases in the Cellular Response to Amino Acids. *Oncogene* (2013) 32:4549–56. doi: 10.1038/onc.2012.465
99. Stegen S, Laperre K, Eelen G, Rinaldi G, Fraisl P, Torrekens S, et al. HIF-1alpha Metabolically Controls Collagen Synthesis and Modification in Chondrocytes. *Nature* (2019) 565:511–5. doi: 10.1038/s41586-019-0874-3
100. Chiavarina B, Whitaker-Menezes D, Migneco G, Martinez-Outschoorn UE, Pavlides S, Howell A, et al. HIF1-Alpha Functions as a Tumor Promoter in Cancer Associated Fibroblasts, and as a Tumor Suppressor in Breast Cancer Cells: Autophagy Drives Compartment-Specific Oncogenesis. *Cell Cycle* (2010) 9:3534–51. doi: 10.4161/cc.9.17.12908
101. Kuchnio A, Moens S, Bruning U, Kuchnio K, Cruys B, Thienpont B, et al. The Cancer Cell Oxygen Sensor PHD2 Promotes Metastasis via Activation of Cancer-Associated Fibroblasts. *Cell Rep* (2015) 12:992–1005. doi: 10.1016/j.celrep.2015.07.010
102. Elia I, Rossi M, Stegen S, Broekaert D, Doglioni G, van Gorsel M, et al. Breast Cancer Cells Rely on Environmental Pyruvate to Shape the Metastatic Niche. *Nature* (2019) 568:117–21. doi: 10.1038/s41586-019-0977-x
103. Bertero T, Oldham WM, Grasset EM, Bourget I, Boulter E, Pisano S, et al. Tumor-Stroma Mechanics Coordinate Amino Acid Availability to Sustain Tumor Growth and Malignancy. *Cell Metab* (2019) 29:124–40.e10. doi: 10.1016/j.cmet.2018.09.012
104. Dooley A, Bruckdorfer KR, Abraham DJ. Modulation of Fibrosis in Systemic Sclerosis by Nitric Oxide and Antioxidants. *Cardiol Res Pract* (2012) 2012:521958. doi: 10.1155/2012/521958
105. Davila HH, Magee TR, Vernet D, Rajfer J, Gonzalez-Cadavid NF. Gene Transfer of Inducible Nitric Oxide Synthase Complementary DNA Regresses the Fibrotic Plaque in an Animal Model of Peyronie's Disease. *Biol Reprod* (2004) 71:1568–77. doi: 10.1095/biolreprod.104.030833
106. Vernet D, Ferrini MG, Valente EG, Magee TR, Bou-Gharios G, Rajfer J, et al. Effect of Nitric Oxide on the Differentiation of Fibroblasts Into Myofibroblasts in the Peyronie's Fibrotic Plaque and in Its Rat Model. *Nitric Oxide* (2002) 7:262–76. doi: 10.1016/S1089-8603(02)00124-6
107. Pavlides S, Vera I, Gandara R, Sneddon S, Pestell RG, Mercier I, et al. Warburg Meets Autophagy: Cancer-Associated Fibroblasts Accelerate Tumor Growth and Metastasis via Oxidative Stress, Mitophagy, and Aerobic Glycolysis. *Antioxid Redox Signal* (2012) 16:1264–84. doi: 10.1089/ars.2011.4243
108. Shi HP, Efron DT, Most D, Tantry US, Barbul A. Supplemental Dietary Arginine Enhances Wound Healing in Normal But Not Inducible Nitric Oxide Synthase Knockout Mice. *Surgery* (2000) 128:374–8. doi: 10.1067/msy.2000.107372
109. Milne K, Sun J, Zaal EA, Mowat J, Celie PHN, Fish A, et al. A Fragment-Like Approach to PYCR1 Inhibition. *Bioorg Med Chem Lett* (2019) 29(18):2626–31. doi: 10.1016/j.bmcl.2019.07.047
110. Christensen EM, Bogner AN, Vandekeere A, Tam GS, Patel SM, Becker DF, et al. In Crystalline Screening for Proline Analog Inhibitors of the Proline Cycle Enzyme PYCR1. *J Biol Chem* (2020) 295:18316–27. doi: 10.1074/jbc.RA120.016106
111. Cai F, Miao Y, Liu C, Wu T, Shen S, Su X, et al. Pyrroline-5-Carboxylate Reductase 1 Promotes Proliferation and Inhibits Apoptosis in Non-Small Cell Lung Cancer. *Oncol Lett* (2018) 15:731–40. doi: 10.3892/ol.2017.7400
112. Ding J, Kuo ML, Su L, Xue L, Luh F, Zhang H, et al. Human Mitochondrial Pyrroline-5-Carboxylate Reductase 1 Promotes Invasiveness and Impacts Survival in Breast Cancers. *Carcinogenesis* (2017) 38:519–31. doi: 10.1093/carcin/bgx022
113. Peng DH, Rodriguez BL, Diao L, Chen L, Wang J, Byers LA, et al. Collagen Promotes Anti-PD-1/PD-L1 Resistance in Cancer Through LAIR1-Dependent CD8(+) T Cell Exhaustion. *Nat Commun* (2020) 11:4520. doi: 10.1038/s41467-020-18298-8
114. Chen Y, Kim J, Yang S, Wang H, Wu CJ, Sugimoto H, et al. Type I Collagen Deletion in alphaSMA(+) Myofibroblasts Augments Immune Suppression and Accelerates Progression of Pancreatic Cancer. *Cancer Cell* (2021) 39:548–65.e6. doi: 10.1016/j.ccell.2021.02.007

**Conflict of Interest:** The authors declare that the research was conducted in the absence of any commercial or financial relationships that could be construed as a potential conflict of interest.

**Publisher's Note:** All claims expressed in this article are solely those of the authors and do not necessarily represent those of their affiliated organizations, or those of the publisher, the editors and the reviewers. Any product that may be evaluated in this article, or claim that may be made by its manufacturer, is not guaranteed or endorsed by the publisher.

Copyright © 2021 Kay, Koulouras and Zanivan. This is an open-access article distributed under the terms of the Creative Commons Attribution License (CC BY). The use, distribution or reproduction in other forums is permitted, provided the original author(s) and the copyright owner(s) are credited and that the original publication in this journal is cited, in accordance with accepted academic practice. No use, distribution or reproduction is permitted which does not comply with these terms.



# Mechanisms Governing Metabolic Heterogeneity in Breast Cancer and Other Tumors

Sayani Patra<sup>1,2†</sup>, Naveed Elahi<sup>1,2†</sup>, Aaron Armorer<sup>1,2†</sup>, Swathi Arunachalam<sup>1,2</sup>, Joshua Omala<sup>1,2</sup>, Iman Hamid<sup>1,2</sup>, Anthony W. Ashton<sup>2,3</sup>, David Joyce<sup>4</sup>, Xuanmao Jiao<sup>1,2\*</sup> and Richard G. Pestell<sup>1,2,5</sup>

<sup>1</sup> Pennsylvania Cancer and Regenerative Medicine Research Center, Baruch S. Blumberg Institute, Wynnewood, PA, United States, <sup>2</sup> Xavier University School of Medicine at Aruba, Oranjestad, Aruba, <sup>3</sup> Program in Cardiovascular Medicine, Lankenau Institute for Medical Research, Wynnewood, PA, United States, <sup>4</sup> Medical School, Faculty of Health and Medical Sciences, The University of Western Australia, Crawley, WA, Australia, <sup>5</sup> Cancer Center, Wistar Institute, Philadelphia, PA, United States

## OPEN ACCESS

### Edited by:

Yong Teng,  
Emory University, United States

### Reviewed by:

Jaromir Gumulec,  
Masaryk University, Czechia  
Abhinav Achreja,  
University of Michigan, United States

### \*Correspondence:

Xuanmao Jiao  
xuanmao.jiao@bbblumberg.org

<sup>†</sup>These authors have contributed  
equally to this work and share  
first authorship

### Specialty section:

This article was submitted to  
Cancer Metabolism,  
a section of the journal  
Frontiers in Oncology

Received: 28 April 2021

Accepted: 30 August 2021

Published: 23 September 2021

### Citation:

Patra S, Elahi N, Armorer A,  
Arunachalam S, Omala J, Hamid I,  
Ashton AW, Joyce D, Jiao X and  
Pestell RG (2021) Mechanisms  
Governing Metabolic Heterogeneity in  
Breast Cancer and Other Tumors.  
Front. Oncol. 11:700629.  
doi: 10.3389/fonc.2021.700629

Reprogramming of metabolic priorities promotes tumor progression. Our understanding of the Warburg effect, based on studies of cultured cancer cells, has evolved to a more complex understanding of tumor metabolism within an ecosystem that provides and catabolizes diverse nutrients provided by the local tumor microenvironment. Recent studies have illustrated that heterogeneous metabolic changes occur at the level of tumor type, tumor subtype, within the tumor itself, and within the tumor microenvironment. Thus, altered metabolism occurs in cancer cells and in the tumor microenvironment (fibroblasts, immune cells and fat cells). Herein we describe how these growth advantages are obtained through either “convergent” genetic changes, in which common metabolic properties are induced as a final common pathway induced by diverse oncogene factors, or “divergent” genetic changes, in which distinct factors lead to subtype-selective phenotypes and thereby tumor heterogeneity. Metabolic heterogeneity allows subtyping of cancers and further metabolic heterogeneity occurs within the same tumor mass thought of as “microenvironmental metabolic nesting”. Furthermore, recent findings show that mutations of metabolic genes arise in the majority of tumors providing an opportunity for the development of more robust metabolic models of an individual patient’s tumor. The focus of this review is on the mechanisms governing this metabolic heterogeneity in breast cancer.

**Keywords:** breast cancer, metabolism, Warburg effect, aerobic glycolysis, reverse Warburg effect, epigenetics, PPAR- $\gamma$ , Cyclin D1

## INTRODUCTION

Breast Cancer. Breast cancer is the most common non-dermatological malignancy in women representing approximately one third of all malignancies diagnosed in US women (1, 2). In approximately 10% of cases breast cancers are associated with gene mutations inherited from one relative. Almost 50% of breast cancer cases occur in less developed countries with incidence rates

ranging from 19 per 100,000 women in Eastern Africa to 90 per 100,000 women in Western Europe. Efforts to provide more precise therapies to patients with breast cancer has led to subclassification using the coding genome, the non-coding genome or more recently, metabolic subtypes.

Precision medicine approaches have identified genetic subtypes of BCa based initially on the coding genome (3). At least five distinct coding genome molecular subtypes are recognized including luminal A, luminal B, human epidermal growth factor receptor 2 (HER2)-enriched, basal-like, and claudin-low and normal-like (4, 5). Triple negative breast cancer (TNBC), which lacks estrogen receptor- $\alpha$  (ER $\alpha$ ), progesterone receptor (PR) and HER2, characteristically includes mutations of DNA damage repair (6), altered PD-L1 expression (7) and increased expression of the G protein coupled receptor CCR5 (8, 9). Breast cancer has also been characterized based on the non-coding genome (10, 11). Altered expression of miRNA was observed in breast cancer (12). In subsequent studies hierarchical clustering of human breast cancers defined four distinct miRNA clusters (G1-G4) associated with distinguishable relapse-free survival by Kaplan-Meier analysis (10). These studies defined a cyclin D1-regulated miRNA signature which included several oncomirs, that was conserved in multiple breast cancer cell lines, and was associated with the G2 tumor miRNA cluster, ER $\alpha$ <sup>+</sup> status, better outcome and activation of the Wnt pathway (10). Of interest these studies showed that the coding and non-coding genome for any given tumor were discordant within breast cancer subtypes. In recent studies metabolic subtyping of breast cancer has revealed distinguishable characteristics. Triple negative breast cancer (TNBC), for example, expresses low levels of glutamine synthetase (GLUL, glutamate-ammonia ligase). Withdrawing glutamine suppresses growth of the basal and claudin low triple negative tumors BCa tumor subtype (13). In contrast, luminal tumor cells express GLUL and are resistant to glutamine deprivation (14). The glutaminase isozyme GLS2, is upregulated and essential in luminal-subtype breast tumors (15).

Currently, therapies for breast cancer rely on surgical, radiotherapeutic, chemotherapeutic and biological therapeutic approaches (16). Despite these advances in medicine, 30% of patients relapse and develop a metastatic cancer (17). Patients with triple negative breast cancer (ER $\alpha$  Negative, HER2 Negative, PR Negative) have a poor outcome and require additional therapy. Historically targeting of the coding genome has improved mortality rates in breast cancer patients, and *in vitro* pre-clinical studies have shown promise in targeting the non-coding genome (18–20). The identification of metabolic dependencies specific to the cancer vs. normal cells therefore represents an important new opportunity for therapeutic intervention. In this regard the xCT antiporter, which is expressed on 1/3 of triple negative tumors *in vivo*, is essential to support environmental cystine acquisition (13). Inhibition of the xCT antiporter with the anti-inflammatory Sulfasalazine decreased tumor growth (13). Targeting GLS1/GLS2 with the small-molecule inhibitor 968 reduced tumor growth in luminal breast cancer (15).

Tumor metabolism. The abnormalities associated with tumor metabolism have been recently reviewed (21–23). In contrast to normal differentiated cells, which rely primarily on mitochondrial oxidative phosphorylation to generate the energy needed for cellular processes, most cancer cells instead rely substantially on cytosolic aerobic glycolysis, a phenomenon termed “the Warburg effect” (Figure 1) (24, 25). In Warburg’s view, so central were metabolic changes to the cancer phenotype that he opined, “From this point of view, mutation and carcinogenic agent are not alternatives, but empty words, unless metabolically specified” (24).

As the analytical tools used to interrogate the characteristics of tumor metabolism have evolved, it has become increasingly clear that metabolic adaptations of tumors are highly heterogeneous (26–30). Historically the understanding of

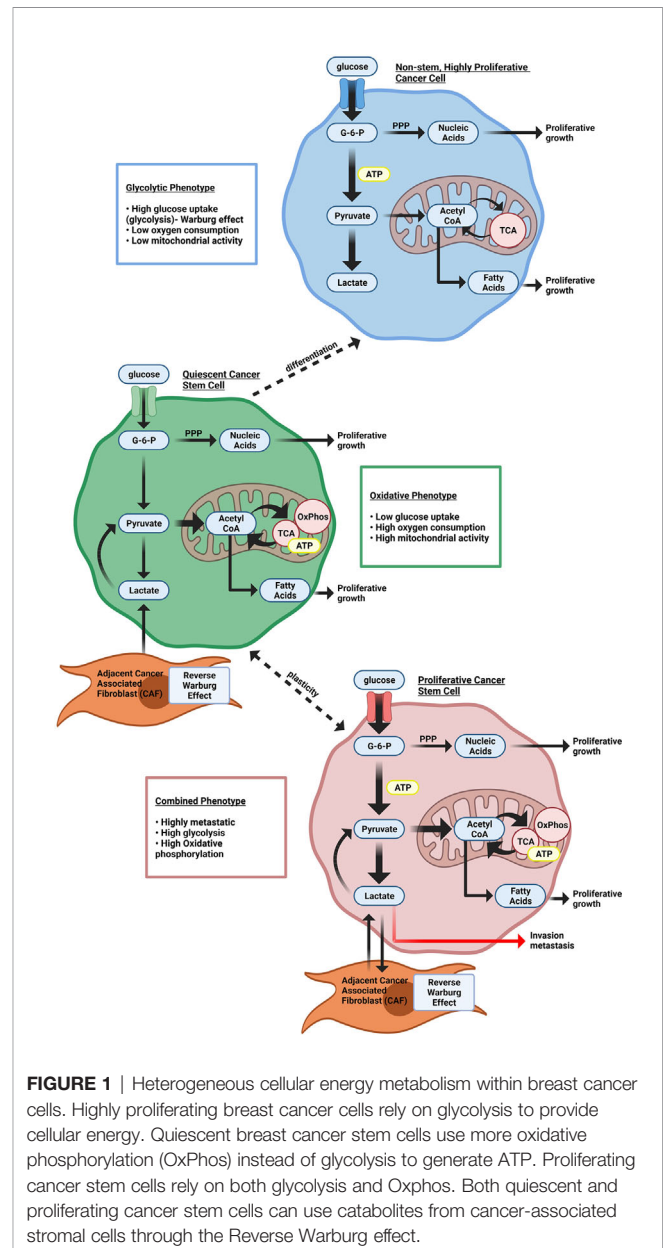


**FIGURE 1 |** Heterogeneous cellular energy metabolism within breast cancer cells. Highly proliferating breast cancer cells rely on glycolysis to provide cellular energy. Quiescent breast cancer stem cells use more oxidative phosphorylation (OxPhos) instead of glycolysis to generate ATP. Proliferating cancer stem cells rely on both glycolysis and Oxphos. Both quiescent and proliferating cancer stem cells can use catabolites from cancer-associated stromal cells through the Reverse Warburg effect.

cancer metabolism was drawn from principles of “convergent” metabolic phenotypes, properties that are governed by diverse factors shared among diverse tumor types. As the resolution of investigative tools has evolved, evidence for “divergent” metabolic pathways has provided compelling evidence for breast cancer metabolic heterogeneity.

Convergent properties include the principal that cancer cells have evolved multiple distinct mechanisms in order to provide metabolic substrates for proliferation within the tumor microenvironment (25). Like all living cells cancer cells need ATP, together with carbon intermediates for the synthesis of DNA, proteins and lipids. Cancer cells augment the procurement of nutrients, scavenge nutrients from alternative sources (alternative substrates), reprogram metabolic process needed for growth, and upregulate the apparatus for processing the nutrients into energy and structural intermediates for replication, growth, and invasion. Cancer-associated metabolic changes have been usefully categorized as: (i) deregulated uptake of glucose and amino acids, (ii) opportunistic nutrient acquisition from both intracellular and environmental sources, (iii) use of glycolysis/TCA cycle intermediates for biosynthesis and NADPH production, (iv) increased demand for nitrogen and means to satisfy it, (v) alterations in metabolite-driven gene regulation, and (vi) metabolic interactions with the tumor microenvironment. Tumors vary in the degree to which they deploy these individual changes (31). Thus, in addition to changes in glucose uptake, increased levels of methionine, glutamine, cystine, tryptophan, tyrosine, and other amino acids have been noted in breast cancer (32–36). Cancer cells with upregulation of amino acid metabolism stimulate increased transport of amino acids into the cell. The increased consumption of amino acids and overexpression of amino acid transporters (L-type amino acid transporter 1) during breast cancer progression, has led to an interest in radiolabeled amino acids imaging agents (37).

“Divergent” properties derive from distinct genetic or epigenetic alterations with a tumor which govern distinct molecular subsets of genes that in turn alter cellular metabolism thereby contributing to metabolic heterogeneity. Distinct oncogenotypes have been characterized in a variety of cancers. IDH1 and IDH2 mutations give rise to accumulation of (R)-2HG (38, 39). In lung cancer distinct somatic mutations (TP53, KRAS, BRAF, NF1, EGFR, KEAP1) appear to be each sufficient to regulate tumor metabolism (26–28). Although less well characterized in breast cancer, genetic alterations that occur in breast cancer (cyclin D1 overexpression (40, 41) and epigenetic changes [FBP1 (42), the Jumonji-domain histone demethylase (JHDM)3C (43)], are sufficient to induces metabolic changes reflected by the Warburg effect.

## “CONVERGENT” GENETIC PROPERTIES DRIVING THE WARBURG EFFECT

Warburg observed that cancer cells primarily supply energy from glucose through avid glycolysis, even in aerobic conditions where

more efficient mitochondrial oxidative phosphorylation (OXPHOS) was potentially available. Per molecule of glucose, glycolysis followed by OXPHOS generates up to 18 times more adenosine 5′-triphosphate (ATP) than glycolysis alone (44). The Warburg effect is pervasive among cancer cells of many but not all cancer types. For example the Warburg effect is not prominent in early prostate cancer (45, 46) and is found in only one of the metabolic subtypes of glioblastoma multiforme (21). Furthermore, the Warburg effects occurs in a heterogeneous manner within tumors, generating an intratumoral “nesting phenomenon”. Aerobic cells proliferate best when they are clustered with some glycolytic cells (44, 47, 48).

Several convergent genetic processes further drive the Warburg effect in tumors. Oncogenic mutations, tumor suppressor deletions and overexpression of collaborative oncogenes contributes to the tumor metabolic shift as these genes govern expression of glycolytic enzymes. In this regard *c-myc*, *k-Ras*, mutant *p53*, cyclin D1 and the  $\beta$ -catenin/TCF signaling pathway augment the Warburg effect (41, 49–52). Hypoxia-inducible factor-1 $\alpha$  (HIF1 $\alpha$ ), which normally contributes to regulation of glycolysis in hypoxia, is also more protected from degradation in some cancer types.

A transition towards aerobic glycolysis is available to normal cells during proliferation (53). In tumor cells that activate the Warburg effect, several metabolic consequences occur. Cancer cells accelerate aerobic glycolysis partly through regulatory processes that are general to proliferating cells (54). Normally, glycolysis proceeds at a rate that reflects negative feedback control of intracellular ATP and NAD<sup>+</sup>/NADH homeostasis. There may be an advantage for an energetically active cancer cell in the speed of ATP production in glycolysis. ATP can be rapidly synthesized by glycolysis, up to 100 times faster than OXPHOS (55). Cancer cells, with diminished OXPHOS-generated ATP and efficient export of NADH reducing equivalents as lactate, maintain a permissive intracellular environment for dysregulated glycolysis. The diversion of pyruvate away from acetyl CoA production to lactate, simultaneously regenerates NAD<sup>+</sup> and deprives the mitochondrial electron transport chain of NADH for ATP synthesis.

Aerobic glycolysis also confers an advantage to cancer cells by generation of macromolecules to increase the cellular biomass (53). Rapid proliferation of cancer cells needs to be sustained by increased macromolecular biosynthesis. As well as its role in providing substrates for mitochondrial OXPHOS, glycolysis intermediates supply the pentose phosphate pathway, support NADPH generation, contribute one-carbon species into the one-carbon cycle and make acetyl CoA available for lipid synthesis (53). Glucose-6-phosphate dehydrogenase action on the first product of glycolysis, glucose-6-phosphate, initiates the pentose phosphate pathway. Products of the pentose phosphate pathway include ribose-5-phosphate for nucleotide synthesis and NADPH. NADPH, an essential intracellular reductant that is consumed in numerous lipid, amino acid and nucleotide anabolic pathways, is created in both the pentose phosphate pathway and in one-carbon cycle reactions (56).



Later steps in glycolysis yield fructose-6-phosphate, which may proceed to hexosamine synthesis and dihydroacetone phosphate, which is a substrate for glycerol-3-phosphate, and thence lipid, synthesis. Enhanced expression of 3-phosphoglycerate dehydrogenase has been described in breast cancer cells (57). In glycolysis, 3-phosphoglycerate is diverted out of the pathway under the action of 3-phosphoglycerate dehydrogenase. This is a quantitatively important source of substrates for the one-carbon cycle, enabling production of glycine, serine and thence S-adenosylmethionine and one-carbon derivatives of tetrahydrofolic acid (58). These are essential for the synthesis of purine and pyrimidine bases for nucleotides and many other biosynthetic processes. The glycolysis product, pyruvate, is available for acetyl CoA generation and thereby lipogenesis (53, 59).

Increased *lactate production* from aerobic glycolysis leading to cellular acidification and results in lactate efflux from cells to maintain cellular pH. Lactate efflux results in an acidic extracellular tumor microenvironment, which promotes angiogenesis (60) increasing HIF1 $\alpha$  stabilization, promoting VEGF production from cancer associated macrophages (61), enhancing hyaluronic acid production from fibroblasts (62), inducing extracellular matrix degrading cathepsins and matrix metalloproteases (63, 64), and augmenting endothelial cell PI3K and NF $\kappa$ B signaling (65) thereby promoting vasculogenesis.

## EPIGENETIC CHANGES IN TUMORS THAT PROMOTE THE WARBURG EFFECT

Epigenetic modifications in breast cancer cells can alter metabolism in a particular tumor, thereby contributing to divergent heterogeneous metabolic changes. Epigenetic changes, which are inheritable, reversible changes in selective gene expression that occur without any alterations to the DNA sequence itself, include DNA methylation, histone modifications, and RNA-mediated gene silencing by non-coding RNAs such as miRNA. DNA methylation has been described of specific key components in glycolytic pathways, glycolysis bypass pathways (i.e. gluconeogenesis and pentose phosphate pathway), as well as mitochondrial and oxygen sensing pathways (66). Furthermore many of the intermediates of cellular metabolic pathways participate in the chemical modifications that epigenetically modify DNA and histones (67). A synopsis of these epigenetic changes that have been described in tumors, shown in **Figure 2**, underscore the growing evidence for heterogeneous drivers of altered tumor metabolism. In addition to epigenetic changes within the tumors, epigenetic changes also occur in the tumor stroma. Distinct epigenetic alterations occur in epithelial and myoepithelial cells, and stromal fibroblasts occur in a tumor stage- and cell type-specific manner (68). Based on unsupervised analysis three methylation patterns of breast cancer (luminal A, luminal B and basal-like molecular subtypes) were identified, whereas HER2-enriched and normal-like subtypes were distributed among the three groups (69). The luminal B were most methylated and basal-like tumors least frequently

methylated. BRCA2-mutated tumors were highly methylated. A large fraction of genes reported as having subtype-specific expression patterns might be regulated through methylation (69).

## Epigenetic Modification of the Tumor

Within the tumor, DNA methylation affects key glycolytic components, including glucose transporters (GLUT1, GLUT3), lactate dehydrogenase genes (*LDH-A*, *LDH-B*), the hexokinase 2 isoform (HK2), glyceraldehyde-3-phosphate dehydrogenase (GAPDH), and the pyruvate kinase (PK) isoform M2 (PKM2), each of which contribute to the Warburg effect (66). DNA hypermethylation-mediated inactivation of the *Derlin-3* gene, which normally contributes to GLUT1 degradation, leads to increased GLUT1 expression (70). Increased GLUT3 expression is regulated by methylation (71). DNA hypermethylation of the *LDH-B* gene in breast cancer (which interconverts lactate and pyruvate), increases the LDH-A to LDH-B ratio (72). Increased LDH-A mediated conversion of pyruvate into lactate promotes aerobic glycolysis (73). LDH-A activity is crucial to the Warburg effect since it oxidizes NADH and regenerates NAD<sup>+</sup>, without which aerobic glycolysis could not continue (74). Aerobic glycolysis is induced by upregulation of the hexokinase isoform HK2 *via* hypomethylation of its promoter (75) and hypomethylation within intron 1 of the pyruvate kinase (*PK* gene) (76). GAPDH upregulation, *via* coactivator-associated arginine methyltransferase 1 (CARM1)-mediated methylation also enhances aerobic glycolysis (77). The pyruvate kinase (PK) isoform M2 undergoes DNA methylation at exon 10 of the PK gene, correlating with increased PKM2 expression in breast cancer cells (78–80). Binding of Brother of Regulator of Imprinted Sites (BORIS) to the alternative exon 10 is thereby enhanced. Inhibiting DNA methylation, depleting BORIS or eliminating the BORIS binding site, switched splicing toward generating the normal PKM1 isoform. Loss of BORIS also suppresses the Warburg effect and growth of breast cancer cells (79).

DNA methylation of mitochondrial components, such as mitochondrial DNA (mtDNA), the mitochondrial quality control protein Mienap, and pyruvate dehydrogenase (PDH) kinase 4 (PDK4), causes mitochondrial dysfunction in cancer cells, triggering the Warburg effect (81). Methylation of mtDNA specifically causes dysfunction of oxidative phosphorylation, which promotes aerobic glycolysis as the primary method for rapid ATP synthesis in cancer cells (82). Mienap normally functions to induce intramitochondrial recruitment of lysosome-like organelles in order to eliminate oxidized mitochondrial proteins while maintaining mitochondrial structural integrity. Methylation of the *Mienap* promoter reduces Mienap abundance, leading to ROS accumulation and mitochondrial destruction (83–85).

DNA methylation changes affect activity of nuclear factor erythroid 2-related factor 2 (NRF2), which in turn regulates expression of transketolase (TKT) like-1 gene (TKT L1), and the fructose-1,6-bisphosphate isoform 1 (FBP1) (66). Methylation in the KEAP1 promoter reduces KEAP1 expression, and thereby abrogates NRF2 degradation (86–88). NRF2 is a transcriptional activator of genes in the pentose phosphate pathway [G6PDH, 6-



## Epigenetic Modification of the Tumor Microenvironment

Epigenetic modification of the tumor microenvironment also contributes to tumor metabolic heterogeneity. Epigenetic reprogramming in CAFs are biomarkers for cancer progression and promote cancer epithelial progression *via* paracrine signaling (100). Multiple epigenetic mechanisms, including DNA methylation, histone modification, and chromatin remodeling, together shape and reprogram the phenotypes of CAFs during tumorigenesis (101). Altered DNA methylation status of genes occurs in CAFs isolated from breast cancer tissues (68) and the prostate (102). CAF-secreted factors and stromal content of breast tumors regulated specific genes characterized by a DNA methylation pattern: hypermethylation at transcription start site and shore regions (103). CAFs from localized prostate cancer display distinct genome-wide changes in DNA methylation, significantly at enhancers and promoters, compared to nonmalignant prostate fibroblasts (NPFs) (104). In pancreatic cancer CAFs adopt unique DNA methylation and expression patterns upon interaction with PDA tumor cells (105). Fibroblasts can be reprogrammed to adopt a pro-invasive phenotype by leukemia inducible factor (LIF), which induced methylation through DNMT3B of the promoter region in the protein phosphatase regulator Src homology 2 domain-containing protein tyrosine phosphatase 1 (*Shp-1*) gene (106).

Immune cells, including tumor-associated macrophages (TAMs), participate in breast cancer onset and progression and contribute to the TME metabolic ecosystem to enhance tumor growth. TAMs generally show increased aerobic glycolysis but may use OXPHOS to generate energy. Bidirectional metabolic feedback occurs between macrophages and breast cancer cells in which M2 like macrophages induce sodium/glucose cotransporter 1 (SGLT1) in breast cancer cells and SGLT1 enhances lactic acid secretion to promote M2 macrophage polarization (107) CCL5 activates the CCR5 receptor, which participates in metastasis of breast (9, 108) and other cancers (109–111). Lactate induces the TAM phenotype, inducing CCL5 expression which promotes breast cancer cellular EMT and aerobic glycolysis *via* AMPK (112). Human mesenchymal stem cells (MSCs) induce the DNA methylation of the *IL1A* and *IL1B* genes when co-cultured with pancreatic ductal adenocarcinoma cells (PDAC) (113). The process of T-cell exhaustion is also controlled by epigenetic regulation and enrichment of T lymphocytes within the TME is a prerequisite for successful cancer immunotherapy (101).

Metabolic substrates from the tumor microenvironment in turn regulate methylation of stromal CAFs (114). The loss of cytosine methylation in de-novo generated CAFs is associated with the induction of inflammatory transcripts. Lactate produced by tumor cells leads to increased production of alpha-ketoglutarate ( $\alpha$ KG) within mesenchymal stem cells (MSCs). In turn,  $\alpha$ KG mediates activation of the demethylase TET enzyme leading to decreased cytosine methylation and increased hydroxymethylation during *de novo* differentiation of MSCs to CAF. Thus, in PDAC, a tumor-mediated lactate flux is

associated with widespread epigenomic reprogramming that is seen during CAF formation.

## THE DEMAND FOR GLUTAMINE

Glutamine is generally required for proliferation of normal and cancer cells (115), however cancer cells have an increased demand for glutamine as a source of nitrogen. Glutamine is used for the synthesis of amino acids and nucleotides (31) (**Figure 3**). In early studies, the optimal growth of cultured HeLa cells was shown to require a 10- to a 100-fold molar excess of glutamine in culture medium compared to other amino acids (116). Furthermore, glutamine is the most rapidly used amino acid (116). The increased use of glutamine has been established in the tumor microenvironment *in vivo* (117–120) and tumors demonstrate increased uptake of  $^{18}\text{F}$ -labeled glutamine using positron emission tomography (121). Breast cancer and other cell lines may develop resistance to this metabolic dependency (122). Glutamine is required for a variety of different cellular functions in proliferating cells, providing a source of nitrogen for the synthesis of purine and pyrimidine nucleotides and for the synthesis of other amino acids (123). Glutamine is deaminated by glutaminase to generate glutamate, which is converted to  $\alpha$ -ketoglutarate. Within the mitochondria,  $\alpha$ -ketoglutarate is converted to oxaloacetate, citrate and malate which in turn contribute to other anabolic pathways (31) (**Figure 2**). Uptake of cellular amino acids is also affected by glutamine as intracellular glutamine exchanges with extracellular leucine *via* LAT, a plasma membrane-localized antiporter for neutral amino acids (124). The cystine/glutamate antiporter, which imports cystine to provide cysteine for protein and glutathione synthesis is also regulated by glutamate which serves as the intracellular substrate for the plasma membrane antiporter (125).

Glutamine metabolism is under physiological control by the serine-threonine kinase, mammalian target of rapamycin (mTOR) pathway. mTOR governs several important cellular functions including cellular growth, survival, protein translation and autophagy. mTOR upregulates glutaminase (GLS) thereby increasing the conversion of glutamine to glutamate. The consequent increased production of  $\alpha$ -ketoglutarate is then used within the TCA cycle (126). Restraint of mTOR activity also increases the ability of a cell to obtain extracellular proteins as a source of amino acids (127). Induction of mTOR correlates with increased HIF and VEGF which contribute to angiogenesis. Increased mTOR activity therefore collectively stimulates glutamine uptake, glutaminolysis, glycolysis, and angiogenesis in cancer cells.

*c-myc* governs glutamine homeostasis, with direct effects and indirect actions on cellular uptake *via* transporters ASCT2 (SLC1AS) (**Figure 2**) and SN2 (SLC38A5) (128). This enhanced uptake is associated with increased conversion to  $\alpha$ -ketoglutarate (129) and incorporation into nucleic acid synthesis (130). The dependence of cancer cells survival on glutamine has

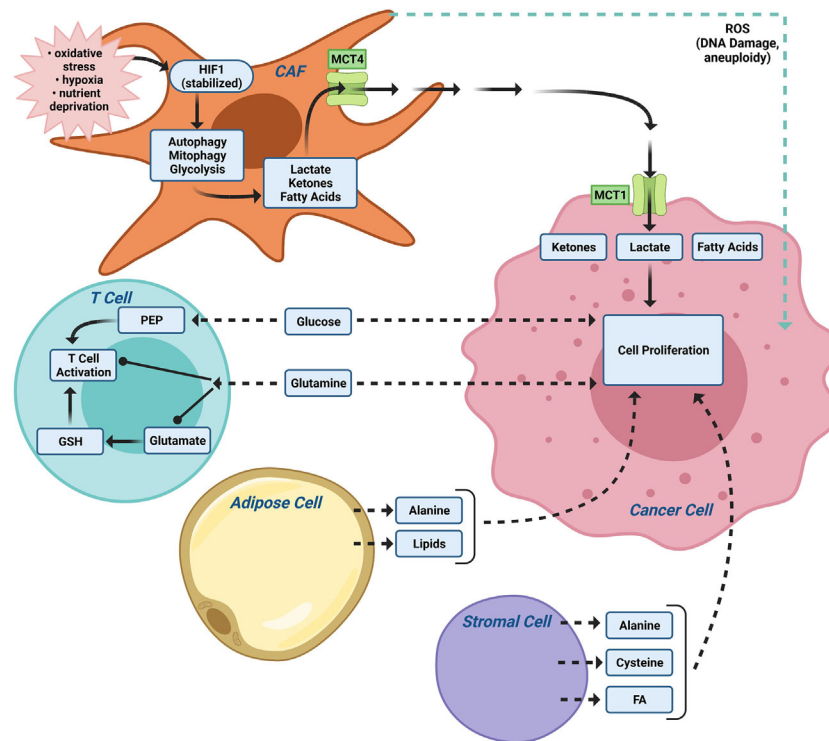


**FIGURE 3 |** The tumor microenvironment (TME) contributes to metabolic tumor heterogeneity. In addition to CAFs (Figure 2), the local TME, including immune cells and adipocytes, provide nutrients for tumor metabolism. The relative importance of the different TME cellular subtypes varies between patients thereby contributing to additional levels of tumor heterogeneity. PEP (the glycolytic metabolite phosphoenolpyruvate).

led to testing of transport inhibitors targeting ASCT2 and the glutaminase (GLS) (Figure 2) inhibitors, CB-839 and BPTES, for anticancer therapies (131–133).

## HETEROGENEOUS OXIDATIVE METABOLISM IN THE BREAST TUMOR AND THE TUMOR MICROENVIRONMENT PROVIDES DIVERSE NUTRIENTS FOR TUMOR GROWTH

Continued tumor growth requires the development of mechanisms to enhance access to diverse intracellular and extracellular nutrients (134, 135). Tumor cells retain a high level of metabolic plasticity, allowing them to both establish and subsequently adapt to the extracellular environment of a developing tumor. Heterogeneous tumor nutrients can be derived from tumor cells with different metabolic characteristics, in part driven by heterogeneous oxygenation within the tumor. In oxygenated tumor cells MCT1, which is expressed in breast cancers, serves as the prominent pathway for lactate uptake, which in turn serves as a substrate for tumor metabolism (47). Thus, there is a symbiosis by which glycolytic and oxidative tumor cells mutually regulate their access to energy

metabolites based on heterogeneous oxygenation within the tumor (136).

## Autophagy

Autophagy provides intracellular nutrients and is upregulated in dormant breast cancer cells promoting cancer cell survival under metabolic stress (137–139). Autophagy includes, macroautophagy, microautophagy and chaperone-mediated autophagy. During macroautophagy intracellular components are enveloped in double-membraned vesicles. Lysosomes fuse with autophagosomes resulting in degradation and recycling of these substrates in the cytosol (140). The autophagic process may either enhance or restrain tumor progression depending upon the stage of tumorigenesis. In a genome-wide screen, genes that negatively regulated autophagy were also involved in cellular growth and proliferation (141). Strong evidence for an association between mitogenic signaling in the restraint of autophagy led to studies wherein the pro-mitogenic, collaborative oncogene cyclin D1, was shown to restrain autophagy in breast cancer cells by modulating the activation of AMPK (142). AMPK enhanced autophagy and in human breast cancer cells cyclin D1 restrained AMPK activity (142). Cyclin D1 reduced activation of AMPK (pT172), via cyclin D1-Cdk4/Cdk6 phosphorylation of LKB1, thereby inhibiting mitochondrial function and promoting glycolysis (40, 41).



## Tumor Microenvironment and Alternative Nutrients

Alternatively, the tumor microenvironment (TME) provides a rich source of distinct nutrients. Distinct cell types within the TME (cancer associated fibroblasts (CAFs), adipocytes, immune cells, tissue plasma/interstitial fluid) provide distinct nutrients to fuel tumor metabolism (**Figure 3**). Cancer-associated fibroblasts (CAFs) and adipocytes (143) can support malignant cells by providing nutrients such as alanine and lipids (143). Macrophages participate in TME metabolism (144) and MCT4 is expressed in macrophages (145). Understanding the source of nutrients for a particular tumor may provide an alternative therapeutic opportunity. Alternative substrates fueling tumor growth, include branched chain amino acids for *de novo* nucleotide and non-essential amino acid (NEAA) biosynthesis (146), acetate for acetyl-CoA and fatty acid synthesis (147), scavenging of extracellular lysophospholipids to bypass *de novo* lipogenesis (148), and macropinocytotic uptake and degradation of extracellular protein to maintain amino acid supply and bioenergetics (149, 150). Macropinocytotic uptake is induced by Ras (149, 151) and other oncogenic stimuli [reviewed in (152)]. Although the relative importance of scavenging pathways in breast cancer remains to be more fully understood, necrosis is a common feature of invasive breast cancer and breast tumor growth often outstrips the vasculature leaving tumor cells in nutrient-limited environment (153). Desmoplasia, a form of excessive fibrosis that limits perfusion, may favor the

outgrowth of breast cancer cells that are capable of nutrient scavenging (154).

## Cancer Associated Fibroblasts

The concept of scavenging alternative substrates to fuel tumor growth is illustrated by the “Reverse Warburg Effect” that was initially characterized in breast cancer cells (44, 47, 48). In the “Reverse Warburg” effect, anabolic cancer cells import lactate, ketones and fatty acids released by either adjacent cancer associated fibroblasts (CAF), other stromal cell types or catabolic cancer cells, in response to oxidative stress (21, 155). The “Autophagic Tumor Stroma Model of Cancer” proposes aerobic glycolysis in cancer associated fibroblasts (CAFs) generates energy-rich metabolites (such as lactate, ketone bodies and pyruvate) that are transferred to adjacent cancer cells, where they then enter the TCA cycle, promoting oxidative phosphorylation and increased ATP production (156–165) (**Figure 4**). In this model, hypoxia, nutrient deprivation and oxidative stress are thought to stabilize HIF1, which in turn causes catabolic autophagy, mitophagy and glycolysis, together with expression of the monocarboxylate transporter (MCT) 4 that exports lactate (21).

The molecular drivers governing the CAF metabolic phenotype may involve downregulation of caveolin-1 (Cav-1) (157). Low expression of stromal Cav-1 correlates with a high rate of tumor recurrence, metastasis, tamoxifen resistance, and poor clinical outcome in breast carcinoma (166, 167). Oxidative stress in the

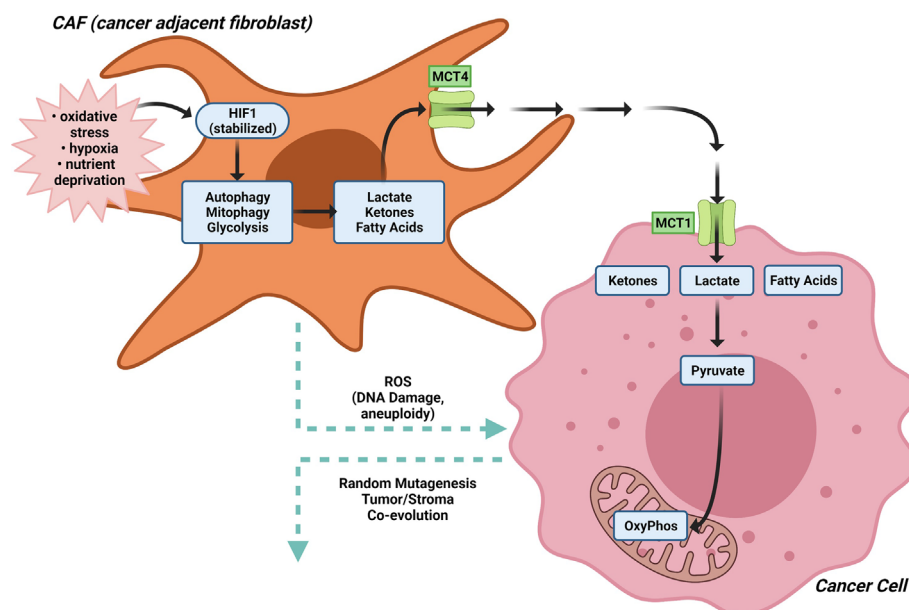


**FIGURE 4** | The Reverse Warburg effect. In the “Reverse Warburg Effect”, which was initially characterized in breast cancer cells, anabolic cancer cells import lactate, ketones and fatty acids released by either adjacent cancer associated fibroblasts (CAF), other stromal cell types or catabolic cancer cells, in response to oxidative stress. In CAFs, hypoxia, nutrient deprivation and oxidative stress stabilize HIF1 $\alpha$ , which in turn causes catabolic autophagy, mitophagy and glycolysis, together with expression of the monocarboxylate transporter (MCT) 4 that exports lactate. Aerobic glycolysis in cancer associated fibroblasts (CAFs) generates energy-rich metabolites (such as lactate, ketone bodies and pyruvate) that are transferred to adjacent cancer cells, where they then enter the TCA cycle, promoting oxidative phosphorylation and increased ATP production.

tumor micro-environment then activates an autophagic program, governed in part by the tumor vasculature, leading to the production of recycled nutrients that can then be used as “fuel” to promote the anabolic growth and aggressive progression of tumor epithelial cells (**Figure 3**). Autophagy in cancer-associated fibroblasts protects tumor cells against apoptotic cell death, in part through the provision of recycled nutrients. Oxidative stress in the tumor microenvironment also has mutagenic consequences (157). ROS production in cancer-associated fibroblasts, induces DNA damage and aneuploidy in adjacent epithelial cancer cells serving as a catalyst for the random mutagenesis of tumor cells and for tumor-stroma co-evolution. Bidirectional metabolic interactions are also observed with glutamine metabolism. Co-targeting glutamine synthetase in stroma and glutaminase in cancer cells reduces tumor weight, nodules, and metastasis (168).

Additional substrates participating in tumor stroma metabolic cross talk have been described in pancreatic cancer for the use of branched-chain amino acids (BCAA) (169). Pancreatic ductal cancer (PDAC)-induces branch chain amino acid transaminase 1 (BCAT1) in CAFs which govern internalization of the extracellular matrix from the tumor microenvironment to supply amino-acid precursors for branched-chain  $\alpha$ -ketoacid (BCKA). BCKA secretion by CAF are utilized by PDCA for protein synthesis and oxidative phosphorylation (169).

## Tumor-Associated Macrophages

Tumor-associated macrophages (TAMs) and cancer cells co-exist in the context of a complex, bidirectional metabolic relationship. M1-like macrophages displaying enhanced glycolysis and reduced oxidative phosphorylation in contrast with more oxidative M2-like macrophages (170). TAMs exposed to hypoxia or lactate secrete multiple cytokines with metabolic functions, including IL6, TNF, C-C motif chemokine ligand 5 (CCL5) (112), and CCL18 (171). CCL5, and CCL18 boost the synthesis of multiple pro-glycolytic factors including HXK2, PGK1, lactate dehydrogenase A (LDHA), glucose-6-phosphate dehydrogenase (G6PD), pyruvate kinase M1/2 (PKM), pyruvate dehydrogenase kinase 1 (PDK1), pyruvate dehydrogenase (PDH), solute carrier family 2 member 1 (SLC2A1, best known as GLUT1), and vascular cell adhesion molecule 1 (VCAM1) and display lower glyceraldehyde 3-phosphate dehydrogenase (GAPDH) and succinate dehydrogenase (SDH) activity than normal macrophages. There are important consequences of tumor metabolites on immune function as Lactate secreted by glycolytic cancer cells, favors the polarization of immune cells to an immunosuppressive phenotype. Inhibiting glutamine synthetase activity in M2 macrophages skews their polarization toward an HIF1 $\alpha$ -mediated M1 state, which impairs cytotoxic T cell recruitment and angiogenesis (172).

## Stromal Adipose Cells, Extracellular Fluids and Exosomes

Stromal adipose cells contribute to the breast tumor metabolic microenvironment. *In silico* deconvolution estimates of cell type composition and molecular profiles of constituent cell types in the

context of breast tumors applied to the TCGA data revealed metabolic coupling occurs between the epithelial and stroma cell types (173). A less adipose dense stroma displayed lower levels of mitochondrial activity and were associated with tumor cells with higher levels of oxidative metabolism. An adipokine, omentin cell-derived circulating ITLN1 (intelectin-1, or omentin), induced a metabolic shift in metastatic ovarian cancer cell and decrease in tumor growth rates (174). Reduced glycolysis was observed in the cancer cells *in vivo* in mice given intraperitoneally injections of ITLN1, while increased glycolysis was observed in the adjacent cancer-associated adipocytes (174).

Tissue plasma and interstitial fluid contains soluble proteins that are normally not utilized as sources of amino acids. Tumor cells may activate processes to utilize these nutrients including entosis (175), [the engulfment and degradation of entire live cells), macropinocytosis, (the bulk uptake of extracellular fluid into large vesicles (176, 177)], and micropinocytosis (178). Micropinocytosis is augmented in cancer cells, through mutations including K-Ras, and c-Src, and activation of the phosphoinositide 3-kinase (PI3 kinase) (149, 179, 180) or Hippo pathway effectors Yap and Taz (181). Pancreatic and prostate cancers bearing oncogenic mutations in *KRAS* or *PTEN*, respectively, use amino acids derived from engulfed extracellular proteins to proliferate in nutrient-limiting environment (127, 182–184).

An additional mechanism providing tumor nutrients involves CAF-derived exosomes which contain intact metabolites, including amino acids, lipids, and TCA-cycle intermediates that are avidly utilized by cancer cells for central carbon metabolism. These metabolites promote tumor growth under nutrient deprivation or nutrient stressed conditions and inhibit mitochondrial oxidative phosphorylation increasing glycolysis and glutamine-dependent reductive carboxylation in cancer cells (185).

## ALTERED LIPID METABOLISM WITHIN THE BREAST TUMOR EPITHELIUM AND TUMOR MICROENVIRONMENT

Lipid synthesis increases in cancer cells, corresponding to an increased requirement for membrane synthesis during proliferation and cell division, cellular signaling and synthesis of hormones. Acetyl CoA carboxylase (ACC) activity is essential for breast cancer cell survival (186). Acetyl CoA carboxylase (ACC) and fatty acid synthase complex (FASN) are commonly upregulated in cancer cells (187, 188). ACC converts acetyl CoA (**Figure 3**) to malonyl CoA, rather than citrate, which in turn is converted by FAS to saturated fatty acids (SFA). Chemical inhibitors of ACC or genetic ablation of FASN by RNAi have shown some efficacy in cancer treatment (189). Lipid precursors are made available through glycolysis and through mitochondrial metabolism of glutamine through  $\alpha$ ketoglutarate to citrate (**Figure 3**). Increased glycolysis in cancer cells ensures the availability of dihydroxyacetone phosphate (DHAP) for

conversion by glycerol-3-phosphate dehydrogenase 1 (GPD1) to glycerol-3-phosphate and thence phospholipids for cell membrane synthesis (190).

Expression of peroxisome proliferator-activated receptor gamma (PPAR $\gamma$ ), a key regulator of lipogenesis, is altered in breast cancer. PPAR $\gamma$  expression is a positive prognostic factor in luminal and ductal breast cancer (191). PPAR $\gamma$  levels are inversely correlated with tumor size, grade and TNM staging (192, 193). PPAR $\gamma$  agonists trigger apoptosis, inhibit cell growth, decrease breast cancer cell motility and inhibit invasion of breast cancer cells (194). Ligands of PPAR $\gamma$  inhibit the expression of several cell cycle regulators thereby reducing cancer cell proliferation (195). The synthetic PPAR $\gamma$  ligands, rosiglitazone and troglitazone and endogenous 15dPGJ2 inhibit cyclin D1 gene expression *via* repression of *cyclin D1* transcription, leading to cell cycle arrest (196). Although the role of PPAR $\gamma$  in tumor progression and metastasis remains controversial, in part because of the potential off target effects of PPAR $\gamma$  ligands (197), consistent with the important role of lipogenesis in breast cancer progression, recent studies showed that genetic deletion of *Ppar $\gamma$ 1* delayed the onset of tumorigenesis by mammary epithelial cell targeted ErbB2 (198).

Recent studies have identified ferroptosis-related gene expression pathways that predict outcome in breast cancer (199). Ferroptosis is a form of regulated necrosis driven by iron-dependent peroxidation of phospholipids, plays an important role in tumor suppression (200–202). Lipid metabolism can govern ferroptosis *via* sterol regulatory element-binding protein 1 (SREBP1), a central transcription factor regulating lipid metabolism. SREBP1m targets include gene governing lipogenesis (such as ACLY, ACC, FASN and stearoyl CoA desaturase 1), gluconeogenesis and the pentose phosphate pathway (**Figure 2**) including pyruvate kinase R isoform (PKLR), phosphoenolpyruvate carboxykinase 1 (PCK1), glucose 6-phosphatase (G6PC), and glucose 6-phosphate dehydrogenase (G6PDH). Sustained activation of mechanistic target of rapamycin complex 1 (mTORC1) through oncogenic activation of the PI<sub>3</sub>K-AKT pathway induces SREBP1 and provides resistance to ferroptosis in breast tumors in mice (203).

## CELL CYCLE REGULATORS GOVERN TUMOR METABOLISM

The cell-cycle governs cellular metabolism and, reciprocally, glycolytic enzyme activity can affect cellular proliferation and tumor aggressiveness, including through actions that are additional to their functions within glycolysis (204). Enhanced activity of the glycolytic enzymes, phosphoglycerate mutase (PGM) or glucose phosphate isomerase (GPI) induces proliferation of mouse embryonic fibroblasts and inhibition of these glycolytic enzymes promotes senescence (205). GPI converts glucose 6 phosphate to fructose 6 phosphate (**Figure 2**)

Regulators of cell cycle progression can also directly affect cellular metabolism. p53 for example downregulates PGM (204).

Cyclin D1 overexpression restrains adipogenesis (206), suppresses mitochondrial function and biogenesis, and augments cytosolic glycolysis. The *cyclin D1* gene is overexpressed in human breast cancer and is required for oncogene-induced tumorigenesis therefore the mechanism by which cyclin D1 governs tumor metabolism is of broad interest. Cyclin D1 encodes the regulatory subunit of the holoenzyme that phosphorylates and inactivates the RB protein. Early observations in cyclin D1 anti-sense transgenic mice targeting the mammary gland showed induction of mitochondrial and lipogenic regulatory gene clusters *in vivo* (41). The induction of cyclin D1 antisense in the mammary epithelial cell of transgenic mice induced acetyl-CoA carboxylase, fatty acid synthase, hexokinase II, and pyruvate kinase (**Figure 2**). A detailed gene expression analysis evidenced the impact of increased cyclin D1 to enhance the Warburg effect (207).

Several additional mechanisms have been described by which cyclin D1 regulates cytosolic glycolysis and induces the Warburg effect. Firstly, the cyclin D1/cdk4 complex phosphorylates NRF1 at a canonical cyclin D1/CDK4 phosphorylation site. NRF1 is a key nuclear transcription factor governing mitochondrial function with targets that include mitochondrial transcription factor A (mTFA). Consequences included reduced D loop transcriptional activity in mitochondrial DNA. Deletion of the *cyclin D1* gene increased mitochondrial mass and mitochondrial activity function (40, 208). Secondly, in hepatocytes, cyclin D1–cyclin dependent kinase-4 (Cdk4) phosphorylates and activates the histone acetyltransferase, general control non-repressed protein 5 (GCN5), which then acetylates and inhibits peroxisome-proliferator-activated receptor- $\gamma$  coactivator-1 $\alpha$  (PGC-1 $\alpha$ ) activity at gluconeogenic genes (209). Thirdly, cyclin D1 increased phosphorylation of AKT<sup>Ser 473</sup> in breast cancer cells and animal models, augmented AKT1 activity (210), which in turn simulates the Warburg effect (211). Collectively these studies illustrate cyclin D1 promotes the Warburg effect in tissue culture and *in vivo*.

## MUTATIONS OF METABOLIC GENES IN CANCER

As noted above, a number of genes and proteins that have direct roles in metabolism are regulated by oncogenes (c-Myc, cyclin D1, Ras, AKT/PI<sub>3</sub>K/mTOR), or tumor suppressors (p53) (212). Additionally, germ line and somatic mutations have been described in genes encoding enzymes that have direct roles in metabolism. Familial germline mutations in succinate dehydrogenase (213–215), and somatic mutations in isocitrate dehydrogenase 1 and 2 (*IDH1* and *IDH2*), fumarate hydratase (*FH*) and isoforms of succinate dehydrogenase (*SDH*) are found in a variety of human cancers (216). *IDH1* and *IDH2* catalyze the decarboxylation of isocitrate to  $\alpha$ -ketoglutarate (**Figure 2**). Fumarate hydratase catalyzes the reversible hydration of fumarate to malate. The multi-component *SDH* complex catalyzes the oxidation of succinate to fumarate, in concert with reducing ubiquinone in the electron transport chain.

Succinate in turn may induce DNA hypermethylation (**Figure 2**). Tumors that accumulate succinate, show inhibition of 2-oxoglutarate-dependent histone and DNA demethylase enzymes, resulting in epigenetic silencing (217).

The metabolite profile itself drives oncogenesis. In the case of the *IDH1* and *IDH2* mutations, there is reduced production of  $\alpha$ KG from isocitrate.  $\alpha$ KG is a rate-limiting substrate for  $\alpha$ -ketoglutarate-dependent dioxygenases that catalyze demethylation of DNA, histones and mRNA, and regulate HIF1 $\alpha$  (212) (**Figure 2**). *IDH1* mutations in some gliomas, and *IDH1* and *IDH2* mutations in some acute myeloblastic leukemias, convert  $\alpha$ KG to R-2-hydroxyglutarate (2HG). 2HG can then suppress activity in  $\alpha$ -ketoglutarate-dependent dioxygenases through competition with  $\alpha$ KG. Inhibition of some dioxygenases by succinate or fumarate has also been rationalized as an effector pathway for loss of function of mutations in fumarate hydratase (FH), succinate dehydrogenase (31). Fumarate derivatization of cysteine residues within the Kelch-like ECH-associated protein 1 (KEAP1) may also occur, freeing NRF2 from KEAP1-mediated degradation (218).

Recent studies of over 900 cell lines revealed diverse metabolic changes with associated potential therapeutic potential. Hypermethylation of the gene encoding asparagine synthetase showed sensitivity to L-asparaginase (219). A comprehensive proteomic analysis combined with metabolomic and gene methylation analysis revealed the metabolic heterogeneity of the cancer cell lines (220). Analysis of 225 metabolites in 928 cell lines from 20 cancer types revealed several broad principles firstly, previously described mutations (*IDH1*, *KEAP1*) revealed the predicted change in metabolites. Secondly, that common oncogenic events (*EGFR*, *KRAS*, *NRAS*, *TP53*, *PTEN*, *TSC1*, *TSC2*) had weak to non-significant associations with profiled metabolites. Thirdly, that DNA hypermethylation influence metabolite production *via* suppressing degradation pathways. For example, methylation of *SLC25A20* (carnitine/acylcarnitine translocase) in breast cancer cell lines led to accumulation of long chain acylcarnitine species. Fourthly, DNA hypermethylation regulates metabolite levels by limiting components of biosynthetic pathways. For example, hypermethylation of the *PYCR* gene, an enzyme that converts pyrroline-5-carboxylate to proline, was associated with reduced proline levels.

## EPIGENETIC REGULATION OF EMT GOVERNS BREAST CANCER METABOLISM

Carcinoma cells undergo an epithelial-to-mesenchymal transition (EMT) although the transition is considered a spectrum of changes, rather than a binary event (221). EMT-inducing transcription factor (EMT-TF) regulate the induction of EMT by repressing the transcription of epithelial genes while activating mesenchymal genes. EMT-TFs are regulated at a transcriptional level by DNA methylation, histone modifications, and RNA-mediated epigenetic regulation (222). Genetic regulators of EMT also directly regulate BCa cellular metabolism (223). Many pathways link EMT-TFs expression

with glycolysis, mitochondrial metabolism, glutaminolysis and lipid metabolism (224), providing the rational basis for metabolic targeting of BCa cancer EMT (223). MDA-MB-231 is a mesenchymal basal-like breast cell line with decreased mitochondrial respiration compared to the epithelial luminal-like breast cell line, MCF-7. The decrease in oxidative phosphorylation correlated with the down regulation of succinate dehydrogenase B (SDHB, complex II), the core catalytic subunit of SDH in MDA-MB-231 cells (225). Decreased SDHB expression leads to metabolic reprogramming and migration and invasion of tumor cells by promoting EMT (226–228).

Most BCa cells express both epithelial and mesenchymal traits. When epithelial cancer cells lose their epithelial features and acquire a mesenchymal phenotype this promotes motility and invasion through loss of cell polarity, disruption E-cadherin/ $\beta$ -catenin leading to loss of cell-cell adhesion involved in cancer invasion and metastasis (225). This E/M hybrid state is facilitated by the differential expression of Snail (Snail and Snai2), bHLH (Twist1 and Twist2), and zinc finger and E-box binding (Zeb1 and Zeb2), collectively termed EMT-inducing transcription factors (EMT-TFs). The mesenchymal-like phenotype is accompanied by the expression of adult stem cell programs, notably, active canonical Wnt signaling.

The EMT transition in BCa is regulated by altered expression of the transcription factors SNAIL/SLUG (229), TGF- $\beta$  (230), Twist, and Goosecoid and the cell-cycle control proteins [p21<sup>CIP1</sup> (231), cyclin D1 (232)]. These EMT inducing agents in turn have been shown to regulate cellular metabolism (reviewed in (233)). For example, the EMT TFs Slug/Twist suppresses succinate dehydrogenase (SDH), thereby repressing mitochondrial respiration, leading to the accumulation of succinate, which suppresses TET2, causes causing DNA hypermethylation, further promoting EMT in paraganglioma (234). Recent studies identified a novel role for the cell fate determination pathway in restraining EMT. Loss of DACH1 expression, a helix-turn helix protein of the Forkhead family that is a key determinant of the cell fate determination pathway, is a predictor of metastasis and poor survival in BCa (235). The *DACH1* gene is silenced by methylation (236), and DACH1 in turns restrains the EMT program (237).

## EMERGING QUESTIONS IN METABOLIC HETEROGENEITY

The increased resolution of investigative technology has provided evidence for distinct sources of metabolic heterogeneity in BCa. Metabolic heterogeneity has been identified between genetic subtypes of breast cancer and within the components of the tumor microenvironment for an individual patient's tumor. Several key questions have emerged as a consequence of the emerging understanding that tumors are highly heterogeneous (238). How can we best harness the knowledge that genetic mutations can alter a particular patient's tumor metabolic in order to identify therapeutic vulnerabilities?



Analysis of large compendiums of tumor cell lines has identified correlates between altered genetic changes and metabolite production (220). However, evidence suggests that most human tumors acquire hundreds of somatic mutations in coding regions (239). Taking a broader definition of a metabolic genes to include the known upstream regulators of the enzymes that actually carry out the metabolic transformation, though, reveals the extent to which mutation or altered copy number pervades human cancers (240). Metabolic gene alterations are frequent and determine tumor aggressiveness and therapy responses (219, 240). High metabolic gene abnormality frequency correlated with worse prognosis (240). The most frequent metabolic gene abnormalities in breast cancer involve lipid metabolism (240). Bystander gene deletion may also contribute to tumor metabolic heterogeneity as metabolic genes may reside in proximity to known tumor suppressor genes that are deleted in cancer. The *MTAP* (methylthioadenosine phosphorylase) gene for example may be co-deleted with *CDKN2A*, resulting in elevated methyl thioadenosine which sensitizes cells to PRMT5 inhibitors (241). How then to discern the functional significance of such ubiquitous mutational loads of metabolic genes in a tumor?

Intratumoral heterogeneity subclonal driver mutations that govern tumor metabolism have been identified in breast cancer (TP53, SMAD4) (238), consistent with studies of subclonal diversification of primary breast cancer revealed by multi region sequencing of the coding region (238), the non-coding region (242) and evidence for further genetic evolution upon relapse (SWI-SNF and JAK2-STAT3) (243). What metabolic vulnerabilities emerge in tumors with metabolically diverse subclonal populations?

Mathematical modeling approaches have been developed to understand the metabolic impact of altered gene expression on tumor metabolism. Modeling analysis of epithelial-to-mesenchymal transition has been conducted, in which metabolic pathway signatures have been used to quantify the activities of glycolysis, and the citric acid cycle with corresponding analysis of enzymes governing the metabolic processes in tumor samples (233, 244). Because tumors exhibit a spectrum of EMT and a spectrum of metabolic changes which may be topologically distinct, for example in the leading vs. the trailing edge of an invasive tumors, more accurate mathematical predictive models are required to provide precise metabolic therapeutics.

Linking the complex patterns of metabolic genetic alterations that occurs within a tumor to therapeutic co-extinction paradigms for individualized patient treatment remains a key challenge for future research.

## AUTHOR CONTRIBUTIONS

All authors listed have made a substantial, direct, and intellectual contribution to the work, and approved it for publication.

## FUNDING

This work was supported in part by NIH R01CA132115, R21CA235139-01 RP and a Breakthrough Breast Cancer Research Program grant award from Department of Defense (W81XWH1810605) RP.

## REFERENCES

- Siegel RL, Miller KD, Jemal A. Cancer Statistics, 2017. *CA Cancer J Clin* (2017) 67(1):7–30. doi: 10.3322/caac.21387
- Gilbert M, Bertucci F, Esterni B, Madroszyk A, Tarpin C, Jacquemier J, et al. Capecitabine After Anthracycline and Taxane Exposure in HER2-Negative Metastatic Breast Cancer Patients: Response, Survival and Prognostic Factors. *Anticancer Res* (2011) 31(3):1079–86.
- Cancer Genome Atlas N. Comprehensive Molecular Portraits of Human Breast Tumours. *Nature* (2012) 490(7418):61–70. doi: 10.1038/nature11412
- Perou CM, Sorlie T, Eisen MB, van de Rijn M, Jeffrey SS, Rees CA, et al. Molecular Portraits of Human Breast Tumours. *Nature* (2000) 406(6797):747–52. doi: 10.1038/35021093
- Cancer Genome Atlas Network. Comprehensive Molecular Portraits of Human Breast Tumours. *Nature* (2012) 490(7418):61–70. doi: 10.1038/nature11412
- Shimelis H, LaDuca H, Hu C, Hart SN, Na J, Thomas A, et al. Triple-Negative Breast Cancer Risk Genes Identified by Multigene Hereditary Cancer Panel Testing. *J Natl Cancer Inst* (2018) 110(8):855–62. doi: 10.1093/jnci/djy106
- Mittendorf EA, Philips AV, Meric-Bernstam F, Qiao N, Wu Y, Harrington S, et al. PD-L1 Expression in Triple-Negative Breast Cancer. *Cancer Immunol Res* (2014) 2(4):361–70. doi: 10.1158/2326-6066.CIR-13-0127
- Velasco-Velazquez M, Jiao X, de la Fuente M, Pestell TG, Ertel A, Lisanti MP, et al. CCR5 Antagonist Blocks Metastasis of Basal Breast Cancer Cells. *Cancer Res* (2012) 72(15):3839–50. doi: 10.1158/0008-5472.CAN-11-3917
- Jiao X, Velasco-Velazquez MA, Wang M, Li Z, Rui H, Peck AR, et al. CCR5 Governs DNA Damage Repair and Breast Cancer Stem Cell Expansion. *Cancer Res* (2018) 78(7):1657–71. doi: 10.1158/0008-5472.CAN-17-0915
- Wang G, Gormley M, Qiao J, Zhao Q, Wang M, Di Sante G, et al. Cyclin D1-Mediated microRNA Expression Signature Predicts Breast Cancer Outcome. *Theranostics* (2018) 8(8):2251–63. doi: 10.7150/thno.23877
- Cedro-Tanda A, Rios-Romero M, Romero-Cordoba S, Cisneros-Villanueva M, Rebollar-Vega RG, Alfaro-Ruiz LA, et al. A lncRNA Landscape in Breast Cancer Reveals a Potential Role for AC009283.1 in Proliferation and Apoptosis in HER2-Enriched Subtype. *Sci Rep* (2020) 10(1):13146. doi: 10.1038/s41598-020-69905-z
- Volinia S, Galasso M, Sana ME, Wise TF, Palatini J, Huebner K, et al. Breast Cancer Signatures for Invasiveness and Prognosis Defined by Deep Sequencing of microRNA. *Proc Natl Acad Sci USA* (2012) 109(8):3024–9. doi: 10.1073/pnas.1200010109
- Timmerman LA, Holton T, Yuneva M, Louie RJ, Padro M, Daemen A, et al. Glutamine Sensitivity Analysis Identifies the xCT Antiporter as a Common Triple-Negative Breast Tumor Therapeutic Target. *Cancer Cell* (2013) 24(4):450–65. doi: 10.1016/j.ccr.2013.08.020
- Kung HN, Marks JR, Chi JT. Glutamine Synthetase Is a Genetic Determinant of Cell Type-Specific Glutamine Independence in Breast Epithelia. *PLoS Genet* (2011) 7(8):e1002229. doi: 10.1371/journal.pgen.1002229
- Lukey MJ, Cluntun AA, Katt WP, Lin MJ, Druso JE, Ramachandran S, et al. Liver-Type Glutaminase GLS2 Is a Druggable Metabolic Node in Luminal-Subtype Breast Cancer. *Cell Rep* (2019) 29(1):76–88.e7. doi: 10.1016/j.celrep.2019.08.076

16. Harbeck N, Penault-Llorca F, Cortes J, Gnant M, Houssami N, Poortmans P, et al. Breast Cancer. *Nat Rev Dis Primers* (2019) 5(1):66. doi: 10.1038/s41572-019-0111-2
17. Anampa J, Makower D, Sparano JA. Progress in Adjuvant Chemotherapy for Breast Cancer: An Overview. *BMC Med* (2015) 13:195. doi: 10.1186/s12916-015-0439-8
18. Baldassari F, Zerbinati C, Galasso M, Corra F, Minotti L, Agnoletto C, et al. Screen for MicroRNA and Drug Interactions in Breast Cancer Cell Lines Points to miR-126 as a Modulator of CDK4/6 and PIK3CA Inhibitors. *Front Genet* (2018) 9:174. doi: 10.3389/fgene.2018.00174
19. Balatti V, Croce CM. MicroRNA Dysregulation and Multi-Targeted Therapy for Cancer Treatment. *Adv Biol Regul* (2020) 75:100669. doi: 10.1016/j.jbior.2019.100669
20. Pekarsky Y, Croce CM. Noncoding RNA Genes in Cancer Pathogenesis. *Adv Biol Regul* (2019) 71:219–23. doi: 10.1016/j.jbior.2018.12.002
21. Martinez-Outschoorn UE, Peiris-Pages M, Pestell RG, Sotgia F, Lisanti MP. Cancer Metabolism: A Therapeutic Perspective. *Nat Rev Clin Oncol* (2017) 14(1):11–31. doi: 10.1038/nrclinonc.2016.60
22. Peiris-Pages M, Martinez-Outschoorn UE, Pestell RG, Sotgia F, Lisanti MP. Cancer Stem Cell Metabolism. *Breast Cancer Res* (2016) 18(1):55. doi: 10.1186/s13058-016-0712-6
23. DeBerardinis RJ, Lum JJ, Hatzivassiliou G, Thompson CB. The Biology of Cancer: Metabolic Reprogramming Fuels Cell Growth and Proliferation. *Cell Metab* (2008) 7(1):11–20. doi: 10.1016/j.cmet.2007.10.002
24. Warburg O. On the Origin of Cancer Cells. *Science* (1956) 123(3191):309–14. doi: 10.1126/science.123.3191.309
25. Schworer S, Vardhana SA, Thompson CB. Cancer Metabolism Drives a Stromal Regenerative Response. *Cell Metab* (2019) 29(3):576–91. doi: 10.1016/j.cmet.2019.01.015
26. Strickaert A, Saiselet M, Dom G, De Deken X, Dumont JE, Feron O, et al. Cancer Heterogeneity Is Not Compatible With One Unique Cancer Cell Metabolic Map. *Oncogene* (2017) 36(19):2637–42. doi: 10.1038/onc.2016.411
27. Hensley CT, Faubert B, Yuan Q, Lev-Cohain N, Jin E, Kim J, et al. Metabolic Heterogeneity in Human Lung Tumors. *Cell* (2016) 164(4):681–94. doi: 10.1016/j.cell.2015.12.034
28. Kim J, DeBerardinis RJ. Mechanisms and Implications of Metabolic Heterogeneity in Cancer. *Cell Metab* (2019) 30(3):434–46. doi: 10.1016/j.cmet.2019.08.013
29. Rao AD, DeBerardinis RJ. Metabolic Vulnerability in Tumours Illuminated. *Nature* (2019) 575(7782):296–7. doi: 10.1038/d41586-019-03239-3
30. Borroughs LK, DeBerardinis RJ. Metabolic Pathways Promoting Cancer Cell Survival and Growth. *Nat Cell Biol* (2015) 17(4):351–9. doi: 10.1038/ncb3124
31. Pavlova NN, Thompson CB. The Emerging Hallmarks of Cancer Metabolism. *Cell Metab* (2016) 23(1):27–47. doi: 10.1016/j.cmet.2015.12.006
32. Baek S, Choi CM, Ahn SH, Lee JW, Gong G, Ryu JS, et al. Exploratory Clinical Trial of (4S)-4-(3-[18F]Fluoropropyl)-L-Glutamate for Imaging xC-Transporter Using Positron Emission Tomography in Patients With Non-Small Cell Lung or Breast Cancer. *Clin Cancer Res* (2012) 18(19):5427–37. doi: 10.1158/1078-0432.CCR-12-0214
33. Xin Y, Cai H. Improved Radiosynthesis and Biological Evaluations of L- and D-1-[(18F)Fluoroethyl-Tryptophan for PET Imaging of IDO-Mediated Kynurenine Pathway of Tryptophan Metabolism. *Mol Imaging Biol* (2017) 19(4):589–98. doi: 10.1007/s11307-016-1024-z
34. Kole AC, Nieweg OE, Pruim J, Paans AM, Plukker JT, Hoekstra HJ, et al. Standardized Uptake Value and Quantification of Metabolism for Breast Cancer Imaging With FDG and L-[1-11C]Tyrosine PET. *J Nucl Med* (1997) 38(5):692–6.
35. Haukaas TH, Euceda LR, Giskeodegard GF, Bathen TF. Metabolic Portraits of Breast Cancer by HR MAS MR Spectroscopy of Intact Tissue Samples. *Metabolites* (2017) 7(2):18. doi: 10.3390/metabo7020018
36. Leskinen-Kallio S, Nagren K, Lehtikoinen P, Ruotsalainen U, Joensuu H. Uptake of 11C-Methionine in Breast Cancer Studied by PET. An Association With the Size of S-Phase Fraction. *Br J Cancer* (1991) 64(6):1121–4. doi: 10.1038/bjc.1991.475
37. Jager PL, Plaat BE, de Vries EG, Molenaar WM, Vaalburg W, Piers DA, et al. Imaging of Soft-Tissue Tumors Using L-3-[Iodine-123]Iodo-Alpha-Methyl-Tyrosine Single Photon Emission Computed Tomography: Comparison With Proliferative and Mitotic Activity, Cellularity, and Vascularity. *Clin Cancer Res* (2000) 6(6):2252–9.
38. Prendergast GC, Malachowski WP, DuHadaway JB, Muller AJ. Discovery of IDO1 Inhibitors: From Bench to Bedside. *Cancer Res* (2017) 77(24):6795–811. doi: 10.1158/0008-5472.CAN-17-2285
39. Muller AJ, DuHadaway JB, Donover PS, Sutanto-Ward E, Prendergast GC. Inhibition of Indoleamine 2,3-Dioxygenase, an Immunoregulatory Target of the Cancer Suppression Gene Bin1, Potentiates Cancer Chemotherapy. *Nat Med* (2005) 11(3):312–9. doi: 10.1038/nm1196
40. Wang C, Li Z, Lu Y, Du R, Katiyar S, Yang J, et al. Cyclin D1 Repression of Nuclear Respiratory Factor 1 Integrates Nuclear DNA Synthesis and Mitochondrial Function. *Proc Natl Acad Sci USA* (2006) 103(31):11567–72. doi: 10.1073/pnas.0603363103
41. Sakamaki T, Casimiro MC, Ju X, Quong AA, Katiyar S, Liu M, et al. Cyclin D1 Determines Mitochondrial Function In Vivo. *Mol Cell Biol* (2006) 26(14):5449–69. doi: 10.1128/MCB.02074-05
42. Dong C, Yuan T, Wu Y, Wang Y, Fan TW, Miriyala S, et al. Loss of FBP1 by Snail-Mediated Repression Provides Metabolic Advantages in Basal-Like Breast Cancer. *Cancer Cell* (2013) 23(3):316–31. doi: 10.1016/j.ccr.2013.01.022
43. Luo W, Chang R, Zhong J, Pandey A, Semenza GL. Histone Demethylase JMJD2C Is a Coactivator for Hypoxia-Inducible Factor 1 That Is Required for Breast Cancer Progression. *Proc Natl Acad Sci USA* (2012) 109(49):E3367–76. doi: 10.1073/pnas.1217394109
44. Cox E, Bonner J. Ecology. The Advantages of Togetherness. *Science* (2001) 292(5516):448–9. doi: 10.1126/science.1060456
45. Gomez-Cebrian N, Rojas-Benedicto A, Albers-Vaquer A, Lopez-Guerrero JA, Pineda-Lucena A, Puchades-Carrasco L. Metabolomics Contributions to the Discovery of Prostate Cancer Biomarkers. *Metabolites* (2019) 9(3):48. doi: 10.3390/metabo9030048
46. Giunchi F, Fiorentino M, Loda M. The Metabolic Landscape of Prostate Cancer. *Eur Urol Oncol* (2019) 2(1):28–36. doi: 10.1016/j.euo.2018.06.010
47. Sonveaux P, Vegran F, Schroeder T, Wergin MC, Verrax J, Rabbani ZN, et al. Targeting Lactate-Fueled Respiration Selectively Kills Hypoxic Tumor Cells in Mice. *J Clin Invest* (2008) 118(12):3930–42. doi: 10.1172/JCI36843
48. Pavlides S, Whitaker-Menezes D, Castello-Cros R, Flomenberg N, Witkiewicz AK, Frank PG, et al. The Reverse Warburg Effect: Aerobic Glycolysis in Cancer Associated Fibroblasts and the Tumor Stroma. *Cell Cycle* (2009) 8(23):3984–4001. doi: 10.4161/cc.8.23.10238
49. Ying H, Kimmelman AC, Lyssiotis CA, Hua S, Chu GC, Fletcher-Sanankone E, et al. Oncogenic Kras Maintains Pancreatic Tumors Through Regulation of Anabolic Glucose Metabolism. *Cell* (2012) 149(3):656–70. doi: 10.1016/j.cell.2012.01.058
50. Jiang P, Du W, Wang X, Mancuso A, Gao X, Wu M, et al. P53 Regulates Biosynthesis Through Direct Inactivation of Glucose-6-Phosphate Dehydrogenase. *Nat Cell Biol* (2011) 13(3):310–6. doi: 10.1038/ncb2172
51. Wahlstrom T, Henriksson MA. Impact of MYC in Regulation of Tumor Cell Metabolism. *Biochim Biophys Acta* (2015) 1849(5):563–9. doi: 10.1016/j.bbaggm.2014.07.004
52. Pate KT, Stringari C, Sprowl-Tanio S, Wang K, TeSlaa T, Hoverter NP, et al. Wnt Signaling Directs a Metabolic Program of Glycolysis and Angiogenesis in Colon Cancer. *EMBO J* (2014) 33(13):1454–73. doi: 10.15252/embj.201488598
53. Vander Heiden MG, Cantley LC, Thompson CB. Understanding the Warburg Effect: The Metabolic Requirements of Cell Proliferation. *Science* (2009) 324(5930):1029–33. doi: 10.1126/science.1160809
54. Brand K, Leibold W, Luppa P, Schoerner C, Schulz A. Metabolic Alterations Associated With Proliferation of Mitogen-Activated Lymphocytes and of Lymphoblastoid Cell Lines: Evaluation of Glucose and Glutamine Metabolism. *Immunobiology* (1986) 173(1):23–34. doi: 10.1016/S0171-2985(86)80086-9
55. Pfeiffer T, Schuster S, Bonhoeffer S. Cooperation and Competition in the Evolution of ATP-Producing Pathways. *Science* (2001) 292(5516):504–7. doi: 10.1126/science.1058079
56. Fan J, Ye J, Kamphorst JJ, Shlomi T, Thompson CB, Rabinowitz JD. Quantitative Flux Analysis Reveals Folate-Dependent NADPH Production. *Nature* (2014) 510(7504):298–302. doi: 10.1038/nature13236

57. Possemato R, Marks KM, Shaul YD, Pacold ME, Kim D, Birsoy K, et al. Functional Genomics Reveal That the Serine Synthesis Pathway Is Essential in Breast Cancer. *Nature* (2011) 476(7360):346–50. doi: 10.1038/nature10350
58. Locasale JW, Grassian AR, Melman T, Lysiotis CA, Mattaini KR, Bass AJ, et al. Phosphoglycerate Dehydrogenase Diverts Glycolytic Flux and Contributes to Oncogenesis. *Nat Genet* (2011) 43(9):869–74. doi: 10.1038/ng.890
59. Wang T, Marquardt C, Foker J. Aerobic Glycolysis During Lymphocyte Proliferation. *Nature* (1976) 261(5562):702–5. doi: 10.1038/261702a0
60. Porporato PE, Payen VL, De Saedeleer CJ, Preat V, Thissen JP, Feron O, et al. Lactate Stimulates Angiogenesis and Accelerates the Healing of Superficial and Ischemic Wounds in Mice. *Angiogenesis* (2012) 15(4):581–92. doi: 10.1007/s10456-012-9282-0
61. Constant JS, Feng JJ, Zabel DD, Yuan H, Suh DY, Scheuenstuhl H, et al. Lactate Elicits Vascular Endothelial Growth Factor From Macrophages: A Possible Alternative to Hypoxia. *Wound Repair Regen* (2000) 8(5):353–60. doi: 10.1111/j.1524-475X.2000.00353.x
62. Stern R, Shuster S, Neudecker BA, Formby B. Lactate Stimulates Fibroblast Expression of Hyaluronan and CD44: The Warburg Effect Revisited. *Exp Cell Res* (2002) 276(1):24–31. doi: 10.1006/excr.2002.5508
63. Rothberg JM, Bailey KM, Wojtkowiak JW, Ben-Nun Y, Bogoy M, Weber E, et al. Acid-Mediated Tumor Proteolysis: Contribution of Cysteine Cathepsins. *Neoplasia* (2013) 15(10):1125–37. doi: 10.1593/neo.13946
64. Estrella V, Chen T, Lloyd M, Wojtkowiak J, Cornell HH, Ibrahim-Hashim A, et al. Acidity Generated by the Tumor Microenvironment Drives Local Invasion. *Cancer Res* (2013) 73(5):1524–35. doi: 10.1158/0008-5472.CAN-12-2796
65. Vegran F, Boidot R, Michiels C, Sonveaux P, Feron O. Lactate Influx Through the Endothelial Cell Monocarboxylate Transporter MCT1 Supports an NF-Kappab/IL-8 Pathway That Drives Tumor Angiogenesis. *Cancer Res* (2011) 71(7):2550–60. doi: 10.1158/0008-5472.CAN-10-2828
66. Zhu X, Xuan Z, Chen J, Li Z, Zheng S, Song P. How DNA Methylation Affects the Warburg Effect. *Int J Biol Sci* (2020) 16(12):2029–41. doi: 10.7150/ijbs.45420
67. Schvartzman JM, Thompson CB, Finley LWS. Metabolic Regulation of Chromatin Modifications and Gene Expression. *J Cell Biol* (2018) 217(7):2247–59. doi: 10.1083/jcb.201803061
68. Hu M, Yao J, Cai L, Bachman KE, van den Brule F, Velculescu V, et al. Distinct Epigenetic Changes in the Stromal Cells of Breast Cancers. *Nat Genet* (2005) 37(8):899–905. doi: 10.1038/ng1596
69. Holm K, Hegardt C, Staaf J, Vallon-Christersson J, Jonsson G, Olsson H, et al. Molecular Subtypes of Breast Cancer Are Associated With Characteristic DNA Methylation Patterns. *Breast Cancer Res* (2010) 12(3):R36. doi: 10.1186/bcr2590
70. Lopez-Serra P, Marcilla M, Villanueva A, Ramos-Fernandez A, Palau A, Leal L, et al. A DERL3-Associated Defect in the Degradation of SLC2A1 Mediates the Warburg Effect. *Nat Commun* (2014) 5:3608. doi: 10.1038/ncomms4608
71. Ha TK, Her NG, Lee MG, Ryu BK, Lee JH, Han J, et al. Caveolin-1 Increases Aerobic Glycolysis in Colorectal Cancers by Stimulating HMGA1-Mediated GLUT3 Transcription. *Cancer Res* (2012) 72(16):4097–109. doi: 10.1158/0008-5472.CAN-12-0448
72. Yen CY, Huang HW, Shu CW, Hou MF, Yuan SS, Wang HR, et al. DNA Methylation, Histone Acetylation and Methylation of Epigenetic Modifications as a Therapeutic Approach for Cancers. *Cancer Lett* (2016) 373(2):185–92. doi: 10.1016/j.canlet.2016.01.036
73. Brown NJ, Higham SE, Perunovic B, Arafat M, Balasubramanian S, Rehman I. Lactate Dehydrogenase-B Is Silenced by Promoter Methylation in a High Frequency of Human Breast Cancers. *PLoS One* (2013) 8(2):e57697. doi: 10.1371/journal.pone.0057697
74. San-Millan I, Brooks GA. Reexamining Cancer Metabolism: Lactate Production for Carcinogenesis Could be the Purpose and Explanation of the Warburg Effect. *Carcinogenesis* (2017) 38(2):119–33. doi: 10.1093/carcin/bgw127
75. Thakur C, Chen F. Connections Between Metabolism and Epigenetics in Cancers. *Semin Cancer Biol* (2019) 57:52–8. doi: 10.1016/j.semcancer.2019.06.006
76. Desai S, Ding M, Wang B, Lu Z, Zhao Q, Shaw K, et al. Tissue-Specific Isoform Switch and DNA Hypomethylation of the Pyruvate Kinase PKM Gene in Human Cancers. *Oncotarget* (2014) 5(18):8202–10. doi: 10.18632/oncotarget.1159
77. Zhong XY, Yuan XM, Xu YY, Yin M, Yan WW, Zou SW, et al. CARM1 Methylates GAPDH to Regulate Glucose Metabolism and Is Suppressed in Liver Cancer. *Cell Rep* (2018) 24(12):3207–23. doi: 10.1016/j.celrep.2018.08.066
78. Christofk HR, Vander Heiden MG, Harris MH, Ramanathan A, Gerszten RE, Wei R, et al. The M2 Splice Isoform of Pyruvate Kinase Is Important for Cancer Metabolism and Tumour Growth. *Nature* (2008) 452(7184):230–3. doi: 10.1038/nature06734
79. Singh S, Narayanan SP, Biswas K, Gupta A, Ahuja N, Yadav S, et al. Intragenic DNA Methylation and BORIS-Mediated Cancer-Specific Splicing Contribute to the Warburg Effect. *Proc Natl Acad Sci USA* (2017) 114(43):11440–5. doi: 10.1073/pnas.1708447114
80. Luo W, Semenza GL. Emerging Roles of PKM2 in Cell Metabolism and Cancer Progression. *Trends Endocrinol Metab* (2012) 23(11):560–6. doi: 10.1016/j.tem.2012.06.010
81. Gaowa S, Futamura M, Tsuneki M, Kamino H, Tajima JY, Mori R, et al. Possible Role of P53/Micap-Regulated Mitochondrial Quality Control as a Tumor Suppressor in Human Breast Cancer. *Cancer Sci* (2018) 109(12):3910–20. doi: 10.1111/cas.13824
82. Menga A, Palmieri EM, Cianciulli A, Infantino V, Mazzone M, Scilimati A, et al. SLC25A26 Overexpression Impairs Cell Function via mtDNA Hypermethylation and Rewiring of Methyl Metabolism. *FEBS J* (2017) 284(6):967–84. doi: 10.1111/febs.14028
83. Miyamoto Y, Kitamura N, Nakamura Y, Futamura M, Miyamoto T, Yoshida M, et al. Possible Existence of Lysosome-Like Organella Within Mitochondria and Its Role in Mitochondrial Quality Control. *PLoS One* (2011) 6(1):e16054. doi: 10.1371/journal.pone.0016054
84. Tsuneki M, Nakamura Y, Kinjo T, Nakanishi R, Arakawa H. Micap Suppresses Murine Intestinal Tumor via Its Mitochondrial Quality Control. *Sci Rep* (2015) 5:12472. doi: 10.1038/srep12472
85. Nakamura Y, Arakawa H. Discovery of Micap-Regulated Mitochondrial Quality Control as a New Function of Tumor Suppressor P53. *Cancer Sci* (2017) 108(5):809–17. doi: 10.1111/cas.13208
86. Muscarella LA, Barbano R, D'Angelo V, Copetti M, Coco M, Balsamo T, et al. Regulation of KEAP1 Expression by Promoter Methylation in Malignant Gliomas and Association With Patient's Outcome. *Epigenetics* (2011) 6(3):317–25. doi: 10.4161/epi.6.3.14408
87. Muscarella LA, Parrella P, D'Alessandro V, la Torre A, Barbano R, Fontana A, et al. Frequent Epigenetics Inactivation of KEAP1 Gene in Non-Small Cell Lung Cancer. *Epigenetics* (2011) 6(6):710–9. doi: 10.4161/epi.6.6.15773
88. Zhang P, Singh A, Yegnasubramanian S, Esopi D, Kombairaju P, Bodas M, et al. Loss of Kelch-Like ECH-Associated Protein 1 Function in Prostate Cancer Cells Causes Chemoresistance and Radioresistance and Promotes Tumor Growth. *Mol Cancer Ther* (2010) 9(2):336–46. doi: 10.1158/1535-7163.MCT-09-0589
89. Taguchi K, Motohashi H, Yamamoto M. Molecular Mechanisms of the Keap1-Nrf2 Pathway in Stress Response and Cancer Evolution. *Genes Cells* (2011) 16(2):123–40. doi: 10.1111/j.1365-2443.2010.01473.x
90. Yang W, Lu Z. Regulation and Function of Pyruvate Kinase M2 in Cancer. *Cancer Lett* (2013) 339(2):153–8. doi: 10.1016/j.canlet.2013.06.008
91. Ristic B, Bhutia YD, Ganapathy V. Cell-Surface G-Protein-Coupled Receptors for Tumor-Associated Metabolites: A Direct Link to Mitochondrial Dysfunction in Cancer. *Biochim Biophys Acta Rev Cancer* (2017) 1868(1):246–57. doi: 10.1016/j.bbcan.2017.05.003
92. Abu-Remaileh M, Aqeilan RI. The Tumor Suppressor WW Domain-Containing Oxidoreductase Modulates Cell Metabolism. *Exp Biol Med (Maywood)* (2015) 240(3):345–50. doi: 10.1177/1535370214561956
93. Ekizoglu S, Bulut P, Karaman E, Kilic E, Buyru N. Epigenetic and Genetic Alterations Affect the WWOX Gene in Head and Neck Squamous Cell Carcinoma. *PLoS One* (2015) 10(1):e0115353. doi: 10.1371/journal.pone.0115353
94. Abu-Remaileh M, Aqeilan RI. Tumor Suppressor WWOX Regulates Glucose Metabolism via HIF1alpha Modulation. *Cell Death Differ* (2014) 21(11):1805–14. doi: 10.1038/cdd.2014.95
95. Huang KT, Takano EA, Mikeska T, Byrne DJ, Dobrovic A, Fox SB. Aberrant DNA Methylation But Not Mutation of CITED4 Is Associated With



- Alteration of HIF-Regulated Genes in Breast Cancer. *Breast Cancer Res Treat* (2011) 130(1):319–29. doi: 10.1007/s10549-011-1657-1
96. Sun W, Liu Y, Glazer CA, Shao C, Bhan S, Demokan S, et al. TKTL1 Is Activated by Promoter Hypomethylation and Contributes to Head and Neck Squamous Cell Carcinoma Carcinogenesis Through Increased Aerobic Glycolysis and HIF1 $\alpha$  Stabilization. *Clin Cancer Res* (2010) 16(3):857–66. doi: 10.1158/1078-0432.CCR-09-2604
97. Jayachandran A, Lo PH, Chueh AC, Prithviraj P, Molania R, Davalos-Salas M, et al. Transketolase-Like 1 Ectopic Expression Is Associated With DNA Hypomethylation and Induces the Warburg Effect in Melanoma Cells. *BMC Cancer* (2016) 16:134. doi: 10.1186/s12885-016-2185-5
98. Foxler DE, Bridge KS, James V, Webb TM, Mee M, Wong SC, et al. The LIMD1 Protein Bridges an Association Between the Prolyl Hydroxylases and VHL to Repress HIF-1 Activity. *Nat Cell Biol* (2012) 14(2):201–8. doi: 10.1038/ncb2424
99. Chakraborty C, Mitra S, Roychowdhury A, Samadder S, Dutta S, Roy A, et al. Deregulation of LIMD1-VHL-HIF-1 $\alpha$ -VEGF Pathway Is Associated With Different Stages of Cervical Cancer. *Biochem J* (2018) 475(10):1793–806. doi: 10.1042/BCJ20170649
100. Mishra R, Haldar S, Suchanti S, Bhowmick NA. Epigenetic Changes in Fibroblasts Drive Cancer Metabolism and Differentiation. *Endocr Relat Cancer* (2019) 26(12):R673–88. doi: 10.1530/ERC-19-0347
101. Pan X, Zheng L. Epigenetics in Modulating Immune Functions of Stromal and Immune Cells in the Tumor Microenvironment. *Cell Mol Immunol* (2020) 17(9):940–53. doi: 10.1038/s41423-020-0505-9
102. Hanson JA, Gillespie JW, Grover A, Tangrea MA, Chuaqui RF, Emmert-Buck MR, et al. Gene Promoter Methylation in Prostate Tumor-Associated Stromal Cells. *J Natl Cancer Inst* (2006) 98(4):255–61. doi: 10.1093/jnci/djj051
103. Mathot P, Grandin M, Devailly G, Souza F, Cahais V, Moran S, et al. DNA Methylation Signal has a Major Role in the Response of Human Breast Cancer Cells to the Microenvironment. *Oncogenesis* (2017) 6(10):e390. doi: 10.1038/oncsis.2017.88
104. Pidsley R, Lawrence MG, Zotenko E, Niranjana B, Statham A, Song J, et al. Enduring Epigenetic Landmarks Define the Cancer Microenvironment. *Genome Res* (2018) 28(5):625–38. doi: 10.1101/gr.229070.117
105. Xiao Q, Zhou D, Rucki AA, Williams J, Zhou J, Mo G, et al. Cancer-Associated Fibroblasts in Pancreatic Cancer Are Reprogrammed by Tumor-Induced Alterations in Genomic DNA Methylation. *Cancer Res* (2016) 76(18):5395–404. doi: 10.1158/0008-5472.CAN-15-3264
106. Albregues J, Bourget I, Pons C, Butet V, Hofman P, Tartare-Deckert S, et al. LIF Mediates Proinvasive Activation of Stromal Fibroblasts in Cancer. *Cell Rep* (2014) 7(5):1664–78. doi: 10.1016/j.celrep.2014.04.036
107. Niu X, Ma J, Li J, Gu Y, Yin L, Wang Y, et al. Sodium/glucose Cotransporter 1-Dependent Metabolic Alterations Induce Tamoxifen Resistance in Breast Cancer by Promoting Macrophage M2 Polarization. *Cell Death Dis* (2021) 12(6):509. doi: 10.1038/s41419-021-03781-x
108. Jiao X, Wang M, Zhang Z, Li Z, Ni D, Ashton AW, et al. Leronlimab, a Humanized Monoclonal Antibody to CCR5, Blocks Breast Cancer Cellular Metastasis and Enhances Cell Death Induced by DNA Damaging Chemotherapy. *Breast Cancer Res* (2021) 23(1):11. doi: 10.1186/s13058-021-01391-1
109. Sicoli D, Jiao X, Ju X, Velasco-Velazquez M, Ertel A, Addya S, et al. CCR5 Receptor Antagonists Block Metastasis to Bone of V-Src Oncogene-Transformed Metastatic Prostate Cancer Cell Lines. *Cancer Res* (2014) 74(23):7103–14. doi: 10.1158/0008-5472.CAN-14-0612
110. Jiao X, Nawab O, Patel T, Kossenkova AV, Halama N, Jaeger D, et al. Recent Advances Targeting CCR5 for Cancer and Its Role in Immuno-Oncology. *Cancer Res* (2019) 79(19):4801–7. doi: 10.1158/0008-5472.CAN-19-1167
111. Novak M, Koprivnikar Krajnc M, Hrstar B, Breznik B, Majc B, Mlinar M, et al. CCR5-Mediated Signaling Is Involved in Invasion of Glioblastoma Cells in Its Microenvironment. *Int J Mol Sci* (2020) 21(12):4199. doi: 10.3390/ijms21124199
112. Lin S, Sun L, Lyu X, Ai X, Du D, Su N, et al. Lactate-Activated Macrophages Induced Aerobic Glycolysis and Epithelial-Mesenchymal Transition in Breast Cancer by Regulation of CCL5-CCR5 Axis: A Positive Metabolic Feedback Loop. *Oncotarget* (2017) 8(66):110426–43. doi: 10.18632/oncotarget.22786
113. Ohlund D, Handly-Santana A, Biffi G, Elyada E, Almeida AS, Ponz-Sarvisse M, et al. Distinct Populations of Inflammatory Fibroblasts and Myofibroblasts in Pancreatic Cancer. *J Exp Med* (2017) 214(3):579–96. doi: 10.1084/jem.20162024
114. Bhagat TD, Von Ahrens D, Dawlaty M, Zou Y, Baddour J, Achreja A, et al. Lactate-Mediated Epigenetic Reprogramming Regulates Formation of Human Pancreatic Cancer-Associated Fibroblasts. *Elife* (2019) 8:e50663. doi: 10.7554/eLife.50663
115. DeBerardinis RJ, Mancuso A, Daikhin E, Nissim I, Yudkoff M, Wehrli S, et al. Beyond Aerobic Glycolysis: Transformed Cells can Engage in Glutamine Metabolism That Exceeds the Requirement for Protein and Nucleotide Synthesis. *Proc Natl Acad Sci USA* (2007) 104(49):19345–50. doi: 10.1073/pnas.0709747104
116. Eagle H. The Minimum Vitamin Requirements of the L and HeLa Cells in Tissue Culture, the Production of Specific Vitamin Deficiencies, and Their Cure. *J Exp Med* (1955) 102(5):595–600. doi: 10.1084/jem.102.5.595
117. Urbano-Marquez A, Estruch R, Navarro-Lopez F, Grau JM, Mont L, Rubin E. The Effects of Alcoholism on Skeletal and Cardiac Muscle. *N Engl J Med* (1989) 320(7):409–15. doi: 10.1056/NEJM198902163200701
118. Rivera SC, Hazen TC, Toranzos GA. Isolation of Fecal Coliforms From Pristine Sites in a Tropical Rain Forest. *Appl Environ Microbiol* (1988) 54(2):513–7. doi: 10.1128/aem.54.2.513-517.1988
119. Roberts E, Frankel S. Free Amino Acids in Normal and Neoplastic Tissues of Mice as Studied by Paper Chromatography. *Cancer Res* (1949) 9(11):645–8, 3 pl.
120. Yuneva MO, Fan TW, Allen TD, Higashi RM, Ferraris DV, Tsukamoto T, et al. The Metabolic Profile of Tumors Depends on Both the Responsible Genetic Lesion and Tissue Type. *Cell Metab* (2012) 15(2):157–70. doi: 10.1016/j.cmet.2011.12.015
121. Lieberman BP, Ploessl K, Wang L, Qu W, Zha Z, Wise DR, et al. PET Imaging of Glutaminolysis in Tumors by 18F-(2S,4R)-4-Fluoroglutamine. *J Nucl Med* (2011) 52(12):1947–55. doi: 10.2967/jnumed.111.093815
122. Kung CP, Budina A, Balaburski G, Bergenstock MK, Murphy M. Autophagy in Tumor Suppression and Cancer Therapy. *Crit Rev Eukaryot Gene Expr* (2011) 21(1):71–100. doi: 10.1615/CritRevEukaryotGeneExpr.v21.i1.50
123. Curi R, Lagranha CJ, Doi SQ, Sellitti DF, Procopio J, Pithon-Curi TC, et al. Molecular Mechanisms of Glutamine Action. *J Cell Physiol* (2005) 204(2):392–401. doi: 10.1002/jcp.20339
124. Yanagida O, Kanai Y, Chairoungdua A, Kim DK, Segawa H, Nii T, et al. Human L-Type Amino Acid Transporter 1 (LAT1): Characterization of Function and Expression in Tumor Cell Lines. *Biochim Biophys Acta* (2001) 1514(2):291–302. doi: 10.1016/S0005-2736(01)00384-4
125. Lo E, Nicolle L, Classen D, Arias KM, Podgorny K, Anderson DJ, et al. Strategies to Prevent Catheter-Associated Urinary Tract Infections in Acute Care Hospitals. *Infect Control Hosp Epidemiol* (2008) 29 Suppl 1:S41–50. doi: 10.1086/591066
126. Jin L, Alesi GN, Kang S. Glutaminolysis as a Target for Cancer Therapy. *Oncogene* (2016) 35(28):3619–25. doi: 10.1038/ncr.2015.447
127. Palm W, Park Y, Wright K, Pavlova NN, Tuveson DA, Thompson CB. The Utilization of Extracellular Proteins as Nutrients Is Suppressed by Mtorc1. *Cell* (2015) 162(2):259–70. doi: 10.1016/j.cell.2015.06.017
128. Li B, Simon MC. Molecular Pathways: Targeting MYC-Induced Metabolic Reprogramming and Oncogenic Stress in Cancer. *Clin Cancer Res* (2013) 19(21):5835–41. doi: 10.1158/1078-0432.CCR-12-3629
129. Gao P, Tchernyshyov I, Chang TC, Lee YS, Kita K, Ochi T, et al. C-Myc Suppression of miR-23a/B Enhances Mitochondrial Glutaminase Expression and Glutamine Metabolism. *Nature* (2009) 458(7239):762–5. doi: 10.1038/nature07823
130. Mannava S, Grachtchouk V, Wheeler LJ, Im M, Zhuang D, Slavina EG, et al. Direct Role of Nucleotide Metabolism in C-MYC-Dependent Proliferation of Melanoma Cells. *Cell Cycle* (2008) 7(15):2392–400. doi: 10.4161/cc.6390
131. Xiang Y, Stine ZE, Xia J, Lu Y, O'Connor RS, Altman BJ, et al. Targeted Inhibition of Tumor-Specific Glutaminase Diminishes Cell-Autonomous Tumorigenesis. *J Clin Invest* (2015) 125(6):2293–306. doi: 10.1172/JCI75836
132. Gross AE, Van Schooneveld TC, Olsen KM, Rupp ME, Bui TH, Forsung E, et al. Epidemiology and Predictors of Multidrug-Resistant Community-Acquired and Health Care-Associated Pneumonia. *Antimicrob Agents Chemother* (2014) 58(9):5262–8. doi: 10.1128/AAC.02582-14



133. Land SC, Tee AR. Hypoxia-Inducible Factor 1alpha Is Regulated by the Mammalian Target of Rapamycin (mTOR) via an mTOR Signaling Motif. *J Biol Chem* (2007) 282(28):20534–43. doi: 10.1074/jbc.M611782200
134. Finicle BT, Jayashankar V, Edinger AL. Nutrient Scavenging in Cancer. *Nat Rev Cancer* (2018) 18(10):619–33. doi: 10.1038/s41568-018-0048-x
135. Palm W, Thompson CB. Nutrient Acquisition Strategies of Mammalian Cells. *Nature* (2017) 546(7657):234–42. doi: 10.1038/nature22379
136. Kennedy KM, Scarbrough PM, Ribeiro A, Richardson R, Yuan H, Sonveaux P, et al. Catabolism of Exogenous Lactate Reveals It as a Legitimate Metabolic Substrate in Breast Cancer. *PLoS One* (2013) 8(9):e75154. doi: 10.1371/journal.pone.0075154
137. Kimmelman AC, White E. Autophagy and Tumor Metabolism. *Cell Metab* (2017) 25(5):1037–43. doi: 10.1016/j.cmet.2017.04.004
138. Flynn AB, Schiemann WP. Autophagy in Breast Cancer Metastatic Dormancy: Tumor Suppressing or Tumor Promoting Functions? *J Cancer Metastasis Treat* (2019) 5:43. doi: 10.20517/2394-4722.2019.13
139. Huo Y, Cai H, Teplova I, Bowman-Colin C, Chen G, Price S, et al. Autophagy Opposes P53-Mediated Tumor Barrier to Facilitate Tumorigenesis in a Model of PALB2-Associated Hereditary Breast Cancer. *Cancer Discov* (2013) 3(8):894–907. doi: 10.1158/2159-8290.CD-13-0011
140. Levine B, Klionsky DJ. Development by Self-Digestion: Molecular Mechanisms and Biological Functions of Autophagy. *Dev Cell* (2004) 6(4):463–77. doi: 10.1016/S1534-5807(04)00099-1
141. Lipinski MM, Hoffman G, Ng A, Zhou W, Py BF, Hsu E, et al. A Genome-Wide siRNA Screen Reveals Multiple Mtorc1 Independent Signaling Pathways Regulating Autophagy Under Normal Nutritional Conditions. *Dev Cell* (2010) 18(6):1041–52. doi: 10.1016/j.devcel.2010.05.005
142. Casimiro MC, Di Sante G, Di Rocco A, Loro E, Pupo C, Pestell TG, et al. Cyclin D1 Restrains Oncogene-Induced Autophagy by Regulating the AMPK-LKB1 Signaling Axis. *Cancer Res* (2017) 77(13):3391–405. doi: 10.1158/0008-5472.CAN-16-0425
143. Zhang M, Di Martino JS, Bowman RL, Campbell NR, Baksh SC, Simon-Vermot T, et al. Adipocyte-Derived Lipids Mediate Melanoma Progression via FATP Proteins. *Cancer Discov* (2018) 8(8):1006–25. doi: 10.1158/2159-8290.CD-17-1371
144. Vitale I, Manic G, Coussens LM, Kroemer G, Galluzzi L. Macrophages and Metabolism in the Tumor Microenvironment. *Cell Metab* (2019) 30(1):36–50. doi: 10.1016/j.cmet.2019.06.001
145. Tan Z, Xie N, Banerjee S, Cui H, Fu M, Thannickal VJ, et al. The Monocarboxylate Transporter 4 Is Required for Glycolytic Reprogramming and Inflammatory Response in Macrophages. *J Biol Chem* (2015) 290(1):46–55. doi: 10.1074/jbc.M114.603589
146. Mayers JR, Torrence ME, Danai LV, Papagiannakopoulos T, Davidson SM, Bauer MR, et al. Tissue of Origin Dictates Branched-Chain Amino Acid Metabolism in Mutant Kras-Driven Cancers. *Science* (2016) 353(6304):1161–5. doi: 10.1126/science.aaf5171
147. Schug SA, Palmer GM, Scott DA, Halliwell R, Trinca J. Acute Pain Management: Scientific Evidence, Fourth Edition, 2015. *Med J Aust* (2016) 204(8):315–7. doi: 10.5694/mja16.00133
148. Kamphorst JJ, Cross JR, Fan J, de Stanchina E, Mathew R, White EP, et al. Hypoxic and Ras-Transformed Cells Support Growth by Scavenging Unsaturated Fatty Acids From Lysophospholipids. *Proc Natl Acad Sci USA* (2013) 110(22):8882–7. doi: 10.1073/pnas.1307237110
149. Commisso C, Davidson SM, Soydaner-Azeloglu RG, Parker SJ, Kamphorst JJ, Hackett S, et al. Macropinocytosis of Protein Is an Amino Acid Supply Route in Ras-Transformed Cells. *Nature* (2013) 497(7451):633–7. doi: 10.1038/nature12138
150. Rajeshkumar NV, Dutta P, Yabuuchi S, de Wilde RF, Martinez GV, Le A, et al. Therapeutic Targeting of the Warburg Effect in Pancreatic Cancer Relies on an Absence of P53 Function. *Cancer Res* (2015) 75(16):3355–64. doi: 10.1158/0008-5472.CAN-15-0108
151. Yoo DY, Barros SA, Brown GC, Rabot C, Bar-Sagi D, Arora PS. Macropinocytosis as a Key Determinant of Peptidomimetic Uptake in Cancer Cells. *J Am Chem Soc* (2020) 142(34):14461–71. doi: 10.1021/jacs.0c02109
152. Recouvreur MV, Commisso C. Macropinocytosis: A Metabolic Adaptation to Nutrient Stress in Cancer. *Front Endocrinol (Lausanne)* (2017) 8:261. doi: 10.3389/fendo.2017.00261
153. Gilchrist KW, Gray R, Fowble B, Tormey DC, Taylor SGT. Tumor Necrosis Is a Prognostic Predictor for Early Recurrence and Death in Lymph Node-Positive Breast Cancer: A 10-Year Follow-Up Study of 728 Eastern Cooperative Oncology Group Patients. *J Clin Oncol* (1993) 11(10):1929–35. doi: 10.1200/JCO.1993.11.10.1929
154. Walker RA. The Complexities of Breast Cancer Desmoplasia. *Breast Cancer Res* (2001) 3(3):143–5. doi: 10.1186/bcr287
155. Wallace DC. Mitochondria and Cancer. *Nat Rev Cancer* (2012) 12(10):685–98. doi: 10.1038/nrc3365
156. Pavlides S, Tsigirig A, Migneco G, Whitaker-Menezes D, Chiavarina B, Flomenberg N, et al. The Autophagic Tumor Stroma Model of Cancer: Role of Oxidative Stress and Ketone Production in Fueling Tumor Cell Metabolism. *Cell Cycle* (2010) 9(17):3485–505. doi: 10.4161/cc.9.17.12721
157. Martinez-Outschoorn UE, Balliet RM, Rivadeneira DB, Chiavarina B, Pavlides S, Wang C, et al. Oxidative Stress in Cancer Associated Fibroblasts Drives Tumor-Stroma Co-Evolution: A New Paradigm for Understanding Tumor Metabolism, the Field Effect and Genomic Instability in Cancer Cells. *Cell Cycle* (2010) 9(16):3256–76. doi: 10.4161/cc.9.16.12553
158. Martinez-Outschoorn UE, Trimmer C, Lin Z, Whitaker-Menezes D, Chiavarina B, Zhou J, et al. Autophagy in Cancer Associated Fibroblasts Promotes Tumor Cell Survival: Role of Hypoxia, HIF1 Induction and NFkappaB Activation in the Tumor Stromal Microenvironment. *Cell Cycle* (2010) 9(17):3515–33. doi: 10.4161/cc.9.17.12928
159. Chiavarina B, Whitaker-Menezes D, Migneco G, Martinez-Outschoorn UE, Pavlides S, Howell A, et al. HIF1-Alpha Functions as a Tumor Promoter in Cancer Associated Fibroblasts, and as a Tumor Suppressor in Breast Cancer Cells: Autophagy Drives Compartment-Specific Oncogenesis. *Cell Cycle* (2010) 9(17):3534–51. doi: 10.4161/cc.9.17.12908
160. Martinez-Outschoorn UE, Curry JM, Ko YH, Lin Z, Tuluc M, Cognetti D, et al. Oncogenes and Inflammation Rewire Host Energy Metabolism in the Tumor Microenvironment: RAS and NFkappaB Target Stromal MCT4. *Cell Cycle* (2013) 12(16):2580–97. doi: 10.4161/cc.25510
161. Salem AF, Whitaker-Menezes D, Lin Z, Martinez-Outschoorn UE, Tanowitz HB, Al-Zoubi MS, et al. Two-Compartment Tumor Metabolism: Autophagy in the Tumor Microenvironment and Oxidative Mitochondrial Metabolism (OXPHOS) in Cancer Cells. *Cell Cycle* (2012) 11(13):2545–56. doi: 10.4161/cc.20920
162. Sotgia F, Whitaker-Menezes D, Martinez-Outschoorn UE, Flomenberg N, Birbe RC, Witkiewicz AK, et al. Mitochondrial Metabolism in Cancer Metastasis: Visualizing Tumor Cell Mitochondria and the "Reverse Warburg Effect" in Positive Lymph Node Tissue. *Cell Cycle* (2012) 11(7):1445–54. doi: 10.4161/cc.19841
163. Pavlides S, Tsigirig A, Vera I, Flomenberg N, Frank PG, Casimiro MC, et al. Loss of Stromal Caveolin-1 Leads to Oxidative Stress, Mimics Hypoxia and Drives Inflammation in the Tumor Microenvironment, Conferring the "Reverse Warburg Effect": A Transcriptional Informatics Analysis With Validation. *Cell Cycle* (2010) 9(11):2201–19. doi: 10.4161/cc.9.11.11848
164. Bonuccelli G, Whitaker-Menezes D, Castello-Cros R, Pavlides S, Pestell RG, Fatatis A, et al. The Reverse Warburg Effect: Glycolysis Inhibitors Prevent the Tumor Promoting Effects of Caveolin-1 Deficient Cancer Associated Fibroblasts. *Cell Cycle* (2010) 9(10):1960–71. doi: 10.4161/cc.9.10.11601
165. Pavlides S, Tsigirig A, Vera I, Flomenberg N, Frank PG, Casimiro MC, et al. Transcriptional Evidence for the "Reverse Warburg Effect" in Human Breast Cancer Tumor Stroma and Metastasis: Similarities With Oxidative Stress, Inflammation, Alzheimer's Disease, and "Neuron-Glia Metabolic Coupling". *Aging (Albany NY)* (2010) 2(4):185–99. doi: 10.18632/aging.100134
166. Del Galdo F, Lisanti MP, Jimenez SA. Caveolin-1, Transforming Growth Factor-Beta Receptor Internalization, and the Pathogenesis of Systemic Sclerosis. *Curr Opin Rheumatol* (2008) 20(6):713–9. doi: 10.1097/BOR.0b013e3283103d27
167. Del Galdo F, Sotgia F, de Almeida CJ, Jasmin JF, Musick M, Lisanti MP, et al. Decreased Expression of Caveolin 1 in Patients With Systemic Sclerosis: Crucial Role in the Pathogenesis of Tissue Fibrosis. *Arthritis Rheum* (2008) 58(9):2854–65. doi: 10.1002/art.23791
168. Yang L, Achreja A, Yeung TL, Mangala LS, Jiang D, Han C, et al. Targeting Stromal Glutamine Synthetase in Tumors Disrupts Tumor

- Microenvironment-Regulated Cancer Cell Growth. *Cell Metab* (2016) 24 (5):685–700. doi: 10.1016/j.cmet.2016.10.011
169. Zhu Z, Achreja A, Meurs N, Animasahun O, Owen S, Mittal A, et al. Tumour-Reprogrammed Stromal BCAT1 Fuels Branched-Chain Ketoacid Dependency in Stromal-Rich PDAC Tumours. *Nat Metab* (2020) 2(8):775–92. doi: 10.1038/s42255-020-0226-5
  170. Biswas SK, Mantovani A. Macrophage Plasticity and Interaction With Lymphocyte Subsets: Cancer as a Paradigm. *Nat Immunol* (2010) 11 (10):889–96. doi: 10.1038/ni.1937
  171. Ye H, Zhou Q, Zheng S, Li G, Lin Q, Wei L, et al. Tumor-Associated Macrophages Promote Progression and the Warburg Effect via CCL18/NF-Kb/VCAM-1 Pathway in Pancreatic Ductal Adenocarcinoma. *Cell Death Dis* (2018) 9(5):453. doi: 10.1038/s41419-018-0486-0
  172. Palmieri EM, Menga A, Martin-Perez R, Quinto A, Riera-Domingo C, De Tullio G, et al. Pharmacologic or Genetic Targeting of Glutamine Synthetase Skews Macrophages Toward an M1-Like Phenotype and Inhibits Tumor Metastasis. *Cell Rep* (2017) 20(7):1654–66. doi: 10.1016/j.celrep.2017.07.054
  173. Onuchic V, Hartmaier RJ, Boone DN, Samuels ML, Patel RY, White WM, et al. Epigenomic Deconvolution of Breast Tumors Reveals Metabolic Coupling Between Constituent Cell Types. *Cell Rep* (2016) 17(8):2075–86. doi: 10.1016/j.celrep.2016.10.057
  174. Au-Yeung CL, Yeung TL, Achreja A, Zhao H, Yip KP, Kwan SY, et al. ITLN1 Modulates Invasive Potential and Metabolic Reprogramming of Ovarian Cancer Cells in Omental Microenvironment. *Nat Commun* (2020) 11 (1):3546. doi: 10.1038/s41467-020-17383-2
  175. Overholtzer M, Mailleux AA, Mounieime G, Normand G, Schnitt SJ, King RW, et al. A Nonapoptotic Cell Death Process, Entosis, That Occurs by Cell-in-Cell Invasion. *Cell* (2007) 131(5):966–79. doi: 10.1016/j.cell.2007.10.040
  176. Sivanand S, Vander Heiden MG. Transcriptional Activation of Macropinocytosis by the Hippo Pathway Following Nutrient Limitation. *Genes Dev* (2020) 34(19–20):1253–5. doi: 10.1101/gad.343632.120
  177. Bryant DM, Kerr MC, Hammond LA, Joseph SR, Mostov KE, Teasdale RD, et al. EGF Induces Macropinocytosis and SNX1-Modulated Recycling of E-Cadherin. *J Cell Sci* (2007) 120(Pt 10):1818–28. doi: 10.1242/jcs.000653
  178. Kapara A, Brunton V, Graham D, Faulds K. Investigation of Cellular Uptake Mechanism of Functionalised Gold Nanoparticles Into Breast Cancer Using SERS. *Chem Sci* (2020) 11(22):5819–29. doi: 10.1039/D0SC01255F
  179. Kim SM, Nguyen TT, Ravi A, Kubiniok P, Finicle BT, Jayashankar V, et al. PTEN Deficiency and AMPK Activation Promote Nutrient Scavenging and Anabolism in Prostate Cancer Cells. *Cancer Discov* (2018) 8(7):866–83. doi: 10.1158/2159-8290.CD-17-1215
  180. Palm W, Araki J, King B, DeMatteo RG, Thompson CB. Critical Role for PI3-Kinase in Regulating the Use of Proteins as an Amino Acid Source. *Proc Natl Acad Sci USA* (2017) 114(41):E8628–36. doi: 10.1073/pnas.1712726114
  181. King B, Araki J, Palm W, Thompson CB. Yap/Taz Promote the Scavenging of Extracellular Nutrients Through Macropinocytosis. *Genes Dev* (2020) 34(19–20):1345–58. doi: 10.1101/gad.340661.120
  182. Davidson SM, Jonas O, Keibler MA, Hou HW, Luengo A, Mayers JR, et al. Direct Evidence for Cancer-Cell-Autonomous Extracellular Protein Catabolism in Pancreatic Tumors. *Nat Med* (2017) 23(2):235–41. doi: 10.1038/nm.4256
  183. Kamphorst JJ, Nofal M, Comisso C, Hackett SR, Lu W, Grabocka E, et al. Human Pancreatic Cancer Tumors Are Nutrient Poor and Tumor Cells Actively Scavenge Extracellular Protein. *Cancer Res* (2015) 75(3):544–53. doi: 10.1158/0008-5472.CAN-14-2211
  184. Redelman-Sidi G, Binyamin A, Gaeta I, Palm W, Thompson CB, Romesser PB, et al. The Canonical Wnt Pathway Drives Macropinocytosis in Cancer. *Cancer Res* (2018) 78(16):4658–70. doi: 10.1158/0008-5472.CAN-17-3199
  185. Zhao H, Yang L, Baddour J, Achreja A, Bernard V, Moss T, et al. Tumor Microenvironment Derived Exosomes Pleiotropically Modulate Cancer Cell Metabolism. *Elife* (2016) 5:e10250. doi: 10.7554/eLife.10250
  186. Chajes V, Cambot M, Moreau K, Lenoir GM, Joulin V. Acetyl-CoA Carboxylase Alpha Is Essential to Breast Cancer Cell Survival. *Cancer Res* (2006) 66(10):5287–94. doi: 10.1158/0008-5472.CAN-05-1489
  187. Menendez JA, Lupu R. Fatty Acid Synthase and the Lipogenic Phenotype in Cancer Pathogenesis. *Nat Rev Cancer* (2007) 7(10):763–77. doi: 10.1038/nrc2222
  188. Santos CR, Schulze A. Lipid Metabolism in Cancer. *FEBS J* (2012) 279 (15):2610–23. doi: 10.1111/j.1742-4658.2012.08644.x
  189. Rohrig F, Schulze A. The Multifaceted Roles of Fatty Acid Synthesis in Cancer. *Nat Rev Cancer* (2016) 16(11):732–49. doi: 10.1038/nrc.2016.89
  190. Migita T, Narita T, Nomura K, Miyagi E, Inazuka F, Matsuura M, et al. ATP Citrate Lyase: Activation and Therapeutic Implications in Non-Small Cell Lung Cancer. *Cancer Res* (2008) 68(20):8547–54. doi: 10.1158/0008-5472.CAN-08-1235
  191. Papadaki I, Mylona E, Giannopoulou I, Markaki S, Keramopoulos A, Nakopoulou L. PPARgamma Expression in Breast Cancer: Clinical Value and Correlation With ERbeta. *Histopathology* (2005) 46(1):37–42. doi: 10.1111/j.1365-2559.2005.02056.x
  192. Jiang Y, Zou L, Zhang C, He S, Cheng C, Xu J, et al. PPARgamma and Wnt/beta-Catenin Pathway in Human Breast Cancer: Expression Pattern, Molecular Interaction and Clinical/Prognostic Correlations. *J Cancer Res Clin Oncol* (2009) 135(11):1551–9. doi: 10.1007/s00432-009-0602-8
  193. Abduljabbar R, Al-Kaabi MM, Negm OH, Jerjees D, Muftah AA, Mukherjee A, et al. Prognostic and Biological Significance of Peroxisome Proliferator-Activated Receptor-Gamma in Luminal Breast Cancer. *Breast Cancer Res Treat* (2015) 150(3):511–22. doi: 10.1007/s10549-015-3348-9
  194. Chou FS, Wang PS, Kulp S, Pinzone JJ. Effects of Thiazolidinediones on Differentiation, Proliferation, and Apoptosis. *Mol Cancer Res* (2007) 5 (6):523–30. doi: 10.1158/1541-7786.MCR-06-0278
  195. Tachibana K, Yamasaki D, Ishimoto K, Doi T. The Role of PPARs in Cancer. *PPAR Res* (2008) 2008:102737. doi: 10.1155/2008/102737
  196. Wang C, Fu M, D'Amico M, Albanese C, Zhou JN, Brownlee M, et al. Inhibition of Cellular Proliferation Through IkkappaB Kinase-Independent and Peroxisome Proliferator-Activated Receptor Gamma-Dependent Repression of Cyclin D1. *Mol Cell Biol* (2001) 21(9):3057–70. doi: 10.1128/MCB.21.9.3057-3070.2001
  197. Augimeri G, Giordano C, Gelsomino L, Plastina P, Barone I, Catalano S, et al. The Role of PPARgamma Ligands in Breast Cancer: From Basic Research to Clinical Studies. *Cancers (Basel)* (2020) 12(9):2623. doi: 10.3390/cancers12092623
  198. Jiao X, Tian L, Zhang Z, Balcerek J, Kossenkova AV, Casimiro MC, et al. Ppargamma1 Facilitates ErbB2-Mammary Adenocarcinoma in Mice. *Cancers (Basel)* (2021) 13(9):2171. doi: 10.3390/cancers13092171
  199. Wu ZH, Tang Y, Yu H, Li HD. The Role of Ferroptosis in Breast Cancer Patients: A Comprehensive Analysis. *Cell Death Discov* (2021) 7(1):93. doi: 10.1038/s41419-020-03329-5
  200. Zhang Y, Shi J, Liu X, Feng L, Gong Z, Koppula P, et al. BAP1 Links Metabolic Regulation of Ferroptosis to Tumour Suppression. *Nat Cell Biol* (2018) 20(10):1181–92. doi: 10.1038/s41556-018-0178-0
  201. Jiang L, Kon N, Li T, Wang SJ, Su T, Hibshoosh H, et al. Ferroptosis as a P53-Mediated Activity During Tumour Suppression. *Nature* (2015) 520 (7545):57–62. doi: 10.1038/nature14344
  202. Gao M, Yi J, Zhu J, Minikes AM, Monian P, Thompson CB, et al. Role of Mitochondria in Ferroptosis. *Mol Cell* (2019) 73(2):354–63.e3. doi: 10.1016/j.molcel.2018.10.042
  203. Yi J, Zhu J, Wu J, Thompson CB, Jiang X. Oncogenic Activation of PI3K-AKT-mTOR Signaling Suppresses Ferroptosis via SREBP-Mediated Lipogenesis. *Proc Natl Acad Sci USA* (2020) 117(49):31189–97. doi: 10.1073/pnas.2017152117
  204. Lu Z, Hunter T. Metabolic Kinases Moonlighting as Protein Kinases. *Trends Biochem Sci* (2018) 43(4):301–10. doi: 10.1016/j.tibs.2018.01.006
  205. Kondoh H, Leonart ME, Gil J, Wang J, Degan P, Peters G, et al. Glycolytic Enzymes can Modulate Cellular Life Span. *Cancer Res* (2005) 65(1):177–85.
  206. Wang C, Pattabiraman N, Zhou JN, Fu M, Sakamaki T, Albanese C, et al. Cyclin D1 Repression of Peroxisome Proliferator-Activated Receptor Gamma Expression and Transactivation. *Mol Cell Biol* (2003) 23 (17):6159–73. doi: 10.1128/MCB.23.17.6159-6173.2003
  207. Icard P, Fournel L, Wu Z, Alifano M, Lincet H. Interconnection Between Metabolism and Cell Cycle in Cancer. *Trends Biochem Sci* (2019) 44(6):490–501. doi: 10.1016/j.tibs.2018.12.007
  208. Zhang J, Wang C, Chen X, Takada M, Fan C, Zheng X, et al. EglN2 Associates With the NRF1-PGC1alpha Complex and Controls Mitochondrial Function in Breast Cancer. *EMBO J* (2015) 34(23):2953–70. doi: 10.15252/emboj.201591437

209. Lee Y, Dominy JE, Choi YJ, Jurczak M, Tolliday N, Camporez JP, et al. Cyclin D1-Cdk4 Controls Glucose Metabolism Independently of Cell Cycle Progression. *Nature* (2014) 510(7506):547–51. doi: 10.1038/nature13267
210. Chen K, Jiao X, Di Rocco A, Shen D, Xu S, Ertel A, et al. Endogenous Cyclin D1 Promotes the Rate of Onset and Magnitude of Mitogenic Signaling via Akt1 Ser473 Phosphorylation. *Cell Rep* (2020) 32(11):108151. doi: 10.1016/j.celrep.2020.108151
211. Robey RB, Hay N. Is Akt the "Warburg Kinase"?-Akt-Energy Metabolism Interactions and Oncogenesis. *Semin Cancer Biol* (2009) 19(1):25–31. doi: 10.1016/j.semcancer.2008.11.010
212. Oermann EK, Wu J, Guan KL, Xiong Y. Alterations of Metabolic Genes and Metabolites in Cancer. *Semin Cell Dev Biol* (2012) 23(4):370–80. doi: 10.1016/j.semcdb.2012.01.013
213. Astuti D, Latif F, Dallol A, Dahia PL, Douglas F, George E, et al. Gene Mutations in the Succinate Dehydrogenase Subunit SDHB Cause Susceptibility to Familial Pheochromocytoma and to Familial Paraganglioma. *Am J Hum Genet* (2001) 69(1):49–54. doi: 10.1086/321282
214. Janeway KA, Kim SY, Lodish M, Nose V, Rustin P, Gaal J, et al. Defects in Succinate Dehydrogenase in Gastrointestinal Stromal Tumors Lacking KIT and PDGFRA Mutations. *Proc Natl Acad Sci USA* (2011) 108(1):314–8. doi: 10.1073/pnas.1009199108
215. Tomlinson IP, Alam NA, Rowan AJ, Barclay E, Jaeger EE, Kelsell D, et al. Germline Mutations in FH Predispose to Dominantly Inherited Uterine Fibroids, Skin Leiomyomata and Papillary Renal Cell Cancer. *Nat Genet* (2002) 30(4):406–10. doi: 10.1038/ng849
216. Baysal BE, Ferrell RE, Willett-Brozick JE, Lawrence EC, Myssiorek D, Bosch A, et al. Mutations in SDHD, A Mitochondrial Complex II Gene, in Hereditary Paraganglioma. *Science* (2000) 287(5454):848–51. doi: 10.1126/science.287.5454.848
217. Yang M, Pollard PJ. Succinate: A New Epigenetic Hacker. *Cancer Cell* (2013) 23(6):709–11. doi: 10.1016/j.ccr.2013.05.015
218. Adam TC, Schmitt RJ, Holbrook SJ, Brooks AJ, Edmunds PJ, Carpenter RC, et al. Herbivory, Connectivity, and Ecosystem Resilience: Response of a Coral Reef to a Large-Scale Perturbation. *PloS One* (2011) 6(8):e23717. doi: 10.1371/journal.pone.0023717
219. Li H, Ning S, Ghandi M, Kryukov GV, Gopal S, Deik A, et al. The Landscape of Cancer Cell Line Metabolism. *Nat Med* (2019) 25(5):850–60. doi: 10.1038/s41591-019-0404-8
220. Nusinow DP, Szpyt J, Ghandi M, Rose CM, McDonald ER3rd, Kalocsay M, et al. Quantitative Proteomics of the Cancer Cell Line Encyclopedia. *Cell* (2020) 180(2):387–402.e16. doi: 10.1016/j.cell.2019.12.023
221. Kroger C, Afeyan A, Mraz J, Eaton EN, Reinhardt F, Khodor YL, et al. Acquisition of a Hybrid E/M State Is Essential for Tumorigenicity of Basal Breast Cancer Cells. *Proc Natl Acad Sci USA* (2019) 116(15):7353–62. doi: 10.1073/pnas.1812876116
222. Skrypek N, Goossens S, De Smedt E, Vandamme N, Berx G. Epithelial-to-Mesenchymal Transition: Epigenetic Reprogramming Driving Cellular Plasticity. *Trends Genet* (2017) 33(12):943–59. doi: 10.1016/j.tig.2017.08.004
223. Georgakopoulos-Soares I, Chartoumpakis DV, Kyriazopoulou V, Zaravinos A, and Metabolic Pathways in Cancer. *Front Oncol* (2020) 10:499. doi: 10.3389/fonc.2020.00499
224. Sciacovelli M, Frezza C. Metabolic Reprogramming and Epithelial-to-Mesenchymal Transition in Cancer. *FEBS J* (2017) 284(19):3132–44. doi: 10.1111/febs.14090
225. Lunetti P, Di Giacomo M, Vergara D, De Domenico S, Maffia M, Zara V, et al. Metabolic Reprogramming in Breast Cancer Results in Distinct Mitochondrial Bioenergetics Between Luminal and Basal Subtypes. *FEBS J* (2019) 286(4):688–709. doi: 10.1111/febs.14756
226. Xiao Z, Liu S, Ai F, Chen X, Li X, Liu R, et al. SDHB Downregulation Facilitates the Proliferation and Invasion of Colorectal Cancer Through AMPK Functions Excluding Those Involved in the Modulation of Aerobic Glycolysis. *Exp Ther Med* (2018) 15(1):864–72. doi: 10.3892/etm.2017.5482
227. Wang H, Chen Y, Wu G. SDHB Deficiency Promotes TGFbeta-Mediated Invasion and Metastasis of Colorectal Cancer Through Transcriptional Repression Complex SNAIL1-Smad3/4. *Transl Oncol* (2016) 9(6):512–20. doi: 10.1016/j.tranon.2016.09.009
228. Aspuri PP, Lunt SY, Varemo L, Vergnes L, Gozo M, Beach JA, et al. Succinate Dehydrogenase Inhibition Leads to Epithelial-Mesenchymal Transition and Reprogrammed Carbon Metabolism. *Cancer Metab* (2014) 2:21. doi: 10.1186/2049-3002-2-21
229. Vega S, Morales AV, Ocana OH, Valdes F, Fabregat I, Nieto MA. Snail Blocks the Cell Cycle and Confers Resistance to Cell Death. *Genes Dev* (2004) 18(10):1131–43. doi: 10.1101/gad.294104
230. Morikawa M, Derynck R, Miyazono K. TGF-Beta and the TGF-Beta Family: Context-Dependent Roles in Cell and Tissue Physiology. *Cold Spring Harb Perspect Biol* (2016) 8(5):a021873. doi: 10.1101/cshperspect.a021873
231. Liu M, Casimiro MC, Wang C, Shirley LA, Jiao X, Katiyar S, et al. P21cip1 Attenuates Ras- and C-Myc-Dependent Breast Tumor Epithelial Mesenchymal Transition and Cancer Stem Cell-Like Gene Expression In Vivo. *Proc Natl Acad Sci USA* (2009) 106(45):19035–9. doi: 10.1073/pnas.0910009106
232. Ju X, Casimiro MC, Gormley M, Meng H, Jiao X, Katiyar S, et al. Identification of a Cyclin D1 Network in Prostate Cancer That Antagonizes Epithelial-Mesenchymal Restraint. *Cancer Res* (2014) 74(2):508–19. doi: 10.1158/0008-5472.CAN-13-1313
233. Jia D, Park JH, Kaur H, Jung KH, Yang S, Tripathi S, et al. Towards Decoding the Coupled Decision-Making of Metabolism and Epithelial-to-Mesenchymal Transition in Cancer. *Br J Cancer* (2021) 124(12):1902–11. doi: 10.1038/s41416-021-01385-y
234. Letouze E, Martinelli C, Lorient C, Burnichon N, Abermil N, Ottolenghi C, et al. SDH Mutations Establish a Hypermethylator Phenotype in Paraganglioma. *Cancer Cell* (2013) 23(6):739–52. doi: 10.1016/j.ccr.2013.04.018
235. Wu GA, Prochnik S, Jenkins J, Salse J, Hellsten U, Murat F, et al. Sequencing of Diverse Mandarin, Pummelo and Orange Genomes Reveals Complex History of Admixture During Citrus Domestication. *Nat Biotechnol* (2014) 32(7):656–62. doi: 10.1038/nbt.2906
236. Wu K, Chen K, Wang C, Jiao X, Wang L, Zhou J, et al. Cell Fate Factor DACH1 Represses YB-1-Mediated Oncogenic Transcription and Translation. *Cancer Res* (2014) 74(3):829–39. doi: 10.1158/0008-5472.CAN-13-2466
237. Popov VM, Wu K, Zhou J, Powell MJ, Mardon G, Wang C, et al. The Dachsund Gene in Development and Hormone-Responsive Tumorigenesis. *Trends Endocrinol Metab* (2010) 21(1):41–9. doi: 10.1016/j.tem.2009.08.002
238. Dentre SC, Leshchiner I, Haase K, Tarabichi M, Wintersinger J, Deshwar AG, et al. Characterizing Genetic Intra-Tumor Heterogeneity Across 2,658 Human Cancer Genomes. *Cell* (2021) 184(8):2239–54.e39. doi: 10.1016/j.cell.2021.03.009
239. Abascal F, Harvey LMR, Mitchell E, Lawson ARJ, Lensing SV, Ellis P, et al. Somatic Mutation Landscapes at Single-Molecule Resolution. *Nature* (2021) 593(7859):405–10. doi: 10.1038/s41586-021-03477-4
240. Sinkala M, Mulder N, Patrick Martin D. Metabolic Gene Alterations Impact the Clinical Aggressiveness and Drug Responses of 32 Human Cancers. *Commun Biol* (2019) 2:414. doi: 10.1038/s42003-019-0666-1
241. Marjon K, Cameron MJ, Quang P, Clasquin MF, Mandley E, Kunii K, et al. MTAP Deletions in Cancer Create Vulnerability to Targeting of the MAT2A/PRMT5/RIOK1 Axis. *Cell Rep* (2016) 15(3):574–87. doi: 10.1016/j.celrep.2016.03.043
242. Rheinbay E, Nielsen MM, Abascal F, Wala JA, Shapira O, Tiao G, et al. Analyses of Non-Coding Somatic Drivers in 2,658 Cancer Whole Genomes. *Nature* (2020) 578(7793):102–11. doi: 10.1038/s41586-020-1965-x
243. Yates LR, Knappskog S, Wedge D, Farmery JHR, Gonzalez S, Martincorena I, et al. Genomic Evolution of Breast Cancer Metastasis and Relapse. *Cancer Cell* (2017) 32(2):169–84.e7. doi: 10.1016/j.cccell.2017.07.005
244. Tripathi S, Xing J, Levine H, Jolly MK. Mathematical Modeling of Plasticity and Heterogeneity in EMT. *Methods Mol Biol* (2021) 2179:385–413. doi: 10.1007/978-1-0716-0779-4\_28

**Conflict of Interest:** RGP holds ownership interests in the companies ProstaGene, CytoDyn, LightSeed, Inc., and EcoGenome. RGP holds ownership interests (value unknown) of several patents and submitted patent applications.

The remaining authors declare that the research was conducted in the absence of any commercial or financial relationships that could be construed as a potential conflict of interest.

**Publisher's Note:** All claims expressed in this article are solely those of the authors and do not necessarily represent those of their affiliated organizations, or those of the publisher, the editors and the reviewers. Any product that may be evaluated in

this article, or claim that may be made by its manufacturer, is not guaranteed or endorsed by the publisher.

Copyright © 2021 Patra, Elahi, Armorer, Arunachalam, Omala, Hamid, Ashton, Joyce, Jiao and Pestell. This is an open-access article distributed under the terms of the

*Creative Commons Attribution License (CC BY). The use, distribution or reproduction in other forums is permitted, provided the original author(s) and the copyright owner(s) are credited and that the original publication in this journal is cited, in accordance with accepted academic practice. No use, distribution or reproduction is permitted which does not comply with these terms.*





# Oncogenic Integration of Nucleotide Metabolism *via* Fatty Acid Synthase in Non-Hodgkin Lymphoma

Dashnamoorthy Ravi<sup>1,2\*</sup>, Afshin Beheshti<sup>3,4</sup>, Nasséra Abermil<sup>5</sup>, Frederick Lansigan<sup>6,7</sup>, William Kinlaw<sup>8</sup>, Nirupa R. Matthan<sup>9</sup>, Maisarah Mokhtar<sup>1</sup>, Frank C. Passero Jr.<sup>10</sup>, Patrick Puliti<sup>1,6,7</sup>, Kevin A. David<sup>1,2</sup>, Gregory G. Dolnikowski<sup>9</sup>, Xiaoyang Su<sup>2,11</sup>, Ying Chen<sup>12</sup>, Mahboubi Bijan<sup>13</sup>, Rohan R. Varshney<sup>14</sup>, Baek Kim<sup>13,15</sup>, Sandeep S. Dave<sup>16</sup>, Michael C. Rudolph<sup>14</sup> and Andrew M. Evens<sup>1,2</sup>

<sup>1</sup> Division of Blood Disorders, Rutgers Cancer Institute of New Jersey, New Brunswick, NJ, United States, <sup>2</sup> Department of Medicine, Robert Wood Johnson Medical School, Rutgers University, New Brunswick, NJ, United States, <sup>3</sup> Stanley Center for Psychiatric Research, Broad Institute of Massachusetts Institute of Technology and Harvard, Cambridge, MA, United States, <sup>4</sup> KBR, Space Biosciences Division, National Aeronautics and Space Administration, Ames Research Center, Moffett Field, CA, United States, <sup>5</sup> Assistance Publique-Hôpitaux de Paris (AP-HP), Hôpital Saint-Antoine, Service d'Hématologie Biologique, Paris, France, <sup>6</sup> Department of Medicine, Norris Cotton Cancer Center, Dartmouth-Hitchcock Medical Center, Lebanon, NH, United States, <sup>7</sup> Department of Medicine, Section of Endocrinology and Metabolism, Geisel School of Medicine at Dartmouth, Hanover, NH, United States, <sup>8</sup> Department of Medicine, Norris Cotton Cancer Center, Geisel School of Medicine at Dartmouth, Lebanon, NH, United States, <sup>9</sup> Jean Mayer United States Department of Agriculture (USDA) Human Nutrition Research Center on Aging, Tufts University, Boston, MA, United States, <sup>10</sup> Department of Medicine, University of Rochester Medical Center, Rochester, NY, United States, <sup>11</sup> Metabolomics Core, Rutgers Cancer Institute of New Jersey, New Brunswick, NJ, United States, <sup>12</sup> Bioinformatics Core, Rutgers Cancer Institute of New Jersey, New Brunswick, NJ, United States, <sup>13</sup> Department of Pediatrics, School of Medicine, Emory University, Atlanta, GA, United States, <sup>14</sup> Harold Hamm Diabetes Center, The University of Oklahoma Health Sciences Center, Oklahoma, OK, United States, <sup>15</sup> Center for Drug Discovery, Children's Healthcare of Atlanta, Atlanta, GA, United States, <sup>16</sup> Department of Medicine, Duke Cancer Institute, Duke University Medical Center, Durham, NC, United States

## OPEN ACCESS

### Edited by:

Andrea Morandi,  
University of Florence, Italy

### Reviewed by:

Sofia Avnet,  
University of Bologna, Italy  
Aleš Dvořák,  
Charles University, Czechia

### \*Correspondence:

Dashnamoorthy Ravi  
ravi.dashnamoorthy@rutgers.edu

### Specialty section:

This article was submitted to  
Cancer Metabolism,  
a section of the journal  
Frontiers in Oncology

**Received:** 14 June 2021

**Accepted:** 04 October 2021

**Published:** 26 October 2021

### Citation:

Ravi D, Beheshti A, Abermil N, Lansigan F, Kinlaw W, Matthan NR, Mokhtar M, Passero FC Jr., Puliti P, David KA, Dolnikowski GG, Su X, Chen Y, Bijan M, Varshney RR, Kim B, Dave SS, Rudolph MC and Evens AM (2021) Oncogenic Integration of Nucleotide Metabolism *via* Fatty Acid Synthase in Non-Hodgkin Lymphoma. *Front. Oncol.* 11:725137. doi: 10.3389/fonc.2021.725137

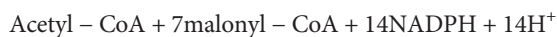
Metabolic dysfunctions enabling increased nucleotide biosynthesis are necessary for supporting malignant proliferation. Our investigations indicate that upregulation of fatty acid synthase (FASN) and *de novo* lipogenesis, commonly observed in many cancers, are associated with nucleotide metabolic dysfunction in lymphoma. The results from our experiments showed that ribonucleotide and deoxyribonucleotide pool depletion, suppression of global RNA/DNA synthesis, and cell cycle inhibition occurred in the presence of FASN inhibition. Subsequently, we observed that FASN inhibition caused metabolic blockade in the rate-limiting step of the oxidative branch of the pentose phosphate pathway (oxPPP) catalyzed by phosphogluconate dehydrogenase (PGDH). Furthermore, we determined that FASN inhibitor treatment resulted in NADPH accumulation and inhibition of PGDH enzyme activity. NADPH is a cofactor utilized by FASN, also a known allosteric inhibitor of PGDH. Through cell-free enzyme assays consisting of FASN and PGDH, we delineated that the PGDH-catalyzed ribulose-5-phosphate synthesis is enhanced in the presence of FASN and is suppressed by increasing concentrations of NADPH. Additionally, we observed that FASN and PGDH were colocalized in the cytosol. The results from these experiments led us to conclude that NADP–NADPH turnover and the reciprocal stimulation of FASN and PGDH catalysis are involved in promoting oxPPP and nucleotide biosynthesis in lymphoma. Finally, a transcriptomic analysis of non-Hodgkin's lymphoma ( $n = 624$ ) revealed the increased

expression of genes associated with metabolic functions interlinked with oxPPP, while the expression of genes participating in oxPPP remained unaltered. Together we conclude that FASN–PGDH enzymatic interactions are involved in enabling oxPPP and nucleotide metabolic dysfunction in lymphoma tumors.

**Keywords:** non-Hodgkin lymphoma, FASN, metabolomics, nucleotides, pentose phosphate pathway, lipid metabolism

## INTRODUCTION

Oncogenic *de novo* lipogenesis, which is catalyzed by the overexpressed fatty acid synthase (FASN), is an important metabolic phenotype observed in many cancers (1). FASN is a 273-kDa cytosolic multi-catalytic enzyme complex consisting of homo-dimeric subunits with head to tail linked configuration, which catalyzes the biosynthesis of palmitic acid (2). FASN activity is entirely dependent on cytosolic glucose metabolism for the substrates acetyl-CoA and malonyl-CoA, both derived through glycolysis/citric acid cycle, and coenzyme NADPH, derived from the pentose phosphate pathway (PPP) (2), as indicated in the following reaction equation.



While other enzymatic sources of cytosolic NADPH are known to exist, PPP is regarded as the primary NADPH source for human FASN activity (3). Palmitic acid, which is the end-product in FASN enzyme activity, is also a key intermediate for lipid metabolism. Palmitic acid is utilized in the biosynthesis of phospholipids, sphingolipids, ether lipids, diacylglycerol, and ceramide. Most importantly, several palmitic acid-derived lipids act as second messengers and are involved in the regulation of growth and immune-related signaling pathways, including, PI3K, MAPK, and NFκB (2, 4–6). Moreover, palmitic acid, through protein palmitoylation, is known to impact receptor aggregation and protein mobilization dynamics on the cell surface (7, 8). In premalignant cells, FASN activity induced by HIF1α is associated with restoring glycolysis and oxidative phosphorylation from hypoxia-induced metabolic suppression (9). In malignant cells, FASN upregulation mediated by oncogenic signals (including HER2, EGFR, MAPK, and PI3K) through sterol response element binding proteins is surmised as lipogenic in nature (2).

We have previously reported the occurrence of PI3K alterations (10) and increased FASN expression in non-Hodgkin lymphoma (NHL) (11). Furthermore, we also observed that an increased FASN expression was correlated with a poor clinical outcome in NHL (11). Collectively, there remains a desire to identify novel targeted therapeutic options with better efficacy and relatively fewer toxic profiles for the treatment of NHL (12, 13). Therefore, we evaluated the potency of several FASN small molecule inhibitors, including cerulenin, orlistat, TVB3166, and TVB3567, in NHL experimental models.

Cerulenin is an antifungal antibiotic FASN inhibitor, which binds irreversibly with the catalytic domain of β-keto acyl synthase subunit and blocks the initial step of FASN-catalyzed condensation of acetyl-CoA with malonyl-CoA (14). The anticancer activity of cerulenin-mediated FASN inhibition has been extensively investigated using multiple *in vivo* and *in vitro* tumor models (5). Similarly, orlistat, a bispecific FASN and pancreatic lipase inhibitor, and the novel small-molecule FASN inhibitors, TVB3166 and TVB3567, have been evaluated in several solid tumor models (15, 16). In the present study, we define the biological consequences and significance of FASN inhibition in NHL.

## METHODS

### Cell Culture, Reagents, And Transfections

ATCC (STR profiling) authenticated bNHL cells, SUDHL2, SUDHL4, SUDHL10, and OCI-LY19. Raji was grown in the RPMI 1640 medium with 10% heat-inactivated fetal bovine serum (FBS) and 200 U of penicillin/streptomycin (Mediatech, Manassas, VA) under 5% CO<sub>2</sub> and at 37°C. Primary DLBCL tumor cells were obtained through Tufts Tumor Repository at Tufts Medical Center (Boston, MA) as de-identified discarded specimens through an exempt institutional review board approval. The FASN inhibitors cerulenin (Sigma Aldrich, St. Louis, MO), TVB3166, and TVB3567 were generous gifts from 3V Biosciences (Menlo Park, CA). Standards from quantitative mass spectrometry nucleotides, 6-phosphogluconate and glucose-6-phosphate, were purchased from Sigma (St. Louis, MO). RNA interference experiments were performed using FASN siRNA Ambion Cat# 4390824 (Thermo Fisher Scientific, Austin, TX) and PGDH shRNA, Mission shRNA clone TRCN0000274974 (Sigma Aldrich, St. Louis, MO).

### Western Blot

We prepared the protein lysates and performed western blots as described before (17) using the following primary antibodies against total and cleaved caspase-3 and PARP. PGDH, FASN, and β-actin were purchased from Cell Signaling Technology (Beverly, MA).

### Cell Viability Assays

MTT assays were performed using bNHL cells treated with cerulenin for 72 h, as described before (17). IC<sub>50</sub> values for drug treatments were derived using Calcsyn version 2.1 software (Biosoft, Ferguson, MO).

## Flow Cytometry

Apoptosis was determined using annexin-V/propidium iodide (PI) staining and flow cytometry, as described before (17).

## Transcriptome Analysis

RNA isolation and transcriptomic analysis by gene set enrichment analysis (GSEA) and ingenuity pathway analysis (IPA) were performed as described before (17–19). All experiments were performed in biological triplicates. Affymetrix Human Genechip 2.0 ST was used for cerulenin-treated Raji and SUDHL10, and Human HT 12 Genechip Illumina was used for cerulenin-, TVB3166-, or TVB3567-treated Raji, SUDHL2, SUDHL10, or SUDHL4 cells. The raw data from these experiments is available at the NCBI Gene Expression Omnibus database, with the following identifiers: GSE102760 for cerulenin-treated Raji and SUDHL10 experiments and GSE102764 for cerulenin-treated SUDHL4 experiments and for cerulenin-, TVB3166-, or TVB3567-treated Raji, SUDHL2 SUDHL10 experiments. Previously published RNA seq data set available from 624 NHL patients (20) were utilized for metabolic gene expression. Lists of metabolic genes were downloaded from KEGG databases, Reactome, and KEGG databases, and a curated gene list was used for gene expression analysis and construction of metabolic pathway models and heatmap by R package (ComplexHeatmap), as described previously (21).

## Metabolic Profiling

bNHL cells cultured in the presence of D-glucose- $^{13}\text{C}_6$  2 g/L (Cambridge Isotopes, Tewksbury, MA) in glucose-free RPMI-1640 (Sigma Aldrich, St. Louis, MO) containing 10% FBS were treated with an appropriate concentration of drugs for 48 h. Lipids were extracted using a modified Folch method (22), followed by saponification using 0.5 N methanolic sodium hydroxide and methylated by boron trifluoride in methanol as described previously (23). The supernatant containing the fatty acid methyl esters was dried under nitrogen and resuspended in acetonitrile for lipid profiling by liquid chromatography–mass spectrometry (LC–MS). For polar metabolites, samples extracted with (40:40:10) methanol, acetonitrile, and water, consisting of 0.5% formic acid and neutralized with sodium bicarbonate, were used for analysis by mass spectrometry. LC–MS was performed using the Q Exactive PLUS hybrid quadrupole-orbitrap mass spectrometer (Thermo Scientific) coupled to hydrophilic interaction chromatography. Metabolite features were extracted using MAVEN with labeled isotope specified and a mass accuracy window of 5 ppm (24). The  $^{13}\text{C}$  isotope natural abundance and the impurity of labeled substrate were corrected using AccuCor written in R as described (25). The corrected ion counts were normalized by cell number. The processed datasets were statistically analyzed, and feature identification by principal component analysis (PCA), partial least squares-discriminant analysis (PLS-DA), PatternHunter, correlation clustering and heat map analysis, and joint pathway analysis were performed using Metaboanalyst 3.0 software (26, 27).

## dNTP Assays

Cellular dNTP levels were determined using a RT-based dNTP assay, as described previously (28).

## Global DNA and RNA Synthesis

DNA synthesis was monitored using EZClick EdU cell proliferation kit (#K946). Confocal microscopy and RNA synthesis, quantified by flow cytometry, were performed using 5-ethynyl-uridine-based EZClick Global RNA synthesis assay kit (#K718) purchased from Biovision (Milpitas, CA), following the instructions supplied by the manufacturer.

## NADP/NADPH Assay

Total NADP/NADPH concentration was determined using NADP/NADPH-Glo assay (Promega, Madison, WI), following the manufacturer-supplied instructions, using NHL cells treated with cerulenin for 48 h.

## Enzyme Activity Assays

Enzymatic activity assays were performed using the following kit purchased from Abcam (Cambridge, MA): phospho-gluconate dehydrogenase (PGDH) #ab155896. The assays were performed following the manufacturer-supplied instructions.

## FASN PGDH Colocalization Analysis

Cytospin preparation consisting of  $1 \times 10^5$  cells was performed using EZ Cytospin starter kit and Cytospin 4 (Thermo Scientific, Waltham, MA). Air-dried and methanol-fixed cell preparations were permeabilized with 0.25% Triton X-100 in phosphate-buffered saline, blocked using 1% bovine serum albumin, and incubated with appropriate antibody concentrations. Stained cells mounted using Prolong Antifade-Gold reagent (Molecular Probes, by Thermo Fisher Scientific, Waltham, MA) were used for image acquisition by a Nikon A1RSi laser confocal microscope. Colocalization analysis was performed using Colocalization and JACoP, plugins available through ImageJ, as described before (29). Primary antibodies mouse anti-human FASN antibody clone 3F2-1F3 (LSBio, LifeSpan, cat. #LS-C104946, Seattle, WA) and rabbit anti-human PGDH (Cell Signaling Technology, cat. #13389, Danvers, MA) and the following secondary antibodies, AlexaFluor-594 goat and anti-mouse and AlexaFluor-488 donkey anti-rabbit (Invitrogen), were used in this study.

## Cell-Free Enzyme Assays

The human recombinant PGDH was purchased from ProSpec Bio (East Brunswick, NJ). The human recombinant FASN is a generous gift from Dr. Michael C. Rudolph. The preparation, purification, reconstitution, and activity assessments are described elsewhere (30, 31). The following substrates and coenzyme factors for cell-free enzyme assays were purchased from Sigma Aldrich (St. Louis, MO): 6-phosphogluconate (6PG), acetyl-CoA, malonyl-CoA,  $\beta$ -NADP, and  $\beta$ -NADPH. The reactions were performed using 250 mM potassium phosphate buffer, pH 7.6, consisting of 1 mM DTT and 5  $\mu\text{M}$  EDTA. The reactions were performed using PGDH (0.25  $\mu\text{g}$ ), FASN (4  $\mu\text{g}$ ), 2 mM 6PG, 40  $\mu\text{M}$  acetyl-CoA, 110  $\mu\text{M}$  malonyl-CoA, and variable concentrations of NADP or NADPH (0–800  $\mu\text{M}$ ) in 100- $\mu\text{l}$  final volume. The reaction kinetics were monitored continuously for 20 min at 340 nM, for NADPH appearance

or disappearance, using 96-well half area U-plate (Costar) and Tecan infinite M200 plate reader. The reactions were quenched by the addition of ice-cold 1:1 methanol and acetonitrile consisting of 0.5% formic acid, and the mixture was incubated on ice for 5 min, neutralized with sodium bicarbonate, and centrifuged. The collected supernatants were used for mass spectrometric analysis.

## Statistical Analysis

All experiments were performed in triplicate. Significant differences between control and treatment were statistically determined by Student's *t*-test for cell viability, apoptosis, and enzyme activity assays. For metabolic profiling experiments, identification of top significant metabolite features by PLS-DA and variable importance in projection (VIP) scoring analysis, statistical correlation analysis by one-way ANOVA, and *post-hoc* analysis and Spearman rank correlation were performed using the software packages included in Metaboanalyst 3.0 (26, 27). The statistical analysis for transcriptomic datasets was performed as previously described (17–19).

## RESULTS

### FASN Inhibition Induces Cell Death in bNHL

Treatment with increasing concentrations of cerulenin for 72 h resulted in a dose-dependent reduction in cell viability with associated induction of apoptosis in bNHL cells (**Figure 1**). The corresponding IC<sub>50</sub> values for the cerulenin treatment were as follows: Raji (14.3  $\mu$ M), SUDHL4 (8.0  $\mu$ M), SUDHL10 (19.4  $\mu$ M), and OCI-LY19 (9.6  $\mu$ M) (**Figure 1A**). In primary bNHL tumor cells, the associated IC<sub>50</sub> values were 5.1  $\mu$ M in DLBCL #1, 4.04  $\mu$ M in DLBCL #2, and 7.8  $\mu$ M in DLBCL #3 (**Figure 1A**). We also noted that the sensitivity of DLBCL cells was significantly low with IC<sub>50</sub> >50  $\mu$ M for orlistat compared with cerulenin (data not shown). The IC<sub>50</sub> values of novel small-molecule FASN inhibitors TVB3166 or TVB3156, respectively, were as follows: Raji—110 and 115 nM, SUDHL2—227 and 222 nM, SUDHL4—78 and 85 nM, and SUDHL10—433 and 863 nM (**Figure 1A**). The annexin-V-based flow cytometry showed a dose-dependent increase in apoptosis in SUDHL4 and Raji, but not in SUDHL10 cells (**Figure 1B**). These results were confirmed by western blot analysis for markers of apoptosis, which showed the presence of cleaved caspase 3 and PARP in the cerulenin-treated bNHL (**Figure 1B**), except in cerulenin-treated SUDHL10, indicating resistance to FASN inhibition in these cells.

### FASN Inhibitory Transcriptome

The global transcriptomic analyses following cerulenin treatment showed significant differential gene changes for DLBCL cells SUDHL2 (141 genes), SUDHL4 (242 genes), and SUDHL10 (1,600 genes) and Raji (Burkitt lymphoma) (1,092 genes) (**Supplementary Figures S1A–D, G**). Inhibition of FASN by TVB3166 or TVB3567 showed differentially expressed

significant genes for SUDHL2 (962 and 600 genes), SUDHL10 (779 and 497 genes), and Raji (2,216 and 2,556 genes) (**Supplementary Figures S1E–G**). The canonical pathway analysis by IPA of these FASN inhibitory transcriptomes identified a conserved upregulation of immune signaling (tumor necrosis factor, interferon, CD27, CD28, IL1, IL6, IL9, and BCR signaling), apoptosis signaling, cAMP, protein kinase A, and NRF-2-mediated oxidative stress response pathways as activated mechanisms by FASN inhibition in NHL cells (**Figure 1C**). Genes down-regulated by FASN inhibition included cell cycle functions (mediated by cyclins, estrogen, and checkpoint proteins) and growth regulation (mediated by p53, PPAR, phospholipase C, p70 S6K, VEGF, IL2, IL22, GM-CSF, and HGF) as identified by the IPA analysis of all NHL cells (**Figure 1C**). The transcriptional network analysis from GSEA showed nucleotide/RNA metabolism and cell cycle as down-regulated mechanisms from cerulenin or TVB3166 and TVB3567 treatment in NHL cells (**Supplementary Figure S2**). Taken together, the gene expression analyses by IPA and GSEA both indicate that cell cycle and its regulatory functions are negatively impacted by FASN inhibition.

### FASN Inhibitory Metabolome

We next performed metabolic profiling to determine the impact of FASN inhibition on cellular metabolism. For this, SUDHL10 cells treated with increasing concentrations of cerulenin for 48 h were utilized for metabolic assessments by mass spectrometry. The PCA score plot comparing the cerulenin (15–30  $\mu$ M) treatment indicated 72% variance by differential loading across the PC1 axis in metabolic alterations compared to untreated SUDHL10 cells (**Figure 2A**). The regression-based PLS-DA of the top 50 metabolic features identified from one-way ANOVA analysis resulted in the selection of 15 metabolites. These identified 15 features were then ranked by VIP scoring analysis with significant *P*-values <0.001, which identified cAMP, 6PG, phosphocholine, CDP-choline, and acetyl-CoA among other metabolites (**Figure 2B**). The heat map of this plot showed that the levels of 6-phosphogluconate, CDP-choline, and acetyl-CoA were increased with cerulenin treatment in a concentration-dependent manner (**Figure 2B**). The correlation matrix analysis comparing the cerulenin dose effect with the responses of significant metabolites revealed four major clusters across the diagonal within the heat map (**Figure 2C**). The first cluster (group 1) consisted of acetoacetate (acetyl-CoA-derived ketone body), reduced and oxidized glutathione, glucose, glucose-6-phosphate, and 6PG (PPP metabolites), CDP-choline, and amino acids (serine and glutamine) (**Figure 2C**). The second cluster (group 2) in the middle section included metabolites predominantly representing nucleotide metabolism (uridine, uracil, nucleotide monophosphates, ribose + ribulose-5-phosphate (R5P), AICAR, coenzymes—reduced (NADH/NADPH), alanine, aspartate, and glycine amino acids related to the *de novo* biosynthesis of nucleotides), and glycolytic intermediates (fructose-6-phosphate, pyruvate, and lactate) (**Figure 2C**). The third minor cluster (group 3) in the middle mid-segment consisted of cAMP, adenine, 3-phosphoglycerate, and phosphoenolpyruvate, representing both nucleotide and





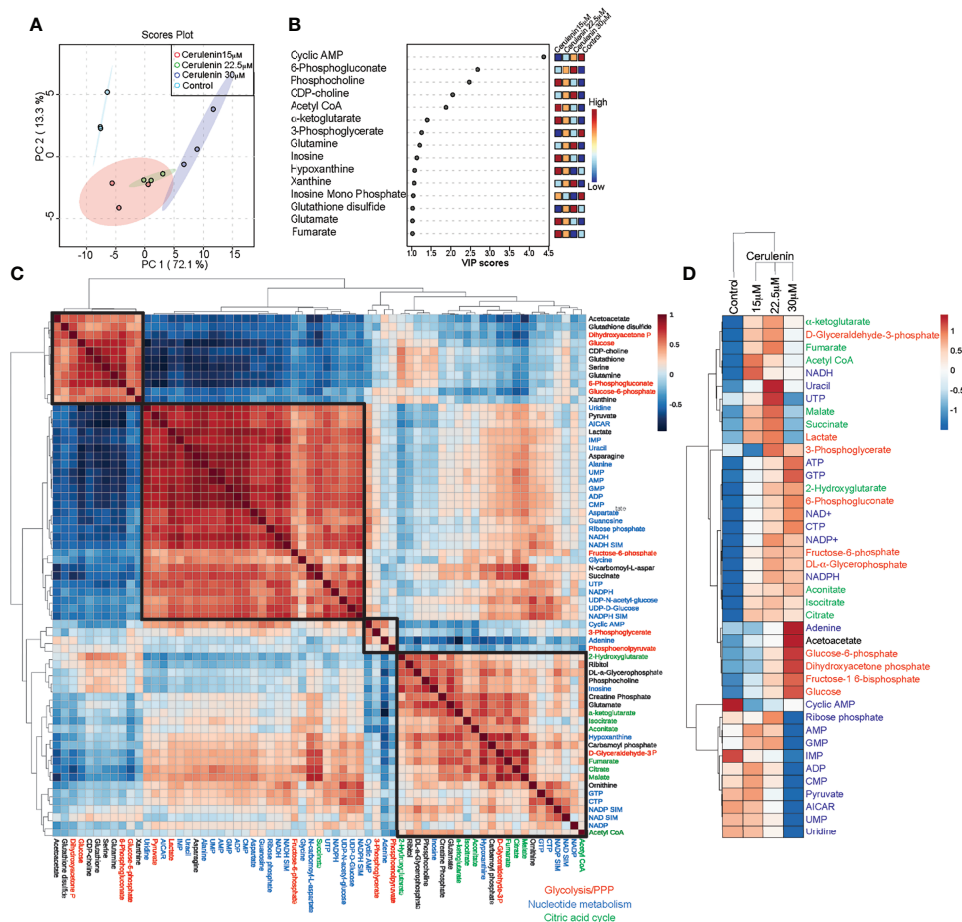


**FIGURE 2 |** Metabolic impacts of cerulenin-mediated FASN inhibition in SUDHL10 cells. **(A)** Score plot from SUDHL10 cells by principal component analysis (PCA) indicates variances (shown within brackets) to metabolic profiles resulting from cerulenin treatment. **(B)** Identification of top significant metabolite features ( $P < 0.001$ ) which contributed to differential PCA loading by partial least squares—discriminant analysis and variable importance in projection scoring analysis. The colored boxes on the right indicate the relative concentrations of the corresponding metabolite in each group. **(C)** Correlation heat map comparing the top 50 significant features with  $p$ -value and false discovery rate  $< 0.05$  determined by one-way ANOVA and *post-hoc* analysis, identified distinct patterns of correlative associations (distance measured by Spearman rank correlation) between metabolites affected by cerulenin treatment in SUDHL10 cells. In the correlation matrix, a positive correlation coefficient between concordant metabolites is represented in red, and a negative correlation coefficient between discordant metabolites is represented as blue. Legend depicting the metabolites shown in colors represents the following: red—glucose metabolism, blue—nucleotide metabolism, and green—citric acid cycle. **(D)** Heat map representing hierarchical clustering by correlation distance and average linkage of  $\log_2$ -transformed; row-centered data show cerulenin dose effect on individual metabolite in experimental triplicates, indicating either increased (in red) or decreased (in blue) pool sizes observed with FASN inhibition in SUDHL10 cells.

## FASN Inhibition Impacts Nucleotide Metabolism

We then fused transcriptomic and metabolomic datasets and performed topological assessment of centrality and determination of pathway enrichment scores, using joint-pathway analysis by Metaboanalyst. This process resulted in the identification of ketone body metabolism, Krebs (citric acid cycle), nucleotide metabolism (purine/pyrimidine metabolism), cell cycle, amino acid and glutathione metabolism, and PPP and NAD metabolism as the most FASN inhibition-impacted pathways with enrichment scores  $> 1$ , false discovery rate (FDR), and  $P$ -values  $< 0.05$  (Figure 3A and Supplementary Table S1). Other high-impact pathways that included several lipid metabolic processes and PI3K/JAK/STAT signaling pathways were identified but were below the cutoff for

statistical stringency (Figure 3A and Supplementary Table S1). In summarizing these observations, FASN inhibition resulted in increasing the levels of metabolic intermediates associated with glycolysis and citric acid cycle that yield acetyl-CoA as substrate for FASN activity (indicated in red) (Figure 3B). The inhibition of FASN is expected to interrupt palmitic acid synthesis; towards this end, we observed decreased palmitic acid synthesis (determined based on  $C^{13}$  fractional labeling) that occurred with cerulenin treatment in SUDHL10 (Figure 3C). Thus, with acetyl-CoA accumulation and decreased palmitic acid synthesis, we also observed pool size reductions in R5P and nucleotides (denoted in blue) occurring with FASN inhibition (Figure 3B). Biochemically, oxidative PPP supplies NADPH for FASN. Thus, the accumulation of 6-phosphogluconate (6PG) (denoted in red) and the reduction in



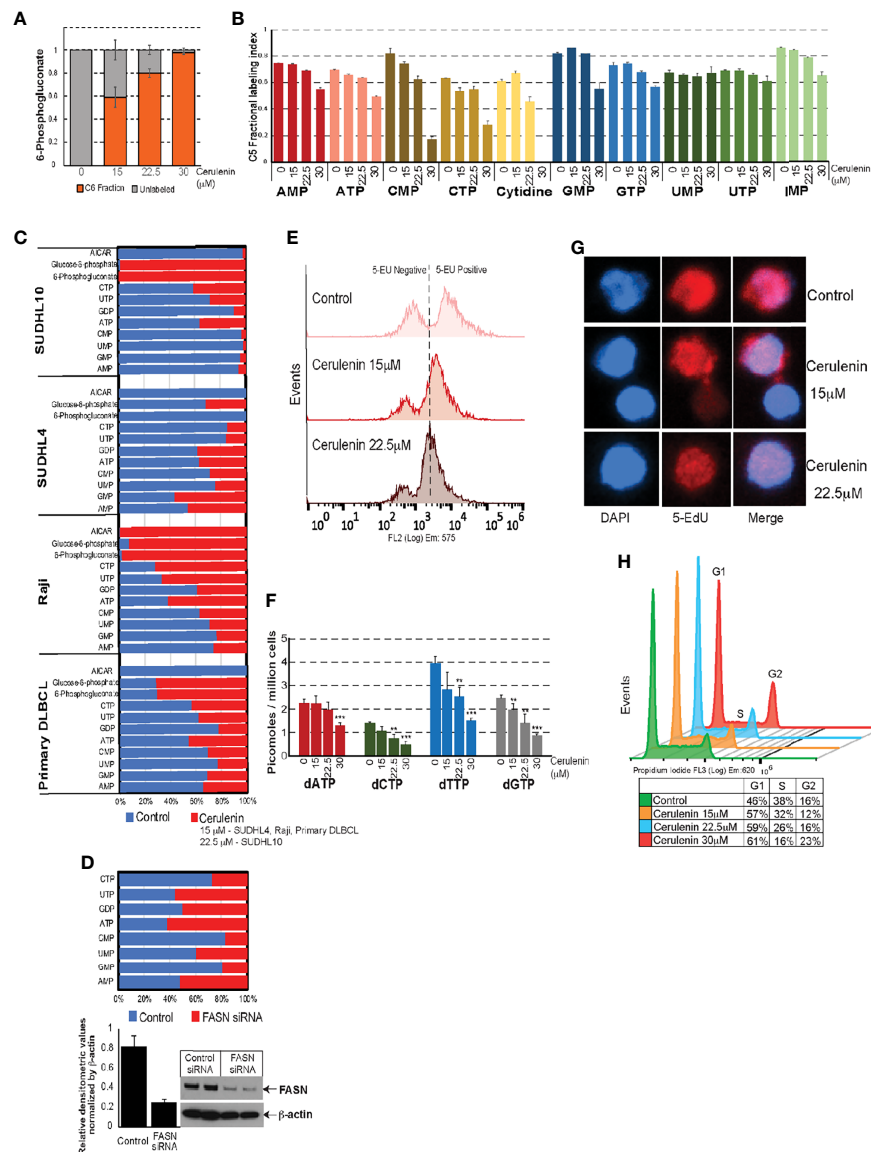


**FIGURE 4 |** Effects of FASN inhibition on nucleotide metabolism. **(A, B)** Bar graphs representing  $C^{13}$  fractional incorporation (in y-axis) in C5 residues of 6PG or nucleotide pools listed on the x-axis, with cerulenin-treated SUDHL10 cells. **(C, D)** Quantitative mass spectrometry analysis of nucleotide pools represented as fold change (by percentage) with the levels of nucleotides occurring with cerulenin treatment in bNHL cells or with FASN siRNA in SUDHL10 cells. Western blot represents the extent of siRNA-mediated FASN knockdown observed in SUDHL10 cells. Bar graph represents the ratio of FASN protein expression normalized by total  $\beta$ -actin for equal loading. Absolute concentrations corresponding to these fold changes are included in **Supplementary Table S1**. **(E)** Flow cytometry of ClickIT 5-EU pulse-labeled SUDHL10 cells show decreased fluorescence intensity indicative of RNA global transcriptional activity occurring with cerulenin treatment in SUDHL10 compared to control. **(F, G)** Bar graph representing changes in the concentration of dNTPs following cerulenin treatment in SUDHL10 cells. Confocal imaging of ClickIT 5-EdU pulse-labeled SUDHL10 cells show decreased 5-EdU (red) incorporation in DNA against DAPI (blue) or merged occurring with cerulenin treatment in SUDHL10 compared to control. All experiments were performed in triplicates; the error bars in all bar graphs represent the standard deviations of mean, and the significant difference between control and treatment is indicated by an asterisk ( $**p < 0.05$  and  $***p < 0.005$ ) statistically determined by Student's *t*-test. **(H)** Histogram representing changes in cell cycle occurring with cerulenin treatment based on the flow cytometry of propidium-stained SUDHL10 cells at 48 h **(H)** Overlaid histogram representing cell cycle changes comparing cerulenin with control at 48 h in SUDHL10 cells, detected by propidium iodide staining and flow cytometry analysis.

## Enzymatic Coupling of FASN-PGDH Activities

FASN inhibition resulted in nucleotide depletion and impacted DNA/RNA metabolism and the cell cycle. It is likely that the

perturbation of PGDH could be relevant for the negative impacts observed with nucleotide metabolism associated with FASN inhibition. We, therefore, focused our investigations towards delineating the mechanistic link between FASN inhibition and the



perturbation of PGDH activity. Sources of cytosolic NADPH for FASN activity include PGDH, malic enzyme, and isocitrate dehydrogenase; however, with FASN inhibition, the metabolic profiles show that only PGDH activity was impacted (shown in blue), while the other enzymes remained unaffected (Figure 5A). Moreover, PGDH is the only rate-limiting unidirectional enzyme susceptible to allosteric inhibition by NADPH. From these evidence, we concluded that PGDH is the only NADPH-yielding enzyme that was responsive to FASN inhibition. The results from NADP/NADPH quantification by NADP/NADPH-Glo assay showed a significant fold increase in both NADP and NADPH levels ( $P < 0.001$ ) occurring with cerulenin treatment in SUDH10 cells (Figure 5B). While NADPH accumulation is expected with FASN inhibition, the reason for the observed NADP increase seems unclear. To better understand these metabolic impacts, we first performed enzyme activity assays, using SUDHL10 cells, and observed a decrease in PGDH activity occurring in a cerulenin-concentration-dependent manner (Figure 5C). Our western blot analysis revealed a stable PGDH protein expression (Supplementary Figure S4), indicating that PGDH is metabolically repressed under FASN inhibition. Similar inhibitions of PGDH enzyme activity by cerulenin were observed in other NHL cells (SUDHL4 and Raji) (data not shown). Notably, the expression of PPP enzyme G6PDH and dependent antioxidant enzymes showed a dynamic increase in protein expression with FASN inhibition, indicating that PGDH is the only unregulated expression function in this pathway (Supplementary Figures S4B–E). Since PGDH is the rate-limiting bridge between PPP and nucleotide biosynthesis, we investigated the impact of PGDH silencing using shRNA. The results from this experiment showed that ribulose-5-phosphate (PGDH product) and inosine monophosphate (precursor associated with *de novo* nucleotide biosynthesis) were reduced (Figure 5D), with decreased PGDH. Therefore, it is now apparent that PGDH perturbation by both FASN inhibition and RNAi results in negatively impacting the nucleotide metabolism.

Mechanistically, perturbation of PGDH activity is feasible through allosteric feedback inhibition caused by NADPH accumulation resulting from FASN inhibition (Figure 5B). PGDH is sensitive to allosteric inhibition by NADPH ( $K_i$  value,  $0.03 \mu\text{M}$ ) (source: BRENDA, www.brenda-enzymes.org). Thus, for NADPH accumulation by FASN inhibition to impact PGDH function, both of these enzymes must be localized in close proximity. The results from colocalization studies based on immunofluorescence staining and confocal imaging analysis of SUDHL10 cells showed that both PGDH (green) and FASN (red) were localized in the cytosol, with few punctate nuclear distributions observed with PGDH (Figure 6A). A colocalization analysis by Manders coefficient method (JaCoP, ImageJ plugin) performed using three independent sets of images determined that  $0.79 \pm 0.04$  fraction of PGDH overlapped with FASN, and  $0.58 \pm 0.12$  fraction of FASN likewise overlapped with PGDH in SUDHL10 cells (Figure 6A). Similar results with overlaps and colocalization patterns for FASN and PGDH were also observed from staining with independent sets of antibodies (FASN #sc-398977 and PGD #sc48357, Santa Cruz Biotechnology, Dallas, TX) and additional SUDHL4 cell line (data not shown).

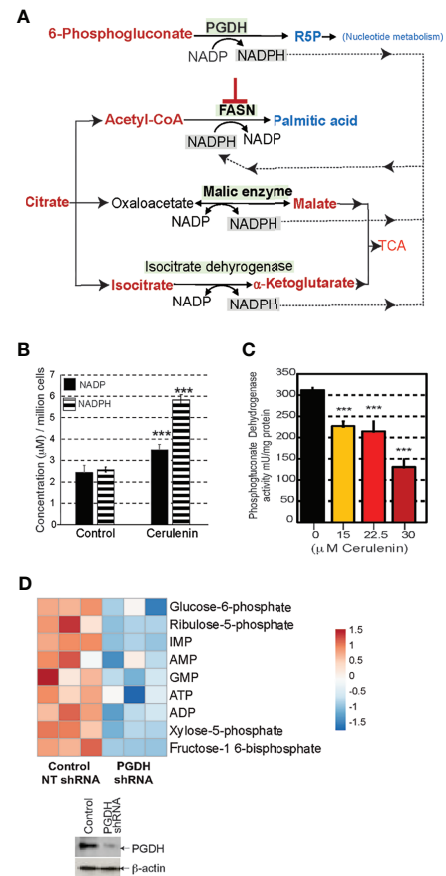


**FIGURE 5 |** FASN inhibition interrupts phosphogluconate dehydrogenase (PGDH) activity. **(A)** Schematic representation of the metabolic impacts of FASN inhibition on potential enzymatic sources of NADPH for FASN activity; elevated metabolites are shown in red, and decreased metabolites are shown in blue. **(B)** Bar graph representing changes in concentrations of NADP or NADPH comparing untreated control and cerulenin treatment (on x-axis), and concentration represented as  $\mu\text{M}$ /million cells (on y-axis) in SUDHL10 cells. Data represented are based on averages from experimental triplicates, comparing cerulenin-treated cells with untreated control, with \*\*\* denoting  $P < 0.001$ . **(C)** Bar graph representing PGDH enzymatic activity in SUDHL10 cells treated with cerulenin, with the concentration shown on x-axis, and enzyme activity normalized by mU/mg of total protein (on y-axis). All experiments were performed in triplicates. The error bars in all bar graphs represent the standard deviations of mean, and the significant difference between control and treatment is indicated by an asterisk (\*\*\*) denoting  $P < 0.005$ , statistically determined by Student's *t*-test. **(D)** Heat map representing the metabolic impacts of shRNA-mediated PGDH knockdown compared with non-targeted control in SUDHL4 cells, shown as  $\log_2$ -transformed, row-centered data from experimental triplicates. Western blot representing the extent of PGDH knockdown observed with shRNA-mediated RNA silencing in SUDHL4 cells.

The FASN and PGDH colocalization patterns indicate that both of these enzymes are proximally localized, and, therefore, shuttling of NADP–NADPH between these enzymes could occur within the cells. In order to determine whether reciprocal shuttling of NADP–NADPH occurs and influences FASN and PGDH, we performed the following cell-free enzyme assays: first, PGDH catalytic activity was quantified in the presence of

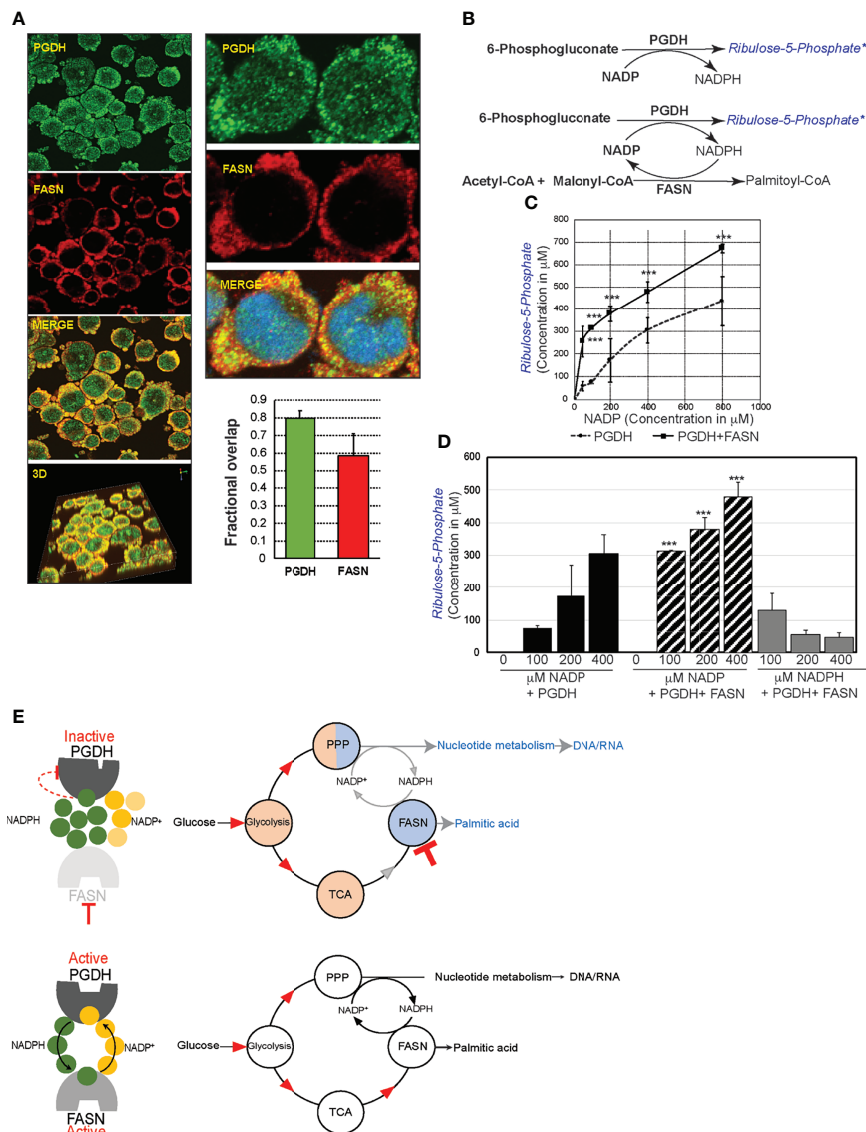


**FIGURE 6 |** FASN and phosphogluconate dehydrogenase (PGDH) are metabolically synergistic enzymes. **(A)** Confocal microscopy of SUDHL10 cells stained with rabbit anti-human PGDH (green) and mouse anti-human FASN antibody (red) as primary antibodies and donkey anti-rabbit AlexaFluor-488 and goat anti-mouse AlexaFluor-594 as secondary antibodies. Images were acquired using  $\times 40$  objectives and  $\times 2.5$  optical zoom, shown as individual channels or merged or 3D-rendered volume. Bar graph representing colocalization as overlap by correlation between PGDH and FASN expression, with error bars representing averages from an analysis of three independent images by ImageJ. **(B)** Schematic representation of cell-free assay experimental design. Shown in black are the reactants supplied in the reaction buffer, and shown in blue are the products. FASN-PGDH double-enzyme reactions were performed with either NADP or NADPH as cofactors. \*\*\* refers to reaction product quantified by mass spectrometry. **(C)** Line graph representing ribulose-5-phosphate quantification (y-axis) by mass spectrometry from PGDH-catalyzed reaction consisting of increasing concentrations of NADP (x-axis). **(D)** Bar graph representing the quantification of ribulose-5-phosphate (y-axis) and comparison of increasing concentrations of NADP-driven PGDH or PGDH+FASN-catalyzed reaction and NADPH-driven PGDH+FASN-catalyzed reactions. The error bars represent the standard deviations of mean and the significant differences between each concentration of NADP-driven PGDH reaction, with NADP- or NADPH-driven PGDH+FASN-catalyzed reaction indicated by an asterisk (\*\*\*)  $p < 0.001$ . **(E)** Diagram representing the allosteric stimulation or inhibitory effects of NADP<sup>+</sup> and NADPH on PGDH and summarizing the impact of FASN inhibition on overall metabolic pools (shaded in red indicating increases or blue indicating decreases) in comparison with metabolic flow in uninhibited cells.

increasing concentrations of cofactor, NADP, and fixed substrate concentration (6PG). The results from mass spectrometry indicate that the stimulation of PGDH activity occurred in the presence of an increased NADP concentration (50–800  $\mu\text{M}$ ), resulting in an increase of ribulose-5-phosphate (R5P) synthesis ( $57 \pm 20$ – $437 \pm 111 \mu\text{M}$ ). Next, we observed that coupling FASN

reaction with NADP-driven PGHD resulted in a significantly increased R5P synthesis at  $256 \pm 68 \mu\text{M}$  ( $P < 0.001$ ), compared to R5P synthesis  $57 \pm 20 \mu\text{M}$  by PGDH alone in the reactions performed using 50  $\mu\text{M}$  NADP (**Figures 6B, D**). Moreover, we observed that FASN presence led to decreasing the  $K_m$  for NADP from 22.1 to 11.5  $\mu\text{M}$  and the acceleration of PGDH

reaction velocity, demonstrating that FASN is exerting a positive influence on PGDH activity. The spectrophotometric monitoring also showed a reduction in the kinetics of NADPH appearance in the presence of FASN (compared to PGDH without FASN) (**Supplementary Figure S4F**). These results together indicate that PGDH activity is stimulated by NADP and that the removal of NADPH in the presence of FASN leads to an accelerated synthesis of R5P by PGDH. Similarly, in FASN–PGDH coupled reactions consisting NADPH, an incremental presence of NADPH resulted in the suppression of R5P synthesis, indicating that NADPH exerts an inhibitory effect on PGDH activity (**Supplementary Figures 6B, D**). In conclusion, FASN enhances PGDH activity *via* the regeneration of allosteric stimulator NADP and reducing the levels of the allosteric inhibitor NADPH (**Figure 6D**). The results observed from these experiments suggest that NADPH accumulation could be biologically responsible for PGDH inactivation in the presence of FASN inhibition (**Figure 5C**). Thus, FASN inhibition and perturbation of PGDH could lead to the accumulation of glycolytic and citric acid cycle intermediates and contributed to nucleotide depletion as observed and summarized in **Figures 3B** and **6E**.

## Onco-Metabolic Implications of Glucose, Nucleotide, and Lipid Metabolism in Lymphoma

The results from *in vitro* metabolic and enzymatic assessments showed FASN and PPP as interrelated metabolic functions linked with nucleotide metabolism. Ample nucleotide supply is necessary for proliferative functions, including for the support of malignant cell proliferation. Therefore, altering nucleotide metabolism is an end-point and major end-point for regulation by oncogenic factors. In this context, we analyzed RNA seq data from  $n = 624$  NHL tumors consisting of genetic mutations ( $n = 361$ ) with unaltered ( $n = 263$ ) TP53, MYC, BCL2, mTOR, MYD88, PIM2, and CREBP and identified differentially expressed metabolic genes (**Figure 7A**). Tumors with mutations ( $n = 361$ ) included 144 tumors with two or more multiple mutations (**Figure 7B**). A total of 116/241 genes were altogether identified as differentially expressed metabolic genes based on significant cutoff ( $P < 0.005$ ) in tumors consisting of mutations in TP53, MYC, BCL2, mTOR, MYD88, PIM2, and CREBP against tumors that are wild type for these genes. The differentially expressed genes represented in the heat map (**Figure 7C**) indicate elevated genes ( $\log_2$  two- to sevenfold) associated with fatty acid, glycolysis, gluconeogenesis, citric acid cycle, ketogenesis, PPP, nucleotide, oxidative phosphorylation, and oxidative stress metabolism (**Figure 7C**).

Alterations in MYD88 and TP53 resulted in the most numbers of metabolic genes being upregulated, 64 and 46, respectively; however, other genetic mutations also yielded similar distributions in the upregulated metabolic gene expression patterns (**Figure 7D**). Furthermore, of 361 tumors with genetic mutations, 144 tumors carried two or more genetic mutations, indicating that the upregulation of metabolic gene expression could be under the influence of multiple oncogenic

mutations in these NHL tumors. Further mapping of elevated genes (red) to corresponding metabolic pathways indicate that >95% of metabolic steps associated with glucose, PPP, lipid, and nucleotide metabolism were increased (**Figure 7D**), but regardless of mutational origins. Interestingly, genes related to oxidative PPP (G6PD, PGLS, and PGDH) were not elevated, but genes relevant to metabolic feeder pathways (glucose and lipid metabolism) and dependent processes (nucleotide metabolism) were found to be elevated in these tumors. These gene expression patterns altogether suggest that the enzymatic modulation of oxidative PPP activity *via* elevated FASN activity could be necessary for influencing PPP and nucleotide biosynthesis in these NHL tumors.

## DISCUSSION

Intracellular nucleotide concentrations fluctuate continuously during cell progression, dictating the overall fate, frequencies, and timings of cell division (32–34). While nucleotide biosynthesis and proliferation are tightly coordinated processes in normal cells, a disproportional increase in nucleotide levels is commonly observed in malignant cells (35). Most importantly, the lack of carrier protein and the presence of negative charges are barriers that require endogenous nucleotide biosynthesis as a metabolic essentiality for sustaining cellular proliferation (36). While *de novo* biosynthesis primarily caters the nucleotide supply for DNA replication, salvage biosynthesis often supports only low-demand functions, such as DNA repair, *etc.* (36). Thus, promotion of *de novo* nucleotide biosynthesis is the landmark and end-point for transcriptional upregulation by various oncogenic factors, including by MYC, RAS, PI3K, AKT, Rb, mTOR, MAPK, NFκB, *etc.* (35, 37). Increased nucleotide metabolism is absolutely necessary for gaining proliferative advantage in malignancy; therefore, malignant cells generally maintain excess (approximately three- to sixfold higher) amounts of nucleotides compared to normal counterparts (38). The correlation between elevated nucleotide metabolism and poor clinical outcome is reported in both hematological and solid tumors (35, 38). Our metabolic and transcriptomic assessments with FASN inhibition demonstrate that NADPH utilization and NADP regeneration by FASN could allow PGDH to remain active and sustain nucleotide biosynthesis. Furthermore, the increased expression of genes relevant to FASN metabolism, glycolysis, citric acid cycle, and nucleotide metabolism, but not of genes associated with oxidative PPP, underscores the presence of FASN as enzymatic necessity for promoting nucleotide metabolism in the tumors.

Lipids are physiologically abundant molecules (free fatty acids, triglycerides, VLDL, LDL, and HDL), and malignant cells are known to utilize and integrate exogenous lipids with greater preference (39). Furthermore, FASN-mediated lipogenesis is an energetically expensive reaction that consumes massive amounts of energy (through seven ATP, 14 NADPH, and eight acetyl-CoA used per molecule of palmitate synthesis) (40). Therefore, *de novo* lipogenesis is a biologically

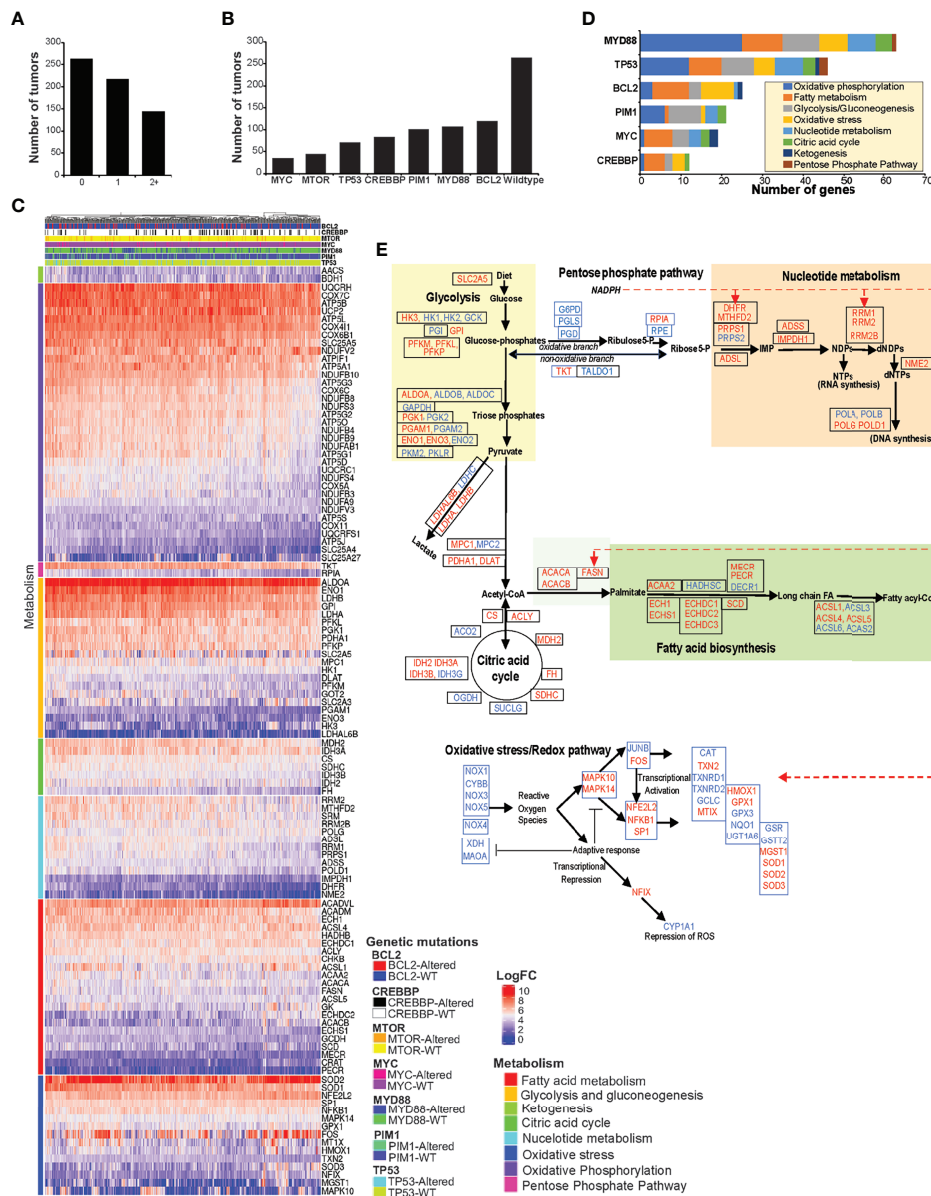


**FIGURE 7 |** DLBCL metabolic transcriptome. **(A, B)** Bar graphs represent the proportion and distribution by number of tumors, consisting of wild-type, single, or multiple mutations in MYC, MTOR, TP53, CREBBP, PIM1, MYD88, and TP53. **(C)** Heat map representing the differential expression of metabolic genes, significant by single-gene mutation with  $P < 0.005$ , comparing tumors that consist of wild-type or mutant MYC, MTOR, TP53, CREBBP, PIM1, MYD88, and TP53 genes ( $n = 624$ ). **(D)** Bar graph representing the number of genes overexpressed by metabolic pathways and distribution by genetic mutations. **(E)** Flow chart representing the mapping of differentially expressed genes corresponding to glucose, pentose phosphate pathway, lipid, and redox metabolic pathways. The upregulated genes are indicated in red color, and the unaffected genes are indicated in blue color. Dashed red lines indicate NADPH-related enzymes.

unfavorable metabolic reaction, an energy competitor which is unbeneficial to malignant cell proliferation. However, in the context of extra-lipogenic function, it has been shown that FASN activity could serve as a positive influencer and metabolic driver of glycolysis and citric acid cycle under hypoxia (9). Similarly, rapid bursts of FASN activity accompanied with increased glucose uptake and metabolism are observed during the proliferative expansion of B and T lymphocytes (41). While in lipogenic tissues *de novo*

lipogenesis could be the primary function of FASN, extra-lipogenic role could be a significant metabolic function of FASN for non-lipogenic tissues.

The results from our experiments demonstrate that extra-lipogenic activity could involve leveraging FASN substrate and co-factor dependency for promoting interlinked metabolic activities. NADP is an allosteric stimulator of PGDH and inhibitor of FASN. Similarly, NADPH is an allosteric stimulator of FASN and inhibitor of PGDH. Thus, NADP and NADPH turnover is reciprocally



beneficial for sustaining FASN and PGDH metabolic activity. Therefore, mitogenic stimulation, triggering *de novo* lipogenic activity as observed in B lymphocytes (41, 42), could be pertinent to diverting glucose carbon *via* PPP and nucleotide biosynthesis for supporting cell proliferation. PPP and nucleotide metabolism is dynamically influenced by the physiological demands. In resting cells, R5P synthesized from PPP is shunted back to glycolysis (43); during oxidative stress and DNA damage, G6PDH-coupled glutathione reaction caters to the supply of nucleotides for DNA repair and NADPH for antioxidant defense (44). G6PDH and PGDH are both rate-limiting PPP metabolic steps subject to allosteric inhibition by NADPH (K<sub>i</sub> for PGDH is ~0.03 and for G6PDH is ~0.017 μM; source: average K<sub>i</sub> values for human enzymes; BRENDA, [www.brenda-enzymes.org](http://www.brenda-enzymes.org)). Interestingly, PGDH exhibits lower K<sub>i</sub> for NADPH compared to G6PDH; thus, PGDH becomes more vulnerable to inhibition by NADPH. Similarly, FASN has remarkably low K<sub>m</sub> for NADPH compared to PPP-dependent antioxidant enzymes (~K<sub>m</sub> values for NADPH: FASN—0.005 μM, GR—0.008 μM, TR—0.088 μM, NQO1—0.24 μM; source: BRENDA, [www.brenda-enzymes.org](http://www.brenda-enzymes.org)). Thus, FASN with low K<sub>m</sub> for NADPH and PGDH with low K<sub>i</sub> NADP could function as ideal enzymatic partners for NADP–NADPH recycling activity. Considering that FASN-inhibition-associated NADPH accumulation inhibits PGDH activity, we conclude that FASN, *via* a NADP–NADPH recycling process, could lead to sustained PGDH activity, as summarized in models shown in **Figure 6E**.

PPP is considered as a central integrator of glucose, nucleotide, lipid, and oxidative stress metabolism (37, 43). Overwhelming evidence indicates that nucleotide metabolism is the end-point for oncogenic functions mediated by MYC, PI3K, NFκB, AP1, c-jun, c-fos, GATA1, FOXO, HOX, E2F, and STAT1 (35, 45). The results from RNA seq data analysis comparing the impact of genetic mutations of TP53, MYD88, MYC, BCL2, PIM1, and CREBBP show that metabolic genes included in nucleotide biosynthesis are upregulated in NHL tumors (**Figure 7**). With FASN upregulation and unapparent effect on oxidative PPP genes, FASN is likely to function as an enzymatic driver of oxidative PPP in lymphoma tumors.

## CONCLUSION

In summary, FASN upregulation, generally ascribed with lipogenic function in malignancy, appears to be necessary for promoting nucleotides in lymphoma. The results from FASN inhibition with cerulenin treatment show the transcriptomic downregulation of nucleotide metabolism and cell cycle processes (**Supplementary Figure S2**) to be correlated with reduced nucleotide biosynthesis, nucleic acid metabolism, and cell cycle impairment (**Figure 4**). Furthermore, impairment of nucleotide biosynthesis caused by NADPH accumulation and interruption of PGDH activity by FASN inhibition resulted in the metabolic accumulations in PPP, while citrate accumulation resulted in the metabolic accumulations within the citric acid cycle and glycolysis (**Figure 3B**). Based on these observations, we conclude that FASN, *via* NADPH and citrate utilization in

palmitic acid biosynthesis, plays a central role in the integration of glucose metabolism with nucleotide biosynthesis. Thus, the results from our experiments and prior reports showing that tumor cells exhibit preferential utilization for extracellular lipids (39) suggest that extralipogenic function should be the primary metabolic dysfunction of FASN in cancer.

The analysis of the NHL transcriptome from *n* = 624 lymphoma patients showing upregulations in the expression of FASN nucleotide metabolic genes, but not with those of oxidative PPP in the presence of lymphomagenic mutations (**Figure 7**), underpins the necessity of FASN to function as a metabolic driver of nucleotide synthesis in cancer. Although targeting FASN impairs the cell cycle (**Figure 4H**), the impact on decreasing nucleotide levels (**Figure 4C**) provides unique opportunities for combining FASN inhibitory drugs with antinucleoside analogs—for example, we observed that combining 5FU with FASN inhibitor in fact resulted in increased apoptotic cell death (**Supplementary Figure S4G**), possibly *via* the robust incorporation of 5FU into the nucleic acid structures. Finally, experiments based on cell-free enzyme assay demonstrating that NADP/NADPH recycling occurs between FASN and PGDH and the resultant increase in the R5P synthesis implicate that PPP is, mechanistically, a FASN-dependent metabolic function (**Figure 6**).

We altogether conclude that FASN PGDH enzymes exhibit metabolic cooperativity and facilitate the flow of glucose carbons through PPP metabolism into the nucleotide biosynthesis in lymphoma.

## DATA AVAILABILITY STATEMENT

The datasets presented in this study can be found in online repositories. The names of the repository/repositories and accession number(s) can be found in the article/**Supplementary Material**.

## ETHICS STATEMENT

The results from the RNA seq of NHL patients were obtained from public datasets previously published and authored by SD. For original investigation, anonymized lymphoma specimens were processed in accordance with protocol approved by the Institutional Review Board at Duke University.

## AUTHOR CONTRIBUTIONS

DR conceptualized the study, conducted experiments, and performed overall research, data analysis, and manuscript writing. AB performed transcriptomic data analysis and manuscript writing. Research interns NA, FP, and PP conducted cell viability assays. MM performed flow cytometry assays. FL and WK provided funding support and performed data analysis and manuscript writing. NM conducted lipid extraction and analysis, and GD provided funding support and performed mass spectrometry lipid assessment, data analysis and

manuscript writing. XS performed mass spectrometry profiling of polar metabolites. RV performed cell-free enzyme assay, and MR provided recombinant FASN and performed the analysis of cell-free enzyme assay data and manuscript review. SD shared RNA seq data, and YC performed bioinformatic analysis. AE provided funding support, designed the research, and performed data analysis and manuscript writing. All authors contributed to the article and approved the submitted version.

## FUNDING

FL, WK, and AE were supported by Our Danny cancer fund. DR, GD, and AE were supported by Tufts Medical Center–Human Nutrition Research Center on Aging pilot fund. NM and GD were supported by the US Department of Agriculture (agreement no. 58-1950-4-401). DR and AE were supported by 3-V Biosciences. The research service of XS was supported by the Metabolomics shared resource of Rutgers Cancer Institute of New Jersey (P30CA072720). BK was supported by NIH/NIAID R01 AI150451 and AI136581. The research service of YC was generated by Biomedical Informatics shared resource of Rutgers Cancer Institute of New Jersey, supported, in part, with funding from NCI-CCSG P30CA072720-5917. 3-V Biosciences was not involved in the study design, collection, analysis, interpretation of data, the writing of this article, or the decision to submit it for publication.

## SUPPLEMENTARY MATERIAL

The Supplementary Material for this article can be found online at: <https://www.frontiersin.org/articles/10.3389/fonc.2021.725137/full#supplementary-material>

**Supplementary Figure S1** | Identification of differentially expressed genes by transcriptomic profiling with FASN inhibitors in bNHL cells. Hierarchical clustering of genes and Euclidean distance calculation for 48 hours of 12.5  $\mu$ M cerulenin treatment on (A) SUDHL2 cells with One-Way ANOVA, FDR < 0.1 (141 genes), (B) SUDHL10 cells with LIMMA analysis, FDR < 0.05 (1600 genes) (C) SUDHL4 cells with One-Way ANOVA, FDR < 0.05 (242 genes), (D) Raji cells with LIMMA analysis, FDR < 0.05 (1092 genes). (E) Hierarchical clustering of genes and Euclidean distance calculation for 48 hours of TVB3166 or 3657 in SUDHL2, SUDHL10 and Raji cells with One-Way ANOVA, FDR < 0.05 (8872 genes). (F) Principal component analysis plot of TVB3166 or TVB3567 treated bNHL cells show global differences between the experimental conditions and the untreated controls for SUDHL2,

SUDHL10 and Raji cells. (G) Scatter plot represents fold changes in the gene expression from the transcriptome of TVB3166 or 3657 or cerulenin treated bNHL cells (no significant difference were detected in the gene expression pattern with cerulenin treatment performed in the presence of 1% or 10% serum containing medium, data not shown), with whiskers showing the range of the outliers, with max and min values as O and the 1 and 99th percentile outliers as X. Individual data points are shown on the left of box plots as filled circles. Dotted red lines show the 1.2 log2 fold-change cutoff.

**Supplementary Figure S2–S3** | GSEA analysis of global biological responses to FASN inhibition. Network representation of Gene Set Enrichment Analysis (GSEA) for Reactome gene sets for (A) cerulenin or (B) and S3 for TVB3166 or TVB3567 treatment, 48 hours versus untreated control bNHL cells, SUDHL2, SUDHL4, SUDHL10 and Raji cells. Leading edge analysis with a FDR < 0.05 determined significant gene sets enriched for each group. The size of each node reflects the amounts of genes involved for each gene set. The edge thickness (green lines) represents the number of genes associated with the overlap of two gene sets (or nodes) that the edge connects. Clusters in each grouping were named according to common functions. Upregulated gene sets denoted with red color and downregulated gene sets were denoted by blue color.

**Supplementary Figure S4** | Metabolic and key gene responses to cerulenin treatment in bNHL cells. (A) Line graphs represents spectrophotometric detection of NADPH appearance (y-axis) as rate of change in OD (optical density at 340nm wavelength from cell-free enzyme assays consisting increasing concentrations of NADP (x-axis) comparing PGDH alone or PGDH+FASN catalyzed reactions. (B) Lineweaver-Burk plot represents PGDH reaction velocity in the presence of increasing NADP concentration, and the effect of coupling this reaction with FASN enzymatic activity. (C) Key significant genes and network analysis identified from transcriptomic analysis of cerulenin treated with SUDHL10 cells reveal interactions occurring between G6PDH (NADPH generating PPP, rate-limiting enzyme from first step) and NADPH dependent enzymes GSR, TXNRD1 and NQO1 with FASN inhibition. (D) Schematic representation of pentose phosphate pathway steps associated with NADPH generation. (E) Bar graphs represents log fold change (y-axis) in G6PDH, GSR, TXNRD1, NQO1 genes expression induced by cerulenin treatment in multiple bNHL cells (x-axis). (F) Western blot analysis show changes in protein levels associated with key gene responses to cerulenin treatment in NHL cells. (G) Annexin-V staining for apoptosis and analysis by flow cytometry show that cerulenin and 5FU combination results in increased cell death compared to single agent treatments in SUDHL10 cells at 96 hours.

**Supplementary Table S1** | Pathway enrichment by multi-omic analysis comparing cerulenin transcriptome and metabolome. List of pathways determined using significant genes and metabolites from cerulenin treated SUDHL10 cells analyzed based on pathway centrality and degree of enrichment for determination of high impact pathways shown in Figure 2E, is included in this table. Impact scores, FDR, P values, number of molecules and hits are included in this table.

**Supplementary Table S2** | Concentration of nucleotide pools in cerulenin treated bNHL cells. Quantitative mass spectrometry analysis of cerulenin treated bNHL cells, normalized per million cells, represented in  $\mu$ M or \*ion counts.

## REFERENCES

- Yoshii Y, Furukawa T, Saga T, Fujibayashi Y. Acetate/acetyl-CoA Metabolism Associated With Cancer Fatty Acid Synthesis: Overview and Application. *Cancer Lett* (2015) 356:211–6. doi: 10.1016/j.canlet.2014.02.019
- Mashima T, Seimiya H, Tsuruo T. De Novo Fatty-Acid Synthesis and Related Pathways as Molecular Targets for Cancer Therapy. *Br J Cancer* (2009) 100:1369–72. doi: 10.1038/sj.bjc.6605007
- Rodwell V, Bender D, Botham K, Kennelly P, Weil P. *Harper's Illustrated Biochemistry*. (2018).
- Frey RS, Gao X, Javadi K, Siddiqui SS, Rahman A, Malik AB. Phosphatidylinositol 3-Kinase Gamma Signaling Through Protein Kinase C $\zeta$  Induces NADPH Oxidase-Mediated Oxidant Generation and NF- $\kappa$ B Activation in Endothelial Cells. *J Biol Chem* (2006) 281:16128–38. doi: 10.1074/jbc.M508810200
- Kuhajda FP. Fatty Acid Synthase and Cancer: New Application of an Old Pathway. *Cancer Res* (2006) 66:5977–80. doi: 10.1158/0008-5472.CAN-05-4673
- Flavin R, Peluso S, Nguyen PL, Loda M. Fatty Acid Synthase as a Potential Therapeutic Target in Cancer. *Future Oncol* (2010) 6:551–62. doi: 10.2217/fon.10.11
- Flaumenhaft R, Sim DS. Protein Palmitoylation in Signal Transduction of Hematopoietic Cells. *Hematology* (2005) 10:511–9. doi: 10.1080/10245330500141507
- Fragoso R, Ren D, Zhang X, Su MW, Burakoff SJ, Jin YJ. Lipid Raft Distribution of CD4 Depends on its Palmitoylation and Association With Lck, and Evidence for CD4-Induced Lipid Raft Aggregation as an Additional

- Mechanism to Enhance CD3 Signaling. *J Immunol* (2003) 170:913–21. doi: 10.4049/jimmunol.170.2.913
9. Menendez JA, Lupu R. Fatty Acid Synthase and the Lipogenic Phenotype in Cancer Pathogenesis. *Nat Rev Cancer* (2007) 7:763–77. doi: 10.1038/nrc2222
  10. Zhang J, Grubor V, Love CL, Banerjee A, Richards KL, Mieczkowski PA, et al. Genetic Heterogeneity of Diffuse Large B-Cell Lymphoma. *Proc Natl Acad Sci USA* (2013) 110:1398–403. doi: 10.1073/pnas.1205299110
  11. Danilova OV, Dumont LJ, Levy NB, Lansigan F, Kinlaw WB, Danilov AV, et al. FASN and CD36 Predict Survival in Rituximab-Treated Diffuse Large B-Cell Lymphoma. *J Hematop* (2013) 6:11–8. doi: 10.1007/s12308-012-0166-4
  12. Nowakowski GS, Czuczman MS. ABC, GCB, and Double-Hit Diffuse Large B-Cell Lymphoma: Does Subtype Make a Difference in Therapy Selection? *Am Soc Clin Oncol Educ Book* (2015), e449–57. doi: 10.14694/EdBook\_AM.2015.35.e449
  13. Baudino TA. Targeted Cancer Therapy: The Next Generation of Cancer Treatment. *Curr Drug Discovery Technol* (2015) 12:3–20. doi: 10.2174/1570163812666150602144310
  14. Funabashi H, Kawaguchi A, Tomoda H, Omura S, Okuda S, Iwasaki S. Binding Site of Cerulenin in Fatty Acid Synthetase. *J Biochem* (1989) 105:751–5. doi: 10.1093/oxfordjournals.jbchem.a122739
  15. Ventura R, Mordec K, Waszczuk J, Wang Z, Lai J, Fridlib M, et al. Inhibition of *De Novo* Palmitate Synthesis by Fatty Acid Synthase Induces Apoptosis in Tumor Cells by Remodeling Cell Membranes, Inhibiting Signaling Pathways, and Reprogramming Gene Expression. *EBioMedicine* (2015) 2:808–24. doi: 10.1016/j.ebiom.2015.06.020
  16. Heuer TS, Ventura R, Mordec K, Lai J, Fridlib M, Buckley D, et al. FASN Inhibition and Taxane Treatment Combine to Enhance Anti-Tumor Efficacy in Diverse Xenograft Tumor Models Through Disruption of Tubulin Palmitoylation and Microtubule Organization and FASN Inhibition-Mediated Effects on Oncogenic Signaling and Gene Expression. *EBioMedicine* (2017) 16:51–62. doi: 10.1016/j.ebiom.2016.12.012
  17. Ravi D, Beheshti A, Abermil N, Passero F, Sharma J, Coyle M, et al. Proteasomal Inhibition by Ixazomib Induces CHK1 and MYC-Dependent Cell Death in T-Cell and Hodgkin Lymphoma. *Cancer Res* (2016) 76:3319–31. doi: 10.1158/0008-5472.CAN-15-2477
  18. Beheshti A, Neuberger D, McDonald JT, Vanderburg CR, Evens AM. The Impact of Age and Sex in DLBCL: Systems Biology Analyses Identify Distinct Molecular Changes and Signaling Networks. *Cancer Inform* (2015) 14:141–8. doi: 10.4137/CIN.S34144
  19. Beheshti A, Wage J, McDonald JT, Lamont C, Peluso M, Hahnfeldt P, et al. Tumor-Host Signaling Interaction Reveals a Systemic, Age-Dependent Splenic Immune Influence on Tumor Development. *Oncotarget* (2015) 6:35419–32. doi: 10.18632/oncotarget.6214
  20. Reddy A, Zhang J, Davis NS, Moffitt AB, Love CL, Waldrop A, et al. Genetic and Functional Drivers of Diffuse Large B Cell Lymphoma. *Cell* (2017) 171:481–94 e15. doi: 10.1016/j.cell.2017.09.027
  21. Gu Z, Eils R, Schlesner M. Complex Heatmaps Reveal Patterns and Correlations in Multidimensional Genomic Data. *Bioinformatics* (2016) 32:2847–9. doi: 10.1093/bioinformatics/btw313
  22. Folch J, Lees M, Sloane Stanley GH. A Simple Method for the Isolation and Purification of Total Lipides From Animal Tissues. *J Biol Chem* (1957) 226:497–509. doi: 10.1016/S0021-9258(18)64849-5
  23. Morrison WR, Smith LM. Preparation of Fatty Acid Methyl Esters and Dimethylacetals From Lipids With Boron Fluoride–Methanol. *J Lipid Res* (1964) 5:600–8. doi: 10.1016/S0022-2275(20)40190-7
  24. Melamud E, Vastag L, Rabinowitz JD. Metabolomic Analysis and Visualization Engine for LC-MS Data. *Anal Chem* (2010) 82:9818–26. doi: 10.1021/ac1021166
  25. Su X, Lu W, Rabinowitz JD. Metabolite Spectral Accuracy on Orbitraps. *Anal Chem* (2017) 89:5940–8. doi: 10.1021/acs.analchem.7b00396
  26. Chong J, Soufan O, Li C, Caraus I, Li S, Bourque G, et al. MetaboAnalyst 4.0: Towards More Transparent and Integrative Metabolomics Analysis. *Nucleic Acids Res* (2018) 46:W486–94. doi: 10.1093/nar/gky310
  27. Xia J, Sinelnikov IV, Han B, Wishart DS. MetaboAnalyst 3.0–Making Metabolomics More Meaningful. *Nucleic Acids Res* (2015) 43:W251–7. doi: 10.1093/nar/gkv380
  28. Diamond TL, Roshal M, Jamburuthugoda VK, Reynolds HM, Merriam AR, Lee KY, et al. Macrophage Tropism of HIV-1 Depends on Efficient Cellular dNTP Utilization by Reverse Transcriptase. *J Biol Chem* (2004) 279:51545–53. doi: 10.1074/jbc.M408573200
  29. Bolte S, Cordelieres FP. A Guided Tour Into Subcellular Colocalization Analysis in Light Microscopy. *J Microsc* (2006) 224:213–32. doi: 10.1111/j.1365-2818.2006.01706.x
  30. Rudolph MC, Karl Maluf N, Wellberg EA, Johnson CA, Murphy RC, Anderson SM. Mammalian Fatty Acid Synthase Activity From Crude Tissue Lysates Tracing (1)(3)C-Labeled Substrates Using Gas Chromatography-Mass Spectrometry. *Anal Biochem* (2012) 428:158–66. doi: 10.1016/j.ab.2012.06.013
  31. Joshi AK, Rangan VS, Smith S. Differential Affinity Labeling of the Two Subunits of the Homodimeric Animal Fatty Acid Synthase Allows Isolation of Heterodimers Consisting of Subunits That Have Been Independently Modified. *J Biol Chem* (1998) 273:4937–43. doi: 10.1074/jbc.273.9.4937
  32. Fornalewicz K, Wiecek A, Wegrzyn G, Lyzen R. Silencing of the Pentose Phosphate Pathway Genes Influences DNA Replication in Human Fibroblasts. *Gene* (2017) 635:33–8. doi: 10.1016/j.gene.2017.09.005
  33. Jing X, Wang XJ, Zhang T, Zhu W, Fang Y, Wu H, et al. Cell-Cycle-Dependent Phosphorylation of PRPS1 Fuels Nucleotide Synthesis and Promotes Tumorigenesis. *Cancer Res* (2019) 79:4650–64. doi: 10.1158/0008-5472.CAN-18-2486
  34. Vizan P, Alcarraz-Vizan G, Diaz-Moralli S, Solovjeva ON, Frederiks WM, Cascante M. Modulation of Pentose Phosphate Pathway During Cell Cycle Progression in Human Colon Adenocarcinoma Cell Line HT29. *Int J Cancer* (2009) 124:2789–96. doi: 10.1002/ijc.24262
  35. Villa E, Ali ES, Sahu U, Ben-Sahra I. Cancer Cells Tune the Signaling Pathways to Empower *De Novo* Synthesis of Nucleotides. *Cancers (Basel)* (2019) 11. doi: 10.3390/cancers11050688
  36. Diab R, Degobert G, Hamoudeh M, Dumontet C, Fessi H. Nucleoside Analogue Delivery Systems in Cancer Therapy. *Expert Opin Drug Deliv* (2007) 4:513–31. doi: 10.1517/17425247.4.5.513
  37. Patra KC, Hay N. The Pentose Phosphate Pathway and Cancer. *Trends Biochem Sci* (2014) 39:347–54. doi: 10.1016/j.tibs.2014.06.005
  38. Traut TW. Physiological Concentrations of Purines and Pyrimidines. *Mol Cell Biochem* (1994) 140:1–22. doi: 10.1007/BF00928361
  39. Louie SM, Roberts LS, Mulvihill MM, Luo K, Nomura DK. Cancer Cells Incorporate and Remodel Exogenous Palmitate Into Structural and Oncogenic Signaling Lipids. *Biochim Biophys Acta* (2013) 1831:1566–72. doi: 10.1016/j.bbalip.2013.07.008
  40. Meisenberg G, Simmons WH. *Principles of Medical Biochemistry* Vol. xii. Philadelphia, PA: Elsevier (2017). p. 617.
  41. Dufort FJ, Gumina MR, Ta NL, Tao Y, Heyse SA, Scott DA, et al. Glucose-Dependent *De Novo* Lipogenesis in B Lymphocytes: A Requirement for Atp-Citrate Lyase in Lipopolysaccharide-Induced Differentiation. *J Biol Chem* (2014) 289:7011–24. doi: 10.1074/jbc.M114.551051
  42. Reitzer LJ, Hele BM, Kennell D. The Pentose Cycle. Control and Essential Function in HeLa Cell Nucleic Acid Synthesis. *J Biol Chem* (1980) 255:5616–26. doi: 10.1016/S0021-9258(19)70674-7
  43. Stincone A, Prigione A, Cramer T, Wamelink MM, Campbell K, Cheung E, et al. The Return of Metabolism: Biochemistry and Physiology of the Pentose Phosphate Pathway. *Biol Rev Camb Philos Soc* (2015) 90:927–63. doi: 10.1111/brv.12140
  44. Roth EF Jr, Ruprecht RM, Schulman S, Vanderberg J, Olson JA. Ribose Metabolism and Nucleic Acid Synthesis in Normal and Glucose-6-Phosphate Dehydrogenase-Deficient Human Erythrocytes Infected With Plasmodium Falciparum. *J Clin Invest* (1986) 77:1129–35. doi: 10.1172/JCI112412
  45. Lane AN, Fan TW. Regulation of Mammalian Nucleotide Metabolism and Biosynthesis. *Nucleic Acids Res* (2015) 43:2466–85. doi: 10.1093/nar/gkv047

**Author Disclaimer:** Any opinions, findings, conclusions or recommendations expressed in this publication are those of the authors and do not necessarily reflect the view of the U S Department of Agriculture.

**Conflict of Interest:** AE: Advisory board (with honorarium): Bayer, Seattle Genetics, Affimed, Verastem, Pharmacyclics, Research to Practice, and Physician Education Resource. Research support: Takeda, Seattle Genetics, Merck, NIH/ NCI, Leukemia and Lymphoma Society, and ORIEN.

The remaining authors declare that the research was conducted in the absence of any commercial or financial relationships that could be construed as a potential conflict of interest.

**Publisher's Note:** All claims expressed in this article are solely those of the authors and do not necessarily represent those of their affiliated organizations, or those of the publisher, the editors and the reviewers. Any product that may be evaluated in this article, or claim that may be made by its manufacturer, is not guaranteed or endorsed by the publisher.

*Copyright © 2021 Ravi, Beheshti, Abermil, Lansigan, Kinlaw, Matthan, Mokhtar, Passero, Puliti, David, Dolnikowski, Su, Chen, Bijan, Varshney, Kim, Dave, Rudolph and Evens. This is an open-access article distributed under the terms of the Creative Commons Attribution License (CC BY). The use, distribution or reproduction in other forums is permitted, provided the original author(s) and the copyright owner(s) are credited and that the original publication in this journal is cited, in accordance with accepted academic practice. No use, distribution or reproduction is permitted which does not comply with these terms.*





# Metabolic Reprogramming of Thyroid Cancer Cells and Crosstalk in Their Microenvironment

Lisha Bao<sup>1,2,3</sup>, Tong Xu<sup>4</sup>, Xixuan Lu<sup>2,3</sup>, Ping Huang<sup>3,4</sup>, Zongfu Pan<sup>3,4\*</sup> and Minghua Ge<sup>2,3\*</sup>

<sup>1</sup> Second Clinical College, Zhejiang Chinese Medical School, Hangzhou, China, <sup>2</sup> ENT-Head & Neck Surgery Center, Department of Head and Neck Surgery, Zhejiang Provincial People's Hospital, Affiliated People's Hospital, Hangzhou Medical College, Hangzhou, China, <sup>3</sup> Key Laboratory of Endocrine Gland Diseases of Zhejiang Province, Zhejiang Provincial People's Hospital, Hangzhou, China, <sup>4</sup> Clinical Pharmacy Center, Department of Pharmacy, Zhejiang Provincial People's Hospital, Affiliated People's Hospital, Hangzhou Medical College, Hangzhou, China

## OPEN ACCESS

### Edited by:

Miriam Martini,  
University of Turin, Italy

### Reviewed by:

Jaroslav Truksa,  
Institute of Biotechnology  
(ASCR), Czechia  
Huakan Zhao,  
Chongqing University, China

### \*Correspondence:

Zongfu Pan  
panzongfu@hmc.edu.cn  
Minghua Ge  
geminghua@hmc.edu.cn

### Specialty section:

This article was submitted to  
Cancer Metabolism,  
a section of the journal  
Frontiers in Oncology

**Received:** 09 September 2021

**Accepted:** 05 November 2021

**Published:** 02 December 2021

### Citation:

Bao L, Xu T, Lu X, Huang P, Pan Z  
and Ge M (2021) Metabolic  
Reprogramming of Thyroid  
Cancer Cells and Crosstalk  
in Their Microenvironment.  
Front. Oncol. 11:773028.  
doi: 10.3389/fonc.2021.773028

Metabolism differs significantly between tumor and normal cells. Metabolic reprogramming in cancer cells and metabolic interplay in the tumor microenvironment (TME) are important for tumor formation and progression. Tumor cells show changes in both catabolism and anabolism. Altered aerobic glycolysis, known as the Warburg effect, is a well-recognized characteristic of tumor cell energy metabolism. Compared with normal cells, tumor cells consume more glucose and glutamine. The enhanced anabolism in tumor cells includes *de novo* lipid synthesis as well as protein and nucleic acid synthesis. Although these forms of energy supply are uneconomical, they are required for the functioning of cancer cells, including those in thyroid cancer (TC). Increasing attention has recently focused on alterations of the TME. Understanding the metabolic changes governing the intricate relationship between TC cells and the TME may provide novel ideas for the treatment of TC.

**Keywords:** metabolic reprogramming, thyroid cancer, microenvironment, metabolic interplay, Warburg effect

## INTRODUCTION

Thyroid cancer (TC) remains the most frequently diagnosed endocrine malignancy; with a sharp increase in incidence worldwide, this disease is projected to become the fourth leading type of cancer globally (1). Based on its histological features, TC is grouped into four types: papillary thyroid carcinoma (PTC), follicular thyroid carcinoma (FTC), medullary thyroid cancer (MTC), and anaplastic thyroid carcinoma (ATC). Approximately 90% of all TCs are differentiated, including PTC, which is the most common histological type of differentiated thyroid cancer, followed by FTC (2). Notably, different TC subtypes exhibit distinct tumor aggressiveness and progression and show heterogeneous responses to different treatments (3). Although well-differentiated TCs have good prognoses, approximately 10% of patients do not respond to radioactive iodine therapy and are more likely to relapse. While the incidence of poorly differentiated TCs such as ATC and MTC is very low, they are characterized by high invasiveness, early metastasis, and poor prognosis (4, 5). Conventional therapy consists of surgery, radiotherapy, and endocrine suppression treatment (6, 7). However, these treatments have various limitations and side effects (8, 9).

The large differences in metabolism between tumor cells and normal human somatic cells are mainly reflected in catabolic and biosynthesis metabolism (10). The metabolic changes in tumor cells are often considered to be closely related to tumor formation and progression (11). Thus, the unique metabolism of tumor cells is both an opportunity and a challenge. Here, we review the catabolic and anabolic metabolism changes in TC cells. We also describe the mutual relationship between metabolic reprogramming and the tumor microenvironment (TME) in TC, which provides the theoretical basis for new therapeutic targets and prognostic indicators.

## METABOLIC CHANGES IN TUMOR CELLS

Cancer cells always acquire energy and material basis for rapid tumor growth by enhanced anabolism, including rapid aerobic glycolysis, glutaminolysis, *de novo* lipid synthesis and nucleotide synthesis (12, 13). Thyroid cancer cells generate energy primarily by increasing glycolysis and glutaminolysis. In addition, the production of glycolysis can also provide materials for nucleic acid synthesis through pentose phosphate pathway (PPP). Nucleic acid synthesis, protein synthesis, and *de novo* lipid synthesis are enhanced to support thyroid cancer cell proliferation. During metastasis, tumor cells rely on catabolism to survive from metabolic stress, mainly through aerobic glycolysis, OXPHOS, glutamine metabolism and autophagy to produce ATP (14). Thyroid tumors acquired aggressive phenotype and epithelial-mesenchymal transformation (EMT) *via* sirtuin 6 (SIRT6)-Autophagy-Warburg Effect Axis (15). AMPK signal is also essential for activating adaptive changes

in cell metabolism such as inhibiting anabolism and promoting catabolism, which is the basis for cell survival under metabolic stress. In TC, AMPK activation inhibits TC cell proliferation and promotes cell migration (16). Moreover, carnitine palmitoyltransferase 1C which is regulated by AMPK, transfers long-chain fatty acids into mitochondria to further oxidation and promotes TC cells survival under metabolic stress conditions (17).

## Changes in Catabolism

### Glucose Metabolism

Cells produce ATP for energy in two main ways: glycolysis and oxidative phosphorylation (OXPHOS). To satisfy the need of energy for proliferation, thyroid tumor cells increased the level of glycolysis. Although aerobic glycolysis is inefficient compared to OXPHOS, it can provide energy for tumor cell proliferation and invasion and a constant supply of material for biosynthesis (18). The Warburg effect suggests that tumor cells require more glucose than normal cells and derive their energy mainly from glycolysis even when oxygenated adequately (19). However, the energy sources of different tumors also show heterogeneity, and even different areas of the same tumor have different energy sources (20–22). It is noteworthy that glycolysis plays a more important role in sustaining the balance of the PPP in thyroid cells, which is more critical for thyroid hormone synthesis than ATP production even in TC (23) (Figure 1).

Hypoxia-inducible factor (HIF) is a transcription factor that is widespread in mammals and humans under hypoxic conditions. HIF plays roles in glycolysis, promote angiogenesis, cell survival or apoptosis. As the basic regulator of glycolysis, HIF can upregulate the activity of 90% of glycolytic reactivity enzymes and inhibit the

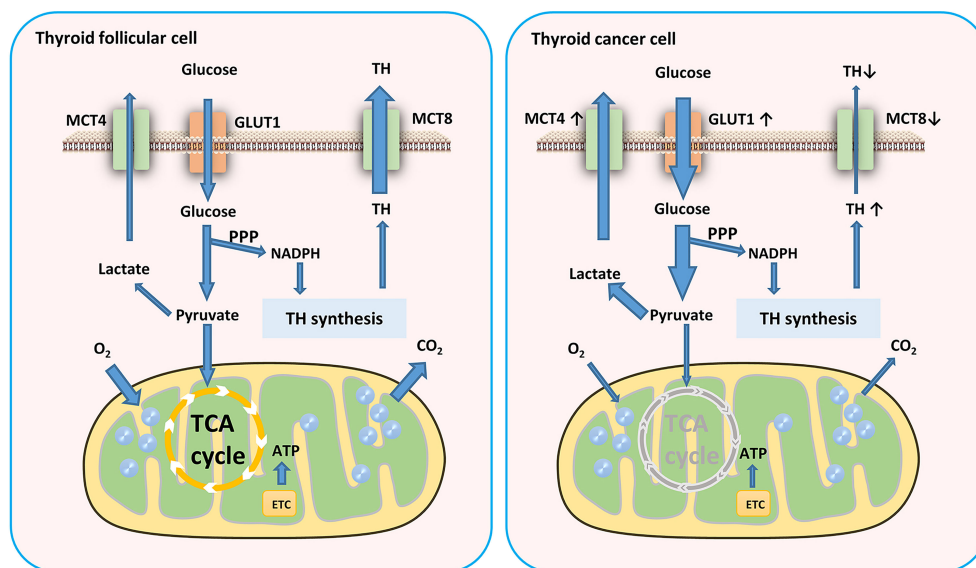


**FIGURE 1** | Glucose metabolism in TC cells. TC cells require more glucose than normal cells and derive their energy mainly from glycolysis. This aerobic glycolytic phenotype generates more lactates which transported by MCT4. MCT8 downregulation in TC cells results in TH accumulation in TC tissues. GLUT, glucose transporter; TH, thyroid hormones; ETC, electron transport chain; MCT, monocarboxylate transporter.

use of pyruvate by mitochondria (24). In TC cells, aerobic glycolysis can be enhanced through the alteration of the HIF1 $\alpha$ -MYC-PGC-1 $\beta$  axis (25). Zhou et al. showed that hypoxia promoted FTC progression by upregulating HIF1 $\alpha$  and programmed death-ligand 1 (PD-L1) (26). In PTC, SIRT6 promotes the EMT of cancer cells through HIF-1 $\alpha$  (27). Klaus et al. demonstrated the critical role of HIF-1 $\alpha$  in the desmoplastic stroma reaction and metastatic processes in FTC (28). HIF can stimulate the expression of MYC, a transcription factor that is highly expressed in tumors and has a variety of biological functions, including cell metabolism. MYC can promote glycolysis and glucose transporter (GLUT) expression, thus transforming tumor energy metabolism into the Warburg effect (29–31). Myc overexpression can also lead to abnormally increased synthesis of lactate dehydrogenase A (LDHA), which catalyzes pyruvate to lactate. Compared to normal thyroid tissues, LDHA expression is higher in PTC. Hou et al. reported that LDHA not only promoted PTC tumorigenesis but also migration and invasion by regulating autophagy and inducing EMT gene transcription. Moreover, they also found that the metabolic products catalyzed by LDHA increased the acetylation of the related H3K27 and induced EMT (32). LDHA is phosphorylated by HER2 and SRC39, resulting in the increased invasive and metastatic potential of head and neck cancer (33).

GLUT is a transporter that helps cells to take up glucose and is the first rate-limiting step in glucose metabolism. Many studies have demonstrated the upregulation of GLUT subtypes during carcinogenesis (34–36). Samih et al. reported that the phosphoinositide 3-kinase (PI3K)/Akt pathway is the key to GLUT1 transfer from the cytoplasm to the plasma membrane (37). GLUT1 overexpression is also associated with cancer cell aggressiveness and dedifferentiation. Mediated by the transcription factor HIF, GLUT3 is upregulated in response to hypoxia. The overexpression of GLUT1 and GLUT3 is generally recognized as one of the characteristics of tumors (38). Józwiak et al. reported that most PTC samples showed higher GLUT1 and GLUT3 expression than the expression in FTC and non-neoplastic thyroid lesions (39). Chai et al. analyzed the expression of GLUT family genes and concluded that the upregulation of the genes encoding GLUT1, GLUT3, GLUT14 was associated with decreased overall survival in patients with PTC (40). The function and tissue distribution of GLUT14 are uncharacterized, although there is some disease association, specifically in inflammatory bowel disease. GLUT14 is a GLUT3 variant that has also been found in the genome as a duplicon of GLUT3. Moreover, the upregulation of GLUT14 was associated with the maintenance of glucose uptake in hypoxia (41). The localization of GLUT1 is heterogeneous among TCs. For example, it exhibits a focal circumferential form in plasma membrane of PTC cells, shows a non-symmetric distribution in the basilar membrane of tumor cells adjacent to the capillary blood supply and stroma, and focal distribution in the center of metastatic tumors or ATC (42). Previous studies indicated that GLUT1 and GLUT3 expression levels may be associated with increased invasion and a worse prognosis of TC. Glucose transported by GLUT involved in glycolysis, the products of which eventually enter the mitochondria to generate ATP for cell

energy through OXPHOS. The mitochondrial pyruvate carrier 1 (MPC1) is a critical channel that connects glycolysis to OXPHOS by regulating the transport of pyruvate into the mitochondrial inner membrane. MPC1 deficiency may cause metabolic reprogramming and is associated with a poor prognosis. MPC1 expression is strongly negatively correlated with tumor purity and immune cell infiltration in TC (43).

Many enzymes are involved in the aerobic glycolysis of tumor cells, including pyruvate kinase M2 (PKM2), hexokinase (HK), phosphofructokinase 1 (PFK1). The PI3K/Akt pathway can enhance the Warburg effect of tumors by increasing the activity of these factors (44). HK is the first rate-limiting enzyme in glycolysis and catalyzes the phosphorylation of glucose into glucose 6-phosphate. HK2 is also highly expressed in TC (45, 46). Huang et al. demonstrated the promotion of thyroid carcinoma cell proliferation and migration through the activation of AKT/mTOR/HK2-mediated glycolysis (47). Feng et al. reported that PKM2 overexpression in PTC was related to poor clinicopathological features such as advanced tumor stages and lymph node metastasis (48). In their proteomic analysis of five PTC specimens, Aurélie Strickaert et al. investigated the cellular distribution of several upregulated metabolic proteins in the cancerous and stromal cells of these tumors. They discovered the upregulation of many metabolism-related proteins including pyruvate carboxylase (PC) (49). Verhagen et al. compared PK in human thyroid carcinomas, follicular adenomas, and normal thyroid tissue and reported a positive correlation between the specific activities of PK and tumor proliferation (50). The results of these studies demonstrated that PK overexpression plays an important role in TC.

## Amino Acid Metabolism

Glutamine is a nonessential amino acid in normal cells and can be converted from glucose. However, tumor cells cannot grow in a culture medium without glutamine; thus, glutamine is an essential amino acid in these cells (51). Ample evidence supports the essential role of glutamine in tumors. Tumor cells consume large amounts of glutamine as an alternative energy supply pathway to glycolysis (52–54). However, the requirements for glutamine in cancer vary in different tissues and situations (55) (Table 1). Several studies demonstrated the changes in glutamine metabolism of thyroid tumors. Inhibition of glutamine metabolism in TC cells results in insufficient energy supply, which inhibits cell proliferation, migration, and invasion (56). Kim et al. performed tissue microarrays of 557 TC cases and immunohistochemical staining of glutaminolysis-related proteins. They reported that glutaminase 1 (GLS1) and glutamate dehydrogenase (GDH) showed the highest expression in ATC compared to other subtypes. Tumoral amino acid transporter-2 expression was higher in MTC but lower in FTC. In PTC, the expression levels of tumoral GLS1 and GDH were higher in the conventional type than those in the follicular variant, and in the BRAF<sup>V600E</sup> mutation than those in cases without the BRAF<sup>V600E</sup> mutation (57). The expression levels of glutaminolysis-related proteins including GLS1, GDH, and GLUD were higher in Hürthle cell neoplasm of the thyroid than in those of follicular neoplasm. The expression of SLC1A5 was highest in Hürthle cell adenomas, followed by FC and FA (58). When glutamine enters the

**TABLE 1 |** The metabolic differences and similarities in cancers.

Metabolic pathways	Tumor types	Difference	Similarity
<b>Glycolysis metabolism</b>	Thyroid cancer	Produce NADPH through the PPP pathway for thyroid hormone synthesis, ATP production (17)	Enhancement of glycolysis and lactate production
	Other cancers	Mainly used for ATP production (13)	
<b>Energy source</b>	Primary thyroid cancer	Glucose and glutamine metabolism(186)	Increased energy demand
	Metastatic thyroid cancer	Unknown	
	Primary breast cancer	Glucose and glutamine metabolism (15)	
	Metastatic breast cancer	Pyruvate (lung metastases) to sustain the TCA cycle (15)	
	Non-small cell lung cancer	Serine and acetate (brain metastases) to sustain the TCA cycle (16) Carbon source: glucose (areas with low perfusion); glucose and other sources (highly perfused areas) (14)	
<b>Lipid metabolism</b>	Thyroid cancer	Low correlation between MUFAs and MUPCs or monosaturated and polyunsaturated lipids (85) ACC2 downregulation (83)	Enhancement of de novo lipid synthesis
	Breast, lung, colorectal, esophageal and gastric cancer	Highly positive correlation between MUFAs and MUPCs negative correlation between monosaturated and polyunsaturated lipids (85)	
	liver, breast and prostate	ACC upregulation (82)	

cell, it is hydrolyzed to glutamic acid and ammonia by glutaminase. Glutamate can be converted into  $\alpha$ -KG to enter the tricarboxylic acid (TCA) cycle, providing intermediate metabolites and energy for cell metabolism. This is particularly evident in the truncated TCA cycle, which can be used as feedstock for the passive TCA cycle due to the lack of citrate (44). This phenomenon, termed anapleurosis, suggests that the use of glutamine affects glucose absorption. Therefore, reducing the use of glutamine can also reduce that of glucose (59). In general, glucose and glutamine metabolism influence each other. Other changes in protein metabolism are present besides glutamine. Sun et al. analyzed 557 different types of TC and found a higher expression level of serine/glycine metabolism-related proteins in PDC and PTC compared to that in MTC. In PTC, the rate of expression was higher in cases with BRAF<sup>V600E</sup> mutation than in those with a follicular variant (60).

## Changes in Biosynthesis Metabolism

### Enhancement of De Novo Lipid Synthesis

Compared to normal tissue, tumor cells synthesize lipids more rapidly and from different sources. Accumulating evidence has demonstrated the important role of lipid metabolism reprogramming in tumor cell development and metastasis (61–67). Liao et al. reported that lysine methyltransferase 5A (KMT5A), a regulator of lipid metabolism in PTC, was significantly associated with extrathyroidal extension and lymph node metastasis in PTC (68). Instead of nutrient uptake, the raw materials of lipid synthesis in tumor cells mainly come from glucose metabolism. Approximately 93% of the fatty acids in tumor cells are synthesized *de novo* (69, 70). The enzymes involved in the fatty acid synthesis, such as ATP citrate lyase (ACLY), Acetyl-CoA carboxylase (ACC), and fatty acid synthase (FASN) are changed in tumor cells (71–83). Citrate, the intermediate product of glucose metabolism, forms Ac-CoA under the catalysis of ACLY, and Ac-CoA forms malonyl CoA (Mal-CoA) under the catalysis of ACC. Ac-CoA and MAL-CoA synthesize palmitic acid catalyzed by

FASN, and palmitic acid forms lipid components required by cells catalyzed by other specific enzymes.

Several studies on thyroid carcinoma also demonstrated lipid metabolism reprogramming. In their transcriptome analysis of lipid metabolism-related genes in PTC, Xu et al. described the use of these genes for PTC classification (84). Recent cases reported by Leng et al. suggested abnormality in the metabolism of fatty acid synthases and lipids. They detected 18 types of FFAs with increased levels in carcinoma tissue compared to the normal tissue of the thyroid (85). Several studies have reported abnormal changes in lipogenic enzymes in TC. FASN is upregulated in various TC subtypes, including PTC, ATC, and FTC (86–88). Under hypoxic conditions, ACC is upregulated in most types of cancer such as liver, breast, and prostate cancer (89) and is downregulated in PTC. The downregulation of ACC2 *via* BRAF<sup>V600E</sup> plays a critical role in PTC and establishes favorable conditions for TC cell proliferation (90). Of the lipogenic enzymes upregulated in ATC, stearoyl-CoA desaturase-1 (SCD1) that can mediate the desaturation of endogenously synthesized saturated fatty acids into monounsaturated fatty acids (MUFAs) and promote the proliferation of various cancer cell types showed the most significant differential expression when compared with that in normal thyroid tissues (91). A highly positive correlation between MUFAs and monounsaturated phosphatidylcholines (MUPCs) and negative correlations between monosaturated and polyunsaturated lipids have been observed in many types of cancers including breast, lung, colorectal, esophageal, and gastric cancer; thus, similar lipogenic mechanisms may exist to generate the lipids. However, it should be noted that a lower correlation than that mentioned above in TC was observed (92) (Table 1). These findings suggest the presence of different lipid metabolism in TC while it is not clear at this stage. Overall, these cases support the view that TC cells are dependent on *de novo* lipogenesis for cell viability (Figure 2).



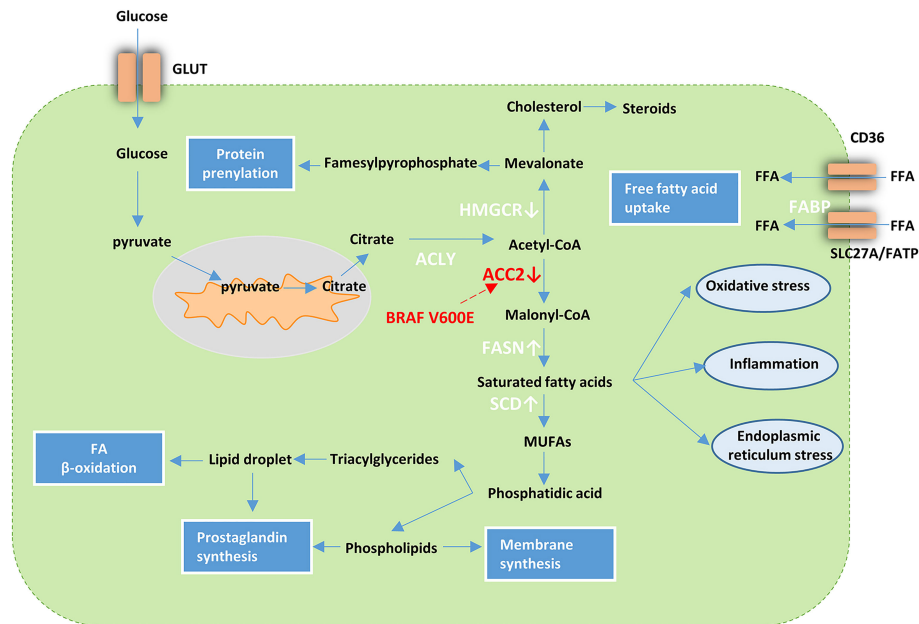


**FIGURE 2 |** Lipid metabolism in cancer cells. Tumor cells increase FFA uptake *via* upregulation of fatty acid transport receptors and chaperones such as Solute Carrier SLC27A/FATP, CD36, and FABP. In addition, metabolic reprogramming that facilitates glycolysis can activate *de novo* lipid synthesis. Acetyl-CoA derived from citrate can be further processed into a variety of lipid species with the help of various enzymes. FASN and SCD are upregulated while ACC2 and HMGCR are downregulated in TC. BRAF<sup>V600E</sup> influences the lipid metabolism in PTC *via* downregulation of ACC2. GLUT, glucose transporter; HMGCR, 3-hydroxy-3-methylglutaryl-CoA reductase; fatty acid synthase ACLY; ACC2, Acetyl-CoA carboxylase 2; FASN fatty acid synthase; SCD, stearoyl-CoA desaturase-1; MUFAs, monounsaturated fatty acids; FFA, free fatty acid; FABP, fatty acid binding protein; SLC27A, Solute Carrier Family 27; FATP, Fatty Acid Transporter.

## Enhancement of Protein Synthesis

As a crucial component of all cells and tissues of the human body, proteins are the material basis of life. Proteins have many functions in organisms, including catalysis, locomotion, transport, mechanical support, immunity, regulation. Protein synthesis consists of five steps, including amino acid activation, initiation of polypeptide chain synthesis, peptide chain extension, peptide chain termination and release, and post-synthesis processing and modification of the protein. This process expresses the genetic information on messenger RNA (mRNA) transcribed from DNA in the form of proteins. As tumor cells are more metabolically active and divide more frequently than normal cells, they require more proteins.

As mentioned above, the PI3K-Akt-mTOR pathway is activated in various kinds of carcinoma. This pathway is also closely associated with protein synthesis. Tumor cells keep their protein synthesis positive to meet the growth needs through this pathway. In addition, tumor cells have different genetic mutations that activate the synthesis of certain proteins and perform certain functions.

Ribosomes, ribonucleoprotein particles in cells, are mainly composed of numerous distinct proteins and rRNA and are responsible for protein synthesis. In recent decades, many studies have demonstrated the causal associations between inherited mutations affecting ribosome biogenesis and increased cancer risk. Recent studies have shown that dysregulated ribosome biogenesis plays a broader role in the development and

progression of most cancers (93–98). Some studies have also assessed the relationship between ribosomes and TC. Saiselet et al. reported that the expression of genes involved in the negative regulation of cell death/apoptosis was also downregulated in five TC cell lines (WRO, FTC133, BCPAP, TPC1, and K1) (99). Jeong et al. discovered the high expression of LXR $\beta$  in TC, which was coordinately associated with ribosome-related genes (100).

## Abnormalities in Nucleic Acid Biosynthesis

Nucleic acid is a biological macromolecule with a nucleotide as its basic unit, which has a complex spatial structure and important biological functions. Nucleic acids can be classified as deoxyribonucleic acid (DNA) and ribonucleic acid (RNA). DNA, which is found in the nucleus and mitochondria, carries genetic information and is passed down through generations through replication. Cell and organismal traits are determined by this genetic information. The two basic pathways of nucleotide synthesis are *de novo* synthesis and remediation. The *de novo* synthesis of nucleotides from simple materials such as ribose phosphate, amino acids, one-carbon units, and CO<sub>2</sub> is the main synthesis pathway in the human body. The *in vivo* use of free bases or nucleosides can generate nucleotides through a simple reaction process known as the salvage pathway. Tumor cells use both pathways because they require significant amounts of nucleic acids for rapid growth. As mentioned above, the catabolism of glutamine is particularly active in tumor cells;

thus, increased amounts of the breakdown products of glutamine are observed when compared with those in normal cells. Ammonia produced by the breakdown of glutamine participates in the ammonia cycle and can be used for the biosynthesis of nucleotides and proteins (101–105).

Tumor cells increase nucleotide synthesis to satisfy their need for growth and proliferation (106). Therefore, the activity of nucleotide synthetase, especially deoxyribonuclease, is higher in tumor cells than that in normal cells (107). The expression of deoxyribonuclease in normal cells fluctuates with changes in the cell cycle. Cancer cells have lost normal regulation and the expression levels are constitutively high, leading to increased DNA synthesis (24). The expression levels of genes involved in DNA replication were upregulated in TC cell lines such as BCPAP and 8505C (99). The occurrence of thyroid tumors is related to abnormal nucleic acid synthesis caused by a variety of gene mutations. The activation of BRAF mutations is a major oncogenic driver of many cancers, especially TC (108, 109). BRAF is the predominant mutation (30–40%) in PTC and is considered an initiating event in papillary thyroid carcinogenesis. Another human gene involved in thyroid carcinogenesis is TERT, which contributes to the distant metastasis (110–112).

## TC CELL METABOLISM AND THE TME

### Tumor Cell Metabolism Shapes the Inflammatory TME

The two major characteristics of the TME are hypoxia and acidification, which are closely related. Tumor cells increase glycolysis to adapt to the hypoxic microenvironment. The lactate produced by glycolysis, in turn, acidifies the TME. In addition, the incomplete vasculature of tumor tissue prevents the timely elimination of metabolites, which is also related to the acidification of the TME. Active metabolism in TME cells can also lead to increased toxic concentrations of certain metabolites, such as increased levels of adenosine, kynurenine, ornithine, reactive oxygen species, and potassium. These metabolites have profound effects on suppressing the tumor immune response. During tumor development, the TME changes continuously with tumor growth and develop its cellular contents by releasing various recruiting factors, leading to the accumulation of specific types of immune cells in the TME, also affects the functions of these immune cells and the complex relationship between these cells and tumor cells. Thus, tumors are no longer simply a problem of cancer cells. Co-evolution occurs between tumor cells and the surrounding stromal cells, forming an inseparable community. Under the influence of tumor cells, tumor stromal fibroblasts, macrophages, and neutrophils become tumor-associated fibroblasts (CAFs), tumor-associated macrophages (TAMs), and tumor-associated neutropenia.

### Metabolic Crosstalk in the TC Microenvironment

#### Nutrient Competition

The high metabolic activity of cancer cells and the disordered vasculature in the TME can contribute to a microenvironment

featuring nutrient depletion and hypoxia, which established a metabolic competition between cancer cells and infiltrating immune cells. This series of changes and metabolic reprogramming plays a significant role in promoting tumor growth and immune escape. Chen et al. compared human normal thyroid and PTC samples and identified metabolites in carbohydrate metabolism, including glucose, that consistently decreased in PTC (113). The lack of glucose impaired the function of immune cells such as TAMs and T cells by regulating mTOR and GAPDH. Glycolysis promotes effector T cell (Teff cell) function by sustaining the production of IFN $\gamma$ . Decreased mTOR activity diminishes IFN $\gamma$  at the transcriptional level in CD8<sup>+</sup> T cells and, thus, impairs T cell function (114, 115). Besides glucose, amino acids also play a role in driving and fueling T cell function and differentiation. The neighboring immune cells in solid tumors are outcompeted due to arginine uptake and catabolism which primarily shifts toward cancer cells (116). Leone et al. reported that tumor cells exposed to glutamine antagonist showed decreased viability, proliferation, and cell cycle progression while Teff cells produce a long-lived, highly activated phenotype by markedly upregulating oxidative metabolism (117).

#### Secreted Metabolites

The accumulation of metabolites such as lactate, kynurenine, and other metabolic by-products of cancer metabolism can be detrimental to immune cells, leading to tumor immunosuppression. Indoleamine 2, 3-dioxygenase (IDO), a rate-limiting enzyme in tryptophan oxidation, promotes tryptophan uptake from the TME and generates kynurenine, which inhibits tryptophan import. Therefore, the amino acids of T cells are depleted and result in immunosuppression and induced T cell apoptosis. IDO-expressing tumor cells are not rejected by specific T cells through the secretion of kynurenines, which can suppress cytotoxic effector functions *via* the downregulation of TCR CD3  $\zeta$ -chain and induced FOXP3<sup>+</sup> regulatory T cell (Treg) differentiation. IDO upregulation impaired the function of NK cell function and boost the high infiltration of FOXP3<sup>+</sup> Tregs in thyroid carcinoma (118, 119). In addition, Foxp3<sup>+</sup> Tregs in lymphocytes facilitate thyroid tumor growth and invasion (120). A large amount of lactate can also cause acidosis in the microenvironment and weaken immune cell function (121). Arts et al. showed that TC-derived lactate-mediated TC-induced TAM reprogramming and inflammation through Akt/mTOR-dependent glycolysis, an increase in inflammation characteristics, and changes in cell metabolism (122). The accumulation of lactate is also detrimental to the function and antitumor response of T and NK cells by inhibiting proliferation and cytokine production (123). These studies suggested that patients with cancer should be cautious when using lactate preparations, as lactate may promote tumor growth.

Tumor cells also secrete vascular endothelial growth factor (VEGF) into the TME, resulting in the upregulation of 6-phosphofructo-2-kinase/fructose-2, 6-biphosphatase 3 (PFKFB3) in endothelial cells, which activates PFK-1 to promote the glycolytic phenotype as well as proliferation (124). Colegio et al. demonstrated that lactate produced by tumor cells promotes M2 macrophage polarization by a HIF1 $\alpha$ -dependent mechanism. In turn, VEGF and Arginase-1 secreted by

M2-polarized macrophages signal back to tumor cells and promote tumor growth (125).

### Metabolic Coupling

In TME, the energy metabolism of CAFs shifts to aerobic glycolysis under the influence of cancer cells. The lactate, ketone body, or pyruvate released by these CAFs can be used as an energy source by epithelial cancer cells to enter the TCA cycle and produce ATP through OXPHOS. This phenomenon is called the reverse Warburg effect. Lactate produced by CAFs is exported *via* the monocarboxylate transporter (MCT)-4 into the TME and taken up by tumor cells *via* the MCT-1 transporter. Such metabolic coupling has been reported in several tumor types including head and neck cancer (126). In addition, the metabolic coupling between PTC cells and adjacent fibroblasts can result in aggressive behavior owing to the large-scale production lactate, which is transported outside the cell by MCT4 (127). CAFs also increased the anabolic metabolism of glutamine which can be consumed by cancer cells to sustain nucleotide generation and OXPHOS. In contrast, glutamate secreted by cancer cells promoted the production of glutathione (GSH), thereby maintaining redox balance and ECM remodeling in CAFs (128). The results of Mestre-Farrera et al. indicated that glutamine deprivation promoted CAFs migration and invasion, which, in turn, promotes tumor epithelial cells to move to nutrient-rich areas (129). CAFs release paracrine signals to induce metabolic reprogramming and epigenetic changes, causing changes similar to KRAS-driven oncogenic transformations (130). Tumors cells release factors such as PDGF and TGF- $\beta$ , resulting in metabolic reprogramming of CAFs toward aerobic glycolysis (131, 132). Fozzatti et al. described the significant increase of GLUT-1 in human fibroblasts *in vitro* when cultured in ATC cells-derived conditioned media. Strikingly, conditioned media obtained from these activated fibroblasts promoted cell proliferation and invasion of follicular TC cell line (133). Rabold et al. performed transcriptome, metabolome, and lipidome analyses on TC-induced macrophages in a human coculture model. The lipidome analysis showed increased total lipid and intracellular lipid content of tumor-induced macrophages, especially phosphoglycerides and sphingolipids. Remarkably, this metabolic shift in lipid synthesis contributes to their protumoral functional characteristics: a block of key enzymes of lipid biosynthesis in tumor-induced macrophages reversed elevated inflammatory cytokines and the ability to produce ROS, two well-known pro-tumoral factors in the TME (134).

These studies show the complicated and dynamic interaction that exists between thyroid tumors and immune cells in TME, which results in the promotion of thyroid tumorigenesis (Figure 3).

## PROGNOSTIC BIOMARKERS AND TREATMENT

### Prognostic Indicators

In conclusion, the expression of metabolism-related molecules revealed the differences in invasiveness and prognosis between different TC subtypes (Figure 4). Numerous studies have demonstrated the relationship between the prognosis of thyroid

carcinoma and glycolysis-related proteins such as GLUT, LDHA, MCT1 (32, 135, 136). Some studies have indicated that GLUT contributed to the increased glucose uptake observed during carcinogenesis (135, 137). The differentiated extent of thyroid cancer is negatively correlated with the expression of GLUTs. Poorly differentiated types such as ATC have high expression levels of GLUT (mainly GLUT-1); in contrast, well-differentiated tumors such as FTC and PTC usually have low GLUT-1 expression levels (45, 137–140). Glutamine, serine, glycine, and other amino acid metabolism-related proteins can also be used as prognostic indicators for thyroid tumors. Stromal GDH positivity was an independent factor associated with poor prognosis. In follicular variant PTC, stromal serine hydromethyl transferase 1 expression was associated with shorter disease-free survival. The serine/glycine metabolism-related molecules phosphoglycerate dehydrogenase, glycine decarboxylase, and phosphoserine phosphatase positivity were associated with shorter overall survival (57, 58, 60, 141). IDO, which was associated with the aggressive features of papillary thyroid microcarcinoma, may disrupt antitumor immunity and contribute to tumor progression by increased infiltration of FOXP3<sup>+</sup> Treg cells (142).

### Metabolism Targeted Therapy

At present, cancer therapeutic regimens face the problem of drug resistance which may associate with metabolic reprogramming in tumor. Therefore, combination therapies that target various tumor cell properties showed great potential value. Metabolic inhibitors in combination with targeted therapy or chemotherapy hold promise for increasing anticancer drug sensitivity.

### Glucose Metabolism as a Therapeutic Target

The energy supply of tumor cells differs from that of normal cells. This unique energy supply pathway is mainly due to increased glycolytic enzyme expression and activity levels. Theoretically, inhibiting specific glycolytic metabolic enzymes with high expression levels can cut off the energy supply of tumor cells, while normal tissues are not affected. When the glycolytic pathway is inhibited, normal tissue cells can utilize fatty acid and amino acid production through alternative pathways. Some glycolytic enzymes, such as HK-II LDHA, and PKM2, are highly expressed in malignant tumors. These highly expressed glycolytic enzymes can be used as targets for tumor treatment (143). Due to tumor cell heterogeneity and TME variability, the expression and activity of glycolytic enzymes may change. Consequently, the therapeutic effect of a single glycolytic enzyme target may not be as good as that for the combination of multiple glycolytic enzyme targets. Combinations involving the inhibition of glycolysis and OXPHOS, or glycolysis and glutaminolysis have been proven in multiple preclinical cancer models to effectively suppress tumor growth (144–148). Glyoxalase I (GLO I) is a rate-limiting enzyme that is involved in the detoxification of cytotoxic methylglyoxal formed in glycolysis. The combination of GLO I inhibitor with shikonin, a PKM2 specific inhibitor, could suppress the cellular proliferation and induction of apoptosis (149).

Various HK2 inhibitors have been identified, including 2-deoxyglucose(2-DG), 3-bromopyruvate (3-BP), and lonidamine (LND). In thyroid tumors, glycolytic inhibitors also show unique

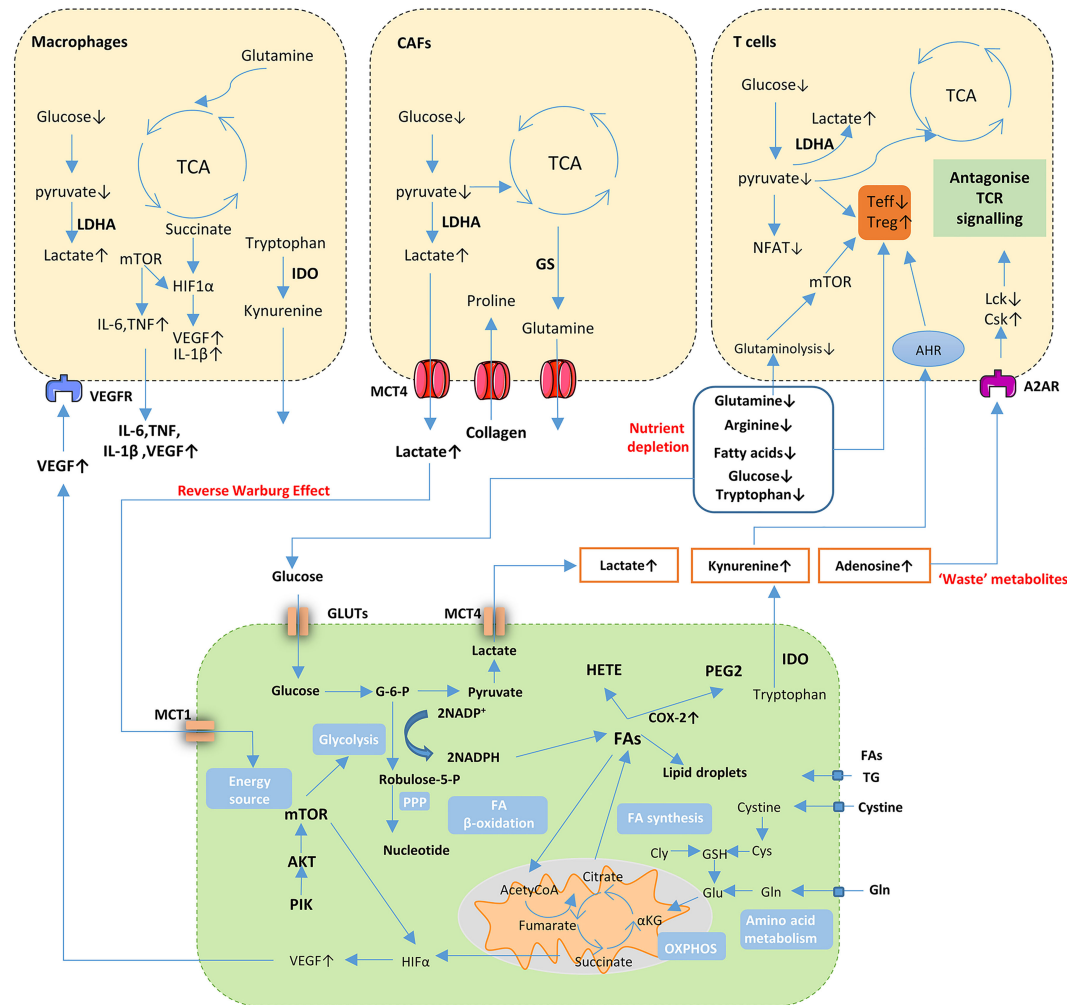


**FIGURE 3 |** Cancer cell metabolism and crosstalk in the TME. Cancer cells undergo metabolic changes including activation of aerobic glycolytic, enhanced FA synthesis and increased uptake of glutamine supply for bioenergetics through tricarboxylic acid (TCA) cycle and support biosynthesis of proteins. Nutrient depletion, accumulation of ‘waste’ metabolites and aberrant signaling molecules in TME influence the function and proliferation of both cancer cells and immune or stromal cells. Gln, glutamine; Glu, Glutamate; Cys, cysteine; GSH, glutathione; Gly, glycine; TG, triglyceride; FA, fatty acids; PPP, pentose phosphate pathway; NADH, nicotinamide adenine dinucleotide; NADPH, nicotinamide adenine dinucleotide phosphate; HETE, thromboxane hydroxyepoxyicosate-trienoic acid; PEG2, prostaglandin E2; COX-2, cyclooxygenase-2; G-6-P, glucose-6-phosphate; IDO, Indoleamine 2, 3-dioxygenase; MCT, monocarboxylate transporter; GLUT, glucose transporter; VEGF, vascular endothelial growth factor; LDHA, lactate dehydrogenase A; GS, glutamine synthetase; NFAT, nuclear factor of activated T cells; AHR, aryl hydrocarbon receptor; A2AR, Adenosine 2A receptor; Csk, C-terminal Src kinase; Lck, lymphocyte-specific protein tyrosine kinase; Teff, effector T cells; Treg, regulatory T cells.

therapeutic effects. Glycolytic inhibition with 3-BP suppress tumor growth and extends survival in a murine model of ATC when combined with the ketogenic diet (150). It has been previously shown that glycolytic inhibitors 2DG significantly enhanced the antitumor effects of other medical treatments and radiotherapy (151–154). Phase I/II clinical trials have been performed for 2-DG as a single-agent therapy in solid tumors and hormone-refractory prostate cancer. However, further research was halted owing to the significant toxicities and limited efficacy (NCT00633087) (155). LND also reached phase II and III clinical trials for the treatment of several tumor types but showed only modest clinical activity and a

lack of specificity. Moreover, due to concerns regarding liver enzyme abnormalities, further research was halted (156, 157). Targeted therapy is a common treatment for thyroid tumors. When blocking platelet-derived growth factor receptor by imatinib, the pro-oncogene  $BRAF^{V600E}$  promotes thyroid tumor cell glycolysis *via* the upregulation of HK2 expression, resulting in drug resistance. However, glucose uptake and metabolism in thyroid tumor cells were downregulated when  $BRAF^{V600E}$  was blocked by vemurafenib. In terms of tumor growth, combination therapy of imatinib and vemurafenib was much more effective than single therapy and led to a near abolition of the tumors (158). The combination of imatinib



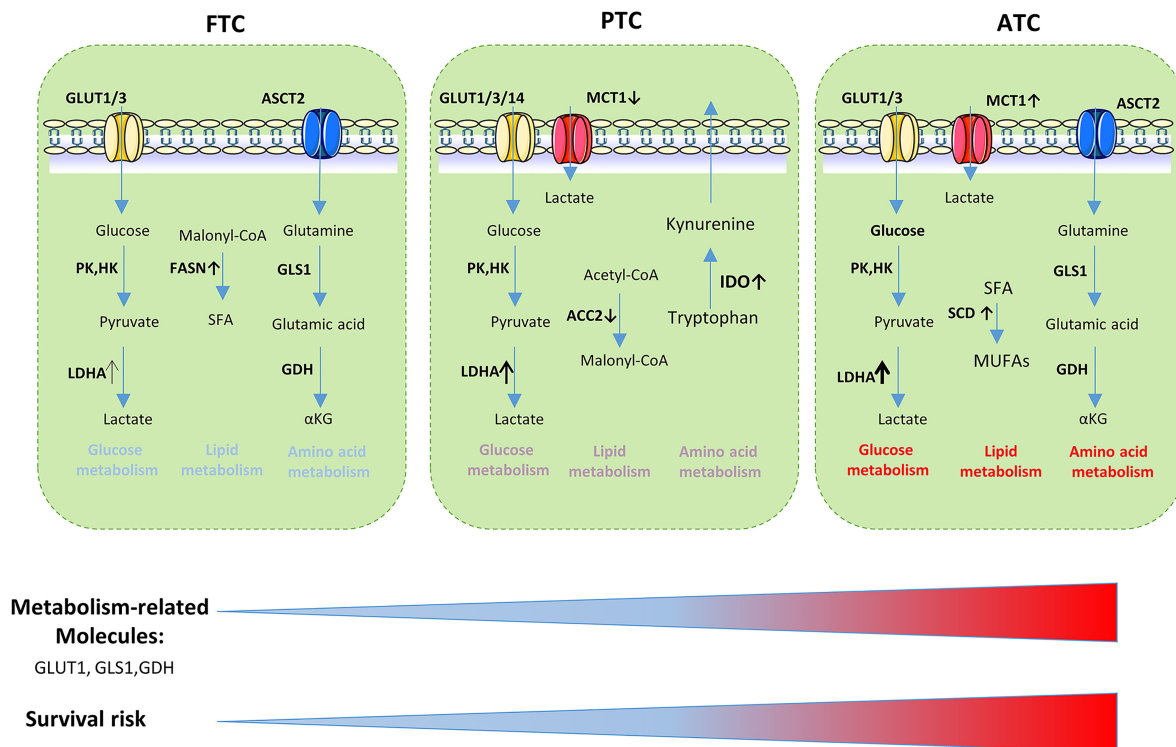


**FIGURE 4 |** Metabolism-related molecules is related to the aggressiveness of thyroid cancer and survival risk. GLUT, glucose transporter; LDHA, lactate dehydrogenase A; PK, Pyruvate kinase; HK, hexokinase; SFA, saturated fatty acids; ASCT, amino acid transporter; FASN, fatty acid synthase; GLS1, glutaminase 1; GDH, glutamate dehydrogenase; ACC2, Acetyl-CoA carboxylase 2; IDO, Indoleamine 2, 3-dioxygenase; SCD1, stearoyl-CoA desaturase-1; MUFAs, monounsaturated fatty acids.

and HK2 inhibitors may solve the problem of drug resistance and also provide better efficacy in TC.

LDH is a critical metabolic enzyme that is considered a hallmark of aggressive malignancies. Radiotherapy is a common therapy in thyroid cancer, indicating the combination therapy of LDHA inhibitor and radiotherapy may be efficient in thyroid cancer. Chen et al. find LDHA suppression monotherapy decreased cellular proliferation and stunted tumor growth temporarily in ATC but cannot achieve tumor cure, due to the maintenance of residual viable cells. Only the combination therapy of chronic LDHA suppression and radiation can achieve a functional cure (159). Various LDHA inhibitors have been developed, such as dichloroacetate (DCA), gossypol, oxamate and FX-11 (160–162). The lactate transporter MCT links intracellular lactate with the TME and plays an indispensable role in tumor lactate metabolism. AZD3965 is an inhibitor of the MCT-1/MCT-2 lactate transporter and reached phase I clinical trials for both solid tumors and large B-cell lymphoma (NCT01791595). However, MCT inhibition also impairs T cell proliferation (Table 2).

### Amino Acid Metabolism as a Therapeutic Target

Amino acids are an essential component of tumor cells and are closely related to tumor development. Thus, amino acid metabolism may provide a new therapeutic perspective.

Lasparaginase is approved by the Food and Drug Administration for the frontline treatment of acute lymphoblastic leukemia (163). Other treatments for amino acid deprivation have also shown encouraging results in clinical trials in several solid malignancies (164–167). The mitochondrial enzyme GLS plays a crucial role in glutaminolysis. Among the GLS inhibitors, CB-839 is more potent, selective and shows greater bioavailability. In phase I clinical trials, CB-839 showed preliminary signs of clinical activity with an acceptable safety profile in multiple tumor types including triple-negative breast cancer, non-small cell lung adenocarcinoma, renal cell carcinoma, mesothelioma, and tumors with mutations in enzymes in the TCA cycle (NCT02071862) (168).

Since tumor cells require glutamine, one possible strategy is to treat tumors by preventing or interfering with glutamine metabolism by tumor cells. The blockade of glutamine in tumor-bearing mice inhibited cancer cell oxidation and glycolytic metabolism, resulting in hypoxia, acidosis, and reduced nutrient consumption (117). However, some studies showed that increasing the intake of glutamine in tumor-bearing rats did not elevate the growth rate of tumors; moreover, clinical work has also shown that glutamine supplementation in patients with tumors improved chemotherapy efficacy and reduced the adverse reactions (169–173). IDO, the ratelimiting enzyme in tryptophan catabolism, is highly expressed in TC cells and suppresses the function of NK cells.

**TABLE 2 |** Metabolism-targeting cancer therapies.

Target pathway and protein		Agent	Study phase	Effects	Interventions	References	Status
Glucose metabolism	HK2	2-DG	Phase II	Limited efficacy on tumor growth and significant toxicities	Single agent	NCT00633087	Terminated
		LND	Phase III	Limited efficacy and produced more myalgias and fatigue	Combined with epirubicin	(150)	
		3-BP	Preclinical	Suppresses tumor growth and improves survival <i>in vivo</i>	combined with the ketogenic diet	(143)	
	MTC1	AZD3965	Phase I		Single agent	NCT01791595	Completed
	LDHA	DCA	Phase I		Single agent	NCT01163487	Completed
		Gossypol	Phase I/II	Safe and well tolerated but shown limited activity.	Single agent	(1153)	
		Oxamate	Preclinical	Inhibits the viability of cancer cells in a dose- and time-dependent manner		(155)	
		FX-11	Preclinical	Block aerobic glycolysis and growth cancer <i>in vitro</i>	Single agent	(154)	
Amino acid metabolism	GL1	CB-839	Phase II		Combined with Paclitaxel	NCT03057600	Completed
	IDO	Epacadostat	Phase III	Effect remains uncertain.	Combined with Pembrolizumab	NCT02752074	Completed
		Indoximod	Phase II		Combined with Chemoradiotherapy	NCT04049669	Recruiting
Lipid metabolism	ACC	ND-654	Preclinical	Inhibits the tumor development <i>in vivo</i> , improve survival rate	Single agent; combined with the sorafenib	(68)	
	SCD	SSI-4	Preclinical	Regulate tumor-initiating cells and sorafenib resistance	Combined with sorafenib	(182)	
		Betulinic acid	Preclinical	Induces rapid cell death	Single agent	(184)	
		MF-438	Preclinical	Achieve better control	Combined with cisplatin	(183)	

IDO inhibitors such as epacadostat have reached phase III trials and show promising efficacy in combination therapies by linking metabolism and immunomodulation. Therefore, IDO inhibitors are likely to be useful for the treatment of thyroid tumors (174).

### Lipid Metabolism as a Therapeutic Target

ACC is a rate-limiting enzyme for *de novo* lipid synthesis and inhibition of fatty acid oxidation. Rescue of ACC2 may be a new molecular strategy to overcome the resistance of refractory PTC to BRAF<sup>V600E</sup> inhibitors (90). SCD is an aliphatic acyl desaturase that catalyzes the transformation of saturated fatty acids into MUFAs by inserting cis-double bonds at the Δ9 position of the carbon chain (175). MUFAs play a role in cell growth, survival, differentiation, metabolic regulation, and signal transduction. SCD has been observed in a wide range of cancer cells (176–179) and this increase is closely associated with cancer aggressiveness and poor prognosis (180–183). Previous research established SCD reduces cell proliferation and invasion by blocking cell migration and membrane fluidity (184–187). In ATC, therapeutic and genetic-

targeted inhibition of SCD enzyme activity promoted a significant reduction in cell proliferation and induced cell death, while normal thyroid cells were unaffected (91). SCD inhibitors such as SSI-4, betulinic acid, and MF-438 that proved effective in antitumor effect (188–190) may show a promising efficiency in the treatment of thyroid cancer.

## CONCLUSION AND PERSPECTIVE

The crucial of metabolic reprogramming in tumor development and metastasis is increasingly recognized (Table 3). The complicated relationship between tumor cell metabolism and the TME is also important. Tumor cell metabolism can cause acidification of the TME and can also recruit immune cells to change immune cell metabolism in the TME. However, the immune microenvironment can also act on tumor cells to promote the immune escape of tumor cells.

Although there has been some progress in the study of metabolic reprogramming of TC in recent years, there remain

**TABLE 3 |** Metabolic reprogramming between proliferation and metastasis in thyroid cancer.

Metabolism pathways	Function	Reference	Evidence
<b>Glucose metabolism</b>	LDHA		(26)
	HK2		(41)
<b>Amino acid metabolism</b>	IDO		(135)
<b>Lipid metabolism</b>	SREBP1, SCD, FASN and ACC		(61)
	SCD1		(84)

many gaps to fill. Some outstanding questions still need to be addressed for the development of specific metabolic targeted therapy. More studies are needed to determine how thyroid tumor cell metabolism interacts with immune cells in the microenvironment, which metabolic targets can be blocked specifically for TC treatment, the possible side effects of metabolism inhibitors, and the solutions to these challenges.

## AUTHOR CONTRIBUTIONS

Conceived the work: LB and ZP. Wrote the manuscript: LB. Generated data for figures: TX and XL. Revised the manuscript:

MG and PH. All authors contributed to the article and approved the submitted version.

## FUNDING

This work was funded by the National Natural Science Foundation, People's Republic of China (Nos. 82173157, U20A20382, 81872170, 81802673), Natural Science Foundation of Zhejiang Provincial under Grant No.Y22H168220, Chinese Medicine Research Program of Zhejiang Province (No. 2021ZA006), and Zhejiang Medical and Health Science and Technology Project (Nos. 2021KY056 and 2022KY042).

## REFERENCES

- Kim J, Gosnell JE, Roman SA. Geographic Influences in the Global Rise of Thyroid Cancer. *Nat Rev Endocrinol* (2020) 16:17–29. doi: 10.1038/s41574-019-0263-x
- Kitahara CM, Sosa JA. The Changing Incidence of Thyroid Cancer. *Nat Rev Endocrinol* (2016) 12:646–53. doi: 10.1038/nrendo.2016.110
- Cabanillas ME, McFadden DG, Durante C. Thyroid Cancer. *Lancet* (2016) 388:2783–95. doi: 10.1016/s0140-6736(16)30172-6
- Nikiforova MN, Nikiforov YE. Molecular Genetics of Thyroid Cancer: Implications for Diagnosis, Treatment and Prognosis. *Expert Rev Mol Diagn* (2008) 8:83–95. doi: 10.1586/14737159.8.1.83
- Molinaro E, Romei C, Biagini A, Sabini E, Agate L, Mazzeo S, et al. Anaplastic Thyroid Carcinoma: From Clinicopathology to Genetics and Advanced Therapies. *Nat Rev Endocrinol* (2017) 13:644–60. doi: 10.1038/nrendo.2017.76
- Filetti S, Durante C, Hartl D, Leboulleux S, Locati LD, Newbold K, et al. Thyroid Cancer: ESMO Clinical Practice Guidelines for Diagnosis, Treatment and Follow-Up†. *Ann Oncol* (2019) 30:1856–83. doi: 10.1093/annonc/mdz400
- Grani G, Lamartina L, Durante C, Filetti S, Cooper DS. Follicular Thyroid Cancer and Hürthle Cell Carcinoma: Challenges in Diagnosis, Treatment, and Clinical Management. *Lancet Diabetes Endocrinol* (2018) 6:500–14. doi: 10.1016/s2213-8587(17)30325-x
- Tuttle RM. Controversial Issues in Thyroid Cancer Management. *J Nucl Med* (2018) 59:1187–94. doi: 10.2967/jnumed.117.192559
- Raue F, Frank-Raue K. Thyroid Cancer: Risk-Stratified Management and Individualized Therapy. *Clin Cancer Res* (2016) 22:5012–21. doi: 10.1158/1078-0432.Ccr-16-0484
- Hay N. Reprogramming Glucose Metabolism in Cancer: Can it be Exploited for Cancer Therapy? *Nat Rev Cancer* (2016) 16:635–49. doi: 10.1038/nrc.2016.77
- Faubert B, Solmonson A, DeBerardinis RJ. Metabolic Reprogramming and Cancer Progression. *Science* (2020) 368:eaaw5473. doi: 10.1126/science.aaw5473
- Cha YH, Yook JI, Kim HS, Kim NH. Catabolic Metabolism During Cancer EMT. *Arch Pharm Res* (2015) 38:313–20. doi: 10.1007/s12272-015-0567-x
- Herst PM, Grasso C, Berridge MV. Metabolic Reprogramming of Mitochondrial Respiration in Metastatic Cancer. *Cancer Metastasis Rev* (2018) 37:643–53. doi: 10.1007/s10555-018-9769-2
- Zhao H, Li Y. Cancer Metabolism and Intervention Therapy. *Mol Biomedicine* (2021) 2:5. doi: 10.1186/s43556-020-00012-1
- Yang Z, Huang R, Wei X, Yu W, Min Z, Ye M. The SIRT6-Autophagy-Warburg Effect Axis in Papillary Thyroid Cancer. *Front Oncol* (2020) 10:1265. doi: 10.3389/fonc.2020.01265
- Chen J, Zhou Q, Feng J, Zheng W, Du J, Meng X, et al. Activation of AMPK Promotes Thyroid Cancer Cell Migration Through Its Interaction With PKM2 and  $\beta$ -Catenin. *Life Sci* (2019) 239:116877. doi: 10.1016/j.lfs.2019.116877
- Wang R, Cheng Y, Su D, Gong B, He X, Zhou X, et al. Cpt1c Regulated by AMPK Promotes Papillary Thyroid Carcinomas Cells Survival Under Metabolic Stress Conditions. *J Cancer* (2017) 239:3675–81. doi: 10.7150/jca.21148
- Kishore M, Cheung KCP, Fu H, Bonacina F, Wang G, Coe D, et al. Regulatory T Cell Migration Is Dependent on Glucokinase-Mediated Glycolysis. *Immunity* (2017) 47:875–89.e10. doi: 10.1016/j.immuni.2017.10.017
- Li L, Liang Y, Kang L, Liu Y, Gao S, Chen S, et al. Transcriptional Regulation of the Warburg Effect in Cancer by SIX1. *Cancer Cell* (2018) 33:368–85.e7. doi: 10.1016/j.ccell.2018.01.010
- Hensley CT, Faubert B, Yuan Q, Lev-Cohain N, Jin E, Kim J, et al. Metabolic Heterogeneity in Human Lung Tumors. *CELL* (2016) 164:681–94. doi: 10.1016/j.cell.2015.12.034
- Christen S, Lorendeau D, Schmieder R, Broekaert D, Metzger K, Veys K, et al. Breast Cancer-Derived Lung Metastases Show Increased Pyruvate Carboxylase-Dependent Anaplerosis. *Cell Rep* (2016) 17:837–48. doi: 10.1016/j.celrep.2016.09.042
- Chen J, Lee HJ, Wu X, Huo L, Kim SJ, Xu L, et al. Gain of Glucose-Independent Growth Upon Metastasis of Breast Cancer Cells to the Brain. *Cancer Res* (2015) 75:554–65. doi: 10.1158/0008-5472.Can-14-2268
- Mulvey PF Jr., Kelleher JJ, Slingerland DW. Oxidation of Glucose-C14 by Human Thyroid Tissues. *Metabolism* (1963) 12:829–32.
- Hengstschläger M, Mudrak I, Wintersberger E, Wawra E. A Common Regulation of Genes Encoding Enzymes of the Deoxynucleotide Metabolism is Lost After Neoplastic Transformation. *Cell Growth Differ* (1994) 5:1389–94.
- Gao Y, Yang F, Yang XA, Zhang L, Yu H, Cheng X, et al. Mitochondrial Metabolism is Inhibited by the HIF1 $\alpha$ -MYC-PGC-1 $\beta$  Axis in BRAF V600E Thyroid Cancer. *FEBS J* (2019) 286:1420–36. doi: 10.1111/febs.14786
- Zhou L, Cha G, Chen L, Yang C, Xu D, Ge M. HIF1 $\alpha$ /PD-L1 Axis Mediates Hypoxia-Induced Cell Apoptosis and Tumor Progression in Follicular Thyroid Carcinoma. *Onco Targets Ther* (2019) 12:6461–70. doi: 10.2147/ott.S203724
- Yang Z, Yu W, Huang R, Ye M, Min Z. SIRT6/HIF-1 $\alpha$  Axis Promotes Papillary Thyroid Cancer Progression by Inducing Epithelial-Mesenchymal Transition. *Cancer Cell Int* (2019) 19:17. doi: 10.1186/s12935-019-0730-4
- Klaus A, Fathi O, Tatjana TW, Bruno N, Oskar K. Expression of Hypoxia-Associated Protein HIF-1 $\alpha$  in Follicular Thyroid Cancer is Associated With Distant Metastasis. *Pathol Oncol Res* (2018) 24:289–96. doi: 10.1007/s12253-017-0232-4
- Yu L, Lu M, Jia D, Ma J, Ben-Jacob E, Levine H, et al. Modeling the Genetic Regulation of Cancer Metabolism: Interplay Between Glycolysis and Oxidative Phosphorylation. *Cancer Res* (2017) 77:1564–74. doi: 10.1158/0008-5472.Can-16-2074
- Matijevic Glavan T, Cipak Gasparovic A, Verrillaud B, Busson P, Pavelic J. Toll-Like Receptor 3 Stimulation Triggers Metabolic Reprogramming in Pharyngeal Cancer Cell Line Through Myc, MAPK, and HIF. *Mol Carcinog* (2017) 56:1214–26. doi: 10.1002/mc.22584

31. Choudhry H, Harris AL. Advances in Hypoxia-Inducible Factor Biology. *Cell Metab* (2018) 27:281–98. doi: 10.1016/j.cmet.2017.10.005
32. Hou X, Shi X, Zhang W, Li D, Hu L, Yang J, et al. LDHA Induces EMT Gene Transcription and Regulates Autophagy to Promote the Metastasis and Tumorigenesis of Papillary Thyroid Carcinoma. *Cell Death Dis* (2021) 12:347. doi: 10.1038/s41419-021-03641-8
33. Jin L, Chun J, Pan C, Alesi GN, Li D, Magliocca KR, et al. Phosphorylation-Mediated Activation of LDHA Promotes Cancer Cell Invasion and Tumour Metastasis. *Oncogene* (2017) 36:3797–806. doi: 10.1038/onc.2017.6
34. Matsuzaki K, Segade F, Matsuzaki U, Carter A, Bowden DW, Perrier ND. Differential Expression of Glucose Transporters in Normal and Pathologic Thyroid Tissue. *Thyroid* (2004) 14:806–12. doi: 10.1089/thy.2004.14.806
35. Grabellus F, Nagarajah J, Bockisch A, Schmid KW, Sheu SY. Glucose Transporter 1 Expression, Tumor Proliferation, and Iodine/Glucose Uptake in Thyroid Cancer With Emphasis on Poorly Differentiated Thyroid Carcinoma. *Clin Nucl Med* (2012) 35:121–7. doi: 10.1097/RLU.0b013e3182393599
36. Ciampi R, Vivaldi A, Romei C, Del Guerra A, Salvadori P, Cosci B, et al. Expression Analysis of Facilitative Glucose Transporters (Gluts) in Human Thyroid Carcinoma Cell Lines and Primary Tumors. *Mol Cell Endocrinol* (2008) 291:57–62. doi: 10.1016/j.mce.2008.05.003
37. Samih N, Hovsepian S, Aouani A, Lombardo D, Fayet G. Glut-1 Translocation in FRTL-5 Thyroid Cells: Role of Phosphatidylinositol 3-Kinase and N-Glycosylation. *Endocrinology* (2000) 141:4146–55. doi: 10.1210/endo.141.11.7793
38. Szablewski L. Expression of Glucose Transporters in Cancers. *Biochim Biophys Acta* (2013) 1835:164–9. doi: 10.1016/j.bbcan.2012.12.004
39. Józwiak P, Krześlak A, Pomorski L, Lipińska A. Expression of Hypoxia-Related Glucose Transporters GLUT1 and GLUT3 in Benign, Malignant and Non-Neoplastic Thyroid Lesions. *Mol Med Rep* (2012) 6:601–6. doi: 10.3892/mmr.2012.969
40. Chai YJ, Yi JW, Oh SW, Kim YA, Yi KH, Kim JH, et al. Upregulation of SLC2 (GLUT) Family Genes is Related to Poor Survival Outcomes in Papillary Thyroid Carcinoma: Analysis of Data From the Cancer Genome Atlas. *Surgery* (2017) 12:188–94. doi: 10.1016/j.surg.2016.04.050
41. Valli A, Morotti M, Zois CE, Albers PK, Soga T, Feldinger K, et al. Adaptation to HIF1 $\alpha$  Deletion in Hypoxic Cancer Cells by Upregulation of GLUT14 and Creatine Metabolism. *Mol Cancer Res* (2019) 17:1531–44. doi: 10.1158/1541-7786.Mcr-18-0315
42. Haber RS, Weiser KR, Pritsker A, Reder I, Burstein DE. GLUT1 Glucose Transporter Expression in Benign and Malignant Thyroid Nodules. *Thyroid* (1997) 7:363–7. doi: 10.1089/thy.1997.7.363
43. Xue C, Li G, Bao Z, Zhou Z, Li L. Mitochondrial Pyruvate Carrier 1: A Novel Prognostic Biomarker That Predicts Favourable Patient Survival in Cancer. *Cancer Cell Int* (2021) 21:288. doi: 10.1186/s12935-021-01996-8
44. Cairns RA, Harris IS, Mak TW. Regulation of Cancer Cell Metabolism. *Nat Rev Cancer* (2011) 11:85–95. doi: 10.1038/nrc2981
45. Nahm JH, Kim HM, Koo JS. Glycolysis-Related Protein Expression in Thyroid Cancer. *Tumour Biol* (2017) 39:1010428317695922. doi: 10.1177/1010428317695922
46. Hoof L, van der Veldt AA, Hoekstra OS, Boers M, Molthoff CF, van Diest PJ. Hexokinase III, Cyclin a and Galectin-3 are Overexpressed in Malignant Follicular Thyroid Nodules. *Clin Endocrinol (Oxf)* (2008) 68:252–7. doi: 10.1111/j.1365-2265.2007.03031.x
47. Huang J, Gao W, Liu H, Yin G, Duan H, Huang Z, et al. Up-Regulated ANP32E Promotes the Thyroid Carcinoma Cell Proliferation and Migration via Activating AKT/Mtor/HK2-Mediated Glycolysis. *Gene* (2020) 750:144681. doi: 10.1016/j.gene.2020.144681
48. Feng C, Gao Y, Wang C, Yu X, Zhang W, Guan H, et al. Aberrant Overexpression of Pyruvate Kinase M2 Is Associated With Aggressive Tumor Features and the BRAF Mutation in Papillary Thyroid Cancer. *J Clin Endocrinol Metab* (2013) 98:E1524–33. doi: 10.1210/jc.2012-4258
49. Strickaert A, Corbet C, Spinette SA, Craciun L, Dom G, Andry G, et al. Reprogramming of Energy Metabolism: Increased Expression and Roles of Pyruvate Carboxylase in Papillary Thyroid Cancer. *Thyroid* (2019) 29:845–57. doi: 10.1089/thy.2018.0435
50. Verhagen JN, van der Heijden MC, de Jong-van Dijken J, Rijkse G, der Kinderen PJ, van Unnik JA, et al. Pyruvate Kinase in Normal Human Thyroid Tissue and Thyroid Neoplasms. *Cancer* (1985) 55:142–8. doi: 10.1002/1097-0142(19850101)55:1<142::aid-cnrc2820550122>3.0.co;2-x
51. Hosios AM, Hecht VC, Danai LV, Johnson MO, Rathmell JC, Steinhauser ML, et al. Amino Acids Rather Than Glucose Account for the Majority of Cell Mass in Proliferating Mammalian Cells. *Dev Cell* (2016) 36:540–9. doi: 10.1016/j.devcel.2016.02.012
52. Zhang J, Pavlova NN, Thompson CB. Cancer Cell Metabolism: The Essential Role of the Nonessential Amino Acid, Glutamine. *EMBO J* (2017) 36:1302–15. doi: 10.15252/embj.201696151
53. Kodama M, Oshikawa K, Shimizu H, Yoshioka S, Takahashi M, Izumi Y, et al. A Shift in Glutamine Nitrogen Metabolism Contributes to the Malignant Progression of Cancer. *Nat Commun* (2020) 11:1320. doi: 10.1038/s41467-020-15136-9
54. Altman BJ, Stine ZE, Dang CV. From Krebs to Clinic: Glutamine Metabolism to Cancer Therapy. *Nat Rev Cancer* (2016) 16:619–34. doi: 10.1038/nrc.2016.71
55. Cluntun AA, Lukey MJ, Cerione RA, Locasale JW. Glutamine Metabolism in Cancer: Understanding the Heterogeneity. *Trends Cancer* (2017) 3:169–80. doi: 10.1016/j.trecan.2017.01.005
56. Chen Z, Lin J, Feng S, Chen X, Huang H, Wang C, et al. SIRT4 Inhibits the Proliferation, Migration, and Invasion Abilities of Thyroid Cancer Cells by Inhibiting Glutamine Metabolism. *Oncotargets Ther* (2019) 12:2397–408. doi: 10.2147/ott.S189536
57. Kim HM, Lee YK, Koo JS. Expression of Glutamine Metabolism-Related Proteins in Thyroid Cancer. *Oncotarget* (2016) 7:53628–41. doi: 10.18632/oncotarget.10682
58. Cha YJ, Jang H, Koo JS. Expression of Glutamine Metabolism-Related Proteins in Hürthle Cell Neoplasm of Thyroid: Comparison With Follicular Neoplasm. *Histol Histopathol* (2019) 34:167–74. doi: 10.14670/hh-18-036
59. Gebregiorgis T, Purohit V, Shukla SK, Tadros S, Chaika NV, Abrego J, et al. Glucose Limitation Alters Glutamine Metabolism in MUC1-Overexpressing Pancreatic Cancer Cells. *J Proteome Res* (2017) 16:3536–46. doi: 10.1021/acs.jproteome.7b00246
60. Sun WY, Kim HM, Jung WH, Koo JS. Expression of Serine/Glycine Metabolism-Related Proteins is Different According to the Thyroid Cancer Subtype. *J Transl Med* (2016) 14:168. doi: 10.1186/s12967-016-0915-8
61. Zhao M, Bu Y, Feng J, Zhang H, Chen Y, Yang G, et al. SPIN1 Triggers Abnormal Lipid Metabolism and Enhances Tumor Growth in Liver Cancer. *Cancer Lett* (2020) 470:54–63. doi: 10.1016/j.canlet.2019.11.032
62. Yi M, Li J, Chen S, Cai J, Ban Y, Peng Q, et al. Emerging Role of Lipid Metabolism Alterations in Cancer Stem Cells. *J Exp Clin Cancer Res* (2018) 16:118. doi: 10.1186/s13046-018-0784-5
63. Röhrig F, Schulze A. The Multifaceted Roles of Fatty Acid Synthesis in Cancer. *Nat Rev Cancer* (2016) 16:732–49. doi: 10.1038/nrc.2016.89
64. Mossman D, Park S, Hall MN. Mtor Signalling and Cellular Metabolism are Mutual Determinants in Cancer. *Nat Rev Cancer* (2018) 18:744–57. doi: 10.1038/s41568-018-0074-8
65. Luo X, Cheng C, Tan Z, Li N, Tang M, Yang L, et al. Emerging Roles of Lipid Metabolism in Cancer Metastasis. *Mol Cancer* (2017) 16:76. doi: 10.1186/s12943-017-0646-3
66. Li H, Feng Z, He ML. Lipid Metabolism Alteration Contributes to and Maintains the Properties of Cancer Stem Cells. *Theranostics* (2020) 10:7053–69. doi: 10.7150/thno.41388
67. Cheng C, Geng F, Cheng X, Guo D. Lipid Metabolism Reprogramming and its Potential Targets in Cancer. *Cancer Commun (Lond)* (2018) 38:27. doi: 10.1186/s40880-018-0301-4
68. Liao T, Wang YJ, Hu JQ, Wang Y, Han LT, Ma B, et al. Histone Methyltransferase KMT5A Gene Modulates Oncogenesis and Lipid Metabolism of Papillary Thyroid Cancer *In Vitro*. *Oncol Rep* (2018) 39:2185–92. doi: 10.3892/or.2018.6295
69. Liu H, Liu JY, Wu X, Zhang JT. Biochemistry, Molecular Biology, and Pharmacology of Fatty Acid Synthase, an Emerging Therapeutic Target and Diagnosis/Prognosis Marker. *Int J Biochem Mol Biol* (2010) 1:69–89.
70. Fantin VR, St-Pierre J, Leder P. Attenuation of LDH-a Expression Uncovers a Link Between Glycolysis, Mitochondrial Physiology, and Tumor Maintenance. *Cancer Cell* (2006) 9:425–34. doi: 10.1016/j.ccr.2006.04.023
71. Zhang C, Liu J, Huang G, Zhao Y, Yue X, Wu H, et al. Cullin3-KLHL25 Ubiquitin Ligase Targets ACLY for Degradation to Inhibit Lipid Synthesis



- and Tumor Progression. *Genes Dev* (2016) 30:1956–70. doi: 10.1101/gad.283283.116
72. Svensson RU, Parker SJ, Eichner LJ, Kolar MJ, Wallace M, Brun SN, et al. Inhibition of Acetyl-CoA Carboxylase Suppresses Fatty Acid Synthesis and Tumor Growth of Non-Small-Cell Lung Cancer in Preclinical Models. *Nat Med* (2016) 22:1108–19. doi: 10.1038/nm.4181
73. Rios Garcia M, Steinbauer B, Srivastava K, Singhal M, Mattijssen F, Maida A, et al. Acetyl-CoA Carboxylase 1-Dependent Protein Acetylation Controls Breast Cancer Metastasis and Recurrence. *Cell Metab* (2017) 26:842–55.e5. doi: 10.1016/j.cmet.2017.09.018
74. Nwosu ZC, Battello N, Rothley M, Piorońska W, Sitek B, Ebert MP, et al. Liver Cancer Cell Lines Distinctly Mimic the Metabolic Gene Expression Pattern of the Corresponding Human Tumours. *J Exp Clin Cancer Res* (2018) 37:211. doi: 10.1186/s13046-018-0872-6
75. Lally JSV, Ghoshal S, DePeralta DK, Moaven O, Wei L, Masia R, et al. Inhibition of Acetyl-CoA Carboxylase by Phosphorylation or the Inhibitor ND-654 Suppresses Lipogenesis and Hepatocellular Carcinoma. *Cell Metab* (2019) 29:174–82.e5. doi: 10.1016/j.cmet.2018.08.020
76. Kapadia B, Nanaji NM, Bhalla K, Bhandary B, Lapidus R, Beheshti A, et al. Fatty Acid Synthase Induced S6Kinase Facilitates USP11-Eif4b Complex Formation for Sustained Oncogenic Translation in DLBCL. *Nat Commun* (2018) 9:829. doi: 10.1038/s41467-018-03028-y
77. Gu L, Zhu Y, Lin X, Lu B, Zhou X, Zhou F, et al. The Ikk $\beta$ -USP30-ACLY Axis Controls Lipogenesis and Tumorigenesis. *Hepatology* (2021) 73:160–74. doi: 10.1002/hep.31249
78. Gouw AM, Margulis K, Liu NS, Raman SJ, Mancuso A, Toal GG, et al. The MYC Oncogene Cooperates With Sterol-Regulated Element-Binding Protein to Regulate Lipogenesis Essential for Neoplastic Growth. *Cell Metab* (2019) 30:556–72.e5. doi: 10.1016/j.cmet.2019.07.012
79. Corbet C, Pinto A, Martherus R, Santiago de Jesus JP, Polet F, Feron O. Acidosis Drives the Reprogramming of Fatty Acid Metabolism in Cancer Cells Through Changes in Mitochondrial and Histone Acetylation. *Cell Metab* (2016) 24:311–23. doi: 10.1016/j.cmet.2016.07.003
80. Che L, Chi W, Qiao Y, Zhang J, Song X, Liu Y, et al. Cholesterol Biosynthesis Supports the Growth of Hepatocarcinoma Lesions Depleted of Fatty Acid Synthase in Mice and Humans. *Gut* (2020) 69:177–86. doi: 10.1136/gutjnl-2018-317581
81. Bort A, Sánchez BG, de Miguel I, Mateos-Gómez PA, Diaz-Laviada I. Dysregulated Lipid Metabolism in Hepatocellular Carcinoma Cancer Stem Cells. *Mol Biol Rep* (2020) 47:2635–47. doi: 10.1007/s11033-020-05352-3
82. Ali A, Levantini E, Teo JT, Goggi J, Clohessy JG, Wu CS, et al. Fatty Acid Synthase Mediates EGFR Palmitoylation in EGFR Mutated Non-Small Cell Lung Cancer. *EMBO Mol Med* (2018) 10. doi: 10.15252/emmm.201708313
83. Abbassi-Ghadi N, Antonowicz SS, McKenzie JS, Kumar S, Huang J, Jones EA, et al. De Novo Lipogenesis Alters the Phospholipidome of Esophageal Adenocarcinoma. *Cancer Res* (2020) 80:2764–74. doi: 10.1158/0008-5472.Can-19-4035
84. Xu M, Sun T, Wen S, Zhang T, Wang X, Cao Y, et al. Characteristics of Lipid Metabolism-Related Gene Expression-Based Molecular Subtype in Papillary Thyroid Cancer. *Acta Biochim Biophys Sin (Shanghai)* (2020) 52:1166–70. doi: 10.1093/abbs/gmaa092
85. Leng J, Guan Q, Sun T, Wu Y, Cao Y, Guo Y. Application of Isotope-Based Carboxy Group Derivatization in LC-MS/MS Analysis of Tissue Free-Fatty Acids for Thyroid Carcinoma. *J Pharm BioMed Anal* (2013) 84:256–62. doi: 10.1016/j.jpba.2013.06.004
86. Uddin S, Siraj AK, Al-Rasheed M, Ahmed M, Bu R, Myers JN, et al. Fatty Acid Synthase and AKT Pathway Signaling in a Subset of Papillary Thyroid Cancers. *J Clin Endocrinol Metab* (2008) 93:4088–97. doi: 10.1210/jc.2008-0503
87. Sekiguchi M, Shiroko Y, Arai T, Kishino T, Sugawara I, Kusakabe T, et al. Biological Characteristics and Chemosensitivity Profile of Four Human Anaplastic Thyroid Carcinoma Cell Lines. *BioMed Pharmacother* (2001) 55:466–74. doi: 10.1016/s0753-3322(01)00087-7
88. Liu J, Brown RE. Immunohistochemical Expressions of Fatty Acid Synthase and Phosphorylated C-Met in Thyroid Carcinomas of Follicular Origin. *Int J Clin Exp Pathol* (2011) 4:755–64.
89. Munir R, Liscic J, Swinnen JV, Zaidi N. Lipid Metabolism in Cancer Cells Under Metabolic Stress. *Br J Cancer* (2019) 120:1090–8. doi: 10.1038/s41416-019-0451-4
90. Valvo V, Iesato A, Kavanagh TR, Priolo C, Zsengeller Z, Pontecorvi A, et al. Fine-Tuning Lipid Metabolism by Targeting Mitochondria-Associated Acetyl-CoA-Carboxylase 2 in BRAF(V600E) Papillary Thyroid Carcinoma. *Thyroid* (2021) 31:1335–58. doi: 10.1089/thy.2020.0311
91. von Roemeling CA, Marlow LA, Pinkerton AB, Crist A, Miller J, Tun HW, et al. Aberrant Lipid Me[Von Roemeling, 2015 #353]tabolism in Anaplastic Thyroid Carcinoma Reveals Stearoyl CoA Desaturase 1 as a Novel Therapeutic Target. *J Clin Endocrinol Metab* (2015) 100:E697–709. doi: 10.1210/jc.2014-2764
92. Guo S, Wang Y, Zhou D, Li Z. Significantly Increased Monounsaturated Lipids Relative to Polyunsaturated Lipids in Six Types of Cancer Microenvironment are Observed by Mass Spectrometry Imaging. *Sci Rep* (2014) 4:5959. doi: 10.1038/srep05959
93. Turi Z, Lacey M, Mistrik M, Moudry P. Impaired Ribosome Biogenesis: Mechanisms and Relevance to Cancer and Aging. *Aging (Albany NY)* (2019) 11:2512–40. doi: 10.18632/aging.101922
94. Prakash V, Carson BB, Feenstra JM, Dass RA, Sekyrova P, Hoshino A, et al. Ribosome Biogenesis During Cell Cycle Arrest Fuels EMT in Development and Disease. *Nat Commun* (2019) 10:2110. doi: 10.1038/s41467-019-10100-8
95. Penzo M, Montanaro L, Treré D, Derenzini M. The Ribosome Biogenesis-Cancer Connection. *Cells* (2019) 8. doi: 10.3390/cells8010055
96. Pelletier J, Thomas G, Volarević S. Ribosome Biogenesis in Cancer: New Players and Therapeutic Avenues. *Nat Rev Cancer* (2018) 18:51–63. doi: 10.1038/nrc.2017.104
97. Kim DS, Camacho CV, Nagari A, Malladi VS, Challa S, Kraus WL. Activation of PARP-1 by Snorans Controls Ribosome Biogenesis and Cell Growth via the RNA Helicase DDX21. *Mol Cell* (2019) 75:1270–85.e14. doi: 10.1016/j.molcel.2019.06.020
98. Catez F, Dalla Venezia N, Marcel V, Zorbas C, Lafontaine DLJ, Diaz JJ. Ribosome Biogenesis: An Emerging Druggable Pathway for Cancer Therapeutics. *Biochem Pharmacol* (2019) 175:74–81. doi: 10.1016/j.bcp.2018.11.014
99. Saiselet M, Floor S, Tarabichi M, Dom G, Hébrant A, van Staveren WC, et al. Thyroid Cancer Cell Lines: An Overview. *Front Endocrinol (Lausanne)* (2012) 3:133. doi: 10.3389/fendo.2012.00133
100. Jeong S, Kim IK, Kim H, Choi MJ, Lee J, Jo YS. Liver X Receptor  $\beta$  Related to Tumor Progression and Ribosome Gene Expression in Papillary Thyroid Cancer. *Endocrinol Metab (Seoul)* (2020) 35:656–68. doi: 10.3803/EnM.2020.667
101. Wang Y, Bai C, Ruan Y, Liu M, Chu Q, Qiu L, et al. Coordinative Metabolism of Glutamine Carbon and Nitrogen in Proliferating Cancer Cells Under Hypoxia. *Nat Commun* (2019) 10:201. doi: 10.1038/s41467-018-08033-9
102. Tardito S, Oudin A, Ahmed SU, Fack F, Keunen O, Zheng L, et al. Glutamine Synthetase Activity Fuels Nucleotide Biosynthesis and Supports Growth of Glutamine-Restricted Glioblastoma. *Nat Cell Biol* (2015) 17:1556–68. doi: 10.1038/ncb3272
103. Kodama M, Nakayama KI. A Second Warburg-Like Effect in Cancer Metabolism: The Metabolic Shift of Glutamine-Derived Nitrogen: A Shift in Glutamine-Derived Nitrogen Metabolism From Glutaminolysis to De Novo Nucleotide Biosynthesis Contributes to Malignant Evolution of Cancer. *BIOESSAYS* (2020) 42:e2000169. doi: 10.1002/bies.202000169
104. Fu S, Li Z, Xiao L, Hu W, Zhang L, Xie B, et al. Glutamine Synthetase Promotes Radiation Resistance via Facilitating Nucleotide Metabolism and Subsequent DNA Damage Repair. *Cell Rep* (2019) 28:1136–43.e4. doi: 10.1016/j.celrep.2019.07.002
105. Bott AJ, Shen J, Tonelli C, Zhan L, Sivaram N, Jiang YP, et al. Glutamine Anabolism Plays a Critical Role in Pancreatic Cancer by Coupling Carbon and Nitrogen Metabolism. *Cell Rep* (2019) 29:1287–98.e6. doi: 10.1016/j.celrep.2019.09.056
106. Lv Y, Wang X, Li X, Xu G, Bai Y, Wu J, et al. Nucleotide De Novo Synthesis Increases Breast Cancer Stemness and Metastasis via Cgmp-PKG-MAPK Signaling Pathway. *PloS Biol* (2020) 18:e3000872. doi: 10.1371/journal.pbio.3000872
107. Chan EM, Shibue T, McFarland JM, Gaeta B, Ghandi M, Dumont N, et al. WRN Helicase is a Synthetic Lethal Target in Microsatellite Unstable Cancers. *NATURE* (2019) 568:551–6. doi: 10.1038/s41586-019-1102-x
108. Robb R, Yang L, Shen C, Wolfe AR, Webb A, Zhang X, et al. Inhibiting BRAF Oncogene-Mediated Radioresistance Effectively Radiosensitizes BRAF

- (V600E)-Mutant Thyroid Cancer Cells by Constraining DNA Double-Strand Break Repair. *Clin Cancer Res* (2019) 25:4749–60. doi: 10.1158/1078-0432.Ccr-18-3625
109. Cabanillas ME, Ferrarotto R, Garden AS, Ahmed S, Busaidy NL, Dadu R, et al. Neoadjuvant BRAF- and Immune-Directed Therapy for Anaplastic Thyroid Carcinoma. *THYROID* (2018) 28:945–51. doi: 10.1089/thy.2018.0060
110. Trybek T, Walczyk A, Gąsior-Perczak D, Palyga I, Mikina E, Kowalik A, et al. Impact of BRAF V600E and TERT Promoter Mutations on Response to Therapy in Papillary Thyroid Cancer. *Endocrinology* (2019) 160:2328–38. doi: 10.1210/en.2019-00315
111. Panebianco F, Nikitski AV, Nikiforova MN, Nikiforov YE. Spectrum of TERT Promoter Mutations and Mechanisms of Activation in Thyroid Cancer. *Cancer Med* (2019) 8:5831–9. doi: 10.1002/cam4.2467
112. Melo M, Gaspar da Rocha A, Batista R, Vinagre J, Martins MJ, Costa G, et al. TERT, BRAF, and NRAS in Primary Thyroid Cancer and Metastatic Disease. *J Clin Endocrinol Metab* (2017) 102:1898–907. doi: 10.1210/jc.2016-2785
113. Chen M, Shen M, Li Y, Liu C, Zhou K, Hu W, et al. GC-MS-Based Metabolomic Analysis of Human Papillary Thyroid Carcinoma Tissue. *Int J Mol Med* (2015) 36:1607–14. doi: 10.3892/ijmm.2015.2368
114. Cham CM, Gajewski TF. Glucose Availability Regulates IFN- $\gamma$  Production and P70s6 Kinase Activation in CD8 $^{+}$  Effector T Cells. *J Immunol* (2005) 174:4670–7. doi: 10.4049/jimmunol.174.8.4670
115. Chang CH, Curtis JD, Maggi LBJr, Faubert B, Villarino AV, O'Sullivan D, et al. Posttranscriptional Control of T Cell Effector Function by Aerobic Glycolysis. *CELL* (2013) 153:1239–51. doi: 10.1016/j.cell.2013.05.016
116. Elia I, Haigis MC. Metabolites and the Tumour Microenvironment: From Cellular Mechanisms to Systemic Metabolism. *Nat Metab* (2021) 3:21–32. doi: 10.1038/s42255-020-00317-z
117. Leone RD, Zhao L, Englert JM, Sun IM, Oh MH, Sun IH, et al. Glutamine Blockade Induces Divergent Metabolic Programs to Overcome Tumor Immune Evasion. *Science* (2019) 366:1013–21. doi: 10.1126/science.aav2588
118. Moretti S, Menicali E, Voce P, Morelli S, Cantarelli S, Sponziello M, et al. Indoleamine 2,3-Dioxygenase 1 (IDO1) is Up-Regulated in Thyroid Carcinoma and Drives the Development of an Immunosuppressant Tumor Microenvironment. *J Clin Endocrinol Metab* (2014) 99:E832–40. doi: 10.1210/jc.2013-3351
119. Park A, Yang Y, Lee Y, Kim MS, Park YJ, Jung H, et al. Indoleamine-2,3-Dioxygenase in Thyroid Cancer Cells Suppresses Natural Killer Cell Function by Inhibiting NKG2D and Nkp46 Expression via STAT Signaling Pathways. *J Clin Med* (2019) 8. doi: 10.3390/jcm8060842
120. Chu R, Liu SY, Vlantis AC, van Hasselt CA, Ng EK, Fan MD, et al. Inhibition of Foxp3 in Cancer Cells Induces Apoptosis of Thyroid Cancer Cells. *Mol Cell Endocrinol* (2015) 399:228–34. doi: 10.1016/j.mce.2014.10.006
121. Ivashkiv LB. The Hypoxia-Lactate Axis Tempers Inflammation. *Nat Rev Immunol* (2020) 20:85–6. doi: 10.1038/s41577-019-0259-8
122. Arts RJ, Plantinga TS, Tuit S, Ulas T, Heinhuis B, Tesselaar M, et al. Transcriptional and Metabolic Reprogramming Induce an Inflammatory Phenotype in Non-Medullary Thyroid Carcinoma-Induced Macrophages. *Oncotarget* (2016) 5:e1229725. doi: 10.1080/2162402x.2016.1229725
123. Brand A, Singer K, Koehl GE, Kolitzus M, Schoenhammer G, Thiel A, et al. LDHA-Associated Lactic Acid Production Blunts Tumor Immunosurveillance by T and NK Cells. *Cell Metab* (2016) 24:657–71. doi: 10.1016/j.cmet.2016.08.011
124. Cantelmo AR, Conradi LC, Brajic A, Goveia J, Kalucka J, Pircher A, et al. Inhibition of the Glycolytic Activator PFKFB3 in Endothelium Induces Tumor Vessel Normalization, Impairs Metastasis, and Improves Chemotherapy. *Cancer Cell* (2016) 30:968–85. doi: 10.1016/j.ccell.2016.10.006
125. Colegio OR, Chu NQ, Szabo AL, Chu T, Rhebergen AM, Jairam V, et al. Functional Polarization of Tumour-Associated Macrophages by Tumour-Derived Lactic Acid. *Nature* (2014) 513:559–63. doi: 10.1038/nature13490
126. Curry JM, Tuluc M, Whitaker-Menezes D, Ames JA, Anantharaman A, Butera A, et al. Cancer Metabolism, Stemness and Tumor Recurrence: MCT1 and MCT4 are Functional Biomarkers of Metabolic Symbiosis in Head and Neck Cancer. *Cell Cycle* (2013) 12:1371–84. doi: 10.4161/cc.24092
127. Curry JM, Tassone P, Cotzia P, Sprandio J, Luginbuhl A, Cognetti DM, et al. Multicompartment Metabolism in Papillary Thyroid Cancer. *Laryngoscope* (2016) 126:2410–8. doi: 10.1002/lary.25799
128. Bertero T, Oldham WM, Grasset EM, Bourget I, Boulter E, Pisano S, et al. Tumor-Stroma Mechanics Coordinate Amino Acid Availability to Sustain Tumor Growth and Malignancy. *Cell Metab* (2019) 29:124–40.e10. doi: 10.1016/j.cmet.2018.09.012
129. Mestre-Farrera A, Bruch-Oms M, Peña R, Rodríguez-Morató J, Alba-Castellón L, Comerma L, et al. Glutamine-Directed Migration of Cancer-Activated Fibroblasts Facilitates Epithelial Tumor Invasion. *Cancer Res* (2021) 81:438–51. doi: 10.1158/0008-5472.Can-20-0622
130. Sherman MH, Yu RT, Tseng TW, Sousa CM, Liu S, Truitt ML, et al. Stromal Cues Regulate the Pancreatic Cancer Epigenome and Metabolome. *Proc Natl Acad Sci USA* (2017) 114:1129–34. doi: 10.1073/pnas.1620164114
131. Cadamuro M, Brivio S, Mertens J, Vismara M, Moncsek A, Milani C, et al. Platelet-Derived Growth Factor-D Enables Liver Myofibroblasts to Promote Tumor Lymphangiogenesis in Cholangiocarcinoma. *J Hepatol* (2019) 70:700–9. doi: 10.1016/j.jhep.2018.12.004
132. Cruz-Bermúdez A, Laza-Briviesca R, Vicente-Blanco RJ, García-Grande A, Coronado MJ, Laine-Menéndez S, et al. Cancer-Associated Fibroblasts Modify Lung Cancer Metabolism Involving ROS and TGF- $\beta$  Signaling. *Free Radic Biol Med* (2019) 130:163–73. doi: 10.1016/j.freeradbiomed.2018.10.450
133. Fozzatti L, Alamino VA, Park S, Giusiano L, Volpini X, Zhao L, et al. Interplay of Fibroblasts With Anaplastic Tumor Cells Promotes Follicular Thyroid Cancer Progression. *Sci Rep* (2019) 9:8028. doi: 10.1038/s41598-019-44361-6
134. Rabold K, Aschenbrenner A, Thiele C, Boahen CK, Schiltmans A, Smit JWA, et al. Enhanced Lipid Biosynthesis in Human Tumor-Induced Macrophages Contributes to Their Protumoral Characteristics. *J Immunother Cancer* (2020) 8. doi: 10.1136/jitc-2020-000638
135. Schönberger J, Rüschhoff J, Grimm D, Marienhagen J, Rümmele P, Meyringer R, et al. Glucose Transporter 1 Gene Expression is Related to Thyroid Neoplasms With an Unfavorable Prognosis: An Immunohistochemical Study. *THYROID* (2002) 12:747–54. doi: 10.1089/105072502760339307
136. Johnson JM, Lai SY, Cotzia P, Cognetti D, Luginbuhl A, Pribitkin EA, et al. Mitochondrial Metabolism as a Treatment Target in Anaplastic Thyroid Cancer. *Semin Oncol* (2015) 42:915–22. doi: 10.1053/j.seminoncol.2015.09.025
137. Matsuzaki K, Segade F, Wong M, Clark OH, Perrier ND, Bowden DW. Glucose Transporters in the Thyroid. *Thyroid* (2005) 15:545–50. doi: 10.1089/thy.2005.15.545
138. Yang H, Zhong JT, Zhou SH, Han HM. Roles of GLUT-1 and HK-II Expression in the Biological Behavior of Head and Neck Cancer. *Oncotarget* (2019) 10:3066–83. doi: 10.18632/oncotarget.24684
139. Suh HY, Choi H, Paeng JC, Cheon GJ, Chung JK, Kang KW. Comprehensive Gene Expression Analysis for Exploring the Association Between Glucose Metabolism and Differentiation of Thyroid Cancer. *BMC Cancer* (2019) 19:1260. doi: 10.1186/s12885-019-6482-7
140. Kim S, Chung JK, Min HS, Kang JH, Park DJ, Jeong JM, et al. Expression Patterns of Glucose Transporter-1 Gene and Thyroid Specific Genes in Human Papillary Thyroid Carcinoma. *Nucl Med Mol Imaging* (2014) 48:91–7. doi: 10.1007/s13139-013-0249-x
141. Huang FQ, Li J, Jiang L, Wang FX, Alolga RN, Wang MJ, et al. Serum-Plasma Matched Metabolomics for Comprehensive Characterization of Benign Thyroid Nodule and Papillary Thyroid Carcinoma. *Int J Cancer* (2019) 144:868–76. doi: 10.1002/ijc.31925
142. Ryu HS, Park YS, Park HJ, Chung YR, Yom CK, Ahn SH, et al. Expression of Indoleamine 2,3-Dioxygenase and Infiltration of FOXP3 $^{+}$  Regulatory T Cells are Associated With Aggressive Features of Papillary Thyroid Microcarcinoma. *Thyroid* (2014) 24:1232–40. doi: 10.1089/thy.2013.0423
143. Hsieh IS, Gopula B, Chou CC, Wu HY, Chang GD, Wu WJ, et al. Development of Novel Irreversible Pyruvate Kinase M2 Inhibitors. *J Med Chem* (2019) 62:8497–510. doi: 10.1021/acs.jmedchem.9b00763
144. Vangapandu HV, Alston B, Morse J, Ayres ML, Wierda WG, Keating MJ, et al. Biological and Metabolic Effects of IACS-010759, an Oxphos Inhibitor, on Chronic Lymphocytic Leukemia Cells. *Oncotarget* (2018) 9:24980–91. doi: 10.18632/oncotarget.25166
145. Bizjak M, Malavašič P, Dolinar K, Pohar J, Pirkmajer S, Pavlin M. Combined Treatment With Metformin and 2-Deoxy Glucose Induces Detachment of Viable MDA-MB-231 Breast Cancer Cells. *vitro Sci Rep* (2017) 7:1761. doi: 10.1038/s41598-017-01801-5

146. Jones AT, Narov K, Yang J, Sampson JR, Shen MH. Efficacy of Dual Inhibition of Glycolysis and Glutaminolysis for Therapy of Renal Lesions in Tsc2(+/-) Mice. *Neoplasia* (2019) 21:230–8. doi: 10.1016/j.neo.2018.12.003
147. Sun Y, Bandi M, Lofton T, Smith M, Bristow CA, Carugo A, et al. Functional Genomics Reveals Synthetic Lethality Between Phosphogluconate Dehydrogenase and Oxidative Phosphorylation. *Cell Rep* (2019) 26:469–82.e5. doi: 10.1016/j.celrep.2018.12.043
148. DeWaal D, Nogueira V, Terry AR, Patra KC, Jeon SM, Guzman G, et al. Hexokinase-2 Depletion Inhibits Glycolysis and Induces Oxidative Phosphorylation in Hepatocellular Carcinoma and Sensitizes to Metformin. *Nat Commun* (2018) 9:446. doi: 10.1038/s41467-017-02733-4
149. Shimada N, Takasawa R, Tanuma SI. Interdependence of GLO I and PKM2 in the Metabolic Shift to Escape Apoptosis in GLO I-Dependent Cancer Cells. *Arch Biochem Biophys* (2018) 638:1–7. doi: 10.1016/j.abb.2017.12.008
150. Zhao B, Aggarwal A, Marshall JA, Barletta JA, Kijewski MF, Lorch JH, et al. Glycolytic Inhibition With 3-Bromopyruvate Suppresses Tumor Growth and Improves Survival in a Murine Model of Anaplastic Thyroid Cancer. *Surgery* (2021). doi: 10.1016/j.surg.2021.05.055
151. Wang SY, Wei YH, Shieh DB, Lin LL, Cheng SP, Wang PW, et al. 2-Deoxy-D-Glucose can Complement Doxorubicin and Sorafenib to Suppress the Growth of Papillary Thyroid Carcinoma Cells. *PLoS One* (2015) 10:e0130959. doi: 10.1371/journal.pone.0130959
152. Sobhakumari A, Orcutt KP, Love-Homan L, Kowalski CE, Parsons AD, Knudson CM, et al. 2-Deoxy-D-Glucose Suppresses the in Vivo Antitumor Efficacy of Erlotinib in Head and Neck Squamous Cell Carcinoma Cells. *Oncol Res* (2016) 24:55–64. doi: 10.3727/096504016x14586627440192
153. Sandulache VC, Skinner HD, Wang Y, Chen Y, Dodge CT, Ow TJ, et al. Glycolytic Inhibition Alters Anaplastic Thyroid Carcinoma Tumor Metabolism and Improves Response to Conventional Chemotherapy and Radiation. *Mol Cancer Ther* (2012) 11:1373–80. doi: 10.1158/1535-7163.Mct-12-0041
154. Robbins RJ, Wan Q, Grewal RK, Reibke R, Gonen M, Strauss HW, et al. Real-Time Prognosis for Metastatic Thyroid Carcinoma Based on 2-[18F]Fluoro-2-Deoxy-D-Glucose-Positron Emission Tomography Scanning. *J Clin Endocrinol Metab* (2006) 91:498–505. doi: 10.1210/jc.2005-1534
155. Li J, Eu JQ, Kong LR, Wang L, Lim YC, Goh BC, et al. Targeting Metabolism in Cancer Cells and the Tumour Microenvironment for Cancer Therapy. *Molecules* (2020) 25. doi: 10.3390/molecules25204831
156. Nancolas B, Guo L, Zhou R, Nath K, Nelson DS, Leeper DB, et al. The Anti-Tumour Agent Lonidamine is a Potent Inhibitor of the Mitochondrial Pyruvate Carrier and Plasma Membrane Monocarboxylate Transporters. *Biochem J* (2016) 473:929–36. doi: 10.1042/bj20151120
157. Berruti A, Bitossi R, Gorzegno G, Bottini A, Alquati P, De Matteis A, et al. Time to Progression in Metastatic Breast Cancer Patients Treated With Epirubicin is Not Improved by the Addition of Either Cisplatin or Lonidamine: Final Results of a Phase III Study With a Factorial Design. *J Clin Oncol* (2002) 20:4150–9. doi: 10.1200/jco.2002.08.012
158. Wagner M, Wuest M, Lopez-Campistrous A, Glubrecht D, Dufour J, Jans HS, et al. Tyrosine Kinase Inhibitor Therapy and Metabolic Remodelling in Papillary Thyroid Cancer. *Endocr Relat Cancer* (2020) 27:495–507. doi: 10.1530/erc-20-0135
159. Chen Y, Maniakas A, Tan L, Cui M, Le X, Niedzielski JS, et al. Development of a Rational Strategy for Integration of Lactate Dehydrogenase a Suppression Into Therapeutic Algorithms for Head and Neck Cancer. *Br J Cancer* (2021) 124:1670–9. doi: 10.1038/s41416-021-01297-x
160. Van Poznak C, Seidman AD, Reidenberg MM, Moasser MM, Sklarin N, Van Zee K, et al. Oral Gossypol in the Treatment of Patients With Refractory Metastatic Breast Cancer: A Phase I/II Clinical Trial. *Breast Cancer Res Treat* (2001) 66:239–48. doi: 10.1023/a:1010686204736
161. Rellinger EJ, Craig BT, Alvarez AL, Dusek HL, Kim KW, Qiao J, et al. FX11 Inhibits Aerobic Glycolysis and Growth of Neuroblastoma Cells. *SURGERY* (2017) 161:747–52. doi: 10.1016/j.surg.2016.09.009
162. Zhao Z, Han F, Yang S, Wu J, Zhan W. Oxamate-Mediated Inhibition of Lactate Dehydrogenase Induces Protective Autophagy in Gastric Cancer Cells: Involvement of the Akt-Mtor Signaling Pathway. *Cancer Lett* (2015) 358:17–26. doi: 10.1016/j.canlet.2014.11.046
163. Pieters R, Appel I, Kuehn HJ, Tetzlaff-Fohr I, Pichlmeier U, van der Vaart I, et al. Pharmacokinetics, Pharmacodynamics, Efficacy, and Safety of a New Recombinant Asparaginase Preparation in Children With Previously Untreated Acute Lymphoblastic Leukemia: A Randomized Phase 2 Clinical Trial. *Blood* (2008) 112:4832–8. doi: 10.1182/blood-2008-04-149443
164. Zhai L, Spranger S, Binder DC, Gritsina G, Lauing KL, Giles FJ, et al. Molecular Pathways: Targeting IDO1 and Other Tryptophan Dioxygenases for Cancer Immunotherapy. *Clin Cancer Res* (2015) 21:5427–33. doi: 10.1158/1078-0432.Ccr-15-0420
165. Joyce JA, Fearon DT. T Cell Exclusion, Immune Privilege, and the Tumor Microenvironment. *SCIENCE* (2015) 348:74–80. doi: 10.1126/science.aaa6204
166. Glazer ES, Piccirillo M, Albino V, Di Giacomo R, Palaia R, Mastro AA, et al. Phase II Study of Pegylated Arginine Deiminase for Nonresectable and Metastatic Hepatocellular Carcinoma. *J Clin Oncol* (2010) 28:2220–6. doi: 10.1200/jco.2009.26.7765
167. Ascierto PA, Scala S, Castello G, Daponte A, Simeone E, Ottaviano A, et al. Pegylated Arginine Deiminase Treatment of Patients With Metastatic Melanoma: Results From Phase I and II Studies. *J Clin Oncol* (2005) 23:7660–8. doi: 10.1200/jco.2005.02.0933
168. Harding JJ, Telli ML, Munster PN, Le MH, Molineaux C, Bennett MK, et al. Safety and Tolerability of Increasing Doses of CB-839, a First-in-Class, Orally Administered Small Molecule Inhibitor of Glutaminase, in Solid Tumors. *J OF Clin Oncol* (2015) 33:2512–2. doi: 10.1200/jco.2015.33.15\_suppl.2512
169. Wu JM, Ho TW, Lai IR, Chen CN, Lin MT. Parenteral Glutamine Supplementation Improves Serum Albumin Values in Surgical Cancer Patients. *Clin Nutr* (2021) 40:645–50. doi: 10.1016/j.clnu.2020.06.015
170. Sands S, Ladas EJ, Kelly KM, Weiner M, Lin M, Ndao DH, et al. Glutamine for the Treatment of Vincristine-Induced Neuropathy in Children and Adolescents With Cancer. *Support Care Cancer* (2017) 25:701–8. doi: 10.1007/s00520-016-3441-6
171. Azman M, Mohd Yunus MR, Sulaiman S, Syed Omar SN. Enteral Glutamine Supplementation in Surgical Patients With Head and Neck Malignancy: A Randomized Controlled Trial. *Head Neck* (2015) 37:1799–807. doi: 10.1002/hed.23839
172. Anderson PM, Lalla RV. Glutamine for Amelioration of Radiation and Chemotherapy Associated Mucositis During Cancer Therapy. *Nutrients* (2020) 12. doi: 10.3390/nu12061675
173. Abe T, Hosoi T, Kawai R, Uemura N, Higaki E, An B, et al. Perioperative Enteral Supplementation With Glutamine, Fiber, and Oligosaccharide Reduces Early Postoperative Surgical Stress Following Esophagectomy for Esophageal Cancer. *Esophagus* (2019) 16:63–70. doi: 10.1007/s10388-018-0630-z
174. Long GV, Dummer R, Hamid O, Gajewski TF, Caglevic C, Dalle S, et al. Epacadostat Plus Pembrolizumab Versus Placebo Plus Pembrolizumab in Patients With Unresectable or Metastatic Melanoma (ECHO-301/KEYNOTE-252): A Phase 3, Randomised, Double-Blind Study. *Lancet Oncol* (2019) 20:1083–97. doi: 10.1016/s1470-2045(19)30274-8
175. Ntambi JM. Regulation of Stearoyl-CoA Desaturase by Polyunsaturated Fatty Acids and Cholesterol. *J Lipid Res* (1999) 1549–58. doi: 10.1016/S0022-2275(20)33401-5
176. Presler M, Wojtczyk-Miaskowska A, Schlichtholz B, Kaluzny A, Matuszewski M, Mika A, et al. Increased Expression of the Gene Encoding Stearoyl-CoA Desaturase 1 in Human Bladder Cancer. *Mol Cell Biochem* (2018) 40:217–24. doi: 10.1007/s11010-018-3306-z
177. Lai KKY, Kweon SM, Chi F, Hwang E, Kabe Y, Higashiyama R, et al. Stearoyl-CoA Desaturase Promotes Liver Fibrosis and Tumor Development in Mice via a Wnt Positive-Signaling Loop by Stabilization of Low-Density Lipoprotein-Receptor-Related Proteins 5 and 6. *Gastroenterology* (2017) 147:1477–91. doi: 10.1053/j.gastro.2017.01.021
178. Gao Y, Li J, Xi H, Cui J, Zhang K, Zhang J, et al. Stearoyl-CoA-Desaturase-1 Regulates Gastric Cancer Stem-Like Properties and Promotes Tumour Metastasis via Hippo/YAP Pathway. *Br J Cancer* (2020) 122:1837–47. doi: 10.1038/s41416-020-0827-5
179. Aljohani A, Khan MI, Bonneville A, Guo C, Jeffery J, O'Neill L, et al. Hepatic Stearoyl CoA Desaturase 1 Deficiency Increases Glucose Uptake in Adipose Tissue Partially Through the PGC-1 $\alpha$ -FGF21 Axis in Mice. *J Biol Chem* (2019) 122:19475–85. doi: 10.1074/jbc.RA119.009868
180. Wang J, Xu Y, Zhu L, Zou Y, Kong W, Dong B, et al. High Expression of Stearoyl-CoA Desaturase 1 Predicts Poor Prognosis in Patients With Clear-Cell Renal Cell Carcinoma. *PLoS One* (2016) 294:e0166231. doi: 10.1371/journal.pone.0166231

181. Peck B, Schulze A. Lipid Desaturation - the Next Step in Targeting Lipogenesis in Cancer? *FEBS J* (2016) 11:2767–78. doi: 10.1111/febs.13681
182. Liu G, Feng S, Jia L, Wang C, Fu Y, Luo Y. Lung Fibroblasts Promote Metastatic Colonization Through Upregulation of Stearoyl-CoA Desaturase 1 in Tumor Cells. *Oncogene* (2018) 283:1519–33. doi: 10.1038/s41388-017-0062-6
183. Gao J, Zhang Z, Liu Y, Zhang Z, Wang M, Gong A, et al. Stearoyl-CoA Desaturase 1 Potentiates Hypoxic Plus Nutrient-Deprived Pancreatic Cancer Cell Ferroptosis Resistance. *Oxid Med Cell Longev* (2021) 37:6629804. doi: 10.1155/2021/6629804
184. Tutino V, Gigante I, Scavo MP, Refolo MG, Nunzio V, Milella RA, et al. Stearoyl-CoA Desaturase-1 Enzyme Inhibition by Grape Skin Extracts Affects Membrane Fluidity in Human Colon Cancer Cell Lines. *Nutrients* (2020) 2021:6629804. doi: 10.3390/nu12030693
185. Pisanu ME, Maugeri-Sacca M, Fattore L, Bruschini S, De Vitis C, Tabbi E, et al. Inhibition of Stearoyl-CoA Desaturase 1 Reverts BRAF and MEK Inhibition-Induced Selection of Cancer Stem Cells in BRAF-Mutated Melanoma. *J Exp Clin Cancer Res* (2018) 12:318. doi: 10.1186/s13046-018-0989-7
186. Piao C, Cui X, Zhan B, Li J, Li Z, et al. Inhibition of Stearoyl CoA Desaturase-1 Activity Suppresses Tumour Progression and Improves Prognosis in Human Bladder Cancer. *J Cell Mol Med* (2019) 37:2064–76. doi: 10.1111/jcmm.14114
187. Ma XL, Sun YF, Wang BL, Shen MN, Zhou Y, Chen JW, et al. Sphere-Forming Culture Enriches Liver Cancer Stem Cells and Reveals Stearoyl-CoA Desaturase 1 as a Potential Therapeutic Target. *BMC Cancer* (2019) 23:760. doi: 10.1186/s12885-019-5963-z
188. Ma MKF, Lau EYT, Leung DHW, Lo J, Ho NPY, Cheng LKW, et al. Stearoyl-CoA Desaturase Regulates Sorafenib Resistance via Modulation of ER Stress-Induced Differentiation. *J Hepatol* (2017) 19:979–90. doi: 10.1016/j.jhep.2017.06.015
189. Pisanu ME, Noto A, De Vitis C, Morrone S, Scognamiglio G, Botti G, et al. Blockade of Stearoyl-CoA-Desaturase 1 Activity Reverts Resistance to Cisplatin in Lung Cancer Stem Cells. *Cancer Lett* (2017) 67:93–104. doi: 10.1016/j.canlet.2017.07.027
190. Potze L, di Franco S, Kessler JH, Stassi G, Medema JP. Betulinic Acid Kills Colon Cancer Stem Cells. *Curr Stem Cell Res Ther* (2016) 11:427–33. doi: 10.2174/1574888x11666151203223512

**Conflict of Interest:** The authors declare that the research was conducted in the absence of any commercial or financial relationships that could be construed as a potential conflict of interest.

**Publisher's Note:** All claims expressed in this article are solely those of the authors and do not necessarily represent those of their affiliated organizations, or those of the publisher, the editors and the reviewers. Any product that may be evaluated in this article, or claim that may be made by its manufacturer, is not guaranteed or endorsed by the publisher.

Copyright © 2021 Bao, Xu, Lu, Huang, Pan and Ge. This is an open-access article distributed under the terms of the Creative Commons Attribution License (CC BY). The use, distribution or reproduction in other forums is permitted, provided the original author(s) and the copyright owner(s) are credited and that the original publication in this journal is cited, in accordance with accepted academic practice. No use, distribution or reproduction is permitted which does not comply with these terms.





# The Metabolism Symbiosis Between Pancreatic Cancer and Tumor Microenvironment

Ying Li<sup>1</sup>, Ju Zhang<sup>2</sup>, Jie Xu<sup>3</sup> and Shanglong Liu<sup>4\*</sup>

<sup>1</sup> Department of Blood Transfusion, The Affiliated Hospital of Qingdao University, Qingdao, China, <sup>2</sup> Department of Operating Room, The Affiliated Hospital of Qingdao University, Qingdao, China, <sup>3</sup> Department of Nursing, Zaozhuang Second Health School, Zaozhuang, China, <sup>4</sup> Department of Gastrointestinal Surgery, The Affiliated Hospital of Qingdao University, Qingdao, China

## OPEN ACCESS

### Edited by:

Monica Montopoli,  
University of Padua, Italy

### Reviewed by:

Georg F. Weber,  
University of Cincinnati, United States  
Gang Yang,  
Peking Union Medical College Hospital  
(CAMS), China

### \*Correspondence:

Shanglong Liu  
liushanglong@qdyu.cn

### Specialty section:

This article was submitted to  
Cancer Metabolism,  
a section of the journal  
Frontiers in Oncology

**Received:** 16 August 2021

**Accepted:** 30 November 2021

**Published:** 16 December 2021

### Citation:

Li Y, Zhang J, Xu J and Liu S  
(2021) The Metabolism Symbiosis  
Between Pancreatic Cancer and  
Tumor Microenvironment.  
Front. Oncol. 11:759376.  
doi: 10.3389/fonc.2021.759376

Complex interactions occur between tumor cells and the tumor microenvironment. Studies have focused on the mechanism of metabolic symbiosis between tumors and the tumor microenvironment. During tumor development, the metabolic pattern undergoes significant changes, and the optimal metabolic mode of the tumor is selected on the basis of its individual environment. Tumor cells can adapt to a specific microenvironment through metabolic adjustment to achieve compatibility. In this study, the effects of tumor glucose metabolism, lipid metabolism, and amino acid metabolism on the tumor microenvironment and related mechanisms were reviewed. Selective targeting of tumor cell metabolic reprogramming is an attractive direction for tumor therapy. Understanding the mechanism of tumor metabolic adaptation and determining the metabolism symbiosis mechanism between tumor cells and the surrounding microenvironment may provide a new approach for treatment, which is of great significance for accelerating the development of targeted tumor metabolic drugs and administering individualized tumor metabolic therapy.

**Keywords:** pancreatic cancer, tumor microenvironment, metabolism symbiosis, metabolic remodeling, crosstalk

## INTRODUCTION

The composition of the tumor microenvironment in pancreatic cancer is complex and involves a dynamic process. A distinctive feature of malignant tumor pathology is the desmoplastic reaction, that is, the cancer cells are surrounded by a large number of dense fibrous matrix components. These matrix components lead tumors to show the characteristics of ischemia, and make it difficult for traditional chemotherapy drugs to enter tumor tissues. The enveloped tumor cells in microenvironment include various mesenchymal cells, a large amount of extracellular matrix extracellular matrix (ECM), and some soluble molecules such as cytokines, chemokines, and pro-angiogenic factors (1). Tumors form specific tumor microenvironments during their occurrence and development that are mainly divided into ecological microenvironments and physical microenvironments. The ecological microenvironment includes immune cells, fibroblasts, endothelial cells, and ECM. The physical microenvironment includes low oxygen, nutrient pressure, low pH, and oxidative pressure. There is an intricate relationship between the

microenvironment and cells that plays an important role in tumor development, invasion and metastasis, chemotherapy resistance, tumor immunosuppression, and tumor cell metabolism remodeling (2).

In recent years, many studies have focused on the remodeling of tumor metabolism by the tumor microenvironment. Metabolic remodeling is one of the salient features of tumorigenesis and development, which can meet the rapid proliferation of tumor cells for energy and biological macromolecular substances. To maintain its malignant characteristics, tumors undergo significant changes in their metabolic patterns and pathways. This change is called metabolic remodeling (3). As early as the beginning of the 20<sup>th</sup> century, Otto Warburg proposed that fast-proliferating cancer cells use “aerobic glycolysis” as their main energy production method. This metabolic pathway can help tumors adapt to the pancreatic cancer microenvironment, enhance their malignant biological behavior, and resistance to radiotherapy and chemotherapy. This process is accompanied by the accumulation of specific metabolites, such as glucose metabolites, lipid metabolites, and amino acids, which can regulate tumor-related signaling pathways through mechanisms such as competitive inhibition of epigenetic regulatory enzymes or post-translational modification of proteins. The pancreatic cancer microenvironment contains a large number of stromal cells, of which cancer-associated fibroblasts (CAFs) account for approximately half of the total number of cells in tumor tissues. Previous studies have shown that CAFs mainly promote tumor cell proliferation and metastasis by secreting large amounts of growth factors and chemokines (4). Furthermore, CAFs also undergo metabolic changes similar to tumor cells, from oxidative phosphorylation to aerobic glycolysis, thus producing and secreting metabolic intermediates such as lactic acid and ketone bodies, and these metabolic intermediates can be directly taken up by tumor cells to promote rapid proliferation (5). Demircioglu et al. reported that loss of focal adhesion kinase (FAK) in a subpopulation of CAFs causes the upregulation of Ccl6, Ccl11, Ccl12 and pentraxin-3 resulting in the enhancement of glycolysis in pancreatic cancers. FAK depletion in CAFs activate protein kinase A and lead to enhanced malignant cell glycolysis *via* CCR1/CCR2 on cancer cells (6). Moreover, it is demonstrated that as regulator of glutamate, glutamine, and cytokine release, Netrin G1 (NetG1) in CAFs and Netrin G1 Ligand (NGL-1) in pancreatic cancer cells enhanced tumorigenesis by allowing cancer cells to survive in low nutrient conditions and reduced death induced by NK cells (7). Limitation of nutrient availability is overcome partly by exchange of metabolites and cytokines between the stromal and cancer cells. Data shows that as the main matrix component in tumor tissues, CAFs not only promote tumor progression, but also directly supply the biomass needed for tumor cell synthesis and metabolism by secreting metabolic intermediate products (8). Metabolic crosstalk with stromal cells in the tumor microenvironment is one of important alternative sources of nutrient acquisition for pancreatic cancer. However, little is known about the molecular mechanism of this metabolic change, and the metabolic relationship between pancreatic cancer tumor cells and the tumor microenvironment remains unclear. This article mainly focuses on the metabolic symbiosis and critical metabolites in the

microenvironment of pancreatic cancer, and discusses the mechanism of metabolites in the regulation of signaling pathways related to tumorigenesis.

## METABOLIC CHARACTERISTICS OF PANCREATIC CANCER AND THE TUMOR MICROENVIRONMENT

Carbohydrates, amino acids and lipids are used by cells to maintain energy balance and support biosynthesis. In normal cells, glucose is metabolized to pyruvate through glycolysis. Pyruvate enters the mitochondrial tricarboxylic acid (TCA) cycle with the assistance of pyruvate transporter, and then is completely oxidized to carbon dioxide and water through the process of oxidative phosphorylation, producing a large amount of ATP to meet the needs of cell metabolism. In tumor cells, glucose generates pyruvate *via* glycolysis. Subsequently, pyruvate no longer enters the TCA cycle, but is converted into lactic acid under the action of lactate dehydrogenase (LDH). Therefore, the glycolytic pathway of tumor cells will not be coupled with mitochondrial oxidative phosphorylation. Other metabolic characteristics of tumors include imbalanced amino acid uptake, increased nitrogen demand, changes in nutrient acquisition patterns, increased glycolysis/TCA cycle intermediates for biosynthesis and nicotinamide adenine dinucleotide phosphate production, metabolite-driven gene regulation changes, and enhanced microenvironmental metabolic interactions (9). Although metabolism remodeling is a general characteristic of cancer, different cancers show distinct metabolic additions, which are mainly determined multiple factors such as their specific genetic mutations or tumor microenvironment. Cancer cells exhibit extraordinary growth advantages mainly in three ways (1): Reprogramming intracellular energy metabolism of nutrients (2). Improving nutrient acquisition by scavenging and recycling (3). Conducting metabolic crosstalk with stromal cells within the microenvironment (10). At present, the mechanism of tumor aerobic glycolysis is not clear, it is generally believed to be related to hypoxia and abnormal tumor gene signals. Studies have pointed out that glucose transporters (GLUTs), a family of proteins on the cell membrane that can transfer glucose into cells, can be significantly upregulated in tumor cells, which accelerates aerobic glycolysis and maintain the proliferative advantage of tumor cells (11). In addition, specific oncogenes such as murine sarcoma virus oncogene (KRAS), phosphatidylinositol 3-kinase (PI3K), c-MYC, and hypoxia-inducible factor 1 (HIF1) can also play the same role by regulating pyruvate kinase M2 (PKM2), hexokinase 2 (HK2), and other crucial enzymes in the glycolytic pathway (12). There is also an interaction between tumor metabolic remodeling and Myc. On the one hand, Myc regulate the glycolytic process of tumor cells by activating glycolysis-related proteins such as HK2, glyceraldehyde-3-phosphate dehydrogenase (GAPDH), and enolase-1. On the other hand, changes in tumor metabolic status also activate mammalian target of rapamycin complex 1 (mTORC1) and increase the translation levels of Myc

by targeting ribosomal S6 protein kinase (S6K1), thereby forming a positive feedback loop (13). The oncogene KRAS is nearly universally mutated in pancreatic cancer. Oncogenic Kras signaling promotes extracellular glucose avidity and capture *via* upregulation of GLUT1 and HK, respectively. Oncogenic Kras diverts glucose flux into the hexosamine biosynthetic pathway to enhance the generation of precursor moieties required for protein glycosylation. Oncogenic Kras activity also leads to enhanced entry of glucose carbon into the pentose phosphate pathway by which proliferating cells make ribose 5-phosphate (R5P) for DNA and RNA biosynthesis (14). Knock down of Kras-regulated enzymes that govern pentose phosphate pathway is strongly growth inhibitory (15). Tumor suppressor genes have an opposite role in tumor metabolic remodeling. P53 can block the expression of GLUT1, GLUT3, and GLUT4 by interfering with nuclear factor kappa-B kinase  $\alpha/\beta$  (I $\kappa$ Bk  $\alpha/\beta$ ). The gene promoters of critical enzymes in the aerobic glycolysis pathway, such as *HK2*, contain p53 binding sites; thus, they can also be inhibited by p53 (16, 17). Therefore, deletion of *TP53* gene in tumor cells will promote aerobic glycolysis.

Cancer-associated fibroblasts are the most important component of stromal cells in pancreatic cancer and are in direct or indirect contact with tumor cells. Our research shows that as an important interstitial component of the pancreatic cancer microenvironment, pancreatic stellate cells have a positive feedback relationship with pancreatic cancer cells. Activated stellate cells promote the progression of malignant biological behavior and chemotherapy resistance of pancreatic cancer (18–20). CAFs are continuously activated in the tumor microenvironment. Compared with normal fibroblasts, CAFs have also undergone significant changes in carbohydrate metabolism, similar to the Warburg effect of tumor cells. Studies have shown that as the rate-limiting enzyme of the TCA cycle in the mitochondria, isocitrate dehydrogenase 3 $\alpha$  (IDH3 $\alpha$ ) plays a crucial regulatory role in the aerobic glycolysis of CAFs. Conversely, IDH3 $\alpha$  allosterically regulates the activity of proline hydroxylase 2 (PHD2) by adjusting the ratio of  $\alpha$ -ketoglutarate ( $\alpha$ -KG) to fumaric acid and succinic acid, resulting in the inhibition of PHD2 activity and HIF1 $\alpha$  stabilization. The accumulation of HIF1 $\alpha$  can strengthen the cell's aerobic glycolysis process and inhibit the level of oxidative phosphorylation (21). However, carbohydrates produced by aerobic glycolysis in CAFs are not used for cell biosynthesis. Some studies have shown that lactic acid and ketone bodies produced by aerobic glycolysis are exported to adjacent tumor tissues, thereby promoting tumor cell proliferation. In CAFs, the expression of monocarboxylic acid transporter-4 (MCT-4), which exports lactate to the ECM, is upregulated. At the same time, the expression of monocarboxylic acid transporter-1 (MCT-1) on the cytoplasmic membrane of tumor cells is increased, and the metabolites of CAFs are absorbed into tumor cells, indicating that the metabolites exported by CAFs could provide materials for tumor proliferation (22). After CAF metabolic reprogramming, the content of anaerobic metabolism-related enzymes increases significantly, especially the critical rate-limiting enzyme PKM2 in anaerobic metabolism. Studies

have shown that overexpression of PKM2 in CAFs can induce larger breast cancer masses in mouse models (23). Glutamine synthetase is the most important enzyme for glutamyl synthesis. Tumor cells can promote the expression of glutamine synthase in CAFs, which is beneficial to mitochondrial metabolism of tumor cells. Glutamine can enhance the autophagy of mitochondria in CAFs, reduce the autophagy of mitochondria in tumor cells, upregulate the expression of glutamine transporters in tumor cells, and enhance mitochondrial biosynthesis in tumor cells (24).

## INTERACTION BETWEEN TUMOR METABOLIC REMODELING AND THE TUMOR MICROENVIRONMENT

Pancreatic cancer not only responds to the tumor microenvironment, but also affects the metabolism of stromal cells in the microenvironment. Tumor-derived exosomes can mediate communication between tumor cells and their microenvironment (25). The vesicles of cancer cells can inhibit glucose uptake by other cells in the metastatic tumor, such as fibroblasts and astrocytes, thereby allowing metastatic cancer cells to preferentially take up glucose. These vesicles contain high levels of *miR-122*, which can inhibit the uptake of glucose by stromal cells *via* downregulating glycolytic enzymes such as pyruvate kinase (26). These findings indicate that metabolism remodeling of stromal cells in the tumor microenvironment is a metabolic adaptation process for tumor cells to facilitate their own proliferation.

Tumor cells can choose different metabolic methods to generate ATP and biological macromolecular substances for their own use according to the content and concentration of nutrients such as glucose, glutamine, or fatty acids in the surrounding environment. Studies have shown that metastatic colorectal cancer cells can affect liver cell metabolites to promote colonization of metastatic tumor cells and the formation of liver metastases. The metastatic tumor cells release brain-type creatine kinase to promote creatine phosphate production, which then enters the metastatic colorectal cancer cells to produce ATP. Under the nutritional pressure of lack of glucose or glutamine, tumor cells activate the oncogene c-Myc, metabolize enzyme expression by regulating the serine synthesis pathway molecules such as PHGDH, PSAT1, and PSPH, use the remaining glutamine or glucose to support the *de novo* serine synthesis pathway, and support tumor cell survival under nutritional stress by maintaining redox homeostasis (27). In tumors with *MYC* gene mutations, the expression of the monocarboxylic acid transporter MCT1 and LDH is significantly increased, which promotes the transport and reuse of lactate. In addition, under serum starvation conditions, tumor cells can activate the mTORC2–AKT–SP1 signaling pathway and upregulate the expression of the rate-limiting enzyme 3-ketoacyl-CoA transferase 1 (OXCT1) of ketone body catabolism. Metabolites produced by ketone body catabolism enter the TCA cycle to provide ATP for tumor cells (28). Under hypoxic or nutritional stress

conditions, tumor cells ingest acetoacetate to produce acetyl-CoA, which provides energy and biological macromolecules for their survival. During pancreatic cancer progression, there is a hypoxic inner area and an oxygen-rich outer area. Lactic acid can be produced, transported, and effectively used between the two areas. The glycolysis of pancreatic cancer cells in the hypoxic zone produces lactic acid and hydrogen ions that are excreted into the tumor microenvironment through monocarboxylic acid transporter 4 (MCT4), and then are taken up by cancer cells in the peripheral oxygen-rich zone that express MCT1. The glycolysis of pancreatic cancer cells in the hypoxic zone produces lactic acid and hydrogen ions that are excreted into the tumor microenvironment through MCT4, and then are taken up by pancreatic cancer cells in the peripheral oxygen-rich zone that expresses MCT1. Lactate dehydrogenase is reduced to pyruvate NADH, which enters the TCA cycle and becomes the fuel for respiration. After inhibiting the expression of MCT1, peripheral cancer cells die of glucose starvation due to the preferential use of lactic acid for oxidative metabolism. The remaining cancer cells are sensitive to radiotherapy, which suggests an effective combination therapy strategy to tumor treatment (29, 30). Therefore, cancer cells can use the metabolites produced in the microenvironment to cope with the metabolic stress encountered at different metastatic sites. The metabolic status of pancreatic cancer cells is not only the result of their own long-term adaptation, but also affects the fate of surrounding cells, such as cancer-related fibroblasts, endothelial cells, and immune cells. As the tumor grows, these cells undergo a series of metabolic remodeling that leads to phenotypic changes.

## Tumor Metabolism and the Inflammatory Microenvironment

Proper inflammatory response in the body can stimulate the body to improve immunity, but long-term stimulation of inflammatory mediators forms a suitable soil for tumor cell proliferation, that is, the inflammatory microenvironment. Studies have confirmed that chronic inflammation is related to tumorigenesis. Tumors are often accompanied by diseases such as gastritis, gastric ulcer (*Helicobacter pylori*) and gastric cancer, chronic cervicitis (papilloma virus), and cervical cancer. Recent studies have found that some metabolic diseases are closely related to the occurrence of tumors, such as obesity, diabetes, and non-alcoholic fatty liver. The carcinogenic pathway is most likely through the inflammatory response. In 2006, Hotamisligil first proposed the concept of the “metabolic inflammatory response”, providing new ideas for studying the relationship between metabolism and the inflammatory response (31). Pancreatic cancer is a highly metabolic disease, in which many inflammatory factors including cytokines, chemokines, and other inflammatory response mediators participate. Inflammatory mediators have a regulatory role in the synthesis, secretion, and metabolism of nutrients such as glucose, fat, and protein in tumor cells. Researchers have studied the relationship between tumor metabolism and the inflammatory response, and paved the way for clinical diagnosis and treatment (Table 1).

The interleukin family is a widely studied inflammatory cytokine that plays an important role in information

transmission and regulation of immune cells. IL-1 (lymphocyte stimulating factor), with two structures (IL-1 $\alpha$  and IL-1 $\beta$ ), is the main inducer of the immune inflammatory response. Many studies have found that IL-1 is closely related to the occurrence and development of pancreatic, gastric, liver, and breast cancer, amongst others. IL-1 induces LIF expression and downstream JAK/STAT activation to generate inflammatory CAFs in pancreatic cancer, thus promoting cancer progression, chemoresistance and other cancer-associated systemic effects, such as cachexia and immune suppression (45). IL-1 $\beta$  is mainly present in the blood circulation and functions within a cascade of cytokines that initiates the inflammatory response and promote the migration of cancer cells. IL-1 may also have an effect on the anti-tumor immune response (46). Studies have found that inflammatory response mediators participate in regulating lipid metabolism. IL-1, IL-6, and TNF- $\alpha$  can inhibit cholesterol hydroxylase. Studies have shown that IL-4 increases occurrence and enhances metabolism of tumors by promoting glycolysis and glutamine metabolism (47, 48). Lactate dehydrogenase A (LDH-A) is one of the critical enzymes in the glucose metabolism pathway, and IL-4 can upregulate the expression of the glucose metabolism-related gene *LDHA*, thereby promoting the proliferation of tumor cells. IL-6 has a role in regulating metabolic balance and anti-inflammatory responses in obesity-related inflammatory reactions and metabolic diseases. Studies have found that there is a direct regulatory relationship between IL-6 and insulin, metabolic pathways, and inflammatory response signals. IL-6 is overexpressed in a variety of cancers, and it can activate the STAT3 signaling pathway to promote tumor occurrence (32). Lesina et al. found that IL-6 was mainly involved in the JAK/STAT pathway activation promoting acute and chronic pancreatitis disease aggravation as well as pancreatic cancer initiation and progression (33). However, some other studies found that IL-6 regulates tumor metabolism and inflammatory response disorders by inhibiting the mTOR pathway through the activation of AMPK rather than STAT signals (34).

Interferon  $\gamma$  (INF- $\gamma$ ) is an important member of the interferon family with broad-spectrum anti-viral, anti-proliferative, and immunomodulatory activities. INF- $\gamma$  mainly induces the production of cytokines such as TNF- $\alpha$  and IL-6 to mediate the Th1 type inflammatory response. The mutual influence of these inflammatory response factors can form a vicious circle, which is the main mechanism leading to a sustained inflammatory response (35). The INF- $\gamma$ -inducing genes (including *CXCL9*, *CXCL10*, and *CXCL11*) encode ligands of chemokine receptor 3 (CXCR3). INF- $\gamma$  not only induces binding to its receptor to clear cells, but also induces the inflammatory response by recruiting inflammatory effector cells. As one of major cytokine involved in cachexia, INF- $\gamma$  demonstrates an antiproliferative and antifibrotic capacity, which modulate local anti-tumor immune response. Weight loss in cancer was associated with INF- $\gamma$  production and administration of an anti-INF- $\gamma$  antibody reduced the depletion of body fat (49).

Hypoxia-inducible factor-1 is a transcriptionally active nuclear protein with a broad spectrum of target genes,



**TABLE 1 |** Inflammatory factor that regulating the metabolic remodeling and cancer microenvironment.

Inflammatory factor	Signaling pathway	Effect of metabolic process	Role in immune response	Role in cancer progress	Refs.
Interleukin family	STAT3; mTOR; AMPK	Inhibit cholesterol hydroxylase; promoting glycolysis and glutamine metabolism;	Induces immune inflammatory response; anti-tumor immune response	Promote occurrence and development of cancer	(32–34)
INF- $\gamma$	JAK/STAT3; PD-L1; (PI3K)/AKT	Induce inflammatory and catabolic response	Mediates Th1 type inflammatory response	Pro-apoptotic activity	(35)
Hypoxia inducible factor-1	VEGF; ET-1; PDGF; GLUT;	Accelerate the efficiency of glucose metabolism	Suppresses antitumor immune responses	Induce tumor angiogenesis; promote tumor growth;	(36–40)
NLRP3	IL-1 $\beta$ ; IL-8; IL-18 IL-33; mTORC1	Glucose metabolism, and amino acid metabolism	Promotes inflammatory responses	Promotes cancer progression and metastasis	(41, 42)
CTRP	PI3K-Akt; TNF- $\alpha$ ; IL-1 $\beta$ ; IL6/STAT3; Akt/ NF- $\kappa$ B	Enhance insulin sensitivity; inhibits gluconeogenesis	Links metabolism, inflammation, and immunity	Promotes tumor cell survival and resistance to chemotherapy-induced apoptosis	(43, 44)

including nearly a hundred target genes related to the development of the inflammatory response, tumor growth, and hypoxia adaptation. Target genes regulated by HIF-1 include vascular endothelial growth factor (*VEGF*), endothelin-1 (*EDN1*), insulin-like growth factor 2 (*IGF2*), and platelet-derived growth factor (*PDGF*). Under the action of these genes, HIF-1 has biological effects such as erythropoiesis, angiogenesis, energy metabolism of amino acids and glucose, cell survival, apoptosis, and drug resistance (50, 51). HIF-1 $\alpha$  makes cancer cells resistant to cisplatin, oxaliplatin, and paclitaxel. The hypoxic microenvironment of pancreatic tumors stabilizes HIF-1 $\alpha$ , which promotes glucose metabolism. Shukla et al. found that HIF-1 $\alpha$  regulated the metabolic phenotype and gemcitabine resistance in pancreatic cancer. Gemcitabine-resistant pancreatic cancer cells increased expression of HIF-1 $\alpha$  by upregulating MUC1 expression, along with increased glycolytic phenotype and dependence on glucose (52). Other studies show that HIF-1 $\alpha$  can accelerate the efficiency of glucose metabolism and provide the energy needs for cancer cells by regulating the activity of GLUT1 and the transcription of *GLUT1* mRNA (36, 37). The roles of HIF-1 $\alpha$  in lipid metabolism reprogramming in cancer is under-studied. Existing evidences show that HIF-1 $\alpha$ , promotes fatty acid uptake through induction of FABPs (FABP3, FABP7, and FABP4) along with PPAR $\gamma$ , and lipid storage by modulating ADRP, AGPAT2, and LIPIN1 expressions. Seo and colleagues determined that the FABP5/HIF-1 $\alpha$  axis regulates lipid metabolism and cell proliferation in hepatocellular carcinoma (38). HIF-1 $\alpha$  can induce vascular target genes, especially vascular endothelial growth factor (*VEGF*), and induce tumor angiogenesis (39, 40). However, VEGF also regulates HIF1 $\alpha$  expression and activation, forming a positive feedback loop between HIF-1 $\alpha$  and VEGF. Shi et al. indicated that VEGF enhanced glycolysis by neuropilin 1 (NRP1)-mediated up-regulation of HIF1 $\alpha$  and its targeted glycolytic enzymes (53).

NLRP3 is a multi-protein complex mainly expressed in neutrophils and macrophages. The main function of NLRP3 is to activate caspase-1 to indirectly regulate the secretion of interleukin 1 $\beta$  (IL-1 $\beta$ ), IL-8, and IL-33. NLRP3 is also identified as a regulator to controls platelet activation and

aggregation. Boone et al. reported the NLRP3 inflammasome was upregulated in a murine model pancreatic cancer and promoted platelet aggregation and tumor growth. Pharmacological inhibition of NLRP3 in platelets resulted in decreased platelet activation and improved survival of tumor-bearing mice (54). Studies have shown that the activation of NLRP3 is related to many factors. The possible mechanisms include potassium efflux, oxidized mitochondrial DNA release, mitochondrial dysfunction and reactive oxygen species (ROS) production, cathepsin B release caused by lysosome destruction, changes in intracellular calcium concentration, and transmembrane hole formation (41). NLRP3 inflammasome has an important role in linking metabolism and inflammation. For example, glycolysis is related to the NLRP3 inflammasome through different metabolites. Intermediates or metabolites in the TCA cycle may also be involved in the regulation of NLRP3. The glycolytic enzyme hexokinase-1 (HK1) directly interacts and activates the NLRP3 inflammasome in the outer mitochondrial membrane. In this process, mTORC1 regulates HK1-dependent glycolysis through Raptor's influence on HK1 expression. Raptor is a regulatory-related protein of the mTORC1 complex and is related to the activation of NLRP3 inflammasomes. Moreover, this activation may in turn promote the expression of HK1 (42). In addition to glucose metabolism, its role in amino acid metabolism is attracting increasing attention and may become a future research hotspot. In addition, NLRP3 inflammasomes are also activated in many diseases, including infections, autoimmune diseases, and various cancers such as stomach, colorectal, liver, lung, and cervical cancer. The main mechanism is mainly related to the activation of IL-1 $\beta$  and IL-6 signaling pathways (41).

Complement-C1q/TNF-related protein (CTRP) is a newly discovered adipokine superfamily, and 15 members have been discovered so far. CTRP contains an amino-terminal signal peptide, a short variable domain, a collagen-like domain, and a carboxy-terminal spherical domain. Recent studies have shown that CTRP family members participate in the regulation of glucose and lipid metabolism and inflammation. CTRP12 is an adipose factor, and it is secreted by adipose tissue that can enhance insulin sensitivity, improve insulin resistance, and

reduce the inflammatory response of adipose tissue. CTRP12 inhibits liver gluconeogenesis and adipocyte glucose uptake by activating the PI3K–AKT signaling pathway. CTRP3 also has similar characteristics. It inhibits gluconeogenesis by downregulating the expression of the rate-limiting enzymes glucose 6-phosphatase and phosphoenolpyruvate carboxykinase, which can also improve the insulin sensitivity of adipocytes and promote the expression of adipokines adiponectin, leptin, and visfatin. CTRP6 expression is significantly increased in the state of high glucose. CTRP6 stimulates the generation of ROS, induces inflammation and ECM accumulation by upregulating the expression levels of tumor necrosis factor- $\alpha$  (TNF- $\alpha$ ), IL-1 $\beta$ , IL-6, and the AKT–NF- $\kappa$ B pathway (43). CTRP4 promotes tumor cell survival and resistance to chemotherapy by effectively inducing the activation of the NF- $\kappa$ B and IL6–STAT3 signaling pathways (44).

Other inflammatory response mediators related to tumor metabolism disorders include proteolysis-inducing factor (PIF), which stimulates and activates the NF- $\kappa$ B pathway, thereby inducing the secretion of a variety of inflammatory factors, such as IL-6/IL-8 and ICAM-1 (55). Lipid-mobilizing factor (LMF) can promote the decomposition of fat tissue under the action of  $\beta$ 3 adrenal receptors. Other cytokines include leukemia inhibitory factor (LIF) and ciliary neurotrophic factor (CNTF). The former can inhibit the activity of lipase and promote lipolysis, while the latter is related to the metabolic disorders of fat and protein. Neutrophil gelatinase-associated lipocalin (NGAL) is a member of the lipocalin family of proteins. NGAL is involved in cell glucose and lipid metabolism and energy regulation. At the same time, NGAL can form a complex with matrix metalloproteinase 9 (MMP9). This MMP9/NGAL complex is related to tumor proliferation, metastasis, and chemotherapy resistance (56).

## Pancreatic Cancer Metabolism and the Acid Microenvironment

The metabolic remodeling of pancreatic cancer is an important reason for the formation of an acidic microenvironment. Low energy but rapid energy supply method generates heat and leads to an increase in the production of lactic acid, thereby inducing the production of an acidic tumor environment (57). Another major feature of the pancreatic cancer microenvironment is hypoxia. Hypoxia is caused by the rapid proliferation of cancer cells. The hypoxic environment of pancreatic cancer cells can activate HIF. In this environment, HIF-1 induces the expression of carbonic anhydrase IX (CA IX) and CA XI to facilitate extracellular acidification. HIF contributes to the formation of glycolytic phenotypes in cancer cells, which is acidified by lactic acid production. HIF converts pyruvate into lactic acid by upregulating lactate dehydrogenase-A (LDH-A) and directly upregulates the expression of GLUT1 and GLUT3. In summary, HIF plays a central role in the regulation of energy metabolism. It promotes the production of lactic acid and forms the acidic microenvironment by converting mitochondrial oxidative phosphorylation to anaerobic glycolysis under hypoxia (58). The acidic tumor microenvironment can induce the expression of MMPs such as MMP-2 and MMP-9 and enhance the invasion

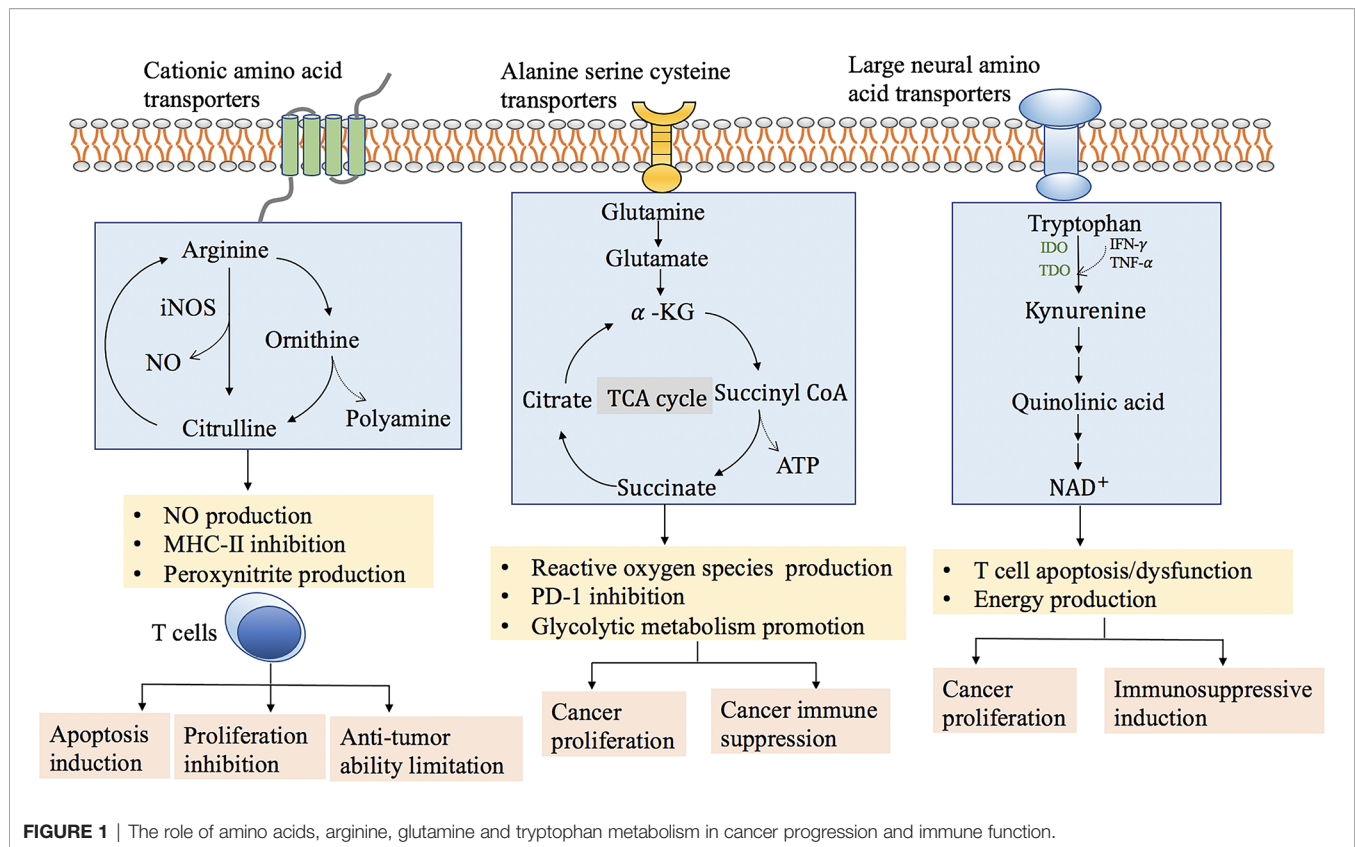
and metastatic ability of tumor cells. Cancer cells exposed to acidosis have the characteristics of an epithelial–mesenchymal transition phenotype, as well as high invasiveness, high anti-apoptotic ability, and anti-drug therapy properties (59). Moreover, aberrant glycolysis is also a promoting factor for tolerance to chemotherapeutic drugs. 2-DG (a synthetic glucose analog)-induced glycolysis inhibition markedly improves pancreatic cancer sensitivity to gemcitabine (60).

CO<sub>2</sub> produced in the process of tumor fatty acid metabolism is hydrated to HCO<sub>3</sub><sup>−</sup> and H<sup>+</sup> by CAs. The process of fatty acid synthesis palmitate in tumor cells produces CO<sub>2</sub> and H<sup>+</sup>. To avoid intracellular acidosis and maintain pH homeostasis, tumor cells increase the expression of transporters and channels to promote H<sup>+</sup> excretion. The main acidic metabolites accumulated in cells are lactic acid and hydrogen ions, which are mainly excreted by MCT1 and MCT4. The hydrogen protons produced in the cell are also discharged outside the cell by Na<sup>+</sup>/H<sup>+</sup> exchangers (NHE), which causes acidification outside the cell. CA IX and CA XII are transmembrane CAs with extracellular catalytic domains that catalyze the hydration of extracellular CO<sub>2</sub> to generate HCO<sub>3</sub><sup>−</sup> and H<sup>+</sup>. Lack of sufficient functional blood vessels is also a common feature of pancreatic cancer that affect the acidification of tumors. The lack of vasculature reduces the oxygen supply and the removal of acidic waste, leading to the accumulation of H<sup>+</sup> in the poorly perfused microenvironment. Therefore, the increase in lactic acid and CO<sub>2</sub> caused by abnormal tumor metabolism, hypoxia, and poor perfusion are the main reasons for the formation of an acidic tumor microenvironment. Ion transporters and CAs can reverse the acidic microenvironment of pancreatic cancer to a certain extent by targeted regulation of the pH gradient of the microenvironment, thereby inhibiting tumor cell proliferation and reducing tumor drug resistance. A study showed that the combined use of proton pump inhibitors and CA inhibitors achieved more effective anti-tumor effects than single-drug therapy (61). The development of drugs that reverse the pH gradient of the tumor microenvironment can provide new strategies for effective anti-cancer treatments.

## Tumor Metabolism and the Immunosuppressive Microenvironment

In the process of pancreatic cancer development, in addition to obtaining the nutrients needed for their rapid proliferation, it is also necessary to escape the attack from immune system. Lactic acid is the final product of glycolysis in tumor cells. The effects of extracellular lactic acid include: (1) preventing the transformation of monocytes into dendritic cells; (2) inhibiting the release of cytokines from dendritic cells and cytotoxic T cells; (3) inhibiting monocyte migration; and (4) decreasing the function of cytotoxic T cells. Pancreatic cancer cells can inhibit the activity of cytotoxic T cells and antigen-presenting cells by controlling the acidity of the tumor microenvironment and further increasing the glycolysis of tumor cells, leading to the immune escape of tumor cells (57).

The metabolic level of amino acids in pancreatic cancer cells changes to adapt to the increase in energy demand. Changes in the amino acid metabolism pathways of pancreatic cancer cells are often driven by multiple signaling pathways and transcription factors (**Figure 1**). A large number of basic research studies and clinical trials have shown that development of new drugs for



regulation of tumor-dependent amino acid metabolism can effectively inhibit tumor growth.

Arginine metabolism is an important mechanism to regulate the responsiveness of immune cells. Arginine and its downstream metabolites (such as ornithine and citrulline) may be essential for T cell activation, thereby regulating innate and adaptive immunity (62). Decreased arginine content in tumors can inhibit the function of T cells, especially CD8<sup>+</sup> T cells. Both myeloid-derived suppressor cells (MDSCs) and macrophages in the tumor microenvironment can induce the expression of arginase (ARG) and nitric oxide synthase (NOS). ARG degrades arginine into ornithine and urea, and NOS oxidizes arginine to citrulline and nitric oxide (NO). NO inhibits the proliferation of T cells by inhibiting the expression of major histocompatibility complex II (MHC-II). Tumor-derived cytokines such as transforming growth factor-β (TGF-β) can induce ROS production in MDSCs. The peroxide molecule (O<sub>2</sub><sup>-</sup>) reacts with NO to produce peroxynitrite (PNT). PNT can induce the apoptosis of T lymphocytes, and also nitrate and nitrosylate T cell receptors and CD8 molecules, rendering T cells resistant to tumor cells. The nitrosylated T cell receptor loses its ability to recognize specific peptides and MHC complexes, thus limiting the anti-tumor ability of CD8<sup>+</sup> T cells.

Tryptophan is necessary for T cell division and proliferation. In the absence of tryptophan and tryptophan breakdown products, activated T cells are stagnant in S phase, unable to synthesize DNA, and are extremely sensitive to Fas-mediated apoptosis, which

indicates that the reduction in tryptophan can lead to immunosuppression. Indoleamine2,3-dioxygenase (IDO) is a tryptophan-decomposing enzyme overexpressed in melanoma, colon cancer, and renal cell carcinoma, and is closely related to the prognosis of tumors (63). In the tumor microenvironment, IDO can be secreted by tumor cells, tumor-associated macrophages, and regulatory T cells. IDO is highly expressed in macrophages and dendritic cells, and directly inhibits T cell functions, thereby making the tumor microenvironment an immune tolerance environment. Except for IDO1, tryptophan catabolism by tryptophan-2,3-dioxygenase (TDO2) is a feature of many tumors, especially malignant gliomas (64, 65). The accumulation of metabolites caused by increased tryptophan metabolism, such as 3-hydroxykynurenine and 3-hydroxyanthranilic acid (3-HAA), can trigger immunosuppression. Kynurenine binds to aryl hydrocarbon receptor (AHR) to inhibit T cell activity. Decreases in tryptophan and tryptophan metabolites lead to downregulation of CD8<sup>+</sup> T cell receptor ζ chain and inhibit CD8<sup>+</sup> T cell expansion *in vitro*. The catabolism of the essential amino acid tryptophan is a crucial metabolic pathway for the formation of the immunosuppressive tumor microenvironment, and thus it is a feasible drug target for tumor immunotherapy.

Glutamine is an important cancer cells metabolism substrate. Pancreatic cancer cells grown in culture are strictly dependent on glutamine for proliferation. Glutamine facilitates generation of reducing equivalents in the form of NADPH is driven by oncogenic Kras. Kras activates the GOT2-GOT1-ME1 pathway

and initiates a nuclear factor (erythroid-derived 2)-like 2 (Nrf2)-dependent reactive oxygen species (ROS) detoxification program. Mutant Kras constitutively activates this antioxidant program to suppress ROS and enhance pancreatic tumorigenesis (66). Glutamine can be converted into  $\alpha$ -ketoglutarate ( $\alpha$ -KG) through following mechanisms; either by glutamate dehydrogenase (GLUD1) or transaminases. Many cancer cells rely on GLUD1-mediated glutamine conversion. However, being different from other cancer models, pancreatic cancer cells metabolize glutamine in a manner that transaminases is critical for glutamine metabolism (67). Glutamine deficiencies in pancreatic cancer can modulate adaptation mechanisms through signal transduction. Recouvreux et al. reported that glutamine depletion increased Slug expression to promote epithelial-mesenchymal transition (EMT) and metastasis (68). Glutamine is required to support optimal lymphocyte proliferation and production of cytokines by lymphocytes and macrophages. Research found that tumor-specific CD8<sup>+</sup> T cells cultured under glutamine-restricted (dGln) conditions or adoptive transfer of CD8<sup>+</sup> T cells treated with specific inhibitors of glutamine metabolism can effectively eliminate tumors. In addition, PD-1 expression on tumor-infiltrating CD8<sup>+</sup> T cells cultured with dGln was downregulated, and the positive rate of Ki67 was increased, indicating that inhibition of glutamine metabolism can prevent CD8<sup>+</sup> T cells from failing *in vivo* (69). The use of glutamine antagonists can destroy the tumor's metabolic immune suppression microenvironment. There is evidence that glutamine blockade in tumor-bearing mice inhibit the oxidation and glycolytic metabolism of cancer cells. In contrast, the response of effector T cells to glutamine antagonism is to significantly upregulate oxidative metabolism and extend cell lifespan (70). Glutamine antagonism reveals a metabolic interaction between tumor cells and effector T cells that can be used as a "metabolic checkpoint" for tumor immunotherapy.

## CONCLUSIONS

Selectively targeted tumor cell metabolic remodeling is an attractive direction for tumor therapy. However, this method has many problems. Because the enzymes in the metabolic pathway often have multiple subtypes, small molecule inhibitors may be unable to distinguish the subtypes of metabolic enzymes expressed in tumor cells from normal cells. Even if specific inhibitors are developed, tumor metabolism is heterogeneous and highly adaptable, and tumors will develop another metabolic pathway. Therefore, to avoid the adaptive

resistance of tumor cells, combination of two metabolic pathway inhibitors can be used, and the metabolic inhibitor can also be tried as an auxiliary treatment plan for other treatment methods.

The metabolic pathways adopted by tumor cells are diverse and heterogeneous, and there is also a metabolic symbiosis with stromal cells in the tumor microenvironment. In addition to aerobic glycolysis, metastatic tumor cells can also adopt complementary metabolic pathways such as oxidative phosphorylation and enable them to quickly adapt to new metabolic needs. This metabolic flexibility limits the effectiveness of single targeted therapy. Metabolism targeted therapy is not yet recommended as regular treatment in most guidelines for treating cancers. Our future challenge is to make a deeper understanding of how tumor cells maximize the use of the surrounding resources to maintain survival by influencing the tumor microenvironment (CAFs, macrophages, fat cells, et al). Understanding the mechanism of tumor metabolic adaptation and the metabolic-dependent symbiosis between tumor cells and the surrounding microenvironment may provide a new approach for tumor treatment. This is of great significance for guiding tumor metabolism research, accelerating the development of targeted tumor metabolism drugs, and developing individualized tumor metabolism treatments.

## AUTHOR CONTRIBUTIONS

YL: Original draft preparation and information collection. JZ: Acquisition of data and revision the manuscript. JX: Interpretation of data and analysis of data. SL: Conception and design of study. All authors contributed to the article and approved the submitted version.

## FUNDING

The study was supported by the National Natural Science Foundation of China (Grant No.81802888) and the Key Research and Development Project of Shandong Province (Grant No.2018GSF118206; No.2018GSF118088).

## ACKNOWLEDGMENTS

We thank H. Nikki March, PhD, from Liwen Bianji (Edanz) ([www.liwenbianji.cn/](http://www.liwenbianji.cn/)), for editing the English text of a draft of this manuscript.

## REFERENCES

- Hinshaw DC, Shevde LA. The Tumor Microenvironment Innately Modulates Cancer Progression. *Cancer Res* (2019) 79:4557–66. doi: 10.1158/0008-5472.CAN-18-3962
- Vasan N, Baselga J, Hyman DM. A View on Drug Resistance in Cancer. *Nature* (2019) 575:299–309. doi: 10.1038/s41586-019-1730-1
- Pavlova NN, Thompson CB. The Emerging Hallmarks of Cancer Metabolism. *Cell Metab* (2016) 23:27–47. doi: 10.1016/j.cmet.2015.12.006
- Chen X, Song E. Turning Foes to Friends: Targeting Cancer-Associated Fibroblasts. *Nat Rev Drug Discov* (2019) 18:99–115. doi: 10.1038/s41573-018-0004-1
- Sung JS, Kang CW, Kang S, Jang Y, Chae YC, Kim BG, et al. ITGB4-Mediated Metabolic Reprogramming of Cancer-Associated Fibroblasts. *Oncogene* (2020) 39:664–76. doi: 10.1038/s41388-019-1014-0
- Demircioglu F, Wang J, Candido J, Costa ASH, Casado P, de Luxan Delgado B, et al. Cancer Associated Fibroblast FAK Regulates Malignant Cell Metabolism. *Nat Commun* (2020) 11:1290. doi: 10.1038/s41467-020-15104-3



7. Francescone R, Barbosa Vendramini-Costa D, Franco-Barraza J, Wagner J, Muir A, Lau AN, et al. Netrin G1 Promotes Pancreatic Tumorigenesis Through Cancer-Associated Fibroblast-Driven Nutritional Support and Immunosuppression. *Cancer Discov* (2021) 11:446–79. doi: 10.1158/2159-8290.CD-20-0775
8. Sazeides C, Le A. Metabolic Relationship Between Cancer-Associated Fibroblasts and Cancer Cells. *Adv Exp Med Biol* (2018) 1063:149–65. doi: 10.1007/978-3-319-77736-8\_11
9. Koppenol WH, Bounds PL, Dang CV. Otto Warburg's Contributions to Current Concepts of Cancer Metabolism. *Nat Rev Cancer* (2011) 11:325–37. doi: 10.1038/nrc3038
10. Qin C, Yang G, Yang J, Ren B, Wang H, Chen G, et al. Metabolism of Pancreatic Cancer: Paving the Way to Better Anticancer Strategies. *Mol Cancer* (2020) 19:50. doi: 10.1186/s12943-020-01169-7
11. Henriques AFA, Matos P, Carvalho AS, Azkargorta M, Elortza F, Matthiesen R, et al. WNK1 Phosphorylation Sites in TBC1D1 and TBC1D4 Modulate Cell Surface Expression of GLUT1. *Arch Biochem Biophys* (2020) 679:108223. doi: 10.1016/j.abb.2019.108223
12. Liu R, Li Y, Tian L, Shi H, Wang J, Liang Y, et al. Gankyrin Drives Metabolic Reprogramming to Promote Tumorigenesis, Metastasis and Drug Resistance Through Activating  $\beta$ -Catenin/C-Myc Signaling in Human Hepatocellular Carcinoma. *Cancer Lett* (2019) 443:34–46. doi: 10.1016/j.canlet.2018.11.030
13. Stine ZE, Walton ZE, Altman BJ, Hsieh AL, Dang CV. MYC, Metabolism, and Cancer. *Cancer Discov* (2015) 5:1024–39. doi: 10.1158/2159-8290.CD-15-0507
14. Halbrook CJ, Lyssiotis CA. Employing Metabolism to Improve the Diagnosis and Treatment of Pancreatic Cancer. *Cancer Cell* (2017) 31:5–19. doi: 10.1016/j.ccell.2016.12.006
15. Ying H, Kimmelman AC, Lyssiotis CA, Hua S, Chu GC, Fletcher-Sananikone E, et al. Oncogenic Kras Maintains Pancreatic Tumors Through Regulation of Anabolic Glucose Metabolism. *Cell* (2012) 149:656–70. doi: 10.1016/j.cell.2012.01.058
16. Zhao M, Zhang Z. Glucose Transporter Regulation in Cancer: A Profile and the Loops. *Crit Rev Eukaryot Gene Expr* (2016) 26:223–38. doi: 10.1615/CritRevEukaryotGeneExpr.2016016531
17. Martin PL, Yin JJ, Seng V, Casey O, Corey E, Morrissey C, et al. Androgen Deprivation Leads to Increased Carbohydrate Metabolism and Hexokinase 2-Mediated Survival in Pten/Tp53-Deficient Prostate Cancer. *Oncogene* (2017) 36:525–33. doi: 10.1038/onc.2016.223
18. Liu SL, Cao SG, Li Y, Sun B, Chen D, Wang DS, et al. Pancreatic Stellate Cells Facilitate Pancreatic Cancer Cell Viability and Invasion. *Oncol Lett* (2019) 17:2057–62. doi: 10.3892/ol.2018.9816
19. Yang XP, Liu SL, Xu JF, Cao SG, Li Y, Zhou YB. Pancreatic Stellate Cells Increase Pancreatic Cancer Cells Invasion Through the Hepatocyte Growth Factor /C-Met/survivin Regulated by P53/P21. *Exp Cell Res* (2017) 357:79–87. doi: 10.1016/j.yexcr.2017.04.027
20. Xu J, Liu S, Yang X, Cao S, Zhou Y. Paracrine HGF Promotes EMT and Mediates the Effects of PSC on Chemoresistance by Activating C-Met/PI3K/Akt Signaling in Pancreatic Cancer *In Vitro*. *Life Sci* (2020) 8:118523. doi: 10.1016/j.lfs.2020.118523
21. Zhang D, Wang Y, Shi Z, Liu J, Sun P, Hou X, et al. Metabolic Reprogramming of Cancer-Associated Fibroblasts by IDH3 $\alpha$  Downregulation. *Cell Rep* (2015) 10:1335–48. doi: 10.1016/j.celrep.2015.02.006
22. Nocquet L, Juin PP, Souazé F. Mitochondria at Center of Exchanges Between Cancer Cells and Cancer-Associated Fibroblasts During Tumor Progression. *Cancers (Basel)* (2020) 12:3017. doi: 10.3390/cancers12103017
23. Sun K, Tang S, Hou Y, Xi L, Chen Y, Yin J, et al. Oxidized ATM-Mediated Glycolysis Enhancement in Breast Cancer-Associated Fibroblasts Contributes to Tumor Invasion Through Lactate as Metabolic Coupling. *EBioMedicine* (2019) 41:370–83. doi: 10.1016/j.ebiom.2019.02.025
24. Wu D, Zhuo L, Wang X. Metabolic Reprogramming of Carcinoma-Associated Fibroblasts and Its Impact on Metabolic Heterogeneity of Tumors. *Semin Cell Dev Biol* (2017) 64:125–31. doi: 10.1016/j.semcdb.2016.11.003
25. Liu SL, Sun P, Li Y, Liu S, Lu Y. Exosomes as Critical Mediators of Cell-to-Cell Communication in Cancer Pathogenesis and Their Potential Clinical Application. *Transl Cancer Res* (2019) 8:298–311. doi: 10.21037/tcr.2019.01.03
26. Fong MY, Zhou W, Liu L, Alontaga AY, Chandra M, Ashby J, et al. Breast-Cancer-Secreted miR-122 Reprograms Glucose Metabolism in Premetastatic Niche to Promote Metastasis. *Nat Cell Biol* (2015) 17:183–94. doi: 10.1038/ncb3094
27. Burlaka AP, Burlaka AA, Virko SV, Ganusevich II. Molecular Mechanisms of Oxidation Damage and Liver Cell Dysfunction in Patients With Metastatic Colorectal Cancer. *Exp Oncol* (2019) 41:328–34. doi: 10.32471/exp-oncology.2312-8852.vol-41-no-4.13796
28. Huang D, Li T, Wang L, Zhang L, Yan R, Li K, et al. Hepatocellular Carcinoma Redirects to Ketolysis for Progression Under Nutrition Deprivation Stress. *Cell Res* (2016) 26:1112–30. doi: 10.1038/cr.2016.109
29. Contreras-Baeza Y, Sandoval PY, Alarcón R, Galaz A, Cortés-Molina F, Alegria K, et al. Monocarboxylate Transporter 4 (MCT4) is a High Affinity Transporter Capable of Exporting Lactate in High-Lactate Microenvironments. *J Biol Chem* (2019) 294:20135–47. doi: 10.1074/jbc.RA119.009093
30. Fiaschi T, Marini A, Giannoni E, Taddei ML, Gandellini P, De Donatis A, et al. Reciprocal Metabolic Reprogramming Through Lactate Shuttle Coordinately Influences Tumor-Stroma Interplay. *Cancer Res* (2012) 72:5130–40. doi: 10.1158/0008-5472.CAN-12-1949
31. Hotamisligil GS. Inflammation and Metabolic Disorders. *Nature* (2006) 444:860–7. doi: 10.1038/nature05485
32. Daou HN. Exercise as an Anti-Inflammatory Therapy for Cancer Cachexia: A Focus on Interleukin-6 Regulation. *Am J Physiol Regul Integr Comp Physiol* (2020) 318:R296–310. doi: 10.1152/ajpregu.00147.2019
33. Lesina M, Wörmann SM, Neuhöfer P, Song L, Algül H. Interleukin-6 in Inflammatory and Malignant Diseases of the Pancreas. *Semin Immunol* (2014) 26:80–7. doi: 10.1016/j.smim.2014.01.002
34. White JP, Puppa MJ, Gao S, Sato S, Welle SL, Carson JA. Muscle Mtorc1 Suppression by IL-6 During Cancer Cachexia: A Role for AMPK. *Am J Physiol Endocrinol Metab* (2013) 304:E1042–52. doi: 10.1152/ajpendo.00410.2012
35. He H, Genovese KJ, Swaggerty CL, MacKinnon KM, Kogut MH. Co-Stimulation With TLR3 and TLR21 Ligands Synergistically Up-Regulates Th1-Cytokine IFN- $\gamma$  and Regulatory Cytokine IL-10 Expression in Chicken Monocytes. *Dev Comp Immunol* (2012) 36:756–60. doi: 10.1016/j.dci.2011.11.006
36. Kim MC, Hwang SH, Kim NY, Lee HS, Ji S, Yang Y, et al. Hypoxia Promotes Acquisition of Aggressive Phenotypes in Human Malignant Mesothelioma. *BMC Cancer* (2018) 18:819. doi: 10.1186/s12885-018-4720-z
37. Heydarzadeh S, Moshtaghi AA, Daneshpoor M, Hedayati M. Regulators of Glucose Uptake in Thyroid Cancer Cell Lines. *Cell Commun Signal* (2020) 18:83. doi: 10.1186/s12964-020-00586-x
38. Seo J, Jeong DW, Park JW, Lee KW, Fukuda J, Chun YS. Fatty-Acid-Induced FABP5/HIF-1 Reprograms Lipid Metabolism and Enhances the Proliferation of Liver Cancer Cells. *Commun Biol* (2020) 3:638. doi: 10.1038/s42003-020-01367-5
39. Xu B, Zhang X, Gao Y, Song J, Shi B. Microglial Annexin A3 Promoted the Development of Melanoma via Activation of Hypoxia-Inducible Factor-1 $\alpha$ /Vascular Endothelial Growth Factor Signaling Pathway. *J Clin Lab Anal* (2020) 29:e23622. doi: 10.1002/jcla.23622
40. Tamura R, Tanaka T, Akasaki Y, Murayama Y, Yoshida K, Sasaki H. The Role of Vascular Endothelial Growth Factor in the Hypoxic and Immunosuppressive Tumor Microenvironment: Perspectives for Therapeutic Implications. *Med Oncol* (2019) 37:2. doi: 10.1007/s12032-019-1329-2
41. Moossavi M, Parsamanesh N, Bahrami A, Atkin SL, Sahebkar A. Role of the NLRP3 Inflammasome in Cancer. *Mol Cancer* (2018) 17:158. doi: 10.1186/s12943-018-0900-3
42. Jiang D, Chen S, Sun R, Zhang X, Wang D. The NLRP3 Inflammasome: Role in Metabolic Disorders and Regulation by Metabolic Pathways. *Cancer Lett* (2018) 419:8–19. doi: 10.1016/j.canlet.2018.01.034
43. Xu E, Yin C, Yi X, Liu Y. Knockdown of CTRP6 Inhibits High Glucose-Induced Oxidative Stress, Inflammation and Extracellular Matrix Accumulation in Mesangial Cells Through Regulating the Akt/NF- $\kappa$ B Pathway. *Clin Exp Pharmacol Physiol* (2020) 47:1203–11. doi: 10.1111/1440-1681.13289
44. Li Q, Wang L, Tan W, Peng Z, Luo Y, Zhang Y, et al. Identification of ClqTNF-Related Protein 4 as a Potential Cytokine That Stimulates the STAT3 and NF- $\kappa$ B Pathways and Promotes Cell Survival in Human Cancer Cells. *Cancer Lett* (2011) 308:203–14. doi: 10.1016/j.canlet.2011.05.005
45. Biffi G, Oni TE, Spielman B, Hao Y, Elyada E, Park Y, et al. IL1-Induced JAK/STAT Signaling Is Antagonized by Tgfb $\beta$  to Shape CAF Heterogeneity in Pancreatic Ductal Adenocarcinoma. *Cancer Discov* (2019) 9:282–301. doi: 10.1158/2159-8290.CD-18-0710

46. Dmitrieva OS, Shilovskiy IP, Khaitov MR, Grivennikov SI. Interleukins 1 and 6 as Main Mediators of Inflammation and Cancer. *Biochem (Mosc)* (2016) 81:80–90. doi: 10.1134/S0006297916020024
47. Venmar KT, Kimmel DW, Cliffl DE, Fingleton B. IL4 Receptor  $\alpha$  Mediates Enhanced Glucose and Glutamine Metabolism to Support Breast Cancer Growth. *Biochim Biophys Acta* (2015) 1853:1219–28. doi: 10.1016/j.bbamcr.2015.02.020
48. Bankaitis KV, Fingleton B. Targeting IL4/IL4R for the Treatment of Epithelial Cancer Metastasis. *Clin Exp Metastasis* (2015) 32:847–56. doi: 10.1007/s10585-015-9747-9
49. Talar-Wojnarowska R, Gasiorowska A, Smolarz B, Romanowicz-Makowska H, Kulig A, Malecka-Panas E. Tumor Necrosis Factor Alpha and Interferon Gamma Genes Polymorphisms and Serum Levels in Pancreatic Adenocarcinoma. *Neoplasma* (2009) 56:56–62. doi: 10.4149/neo\_2009\_01\_56
50. Lin CM, Chiu JH, Wu IH, Wang BW, Pan CM, Chen YH. Ferulic Acid Augments Angiogenesis via VEGF, PDGF and HIF-1 Alpha. *J Nutr Biochem* (2010) 21:627–33. doi: 10.1016/j.jnutbio.2009.04.001
51. Tirpe AA, Gulei D, Ciortea SM, Crivii C, Berindan-Neagoe I. Hypoxia: Overview on Hypoxia-Mediated Mechanisms With a Focus on the Role of HIF Genes. *Int J Mol Sci* (2019) 20:6140. doi: 10.3390/ijms20246140
52. Shukla SK, Purohit V, Mehla K, Gunda V, Chaika NV, Vernucci E, et al. MUC1 and HIF-1alpha Signaling Crosstalk Induces Anabolic Glucose Metabolism to Impart Gemcitabine Resistance to Pancreatic Cancer. *Cancer Cell* (2017) 32:71–87.e7. doi: 10.1016/j.ccell.2017.06.004
53. Shi S, Xu J, Zhang B, Ji S, Xu W, Liu J, et al. VEGF Promotes Glycolysis in Pancreatic Cancer via HIF1 $\alpha$  Up-Regulation. *Curr Mol Med* (2016) 16:394–403. doi: 10.2174/1566524016666160316153623
54. Boone BA, Murthy P, Miller-Ocui JL, Liang X, Russell KL, Loughran P, et al. The Platelet NLRP3 Inflammasome is Upregulated in a Murine Model of Pancreatic Cancer and Promotes Platelet Aggregation and Tumor Growth. *Ann Hematol* (2019) 98:1603–10. doi: 10.1007/s00277-019-03692-0
55. Watchorn TM, Dowidar N, Dejong CH, Waddell ID, Garden OJ, Ross JA. The Cachectic Mediator Proteolysis Inducing Factor Activates NF-kappaB and STAT3 in Human Kupffer Cells and Monocytes. *Int J Oncol* (2005) 27:1105–11.
56. Chappell WH, Candido S, Abrams SL, Russo S, Ove R, Martelli AM, et al. Roles of P53, NF-kb and the Androgen Receptor in Controlling NGAL Expression in Prostate Cancer Cell Lines. *Adv Biol Regul* (2018) 69:43–62. doi: 10.1016/j.jbior.2018.05.002
57. Wang JX, Choi SYC, Niu X, Kang N, Xue H, Killam J, et al. Lactic Acid and an Acidic Tumor Microenvironment Suppress Anticancer Immunity. *Int J Mol Sci* (2020) 21:E8363. doi: 10.3390/ijms21218363
58. Vaupel P, Multhoff G. Fatal Alliance of Hypoxia-/HIF-1 $\alpha$ -Driven Microenvironmental Traits Promoting Cancer Progression. *Adv Exp Med Biol* (2020) 1232:169–76. doi: 10.1007/978-3-030-34461-0\_21
59. Andreucci E, Peppicelli S, Ruzzolini J, Bianchini F, Biagioni A, Papucci L, et al. The Acidic Tumor Microenvironment Drives a Stem-Like Phenotype in Melanoma Cells. *J Mol Med (Berl)* (2020) 98:1431–46. doi: 10.1007/s00109-020-01959-y
60. Dai S, Peng Y, Zhu Y, Xu D, Zhu F, Xu W, et al. Glycolysis Promotes the Progression of Pancreatic Cancer and Reduces Cancer Cell Sensitivity to Gemcitabine. *BioMed Pharmacother* (2020) 121:109521. doi: 10.1007/s00277-019-03692-0
61. Federici C, Lugini L, Marino ML, Carta F, Iessi E, Azzarito T, et al. Lansoprazole and Carbonic Anhydrase IX Inhibitors Synergize Against Human Melanoma Cells. *J Enzyme Inhib Med Chem* (2016) 31(sup1):119–25. doi: 10.1080/14756366.2016.1177525
62. Kim SH, Roszik J, Grimm EA, Ekmekcioglu S. Impact of L-Arginine Metabolism on Immune Response and Anticancer Immunotherapy. *Front Oncol* (2018) 8:67. doi: 10.3389/fonc.2018.00067
63. Wang S, Wu J, Shen H, Wang J. The Prognostic Value of IDO Expression in Solid Tumors: A Systematic Review and Meta-Analysis. *BMC Cancer* (2020) 20:471. doi: 10.1186/s12885-020-06956-5
64. Kudo T, Prentzell MT, Mohapatra SR, Sahm F, Zhao Z, Grummt I, et al. Constitutive Expression of the Immunosuppressive Tryptophan Dioxygenase TDO2 in Glioblastoma Is Driven by the Transcription Factor C/EBP $\beta$ . *Front Immunol* (2020) 11:657. doi: 10.3389/fimmu.2020.00657
65. Adam I, Dewi DL, Mooiweer J, Sadik A, Mohapatra SR, Berdel B, et al. Upregulation of tryptophanyl-tRNA Synthetase Adapts Human Cancer Cells to Nutritional Stress Caused by Tryptophan Degradation. *Oncoimmunology* (2018) 7:e1486353. doi: 10.1080/2162402X.2018.1486353
66. Chio IIC, Jafarnejad SM, Ponz-Sarvis M, Park Y, Rivera K, Palm W, et al. NRF2 Promotes Tumor Maintenance by Modulating mRNA Translation in Pancreatic Cancer. *Cell* (2016) 166:963–76. doi: 10.1016/j.cell.2016.06.056
67. Son J, Lyssiotis CA, Ying H, Wang X, Hua S, Ligorio M, et al. Glutamine Supports Pancreatic Cancer Growth Through a KRAS-Regulated Metabolic Pathway. *Nature* (2013) 496:101–5. doi: 10.1038/nature12040
68. Recouvreur MV, Moldenhauer MR, Galenkamp KMO, Jung M, James B, Zhang Y, et al. Glutamine Depletion Regulates Slug to Promote EMT and Metastasis in Pancreatic Cancer. *J Exp Med* (2020) 217:e20200388. doi: 10.1084/jem.20200388
69. Nabe S, Yamada T, Suzuki J, Toriyama K, Yasuoka T, Kuwahara M, et al. Reinforce the Antitumor Activity of CD8<sup>+</sup> T Cells via Glutamine Restriction. *Cancer Sci* (2018) 109:3737–50. doi: 10.1111/cas.13827
70. Leone RD, Zhao L, Englert JM, Sun IM, Oh MH, Sun IH, et al. Glutamine Blockade Induces Divergent Metabolic Programs to Overcome Tumor Immune Evasion. *Science* (2019) 366:1013–21. doi: 10.1126/science.aav2588

**Conflict of Interest:** The authors declare that the research was conducted in the absence of any commercial or financial relationships that could be construed as a potential conflict of interest.

**Publisher's Note:** All claims expressed in this article are solely those of the authors and do not necessarily represent those of their affiliated organizations, or those of the publisher, the editors and the reviewers. Any product that may be evaluated in this article, or claim that may be made by its manufacturer, is not guaranteed or endorsed by the publisher.

Copyright © 2021 Li, Zhang, Xu and Liu. This is an open-access article distributed under the terms of the Creative Commons Attribution License (CC BY). The use, distribution or reproduction in other forums is permitted, provided the original author(s) and the copyright owner(s) are credited and that the original publication in this journal is cited, in accordance with accepted academic practice. No use, distribution or reproduction is permitted which does not comply with these terms.



# Effects of Metformin Combined With Antifolates on HepG2 Cell Metabolism and Cellular Proliferation

Sherouk M. Tawfik<sup>1,2,3</sup>, Maha R. A. Abdollah<sup>2,3</sup>, Mohey M. Elmazar<sup>2</sup>, Hassan A. N. El-Fawal<sup>4</sup> and Anwar Abdelnaser<sup>4\*</sup>

<sup>1</sup> Department of Chemistry, School of Sciences and Engineering, The American University in Cairo, Cairo, Egypt,

<sup>2</sup> Department of Pharmacology and Biochemistry, Faculty of Pharmacy, The British University in Egypt (BUE), Cairo, Egypt,

<sup>3</sup> The Center for Drug Research and Development (CDRD), Faculty of Pharmacy, The British University in Egypt (BUE), Cairo, Egypt, <sup>4</sup> Institute of Global Public Health, School of Sciences and Engineering, The American University in Cairo, Cairo, Egypt

## OPEN ACCESS

### Edited by:

Miriam Martini,  
University of Turin, Italy

### Reviewed by:

Keith R. Laderoute,  
Consultant, Redwood City, CA,  
United States  
Wamidh Hadi Talib,  
Applied Science Private University,  
Jordan

### \*Correspondence:

Anwar Abdelnaser  
anwar.abdelnaser@aucegypt.edu

### Specialty section:

This article was submitted to  
Cancer Metabolism,  
a section of the journal  
Frontiers in Oncology

**Received:** 04 December 2021

**Accepted:** 11 January 2022

**Published:** 02 February 2022

### Citation:

Tawfik SM, Abdollah MRA, Elmazar MM, El-Fawal HAN and Abdelnaser A (2022) Effects of Metformin Combined With Antifolates on HepG2 Cell Metabolism and Cellular Proliferation. *Front. Oncol.* 12:828988. doi: 10.3389/fonc.2022.828988

Hepatocellular carcinoma (HCC), one of the most prevalent types of cancers worldwide, continues to maintain high levels of resistance to standard therapy. As clinical data revealed poor response rates, the need for developing new methods has increased to improve the overall wellbeing of patients with HCC. Furthermore, a growing body of evidence shows that cancer metabolic changes are a key feature of many types of human malignancies. Metabolic reprogramming refers to cancer cells' ability to change their metabolism in order to meet the increased energy demand caused by continuous growth, rapid proliferation, and other neoplastic cell characteristics. For these reasons, metabolic pathways may become new therapeutic and chemopreventive targets. The aim of this study was to investigate the metabolic alterations associated with metformin (MET), an anti-diabetic agent when combined with two antifolate drugs: trimethoprim (TMP) or methotrexate (MTX), and how metabolic changes within the cancer cell may be used to increase cellular death. In this study, single drugs and combinations were investigated using *in vitro* assays including cytotoxicity assay (MTT), RT-qPCR, annexin V/PI apoptosis assay, scratch wound assay and Seahorse XF analysis, on a human HCC cell line, HepG2. The cytotoxicity assay showed that the IC<sub>50</sub> of MET as single therapy was 44.08 mM that was reduced to 22.73 mM and 29.29 mM when combined with TMP and MTX, respectively. The co-treatment of both drugs increased p53 and Bax apoptotic markers, while decreased the anti-apoptotic marker; Bcl-2. Both combinations increased the percentage of apoptotic cells and halted cancer cell migration when compared to MET alone. Furthermore, both combinations decreased the MET-induced increase in glycolysis, while also inducing mitochondrial damage, altering cancer cell bioenergetics. These findings provide an exciting insight into the anti-proliferative and apoptotic effects of MET and anti-folates on HepG2 cells, and how in combination, may potentially combat the aggressiveness of HCC.

**Keywords:** hepatocellular carcinoma, metformin, trimethoprim, methotrexate, antifolates, glycolysis, oxidative phosphorylation, seahorse

## INTRODUCTION

Hepatocellular carcinoma (HCC), a liver disease predominant in patients suffering from cirrhosis and chronic liver disease, is a prominent cause of worldwide deaths which occur due to cancer. As the third main cause of cancer world-wide, HCC occurs most frequently in Asia and Africa (1, 2). Due to its high mortality rates, HCC poses as a worldwide health burden. Researchers have informatively suggested that the development of HCC originates from the concept that hepatic stem cells proliferate due to continuous regeneration induced by viral injury (3). Hence, HCC is known for the inflammation, fibrosis, and necrosis of hepatic cells due to the presence of hepatic cirrhosis or hepatitis B virus (HBV), which are vital risk factors in the progression of HCC.

One of the hallmarks of cancer is altered energy metabolism, which is a molecular fingerprint of cancer cells. This metabolic phenotype is defined by an oxygen-independent preferential reliance on glycolysis (the process of converting glucose into pyruvate followed by lactate generation) for energy production. As a result, cancer cells utilize higher levels of glucose to accommodate their altered metabolic state, known as the Warburg effect (4). As cancer cells can become reliant on certain metabolic pathways, new medications targeting these vulnerabilities pose an exciting alternative to cancer therapy.

Metformin (MET) (1,1-dimethyl biguanide), an orally administered drug, is used to decrease the level of blood glucose in patients with non-insulin-dependent diabetes mellitus (NIDDM) by improving insulin sensitivity and decreasing insulin resistance. Recommended as first-line oral therapy in the treatment of diabetes by the American Diabetes Association (ADA), MET exerts its anti-hyperglycemic action by suppressing the production of hepatic glucose, in a process known as hepatic gluconeogenesis (5). As previously stated, MET inhibits complex I of the electron transport chain (ETC) and consequently decreases ATP production by oxidative phosphorylation (OXPHOS). This ultimately disrupts the AMP : ATP ratio, resulting in the activation of 5' AMP- activated protein kinase (AMPK), an enzyme which constantly detects the cellular energy status by monitoring AMP, ADP, and ATP levels (6). To counteract the improper energy balance upon MET administration, AMPK works to restore ATP levels by impeding biosynthetic pathways and promoting pathways which restore energy balance. AMPK stimulates key processes such as glycolysis,  $\beta$ - oxidation of fatty acids, mitochondrial biogenesis and glucose uptake, while it also switches off protein, glycogen and sterol synthesis in order to salvage ATP (7). AMPK phosphorylates enzymes such as acetyl-CoA carboxylase (ACC) to promote fatty acid oxidation and inhibit fatty acid synthesis, hence altering insulin signaling (8); in addition, AMPK initiates glycolysis through the phosphorylation of phosphofructokinase-2 (PFK-2) (9). Moreover, AMPK promotes the translocation of GLUT4 from intracellular vesicles to the plasma membrane, allowing hepatocytes, skeletal muscles, and adipocytes to take up more glucose (10). The nature of MET in that it allows for the activation of AMPK which consequently affects crucial pathways renders it a potent hypoglycemic drug (11).

Furthermore, one study depicted that in response to MET, *de novo* synthesis of glutathione, a folate-dependent process linked to one-carbon metabolism, was also decreased (12). Accordingly, these findings imply that MET can also act as an antifolate chemotherapeutic drug.

Trimethoprim (TMP) (a synthetic compound), used widely for the treatment of microbial infections, has been shown to inhibit various respiratory and urinary tract pathogens by blocking DHFR (dihydrofolate reductase), an enzyme that catalyzes the reduction of dihydrofolate to tetrahydrofolate (13, 14). Moreover, methotrexate (MTX), which also potently inhibits the synthesis of tetrahydrofolate, the active form of folic acid, was used to treat childhood acute leukemia (15). Interestingly, TMP was shown to cause significant cytotoxicity in bladder cancer cells, suggesting the use of antifolate agents in preventing cancer cell seeding, and hence recurrence (16).

To the best of our knowledge, MET has never been used in conjunction with anti-folates in the treatment of HCC and the impact of this combination on cellular energetics has not been examined using Seahorse analysis. For this reason, in this study, we tested whether MET, when combined with either TMP or MTX, could contribute to abrogating HCC cell survival by combating the compensatory increase in glycolysis due to MET.

## MATERIALS AND METHODS

### Materials

MET and TMP were kind donations from Nile Company for Pharmaceuticals and Chemical Industries (Cairo, Egypt). MTX vials 50 mg/2 mL (Mylan-Merck Generiques) were purchased, in their formulated commercial preparations, from a community pharmacy (Cairo, Egypt). RevertAid cDNA kit (K1621), PowerUP SYBR Green Master Mix (A25741), mRNA primers (10629186; designed by NCBI primer blast tool), Dulbecco's Modified Eagle Medium Gibco™ DMEM, High Glucose (41965-039), Fetal Bovine Serum Gibco™ FBS (10270-106), Dimethyl sulfoxide DMSO (67-68-5), Chloroform (HPLC grade; C607SK-1), Isopropanol (HPLC grade; BP26324), and Ethanol (HPLC grade; 64-17-5) were all purchased from ThermoFisher Scientific (MA, USA). QIAzol lysis buffer (79306), RNase/DNase free water (129114) were purchased from Qiagen (Hilden, Germany). Penicillin-Streptomycin Mixture Pen/Strep (09-757F), and Phosphate Buffered Saline (1X) (PBS) (17-516Q) were obtained from Lonza-Bioscience (Billerica, MA, USA). Seahorse cell mitochondrial stress test (MST) containing oligomycin, carbonyl cyanide p-trifluoromethoxyphenylhydrazone (FCCP), rotenone + antimycin A (Rot/AA) and glycolytic rate assay kit including Rot/AA and 2-deoxyglucose (2-DG) were obtained from Seahorse Bioscience Inc. (Basel, Switzerland). XF96 cell culture plates, sensor cartridges and XF base medium were also procured from Seahorse Bioscience Inc. Annexin V and propidium iodide were purchased from ThermoFisher Scientific (MA, USA).

### Cell Culture

HepG2 cells (ATCC® HB-8065) were obtained from the National Research Centre (NRC) Cairo, Egypt. HepG2 cells



were grown in 75 cm<sup>2</sup> flasks in a 5% CO<sub>2</sub> incubator at 37°C, until they reached 80% confluency. HepG2 cells were cultured in Dulbecco's modified Eagle's medium (DMEM) high glucose media (Gibco®, Thermo Fisher Scientific) supplemented with 10% fetal bovine serum (FBS) (Gibco), 1% Pen-Strep (100 units/mL penicillin, and 100 µg/mL streptomycin (Gibco, MA, USA).

### Cell Viability Assay (MTT Assay)

HepG2 cells were seeded in 96-well plates at a density of 15,000 cells/well. Twenty-four hours later, adherent cells were treated with increasing concentrations of single drugs: MET (12.5, 25, 50, 100, 200 mM), TMP (32.29, 64.58, 129.17, 258.34, 516.67 µM) and MTX (1.56, 3.125, 6.25, 12.5, 25, 50 mM) in fresh DMEM media. The culture medium for dual drugs was composed of increasing concentrations of MET (12.5, 25, 50, 100, 200 mM) and either 516.67 µM TMP or 1.5 mM MTX. Following 24 h incubation with the drugs, culture medium was replaced with 100 µL/well of 10 mg/ml MTT (3-(4,5-Dimethylthiazol-2-yl)-2,5-diphenyltetrazolium bromide) solution prepared in complete DMEM medium. Cells were then incubated for 1 h inside the incubator. MTT media was then removed from the wells and formazan crystals were dissolved in 100 µL/well DMSO. Optical density (absorbance) was measured at 570 nm by using Nano SPECTROstar microplate reader (BMG LABTECH, Ortenberg, Germany). Furthermore, the IC<sub>50</sub> of the drugs when used as monotherapies or in combination were determined *via* GraphPad Prism software using the non-linear regression analysis.

The isobologram equation was used to determine the combination index (CI) of the tested compounds to elucidate whether the combination was synergistic, additive or antagonistic.

$$\text{Combination index (CI)} = \frac{d1}{D1} + \frac{d2}{D2}$$

where d1 and d2 are the respective MET and either TMP or MTX concentrations used in combination to reach a certain level of growth inhibition, and D1 and D2 are their concentrations capable of causing the same magnitude of growth inhibition when employed alone. The effect of combination is said to be synergistic if CI < 0.8; antagonistic if CI > 1.2; additive if CI ranges from 0.8-1.2 (17).

### RTqPCR

HepG2 cells were seeded in 6-well plates overnight at a seeding density of 250,000 cells/well. Cells were then treated with MET, TMP or MTX and the combinations at concentrations of 20 mM, 516.67 µM and 10 mM, respectively for 48 h. Concentrations of MET and MTX correspond to their respective IC<sub>40</sub> concentrations, while TMP was used at the maximum concentration possible, given its solubility in DMSO. Total RNA was then isolated using QIAzol Lysis Reagent, Qiagen, Hilden, Germany) according to the manufacturer's instructions. RNA samples were then assessed to detect purity by measuring the absorbance of the RNA samples at 260 nm (ng/µL) and calculating the A260/280 ratio which was measured using NanoDrop Spectrophotometer (BMG LABTECH, Ortenberg, Germany). cDNA was synthesized using the Revertaid

cDNA synthesis kit (K1621; ThermoFisher Scientific, MA, USA), according to the manufacturer's instructions. Primers sequences, shown in **Table 1**, were generated using the online NCBI primer blast tool and purchased from ThermoFischer (MA, USA). Gene expression levels were calculated as follows:  $2^{-\Delta\Delta CT} \pm$  standard error of mean (SEM).

### Cell Apoptosis Assay

The percentage of apoptotic cells was evaluated by using Annexin V and propidium iodide (PI) staining. Cells were grown in T25 flasks and subsequently treated with MET, TMP or MTX and the combinations at concentrations of 20 mM, 516.67 µM and 10 mM, respectively for 48 h. Cells were then harvested, washed with cold 1x PBS, centrifuged three times at 280 x g for 7 min and resuspended in PBS. Aliquots of 100 µL were stained with 5 µL Annexin V-FITC and 1 µL PI stock (100 µg/mL) and incubated for 15 min at room temperature in the dark. 1x Annexin binding buffer (400 µL) was then added to each sample and analyzed by CytoFlex flow cytometer (Beckman Coulter, CA, USA). according to the manufacturers' instructions. A minimum of 30,000 events were recorded for each sample. Data analysis was performed in CytExpert software.

### Scratch Wound Assay

Briefly, 10<sup>6</sup> HepG2 cells were seeded in 6-well plates and allowed to attach overnight. Once the cells reached confluency, a wound was made by scratching the surface with a 200 µL pipette tip held vertically. To remove floating cells, the cells were washed twice with PBS. The cells were then treated with complete DMEM medium and either 3 mM MET, 344.45 µM TMP or 0.2 mM MTX or the combinations MET + TMP and MET + MTX (lower concentrations were used to avoid the detachment of cells). The initial wound area was measured at time 0 using an inverted microscope (magnification power of 400x) (Labomed Inc., LA, CA, USA) connected to a digital camera. The wound distance was then assessed by ImageJ software.

### Seahorse Analysis

Cells were seeded in XF96-well plates (15,000 cells/80 µL medium/well) and left in the incubator to adhere overnight. The next day, the cells were treated with different concentrations MET (3 mM), TMP (86.11 µM), MTX (1.5 mM) and

**TABLE 1** | List of primer sequences and their National Center for Biotechnology Information (NCBI) accession numbers.

Gene name	Primer sequences (5'-3')	Accession number	Tm (°C)
Bax	F: AAGCTGAGCGAGTGTCTCAAG	NM_138764.5	60.34
	R: CAAAGTAGAAAAGGGCGACAAC		58.11
Bcl-2	F: CTTTGAGTTCGGTGGGGTCA	NM_000633.3	59.89
	R: GGGCCGTACAGTTCCACAAA		60.54
p53	F: CCCTTCCCAGAAAACCTACC	NM_001126118.2	57.49
	R: CTCGTCATGTGCTGTGACT		60.04
AMPK	F: AAGAAAGTCGGCGTCTGTTC	NM_206907.4	58.50
	R: TTCTGGTGCAGCATAGTTGG		58.17
β-actin	F: AGCACAGAGCCTCGCCTTT	NM_001101.5	61.89
	R: CACGATGGAGGGGAAGAC		56.74

combinations for the glycolytic rate assay (concentrations were lowered to reach optimal basal OCR values). Similar concentrations, as well as higher concentrations were used for the ATP rate assay; MET (6.5 mM), TMP (189.45  $\mu$ M), MTX (3 mM) and combinations. The higher concentrations only were used for the MST. Twenty-four hours before the start of the experiment, cartridges were soaked in calibrant solution and left in a non-CO<sub>2</sub> incubator overnight. Before analysis, the culture medium on the plates was removed and cells were washed with 150  $\mu$ L of XF Seahorse media (supplemented with 2 mM glutamine, 1 mM pyruvate and 10 mM glucose). Then, 180  $\mu$ L of Seahorse media was added to each of the wells and the plates were incubated for 45 min in a non-CO<sub>2</sub> incubator. For each of the assays, compounds were prepared, diluted using XF base medium into designed concentrations and added in the corresponding cartridge ports; (Glycolytic Rate Assay; Rot/AA: 5  $\mu$ M, 2-DG: 500 mM; ATP Rate Assay; 15  $\mu$ M Oligomycin and 5  $\mu$ M Rot/AA; MST; Oligomycin: 15  $\mu$ M, FCCP: 10  $\mu$ M and Rot/AA: 5  $\mu$ M). After calibration, all assays were conducted as per manufacturer's instructions.

## Statistical Analysis

Each experiment was repeated at least 3 times with 3 to 6 replicates per treatment (representative data are shown in the *Results* section). Data are depicted as means  $\pm$  SEM for each experiment. Comparisons between treated versus untreated cells for MTT, RT qPCR, apoptosis assay, wound healing assay and Seahorse analysis were done by performing one way ANOVA followed by Tukey *post-hoc* test to assess the statistical significance between multiple groups. A *p*-value < 0.05 was considered statistically significant. SigmaPlot was used to compare the results obtained from the tested compound groups and their relative controls (Version 12.0; Systat Software, Chicago, IL, USA). Graphs were drawn using SigmaPlot software. XF Glycolytic Rate Assay, XF ATP Rate Assay and XF MST parameters were automatically generated using Wave software (Agilent Technologies) to determine OCR (oxygen consumption rate) and ECAR (extracellular acidification rate) values, depicting respiration and acidification rates. Graphs pertaining to the Seahorse data were exported to GraphPad Prism 6 software.

## RESULTS

### Effect of MET, TMP and MTX on HepG2 Cell Viability

To evaluate the effect of MET, TMP and MTX on HepG2 cell viability, cells were exposed to increasing concentrations of MET (12.5–100 mM), TMP (32.29–516.67  $\mu$ M) and MTX (3.125–50 mM). Both MET and MTX significantly reduced HepG2 cell viability in a dose-dependent manner (**Figures 1A, C**). MET individually inhibited cell viability with an IC<sub>50</sub> value of 44.08 mM, while MTX inhibited cell viability with an IC<sub>50</sub> value of 14.3 mM. TMP reduced HepG2 cell viability at 516.67  $\mu$ M, then plateaued at the subsequent concentrations (**Figure 1B**).

Notably, due to the limited solubility of TMP in DMSO at non-toxic concentrations, the IC<sub>50</sub> concentration of TMP was not calculated and is well above the concentrations used in the present study. Hence, all subsequent experiments were conducted using 516.67  $\mu$ M TMP.

### Effect of MET When Combined With TMP or MTX on HepG2 Cell Viability

To evaluate the cytotoxicity of MET in combination with both antifolate agents, TMP and MTX, cells were co-exposed with increasing concentration of MET (12.5–100 mM) and either 516.67  $\mu$ M TMP or 1.5 mM MTX for 24 h. The IC<sub>50</sub> value of MET was decreased from 44.06 mM to 22.73 mM upon the addition of TMP (CI = 0.998, i.e., an additive effect). As presented in **Figure 2**, all combinations of MET with TMP had more cytotoxic effects compared to MET individually. Furthermore, IC<sub>50</sub> value of MET was decreased from 44.06 mM to 29.29 mM upon the addition of MTX (CI = 0.763, i.e., a synergistic effect).

### Effect of MET, TMP, MTX and Combinations on Bax, Bcl-2 and p53 mRNA Expression in HepG2 Cells

The expression levels of apoptosis associated genes, Bax, Bcl-2, p53 were evaluated using the real time quantitative polymerase chain reaction technique. The expression of Bax and p53 were significantly (*P*<0.05) increased in both combinations, when compared with both the control and cells treated with MET alone, as shown below (**Figure 3**). Contrastingly, the anti-apoptotic gene Bcl-2 decreased significantly, when compared to the control. Our data revealed that Bax was upregulated by 1.77, 3.79, 3.03, 3.78 and 6.20 folds after treatment with MET, TMP, MTX, MET + TMP and MET + MTX, respectively compared to the control. The gene expression of p53 exhibited comparable results and was also upregulated by 1.17, 1.06, 1.27, 1.83- and 2.39-folds following treatment with MET, TMP, MTX, MET + TMP and MET + MTX, respectively compared to the control. In contrast, the gene expression of Bcl-2 was shown to decrease by 0.29, 0.59, 0.4, 0.08 and 0.15 folds when treated with MET, TMP, MTX, MET + TMP and MET + MTX, respectively compared to the control. A comprehensive comparison of the fold changes of each of the tested compounds, singly or in combination, revealed an upregulation of key apoptotic markers and downregulation of an anti-apoptotic gene. Combining MET, with either TMP or MTX, exhibited higher fold change values than that of MET only for both apoptotic markers. These data suggest that the tested compounds in combination significantly trigger apoptosis through the mitochondrial apoptotic pathway.

### Effect of MET, TMP, MTX and Combinations on the Percentage of Apoptosis in HepG2 Cells

To examine the role of apoptosis in the cytotoxic effect of MET, TMP, MTX or combinations, the percentage of apoptotic cells was detected *via* Annexin/PI staining that was measured by the flow cytometry analysis, as previously described. Our results

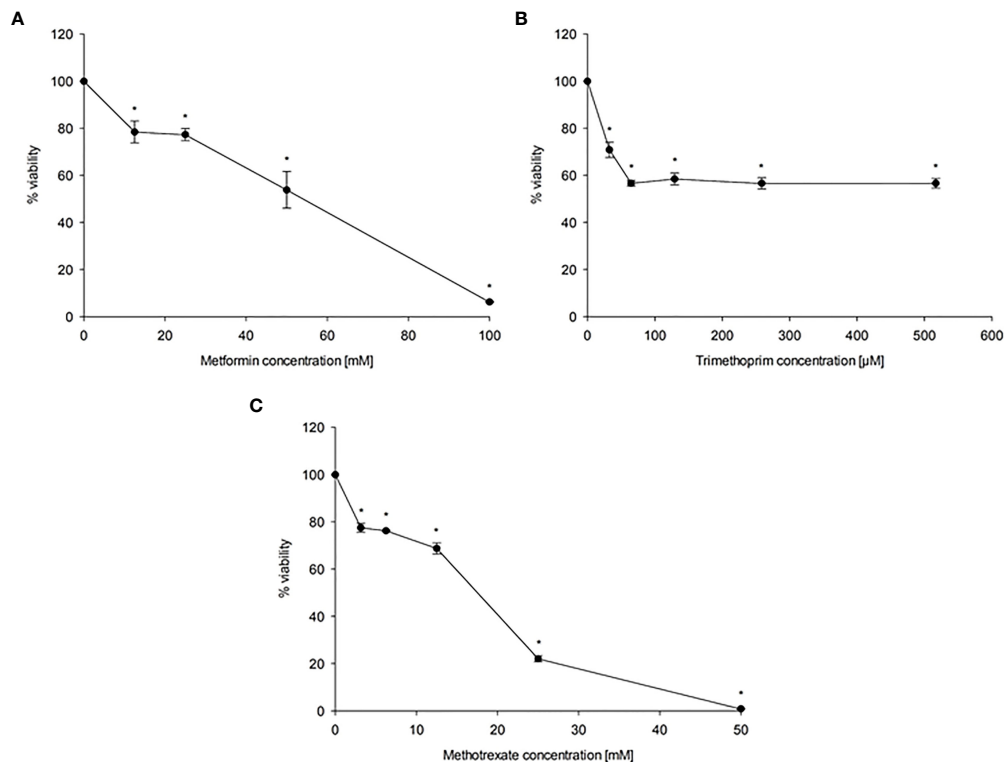


**FIGURE 1 |** Effect of MET (A), TMP (B) and MTX (C) on HepG2 cell viability. HepG2 cells were exposed to increasing concentrations of MET (12.5–100 mM), MTX (3.125–50 mM) and TMP (32.29–516.67  $\mu$ M) for 24 h. The MTT assay was done to assess the inhibitory effects of the tested compounds at the used concentrations. Data are depicted as a percentage of the untreated control. The error bars represent the standard error of mean (SEM) (n=6). Comparisons were made using ANOVA followed by Tukey *post-hoc* test. \*, indicates statistical significance when compared to the control.

showed that cells co-treated with both combinations induced cell death in HepG2 cells when compared with the control as well as single treatment of MET. MET significantly increased apoptosis at 20 mM and the percentage of viable cells, early apoptotic, late apoptotic and necrotic cells was  $85.38 \pm 3.88$ ,  $8.82 \pm 2.78$ ,  $4.22 \pm 1.08$ ,  $1.58 \pm 0.08$ , respectively. TMP at 516.67  $\mu$ M induced apoptosis and the percentage of viable cells, early apoptotic, late apoptotic and necrotic cells was  $88.42 \pm 1.37$ ,  $2.35 \pm 0.45$ ,  $3.60 \pm 0.81$ ,  $5.63 \pm 0.16$ , respectively. It is also of interest that cells treated with MTX (10 mM) did not significantly increase apoptosis. Contrastingly, the percentage of early and late apoptotic cells in the combined treatment of MET and TMP was  $4.73 \pm 2.15\%$  and  $18.57 \pm 4.44$ , respectively. Moreover, the combination of MET with MTX depicted a rise in the percentage of early apoptotic cells,  $18.69 \pm 1.62$ , while the percentage of late apoptotic cells was nearly the same,  $3.93 \pm 0.41$ . The total percentage of apoptotic cells significantly increased when both drug combinations were used simultaneously ( $P < 0.05$ ), as shown in **Figure 4**, as compared with the control or single treatment. These findings suggest that MET combined with TMP or MTX effectively induced early and late apoptosis in HepG2 cells. Changes in the percentage of total apoptotic cells were consistent with the data obtained from the increase in mRNA expression of key apoptotic markers. Hence, the combination of

MET and either TMP or MTX considerably inhibited cell growth in HepG2 cells by inducing apoptosis.

### Effect of MET, TMP, MTX, Alone and in Combination, on HepG2 Cell Migration

Carcinoma cell migration is due to the cancer cells' ability to undergo various biological processes, specifically related to coordination. As metastasis and angiogenesis are closely related (18), therefore, it was crucial to examine the impact of the drugs on HepG2 cell motility. The ability of MET, TMP, MTX and respective combinations to alter cell migration was analyzed *via* the scratch wound healing assay, which investigates the ability of cells to undergo migration and hence, increase tumorigenesis.

The effects of MET, TMP, MTX and combinations on cell migration were observed in HepG2 cell line. Cells were cultured in 6-well plates and gaps were made using a 200  $\mu$ L tip to ensure a cell-free gap in each well. HepG2 cells were then treated with 3 mM MET, 344.45  $\mu$ M TMP or 0.2 mM MTX or the combinations (MET +TMP) and (MET+MTX) and incubated for up to 72 h. Images were taken every 24 h for three consecutive days. Co-presence of MET and TMP resulted in a significantly lower percentage of wound closure when compared to the presence of MET (3 mM) from  $29.75 \pm 3.94\%$  to  $1.97 \pm 0.53\%$  at 24 h, from  $52.29 \pm 2.2\%$  to  $6.79 \pm 4.56\%$  at 48 h and from  $54.93 \pm 2.83\%$  to

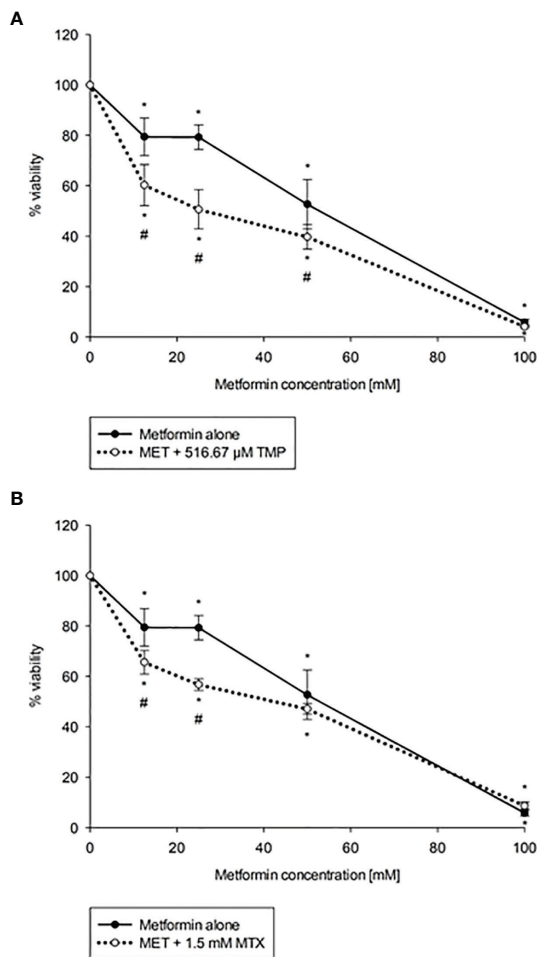


**FIGURE 2 |** Effect of MET when combined with TMP (A) or MTX (B) on HepG2 cell viability. Cytotoxicity of various concentrations of MET individually or in combination with TMP or MTX in HepG2 cells were shown above. TMP and MTX increase the cytotoxic effect of MET on HepG2 cells *in vitro*. The MTT assay was done to assess the combinatory effects of MET (12.5–100 mM) and TMP (516.67 μM) or MTX (1.5 mM). Cells were treated with the above concentrations for 24 hours. The  $IC_{50}$  of MET was calculated as 44.06 mM, while upon the addition of TMP, the  $IC_{50}$  was markedly reduced to 22.73 mM and upon the addition of MTX, the  $IC_{50}$  was markedly reduced to 29.29 mM; the error bars represent the SEM ( $n=6$ ). Comparisons were made using ANOVA followed by Tukey *post-hoc* test. \*, indicates statistical significance when compared to the control.

$10.8 \pm 4.70\%$  at 72 h, respectively (Figure 5). Contrastingly, MET when combined with MTX inhibited cell migration, to a much less extent when compared to MET alone; from  $29.75 \pm 3.94\%$  to  $11.94 \pm 2.61\%$  at 24 h, from  $52.29 \pm 2.2\%$  to  $38.5 \pm 4.38\%$  at 48 h and from  $54.93 \pm 2.83\%$  to  $41.35 \pm 3.92\%$  at 72 h, respectively. TMP and MTX alone significantly decreased HepG2 cellular migration, when compared to the control at the same time points. TMP alone resulted in a percentage of wound closure of  $25.45 \pm 2.42\%$  at 24 h,  $42.24 \pm 2.19\%$  at 48 h and  $43.86 \pm 3.07\%$  at 72 h. Moreover, MTX caused a percentage of wound closure of  $23.99 \pm 2.92\%$  at 24 h,  $43.43 \pm 2.11\%$  at 48 h and  $44.31 \pm 1.63\%$  at 72 h.

## Effect of MET, TMP and MTX, Alone and in Combination, on Rates of Basal and Compensatory Glycolysis in HepG2 Cells

To examine if the tested compounds influence the Warburg effect, MET, TMP, MTX, MET + TMP and MET + MTX treated groups were examined in terms of rate of glycolysis. MET alone, or in combination, activated glycolysis up to the maximum level, as shown by the insensitivity to oligomycin. MET caused an increase in basal glycolysis depicted by a 68% increase, when compared to the control (Figure 6). Contrastingly, TMP and MTX alone decreased basal glycolysis rates by 11% and 27%, respectively, also when compared to the control. Of significance, co-treatment of MET and TMP or MET and MTX, decreased basal glycolysis rates by 17% and 25%, when compared to MET alone. Furthermore, MET caused a slight decrease in the rates of compensatory glycolysis by 4%, when compared to the control, while TMP and MTX decreased compensatory glycolysis by 14% and 26%, respectively. Rates of compensatory glycolysis were significantly decreased upon co-therapy of MET and TMP or MET and MTX by 13% and 21%, respectively, when compared to MET alone. These data bring to light the suggestion that both TMP and MTX significantly combat the MET-induced shift in glycolysis.

## Effect of MET, TMP and MTX and Combinations on the Total ATP Production Rate in HepG2 Cells

To analyze living cells, sub- $IC_{50}$  values were used to measure the total ATP production rates in HepG2 cells. Two concentrations were used for the tested compounds, alone and in combination (Figure 7). At low and high concentrations, MET increased total ATP production rates by 30% and 26%, respectively, when compared to the control. Contrastingly, TMP and MTX (at low concentrations) induced an increase in total ATP production rate by 16% and 1%, respectively, when compared to the control. Contrastingly, TMP induced a decrease in total ATP production by 23% at high concentrations, while MTX, similarly, induced a decrease by 9%, when compared to the control. MET + TMP and MET + MTX significantly decreased ATP production in a dose dependent manner compared with MET alone at both low and high concentrations, respectively; MET + TMP (15% and 39%) and MET + MTX (30% and 58%).

## Effect of MET, TMP and MTX, Alone and in Combination, on the Glycolytic and Mitochondrial ATP Production Rates in HepG2 Cells

Consistent with the percentage of basal and compensatory glycolysis rates depicted in Figure 6, treatment of MET led to an increase in rate of glycolysis, while the combinations led to a decrease in glycolysis rate (Figure 8). Both concentrations of MET increased the glycolytic ATP production rate by 57% and 105%, respectively, when compared to the control. TMP, on the other hand, increased glycolysis by 26% at low concentration and decreased the rate of glycolysis by 11% at higher concentrations. Similarly, MTX increased glycolysis by 15% when administered



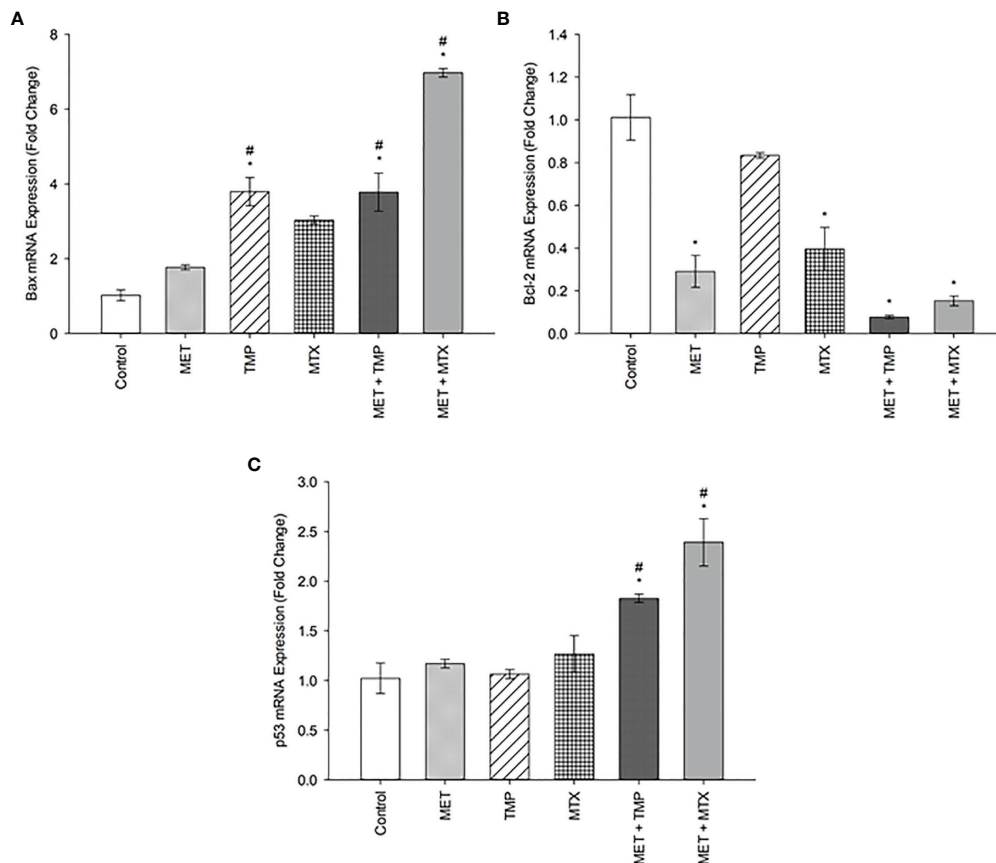


**FIGURE 3 |** Effect of MET, TMP, MTX and combinations on Bax (A), Bcl-2 (B) and p53 (C) mRNA expression in HepG2 cells. HepG2 cells were treated for 48 h with MET (20 mM), TMP (516.67  $\mu$ M), MTX (10 mM), MET + TMP (20 mM + 516.67  $\mu$ M) or MET + MTX (20 mM + 10 mM). Bax, Bcl-2 and p53 mRNA levels were quantified using qRT-PCR and normalized to  $\beta$ -actin. Data are expressed as mean  $\pm$  SEM ( $n=3$ ). Comparisons were made with ANOVA followed by Tukey *post-hoc* test; \*, indicates a statistically significant difference between the control and drug-treated groups at  $P < 0.05$  versus the control group; #; indicates a statistically significant difference between the MET treated group and other drug-treated groups at  $p < 0.05$ .

at a low concentration, while decreased the glycolytic rate by 8% at higher concentrations, when compared to the control. Combining MET and TMP or MET and MTX at low concentrations decreased the rate of glycolysis by 12% and 36%, respectively, when compared to MET alone. Interestingly, both combinations (MET + TMP and MET + MTX) effectively led to a more prominent decrease in the rate of glycolysis at higher concentrations; 36% and 55%, respectively when compared to MET alone. Hence, our results confirmed the findings obtained from the Glycolytic Rate Assay depicted above.

Of significance, the rate of mitochondrial ATP production was also impacted as a result of drug treatments. MET and MTX (at low concentrations) decreased mito-ATP production by 0.92% and 13%, respectively when compared to the control. Contrastingly, TMP slightly increased the mito-ATP production rate by 4%. Both combinations, on the other hand, declined these rates by 21% and 19%, when compared to MET alone. Furthermore, MET, TMP and MTX (at high concentrations) elucidated a higher decrease in mito-ATP production by 69%,

38% and 11%, respectively, when compared to the control. Of note, co-treatment of MET + TMP and MET + MTX further led to a decrease in mitochondrial ATP production by 65% and 75%, respectively, when compared to MET alone.

### Effect of MET, TMP, MTX and Combinations on AMPK mRNA Expression in HepG2 Cells

MET is well known to inhibit complex I of the mitochondrial respiratory chain, resulting in a decrease in the ATP/AMP ratio, and consequent AMPK activation (19, 20). Therefore, we decided to monitor the gene expression of AMPK following drug incubation.

Our data revealed that AMPK was upregulated by 1.29, 1.10, 2.55, 2.11 and 2.03 folds after treatment with MET, TMP, MTX, MET + TMP and MET + MTX, respectively compared to the control (Figure 9). The increasing pattern in terms of fold change confirmed the results obtain *via* the ATP Rate assay, though none of the values above were considered significant.

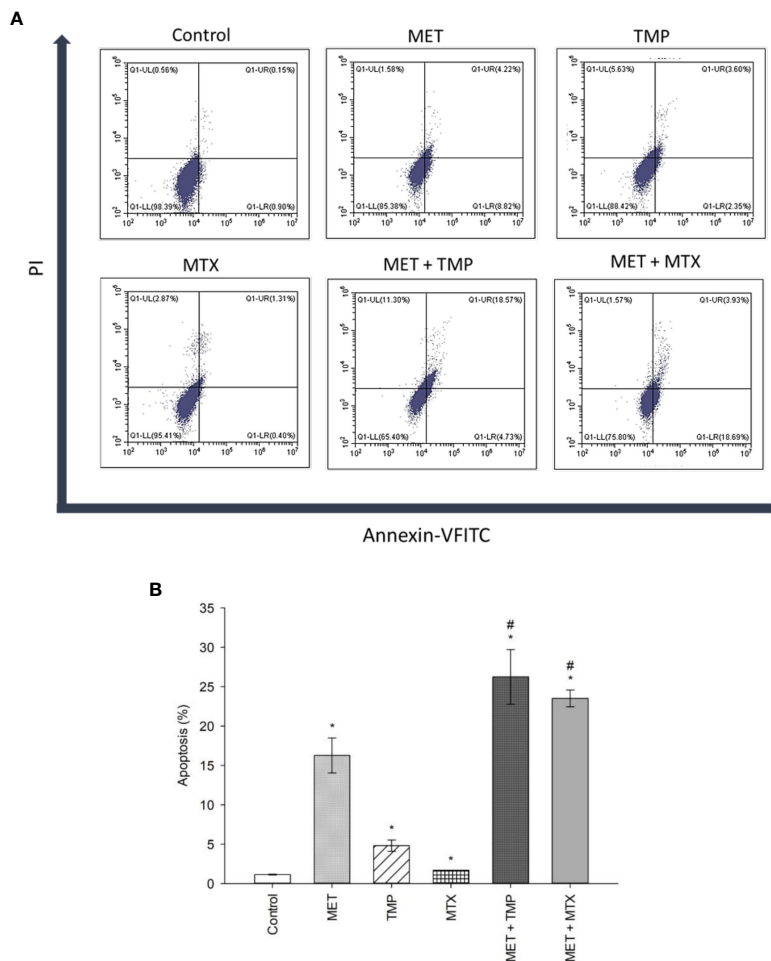


**FIGURE 4 |** Effect of MET, TMP, MTX and combinations on the percentage of apoptosis in HepG2 cells. **(A)** Flow cytometry dot plots (Annexin-V-FITC against PI) for apoptosis assay. Squares depict populations of cells depending on the presence/absence of phosphatidylserine on the outer surface of the plasma membrane as well as the integrity of the membrane; population of viable cells (LL), early apoptotic cells (LR), late apoptotic cells (UR) and necrotic cells (UL). Annexin V/PI flow cytometry of HepG2 cells treated singly or concurrently with either MET +TMP or MET + MTX for 48 h. Representative data of three independent experiments ( $n = 3$ ) are shown. MET + TMP and MET + MTX combinations significantly induced a higher total percentage of apoptosis in HepG2 cells, compared to single drug treatments. **(B)** Total percentage of apoptosis (early + late apoptosis) in different treatment groups. Each bar represents the mean of three independent experiments. HepG2 cells were treated for 48 h with MET (20 mM), TMP (516.67  $\mu$ M), MTX (10 mM), MET + TMP (20 mM + 516.67  $\mu$ M) or MET + MTX (20 mM + 10 mM). Error bars represent the SEM. Some error bars are too small to be seen. Comparisons were made using ANOVA followed by Tukey *post-hoc* test. \*,  $p$ -value < 0.05 versus control and #,  $p$ -value < 0.05 versus cells treated with MET only.

## Effect of MET, TMP, MTX, Alone and in Combination, on Mitochondrial Bioenergetics

Combining MET to either TMP or MTX leads to inhibition of mitochondrial bioenergetics.

As MET has been previously known to inhibit OXPHOS, the tested compounds were examined alone and in combination (at high concentrations) to further investigate the effects of the combinations on mitochondrial function using the MST. HepG2 cells were incubated with MET, TMP, MTX or respective combinations at sub- $IC_{50}$  concentrations for 24 h. Following incubation, cells were incubated in a non- $CO_2$  incubator for 45 min and then examined using the Seahorse XFe96 Analyzer. Real-time measurements of OCR were measured (**Figure 10**). MET

caused a decrease in mitochondrial function as elucidated by a sharp reduction in mitochondria basal activity (calculated as the difference between basal OCR and non-mitochondrial OCR), maximal respiration (maximal OCR after the addition of the uncoupler FCCP), proton leak (remaining basal respiration not coupled to ATP production) and spare respiratory capacity (the difference between basal and maximal rates) by 86%, 69%, 42% and 53%, respectively, when compared to the control. Similarly, TMP alone reduced basal respiration, maximal respiration, proton leak and spare respiratory capacity by 64%, 78%, 24% and 91%, respectively, when compared to untreated cells. Furthermore, MTX decreased the above assessed parameters, in the same order, by 16%, 22%, 4% and 28%, respectively, when compared to the control. Interestingly, the mitochondrial inhibitory functions of MET were increased upon

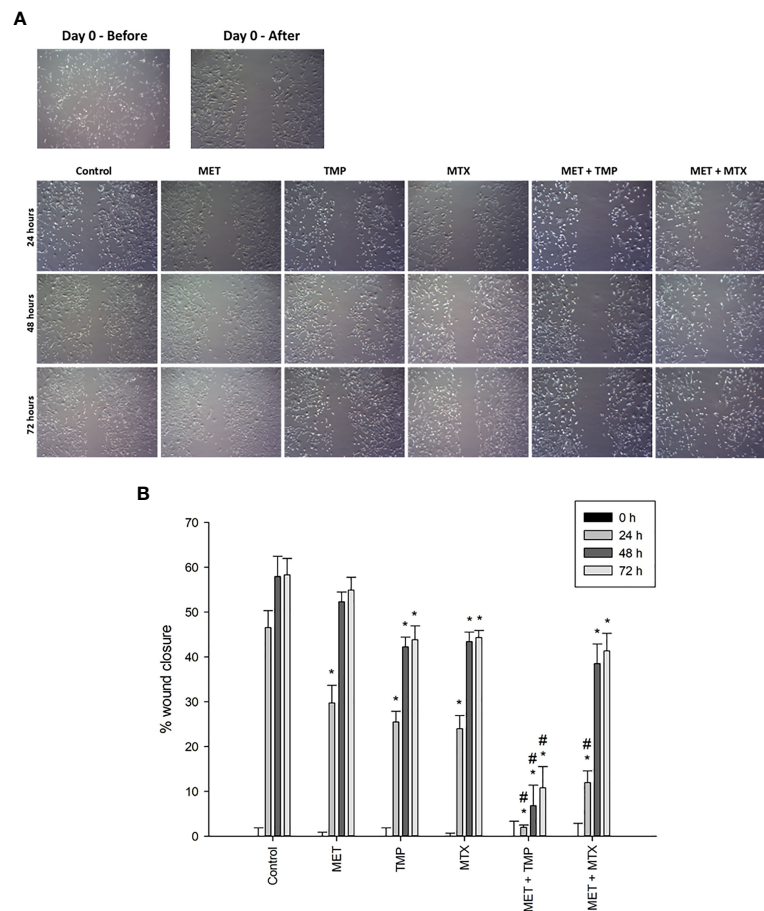


**FIGURE 5 |** Effect of MET, TMP, MTX, alone and in combination, on HepG2 cell migration. **(A)** Migration of HepG2 cells in response to the treated compounds was determined by the wound healing assay at 24, 48 and 72 h using an inverted microscope at 400x magnification. **(B)** Percentage of wound closure was calculated at 0, 24, 48 and 72 h by measuring the gap width with respect to the initial scratch area. Error bars represent the SEM. Comparisons were made using ANOVA followed by Tukey *post-hoc* test. \*, *p*-value < 0.05 versus control at equal time points and #, *p*-value < 0.05 versus cells treated with MET only at equal time points.

the addition of either TMP or MTX. Following 24 h incubation with MET + TMP, cells depicted a basal respiration and maximal respiration reduction by 6% and 86%, respectively, when compared to MET alone. MET + TMP also induced a decrease in proton leak, which reached 25%, while the spare respiratory capacity was completely abolished at 24 h. Moreover, MET when combined with MTX also exhibited a decrease in basal and maximal respiration by 18% and 36%, respectively, when compared to MET alone. In congruence with these findings, the proton leak and spare respiratory capacity were also reduced by 26% and 41% upon co-treatment of tested compounds, compared to MET alone. These data suggest that TMP and MTX may potentiate the detrimental action of MET on mitochondrial function in HepG2 cells.

## DISCUSSION

Inhibiting glycolysis appears to be a logical treatment strategy for cancer cells which rely heavily on this pathway. Due to cancer cells' metabolic adaptability, combining drugs that target different

metabolic pathways to acquire better therapeutic activity is necessary. Furthermore, clinical evidence has emerged that the use of a single therapeutic agent for treatment has proven to be less effective in preventing the recurrence of various cancers (21). Moreover, cancer cells are known to exemplify resistance to pharmacological therapeutics through signaling pathways, thereby increasing mortality rates in liver cancer patients (22). Furthermore, HCC, one of the most common types of cancers worldwide, portrays poor prognosis in currently existing treatment options. Combination therapy hence provides an exciting alternative for improving therapeutic outcomes and reducing recurrence in HCC. Additionally, repurposing FDA approved drugs provides a more economical approach to drug development. The co-treatment of drugs that alter cancer cell metabolism and antifolate agents may yield more effective results (23).

MET, used as first-line treatment of type 2 DM, is a safe and economical therapeutic agent which stands to be one of the most widely prescribed drugs worldwide (24, 25). Several studies have shown the potential of MET as a chemotherapeutic agent in

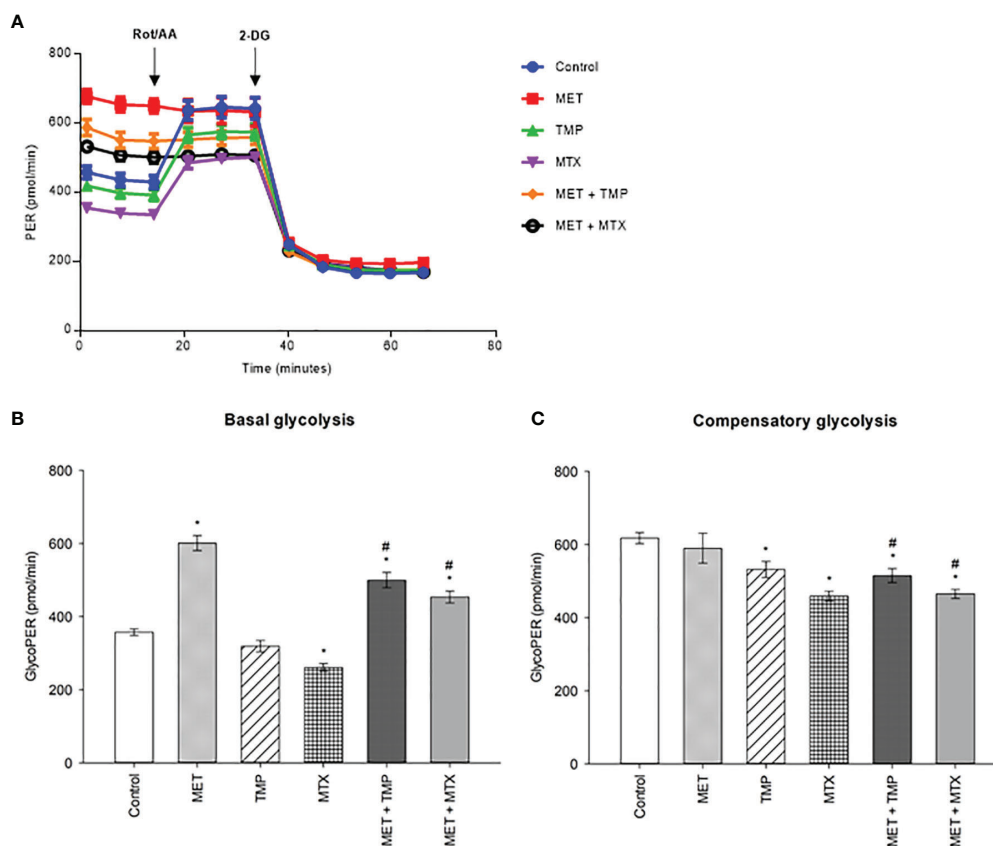


**FIGURE 6 |** Effect of MET, TMP and MTX, alone and in combination, on rates of basal and compensatory glycolysis in HepG2 cells. Cells were seeded in Seahorse tissue culture microplates, treated with MET (3 mM), TMP (86.11  $\mu$ M), MTX (1.5 mM), MET + TMP (3 mM + 86.11  $\mu$ M) or MET + MTX (3 mM + 1.5 mM) for 24 hours and examined by the Glycolytic Rate Assay in which Rot/AA and 2-DG were added as shown above. **(A)** Representative Glycolytic Rate Assay profile. **(B)** Calculated basal glycolytic proton efflux rate (glycoPER). **(C)** Calculated compensatory glycolytic proton efflux rate (glycoPER). Data are expressed as mean  $\pm$  SEM (n=6). Comparisons were made using ANOVA followed by Tukey *post-hoc* test. \*, *p*-value < 0.05 versus control and #, *p*-value < 0.05 versus cells treated with MET only.

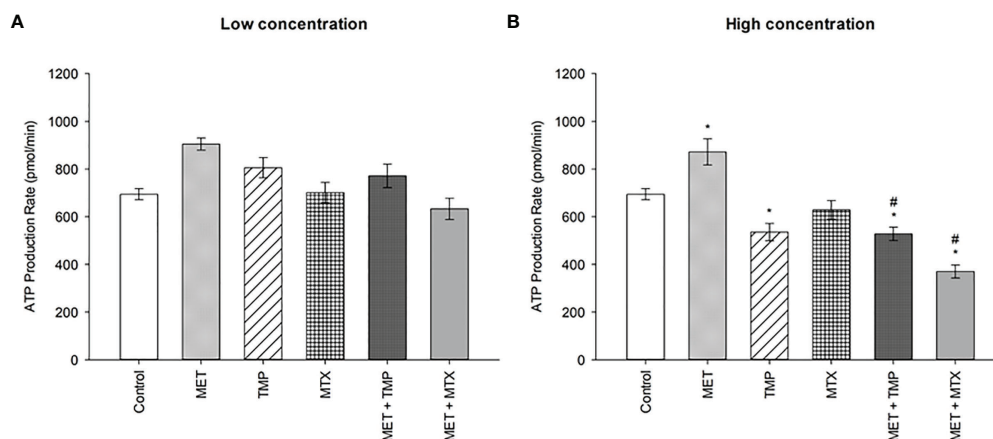


**FIGURE 7 |** Effect of MET, TMP and MTX and combinations on the total ATP production rate in HepG2 cells. **(A)** HepG2 cells were treated for 24 h with MET (3 mM), TMP (86.11  $\mu$ M), MTX (1.5 mM), MET + TMP (3 mM + 86.11  $\mu$ M) or MET + MTX (3 mM + 1.5 mM). **(B)** HepG2 cells were treated for 24 h with MET (6.5 mM), TMP (189.45  $\mu$ M), MTX (3 mM), MET + TMP (6.5 mM + 189.45  $\mu$ M) or MET + MTX (6.5 mM + 3 mM) and measured by Seahorse XF Real-Time ATP rate assays. Data are expressed as mean  $\pm$  SEM (n=6). Comparisons were made using ANOVA followed by Tukey *post-hoc* test. \*, *p*-value < 0.05 versus control and #, *p*-value < 0.05 versus cells treated with MET only.



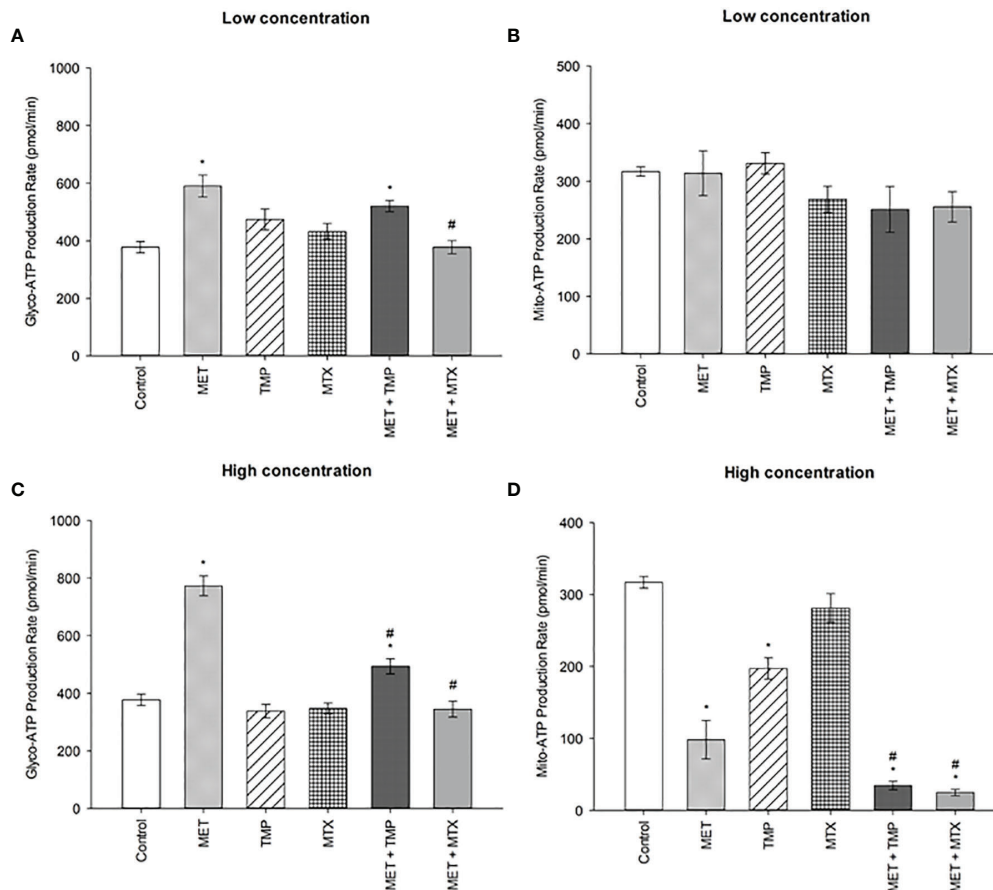


**FIGURE 8 |** Effect of MET, TMP and MTX, alone and in combination, on the glycolytic and mitochondrial ATP production rates in HepG2 cells. **(A, B)** Glycolytic and mitochondrial ATP production rates decreased upon co-treatment of MET with TMP or MTX. HepG2 cells were treated for 24 h with MET (3 mM), TMP (86.11  $\mu$ M), MTX (1.5 mM), MET + TMP (3 mM + 86.11  $\mu$ M) or MET + MTX (3 mM + 1.5 mM). **(C, D)** Percentage of ATP production from glycolysis and mitochondria significantly decreased upon combination of MET with either TMP or MTX, when compared to MET only. HepG2 cells were treated for 24 h with MET (6.5 mM), TMP (189.45  $\mu$ M), MTX (3 mM), MET + TMP (6.5 mM + 189.45  $\mu$ M) or MET + MTX (6.5 mM + 3 mM) and measured by Seahorse XF Real-Time ATP rate assays. Data are expressed as mean  $\pm$  SEM (n=6). Comparisons were made using ANOVA followed by Tukey *post-hoc* test. \*, *p*-value < 0.05 versus control and #, *p*-value < 0.05 versus cells treated with MET only.

various cancer types, such as breast cancer, lung cancer, gastric and colorectal cancer (26–28). Mechanistic investigations on the mode of action of MET have also demonstrated the ability of MET to inhibit cancer cell proliferation and induce apoptosis *in vitro* in a number of human cancer cell lines (29, 30). In another study, MET served to combat thyroid cancer in a dose dependent manner (31). Furthermore, MET significantly inhibited breast and lung cancer cell proliferation when combined with Paclitaxel by inducing AMPK activation and inhibiting mTOR levels (30).

MET has shown to be more effective in combination with other anti-cancer agents when compared to single therapy; i.e. doxorubicin and cisplatin (32). However, to the best of our knowledge, MET has not been previously investigated with either TMP or MTX on HCC. In the present study, the molecular mechanisms associated with the cytotoxic effects of MET + TMP and MET + MTX were tested to assess the effectiveness of the respective combinations in the treatment of HCC.

In the present study, we found that treatment of HepG2 cell line with either MET, TMP or MTX directly inhibits cell survival. In addition, the co-treatment of MET and either TMP or MTX effectively inhibited HepG2 cell survival at sub-IC<sub>50</sub> concentrations, causing a reduction in the IC<sub>50</sub> concentration of MET alone. Our findings are consistent with previous studies that depicted the cytotoxic effects of MET and WP 631 (a structural analogue of doxorubicin) on HepG2 cells (33).

Alternatively, the combination of WP 631 and sitagliptin (a dipeptidyl peptidase-4 inhibitor used for the treatment of type 2 diabetes) did not enhance the cytotoxic effects of WP 631 on HepG2 cells. Moreover, our results are in strong agreement with previous reports of MET in combination with potential chemotherapeutic agents on various breast cancer cell lines (34). Another study also reported that the combined treatment of MET with aloin (an extract of Aloe vera) inhibits HCC growth *in vitro* and *in vivo* (35). Their findings were in uniformity with

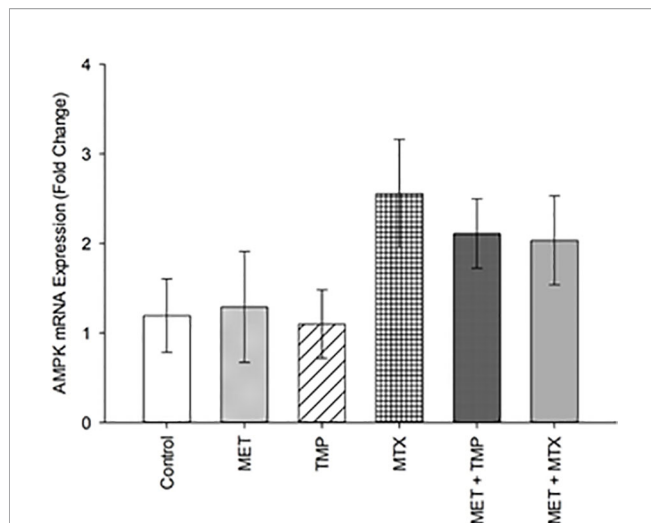


**FIGURE 9 |** Effect of MET, TMP, MTX and combinations on AMPK mRNA expression in HepG2 cells. HepG2 cells were treated with MET (6.5 mM), TMP (189.45  $\mu$ M), MTX (3 mM), MET + TMP (6.5 mM + 189.45  $\mu$ M) or MET + MTX (6.5 mM + 3 mM). AMPK mRNA levels were quantified using qRT-PCR and normalized to  $\beta$ -actin. Data are expressed as mean  $\pm$  SEM. (n=3).

our results in that MET also elucidated a stronger anti-cancer effect when compared to either drug alone; however, upon combination, the added therapeutic agent increased the cytotoxicity of MET in HepG2 cells. Additionally, MET and curcumin were reported to have inhibited the growth, metastasis and angiogenesis of HCC (36). Co-treatment of MET and sorafenib (an FDA approved drug for the treatment of advanced HCC) also effectively decreased the growth of HCC cells, when compared to each drug alone (37–39). MET was also previously reported to have improved the sensitivity of ovarian cancer cells to MTX, compared with the chemotherapeutic agent MTX alone (40). Furthermore, another study reported that MET when used in combination with rapamycin decreased cancer cell viability in HepG2 cells by inducing cell apoptosis (41).

All subsequent experiments were carried out by the calculated sub-IC<sub>50</sub> values of the tested compounds, alone and in combination. Our findings were consistent with the previously mentioned studies which were conducted on HepG2 cells confirming that the combination of MET with both tested antifolate compounds dramatically inhibited cell viability, when compared with single therapy of MET alone. To examine the effect of the tested chemotherapeutic agents on induction of apoptosis, we investigated the effect of MET, TMP, MTX and respective combinations on the expression of p53, Bax and Bcl-2 on HepG2 cells.

Apoptosis is initiated *via* two signaling pathways; intrinsic or extrinsic (42, 43). Bax, Bcl-2 and p53 are associated with mitochondrial-associated intrinsic apoptosis (44). Bax induces apoptotic cell death by forming pores in the mitochondrial outer membrane. Cytochrome C molecules, which are proapoptotic factors, are then able to translocate from the mitochondria to the cytoplasm, disabling the production of ATP and initiating

proteolytic caspase cascade (45). Numerous studies have also suggested that the levels of p53, a tumor suppressor gene, is involved in cell cycle regulation and DNA repair. Once activated, p53 has also been seen to induce AMPK-mediated cell cycle arrest (46). In this aspect, the combined treatment of cells with MET and either TMP or MTX increased p53 and Bax gene levels, while decreasing Bcl-2 levels. Hence, the co-treatment of MET with the antifolate agents (TMP or MTX) on HepG2 cells enhanced the decrease in cancer cell viability through changes in levels of genes involved in the intrinsic pathway of apoptosis; p53, Bax and Bcl-2. When compared to MET alone, both combinations stimulated apoptosis more prominently.

Our results are in agreement with other findings that indicated that an increase in the levels of Bax and a decrease in the Bcl-2 levels are linked to cytochrome C release and increased apoptosis (47). Similar to the findings presented in the section 3, the combination of MET and DSF-Cu (an FDA approved repurposed drug used for the treatment of alcohol abusers) also increased the expression of key apoptotic markers, Bax and p53, but at lower concentrations of MET (48). The decrease in MET concentration may be due to the difference in experimental conditions and diverse cell line used. In another recent study, MET when combined with EGCG (epigallocatechin-3-gallate, a polyphenol present in green tea), increased the levels of caspase-3 and decreased levels of survivin, thereby significantly promoting apoptosis in HCC cells (49). Additionally, another study showed that the co-treatment of HepG2 cells with ATO (arsenic trioxide, a therapeutic agent used in the treatment of acute promyelocytic leukemia) potentiated the anti-HCC efficacy of ATO and increased apoptosis *in vitro* by decreasing the levels of Bcl-2 (50).

Apoptosis was also evaluated in HepG2 cells by flow cytometry after double staining with Annexin V and PI. The percentage of total apoptotic cells (early and late apoptosis) in cells treated with the combined therapy was also consistent with the increase in gene expression of pro-apoptotic molecules. The presence of apoptotic or necrotic cells is not the only indication of cytotoxicity of the tested combinations; for this reason, the impact of treatments on the migration of HepG2 cells was also examined.

In line with the previous results, drug combinations potentially inhibited migration of HepG2 cells *via* decreasing proliferation and increasing the percentage of apoptotic cells. Cell migration, a mechanism involved in the metastatic progression of cancer, is associated with lack of cell-cell adhesion, accelerated migration and cancer cell invasion (51). While higher concentrations of MET elucidate both a decrease in cancer cell viability and induction of apoptosis, the effect of MET on cancer cell migration is prominent even at lower doses (3 mM causing an inhibition in the wound healing assay) (Figure 5), suggesting that MET targets various pathways to differing extents.

Our findings suggest the potential effects of MET and combinations on the inhibition of migration of HepG2 cells. Interestingly, upon the addition of MTX to MET, cancer cell migration was not significantly altered, suggesting a potential

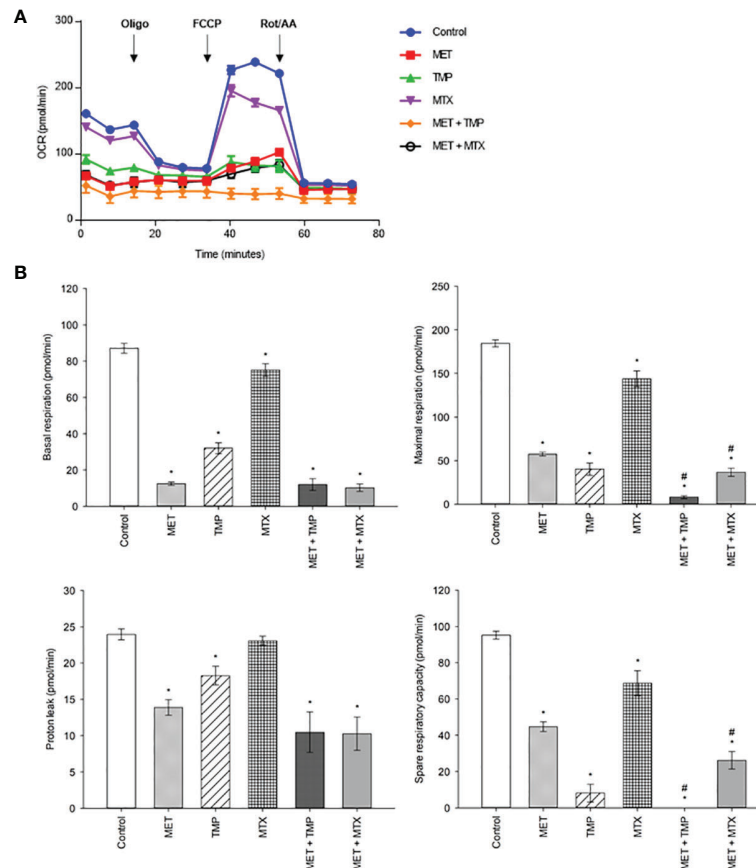


**FIGURE 10 |** Effect of MET, TMP, MTX, alone and in combination, on mitochondrial bioenergetics. Combining MET to either TMP or MTX leads to inhibition of mitochondrial bioenergetics. **(A)** The effect of treatment of MET, TMP, MTX and combinations on the rate of mitochondrial respiration (OCR) in HepG2 cells after 24 h. TMP and MTX combined with MET induced mitochondrial dysfunction in HepG2 cells. A decrease in OCR of cells is seen following combination therapy, when compared to the control. **(B)** Basal respiratory rate, maximal respiration, proton leak and spare respiratory capacity of HepG2 cells following treatment of MET (6.5 mM), TMP (189.45  $\mu$ M), MTX (3 mM), MET + TMP (6.5 mM + 189.45  $\mu$ M) or MET + MTX (6.5 mM + 3 mM) for 24 h. Following measurements of basal respiration, oligomycin (1.5  $\mu$ M), FCCP (1 mM) and Rot/AA (0.5  $\mu$ M) were injected to measure key mitochondrial parameters. The combination treatment clearly caused a significant decrease in mitochondrial function in HepG2 cells. Data are expressed as mean  $\pm$  SEM (n=6). Comparisons were made using ANOVA followed by Tukey *post-hoc* test. \*, *p*-value < 0.05 versus control and #, *p*-value < 0.05 versus cells treated with MET only.

antagonistic role of MET on the effect of MTX on HepG2 cell migration. Contrastingly, our data suggest a strong effect of MET + TMP on migration by significantly reducing wound closure, demonstrating that the sub-IC<sub>50</sub> concentrations of both drugs may be significant in preventing the metastasis of HCC.

In one study, MET slightly increased HER+ cell migration, while the combination of MET with aspirin inhibited cancer cell migration in triple-negative breast cancer as well as MCF-7 cell lines, in alignment with our results. To the contrary, the co-treatment of MET with aspirin did not induce a significant change in MDA-MB-231 and SK-BR-3 cell lines (52). Additionally, another study depicted a reduction in MDA-MB-231 cell migration upon treatment of the same concentration of MET used in the present study (53). Therefore, the effects of MET on cancer cell migration, alone or in combination, vary according to the cancer cell type.

Recent studies have shown that metabolic alterations are crucial for the survival and proliferation of cancer cells. There

is emerging evidence that glycolysis and OXPHOS are essential drivers in cancer cell metastasis (54). Enzymes involved in glycolysis have been shown to play a key role in tumor migration and invasion. Phosphoglucose isomerase (PGI), for instance, is a cytosolic enzyme that catalyzes the conversion of glucose-6-phosphate to fructose-6-phosphate in the second step of glycolysis (55). Studies have depicted that PGI is an autocrine motility factor (AMF) and a tumor-secreted cytokine, which induces cell migration *in vitro* and metastasis *in vivo* (56). Hence, PGI/AMF is required for tumor cell migration, invasion, and metastasis, and has anti-apoptotic effects on malignant cancer cells, as well as other roles in tumor progression (57, 58). Furthermore, by altering the cancer microenvironment *via* accumulating lactate, excessive glycolysis has been shown to enhance cancer stem cell phenotypic, angiogenesis, migration, and immune evasion (59, 60). Additionally, growth factor-stimulated or cancerous cells require an adequate amount of nutrients to meet the metabolic demands of cellular migration

and proliferation. In the absence of nutrition, metabolic checkpoints are triggered, resulting in cell cycle arrest and activation of the intrinsic apoptotic cascade *via* a mechanism involving the Bcl-2 family of proteins (61).

For this reason, the effect of the tested compounds, alone and in combination, on mitochondrial function was assessed. Cancer cells tend to utilize glycolysis to produce ATP, while also maintain OXPHOS for energy production. Since tumors proliferate more quickly than normal tissues, they require a larger amount of ATP as a source of energy. Therefore, drugs targeting the metabolic pathway of cancer cells pose as potential chemotherapeutics. MET has been widely known to inhibit mitochondrial function, by inhibiting complex I of the ETC (62). Consequently, cancer cells treated with MET exhibit an increase in rate of glycolysis as a compensatory mechanism in the aim of increasing ATP production (63). However, if the compensatory increase in glycolysis fails to meet the cellular ATP demands, AMPK is activated to potentiate catabolic metabolism, while inhibiting anabolic processes (64–66). AMPK phosphorylation and activation causes acetyl-CoA carboxylase (ACC), one of the most well-studied AMPK targets, to be phosphorylated and inactivated, resulting in the reduction of lipogenesis (67, 68). Furthermore, MET increases the levels of AMP, leading to the inhibition of adenylate cyclase (69). MET also inhibits mTOR signaling, leading to decreased protein synthesis (70, 71). Overall, MET causes a reduction in cellular energy status, resulting in a decrease in ATP-consuming processes. This may result in a cytostatic condition in proliferating cells, which is associated with lower proliferation and could explain the anti-cancer effects of MET. In a similar vein, cancer cells that are unable to compensate for their reduced energy status may undergo apoptosis, rendering MET cytotoxic (72, 73). Hence, preventing this compensatory metabolic event would directly impact cancer cell survival.

We aimed to test whether MET in combination with antifolates would inhibit the growth of cancer cells, by decreasing the MET-induced increase in glycolysis, hence, potentiating cell death. As the Seahorse XFe96 Analyzer measures glycolytic and mitochondrial parameters in real-time, optimization of the respective drug concentrations used was done to ensure adequate measurements of parameters within the allowed range (20–200 OCR). After 24 h of incubation with the tested compounds, alone or in combination, the glycolytic rate assay was performed to examine the rate of glycolysis in these cells. MET significantly increased the basal rate of glycolysis, when compared to the control. These results are consistent with published literature reporting the MET-associated inhibition of OXPHOS and hence, rise in glycolysis (74). Furthermore, both TMP and MTX alone decreased basal glycolysis rates, when compared to the control. Combined treatment of MET and TMP or MTX exhibited a significant decrease in the basal rate of glycolysis in HepG2 cells, when compared to MET alone (**Figure 6B**).

To further confirm the findings obtained from the glycolytic rate assay, we further went on to perform the ATP rate assay. MET alone induced an increase in the total ATP production rate

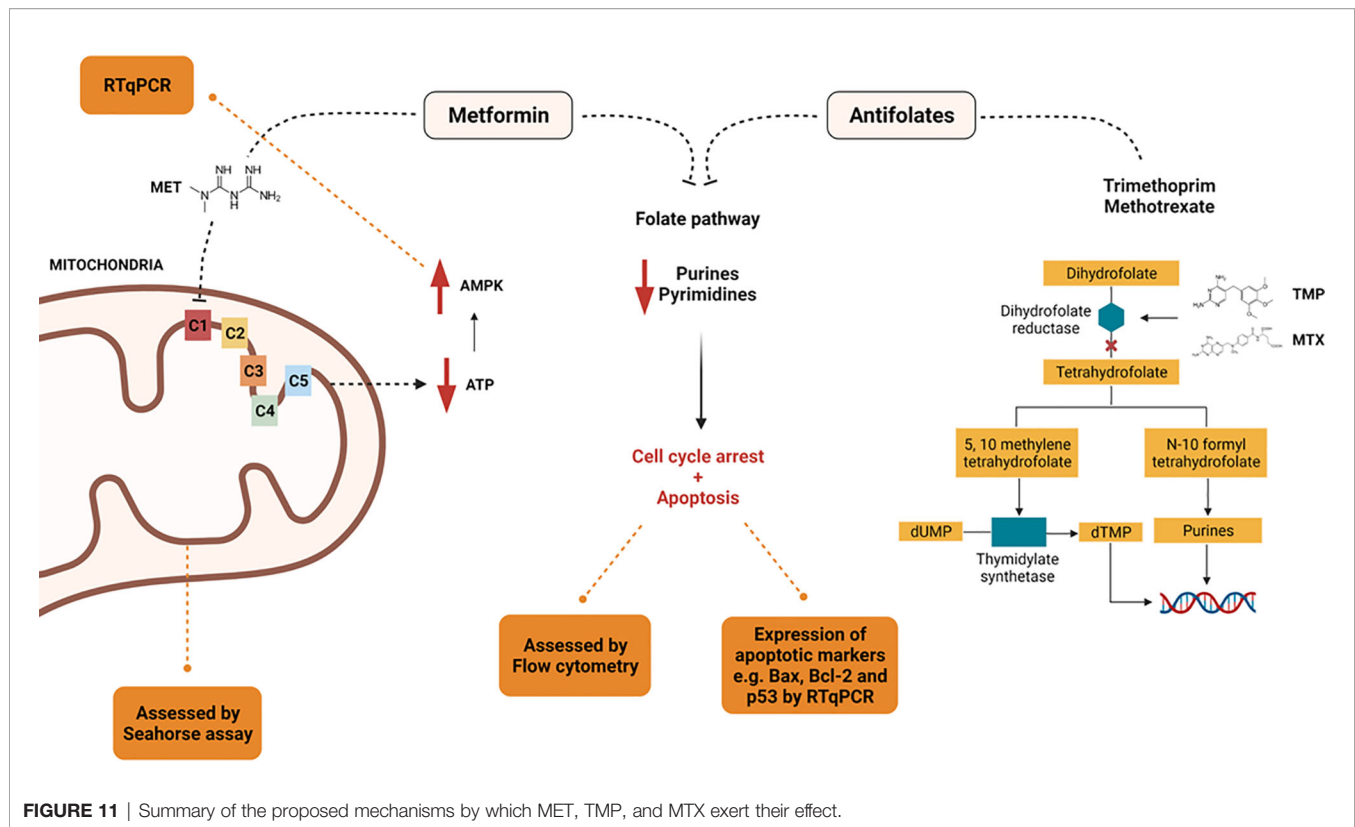
in HepG2 cells (**Figure 7**). Moreover, both TMP and MTX increased the total ATP production when used alone. Consistent with our previous findings, both combinations decreased the percentage of total ATP production in HepG2 cells and significantly impacted the percentage of ATP production produced *via* glycolysis. The ATP rate assay also shed light on the effect of tested compounds on the mitochondrial ATP production. Both combinations elucidated a decrease in the rate of ATP production *via* the mitochondria (**Figure 8**), yet further analysis was needed to confirm these results. AMPK mRNA expression was also evaluated as AMPK values increase with decrease in ATP levels (75). Both combinations depicted an increase in AMPK levels, confirming our findings, though they were not significant (**Figure 9**). However, evaluation of the different AMPK subunits phospho-isoforms at the protein level would further elucidate the role of AMPK in controlling cancer cell bioenergetics.

We then conducted the MST on HepG2 cells treated with the compounds alone and in combination for 24 h. Following MST, data confirmed that MET induced mitochondrial injury, consistent with previous findings. Interestingly, both TMP and MTX also inhibited mitochondrial function, but to a lesser extent. Co-treatment of MET and either antifolate resulted in the significant decrease of OCR, compared to the control. Basal respiration as well as proton leak decreased, but not significantly, when compared to MET alone. Contrastingly, maximal respiration and the spare respiratory capacity significantly declined, compared with MET treatment alone (**Figure 10B**). In conclusion, these data suggest that MET in combination with antifolates (TMP or MTX) impact the energy production in HepG2 cells *via* two main pathways: OXPHOS and glycolysis. Furthermore, the powerful anti-metastatic characteristics of the tested compounds are likely a result of the ability of both combinations to inhibit the mitochondrial bioenergetics. These combinations might be particularly useful in preventing liver cancer metastases and recurrence, as increased oxidative metabolism is linked to increased tumor cell survival and proliferation (76). Through the inhibition of both energy production routes, cancer cell viability, hence, was significantly reduced.

## CONCLUSION

To the best of our knowledge, no prior studies have been performed examining the bioenergetic effects of combining MET with either TMP or MTX. In this study, the effects of MET alone as opposed to both combinations were compared, underlying the mechanisms involved in this combination *in vitro* on HepG2 cell line (**Figure 11**). Our data suggest that treatment of HepG2 cells with a combination of MET and antifolate agent (TMP or MTX) increases cell death than MET alone *via* mitochondrial inhibition and relative decrease in glycolysis. We suggest that the anti-cancer effect of MET combined with either antifolate agent occurs through the inhibition of cancer cell progression,





increase expression of p53 and Bax, decrease expression of Bcl-2, rise in the number of total apoptotic cells, inhibition of migration ability, decrease in ATP production, inhibition of the glycolysis pathway and induction of mitochondrial damage.

## DATA AVAILABILITY STATEMENT

The raw data supporting the conclusions of this article will be made available by the authors, without undue reservation.

## AUTHOR CONTRIBUTIONS

Experiments and data collection were performed by ST, AA, and MA. Data analysis were carried out by ST, AA, MA, and ME. The study was designed by AA, MA, and HE-F. The first draft of the

manuscript was written by ST and all authors revised the previous versions of the manuscript. The revised manuscript was written by ST and edited by AA and MA. All authors read and approved the final manuscript.

## FUNDING

This work was supported by AUC graduate research grant and AUC internal grant [FY19-RG (1-18)], Egyptian Academy of Scientific Research and Technology Grants (JESOR-2019-5305), and (ASRT-2019-4903), a Bartlett Fund for Critical Challenges Grant and an AUC COVID-19 Pandemic Research & Innovation Initiative Grant. Part of the work was funded by the British University in Egypt Young Investigator Research Grant (BUE-YIRG2018-07).

## REFERENCES

- Altekruse SF, McGlynn KA, Reichman ME. Hepatocellular Carcinoma Incidence, Mortality, and Survival Trends in the United States From 1975 to 2005. *J Clin Oncol* (2009) 27(9):1485. doi: 10.1200/JCO.2008.20.7753
- Dhanasekaran R, Limaye A, Cabrera R. Hepatocellular Carcinoma: Current Trends in Worldwide Epidemiology, Risk Factors, Diagnosis, and Therapeutics. *Hepatic Med: Evid Res* (2012) 4:19. doi: 10.2147/HMER.S16316
- Waller LP, Deshpande V, Prysopoulos N. Hepatocellular Carcinoma: A Comprehensive Review. *World J Hepatol* (2015) 7(26):2648–63. doi: 10.4254/wjh.v7.i26.2648
- Warburg O. On the Origin of Cancer Cells. *Science* (1956) 123(3191):309–14. doi: 10.1126/science.123.3191.309
- Foretz M, Guigas B, Bertrand L, Pollak M, Viollet B. MET: From Mechanisms of Action to Therapies. *Cell Metab* (2014) 20(6):953–66. doi: 10.1016/j.cmet.2014.09.018
- Hardie DG. AMP-Activated Protein Kinase: Maintaining Energy Homeostasis at the Cellular and Whole-Body Levels. *Annu Rev Nutr* (2014) 34:31–55. doi: 10.1146/annurev-nutr-071812-161148
- Viollet B, Athes Y, Mounier R, Guigas B, Zarrinpashneh E, Horman S, et al. AMPK: Lessons From Transgenic and Knockout Animals. *Front Biosci (Landmark edition)* (2009) 14:19. doi: 10.2741/3229

8. Galic S, Loh K, Murray-Segal L, Steinberg GR, Andrews ZB, Kemp BE. AMPK Signaling to Acetyl-CoA Carboxylase Is Required for Fasting- and Cold-Induced Appetite But Not Thermogenesis. *Elife* (2018) 7:e32656. doi: 10.7554/eLife.32656.030
9. Marsin A-S, Bertrand L, Rider MH, Deprez J, Beauloye C, Vincent MF, et al. Phosphorylation and Activation of Heart PFK-2 by AMPK Has a Role in the Stimulation of Glycolysis During Ischaemia. *Curr Biol* (2000) 10(20):1247–55. doi: 10.1016/S0960-9822(00)00742-9
10. Fritah A, Steel JH, Parker N, Nikolopoulou E, Christian M, Carling D, et al. Absence of RIP140 Reveals a Pathway Regulating Glut4-Dependent Glucose Uptake in Oxidative Skeletal Muscle Through UCP1-Mediated Activation of AMPK. *PLoS One* (2012) 7(2):e32520. doi: 10.1371/journal.pone.0032520
11. Zhou G, Myers R, Li Y, Chen Y, Shen X, Fenik-Melody J, et al. Role of AMP-Activated Protein Kinase in Mechanism of MET Action. *J Clin Invest* (2001) 108(8):1167–74. doi: 10.1172/JCI13505
12. Corominas-Faja B, Quirantes-Piné R, Oliveras-Ferraro C, Vazquez-Martin A, Cufi S, Martin-Castillo B, et al. Metabolomic Fingerprint Reveals That MET Impairs One-Carbon Metabolism in a Manner Similar to the Antifolate Class of Chemotherapy Drugs. *Aging (Albany NY)* (2012) 4(7):480. doi: 10.18632/aging.100472
13. JD Smilack ed. “Trimethoprim-Sulfamethoxazole”. In: *Mayo Clinic Proceedings*. Elsevier.
14. Darrell J, Garrod L, Waterworth PM. Trimethoprim: Laboratory and Clinical Studies. *J Clin Pathol* (1968) 21(2):202. doi: 10.1136/jcp.21.2.202
15. McGuire JJ. Anticancer Antifolates: Current Status and Future Directions. *Curr Pharm Des* (2003) 9(31):2593–613. doi: 10.2174/1381612033453712
16. Kamat AM, Lamm DL. Antitumor Activity of Common Antibiotics Against Superficial Bladder Cancer. *Urology* (2004) 63(3):457–60. doi: 10.1016/j.urol.2003.10.038
17. Chou T-C. Theoretical Basis, Experimental Design, and Computerized Simulation of Synergism and Antagonism in Drug Combination Studies. *Pharmacol Rev* (2006) 58(3):621–81. doi: 10.1124/pr.58.3.10
18. Nishida N, Yano H, Nishida T, Kamura T, Kojiro M. Angiogenesis in Cancer. *Vasc Health Risk Manag* (2006) 2(3):213–9. doi: 10.2147/vhrm.2006.2.3.213
19. Owen MR, Doran E, Halestrap AP. Evidence That MET Exerts Its Anti-Diabetic Effects Through Inhibition of Complex 1 of the Mitochondrial Respiratory Chain. *Biochem J* (2000) 348(3):607–14. doi: 10.1042/bj3480607
20. El-Mir M-Y, Nogueira V, Fontaine E, Avéret N, Rigoulet M, Leverve X. Dimethylbiguanide Inhibits Cell Respiration via an Indirect Effect Targeted on the Respiratory Chain Complex I. *J Biol Chem* (2000) 275(1):223–8. doi: 10.1074/jbc.275.1.223
21. M Wu, M Sirota, AJ Butte, B Chen eds. *Characteristics of Drug Combination Therapy in Oncology by Analyzing Clinical Trial Data on ClinicalTrials.gov*. Pacific Symposium on Biocomputing Co-Chairs. Kohala Coast, Hawaii, USA: World Scientific (2014).
22. Rexer BN, Ham AL, Rinehart C, Hill S, de Matos Granja-Ingram N, Gonzalez-Angulo A, et al. Phosphoproteomic Mass Spectrometry Profiling Links Src Family Kinases to Escape From HER2 Tyrosine Kinase Inhibition. *Oncogene* (2011) 30(40):4163–74. doi: 10.1038/ncr.2011.130
23. Janjetovic K, Vucicevic L, Misirkic M, Vilimanovich U, Tovilovic G, Zogovic N, et al. MET Reduces Cisplatin-Mediated Apoptotic Death of Cancer Cells Through AMPK-Independent Activation of Akt. *Eur J Pharmacol* (2011) 651(1–3):41–50. doi: 10.1016/j.ejphar.2010.11.005
24. Pryor R, Cabreiro F. Repurposing MET: An Old Drug With New Tricks in its Binding Pockets. *Biochem J* (2015) 471(3):307–22. doi: 10.1042/BJ20150497
25. Kim HG, Hien TT, Han EH, Hwang YP, Choi JH, Kang KW, et al. MET Inhibits P-Glycoprotein Expression via the NF- $\kappa$ B Pathway and CRE Transcriptional Activity Through AMPK Activation. *Br J Pharmacol* (2011) 162(5):1096–108. doi: 10.1111/j.1476-5381.2010.01101.x
26. Libby G, Donnelly LA, Donnan PT, Alessi DR, Morris AD, Evans JM. New Users of MET are at Low Risk of Incident Cancer: A Cohort Study Among People With Type 2 Diabetes. *Diabetes Care* (2009) 32(9):1620–5. doi: 10.2337/dc08-2175
27. Ruiter R, Visser LE, van Herk-Sukel MP, Coebergh J-WW, Haak HR, Geelhoed-Duijvestijn PH, et al. Lower Risk of Cancer in Patients on MET in Comparison With Those on Sulfonurea Derivatives: Results From a Large Population-Based Follow-Up Study. *Diabetes Care* (2012) 35(1):119–24. doi: 10.2337/dc11-0857
28. Bosco JLF, Antonsen S, Sørensen HT, Pedersen L, Lash TL. MET and Incident Breast Cancer Among Diabetic Women: A Population-Based Case-Control Study in Denmark. *Cancer Epidemiol Prev Biomarkers* (2011) 20(1):101–11. doi: 10.1158/1055-9965.EPI-10-0817
29. Alimova IN, Liu B, Fan Z, Edgerton SM, Dillon T, Lind SE, et al. MET Inhibits Breast Cancer Cell Growth, Colony Formation and Induces Cell Cycle Arrest *In Vitro*. *Cell Cycle* (2009) 8(6):909–15. doi: 10.4161/cc.8.6.7933
30. Rocha GZ, Dias MM, Ropelle ER, Osório-Costa F, Rossato FA, Vercesi AE, et al. MET Amplifies Chemotherapy-Induced AMPK Activation and Antitumoral Growth. *Clin Cancer Res* (2011) 17(12):3993–4005. doi: 10.1158/1078-0432.CCR-10-2243
31. González DCF. MET Inhibits Growth of Thyroid Carcinoma Cells, Suppresses Self-Renewal of Derived Cancer Stem Cells, and Potentiates the Effect of Chemotherapeutic Agents. *Rev Endocrinología y Nutrición* (2012) 20(3):131–3. doi: 10.1210/jc.2011-1754
32. Chen G, Xu S, Renko K, Derwahl M. MET Inhibits Growth of Thyroid Carcinoma Cells, Suppresses Self-Renewal of Derived Cancer Stem Cells, and Potentiates the Effect of Chemotherapeutic Agents. *J Clin Endocrinol Metab* (2012) 97(4):E510–E20. doi: 10.1210/jc.2011-1754
33. Sliwiska A, Rogalska A, Marczak A, Kasznicki J, Drzewoski J. MET, But Not Sitagliptin, Enhances WP 631-Induced Apoptotic HepG2 Cell Death. *Toxicol Vitro* (2015) 29(5):1116–23. doi: 10.1016/j.tiv.2015.04.019
34. Liu H, Scholz C, Zang C, Schefe JH, Habel P, Regierer A-C, et al. MET and the mTOR Inhibitor Everolimus (RAD001) Sensitize Breast Cancer Cells to the Cytotoxic Effect of Chemotherapeutic Drugs *In Vitro*. *Anticancer Res* (2012) 32(5):1627–37.
35. Sun R, Zhai R, Ma C, Miao W. Combination of Aloiin and MET Enhances the Antitumor Effect by Inhibiting the Growth and Invasion and Inducing Apoptosis and Autophagy in Hepatocellular Carcinoma Through PI3K/AKT/mTOR Pathway. *Cancer Med* (2020) 9(3):1141–51. doi: 10.1002/cam4.2723
36. Zhang HH, Zhang Y, Cheng YN, Gong FL, Cao ZQ, Yu LG, et al. MET Incombination With Curcumin Inhibits the Growth, Metastasis, and Angiogenesis of Hepatocellular Carcinoma *In Vitro* and *In Vivo*. *Mol Carcinog* (2018) 57(1):44–56. doi: 10.1002/mc.22718
37. Guo Z, Cao M, You A, Gao J, Zhou H, Li H, et al. MET Inhibits the Prometastatic Effect of Sorafenib in Hepatocellular Carcinoma by Upregulating the Expression of TIP30. *Cancer Sci* (2016) 107(4):507–13. doi: 10.1111/cas.12885
38. Ling S, Feng T, Ke Q, Fan N, Li L, Li Z, et al. MET Inhibits Proliferation and Enhances Chemosensitivity of Intrahepatic Cholangiocarcinoma Cell Lines. *Oncol Rep* (2014) 31(6):2611–8. doi: 10.3892/or.2014.3151
39. Ling S, Song L, Fan N, Feng T, Liu L, Yang X, et al. Combination of MET and Sorafenib Suppresses Proliferation and Induces Autophagy of Hepatocellular Carcinoma via Targeting the mTOR Pathway. *Int J Oncol* (2017) 50(1):297–309. doi: 10.3892/ijo.2016.3799
40. Yang C, Zhao N, Li D, Zou G, Chen Y. MET Improves the Sensitivity of Ovarian Cancer Cells to Chemotherapeutic Agents. *Oncol Lett* (2019) 18(3):2404–11. doi: 10.3892/ol.2019.10564
41. Rastegar M, Marjani H-A, Yazdani Y, Shahbazi M, Ghalipour M, Farazmandfar T. Investigating Effect of Rapamycin and MET on Angiogenesis in Hepatocellular Carcinoma Cell Line. *Adv Pharm Bull* (2018) 8(1):63. doi: 10.15171/apb.2018.008
42. Green DR, Kroemer G. The Pathophysiology of Mitochondrial Cell Death. *Science* (2004) 305(5684):626–9. doi: 10.1126/science.1099320
43. Cory S, Adams JM. The Bcl2 Family: Regulators of the Cellular Life-or-Death Switch. *Nat Rev Cancer* (2002) 2(9):647–56. doi: 10.1038/nrc883
44. Fulda S, Debatin KM. Extrinsic Versus Intrinsic Apoptosis Pathways in Anticancer Chemotherapy. *Oncogene* (2006) 25(34):4798–811.
45. Breckenridge DG, Xue D. Regulation of Mitochondrial Membrane Permeabilization by BCL-2 Family Proteins and Caspases. *Curr Opin Cell Biol* (2004) 16(6):647–52. doi: 10.1016/j.ceb.2004.09.009
46. Jones RG, Plas DR, Kubek S, Buzzai M, Mu J, Xu Y, et al. AMP-Activated Protein Kinase Induces a P53-Dependent Metabolic Checkpoint. *Mol Cell* (2005) 18(3):283–93. doi: 10.1016/j.molcel.2005.03.027
47. Ibrahim MY, Hashim NM, Mohan S, Abdulla MA, Kamalidehghan B, Ghaderian M, et al.  $\alpha$ -Mangostin From *Cratoxylum Arborescens* Demonstrates Apoptogenesis in MCF-7 With Regulation of NF- $\kappa$ B and

- Hsp70 Protein Modulation *In Vitro*, and Tumor Reduction *In Vivo*. *Drug Des Dev Ther* (2014) 8:1629. doi: 10.2147/DDDT.S66105
48. Rezaei N, Neshasteh-Riz A, Mazaheri Z, Koosha F, Hoormand M. The Combination of MET and Disulfiram-Cu for Effective Radiosensitization on Glioblastoma Cells. *Cell J (Yakhteh)* (2020) 22(3):263. doi: 10.22074/cellj.2020.6798
  49. Sabry D, Abdelaleem OO, Ali AMEA, Mohammed RA, Abdel-Hameed ND, Hassouna A, et al. Anti-Proliferative and Anti-Apoptotic Potential Effects of Epigallocatechin-3-Gallate and/or MET on Hepatocellular Carcinoma Cells: *In Vitro* Study. *Mol Biol Rep* (2019) 46(2):2039–47. doi: 10.1007/s11033-019-04653-6
  50. Yang X, Sun D, Tian Y, Ling S, Wang L. MET Sensitizes Hepatocellular Carcinoma to Arsenic Trioxide-Induced Apoptosis by Downregulating Bcl2 Expression. *Tumor Biol* (2015) 36(4):2957–64. doi: 10.1007/s13277-014-2926-5
  51. Yamaguchi H, Wyckoff J, Condeelis J. Cell Migration in Tumors. *Curr Opin Cell Biol* (2005) 17(5):559–64. doi: 10.1016/j.ccb.2005.08.002
  52. Amaral MEA, Nery LR, Leite CE, de Azevedo Junior WF, Campos MM. Pre-Clinical Effects of MET and Aspirin on the Cell Lines of Different Breast Cancer Subtypes. *Invest New Drugs* (2018) 36(5):782–96. doi: 10.1007/s10637-018-0568-y
  53. Fan C, Wang Y, Liu Z, Sun Y, Wang X, Wei G, et al. MET Exerts Anticancer Effects Through the Inhibition of the Sonic Hedgehog Signaling Pathway in Breast Cancer. *Int J Mol Med* (2015) 36(1):204–14. doi: 10.3892/ijmm.2015.2217
  54. Porporato PE, Payen VL, Baselet B, Sonveaux P. Metabolic Changes Associated With Tumor Metastasis, Part 2: Mitochondria, Lipid and Amino Acid Metabolism. *Cell Mol Life Sci* (2016) 73(7):1349–63. doi: 10.1007/s00018-015-2100-2
  55. Achari A, Marshall S, Muirhead H, Palmieri R, Noltmann E. Glucose-6-Phosphate Isomerase. *Philos Trans R Soc Lond B Biol Sci* (1981) 293(1063):145–57. doi: 10.1098/rstb.1981.0068
  56. Watanabe H, Takehana K, Date M, Shinozaki T, Raz A. Tumor Cell Autocrine Motility Factor is the Neuroleukin/Phosphohexose Isomerase Polypeptide. *Cancer Res* (1996) 56(13):2960–3.
  57. Haga A, Funasaka T, Niinaka Y, Raz A, Nagase H. Autocrine Motility Factor Signaling Induces Tumor Apoptotic Resistance by Regulations Apaf-1 and Caspase-9 Apoptosome Expression. *Int J Cancer* (2003) 107(5):707–14. doi: 10.1002/ijc.11449
  58. Tsutsumi S, Yanagawa T, Shimura T, Kuwano H, Raz A. Autocrine Motility Factor Signaling Enhances Pancreatic Cancer Metastasis. *Clin Cancer Res* (2004) 10(22):7775–84. doi: 10.1158/1078-0432.CCR-04-1015
  59. Valvona CJ, Fillmore HL, Nunn PB, Pilkington GJ. The Regulation and Function of Lactate Dehydrogenase a: Therapeutic Potential in Brain Tumor. *Brain Pathol* (2016) 26(1):3–17. doi: 10.1111/bpa.12299
  60. Romero-García S, Moreno-Altamirano MMB, Prado-García H, Sánchez-García FJ. Lactate Contribution to the Tumor Microenvironment: Mechanisms, Effects on Immune Cells and Therapeutic Relevance. *Front Immunol* (2016) 7:52. doi: 10.3389/fimmu.2016.00052
  61. Mason EF, Rathmell JC. Cell Metabolism: An Essential Link Between Cell Growth and Apoptosis. *Biochim Biophys Acta (BBA)-Mol Cell Res* (2011) 1813(4):645–54. doi: 10.1016/j.bbamcr.2010.08.011
  62. Fujita H, Hirose K, Sato M, Fujioka I, Fujita T, Aoki M, et al. MET Attenuates Hypoxia-Induced Resistance to Cisplatin in the HepG2 Cell Line. *Oncol Lett* (2019) 17(2):2431–40. doi: 10.3892/ol.2018.9869
  63. Andrzejewski S, Gravel S-P, Pollak M, St-Pierre J. MET Directly Acts on Mitochondria to Alter Cellular Bioenergetics. *Cancer Metab* (2014) 2(1):1–14. doi: 10.1186/2049-3002-2-12
  64. Griss T, Vincent EE, Egnatchik R, Chen J, Ma EH, Faubert B, et al. MET Antagonizes Cancer Cell Proliferation by Suppressing Mitochondrial-Dependent Biosynthesis. *PLoS Biol* (2015) 13(12):e1002309. doi: 10.1371/journal.pbio.1002309
  65. Bogachus LD, Turcotte LP. Genetic Downregulation of AMPK- $\alpha$  Isoforms Uncovers the Mechanism by Which MET Decreases FA Uptake and Oxidation in Skeletal Muscle Cells. *Am J Physiol-Cell Physiol* (2010) 299(6):C1549–C61. doi: 10.1152/ajpcell.00279.2010
  66. Rena G, Hardie DG, Pearson ER. The Mechanisms of Action of MET. *Diabetologia* (2017) 60(9):1577–85. doi: 10.1007/s00125-017-4342-z
  67. Dolphin AC. Calcium Channel Auxiliary  $\alpha 2 \delta$  and  $\beta$  Subunits: Trafficking and One Step Beyond. *Nat Rev Neurosci* (2012) 13(8):542–55. doi: 10.1038/nrn3311
  68. Loubière C, Goiran T, Laurent K, Djabari Z, Tanti J-F, Bost F. MET-Induced Energy Deficiency Leads to the Inhibition of Lipogenesis in Prostate Cancer Cells. *Oncotarget* (2015) 6(17):15652. doi: 10.18632/oncotarget.3404
  69. Miller RA, Chu Q, Xie J, Foretz M, Viollet B, Birnbaum MJ. Biguanides Suppress Hepatic Glucagon Signalling by Decreasing Production of Cyclic AMP. *Nature* (2013) 494(7436):256–60. doi: 10.1038/nature11808
  70. IG DRZMF, Pollak M, Sonenberg N. MET Inhibits Mammalian Target of Rapamycin-Dependent Translation Initiation in Breast Cancer Cells. *Cancer Res* (2007) 67:10804–12. doi: 10.1158/0008-5472.CAN-07-2310
  71. Liu X, Chhipa RR, Pooya S, Wortman M, Yachyshin S, Chow LM, et al. Discrete Mechanisms of mTOR and Cell Cycle Regulation by AMPK Agonists Independent of AMPK. *Proc Natl Acad Sci* (2014) 111(4):E435–E44. doi: 10.1073/pnas.1311121111
  72. Bhat M, Yanagiya A, Graber T, Razumilava N, Bronk S, Zammit D, et al. MET Requires 4E-BPs to Induce Apoptosis and Repress Translation of Mcl-1 in Hepatocellular Carcinoma Cells. *Oncotarget* (2017) 8(31):50542. doi: 10.18632/oncotarget.10671
  73. Takahashi A, Kimura F, Yamanaka A, Takebayashi A, Kita N, Takahashi K, et al. MET Impairs Growth of Endometrial Cancer Cells via Cell Cycle Arrest and Concomitant Autophagy and Apoptosis. *Cancer Cell Int* (2014) 14(1):1–12. doi: 10.1186/1475-2867-14-53
  74. Chen L, Ahmad N, Liu X. Combining P53 Stabilizers With MET Induces Synergistic Apoptosis Through Regulation of Energy Metabolism in Castration-Resistant Prostate Cancer. *Cell Cycle* (2016) 15(6):840–9. doi: 10.1080/15384101.2016.1151582
  75. Ke R, Xu Q, Li C, Luo L, Huang D. Mechanisms of AMPK in the Maintenance of ATP Balance During Energy Metabolism. *Cell Biol Int* (2018) 42(4):384–92. doi: 10.1002/cbin.10915
  76. Liberti MV, Locasale JW. The Warburg Effect: How Does it Benefit Cancer Cells? *Trends Biochem Sci* (2016) 41(3):211–8. doi: 10.1016/j.tibs.2015.12.001

**Conflict of Interest:** The authors declare that the research was conducted in the absence of any commercial or financial relationships that could be construed as a potential conflict of interest.

**Publisher's Note:** All claims expressed in this article are solely those of the authors and do not necessarily represent those of their affiliated organizations, or those of the publisher, the editors and the reviewers. Any product that may be evaluated in this article, or claim that may be made by its manufacturer, is not guaranteed or endorsed by the publisher.

Copyright © 2022 Tawfik, Abdollah, Elmazar, El-Fawal and Abdelnaser. This is an open-access article distributed under the terms of the Creative Commons Attribution License (CC BY). The use, distribution or reproduction in other forums is permitted, provided the original author(s) and the copyright owner(s) are credited and that the original publication in this journal is cited, in accordance with accepted academic practice. No use, distribution or reproduction is permitted which does not comply with these terms.



# Tryptophan Metabolites as Biomarkers for Esophageal Cancer Susceptibility, Metastasis, and Prognosis

Yun Chen<sup>1†</sup>, Jianliang Chen<sup>2†</sup>, Dainian Guo<sup>3†</sup>, Peixuan Yang<sup>4†</sup>, Shuang Chen<sup>5</sup>, Chengkuan Zhao<sup>1,5</sup>, Chengcheng Xu<sup>1,5</sup>, Qiuzhen Zhang<sup>1,5</sup>, Chaoxian Lin<sup>6</sup>, Shilong Zhong<sup>5,7\*</sup> and Shuyao Zhang<sup>1\*</sup>

<sup>1</sup> Department of Pharmacy, Guangzhou Red Cross Hospital, Jinan University, Guangzhou, China, <sup>2</sup> Clinical Laboratory, Cancer Hospital of Shantou University Medical College, Shantou, China, <sup>3</sup> Department of Pharmacy, Cancer Hospital of Shantou University Medical College, Shantou, China, <sup>4</sup> Health Management Center, The First Affiliated Hospital of Shantou University Medical College, Shantou, China, <sup>5</sup> Department of Pharmacology, Shantou University Medical College, Shantou, China, <sup>6</sup> Department of Pharmacology, Shantou Chaonan Minsheng Hospital, Shantou, China, <sup>7</sup> Department of Pharmacy, Guangdong Provincial People's Hospital, Guangdong Academy of Medical Sciences, Guangzhou, China

## OPEN ACCESS

### Edited by:

Monica Montopoli,  
University of Padua, Italy

### Reviewed by:

Rajeev K. Singla,  
Sichuan University, China  
Zhe-Sheng Chen,  
St. John's University, United States

### \*Correspondence:

Shuyao Zhang  
shuyao0754@qq.com  
Shilong Zhong  
gdph\_zhongs@gd.gov.cn

<sup>†</sup>These authors have contributed  
equally to this work

### Specialty section:

This article was submitted to  
Cancer Metabolism,  
a section of the journal  
Frontiers in Oncology

**Received:** 22 October 2021

**Accepted:** 05 January 2022

**Published:** 28 February 2022

### Citation:

Chen Y, Chen J, Guo D, Yang P,  
Chen S, Zhao C, Xu C, Zhang Q, Lin C,  
Zhong S and Zhang S (2022)  
Tryptophan Metabolites as Biomarkers  
for Esophageal Cancer Susceptibility,  
Metastasis, and Prognosis.  
Front. Oncol. 12:800291.  
doi: 10.3389/fonc.2022.800291

**Background:** Perturbation of tryptophan (TRP) metabolism contributes to the immune escape of cancer; however, the explored TRP metabolites are limited, and their efficacy in clarifying the susceptibility and progression of esophageal cancer (EC) remains ambiguous. Our study sought to evaluate the effects of the TRP metabolic profile on the clinical outcomes of EC using a Chinese population cohort; and to develop a risk prediction model targeting TRP metabolism.

**Method:** A total of 456 healthy individuals as control subjects and 393 patients with EC who were followed up for one year as case subjects were enrolled. Quantification of the plasma concentrations of TRP and its metabolites was performed using HPLC-MS/MS. The logistic regression model was applied to evaluate the effects of the clinical characteristics and plasma metabolites of the subjects on susceptibility and tumor metastasis events, whereas Cox regression analysis was performed to assess the overall survival (OS) of the patients.

**Results:** Levels of creatinine and liver enzymes were substantially correlated with multiple metabolites/metabolite ratios in TRP metabolism, suggesting that hepatic and renal function would exert effects on TRP metabolism. Age- and sex-matched case-control subjects were selected using propensity score matching. Plasma exposure to 5-HT was found to be elevated 3.94-fold in case subjects (N = 166) compared to control subjects (N = 203), achieving an AUC of 0.811 for predicting susceptibility event. Subsequent correlation analysis indicated that a higher plasma exposure to 5-HIAA significantly increased the risk of lymph node metastasis (OR: 2.16,  $p = 0.0114$ ). Furthermore, it was figured out that OS was significantly shorter for patients with elevated XA/KYN ratio (HR: 1.99,  $p = 0.0016$ ), in which medium and high levels of XA/KYN versus low level had a significantly lower OS (HR: 0.48,  $p = 0.0080$  and HR: 0.42,  $p = 0.0031$ , respectively).



**Conclusion:** This study provides a pivotal basis for targeting endogenous TRP metabolism as a potential therapeutic intervention.

**Keywords:** tryptophan metabolism, esophageal cancer, susceptibility, metastasis, prognosis, circulating biomarker

## 1 INTRODUCTION

Esophageal cancer (EC) refers to a malignant digestive tract cancer that develops from the aberrant proliferation of the esophageal squamous epithelium or glandular epithelium. Owing to its insidious onset and scarce early detection methods, EC is usually diagnosed as advanced or metastatic cancer, with a five-year survival rate of less than 16.8% (1). Metabolic reprogramming often occurs in the cancer microenvironment (2). Increasing evidence suggests that the rapid progression of cancer is due to the uncontrolled maintenance of immune homeostasis (3, 4), whereas the depletion of tryptophan (TRP) is a pivotal factor in cancer progression (5, 6). Immune homeostasis is susceptible to low extracellular TRP concentration, and the resultant TRP depletion leads to a proliferative block of T cells through the GCN2 pathway, thereby establishing the significant role of TRP metabolism in maintaining immune homeostasis (7).

Catalyzed by specific enzyme activities, TRP serves as a substrate for three different branches (i.e., kynurenine pathway (KP), 5-hydroxytryptamine (5-HT) pathway, and indole pathway) (8, 9), thereby giving rise to the formation of several molecules such as kynurenine (KYN), 5-HT, and 3-indolepropionic acid (IPA). KP metabolites, namely, kynurenic acid (KYNA), 3-hydroxykynurenine (3-HK), 3-hydroxyanthranilic acid (3-HAA), and xanthurenic acid (XA), might be subsequently released into the surroundings. While binding to aromatic receptors (AHRs), KP metabolites constitute the link between chronic inflammation and cancer progression, and further facilitate the decrease in immune surveillance (10, 11). Under the transformation of tryptophan hydroxylase, 5-HT and 5-hydroxyindoleacetic acid (5-HIAA) are generated, of which excessive upregulation of 5-HT could trigger overstimulation of growth function and accelerate cancer progression (5, 6). The remaining pathway mediated by the action of intestinal flora is the channel of IPA and 3-indoleacetic acid (IAA) formation, of which IPA is considered an effective free radical scavenger of indoleamine (12).

Given the rather complex network of TRP metabolic reactions, the regulation of vital immunosuppressive metabolites has become an attractive target for cancer therapy. Nevertheless, pathological shifts in the TRP metabolic profile have shown inconsistent trends in patients with different cancers. Previously, a nested case-control study was conducted which found that serum levels of 3-HAA and 3-HAA/3-HK were negatively correlated with the risk of pancreatic cancer, while KYN/TRP was not significantly correlated with the risk of pancreatic cancer (13). Another prospective trial revealed that the plasma levels of KYN, TRP, and KYN/TRP were significantly higher in healthy individuals than in patients with breast cancer (14). In addition, the only published study in regard to variation in the TRP metabolic profile

in patients with EC merely incorporated a partial profile into a small-scale cohort (15). The association between circulating TRP and its metabolites and EC clinical outcomes has not been fully evaluated in a large-scale prospective study. Hence, current research has proven inconclusive in patients with EC, and more detailed characterization and quantification are urgently needed to systematically elucidate the extent to which the TRP metabolites can explain the EC disease state.

Herein, along the metabolite-clinical phenotype-study endpoint axis, we performed this study to investigate the impact of the TRP metabolic profile on the clinical primary outcomes of EC (i.e., events of susceptibility, lymph node metastasis, distant metastasis, and overall survival (OS) of patients) using a Chinese population cohort.

## 2 MATERIALS AND METHODS

### 2.1 Study Design

A prospective study of the Chinese population was performed. First, clinical indexes were investigated in all subjects (456 healthy individuals and 393 patients with EC) to explain individual differences in the TRP metabolic profile. Later, the effects of plasma exposure to TRP and its metabolites on clinical endpoint events were assessed, namely, susceptibility, lymph node metastasis, distant metastasis, and OS.

### 2.2 Study Population

From August 2018 to November 2018, the study population, namely, 456 healthy individuals (control subjects) and 393 patients with histologically confirmed EC (case subjects), were sequentially recruited at the Cancer Hospital of Shantou University Medical College and the First Affiliated Hospital of Shantou University Medical College. Consistent baseline information was obtained for both groups from the hospital database, namely, demographics, blood routine examination, and biochemical measurements.

The exclusion criteria for the selected subjects were as follows: (1) age <18 years; (2) renal insufficiency (defined as serum creatinine [CREA] concentration >3 times the upper limit of normal [345  $\mu$ mol/L], renal transplantation, or dialysis); (3) liver insufficiency (defined as serum transaminase concentrations >3 times the upper limit of normal [120 U/L] or a cirrhosis diagnosis); (4) pregnancy or lactation; (5) poor compliance or inability to complete the test; (6) patients who underwent anti-cancer treatments during this period; and (7) a history of other malignancies.

An additional exclusion criterion was required for control subjects: metabolic diseases such as diabetes, cancer,

cardiovascular disease, severe infections, gout, and other end-stage diseases.

The study was approved by the Ethics Committee of Guangzhou Red Cross Hospital (2020-109-02) and conducted in accordance with the Declaration of Helsinki principles. All subjects signed informed consent documentation. The workflow of sample selection is depicted in **Figure 1**.

## 2.3 Plasma Sample Preparation

Fasting blood collection in the early morning for both groups of subjects was required to minimize the influence of nutrition on the plasma levels of TRP metabolites. The patients pathologically diagnosed with EC did not receive radiotherapy or chemotherapy at this stage. Each blood sample was placed in EDTA anticoagulation tubes and centrifuged at 2,095×g for 10 min at 4°C within 2 h. Plasma and blood cells were separated and stored at −80°C for future analysis.

## 2.4 Clinical Endpoint

Clinical endpoints included susceptibility event, tumor metastasis event, and OS of patients.

A case-control study was conducted on susceptibility event. The initial sample population included 393 patients with EC and 456 healthy individuals. According to the propensity score matching (PSM) principle, 166 patients with EC and 203 healthy individuals were selected ( $p > 0.05$ ).

Tumor metastasis refers to the continued growth of cancer cells from the primary site (i.e., squamous or glandular epithelium of the esophagus) to other sites *via* lymphatic channels, blood vessels, or body cavities, including lymph node metastasis and distant metastasis. Lymph node metastasis refers

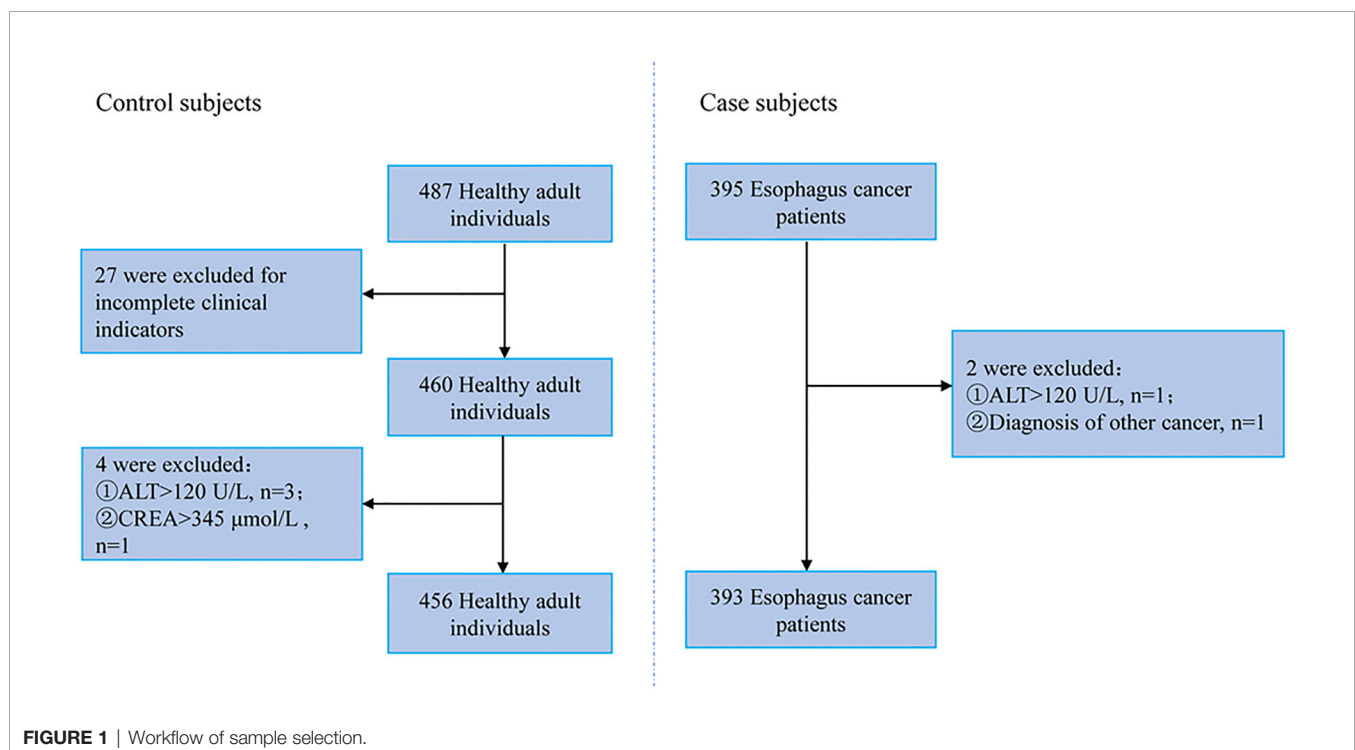
to mediastina, neck, clavicle, axilla, abdomen, and peritoneum lymph node metastasis. Distant metastasis refers to metastasis to the lung, liver, bone, and other sites. The evaluation of tumor metastasis was mainly based on the clinical diagnosis, tumor staging, pathology, and imaging examination (abdominal and pelvic CT or MRI and chest X-ray) of patients at the Cancer Hospital of Shantou University Medical College.

OS was defined as the time from the start of randomization to the death of any cause and was mainly evaluated based on in-hospital outpatient follow-up and out-of-hospital telephone follow-up. Follow-up information for each patient was obtained from the hospital database and telephone interviews. The telephone follow-up period was as follows: advanced-stage patients were followed-up every 3 months, and early stage patients were followed-up every 6 months. The last follow-up period of this study was December 2019, and the patients were followed up for 1 year.

## 2.5 Quantification of Plasma Concentrations of TRP and Their Metabolites

A sensitive high-performance liquid chromatography-tandem mass spectrometry (HPLC-MS/MS) assay was established for the simultaneous quantification of TRP, KYN, KYNA, 3-HAA, XA, 5-HT, 5-HIAA, IPA, and IAA in human plasma. Analysis was performed using an HPLC system (LC-20A, Shimadzu) coupled with an API 4000 triple-quadrupole mass spectrometer (AB, Sciex).

Nine analytes and internal standards (TRP-*d*5 and KYN-*d*4) were isolated from human plasma by liquid-liquid extraction with prechilled acetonitrile and then separated on an Acquity XSelect HSS T3 column (2.1 mm × 100 mm, 3.5 μm) at a flow



rate of 0.30 ml/min by the gradient of the mobile phase consisting of 0.01% (*v/v*) formic acid in water (A) and acetonitrile (B). The following gradient program was used: 0–0.1 min 5% B; 0.1–0.5 min 5→60% B; 0.5–2.8 min 60% B; 2.8–2.9 min 60→5% B; 2.9–5.0 min 5% B.

Mass detection was performed using an API 4000 triple-quadrupole mass spectrometer under the positive electrospray ionization mode. Electrospray voltage (IS) was set at 5,500 V, desolvation gas temperature was set at 550°C, and ion source gas 1 (CS1) and ion source gas 2 (CS2) were set at 50 psi. The air curtain gas (CUR) was 25 psi. Declustering potential (DP) and collision energy (CE) were optimized for each analyte and internal standard. Ion transitions and optimized multiple reaction monitoring (MRM) parameters are shown in **Table S1**.

## 2.6 Data Preprocessing and Analysis

Demographic and clinical characteristics were summarized using counts (percentages) for categorical variables and medians (interquartile ranges [IQR]) for continuous variables. Considering that the concentration ranges of all metabolites were skewed, logarithmic transformation was performed prior to analysis. Spearman correlation analysis was applied to study the association between plasma concentrations of upstream and downstream metabolites (i.e., TRP with all downstream metabolites, KYN with KP downstream metabolites and 5-HT with 5-HIAA). If  $p < 0.05$ , metabolite ratios were also included in the list of dependent variables.

Linear regression analysis was performed to assess the effects of baseline demographic and clinical characteristics on the plasma metabolites/metabolite ratios. Factors with  $p < 0.05$  after univariate linear regression were employed into the multivariate regression model, in which  $p < 0.05$  was considered as the independent factor of metabolites/metabolite ratios. The  $R^2$  was used to evaluate the interpretability of the model.

Based on the propensity index, the appropriate PSM method ("MatchIt" package) was employed to correct the imbalance of baseline data between the study population of case subjects and control subjects for inclusion of the population in the susceptibility event study calculated using the nearest neighbor method. Age and sex were used as covariates to condense a comprehensive score, with a paired caliper value of 0.02. A logistic regression model was applied to evaluate the effects of clinical characteristics and plasma metabolites of the subjects on susceptibility and tumor metastasis events, and Cox regression analysis was performed to assess the OS of patients, while the odds ratio (OR), hazard ratio (HR), and 95% confidence interval (95%CI) were calculated. Variables with  $p < 0.05$  were entered into the multivariate model, and only variables with  $p < 0.05$  considered as independent impact factors, were retained in the model. Furthermore, prognostic models of clinical events were constructed for each predictive variable by receiver-operating characteristic (ROC) curves using the area under the curve (AUC) to measure the diagnostic effectiveness. The optimal cutoffs were calculated by selecting the data point that maximized the true-positive rate and minimized the false-positive rate. The Kaplan–Meier method was conducted to assess the effects of every independent variable associated with

OS, in which patients were further stratified into three groups: low, moderate, and high in terms of the quartiles of their plasma levels, and the  $p$ -value was analyzed with the log-rank test.

The criterion for statistical significance was set at  $p < 0.05$ . All data were analyzed using SAS 9.4 (SAS Institute, Cary, NC, USA), R (version 3.2.3, <http://www.R-project.org/>), and GraphPad Prism 6. A flowchart of the experimental design and sample selection process is depicted in **Figure 2**.

## 3 RESULTS

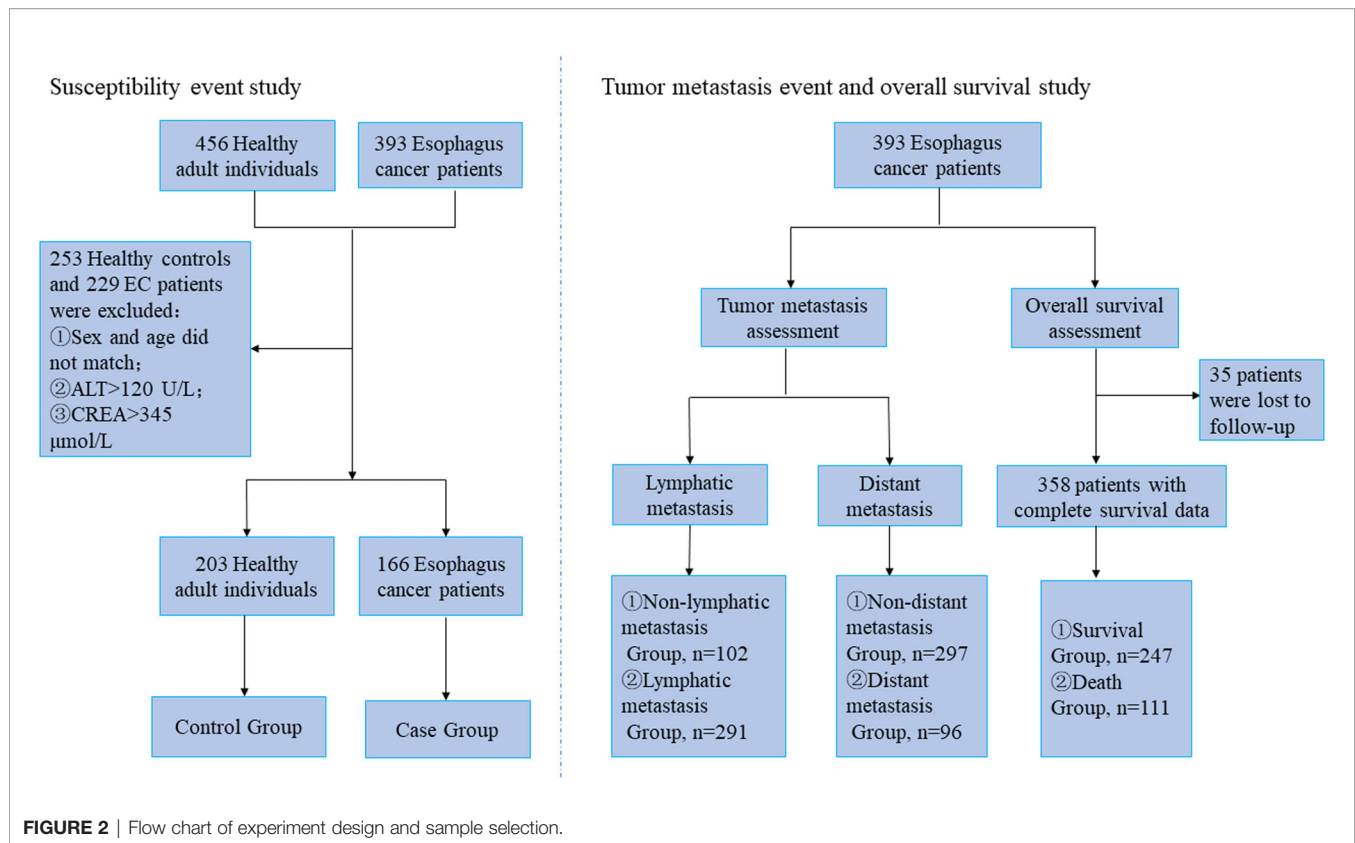
### 3.1 General Characteristics and Metabolite-to-Metabolite Correlation Analysis of the Participants

Based on these criteria, we ultimately included 456 healthy individuals and 393 patients with EC. The demographic characteristics and clinical data of the enrolled subjects are shown in **Tables S2, S3**. Of the 849 participants eligible for this study, 456 healthy individuals were assigned to the control cohort, and 393 patients with EC were assigned to the case cohort. In the metabolite-to-metabolite correlation analysis (**Table S4**), all subjects revealed that the concentration of TRP was significantly and positively associated with the concentrations of five metabolites (KYN, KYNA, XA, 3-HAA, and IAA), and KYN was positively correlated with KYNA, XA, and 3-HAA ( $r > 0$ ,  $p < 0.05$ ), whereas a significant negative correlation was found between TRP and IPA in control subjects ( $r < 0$ ,  $p < 0.05$ ). Therefore, the corresponding ratios were included in the list of dependent variables for further correlation analyses.

### 3.2 Effects of Baseline Characteristics on the Plasma Exposure of TRP and Its Metabolites in Case Subjects

Univariate linear regression analysis revealed the following: (1) high CREA levels were associated with the plasma levels of KYN, KYNA, 5-HIAA, IPA, and IAA; (2) coagulation index of patients, namely, platelet (PLT), was correlated with plasma exposure to multiple metabolites, namely, TRP, KYNA, 5-HT, and IPA; (3) male patients showed higher plasma exposure to TRP, XA, and 3-HAA; (4) other clinical indexes for hepatic function [i.e., aspartate aminotransferase (AST)], nutrition [i.e., albumin (ALB), globulin (GLB), and total protein (TPROT)], coagulation (i.e., PLT), and immune [i.e., red blood cell (RBC) and hemoglobin (HGB)] exhibited certain effects on plasma exposure of metabolites (**Table S2**).

Similarly, univariate linear regression analysis of the baseline characteristics of plasma metabolite ratios showed that low ALB levels significantly affected multiple metabolite ratios, namely, KYN/TRP, KYNA/TRP, XA/TRP, 3-HAA/TRP, and 3-HAA/KYN ratios. Second, age, CREA level, and RBC count were the secondary impact factors influencing the plasma levels of KYN/TRP, KYNA/TRP, XA/TRP, 3-HAA/TRP, XA/KYN, and 3-HAA/KYN. Other indexes that characterized hepatic function (i.e., AST), nutrition (i.e., TPROT), and cardiac function [i.e.,



lactate dehydrogenase (LDH)] exhibited certain effects on plasma exposure to metabolites (**Table S2**).

Based on the results of the univariate linear regression analysis, significant factors serving as covariates were incorporated into the multivariate linear regression model of each metabolite/metabolite ratio. Among these variables, it was found that the CREA level in the case subjects independently affected several metabolites/metabolite ratios of the TRP metabolic profile, namely, KYN, KYNA, 5-HIAA, IPA, KYN/TRP, KYNA/TRP, XA/KYN, and 3-HAA/KYN. The AST level was considered the secondary factor, correlating with the plasma levels of KYN, 5-HIAA, IPA, KYN/TRP, KYNA/KYN, and XA/KYN. It was speculated that the hepatic and renal functions of the patients might be involved in the dynamic changes in the TRP metabolic profile. Corresponding interpretations of the TRP metabolic profile to the clinical baseline are presented in **Table S2**. Of note, platelet count was considered significantly associated with plasma exposure to 5-HT, which was consistent with a previous report published in *Blood* (16), demonstrating the reliability of the present experimental results.

### 3.3 Effects of Baseline Characteristics on the Plasma Exposure of TRP and Its Metabolites in Control Subjects

Univariate linear regression analysis showed that plasma exposure to multiple metabolites was significantly influenced by the levels of ALB, GLB, ALB/GLB, RBC, and HGB, associated metabolites, namely, TRP, KYN, KYNA, XA, 3-HAA, 5-HIAA, and IPA. Second, except for 3-HAA, plasma exposure to TRP

and its metabolites could be significantly affected by two demographic indexes (i.e., sex and age). Hepatic and renal function indexes (alanine aminotransferase [ALT], AST, and CREA) and neutrophil ratio (NE) were correlated with plasma exposure to TRP, KYN, KYNA, XA, 3-HAA, 5-HIAA, and IAA. The effects of the remaining factors on the metabolites in the control subjects are shown in **Table S3**.

Similarly, univariate linear regression analysis showed that age significantly affected the metabolite ratios in the control subjects except for 3-HAA/TRP. In accordance with the above results, the plasma levels of multiple metabolite ratios were still significantly affected by sex and the levels of ALB, GLB, and ALB/GLB; the effects of the remaining factors on the metabolite ratios are shown in **Table S3**.

These factors were incorporated into a multivariate linear regression model of individual metabolites/metabolite ratios. Multivariate linear regression identified that the CREA levels in the control subjects independently affected several metabolites/metabolite ratios in the TRP metabolic profile, namely, IAA, KYN/TRP, KYNA/TRP, IAA/TRP, and 3-HAA/KYN. Hepatic function indexes (i.e., alkaline phosphatase [ALP] and ALT) were considered as secondary factors involving metabolites/metabolite ratios, namely, TRP, KYN, KYNA, 3-HAA, 5-HT, KYN/TRP, and KYNA/KYN. Consistent with the case cohort, hepatic and renal function were similarly involved in the dynamics of the TRP metabolic profile in control subjects, and platelets in the control cohort were similarly independent influencers of plasma exposure to 5-HT. According to previous studies, platelets and mast cells



were proposed to be the vital reservoirs of 5-HT, and secretion of 5-HT would lead to increased uptake of 5-HT by circulating platelets and mast cells (17, 18).

### 3.4 Contribution of Plasma Exposure of TRP and Its Metabolites to Susceptibility, Metastasis, and OS

#### 3.4.1 Results of the PSM

Given the significant differences in age and sex in the original two cohorts, confounding bias could alter the veracity of the findings on cancer susceptibility event; therefore, matching the two cohorts was required to increase the statistical power of the present case-control study.

The MatchIt package of R was used to match the age and sex of the case and control subjects. Before matching, the age of the control subjects was 48.00 (37.50, 56.00) years, accounting for 53.73% of males and 46.27% of females, while the age of case subjects was 63.00 (58.00, 67.00) years, accounting for 77.35% of males and 22.65% of females. The PSM scores of the control and case subjects were  $0.28 \pm 0.27$  and  $0.67 \pm 0.27$ , respectively.

Via the nearest neighbor method of PSM, the age of control subjects was 57.00 (52.00, 62.00) years old, of which 63.55% were male and 36.45% were female, while the age of case subjects was 58.00 (53.00, 63.00) years old, of which 68.67% were male, and 31.33% were female. There was no statistically significant difference between the two groups ( $p > 0.05$ ). The PSM scores of the two groups were  $0.55 \pm 0.22$  in control subjects and  $0.55 \pm 0.22$  in case subjects, which proved that the age and sex of both groups were balanced and comparable (Figure 3). After

matching, the two cohorts were subjected to a subsequent case-control statistical study, as detailed in Table S5 and Figure 2.

#### 3.4.2 Effects of TRP and Its Metabolites on Susceptibility Event of the EC and Their Predictive Value

Subjects with susceptibility events included 166 age- and sex-matched patients with EC and 203 healthy individuals. Univariate logistic regression showed that plasma exposure to TRP and its eight metabolites, six metabolite ratios, NE, RBC, HGB, PLT, ALT, AST, glutamyl transferase (GGT), and ten other biochemical indicators were associated with susceptibility to EC (Table 1). Furthermore, the significantly related factors were included in the multivariate logistic regression model. It was found that only high levels of 5-HT and ALP and low levels of HGB were independent factors influencing susceptibility to EC. Compared with the control group, the plasma exposure to 5-HT in the case group increased 3.94 times, ALP level increased 1.58 times, and HGB level decreased 1.28 times. In the whole multivariate regression model, the concordant part accounted for 99.5% and the discordant part accounted for 0.5%, indicating that the prediction accuracy of the whole regression model was high. The results of this section imply that a high level of 5-HT incorporating ALP and a low HGB level would increase the susceptibility to EC.

Subsequently, we constructed ROC curves with the variables constituted by three independent factors and three merging factors individually to obtain the predictive efficacy for susceptibility events, as shown in Figure 4. ROC analysis of 5-

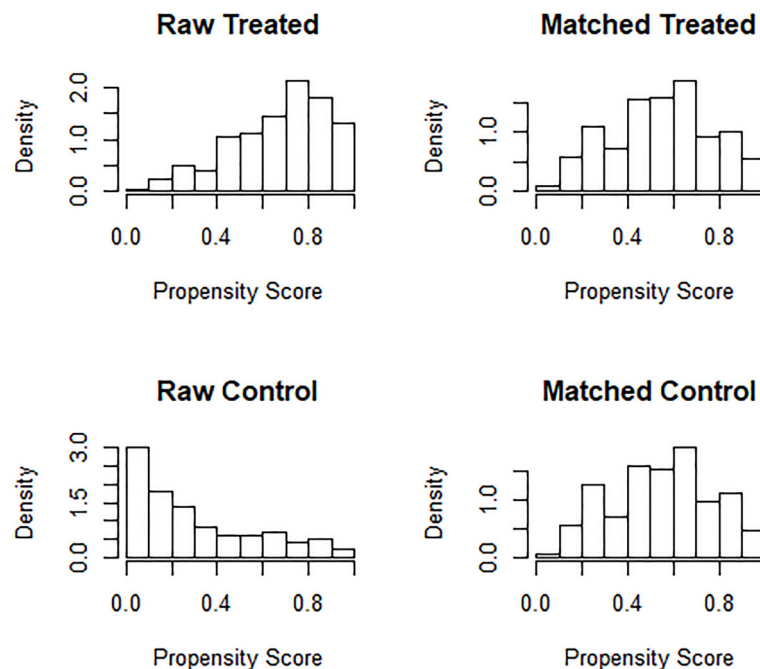


**FIGURE 3** | Histogram of propensity scores of two groups before and after matching.

**TABLE 1 |** Associations of metabolites and baseline data with susceptibility event.

Characteristics	Control subjects	Case subjects	Univariable Analysis		Multivariable Analysis	
	N (%) or Median (IQR)	N (%) or Median (IQR)	OR (95%CI)	p	OR(95%CI)	p
<b>Demographic data</b>						
Total number	203	166				
Age, years	57.00 (52.00, 62.00)	58.0 (53.00, 63.00)	1.02 (1.00–1.05)	0.0905		
Sex						
Female	74 (36.45)	52 (31.33)	1.02 (1.00–1.94)	0.3018		
Male	129 (63.55)	114 (68.67)				
<b>Blood routine examination</b>						
WBC, 10 <sup>9</sup> /L	6.54 (5.67, 7.62)	5.85 (4.20, 8.07)	0.95 (0.88–1.03)	0.2498		
NE, %	54.00 (48.64, 60.00)	66.71 (56.26, 75.00)	1.10 (1.08–1.13)	<.0001		
RBC, 10 <sup>12</sup> /L	4.81 (4.54, 5.16)	4.21 (3.68, 4.69)	0.15 (0.09–0.24)	<.0001		
HGB, g/L	151.00 (141.00, 161.00)	118.95 (105.20, 133.20)	0.89 (0.87–0.91)	<.0001	0.83 (0.75–0.91)	0.0002
PLT, 10 <sup>9</sup> /L	215.00 (186.00, 246.00)	228.00 (172.00, 283.90)	1.00 (1.00–1.00)	0.0119		
<b>Biochemical measurements</b>						
ALT, U/L	24.00 (20.00, 32.00)	20.00 (14.00, 28.00)	0.97 (0.96–0.99)	0.0010		
AST, U/L	28.00 (25.00, 33.00)	19.00 (16.00, 23.00)	0.84 (0.81–0.88)	<.0001		
CREA, $\mu$ mol/L	79.00 (66.00, 89.00)	76.00 (67.00, 87.00)	1.00 (0.99–1.01)	0.4065		
GGT, U/L	30.00 (21.00, 45.00)	20.00 (16.00, 32.00)	0.99 (0.99–1.00)	0.0211		
ALP, U/L	78.50 (64.00, 94.00)	126.00 (104.00, 140.00)	1.06 (1.04–1.07)	<.0001	1.07 (1.03–1.12)	0.0003
LDH, U/L	178.00 (163.00, 207.00)	152.00 (135.00, 177.00)	0.99 (0.98–0.99)	0.0001		
TPROT, g/L	75.00 (72.10, 77.90)	67.80 (62.60, 71.70)	0.78 (0.75–0.83)	<.0001		
ALB, g/L	45.50 (43.40, 46.70)	39.60 (35.90, 42.70)	0.57 (0.50–0.64)	<.0001		
GLB, g/L	29.50 (26.80, 32.30)	28.05 (24.70, 30.60)	0.91 (0.86–0.95)	0.0001		
ALB/GLB	1.52 (1.38, 1.69)	1.44 (1.23, 1.61)	0.16 (0.06–0.38)	<.0001		
GLU, mmol/L	5.56 (5.24, 6.23)	5.02 (4.60, 5.45)	0.55 (0.43–0.71)	<.0001		
<b>Plasma concentrations and Plasma ratios</b>						
TRP, ng/ml	10,900.00 (9,600.00, 12,300.00)	8,235.00 (6,960.00, 9,790.00)	0.01 (0.01–0.04)	<.0001		
KYN, ng/ml	323.00 (272.00, 382.00)	260.00 (216.00, 345.00)	0.14 (0.07–0.29)	<.0001		
KYNA, ng/ml	8.33 (6.76, 10.20)	6.42 (5.05, 8.09)	0.11 (0.06–0.22)	<.0001		
XA, ng/ml	9.11 (7.17, 11.00)	6.59 (5.17, 8.13)	0.10 (0.05–0.20)	<.0001		
3-HAA, ng/ml	0.92 (0.71, 1.15)	1.10 (0.80, 1.55)	2.50 (1.41–4.42)	0.0017		
5-HT, ng/ml	6.89 (4.90, 9.86)	16.60 (9.70, 28.60)	5.57 (3.71–8.36)	<.0001	98.47 (8.00– $\infty$ )	0.0003
5-HIAA, ng/ml	10.30 (7.44, 16.30)	9.13 (7.48, 14.80)	0.77 (0.48–1.25)	0.2902		
IPA, ng/ml	90.30 (56.40, 172.00)	53.20 (31.00, 101.00)	0.64 (0.51–0.80)	0.0001		
IAA, ng/ml	183.00 (137.00, 239.00)	152.00 (105.00, 244.00)	0.60 (0.41–0.88)	0.0087		
KYN/TRP	2.91E–02 (2.50E–02, 3.45E–02)	3.27E–02 (2.64E–02, 4.23E–02)	2.97 (1.50–5.89)	0.0018		
KYNA/TRP	7.40E–04 (6.20E–04, 9.18E–04)	7.35E–04 (6.33E–04, 8.86E–04)	1.07 (0.57–2.02)	0.8400		
XA/TRP	8.40E–04 (6.59E–04, 1.01E–03)	8.13E–04 (5.97E–04, 1.04E–03)	0.66 (0.35–1.21)	0.1777		
3-HAA/TRP	8.47E–05 (6.30E–05, 1.13E–04)	1.35E–02 (9.07E–05, 1.84E–04)	6.52 (3.59–11.86)	<.0001		
IPA/TRP	8.15E–03 (4.82E–03, 1.62E–02)	6.59E–03 (3.51E–03, 1.36E–02)	0.86 (0.69–1.06)	0.1511		
IAA/TRP	1.70E–02 (1.29E–02, 2.32E–02)	1.94E–02 (1.35E–02, 2.75E–02)	1.64 (1.12–2.40)	0.0116		
KYNA/KYN	2.55E–02 (2.20E–02, 3.02E–02)	2.33E–02 (1.88E–02, 2.85E–02)	0.32 (0.16–0.67)	0.0024		
XA/KYN	2.78E–02 (2.18E–02, 3.36E–02)	2.42E–02 (1.86E–02, 3.17E–02)	0.43 (0.26–0.72)	0.0012		
3-HAA/KYN	2.80E–03 (2.13E–03, 3.54E–03)	3.78E–03 (2.79E–03, 5.53E–03)	4.46 (2.50–7.97)	<.0001		

Variables with  $p < 0.05$  were entered into the multivariable model, and only variables with  $p < 0.05$  were retained in the model.

WBC, white blood cell; NE, neutrophil ratio; RBC, red blood cell; HGB, hemoglobin; PLT, platelet; ALT, alanine aminotransferase; AST, aspartate aminotransferase; CREA, creatinine; GGT, glutamyl transferase; ALP, alkaline phosphatase; LDH, lactate dehydrogenase; TPROT, total protein; ALB, albumin; GLB, globulin; GLU, glucose; TRP, tryptophan; KYN, kynurenine; KYNA, kynurenic acid; XA, xanthurenic acid; 3-HAA, 3-hydroxyanthranilic acid; 5-HT, 5-hydroxytryptamine; 5-HIAA, 5-hydroxyindoleacetic acid; IPA, 3-indolepropionic acid; IAA, 3-indoleacetic acid; IQR, interquartile range; OR, odd ratio; CI, confidence interval.

HT for predicting susceptibility events achieved an AUC of 0.811, with the best cutoff of 10.75 ng/ml, sensitivity of 0.721, and specificity of 0.791. After integrating three independent factors, 5-HT, ALP, and HGB, the predictive effectiveness of the combined variables was increased substantially to 0.978.

### 3.4.3 Effects of TRP and Its Metabolites on EC Metastasis

In this subsection, we discuss lymph node and distant metastases. A total of 291 patients with lymph node metastasis and 102 patients without lymph node metastasis were included in the

analysis of lymph node metastasis events, and the results of univariate logistic regression analysis showed that 5-HT, 5-HIAA, and TPROT were significantly associated with lymph node metastasis (**Table 2**). Further significant correlation factors were included in the multivariate logistic regression model, and only high plasma exposure to 5-HIAA remained an independent factor for lymph node metastasis. Plasma exposure to 5-HIAA exhibited a 1.24-fold increase in the lymph node metastasis subjects compared to non-lymph node metastasis subjects. The consistent and inconsistent parts of the multivariate regression model accounted for 61.4 and 38.0%, respectively. In contrast, 96 patients with distant metastasis and 297 patients with non-distant

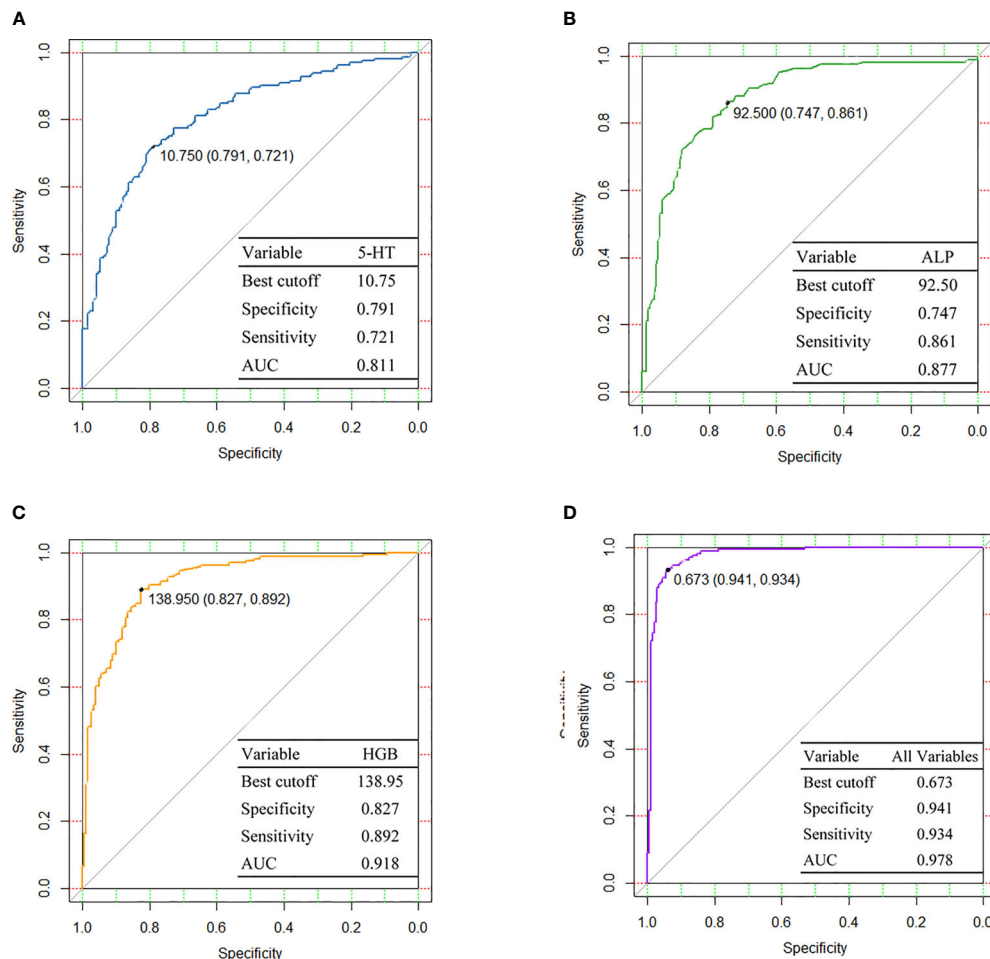


**FIGURE 4** | Diagnostic performances are shown by ROC curves among (A) 5-HT, (B) ALP, (C) HGB, and (D) All variables. 5-HT, 5-hydroxytryptamine; ALP, alkaline phosphatase; HGB, hemoglobin; AUC, area under curve.

metastasis were included, and univariate logistic regression analysis revealed that the plasma levels of IPA and XA/KYN, age, several blood routine indexes [i.e., white blood cell (WBC) and NE], and several biochemical indexes (i.e., AST, GGT, and ALP) of patients were correlated with distant metastasis (**Table 3**). However, multivariate logistic regression analysis revealed that only low WBC and high GGT levels were independent factors for distant metastatic event, whereas metabolites exerted no significant effect on distant metastatic event.

### 3.4.4 Effects of TRP and Its Metabolites on the OS of Patients With EC

Follow-up for this study was completed in December 2019, with survival data available for 358 patients. Of the enrolled patients with EC, 111 died, 247 survived, and 35 were lost to follow-up. Univariate Cox regression analysis showed that plasma levels of XA/TRP, 3-HAA/TRP, XA/KYN, and 3-HAA/KYN, male sex, comorbid hypertension, several blood routine indexes, and

several biochemical indexes were significantly associated with the OS of patients (**Table 4**). Furthermore, significantly associated factors were included in the multivariate Cox regression model, and it was found that high levels of XA/KYN, NE, and low ALB levels independently and significantly affected the OS of patients. To clarify the risk of this event by XA/KYN, we further stratified the patients by quartiles of plasma XA/KYN levels and divided the patients into three groups: high, medium, and low. The Kaplan–Meier method was applied to analyze the differences in survival curves among different groups, as shown in **Figure 5**. Survival prognosis revealed that patients with a low plasma level of XA/KYN showed a significantly lower OS than patients with a medium plasma level of XA/KYN (HR: 0.48,  $p = 0.0080$ ). A similar trend was observed between patients with low and high plasma levels of XA/KYN (HR: 0.42,  $p = 0.0031$ ). However, there was no significant difference between patients with medium and high plasma XA/KYN levels (HR: 0.86,  $p = 0.4634$ ), as depicted in **Figure 5**.

**TABLE 2 |** Associations of metabolites and baseline data with lymph node metastasis event.

Characteristics		Non-lymphatic metastasis Group	Lymphatic metastasis Group	Univariable Analysis		Multivariable Analysis	
		N (%) or Median (IQR)	N (%) or Median (IQR)	OR (95%CI)	p	OR (95%CI)	p
<b>Demographic data</b>							
Total number		102	291				
Age, years		64.00 (59.00, 68.00)	63.0 (57.00, 67.00)	0.98 (0.95–1.01)	0.1471		
Sex	Female	27 (26.47)	62 (21.31)	1.33 (0.79–2.24)	0.2844		
	Male	75 (73.53)	229 (78.69)				
<b>Medical history</b>							
Hypertension	No	81 (79.41)	230 (79.04)	1.02 (0.59–1.79)	0.9365		
	Yes	21 (20.59)	61 (20.96)				
Diabetes	No	95 (93.14)	262 (90.03)	1.50 (0.64–3.54)	0.3530		
	Yes	7 (6.86)	29 (9.97)				
Cerebral Infarction	No	98 (96.08)	284 (97.59)	0.60 (0.17–2.11)	0.4286		
	Yes	4 (3.92)	7 (2.41)				
Family History of Cancer	No	97 (95.10)	279 (95.88)	0.83 (0.29–2.43)	0.7398		
	Yes	5 (4.90)	12 (4.12)				
<b>Blood routine examination</b>							
WBC, 10 <sup>9</sup> /L		6.54 (5.67, 7.62)	5.47 (4.20, 7.74)	0.96 (0.91–1.02)	0.1766		
NE, %		65.26 (53.70, 75.92)	67.02 (56.91, 74.97)	1.00 (0.99–1.02)	0.6830		
RBC, 10 <sup>12</sup> /L		4.20 (3.57, 4.65)	4.14 (3.60, 4.61)	0.94 (0.68–1.30)	0.6946		
HGB, g/L		122.20 (108.80, 135.60)	119.20 (108.30, 132.50)	0.99 (0.98–1.00)	0.1880		
PLT, 10 <sup>9</sup> /L		233.00 (178.00, 288.00)	223.00 (168.00, 281.70)	1.00 (1.00–1.00)	0.2223		
<b>Biochemical measurements</b>							
ALT, U/L		19.00 (13.00, 26.00)	19.00 (14.00, 28.00)	1.01 (0.99–1.02)	0.4163		
AST, U/L		18.00 (15.00, 22.00)	19.00 (15.00, 24.00)	1.03 (1.00–1.06)	0.0893		
CREA, $\mu$ mol/L		79.00 (66.00, 92.00)	78.00 (68.00, 88.00)	1.00 (0.99–1.01)	0.6656		
GGT, U/L		20.00 (16.00, 29.00)	21.00 (16.00, 32.00)	1.00 (0.99–1.01)	0.7067		
ALP, U/L		120.00 (103.00, 135.00)	121.00 (104.00, 142.00)	1.00 (1.00–1.00)	0.9988		
LDH, U/L		145.00 (129.00, 168.00)	153.00 (133.00, 181.00)	1.00 (1.00–1.01)	0.1395		
TPROT, g/L		69.90 (61.80, 74.50)	67.40 (61.80, 71.30)	0.96 (0.94–0.99)	0.0132		
ALB, g/L		40.00 (36.90, 42.70)	39.20 (35.50, 41.90)	0.95 (0.90–1.00)	0.0514		
GLB, g/L		28.40 (24.60, 31.90)	27.70 (24.70, 30.70)	0.97 (0.93–1.02)	0.2661		
ALB/GLB		1.42 (1.27, 1.56)	1.42 (1.23, 1.58)	0.87 (0.34–2.19)	0.7646		
GLU, mmol/L		5.18 (4.71, 5.75)	5.03 (4.65, 5.54)	0.97 (0.82–1.15)	0.6966		
<b>Living habit</b>							
Smoking	No	43 (42.16)	114 (39.31)	1.13 (0.71–1.78)	0.6139		
	Yes	59 (57.84)	176 (60.69)				
Drinking	No	71 (69.61)	194 (66.90)	1.13 (0.70–1.85)	0.6149		
	Yes	31 (30.39)	96 (33.10)				
<b>Plasma concentrations</b>							
TRP, ng/ml		8,725.00 (6,960.00, 10,000.00)	8,250.00 (6,980.00, 9,580.00)	0.83 (0.42–1.65)	0.5988		
KYN, ng/ml		261.50 (214.00, 339.00)	275.00 (224.00, 350.00)	1.21 (0.64–2.29)	0.5565		
KYNA, ng/ml		6.56 (5.15, 7.94)	6.49 (5.29, 8.09)	1.31 (0.71–2.42)	0.3916		
XA, ng/ml		6.54 (5.08, 7.98)	6.65 (5.06, 8.60)	1.07 (0.67–1.71)	0.7727		
3-HAA, ng/ml		1.09 (0.78, 1.48)	1.13 (0.82, 1.54)	1.07 (0.62–1.85)	0.8203		
5-HT, ng/ml		12.90 (8.55, 23.50)	16.40 (9.50, 28.40)	1.33 (1.03–1.72)	0.0303		
5-HIAA, ng/ml		8.04 (6.72, 13.40)	11.00 (8.01, 16.80)	2.18 (1.21–3.97)	0.0095	2.16 (1.19–3.93)	0.0114
IPA, ng/ml		53.30 (28.40, 145.00)	52.60 (28.40, 98.60)	0.93 (0.74–1.17)	0.5280		
IAA, ng/ml		155.00 (115.00, 256.00)	159.00 (107.00, 254.00)	1.02 (0.73–1.41)	0.9156		
<b>Plasma ratios</b>							
KYN/TRP		3.22E–02 (2.73E–02, 3.75E–02)	3.34E–02 (2.79E–02, 4.39E–02)	1.42 (0.75–2.69)	0.2795		
KYNA/TRP		7.68E–04 (6.31E–04, 9.05E–04)	7.91E–04 (6.48E–04, 9.38E–04)	1.61 (0.75–3.44)	0.2201		
XA/TRP		7.94E–04 (5.85E–04, 9.98E–04)	8.13E–03 (6.00E–04, 1.09E–03)	1.25 (0.70–2.22)	0.4549		
3-HAA/TRP		1.28E–04 (9.00E–05, 1.85E–04)	1.39E–04 (9.87E–05, 1.89E–04)	1.06 (0.65–1.74)	0.8209		
IAA/TRP		1.89E–02 (1.46E–02, 2.80E–02)	2.02E–02 (1.32E–02, 3.24E–02)	1.06 (0.77–1.45)	0.7272		
KYNA/KYN		2.47E–02 (1.91E–02, 2.91E–02)	2.29E–02 (1.86E–02, 2.86E–02)	1.02 (0.53–1.99)	0.9454		
XA/KYN		2.38E–02 (1.80E–02, 3.22E–02)	2.38E–02 (1.75E–02, 3.29E–02)	0.96 (0.62–1.51)	0.8706		
3-HAA/KYN		3.11E–03 (1.34E–03, 4.83E–03)	3.09E–03 (0.00, 4.73E–03)	0.91 (0.55–1.52)	0.7246		

Variables with  $p < 0.05$  were entered into the multivariable model, and only variables with  $p < 0.05$  were retained in the model.

Abbreviations as in **Table 1**.



**TABLE 3 |** Associations of metabolites and baseline data with distant metastasis event.

Characteristics		Non-distant metastasis Group	Distant metastasis Group	Univariable Analysis		Multivariable Analysis	
		N (%) or Median (IQR)	N (%) or Median (IQR)	OR (95%CI)	p	OR (95%CI)	p
<b>Demographic data</b>							
Total number		297	96				
Age, years		64.00 (59.00, 68.00)	60.00 (56.00, 66.00)	0.96 (0.93–0.99)	0.0047		
Sex	Female	64 (21.55)	25 (26.04)	0.78 (0.46–1.33)	0.3612		
	Male	233 (78.45)	71 (73.96)				
<b>Medical history</b>							
Hypertension	No	230 (77.44)	81 (84.38)	0.63 (0.34–1.18)	0.1488		
	Yes	67 (22.56)	15 (15.63)				
Diabetes	No	268 (90.24)	89 (92.71)	0.73 (0.31–1.72)	0.4671		
	Yes	29 (9.76)	7 (7.29)				
Cerebral Infarction	No	288 (96.97)	94 (97.92)	0.68 (0.15–3.21)	0.6272		
	Yes	9 (3.03)	2 (2.08)				
Family History of Cancer	No	281 (94.61)	95 (98.96)	0.19 (0.02–1.41)	0.1037		
	Yes	16 (5.39)	1 (1.04)				
<b>Blood routine examination</b>							
WBC, 10 <sup>9</sup> /L		5.98 (4.30, 8.23)	5.00 (3.80, 8.23)	0.90 (0.83–0.97)	0.0090	0.91 (0.83–0.99)	0.0292
NE, %		67.50 (57.07, 75.91)	65.70 (53.10, 73.90)	0.98 (0.97–1.00)	0.0148		
RBC, 10 <sup>12</sup> /L		4.20 (3.60, 4.62)	4.14 (3.68, 4.62)	0.87 (0.63–1.20)	0.3926		
HGB, g/L		120.80 (109.60, 133.60)	118.50 (105.50, 131.60)	1.00 (0.99–1.01)	0.4068		
PLT, 10 <sup>9</sup> /L		232.40 (170.65, 287.00)	209.50 (169.00, 275.00)	1.00 (1.00–1.00)	0.2516		
<b>Biochemical measurements</b>							
ALT, U/L		18.00 (14.00, 26.00)	20.00 (14.00, 30.00)	1.02 (1.00–1.03)	0.0785		
AST, U/L		18.00 (15.00, 23.00)	19.00 (16.00, 25.00)	1.03 (1.01–1.06)	0.0081		
CREA, $\mu$ mol/L		79.00 (68.00, 90.00)	74.00 (66.00, 86.00)	0.99 (0.97–1.00)	0.0896		
GGT, U/L		21.00 (16.00, 30.00)	22.00 (17.00, 39.00)	1.01 (1.00–1.02)	0.0024	1.02 (1.01–1.03)	0.0001
ALP, U/L		117.50 (103.00, 138.50)	126.00 (104.00, 148.00)	1.01 (1.00–1.01)	0.0231		
LDH, U/L		151.00 (133.00, 175.00)	158.00 (126.00, 197.00)	1.00 (1.00–1.00)	0.3640		
TPROT, g/L		67.60 (61.60, 72.10)	67.40 (62.10, 71.50)	1.00 (0.97–1.03)	0.9952		
ALB, g/L		39.55 (35.85, 42.20)	39.20 (35.30, 42.10)	0.99 (0.94–1.04)	0.5556		
GLB, g/L		27.65 (24.60, 30.95)	28.20 (25.10, 31.10)	1.01 (0.97–1.06)	0.6247		
ALB/GLB		1.42 (1.25, 1.58)	1.40 (1.22, 1.60)	0.77 (0.30–1.96)	0.5789		
GLU, mmol/L		5.09 (4.65, 5.64)	5.07 (4.68, 5.68)	1.06 (0.89–1.25)	0.5339		
<b>Living habit</b>							
Smoking	No	114 (38.51)	43 (44.79)	0.77 (0.49–1.23)	0.2759		
	Yes	182 (61.49)	53 (55.21)				
Drinking	No	202 (68.24)	63 (65.63)	1.13 (0.69–1.83)	0.6339		
	Yes	94 (31.76)	33 (34.38)				
<b>Plasma concentrations</b>							
TRP, ng/ml		8,180.00 (6,910.00, 9,650.00)	8,390.00 (7,040.00, 9,580.00)	1.31 (0.65–2.65)	0.4494		
KYN, ng/ml		262.00 (222.00, 339.00)	286.00 (229.00, 375.00)	1.83 (0.94–3.59)	0.0776		
KYNA, ng/ml		6.39 (5.23, 7.92)	6.62 (5.32, 8.52)	1.51 (0.81–2.83)	0.1982		
XA, ng/ml		6.62 (5.09, 8.51)	6.51 (4.68, 8.41)	0.82 (0.51–1.31)	0.4079		
3-HAA, ng/ml		1.10 (0.78, 1.56)	1.21 (0.88, 1.49)	1.11 (0.65–1.91)	0.7003		
5-HT, ng/ml		15.55 (9.26, 28.00)	15.50 (9.25, 26.95)	1.03 (0.80–1.31)	0.8399		
5-HIAA, ng/ml		10.55 (7.48, 16.80)	10.60 (7.85, 16.20)	0.83 (0.47–1.48)	0.5282		
IPA, ng/ml		50.60 (25.60, 95.80)	55.65 (32.55, 118.50)	1.28 (1.02–1.61)	0.0330		
IAA, ng/ml		158.00 (112.00, 257.00)	152.00 (102.00, 226.00)	0.83 (0.59–1.17)	0.2890		
<b>Plasma ratios</b>							
KYN/TRP		3.27E–02 (2.76E–02, 4.09E–02)	3.30E–02 (2.78E–02, 4.74E–02)	1.42 (0.74–2.73)	0.2984		
KYNA/TRP		7.82E–04 (6.38E–04, 9.37E–04)	8.07E–04 (6.72E–04, 9.66E–04)	1.15 (0.56–2.37)	0.7117		
XA/TRP		8.37E–04 (5.98E–04, 1.08E–03)	7.83E–04 (5.96E–04, 1.01E–03)	0.62 (0.34–1.11)	0.1064		
3-HAA/TRP		1.35E–04 (9.35E–05, 1.95E–04)	1.46E–04 (1.03E–04, 1.82E–04)	0.99 (0.60–1.62)	0.9629		
IAA/TRP		2.07E–02 (1.34E–02, 3.10E–06)	1.73E–02 (1.32E–02, 2.87E–02)	0.79 (0.57–1.11)	0.1704		
KYNA/KYN		2.38E–02 (1.90E–02, 2.92E–02)	2.36E–02 (1.76E–02, 2.79E–02)	0.81 (0.41–1.61)	0.5469		
XA/KYN		2.47E–02 (1.83E–02, 3.38E–02)	2.05E–02 (1.63E–02, 2.88E–02)	0.63 (0.40–0.99)	0.0460		
3-HAA/KYN		3.01E–03 (0.00, 4.86E–03)	3.25E–03 (2.18E–03, 4.66E–03)	0.76 (0.45–1.29)	0.3064		

Variables with  $p < 0.05$  were entered into the multivariable model, and only variables with  $p < 0.05$  were retained in the model.

Abbreviations as in **Table 1**.

**TABLE 4 |** Associations of metabolites and baseline data with overall survival of patients.

Characteristics		Survival Group	Death Group	Univariable Analysis		Multivariable Analysis	
		N (%) or Median (IQR)	N (%) or Median (IQR)	HR (95%CI)	p	HR (95%CI)	p
Demographic data							
Total number		247	111				
Age, years		63.00 (58.00, 67.00)	63.00 (59.00, 70.00)	1.02 (0.99–1.04)	0.1745		
Sex	Female	65 (26.32)	15 (13.51)	2.03 (1.18–3.50)	0.0109		
	Male	182 (73.68)	96 (86.49)				
Medical history							
Hypertension	No	203 (82.19)	81 (72.97)	1.61 (1.06–2.45)	0.0255		
	Yes	44 (17.81)	30 (27.03)				
Diabetes	No	228 (92.31)	102 (91.89)	1.01 (0.51–2.00)	0.9753		
	Yes	19 (7.69)	9 (8.11)				
Cerebral Infarction	No	242 (97.98)	106 (95.50)	1.93 (0.79–4.74)	0.1499		
	Yes	5 (2.02)	5 (4.50)				
Family History of Cancer	No	236 (95.55)	107 (96.40)	0.96 (0.35–2.60)	0.9339		
	Yes	11 (4.45)	4 (3.60)				
Stage	Early stage	52 (21.49)	7 (6.60)	3.30 (1.53–7.10)	0.0023		
	Advanced stage	190 (78.51)	99 (93.40)				
Blood routine examination							
WBC, 10 <sup>9</sup> /L		5.50 (4.20, 7.74)	5.78 (4.06, 8.80)	1.05 (1.00–1.10)	0.0512	1.02 (1.00–1.03)	0.0240
NE, %		65.00 54.20, 72.64)	71.45 (62.61, 79.05)	1.03 (1.02–1.04)	<.0001		
RBC, 10 <sup>12</sup> /L		4.30 (3.78, 4.67)	3.89 (3.47, 4.31)	0.55 (0.43–0.71)	<.0001		
HGB, g/L		123.40 (111.80, 135.30)	114.75 (101.90, 128.40)	0.99 (0.98–0.99)	0.0001		
PLT, 10 <sup>9</sup> /L		220.00 (169.00, 279.20)	234.50 (174.00, 304.00)	1.00 (1.00–1.00)	0.0210		
Biochemical measurements							
ALT, U/L		20.00 (14.00, 28.00)	16.00 (12.00, 27.00)	0.98 (0.96–1.00)	0.0282	0.86 (0.82–0.90)	<.0001
AST, U/L		19.00 (16.00, 24.00)	17.00 (13.00, 23.00)	0.99 (0.97–1.01)	0.4240		
CREA, μmol/L		79.00 (70.00, 89.00)	76.00 (67.00, 90.00)	1.00 (0.98–1.01)	0.4003		
GGT, U/L		20.00 (16.00, 30.00)	22.50 (16.00, 39.00)	1.00 (1.00–1.01)	0.0111		
ALP, U/L		118.00 (101.00, 135.00)	123.00 (106.00, 145.00)	1.00 (1.00–1.01)	0.1912		
LDH, U/L		153.00 (133.00, 177.00)	150.50 (130.00, 174.00)	1.00 (1.00–1.00)	0.0171		
TPROT, g/L		69.20 (63.90, 73.00)	64.25 (58.30, 69.20)	0.97 (0.95–0.98)	<.0001		
ALB, g/L		40.50 (37.50, 42.70)	36.65 (33.50, 40.00)	0.87 (0.84–0.90)	<.0001		
GLB, g/L		28.20 (25.10, 31.00)	27.40 (23.60, 31.10)	0.97 (0.94–1.01)	0.1875		
ALB/GLB		1.42 (1.29, 1.58)	1.31 (1.18, 1.57)	0.30 (0.13–0.68)	0.0038		
GLU, mmol/L		5.04 (4.67, 5.49)	5.14 (4.63, 5.67)	1.09 (0.96–1.25)	0.1701		
Living habit							
Smoking	No	103 (41.87)	43 (38.74)	1.10 (0.75–1.61)	0.6327		
	Yes	143 (58.13)	68 (61.26)				
Drinking	No	170 (69.11)	71 (63.96)	1.18 (0.80–1.73)	0.4099		
	Yes	76 (30.89)	40 (36.04)				
Plasma concentrations							
TRP, ng/ml		8,550.00 (6,990.00, 9,920.00)	7,980.00 (6,740.00, 9,240.00)	1.00 (0.58–1.73)	0.9907		
KYN, ng/ml		274.00 (229.00, 349.00)	274.00 (229.00, 349.00)	0.78 (0.46–1.33)	0.3637		
KYNA, ng/ml		6.54 (5.33, 7.96)	6.54 (5.33, 7.96)	1.13 (0.66–1.94)	0.6512		
XA, ng/ml		6.49 (4.63, 8.35)	6.49 (4.63, 8.35)	1.73 (1.14–2.63)	0.0107		
3-HAA, ng/ml		1.09 (0.78, 1.48)	1.09 (0.78, 1.48)	1.48 (0.97–2.26)	0.0691		
5-HT, ng/ml		16.60 (9.07, 29.00)	16.60 (9.07, 29.00)	0.94 (0.77–1.15)	0.5514		
5-HIAA, ng/ml		9.89 (7.24, 16.30)	9.89 (7.24, 16.30)	1.29 (0.85–1.96)	0.2348		
IPA, ng/ml		52.80 (26.60, 109.00)	52.80 (26.60, 109.00)	1.15(0.95–1.38)	0.1529		
IAA, ng/ml		159.00 (108.00, 263.00)	159.00 (108.00, 263.00)	0.95 (0.73–1.24)	0.6856		
Plasma ratios							
KYN/TRP		3.33E–02 (2.76E–02, 4.23E–02)	3.26E–02 (2.76E–02, 4.41E–02)	0.77 (0.44–1.34)	0.3460	1.99 (1.30–3.04)	0.0016
KYNA/TRP		7.84E–04 (6.46E–04, 9.09E–04)	7.76E–04 (6.35E–04, 9.77E–04)	1.33 (0.74–2.40)	0.3429		
XA/TRP		7.54E–04 (5.73E–04, 1.02E–03)	8.96E–04 (6.94E–04, 1.13E–03)	2.20 (1.34–3.61)	0.0019		
3-HAA/TRP		1.30E–04 (9.48E–05, 1.77E–04)	1.55E–04 (1.01E–04, 2.11E–04)	1.47 (1.01–2.12)	0.0427		
IAA/TRP		1.97E–02 (1.34E–02, 3.30E–02)	2.11E–02 (1.36E–02, 2.80E–02)	0.95 (0.74–1.23)	0.6955		
KYNA/KYN		2.28E–02 (1.89E–02, 2.85E–02)	2.43E–02 (1.86E–02, 2.94E–02)	1.74 (0.96–3.15)	0.0668		
XA/KYN		2.32E–02 (1.63E–02, 3.03E–02)	2.70E–02 (1.96E–02, 3.53E–02)	1.95 (1.29–2.93)	0.0015		
3-HAA/KYN		3.00E–03 (0.00, 4.55E–03)	3.45E–03 (1.78E–03, 5.68E–03)	1.72 (1.16–2.55)	0.0073		

Variables with  $p < 0.05$  were entered into the multivariable model, and only variables with  $p < 0.05$  were retained in the model.

Abbreviations as in **Table 1**.

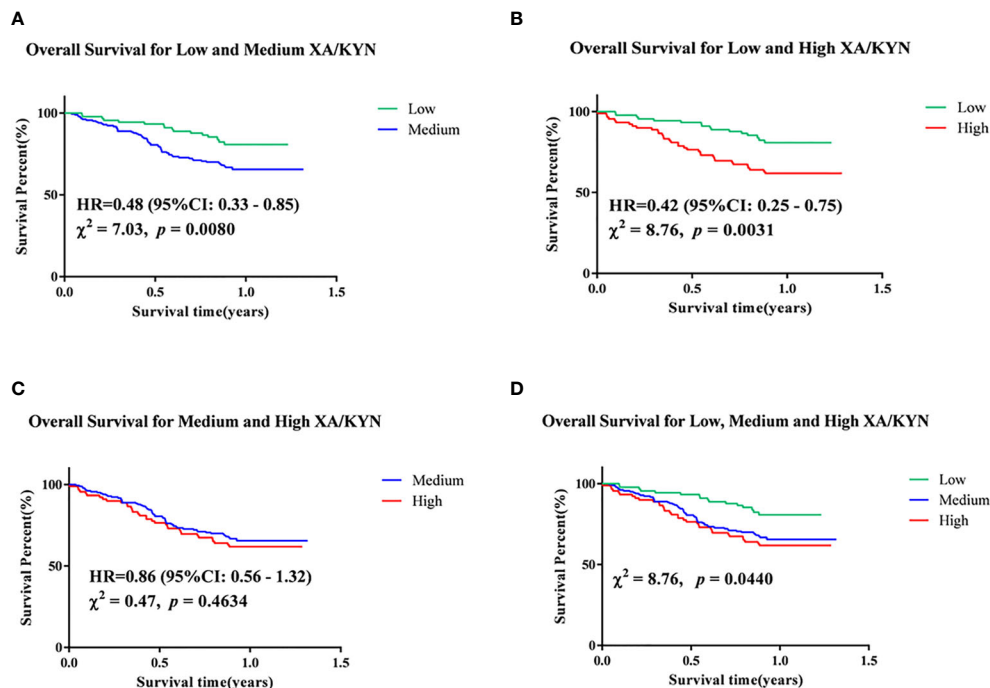


**FIGURE 5 |** Kapan-Meier analyses of (A) low and medium XA/KYN, (B) low and high XA/KYN, (C) medium and high XA/KYN, and (D) low, medium and high XA/KYN for overall survival of patients. XA, xanthurenic acid; KYN, kynurenine.

## DISCUSSION

Reprogrammed TRP metabolism has been proven to directly cause carcinogenesis and cancer progression as an adaptive mechanism for tumors to escape immune surveillance and metastasize, rendering it critical for tight control to maintain healthy homeostasis (19). However, given the relatively complex profile of TRP metabolism, a simple one-branch model could not capture the complex dynamics of the multi-branched TRP metabolic network, whereas evidence to elucidate the dynamic shifts of tryptophan metabolite concentrations involved in the different disease states of EC was sparse. To the best of our knowledge, this work is the first systematic assessment of clinical endpoint events of EC between TRP metabolic profiles and clinical phenotypes, namely, susceptibility event, lymph node metastasis event, distant metastasis event, and OS. A comprehensive mathematical model was established to provide a predictive tool that could facilitate identification of potential pathological changes in TRP metabolism.

Existing reports suggest that hepatic and renal functions assumed the biological roles in the metabolic network of TRP, as our results indicated (20–22). Similarly, this study found that clinical hepatic and renal function indexes were tightly correlated with TRP metabolites. In addition to the reported KP metabolites, corresponding increases in IPA and 5-HIAA levels were also found in patients with EC with liver and kidney insufficiency. Under normal conditions, the TDO enzyme controls TRP flux in the liver and its availability in plasma, and may supply KYN to the

extrahepatic pathway (21). Not to be stated, hepatic function exerted its prominent regulatory effect on the metabolic network of TRP. In an association study of renal function, Yilmaz et al. suggested that the ratio of TRP to KYN could reflect the oxidative stress status in chronic kidney disease patients undergoing hemodialysis and peritoneal dialysis (20). Numerous studies have also shown that TRP metabolism is associated with the severity of chronic kidney disease. Early reports showed that renal insufficiency would lead to decreased TRP levels and KYN accumulation in rats and humans. Moreover, a targeted metabolomic profiling of plasma exposure to TRP in terms of the diagnostic value of acute kidney injury was carried out in renal transplant patients, reaching a decision that low plasma exposure to TRP and high levels of KYN and KYN/TRP were powerful predictors of kidney injury (22). Consistent with previous studies, our data suggest that hepatic and renal function might directly contribute to TRP metabolism.

Additionally, after adjusting for several potential confounding variables, we evaluated whether the metabolic pathways and associated metabolites were altered in the different disease states of the EC. The principal findings were as follows: (1) TRP metabolism was significantly imbalanced in patients with EC. Three major metabolic pathways were severely dysregulated in both groups, in which the population with high plasma exposure to 5-HT significantly increased the risk of EC; (2) 5-HIAA was independently associated with increased lymph node metastasis risk; and (3) high plasma levels of XA/KYN conferred a risk effect on the occurrence of death, since KYN metabolism towards XA

was significantly increased in the high-risk group of death events. The above results characterized their roles in carcinogenesis and potency as risk markers for EC metastasis and prognosis.

Recently, both *in vivo* and *in vitro* studies have shown that 5-HT serves as an effective mitogen in various cell types (23). Its specific receptor subtypes are associated with the progression of solid cancers and can affect the growth of various cancers (24). Accumulating evidence has shown that the level of platelet-derived 5-HT in the cancer microenvironment is higher than that in healthy individuals (25). Moreover, platelet aggregation is frequent in the environment of cancer thrombosis, resulting in the release of a large amount of 5-HT, which is one of the mechanisms of cancer progression and angiogenesis. Our results are consistent with these results. Univariate analysis demonstrated that the PLT level in patients with EC was significantly higher than that in healthy individuals and was significantly associated with plasma exposure to 5-HT in both groups (Tables S2 and S3). Previous studies have shown that 5-HT executes physiological functions in the gastrointestinal tract, participates in esophageal and gastrointestinal motility, and is a mediator of the brain-gut connection (26). Additionally, 5-HT<sub>1</sub>, 5-HT<sub>2</sub>, 5-HT<sub>3</sub>, and 5-HT<sub>4</sub> receptors perform local and systemic functions in human esophageal motility and the transient contraction of the esophageal sphincter (27). Among them, the 5-HT<sub>3</sub> receptor also participates in visceral sensitization of esophageal sensitivity (28). Another study by Hempfling et al. showed that the esophagus had a wealth of 5-HT positive internal nerves, in which 5-HT could regulate the vagus nerve movement of the esophageal striated muscle (29), which suggests that 5-HT serves as an essential biomolecule in the regulation of the physiological state of the esophagus. Consistent with previous studies, our results suggested that 5-HT plays a crucial role in EC susceptibility and may be a potential biomarker for EC.

Regarding 5-HIAA, it has been recognized as a biomarker of neuroendocrine cancer and carcinoid syndrome, since the digestive tract is one of the primary sources of 5-HT and its metabolites (such as 5-HIAA), and the presence of non-endocrine malignant cells in the digestive tract might lead to an increase in these metabolites in body fluid and urine (1). To date, carcinoid cancer has been the only cancer diagnosed explicitly by measuring the urinary level of 5-HIAA in suspected patients (30). Nonetheless, as an effective marker of neuroendocrine cancer, there are limited data to support the prognostic role of 5-HIAA due to its differential expression and secretion. Insufficient evidence was observed for 5-HIAA as a prognostic marker owing to its limitation of high specificity yet low sensitivity (31). Van et al. indicated that the urinary level of 5-HIAA was an independent prognostic factor for the survival of patients with midgut cancers, whereas cumulative urinary 5-HIAA could not predict the survival rate in multivariate analysis (32).

Other studies have also pointed out that urinary 5-HIAA is an effective index of survival and prognosis in univariate analysis, except for multivariate analysis (33, 34). In our correlation study between metabolites and prognosis of patients, 5-HIAA was not found to be associated with OS (HR: 1.29, 95%CI: 0.85–1.96,  $p =$

0.2348), thus revealing that this metabolite could not serve as a biomarker to aid in determining the prognosis of patients with EC yielded insufficient evidence. Previously, Cheng et al. found that the serum 5-HIAA/TRP level in EC patients with metastasis was higher than that non-metastatic patients, which is consistent with our results (15). In this study, we compared the TRP metabolic profile between patients with and without lymph node metastasis. Univariate analysis showed that 5-HT and 5-HIAA levels were increased in patients with lymph node metastasis, and high plasma exposure to 5-HIAA was the only independent factor influencing lymph node metastasis. Based on the above results, we speculated that plasma exposure to 5-HIAA can be used as an effective biomarker to assist in diagnosing the risk of lymph node metastasis in patients with EC.

Interestingly, after exploring the association between metabolites and clinical endpoint events, this study suggested that the plasma level of XA/KYN significantly affected OS (HR: 1.99, 95%CI: 1.30–3.04,  $p = 0.0016$ ), speculating that the metabolism of KYN in the direction of XA increased the risk of death. Moreover, it is significant to point out that this metabolite ratio was the first discovery of an association between the TRP metabolic profile and the prognosis of cancer patients.

The high enzyme activity of KP has been proposed to trigger anti-inflammatory and immunosuppressive mechanisms, thereby executing pathological functions such as activation of cancer and aromatic hydrocarbon receptor (AHR). Remarkably, activation of AHR drives the transformation of naive CD4<sup>+</sup> cells to inhibit the Treg phenotype by reducing inflammatory cytokines and upregulating cytokines, thus promoting the occurrence and growth of malignant cancers (35). In addition, KYN, KYNA, and XA are all inducers of AHR activity, which could drive AHR activity and promote cancer cell migration (19). Furthermore, XA has been recognized as a regulator of glutamate synaptic transmission and a promising candidate as a peripheral biomarker of schizophrenia; however, the detailed mechanisms of cancer development have not been reported (36, 37). Additionally, it was worth noting that several prospective population-based studies had suggested that deficiency of vitamin B6 was associated with the increased risk of colorectal cancer and lung cancer (38–40). Several scientists have demonstrated that this association may be related to the inflammatory state, angiogenesis, DNA methylation, cell-mediated immune response, and other mechanisms (41). Moreover, if the body is deficient in vitamin B6, KYN metabolism would shift from NAD<sup>+</sup> formation to XA and KYNA production (42). Hence, we envisioned the possibility that XA/KYN might affect the survival and prognosis of patients by affecting the concentration of vitamin B6; however, this hypothesis requires further examination.

However, a limitation of this study is that the sample size was relatively small. Nonetheless, we conducted a strict screening and quality control process on the original sample population, and conducted sample screening and correlation discussions for different clinical endpoint events. Most of our findings are in line with those of previous studies, proving the reliability of our results. There is no denying that a more extensive study cohort would be more convincing to clarify the association with clinical



endpoint events. In the future, broader and more comprehensive inclusion of the study population would address this limitation.

## CONCLUSION

A comprehensive evaluation of the clinical predictive value of tryptophan metabolism in carcinogenesis and its potential as biomarkers for metastasis and prognosis of EC emerged from the present study. Our results demonstrated that elevated levels of 5-HT, 5-HIAA, and XA/KYN were observed in EC and might be part of the mechanism underlying the susceptibility, lymph node metastasis, and poor prognosis of EC, respectively. This study provides an essential theoretical basis for targeting endogenous TRP metabolism as a potential therapeutic intervention.

## DATA AVAILABILITY STATEMENT

The original contributions presented in the study are included in the article/**Supplementary Material**. Further inquiries can be directed to the corresponding authors.

## ETHICS STATEMENT

The studies involving human participants were reviewed and approved by the Guangzhou Red Cross Hospital. The patients/

participants provided their written informed consent to participate in this study.

## AUTHOR CONTRIBUTIONS

YC, JC, DG, and PY performed the experiment, performed data analysis, and wrote the manuscript. SC participated in the experiment. CZ, CX, and QZ participated in patient recruitment. CL revised the manuscript; ShiZ and ShoZ designed the study and revised manuscript. All authors contributed to the article and approved the submitted version.

## FUNDING

This study was funded by the 2020 Guangdong Science and Technology Special Fund ("Large Special + Task List") item (No: 200113165875501).

## SUPPLEMENTARY MATERIAL

The Supplementary Material for this article can be found online at: <https://www.frontiersin.org/articles/10.3389/fonc.2022.800291/full#supplementary-material>

## REFERENCES

- Mokhtari M, Rezaei A, Ghasemi A. Determination of Urinary 5-Hydroxyindoleacetic Acid as a Metabolomics in Gastric Cancer. *J Gastrointest Cancer* (2015) 46:138–42. doi: 10.1007/s12029-015-9700-9
- Jiayong Z, Jianjun X, Yongzhong O, Junwen L, Haiyan L, Dongliang Y, et al. Rapid Discrimination of Human Oesophageal Squamous Cell Carcinoma by Mass Spectrometry Based on Differences in Amino Acid Metabolism. *Sci Rep* (2017) 7:3738. doi: 10.1038/s41598-017-03375-8
- Hargadon Km, Johnson Ce, Williams CJ. Immune Checkpoint Blockade Therapy for Cancer: An Overview of FDA-Approved Immune Checkpoint Inhibitors. *Int Immunopharmacol* (2018) 62:29–39. doi: 10.1016/j.intimp.2018.06.001
- Fan L, Li Y, Chen JY, Zheng YF, Xu XM. Immune Checkpoint Modulators in Cancer Immunotherapy: Recent Advances and Combination Rationales. *Cancer Lett* (2019) 456:23–8. doi: 10.1016/j.canlet.2019.03.050
- Amobi A, Qian F, Lugade AA, Odunsi K. Tryptophan Catabolism and Cancer Immunotherapy Targeting IDO Mediated Immune Suppression. *Adv Exp Med Biol* (2017) 1036:129–44. doi: 10.1007/978-3-319-67577-0\_9
- Labadie BW, Bao R, Luke JJ. Reimagining IDO Pathway Inhibition in Cancer Immunotherapy via Downstream Focus on the Tryptophan-Kynurenine-Aryl Hydrocarbon Axis. *Clin Cancer Res: an Off J Am Assoc Cancer Res* (2019) 25:1462–71. doi: 10.1158/1078-0432.ccr-18-2882
- Sonner JK, Deumelandt K, Ott M, Thomé CM, Rauschenbach KJ, Schulz S, et al. The Stress Kinase GCN2 Does Not Mediate Suppression of Antitumor T Cell Responses by Tryptophan Catabolism in Experimental Melanomas. *Oncimmunology* (2016) 5:e1240858. doi: 10.1080/2162402x.2016.1240858
- Roager HM, Licht TR. Microbial Tryptophan Catabolites in Health and Disease. *Nat Commun* (2018) 9:3294. doi: 10.1038/s41467-018-05470-4
- Georghe CE, Martin JA, Manriquez FV, Dinan TG, Cryan JF, Clarke G. Focus on the Essentials: Tryptophan Metabolism and the Microbiome-Gut-Brain Axis. *Curr Opin Pharmacol* (2019) 48:137–45. doi: 10.1016/j.coph.2019.08.004
- Du L, Xing Z, Tao B, Li T, Yang D, Li W, et al. Both IDO1 and TDO Contribute to the Malignancy of Gliomas via the Kyn-AhR-AQP4 Signaling Pathway. *Signal Transduct Target Ther* (2020) 5:10. doi: 10.1038/s41392-019-0103-4
- Guarnieri T, Abruzzo PM, Bolotta A. More Than a Cell Biosensor. Aryl Hydrocarbon Receptor at the Intersection of Physiology and Inflammation. *Am J Physiol Cell Physiol* (2020) 318(6):C1078–82. doi: 10.1152/ajpcell.00493.2019
- Dodd D, Spitzer MH, Van Treuren W, Merrill BD, Hryckowian AJ, Higginbottom SK, et al. A Gut Bacterial Pathway Metabolizes Aromatic Amino Acids Into Nine Circulating Metabolites. *Nature* (2017) 551:648–52. doi: 10.1038/nature24661
- Huang JY, Butler LM, Midttun Ø, Ulvik A, Wang R, Jin A, et al. A Prospective Evaluation of Serum Kynurenine Metabolites and Risk of Pancreatic Cancer. *PLoS One* (2018) 13:e0196465. doi: 10.1371/journal.pone.0196465
- Onesti CE, Boemer F, Josse C, Leduc S, Bours V, Jerusalem G. Tryptophan Catabolism Increases in Breast Cancer Patients Compared to Healthy Controls Without Affecting the Cancer Outcome or Response to Chemotherapy. *J Trans Med* (2019) 17:239. doi: 10.1186/s12967-019-1984-2
- Cheng J, Jin H, Hou X, Lv J, Gao X, Zheng G. Disturbed Tryptophan Metabolism Correlating to Progression and Metastasis of Esophageal Squamous Cell Carcinoma. *Biochem Biophys Res Commun* (2017) 486:781–7. doi: 10.1016/j.bbrc.2017.03.120
- Masri MFB, Mantri CK, Rathore APS, John ALS. Peripheral Serotonin Causes Dengue Virus-Induced Thrombocytopenia Through 5HT2 Receptors. *Blood* (2019) 133:2325–37. doi: 10.1182/blood-2018-08-869156
- Mann DA, Oakley F. Serotonin Paracrine Signaling in Tissue Fibrosis. *Biochim Biophys Acta* (2013) 1832:905–10. doi: 10.1016/j.bbdis.2012.09.009
- Sarrouille D, Mesnil M. Serotonin and Human Cancer: A Critical View. *Biochimie* (2019) 161:46–50. doi: 10.1016/j.biochi.2018.06.016
- Platten M, Nollen EAA, Röhrig UF, Fallarino F, Opitz CA. Tryptophan Metabolism as a Common Therapeutic Target in Cancer, Neurodegeneration and Beyond. *Nat Rev Drug Discov* (2019) 18:379–401. doi: 10.1038/s41573-019-0016-5

20. Yilmaz N, Ustundag Y, Kivrak S, Kahvecioglu S, Celik H, Kivrak I, et al. Serum Indoleamine 2,3 Dioxygenase and Tryptophan and Kynurenine Ratio Using the UPLC-MS/MS Method, in Patients Undergoing Peritoneal Dialysis, Hemodialysis, and Kidney Transplantation. *Renal Fail* (2016) 38:1300–9. doi: 10.1080/0886022x.2016.1209389
21. Badawy Aa. Tryptophan Availability for Kynurenine Pathway Metabolism Across the Life Span: Control Mechanisms and Focus on Aging, Exercise, Diet and Nutritional Supplements. *Neuropharmacology* (2017) 112:248–63. doi: 10.1016/j.neuropharm.2015.11.015
22. Zhang F, Wang Q, Xia T, Fu S, Tao X, Wen Y, et al. Diagnostic Value of Plasma Tryptophan and Symmetric Dimethylarginine Levels for Acute Kidney Injury Among Tacrolimus-Treated Kidney Transplant Patients by Targeted Metabolomics Analysis. *Sci Rep* (2018) 8:14688. doi: 10.1038/s41598-018-32958-2
23. Ruddell RG, Mann DA, Ramm GA. The Function of Serotonin Within the Liver. *J Hepatol* (2008) 48:666–75. doi: 10.1016/j.jhep.2008.01.006
24. Sarrouilhe D, Clarhaut J, Defamie N, Mesnil M. Serotonin and Cancer: What Is the Link? *Curr Mol Med* (2015) 15:62–77. doi: 10.2174/1566524015666150114113411
25. Leboyer M, Philippe A, Bouvard M, Guilloud-Bataille M, Bondoux D, Tabuteau F, et al. Whole Blood Serotonin and Plasma Beta-Endorphin in Autistic Probands and Their First-Degree Relatives. *Biol Psychiatry* (1999) 45:158–63. doi: 10.1016/s0006-3223(97)00532-5
26. Ni W, Watts SW. 5-Hydroxytryptamine in the Cardiovascular System: Focus on the Serotonin Transporter (SERT). *Clin Exp Pharmacol Physiol* (2006) 33:575–83. doi: 10.1111/j.1440-1681.2006.04410.x
27. Wu L, Oshima T, Tomita T, Ohda Y, Fukui H, Watari J, et al. Serotonin Disrupts Esophageal Mucosal Integrity: An Investigation Using a Stratified Squamous Epithelial Model. *J Gastroenterol* (2016) 51:1040–9. doi: 10.1007/s00535-016-1195-z
28. Barnette MS, Grous M, Manning CD, Price WJ, Nelson AH, Bondinell WE, et al. 5-Hydroxytryptamine (5-HT) and SK&F 103829 Contract Canine Lower Esophageal Sphincter Smooth Muscle by Stimulating 5-HT<sub>2</sub> Receptors. *Receptor* (1992) 2:155–67.
29. Hempling C, Neuhauser WL, Worl J. Serotonin-Immunoreactive Neurons and Mast Cells in the Mouse Esophagus Suggest Involvement of Serotonin in Both Motility Control and Neuroimmune Interactions. *Neurogastroenterol Motil* (2012) 24:e67–78. doi: 10.1111/j.1365-2982.2011.01797.x
30. Tohmola N, Ikonen O, Sane T, Markkanen H, Joensuu A, Renkonen R, et al. Analytical and Preanalytical Validation of a New Mass Spectrometric Serum 5-Hydroxyindoleacetic Acid Assay as Neuroendocrine Tumor Marker. *Clin Chim Acta; Int J Clin Chem* (2014) 428:38–43. doi: 10.1016/j.cca.2013.10.025
31. Modlin IM, Oberg K, Taylor A, Drozdov I, Bodei L, Kidd M. Neuroendocrine Tumor Biomarkers: Current Status and Perspectives. *Neuroendocrinology* (2014) 100:265–77. doi: 10.1159/000368363
32. van der Horst-Schrivers AN, Post WJ, Kema Ip, Links TP, Willemsse PH, Wymenga AN, et al. Persistent Low Urinary Excretion of 5-HIAA Is a Marker for Favourable Survival During Follow-Up in Patients With Disseminated Midgut Carcinoid Tumours. *Eur J Cancer (Oxf Engl: 1990)* (2007) 43:2651–7. doi: 10.1016/j.ejca.2007.07.025
33. Janson ET, Holmberg L, Stridsberg M, Eriksson B, Theodorsson E, Wilander E, et al. Carcinoid Tumors: Analysis of Prognostic Factors and Survival in 301 Patients From a Referral Center. *Ann Oncol: Off J Eur Soc Med Oncol* (1997) 8:685–90. doi: 10.1023/a:1008215730767
34. Zandee WT, Kamp K, Van Adrichem RC, FeeldersRa, De Herder WW. Limited Value for Urinary 5-HIAA Excretion as Prognostic Marker in Gastrointestinal Neuroendocrine Tumours. *Eur J Endocrinol* (2016) 175:361–6. doi: 10.1530/eje-16-0392
35. Kesarwani P, Kant S, Prabhu A, Chinnaiyan P. The Interplay Between Metabolic Remodeling and Immune Regulation in Glioblastoma. *Neuro-Oncology* (2017) 19:1308–15. doi: 10.1093/neuonc/nox079
36. Roussel G, Bessede A, Klein C, Maitre M, Mensah-Nyagan AG. Xanthurenic Acid Is Localized in Neurons in the Central Nervous System. *Neuroscience* (2016) 329:226–38. doi: 10.1016/j.neuroscience.2016.05.006
37. Fazio F, Lionetto L, Curto M, Iacovelli L, Copeland CS, Neale SA, et al. Cinnabarinic Acid and Xanthurenic Acid: Two Kynurenine Metabolites That Interact With Metabotropic Glutamate Receptors. *Neuropharmacology* (2017) 112:365–72. doi: 10.1016/j.neuropharm.2016.06.020
38. Larsson SC, Orsini N, Wolk A. Vitamin B6 and Risk of Colorectal Cancer: A Meta-Analysis of Prospective Studies. *JAMA* (2010) 303:1077–83. doi: 10.1001/jama.2010.263
39. Le Marchand L, Wang H, Selhub J, Vogt TM, Yokochi L, Decker R. Association of Plasma Vitamin B6 With Risk of Colorectal Adenoma in a Multiethnic Case-Control Study. *Cancer Causes Control: CCC* (2011) 22:929–36. doi: 10.1007/s10552-011-9759-y
40. Theofylaktopoulou D, Midttun Ø, Ueland PM, Meyer K, Fanidi A, Zheng W, et al. Impaired Functional Vitamin B6 Status Is Associated With Increased Risk of Lung Cancer. *Int J Cancer* (2018) 142:2425–34. doi: 10.1002/ijc.31215
41. Zuo H, Ueland PM, Eussen SJ, Tell GS, Vollset SE, Nygård O, et al. Markers of Vitamin B6 Status and Metabolism as Predictors of Incident Cancer: The Hordaland Health Study. *Int J Cancer* (2015) 136:2932–9. doi: 10.1002/ijc.29345
42. Oxenkrug G, Ratner R, Summergrad P. Kynurenines and Vitamin B6: Link Between Diabetes and Depression. *J Bioinf Diabetes* (2013) 1(1). doi: 10.14302/issn.2374-9431.jbd-13-218

**Conflict of Interest:** The authors declare that the research was conducted in the absence of any commercial or financial relationships that could be construed as a potential conflict of interest.

**Publisher's Note:** All claims expressed in this article are solely those of the authors and do not necessarily represent those of their affiliated organizations, or those of the publisher, the editors and the reviewers. Any product that may be evaluated in this article, or claim that may be made by its manufacturer, is not guaranteed or endorsed by the publisher.

Copyright © 2022 Chen, Chen, Guo, Yang, Chen, Zhao, Xu, Zhang, Lin, Zhong and Zhang. This is an open-access article distributed under the terms of the Creative Commons Attribution License (CC BY). The use, distribution or reproduction in other forums is permitted, provided the original author(s) and the copyright owner(s) are credited and that the original publication in this journal is cited, in accordance with accepted academic practice. No use, distribution or reproduction is permitted which does not comply with these terms.

# Advantages of publishing in Frontiers



## OPEN ACCESS

Articles are free to read  
for greatest visibility  
and readership



## FAST PUBLICATION

Around 90 days  
from submission  
to decision



## HIGH QUALITY PEER-REVIEW

Rigorous, collaborative,  
and constructive  
peer-review



## TRANSPARENT PEER-REVIEW

Editors and reviewers  
acknowledged by name  
on published articles

## Frontiers

Avenue du Tribunal-Fédéral 34  
1005 Lausanne | Switzerland

Visit us: [www.frontiersin.org](http://www.frontiersin.org)

Contact us: [frontiersin.org/about/contact](http://frontiersin.org/about/contact)



## REPRODUCIBILITY OF RESEARCH

Support open data  
and methods to enhance  
research reproducibility



## DIGITAL PUBLISHING

Articles designed  
for optimal readership  
across devices



## FOLLOW US

@frontiersin



## IMPACT METRICS

Advanced article metrics  
track visibility across  
digital media



## EXTENSIVE PROMOTION

Marketing  
and promotion  
of impactful research



## LOOP RESEARCH NETWORK

Our network  
increases your  
article's readership